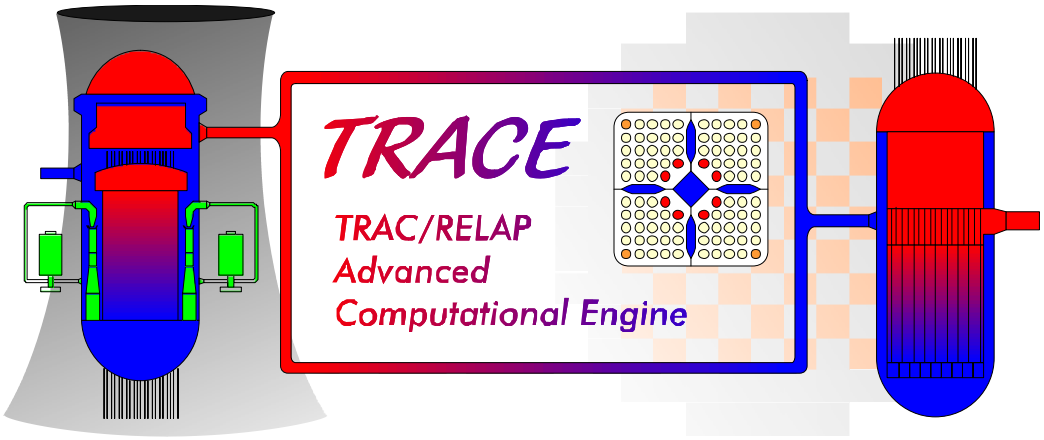

TRACE V5.0
ASSESSMENT MANUAL

Appendix C: Integral Effects Tests

Division of Risk Assessment and Special Projects
Office of Nuclear Regulatory Research
U. S. Nuclear Regulatory Commission
Washington, DC 20555-0001

This page intentionally left blank

PWR Large Break Integral Tests

C.1. LOFT Large Break Tests

Author(s): William A. Macon, Jr.

Affiliation: USNRC

Code Version: TRACE V5.0

Platform and Operating System: Intel x86, Windows XP

C.1.1. Introduction

Three Loss-of-Fluid Test (LOFT) large break loss-of-coolant accident (LBLOCA) tests, L2-5, L2-6 and LB-1, were simulated with the TRACE thermal-hydraulic computer program. The purpose of this report is to document the assessment of these simulations against measured data from these tests. The simulations were performed with TRACE V5.0. These tests were previously simulated with earlier versions of TRACE; the results can be examined in Reference 1 and Reference 2.

C.1.2. Test Facility Description

The LOFT Integral Test facility was a 50-MWt pressurized water reactor (PWR) system designed to simulate the major components and system responses of a commercial PWR during postulated LOCAs and anticipated transients. The facility was built at the Idaho National Engineering Laboratory during the 1970s and forty-four tests were completed over a nine-year period ending in July 1985. The LOFT facility is shown in Figure C.1-1 and described in detail in Reference 3 and Reference 4. The facility consisted of five major systems: the Reactor System with the nuclear core; Primary Coolant System; Blowdown Suppression System; Emergency Core Cooling System; and a Secondary Coolant System. These systems were extensively instrumented to measure the bahavior of system parameters during the tests.

The LOFT facility was scaled to represent a 1/60-scale model of a typical 1000-MWe (electric) commercial four-loop PWR. The unique feature of the facility was that the Reactor System had a UO_2 powered core. The entire nuclear core consisted of five square and four triangular fuel bundles with a total of 1300 fuel pins. The length of the core was 5.5 feet (1.68 m) instead of 12 feet, about one-half the length of typical reactor cores in commercial plants. However, this was the only compromise made in the nuclear fuel for the LOFT core. PWR 15x15 array fuel rod assemblies were used, complete with upper and lower end boxes and fuel rod spacer grids at five

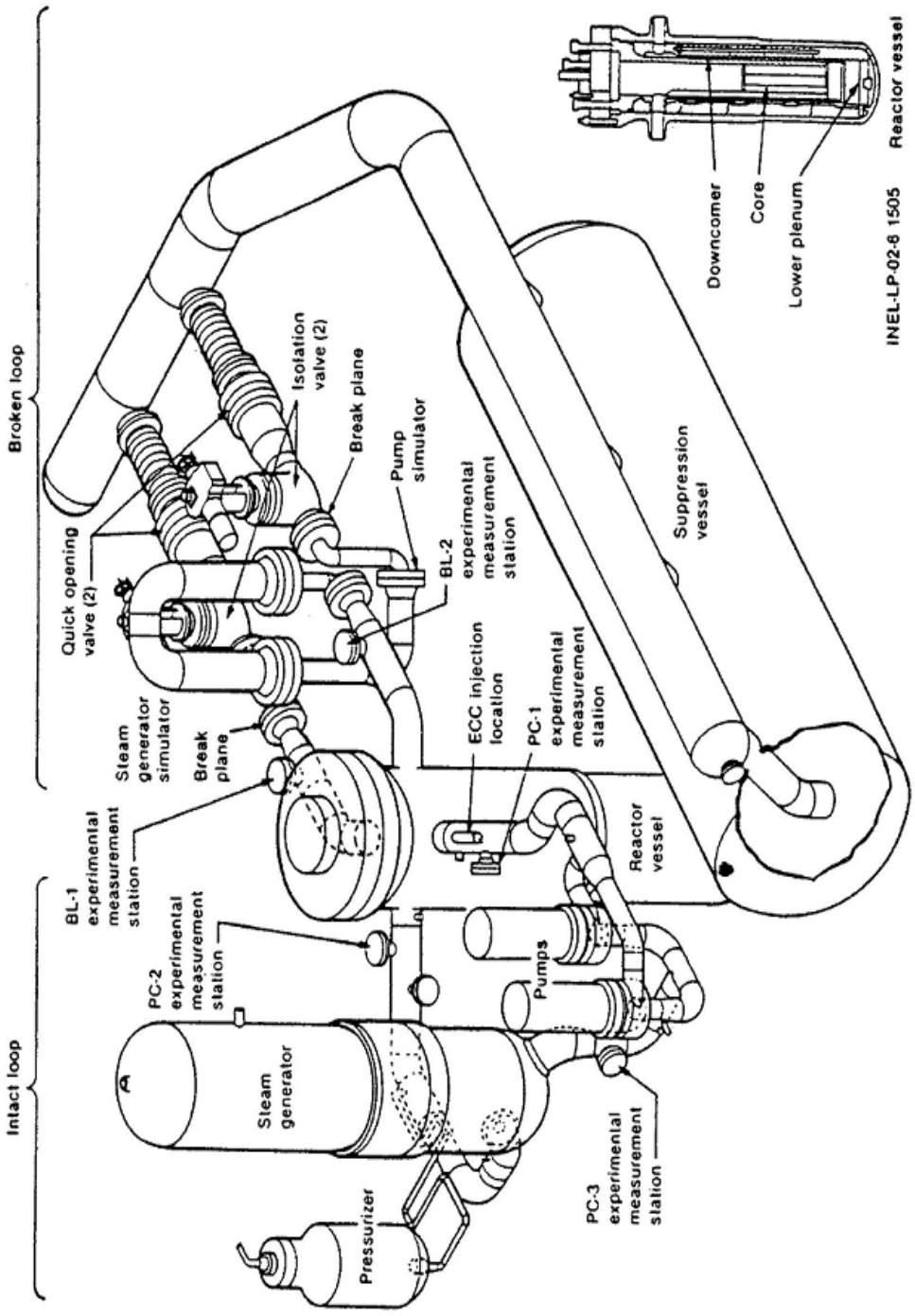

Figure C.1-1. Sketch of the LOFT facility.

locations. The LOFT fuel was designed to have the same physical, chemical and metallurgical properties as commercial fuel.

The Primary Coolant System consisted of an operating loop (with steam generator, two primary coolant pumps in parallel, pressurizer and connecting piping) representing three intact loops of a four-loop PWR. A “broken loop” simulated the broken loop of a four-loop PWR during LOCA conditions. The broken loop consisted of hot and cold legs that connect the Reactor System to the Pressure Suppression System, and was equipped with steam generator and pump simulators and quick-opening blowdown valves. The piping arrangement was variable to simulate either hot or cold leg breaks.

The Blowdown Suppression System was designed to simulate the containment backpressure in large PWRs during LOCA events. It consisted of a large pressure suppression tank, downcomers and a header connected to the Primary Coolant System via the quick-opening blowdown valves.

The Emergency Core Cooling System (ECCS) consisted of the same three systems used in commercial PWRs: the high-pressure injection system (HPIS), the accumulator, and the low-pressure injection system (LPIS). The systems were actuated similarly to their generic counterparts to inject scaled amounts of emergency core coolant (ECC) typical of the ECC delivery behavior in commercial PWRs. The LOFT ECCS had the capability of injecting ECC to any of several locations including the intact loop hot or cold legs, the reactor vessel downcomer, lower plenum, or upper plenum.

The Secondary System was designed to remove the heat transferred into the steam generator to the environment. However, this system could not be controlled for full simulation of secondary system response in large PWRs.

The component and system volumes of the Reactor and Primary Coolant Systems were designed proportional to their respective volumes in a commercial PWR and scaled to have the same volume-to-power ratio. The design objective for the LOFT facility was to produce the significant thermal-hydraulic phenomena with approximately the same conditions and sequence of events that could occur during postulated accidents in commercial PWR systems.

C.1.3. LOFT Test Descriptions

LOFT LBLOCA Tests L2-5, L2-6, and LB-1 are all 200% cold leg break tests. They differ in initial conditions such as power and loop flow. Table C.1.1 gives the measured initial conditions for the three tests. Detailed descriptions of these tests are given in Reference 5 for Test L2-5, Reference 6 and Reference 7 for Test L2-6, and Reference 8 for Test LB-1.

Table C.1.1. LOFT Measured Initial Conditions.

Parameter	L2-5	L2-6	LB-1
Reactor Power (MW)	36.0	46.0	49.3

Table C.1.1. LOFT Measured Initial Conditions.

Parameter	**L2-5**	**L2-6**	**LB-1**
Low Pressure Reactor Scram Set Point (MPa)	14.19	Unknown	14.5
Intact Loop Mass Flow (kg/s-m^2)	192.4	248.7	305.8
Hot Leg Pressure (MPa)	14.94	15.09	14.90
Hot Leg Temperature (K)	589.7	589.0	587.8
Cold Leg Temperature (K)	556.6	555.9	556.0
Pump Speed (rad/s)	131	173	209
Pressurizer Steam Volume (m^3)	0.32	0.39	0.37
Pressurizer Liquid Volume (m^3)	0.61	0.607	0.56
Steam Generator Pressure (MPa)	5.85	5.63	5.53
Steam Generator Mass Flow (kg/s)	19.1	24.3	25.4
Accumulator Pressure (MPa)	4.29	4.11	4.21
Accumulator Temperature (K)	303.2	302	305
Accumulator Initial Level (m)	2.105	2.11	2.31
Accumulator Level at End of Discharge (m)	0.97	1.07	1.75
Accumulator Liquid Level Change (m)	1.135	1.04	0.56
Accumulator Liquid Volume Discharged (m^3)	1.43	1.304	0.76
Accumulator Initial Gas Volume (m^3)	0.96	0.96	0.65
Accumulator Initial Gas/Liquid Fraction	0.67	0.75	0.85

C.1.4. Description of the TRACE Model

The TRACE LOFT input model consists of 67 components including PIPEs, PUMPS, TEEs, HTSTRs, and a VESSEL. Vessel and loop noding diagrams of the TRAC input model are shown in Figure C.1-2 (vessel), Figure C.1-3 (intact loop), Figure C.1-4 (intact loop steam generator secondary), and Figure C.1-5 (broken loop). The input evolved from a TRAC-PD2 model, which was modified for TRAC-PF1/MOD1 by Los Alamos National Laboratory (LANL), improved and modified by United Kingdom Atomic Energy Authority (UKAEA), and then again modified by LANL (Ref. 6) for TRAC-PF1/MOD2. The model does not activate any level tracking logic.

The VESSEL component has 12 axial levels, 4 radial rings and 4 theta sectors. The core is modelled as a ROD component with rods in each of the 3 inner rings from levels 4 through 8. The input file has reflood logic turned on.

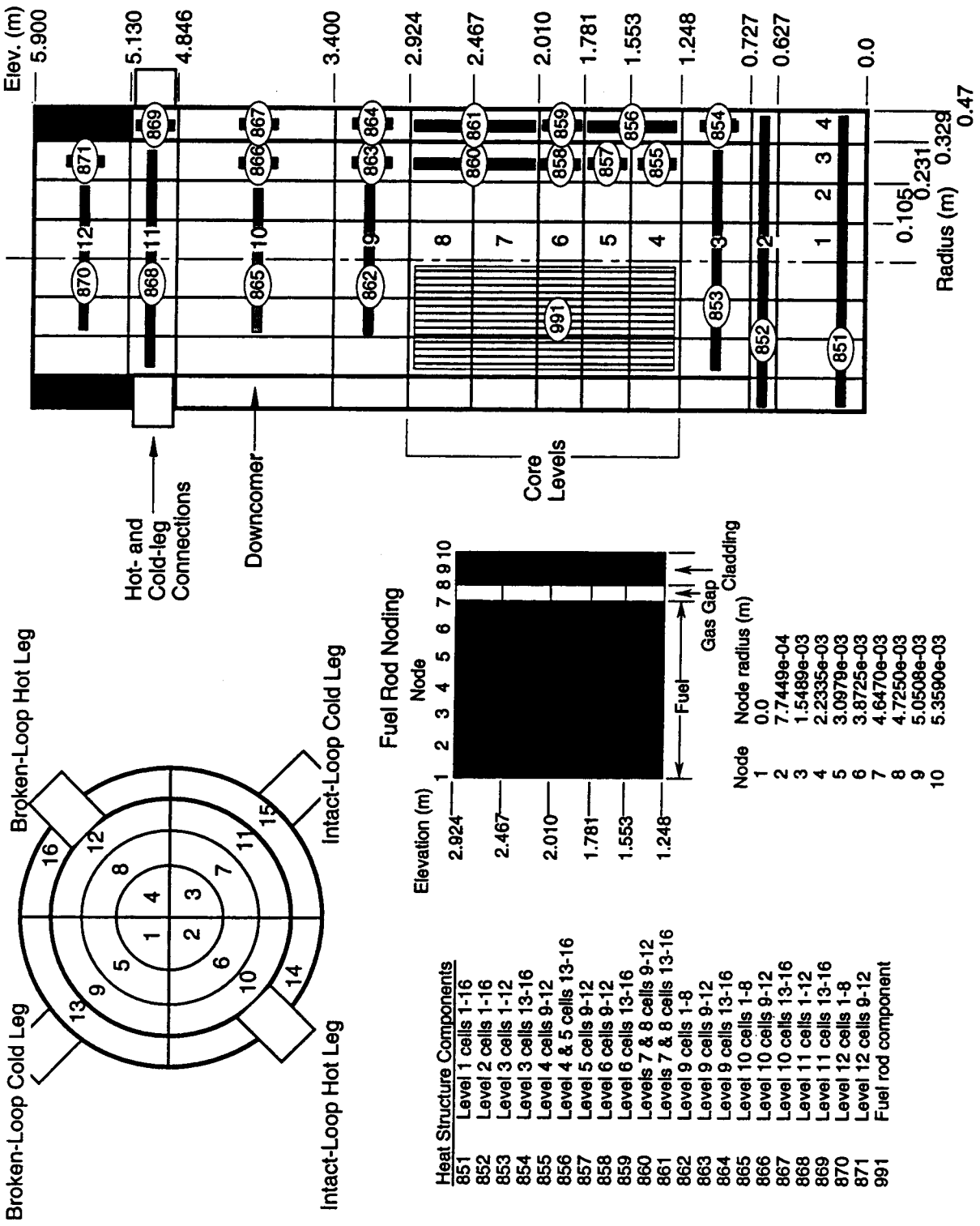

Figure C.1-2. LOFT Reactor Vessel Noding Diagram.

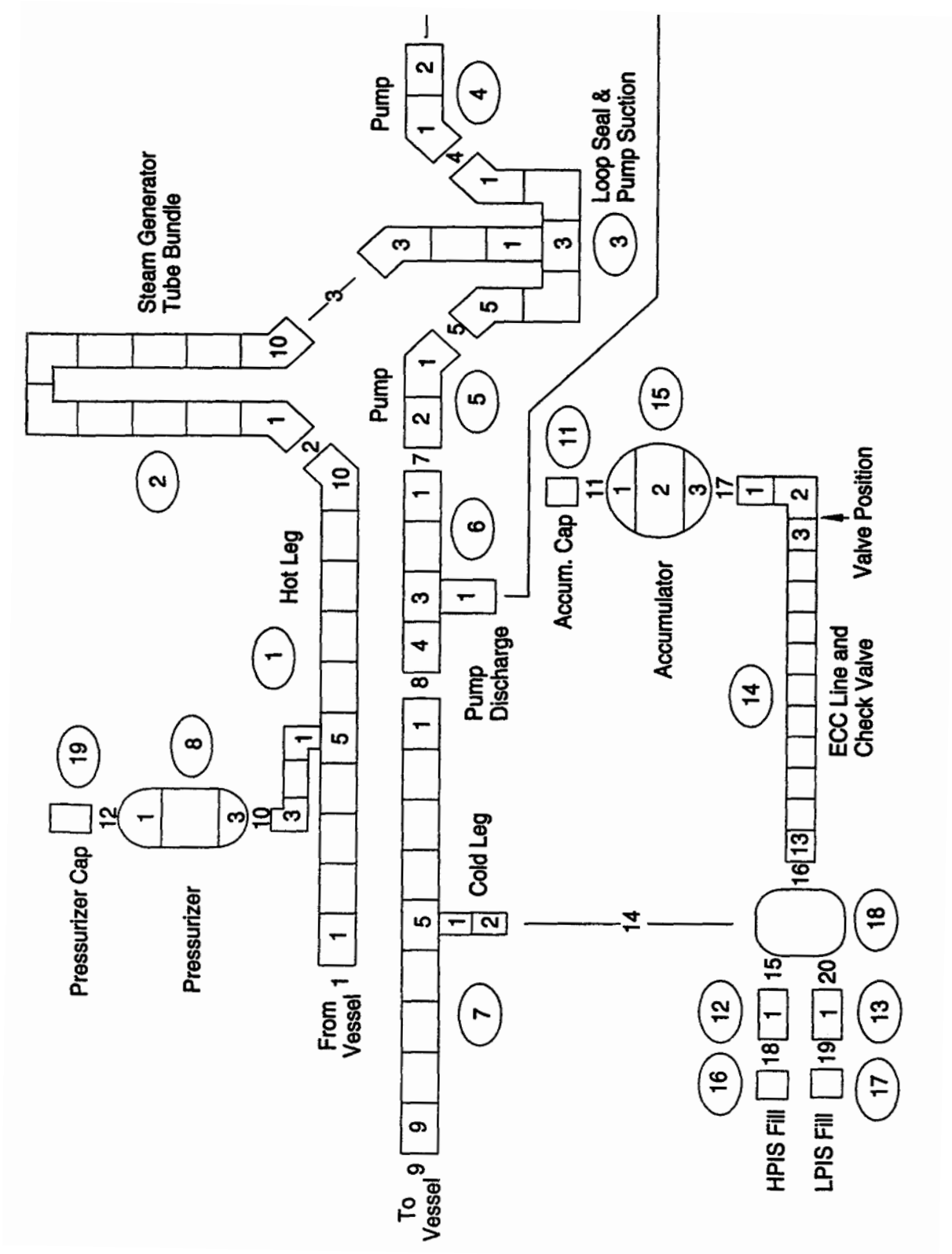

Figure C.1-3. LOFT Intact Loop Noding Diagram.

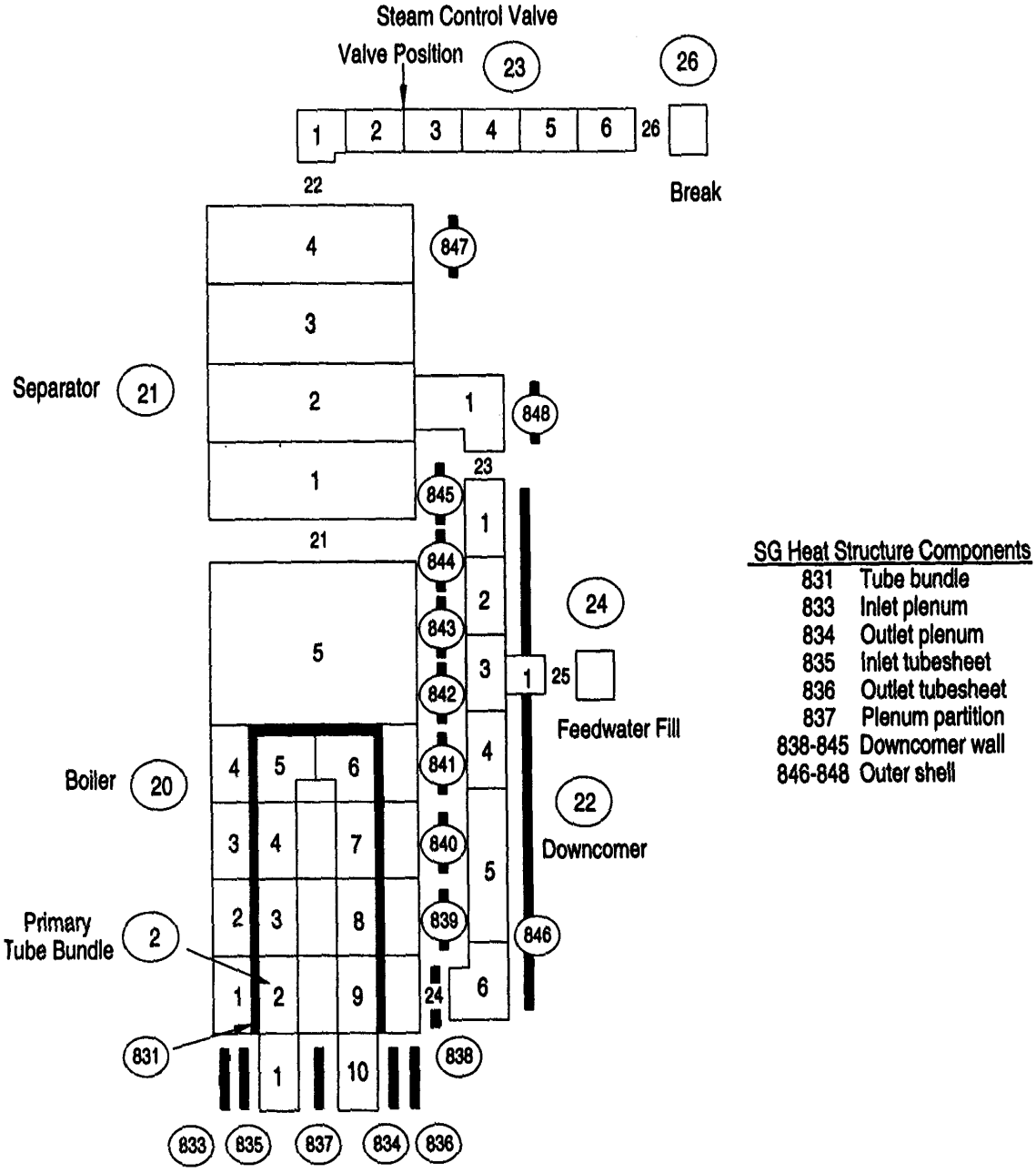

Figure C.1-4. LOFT Intact Loop Secondary Side Steam Generator Noding Diagram.

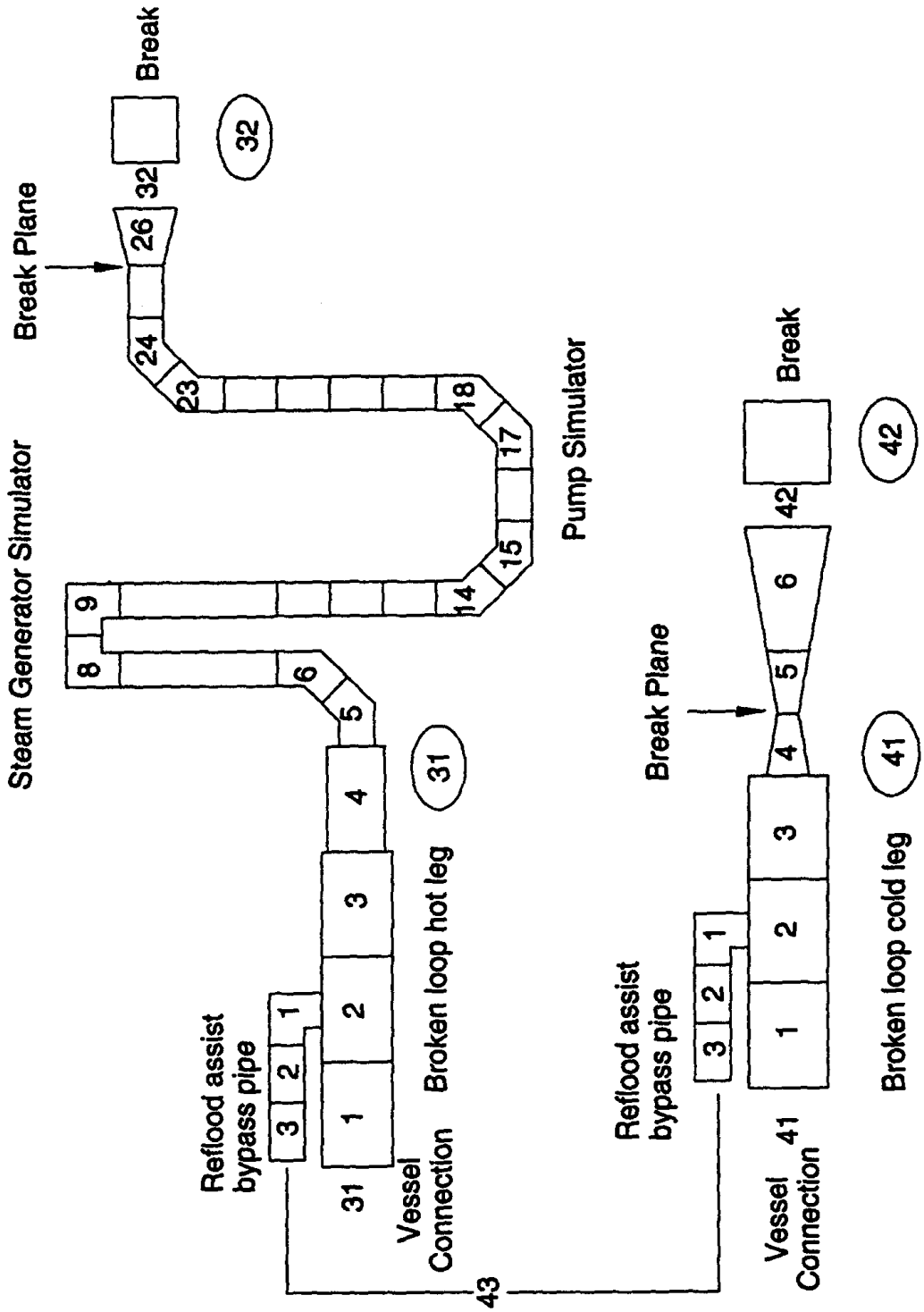

Figure C.1-5. LOFT Broken Loop Noding Diagram.

The nozzles installed in the broken loop cold and hot legs have an inside diameter of 0.1032 m. The broken hot leg nozzle is downstream from the passive steam generator and pump simulators. The break is initiated by opening quick-opening blowdown valves (downstream from the nozzles) that open in about 20 ms.

The ECCS injects into the intact cold leg and provides a scaled amount of ECC to represent the injection into three loops. The primary coolant pumps trip at 0.8 s and coast down under the influence of the flywheels; when the pump speed drops below 73.54 rad/s, the flywheel uncouples from the pump and effectively reduces the pump moment of inertia. The assumption of loss of offsite power at the initiation of the transient results in a delay in the availability of the HPIS and LPIS.

There are 5 spacer grids along the axial length of each fuel bundle assembly. The axial power profile used in the model and the spacer grid locations are shown in Figure C.1-6. The spacer grids are not modeled in the TRACE model. .

C.1.5. LOFT Large Break Test L2-6

Test L2-6 is discussed first since the other input files are based on this test. Steady-state and then transient results are presented.

LOFT Test L2-6 (Experiment LP-02-6) was performed to analyze the effects of a 200% double-ended break of a commercial PWR main cold leg coolant pipe. The major objective of this test was to provide data to assess the capability of computer codes to predict PWR system response during a design basis accident. The test was initiated from a power level of 46.0 MW, yielding a maximum linear generation rate of 48.8 kW/m. The initial conditions for this test were representative of USNRC licensing limits in a commercial PWR and included loss of offsite power coincident with LOCA initiation and minimum ECC injection.

Significant initial conditions for Test L2-6 were: system pressure 15.09 MPa; core outlet temperature 589.0 K; and intact loop mass flow rate 248.7 kg/s. The test was initiated by opening the quick-opening blowdown valves in the broken loop hot and cold legs. The reactor was scrammed on a low pressure signal at 0.1 s in the test. Following the reactor scram, the primary coolant pumps were tripped at 0.8 s and allowed to coast down until 16.5 s when their rotational speed fell below the trip setpoint and they were decoupled from their flywheels.

Flow in the core reversed almost instantaneously with test initiation, and the fuel rod cladding temperatures started to increase due to stored thermal energy at 0.9 s. The entire core heated up until 5.2 s, when positive core flow was again established due to choking of the flow in the broken cold leg. This positive core flow quenched the lower 2/3 of the core until about 10 s when flow in the intact cold leg decreased to below that of the broken cold leg and the core again started to heat up. A partial top-down core quench initiated at 14.8 s and lasted until 18.6 s. Accumulator injection of ECC to the intact loop cold leg began at 17.5 s. Delayed ECC injection from the HPIS and LPIS began at 21.8 s and 34.8 s, respectively. The fuel rod peak cladding temperature of

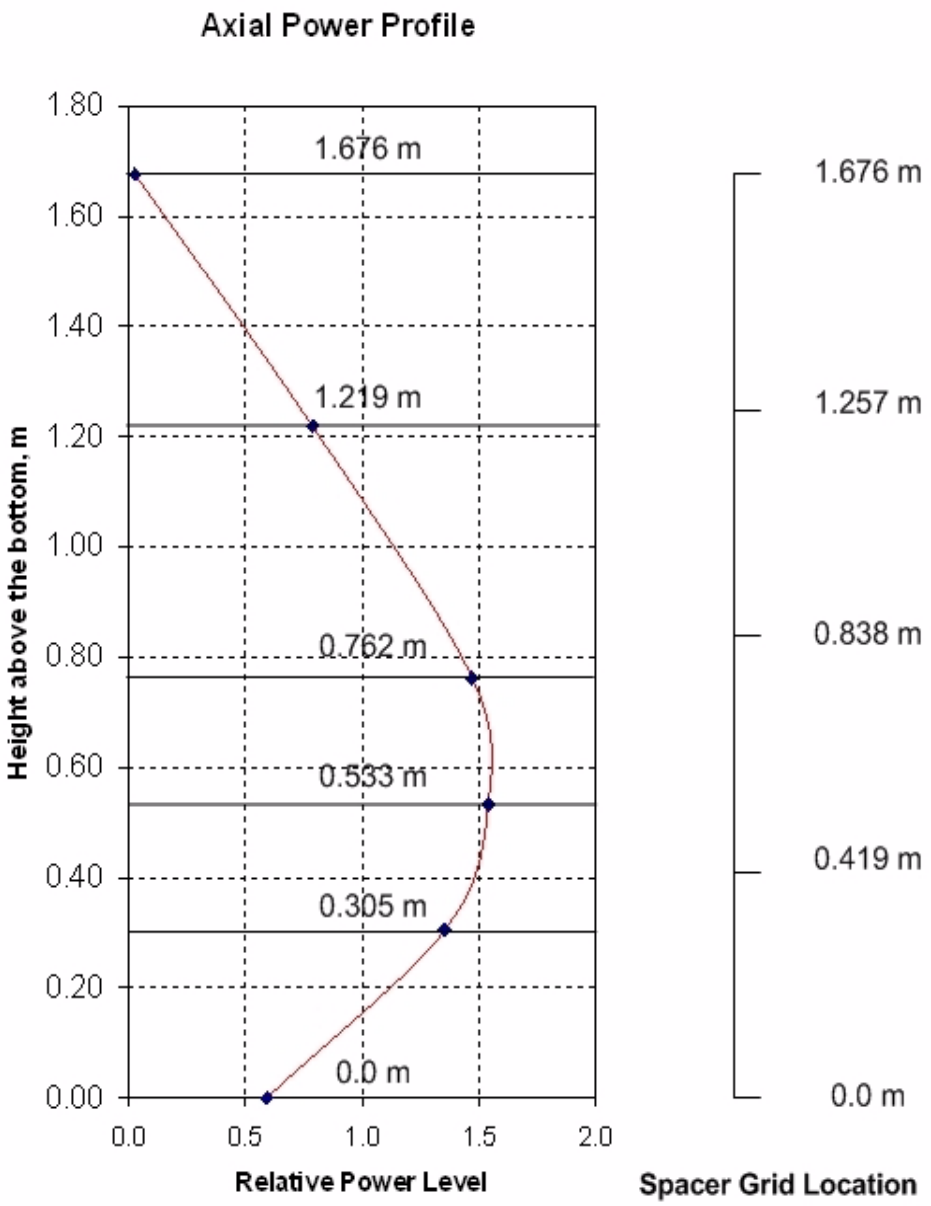

Figure C.1-6. LOFT Reactor Core Axial Power Profile and Spacer Grid Locations.

1055 K was attained at 41.0 s. The lower plenum was filled by 30.7 s, the core quench was complete by 56.0 s, and core reflood was complete by 59.0 s.

C.1.6. Steady-State Calculations for LOFT Test L2-6

Constrained steady-state (CSS) controllers drive the steady-state solution to the user desired loop flow rate, secondary side pressure, and cold leg temperature. The resulting initial conditions for Test L2-6 are given in Table C.1.2

.

Table C.1.2. L2-6 Initial Conditions - Measured and TRACE V5.0.

Parameter	**Measured**	**TRACE**
Reactor Power (MW)	46.0 ± 1.2	46.0
Intact Loop Mass Flow Rate (kg/s)	248.7 ± 2.6	248.0
Cold Leg Temperature (K)	555.9 ± 1.1	556.9
Hot Leg Temperature (K)	589 ± 1.1	590.7
Pressurizer Pressure (MPa)	15.0 ± 0.11	15.0
Pressurizer Level (m)	1.04 ± 0.04	1.10
Steam Generator Pressure (MPa)	5.63 ± 0.2	5.63

Predicted steady-state results are shown in Figure C.1-7, Figure C.1-8, Figure C.1-9 and Figure C.1-10 to demonstrate that initial conditions prior to blowdown were steady. Plots show intact loop mass flow rate, hot and cold leg temperatures, pressurizer and steam generator pressures, and pressurizer level, respectively.

C.1.6.1. Transient Calculations for LOFT Test L2-6

The transient sequence of events for Test L2-6 are shown in Table C.1.3. Reactor power was scrammed on a low pressure signal at 0.1 s in the test. However, the low pressure set point for

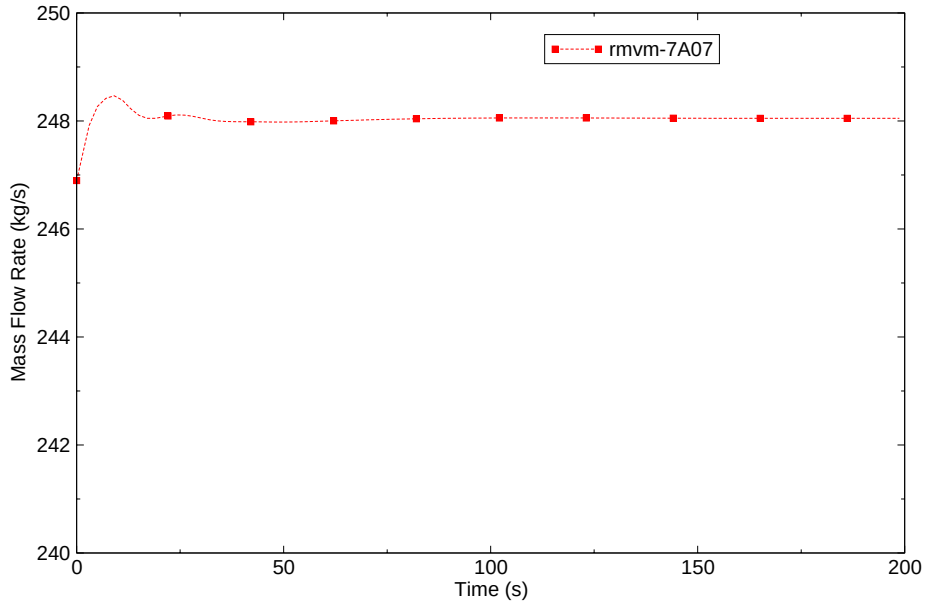

Figure C.1-7. L2-6 Intact Loop Mass Flow Rate.

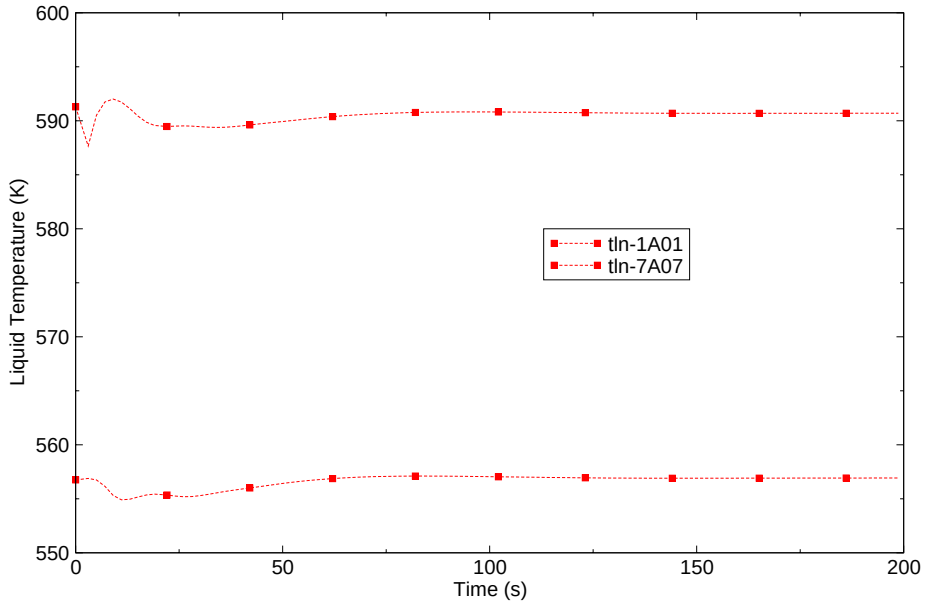

Figure C.1-8. L2-6 Predicted Steady-State Hot and Cold Leg Temperatures.

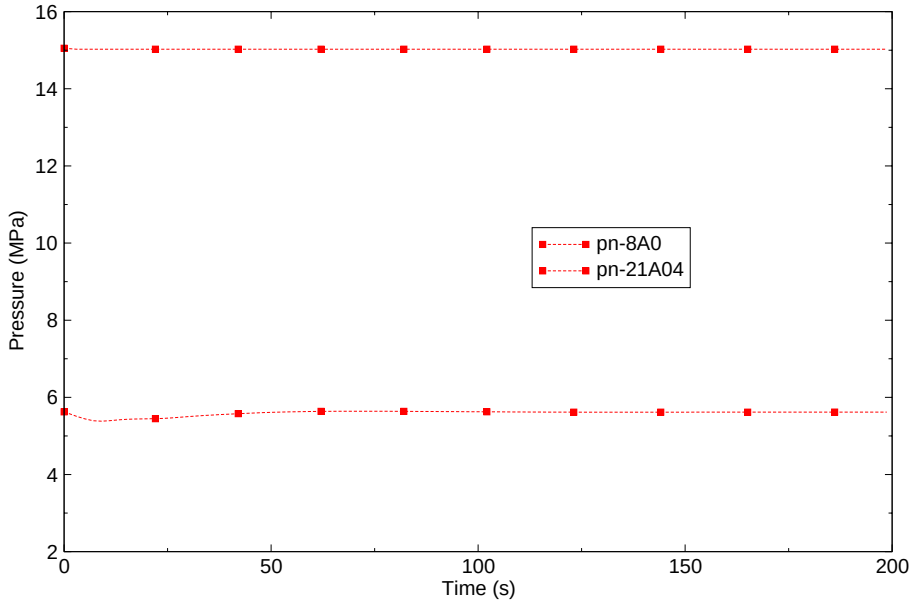

Figure C.1-9. L2-6 Predicted Steady-State Pressurizer and Steam Generator Pressures.

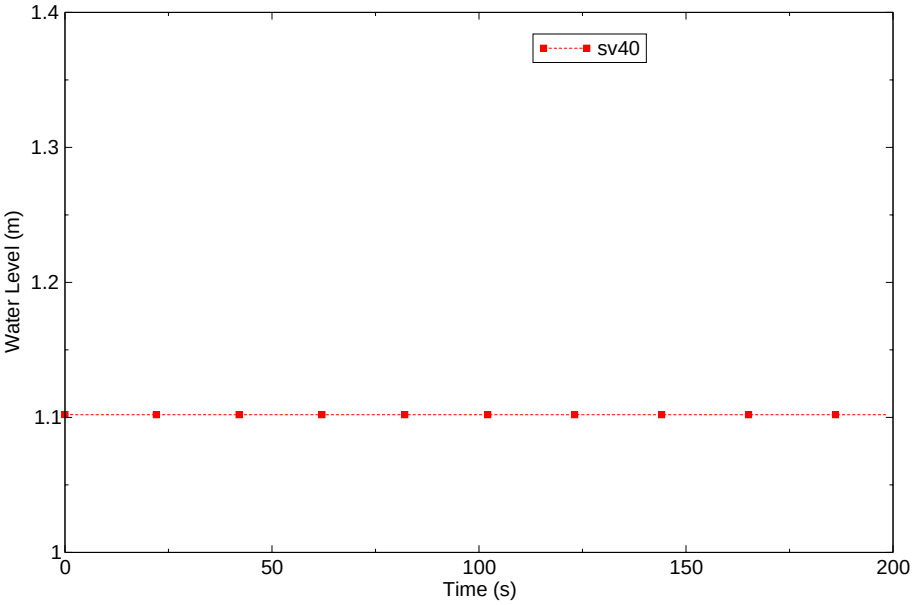

Figure C.1-10. L2-6 Predicted Steady-State Pressurizer Level.

scramming the reactor was not known. Therefore, the reactor in the simulation was scrammed on time as shown in Table C.1.3. .

Table C.1.3. L2-6 Sequence of Event Timing.

Event	**Measured**	**TRACE V5.0**
Break Initiated (s)	0.0	0.0
Reactor Scrammed (s)	0.1 ± 0.01	0.1
Primary Coolant Pumps Tripped (s)	0.8 ± 0.01	0.8
Pressurizer Emptied (s)	15.5 ± 0.5	14.8, void in bottom cell=0.92
Accumulator A Injection Initiated (s)	17.5 ± 0.5	15.2
Reflood Tripped On (s)	NA	0.0
HPIS Injection Initiated (s)	21.8 ± 0.01	21.8
LPIS Injection Initiated (s)	36.96 ± 0.01	36.6
Maximum Cladding Temperature Reached (K)	1074 ± 13.3	1065

The reflood model was active during both steady-state and transient calculations. The choked flow model was turned on in the BREAK components (ICFLOW = 2) with user input multipliers in the choked flow model set at CHM12 = 1.0, CHM22 = 0.84, and CHM13 = CHM23 = CHM14 = CHM 24 = CHM15 = CHM25 = 1.0. The noding upstream of the break was not changed from the steady-state noding.

The transient plots show the measured data as black lines with the TRACE calculation shown in red. The channel identifiers are shown in the legend box.

A comparison of the TRACE calculated pressure and the measured pressure for the intact loop hot leg is shown in Figure C.1-11. The pressure comparison is excellent through the subcooled blowdown and the initial phase of the two-phase blowdown (0 s to about 15 s). During the two-phase blowdown (15 s to about 25 s), TRACE shows a slightly faster depressurization than indicated by the data, but the difference is not significant. During the reflood phase of the transient (25 s to about 60 s), the TRACE predicted pressure is in reasonable agreement with the data. The pressure data uncertainty is given in Reference 3 as 0.214 MPa plus 1% of reading during subcooled blowdown and 0.081 MPa plus 0.1% of reading during saturated blowdown. Generally, the predicted results lie within the data uncertainty.

The calculated and measured intact loop hot leg mass flow rates are shown in Figure C.1-12. Between 0 s and 5 s the predicted mass flow rate is higher than the data. Between 5 s and 25 s, a high negative mass flow rate is predicted by the code that is not observed in the data. An examination of the measured intact loop hot leg differential pressure shown in Figure C.1-13 indicates there was a flow reversal. According to Reference 9, the flow venturi measured only the magnitude of the mass flow rate and not its direction. Consequently, the absolute values of the mass flow rate as shown in Figure C.1-14 provide a more direct indication of the agreement

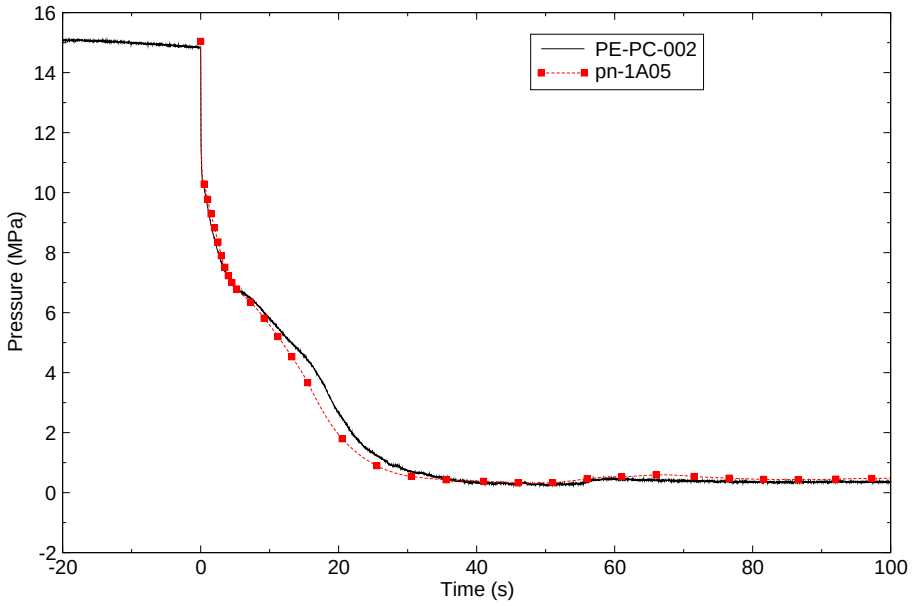

Figure C.1-11. L2-6 Intact Loop Hot Leg Pressure.

between the calculated and measured results. Reference 1 gives the intact loop venturi meter flow rate accuracy as ±5 kg/s; thus, the predicted mass flow rate is generally within the data error.

The calculated and measured intact loop cold leg mass flow rates between the pumps and the ECC injection location are compared in Figure C.1-15. The cold leg flow decreased after the pump trips in both the calculations and the test. Generally, the predicted cold leg mass flow rate compares well with the data. Between 8 s and 20 s, TRACE over-predicted the break mass flow rate but the results were generally within the uncertainty of the data. After 20 s, the calculated results were generally smoother and under-predicted, particularly during the reflood period in the core. Further investigation as to the reasons for the under-prediction is warranted.

The calculated and measured impeller rotational speeds for pump 1 and pump 2 in the intact loop cold leg are shown in Figure C.1-16. Both pumps responded in a similar manner. The measured speeds were nearly constant until the pump trips and then decreased rapidly as the pumps coasted down after they were decoupled from their flywheels. In the calculation, the pumps were decoupled at OMTEST = 118 rad/s, the equivalent rotational speed at 16.5 s in the test, and resulted in the pumps being decoupled slightly earlier. One reason for this discrepancy is that the LOFT pump curves in TRACE use the Semiscale pump curve tables and needs to be updated. Rather than decreasing to zero speed, as might have been expected because the pumps were disconnected from their flywheels, the speeds remained relatively constant near 50 rad/s between 30 s and 60 s and then increased until 75 s. The speed increased because the volumetric flow through the intact loop cold leg was sufficient to accelerate the pump rotors. The steam flow through the intact loop decreased after this time, causing the pump speeds to decrease. Although

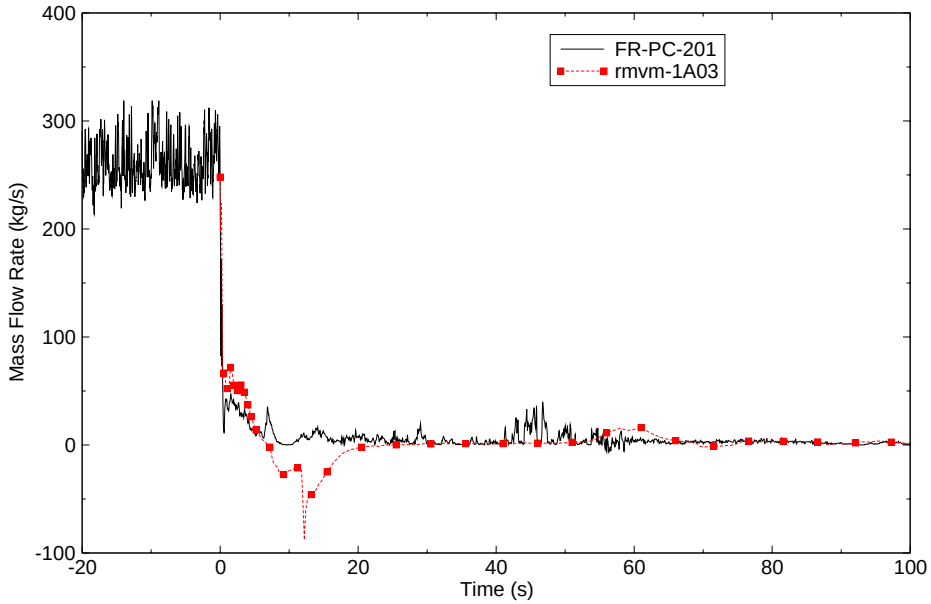

Figure C.1-12. L2-6 Intact Loop Hot Leg Mass Flow Rate.

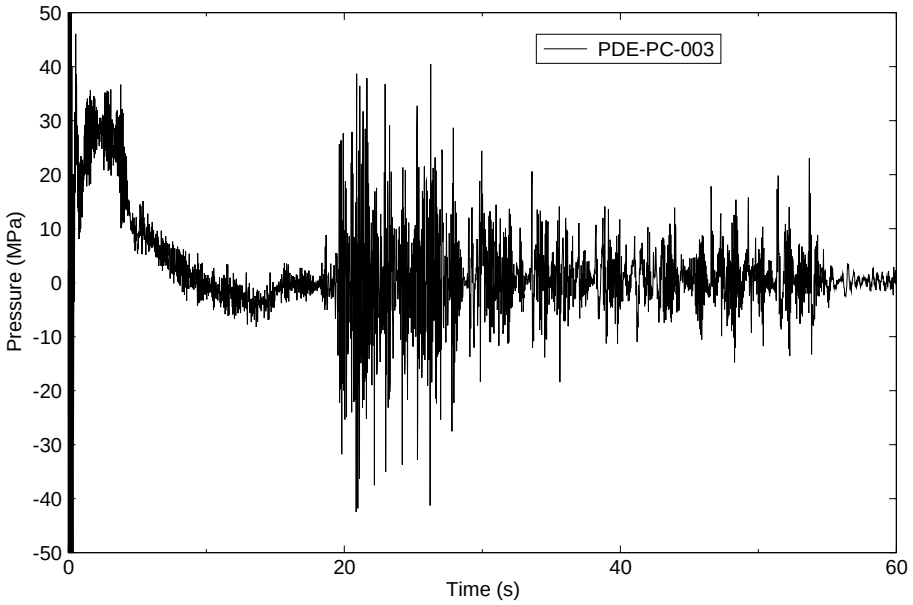

Figure C.1-13. L2-6 Measured Intact Loop Hot Leg Differential Pressure.

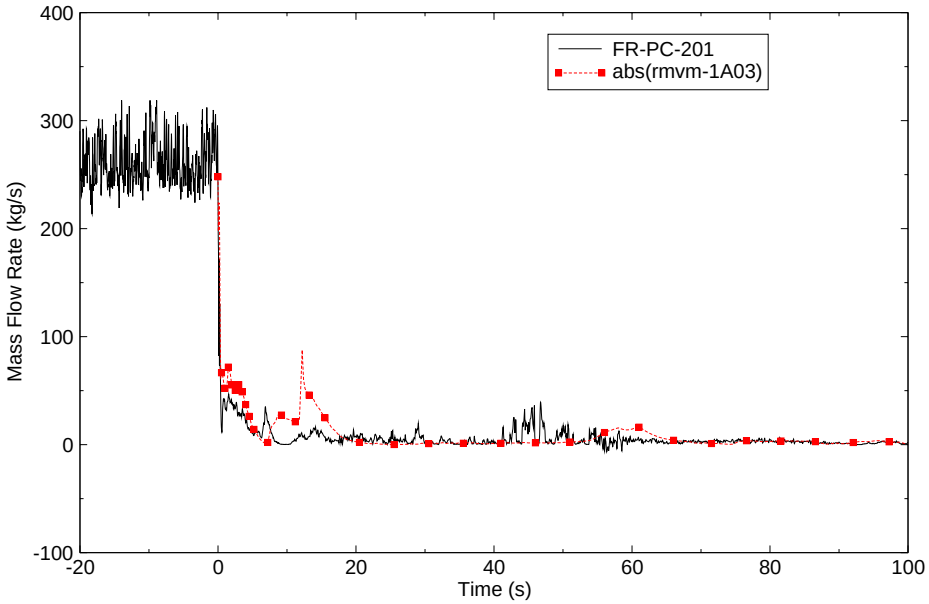

Figure C.1-14. L2-6 Intact Loop Hot Leg Mass Flow Rate.

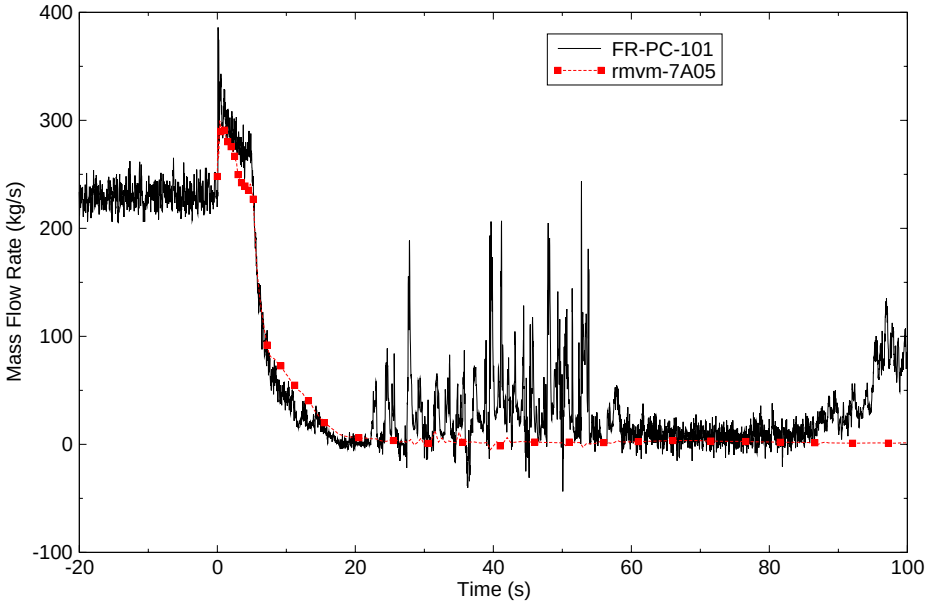

Figure C.1-15. L2-6 Intact Loop Cold Leg Mass Flow Rate.

there were differences in magnitude and timing, the trends of the calculations were similar to those observed in the test.

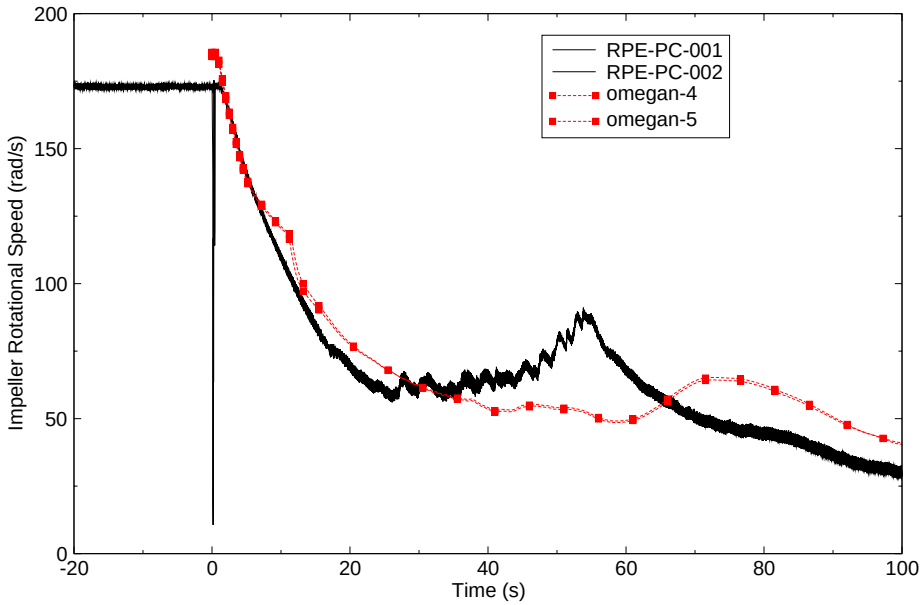

Figure C.1-16. L2-6 Pump Impeller Rotational Speed.

The calculated and measured secondary pressures are shown in Figure C.1-17. The pressure initially began to rise when the steam control valve began to close following reactor trip. The pressure reached a peak and began to decrease due to reduction in heat transfer from the primary side, and the calculated results were in excellent agreement with the measurement for the first several seconds. The pressure decreased relatively rapidly until the steam control valve was completely closed at 11 s, and TRACE over-predicted the pressure drop. The pressure then decreased at a more gradual rate due to heat transfer from the secondary side to the primary side of the steam generator. Further investigation of the heat transfer coefficient in the steam generator tubes may be warranted as shown here and for Test LB-1, but Test L2-5 results were in better agreement.

The calculated and measured mass flow rates in the broken loop hot leg and broken loop cold leg are shown in Figure C.1-18 and Figure C.1-19. The predictions are within the data error bands. At the initiation of the break the measured and calculated mass flow rate is high until two phase flow occurred at the break. Choking occurred and the break mass flow rate decreased. The predicted mass flow rate agrees quite well during the subcooled blowdown and the onset of choked flow at the break. The measured flow in the broken loop cold leg was substantially larger than the flow in the broken loop hot leg, particularly during the first 5 s of the transient. The fluid in the broken loop cold leg, which was supplied by the downcomer, remained subcooled for several seconds. The fluid in the broken loop hot leg, which was supplied by the upper plenum, was relatively hot compared to that in the downcomer. Consequently, the fluid downstream of the broken loop hot

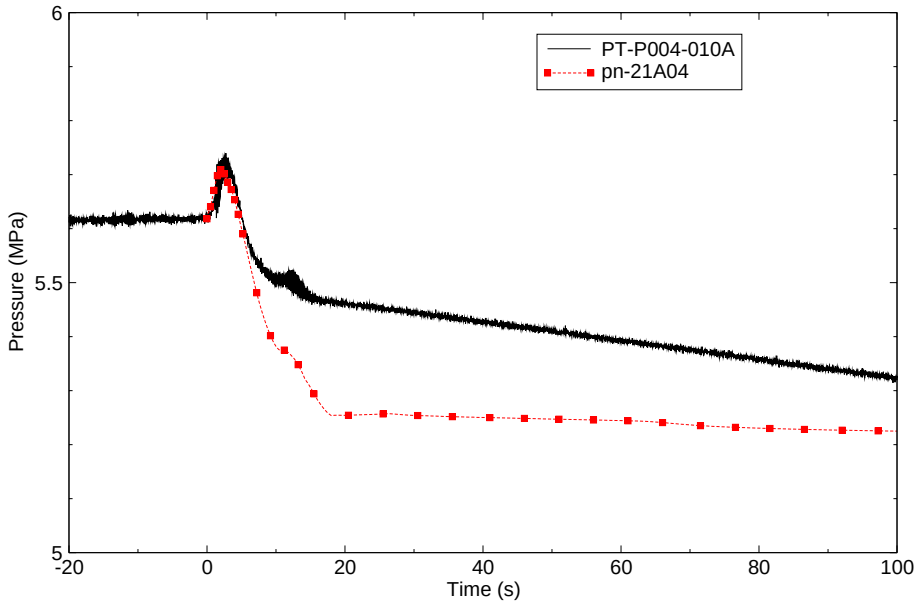

Figure C.1-17. L2-6 SG Secondary System Pressure.

leg reached the saturation temperature almost immediately after the breaks opened. Since the critical mass flow increases with subcooling, higher mass flow rates were obtained at the cold leg break connected to the downcomer. The calculation slightly under-predicted the cold leg mass flow during the first couple of seconds and slightly over-predicted the hot leg mass flow at about 5-10 s, but the calculated results are generally within the uncertainties of the measurements and are thus considered to be in excellent agreement with the data.

The calculated and measured fluid densities in the intact loop cold leg between the pump discharge and the ECC line connection are shown in Figure C.1-20. The density in the cold leg remained near its initial value until about 6 s in both the calculations and the test. Flashing then began in the cold legs and the density decreased rapidly. The calculated results were in reasonable agreement with the measurements until about 24 s, when a series of large-amplitude density oscillations were measured in the test. Oscillations of about the correct frequency were calculated, but the magnitude of the oscillations was generally much smaller in the calculations than in the test. The oscillations appear to be related to the condensation associated with accumulator injection because the oscillations started after accumulator injection began and died out soon after accumulator injection ended. In the test, the cold leg density indicated that the pipe was nearly full of liquid at times, which implies that almost all of the steam then flowing through the intact loop pumps was condensing in the cold leg.

The calculated and measured fluid densities in the broken loop cold leg are shown in Figure C.1-21. The density remained near its initial value for several seconds in both the calculations and the test. The subsequent decrease in density indicated the end of subcooled flow out of the broken

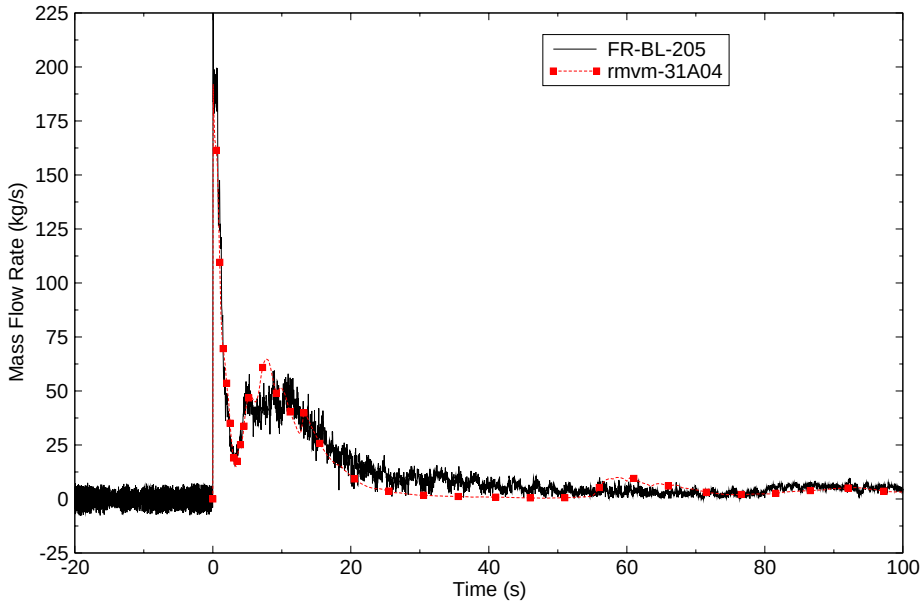

Figure C.1-18. L2-6 Broken Loop Hot Leg Mass Flow Rate.

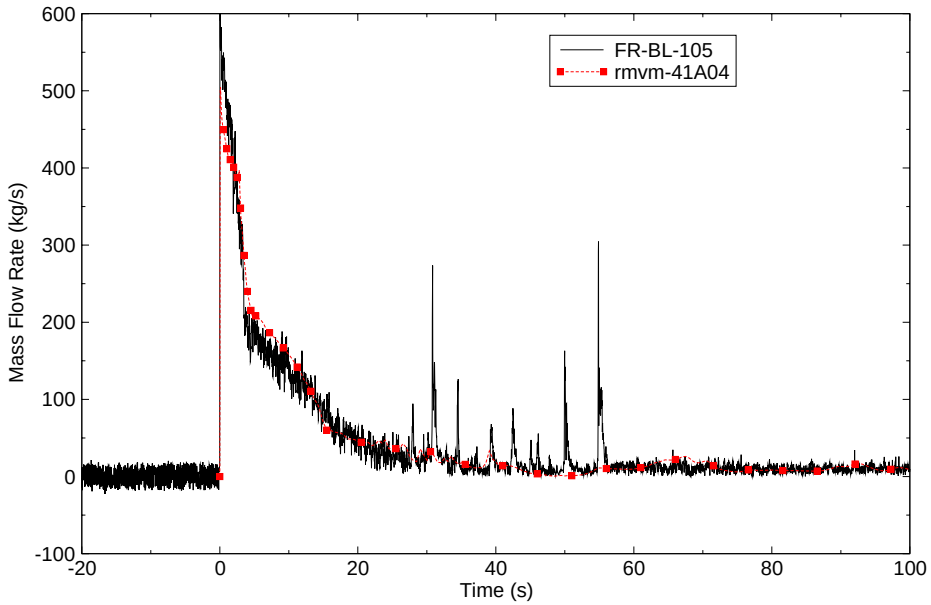

Figure C.1-19. L2-6 Broken Loop Cold Leg Mass Flow Rate.

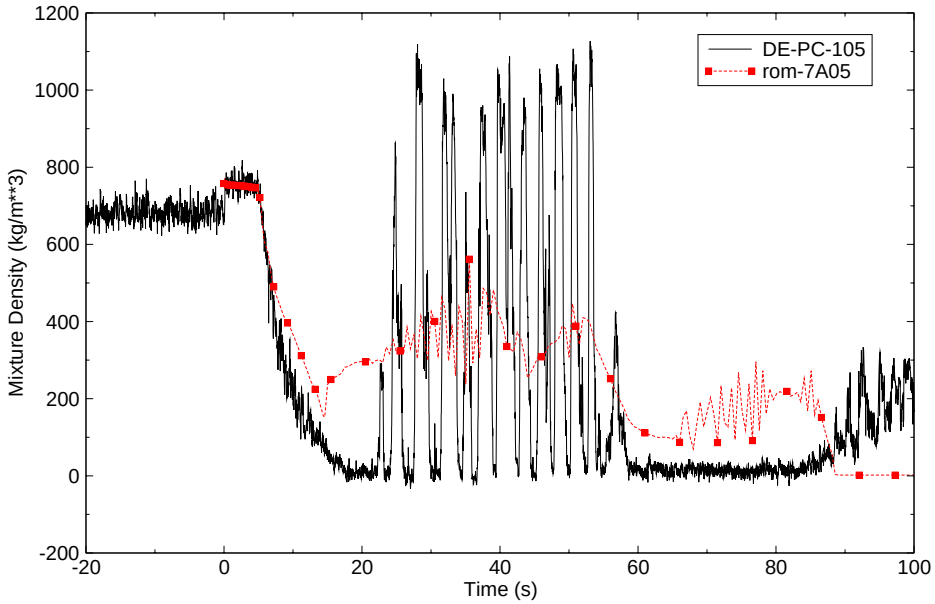

Figure C.1-20. L2-6 Intact Loop Cold Leg Mixture Density.

loop cold leg. The density then gradually decreased until after the start of accumulator injection in both the calculations and the test. There were several increases in density in both the calculations and the test during the period of accumulator injection, which was roughly between 17 s and 50 s. These increases in density indicated that some of the ECC was flowing across the downcomer and out the cold leg break rather than down the downcomer and through the core.

The calculated and measured level for the accumulator is shown in Figure C.1-22. Accumulator injection began near 17 s and ended near 50 s in both the calculation and the test. In the test, the accumulator drained to the elevation of the standpipe. The residual liquid remaining below the elevation of the standpipe was not injected into the primary coolant system. The accumulator model represented only the liquid above the elevation of the standpipe; the liquid below the standpipe was accounted for in the control variable that calculated the liquid level. Nitogen flowed from the accumulator into the primary coolant system after accumulator injection ended near 50 s in both the calculation and the test.

The calculated and measured LPIS mass flow rates are shown in Figure C.1-23. The average calculated LPIS mass flow rate was about 6 kg/s. LPIS flow versus primary system pressure was accurately modeled in the calculation, but the calculations under-predicted LPIS flow. Once the system was depressurized following the blowdown phase, it is not clear why LPIS flow continued to increase to 7 kg/s in the test and what corrections should be made in the model. Regardless, the accumulator supplied most of the ECC to the primary coolant system during the test with an average accumulator flow rate of about 45 kg/s. The ECC was generally swept across the downcomer and into the broken loop cold leg until it began to reach the lower plenum.

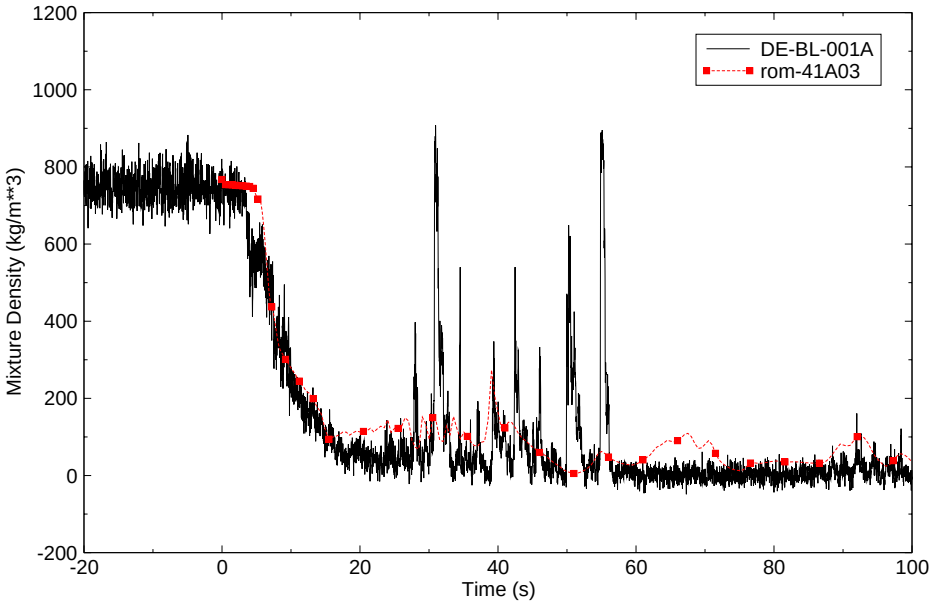

Figure C.1-21. L2-6 Broken Loop Cold Leg Mixture Density.

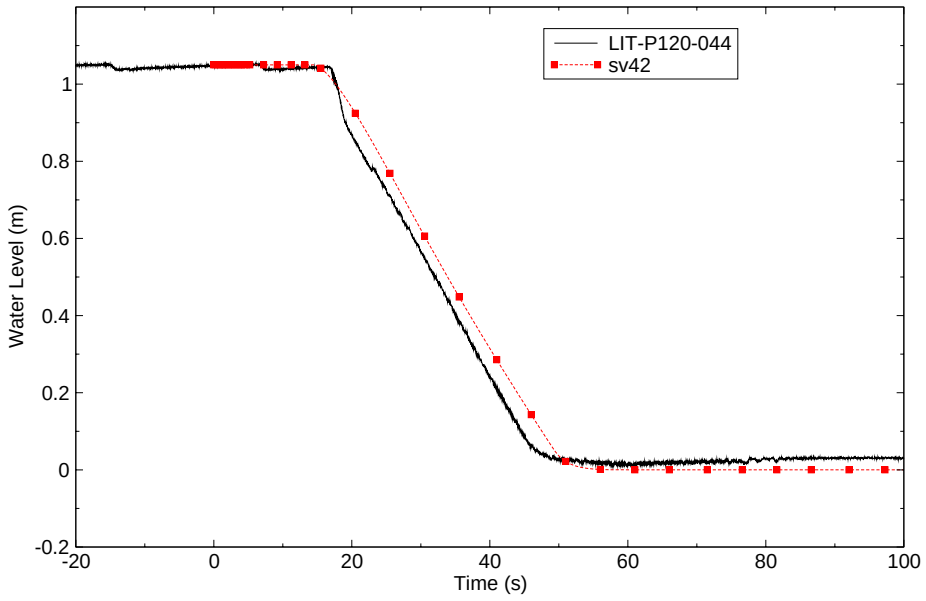

Figure C.1-22. L2-6 Accumulator Level.

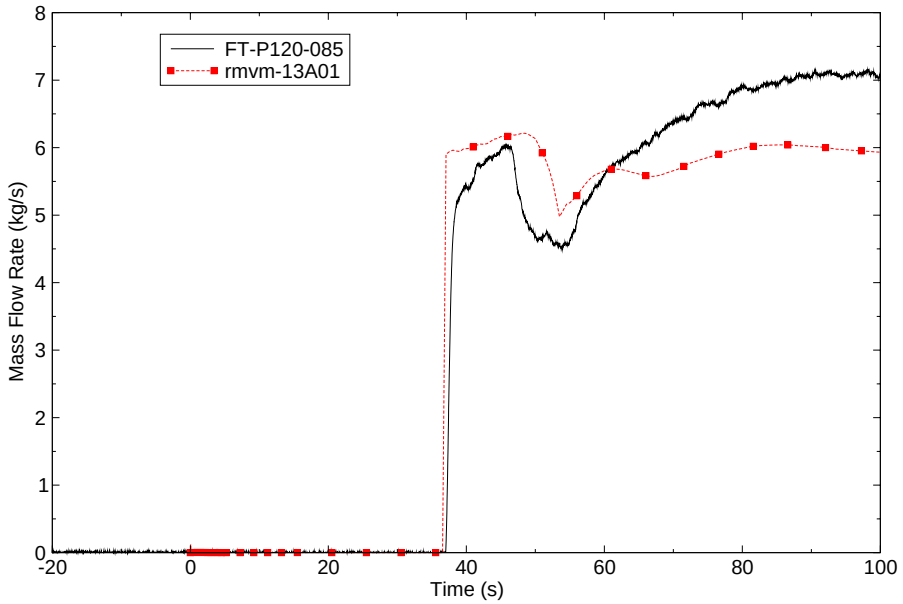

Figure C.1-23. L2-6 LPIS Mass Flow Rate.

A comparison of calculated and measured liquid temperatures in the upper and lower plenums are shown in Figure C.1-24 and Figure C.1-25. The agreement between the calculated and measured values was considered reasonable. The temperatures generally followed the saturation temperature in both the calculations and the test. A small amount of superheat was measured near 45 s. The calculated temperatures were about 10-20 K less than the measured values during the blowdown phase. This underprediction in temperature is consistent with the underprediction in primary coolant pressure previously shown in Figure C.1-11.

The calculated and measured downcomer liquid temperature is shown in Figure C.1-26. The predicted temperature seems reasonable out to about 50 s. The slight under-prediction in temperature is related to the under-prediction in system pressure between 10 s and 20 s shown in Figure C.1-11. The rapid decline in the predicted downcomer liquid temperature just after 50 s results from cold water and noncondensible gases injected into the cold leg from the accumulator. At around 55 s the accumulator became empty, the injection stopped and the liquid in the downcomer warmed up. Wall-to-fluid heat transfer effects may also be influencing the predicted downcomer fluid temperature. Possibly the wall heat transfer coefficients may be too small resulting in less heat being transfer to the fluid from the wall. Further investigation into the wall heat transfer coefficients is warranted. Fluid temperature measurement accuracies are given as 2 K ± 4.2% of reading.

The fuel centerline temperature comparison is shown in Figure C.1-27. A hand calculation indicates the TRACE prediction is reasonable for the initial centerline temperature. The measured

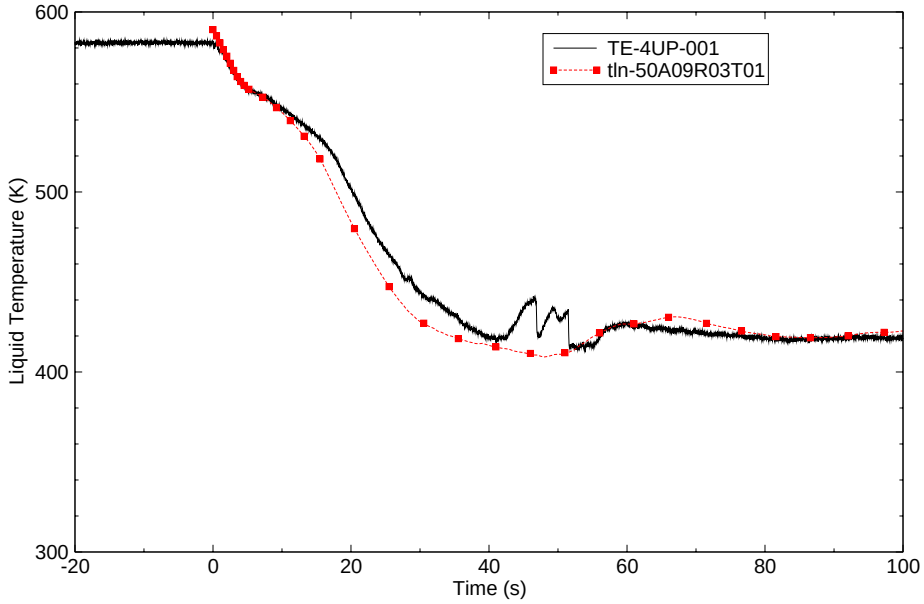

Figure C.1-24. L2-6 Upper Plenum Liquid Temperature.

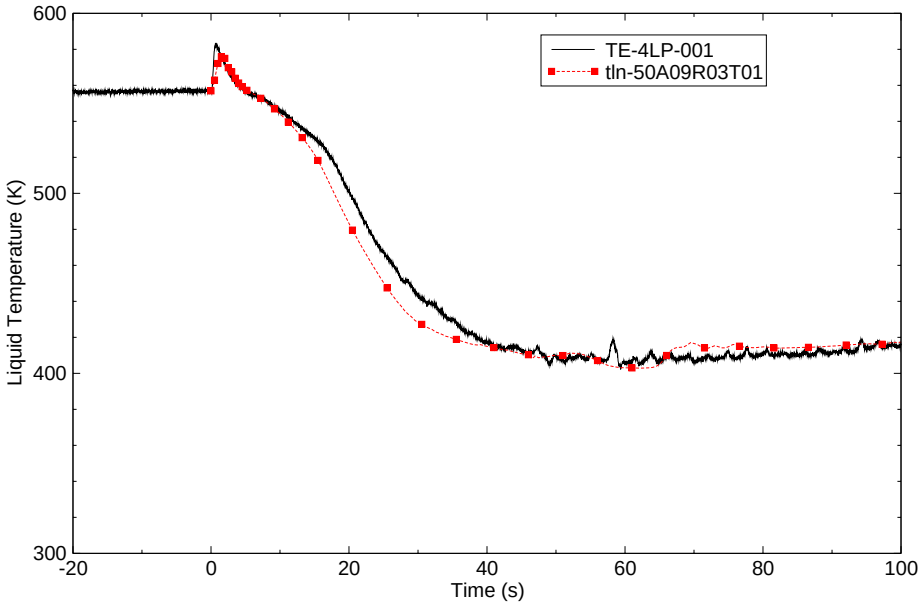

Figure C.1-25. L2-6 Lower Plenum Liquid Temperature.

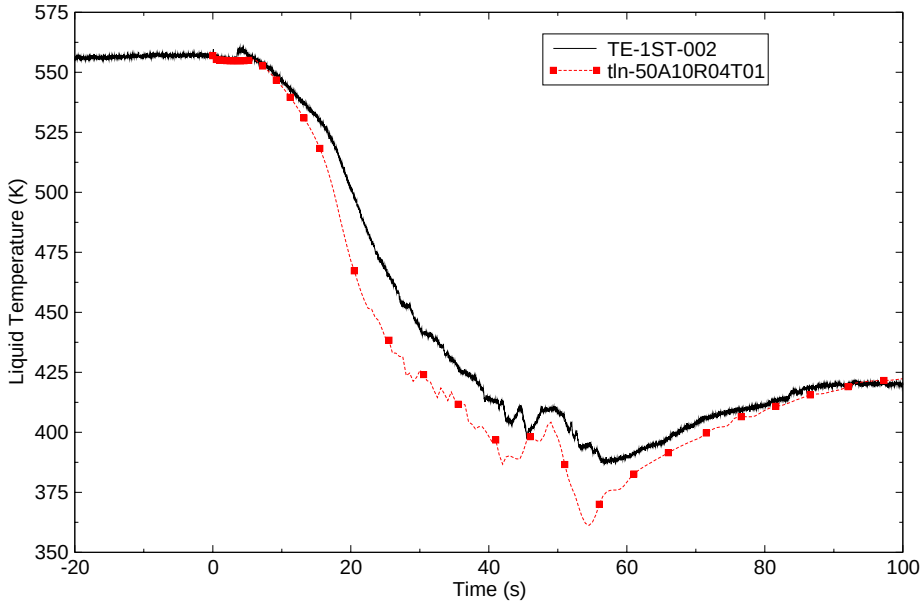

Figure C.1-26. L2-6 Downcomer Liquid Temperature.

centerline temperature may be questionable. The temperatures predicted during the transient are higher than the data. Reference 1 presents some aspects of this issue.

Rod surface temperature comparisons at 0.20, 0.66 and 1.57 m are shown in Figure C.1-28, Figure C.1-29 and Figure C.1-30. The data shows an initial rod heat-up that is well predicted by TRACE. However, the initial quench shown in the measured data is not as well represented. The code seems to do a better job predicting the measured rod clad temperature behavior near the bottom of the core. The predicted clad temperatures after the initial rod heat-up and quench are over-calculated. Possible reasons for the over-prediction may be too much liquid entrained out of the core and insufficient liquid penetrating the core due to ocsillatory core inlet behavior predicted by the code (see Figure C.1-31 and Figure C.1-32). Further investigation into the predicted entrainment and oscillatory behavior is warranted. ,

C.1.6.2. L2-6 Prediction Conclusions.

TRACE predictions of LOFT Test L2-6 showed reasonable agreement with the data. The calculated system pressure and loop mass flow rates reasonably predicted the data trends. The exception is the fuel and cladding temperatures. Fuel rod surface temperatures during the first few seconds of blowdown agree with data. However, steady-state fuel centerline temperatures do not match and transient results following the peak are different. Previous assessments have noted that the LOFT external fuel thermocouples do not measure the cladding surface temperature

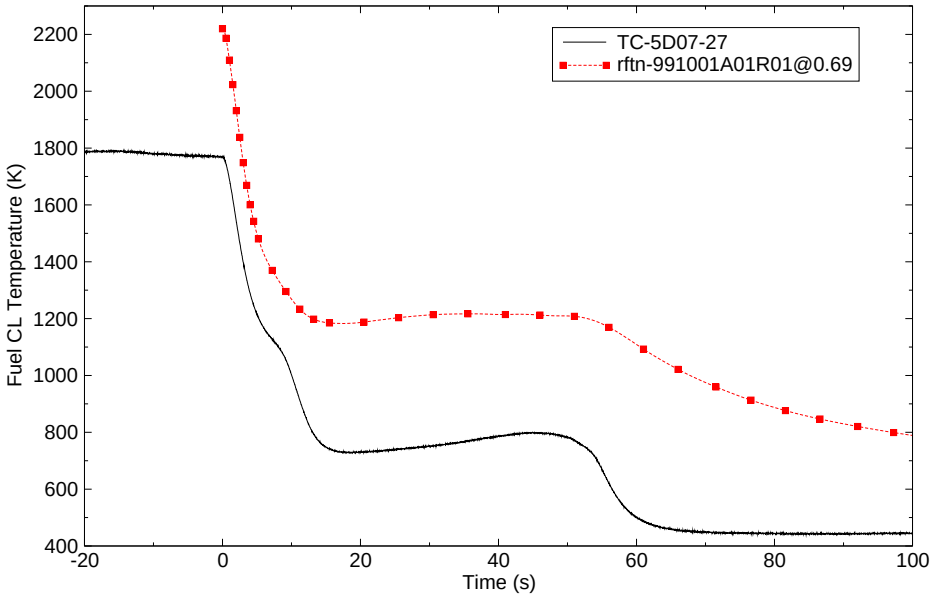

Figure C.1-27. L2-6 Fuel Centerline Temperature at 0.69 m.

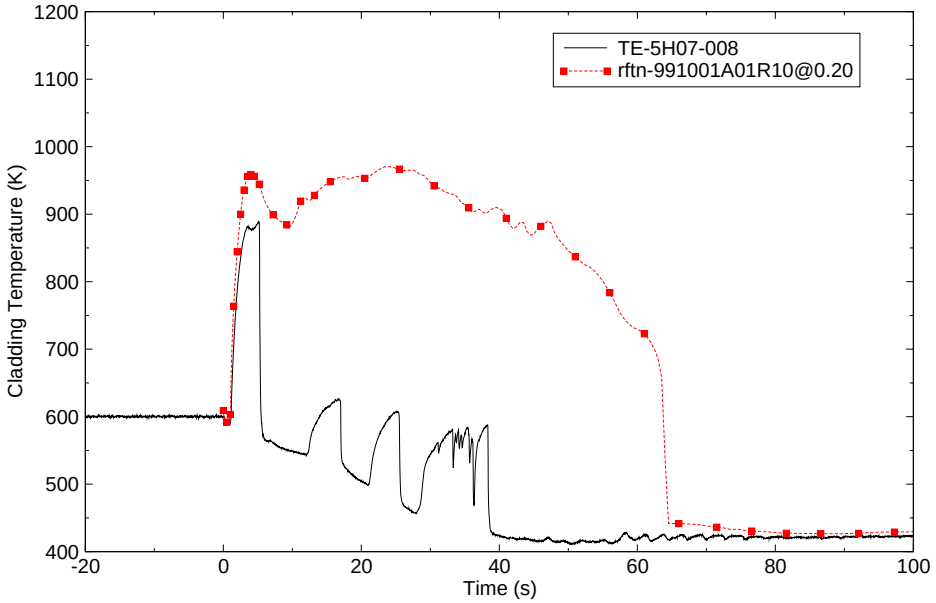

Figure C.1-28. L2-6 Cladding Temperature at 0.20 m.

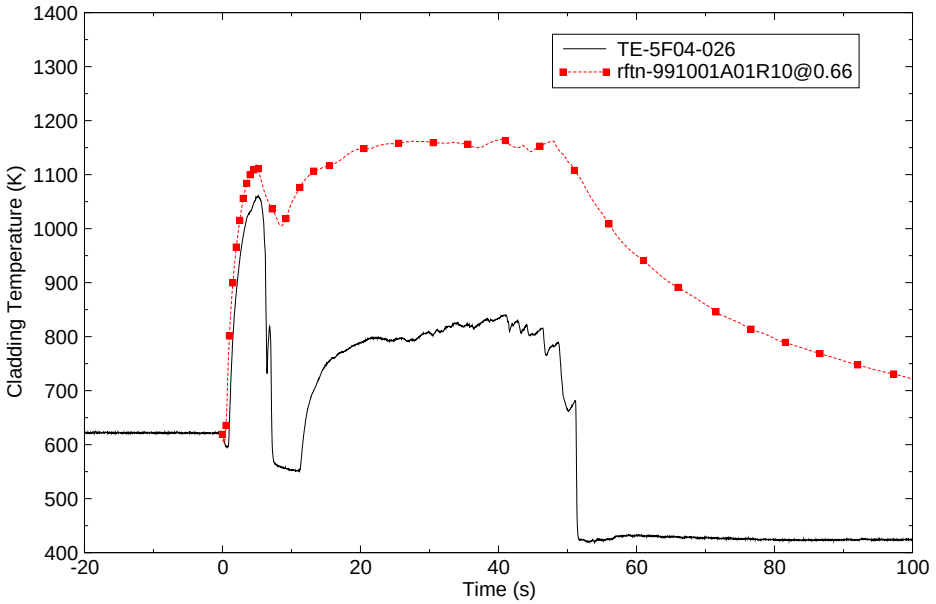

Figure C.1-29. L2-6 Cladding Temperature at 0.66 m.

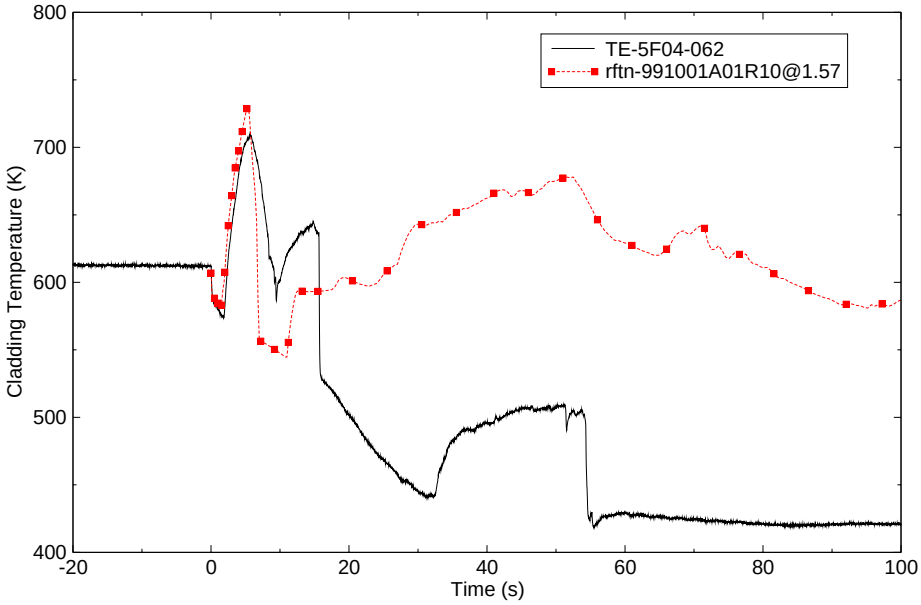

Figure C.1-30. L2-6 Cladding Temperature at 1.57 m.

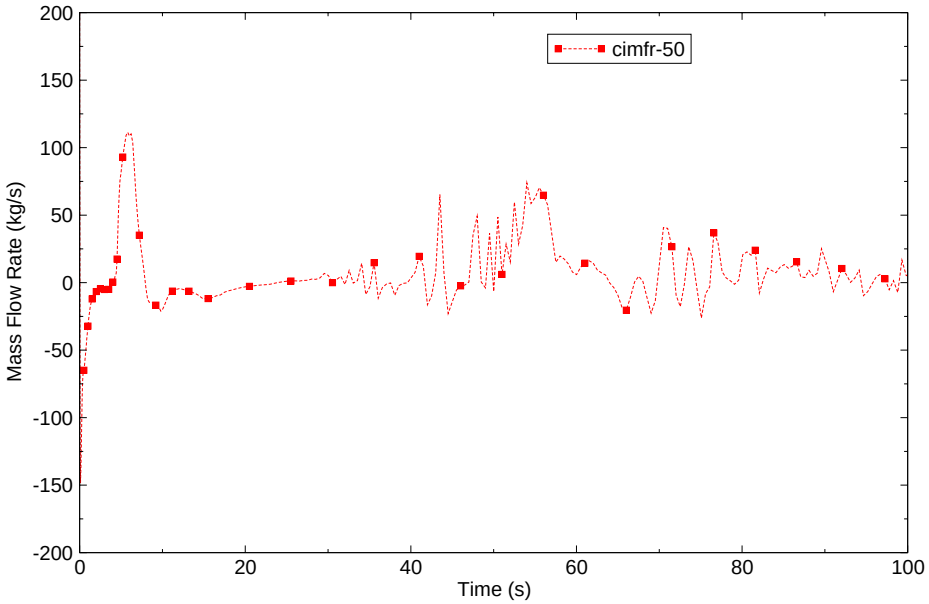

Figure C.1-31. L2-6 Core Inlet Mass Flow Rate.

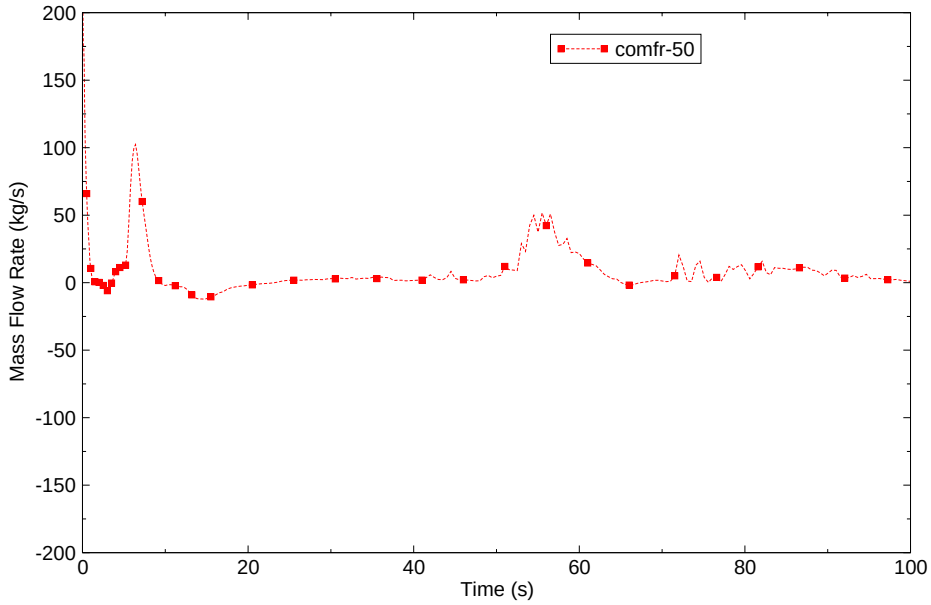

Figure C.1-32. L2-6 Core Outlet Mass Flow Rate.

accurately because of the fin-cooling effect. The external thermocouples are preferentially cooled during the quenching process and do not accurately measure cladding temperature during reflood.

C.1.7. LOFT Large Break Test L2-5

LOFT Test L2-5 was performed to analyze the effects of a 200% double-ended cold leg break with an immediate primary coolant pump trip. The test was conducted at 36 MW (instead of 46 MW as for Test L2-6), yielding a maximum linear generation rate of 40.1 kW/m. This test was designed to provide experimental data to demonstrate that 10 CFR 50 Appendix K assumptions result in a conservative prediction of peak cladding temperature, even without early rewet.

Significant initial conditions for Test L2-5 were: system pressure 14.94 MPa; core outlet temperature 589.7 K; and intact loop mass flow rate 192.4 kg/s. The test was initiated by opening the quick-opening blowdown valves in the broken loop hot and cold legs. The reactor scrammed on a low pressure signal at 0.24 s in the test.

Following the reactor scram, the operators tripped the primary coolant pumps at 0.94 s. The pumps were not connected to the flywheels in this test as they were for Test L2-6. This was done to provide an early rapid coastdown which would prevent the early core rewet phenomena and result in higher fuel cladding temperatures.

A rewet of the upper portion of the center fuel assembly began at approximately 12 s and ended at approximately 23 s. Accumulator injection of ECC to the intact loop cold leg began at 16.8 s. Delayed ECC injection from the HPIS and LPIS began at 23.90 s and 37.32 s, respectively. The fuel rod peak cladding temperature of 1078 K was attained at 28.47 s. The cladding was quenched at 65 s, following the core reflood. The LPIS injection was stopped at 107.1 s, after the test was considered complete.

C.1.7.1. Steady-State Calculations for LOFT Test L2-5

CSS controllers drive the steady-state solution to the user desired loop flow rate, secondary side pressure, and cold leg temperature. The resulting initial conditions for Test L2-5 are given in Table C.1.4.

.

Table C.1.4. L2-5 Initial Conditions - Measured and TRACE V5.0.

Parameter	Measured	TRACE V5.0
Reactor Power (MW)	36.0 ± 1.2	36.0
Intact Loop Mass Flow Rate (kg/s)	192.4 ± 7.8	192.1
Cold Leg Temperature (K)	556.6 ± 4.0	556.9

Table C.1.4. L2-5 Initial Conditions - Measured and TRACE V5.0.

Parameter	Measured	TRACE V5.0
Hot Leg Temperature (K)	589.7 ± 1.6	590.7
Pressurizer Pressure (MPa)	15.0 ± 0.1	15.0
Pressurizer Level (m)	1.13 ± 0.18	1.21
Steam Generator Pressure (MPa)	5.85 ± 0.06	5.88

Predicted steady-state results are shown in Figure C.1-33, Figure C.1-34, Figure C.1-35 and Figure C.1-36 to demonstrate that initial conditions prior to blowdown were steady. Plots show intact loop mass flow rate, hot and cold leg temperatures, pressurizer and steam generator pressures, and pressurizer level, respectively.

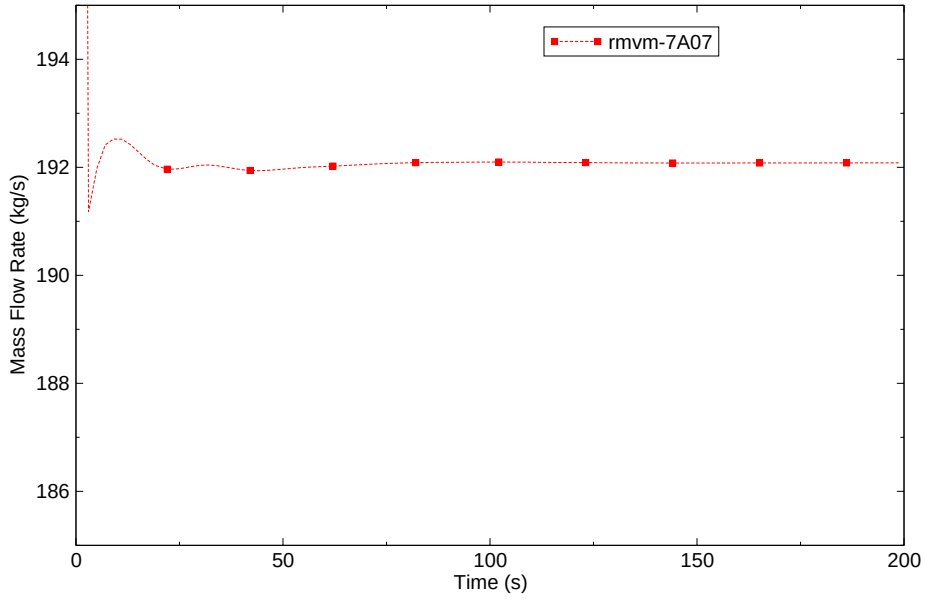

Figure C.1-33. L2-5 Predicted Steady-State Intact Loop Mass Flow Rate.

C.1.7.2. Transient Calculations for LOFT Test L2-5

The transient sequence of events for Test L2-5 are shown in Table C.1.5. Reactor power was scrammed on a low pressure signal at 0.34 s in the experiment. The reactor in the simulation was scrammed on time as shown in Table C.1.5.

A comparison of the calculated and measured pressure for the intact loop hot leg is shown in Figure C.1-37. The calculated pressure does well in predicting the data trends during the subcooled and early two-phase blowndown phase of the transient. The measured curve contains

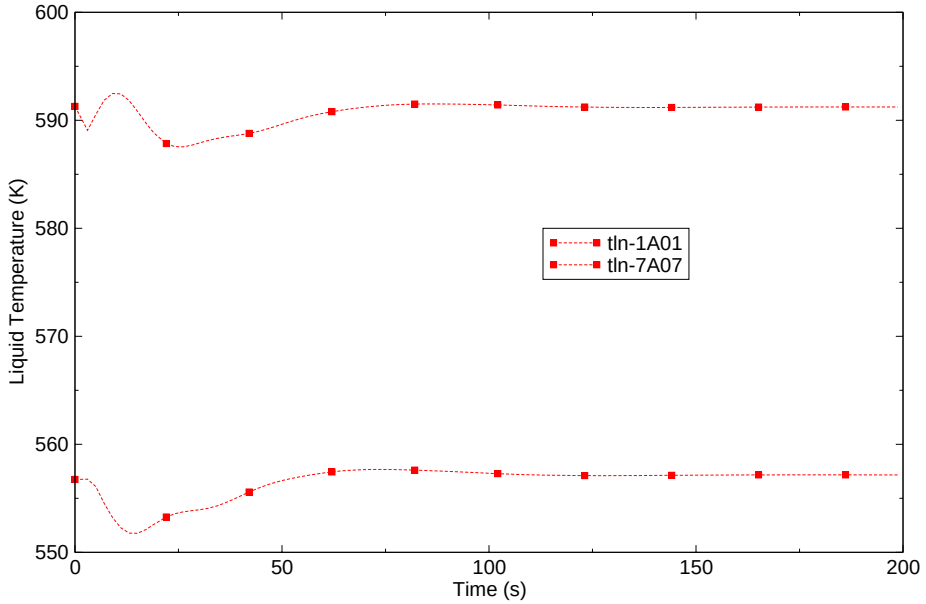

Figure C.1-34. L2-5 Predicted Steady-State Hot and Cold Leg Liquid Temperatures.

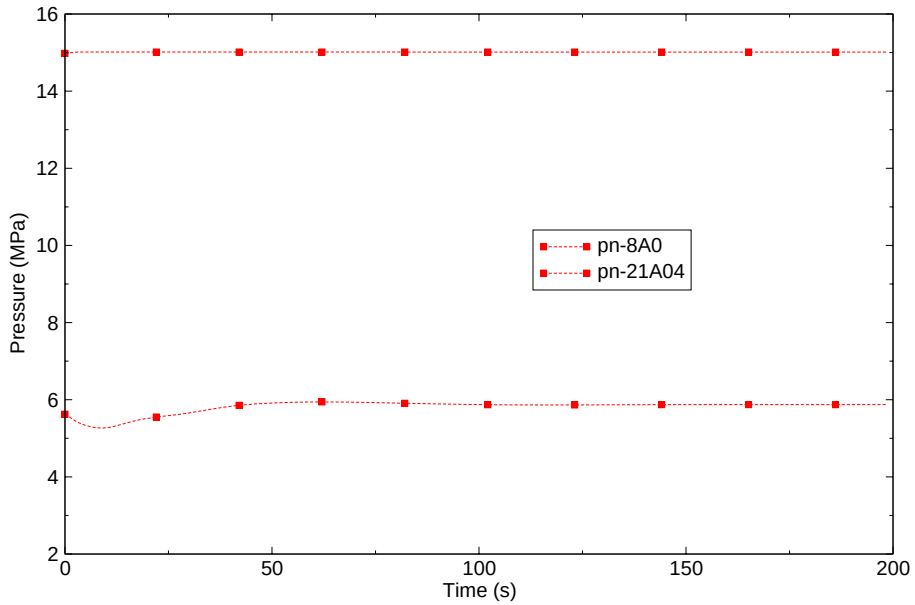

Figure C.1-35. L2-5 Predicted Steady-State Pressurizer and Steam Generator Pressures.

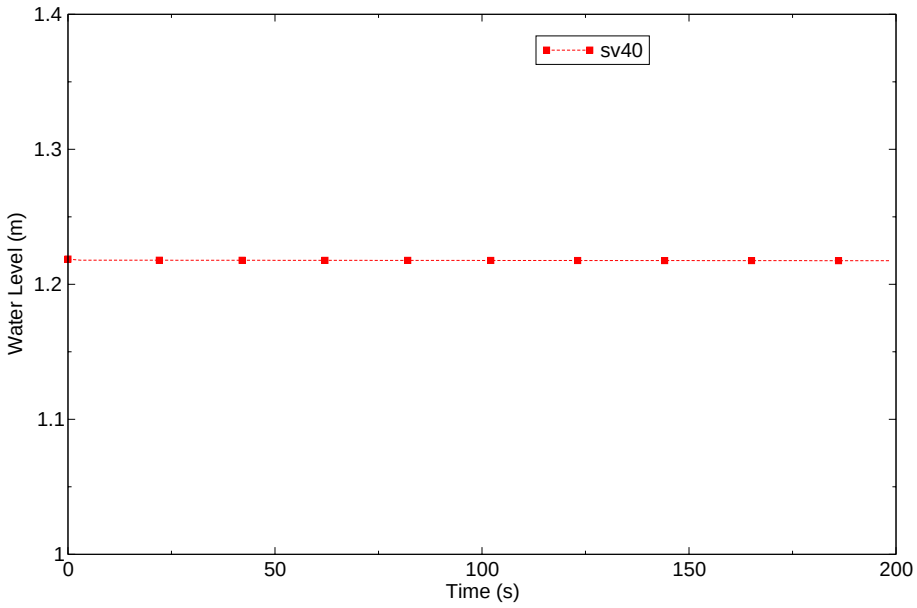

Figure C.1-36. L2-5 Predicted Steady-State Pressurizer Level.

Table C.1.5. L2-5 Sequence of Event Timing.

Event	**Measured**	**TRACE V5.0**
Break Initiated (s)	0.0	0.0
Reactor Scrammed (s)	0.24 ± 0.01	0.24
Primary Coolant Pumps Tripped (s)	0.94 ± 0.01	0.93
Pressurizer Emptied (s)	15.4 ± 1.0	15.0, void in bottom cell=0.92
Accumulator A Injection Initiated (s)	16.8 ± 0.1	14.2
Reflood Tripped On (s)	NA	0.0
HPIS Injection Initiated (s)	23.90 ± 0.02	23.5
LPIS Injection Initiated (s)	37.32 ± 0.02	37.0
Maximum Cladding Temperature (K)	1078 ± 12.8	1123

an inflection point at about 16 s, roughly corresponding to the initiation of accumulator injection. At about 15 s, the predicted depressurization rate was faster and lead to a slightly earlier (2.3 s) initiation of accumulator injection (see Table C.1.5).

The calculated and measured intact loop hot leg mass flow rates are shown in Figure C.1-38. A negative flow rate is predicted by the code that is not observed in the data. This same behavior was observed in the simulation of Test L2-6 discussed in **Section C.1.5.** above. The same

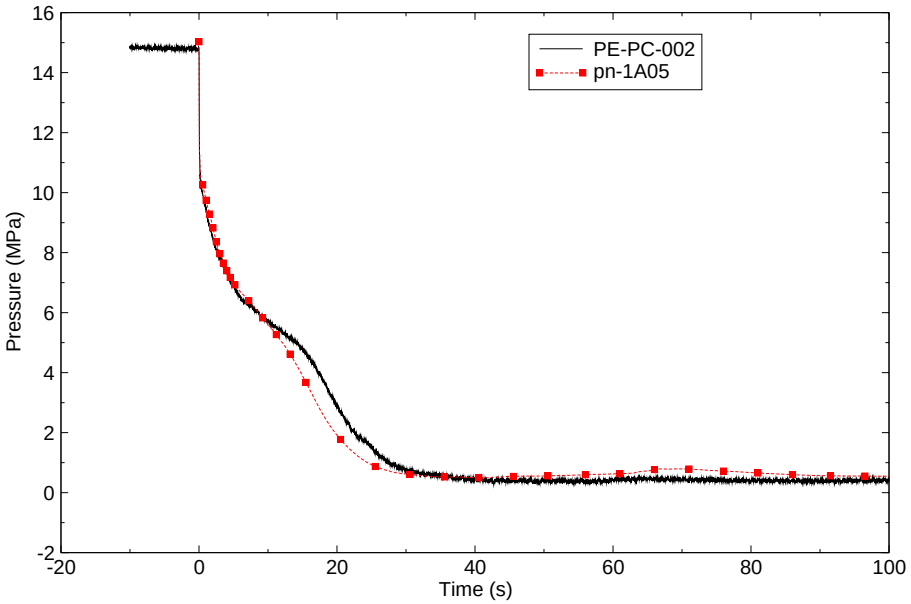

Figure C.1-37. L2-5 Intact Loop Hot Leg Pressure.

argument for the reverse flow applies here; i.e., the instrumentation does not detect direction. An examination of the intact loop hot leg differential pressure indicates there was a flow reversal; consequently, the absolute values of the calculated mass flow rate are shown. Compared to the data, the predicted intact loop hot leg mass flow rate is deemed reasonable.

The calculated and measured intact loop cold leg mass flow rates between the pumps and the ECC injection location are shown in Figure C.1-39. Prior to 30 s, the predicted mass flow rate compares reasonably to the measured value. Between 30 s and 60 s, TRACE under-predicts the mass flow rate. Further investigation as to the reasons for the under-prediction is warranted.

The calculated and measured impeller rotational speeds for pump 1 and pump 2 in the intact loop cold leg are shown in Figure C.1-40. Both pumps responded in a similar manner. The measured speeds were nearly constant until the pump trips. Following the reactor scram, the operators tripped the primary coolant pumps at 0.94 s. The pumps were not connected to the flywheels in this test. In the calculation, the pumps were decoupled at OMTEST = 131.0 rad/s, the equivalent rotational speed at 0.94 s when the pumps were tripped in the test. The pump speeds remained relatively constant near 50 rad/s between 30 s and 60 s and then increased until 80 s due to the volumetric flow through the intact loop cold leg. The steam flow through the intact loop decreased after this time. Although there were differences in magnitude and timing, the trends of the calculations were similar to those observed in the test.

The calculated and measured secondary pressures are shown in Figure C.1-41. The calculated secondary system pressures were in excellent agreement with the measurement. The pressure

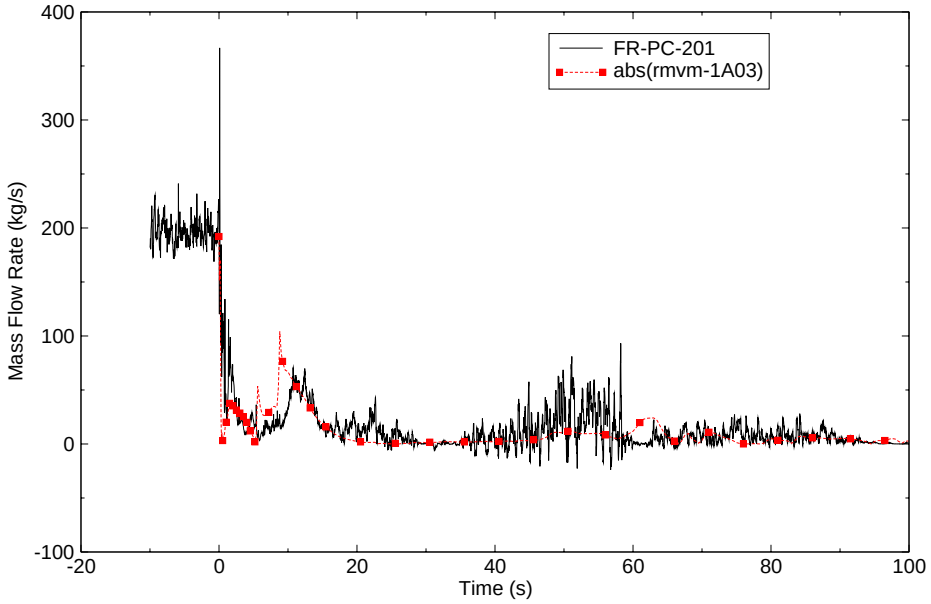

Figure C.1-38. L2-5 Intact Loop Hot Leg Mass Flow Rate.

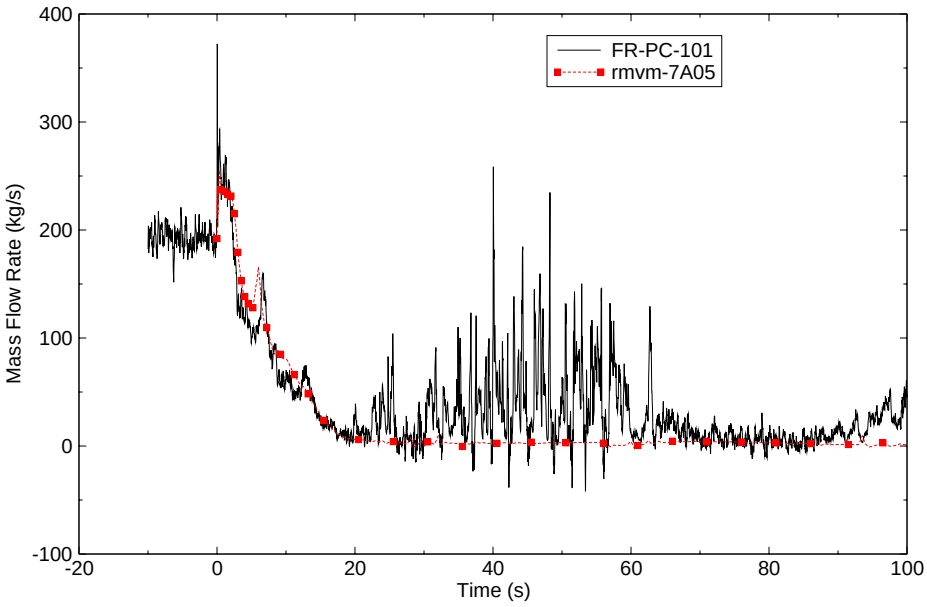

Figure C.1-39. L2-5 Intact Loop Cold Leg Mass Flow Rate.

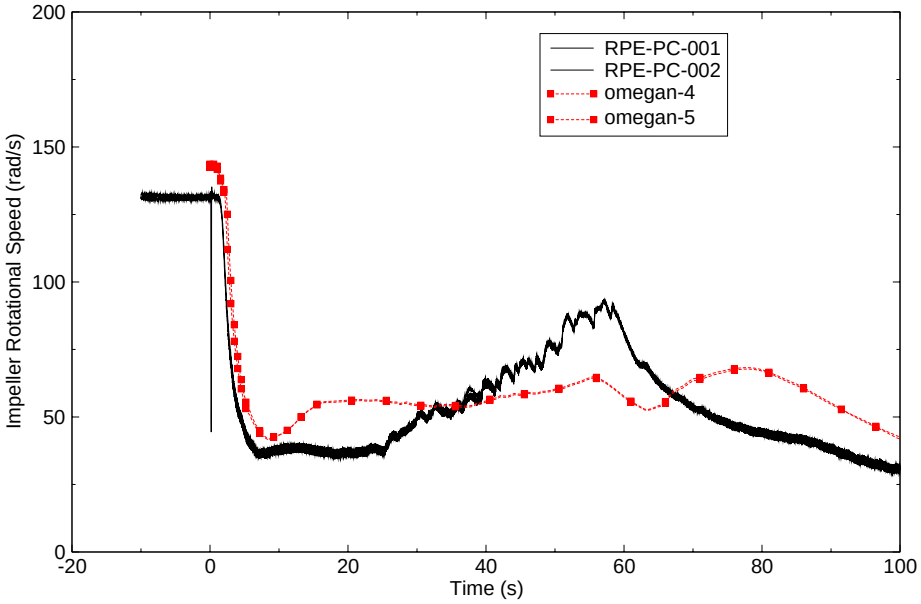

Figure C.1-40. L2-5 Pump Impeller Rotational Speed.

initially began to rise when the steam control valve began to close following reactor trip. The pressure reached a peak and began to decrease due to reduction in heat transfer from the primary side. The pressure decreased relatively rapidly until the steam control valve was completely closed at 9.38 s. The pressure then decreased at a more gradual rate due to heat transfer from the secondary side to the primary side of the steam generator.

The calculated and measured mass flow rate in the broken loop hot leg is shown in Figure C.1-42. The predicted mass flow rate is deemed to be reasonable compared to the data. All of the trends of the data are represented by the calculation. At around 10 s the mass flow rate is slightly under-predicted. The differences may be related to two-phase conditions at the break. It is suspected the void fraction at the break was higher in the calculation, thus a lower mass flow rate.

The calculated and measured mass flow rates in the broken loop cold leg are shown in Figure C.1-43. The fluid in the broken loop cold leg, which was supplied by the downcomer, remained subcooled for several seconds. The TRACE calculation under-predicted the mass flow rate during the first 5 s of the transient and over-predicted the mass flow rate at about 5-15 s, but the calculated results are generally within the uncertainties of the measurements and thus considered to be in good agreement with the data.

The calculated and measured fluid densities in the intact loop cold leg between the pump discharge and the ECC line connection are shown in Figure C.1-44. The density in the cold leg remained near its initial value until about 6 s in both the calculations and the test. Flashing then began in the cold legs and the density decreased rapidly. The calculated results were in reasonable

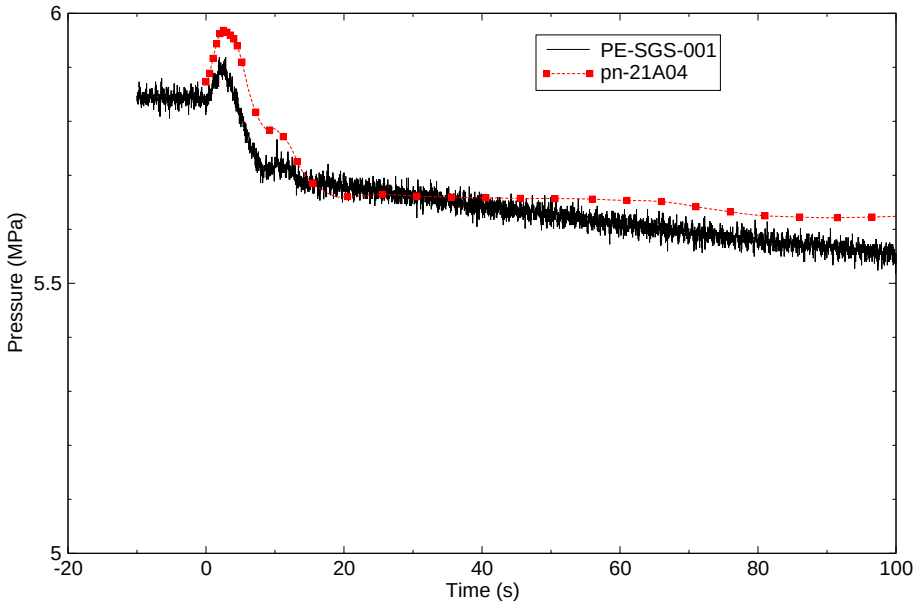

Figure C.1-41. L2-5 SG Secondary System Pressure.

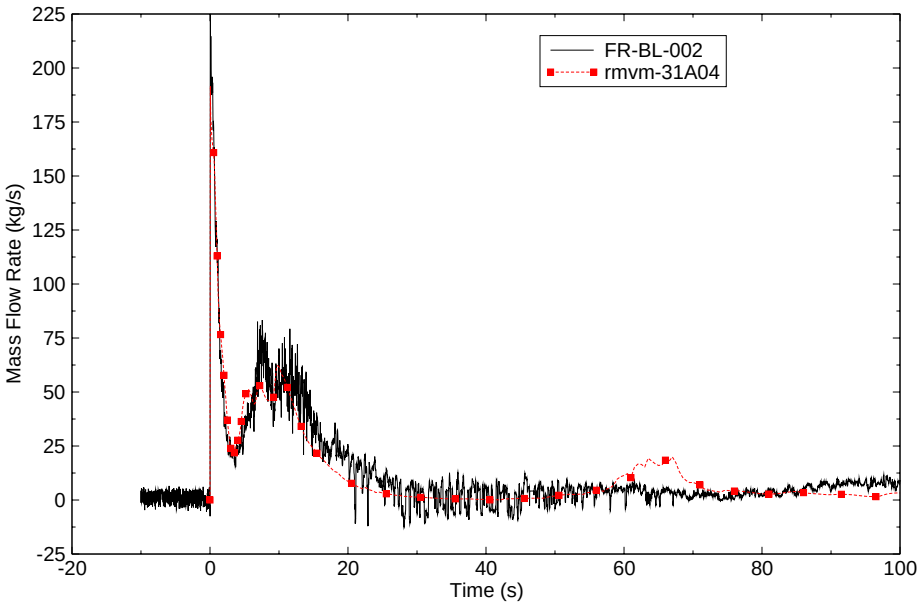

Figure C.1-42. L2-5 Broken Loop Hot Leg Mass Flow Rate.

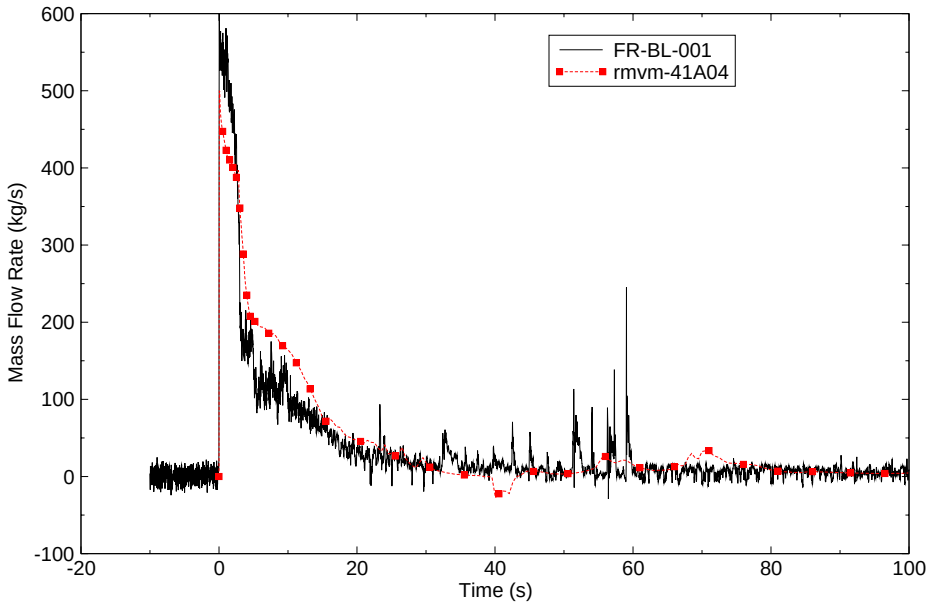

Figure C.1-43. L2-5 Broken Loop Cold Leg Mass Flow Rate.

agreement with the measurements until about 24 s, when a series of large-amplitude density oscillations related to the condensation associated with accumulator injection were measured in the test. Oscillations of about the correct frequency were calculated, but the magnitude of the oscillations was generally much smaller in the calculations than in the test.

Calculated and measured densities in the broken loop cold leg are shown in Figure C.1-45. The density remained near its initial value for several seconds in both the calculations and the test. The density then generally decreased until after the start of accumulator injection in both the calculations and the test. There were several increases in density in both the calculations and the test during the period of accumulator injection, which was roughly between 16 and 50 s. These increases in density indicated that some of the ECC was flowing across the downcomer and out the cold leg break rather than down the downcomer and through the core.

The calculated and measured level for the accumulator is shown in Figure C.1-46. Accumulator injection began near 17 s and ended near 53 s in both the calculation and the test. Although there were differences in timing, the predictions are in excellent agreement with the data.

The calculated and measured LPIS mass flow rates are shown in Figure C.1-47. LPIS injection was initiated at about 37 s and the mass flow rate immediately increased to about 6 kg/s. LPIS flow then decreased slightly when nitrogen flowed out from the accumulators into the primary coolant system after accumulator injection ended near 50 s in the calculations and in the test. In the calculations, the ECC was generally swept across the downcomer and into the broken loop cold leg until it began to reach the lower plenum near 30 s.

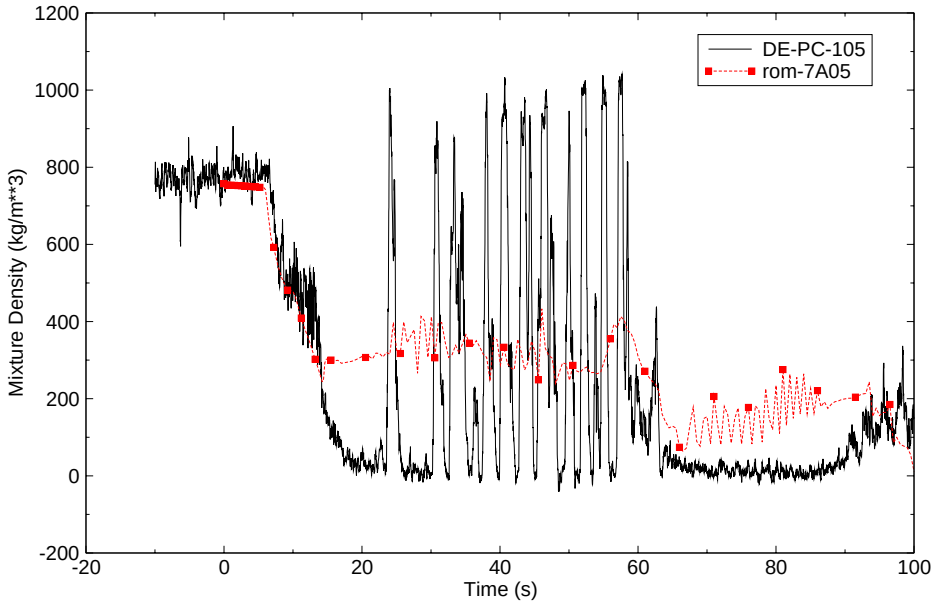

Figure C.1-44. L2-5 Intact Loop Cold Leg Mixture Density.

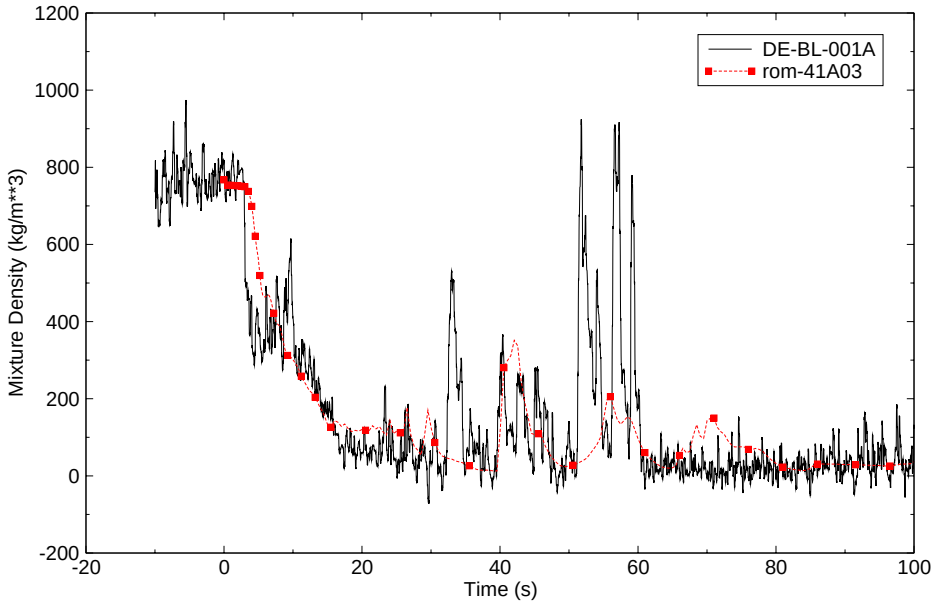

Figure C.1-45. L2-5 Broken Loop Cold Leg Mixture Density.

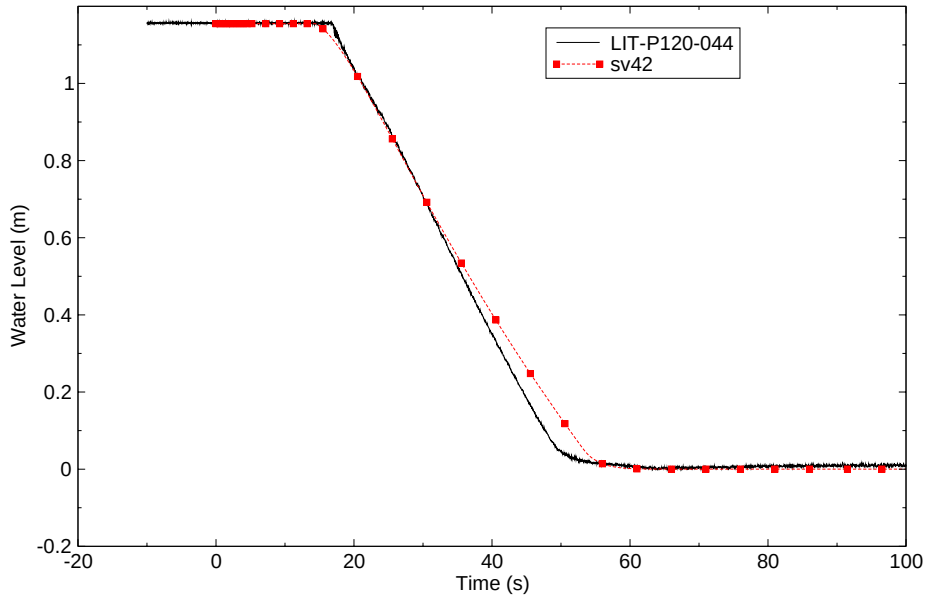

Figure C.1-46. L2-5 Accumulator Level.

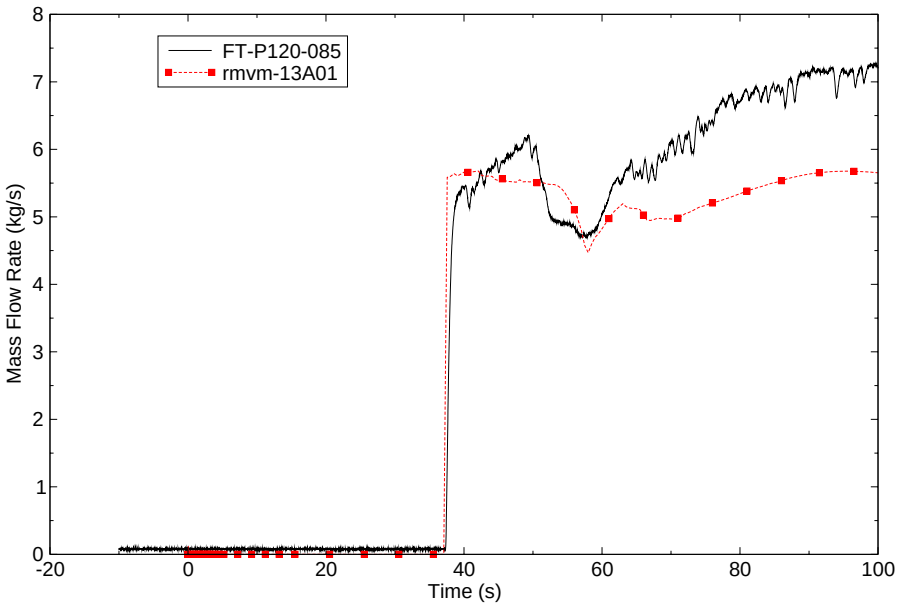

Figure C.1-47. L2-5 LPIS Mass Flow Rate.

A comparison of calculated and measured liquid temperatures in the upper and lower plenums is shown in Figure C.1-48 and Figure C.1-49. The agreement between the calculated and measured values was considered reasonable. The temperatures generally followed the saturation temperature in both the calculations and the test.

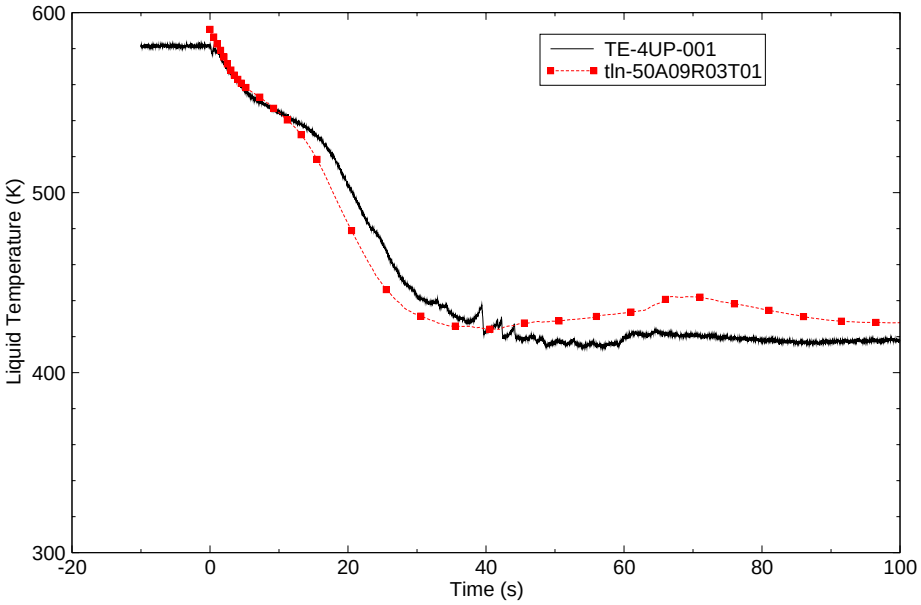

Figure C.1-48. L2-5 Upper Plenum Liquid Temperature.

The calculated and measured downcomer fluid temperature is shown in Figure C.1-50. The predicted downcomer liquid temperature is reasonable out to about 50 s. The slight under-prediction in temperature is related to the under-prediction in system pressure between 10 and 20 s shown in Figure C.1-37. The rapid decline in the predicted downcomer liquid temperature just after 50 s results from cold water and noncondensible gases injected into the cold leg from the accumulator. At around 55 s the accumulator became empty, the injection stopped and the liquid in the downcomer warmed up.

The fuel centerline temperature comparison is shown in Figure C.1-51. Similar to the prediction of the Test L2-6 centerline rod temperature, the initial fuel centerline temperature was higher than the measured value. Throughout the transient the predicted centerline temperature was generally over-predicted until after quenching occurred at about 80 s.

Rod surface temperatures comparisons at 0.20, 0.66 and 1.57 m elevations are shown in Figure C.1-52, Figure C.1-53, and Figure C.1-54. At the lower elevations, the code predicted the rod clad temperature and the time of quench reasonably well. At the 1.57 m elevation, the code did not predict the first rod heat-up and quench and over-predicted the second heat-up and quench. Additional assessment with similar data would be helpful in understanding the code behavior.

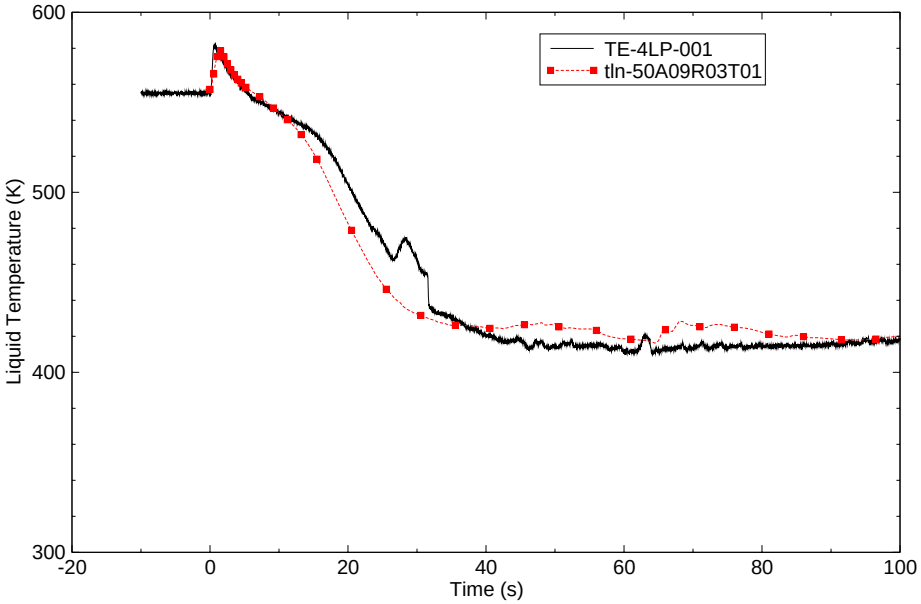

Figure C.1-49. L2-5 Lower Plenum Liquid Temperature.

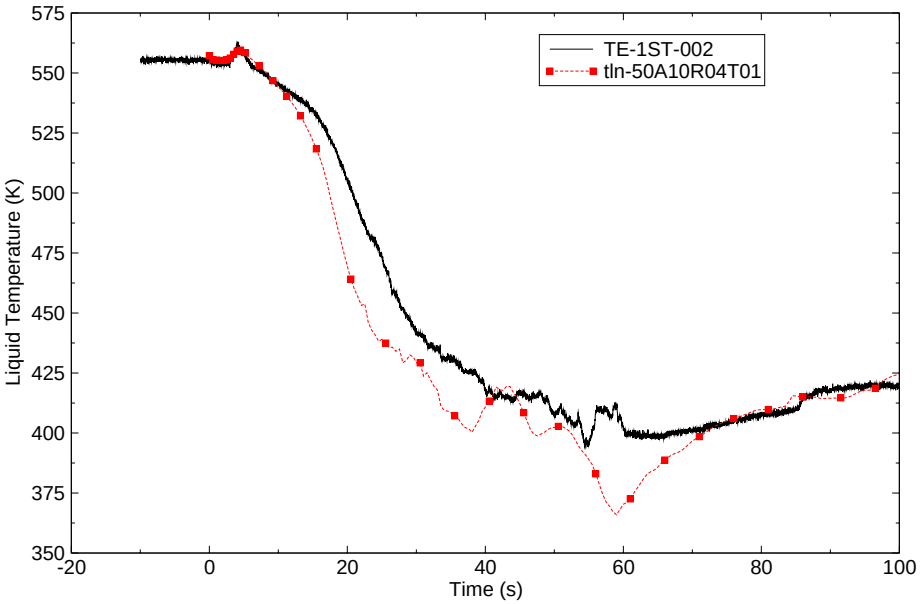

Figure C.1-50. L2-5 Downcomer Liquid Temperature.

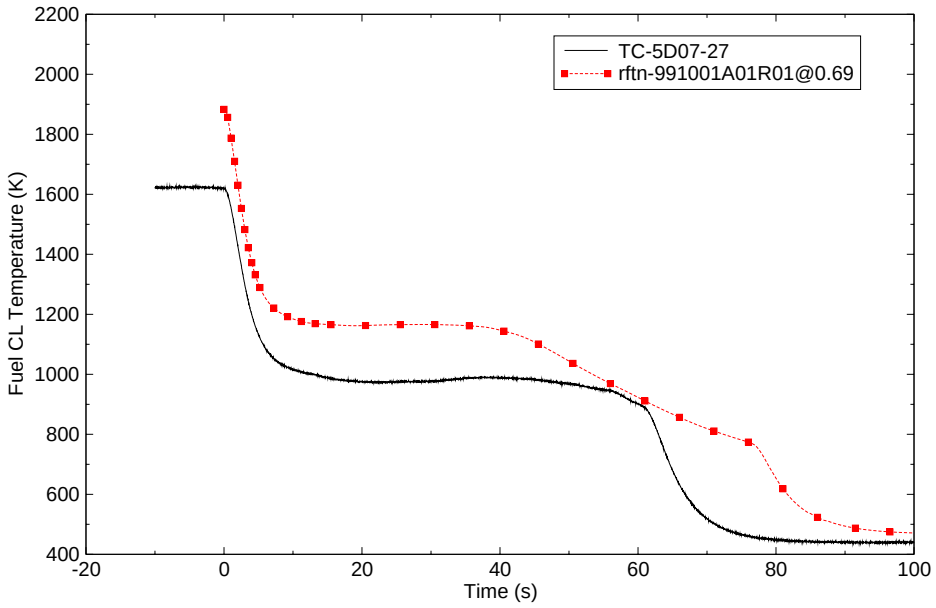

Figure C.1-51. L2-5 Fuel Centerline Temperature at 0.69 m.

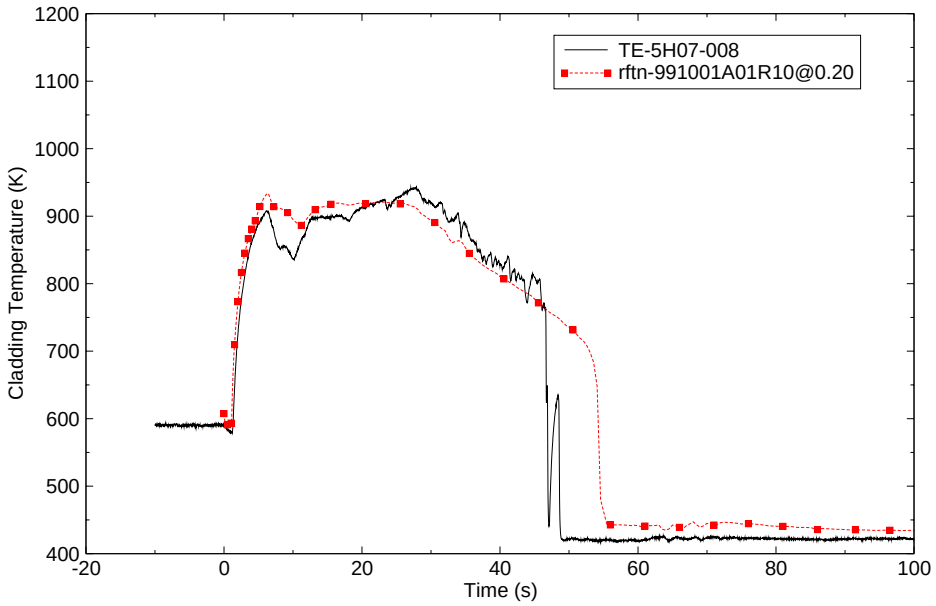

Figure C.1-52. L2-5 Cladding Temperature at 0.20 m.

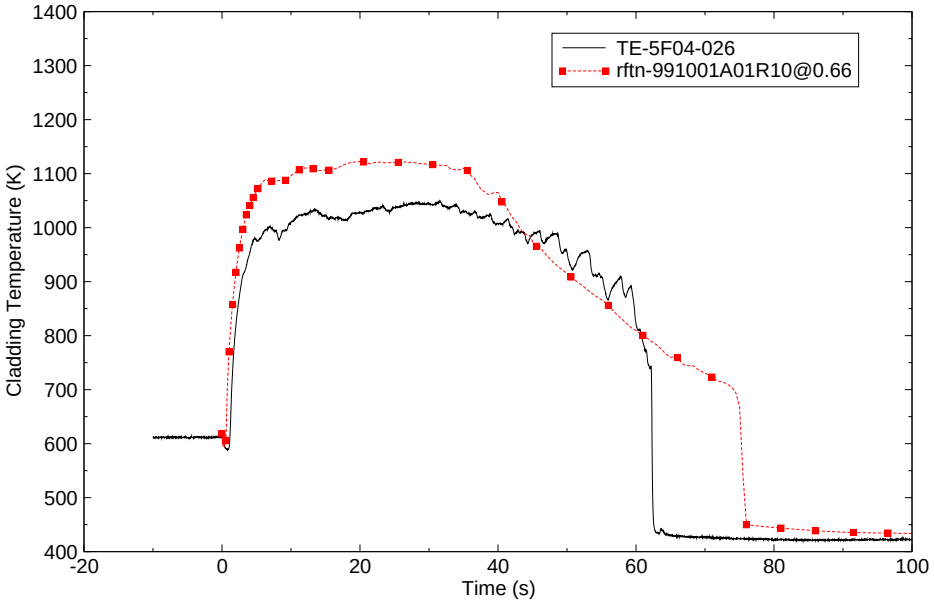

Figure C.1-53. L2-5 Cladding Temperature at 0.66 m.

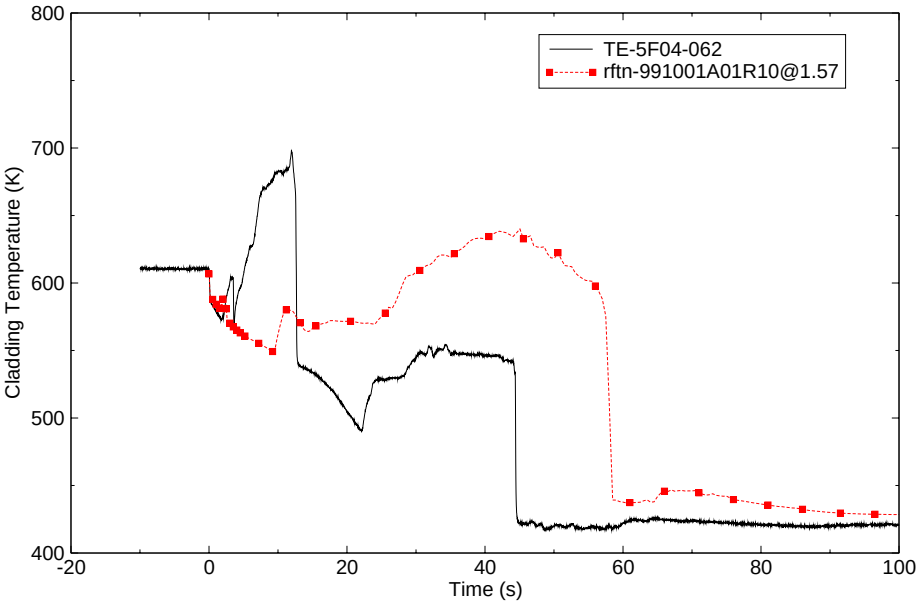

Figure C.1-54. L2-5 Cladding Temperature at 1.57 m.

Core inlet and outlet mass flow rates are shown in Figure C.1-55 and Figure C.1-56. A large negative core inlet flow immediately following the pipe break is predicted. No measured value for the core inlet mass flow rate is available to compare with. Core outlet flow also reversed. Predicted core flow normally reverses when large break LOCA's are simulated.

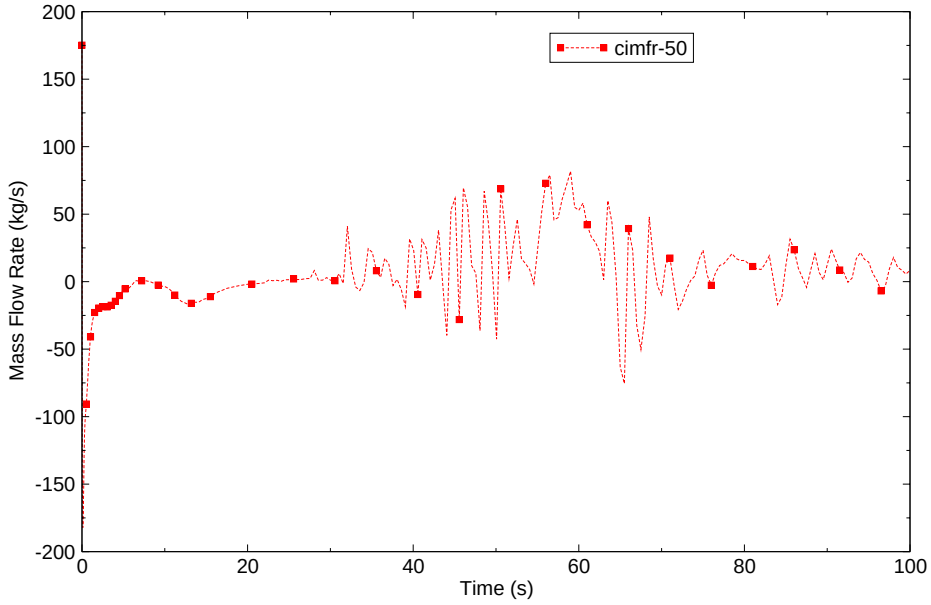

Figure C.1-55. L2-5 Core Inlet Mass Flow Rate.

C.1.7.3. L2-5 Prediction Conclusions

Generally, the TRACE predictions of LOFT Test L2-5 showed reasonable agreement with the data. The calculated system pressure and loop mass flow rates reasonably predicted the data trends. The fuel and cladding temperatures also compared well to measured data.

C.1.8. LOFT Large Break Test LB-1

LOFT Test LB-1 (Experiment LP-LB-1) was designed to reproduce conditions representative of United Kingdom licensing limits and was similar to Tests L2-5 and L2-6. The test was conducted at 49.3 MW, yielding a maximum linear generation rate of 51.7 kW/m. The initial conditions for this test were set to simulate loss of offsite power coincident with LOCA initiation and United Kingdom minimum safeguard ECC injection. These assumptions resulted in utilization of 70% of the accumulator volume and 50% of the pumped ECC injection of that used in L2-6 which represented U.S. licensing limits.

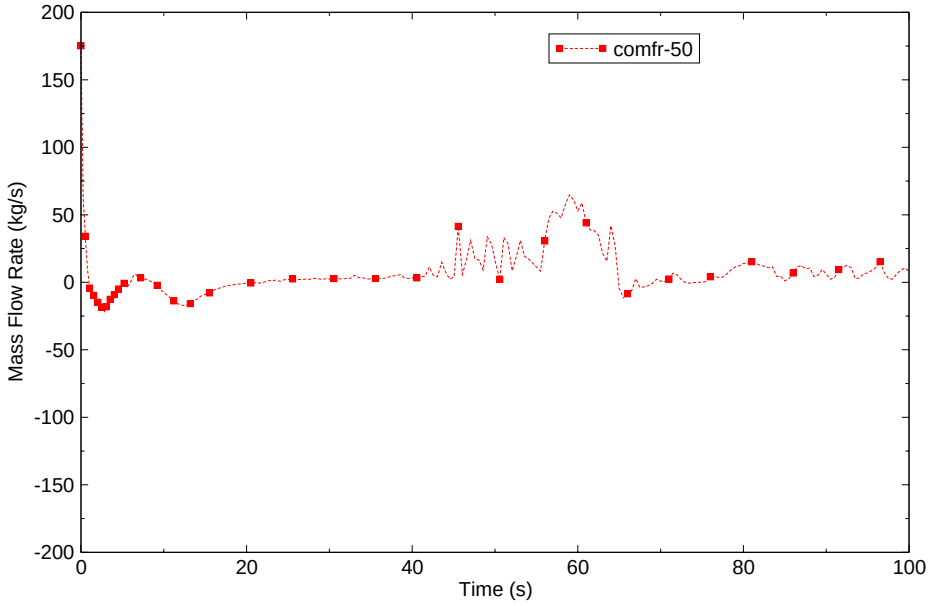

Figure C.1-56. L2-5 Core Outlet Mass Flow Rate.

Significant initial conditions for Test LB-1 were: system pressure 14.92 MPa; core outlet temperature 587.8 K; and intact loop mass flow rate 305.8 kg/s. The test was initiated by opening the quick-opening blowdown valves in the broken loop hot and cold legs. The reactor was scrammed on a low pressure signal at 0.13 s in the test. The primary coolant pumps were tripped slightly later at 0.24 s and disconnected from the flywheels at 0.63 s.

The early decoupling of the primary pumps from their flywheels resulted in insufficient flow into the vessel from the intact cold leg to produce a bottom up flow into the core and an early fuel cladding quench that also occurred in Test L2-6. The rapid cladding temperature rise had stopped at about 13 s because of liquid fallback from the upper plenum. This top-down liquid flow resulted in quench of the upper part of the central fuel assembly and more extensive cooling in the peripheral fuel bundles. The maximum cladding temperature during the blowdown phase was reached shortly before the top-down cooling trend started and reahed 1261 K. The top-down cooling lasted until about 25 s when fuel cladding heatup started again. ECC injection from the accumulators began at 17 s and from LPIS at 32 s and resulted in a core quench at about 34 s. The core quench started at both bottom and top of the core and progressed toward the peak power elevation and was completed at 72 s. The maximum cladding temperature recorded during the ECC injection phase was 1257 K.

C.1.8.1. Steady-State Calculations for LOFT Test LB-1

CSS controllers drive the steady-state solution to the user desired loop flow rate, secondary side pressure, and cold leg temperature. The resulting initial conditions for Test LB-1 are given in Table C.1.6.

Table C.1.6. LB-1 Initial Conditions - Measured and TRACE V5.0.

Parameter	**Measured**	**TRACE V5.0**
Reactor Power (MW)	49.3 ± 1.2	49.3
Intact Loop Mass Flow Rate (kg/s)	305.8 ± 2.6	305.3
Cold Leg Temperature (K)	556.0 ± 1.0	557.0
Hot Leg Temperature (K)	587.8 ± 1.2	586.7
Pressurizer Pressure (MPa)	14.92 ± 0.11	14.85
Pressurizer Level (m)	1.04 ± 0.04	1.13
Steam Generator Pressure (MPa)	5.53 ± 0.02	5.54

Predicted steady-state results are shown in Figure C.1-57, Figure C.1-58, Figure C.1-59 and Figure C.1-60 to demonstrate that initial conditions prior to blowdown were steady. Plots show intact loop mass flow rate, hot and cold leg temperatures, pressurizer and steam generator pressures, and pressurizer level, respectively.

C.1.8.2. Transient Calculations for LOFT Test LB-1

Event timing sequences are shown in Table C.1.7. The reactor was scrammed on a low pressure signal at 0.13 s in the experiment. The reactor in the simulation was scrammed on time as shown in Table C.1.7.

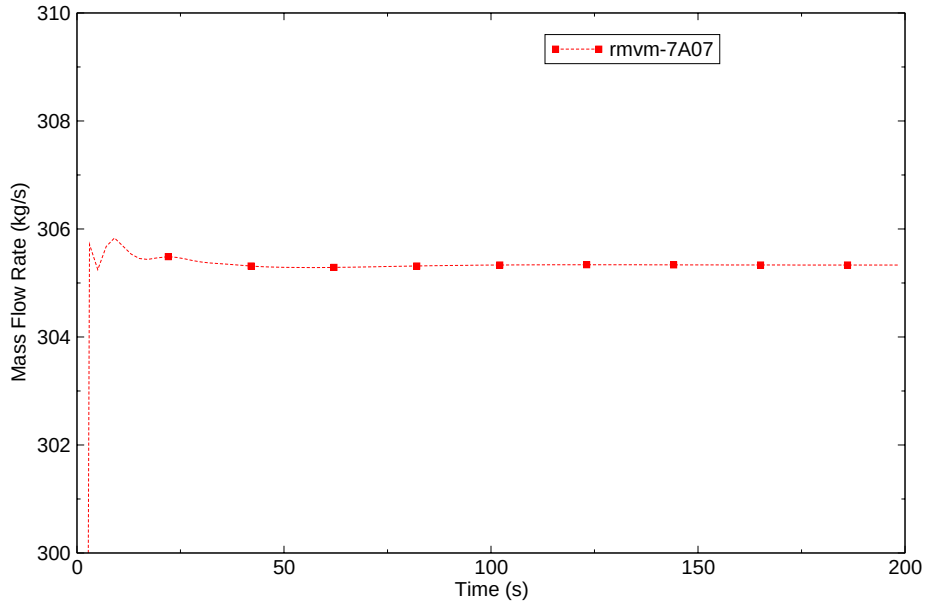

Figure C.1-57. LB-1 Predicted Steady-State Intact Loop Mass Flow Rate.

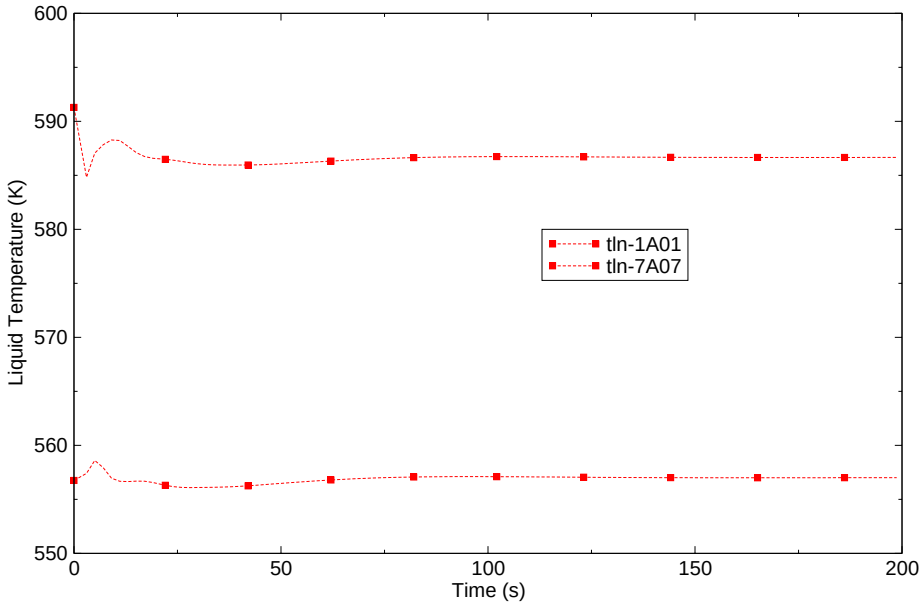

Figure C.1-58. LB-1 Predicted Steady-State Hot and Cold Leg Liquid Temperatures.

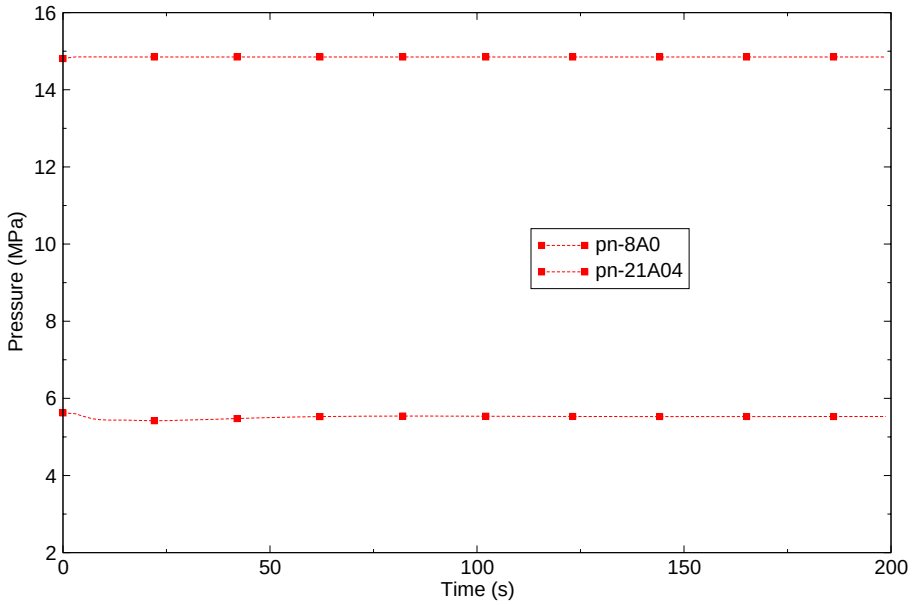

Figure C.1-59. LB-1 Predicted Steady-State Pressurizer and Steam Generator Pressures.

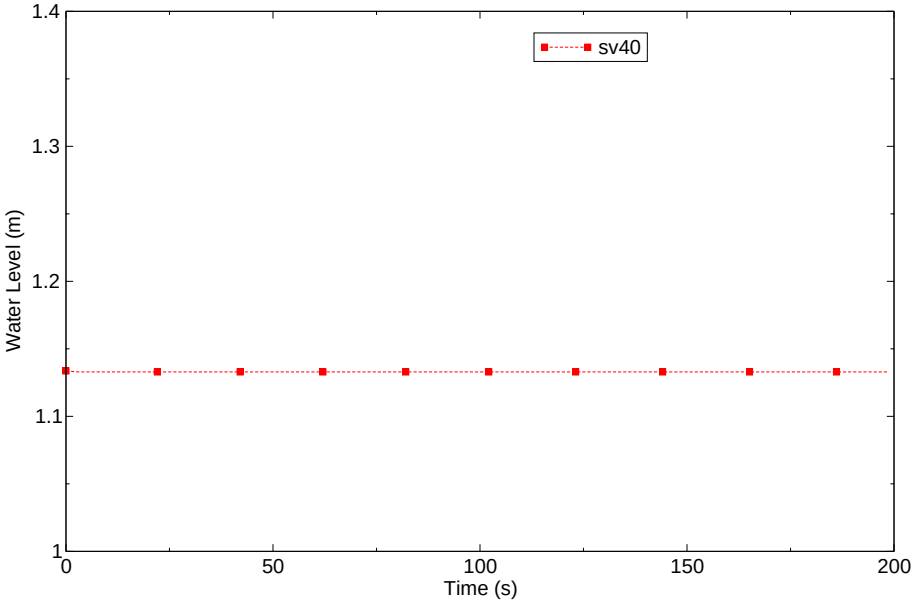

Figure C.1-60. LB-1 Predicted Steady-State Pressurizer Level.

Table C.1.7. LB-1 Sequence of Event Timing.

Event	Measured	TRACE
Break Initiated (s)	0.0	0.0
Reactor Scrammed (s)	0.13 ± 0.01	0.13
Primary Coolant Pumps Tripped (s)	0.24 ± 0.01	0.24
Pressurizer Emptied (s)	15 ± 1	14.4, void in bottom cell=0.92
Accumulator A Injection Initiated (s)	17.5 ± 0.05	14.7
Reflood Tripped On (s)	NA	0.0
HPIS Injection Initiated (s)	0.08 ± 0.1	0.1
LPIS Injection Initiated (s)	30.88 ± 0.1	30.9
Maximum Cladding Temperature (K)	1261 ± 16	1221

The predicted results of the TRACE simulation of LOFT Test LB-1 are similar to those of Tests L2-6 and L2-5 presented in **Section C.1.5.** and **Section C.1.7.** above.

A comparison of calculated and measured intact loop hot leg pressure is shown in Figure C.1-61. As in the predictions for the other LOFT tests, the prediction of the system pressure shows good agreement. Similar predicted behavior is also exhibited; i.e., at the initiation of accumulator injection the depressurization rate increased slightly. After the accumulator emptied the predicted pressure agreed well with the data.

The calculated and measured intact loop hot and cold leg mass flow rates are compared in Figure C.1-62 and Figure C.1-63. The code predicts the intact loop mass flow rate behavior reasonably well.

The calculated and measured impeller rotational speeds for pump 1 and pump 2 in the intact loop cold leg are shown in Figure C.1-64. Both pumps responded in a similar manner. In the calculation, the pumps were decoupled from their flywheels at OMTEST = 118.0 rad/s, the equivalent rotational speed at 16.5 s in the test, and resulted in the pumps being decoupled slightly earlier. The predicted speeds then increased until 20 s, peaking at about 50 rad/s, and then decreased after this time. Although there were differences in magnitude and timing, the trends of the calculations were similar to those observed in the test.

The calculated and measured secondary pressures are shown in Figure C.1-65. The predicted results were in excellent agreement with the measurement for the first several seconds. The pressure decreased relatively rapidly until the steam control valve was completely closed at 12 s, and then TRACE over-predicted the pressure drop. The pressure then decreased at a more gradual rate consistent with the data.

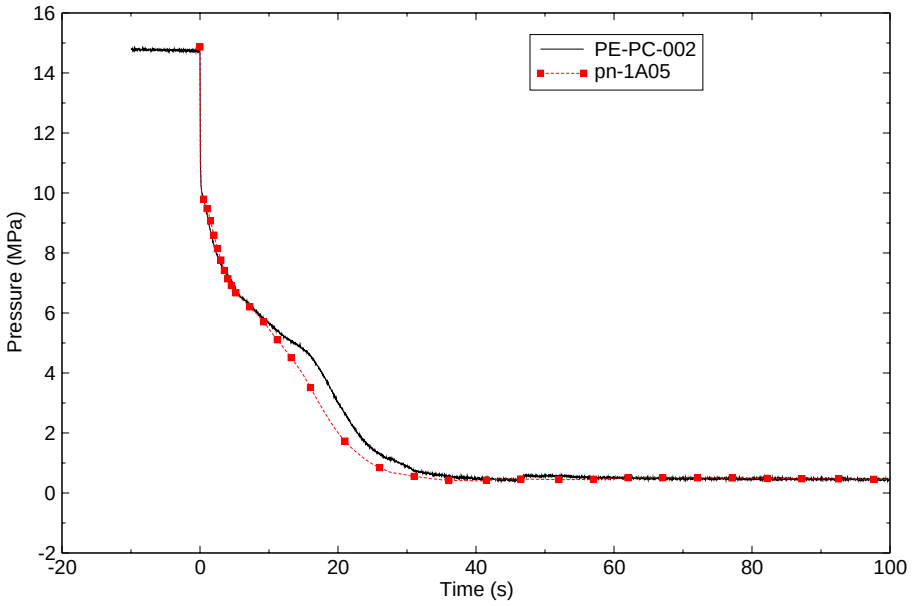

Figure C.1-61. LB-1 Intact Loop Hot Leg Pressure.

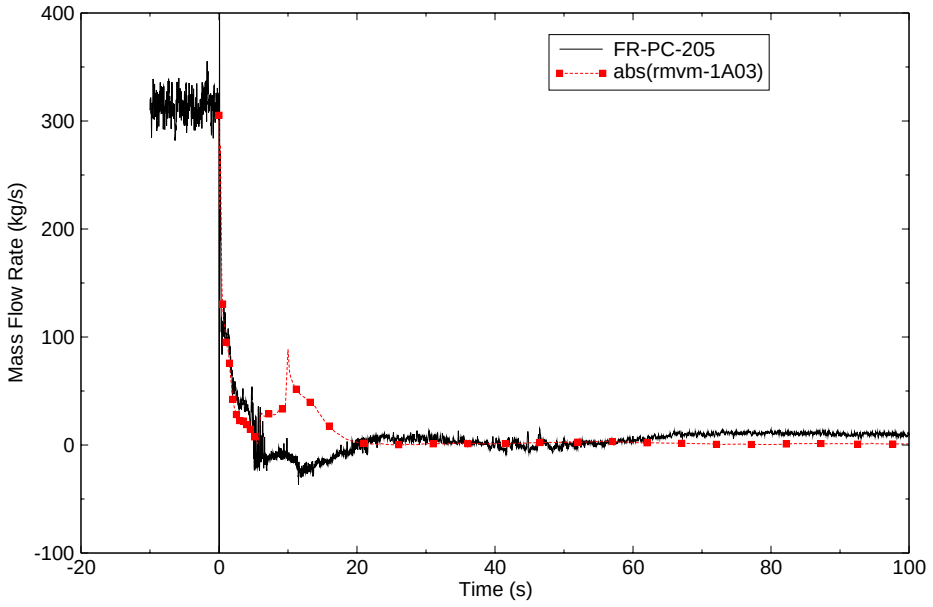

Figure C.1-62. LB-1 Intact Loop Hot Leg Mass Flow Rate.

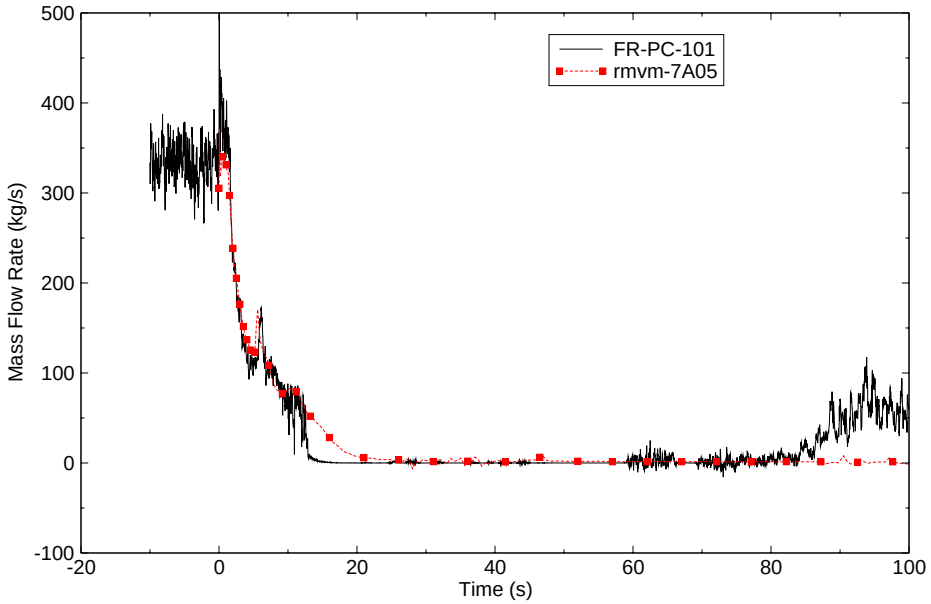

Figure C.1-63. LB-1 Intact Loop Cold Leg Mass Flow Rate.

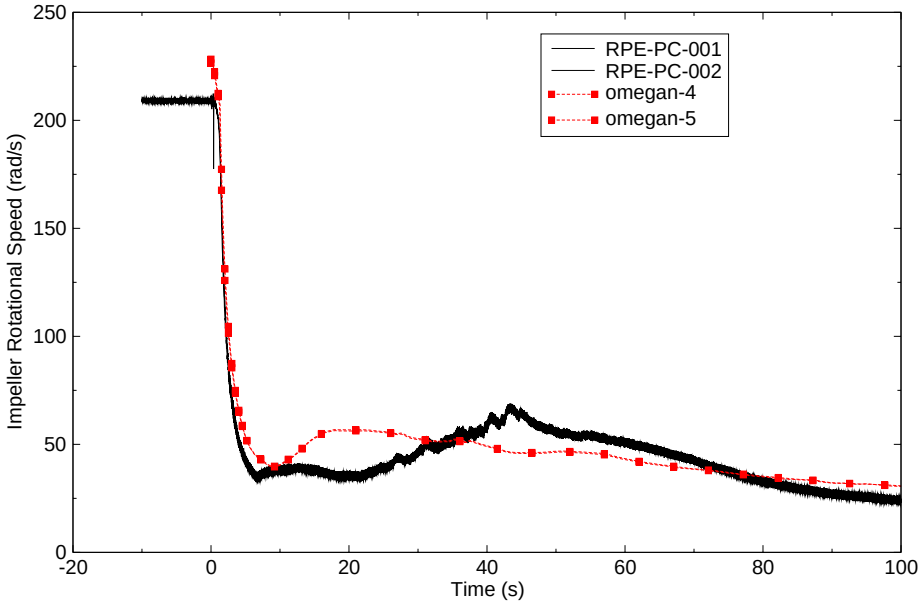

Figure C.1-64. LB-1 Pump Impeller Rotational Speed.

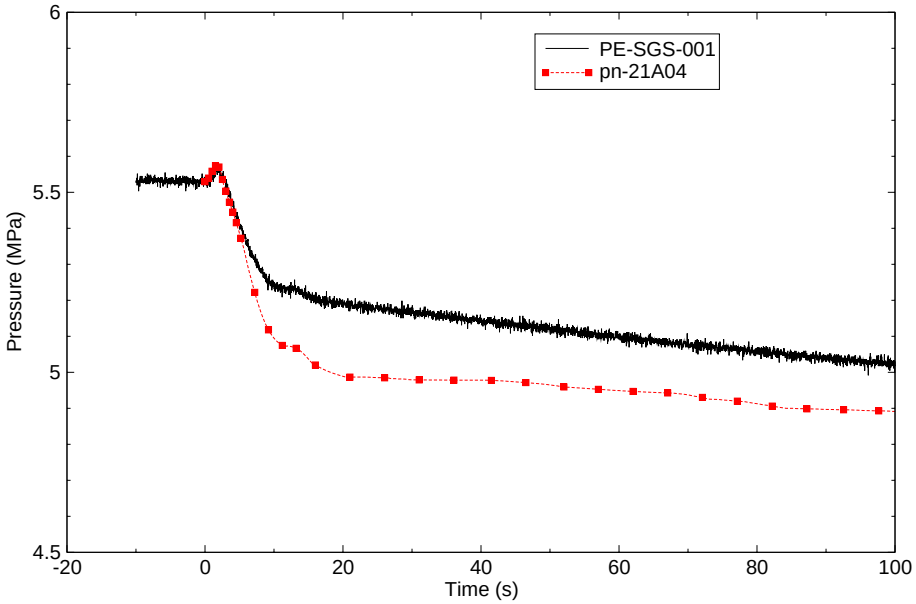

Figure C.1-65. LB-1 SG Secondary System Pressure.

The broken loop hot leg and cold leg mass flow rates are compared in Figure C.1-66 and Figure C.1-67. The predicted mass flow rate compares well with the measured data. The measured broken loop cold leg mass flow rate shown in Figure C.1-67 shows a momentary decrease in the mass flow rate at around 5 s. The decrease in the measured mass flow rate may be a result of some high quality steam passing through the cold leg. The code does not predict the momentary decrease in the break mass flow rate.

The calculated and measured fluid densities in the intact loop cold leg between the pump discharge and the ECC line connection are shown in Figure C.1-68. The density in the cold leg remained near its initial value until about 6 s in both the calculations and the test. Flashing then began in the cold legs and the density decreased rapidly. The calculated results were in reasonable agreement with the measurements until about 24 s, when a series of large-amplitude density oscillations were measured in the test. Oscillations of about the correct frequency were calculated, but the magnitude of the oscillations was generally much smaller in the calculations than in the test. The oscillations appear to be related to the condensation associated with accumulator injection because the oscillations started after accumulator injection began and died out soon after accumulator injection ended. In the test, the cold leg density indicated that the pipe was nearly full of liquid at times, which implies that almost all of the steam then flowing through the intact loop pumps was condensing in the cold leg.

The calculated and measured fluid densities in the broken loop cold leg are shown in Figure C.1-69. The density gradually decreased until after the start of accumulator injection in both the

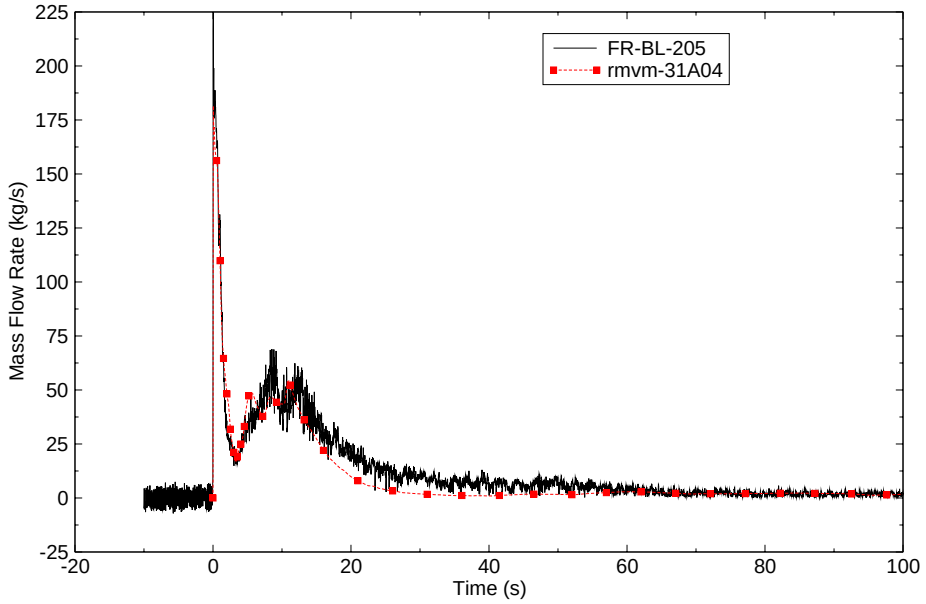

Figure C.1-66. LB-1 Broken Loop Hot Leg Mass Flow Rate.

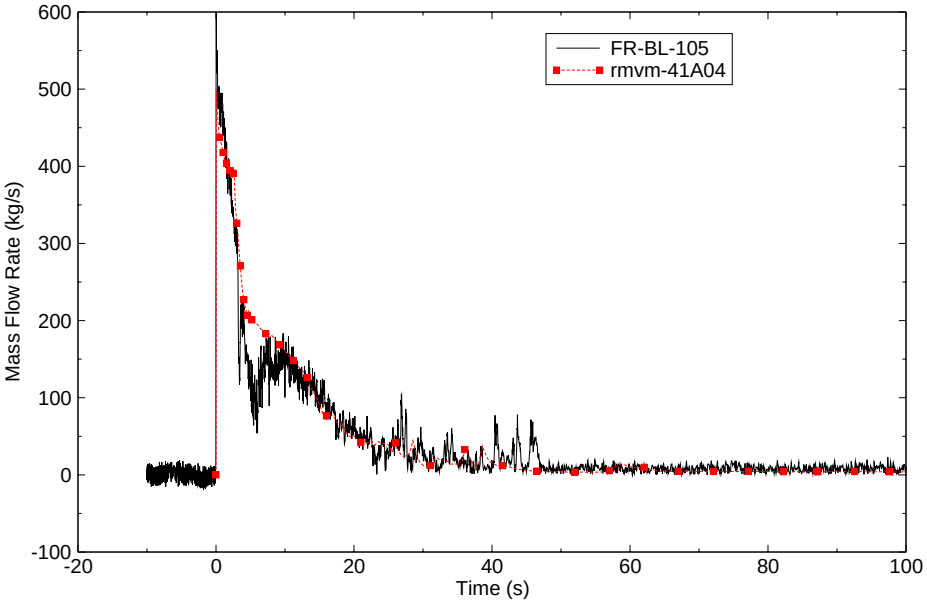

Figure C.1-67. LB-1 Broken Loop Cold Leg Mass Flow Rate.

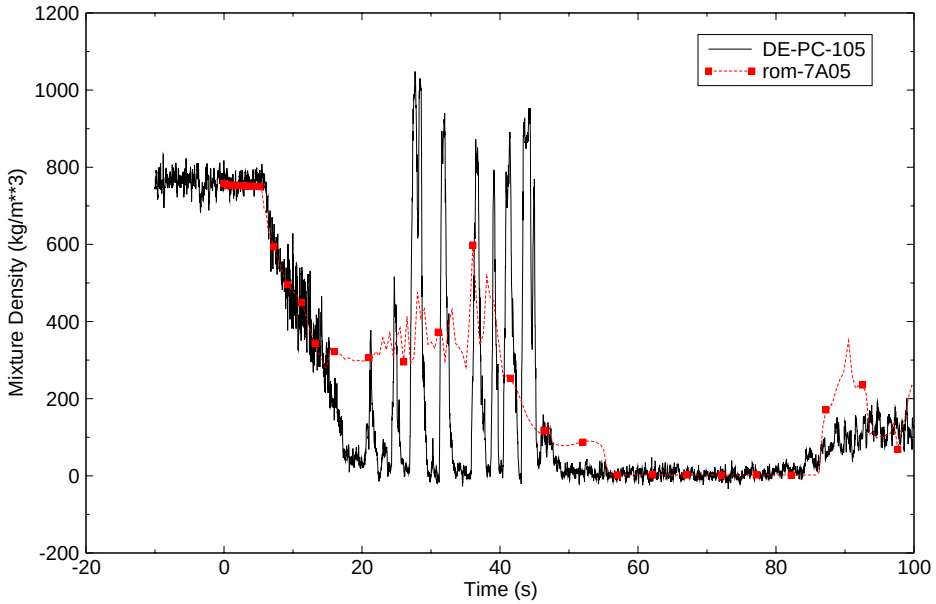

Figure C.1-68. LB-1 Intact Loop Cold Leg Mixture Density.

calculations and the test. There were several increases in density in both the calculations and the test during the period of accumulator injection.

The calculated and measured level for the accumulator is shown in Figure C.1-70. The initial injection rate is higher in the data than in the prediction. Steam condensation on the injected accumulator water has an effect on the predicted injection rate. A lower condensation rate may improve the system pressure response during accumulator injection.

The calculated and measured LPIS mass flow rates are shown in Figure C.1-23. The average predicted LPIS mass flow rate was about 3 kg/s, based on the 50% injection assumption made for Test LB-1. The calculations under-predicted LPIS flow, which reached a maximum of 4 kg/s and then averaged out to about 3.5 kg/s in the data. As for the L2-5 and L2-6 tests, it is not clear why LPIS flow continued to increase in the test and what corrections should be made in the model.

A comparison of calculated and measured liquid temperatures in the upper and lower plenums are shown in Figure C.1-24 and Figure C.1-25. The agreement between the calculated and measured values was considered reasonable.

The calculated and measured downcomer fluid temperature is shown in Figure C.1-26. The predicted downcomer liquid temperature seems reasonable out to about 40 s, when the cold water and noncondensible gases are injected into the cold leg from the accumulator.

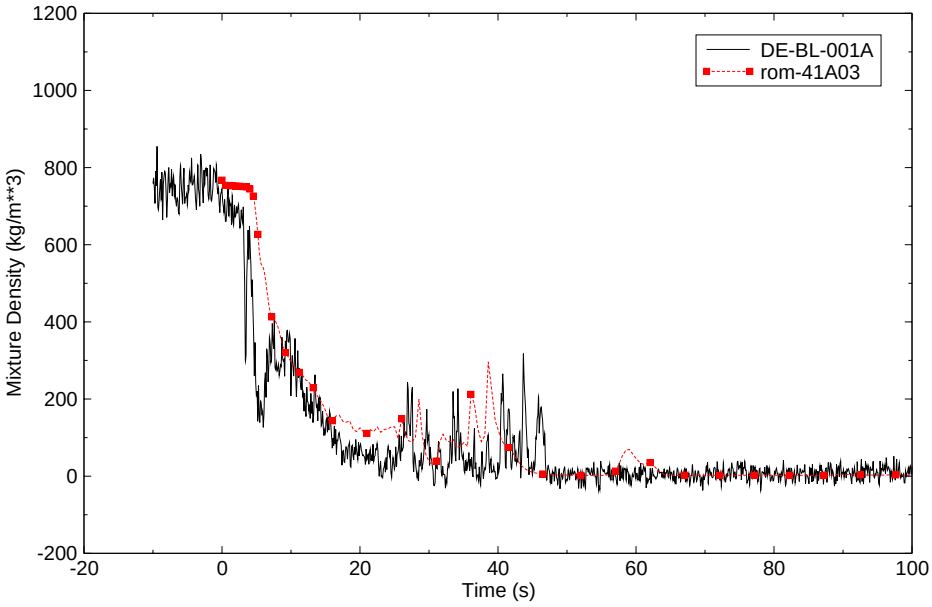

Figure C.1-69. LB-1 Broken Loop Cold Leg Mixture Density.

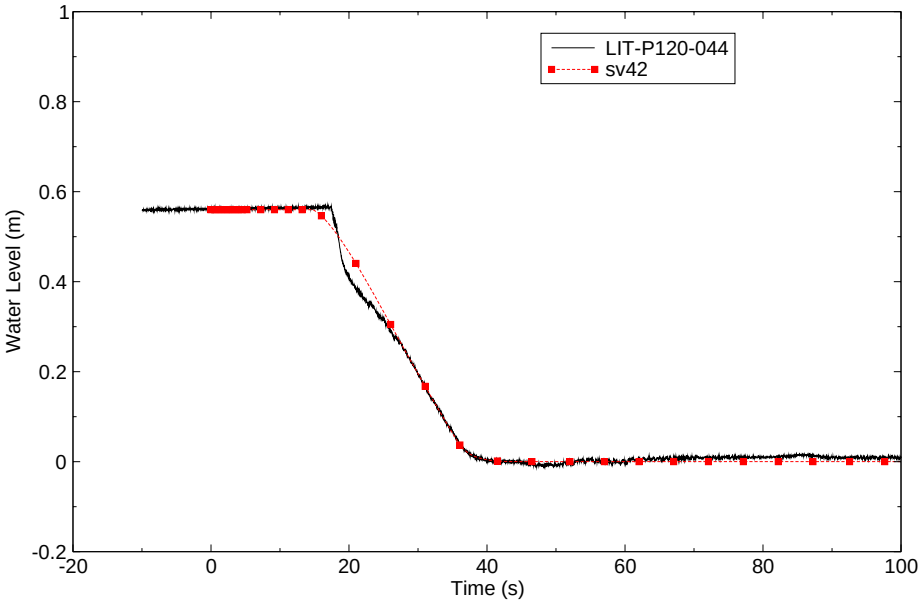

Figure C.1-70. LB-1 Accumulator Level.

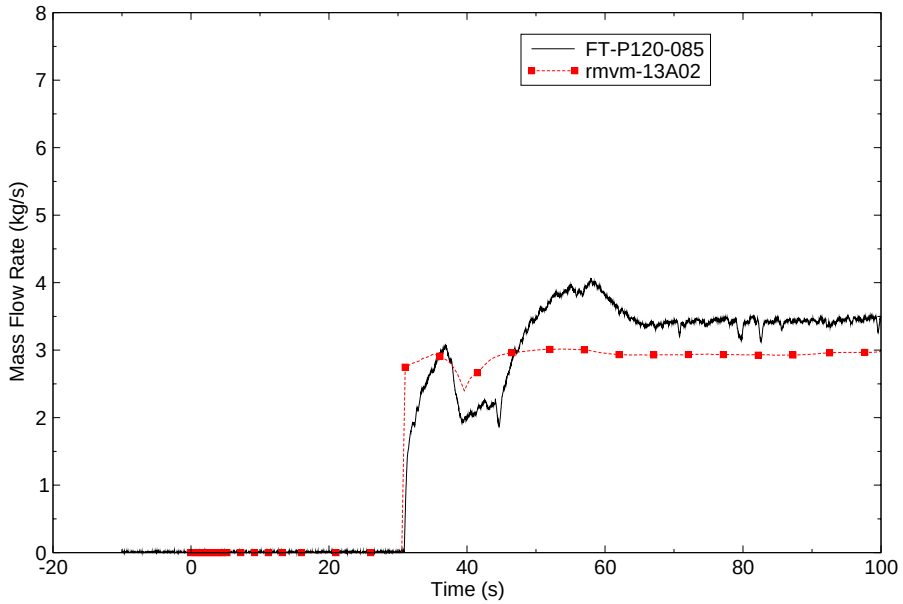

Figure C.1-71. LB-1 LPIS Mass Flow Rate.

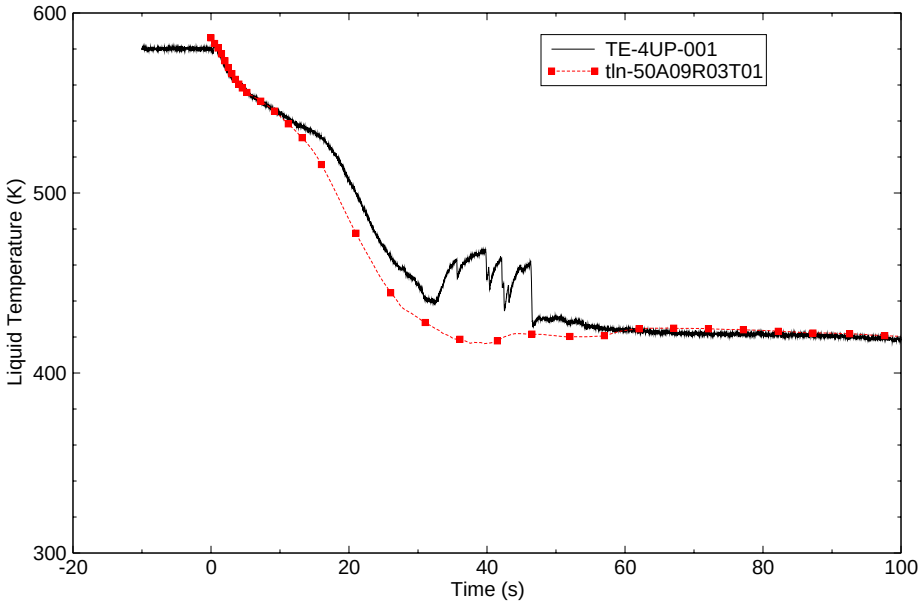

Figure C.1-72. LB-1 Upper Plenum Liquid Temperature.

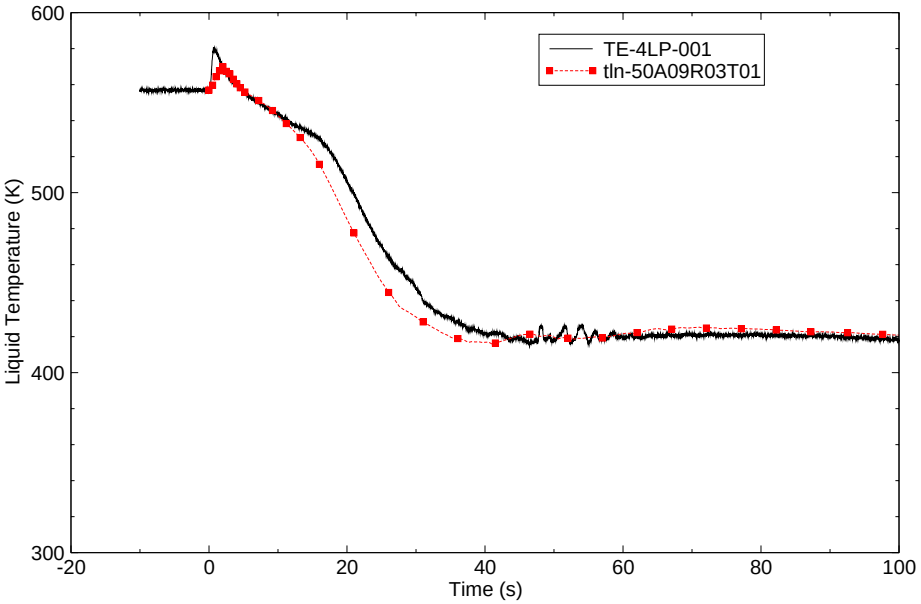

Figure C.1-73. LB-1 Lower Plenum Liquid Temperature.

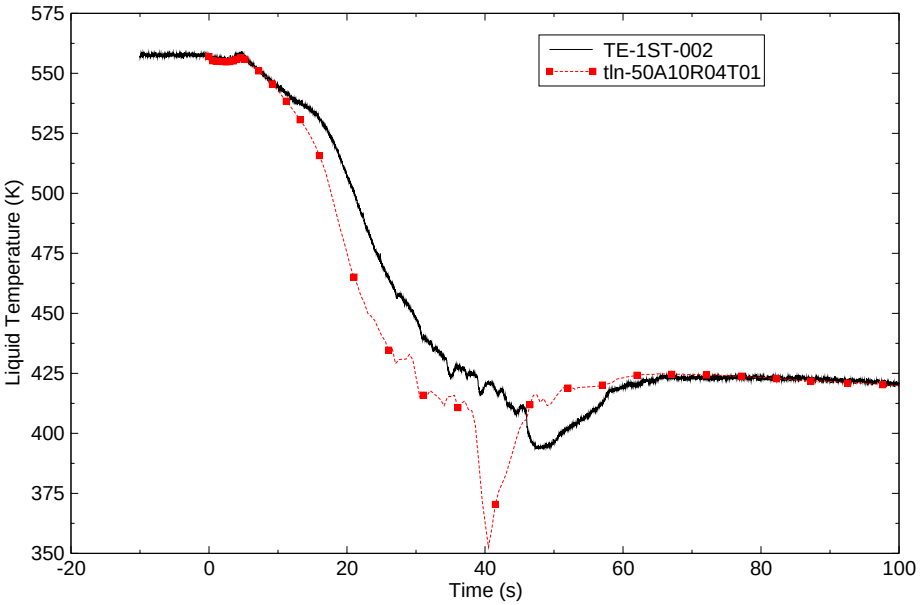

Figure C.1-74. LB-1 Downcomer Liquid Temperature.

The fuel centerline temperature comparison is shown in Figure C.1-75. As in the other simulations presented here, the code over-predicted the centerline rod temperature.

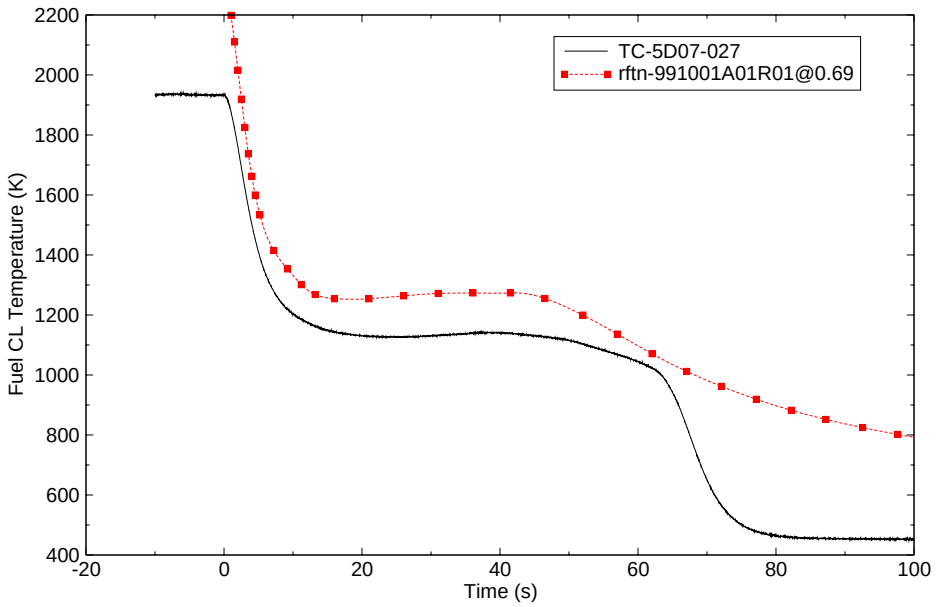

Figure C.1-75. LB-1 Fuel Centerline Temperature.

The rod clad temperatures at elevations 0.38, 0.66, and 1.57 m are compared in Figure C.1-76, Figure C.1-77, and Figure C.1-78 respectively. At the 0.38 m elevation the code predicted the heat removal rate and the peak clad temperature reasonably well but over-predicted the onset of quench. The rod clad temperature prediction at 0.66 m also compares well against the data; i.e., the peak clad temperature is only about 100 K more than the measured. However, the code predicted a longer time for the rods to quench. At the 1.57 m elevation the data shows a double heat-up. The code only predicts one heat-up. As for the lower elevation, the code predicted a longer time for the rods to quench. It appears that not enough entrained liquid is predicted to reach the upper regions of the core and the quench time is delayed.

Core inlet and outlet mass flow rates are shown in Figure C.1-79 and Figure C.1-80. Predicted core flow normally reverses when large break LOCA's are simulated, and this is observed in the calculations. The predictions appear reasonable, since the code prediction of the cladding temperature histories compare well with the data.

C.1.8.3. LB-1 Prediction Conclusions

TRACE predictions of LOFT Test LB-1 showed reasonable agreement with the data. The calculated system pressure and loop mass flow rates reasonably predicted the data trends. As for Test L2-6, the exception is the fuel and cladding temperatures. Fuel rod surface temperatures

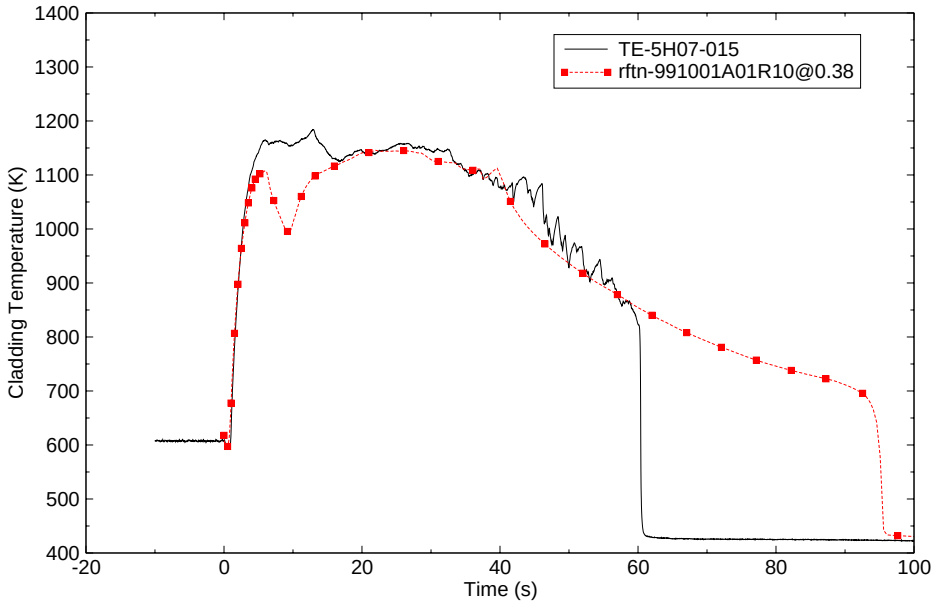

Figure C.1-76. LB-1 Cladding Temperature at 0.38 m.

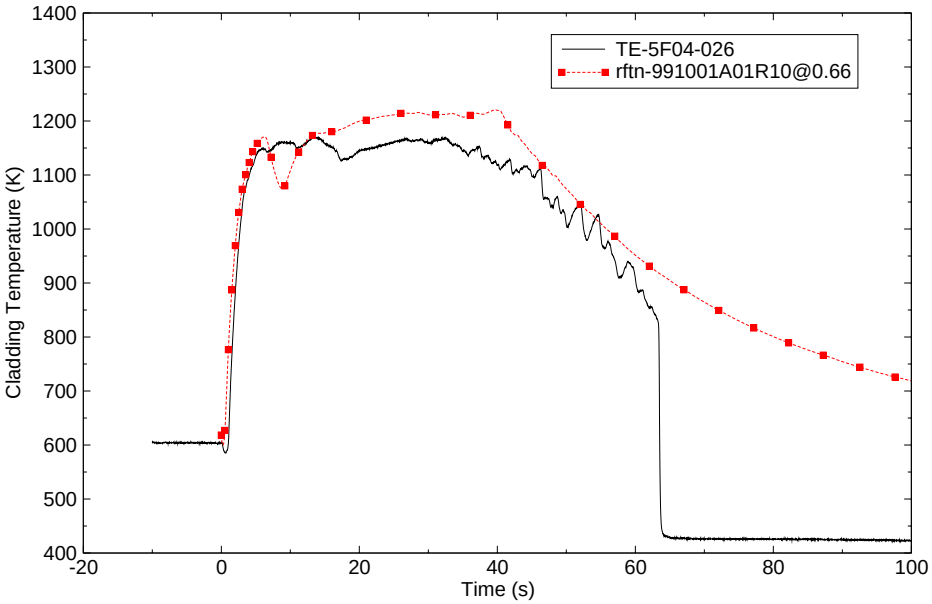

Figure C.1-77. LB-1 Cladding Temperature at 0.66 m.

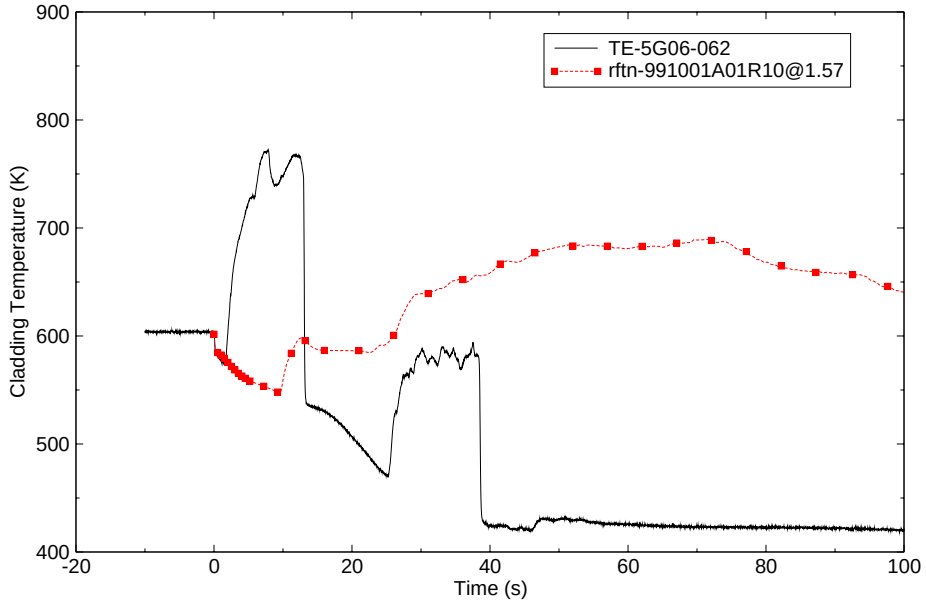

Figure C.1-78. LB-1 Cladding Temperature at 1.57 m.

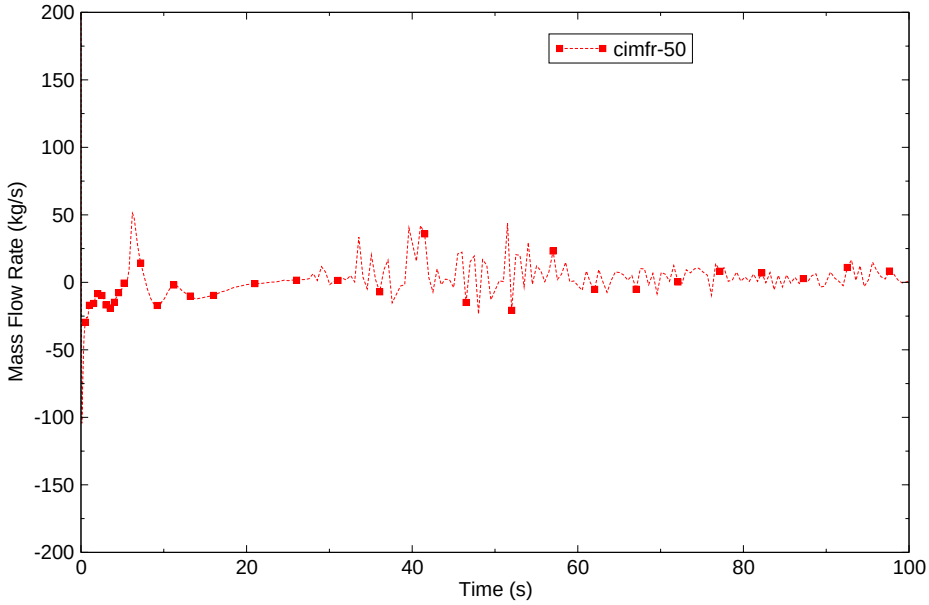

Figure C.1-79. LB-1 Core Inlet Mass Flow Rate.

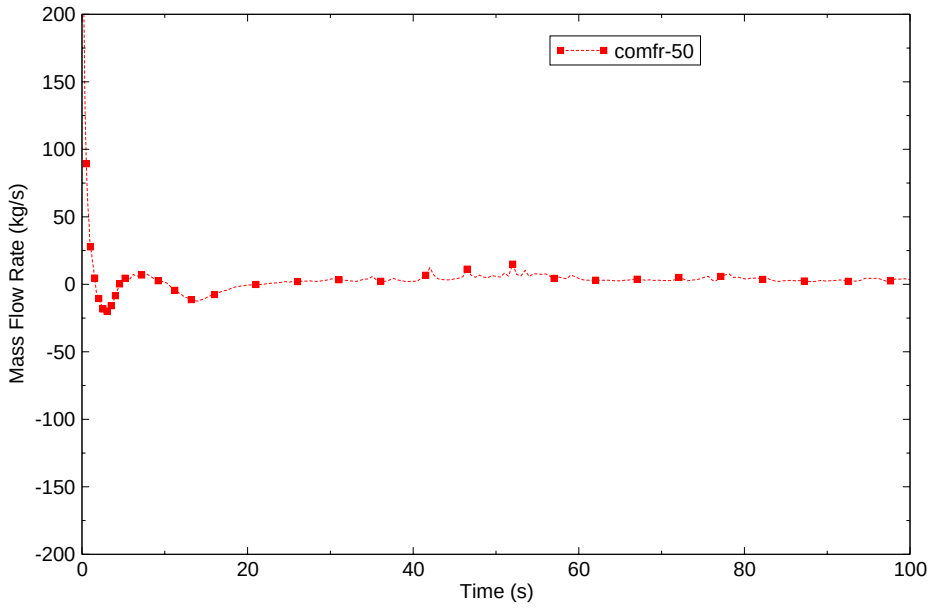

Figure C.1-80. LB-1 Core Outlet Mass Flow Rate.

during the first few seconds of blowdown agree with data but transient results following the peak are different. As noted previously, the external thermocouples do not accurately measure cladding temperature during reflood, particularly at the high power levels for Tests L2-6 and LB-1.

C.1.9. Summary

LOFT Tests L2-5, L2-6, and LB-1 transient results have been assessed using TRACE Version V5.0. Results were compared to measured data. Prediction of thermal-hydraulic parameters in all of the tests simulated were reasonable. TRACE predictions of fuel rod cladding temperatures with the interim reflood model were not as well represented. Insufficient liquid entrainment at the upper regions of the core resulted in over-predictions of the rod clad temperature. Also, the external fuel rod cladding thermocouples used in LOFT do not accurately measure cladding temperature during reflood. Further investigation into the rod clad temperature behavior is warranted. Future versions of TRACE are expected to implement grid spacer models for fuel assemblies and droplet field modeling for core cooling, and these enhancements may improve cladding temperature predictions.

C.1.10. References

1 David L. Caraher and Rex W. Shumway, "TRAC-M Simulations of LOFT Large Break Tests, Task Order No. 6 Task 1", Nuclear Systems Analysis Division, Information Systems Laboratories, Inc., December 2002.

2 Dean Wang and Rex W. Shumway, "TRACE Simulations of LOFT Large Break Tests, Task Order No. 6 Task 9", Nuclear Systems Analysis Division, Information Systems Laboratories, Inc., November 2004. (ADAMS Accession No. ML061800497)

3 Douglas L. Reeder, "LOFT SYSTEM AND TEST DESCRIPTION (5.5-FT NUCLEAR CORE 1 LOCES)", NUREG/CR-0247, July 1978. (ADAMS Accession No. ML070250396)

4 "LOFT Program Description," LPD-1, October 1974. (ADAMS Accession No. ML063070483)

5 Paul D. Bayless, Janice M. Divine, "Experiment Data Report for LOFT Large Break Loss-of-Coolant Experiment L2-5", NUREG/CR-2826, EGG-2210, August 1982.

6 B. E. Boyack, J. F. Lime, D. A. Pimentel, J. W. Spore, J. L. Steiner, "TRAC-M/F77, Version 5.5 Developmental Assessment Manual", NUREG/CR-6730 Vol 1, July 2001.

7 J.C. Lin, et.al., "TRAC-PF1/MOD2 Developmental Assessment Manual", Los Alamos National Laboratory, August 1993.

8 OECD LOFT Experiment LP-LB-1 Data Results, Document Number 09010002, March 1984.

9 S. L. Thompson, and L. N. Kmetyk, "RELAP5 Assessment: LOFT Large Break L2-5", NUREG/CR-3608, SAND83-2549-R4, February 1984.

C.2. CCTF Gravity Reflood Tests

Author(s): Mark Bolander[1], Andrew Ireland[2]

Affiliation: [1]ISL, Inc., [2]US NRC

Code Version: TRACE V5.0

Platform and Operating System: Intel x86, Windows XP

C.2.1. Introduction

The Cylindrical Core Test Facility (CCTF) was an integral test facility located at the Japan Atomic Energy Research Institute (JAERI). Several reflood experiments were conducted at JAERI using CCTF during the 1980's. The objectives of the CCTF tests were to:

1. Demonstrate ECC behavior during refill and reflood period;
2. Verify reflood analysis codes; and
3. Collect information to improve the thermal-hydraulic models in such analysis codes as (a) multidimensional core thermal hydrodynamics, including the radial power distribution effect, fallback effect, and spatial oscillatory behavior; (b) flow behavior in the upper plenum and hot legs; (c) behavior of accumulated water at the bottom of the upper plenum, including possible countercurrent flow and sputtering effects; (d) hydrodynamic behavior of the injected ECC water and the water passing through the steam generator; (e) multidimensional thermal-hydrodynamic behavior in the hot annular downcomer; and (f) overall oscillatory behavior in the system.

Data from several tests conducted at the test facility were used to assess the reflood model incorporated into the TRACE computer program. The tests include C2-4 (Run 62), C2-5 (Run 63), C2-6 (Run 64), C2-8 (Run 67), C2-1 (Run 55), C2-AA2 (Run 58), and C2-12 (Run 71). These tests include variations in total power, radial power profile, system pressure, and ECC injection locations. Throughout this document, the tests will be referred to by their run number (e.g. Run 62).

Previous TRACE assessments using CCTF reflood data is given in Reference 1.

C.2.2. CCTF Facility Description

The CCTF was an experimental test facility designed to model a full-height core section and four primary loops with components of a PWR (Ref. 2). Figure C.2-1 shows an isometric view of the facility. The facility was designed and operated by JAERI and was used to provide information on fluid behavior in the core, downcomer, and upper plenum, including steam and water carryover (steam binding) and integral system (steam generator and pump simulator) effects during the refill and reflood phases of a hypothetical cold leg LOCA in a PWR. The central part of the test facility was a non-nuclear core that consisted of 32 rod bundles housing 1824 electrically heated rods and 224 non-heated rods. The bundles were arranged in a cylindrical array. The core was housed in a test vessel that included a downcomer, lower plenum, upper plenum, and core region. The core design was based on 8 x 8 rod assemblies that modeled a typical 15 x 15 fuel assembly of a PWR.

The primary loops consisted of three intact loops and a broken loop. Each loop consisted of hot and cold leg piping, steam generator u-tubes and a pump simulator. The steam generator u-tubes of two loops were housed in a single shell assembly. The cold leg break was simulated in the broken loop. The broken cold leg was connected to two containment tanks through blowdown valves. The primary loop arrangement is also shown in Figure C.2-1.

The ECCS consisted of an accumulator and LPCI. The injection points were at each cold leg and at the lower plenum. The upper plenum and downcomer injection system were available for alternative ECCS tests.

The facility instrumentation was divided into two groups. One group consists of JAERI supplied instruments that measured the temperatures, absolute pressure, differential pressures, water levels, and flow rates. The other group of instrumentation consisted of the US Nuclear Regulatory Commission (NRC) supplied advanced instrumentation for the two-phase flow measurement.

C.2.3. TRACE Model Description

The TRACE input file for the CCTF facility was derived from the CCTF input file used to simulate CCTF Run 54 in the TRAC-M/F77, Version 5.5 developmental assessment effort (Ref. 3). The base input file was converted to the current TRACE format using the SNAP software program. The base input model consisted of two loops and a vessel. One modeled loop represented the three intact loops and the other modeled loop represented the broken loop. The vessel model included 26 axial levels, 4 radial rings and 2 azimuthal sectors. The base modeled was modified to explicitly model all 4 loops and model the VESSEL with 22 axial levels, 5 radial rings, and 8 azimuthal sectors. All of the major flow paths in the CCTF facility were modeled.

Figure C.2-2 shows the VESSEL component radial and azimuthal noding along with the loop connections points. Figure C.2-3 shows the VESSEL axial nodalization and loop noding scheme

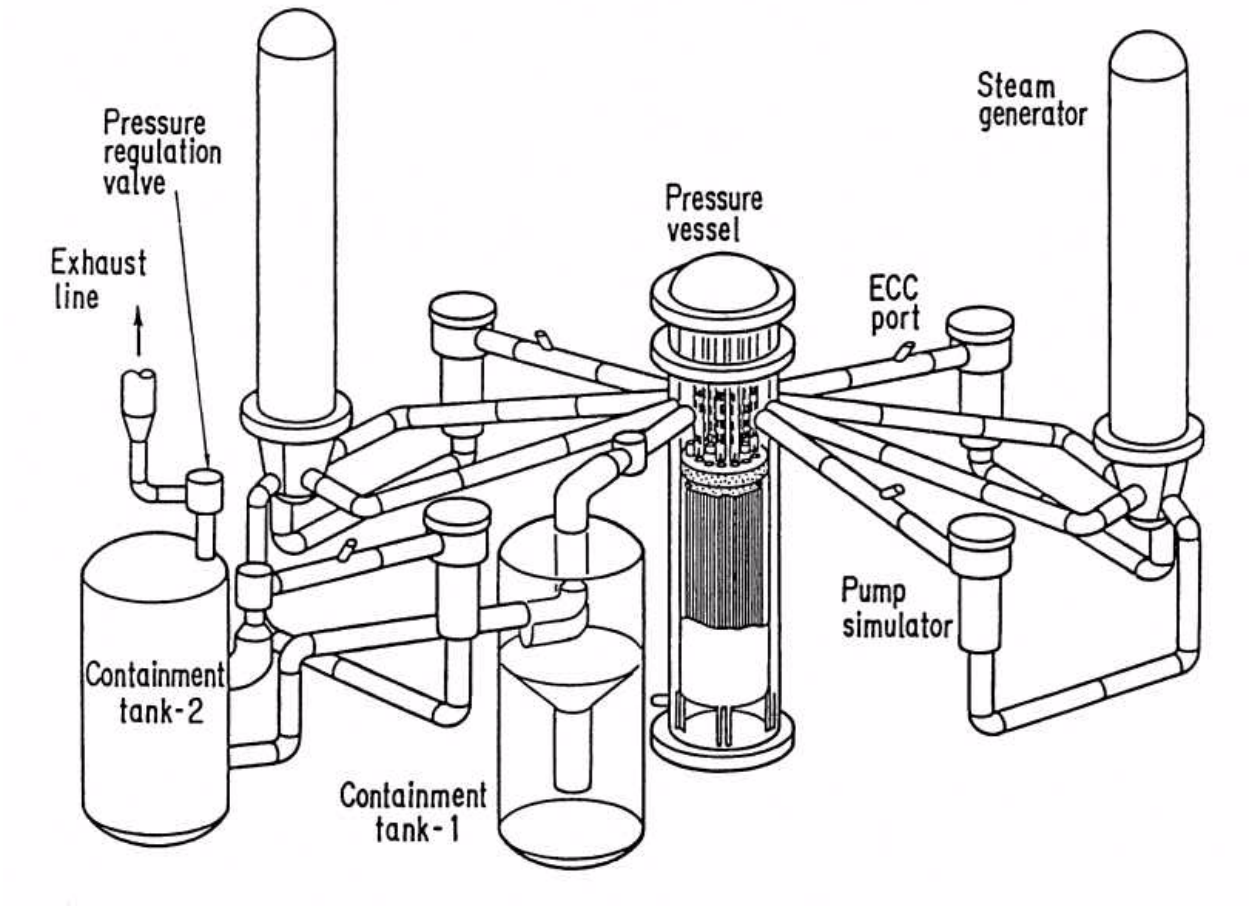

Figure C.2-1. Isometric view of the CCTF facility.

for the TRACE CCTF input model. The connections are consistent with the vessel connections in the physical facility. Modeled loops 1 and 2 share a common steam generator shell while loops 3 and 4 share the other common steam generator shell. The broken loop was modeled out to the containment tanks. These tanks were modeled as BREAK components.

The lower plenum resides in the bottom three axial levels in the VESSEL component. The core region is defined by axial levels 4 through 15 and rings 1 through 3. The upper plenum is represented in VESSEL levels 18 through 22. The downcomer is represented by ring 5.

The CCTF TRACE model contains 204 components in all: 43 hydro components, 160 heat structure components, and 1 power component. There are 343 control blocks, signal variables, and trips that make up the control system. The control system is used to define plottable parameters such as downcomer, core and loop differential pressure. A detailed description of the model and modifications is given in Reference 4.

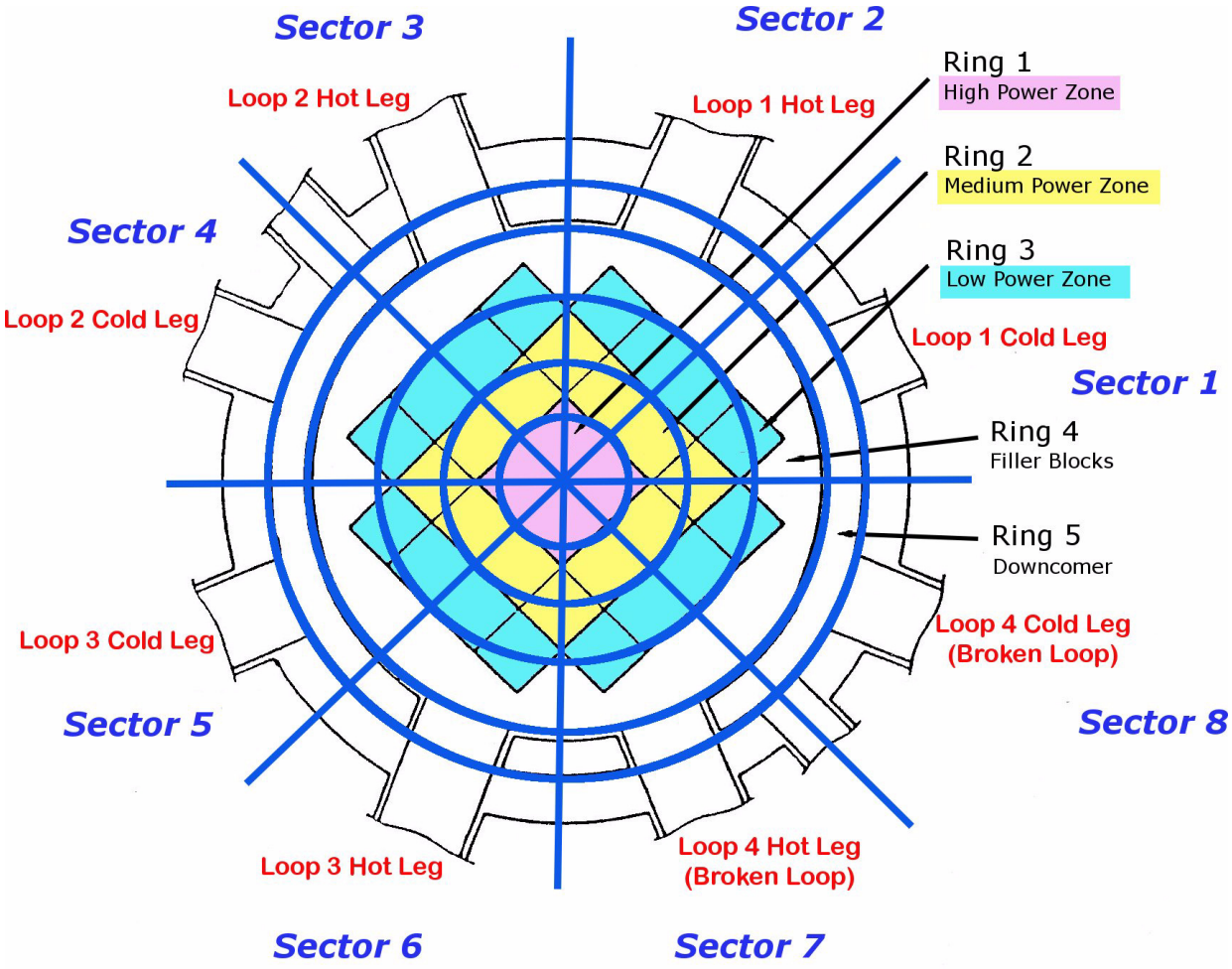

Figure C.2-2. Radial and Azimuthal Noding of the VESSEL Component.

C.2.4. Tests Simulated with TRACE

There were seven CCTF reflood experiments simulated with the TRACE computer code. The tests simulated are: Run 62, Run 63, Run 64, Run 67, Run 55, Run 58, and Run 71. A brief description of the test procedure is given followed by a description of the tests simulated. A detailed description of the tests and test results can be found in References 5 through 11.

C.2.4.1. Test Procedure and Initial Conditions

In preparation for the tests, the accumulator tank, LPCI tank, saturated water tank, and secondary sides of the steam generator simulators were filled with purified water. The instruments were checked for their zero points and sensitivity after all of the components and instruments were inspected for mechanical and electrical leakage.

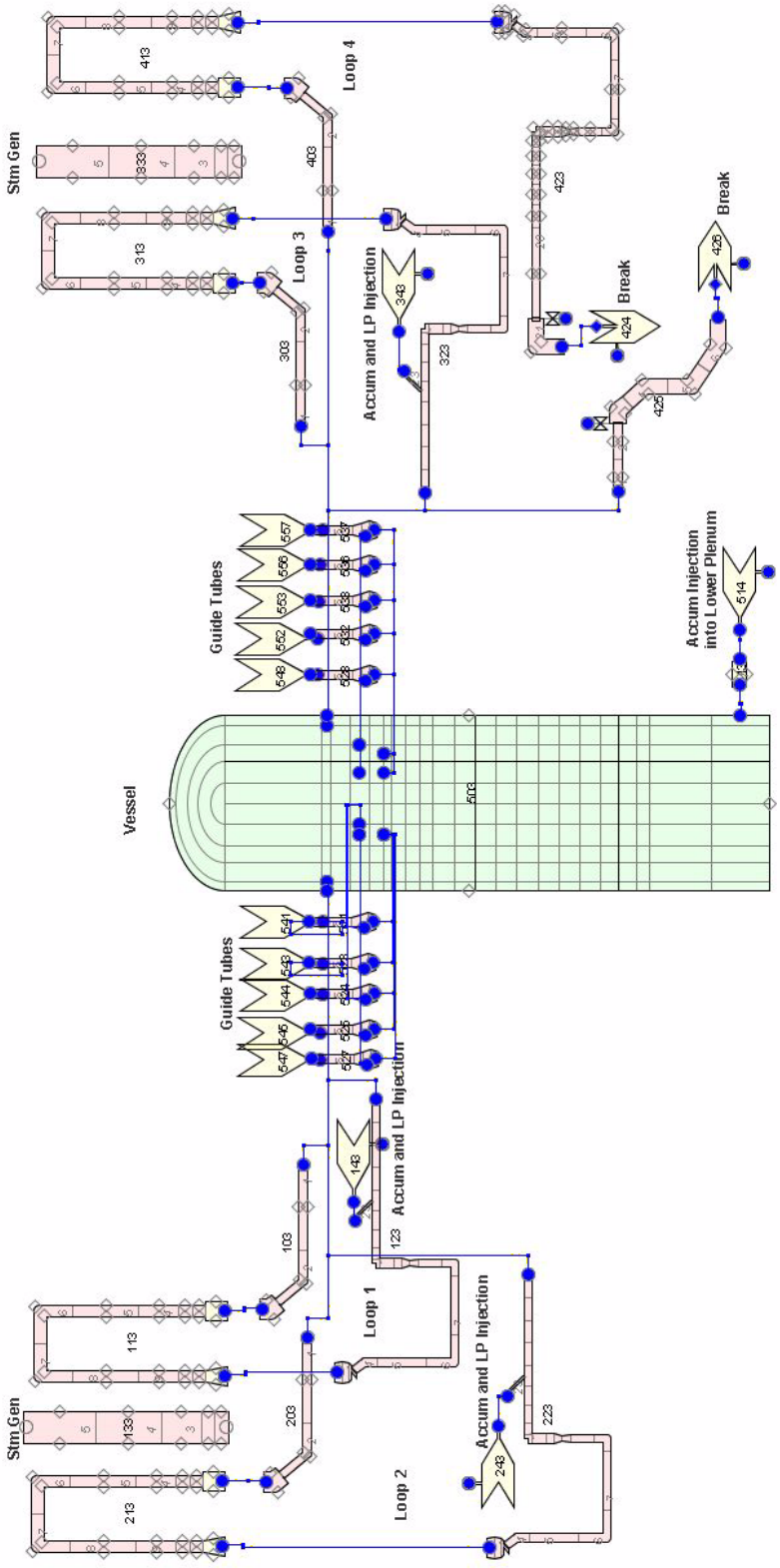

Figure C.2-3. TRACE Nodalization Diagram of the CCTF Facility.

After the preparatory operations, the primary system was heated to its specified temperatures with pre-heaters and pressurized to the specified initial condition pressure by substituting steam for nitrogen gas in the system. The water in the accumulator tank was electrically heated to its specified temperature and pressurized with nitrogen gas to provide sufficient head to drive the injection flow required. The water in the LPCI tank was also heated to its specified temperature and was circulated through the circulation line, including the LPCI line, to preheat the line to the same temperature as the water. The water in the saturated water tank was heated close to the saturation temperature of the expected primary system pressure. The water in the secondary side of each steam generator simulator was also heated and pressurized to the specified temperature and pressure.

After the initial conditions of the test were established, the electric power for preheating was turned off and the lower plenum was filled directly from the saturated water tank until the desired initial level was obtained. Electric power was applied to the heater rods in the core and the data recording was started when the water level in the lower plenum reached the specified level and other initial conditions of the test stabilized at the allowable tolerance. When a specified, test dependent, initial clad temperature was reached, direct injection of the accumulator water into the lower plenum was initiated. The system pressure was maintained at the specified initial pressure throughout the test by controlling the outlet valve of containment tank 2. Decay of power input to the rods was programmed to begin when the water reached the bottom of the heated region of the core.

When the water level in the lower plenum reached a specified level (about 0.5 m) below the bottom of the heated region of the core, the accumulator injection was switched to the three intact cold leg ECC injection ports. This injection procedure was employed to minimize oscillatory core flow behavior. The accumulator injection flow was reduced during the cold leg injection period. At a specified time after the time of core bottom recovery, actions were taken to switch from accumulator injection to LPCI injection. The LPCI injection was maintained throughout the remainder of the test.

The generated steam and the entrained water flowed via the broken and intact loops to the containment tanks. The steam was then vented to the atmosphere to maintain a constant pressure in the containment tanks.

When all thermocouples on the surface of the heater rods indicated quenching of the rods, the power supply to the heater rods and the ECC water injection were turned off. Data recording was terminated and the test ended (about 1000 s).

Table C.2.1 presents the initial conditions for each of the tests simulated.

Table C.2.1. Initial Conditions for the CCTF Tests Simulated.

Parameter							
Test Number	C2-4	C2-5	C2-6	C2-8	C2-1	C2-AA2	C2-12
Run Number	62	63	64	67	55	58	71
Initial Total Power (MW)	9.37	7.10	7.11	9.32	9.35	9.36	7.12

Table C.2.1. Initial Conditions for the CCTF Tests Simulated. (Continued)

Parameter							
Power Decay:							
ANS decay heat factor	1.2	1.0	1.0	1.2	1.2	1.2	1.0
Actinide factor	1.1	1.0	1.1	1.1	1.0	1.0	1.1
Time after scram (s)	30	40	40	30	30	30	40
Radial Power Ratio:							
High Power	1.37	1.37	0.99	1.36	1.36	1.36	1.0
Medium Power	1.19	1.20	1.00	1.20	1.20	1.20	1.0
Low Power	0.76	0.76	1.00	0.76	0.76	0.76	1.0
Initial System pressure (MPa)	0.2	0.2	0.2	0.15	0.42	0.2	0.3
Initial Containment Pressure (MPa)	0.2	0.2	0.2	0.15	0.42	0.2	0.3
Initial Temperatures (K):							
Downcomer wall	467	470	465	461	491	481	472
Primary piping	394	392	394	387	425	395	407
SG secondary	539	540	540	540	538	540	540
ECC Water	308	308	310	310	309	308	308
Initial Lower Plenum Water Level (m)	0.81	0.86	0.87	0.86	0.86	0.86	0.9
Pump K Factor	15	15	15	15	15	15	15
Vent Valve Position	Shut	Shut	Shut	Shut	Shut	Shut	Shut
Loops Sealed	No	No	No	No	No	No	No
ACC flow Rate (m^3/s):							
Into lower plenum	0.105	0.106	0.105	0.105	0.103	0.096	0.105
Into intact cold legs	0.091	0.091	0.091	0.091	0.089	0.080	0.089
Into downcomer	N/A	N/A	N/A	N/A	N/A	0.0089	N/A
LPCI Flow Rate (m^3/s):							
Into intact cold legs	0.011	0.011	0.011	0.011	0.011	0.0022	0.019
Into downcomer	N/A	N/A	N/A	N/A	N/A	0.0089	N/A
Into lower plenum	N/A	N/A	N/A	N/A	N/A	N/A	N/A

C.2.4.2. Run 62

Run 62 was conducted to investigate the reproducibility of Run 53 (Test C2-SH1), the first base case test run in the CCTF-II facility. This test was performed using essentially the same initial and boundary conditions as those used in Run 53 to verify the reproducibility of results in the CCTF-II testing. The initial pressure and power for this test was 0.2 MPa and 9.37 MW, respectively.

C.2.4.3. Run 63

Run 63 investigated the effect of decay power level on reflood thermal-hydrodynamic behavior. The initial total power supplied to the core was set at 7.1 MW. Other test conditions were set almost equal to those of the base case test (Run 62) in which the initial total power was set at 9.4 MW. (see Table C.2.1)

C.2.4.4. Run 64

Run 64 studied the core radial power profile effect on the system and core cooling behavior. The test used a flat radial power profile in the core instead of the steep radial power profile of Run 63. The initial total power of Run 64 was planned to be identical to Run 63.

C.2.4.5. Run 67

Run 67 studied the system pressure effect on the system and core cooling behavior. The test was perform with a system pressure of 0.15 MPa and is a counter part to Run 55, a high pressure test (0.42 MPa), and Run 62, the base case test with a system pressure of 0.2 MPa.

C.2.4.6. Run 55

Run 55 investigated the effect of system pressure on reflood behavior during a Loss of Coolant Accident (LOCA). The initial conditions were the same as those of the base case test of the Core-II facility configuration except for the system pressure. The initial system pressure for Run 55 was 0.42 MPa; twice that of the system pressure in the base case test.

C.2.4.7. Run 58

Run 58 investigated the effects of emergency core cooling (ECC) injection locations. In this test ECC water was injected into the downcomer as well as into the intact cold legs in order to study the characteristics of thermal-hydrodynamic behavior in a downcomer injection situation. The test conditions were the same as those for Run 62 except for the ECC water injection locations.

C.2.4.8. Run 71

Run 71 investigated the thermal-hydraulic behavior of reflood with best estimate conditions and to confirm the conservatism of the initial and boundary conditions used in previous CCTF experiments.

C.2.5. TRACE Simulations of the CCTF Reflood Tests

The following presents the results of the TRACE simulations of the reflood experiments simulated. The general predicted behavior of the tests simulated are similar. The results of the base test, Run 62, are discussed in detail. Differences between the base test and the other tests simulated are presented.

C.2.5.1. Simulation of Run 62.

The results of the TRACE simulation of Run 62 compared to data are presented here.

C.2.5.1.1. Loop Mass Flow Rate Comparisons

The predicted Loop 1 hot leg mass flow rate is compared to data in Figure C.2-4. Generally, the predicted loop mass flow rate compares well with the data. The flow spikes predicted by the code are a result of liquid droplets periodically entering the hot leg from the vessel upper plenum as shown in Figure C.2-5. Most of the liquid is de-entrained before entering the steam generator in the calculation and the liquid is pooled in the hot leg pipe (see Figure C.2-5). The predicted hot leg mass flow rates for loops 2, 3 and 4 show similar behavior.

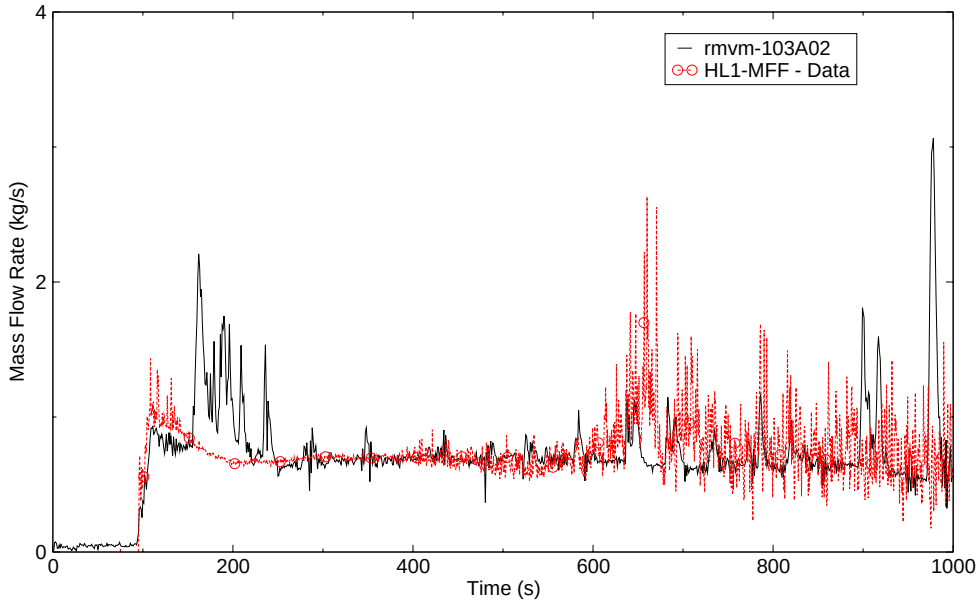

Figure C.2-4. Loop 1 Hot Leg Mass FLow Rate Comparison - Run 62.

Figure C.2-6 shows the comparison of the predicted Loop 1 cold leg mass flow rate with data. The measurement location for the cold leg mass flow rate is downstream of the ECC injection port.

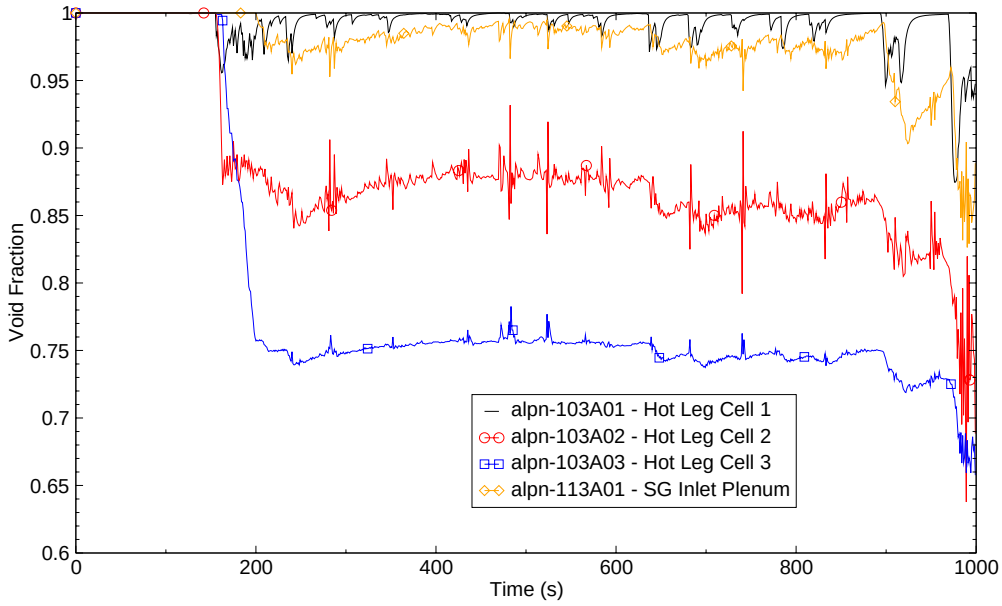

Figure C.2-5. Loop 1 Predicted Void Fraction in the Hot Leg and Steam Generator Inlet Plenum - Run 62.

The predicted mass flow rate is higher than the measured data. Reference 2 indicates the water entrained in the steam exiting the upper plenum was evaporated in the steam generator u-tubes because the secondary side fluid was hotter than the primary side. If very little water was de-entrained in the hot legs, then the mass flow rate in the cold leg just before the ECC injection port would be nearly the same as the hot leg mass flow rate. Thus adding the ECC injection flow rate to the hot leg flow rate should be nearly the same as the measured cold leg flow rate downstream of the ECC injection port. Figure C.2-6 also shows ECC injection rate and the measured hot leg flow rate plus the ECC mass flow rate. As shown, the measured ECC flow rate is higher than the measured cold leg mass flow rate. An examination of the measured loop differential pressure indicates the loop flow rate was always positive, thus none of the injected ECC flowed back to the pump suction piping. Therefore it is concluded that the measured cold leg flow rate is not correct. When compared with the measured hot leg and ECC combined flow rate the calculated cold leg mass flow rate agrees well with the data as shown in Figure C.2-6. The predicted cold leg mass flow rates in the other intact loops show similar behavior.

Figure C.2-7 shows the predicted Loop 4 cold leg mass flow rate compared to data. The measurement location in this loop is in the bottom of the pump suction pipe. There is no ECC injection in this loop. As shown the predicted cold leg mass flow rate agrees well with the data.

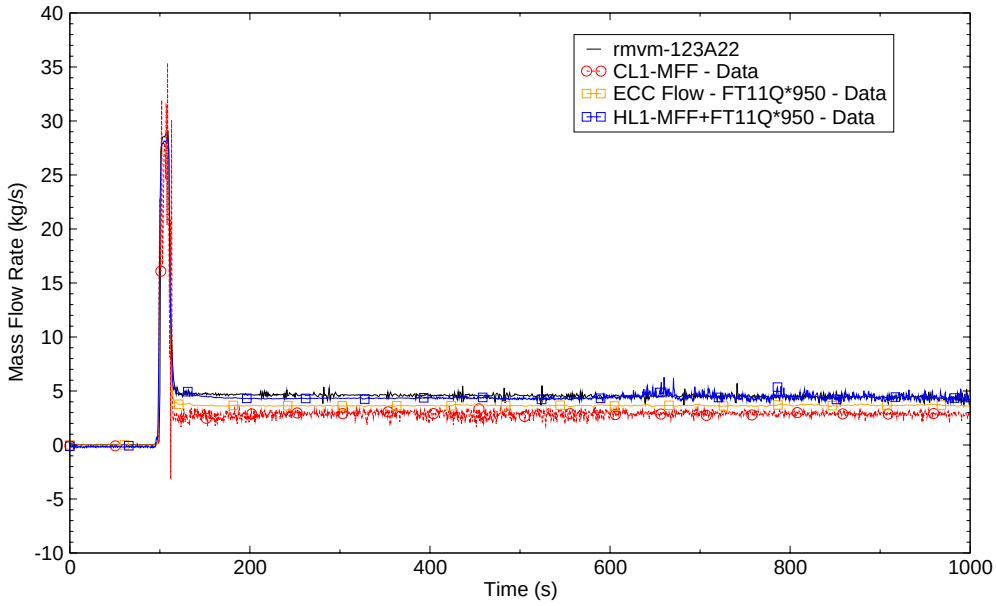

Figure C.2-6. Loop 1 Cold Leg Mass Flow Rate Comparison - Run 62.

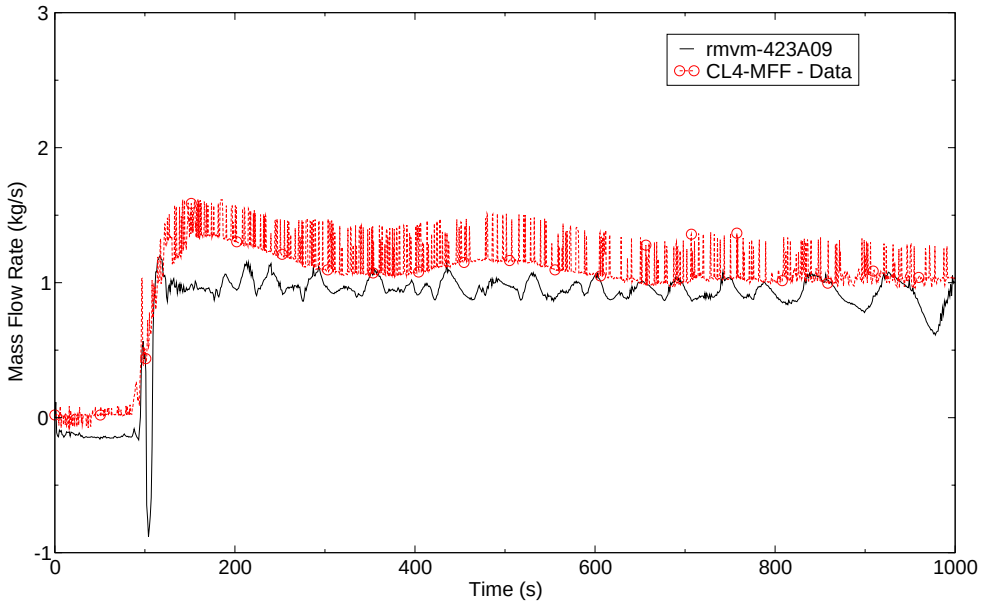

Figure C.2-7. Loop 4 Cold Leg Mass Flow Rate Comparison - Run 62.

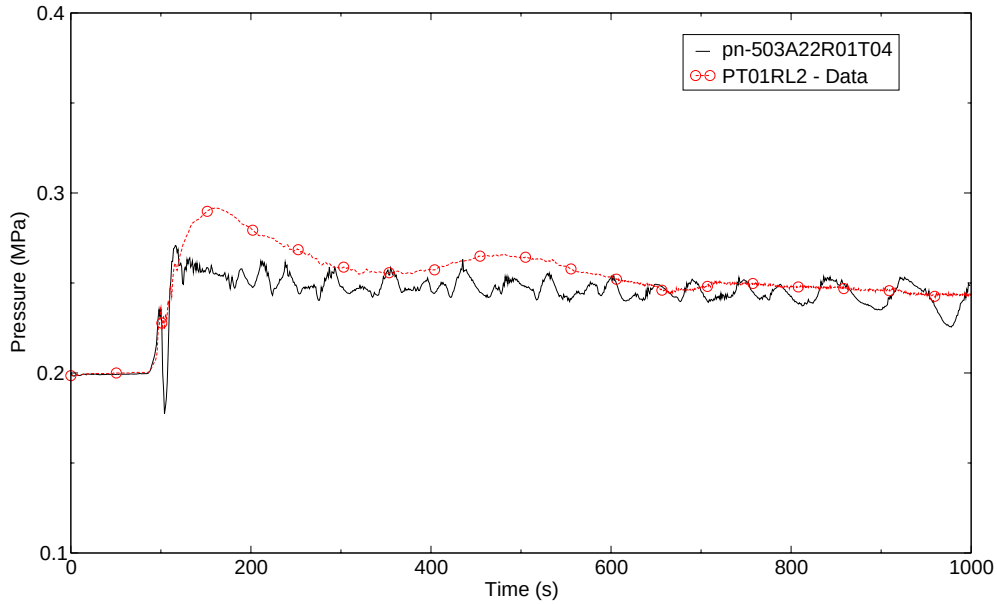

Figure C.2-8. Upper Plenum Pressure Comparison - Run 62.

C.2.5.1.2. Upper Plenum Pressure Comparison

A comparison of the predicted and measured upper plenum pressure is shown in Figure C.2-8. The calculated response predicts the measured response reasonably well. At about 84 seconds accumulator injection began in the lower plenum. By 93 seconds power decay was initiated and at about 94 seconds the liquid level had reached the bottom of the heated core. Accumulator injection was switched from the lower plenum to the intact loop cold legs at around 97 seconds. Accumulator injection in the cold legs continued until about 115 seconds. During the accumulator injection period, the lower plenum and downcomer filled and coolant began to enter the heated core region. As the injected coolant began to flood the hot rods, steam was produced and the system pressure increased. The predicted upper plenum pressure during this time period matched the data very well.

Between 120 and 200 seconds the upper plenum pressure is under-predicted. Three contributors to the under-prediction of the upper plenum pressure include: under-prediction of the core inlet fluid temperature, poor simulation of the heat transfer in the upper core and under-prediction of entrainment to the steam generator tubes.

An examination of the core inlet temperature (Figure C.2-9 and Figure C.2-10) shows the predicted fluid temperature is much more subcooled between 100 and 200 seconds. The colder water entering the core results in less steaming and consequently a lower pressure.

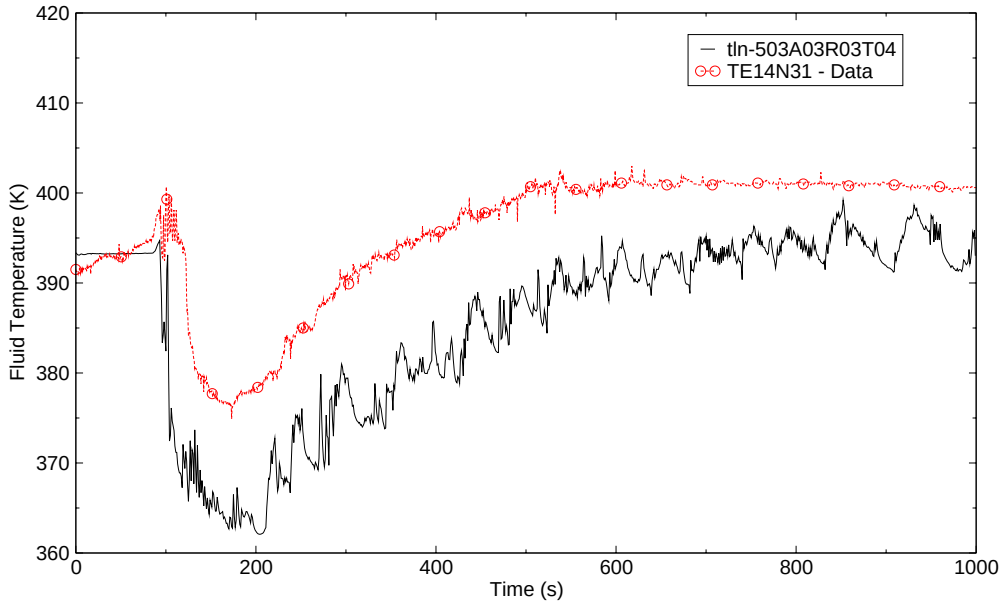

Figure C.2-9. Core Inlet Temperature Comparison in the Low Power Region - Run 62.

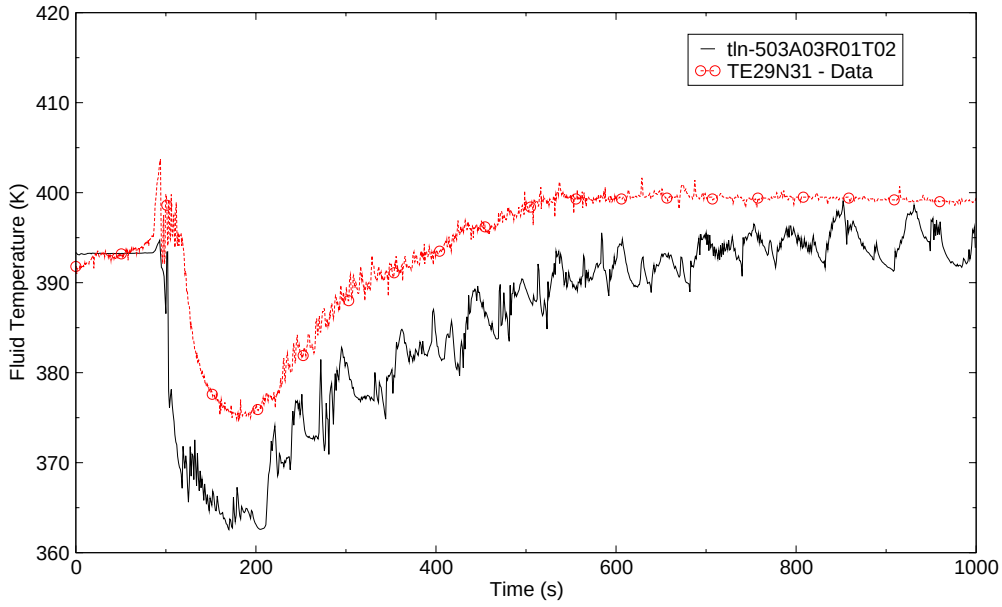

Figure C.2-10. Core Inlet Temperature Comparison in the High Power Region - Run 62.

One explanation for the difference in the core inlet fluid temperature is twofold. First, during the accumulator injection into the lower plenum, the data indicates there was some thermal stratification of the saturated water initially in the lower plenum with the colder accumulator liquid injected into the lower plenum in the experiment. As the lower plenum filled with water, the saturated water remained on top, reaching the thermocouple probe located at the core inlet (Figure C.2-9) before the cold accumulator water. The code predicted more thermal mixing of the cold accumulator and the initial saturated water in the lower plenum during the lower plenum injection period. Thus a colder fluid is predicted just below the core inlet. Second, when the accumulator injection was switched from the lower plenum to the cold legs, steam condensation occurred and warmed the incoming accumulator water. Similar behavior was observed in the calculation. However, the incoming accumulator water did not warm up as much as shown in Figure C.2-11. Thus colder water entered the lower plenum in the calculation. Further, when accumulator injection ended and LPI injection began, there was enough steam condensation occurring to bring the injected LPI water to saturation. While steam condensation in the cold leg occurred in the calculation, it did not warm the injected LPI fluid up to saturation as shown in Figure C.2-11. As the injected cold leg ECC fluid entered and flowed down the downcomer, the hot vessel wall kept the fluid at saturation in the experiment. Although the hot vessel wall warmed the downcomer fluid in the calculation, the fluid temperature remained subcooled as shown in Figure C.2-13.

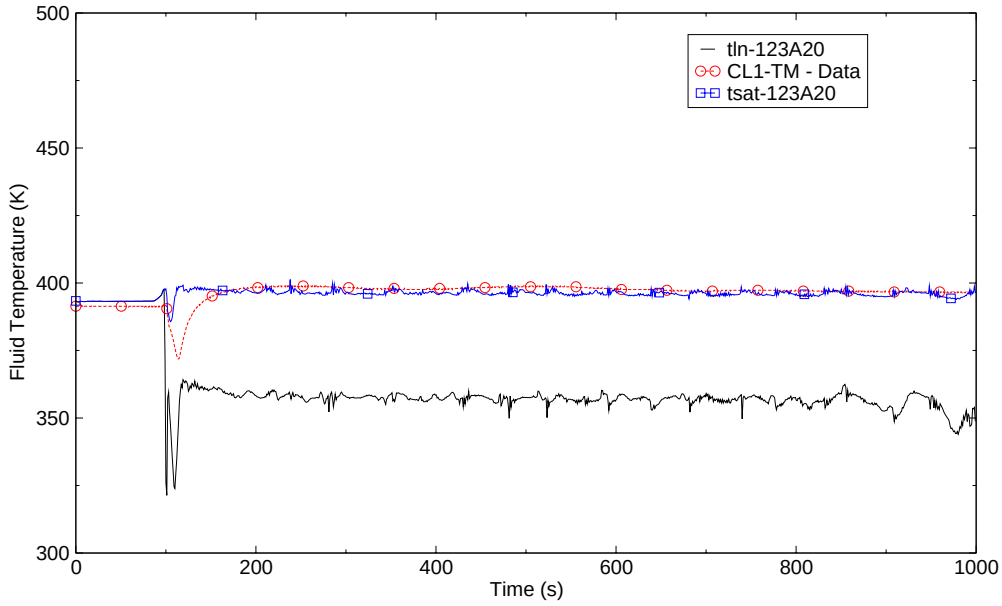

Figure C.2-11. Loop 1 Cold Leg Fluid Temperature Comparison - Run 62.

In the prediction, the steam not condensed in the cold legs from ECC injection flowed around the downcomer and out the vessel-side of the break as shown in Figure C.2-12. The difference between the steam coming into the downcomer from the cold legs and that going out the break is steam condensation in the downcomer.

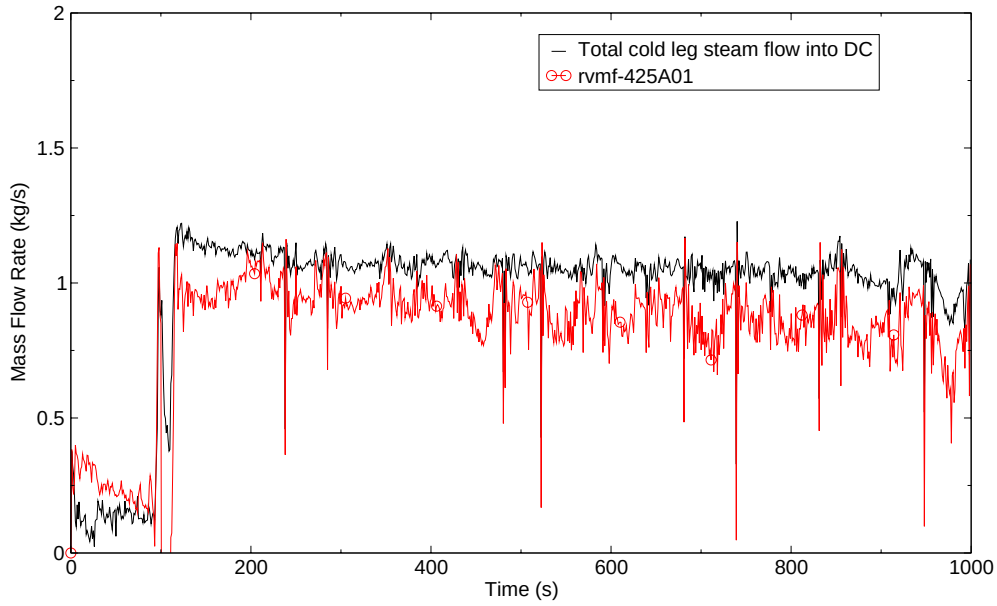

Figure C.2-12. Total Steam Flow Rate from the Cold Legs and the Steam Flow Rate Out the Break.

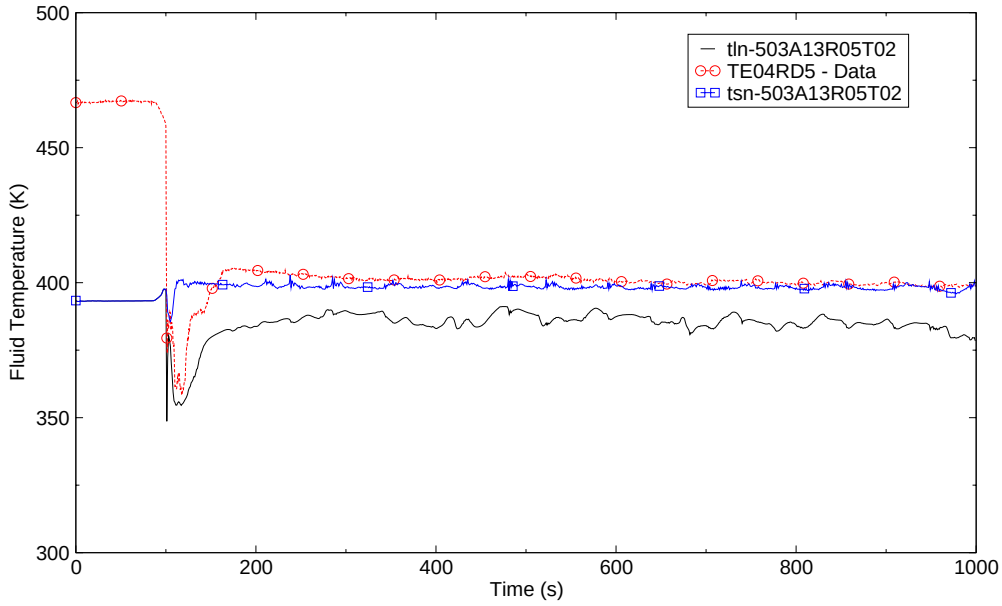

Figure C.2-13. Downcomer Fluid Temperature Comparison at 5.303 meters - Run 62.

After 200 seconds, the predicted upper plenum pressure response matched the data quite well. The low frequency oscillations in the predicted pressure response appear to be related to the build up of liquid in the hot legs as shown in Figure C.2-5.

C.2.5.1.3. Differential Pressure Comparison

Figure C.2-14 through Figure C.2-18 show the differential pressures in Loop 1 (intact loop) between the upper plenum and the SG inlet, across the SG, across the pump orifice, from the upper plenum to the pump discharge and from the upper plenum to the cold leg nozzle. Generally, the predicted loop differential pressure agrees well with the measured data. The predicted liquid buildup in the hot legs is evident in Figure C.2-14. The differential pressures in the other intact loops are similar.

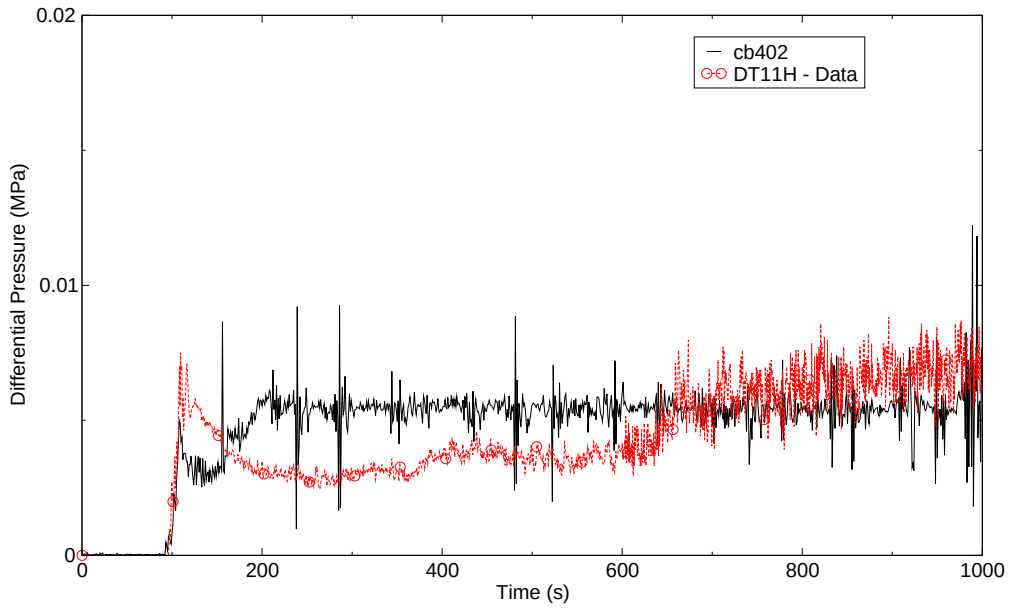

Figure C.2-14. Loop 1 Upper Plenum to SG Inlet Plenum Differential Pressure Comparison - Run 62.

Figure C.2-19 and Figure C.2-20 show the comparison of the differential pressure from the upper plenum to containment tank 1 and containment tank 2, respectively. Between 120 and 200 seconds, the differential pressure is under-predicted because the upper plenum pressure during this time was under-predicted due to a smaller steaming rate in the core region and perhaps droplet evaporation in the steam generator tubes. After 200 seconds, the differential pressure response looks reasonable. The water build up in the loop 4 hot leg is implied by the low frequency oscillations observed in the calculated differential pressure.

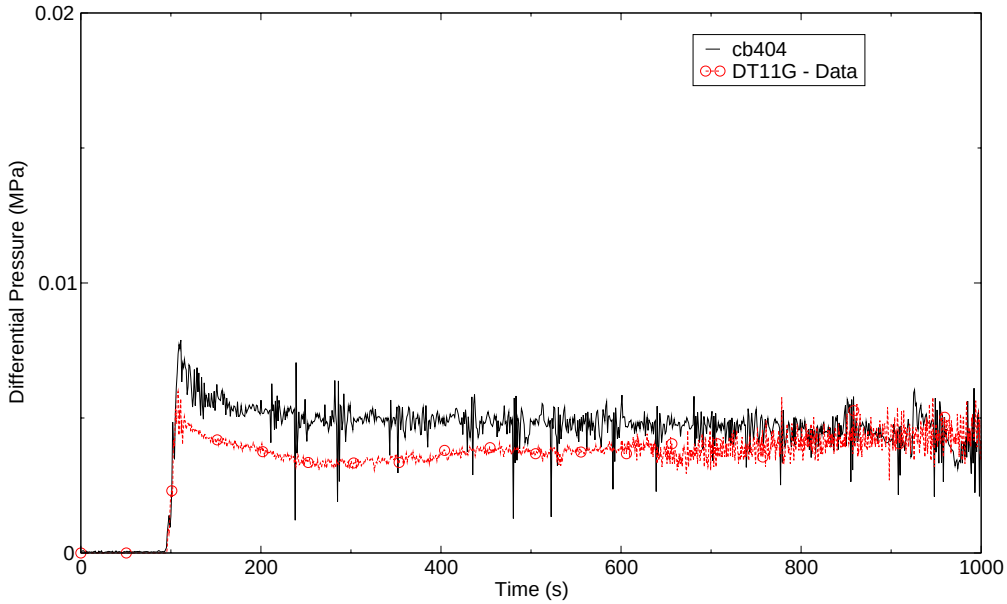

Figure C.2-15. Loop 1 SG Inlet to Outlet Differential Pressure Comparison - Run62.

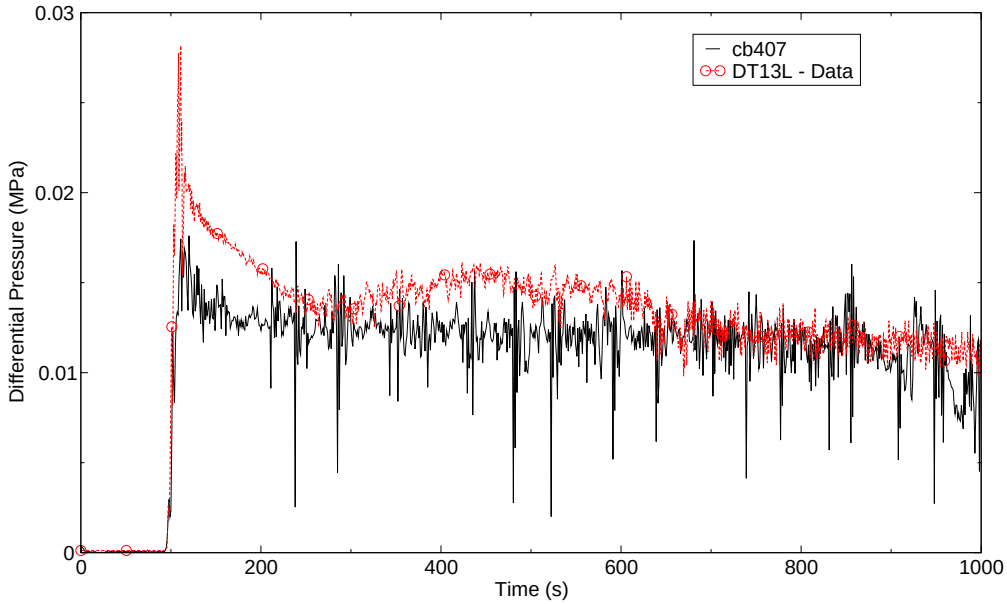

Figure C.2-16. Loop 1 Pump Orifice Differential Pressure Comparison - Run 62.

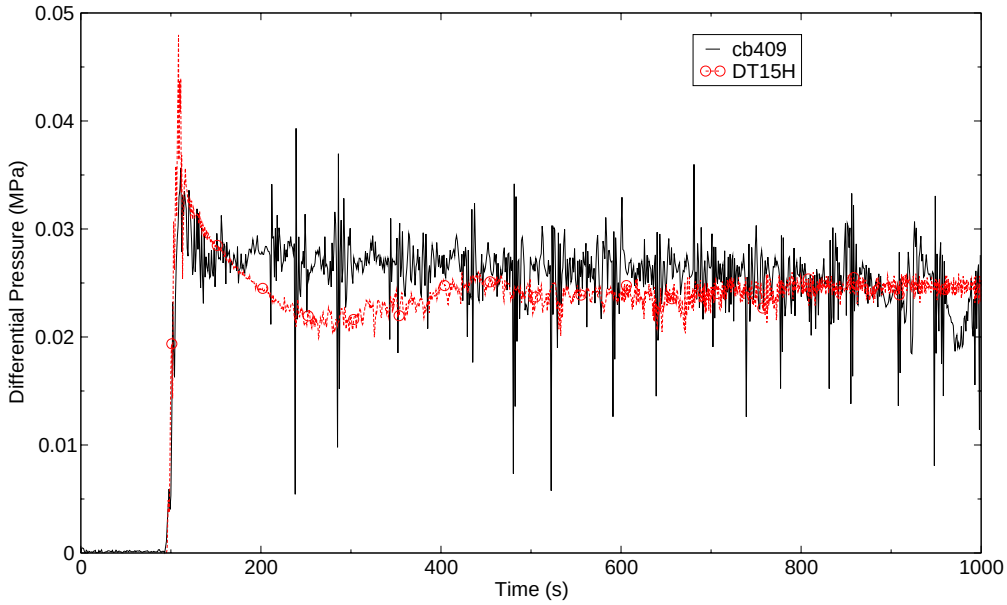

Figure C.2-17. Loop 1 Upper Plenum to Pump Discharge Differential Pressure Comparison - Run 62.

The predicted vessel downcomer differential pressure is compared to data in Figure C.2-21. The predicted differential pressure compares reasonably well with the data. After the accumulator injection ended, the rapid filling of the lower plenum and the downcomer stopped and the core reflooding stabilized. As the rods in the lower part of the core cooled and quenched the core level slowly rose. The downcomer level decreased slightly as implied by the decrease in the downcomer differential pressure (Figure C.2-21). The code did not predict the slight decline in the downcomer level. From about 400 seconds to the end of the transient, the calculation matched the data quite well.

Most of the 12.2 kg/s total intact loop flow (LPI plus steam flow) exited the system through the broken cold leg nozzle into the containment (Ref. 2). Mass balance calculations indicated only about 4.5 kg/s (1/3) of this mass flowed into the downcomer and into the core. Figure C.2-22 shows the difference between the total intact loop mass flow rate and the flow rate out the break (Containment 1), or the mass flow rate down the downcomer and into the core, predicted by the code. The calculated average is 4.4 kg/s. Thus the mass flow rate predicted through the downcomer and core agrees well with the experimental calculations. Based on the intact loop flow rate comparisons (see Figure C.2-6) this implies the predicted break flow rate, from the vessel side of the break, agrees with the experimental value.

Figure C.2-23 compares the predicted lower plenum differential pressure with data. The prediction shows excellent agreement with the data.

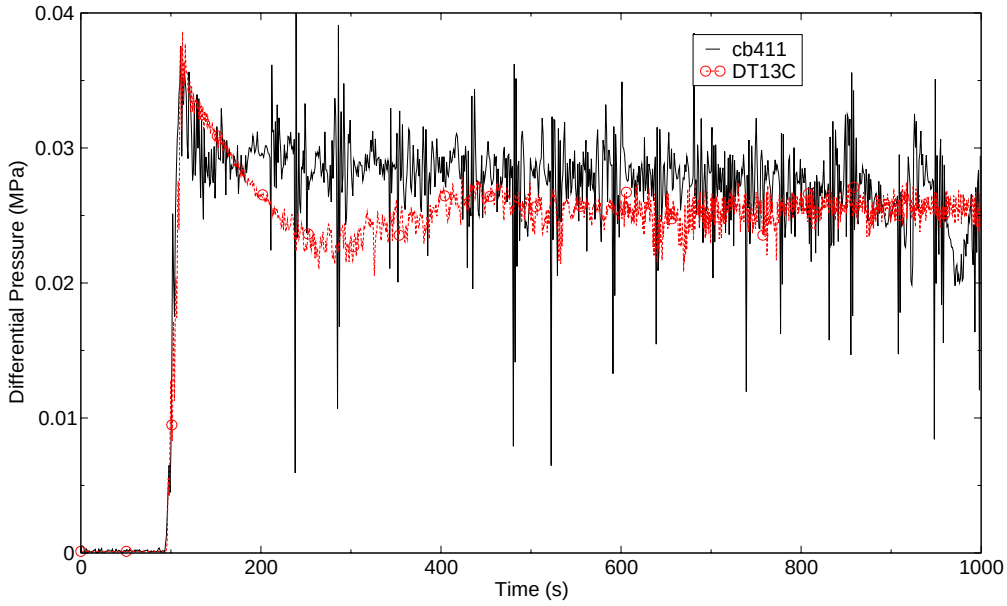

Figure C.2-18. Loop 1 Upper Plenum to Cold Leg Nozzle Differential Pressure Comparison - Run62.

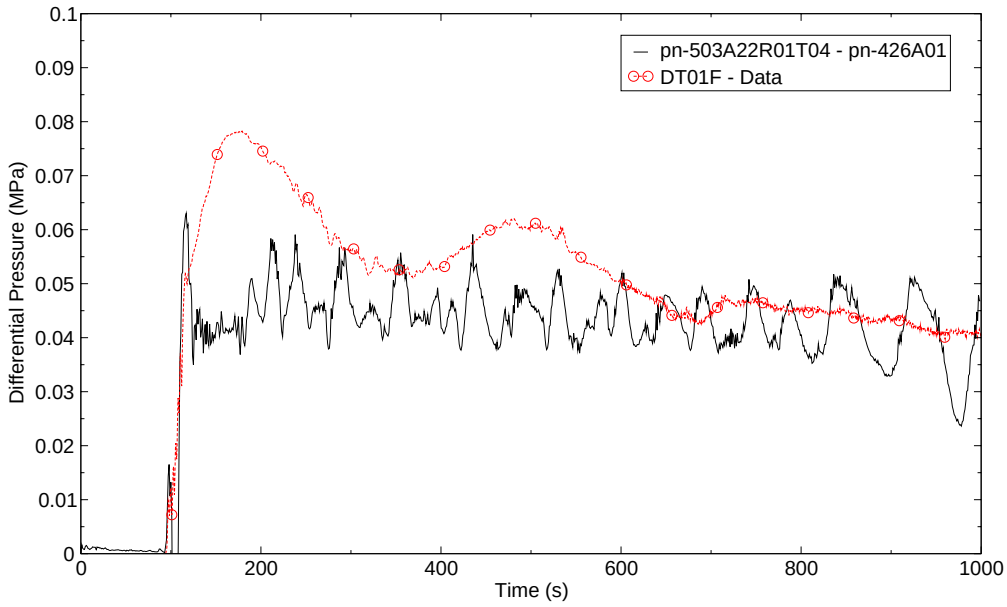

Figure C.2-19. Loop 4 Upper Plenum to Containment Tank 1 Differential Pressure Comparison - Run 62.

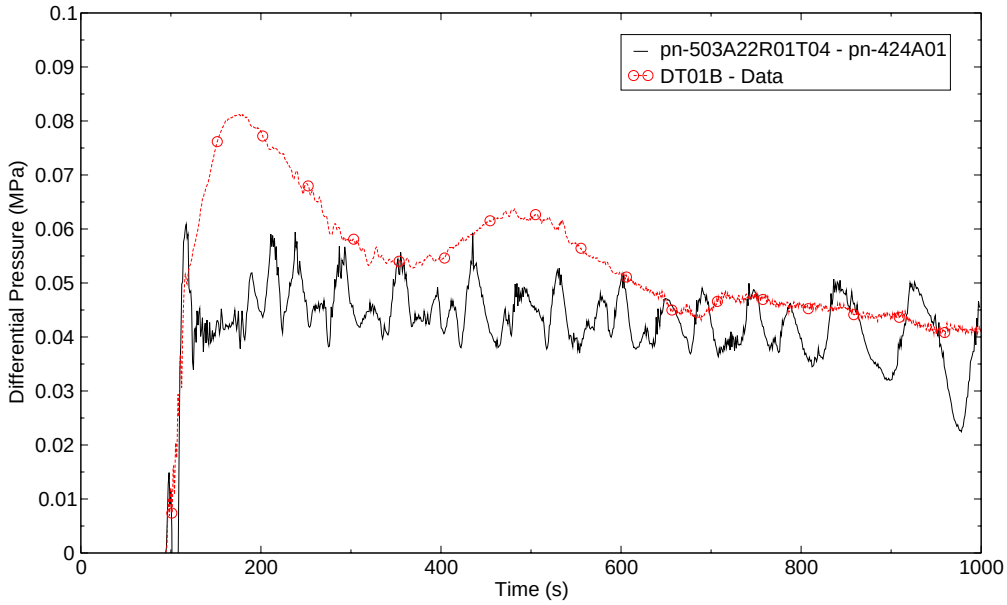

Figure C.2-20. Loop 4 Upper Plenum to Containment Tank 2 Differential Pressure Comparison - Run 62.

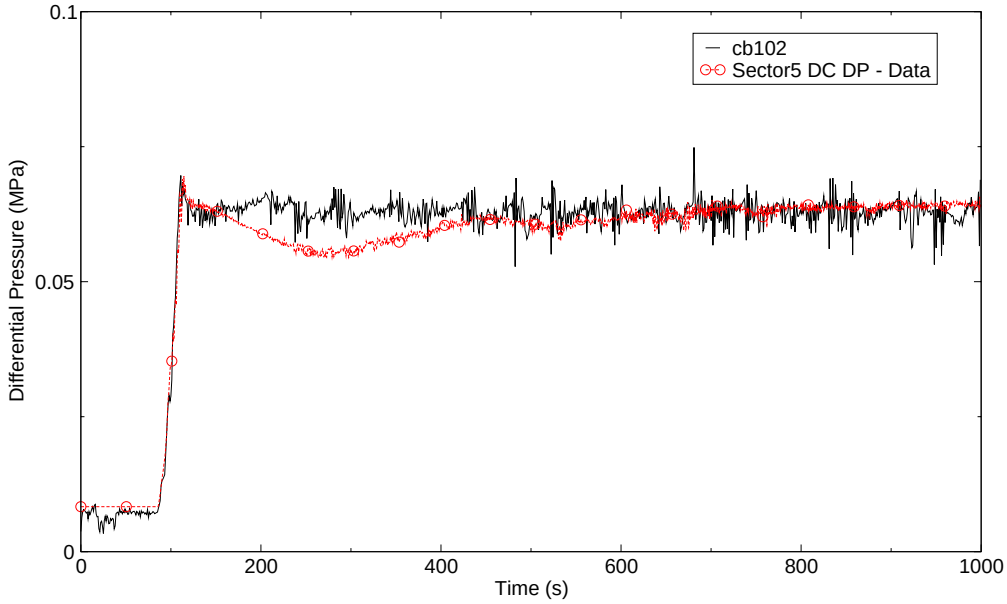

Figure C.2-21. Vessel Downcomer Differential Pressure Comparison - Run 62.

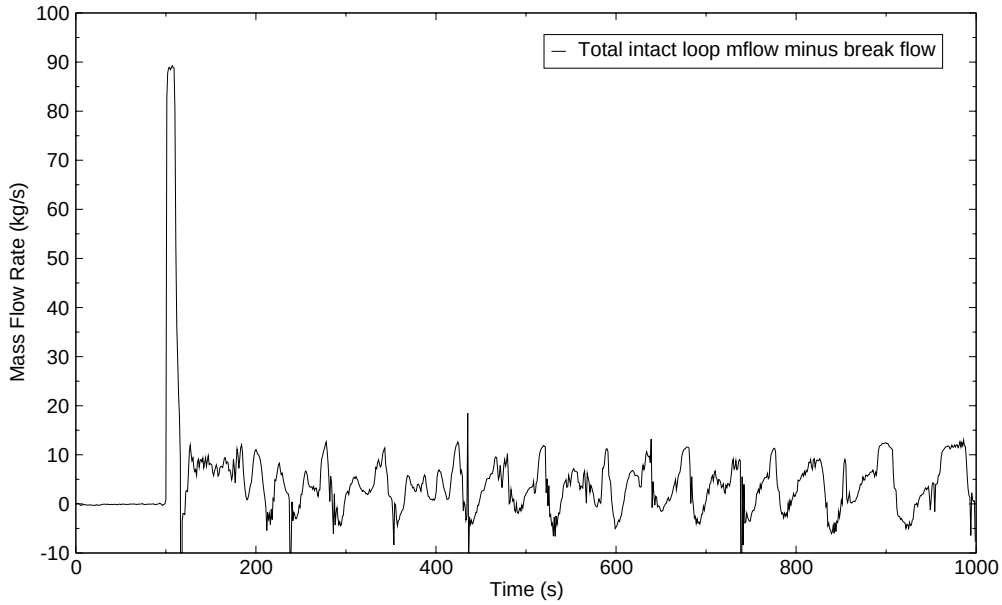

Figure C.2-22. Predicted Downcomer Mass Flow Rate Based on Total Intact Loop Mass Flow and Break Mass Flow - Run 62.

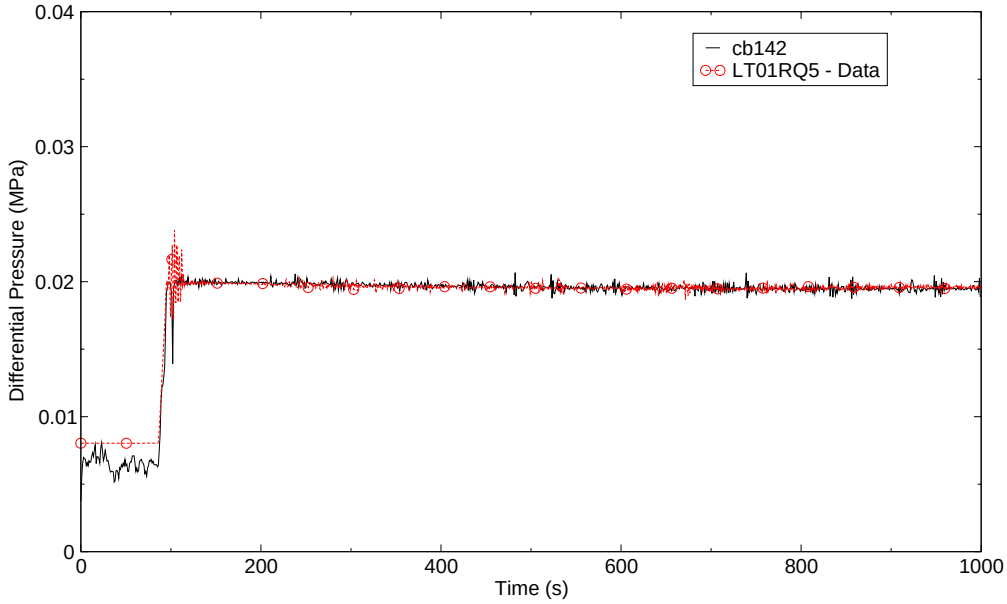

Figure C.2-23. Lower Plenum Differential Pressure Comparison - Run 62.

The predicted core overall differential pressure compared to data is shown in Figure C.2-24. The predicted differential pressure shows excellent agreement with the data. The calculation predicts the lower half of the core fills at a rate consistent with the experiment as shown in Figure C.2-25 through Figure C.2-28. However, in the upper half of the core the amount of liquid present is slightly under-predicted as implied by the differential pressure comparisons shown in Figure C.2-29 and Figure C.2-30. The code is over-predicting the entrainment rate. This is evident in the upper plenum differential pressure comparison shown in Figure C.2-31. The code predicts more liquid in the upper plenum early in time, however, once the liquid gets in the upper plenum it stays fairly constant. As the rods cool and quench in the upper core region, steaming declines and the core liquid level rises at a slightly faster rate in both the experiment (600 seconds) and the prediction (850 seconds) as indicated in the upper core differential pressure comparison shown in Figure C.2-30. Another indication of the code's of over-prediction of the liquid entrainment in the core is the liquid build up in the hot legs as shown in Figure C.2-14 and Figure C.2-5. The lack of liquid in the upper core results in an over-prediction of the peak cladding temperature and delayed rod quench time in that region.

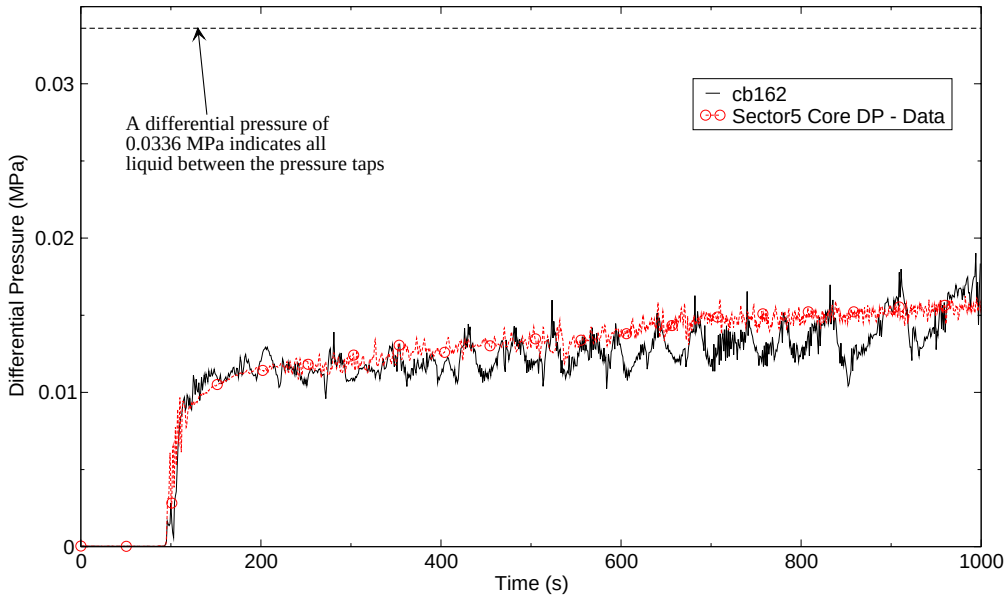

Figure C.2-24. Core Overall Differential Pressure Comparison - Run 62.

C.2.5.1.4. Rod Cladding Temperature Comparison

The core is divided into three power regions radially; a high power region which encompasses the four center bundles, a medium power region that includes the middle ring of rod bundles, and a low power region that includes the outer ring of rod bundles (see Figure C.2-2). Rod clad temperatures along the axial direction as well as the radial direction are compared to data. The

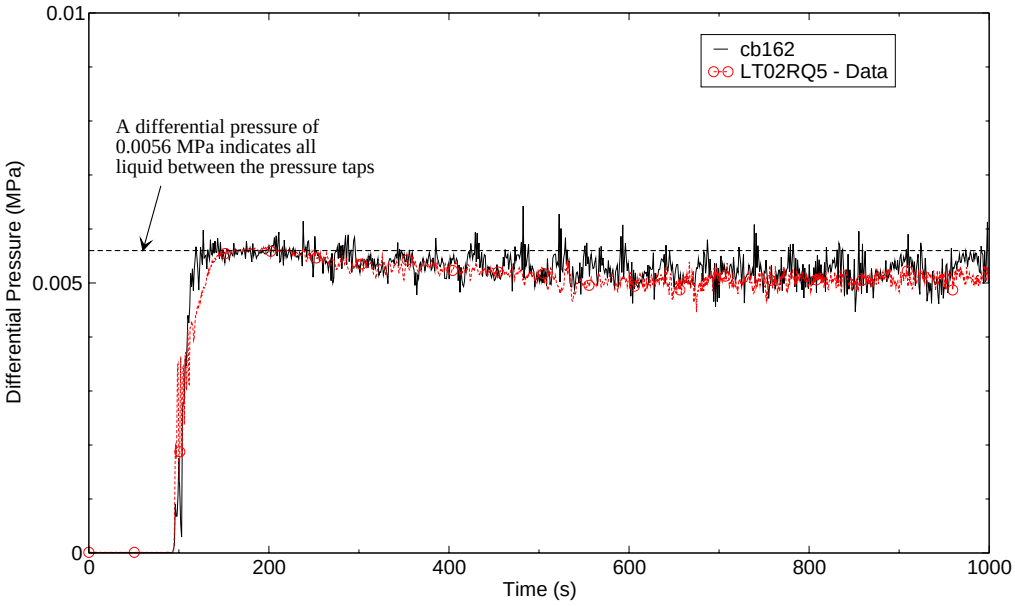

Figure C.2-25. Core Differential Pressure Comparison between 0.0 and 0.61 Meters from the bottom of the Heated Rods - Run 62.

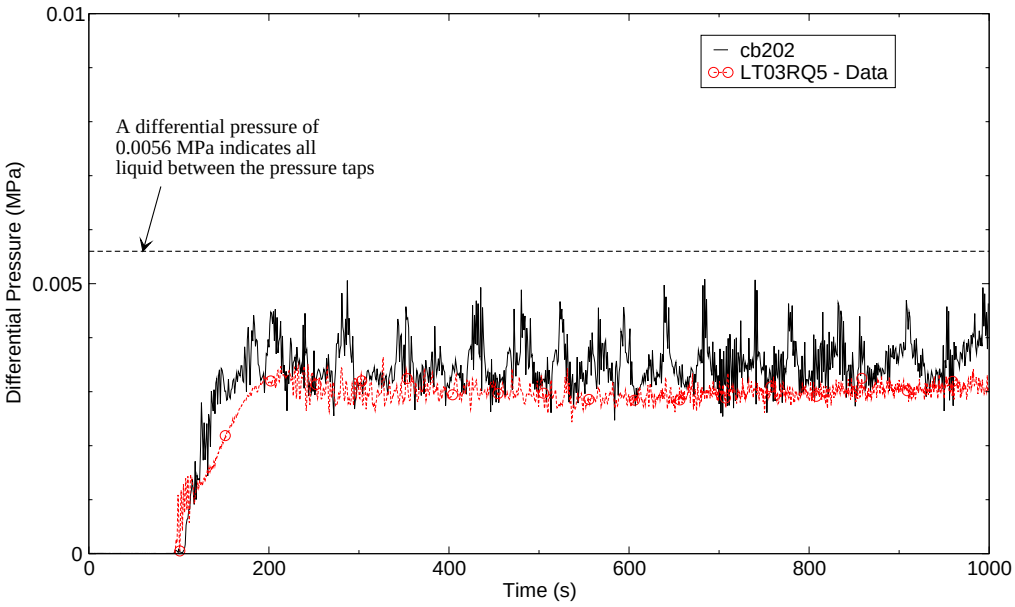

Figure C.2-26. Core Differential Pressure Comparison between 0.61 and 1.22 Meters from the bottom of the Heated Rods - Run 62.

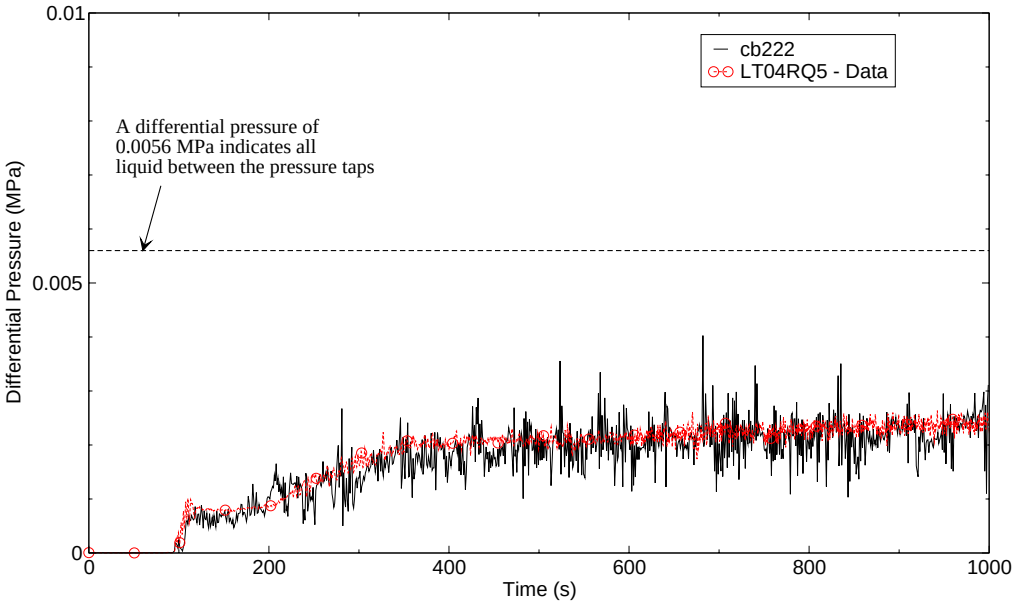

Figure C.2-27. Core Differential Pressure Comparison between 1.22 and 1.83 Meters from the bottom of the Heated Rods - Run 62.

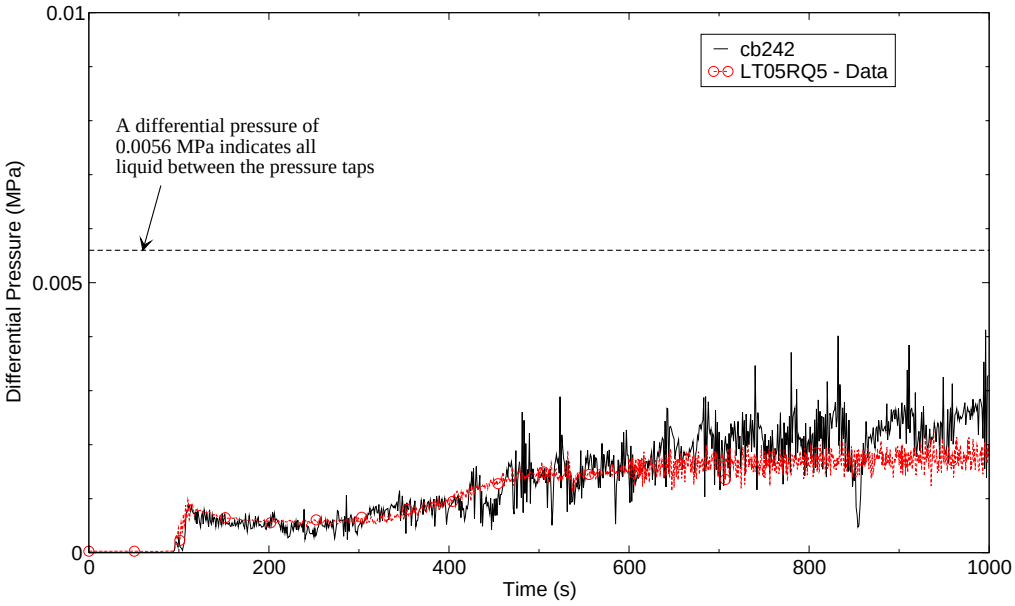

Figure C.2-28. Core Differential Pressure Comparison between 1.83 and 2.44 Meters from the bottom of the Heated Rods - Run 62.

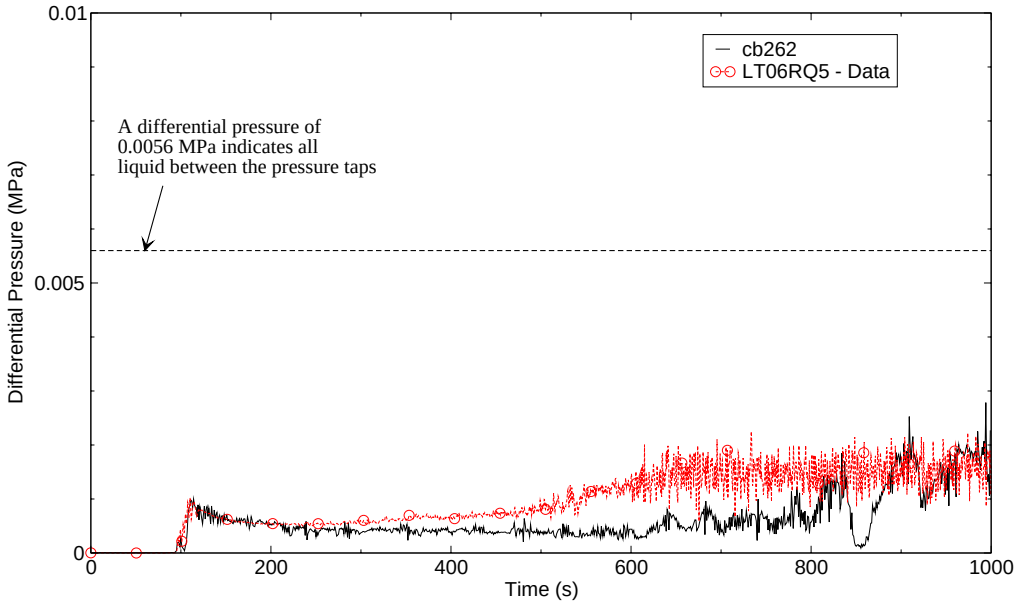

Figure C.2-29. Core Differential Pressure Comparison between 2.44 and 3.05 Meters from the bottom of the Heated Rods - Run 62.

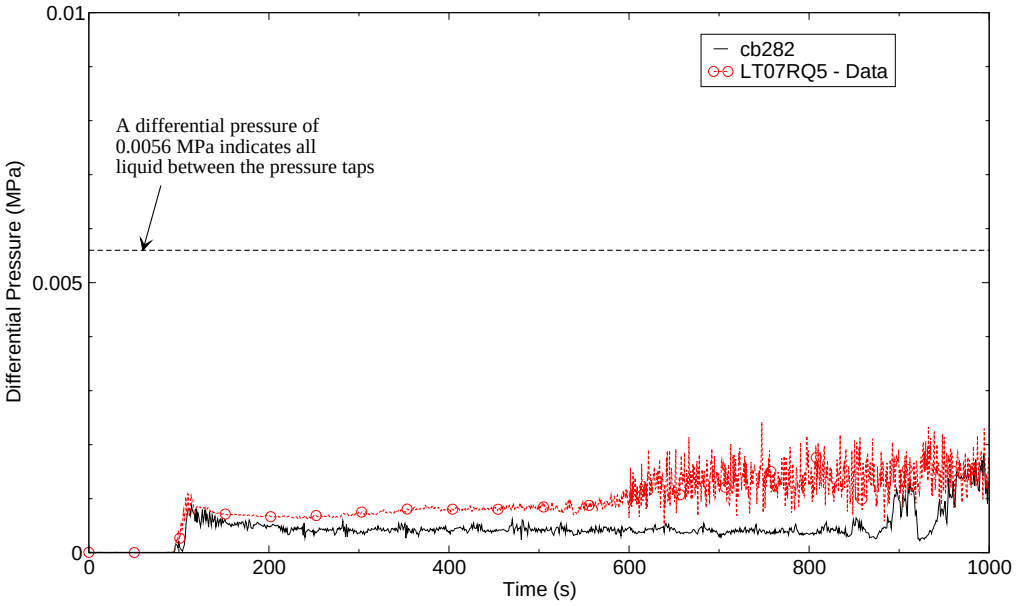

Figure C.2-30. Core Differential Pressure Comparison between 3.05 and 3.66 Meters from the bottom of the Heated Rods - Run 62.

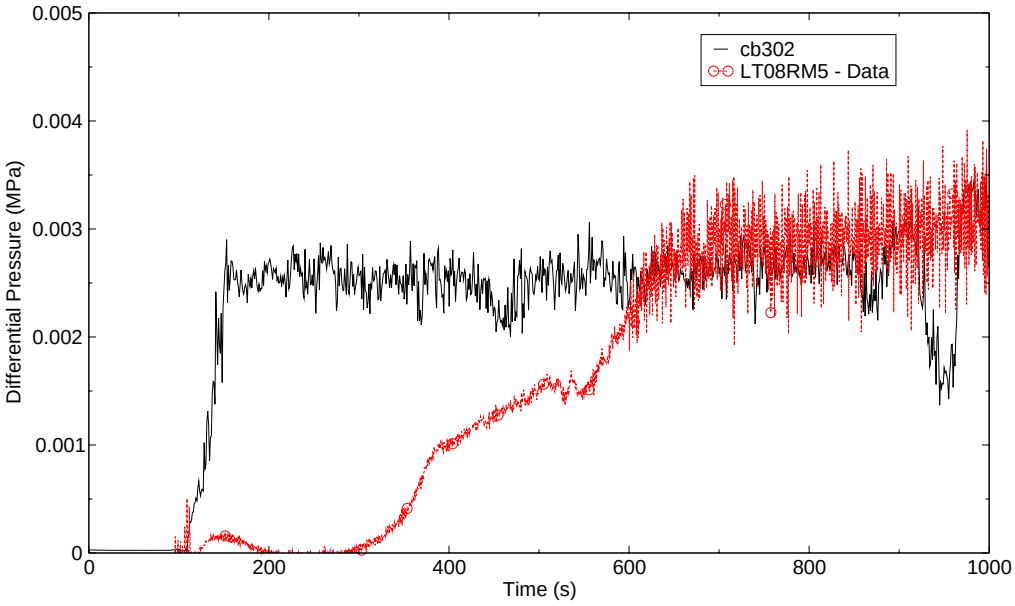

Figure C.2-31. Upper Plenum Differential Pressure Comparison - Run 62.

comparisons presented are divided into three parts: rod temperatures below the mid-plane, rod temperatures at the mid-plane, and rod temperatures above the mid-plane.

Figure C.2-32 through Figure C.2-34 show the predicted rod clad temperatures compared to data at 1.015 meters above the bottom of the heated rods for the high, medium, and low powered regions, respectively. The calculated rod clad temperature compares well, especially in the high powered region. The predicted rod temperature peaked higher than the data in all three power regions. The predicted rod temperature turn over time is about right. The clad temperature declines at about the same rate shown in the data while the rods are transitioning from film boiling to nucleate boiling. At the time of quench, the prediction displays the sharp rapid temperature decrease exhibited in the data. In all three power zones the predicted time of rod quench is earlier because of the cooler core inlet fluid temperature (see Figure C.2-9 and Figure C.2-10). Since the rods are cooler in the low power region more liquid is present in that region and the rods quench earlier as evident in both the experiment and the prediction (see Figure C.2-34).

Rod temperature comparisons at the mid-plane for the three power zones are shown in Figure C.2-35 through Figure C.2-37. Rod heat up, peak clad temperature and the time of temperature turn over are simulated by the code reasonably well. The calculation shows the rods in the outer bundle ring cooling earlier than the data. From the differential pressure comparisons it appears there is about the same amount of coolant predicted in the calculation as in the data. Therefore, it is expected the predicted rod clad temperature should behave similar to the experiment. However, an examination of the void fraction in the outer core ring in the calculation showed more liquid present than in the two inner core rings, thus an earlier quench. The transition from film boiling to

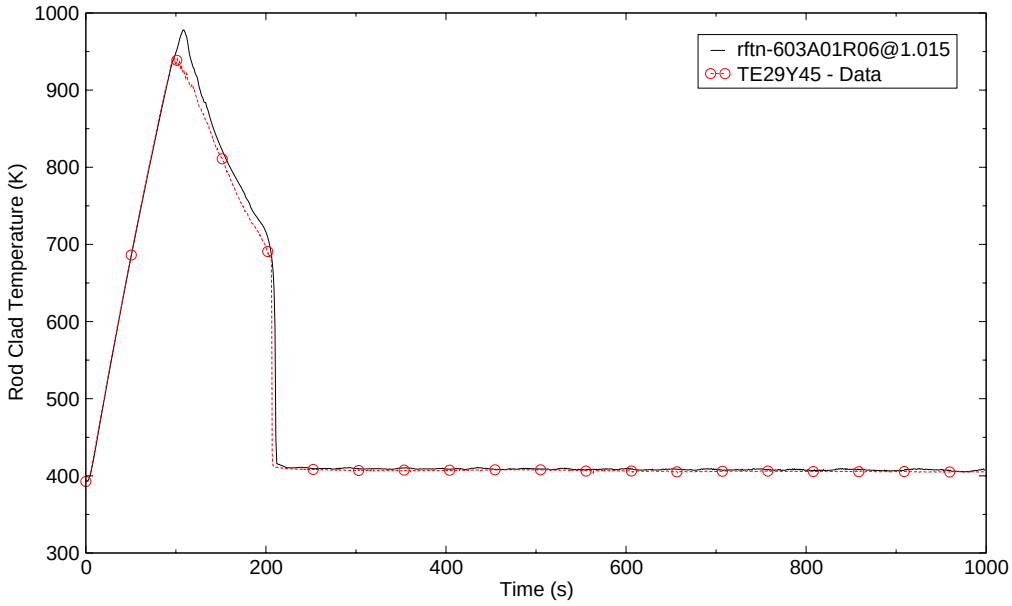

Figure C.2-32. Rod Clad Temperature Comparison at 1.015 Meters above the Bottom of the Heated Rods in the High Powered Region - Run 62.

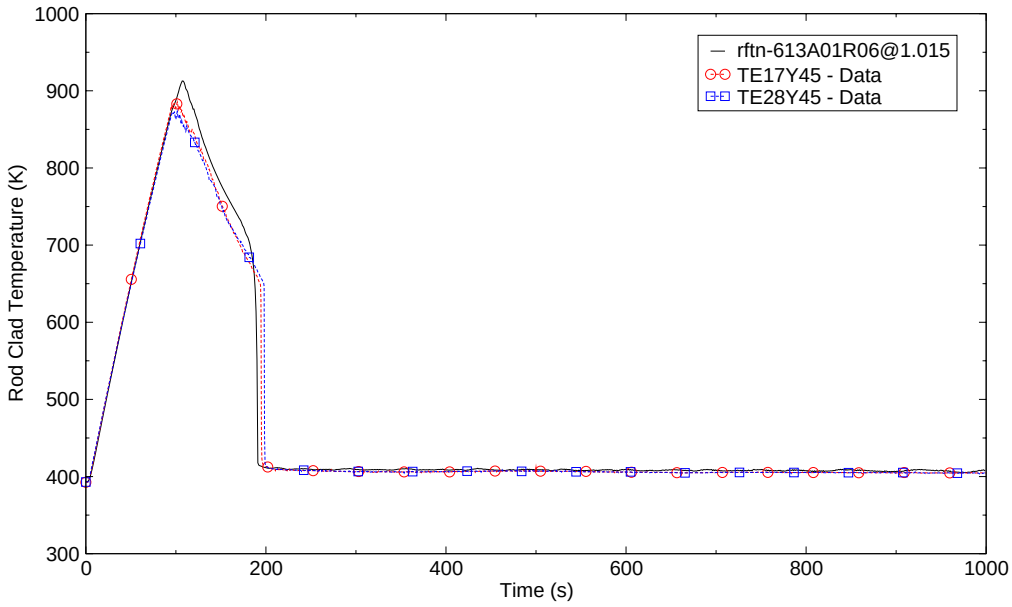

Figure C.2-33. Rod Clad Temperature Comparison at 1.015 Meters above the Bottom of the Heated Rods in the Medium Powered Region - Run 62.

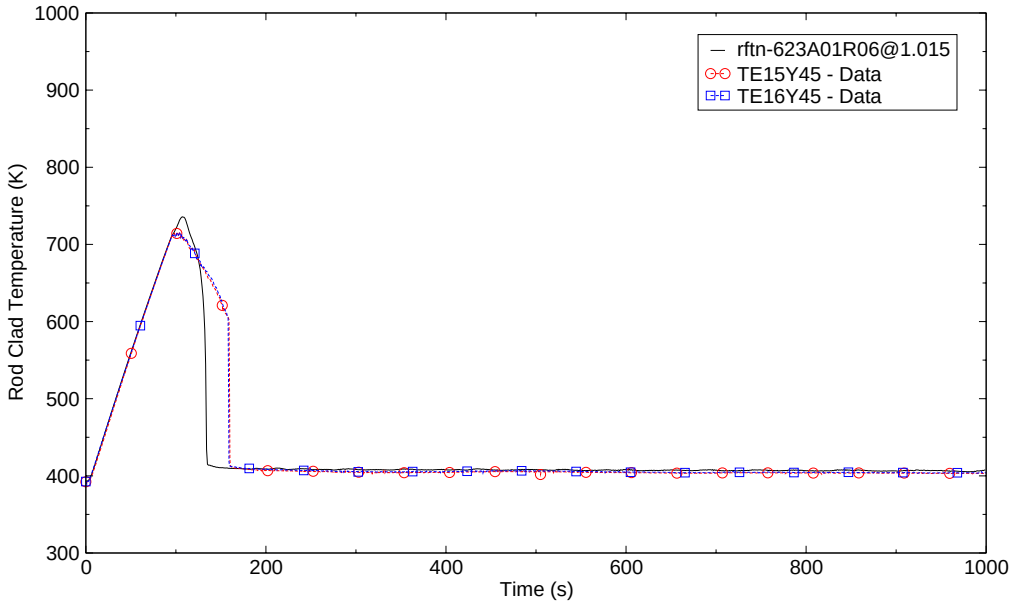

Figure C.2-34. Rod Clad Temperature Comparison at 1.015 Meters above the Bottom of the Heated Rods in the Low Powered Region - Run 62.

nucleate boiling in the middle core ring seems reasonable in the calculation, although it takes a little longer to bring the temperature down to the quench temperature. Similar behavior is observed in the high power region although the transition is not quite as good. Apparently TRACE is predicting a lower heat transfer coefficient (HTC). At the time of rod quench, the calculation displays the same sharp temperature decline as exhibited in the data.

Figure C.2-38 through Figure C.2-40 show the rod clad temperature comparison in the high, medium and low power regions at the 3.05 meter elevation. As expected the initial rod heat up before ECC injection shows excellent agreement. However, after the initiation of ECC injection, the predicted rod clad temperature rose at a higher rate than the data. The peak clad temperature was over-predicted and the time to quench was prolonged. In the calculation the upper one-third of the core, after the initiation of ECC injection into the system, is highly voided as shown in Figure C.2-41. The vapor temperature is nearly that of the rod surface temperature while the liquid temperature is at saturation as shown in Figure C.2-42. The calculated liquid and vapor velocities in the upper core, shown in Figure C.2-43, are on the order of 2.5 and 13 m/s, respectively. Two things are noted. First, it appears interfacial drag is under-predicted. For small droplet sizes (2 mm or less) liquid and vapor velocities should be closer together. Second, it appears the interfacial heat transfer is under-calculated. With hot vapor and rod surface temperatures, the small amount of saturated liquid should vaporize. The interfacial heat transfer is a function of the liquid droplet size which is a function of the Weber number. Possibly the calculated droplet size is too large and thus the interfacial area is too small. If the liquid were

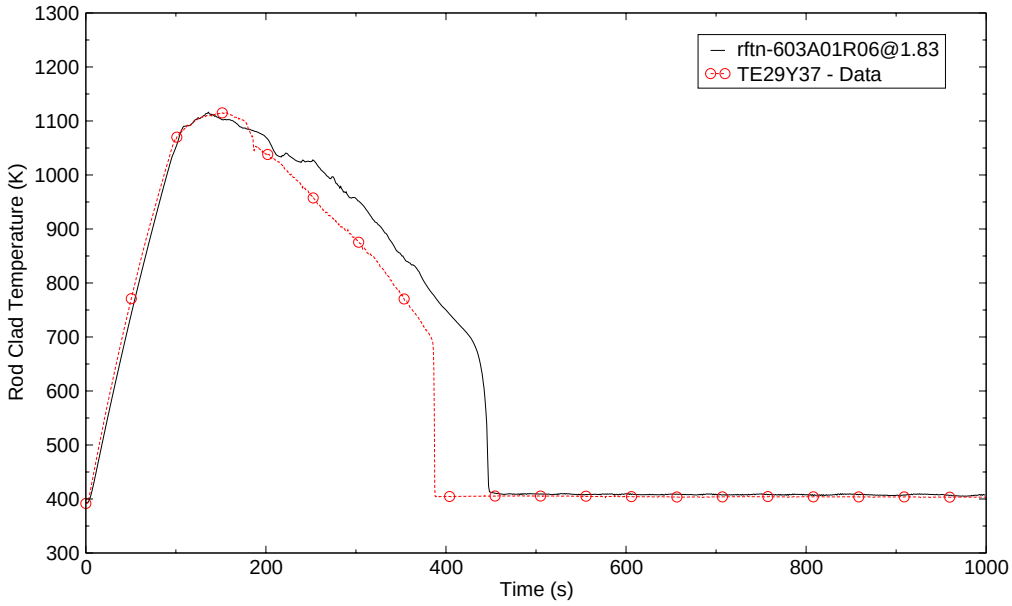

Figure C.2-35. Rod Clad Temperature Comparison at 1.83 Meters above the Bottom of the Heated Rods in the High Powered Region - Run 62.

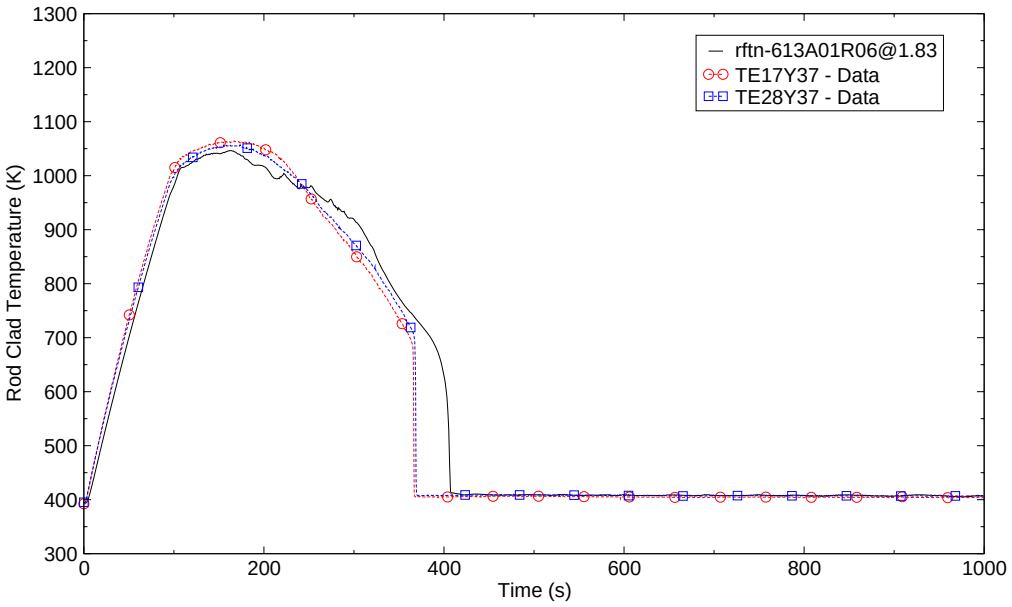

Figure C.2-36. Rod Clad Temperature Comparison at 1.83 Meters above the Bottom of the Heated Rods in the Medium Powered Region - Run 62.

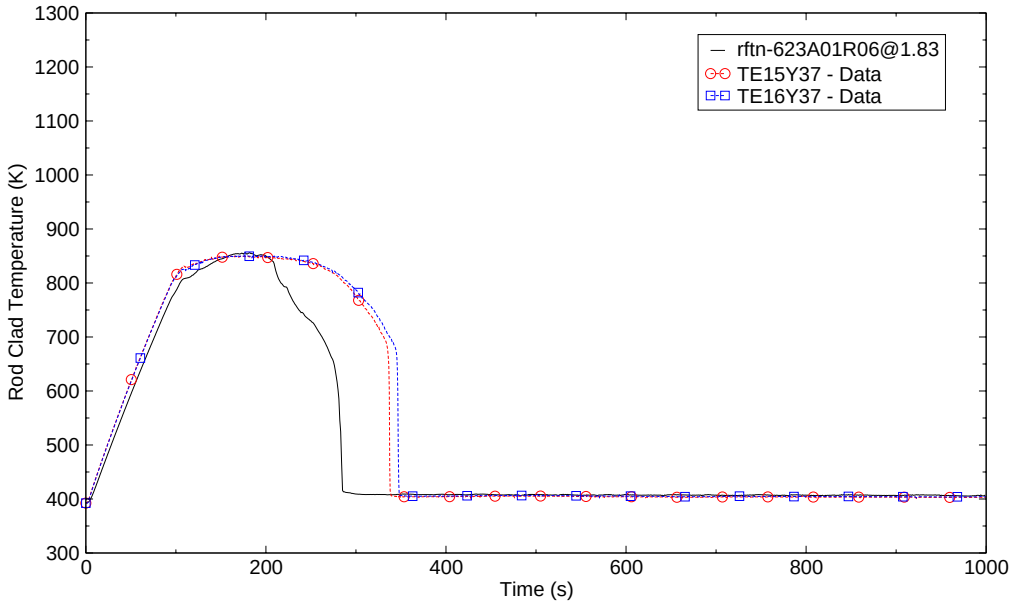

Figure C.2-37. Rod Clad Temperature Comparison at 1.83 Meters above the Bottom of the Heated Rods in the Low Powered Region - Run 62.

calculated to vaporize, the vapor temperature would be lower due to the energy expended in vaporizing the liquid. This in turn would lead to a lower calculated rod temperature.

C.2.5.1.5. Rod Quench Comparison

A comparison of the rod quench time versus elevation in the core for the high, medium, and low power regions are shown in Figure C.2-44 through Figure C.2-46. The predicted rod quench time matches the data reasonably well in all three power zones for elevations below the mid-plane. Above the mid-plane the predicted quench time is much longer. Although there may be sufficient coolant above the mid-plane to quench the rods, it passes through without vaporizing which would lead to a lower vapor temperature and consequently colder rods. The data shows that near the core outlet (elevation 3.56 meters) the rods cool early due to some top down quenching not predicted by the code.

C.2.5.1.6. Peak Clad Temperature Comparison

Measured versus calculated peak clad temperature (PCT) for each radial power zone[1] and each modeled azimuthal sector is shown in Figure C.2-47. Also shown is the 45^{o} line that represents a

1. PCTs occur near the mid-plane in the test and 15 to 20 cm downstream of the mid-plane in the calculation.

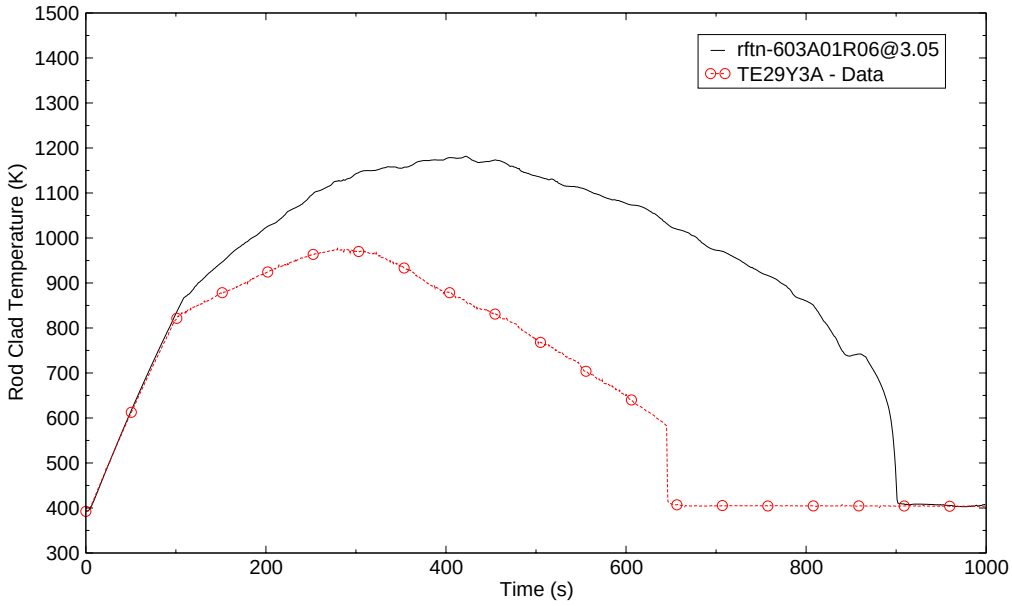

Figure C.2-38. Rod Clad Temperature Comparison at 3.05 Meters above the Bottom of the Heated Rods in the High Powered Region - Run 62.

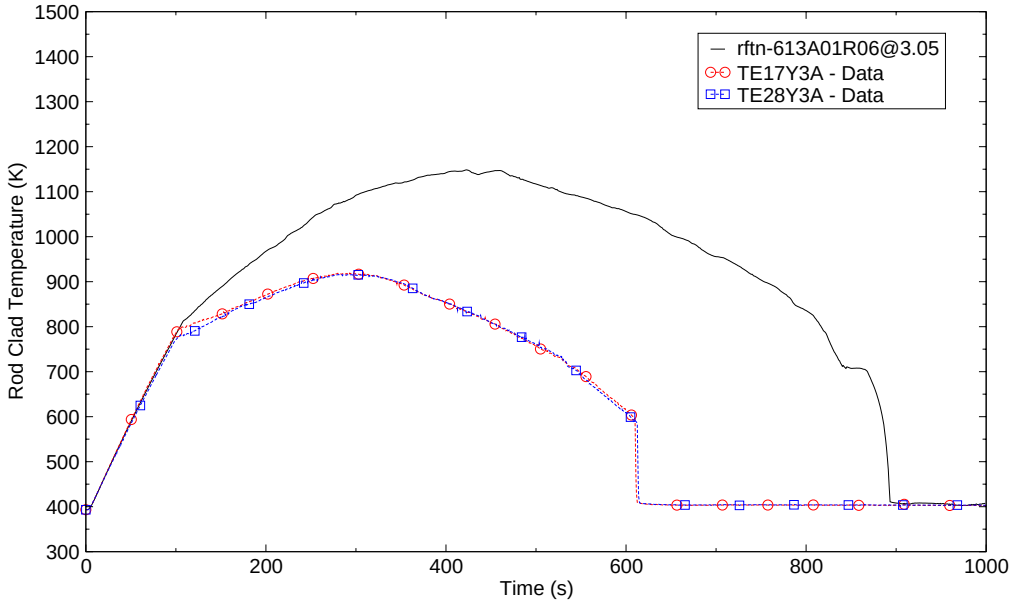

Figure C.2-39. Rod Clad Temperature Comparison at 3.05 Meters above the Bottom of the Heated Rods in the Medium Powered Region - Run 62.

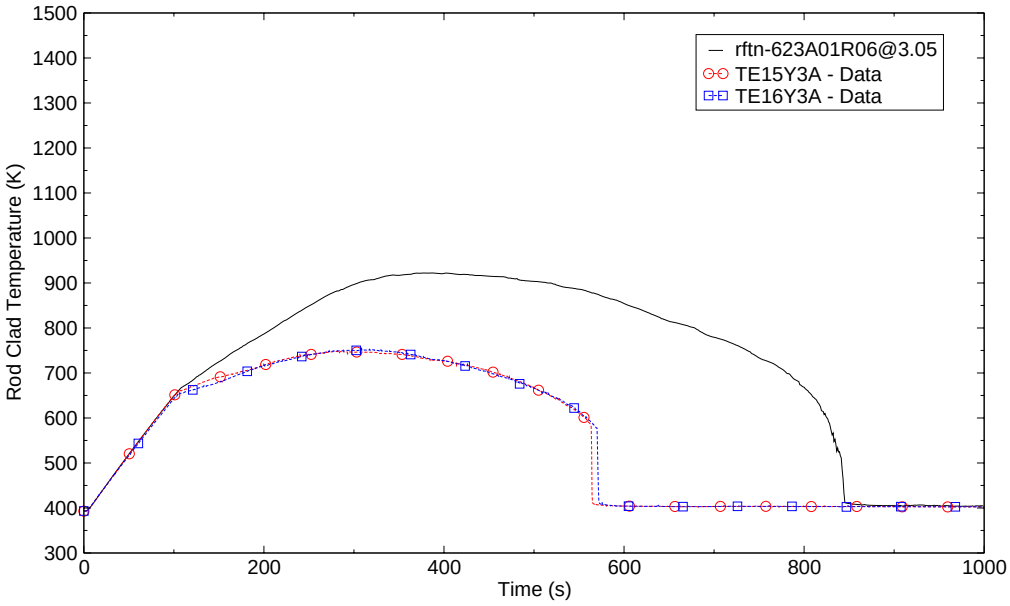

Figure C.2-40. Rod Clad Temperature Comparison at 3.05 Meters above the Bottom of the Heated Rods in the Low Powered Region - Run 62.

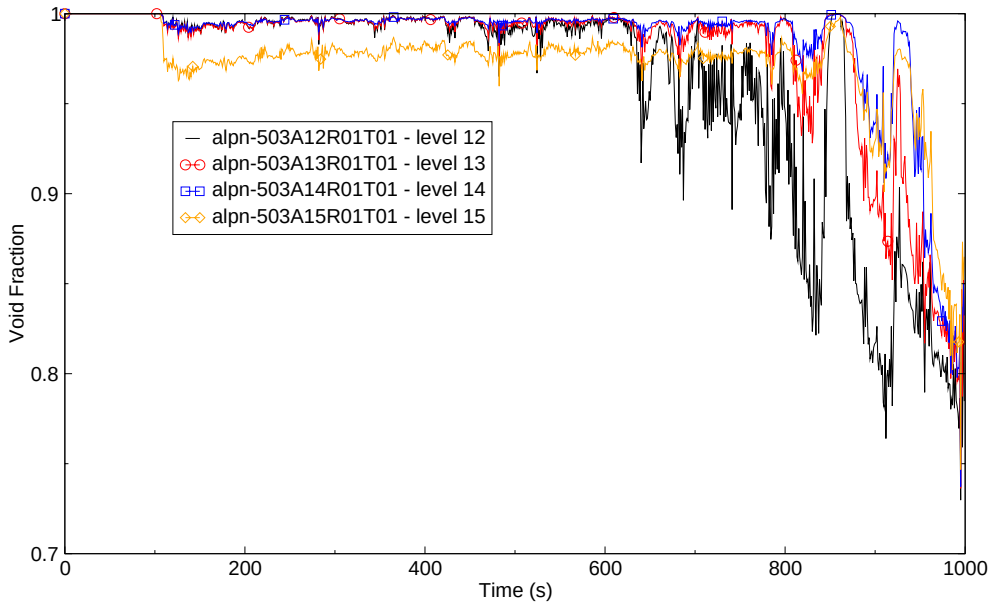

Figure C.2-41. Predicted Void Fraction in the Upper One-Third of the Core - Run 62.

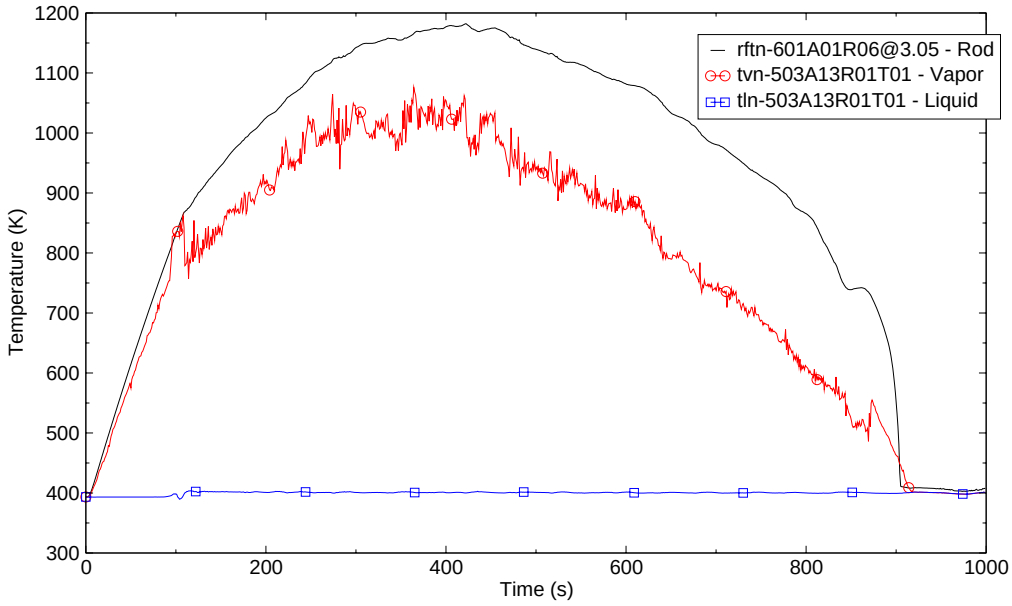

Figure C.2-42. Predicted Rod Surface, Vapor, and Liquid Temperatures in Cell 1, Vessel Level 13 - Run 62.

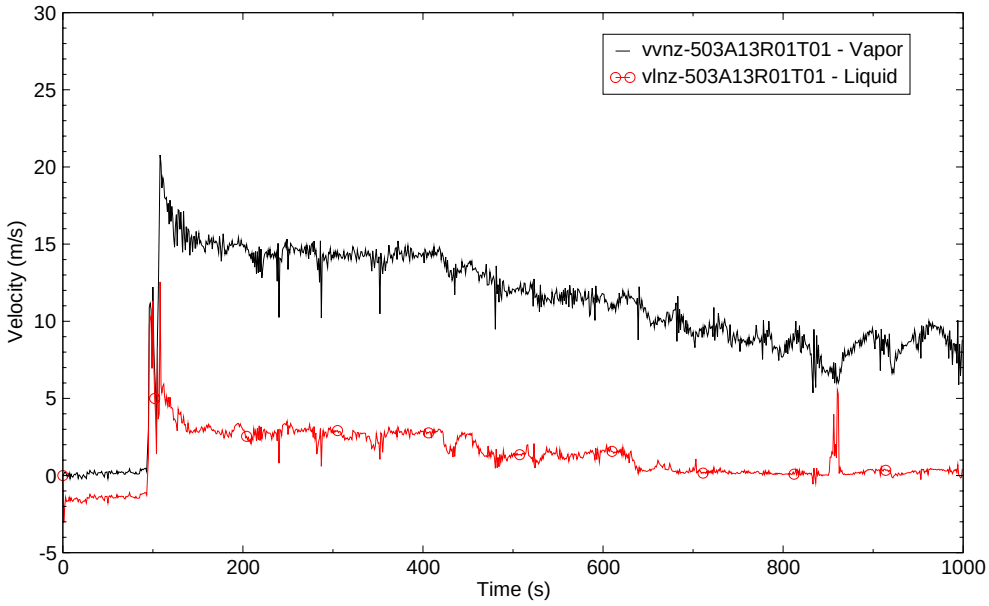

Figure C.2-43. Predicted Liquid and Vapor Velocities in Cell 1 of Vessel Level 13 - Run 62.

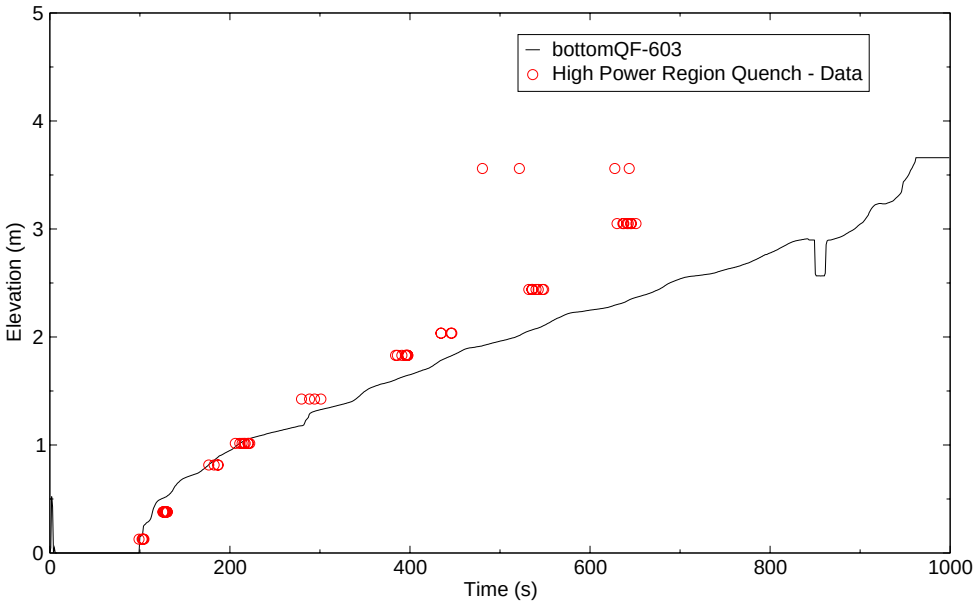

Figure C.2-44. Rod Quench Time Profile Comparison in the High Power Region - Run 62.

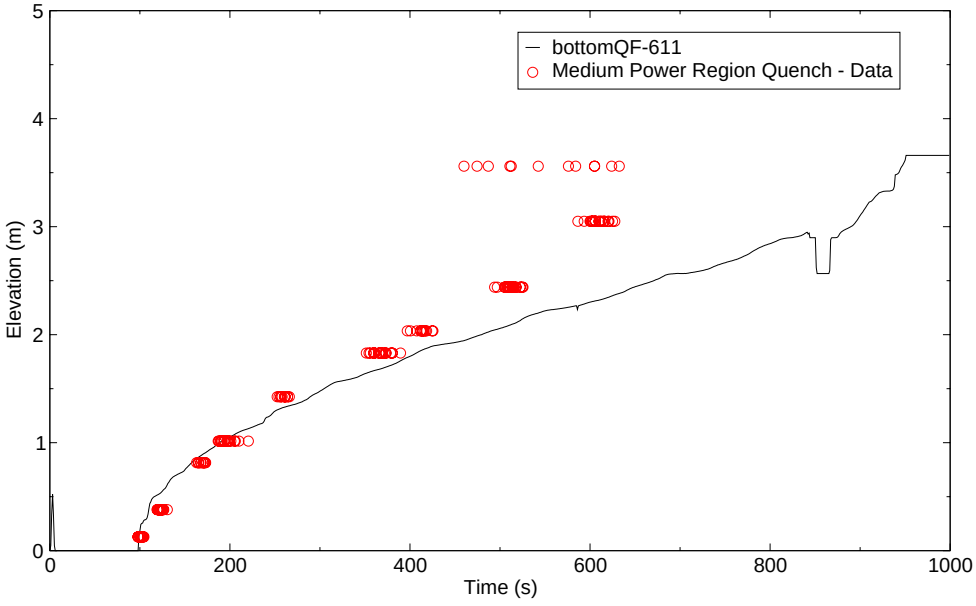

Figure C.2-45. Rod Quench Time Profile Comparison in the Medium Power Region - Run 62.

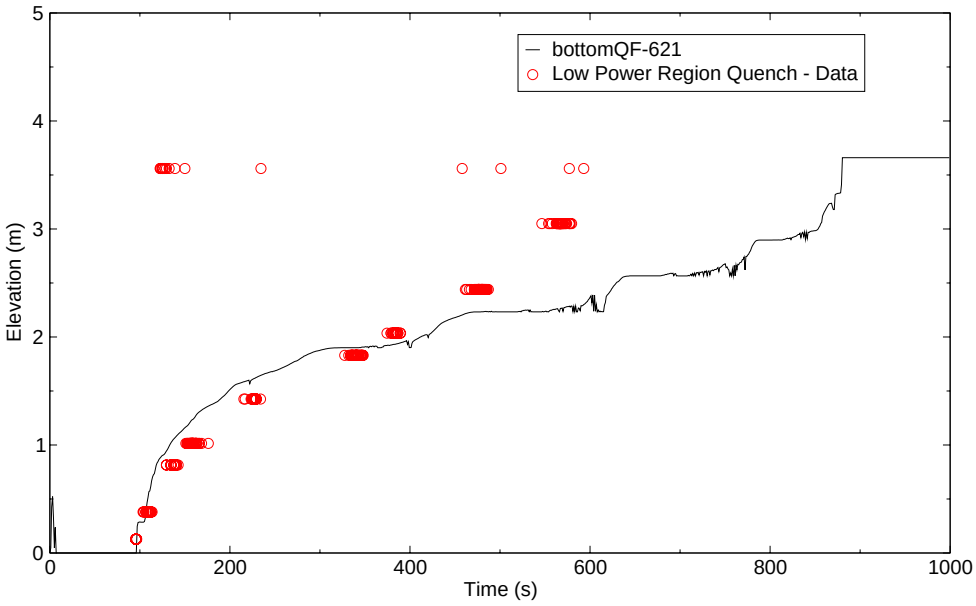

Figure C.2-46. Rod Quench Time Profile Comparison in the Low Power Region - Run 62.

perfect match of the measured and calculated PCT. The calculation over-predicts the PCT in all three radial power zones. The predicted PCT in the low power region comes closer to matching the measured data than it does in the other two power zones. A lack of sufficient cooling in the upper half of the core resulted in higher predicted PCTs.

C.2.5.2. Core Power Effects - Simulation of Run 62 and Run 63.

The purpose of Run 63 was to investigate the effect of decay power level on reflood thermal-hydrodynamic behaviors. The initial total power supplied to the core for this test was set at 7.1 MW, whereas the power for the base test (Run 62) was set at 9.4 MW. The other thermal-hydraulic conditions were nearly the same for the two tests (see Table C.2.1).

The primary hydraulic effect of lower core power is reduced steam generation and flow rate. Figure C.2-48 compares the predicted core outlet steam flow rate for Runs 62 and 63 (The time for bottom of core recovery (BOREC) was different for the two tests, 94 s for Run 62 and 126 for Run 63, therefore the time scale was adjusted so BOREC is at time zero in the figures). As shown the steam flow out of the core is slightly higher for Run 62 (higher power) than for Run 63. After about 600 seconds most of the heater rods had quenched in the simulation of Run 63 and steam production decreased.

Comparison of measured and predicted core differential pressures for Runs 62 and 63 are shown in Figure C.2-49. The data shows a higher core differential pressure (core liquid level) for the

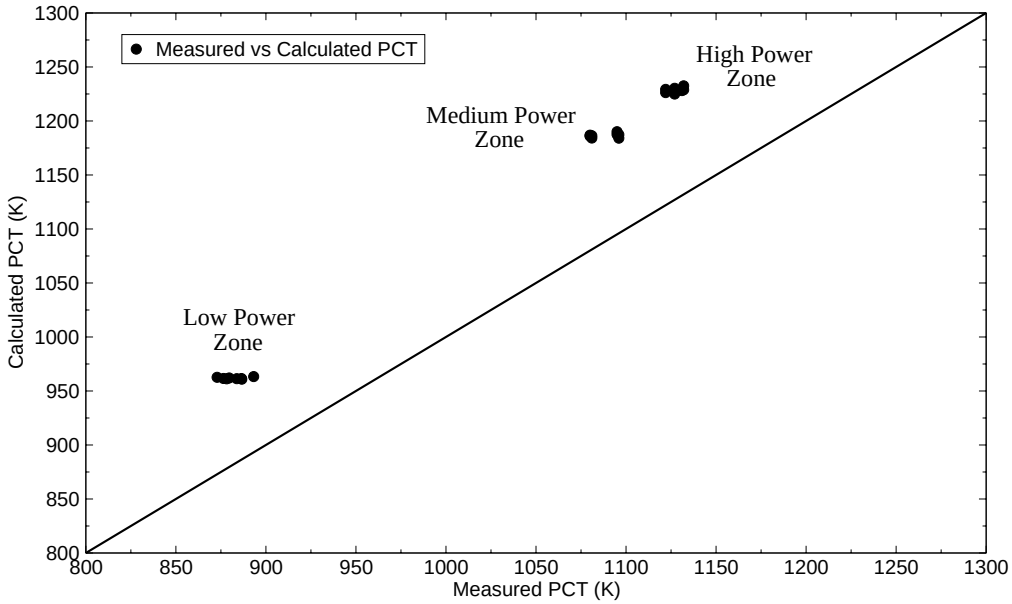

Figure C.2-47. Measured Versus Calculated Peak Clad Temperature for the Three Radial Power Zones - Run 62.

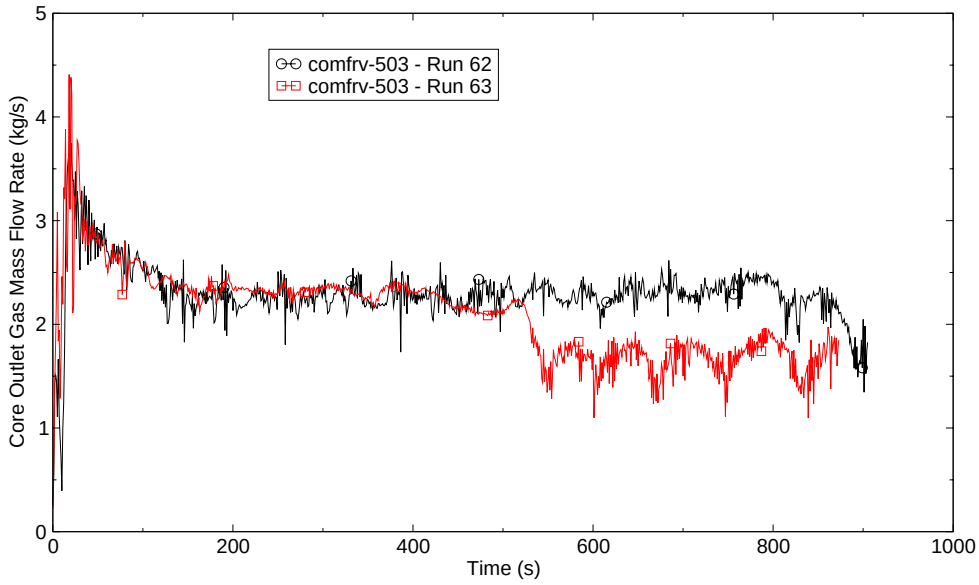

Figure C.2-48. Comparison of the Predicted Core Outlet Steam Mass Flow Rate for Run 62 and Run 63 - Power Effects.

lower power test as expected. Less power results in lower heater rod temperatures, less steam production and consequently a higher liquid level in the core. TRACE also exhibits the same behavior.

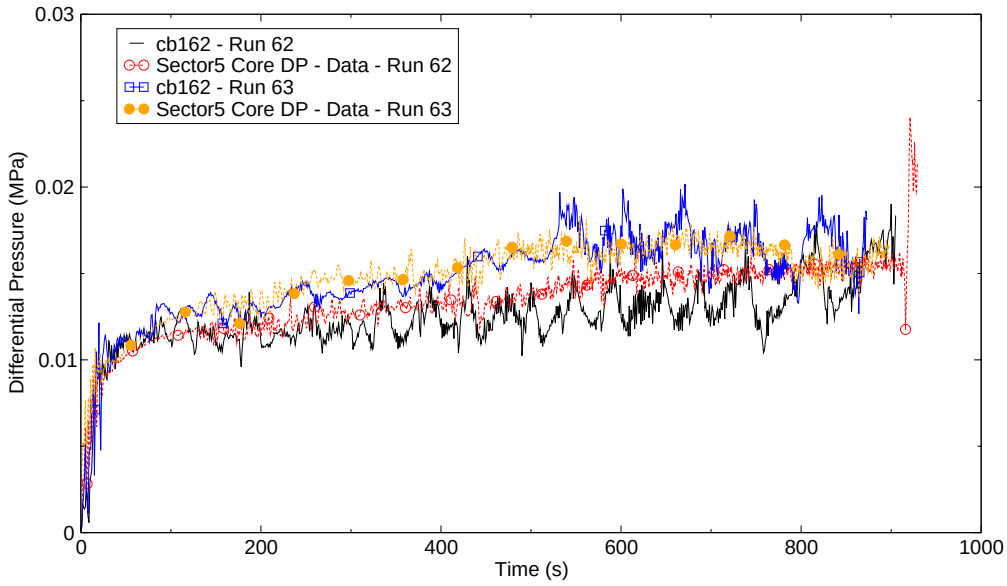

Figure C.2-49. Measured and Predicted Core Differential Pressures for Run 62 and Run 63 - Power Effects.

The primary thermal effect of variations in core power is higher clad temperatures and later core quench times with increasing power. Figure C.2-50 through Figure C.2-52 show the measured and predicted rod clad temperatures in the high powered region at 1.015, 1.83 and 3.05 m, respectively, for Runs 62 and 63. At the higher power, TRACE predicts higher clad temperatures as exhibited by the data. TRACE does a better job predicting the clad temperature in the low power case.

Figure C.2-53 shows the measured and calculated quench front for Runs 62 and 63. The low power test shows an earlier rod quench time as expected. The TRACE calculation also predicts an earlier quench time for the low power test. As shown, TRACE does a better job predicting the quench front for the low power case.

Measured versus calculated maximum peak clad temperatures for each radial power zone and each modeled azimuthal sector for Runs 62 and 63 are shown in Figure C.2-54. Also shown is the 45^{o} line that represents a perfect match of the measured and calculated PCT. The predicted PCT for the low power test compares well with the data.

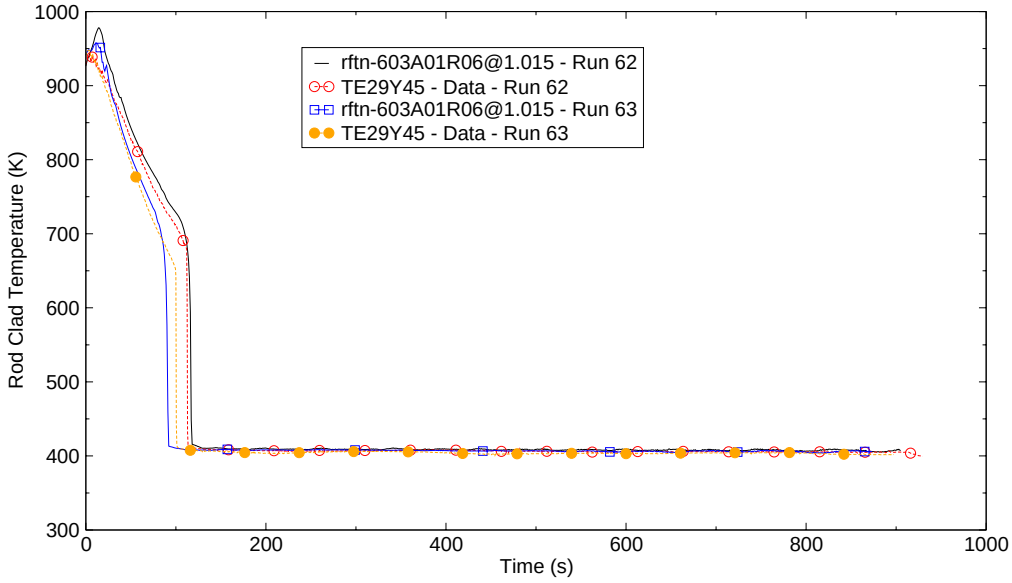

Figure C.2-50. Measured and Predicted Rod Clad Temperature in the High Power Region at 1.015 m for Run 62 and Run 63 - Power Effects.

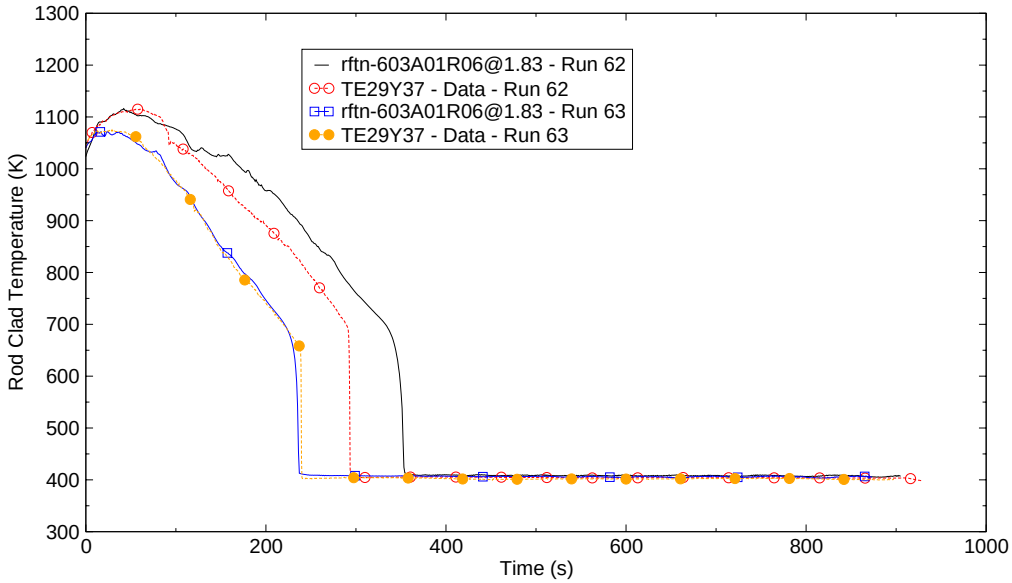

Figure C.2-51. Measured and Predicted Rod Clad Temperatures in the High Power Region at 1.83 m for Run 62 and Run 63 - Power Effects.

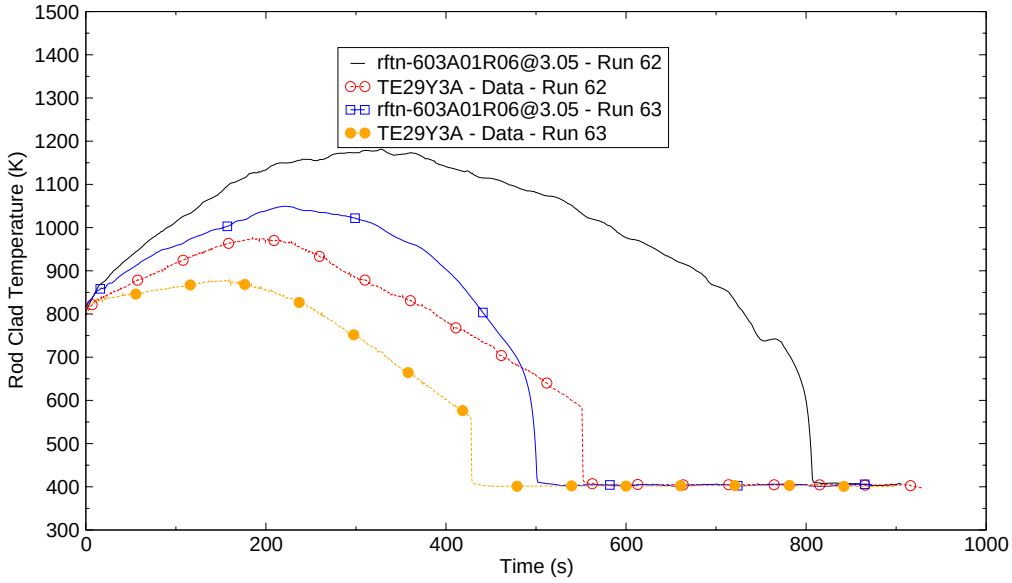

Figure C.2-52. Measured and Predicted Rod Clad Temperatures in the High Power Region at 3.05 m for Run 62 and Run 63 - Power Effects.

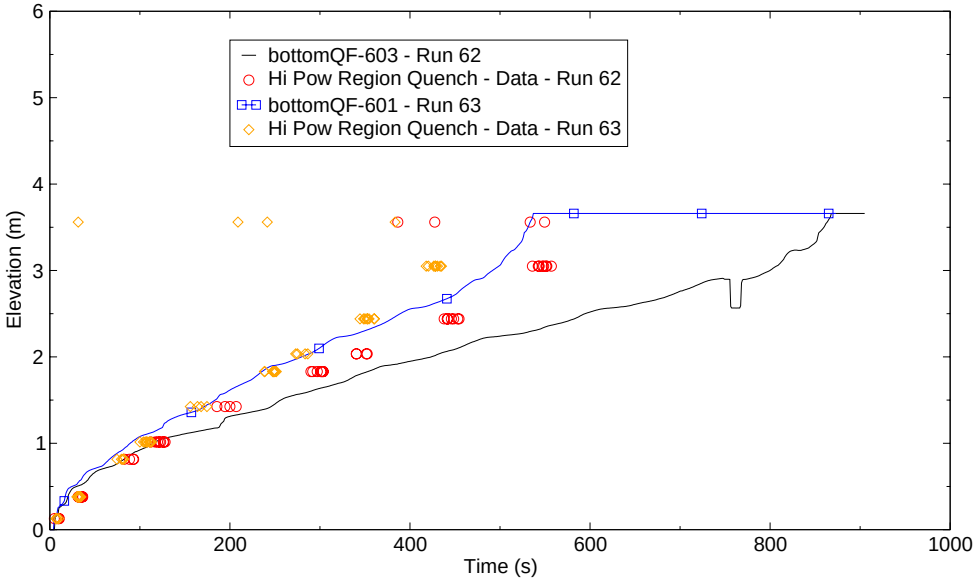

Figure C.2-53. Measured and Predicted Quench Front in the High Power Region for Run 62 and Run 63 - Power Effects.

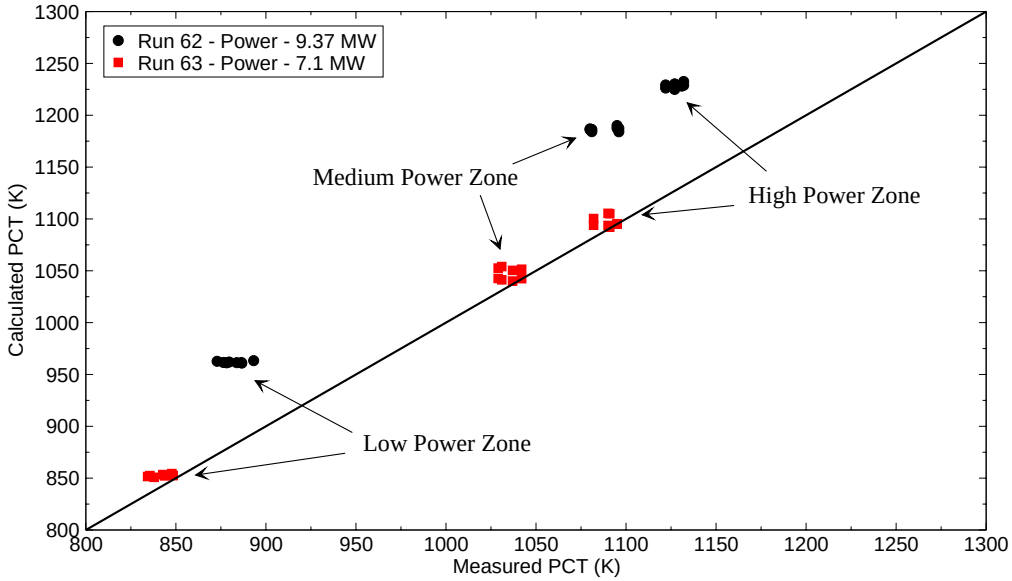

Figure C.2-54. Measured versus Predicted Peak Clad Temperature for the Three Radial Zones for Run 62 and Run 63 - Power Effects.

C.2.5.3. Radial Power Distribution Effects - Simulation of Run 63 and Run 64.

PWRs can operate with a variety of radial power profiles. Generally, PWR operators attempt to keep the radial profile relatively flat. However, it is possible to obtain significant radial profiles. Most of the CCTF tests were performed with a steep radial profile. To determine the effect of power profile on core behavior Run 64 was performed using a flat radial power profile. The test conditions for Run 64 were nearly identical to those of Run 63 except for the radial profile. Therefore the results of Run 64 are compared to the results of Run 63. Since the BOREC for these two tests are nearly the same (126 s versus 122 s) the time scale is not adjusted as was done in the previous section.

The hydraulic behavior was basically the same for these two tests. The predicted hydraulic behavior was basically the same also. Figure C.2-55 compares the measured and predicted Loop 1 hot leg mass flow rate for Runs 63 and 64. The predictions show good agreement with the data and with each other. Figure C.2-56 compares the measured and predicted core differential pressures. Again, the predicted response from the two calculations agrees well with the data and each other. Thus it is shown that TRACE can predict the expected hydraulic behavior for variance in radial power profiles.

Figure C.2-57 through Figure C.2-59 compare the measured and predicted rod clad temperature at the mid-plane for the three radial power zones. As expected, the peak clad temperature is nearly the same radially for the flat profile test. This same behavior is exhibited in the prediction. The

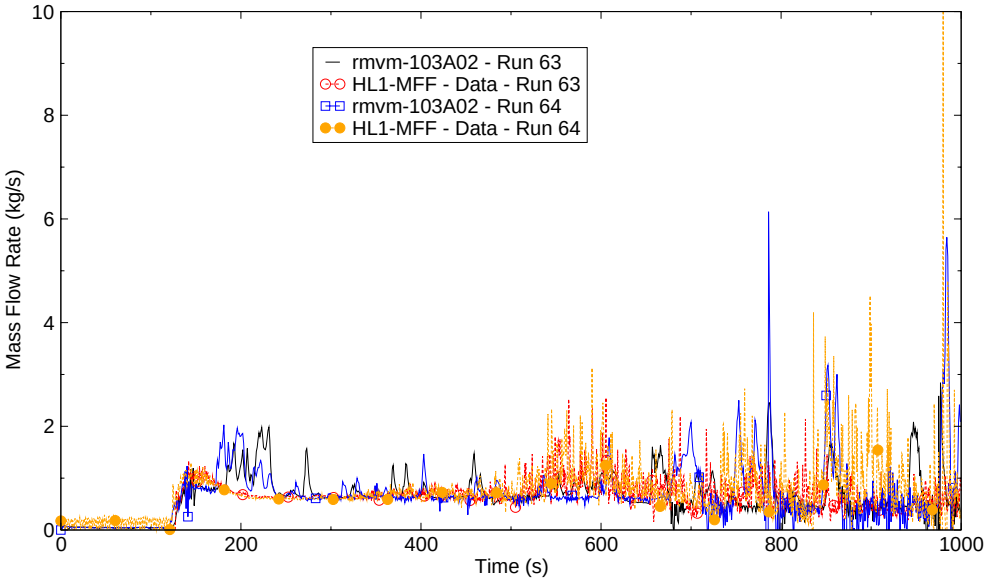

Figure C.2-55. Comparison of Measured and Predicted Loop 1 Hot Leg Mass Flow Rate for Tests 63 and 64 - Radial Profile Effects.

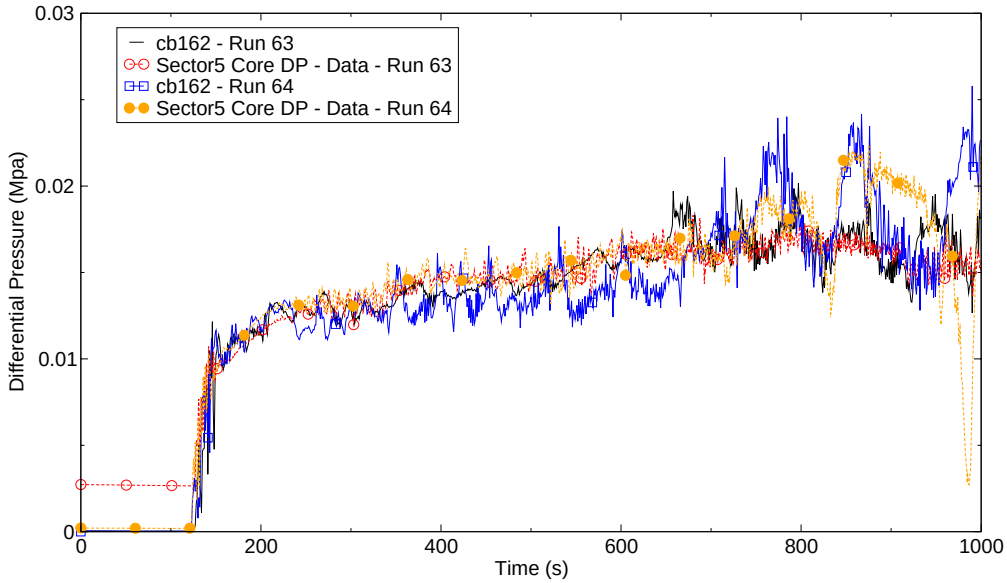

Figure C.2-56. Comparison of Measured and Predicted Core Differential Pressures for Run 63 and 64 - Radial Profile Effects.

under-prediction of the rod clad temperature in the outer ring is due to the presence of more liquid in that region.

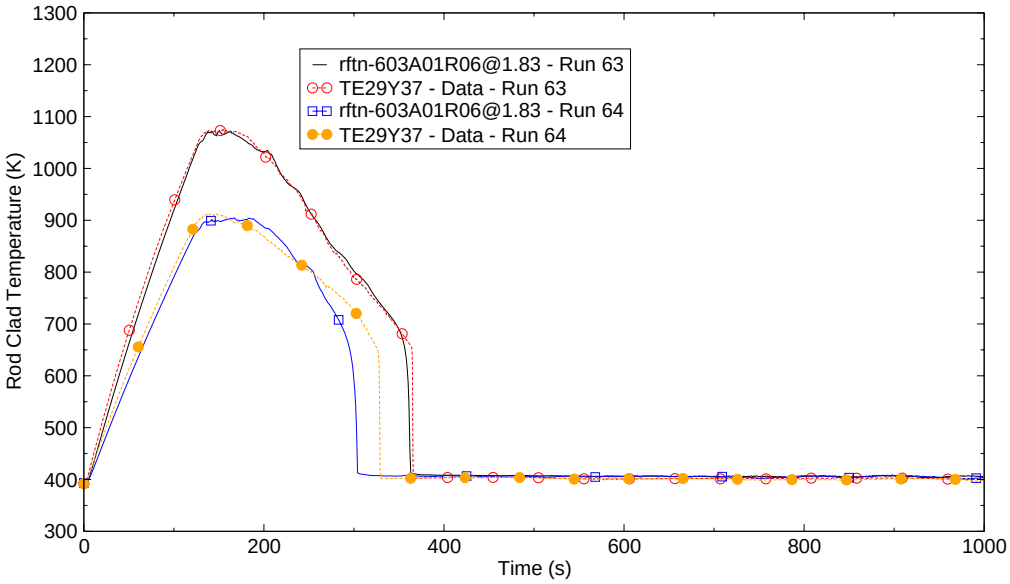

Figure C.2-57. Comparison of Measured and Predicted Rod Clad Temperature in the High Power Region at 1.83 m for Runs 63 and 64 - Radial Profile Effects.

Figure C.2-60 through Figure C.2-62 shows the quench profile for the three power zones. In the flat radial power test quenching of each bundle occurred between 350 and 400 seconds after BOREC. In the steep radial power test, the quench times varied (350-360 s - low-powered bundles, 390-420 s - intermediate bundles, and 420-440 s for the central bundles). This is expected since the central bundles had higher power than the intermediate or low-powered bundles. Thus the quench times were longer than the other regions and also longer than the average powered bundles in the flat radial power test. The same quenching behavior was observed in the calculation. The quench times predicted by TRACE compare reasonably well, especially in the intermediate and low-powered regions.

Measured versus calculated maximum peak clad temperatures for each radial power zone and each modeled azimuthal sector for Runs 63 and 64 are shown in Figure C.2-63. Also shown is the 45^{o} line that represents a perfect match of the measured and calculated PCT. The predicted PCT for Runs 63 and 64 compares quite well with the data .

C.2.5.4. System Pressure Effect - Simulation of Run 67, Run 62 and Run 55.

The effect of system pressure on core reflood is examined with Runs 67, 62 and 55. The system pressure for Run 67 was 0.15 MPa, for Run 62 was 0.2 MPa, and for Run 55 was 0.42 MPa. An

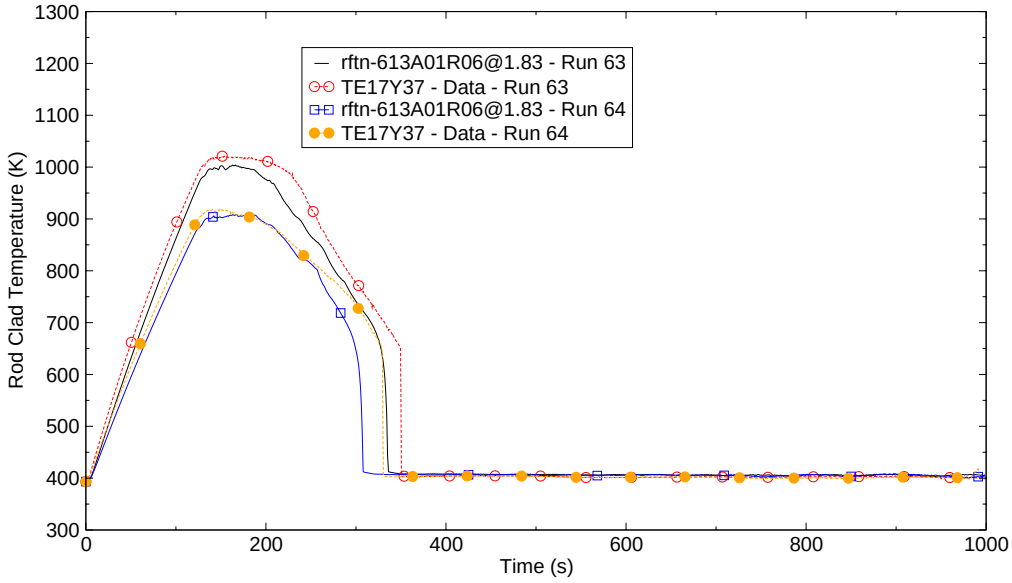

Figure C.2-58. Comparison of Measured and Predicted Rod Clad Temperature in the Medium Power Region at 1.83 m for Runs 63 and 64 - Radial Profile Effects.

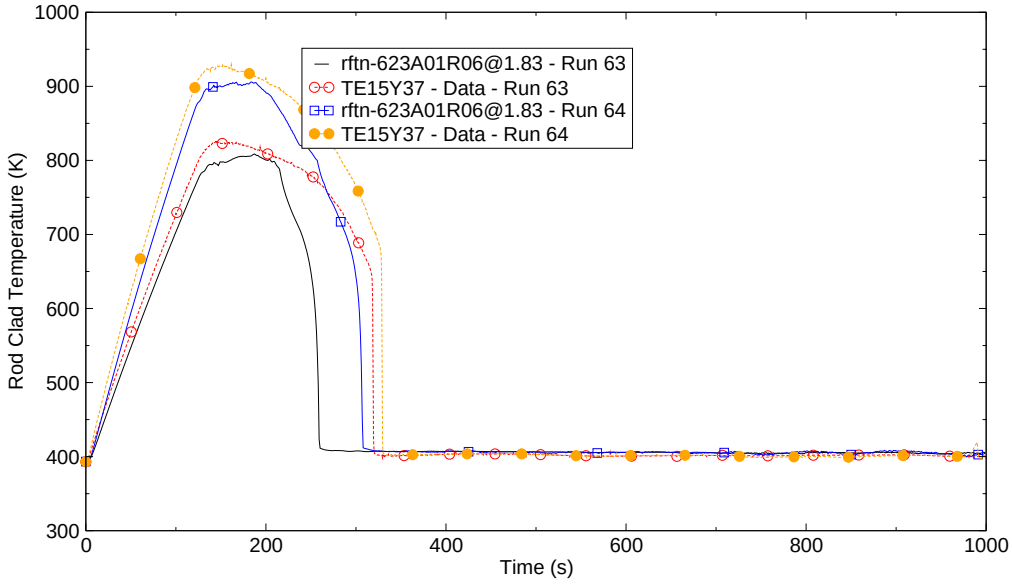

Figure C.2-59. Comparison of Measured and Predicted Rod Clad Temperature in the Low Power Region at 1.83 m for Runs 63 and 64 - Radial Profile Effects.

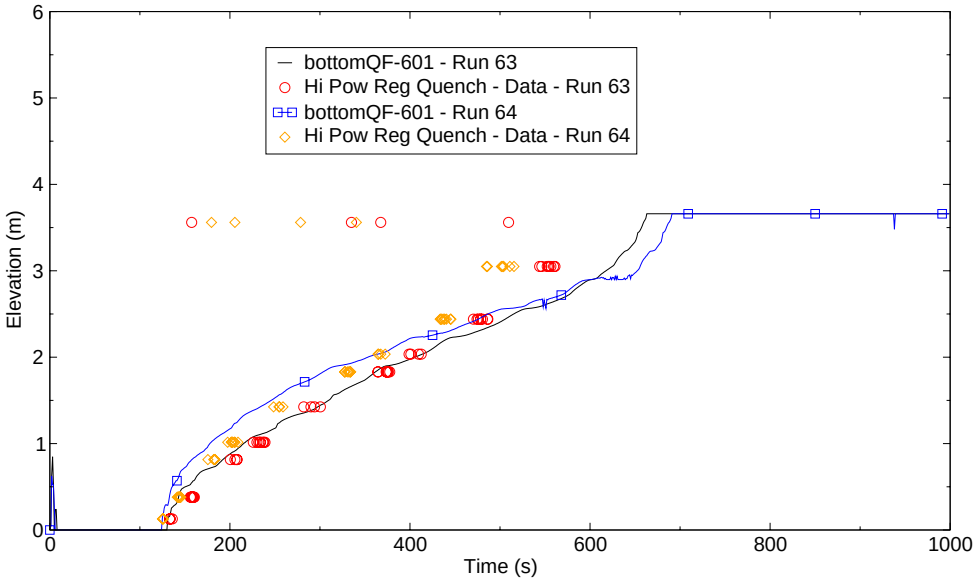

Figure C.2-60. Measured and Predicted Quench Front in the High Power Region for Runs 63 and 64 - Radial Profile Effects.

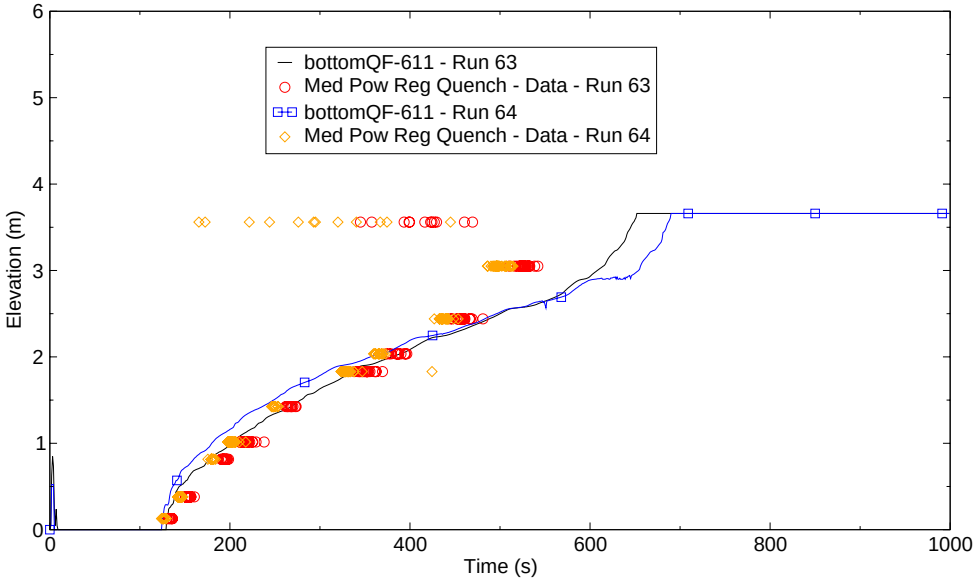

Figure C.2-61. Measured and Predicted Quench Front in the Medium Power Region for Runs 63 and 64 - Radial Profile Effects.

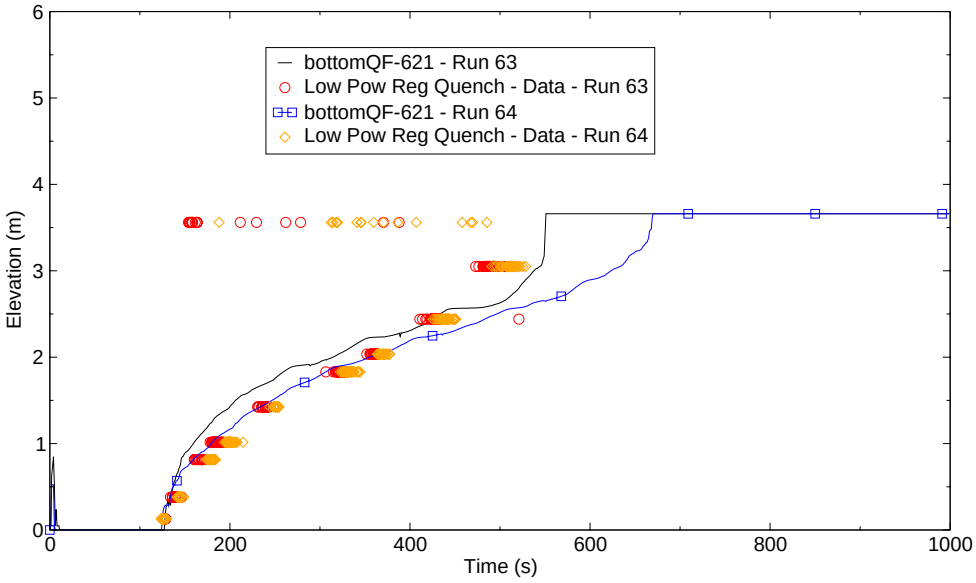

Figure C.2-62. Measured and Predicted Quench Front in the Low Power Region for Runs 63 and 64 - Radial Profile Effects.

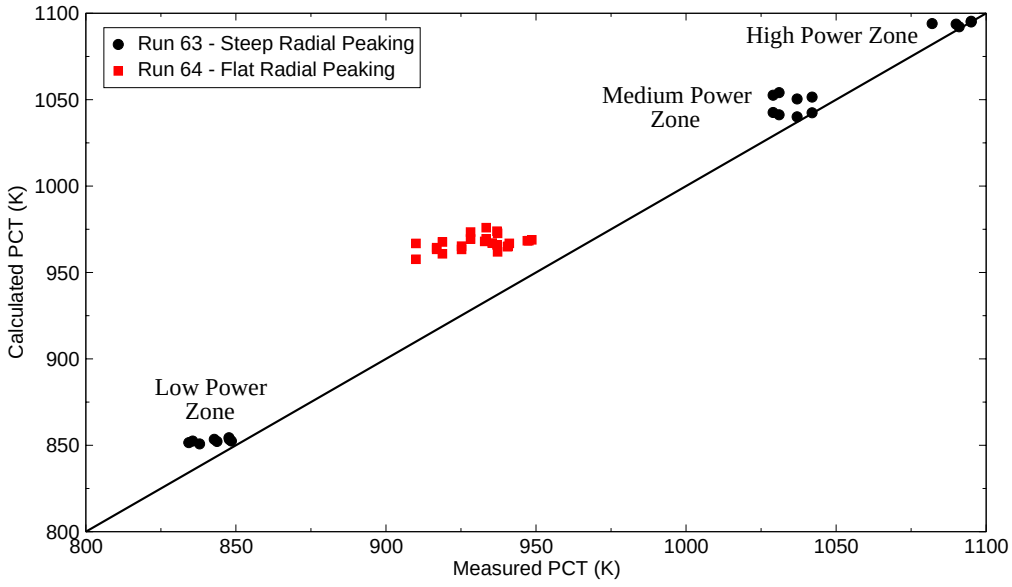

Figure C.2-63. Measured versus Predicted Peak Clad Temperature for the Three Radial Zones for Run 63 and Run 64 - Radial Profile Effects.

increase in system pressure causes an increase in steam density. Higher steam density leads to an increase in local heat transfer coefficients in the core due to a larger mass of steam in contact with the rods. Higher steam density also results in a decrease in loop pressure drop and thus an increase in core mass inventory. The net effect of an increase in pressure is lower PCT and earlier quench times.

Figure C.2-64 compares measured and predicted rod clad temperatures in the high power zone at the mid-plane (1.83 m) for Runs 67, 62 and 55. As shown, TRACE predicts the effects of various system pressure reasonably well, i.e. higher system pressure result in lower PCT and earlier quench times. TRACE under-predicts the PCT in all three simulations; more so for the higher pressure case. Since the rod clad temperature trend is being calculated correctly for a given system pressure suggests the heat transfer coefficient being calculated by the code is being done correctly. However it is apparent the code predicts higher heat transfer coefficients at higher pressures.

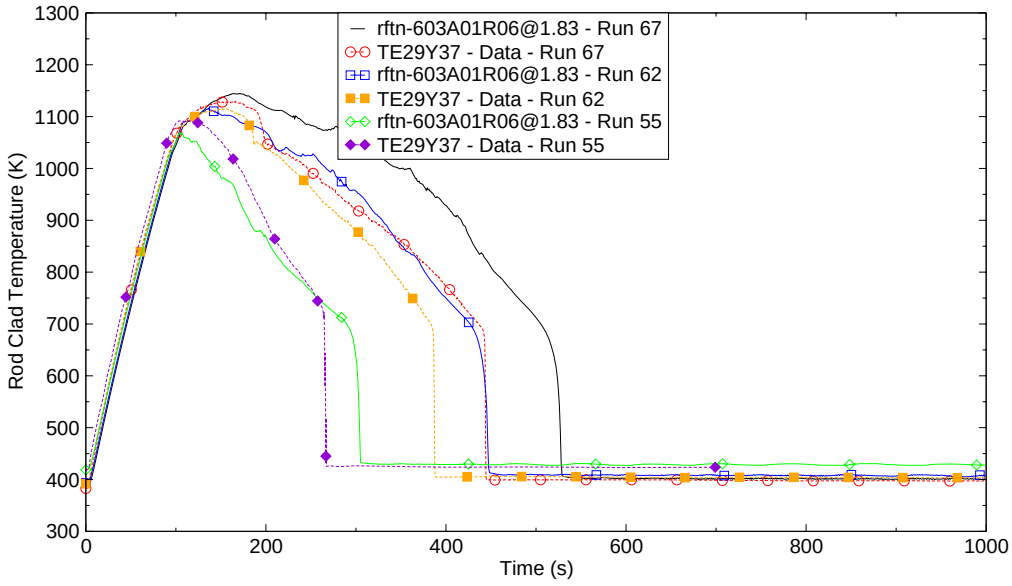

Figure C.2-64. Comparison of Measured and Predicted Rod Clad Temperature in the High Power Region at 1.83 m for Runs 67, 62 and 55 - System Pressure Effects.

Figure C.2-65 compares the measured and predicted quench profile in the high powered region. TRACE calculates the trend of the data reasonably well, i.e. earlier quench times at higher pressures. TRACE comes closer to matching the data in the higher system pressure case. This is probably due to a higher predicted heat transfer coefficient.

Measured versus calculated maximum peak clad temperatures for each radial power zone and each modeled azimuthal sector for Runs 67, 62 and 55 are shown in Figure C.2-66. Also shown is the 45^{o} line that represents a perfect match of the measured and calculated PCT. As expected, the

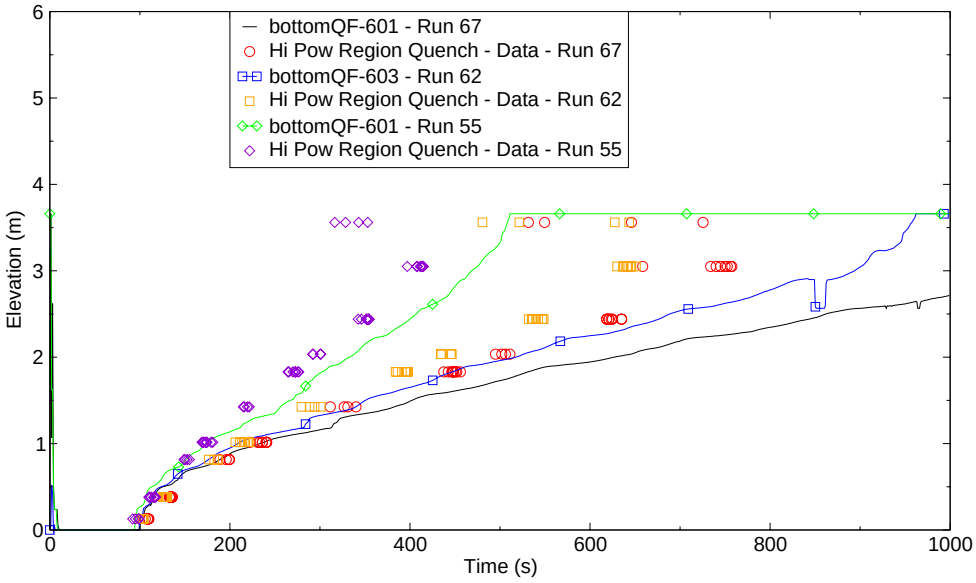

Figure C.2-65. Measured and Predicted Quench Front in the High Power Region for Runs 67, 62 and 55 - System Pressure Effects.

PCT is under-predicted for the higher system tests and over-predicted for the low system pressure test.

C.2.5.5. Downcomer ECC Injection - Simulation of Run 58 and Run 62.

Run 58 was nearly the same as Run 62 in initial and boundary conditions. However, after ECC flow was switched from lower plenum injection to cold leg injection about 10% of the accumulator flow and 80% of the LPCI flow was injected directly into the downcomer.

The simulation of CCTF Run 58 was not successful in completing. The problem failed on "cannot reduce time step further" during the initial rod heatup period when the system was stagnant (i.e. no ECC injection). Attempts were made to work around the failure by reducing the maximum time step size to 2 and 1 milliseconds, but without success. This failure problem has been reported as Bug Report #307. This simulation has run successfully with previous code versions.

C.2.5.6. Best-Estimate Reflood - Simulation of Run 71.

Run 71 was performed under "best estimate" conditions. Boundary and initial conditions for the test are listed in Table C.2.1 The radial power profile for this test was flat. The time of BOREC for this test was 37.5 seconds. TRACE exhibited its capability to predict reflood behavior under "best estimate" conditions.

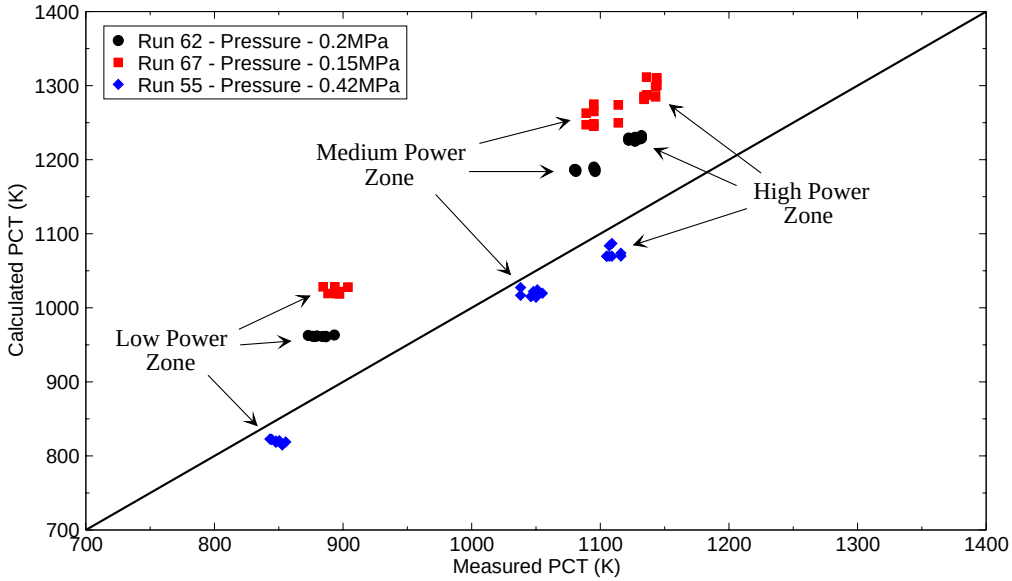

Figure C.2-66. Measured versus Predicted Peak Clad Temperature for the Three Radial Zones for Runs 67, 62 and 55 - System Pressure Effects.

Figure C.2-67 and Figure C.2-68 show the measured and predicted differential pressures in the loop and core, respectively. In general, the predicted differential pressures followed the trend of the data. Both the data and the calculation show the differential pressures in the core and intact loops oscillated in opposite phase throughout the first 200 seconds. Because of the relatively high pressure and low core power, steam generation was low; hence, water accumulated in the upper plenum and eventually overflowed into the steam generator through the hot leg. The overflow water vaporized in the steam generator, resulting in an increased differential pressure across the primary loops. The increased loop differential pressure depressed the water level in the core and upper plenum terminating water flow into the steam generator. Vapor generation gradually ceased in the steam generator as the flow of water from the upper plenum stopped. Consequently loop pressure drop decreased, core water level increased and the cycle repeated. The high LPCI flow was sufficient to condense all the core steam generation resulting in no net steam flow through the downcomer and out the broken cold leg. This gave a higher downcomer driving head and greater water carryover to the hot legs. The period of the oscillation was apparently controlled by the amount of water evaporated in the steam generator per cycle of the oscillation.

The secondary oscillations observed in the calculation are related to the oscillatory behavior of the water exiting the vessel side broken cold leg. The water level in the downcomer hovered around the cold leg connection port. Two phase flow exited through the break. As the level in the downcomer rose, more water exited the break and the differential pressure between the downcomer and broken cold leg increased resulting in an increase in pressure. The increase in pressure depressed the downcomer level, more steam exited the break and the differential

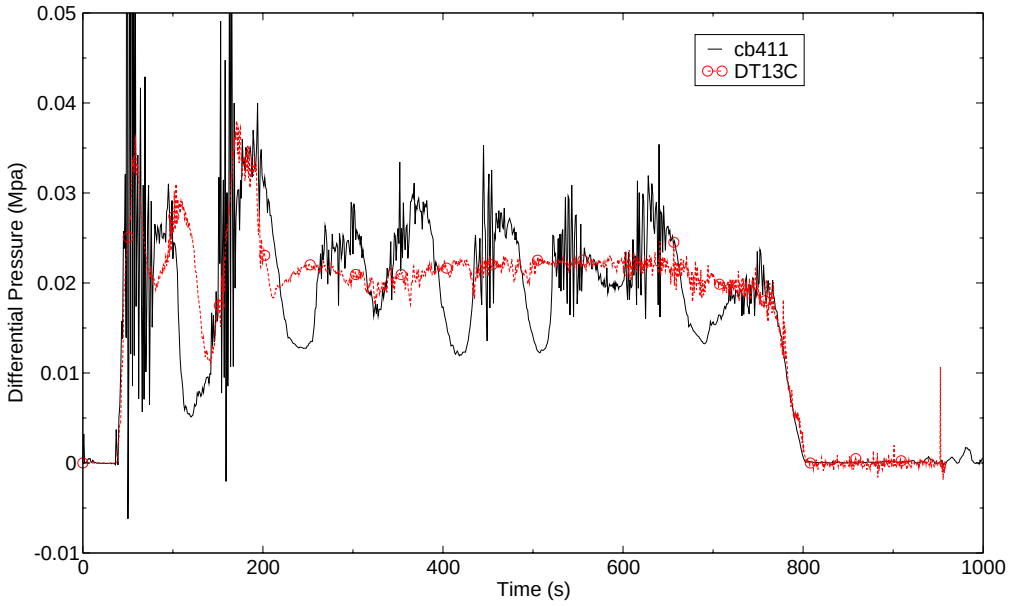

Figure C.2-67. Measured and Predicted Upper Plenum to Loop 1 Cold Leg Nozzle Differential Pressure - Run 71.

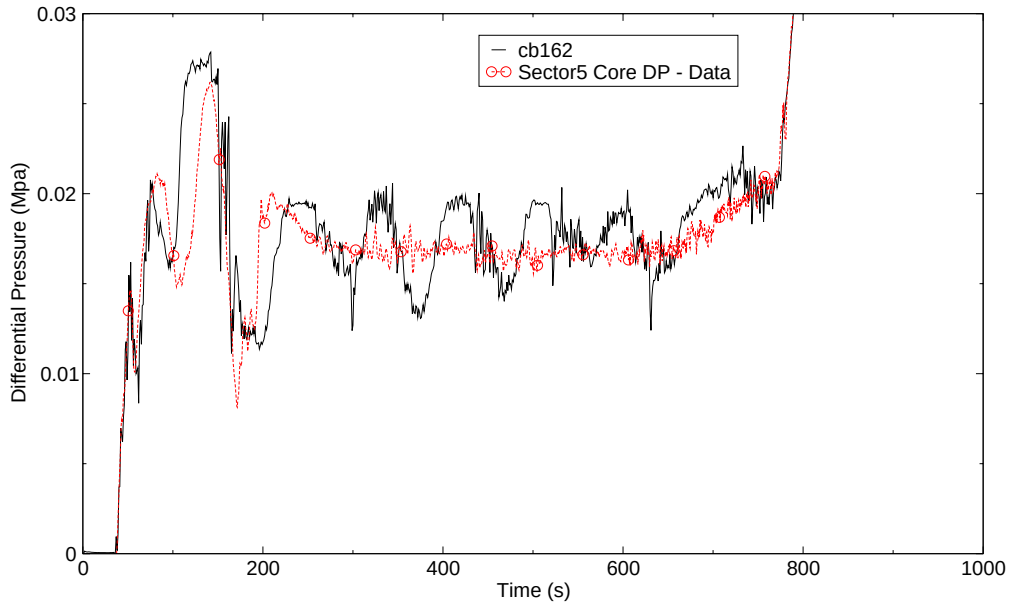

Figure C.2-68. Measured and Predicted Core Differential Pressure - Run 71.

pressure between the downcomer and the broken cold leg decreased. The cycle was repeated through out the calculation, as shown in Figure C.2-69, until the rods were quenched.

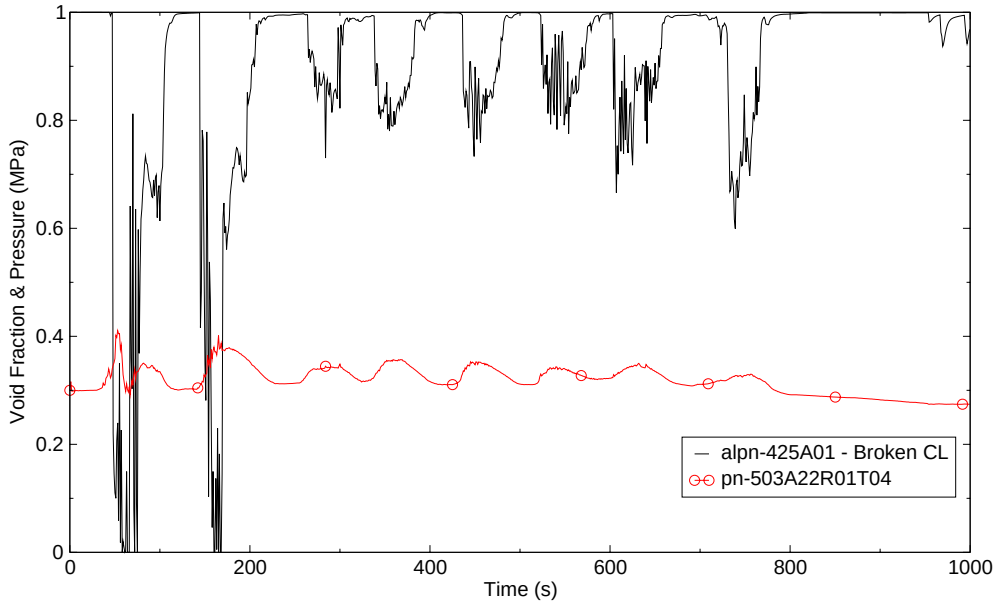

Figure C.2-69. Predicted Void Fraction in the Broken Cold Leg and Pressure in the Upper Plenum - Run 71.

The oscillations throughout the first 200 seconds are earlier and larger in the calculation and resulted in an earlier predicted rod quench as indicated by the rod temperature response shown in Figure C.2-70 through Figure C.2-72. The flow oscillations were high enough to cause a core flow reversal that uncovered the rods in the upper part of the core and lead to a second rod heat up. The code was unable to predict the second rod heat up as shown in Figure C.2-71 and Figure C.2-72.

Figure C.2-73 shows the measured and predicted rod quench profile for the central bundles. The rod quench from the second heat up is not shown in the data and is very short in duration in the predition. Overall, the predicted rod quench shows reasonable agreement with the data.

Measured versus calculated maximum peak clad temperatures for each radial power zone and each modeled azimuthal sector for Run 71 are shown in Figure C.2-74. Also shown is the 45^{o} line that represents a perfect match of the measured and calculated PCT. In gerneral, the PCT was slightly underpredicted by the code.

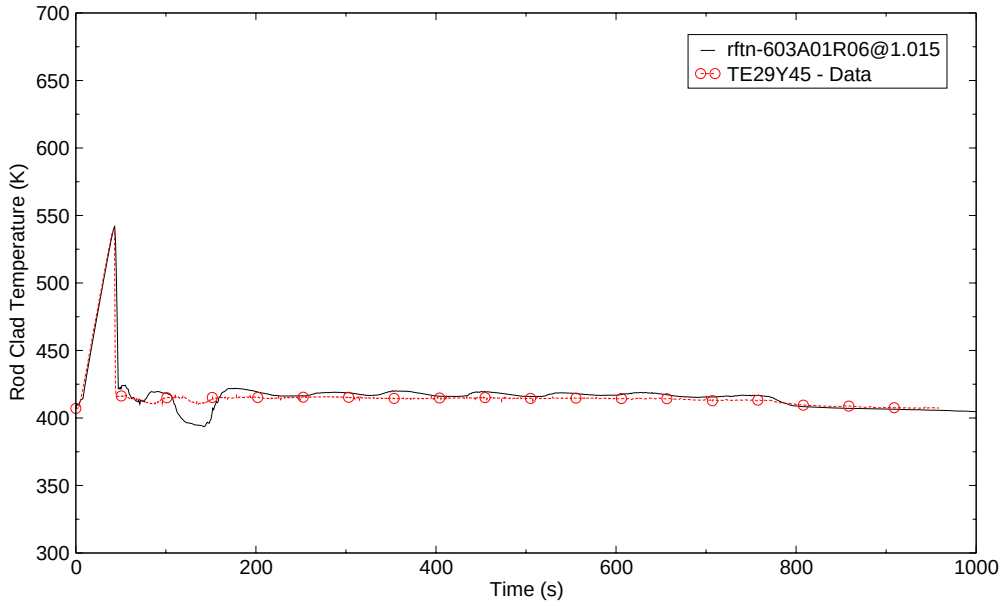

Figure C.2-70. Measured and Predicted Rod Clad Temperature at 1.015 m - Run 71.

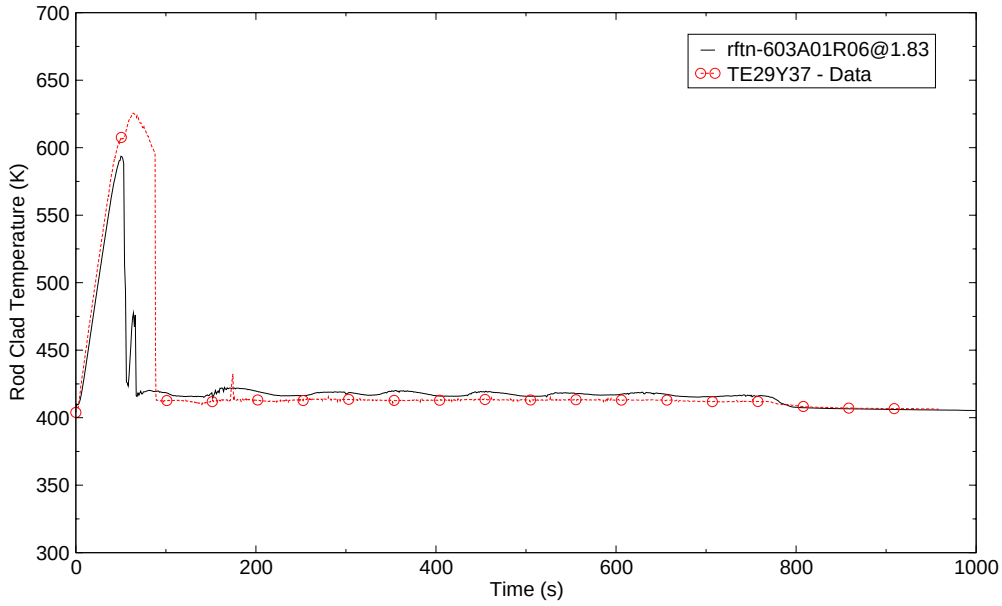

Figure C.2-71. Measured and Predicted Rod Clad Temperature at 1.83 m - Run 71.

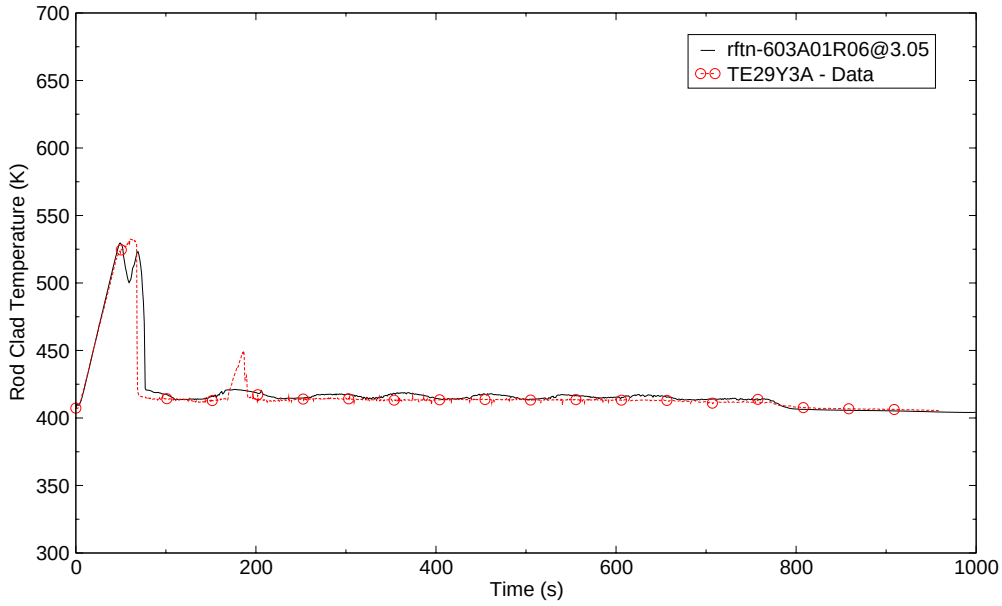

Figure C.2-72. Measured and Predicted Rod Clad Temperature at 3.05 m - Run 71.

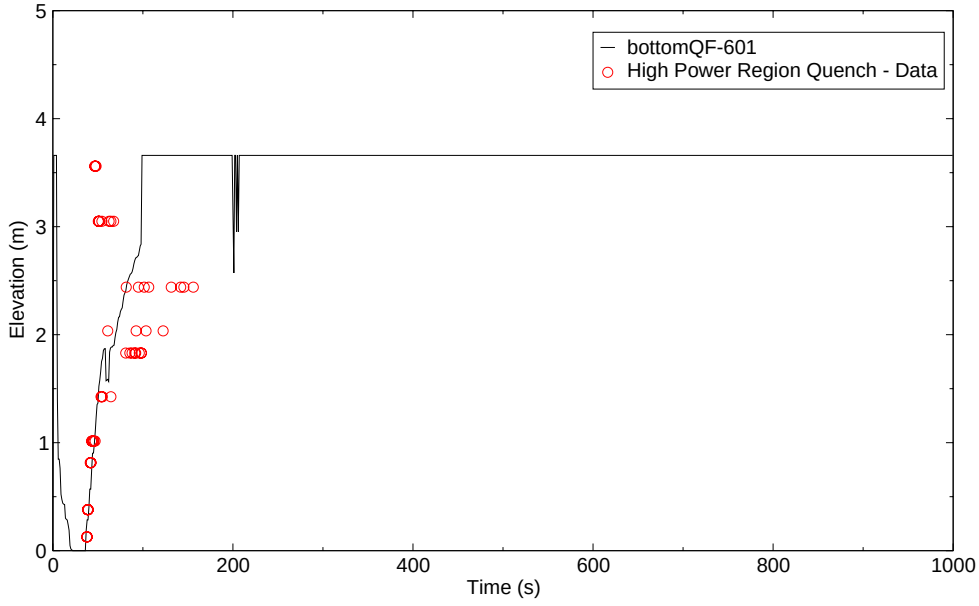

Figure C.2-73. Measured and Predicted Rod Quench Profile for the Central Bundles - Run 71.

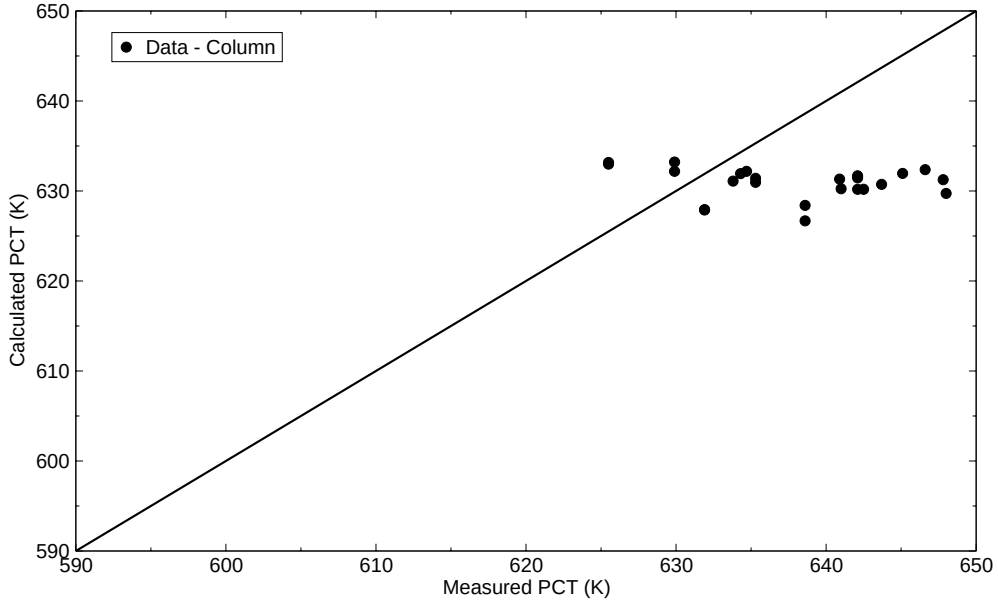

Figure C.2-74. Measured versus Predicted Peak Clad Temperature for the Three Radial Zones for Run 71.

C.2.6. Run Time Statistics

Run time statistics for the seven TRACE CCTF simulations are given in Table C.2.2. The values in the table consist of problem end time, the total number of time steps taken to complete the calculation, the total CPU time used to run the transient, and the CPU time per time step per fluid volume

.

Table C.2.2. Run Time Statistics for the TRACE CCTF Simulations.

Run Number	End Time	Total Number of Time Steps	Total CPU time to Run the Transient	CPU Time per Time Step per Fluid Volume
62	1000.001	136083	79281.094	5.3011E-04
63	1000.005	193041	67928.359	3.2019E-04
64	1000.002	328635	161787.484	4.4795E-04

Table C.2.2. Run Time Statistics for the TRACE CCTF Simulations.

Run Number	End Time	Total Number of Time Steps	Total CPU time to Run the Transient	CPU Time per Time Step per Fluid Volume
67	1000.000	265266	104751.578	3.5932E-04
55	1000.004	101249	34682.781	3.1169E-04
58	1000.005	201300	105548.828	4.7624E-04
71	1000.002	212300	99252.328	4.2540E-04

C.2.7. Assessment Results Summary

TRACE has shown it is capable of calculating the data trends during core reflood for different variations in boundary and initial conditions. TRACE demonstrated its capability to correctly calculate reflood behavior for variations in core power, radial power profile, and system pressures. TRACE exhibited its capability to predict reflood behavior reasonably well under "best estimate" conditions (Run 71). TRACE was not successful in the simulation of Run 58. Code failures prevented the simulation from advancing past the initial rod heatup period when the system was stagnant.

The rod clad temperature in the upper core half was over-predicted and resulted in a longer time to quench. The upper one-third of the core is highly voided. The vapor temperature is nearly that of the rod surface temperature while the liquid temperature is at saturation. The calculated liquid and vapor velocities in the upper core are on the order of 2.5 and 13 m/s, respectively. It appears interfacial drag is under-predicted. For small droplet sizes (2 mm or less) liquid and vapor velocities should be closer together. It also appears the interfacial heat transfer is under-calculated.

C.2.8. References

1 M. Bolander, "CCTF Gravity Reflood Tests", ADAMS No. ML061710558.

2 MPR Associates, Inc., “Research Information Report for the Cylindrical Core Test Facility (CCTF) Core-II Test Series (Excluding Tests Involving Upper Plenum Injection), Volumes I and II, MPR-934, April, 1988.

3 B.E. Boyack, et. al., “TRAC-M/F77, Version 5.5 Developmental Assessment Manual”, Vol.1, NUREG/CR-6730, July 2001.

4 M. Bolander, "TRACE Calculation Notebook for CCTF Reflood Analysis", April 2006.

5 Tsutomu Okubo, et al, “Data Report on Large Scale Reflood Test-82 - CCTF Core-II Test C2-4 (Run 062) - ”, JAERI-memo 59-450, February 1985.

6 Tadashi Iguchi, et al, “Data Report on Large Scale Reflood Test-83 - CCTF Core-II Test C2-5 (Run 063) - ”, JAERI-memo 59-451, February 1985.

7 Hajime Akimoto, et al, “Data Report on Large Scale Reflood Test-84 - CCTF Core-II Test C2-6 (Run 064) - ”, JAERI-memo 59-452, February 1985.

8 Hajime Akimoto, et al, “Data Report on Large Scale Reflood Test-86 - CCTF Core-II Test C2-8 (Run 067) - ”, JAERI-memo 59-453, February 1985.

9 Tadashi Iguchi, et al, “Data Report on Large Scale Reflood Test-44 - CCTF Core-II Test C2-1 (Run 055) - ”, JAERI-memo 58-156, May 1983.

10 Tsutomu Okubo, et al, “Data Report on Large Scale Reflood Test-78 - CCTF Core-II Test C2-AA2 (Run 058) - ”, JAERI-memo 59-446, February 1985.

11 Tsuneyuki Hojo, et al, “Data Report on Large Scale Reflood Test-95 - CCTF Core-II Test C2-12 (Run 071) - ”, JAERI-memo 59-450, July 1985.

C.3. SCTF Reflood Tests

Author(s): David Caraher[1], Andrew Ireland[2]

Affiliation: [1]ISL, Inc., [2]US NRC

Code Version: TRACE V5.0

Platform and Operating System: Intel x86, Windows XP

C.3.1. Introduction

TRACE simulations of seven SCTF (Slab Core Test Facility) reflood tests have been run and compared with experimental data. The objective of these code-to-data comparisons is to evaluate TRACE capabilities for predicting reflood phenomena.

C.3.2. Test Facility Description

The Slab Core Test Facility (SCTF) experimental program (Refs. 1,2) was operated by the Japan Atomic Energy Research Institute (JAERI) during the 1980s as part of the 2D/3D project. These tests were sponsored by JAERI, the U.S. Nuclear Regulatory Commission (USNRC) and the Federal Republic of Germany. A unique feature of the facility was that eight rod bundles were placed side-by-side. Test objectives were to study two-dimensional heat transfer and hydrodynamics during the reflood phase of a postulated LOCA. The SCTF facility is depicted in Figure C.3-1 and Figure C.3-2.

The core was simulated with eight electrically heated rod bundles. The axial power distribution had 17 power steps in a chopped cosine shape with a 1.4 axial peaking factor. Each heater bundle was a 16x16 rod array with 234 electrically heated rods and 22 unpowered rods. All rods within a bundle had the same power. Total core power (all 8 bundles) was approximately 7 MW.

The core heated length was 3.66 meters long and used rods with a pitch and diameter of the Westinghouse 15x15 bundle. Heated rod diameter was 10.7 mm and rod pitch was 14.3 mm.

The nominal core flow area and fluid volume scaling was 1/21. The intact loop piping was sized to represent three lumped loops and the broken loop was sized to represent the single fourth loop.

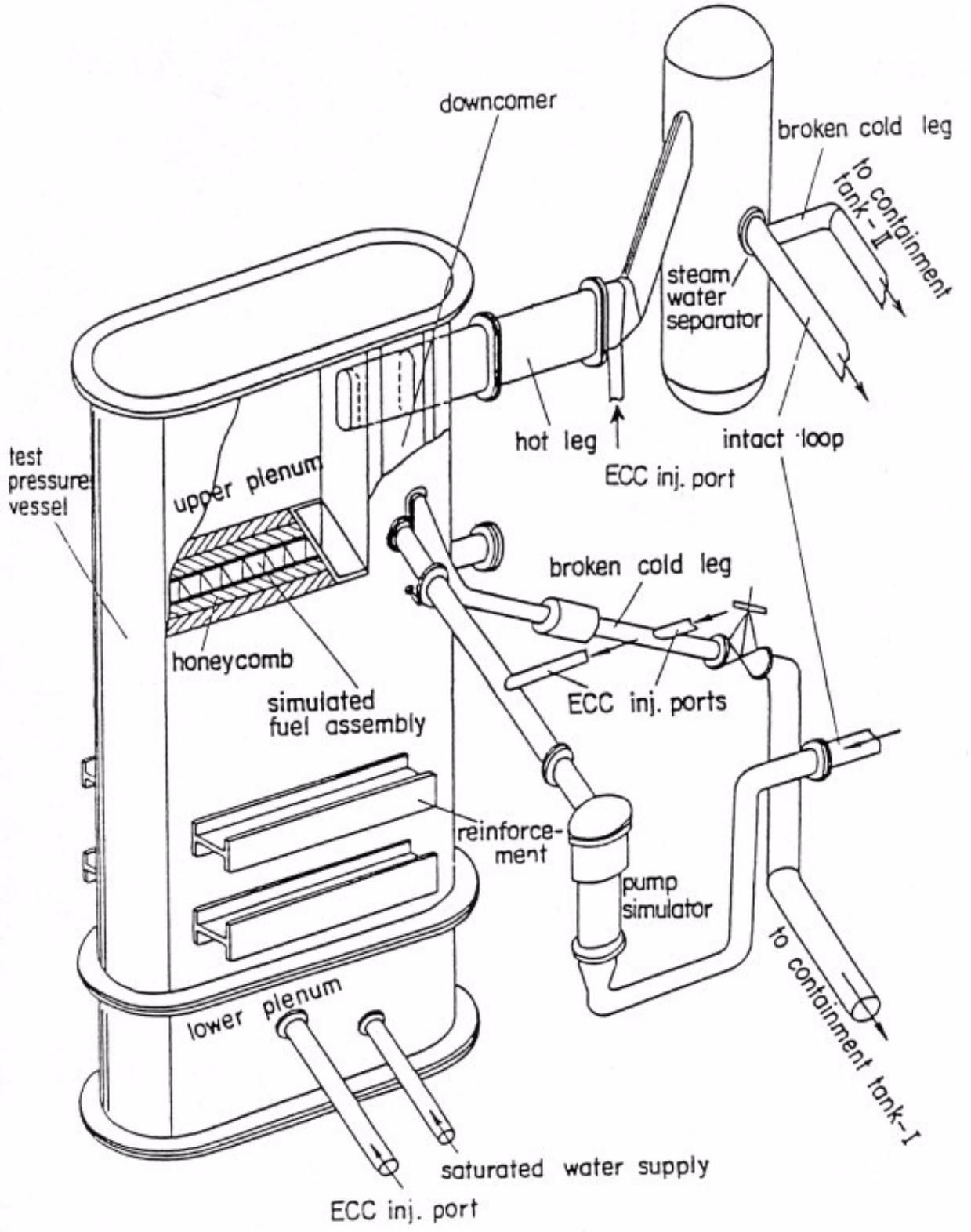

Figure C.3-1. Overview of the SCTF

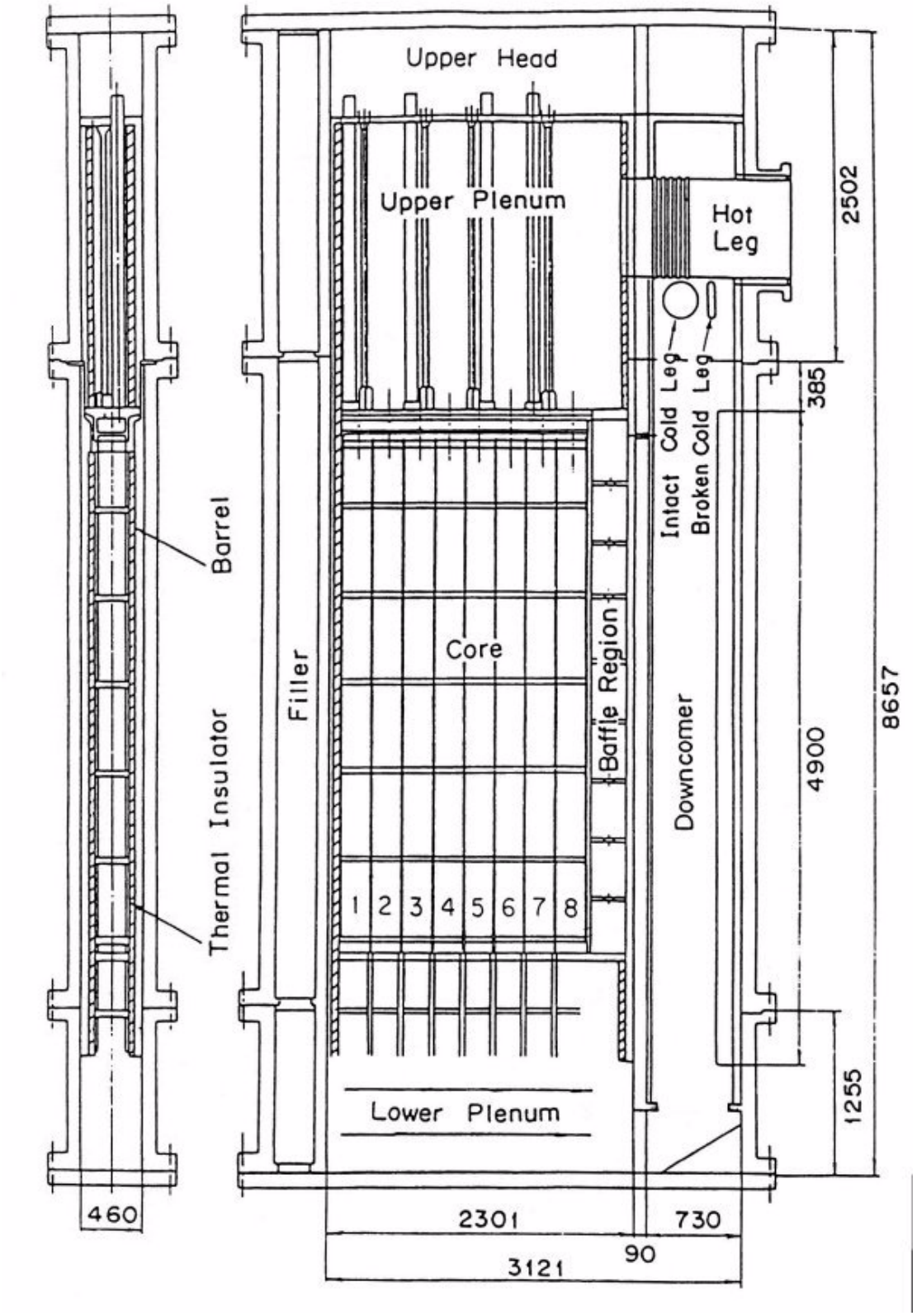

Figure C.3-2. Side and End Views of the SCTF

One hot leg delivered core effluent to one steam generator simulator known as the steam/water (S/W) separator. It simulated the resistance of a steam generator, but did not contain a tube bundle or secondary side water. Hot leg flow entered the side of the S/W separator tank which had a vertical wall in it. Steam flowed through a perforated plate near the top on the inlet side and down the opposite side. De-entrained water could collect in the bottom of the S/W separator tank. Since the 'steam binding' effect of hot secondary water flashing entrained droplets was not simulated by using active steam generator tubes, extra flow resistance was placed in the pump simulator in the intact loop cold leg. The intact and broken loop simulator cold leg pipes are both connected to the S/W separator vessel outlet plenum. A pipe representing the intact cold leg returned steam to the pressure vessel downcomer and a broken cold leg connected to one of two containment tanks. The other half of the broken cold leg connected the vessel downcomer to a second containment tank. The two containment tanks were connected to one another and held at a specified pressure via a pressure control valve.

The SCTF heated rod thermocouple elevations shown in Figure C.3-3 are relative to the bottom of heated length (BOHL) and the thermocouple Level Numbers 1-10 is the numbering scheme used in the SCTF facility to designate heater rod thermocouple axial locations. The horizontal positioning and numbering scheme of the SCTF instrumented heated rods is shown in Figure C.3-4.

Most of the cladding temperature comparisons in this report are for axial level 6, the 1.91 m elevation. When comparing to TRACE all measured cladding temperatures near unheated surfaces were omitted. Thus, only the measurements designated 1B, 1C, and 2A (Figure C.3-4) were used for comparison to TRACE. Since location 2A is near an unheated wall for bundle 8, the bundle 8 measurement at this location was not used for comparisons to TRACE.

C.3.3. TRACE Model Description

The TRACE nodalization of the SCTF test facility is depicted in Figure C.3-5.The development of the input for the TRACE SCTF model is documented in References 10, 11, and 12.

There are a total of 76 components in the TRACE model. Fifty-three of the components are HTSTRs. Eight of the core HTSTRs are powered by eight POWER components.

A noding diagram of the SCTF TRACE model's 2D slab geometry pressure vessel is shown in Figure C.3-6. There are 21 levels, 12 rings or delta-y sectors and 1 cell of theta or delta-x thickness.

A noding diagram of the SCTF TRACE model's loop piping and steam/water separator is shown in Figure C.3-7. Junction numbers are shown in red. Component numbers used are: 2 for the hot leg PIPE; 33, 34, 44 and 45 for the broken cold leg PIPEs; 8 for the intact cold leg TEE; 30 series for the accumulator injection flow to the pressure vessel lower plenum; 12 for the LPCI FILL to the intact cold leg pipe, and 1 for the pressure VESSEL.

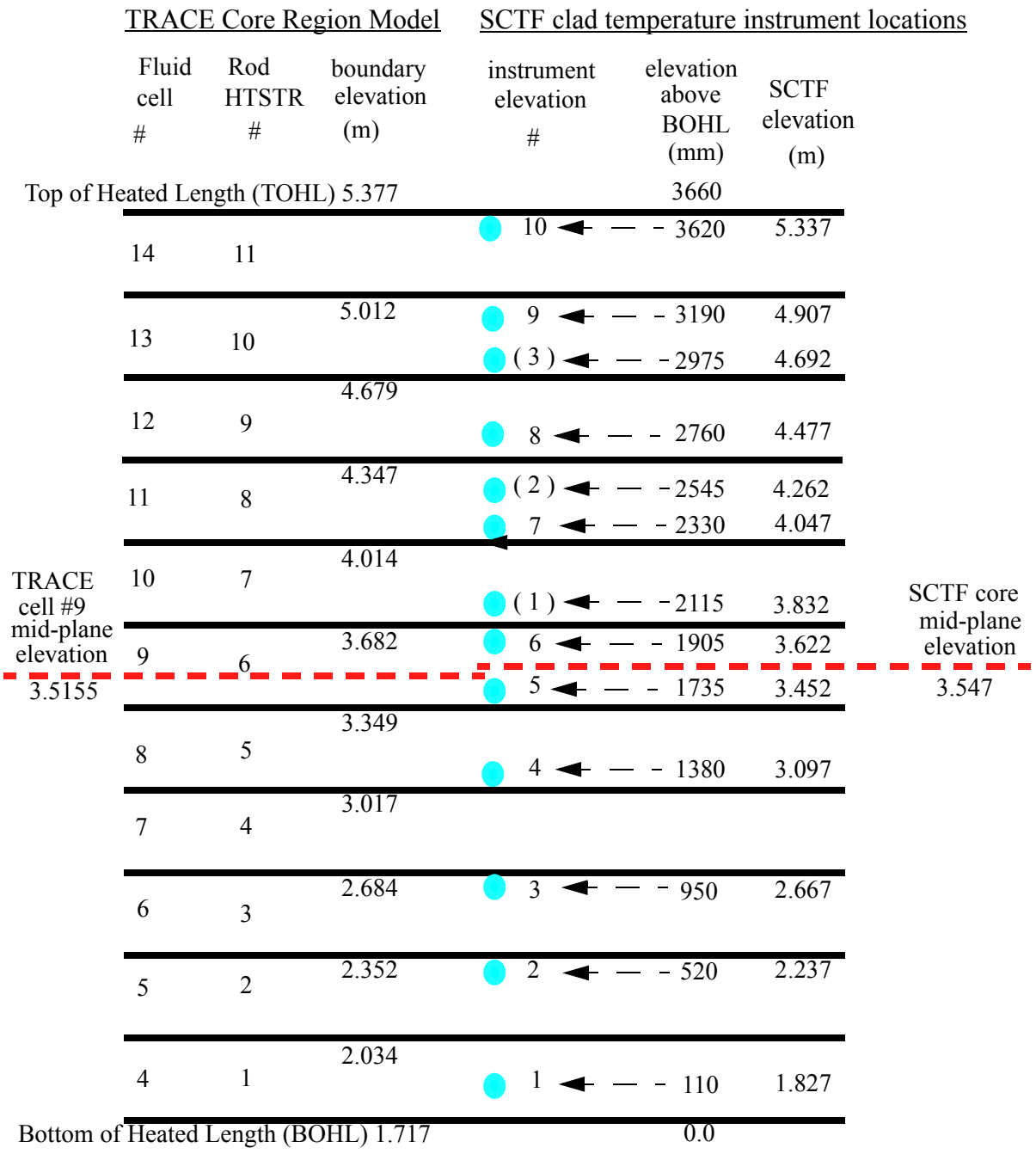

Figure C.3-3. SCTF clad temperature instrument locations vs. TRACE core region hydraulic cell elevations and heat conductor node elevations.

A second VESSEL component, component number 6, models the SCTF S/W separator. The S/W separator has 4 axial levels, 1 radial ring, and 2 theta sectors. VESSEL 6 HTSTRs use the 800 series for HTSTR component numbers.

Clad Temperature Instrument Tag-ID Naming Convention = T E XX Y ZZ, where

XX = Instrument Elevation #, as shown in Figure 3.12-12 = 1 through 10 and 1 through 3

Y = Heater Rod Bundle # = 1 through 8

ZZ = Horizontal Location in Heater Rod Bundle, see below = 1A, etc.

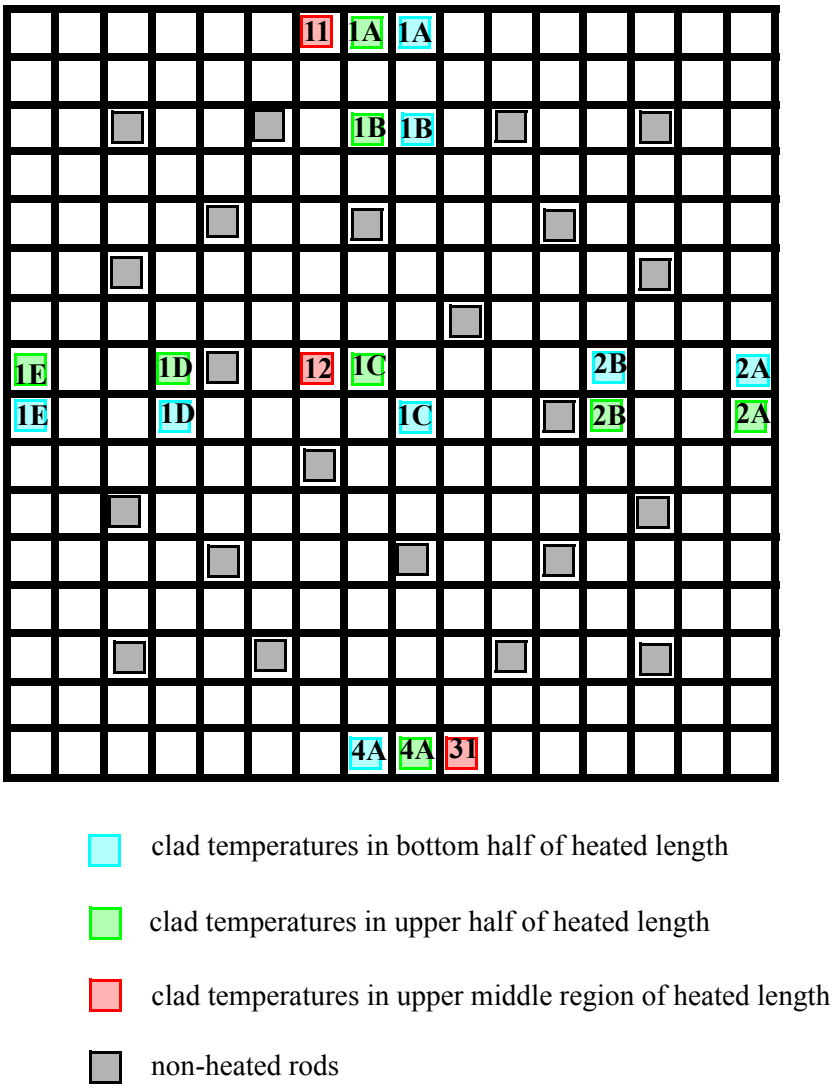

Figure C.3-4. SCTF clad temperature instrument horizontal position in each 16x16 heater rod bundle.

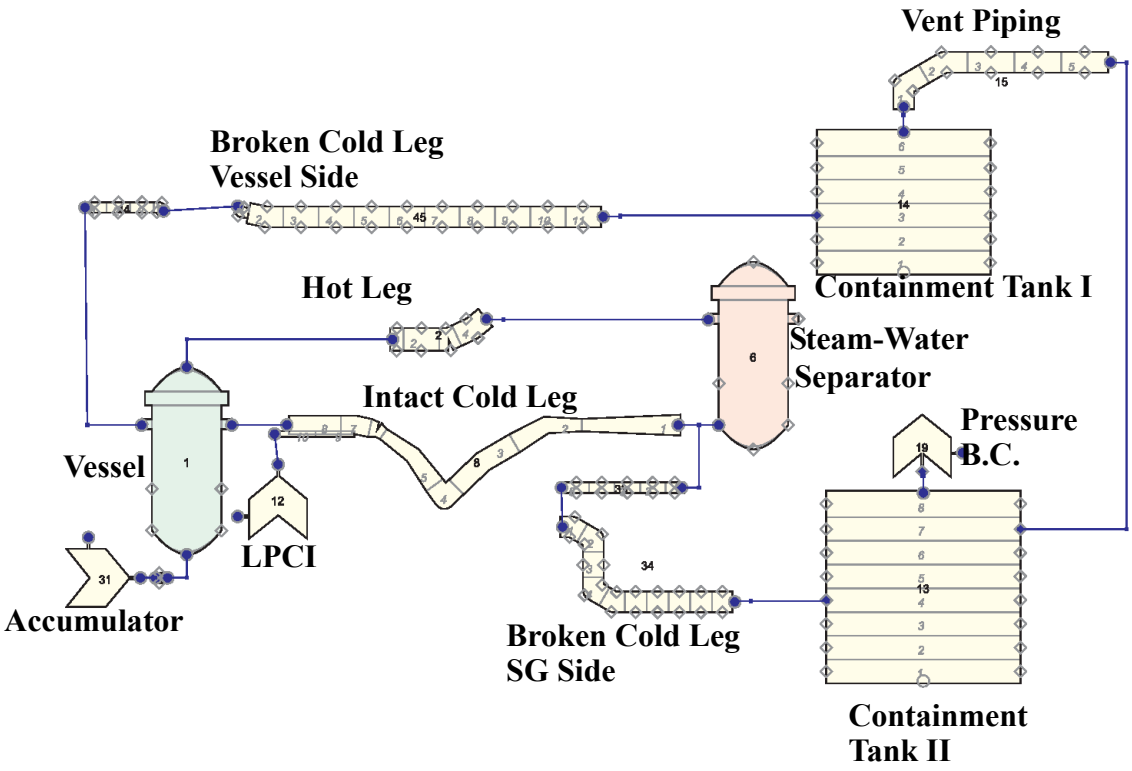

Figure C.3-5. Schematic of the TRACE SCTF Model

The heated bundle noding uses two TRACE VESSEL levels between each spacer grid elevation. This results in an axial level boundary approximately every 0.333 meters in the heated bundle length. This node scheme was judged to be adequate for modeling the TRACE calculated reflood behavior in the core region.

PIPE components 13 and 14 represent two large containment tanks which caught fluid discharged from each side of the break. A pressure boundary condition is imposed on containment tank II.

Vessel heat structure components are numbered with the 700 and 900 series. Figure C.3-8 illustrates the VESSEL 1 and 6 heat structures. HTSTR number 951 through 958 represent rods in the 8 rod bundles.

The loop flow resistances were calibrated by modeling SCTF loop steam flow tests as discussed in Reference 12. Vessel resistance flow tests were not reported. Therefore, since the geometry of the SCTF core is similar to the CCTF core, the vessel flow resistance (core inlet, core outlet, and grids loss values) was set to be the same as what was used in CCTF.

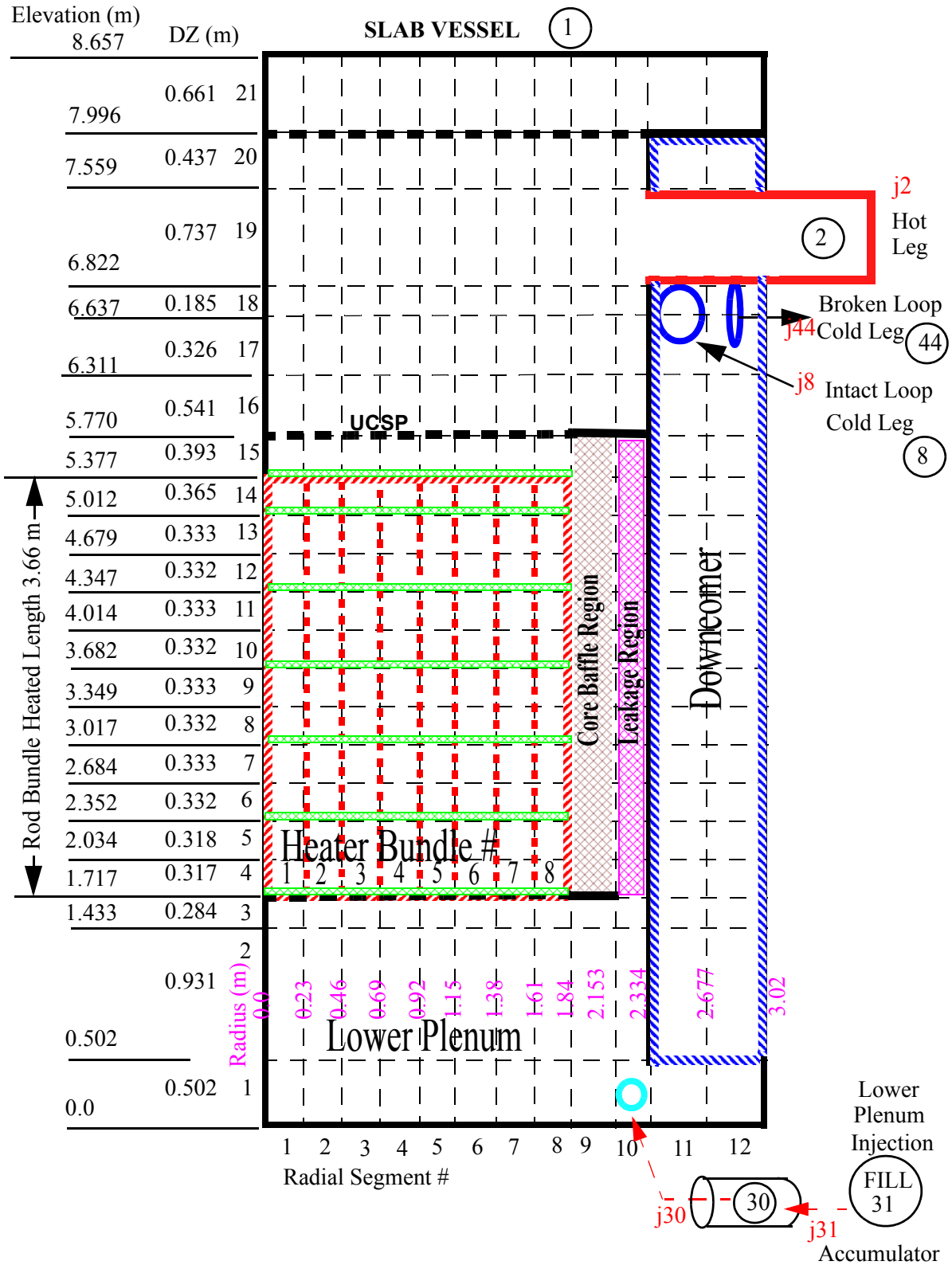

Figure C.3-6. TRACE Model of SCTF Vessel (Component # 1)

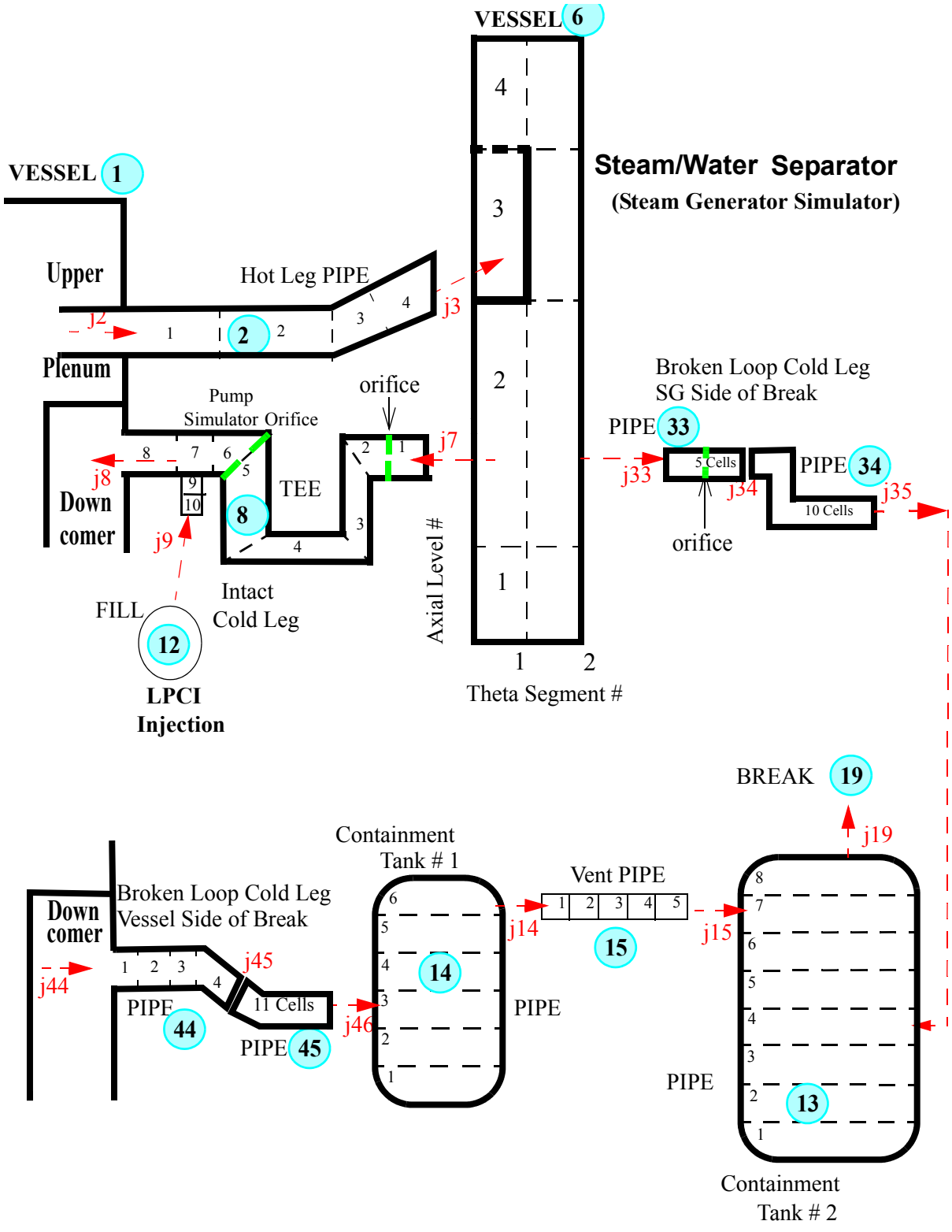

Figure C.3-7. TRACE Model of SCTF Loop Piping and Steam/Water Separator.

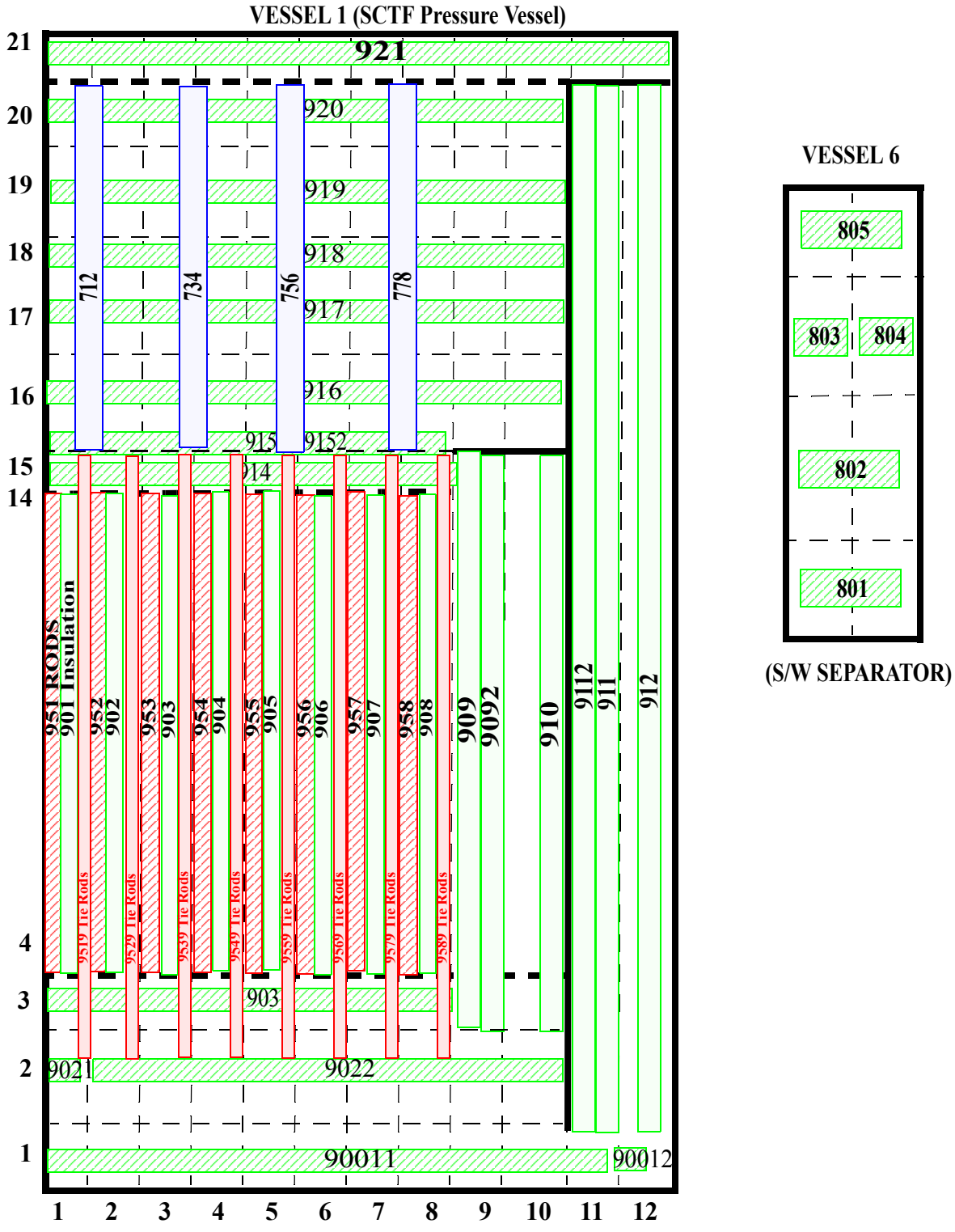

Figure C.3-8. TRACE Heat Structures in the Pressure Vessel and S/W Separator.

C.3.4. Tests Simulated

The seven tests simulated with TRACE code were Runs 604, 605, 606, 607, 611, 621, and 622 (Refs. 3 through 9). They are simulated PWR reflood tests, assuming a full double ended cold leg pipe break, accumulator flow into the lower plenum and LPCI flow into either the intact loop cold leg pipe or the lower plenum. The tests were conducted as follows: First the desired initial system pressure was established with the system steam-filled except for the lower plenum which was partially filled (up to the 1.6 m level) with saturated water. At time zero power was delivered to the core. When four cladding temperatures exceeded a specified setpoint (1013 K to 1137 K, depending upon the test) accumulator injection into the lower plenum began. BOCREC (beginning of core recovery) began when liquid began entering the core, about 2 - 3 seconds after the start of accumulator injection. Core power was held steady for 40 seconds after the beginning of accumulator injection and thereafter followed a "1.02 ANS Standard + Actinides" decay curve. Accumulator injection was stopped at ~55 seconds after it began and LPCI was initiated.

Runs 604, 605, 606, 607 and 611 were gravity reflood tests. In the gravity reflood tests, the vessel downcomer was open to the lower plenum region. LPCI flow was injected into the intact loop cold leg pipe. The accumulator injection rate was nominally 19.5 kg/s and the LPCI rate was nominally 5.1 kg/s for the gravity reflood tests

Runs 621 and 622 were forced reflood tests. In the forced reflood tests, the vessel downcomer bottom was blocked off from the lower plenum. Both accumulator flow and LPCI flow were into the bottom of the lower plenum; the downcomer was isolated from reflood water. For the forced reflood tests the accumulator injection rate was nominally 12 kg/s and the LPCI rate was 5.5 kg/s.

Run 604 is a base case test with nominal power and a nominal radial power distribution. The remaining gravity reflood runs are variations on the base case run - different radial power profiles and/or different system pressure.

Forced reflood Run 621 is a counterpart to gravity reflood Run 611 (Steep radial power profile and nominal system pressure). Run 622 is a counterpart to Run 605 (flat radial power profile and nominal pressure). The seven tests being simulated with the TRACE code are summarized in Table C.3.1. Each test was assigned both a run number and a test number.

A TRACE model was constructed for each of the tests in Table C.3.1 using boundary conditions (radial power distribution, system pressure, and ECC flow vs. time) from the test data. Each test was simulated by initiating power to the bundles. ECC injection was initiated at the times shown in Table C.3.1. The core power was held constant for forty seconds after ECC started and then followed the same decay curve as the test. Each simulation was terminated at 700 seconds.

Table C.3.1. SCTF Test Summary

Test/Run	Forced or Gravity Reflood	Radial Power Profile [a]	Containment Pressure (MPa)	Accumulator Injection Started (s)	BOCREC [b] Time (s)	Max. Rod Temp. at BOCREC (K)	PCT [c] (K)
S2-SH1/604	Gravity	Nominal	0.20	143.	146.	1076	1166
S2-SH2/605	Gravity	Flat	0.20	136.5	139.	1067	1142
S2-01/606	Gravity	Steep	0.24	148.	150.	1167	1167
S2-02/607	Gravity	Nominal	0.15	146.	149.5	1081	1205
S2-06/611	Gravity	Steep	0.20	146.5	150.	1163	1244
S2-16/621	Forced	Steep	0.20	145.	148.	1158	1224
S2-17/622	Forced	Flat	0.20	135	138	1033	1080

a. Power in each pair of radial bundles 1-2/3-4/5-6/7-8 (kW): nominal: 891/948/903/818; Flat: 890/890/890/890; Steep: 890/1068/890/712

b. BOCREC = Bottom of Core Recovery

c. PCT = Peak Clad Temperature. The highest cladding temperature observed in the test.

C.3.4.1. Simulation of SCTF Run 604.

Figure C.3-9 through Figure C.3-11 show the measured and calculated delta-P's for the downcomer, bundle 4, and the upper plenum. These dPs are indicative of the water level at the respective locations.

The calculated and measured dP for the downcomer (Figure C.3-9) are in very good agreement through the first 400 seconds of the test, when accumulator injection stopped. After that the calculated downcomer dP rises above the data mainly because the quenching of the upper half of the core was delayed in TRACE relative to the data. The data report for Run 604 states that there was almost no ECC bypass during Run 604. The TRACE simulation was in substantial agreement with this result, showing a slight but steady bypass flow of 0.3 kg/s (about 5% of the LPCI flow) from 210 seconds onward.

The measured mass inventory in bundle 4 (Figure C.3-10) increased smoothly and rapidly during accumulator injection and steadily increased at a slower rate once accumulator injection stopped and LPCI began at 200 seconds. The TRACE calculation of bundle 4 dP is quite erratic throughout the transient and is generally higher than the data for the first 400 seconds, and below the data for subsequent times.

The dP measurement above the bundle 4 upper core support plate shows an initial accumulation of liquid followed by a 150 s period of no further accumulation followed by a steadily greater accumulation (Figure C.3-11) as the core quenched. The TRACE simulation showed no accumulation of liquid in the upper plenum until 320 seconds followed by a gradual increase and

a leveling off. The simulation did not show the large UP level increase measured in the last 150 seconds because in the simulation the core quenching process was delayed relative to the test.

The calculated upper plenum pressure response (Figure C.3-12) agrees quite well with the measured response. The measured pressure drops below the calculated pressure after 450 seconds due to wholesale core quenching occurring in the test but not in the TRACE simulation. This drop in the measured pressure is accompanied by a rapid rise in the upper plenum measured mass inventory.

Measured and calculated cladding temperatures at four elevations are shown in Figure C.3-13 through Figure C.3-16. At every elevation shown there were at least six different rod surface temperature measurements. At most elevations there was a fairly large variation (20 K - 40 K) in the measured temperatures when accumulator injection began. The measured temperatures shown in the figures are for only rods which were not adjacent to an unheated surface.

At the 0.95 m elevation all the measured temperatures had a similar response both during heatup and after. TRACE calculated a PCT higher than what was measured primarily because its temperature was higher than the measured temperature when reflood began at 143 seconds. Rod quench occurred simultaneously in TRACE and in the test.

The highest temperatures in Run 604 occurred at the 1.91 m elevation (1166 K). From Figure C.3-14 it can be seen that the calculated PCT is in excellent agreement with the measured PCTs at this elevation. Moreover, the calculated temperature history is nearly identical to the measured one.

At the 2.76 m elevation (Figure C.3-15) TRACE's PCT was higher than the highest recorded temperature at that elevation. The calculated temperature turn-around and subsequent decline and quench occurred more slowly and later than actual.

At the 3.62 m elevation (Figure C.3-16) TRACE calculated a peak temperature that was quite close to what was measured for one rod, but considerably higher than other measurements. The calculated quench time was much later than what was measured.

The calculated quench envelope (Figure C.3-17) agrees reasonable well with the actual in the bottom half of the core but lags the actual quench in the upper half, the lag increasing with increasing elevation.

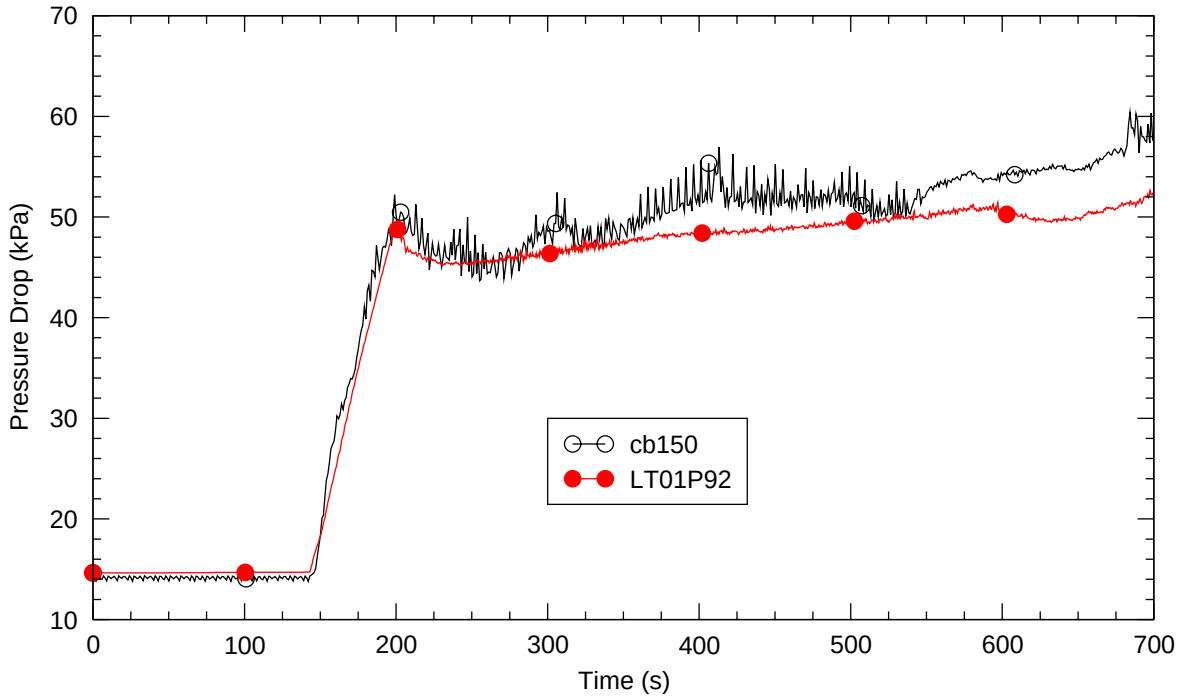

Figure C.3-9. Measured and Calculated Pressure Differential in the Vessel Downcomer - SCTF Run 604

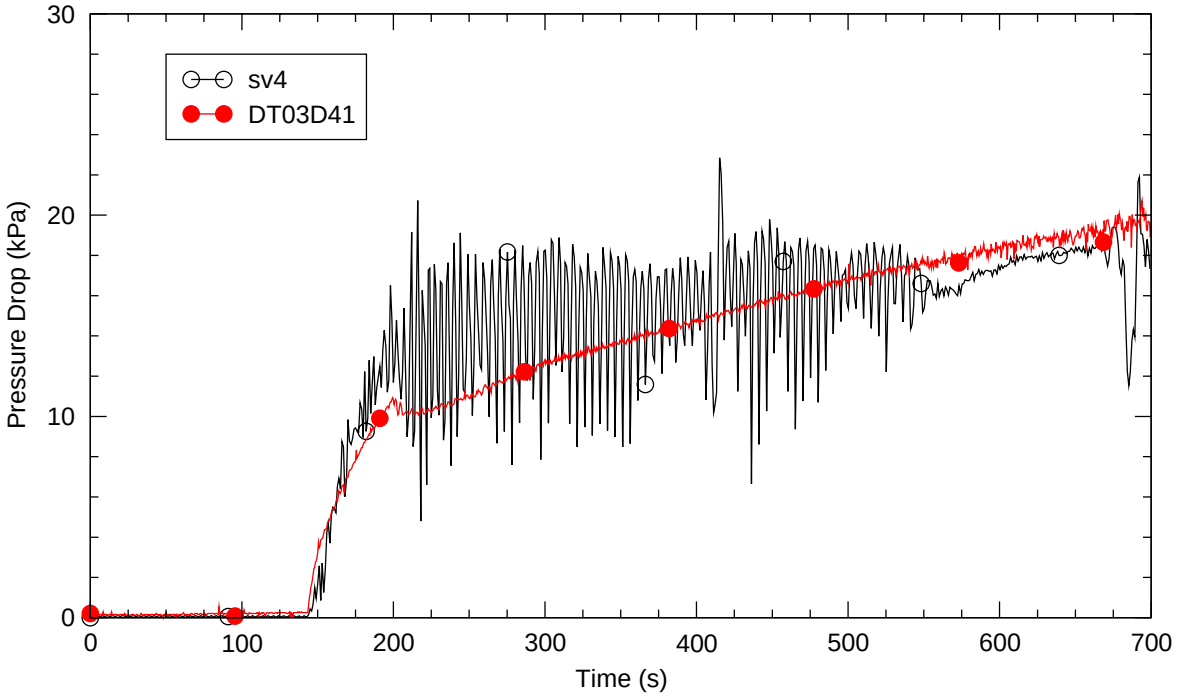

Figure C.3-10. Measured and Calculated Differential Pressure in Bundle 4 - SCTF Run 604

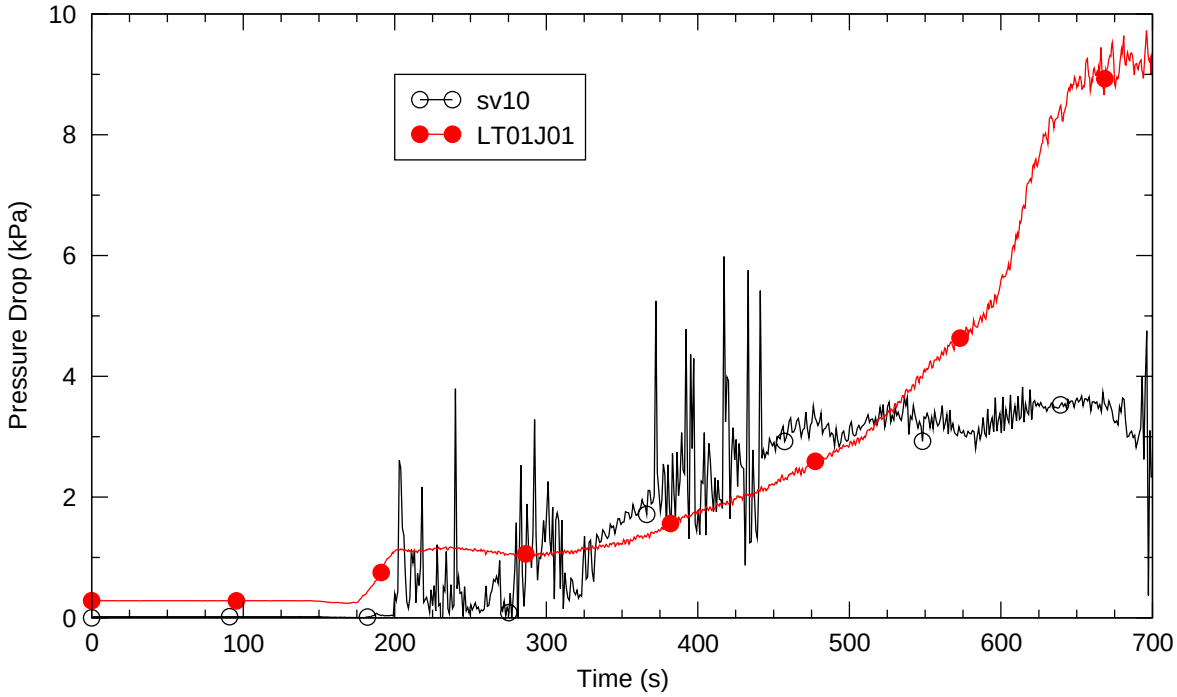

Figure C.3-11. Measured and Calculated Differential Pressure in the Upper Plenum - SCTF Run 604

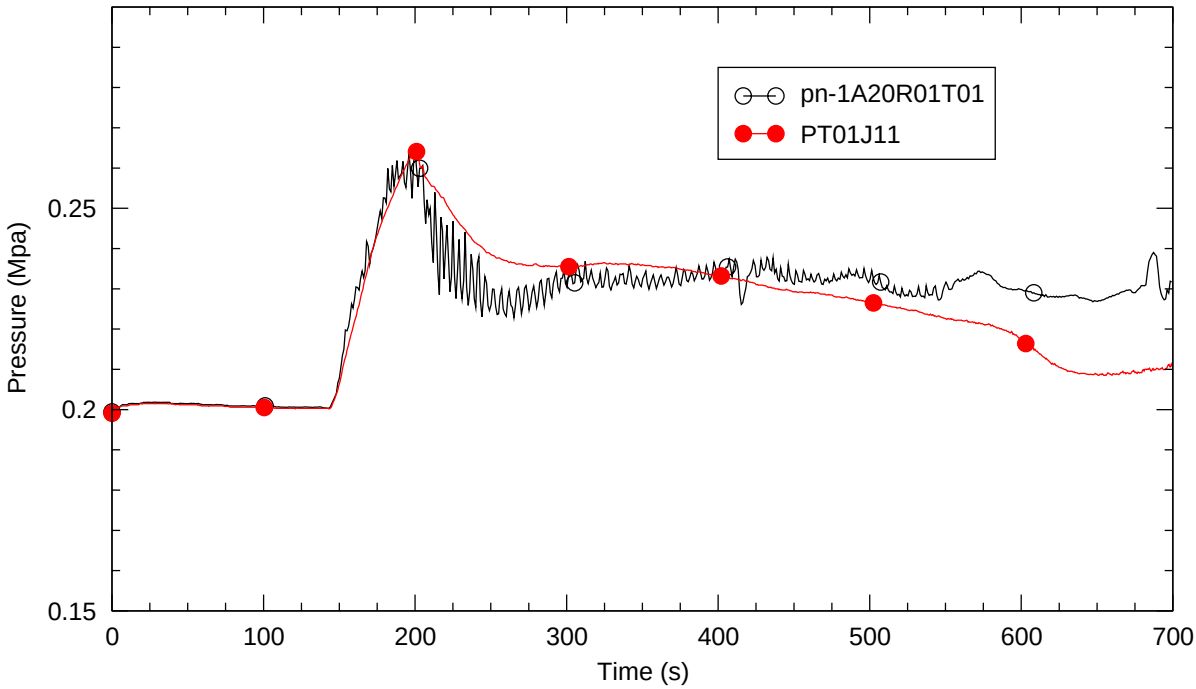

Figure C.3-12. Measured and Calculated Upper Plenum Pressure - SCTF Run 604

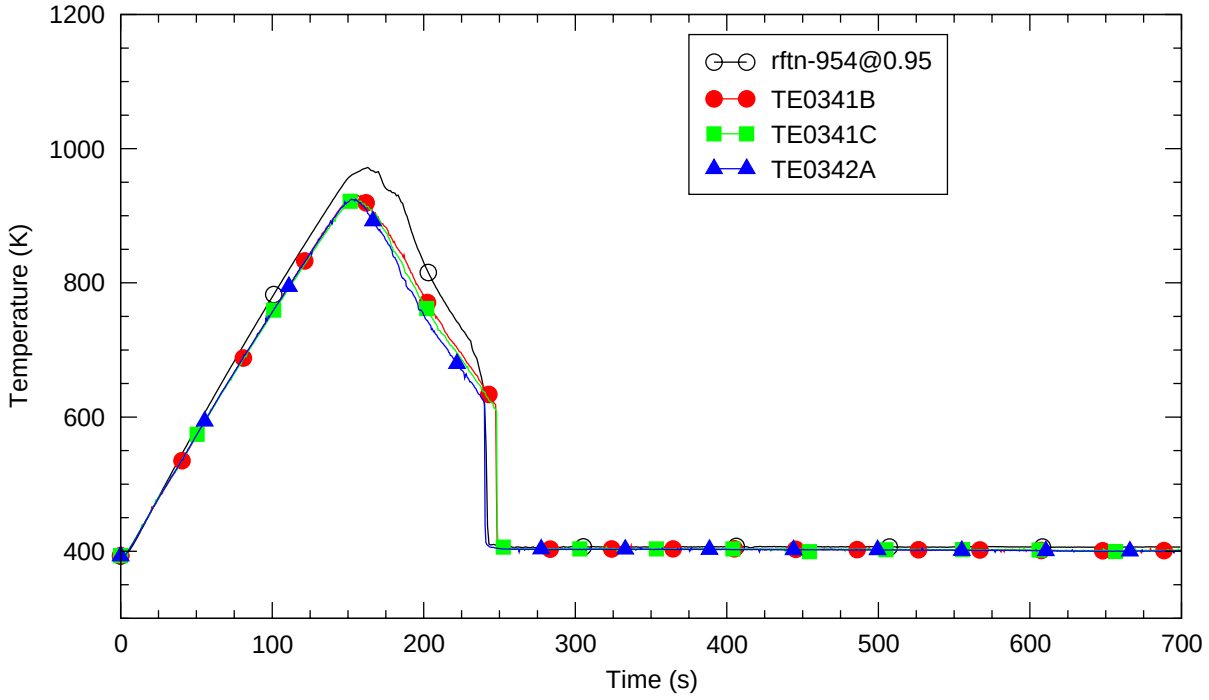

Figure C.3-13. Measured and Calculated Primary Cladding Temperature at the 0.95 m elevation in Bundle 4 - SCTF Run 604

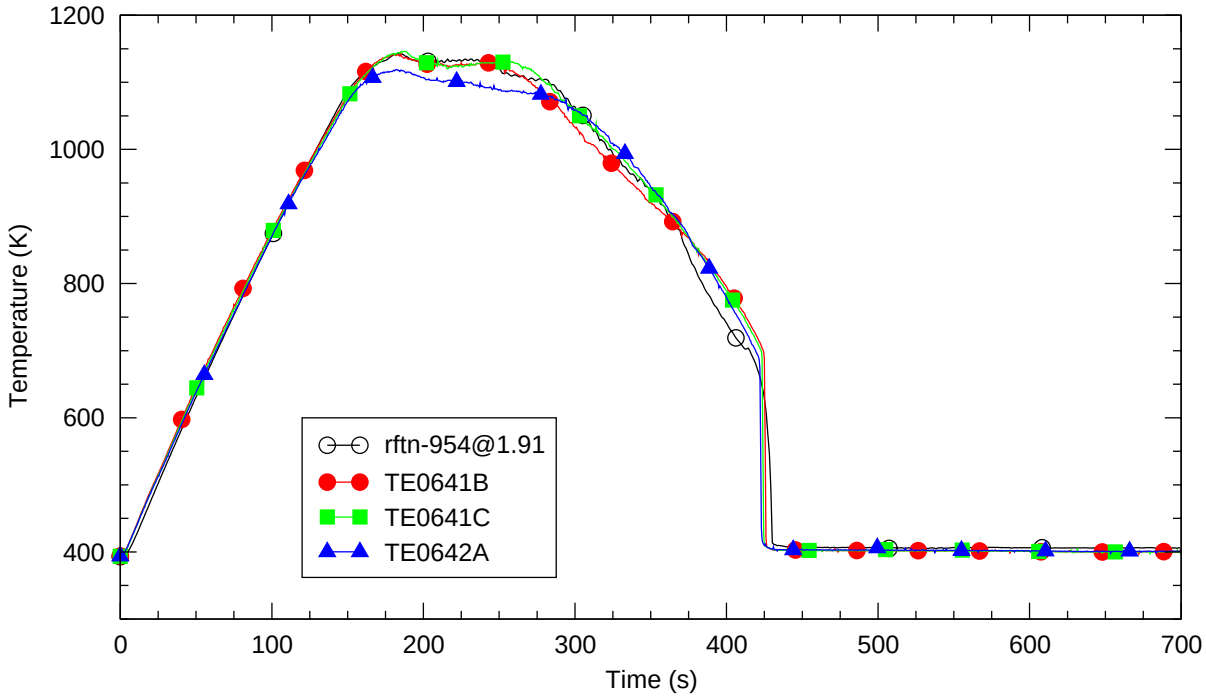

Figure C.3-14. Measured and Calculated Primary Cladding Temperature at the 1.91 m elevation in Bundle 4 - SCTF Run 604

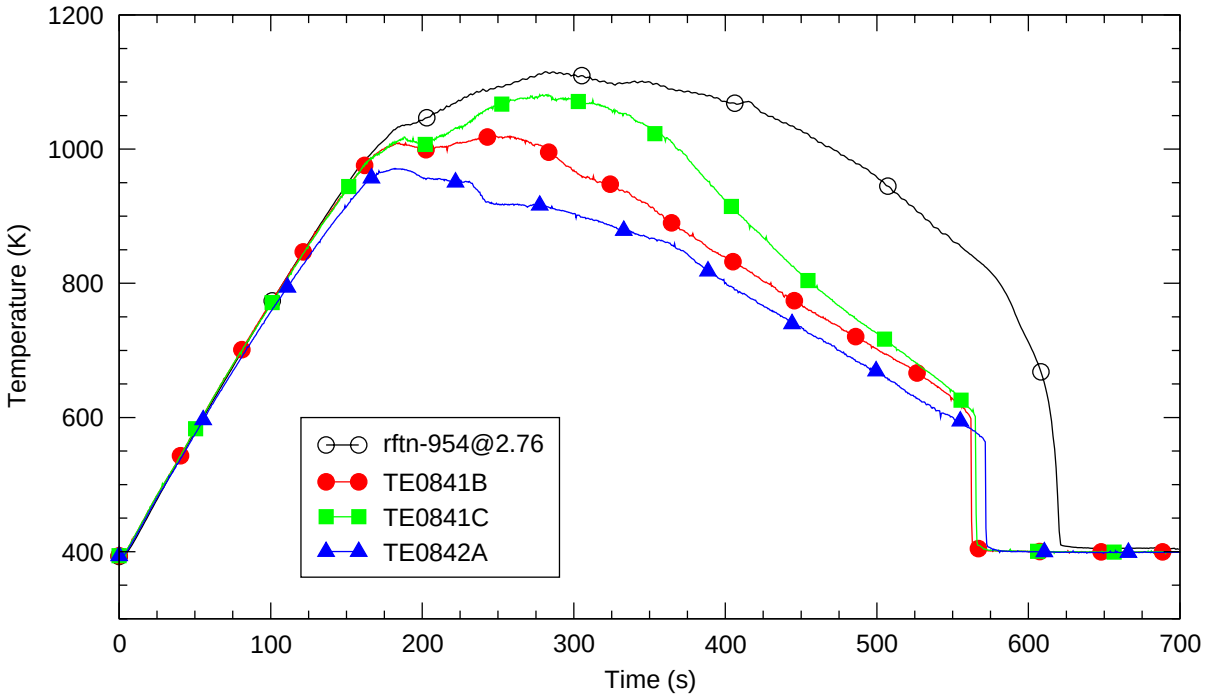

Figure C.3-15. Measured and Calculated Primary Cladding Temperature at the 2.76 m elevation in Bundle 4 - SCTF Run 604

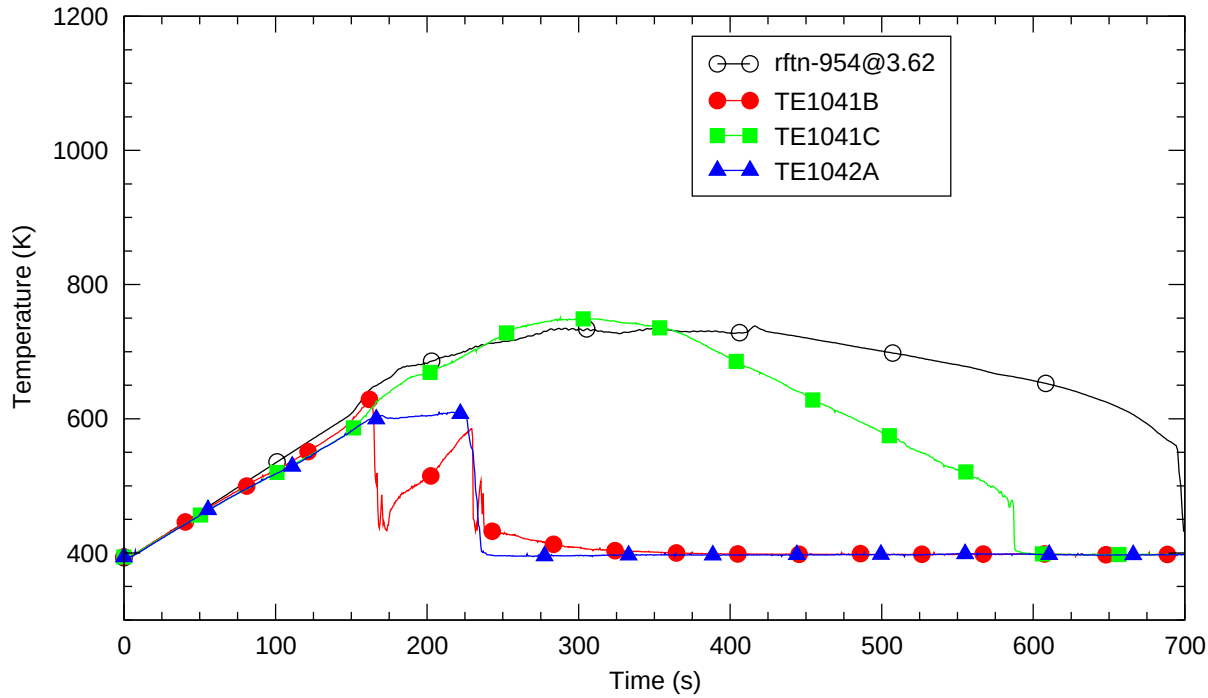

Figure C.3-16. Measured and Calculated Primary Cladding Temperature at the 3.62 m elevation in Bundle 4 - SCTF Run 604

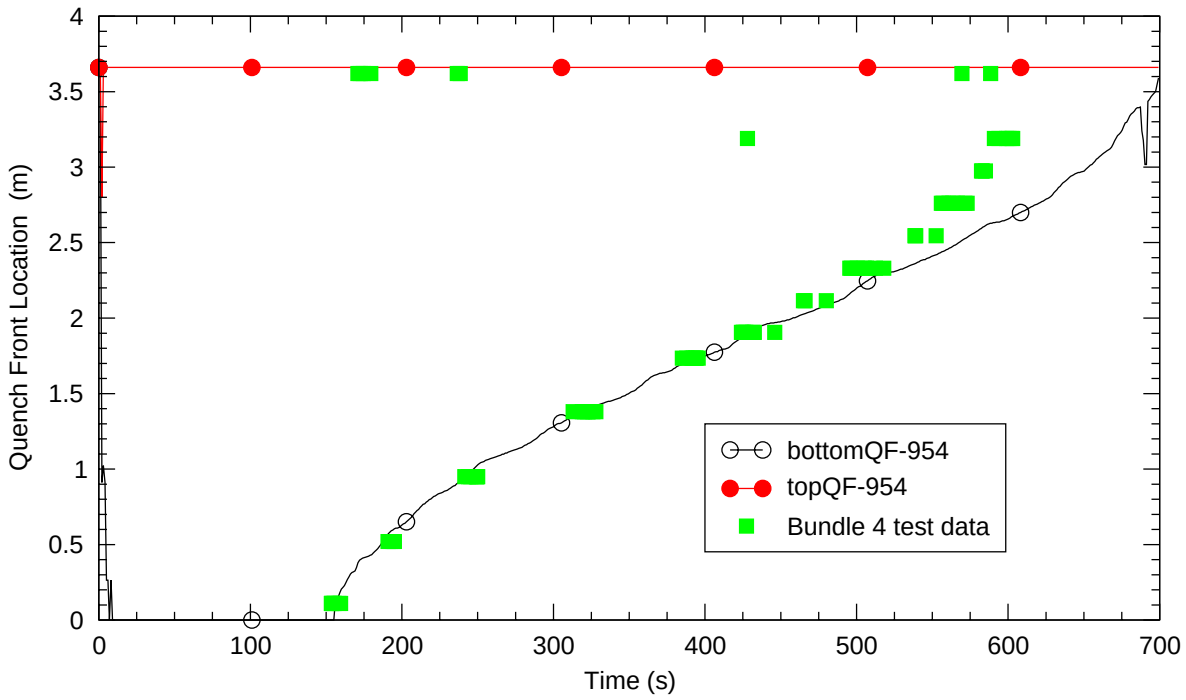

Figure C.3-17. Measure and Calculated Quench Fronts in Bundle 4 - SCTF Run 604

C.3.4.2. SCTF Runs 605 and 611 - Power Profile Effects

Run 605 and Run 611 are the same as Run 604 except for their radial power profile. The purpose of these tests was to experimentally determine the effect of lateral distributions in core power and stored energy. The lateral peaking was 1.0 in Run 605 (flat profile), 1.07 in Run 604 (base profile), and 1.2 in Run 611 (steep profile).

According to section 5.2.2 of Reference 2 the three tests behaved very similarly hydraulically. So did the three TRACE simulations of these tests. The only significant differences were rod temperature responses, with the PCT being higher the more steeped the power profile.

Figure C.3-18 indicates the collapsed level in bundle 4. The three measured dPs are essentially overlays of one another as are the three calculated dPs.

Figure C.3-19 compares the calculated and measured PCTs for bundles 3 and 4. The figure shows that TRACE and the measured PCTs behave very similarly in response to the change in radial power profile. TRACE does a very good job of simulating the effect of power change on PCT.

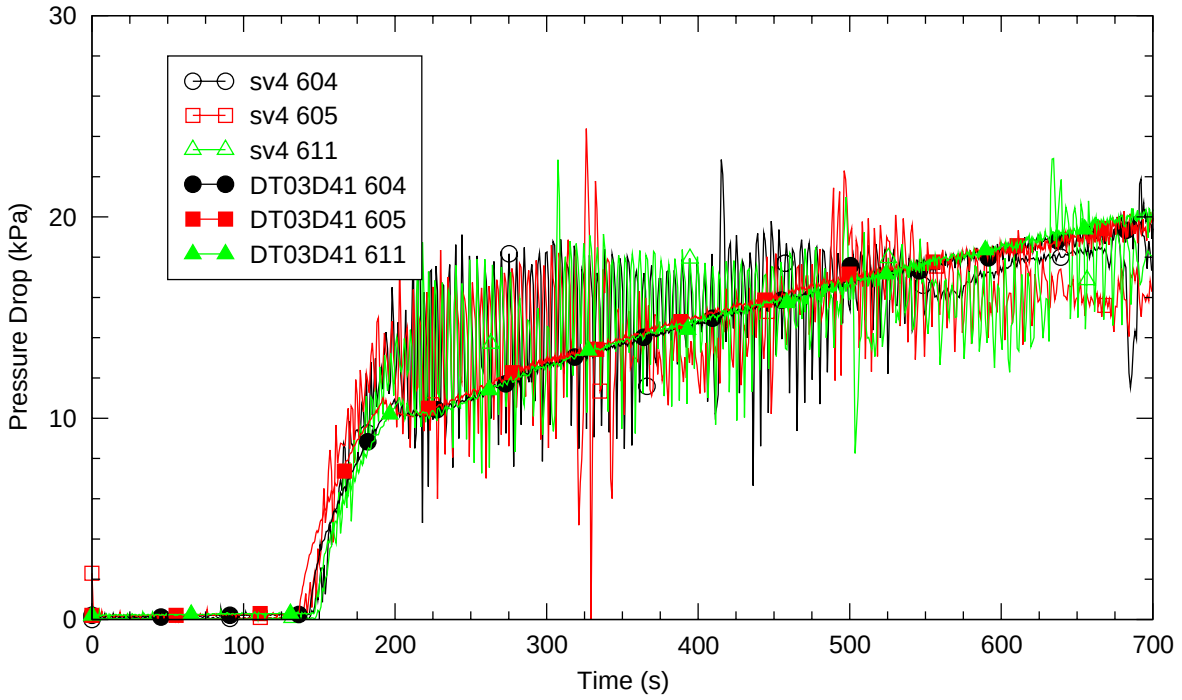

Figure C.3-18. Calculated and Measured dP for Bundle 4 for Runs 604, 605, and 611

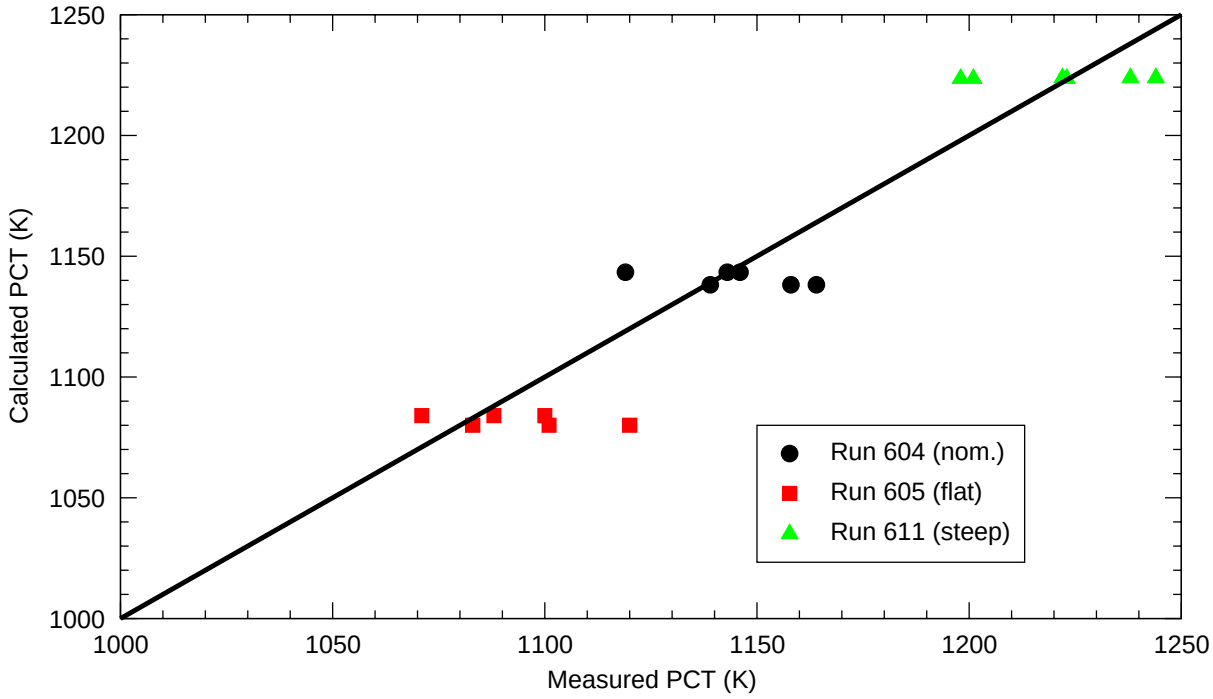

Figure C.3-19. Calculated and Measured PCTs Bundles 3 and 4 for Runs 604, 605, and 611, 1.91 m Elevation

C.3.4.3. SCTF Runs 606 and 607 - Pressure Effects

This section describes the results of Run 606, the gravity reflood, steep power profile, high pressure test and Run 607, the gravity reflood, nominal power profile, low pressure test. The results are compared to the corresponding base case tests. Run 607 (P_{cont} = 0.15 MPa) is compared to Run 604 (0.20 MPa) and Run 606 (P_{cont} = 0.20 MPa) is compared to Run 611 (0.24 MPa).

An increase in system pressure causes an increase in steam density. Higher steam density leads to an increase in local heat transfer coefficients in the core due to a greater mass of steam in contact with the rods at any given time. Higher steam density also results in a decrease in loop pressure drop and hence an increase in core mass inventory. The net effect of an increase in pressure is lower PCT and earlier quench times.

Figure C.3-20 shows the pressure drop across bundle 4 for Runs 604 and 607 while Figure C.3-21 shows the same pressure drop for Runs 606 and 611. In both figures one sees that the run with the higher system pressure also has the greater bundle pressure drop, indicating a higher collapsed liquid level in the bundle. This is apparent for the test data but less so for the calculations because the pressure traces are so erratic.

Figure C.3-22 shows the cladding temperature at the 1.91 m elevation in bundle 4 for Runs 604 and 607 (nominal radial power profile). TRACE calculated about the same PCT for Run 604 (higher pressure case) as it did for Run 607 (lower pressure case). The measurement (TE0641C) showed a PCT of 1146 K for Run 604 and 1168 K for Run 607. The TRACE calculation of the change in PCT due to 50 kPa reduction in pressure is smaller than what was measured. TRACE calculated a delay in quench time due to the pressure reduction that was nearly the same as what was measured. This indicates that TRACE is correctly calculating the influence of pressure on system response.

Figure C.3-23 shows the 1.91 m elevation, bundle 4 cladding temperature for Runs 606 and 611 (steep radial power profile). In this case TRACE again calculated only a slight change in PCT for a 40 kPa reduction in system pressure, similar to what the data show. TRACE calculated a delay in quench time due to the pressure decrease. The magnitude of the delay was the same as what was measured.

C.3.4.4. Run 621 - Forced Reflood with Steep Radial Power Profile

Run 621 was a forced reflood test. The bottom of the downcomer was blocked so no ECC could enter it. Also, LPCI was switched from the cold leg to the lower plenum. In Run 621 the ECC flow was reduced from that of Run 611 to compensate for not having to fill the downcomer. Run 621 had a steep radial power profile and is a counterpart to gravity reflood test Run 611.

Figure C.3-24 and Figure C.3-25 show the delta-p across bundle 4 for Run 621 and Run 611, respectively. The calculated dP for Run 621 is much smoother than that for Run 611 because

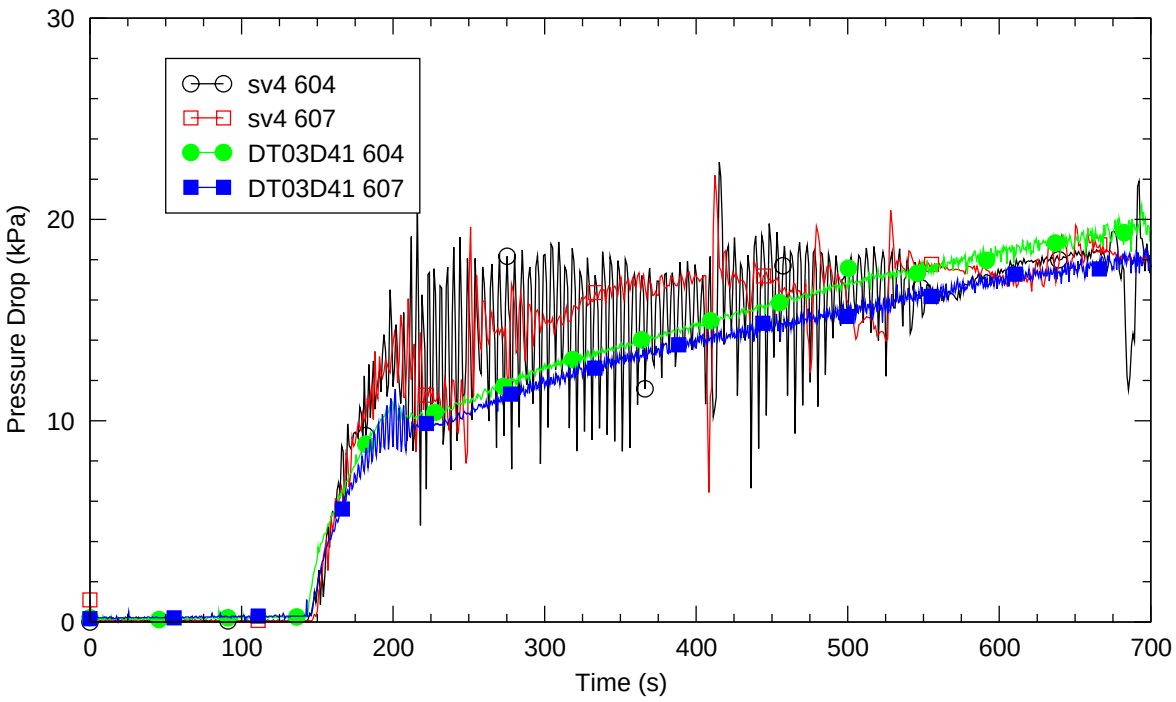

Figure C.3-20. Calculated and Measured dP for Bundle 4 for Runs 604 and 607

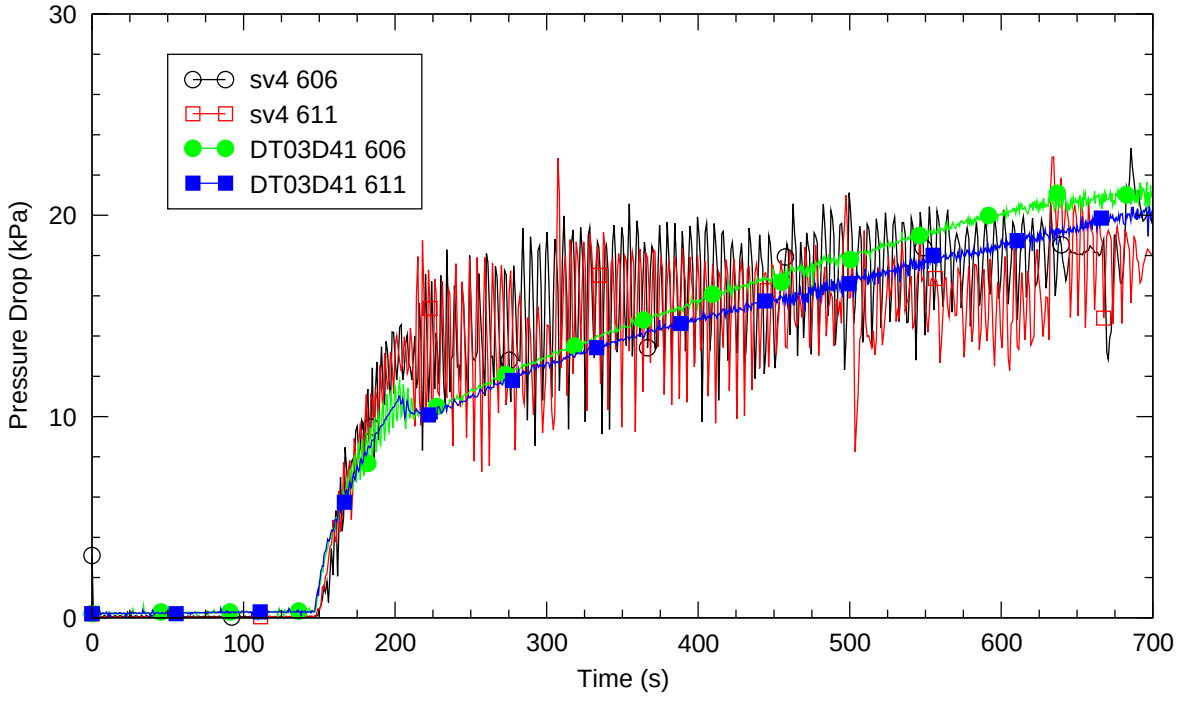

Figure C.3-21. Calculated and Measured dP for Bundle 4 for Runs 606 and 611

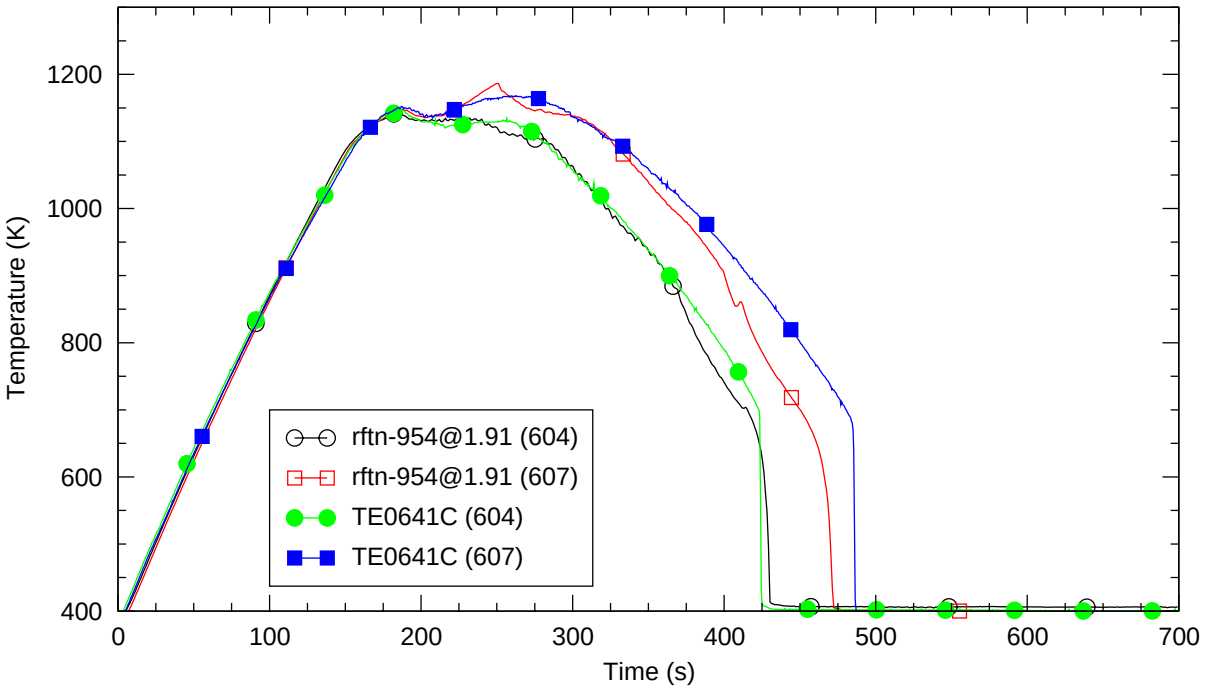

Figure C.3-22. Calculated and Measured Cladding Temperatures at 1.91 m for Runs 604, 607

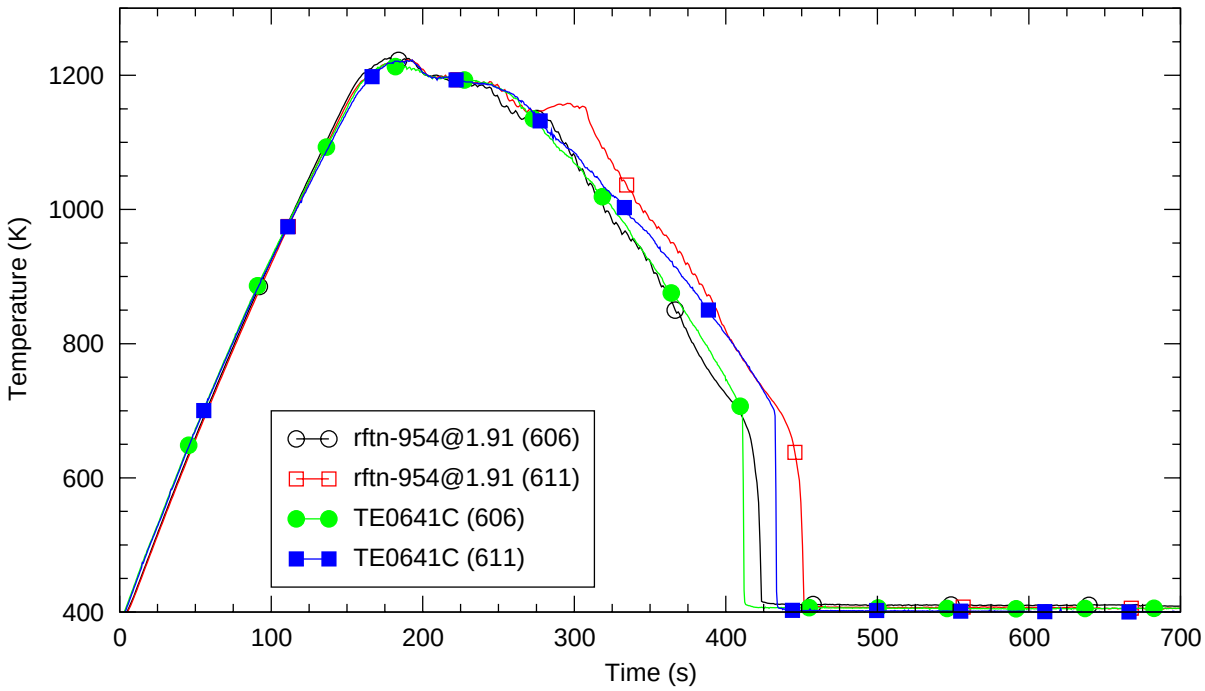

Figure C.3-23. Calculated and Measured Cladding Temperatures at 1.91 m for Runs 606 and 611

gravity driven downcomer-core level oscillations cannot occur when the downcomer is blocked. Note that no reflood oscillations are evident in the data. The agreement between calculated and measured delta-p is better in Run 621. The measured and calculated bundle dPs depart from one another at about 450 s. This is due to the upper part of the core quenching in the tests but not in the simulations. From Figure C.3-26 one sees that the calculated water level in the upper plenum began much sooner in the forced reflood test (621) simulation as compared to the gravity reflood simulation (611) According to the Run 621 data report there was no significant accumulation of liquid in the S/W separator during the test. The TRACE simulation also shows no carry out of water from the upper plenum until the final 50 seconds of the simulation.

Run 611 and Run 621 measured and calculated bundle PCTs are depicted in Figure C.3-27. The points on the lower left side are from bundles 7 and 8; those on the upper right are from bundles 3 and 4; and those in the middle are from bundles 1, 2, 5, and 6. Overall, TRACE did a better job of calculating the PCTs for the forced reflood test (Run 621): the RMS difference between TRACE and the data is 20.1 K for Run 621 and 26.7 K for Run 611.

Measured and calculated quench fronts for Run 621 are shown in Figure C.3-28 while those for Run 611 are shown in Figure C.3-29. TRACE did a much better job of matching the quench front data for the forced reflood test (Run 621) than it did for the gravity reflood test (Run 611). Even so, TRACE still missed the quenching of the upper 1/4 of the core, calculating quench to occur later than what was measured.

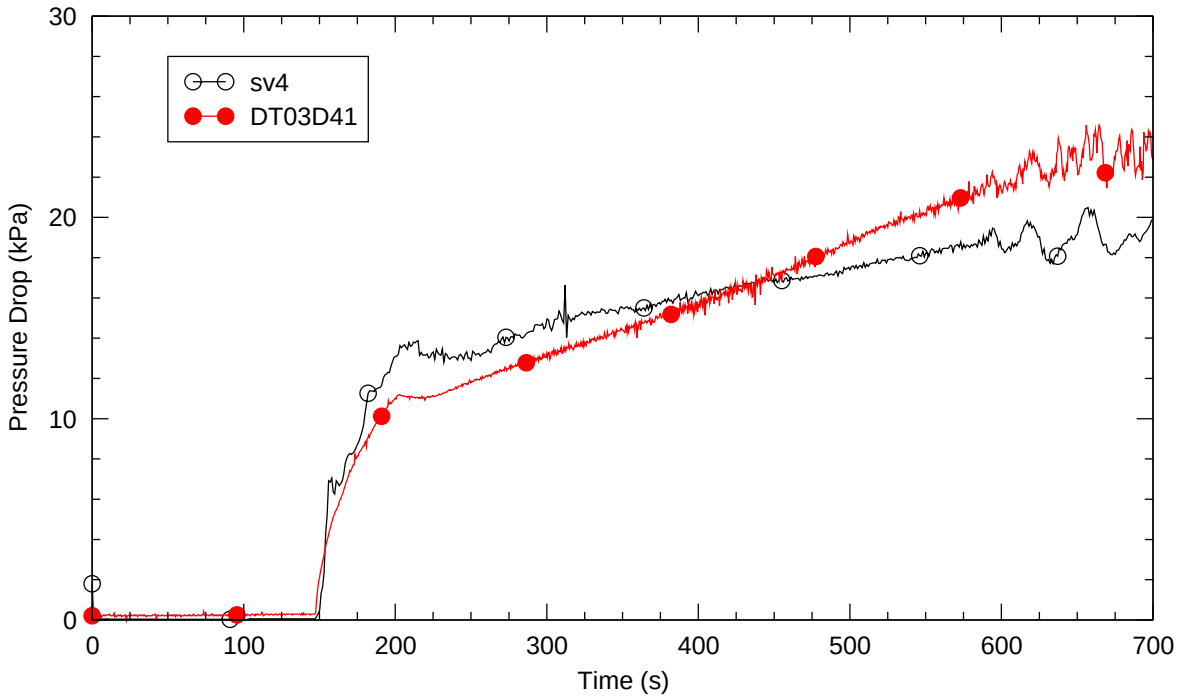

Figure C.3-24. Calculated and Measured dP for Bundle 4 for Run 621

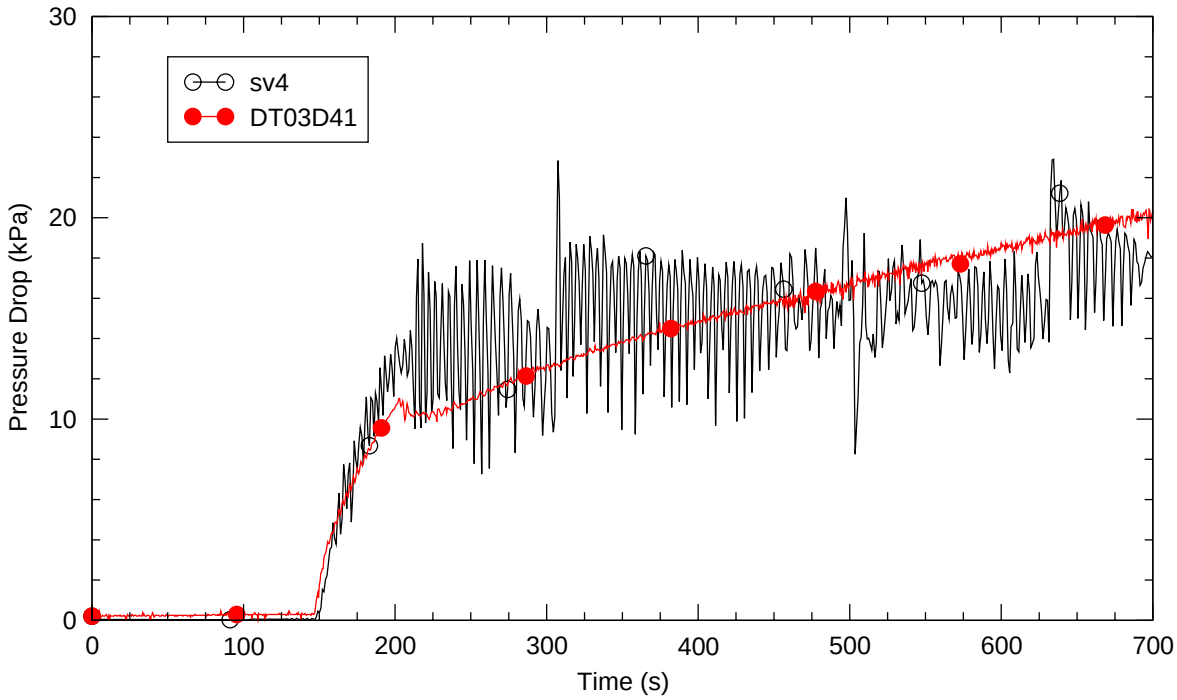

Figure C.3-25. Calculated and Measured dP for Bundle 4 for Run 611

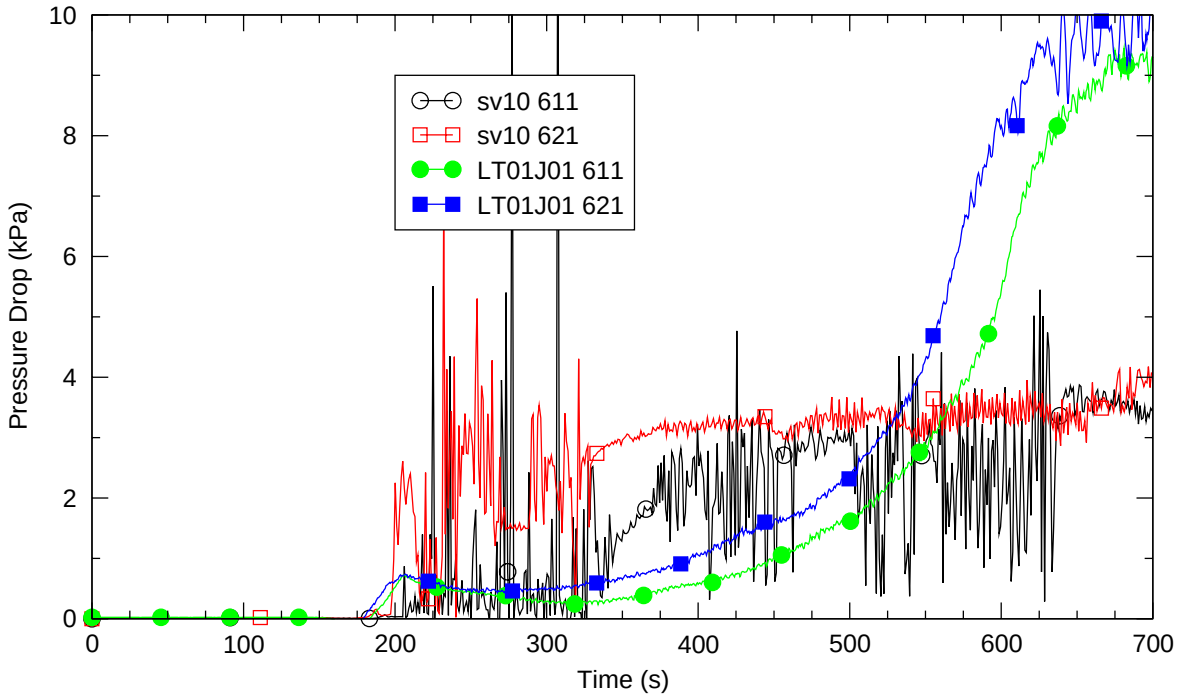

Figure C.3-26. Calculated and Measured dP in the Upper Plenum for Run 621 and 611.

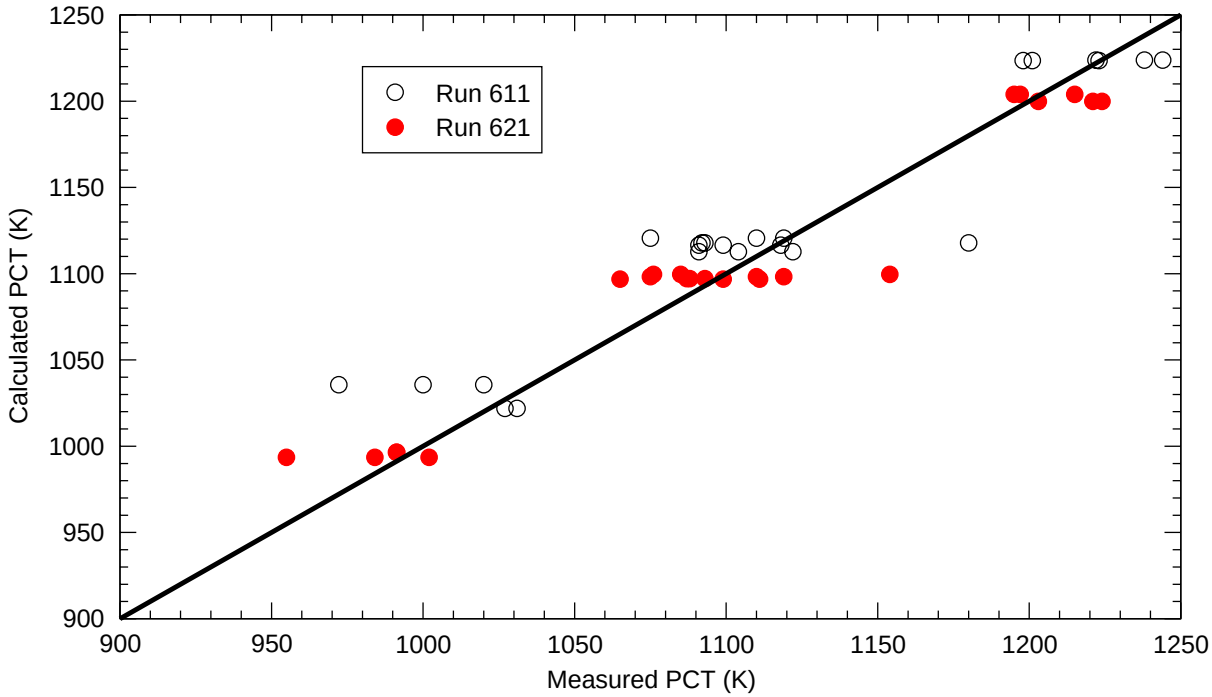

Figure C.3-27. Calculated and Measured PCTs for all bundles - Run 611 and Run 621, 1.91 m Elevation

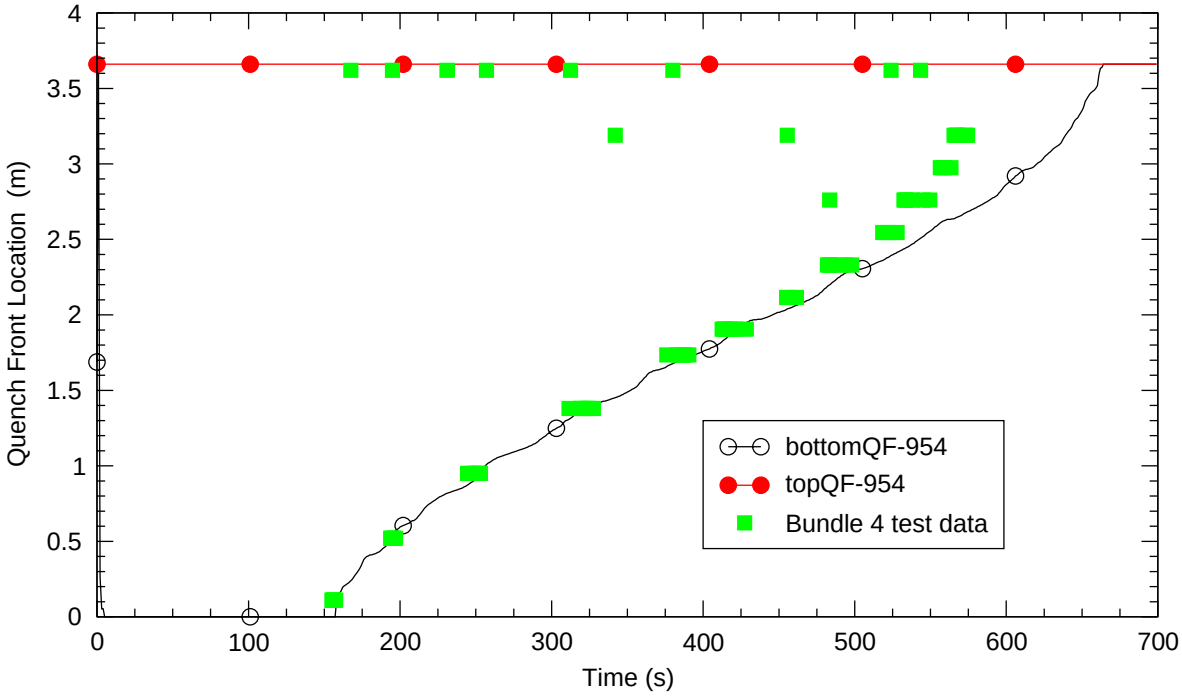

Figure C.3-28. Calculated and Measured Bundle 4 Quench Fronts for Run 621.

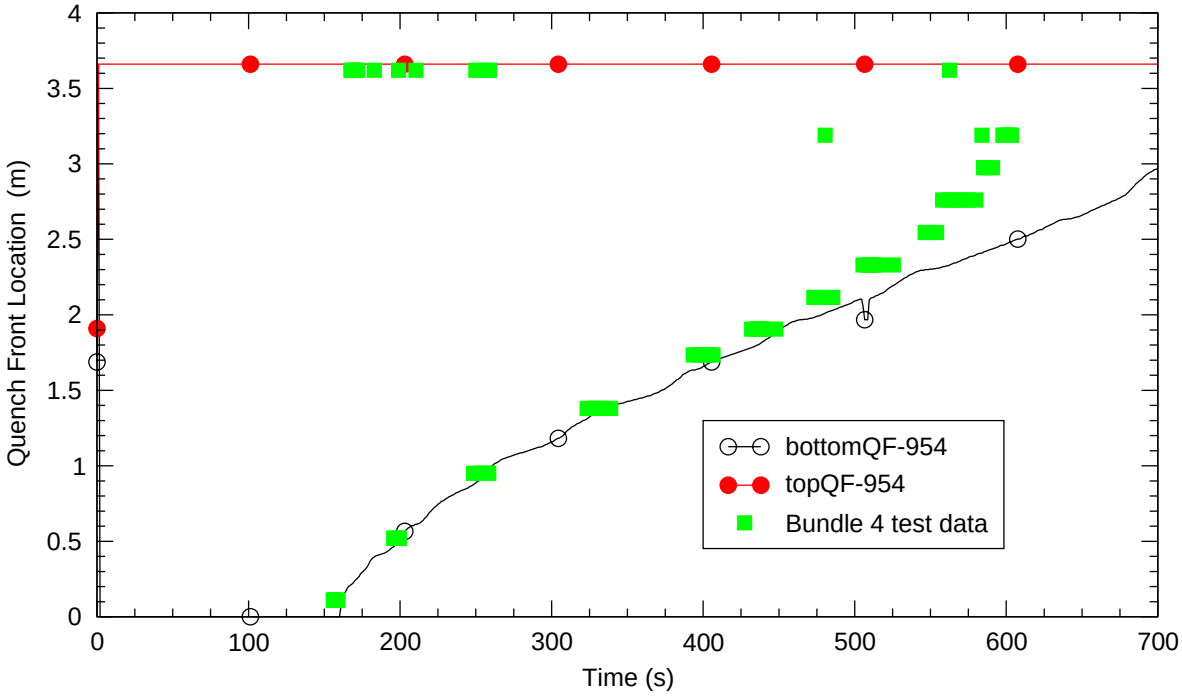

Figure C.3-29. Calculated and Measured Bundle 4 Quench Fronts for Run 611

C.3.4.5. Run 622 - Forced Reflood with Flat Radial Power Profile

Run 622, like Run 621, was a forced reflood test - the bottom of the downcomer was blocked so no ECC could enter it. LPCI was into the lower plenum rather than into the cold leg. Run 622 had a flat radial power profile and is a counterpart to gravity reflood test Run 605. In Run 622 the ECC flow was reduced from that of Run 605 to compensate for not having to fill the downcomer.

The hydraulic behavior of Run 605 and 611 are similar, as is the hydraulic behavior of Run 621 and 622. A comparison of core and upper plenum dPs for runs 622 and 605 is therefore not given here. The discussion given for Run 621 vs. 611 regarding core and upper plenum behavior also applies to Run 622 vs. Run 605.

Run 605 and Run 622 measured and calculated bundle PCTs are depicted in Figure C.3-30 With respect to PCT TRACE did an slightly better job of calculating the PCTs for the forced reflood test (Run 622) than it did for the reflood test (Run 605). The RMS difference between TRACE and the data is 20.0 K for Run 622 and 20.8 K for Run 605, with TRACE on the whole over predicting the data.

Measured and calculated quench fronts for Run 622 are shown in Figure C.3-31 while those for Run 605 are shown in Figure C.3-32. TRACE did a better job of matching the quench front data

for the forced reflood test (Run 622) than it did for the gravity reflood test (Run 605). In the upper 1/3 of the core the calculated quench occurred later than what was measured.

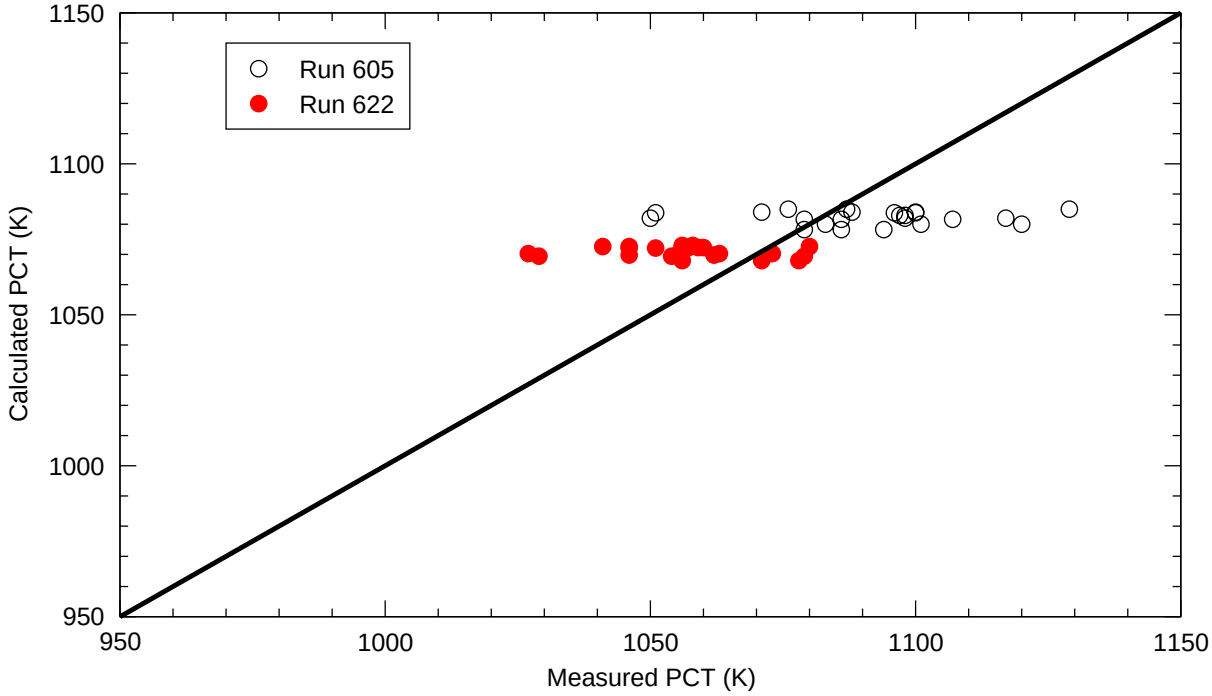

Figure C.3-30. Calculated and Measured PCTs for all bundles - Run 605 and Run 622, 1.91 m Elevation

C.3.5. Assessment Results Summary

The TRACE simulations of SCTF are in reasonable agreement with the experimental data overall and in quite good agreement with measured PCTs at the core midplane. Calculated PCTs at the upper core elevations exceed measured PCTs by between 50 and 200 K. It is believed that this over prediction of upper elevation temperatures is due to the lack of a grid spacer model in TRACE.

The TRACE simulations all show the amount of liquid in the upper plenum is greater than what was measured during the first half of each test, but less than what was measured in the latter half of the tests. TRACE calculated that almost no liquid was carried from the upper plenum into the steam/water separator, in agreement with the test data.

Calculated quench times are in good agreement with measured ones for the bottom 1/3 of the core. For higher elevations the calculated quench times fall further and further behind that data as elevation increases. For the top 1/3 of the core calculated quench times lag the data by up to 200 seconds. In the tests many of the heater rods exhibited very early quench at the core outlet measurement location. This quenching phenomena never occurred in the TRACE simulations.

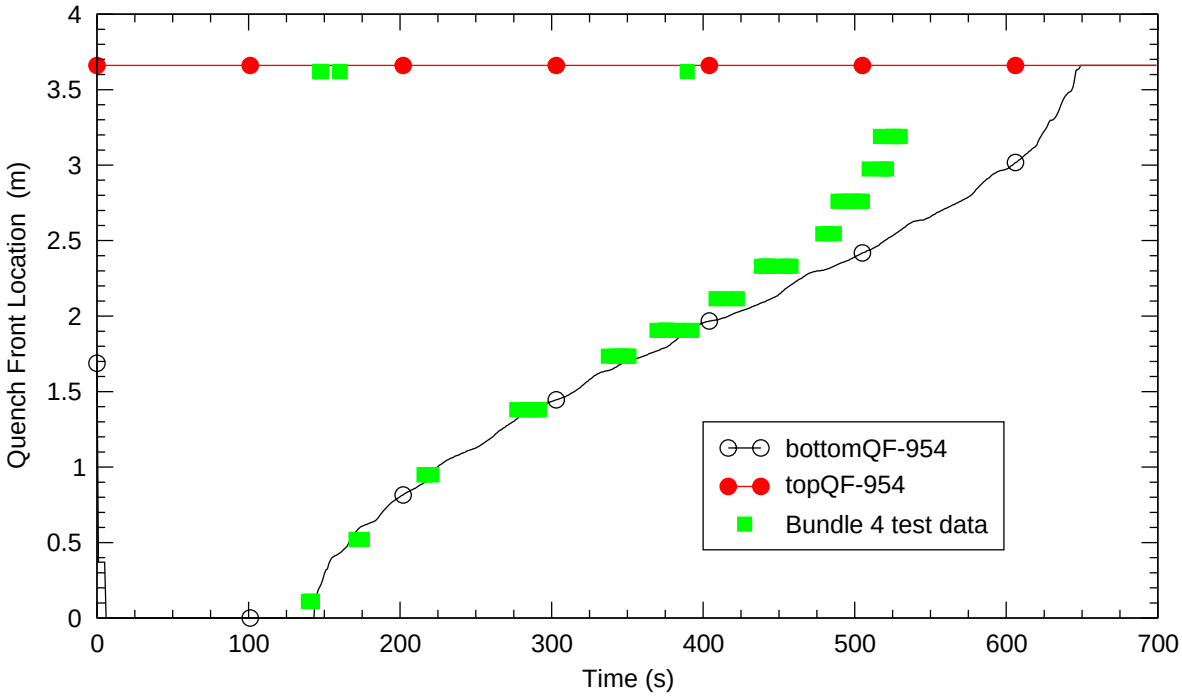

Figure C.3-31. Calculated and Measured Bundle 4 Quench Fronts for Run 622.

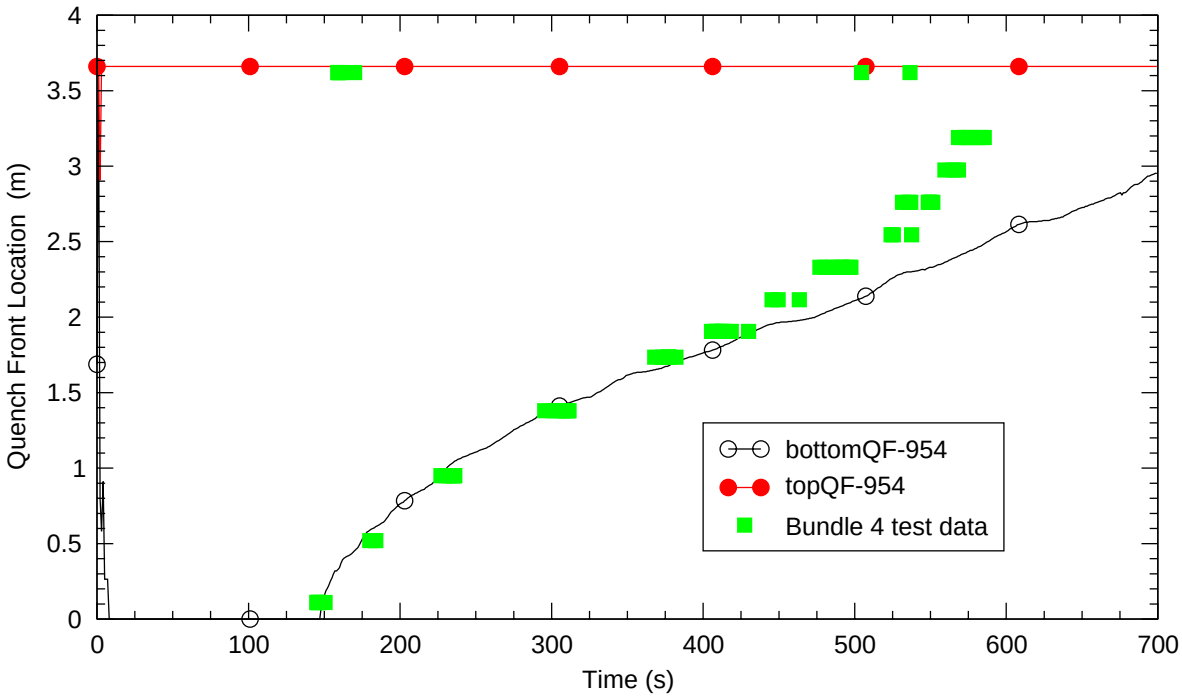

Figure C.3-32. Calculated and Measured Bundle 4 Quench Fronts for Run 605

TRACE did a better job of matching measured quench fronts for the forced reflood tests than it did for the gravity feed tests.

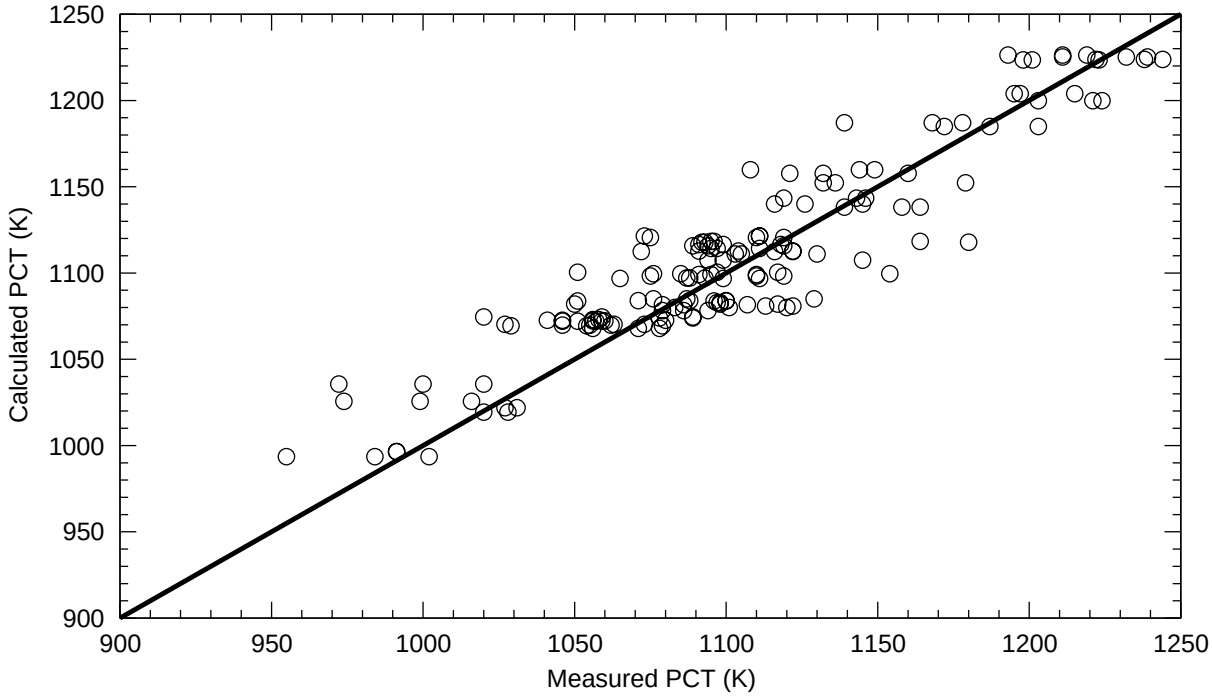

Figure C.3-33. Calculated versus Measured PCTs at the 1.91 m Elevation for All Bundles in All the SCTF Tests which were Simulated

C.3.5.1. Figure of Merit

A significant safety parameter for reflood analysis is the core PCT. The SCTF data show a wide variation in PCTs (50 K is not uncommon) for a set of rods at a common elevation and power level. In large part, this is due to the rods having different temperatures at the beginning of core recovery (BOCREC). In the TRACE model all rods in a bundle are represented by a single equivalent rod[1]. Measured bundle PCTs always occurred on rods that were hotter than the TRACE rod at BOCREC. Some of the differences between TRACE and bundle PCTs can therefore be attributed to initial conditions rather than to TRACE's simulation of the bundle thermal-hydraulics. A comparison of TRACE and measured rods' PCTs at the 1.91 m elevation is given in Figure C.3-33 Only the measured temperatures of rods not adjacent to an unheated surface are included (locations 1B, 1C, and 2A for all bundles, except that 2A is not used for bundle 8).

1. The TRACE rod was modeled so that, at BOCREC for Run 604, its surface temperature for the 1.91 m elevation for each bundle was near the average of all the measured surface temperatures (7 of them) at that location.

Figure C.3-33 shows that, in spite of significant differences between measured and calculated hydraulic behavior for SCTF, TRACE's bundle PCTs are in excellent agreement with the data. The RMS difference between calculated and measured PCTs shown in Figure C.3-33 is 22.7 K.

C.3.6. References

1 Makato Sobajima, Hiromichi Adachi, Isao Arase, Yoshio Fukaya, Tsutomu Oyama, Yaushi Niitsuma, Takao Wakabayashi, Takamichi Iwamura, Akira Ohnuki, Yutaka Abe and Yoshio Murao, *Design of Slab Core Test Facility (SCTF) In Large Scale Reflood Test Program, Part II: Core II*, Japan Atomic Energy research Institute, JAERI-Memo 59-396, December 1984.

2 MPR Associates, Inc, "Research Information Report on the SLAB Core Test Facility (SCTF) Core-II Test Series", MPR-1115 Volume I of II, July 1989.

3 M. Sobajima, et. al; "Data Report On Large Scale Reflood Test-66 SCTF Test S2-SH1 (Run 604)", JAERI-memo 59-282, September 1984.

4 T. Iwamura, et. al; "Data Report On Large Scale Reflood Test-67 SCTF Test S2-SH2 (Run 605)", JAERI-memo 59-287, September, 1984.

5 Y. Abe, et. al; "Data Report On Large Scale Reflood Test-68 SCTF Test S2-01 (Run 606)", JAERI-memo 59-288, September 1984.

6 M. Sobajima, et. al; "Data Report On Large Scale Reflood Test-69 SCTF Test S2-02 (Run 607)", JAERI-memo 59-283, September 1984.

7 M. Sobajima, et. al; "Data Report On Large Scale Reflood Test-73 SCTF Test S2-06 (Run 611)", JAERI-memo 59-435, February 1985.

8 M. Sobajima, et. al; "Data Report On Large Scale Reflood Test-100 SCTF Test S2-16 (Run 621)", JAERI-memo 60-259, October 1985.

9 T. Iwamura, et. al; “Data Report On Large Scale Reflood Test-101 SCTF Test S2-17 (Run 622)”, JAERI-memo 60-260, October 1985.

10 R. Shumway and J. Atkinson, "TRACE Assess Using SCTF Reflood Data", ISL-NSAD-TR-04-20, December 2004.

11 R. Shumway, et. al, “TRACE Calculation Notebook - SCTF”, NRC ADAMS Access No. ML061660015, ML061660016. June 2006.

12 D. Caraher, TRACE Calculation Notebook - SCTF (Rev. 1). November 2006.

PWR Small Break Integral Tests

C.4. LOFT Small Break Tests

Author(s): William A. Macon, Jr.

Affiliation: USNRC

Code Version: TRACE V5.0

Platform and Operating System: Intel x86, Windows XP

C.4.1. Introduction

Two Loss-of-Fluid Test (LOFT) small break loss-of-coolant accident (SBLOCA) tests, L3-7 and L3-1, were simulated with the TRACE thermal-hydraulic computer program. The purpose of this report is to document the assessment of these simulations against measured data from these tests. The simulations were performed with TRACE Version V5.0.

C.4.2. Test Facility Description

The LOFT Integral Test facility was a 50-MWt pressurized water reactor (PWR) system designed to simulate the major components and system responses of a commercial PWR during postulated LOCAs and anticipated transients. The facility was built at the Idaho National Engineering Laboratory during the 1970s and forty-four tests were completed over a nine-year period ending in July 1985. The LOFT facility is shown in Figure C.4-1 and described in detail in Reference 1 and Reference 2. The facility consisted of five major systems: the Reactor System with the nuclear core; Primary Coolant System; Blowdown Suppression System; Emergency Core Cooling System; and a Secondary Coolant System. These systems were extensively instrumented to measure the behavior of system parameters during the tests.

The LOFT facility was scaled to represent a 1/60-scale model of a typical 1000-MWe (electric) commercial four-loop PWR. The unique feature of the facility was that the Reactor System had a UO_2 powered core. The entire nuclear core consisted of five square and four triangular fuel bundles with a total of 1300 fuel pins. The length of the core was 5.5 feet (1.68 m) instead of 12 feet, about one-half the length of typical reactor cores in commercial plants. However, this was the only compromise made in the nuclear fuel for the LOFT core. PWR 15x15 array fuel rod assemblies were used, complete with upper and lower end boxes and fuel rod spacer grids at five locations. The LOFT fuel was designed to have the same physical, chemical and metallurgical properties as commercial fuel.

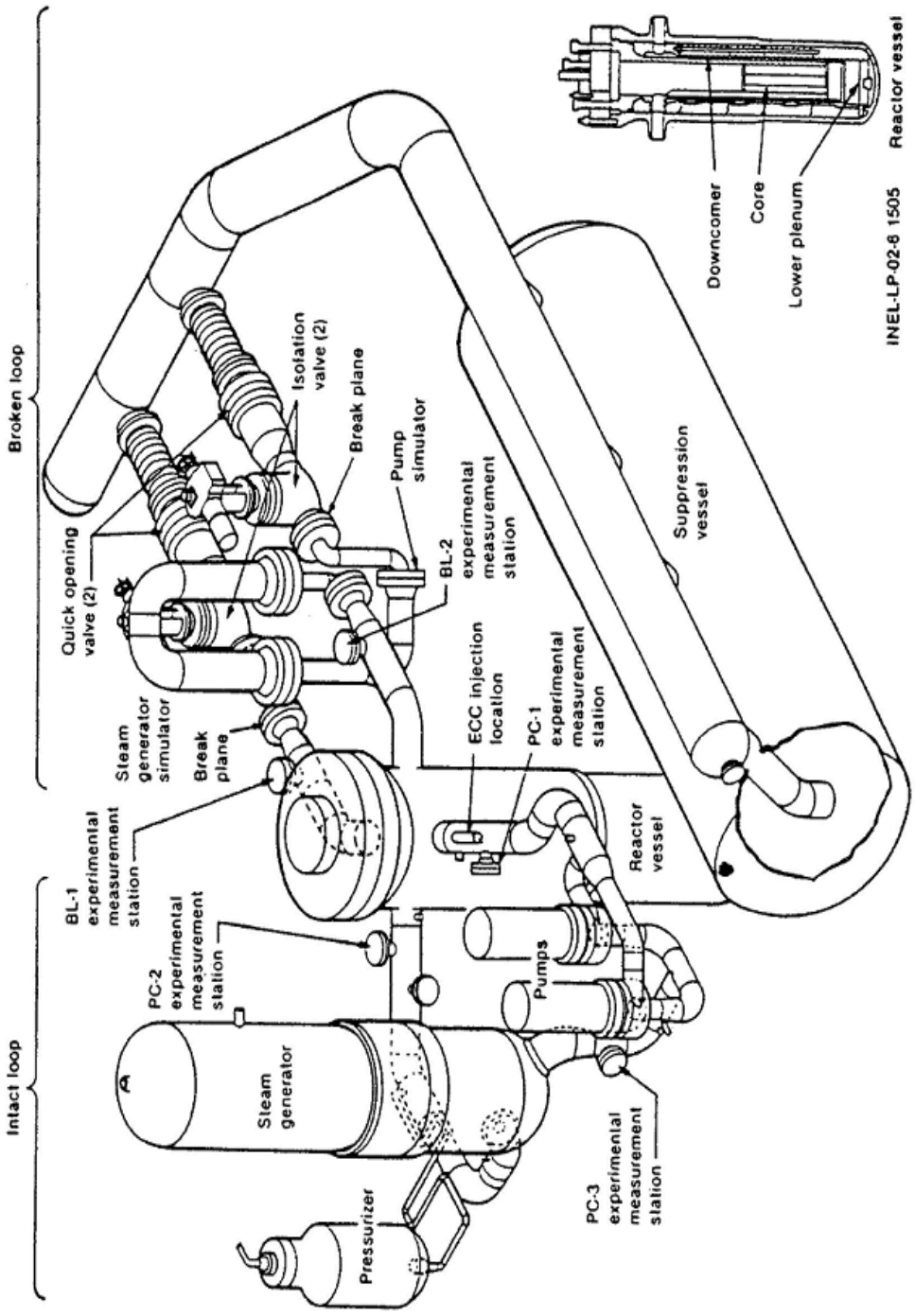

Figure C.4-1. Sketch of the LOFT facility.

The LOFT experimental facility was a 50-MWt PWR at the Idaho National Engineering Laboratory which was instrumented to measure and provide data on the thermal-hydraulic conditions during accidents. The facility was configured to represent a 1/60-scale model of a typical 1000-MWe commercial four-loop pressurized water reactor. In LOFT, three PWR primary-coolant loops are simulated by a single intact loop, scaled to have the same volume-to-power ratio as the PWR. A LOFT broken loop simulates the fourth PWR primary coolant loop where a break may be postulated to occur.

The Primary Coolant System consisted of an operating loop (with steam generator, two primary coolant pumps in parallel, pressurizer and connecting piping) representing three intact loops of a four-loop PWR. A “broken loop” simulated the broken loop of a four-loop PWR during LOCA conditions. The broken loop consisted of hot and cold legs that connect the Reactor System to the Pressure Suppression System, and was equipped with steam generator and pump simulators and quick-opening blowdown valves. The piping arrangement was variable to simulate either hot or cold leg breaks.

The Blowdown Suppression System was designed to simulate the containment backpressure in large PWRs during LOCA events. It consisted of a large pressure suppression tank, downcomers and a header connected to the Primary Coolant System via the quick-opening blowdown valves.

The Emergency Core Cooling System (ECCS) consisted of the same three systems used in commercial PWRs: the high-pressure injection system (HPIS), the accumulator, and the low-pressure injection system (LPIS). The systems were actuated similarly to their generic counterparts to inject scaled amounts of emergency core coolant (ECC) typical of the ECC delivery behavior in commercial PWRs. The LOFT ECCS had the capability of injecting ECC to any of several locations including the intact loop hot or cold legs, the reactor vessel downcomer, lower plenum, or upper plenum.

The Secondary System was designed to remove the heat transferred into the steam generator to the environment. However, this system could not be controlled for full simulation of secondary system response in large PWRs.

The component and system volumes of the Reactor and Primary Coolant Systems were designed proportional to their respective volumes in a commercial PWR and scaled to have the same volume-to-power ratio. The design objective for the LOFT facility was to produce the significant thermal-hydraulic phenomena with approximately the same conditions and sequence of events that could occur during postulated accidents in commercial PWR systems.

C.4.3. TRACE Model Description

The calculations reported here were performed using the TRACE Version V5.0 computer code. The TRACE input model for the LOFT facility for this SBLOCA assessment is based on the model used for the LOFT SBLOCA simulations using TRACE Version 3.1115 (Reference 3). The Reference 3 simulations were performed by running a steady-state calculation and then running

multiple transient calculations to piece-wise simulate the experiments. These simulations were updated in Reference 4 using TRACE Version 4.271. For the simulations presented in Reference 4 and also here in this assessment, the model inlcudes modifications so that a 200 second steady-state followed by the transient calculations could be performed as a single run. The development of the TRACE input model is described in Reference 5. The TRACE nodalization of the LOFT facility is shown in Figure C.4-2.

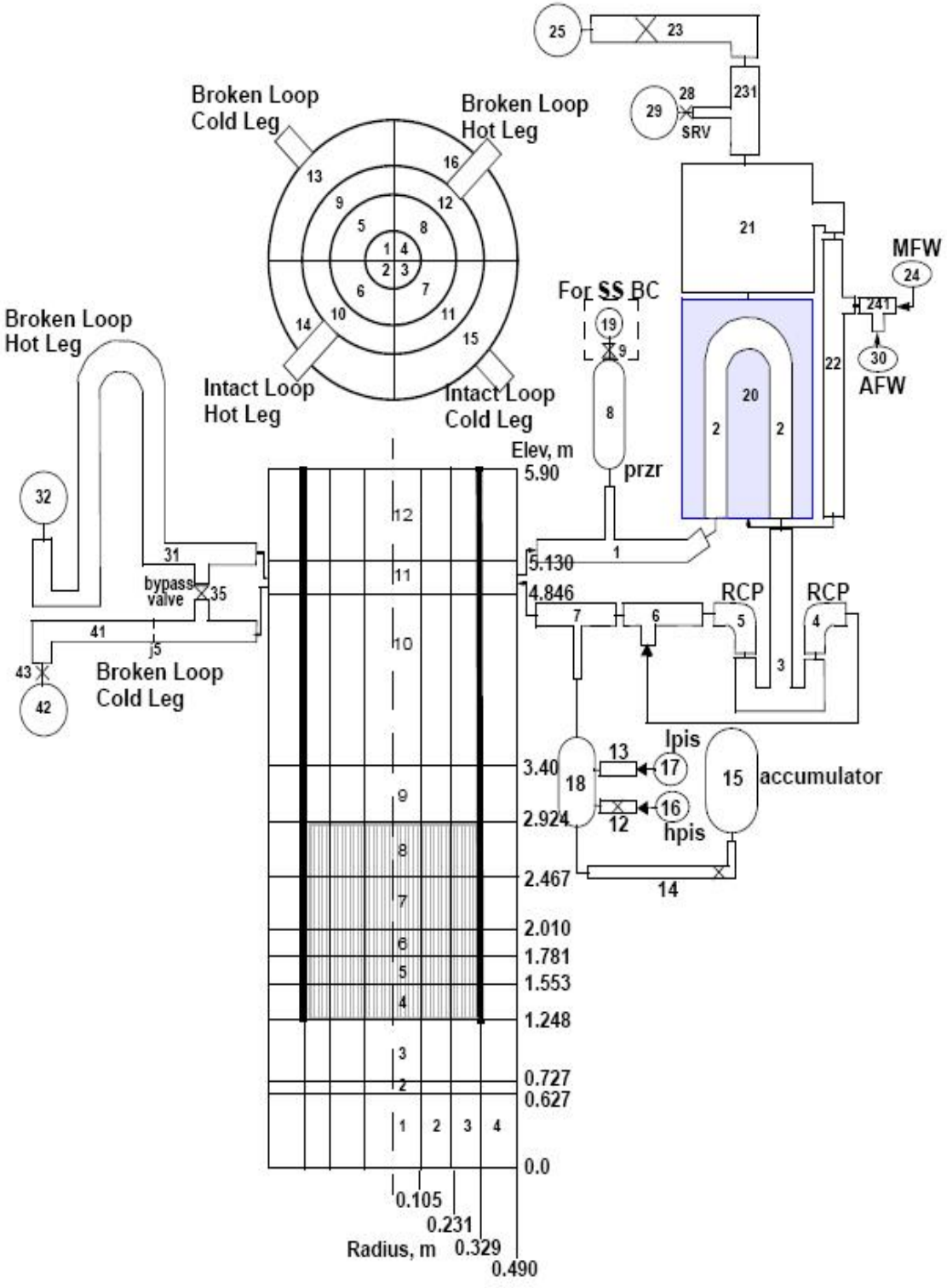

Figure C.4-2. TRACE Nodalization for the LOFT SBLOCA Simulations.

C.4.4. LOFT Tests Simulated with TRACE

Two LOFT SBLOCA tests were simulated using TRACE. Tests L3-7 and L3-1 represent equivalent 1-inch (2.54-cm) and 4-inch (10.16-cm) diameter breaks in the cold leg of a four-loop PWR. The test facility, initial conditions, procedures and results for Test L3-7 and Test L3-1 are described in the experimental data reports, Reference 6 and Reference 7, respectively. The nominal measured experimental initial conditions (at the time of break opening) for the two tests are shown in Table C.4.1. Most of the system initial conditions of the two tests agree very closely; Test L3-1 was run at slightly lower core power, steam generator (SG) pressure and reactor coolant system (RCS) temperatures than Test L3-7. The initial conditions for the TRACE simulations, taken from the large edit just prior to break opening (200 s), are also shown in Table C.4.1

Table C.4.1. LOFT SBLOCA Experiment Measured and TRACE Initial Conditions.

Parameter (units)	Test L3-7	TRACE L3-7	Test L3-1	TRACE L3-1
Reactor Power (MW)	49.0	49.0	48.9	48.9
Intact Loop Mass Flow Rate (kg/s)	481.3	480.0	484.0	481.7
Intact Loop Hot Leg Pressure (MPa)	14.90	14.92	14.85	14.92
Intact Loop Hot Leg Temperature (K)	577.3	577.6	574.0	575.6
Intact Loop Cold Leg Temperature (K)	559.4	558.4	554.0	556.7
Pressurizer Level (m)	1.10	1.12	1.10	1.07
Steam Generator Secondary Pressure (MPa)	5.576	5.560	5.43	5.43
Steam Generator Secondary Level (m)	0.25	---	0.20	---
Broken Loop Hot Leg Temperature (K)	561.4	561.4	562.0	556.3
Broken Loop Cold Leg Temperature (K)	557.7	557.7	557.3	556.5

Test L3-7 represented an equivalent 1-inch (2.54 cm) diameter break in the cold leg of a four-loop PWR. The first 30 minutes of Test L3-7 was a simulation of a 1-inch diameter equivalent break in the cold leg of a PWR which is in full-power operation; normal safety system functions were simulated during this period. The reactor scrammed on a low pressurizer pressure signal and the pumps were tripped 3.3 s after scram. After 30 minutes, the experiment investigated PWR behavior assuming loss of the HPIS and AFW functions and accident mitigation techniques to counter the effects of the loss of those functions. From 30 to 60 minutes the primary system inventory was allowed to be partially, but significantly, depleted as a result of the break flow. At 60 minutes, a SG secondary-side feed-and-bleed operation was instituted; AFW was reinstated and the SGs were depressurized in a controlled manner. At 100 minutes, HPIS flow was reinstated. The break was isolated at 122 minutes, effectively ending the experiment.

Test L3-1 represented an equivalent 4-inch (10.16 cm) diameter break in the cold leg of a four-loop PWR. The reactor was manually tripped just prior to the break opening. Normal functioning of the ECCS systems (HPIS, LPIS, accumulators) is represented in this test. AFW flow was initiated for a period of 30 minutes, starting 75 s after the break opened.

The experimental initial conditions and the TRACE initial conditions are given in Table C.4.1 The TRACE initial conditions were taken from the major edit at 200 s just prior to opening the break.

C.4.4.1. Simulation of Test L3-7.

The first 200 s of the TRACE calculation was used to establish a steady-state. The break was opened at 200 s and the run was carried out to 7700 s. (All figures in this section have had the TRACE time shifted so that time zero on the figures corresponds with the break opening time in Test L3-7.)

Table C.4.2 compares the measured sequence of events for LOFT Test L3-7 (from Table 4-1 of Reference 6) with the TRACE calculated sequences of events. The table shows a generally favorable comparison between the calculated event times and the event times that were measured during the experiment. Because the experiment featured a variety of operator actions, many of the calculated event times simply represent times during the calculations when events were specified to occur. The table shows that the TRACE reactor and pump trip times agreed well with the test data.

Table C.4.2. Measured and Calculated Sequences of Events for LOFT Test L3-7.

Events	LOFT L3-7 Measured Time (s)	TRACE Calculated Time (s)
1” equivalent diameter cold leg break opens	0.0	0.0
Reactor scram initiated	36.0	36.4
Reactor coolant pumps begin coastdown	39.3	36.4
Reactor coolant pump coast-down completed	56.2	98.4
HPIS injection initiated	65.6	50.5
AFW flow initiated	75.0	75.0
Pressurizer empty	264	296
AFW flow terminated	1800	1800
HPIS injection terminated	1805	1805
SG steam bleed initiated, AFW flow reinstated	3603	3603
HPIS injection reinstated	5974	5974
Accumulator injection begins	6028	6107
Cold leg break isolated, TRACE calculation terminated	7302	aborted at 6555

The calculated and measured responses for significant test parameters are compared in Figure C.4-3 through Figure C.4-25. The instrumentation measurement uncertainties cited in the following discussion are from Tables 5-1, 5-2 and B-2 of Reference 6.

Figure C.4-3 compares the primary system pressure responses from the two calculations with the test data. The measurement uncertainty is ±0.223 MPa. After HPIS injection and AFW were terminated at 1800 s, TRACE calculated a hot leg pressure that was, on the average, about 0.4 MPa greater than the data.

The break mass flow comparison is shown in Figure C.4-4. Experimental break flow data are only available for the first 1800 s of the test. The measurement uncertainty is ±10%. Over this period, the calculated break flow rate is in fair agreement with the test data. In the 500 - 1800 s time period the TRACE flow rate is about 30% below the data.

Figure C.4-5 and Figure C.4-6 compare the pressurizer level responses. The measurement uncertainty is ±0.04 m. The TRACE calculated level is in excellent agreement with the data until the reactor trips. At that time the calculated level rapidly drops 15 cm below the calculated level. Thereafter, the two levels parallel one another until the pressurizer is empty.

Figure C.4-7 shows that the TRACE-calculated SG secondary system pressure agrees well with the test data over the first 1000 s, but then stays above the data for the rest of the transient. In the calculation, the SG pressure remained at the relief valve's setpoint until controlled depressurization began at 3600 s. The measurement uncertainty is ±0.110 MPa.

There is some uncertainty as to how the SG steam relief system worked in Test L3-7. There was not a separate relief valve on the LOFT SG; rather, the steam control valve was modulated after reactor trip to maintain SG pressure below 6.56 MPa. The steam valve position data indicate that the valve was about 2% open throughout the test. It appears likely that the overprediction of the steam generator pressure is due to the TRACE model not mimicking the SG pressure control system used in the test. There is insufficient information in the LOFT facility and test description documents to do this. It will be demonstrated later that if the TRACE calculation were to match the measure SG pressure, primary pressures and temperatures would be in excellent agreement with the data.

The liquid temperatures in the hot and cold legs are shown in Figure C.4-8 and Figure C.4-9, respectively. The measurement uncertainty is ±2.6 K. After 1800 s calculated temperatures are well above measured ones. This is a direct result of the overprediction of SG secondary pressure. The agreement is generally good (measurement uncertainity is 4.2% of reading) until HPIS injection is restarted at 6000 s. The disagreement at this point is probably due to TRACE calculating the cold leg to be full of liquid whereas a stratified flow regime actually existed in the experiment. Instrument TE-PC-004 is located near the top of the cold leg. Instrument TE-PC-008, which is located at the bottom of the cold leg behaves like the TRACE temperature, dropping rapidly when HPIS injection is restarted.

Figure C.4-10 shows the fuel rod cladding temperature comparisons in the middle region of the core. No fuel rod heatup above the fluid saturation temperature was observed in the experiment or in the TRACE calculation. The comparison is made at the 1.14 m elevation within the 1.68 m core length (58% of the heated core height). The measurement uncertainty is ±3.2 K. After 1800 s, the calculated temperature differs from the data by about 8 K, with TRACE overpredicting it. The measured and calculated HPIS injection flows are compared in Figure C.4-11.

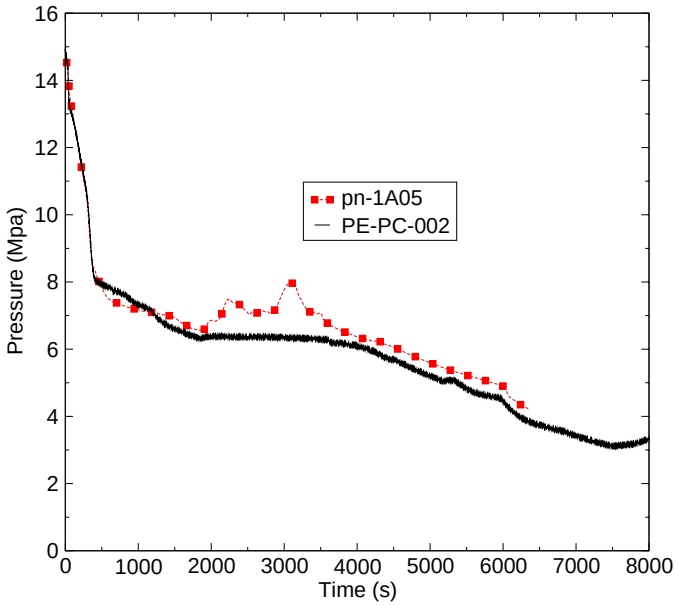

Figure C.4-3. Intact Hot Leg Pressure Comparison for LOFT Test L3-7.

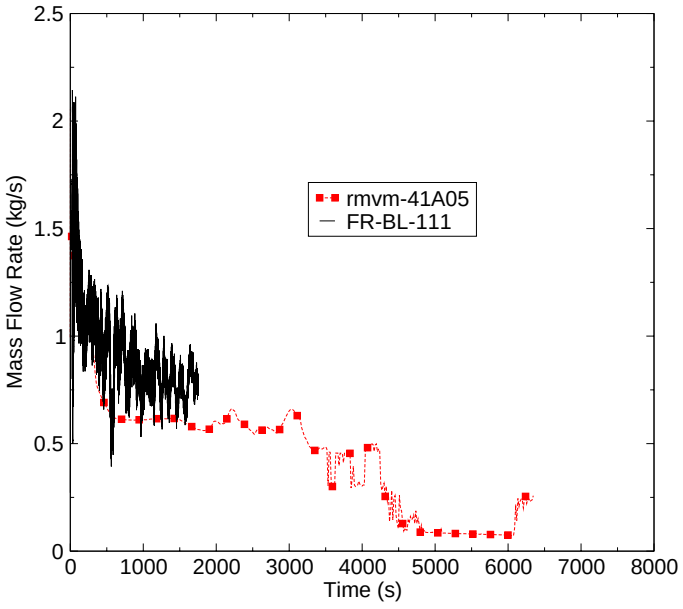

Figure C.4-4. Break Mass Flow Comparison for LOFT Test L3-7.

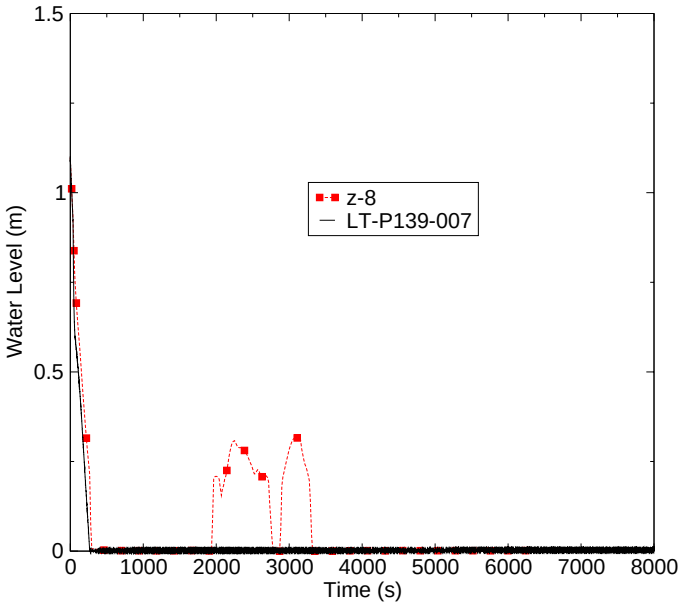

Figure C.4-5. Pressurizer Level Comparison for LOFT Test L3-7.

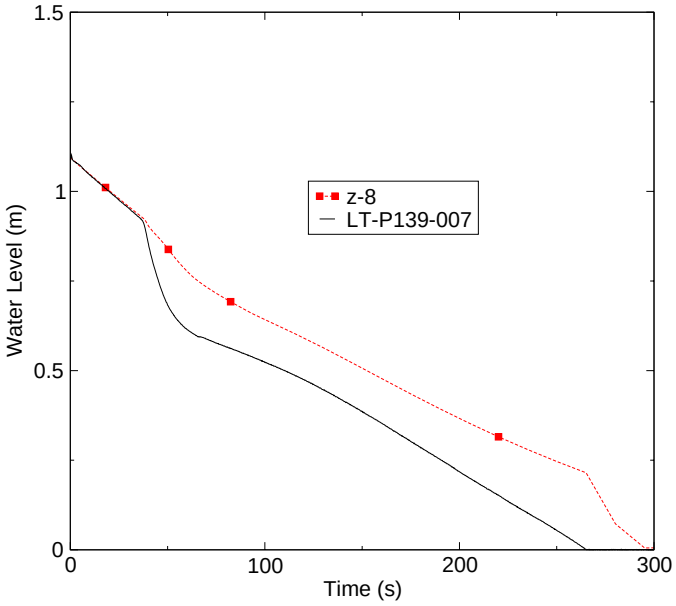

Figure C.4-6. Pressurizer Level Comparison for Test L3-7.

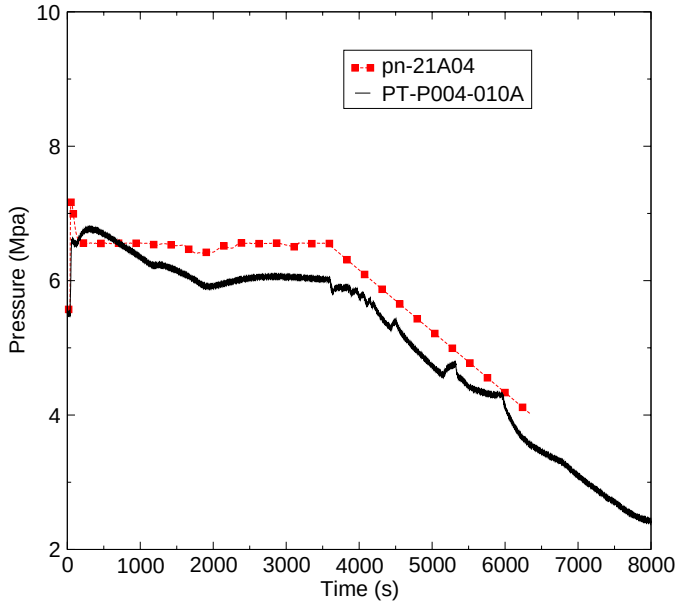

Figure C.4-7. SG Secondary Pressure Comparison for LOFT Test L3-7.

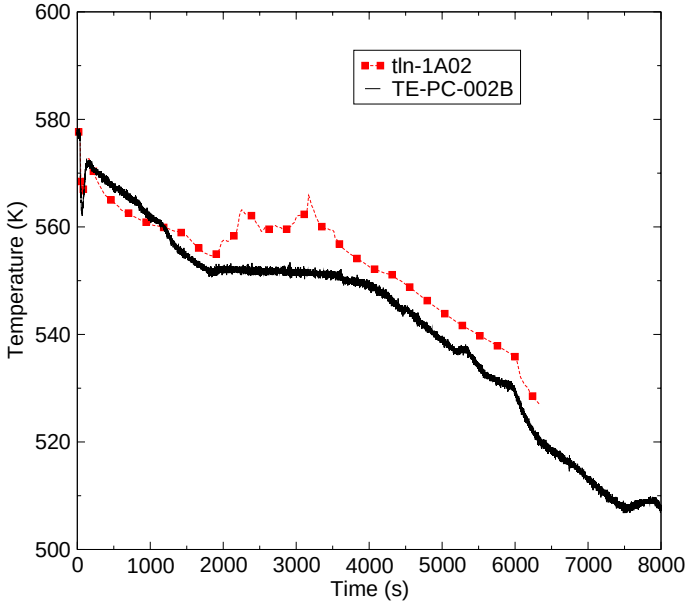

Figure C.4-8. Hot Leg Liquid Temperature Comparison for LOFT Test L3-7.

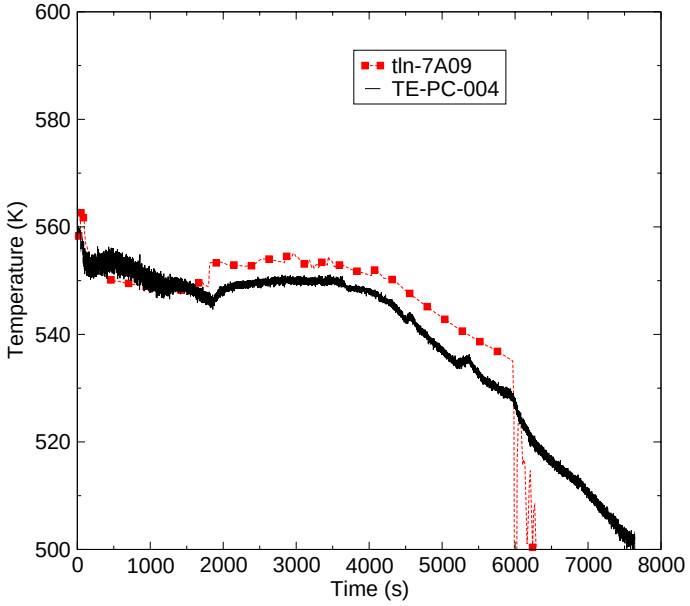

Figure C.4-9. Cold Leg Liquid Temperature Comparison for LOFT Test L3-7.

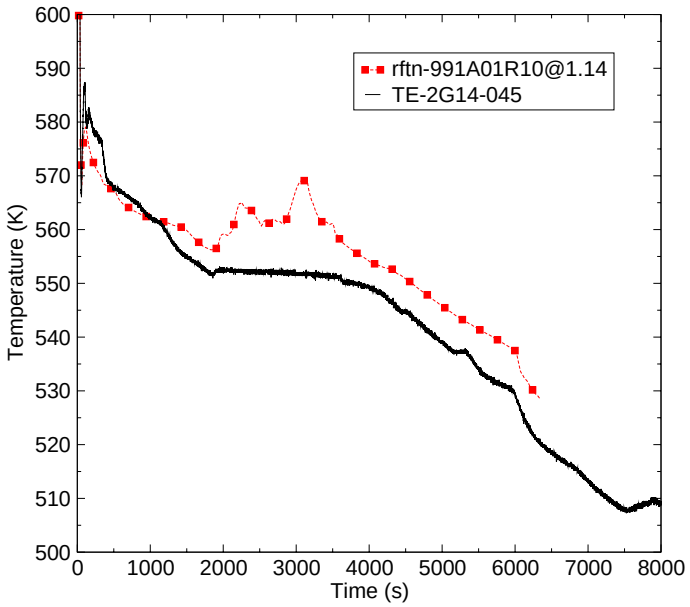

Figure C.4-10. Middle Core Region Fuel Rod Cladding Temperature Comparison for LOFT Test L3-7.

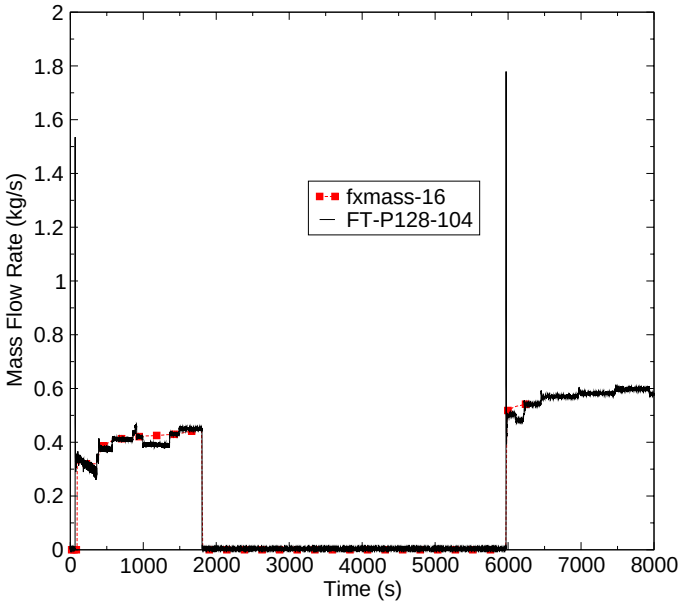

Figure C.4-11. HPI Flow Comparison for LOFT Test L3-7.

Figure C.4-12 shows the intact hot leg fluid density comparison. The measurement uncertainty is $\pm$100 kg/m^3. Prior to 1800 s, the agreement between TRACE and the test data is very good. After 1800 s TRACE calculated a hot leg fluid density which is more voided than the test data indicate. The difference between TRACE and the data is likely a consequence of TRACE not correctly calculating the draining of the cold leg into the vessel when HPIS injection was terminated.

Figure C.4-13 shows the intact cold leg fluid density comparison. The measurement uncertainty is $\pm$76 kg/m^3. The test data show a sharp density drop of about 50% when the HPIS and AFW are terminated at 1800 s. The calculation incorrectly shows that the cold leg remains liquid-filled until the SG feed-and-bleed operation is started at 3600 s. In the TRACE calculation there are no leakage paths between the vessel downcomer and the upper head or the hot leg. It may be that in the test such leakage paths existed and allowed steam in the upper head to leak back into the upper downcomer when HPIS injection was terminated, thus helping the downcomer and cold leg fluid to drain into the core. During the RCS refill period, which starts at about 6000 s, TRACE shows a tendency to refill the cold leg too quickly from the effects of resuming the HPIS injection at 5974 s and the onset of accumulator injection at 6107 s (Figure C.4-14).

As discussed earlier, there is some uncertainty about how the SG pressure was controlled in test L3-7. In other analyses of this test, both with TRACE and RELAP5, HPIS injection flow tables that are different from the data have been used to try to improve the agreement between calculated and measured primary pressure. Analysts have believed the measured HPIS flow record to be in error. To address this issue, a second calculation of Test L3-7 was performed (input file = L37tr02.inp). In this calculation, the measured SG pressure was specified as the TRACE SG pressure (Figure C.4-15).

Figure C.4-16 shows the comparison of calculated and measured pressures in the hot leg. The agreement between the two is excellent.

Figure C.4-17 is a comparison of calculated and measured hot leg liquid temperatures. Again, the agreement between the two parameters is excellent except for the 1200 s following the closure of the SG steam control valve. The reason for this period of disagreement can be traced to differences in SG heat transfer between 50 and 150 s, a period of very dynamic thermal-hydraulic behavior on the secondary side. The measured temperature dropped from 578 K at 41 s (reactor scram and steam valve closure) to 563 K at 64 s and then recovered to 572 K by 140 s. TRACE calculated a slightly greater drop in temperature (to 560 K at 73 s) and less of a temperature rebound (to 566 K at 160 s).

Figure C.4-18 compares calculated and measured cold leg temperatures. The agreement is excellent (measurement uncertainity is 4.2% of reading) until HPIS injection is restarted at 6000 s. As previously discussed, the disagreement at this point is probably due to TRACE calculating the cold leg to be full of liquid whereas a stratified flow regime actually existed in the experiment. Discrepancies between calculated and measured cold leg flow regimes during ECC injection are seen with other codes besides TRACE and is a difficult modelling issue.

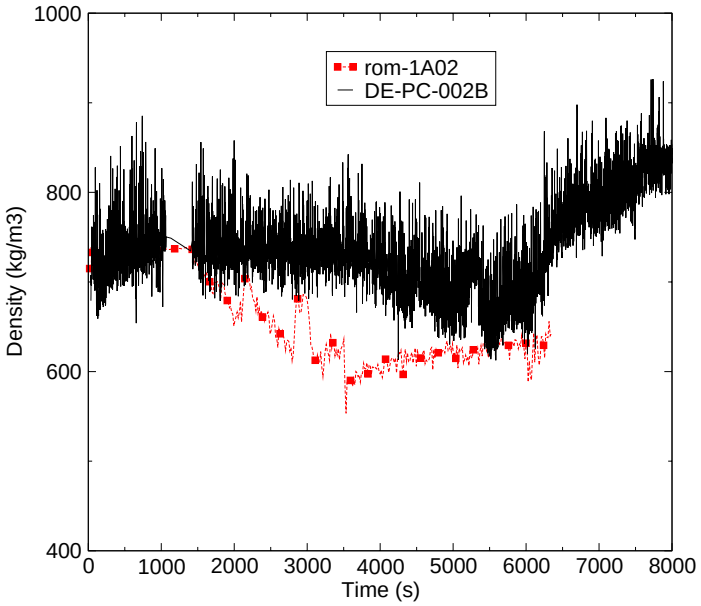

Figure C.4-12. Intact Hot Leg Fluid Density Comparison for LOFT Test L3-7.

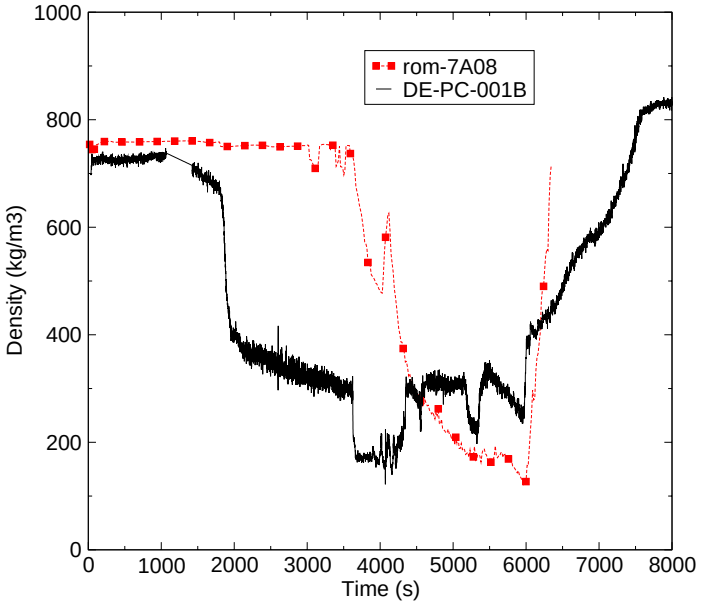

Figure C.4-13. Intact Cold Leg Fluid Density Comparison for LOFT Test L3-7.

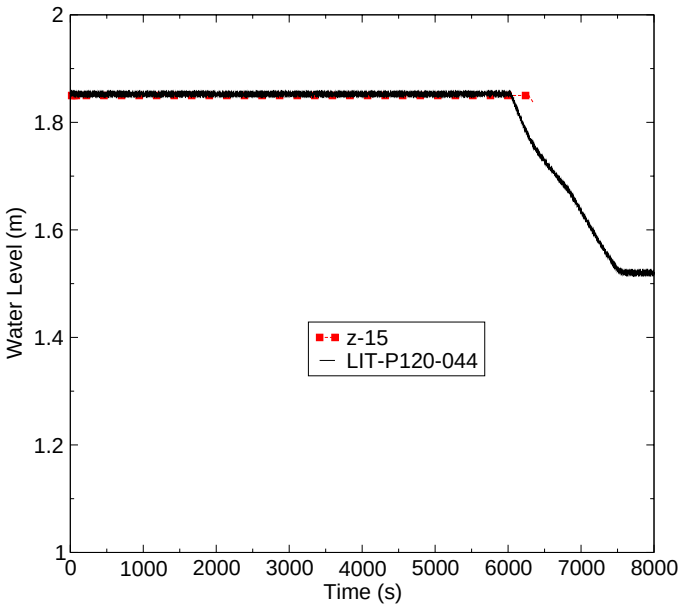

Figure C.4-14. Accumulator Level Comparison for LOFT Test L3-7.

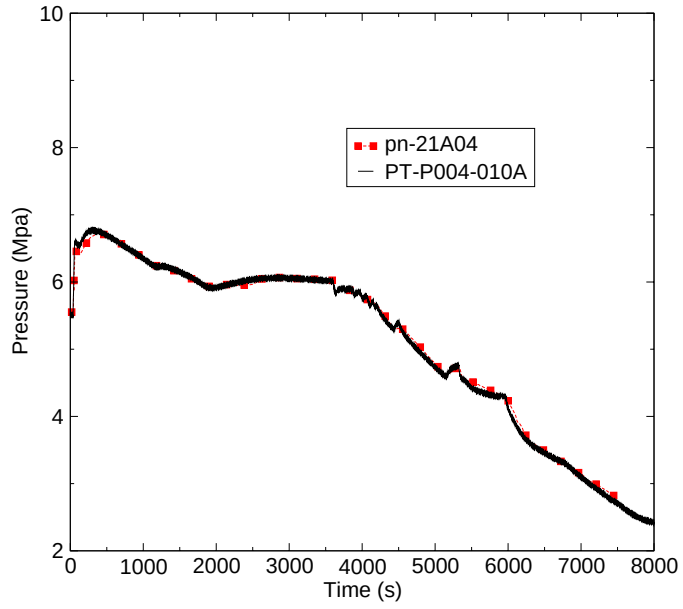

Figure C.4-15. Secondary Pressure Comparison for LOFT Test L3-7.

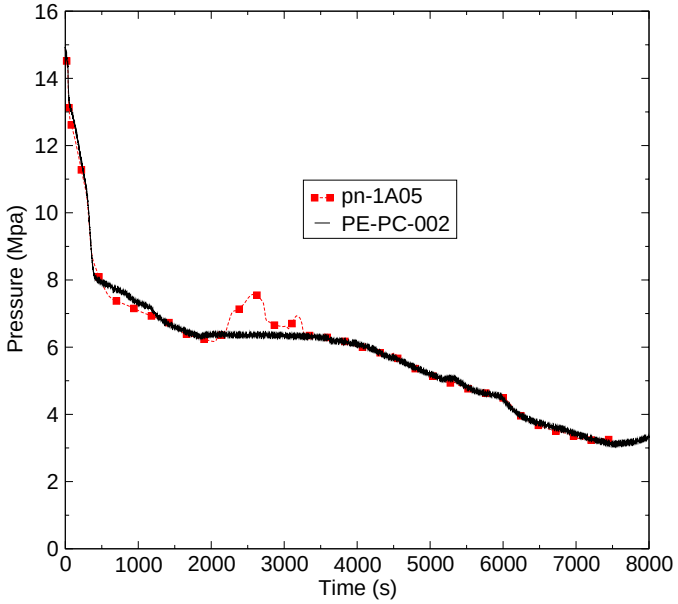

Figure C.4-16. Hot Leg Pressure Comparison for LOFT Test L3-7.

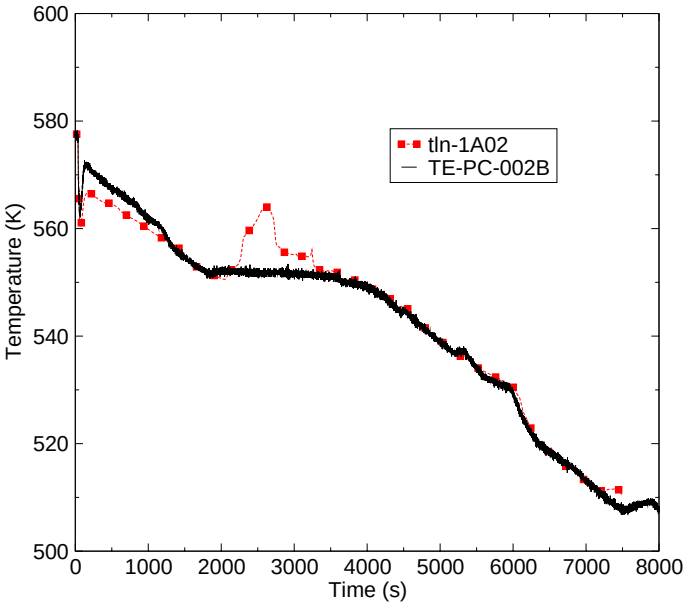

Figure C.4-17. Hot Leg Liquid Temperature Comparison for LOFT Test L3-7.

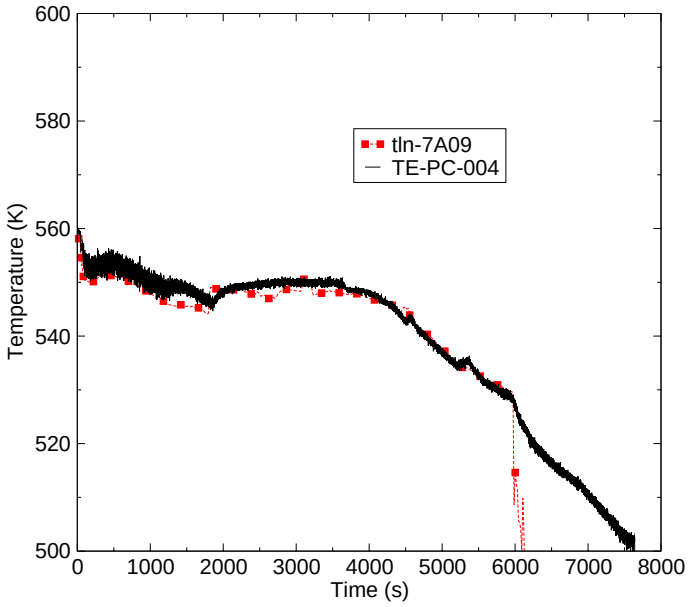

Figure C.4-18. Cold Leg Liquid Temperature Comparison for LOFT Test L3-7.

Figure C.4-19 and Figure C.4-20 shows measured and computed fluid temperatures in the vessel downcomer at two different elevations. Calculated temperatures are lower than measured temperatures during the period of natural circulation ($t < 1800$ s).

Figure C.4-21 shows that modeling the SG pressure response exactly did not result in any improvement in the agreement between measured and calculated cold leg densities.

The TRACE model has no leakage paths between the downcomer and the upper head or hot leg. The degree of leakage in the facility was never reported. It may be, however, that allowing some leakage would allow the downcomer level to recede in TRACE when HPIS injection is terminated at 1800 s, thus improving the agreement between calculated and measured cold leg densities.

The TRACE model which matched the test's SG pressure was further modified to have approximately 2% leakage flow (11.1 kg/s actual) from the downcomer to the upper head. At the same time, the break orifice area was increased by 33% to try to better match the measured break flow.

Figure C.4-22 and Figure C.4-23 show that allowing leakage and increasing the break flow in TRACE resulted in improved agreement of calculated and measured intact loop densities, particularly for the intact hot leg (compare with Figure C.4-12). The calculated time where the cold leg density rapidly declines is now closer to the observed time (compare Figure C.4-22 with Figure C.4-21).

The TRACE calculated pressure shown in Figure C.4-24 now is not in as good agreement as it was when the break flow was lower (compare with Figure C.4-3). However, the present model's break flow shown in Figure C.4-25 is still below the measured break flow in the 400 - 1800 s time range. In the TRACE simulation, the break flow area was simply increased by 33%. Figure C.4-25 suggests that the calculated pressure could be brought into better agreement with the data if break flow were modeled to keep the original (unaltered break area) simulation's flow for the first few hundred seconds and then increase the calculated break flow from 400 - 1800 s.

This final simulation strongly suggests that TRACE, given the actual break area, is underpredicting the break flow for Test L3-7 throughout much of the subcooled blowdown period (0 - 1800 s).

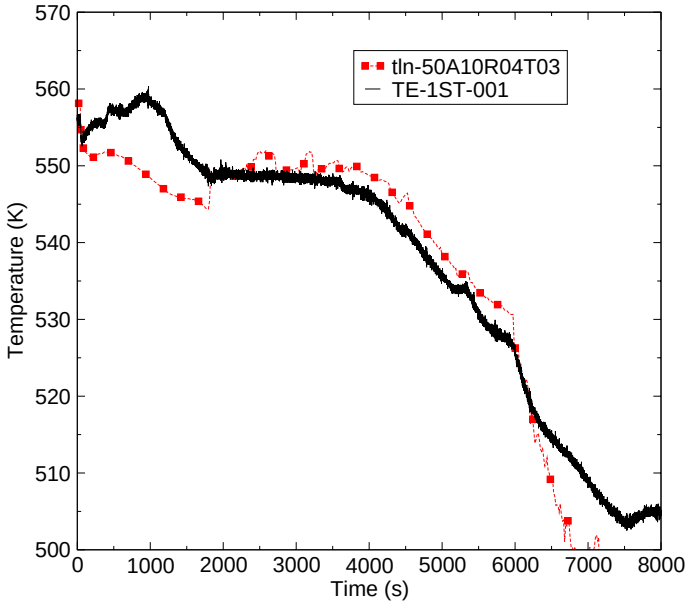

Figure C.4-19. Comparison of Downcomer (4.808 m) Temperature for LOFT Test L3-7.

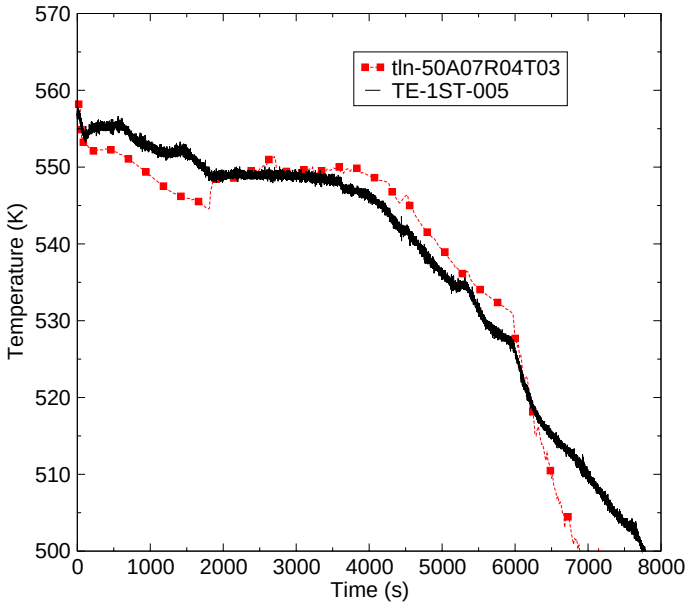

Figure C.4-20. Comparison of Downcomer (2.37 m) Temperature for LOFT Test L3-7.

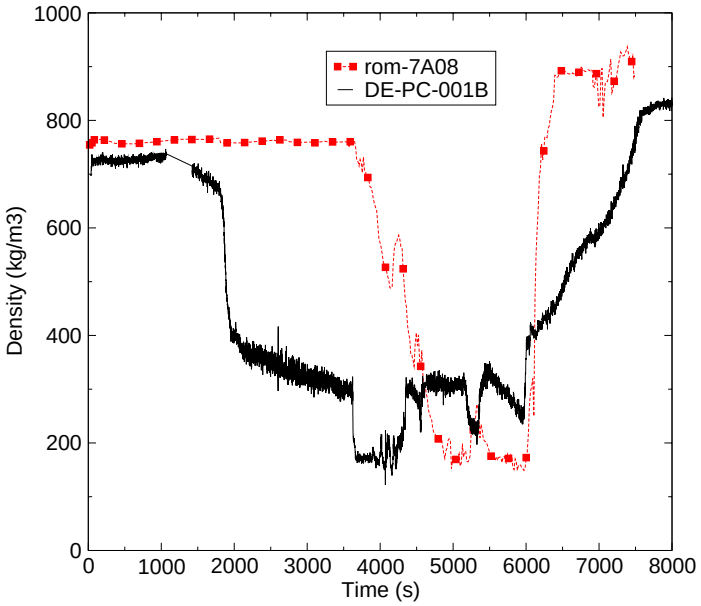

Figure C.4-21. Intact Cold Leg Density Comparison for LOFT Test L3-7.

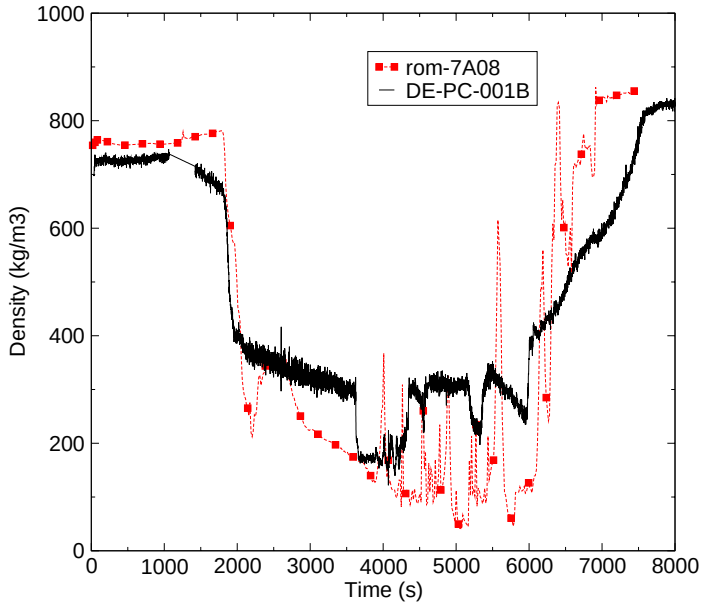

Figure C.4-22. LOFT L3-7 Intact Cold Leg Density - 2% DC/UH Leakage and Increased Break Flow in TRACE.

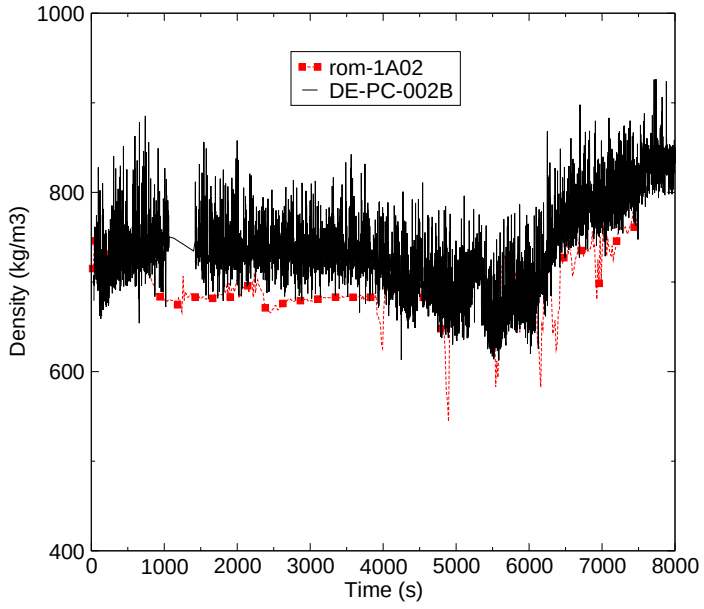

Figure C.4-23. LOFT L3-7 Intact Hot Leg Density - 2% DC/UH Leakage and 33% increased Break Area in TRACE.

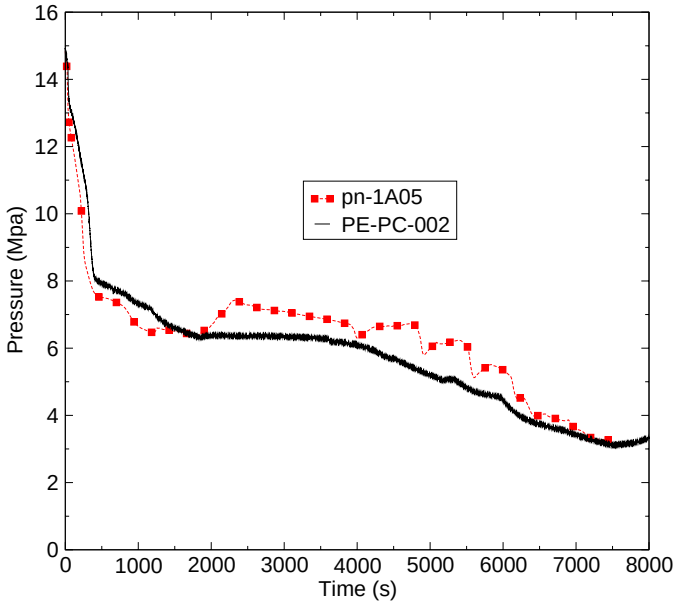

Figure C.4-24. Hot Leg Pressure Comparison for LOFT Test L3-7. TRACE has 2% DC/UH Leakage and 33% Increase in Break Area.

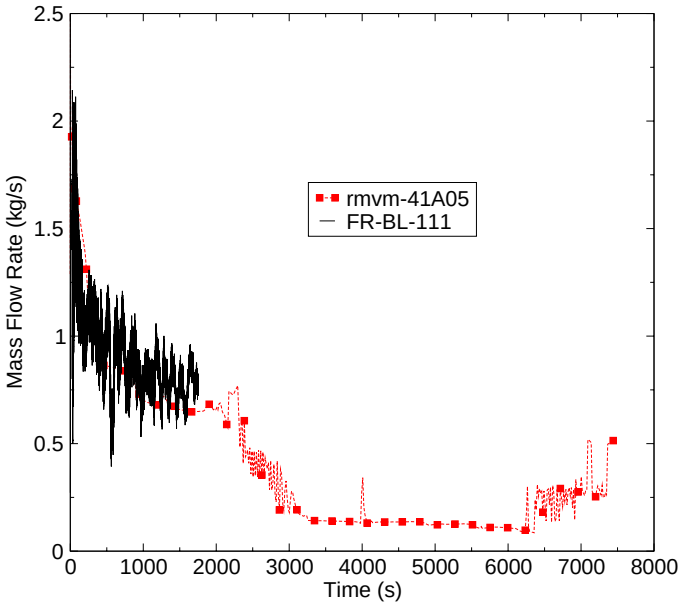

Figure C.4-25. Break Flow Comparison for LOFT Test L3-7. TRACE has 2% DC/UH Leakage and 33% Increase in Break Area.

C.4.4.2. Simulation of Test L3-1.

The first 200 s of the TRACE calculation was used to establish a steady-state (input file = L31tr01.inp). The break was opened at 200 s and the run was carried out to 3600 s. All figures in this section have had the TRACE time shifted so that time zero on the figures corresponds with the break opening time in Test L3-1.

Table C.4.3 compares the measured sequence of events for LOFT Test L3-1 (from Table 2 of Reference 7) with the TRACE calculated sequences of events. The table shows a generally poor comparison between the calculated event times and the event times that were measured during the experiment. The reason for this poor agreement is TRACE's overprediction of the primary system pressure.

Table C.4.3. Measured and Calculated Sequences of Events for LOFT Test L3-1.

Events	LOFT L3-1 Measured Time (s)	TRACE Calculated Time (s)
4" equivalent diameter cold leg break opens	0.0	0.0
Reactor scram initiated	0.0	0.0
Reactor coolant pumps tripped	0.04	0.0
HPIS injection initiated	4.6	18.0
Pressurizer empty	17.0	26.0
Reactor coolant pump coast-down complete	19.0	40.
Reactor vessel upper plenum reaches saturated condition	24.4	46
AFW flow initiated	75.0	75.0
Accumulator injection begins	634	1152
Accumulator empty	1570	n/a
AFW flow terminated	1875	1875
SG feed-and-bleed operation started, leading to end of experiment, TRACE calculation terminated	3623	aborted at 1636

Figure C.4-26 compares the primary system pressure responses from TRACE and the test data. The measurement uncertainty is $\pm$0.223 MPa. TRACE over-predicted hot leg pressure for the first 1600 s until the calculation aborted.

The break mass flow comparison is shown in Figure C.4-27. TRACE greatly underpredicted the break flow for the first couple of hundred seconds, but was in reasonable agreement with the Test L3-1 data thereafter.

The liquid temperatures in the hot and cold legs are shown in Figure C.4-28 and Figure C.4-29, respectively. The measured and calculated HPIS flows are compared in Figure C.4-30.

In Test L3-1, the break was large enough so that the primary pressure quickly fell below the secondary pressure. Once this happened, the decline in secondary pressure was a result of heat being transferred from the secondary to the primary. Since the TRACE primary pressure is considerably greater than what was measured, so is the secondary side pressure as shown in Figure C.4-31.

The TRACE simulation was rerun with a 2% downcomer-to-upper head leakage flow simulated (input file L31tr04.inp). Simulating a leakage flow did not improve the primary system pressure calculated by TRACE (Figure C.4-32).

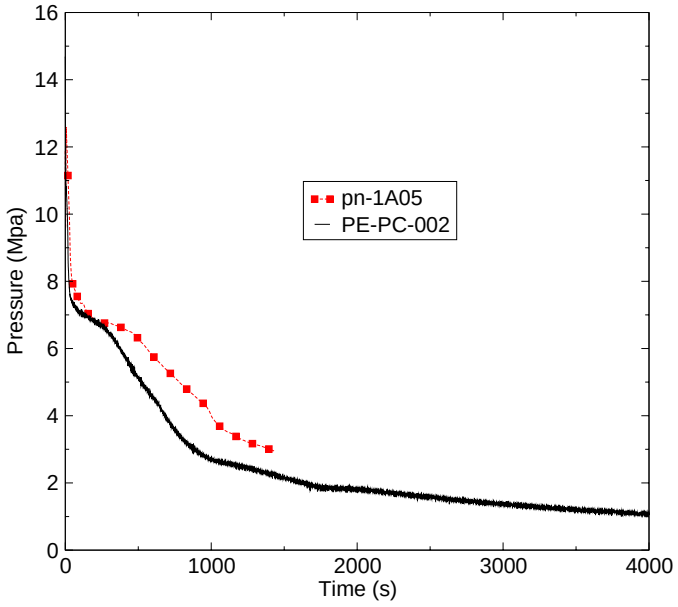

Figure C.4-26. Intact Hot Leg Pressure Comparison for LOFT Test L3-1.

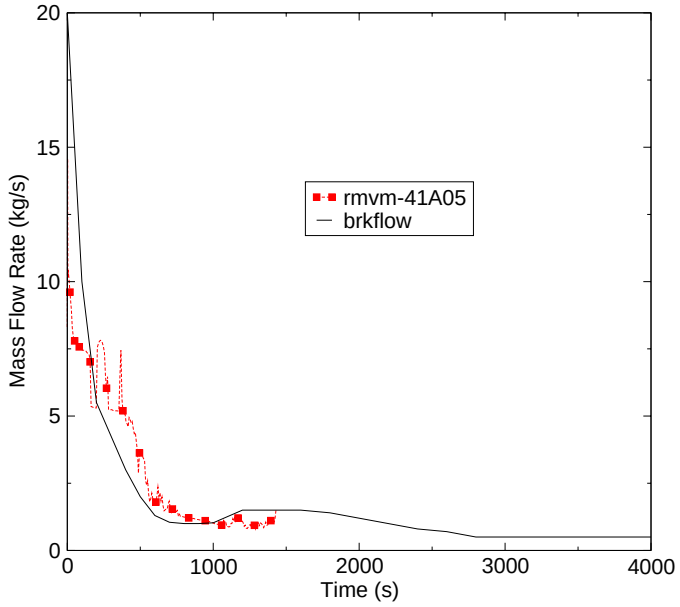

Figure C.4-27. Break Mass Flow Comparison for LOFT Test L3-1.

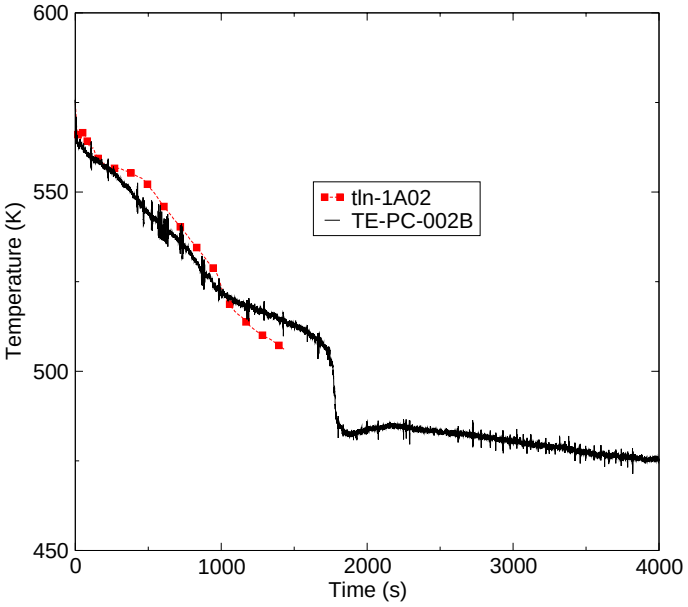

Figure C.4-28. Hot Leg Liquid Temperature Comparison for LOFT Test L3-1.

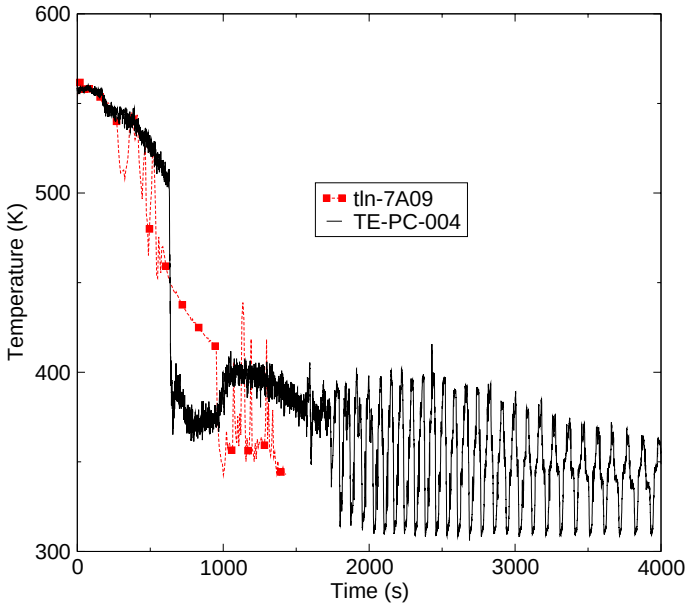

Figure C.4-29. Cold Leg Liquid Temperature Comparison for LOFT Test L3-1.

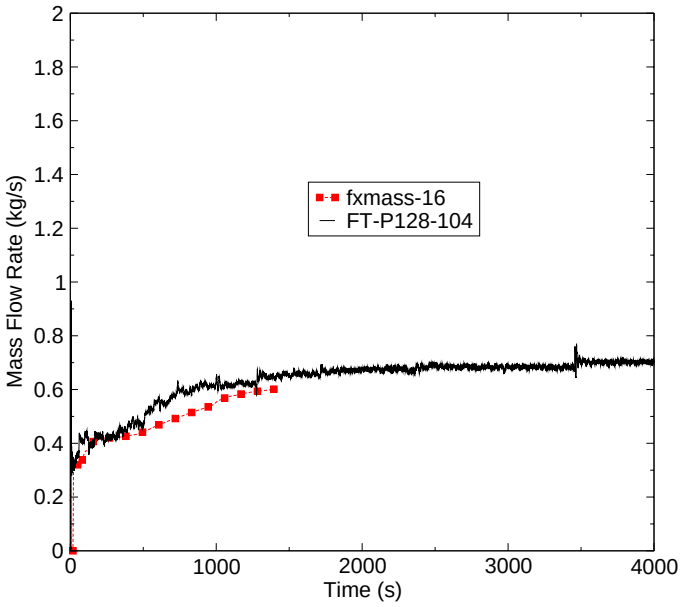

Figure C.4-30. HPIS Flow Comparison for LOFT Test L3-1.

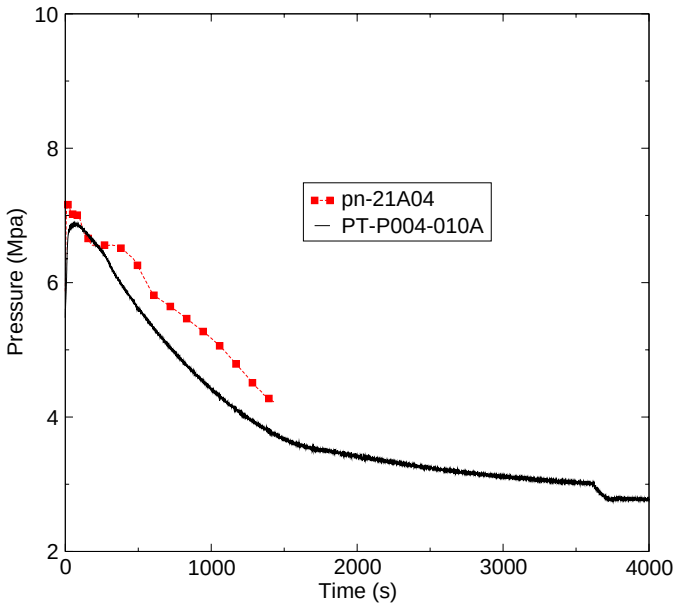

Figure C.4-31. Secondary Side Pressure comparison for LOFT Test L3-1.

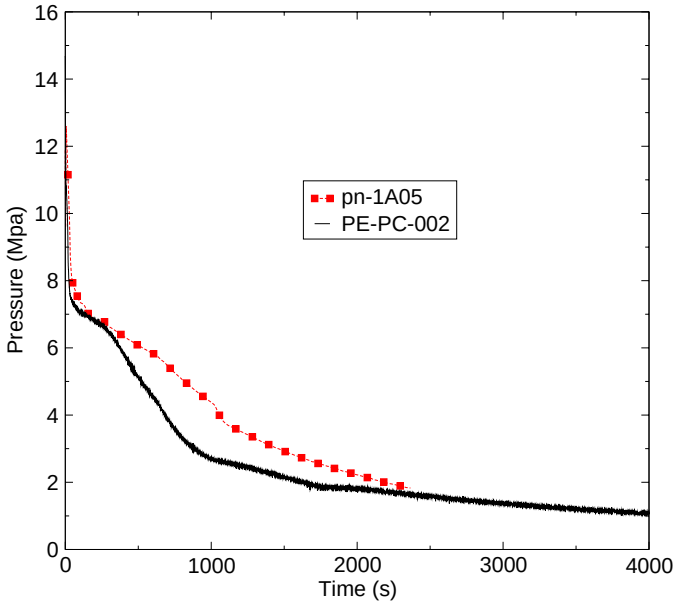

Figure C.4-32. Pressure Comparison. TRACE has 2% DC/UH Leakage Flow.

C.4.4.3. Assessment Results Summary

The TRACE simulation of LOFT Test L3-7 compared very well with the measured data except for hot and cold leg densities. TRACE overpredicted both primary and secondary side pressures when the SG steam control valve was modeled to behave as described in the experimental data report. However, the measured secondary side pressure, as well as the measured position of the steam valve, suggest that there may have been considerable steam leakage through the valve. To simulate the implied experimental steam leakage, the TRACE calculation was rerun with the secondary side pressure the same as the measured pressure. In this case, the TRACE calculation was in excellent agreement with primary side measured pressures and temperatures.

TRACE did not accurately simulate the drainage of the cold leg when HPIS injection was terminated at 1800 s in Test L3-7. This may be because there is no downcomer to upper head leakage in the TRACE model and there is too much inventory in the vessel in TRACE. A revised TRACE simulation was made with 2% DC/UH leakage flow and a 33% increase in break area. This simulation resulted in hot and cold leg densities that were in much better agreement with the data. However, the agreement of primary system pressure was not as good. The simulation stongly suggests that TRACE, given the actual break geometry, is accurately predicting break flow for the first 400 s of the test but is then underpredicting the break flow throughout the rest of the subcooled blowdown.

The TRACE simulation of LOFT Test L3-1 did not compare well with the test data. The TRACE calculation of primary and secondary pressures were well above the data. The Test L3-1 code-data comparison indicates that an under-prediction of critical flow may be responsible for TRACE's overprediction of pressures.

Reference 5 recommended that Test L3-1 be dropped from the TRACE assessment matrix unless it is demonstrated via separate effects assessment that the TRACE break flow model does indeed under-predict break flows for nozzle sizes typical of those used in Test L3-1. As mentioned previously, future TRACE assessments will update the LOFT model for use in both small break and large break LOCA simulations. Future versions of TRACE are also expected to implement new features, and these enhancements may improve the LOFT SBLOCA predictions.

C.4.5. References

1 Douglas L. Reeder, "LOFT SYSTEM AND TEST DESCRIPTION (5.5-FT NUCLEAR CORE 1 LOCES)", NUREG/CR-0247, July 1978. (ADAMS Accession No. ML070250396)

2 "LOFT Program Description," LPD-1, October 1974. (ADAMS Accession No. ML063070483)

3 C. D. Fletcher, "Comparison of TRACE and RELAP5 Calculations with Test Data for LOFT Experiments L3-7 and L3-1," Information Systems Laboratories, Inc., ISL-NSAD-TR-03-11, April 2003.

4 D. L. Caraher, "LOFT SBLOCA Tests," Information Systems Laboratories, Inc., December 2005. (ADAMS Accession No. ML061710609)

5 D. L. Caraher, "TRACE CALCULATION NOTEBOOK - LOFT Small Break Tests L3-1 and L3-7", December 2005. (ADAMS Accession No. ML061710610)

6 Dawn L. Gills and Janice M. Carpenter, "Experimental Data Report for LOFT Nuclear Small Break Experiment L3-7," Idaho National Engineering Laboratory, EG&G Idaho, Inc., NUREG/CR-1570, EGG-2049, August 1980.

7 P. D. Bayless, J. Bruce Marlow and Rahland H. Averill, "Experimental Data Report for LOFT Nuclear Small Break Experiment L3-1," Idaho National Engineering Laboratory, EG&G Idaho, Inc., NUREG/CR-1145, EGG-2007, January 1980.

C.5. ROSA-IV Tests

Author(s): Lichao Du, Millan Straka, Shawn Marshall

Affiliation: AdSTM Inc., USNRC

Code Version: TRACE V5.0

Platform and Operating System: Intel x86, Windows XP

C.5.1. Introduction

This chapter presents TRACE analysis results for a series of cold-leg small break loss-of-coolant tests conducted in the ROSA-IV Large Scale Test Facility (LSTF). The TRACE input model documented here includes all the major components of the test facility. Judgements concerning the adequacy of the input model and its initial thermal-hydraulic conditions were made through comparisons against the steady-state test data of test run SB-CL-18. The transient simulation results for a series of experiments were compared to test measurements and conclusions drawn concerning the ability of the code to simulate these types of small break loss-of-coolant accidents (SBLOCAs). Assessment involved comparisons to data from the following tests:

Test #	Description
SB-CL-01	2.5% cold leg side break, HPIS/LPIS injection purposely delayed (until 1200 sec), auxiliary feedwater available.
SB-CL-05	5% cold leg side break, HPIS/LPIS injection, auxiliary feedwater available.
SB-CL-14	10% cold leg side break, LPIS injection, no HPIS, no auxiliary feedwater.
SB-CL-15	0.5% cold leg bottom break, no HPIS/LPIS injection, no auxiliary feedwater.
SB-CL-16	0.5% cold leg top break, HPIS/LPIS injection (manual after loops cleared), no auxiliary feedwater.
SB-CL-18	5.0% cold leg side break, LPIS injection, no HPIS injection, no auxiliary feedwater

The key SBLOCA phenomena are identified by major system components and a ranking via a Phenomena Identification and Ranking Table (Ref. 6) (PIRT) is assigned for each phase of the SBLOCA with the principal Figure of Merit (FOM) from the PIRT being the core collapsed liquid level.

The core collapsed liquid level indicates the degree of core uncovery and is measured by the pressure difference across the reactor core in the test and the TRACE simulation. The early core uncovery during a SBLOCA is the result of a manometric balance of liquid in the loops and the vessel. For each loop, one leg (or the hot side) of the "manometer" includes the upflow side of SG U-tubes, the hot leg, upper plenum and core. The other leg (or the cold side) includes the downflow side of SG U-tubes, the cold leg, the loop seal, and the downcomer. The two legs are connected through the vessel lower plenum. In the late stage of core liquid depression, the mass flow rate in the loops becomes very low. One can assume that no fluid flows over the top of the SG U-tubes. The gravity head is essentially the same in the two legs. In this situation, if there is more liquid holdup in the uphill side of the U-tubes than in the downhill side of the U-tubes, the core water level would be depressed to maintain the gravity head balance in the two legs of the "manometer." When the loop seal is cleared, there is no liquid holdup in the U-tubes, and both cold and hot legs are almost empty. Therefore, the core coolant mixture level will swell and recover after all liquid flows back to the core.

Other measurable high ranking phenomena were considered in the code-to-data comparison as well. These phenomena are

1. Fuel Rod Decay Heat (high in phases 1 through 5) - *an input parameter; it is initiated by a reactor trip signal in the TRACE calculation.*
2. Break Upstream Flow Regime (phases 1 through 5) - *measured by a series of densitometers at three locations: top, middle, and bottom in the broken cold leg and the break unit. However, it can only be shown as the mixture density and flow-regime number in the TRACE calculation.*
3. Break Flow (phases 1 through 5) - *measured by catch tank level and a flow rate meter. The flow rate meters are invalid during two-phase flow conditions and therefore not presented in this analysis. TRACE calculates the break flow rate.*
4. Steam Generator Primary Side Heat Transfer (condensation in the U-tubes), (phases 1 and 3) - *indirectly measured by the pressure difference in the U-tubes in the test and the calculation.*
5. Core Mixture Level (phases 3 to 5) - *indirectly measured by the pressure difference across the core in the test and the calculation.*

6. Downcomer-Hot Leg Gap Flow (phase 3), - *measured by the leakage flow rate between the downcomer and the hot leg in the test and the calculation.*
7. Steam Generator Tube Voiding/CCFL (phase 3) - *measured by the pressure difference in the U-tubes in the test and the calculation.*
8. Loop Seal Clearance - Entrainment/Flow Regime/Interfacial Drag (phase 3) - *indirectly measured by the pressure difference in the loop seal in the test and the calculation.*
9. Cold Leg Horizontal Stratification/Flow Regime (phases 3 to 5) - *measured by a set of densitometers in the cold legs in the test and the mixture density in the calculation.*
10. Downcomer/Lower Plenum-Mixture Level/Flashing/Void Fraction (phases 3 to 5) - *measured by the pressure difference across downcomer in the test and the calculation.*
11. 3D Core Power Distribution (phases 4 to 5) - *an input parameter to the TRACE code from test data.*

C.5.2. Test Facility Description

The ROSA-IV Large Scale Test Facility (LSTF) is a large integral effects test facility used to simulate LOCA and operational transient behavior in PWRs. It is a 1/48 volumetrically scaled, full height, full pressure model of a reference 3423 MWt Westinghouse four-loop Trojan class PWR. A diagram of the test facility is shown in Figure C.5-1. The LSTF facility operated at the temperature and pressure of the reference PWR. It had two loops (such that the volume scaling ratio in the loop piping was 1/24), each containing all the components of the reference plant. Both loops were the same size but had different break geometries, and the hot leg in loop A had a pressurizer. The core consisted of 1064 electrical heater rods and could produce a maximum power of 10 MW. This represented only 14% of the scaled full power of 71 MW (1/48 of 3423 MW). The heater-rod dimensions simulated 17x17 fuel assemblies. The test facility was equipped with over 2000 instruments for various parameter measurements. The LSTF system description (Ref. 1) depicts the test facility in detail.

All the tests were carried out to examine the core liquid level depression phenomena. In order for LSTF to deliver the 14% rated, scaled core power at steady state initial conditions, the coolant pumps were operated to deliver 14% of rated, scaled primary mass flow. The primary to secondary energy transfer rate was maintained at a 14% rated, scaled value by controlling the secondary system pressure to 7.4 MPa. Small break experiments, such as the SB-CL-18 test, were conducted to investigate safety margins during core liquid level depression. An SBLOCA PIRT (Ref. 1) includes major events and the important core depression phenomena that occurred during these tests; the following is its summary.

1. The initiation event of break followed by primary system rapid depressurization;
2. Beginning of boiling and flashing which resulted in break flow becoming two-phase;
3. Void formation in the primary system; loss of additional coolant through the break, which resulted in the first core uncovery. Subsequent core flushing led to the quick core recovery.
4. Loop seal clearing event when the liquid plug is expelled from the U-bend section of the cold leg piping.
5. Core liquid level depression and core heatup resulted in the second core uncovery;
6. Core collapsed level recovery and the establishment of adequate core cooling.

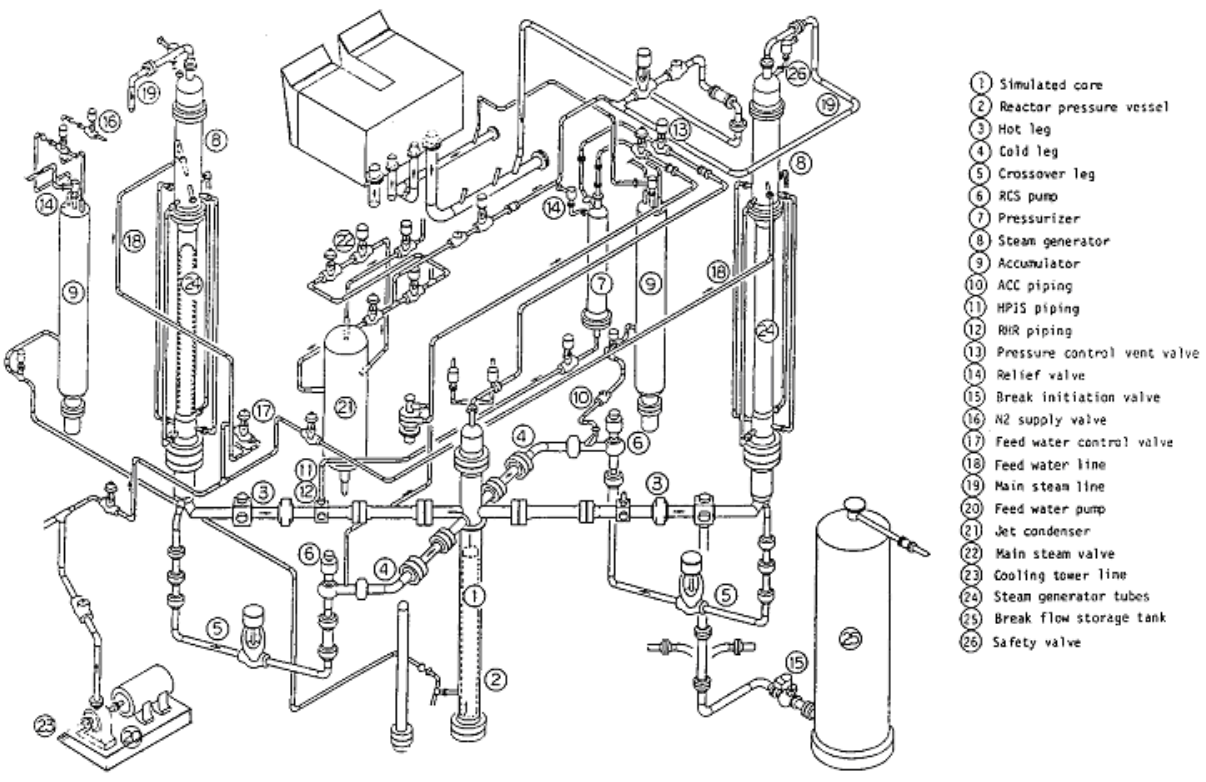

Figure C.5-1. Facility Overview

C.5.3. TRACE Model Description

This section describes the TRACE input model for the ROSA-IV facility. The geometric information used to develop the model is based on the system description documents (Refs. 2, 5), a Los Alamos calculation notebook (Ref. 4), and a TRAC-P ROSA-AP600 input deck.(Ref. 3).

The TRACE input model is shown in Figure C.5-2. It consists of a 3D reactor vessel model, two identical primary coolant loops, Loop A and Loop B, and a pressurizer. Each loop consists of a reactor coolant pump, a steam generator, and connecting piping. The primary loop piping is divided into three segments: hot leg, loop seal, and cold leg. The pressurizer is connected to the hot leg of Loop A through the surge line. The pressurizer spray draws water from the cold leg of Loop A. Two accumulators connect to each of the cold legs. The pump model was obtained from a TRAC-P ROSA/AP600 input deck (Ref. 3) although the pump coast-down curve was modified to match the ROSA-IV test conditions.

C.5.3.1. Reactor Vessel Model

The reactor vessel of the ROSA-IV facility is modeled with a VESSEL component and a number of heat structure components with and without power. The power supply and the core power distribution are modeled using a POWER component. The data for the reactor vessel model is based on a Los Alamos calculation notebook (Ref. 4) for a TRAC model of the ROSA-IV facility. It is modified by adding two more sectors and six more axial levels in the core region. Figure C.5-3 demonstrates the vessel model, which consists of four rings, four sectors, and twenty two levels. It has eighteen sources: two for cold leg nozzles, two for hot leg nozzles, two for hot leg leakage paths, and twelve for the control rod guide tubes. Figure C.5-4 demonstrates the heat structure arrangement in the one-half vessel as well as the nodalization of a single fuel rod.

Inside the core barrel are three rings as demonstrated in Figure C.5-3. They reflect the core power zoning of the ROSA-IV. The core power zoning is schematically demonstrated in Figure C.5-5. (Ref. 1). In the center are four low power bundles (Bundles 21 to 24), followed by eight high power bundles (Bundles 13 to 20). In the periphery of the core are arranged twelve low power bundles. The outer ring (ring 4) is occupied by the vessel downcomer. In the azimuthal direction, the model has four symmetrical sectors. Along the axial direction, twenty two levels are used to model the lower plenum, the heated core region, the upper plenum, and the vessel head. Specifically, the lower plenum is modeled by levels 1 and 2; the heated core section by the levels from 3 to 14; the upper plenum by the levels from 15 to 19; and the vessel head by the upper 3 levels. The primary loops are connected to the vessel at level 18.

A total of 144 heat structure components are coupled with the vessel model to represent the heater rod bundles, the internal structures, and the vessel wall. The arrangement of these heat structures is illustrated in Figure C.5-4(a) for one half of the vessel. As summarized in Table C.5.1, twelve powered heat structure components, HTSTR 901 to 912, are used to model the core power distribution. Figure C.5-4(b) and Figure C.5-6 illustrate the radial nodalization of a single heater rod and the axial power profile, respectively.

C.5.3.2. Steam Generator Model

Figure C.5-7 provides the steam generator model with the secondary piping for Loop B. The steam generator and the secondary side configuration of Loop A are identical to those of Loop B. The model is derived from the steam generator model of the TRAC-P deck of ROSA/AP600 (Ref. 3). The heat structures were converted from ROD/SLAB components to TRACE HTSTR components, with the nodes made coincident with the fluid cell centers.

The steam generator model is represented using an assembly of PIPE and TEE components. A single PIPE component is used to model the steam generator U-tube bundle. On the secondary side, the steam generator is divided into the upper downcomer, the downcomer annulus, boiler/ riser section/steam separator, and steam dome sections, with each section modeled by a TEE component.

The feedwater system is represented by a FILL component. Feedwater conditions are specified according to test procedures and requirements. The steam from each steam generator flows through the main steam lines and into the steam header, where the heat is dumped.

C.5.3.3. Pressurizer Model

The pressurizer, as shown in Figure C.5-8, is modeled by three separate components. At the top is a PRIZER component (112), which is used to specify the operating pressure. The pressurizer spray is modeled with a FILL (802) that connected to the PRIZER. The middle section is modeled with a TEE component (111), which serves as a water reservoir. The heater section of the pressurizer is modeled with a PIPE component (110) and its wall functions as the heater assemblies of the pressurizer, providing heat in a controlled manner. The pressurizer is connected to the hot leg of Loop A through the surge line (160).

C.5.3.4. Primary Loop Piping

The hot leg of Loop A (see Figure C.5-9) is modeled with two TEE components (TEE 101 and TEE 102). One end of the hot leg is connected to the vessel nozzle and the other to the inlet plenum of the steam generator (SG A). The side tube of TEE 101 is connected to the vessel downcomer through a PIPE component (PIPE 100), forming a simulated hot leg leakage path. The side tube of TEE 102 is connected to the surge line.

Between the outlet of SG A and the reactor pump suction (RCP A) is the loop seal section. The nodalization of the loop seal is modeled by two pipe components as demonstrated in Figure C.5-11. The pump model used in the TRAC-P deck (Ref. 3) is adopted for the ROSA-IV model. The test facility specific homologous pump curves are built into the model in accordance to the pump specifications given in the system description (Ref. 1).

The cold leg, from the pump suction to the pump delivery, is shown in Figure C.5-10. It is modeled with two TEE components 105 and 106. The emergency core cooling system (ECCS)

and accumulators are connected to the primary system through the side tube of TEE 108 and 207. The side tube of TEE 107 models the pressurizer spray nozzle (155).

The nodalization of Loop B is given in Figure C.5-12 to Figure C.5-14. The components follow a numbering convention such that the components in primary Loop A take the form 1##, while the equivalent components in primary loop B take the form 2##. A similar convention is followed in the secondary side with components numbered 3## for Loop A and 4## for Loop B.

The primary loop piping of Loop A and Loop B are identical except some nozzles could be used for different purposes in the two loops. The piping of Loop A is given in Figure C.5-9 to Figure C.5-11. The dimensions are based on the system description for the ROSA-IV facility (Ref. 1).

The two loops are identical except for the use of two nozzles:

- The side tube of TEE 202 is reserved for hot leg break tests;
- The side tube of TEE 208 is connected to a break model for cold leg break simulation.

Table C.5.1. Powered HTSTRs for Fuel Rods

HTSTR ID	Axial Location (Cell #)	Power Zone[a]	No. of Fuel Rods	Relative Power Density
901	1	23,24	45	1.000
902	2	22,23	45	1.000
903	3	21,22	45	1.000
904	4	21,24	45	1.000
905	5	17,18	90	1.435
906	6	15,16	90	1.435
907	7	13,14	90	1.435
908	8	19,20	90	1.435
909	9	5,6,11,12	131	0.710
910	10	3,4,10,11	131	0.710
911	11	1,2,9,10	131	0.710
912	12	7,8,9,12	131	0.710

a. See Figure C.5-5

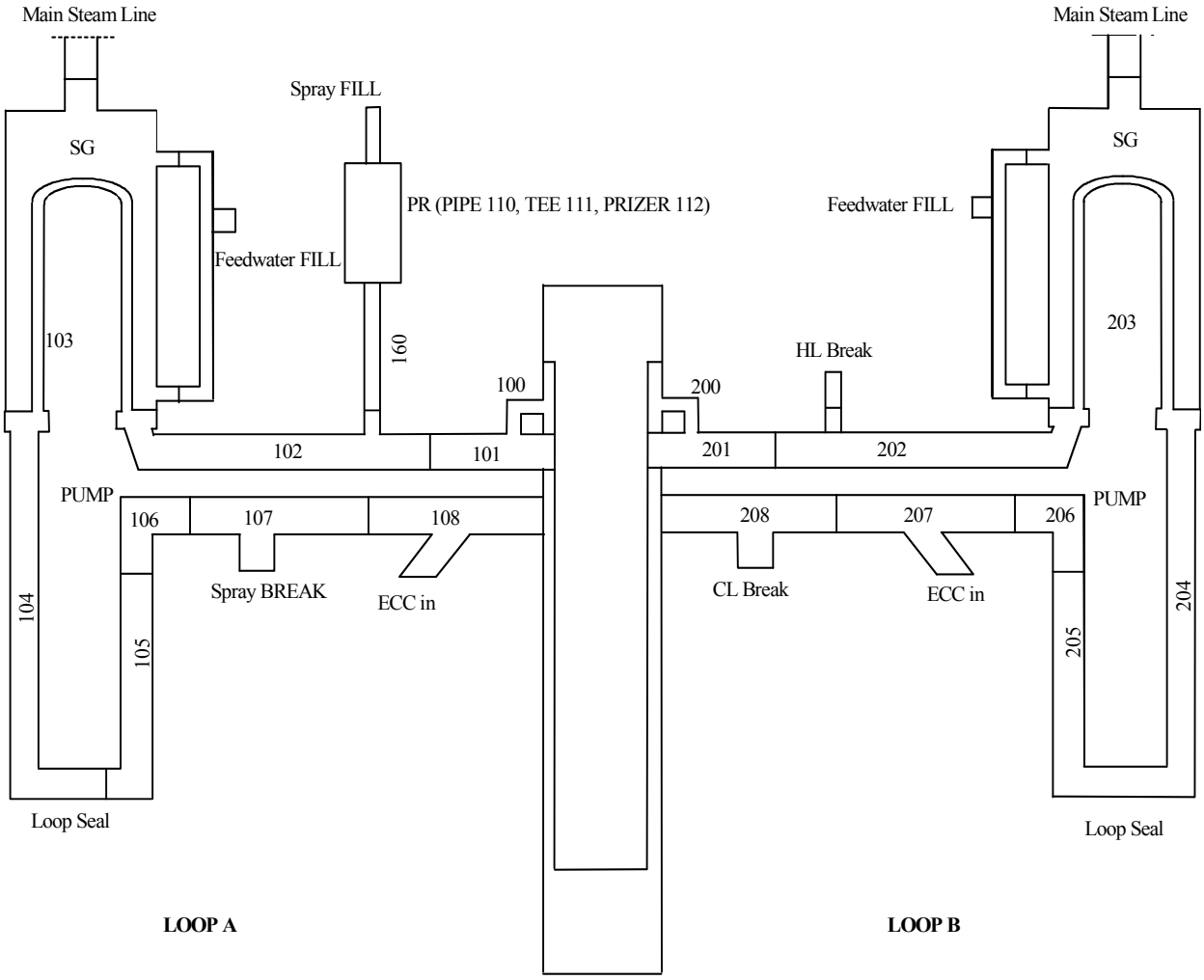

Figure C.5-2. An Overall Description of the TRACE ROSA-IV Plant Model

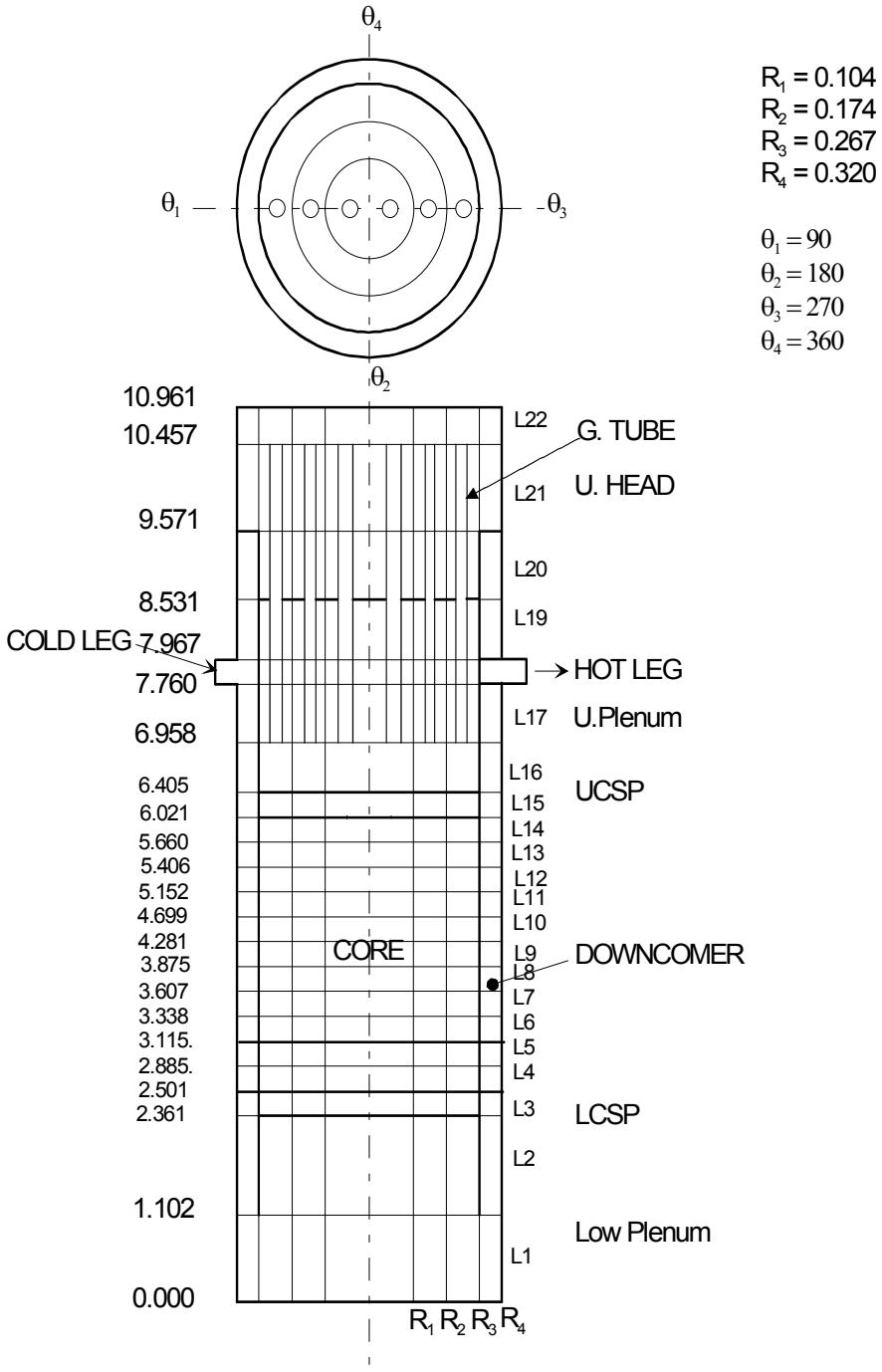

Note: Elevations are in meters

Figure C.5-3. Vessel Nodalization

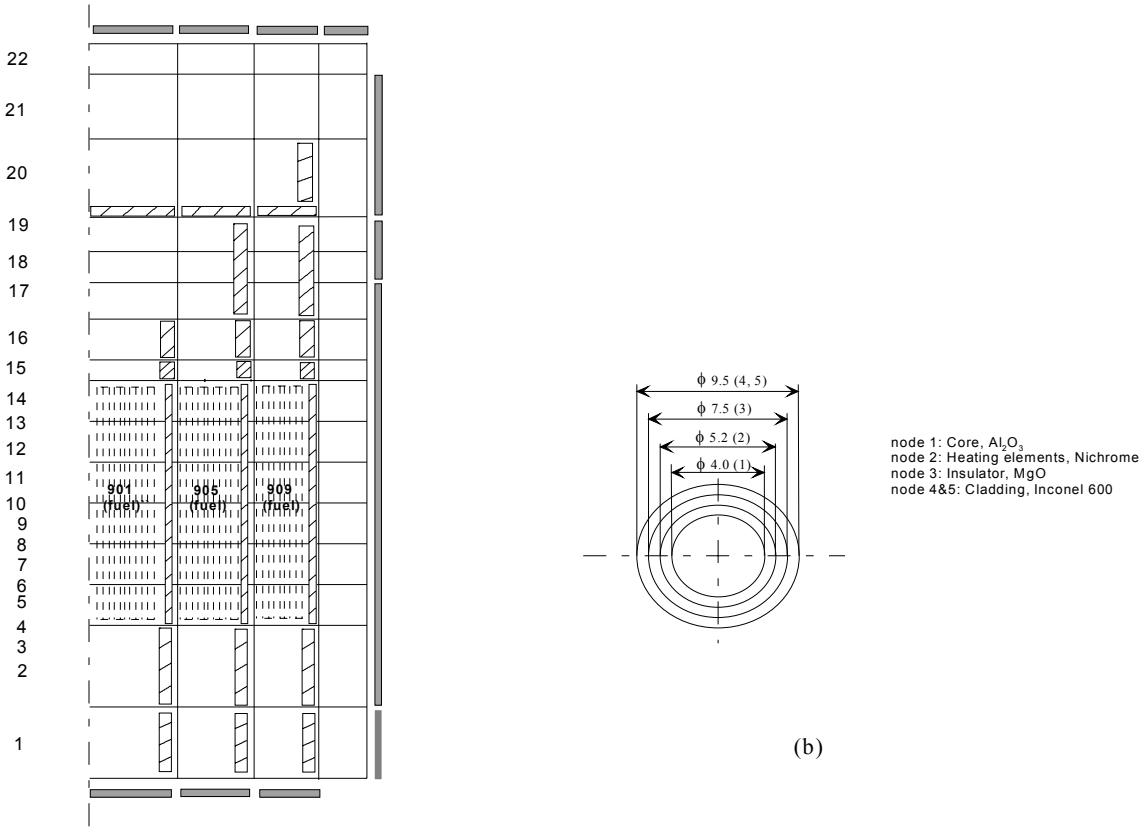

Figure C.5-4. (a) Heat Structure Arrangement in One-Quarter Vessel (b) and Radial Nodalization of a Single Fuel Rod

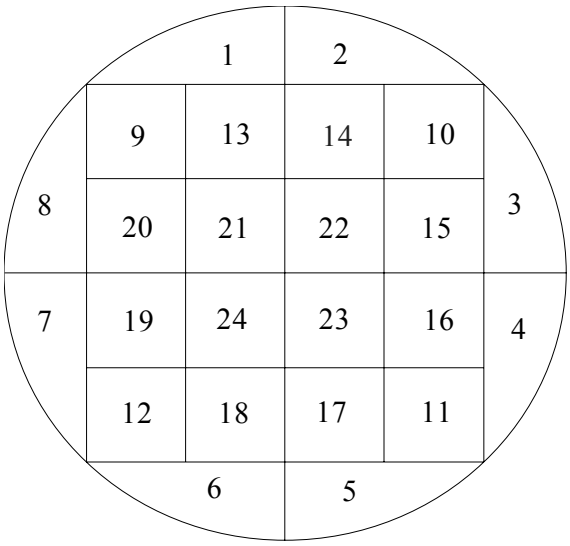

Figure C.5-5. Power Zoning of ROSA-IV Core

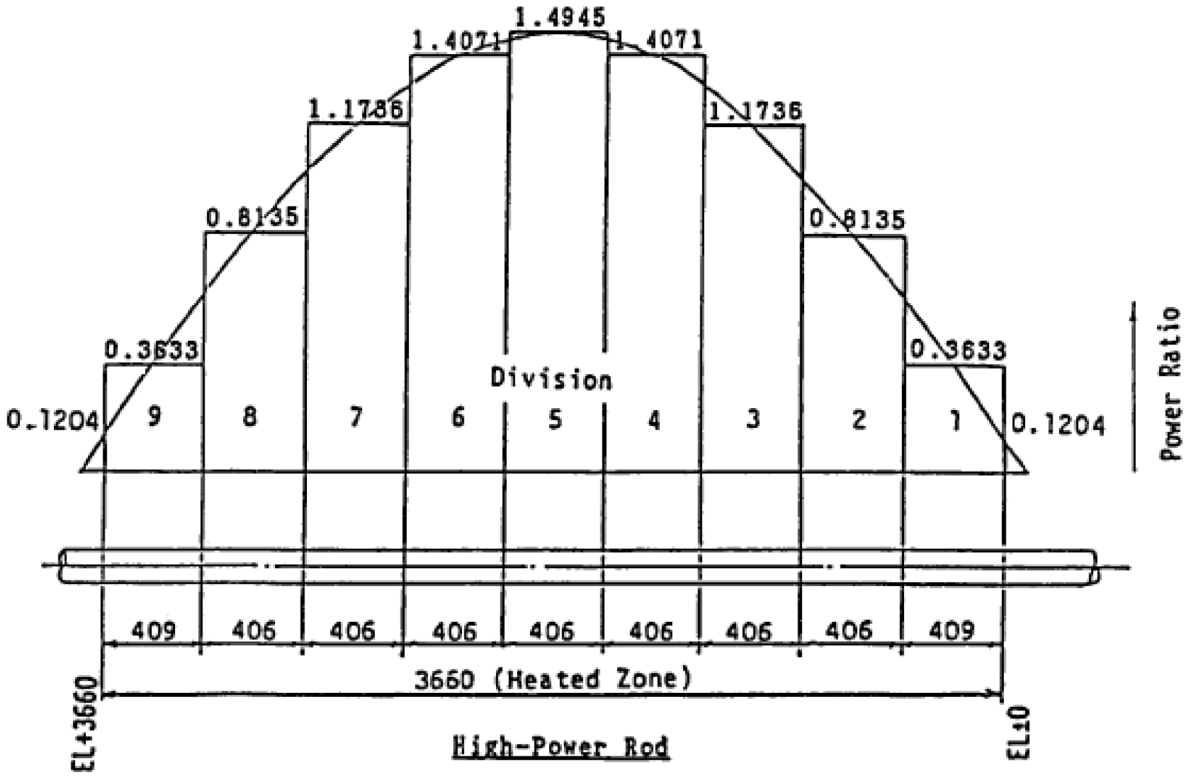

Figure C.5-6. Core Axial Power Profile

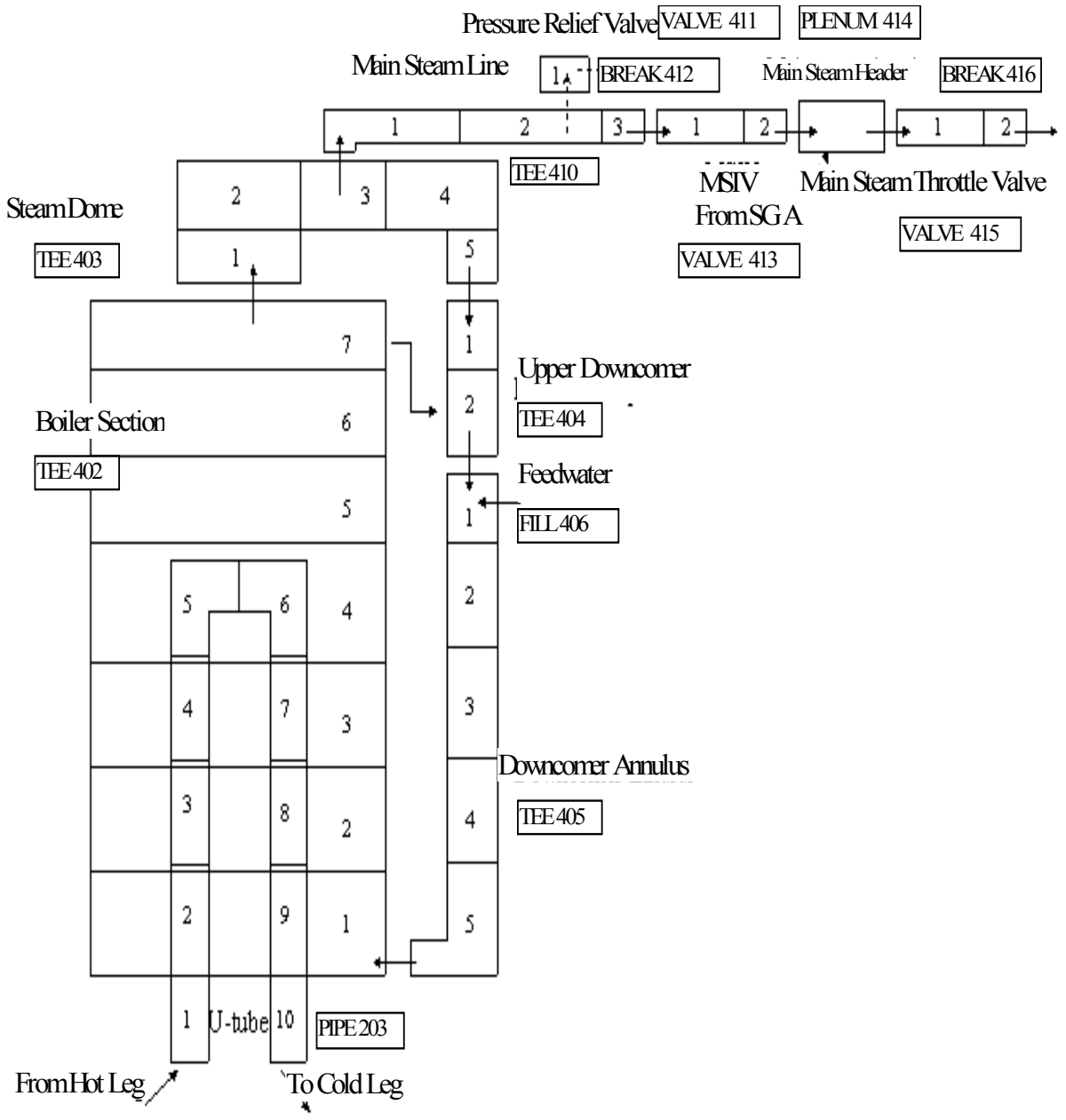

Figure C.5-7. Steam Generator Model and the Secondary Loop (Loop B)

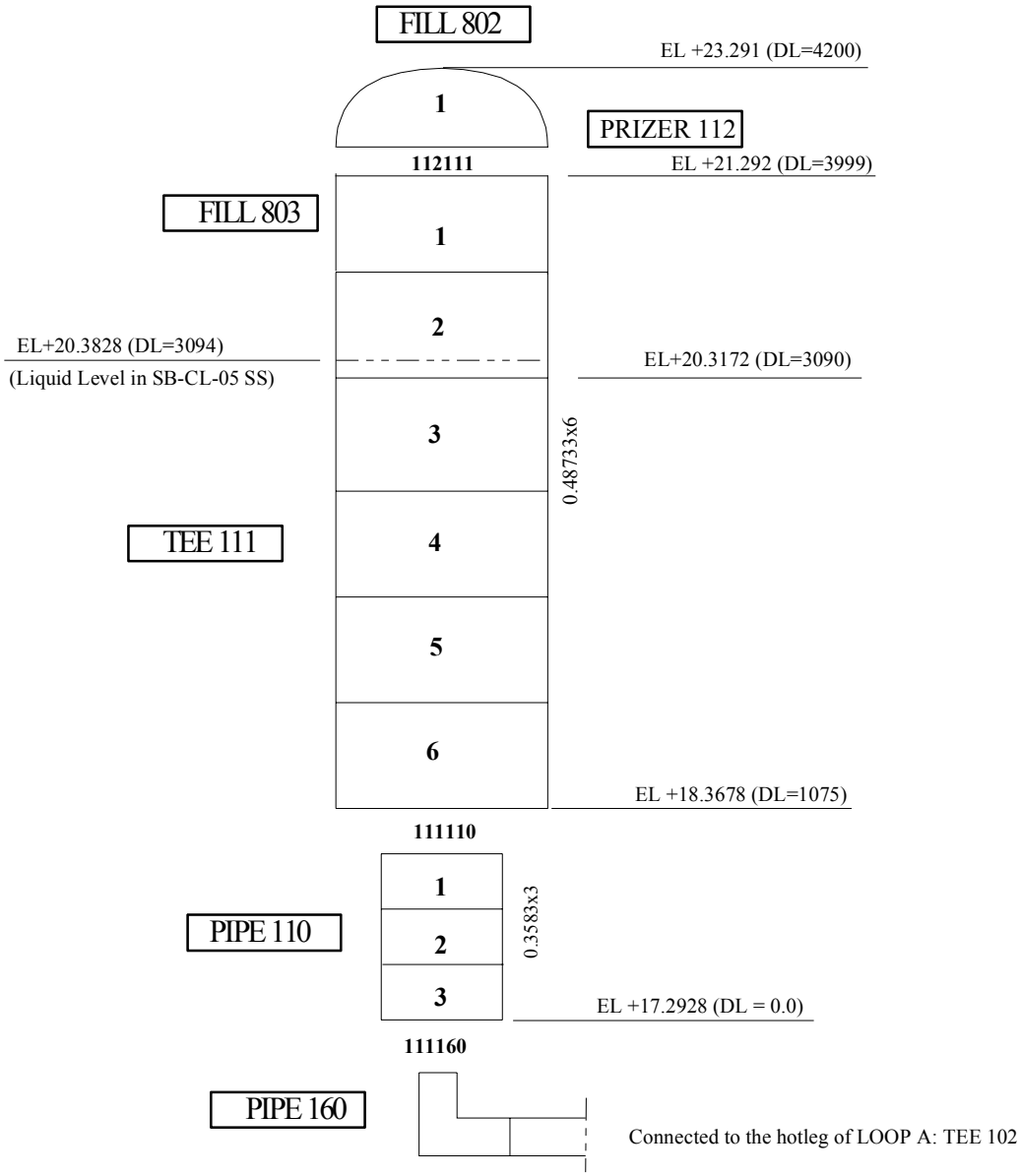

Figure C.5-8. Pressurizer Model

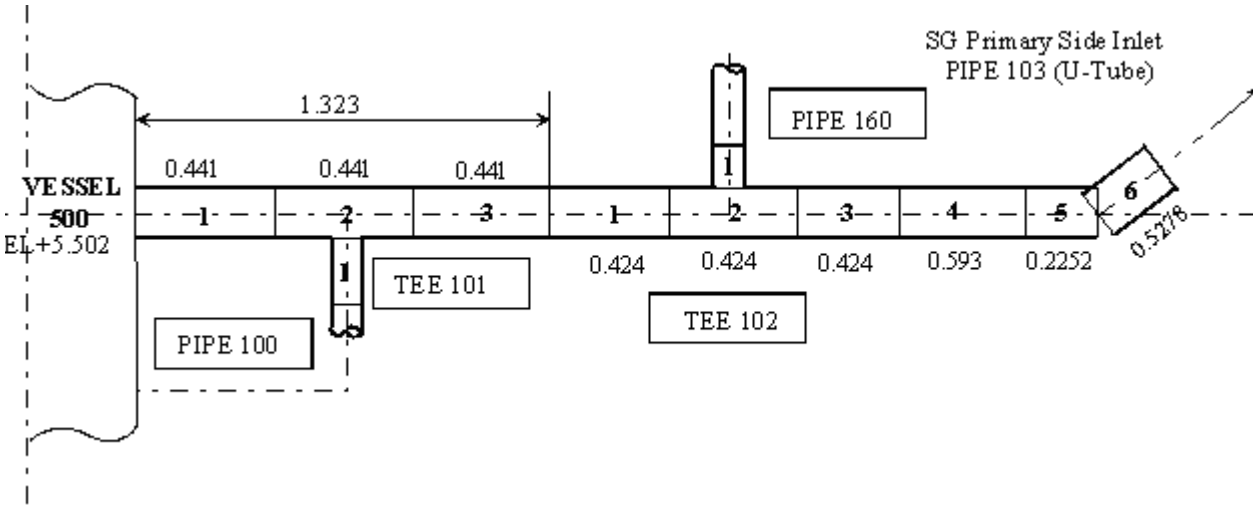

Figure C.5-9. Hot Leg of Loop A

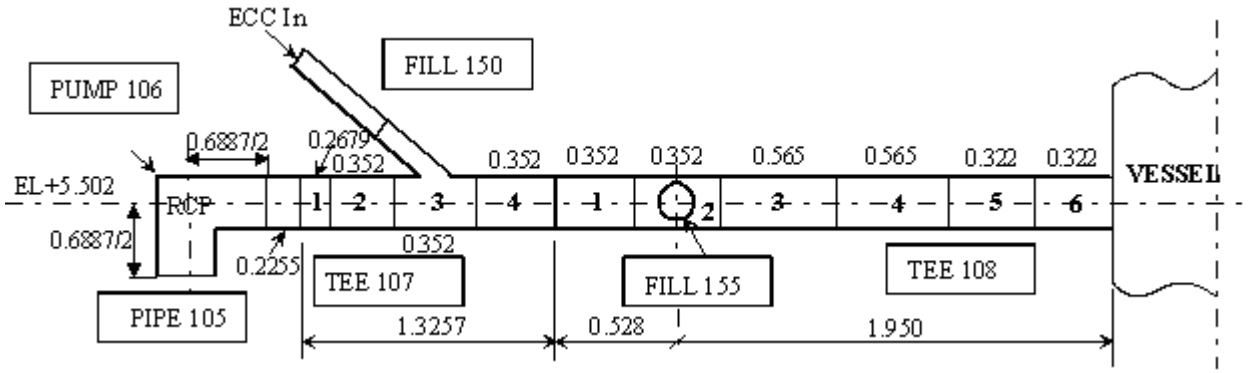

Figure C.5-10. Cold Leg of Loop A

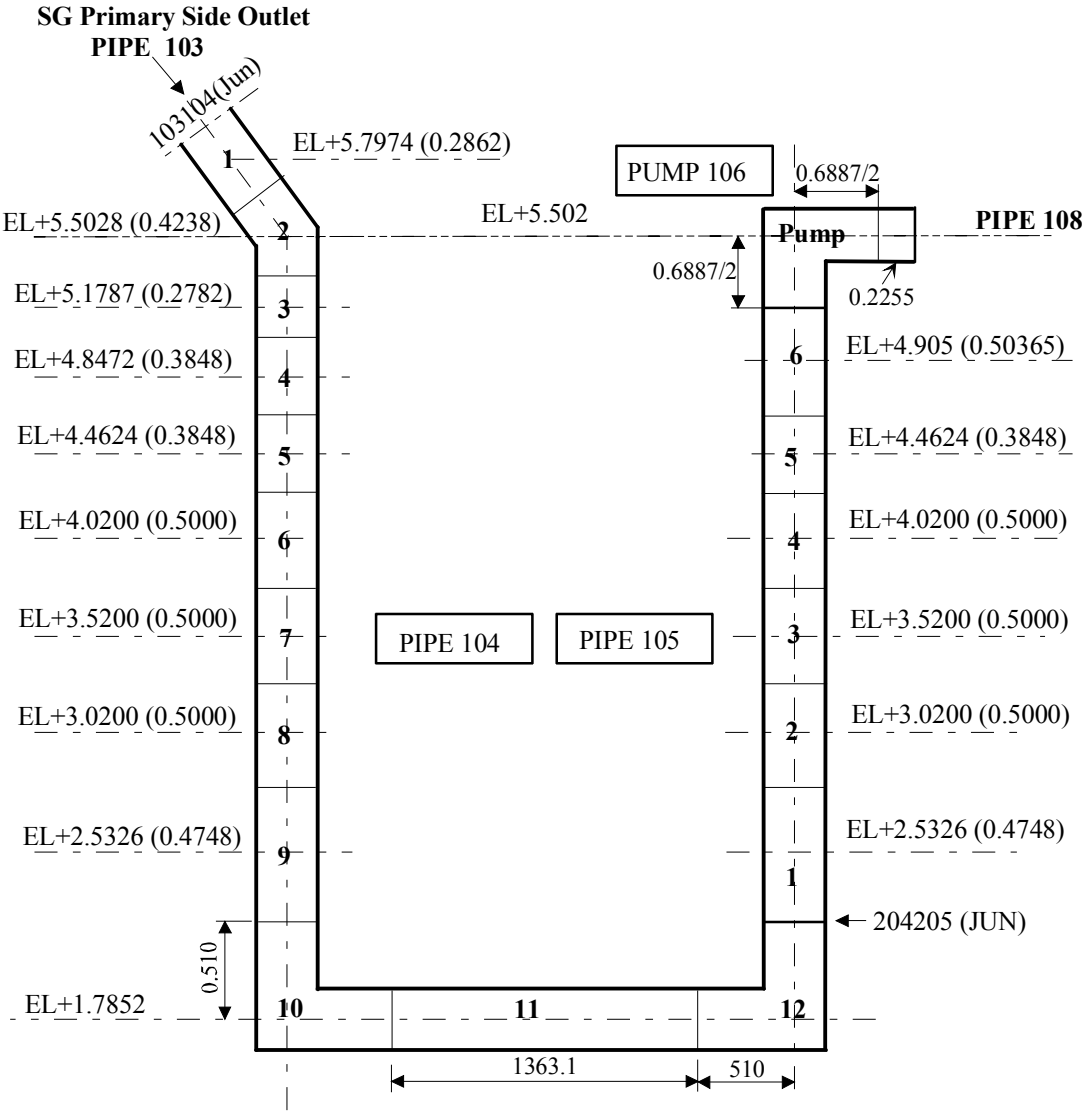

Figure C.5-11. Loop Seal of Loop A

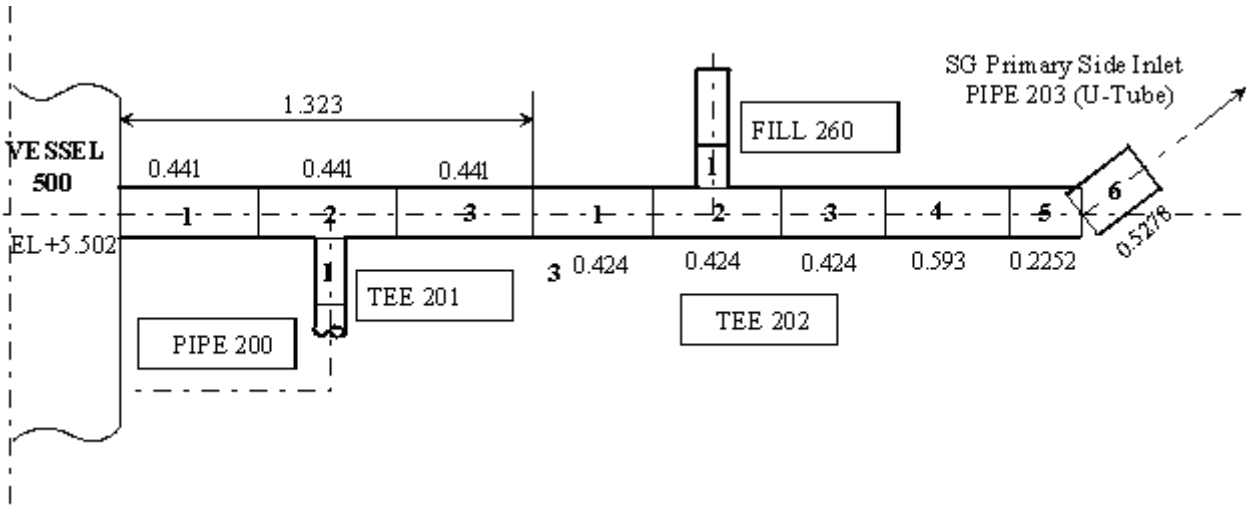

Figure C.5-12. Hot Leg of Loop B

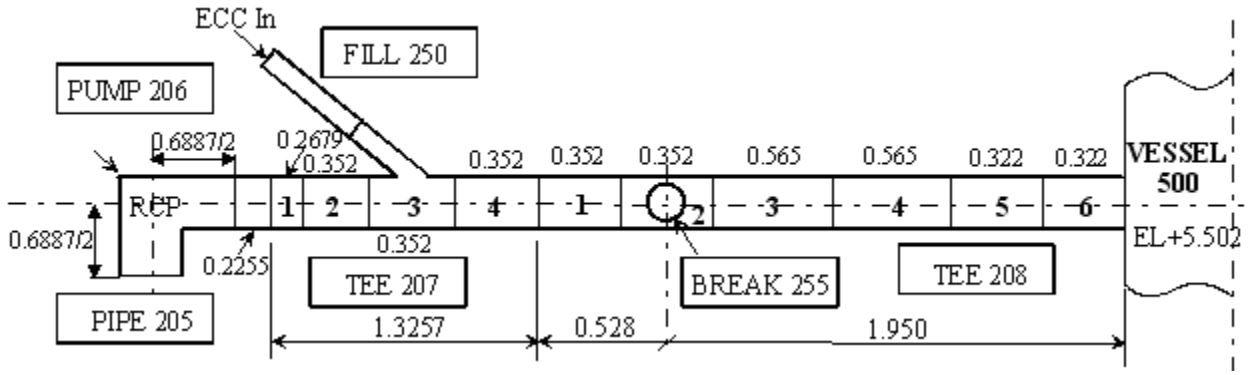

Figure C.5-13. Cold Leg of Loop B

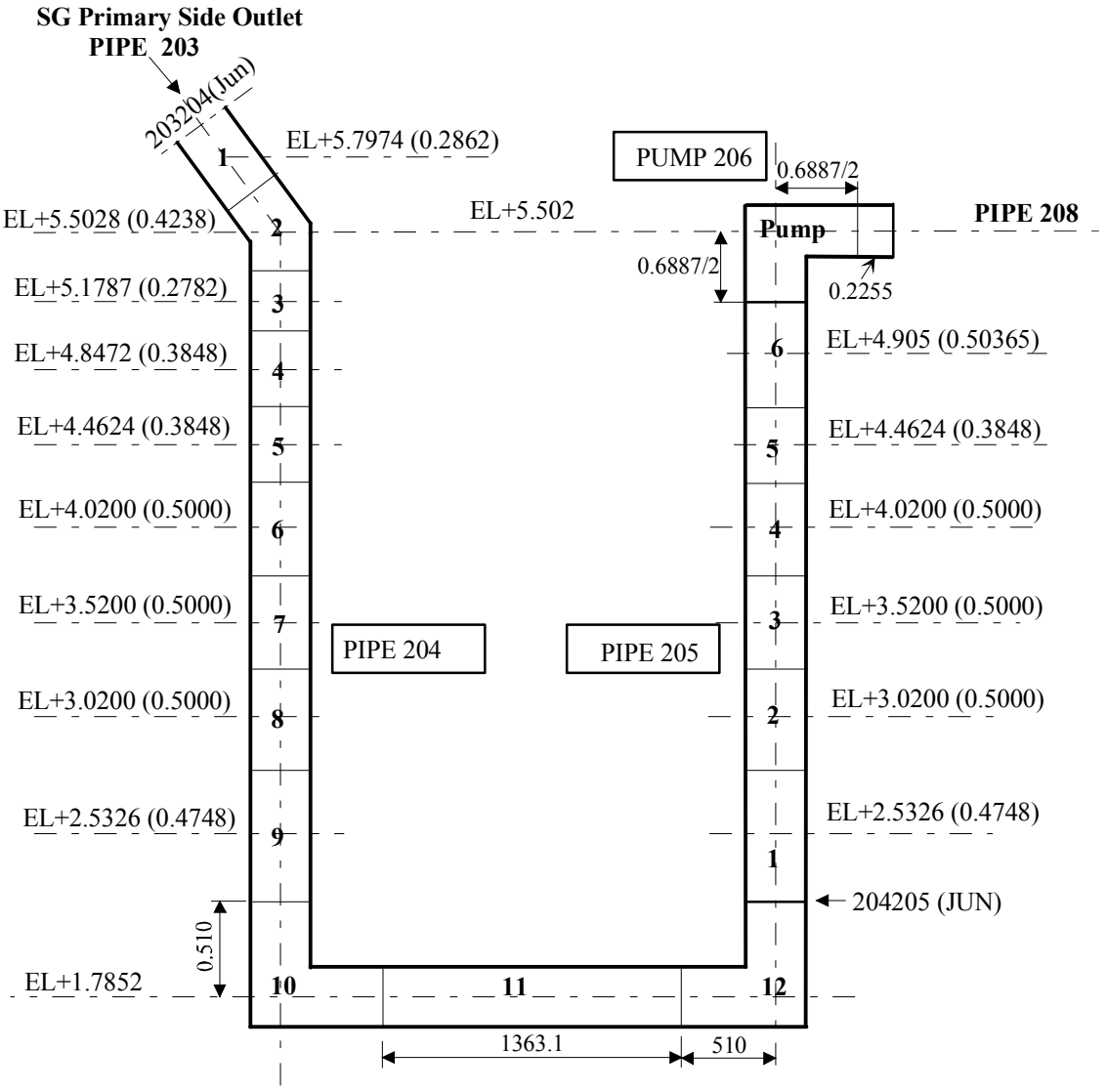

Figure C.5-14. Loop Seal of Loop B

C.5.4. TRACE Input Model Adequacy Assessment

The TRACE ROSA-IV plant input model is evaluated by comparing the calculated steady-state results with the steady-state data from the SB-CL-18 test. The steady-state condition for other tests are basically the same as SB-CL-18 test. Only a minor difference of a few degrees Kelvin exist for feedwater temperature among the test cases. Although steady state calculations are performed for all of the tests, SB-CL-18 will be documented here as the representative case for the steady-state condition assessment.

C.5.4.1. Plant Steady-State Conditions

Some major system parameters are plotted in Figure C.5-15 through Figure C.5-22 to illustrate the steady-state calculation process. It indicates that the steady-state calculation converges within 250 seconds. It is also noticeable that the secondary-side steam flow and pressure show density-wave-like oscillations of small magnitudes after the two parameters are stabilized for a period of time. This could be superficial because of the feedback control systems introduced through the steady-state controllers. The steady state of the model is effectively reached.

Table C.5.3 gives the calculated plant steady-state parameters and the steady-state data of the SB-CL-18 test run. Based on the acceptance criteria provided in Table C.5.2, the calculation results agree well with the test data except for the hot leg temperature and the loop average temperature.

The calculated hot leg temperature is higher than the measured value by 0.5 K, while the suggested error margin is 1.1 K. The uncertainties in the hot leg temperature measurements may have contributed to the deviation. The average of the measurements from TE011A, TE011B and TE011C was 599 K (see Table C.5.3). The average of the measurements from TE010A - TE010E was 601.2 K, and the average of the measurements from TE040A - TE040E was 600.76 K. Considering the measurement uncertainties, the calculated hot leg temperature and the calculated loop average temperature are acceptable.

Because of its importance in the transient analysis (SB-CL-18), the initial mass inventories of the pressurizer are listed in Table C.5.4 for the model and the test SB-CL-18. The initial mass inventory in the model is made as close as possible to the test value.

C.5.4.2. Fluid Inventory Distribution

The coolant inventory and its distribution in the primary loop play an important role in determining the transient behavior of a reactor system in the event of a loss-of-coolant accident. Table C.5.4 lists the fluid inventories of various sections or components for the primary system. According to this table, the TRACE model demonstrates a good agreement with the facility data.

The facility data is obtained from Table 2.1 of the supplemental system description for the facility (Ref. 5). The total primary system volume of the TRACE model and ROSA-IV deviate by about 0.6%. Likewise, for each section or component, the fluid volume from the model agrees quite well with the data.

C.5.4.3. Summary

It is concluded that the steady-state simulation results agree with the test data.

In the evaluation of the TRACE model, system parameters, and the fluid inventory distribution along the primary loop, mass and energy balances have been examined. The geometric volumes

for each component in the TRACE model match the ROSA-IV/LSTF. Energy balance is confirmed by comparing energy removed by the secondary steam flow to the total core input power. Based on the discussion above, the current TRACE model represents a reasonably accurate description of the ROSA-IV facility.

Table C.5.2. Steady-State Parameter Checklist

Parameters	**Margin of Error**
Core power	±0.5% for test facilities
RCS pressure	±0.1379 MPa (20 psi)
Cold leg temperature	±1.1 K (2 F)
Hot leg temperature	±1.1 K (2 F)
Loop average temperature	±1.1 K (2 F)
RCS loop flow	±1%
SG secondary pressure	±0.1379 MPa (20 psi)
SG steam flow rate	±1%
SG Feedwater temperature	±5.556 K (10 F)
SG recirculation ratio	±50%
RCP speed (rad/s)	±25%
Liquid level in PR	Within normal operation band
Vessel head temperature	±2.78 K (5 F)
Upper head bypass	±50%
Core bypass flow	±50%
Vessel inlet to outlet DP	±25%
Core DP (KPa)	±25%
Hot leg nozzle DP	±25%
Cold leg nozzle DP	±25%
SG DP	±25%
Cold leg DP	±25%
Hot leg DP	±25%

Table C.5.3. Plant Steady-State Conditions

Parameters	**Steady-state calculation**	**Test Data**
Core power (MW)	10.045	10.045
RCS pressure (MPa)	15.63	15.58‘
Cold leg temperature (K)	564.9	564.5
Hot leg temperature (K)	598.5	599.0
Loop average temperature	581.7	581.75
RCS loop flow (kg/s)	24.6	24.6
SG secondary pressure (Mpa)	7.42	7.4
SG steam flow rate (kg/s)	2.72	2.74
Feedwater temperature (K)	494.0	494.0
SG recirculation ratio	4.17	5.22
RCP speed (rad/s)	86.8	83.52
Vessel head temperature (K)	597.5	598.2
Hot leg leakage (kg/s)	0.038	0.05

Table C.5.4. Geometric Volumes

Components	ROSA-IV/LSTF[a] (m^3)	TRACE Model (m^3)
Primary loop A (total)	2.038	2.0568
Hot leg	0.124	0.1328
Cold leg	0.116	0.1196
Cross leg	0.212	0.2193
Primary coolant pump	0.024	0.0241
SGA plenums	0.695	0.695
SGA U-tubes and tube sheet	0.867	0.866
Primary loop B (total)	2.038	2.0568
Hot leg	0.124	0.1328
Cold leg	0.116	0.1196
Cross leg	0.212	0.2193
Primary coolant pump	0.024	0.0241
SGA plenums	0.695	0.695
SGA U-tubes and tube sheet	0.867	0.866
Vessel (Total)	2.675	2.5516
Upper Head	0.5100	0.5100
Upper Plenum	0.5472	0.5603
Core	0.408	0.4181
Lower Plenum	0.5802	0.5808
Downcomer	0.8264	0.8435
Pressurizer (total)	1.256	1.223
Spray, Surge, SRV lines	0.105	0.0731[b]
Pressurizer	1.147	1.15
Total Fluid Volume in the Primary System	8.007	7.910

a. Data is from Table 2.1 of Reference 5

b. The value is the volume of the surge line

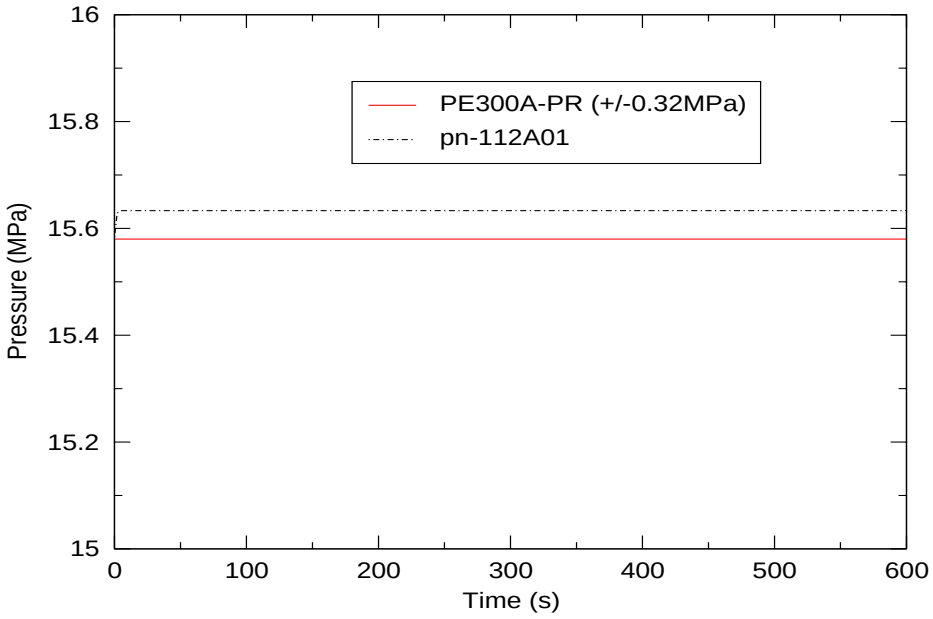

Figure C.5-15. Pressurizer Pressure

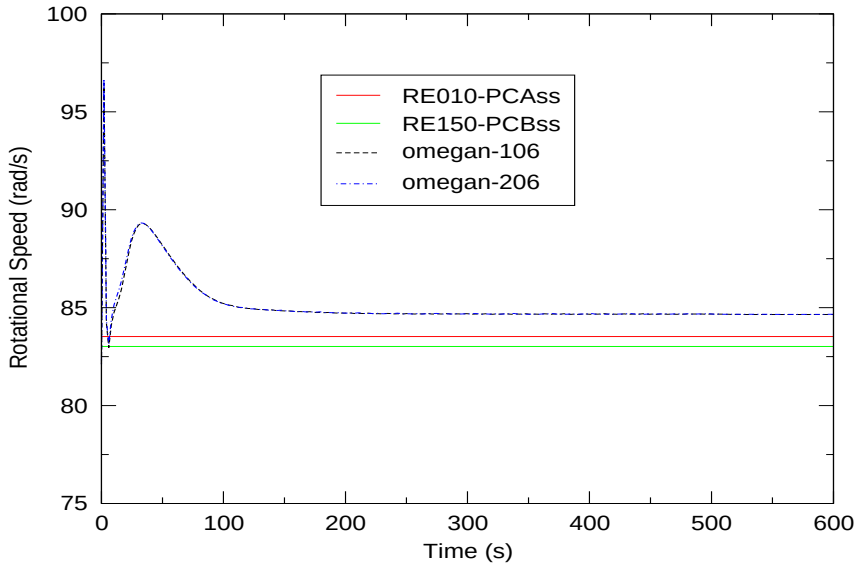

Figure C.5-16. Reactor Coolant Pump Impeller Rotation Speed

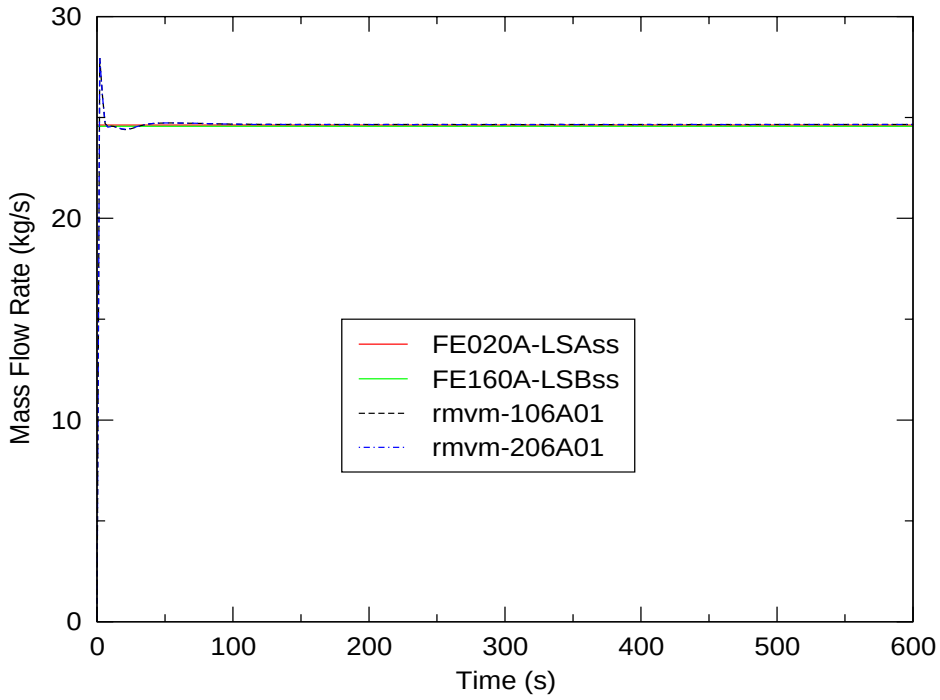

Figure C.5-17. Primary Loop Mass Flowrate

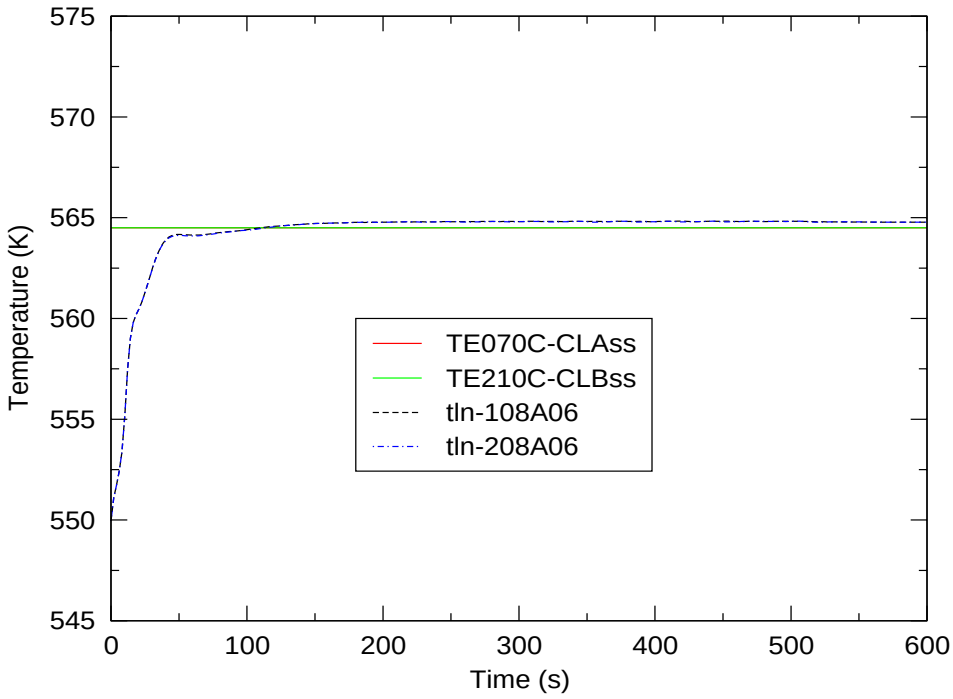

Figure C.5-18. Cold Leg Temperature

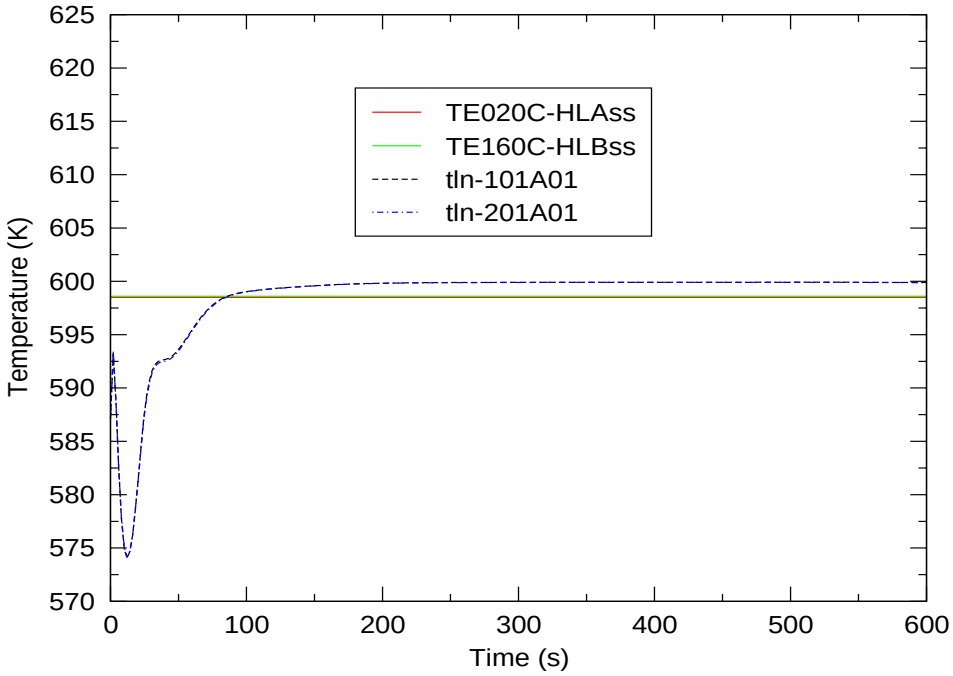

Figure C.5-19. Hot leg Temperature

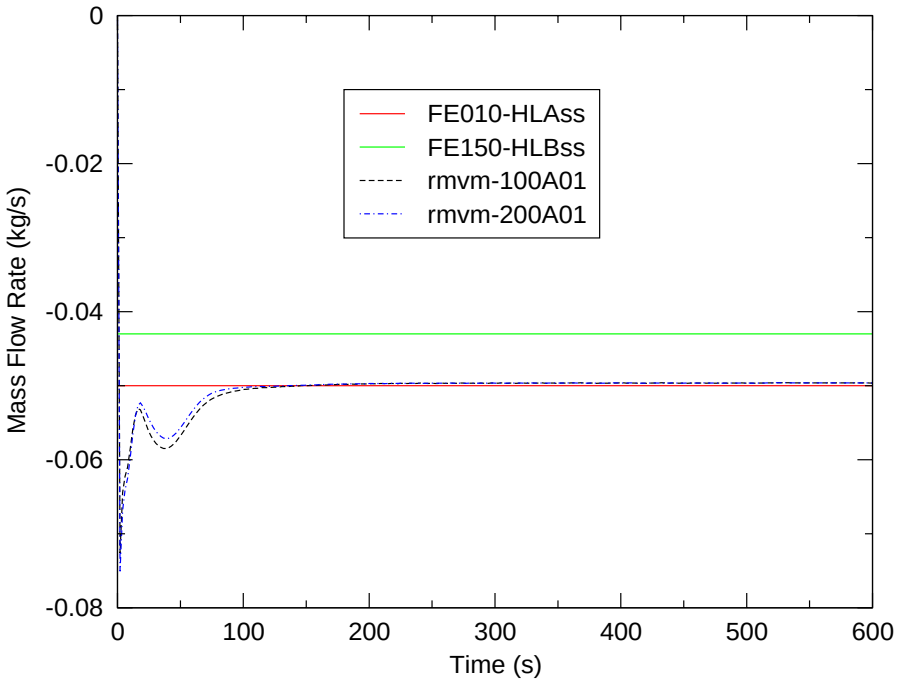

Figure C.5-20. Hot Leg Leakage Flow Rate

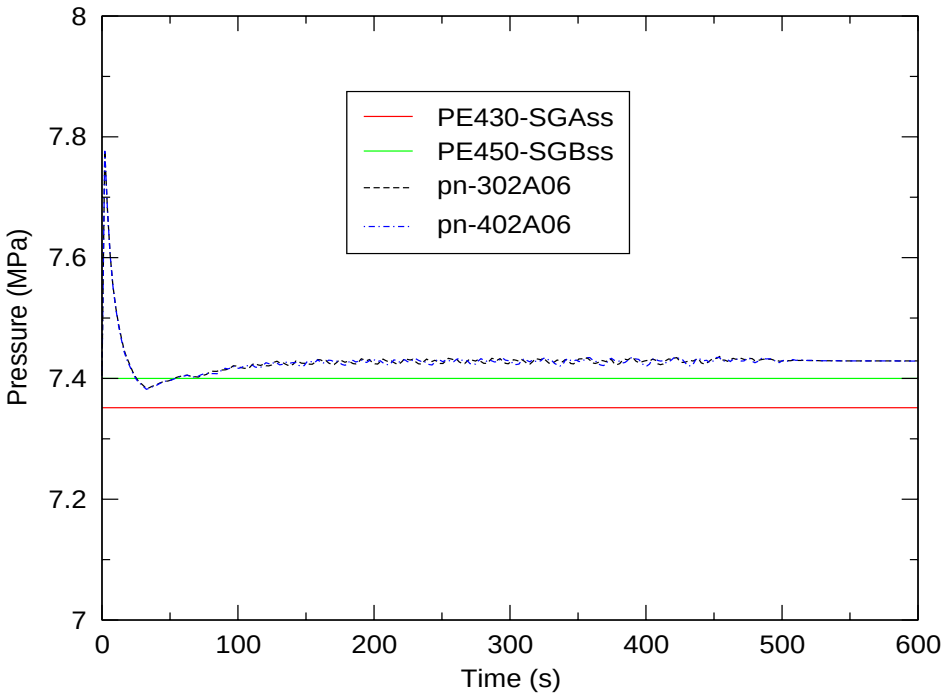

Figure C.5-21. Steam Generator Pressure

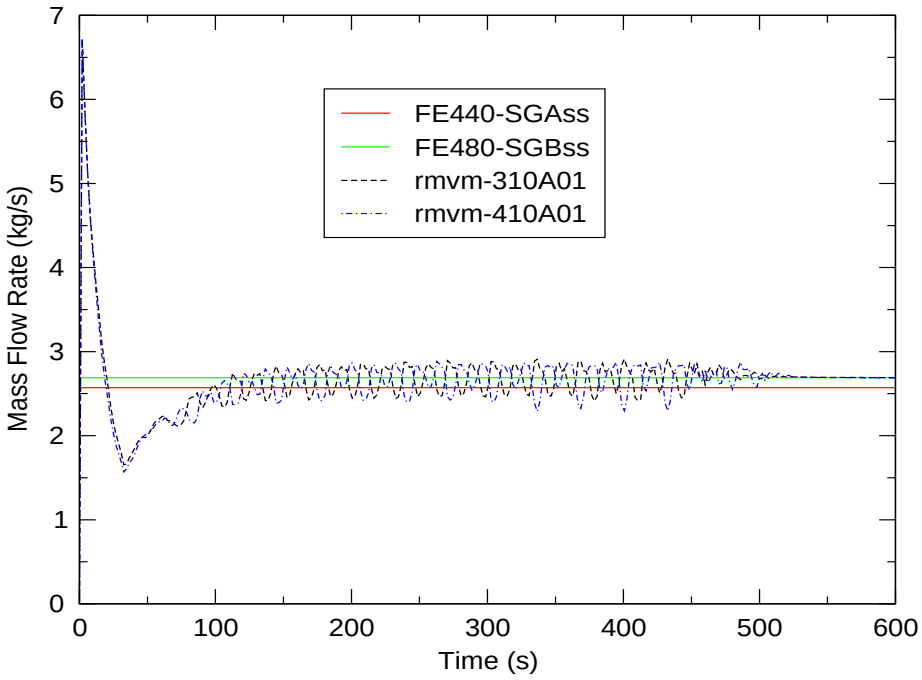

Figure C.5-22. Steam Mass Flow Rate

C.5.5. Tests Simulated with TRACE

This section presents the TRACE simulation results of six ROSA tests. Table C.5.5 shows each test analyzed for this assessment activity and the break locations that characterize each test.

Table C.5.5. Summary of the Analyzed ROSA Tests

Case Name	Break Size (%)	Break Orientation
SB-CL-01	2.5	Side
SB-CL-05	5.0	Side
SB-CL-14	10.0	Side
SB-CL-15	0.5	Bottom
SB-CL-16	0.5	Top
SB-CL-18	5.0	Side

The objective is to assess how accurately the code can predict the dominant phenomena observed in the ROSA tests. The ROSA tests given in Table C.5.5 were selected by the NRC as part of a series of SBLOCA tests carried out on the ROSA-IV facility. The break sizes of ROSA tests are based on the size of one cold leg. The break is located on the cold leg of Loop B (see Figure C.5-13).

It is useful to divide the small break transient into several phases in order to identify and rank the various phenomena. Some phenomena are important for certain periods of time but are insignificant at other times. Correct prediction of phenomena during the time of their respective importance may be crucial to the accurate prediction of the overall transient. The small break transient is characterized by five phases: blowdown, natural circulation, loop seal clearance, boil-off, and core recovery, and the duration of each phase is break size dependent.

The principal Figure of Merit (FOM) in each of the ROSA tests is the core collapsed liquid level. It can be inferred from the pressure difference across the reactor core in the test and the TRACE simulation.

Other measurable high-ranking phenomena are chosen as subsidiary FOM as shown in **Section C.5.1.**; those phenomena will be analyzed in the transient analysis.

The following sections document the analysis for each ROSA test simulation based on the principle FOM and the subsidiary FOM, as well as variables that are useful in the analyses.

C.5.5.1. Simulation of SB-CL-01

Test SB-CL-01 was a 2.5% cold leg break test. The break was located on the side of the cold leg in Loop B. Two input decks were developed for the analysis: one constrained steady-state (CSS) input model and one transient input model. The CSS model contained most of the model information and plant control procedures. It was used to obtain initial plant conditions for the transient calculations.

The control system and control procedures of the ROSA-IV facility were designed to accommodate a wide range of plant operational transients and accident scenarios. The TRACE control procedure was derived from a series of SBLOCA tests.

SB-CL-01 test conditions and control actions implemented in the TRACE transient analysis are discussed below.

C.5.5.1.1. SB-CL-01 Test Conditions

Some of the test conditions or control procedures were different from those in the reference PWR reactor. Special control procedures or test conditions were designed to account for some scaling issues in the design of the test facility (Refs.1, 7).

The plant initial conditions are summarized in Table C.5.3**.** In the test, it was assumed that a loss-of-offsite power occurred concurrently with reactor scram. Also, failure of one of the two diesel-generators for the emergency coolant and auxiliary feedwater pumps was assumed. Table C.5.6 summarizes the operational setpoints for Run SB-CL-01. Table C.5.7 provides the event sequence recorded by the facility instrumentation system; individual items are described below.

- Coolant pumps

Upon the initiation of the break, the pump speed was increased before the pump started to coast down following the reactor scram signal (Ref. 7). The pump impeller rotation speed after the initiation of break is demonstrated in Figure C.5-23 and Figure C.5-24. The dashed line is the pump curve obtained in the TRACE simulation of SB-CL-01. The solid line is the measured pump curve in the SB-CL-01 test.

- Reactor trip and core power after break

As indicated in Table C.5.7, the reactor was tripped 15 seconds after the break was initiated. Two power curves are shown in Figure C.5-25. The solid line is the measured power curve in the SB-CL-01 test. The dashed line is the power curved obtained in the transient simulation.

- Emergency Core Cooling System (ECCS)

During the SB-CL-01 transient, the subsystems of the ECCS system were actuated in the manner provided in Table C.5.6 and Table C.5.7. For each loop, the ECCS subsystems injected water into

the loop through the same nozzle (Figure C.5-2). Figure C.5-26 shows the calculated ECCS injection flow rate into each loop, which is the sum of the injection flow of the ECCS subsystems (high pressure charging and high pressure injection). In the test, the desired ratio of the accumulator (ACC) injection flow into the loop A cold leg to the ACC injection flow into the loop B cold leg was 3:1. Assuming the ratio was maintained, the ACC injection flow rate into each loop can be calculated based on the discharging flow rate of the ACC tank, which is derived from the ACC tank level measurement (LE14). In this particular test, however, it was determined that the data collected in the loop-B accumulator loop was inaccurate; therefore, no data is shown in Figure C.5-28 to compare with the code prediction for loop-B accumulator injection flow.

Figure C.5-27 and C.5-28 show calculated and measured ACC injection flow rates for loops A and B. The data recorded for loop B was found to be unusable, so no data is present in Figure C.5-28. However, it is clear from both plots that the injections occurred at the precise time and with the appropriate 3:1 ratio.

- Auxiliary Feedwater System

After the main feedwater was cut off, the auxiliary feedwater system was actuated with some delay to supply water to the SG's secondary side. The auxiliary system of the test facility used a single pump and branched piping of unequal hydraulic resistance. In SB-CL-01, the auxiliary feedwater was supplied only to the SG A after a 52-second delay.

- Pressurizer heaters

Power to the pressurizer heaters was cut off with the initiation of break.

C.5.5.1.2. TRACE Control Procedure

Using the strategy outlined at the beginning of this chapter, the control procedure for the TRACE model is simplified. As a result, the TRACE control procedure mainly consists of a number of trips**.** In general, a trip is initiated by either time or the system pressure. Specifically

1. At time 0, the break is initiated and the pressurizer heater power is cut off.
2. The pump speed is increased after the break and coasts down with the reactor trip as shown in Figure C.5-19 and Figure C.5-20
3. The reactor is tripped when the system pressure reaches 12.97 MPa. Figure C.5-25 shows the measured power curve after the break and the power curve obtained from the transient calculation.
4. The Safety Injection (SI) signal is generated as the system pressure reaches 12.27 MPa. With a 12-second delay, the Emergency Core Cooling System (ECCS) is actuated. The HPIS/LPIS system is simply modeled as a boundary condition. The accumulators are

modeled as the two pressurized water tanks connected to each cold leg, where flow injection through the check valve is activated when system pressure is below 4.51 MPa.

5. Main steam line valve closure, main feedwater cut off and auxiliary feedwater on are initiated with proper time delays following the reactor trip.

Table C.5.6. Operational Setpoints for Run SB-CL-01

Event	Setpoint
Reactor scram signal	12.97 MPa (system pressure)
Pump coast down	With reactor scram
Safety Injection (SI) signal	12.27 MPa (system pressure)
High Pressure charging	1199 seconds after the break
Accumulator injection	4.51 MPa
Low Pressure Injection	1446 seconds after the break
Main feedwater cutoff	With reactor scram
Turbine throttle valve closure	With reactor scram
Auxiliary feedwater initiation	52 seconds after the break

Table C.5.7. Chronology of Events for Run SB-CL-01

Events	Time (s)
Break	0
Reactor trip	15
Safety Injection Signal	19
Main Steam Line Valve Closure	20
SG Feedwater stop	23
Auxiliary feedwater ON	52
Reactor coolant pump stop	272
Loop Seal clearing	~380
Primary/Secondary Pressure Reversal	380~460
Core dryout	600~980
Accumulator Injection ON	835
Core Power Trip	872
High Pressure Charging Injection	1199
High Pressure Safety Injection	1200
Low Pressure Injection System ON	1446
Accumulator Injection OFF	1460

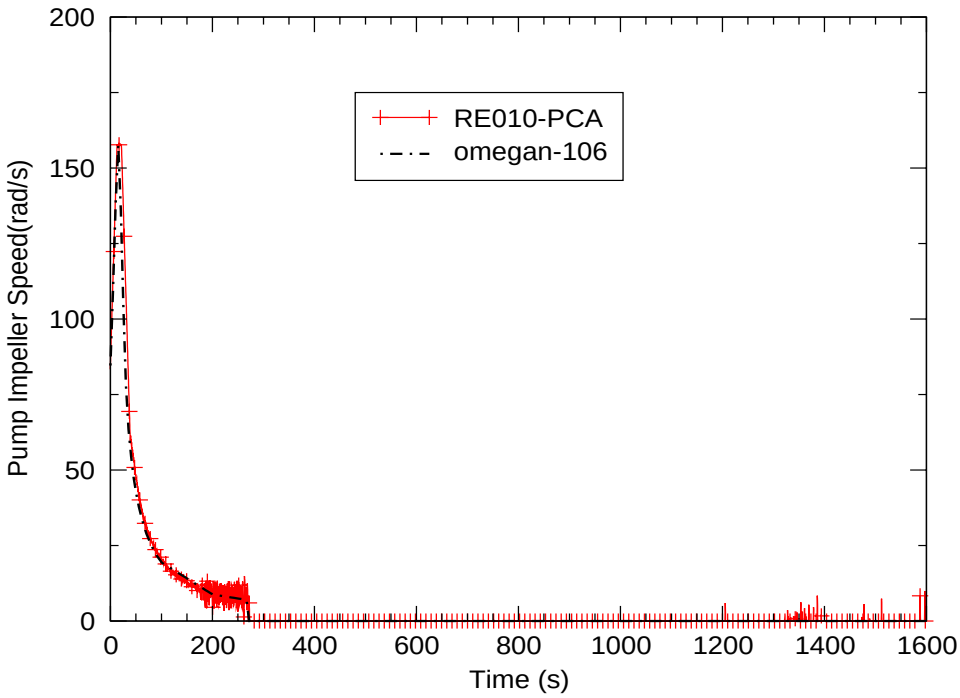

Figure C.5-23. Pump A Impeller Speed After Break

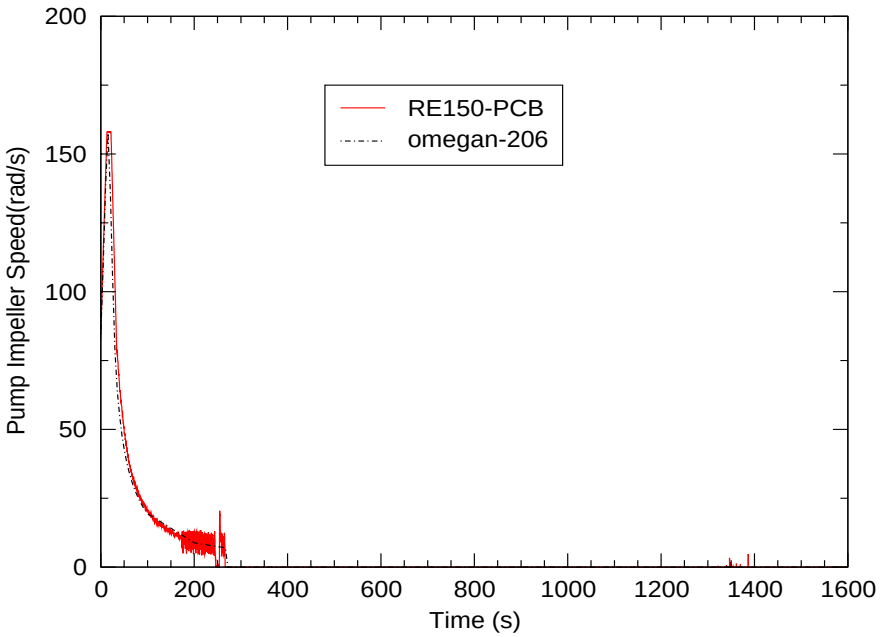

Figure C.5-24. Pump B Impeller Speed After Break

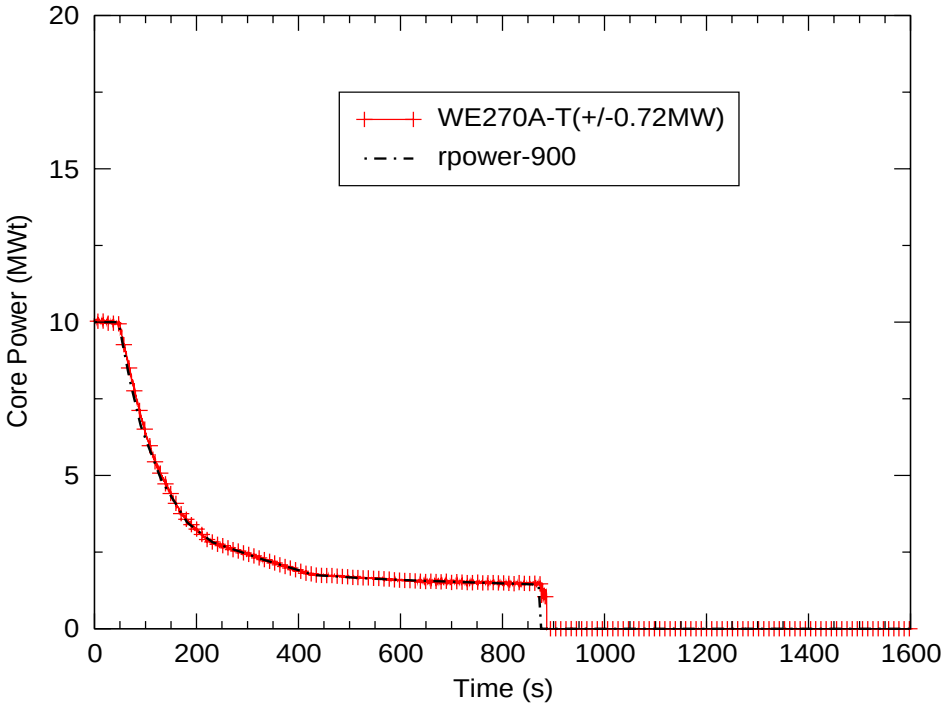

Figure C.5-25. Core Power after Break

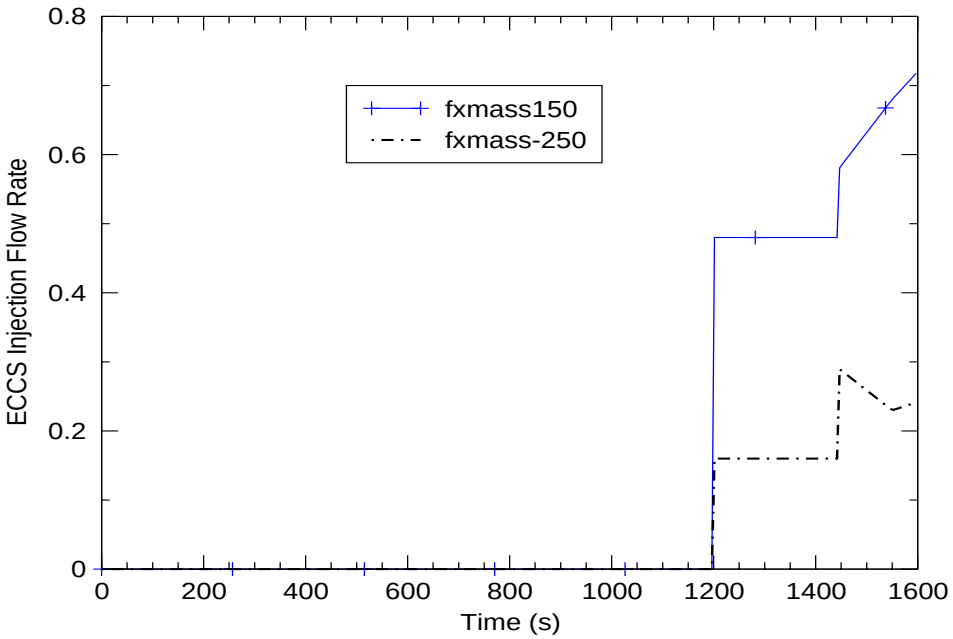

Figure C.5-26. ECCS Injection Flowrates for Loop A and Loop B

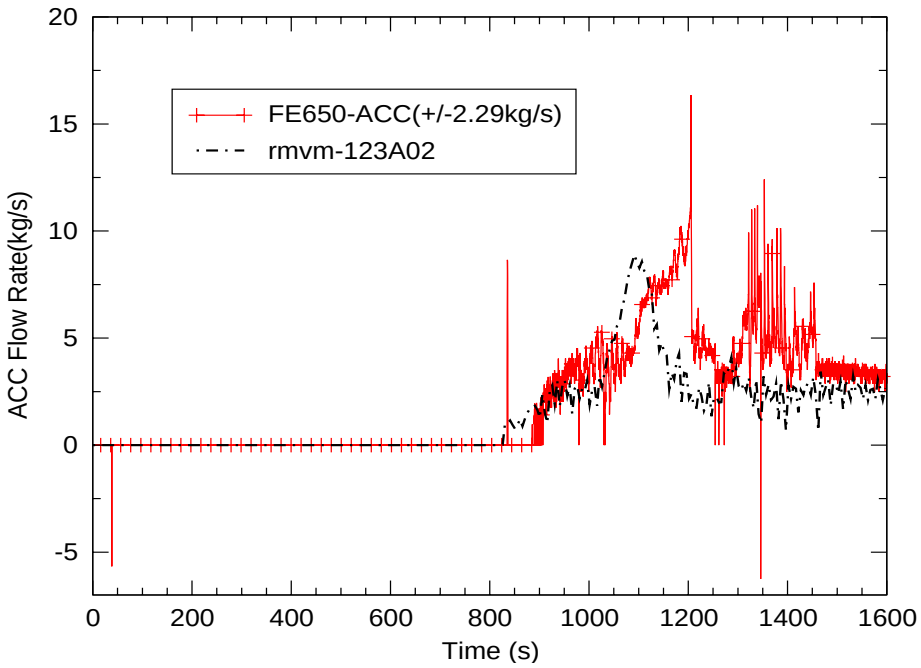

Figure C.5-27. Accumulator Injection Flow to Cold Leg A

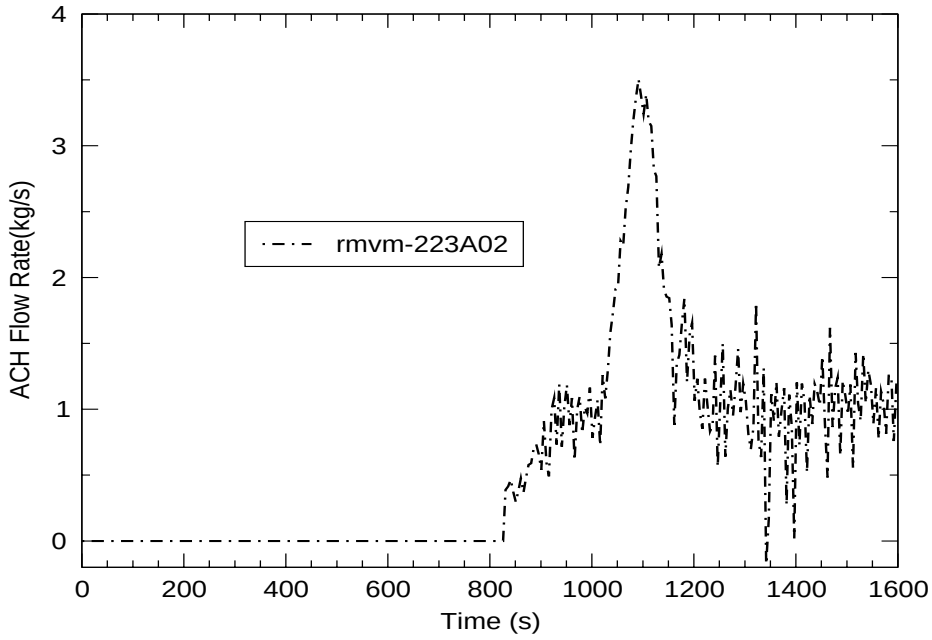

Figure C.5-28. Accumulator Injection Flow to Cold Leg B

C.5.5.1.3. Experimental Observations

The main objective of test SB-CL-01 was to investigate the thermal-hydraulic mechanisms of early core uncovery and heatup. Early core uncovery might have been caused by a manometric effect resulting from an imbalance between the water hold up in the upflow and downflow sections of the primary coolant in the steam generator U-tubes (Ref. 7). Table C.5.7 lists the event sequence recorded by the facility's instrumentation system during the test.

Soon after the start of the transient, the pressure started to drop rapidly and the core power decay curve was initiated at a pressurizer pressure of 12.97 MPa together with the closing of the MSIV, starting of the programmed pump speed curve and termination of the main feedwater to the steam generators.

The safety injection signal occurred at 19 seconds at a pressurizer pressure of 12.27 MPa. However, the charging pump and the high-pressure injection pump were delayed to 1199 and 1200 seconds, respectively. The secondary pressure increased to and remained at approximately 8 MPa due to the SG relief valve operation. The SG secondary-side water mass inventory was maintained at the initial level by the auxiliary feedwater supply, activated at 52 seconds after the break.

During the time interval leading up to the loop seal clearance (which took place at 380 s), the core was becoming partially uncovered, but without a measurable heat-up. Both loops experienced loop seal clearing at about 380 s, which led to a partial core liquid level recovery. Loop seal clearing allowed a mixture of steam and water to discharge from the break, which in turn reduced the mass flow rate and accelerated the depressurization of the primary loop. Soon after that, the primary loop pressure began to decrease below the steam generator secondary side pressure. Consequently, the steam generators no longer served as a heat sink and the energy removal was through the cold leg break.

C.5.5.1.4. Transient Analysis

The SB-CL-01 transient calculation was performed for 1800 seconds. The transient simulation results and the comparison to the test data are presented in Figure C.5-23 to Figure C.5-59. In these figures, the test data is plotted in solid, colored lines with symbols and the calculation results are plotted in solid black or blue lines without symbols.

C.5.5.1.4.1. System Behavior

The overall primary system behavior determines the boundary conditions of the transient event since most of the control signals are based on the system pressure setpoints. The predicted system pressure is in good agreement (in accordance with the acceptance criteria outlined (Ref. 8)) with the data as shown in Figure C.5-29. Therefore, the sequence of the events based on the system pressure setpoints are also in good agreement with the test data.

Table C.5.8 shows a comparison of the sequence of events for the SB-CL-01 simulation results and test data.

Table C.5.8. Sequence of the Event Comparison for SB-CL-01 Test

Event	Test Data	TRACE Model
Break	0 sec	0 sec
Reactor Trip	15 sec	15 sec
Safety Injection Signal	19 sec	19 sec
Main Steam Line Valve Close	20	20 sec
SG Feedwater Stop	23	23 sec
Auxiliary Feedwater ON	52	52 sec
Reactor Coolant Pumps (PC-A/B) Stop	272	272 sec
Loop-A Seal Begins Clearing [a]	388 sec	325 sec
Loop-B Seal Begins Clearing [a]	388 sec	337 sec
Primary/Secondary Pressure Reversal	400 sec	400 sec
Core Dryout	550 - 870 s	600 - 925 sees
Accumulator (A) ON	835 sec[a]	850 sec
High Pressure Charging Injection	1199 sec	1199 sec
High Pressure Safety Injection	1200 sec	1200 sec
Low Pressure Safety Injection	1446 sec	1446 sec
Accumulator (A) OFF	1460 sec	-
End Time	1800 sec	1800 sec

a. The beginning of loop-seal clearance is the time at which the differential pressure across the uphill portion of the loop seal begins to rapidly descend toward zero.

b. Bulk accumulator injection does not begin until 890 secs

C.5.5.1.4.2. Analysis Results

As discussed in **Section C.5.5.**, the PIRT (Ref. 6) identifies the high-ranked phenomena for each phase of the transient. To evaluate the performance of TRACE, each phase will be discussed separately, and the TRACE-simulation results for the highly-ranked phenomena will be compared to the data. The principal Figure of Merit (FOM) of the transient event is the core collapsed liquid level, which is evaluated in terms of the core differential pressure.

Certain input parameters, such as decay heat, core power, and feedwater temperature, are taken directly from the test data as boundary conditions. Therefore, although they are identified as important in some of the phases, they will not be discussed in terms of code performance.

Blowdown phase

The blowdown phase is marked by a rapid depressurization of the primary coolant system until the hot coolant begins to flash into steam. The rate of depressurization is strongly influenced by the rate and enthalpy of the break flow, and it changes when flashing and boiling start in the core. In this phase, the most important parameters defining the evolution of the transient are decay heat, primary side heat transfer, critical break flow, and the flow regime upsteam of the break flow.

In test SB-CL-01, the blowdown phase lasted from 0 to 150 seconds. Throughout this time, good agreement is observed between the simulation results for each highly-ranked parameter and the test data. The core pressure is shown in Figure C.5-29, and the core differential pressure (DP) is shown in Figure C.5-30**.** Primary side heat transfer is evaluated using the fluid temperatures in the steam generator (SG) tubes and the cold legs. These parameters can be seen in Figure C.5-31 through Figure C.5-34. The integrated break flow shown in Figure C.5-35 is used in evaluating critical break flow, and cold-leg-density predictions, shown in Figure C.5-36 and Figure C.5-37, are used to evaluate the flow regime upstream of the break. The data for the density comparisons is taken from three densitometers located along the cross-section of each cold leg.

Other key results that are not ranked high in this phase are the DPs in the upper head and upper plenum, the pressurizer level, and the flow regime in the hot legs. These results will be discussed to further illuminate the evolution of the transient and to thoroughly evaluate the code.

Figure C.5-38 shows the vessel-head DP. Here, the depressurization can be observed, but unlike the data, the code is predicting large spikes in the differential pressure. The reason for this behavior is unclear, as the void fraction in the upper head appears to evolve as it should. As can be seen in Figure C.5-39, flashing occurs in the uppermost region of the upper head, Level 22, and the void fraction in the lower region, level 21, gradually progresses toward single-phase vapor. Such spiking is not seen in the upper-plenum DP predictions shown in Figure C.5-40, which shows excellent agreement between the prediction and the data.

There is also good agreement between the calculated and measured pressurizer level. In Figure C.5-41, both the code prediction and the data show the rapid decrease in level, but unlike the data, the code tends to over-predict the pressure increase caused by the formation of the steam bubble in the SG tubes.

The flow regimes in the hot legs are evaluated in terms of hot-leg fluid density. Figure C.5-42 and C.5-43 show the code predicting the correct mixture densities.

Natural Circulation phase

The natural-circulation phase begins at the end of the pump coastdown and ends when the buoyancy forces caused by differences in loop-fluid densities are no longer able to overcome the flow resistance of the loop components. In the experiment, the natural-circulation phase began at around 151 seconds and lasted until around 240 seconds. This phase can be seen in Figure C.5-45 as the beginning and end of the rapid decrease in SG-tube differential pressure.

The measurable highly-ranked processes in this phase are those that most significantly influence the primary mass inventory, and subsequently, the maximum core liquid level depression. These processes include the decay heat, counter-current flow in the upper-plenum region, and critical break flow. The accuracy in simulating each of these processes is demonstrated in the good agreement between the predicted and measured core level shown in Figure C.5-30. It is apparent that the steaming rates, which are produced by the decay heat prescribed as a boundary condition, are leading to accurate predictions of liquid hold-up and counter-current flow in the SG and

upper-plenum regions. More explicitly, the accuracy of the break-flow prediction can be seen in Figure C.5-35.

Other parameters of interest during this phase are primary-system pressure, U-bend voiding, fuel rod temperature, and secondary-side pressure. Voiding in the U-bend of the SG tubes, which is indicative of the state of primary-side heat transfer, can be evaluated in terms of SG tube DP. Figure C.5-45 through Figure C.5-48 show the SG tube DPs along the uphill and downhill sides of each set of SG tubes. These figures give an indication of the degree of voiding occurring in the tubes, and they show excellent agreement between the simulation and the data.

The temperature of the fuel can be seen in Figure C.5-49. As the natural circulation phase progresses, the temperature of the fuel gradually decreases. As shown in the figure, the code accurately captures this decrease.

Figure C.5-50 and Figure C.5-51 show comparisons of predicted and measured pressures from the shell-side of each SG. During this phase, the pressure fluctuates as a result of the relief valves opening and closing. TRACE captures this process, but the cycling frequency predicted is much greater than the measurements.

Loop Seal Clearing phase

The loop seal clearing phase begins when the trapped primary-side steam volume reaches the top of the loop seal piping. From this point, the steam volume depresses the liquid in the downhill side of the loop seal and in the core until a minimum core level is reached (maximum core-level depression). As steam moves through the seal to the break plane, the liquid it displaces is forced into the core, quenching the heatup caused by the drop in core level. In the test, this sequence of events occurred between 241 and 380 seconds.

As in the Natural Circulation Phase, the highly ranked processes listed below are those affecting primary-system inventory:

1. Decay heat
2. Mixture level in the core region
3. Hot-leg downcomer gap flow
4. Counter-current flow and CCFL in Upper Plenum region
5. SG primary-side heat transfer in the U-tubes
6. SG primary-side flow resistance
7. SG primary-side tube voiding
8. Flow regime/entrainment in the pump suction / loop seal
9. Horizontal stratification in the cold leg

10. Critical break flow

The mixture level in the core is related to the core DP shown in Figure C.5-30**.** As shown in the figure, the loop seals are predicted to clear approximately 50 seconds earlier than the test. At approximately 330 seconds, the sharp increase in DP that indicates clearance of the loop seals is predicted to occur, but in the test, the seals do not clear until around 380 seconds. The potential causes for this discrepancy are an under-prediction of primary-side inventory, which is due to inaccuracies in primary-side cell volumes, and the under-prediction of the hot-leg to downcomer bypass flow shown in Figure C.5-52 and Figure C.5-53. These figures show the calculated leakage flows to be approximately 0.05 kg/s lower than the data.

As for counter-current flow or flooding in the upper plenum region, the DP measurements along the uphill and downhill portions of the SG-tubes, shown in Figure C.5-45 through Figure C.5-48, are indicative of the extent of voiding and liquid-hold up in the SG-tubes. In these figures, the predictions are in good agreement with the data.

Evidence concerning the flow regime established in the loop seals and downstream of the cool-pump suction can be gathered from the loop-seal DPs and the void fraction in the pump-suction piping. Figure C.5-54 through Figure C.5-57 show the DP comparisons along the uphill and downhill sides of the loop seals. These figures further illustrate the early clearing of the loop seals. The predicted density in the pump suction piping is plotted in Figure C.5-58 to determine if any trapped liquid was being entrained into the pumps. This figure shows that after the loop seals clear, no liquid enters the pumps again until after the ECCS injects.

The density of the fluid mixture in the cold legs is used to make inferences about the cold-leg flow regime. Figure C.5-36 and Figure C.5-37 show the predicted cold-leg densities falling at the correct time and reaching values that are in excellent agreement with the data.

Like the cold-leg density, Figure C.5-35 shows the break flow transition from single-phase liquid to a two-phase mixture, but at around 50 s earlier than the data. This early transition is caused by the early clearance of the loop seals. From this point on, the flow is consistently under predicted.

Boil Off phase

As the transient proceeds, the primary system continues to loose inventory and the core inventory continues to boil. During the test, this boil-off phase lasted from 381 to 850s. The highly-ranked processes in this phase are listed below:

1. Fuel Decay heat and local power
2. Mixture level in the core
3. Downcomer mixture level
4. Critical break flow

Figure C.5-30 shows the code predicting a higher level in the core following clearance of the loop seals. As a result, the core remains covered approximately 100s longer than in the test. Also, there is a delay and reduction in the fuel heatup shown in Figure C.5-49.

Like the core level, the level in the downcomer is represented by DP measurements. As seen in Figure C.5-59, the predicted level in the downcomer follows the downward trend of the data, but it remains over 10 kPa higher than the measurements. The reason for this is unclear.

Unlike the downcomer level, the break flow in this phase continues to be under-predicted (Figure C.5-35), but not to a large extent. From 600 seconds until the end of the phase, it remains within the scatter of the data, but lower than the median values.

Also of note during this phase are the SG pressures and the temperatures in the cold legs. Figure C.5-50 and Figure C.5-51 show the calculated SG pressures. In SGA, the predicted pressure is similar to the data, but it does not fall as rapidly as in the test. The predicted pressure in SGB is also similar in magnitude to the data, but its decent is slightly more rapid. The temperatures of the cold-leg mixtures are shown in Figure C.5-33 and Figure C.5-34. For loop-A the predictions and the data agree well, but for loop-B, the predicted temperature begins to trend lower than the data after the loop seals clear.

Core Recovery phase

The final stage of this transient is the core-recovery phase. During this phase, safety systems inject liquid into the core to establish and maintain core cooling. For this particular test, HPIS and LPIS injections are delayed until 1200 seconds.

The highly ranked processes in the recovery-phase (851s – 1800s) are as listed below:

1. Fuel Decay heat and local power
2. Mixture level in the core
3. Downcomer mixture level
4. Critical break flow

Following the injection of the accumulators at around 830 s, the level in the core, shown in Figure C.5-30, rebounds in a manner quite similar to the test, but after 1200 seconds, it settles at a level significantly higher than the data. This increased level appears to be due to the code's difficulty in determining the temperature distribution in the cold leg following the injection of the accumulator flow. In Figure C.5-33 and Figure C.5-34, the predicted cold-leg temperatures are significantly lower than the data, which leads to over-estimations in the density of the fluid leaving the cold leg and entering the vessel. The resulting elevated density can be seen in Figure C.5-36 and Figure C.5-37 after about 1400 seconds.

Figure C.5-59 shows the mixture level in the downcomer. Although the trends in the graph follow the major events of each phase, the values remain throughout the transient at approximately 10 kPa higher than the data.

In Figure C.5-35, the break flow appears to undergo the necessary increase following ECCS injection. However, the amount of mass predicted to leave through the break remains consistently lower than the median data value. The somewhat lower break flow can also be a contributor to the over-predicted core liquid level.

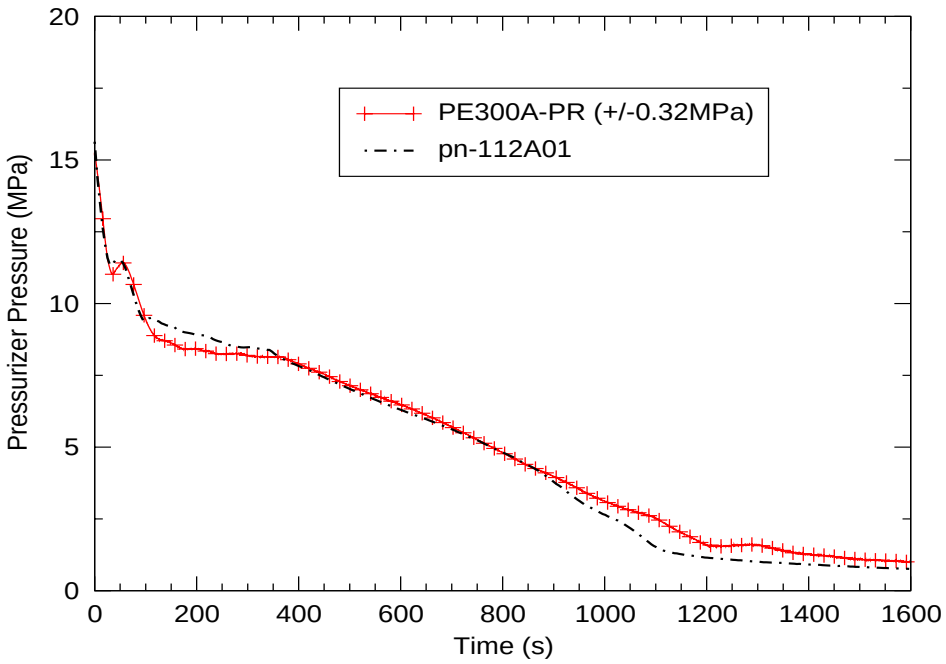

Figure C.5-29. Pressurizer Pressure

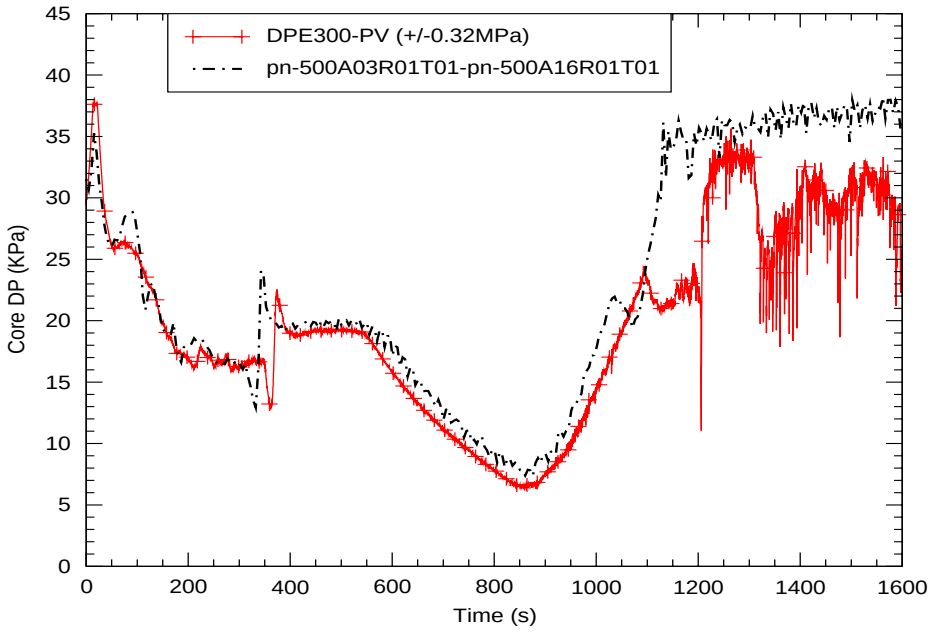

Figure C.5-30. Reactor Core Differential Pressure

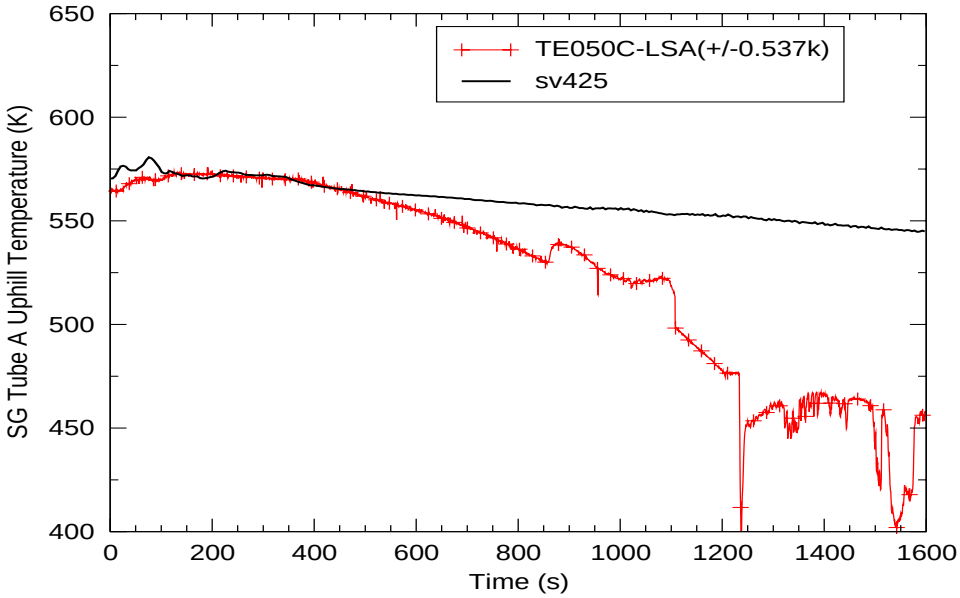

Figure C.5-31. Fluid Temperature in SGA Uphill Tube

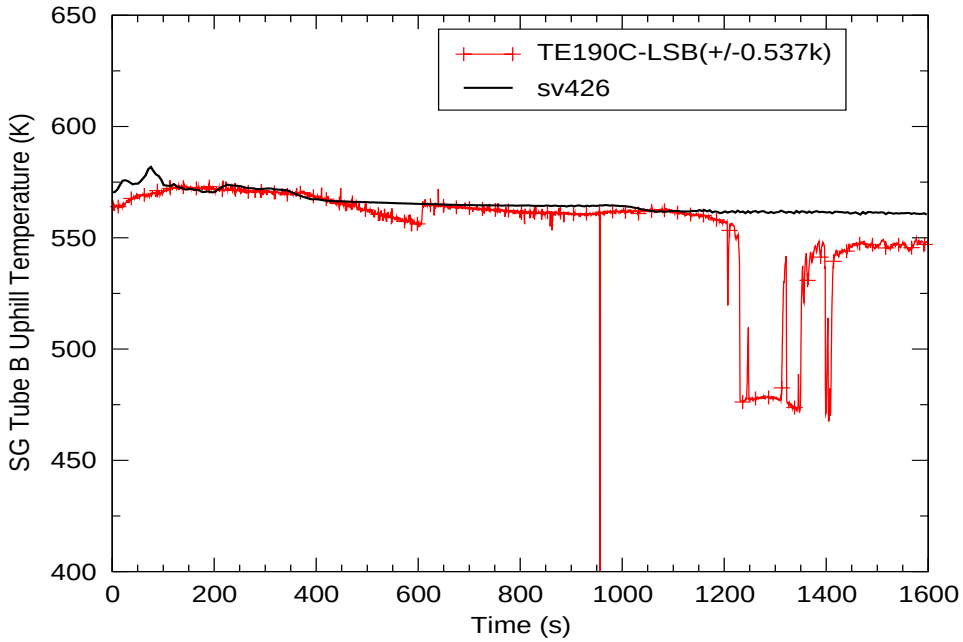

Figure C.5-32. Fluid Temperature, Steam Generator Tubes, Uphill, Loop-B

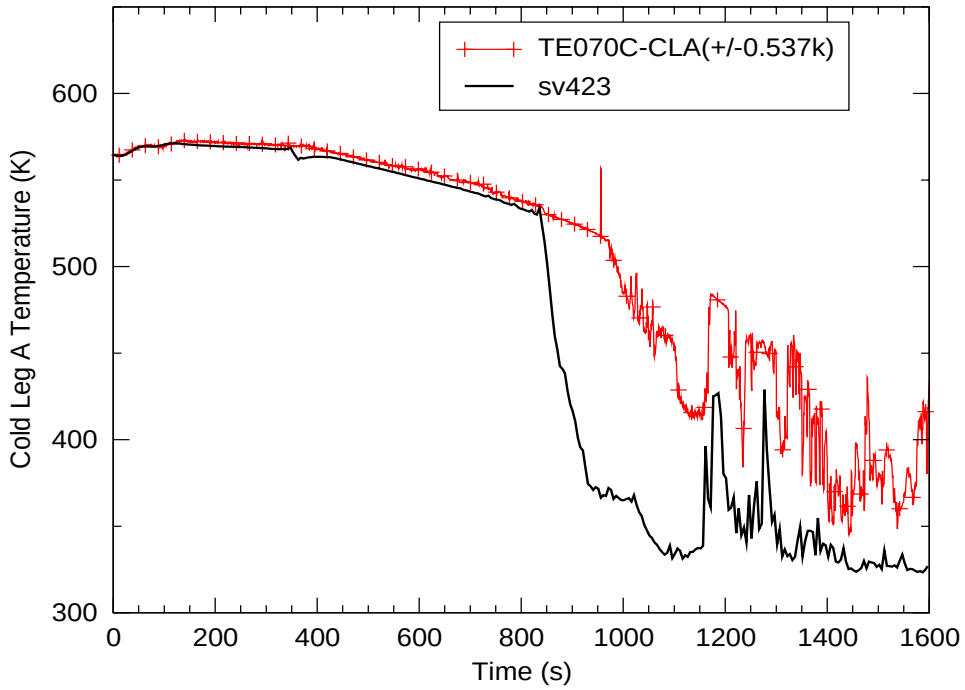

Figure C.5-33. Liquid and Vapor Temperatures in Cold Leg, Loop-A

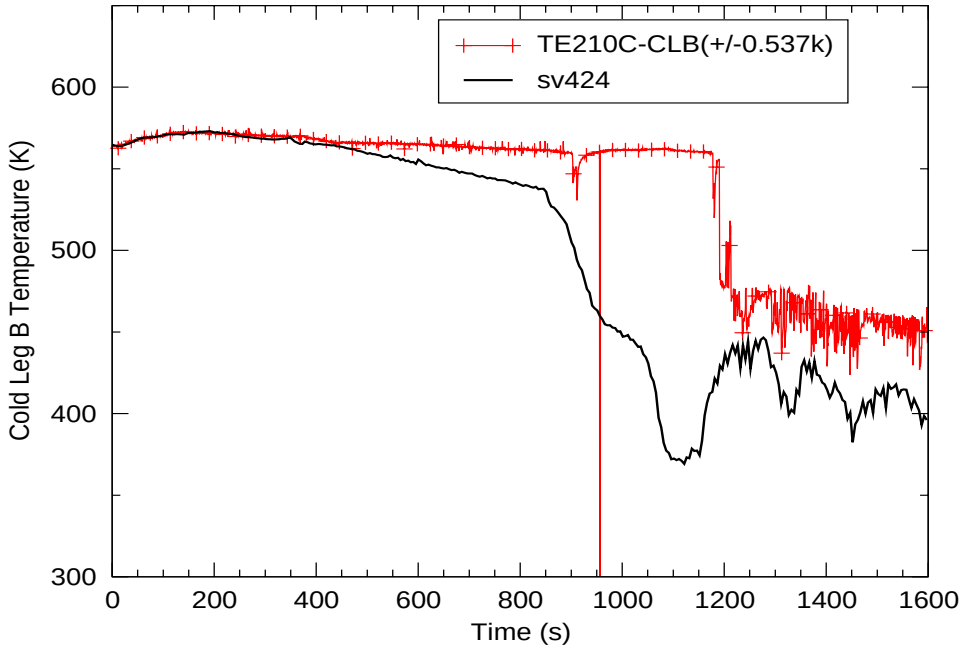

Figure C.5-34. Fluid Temperature in Cold Leg B (Broken Loop)

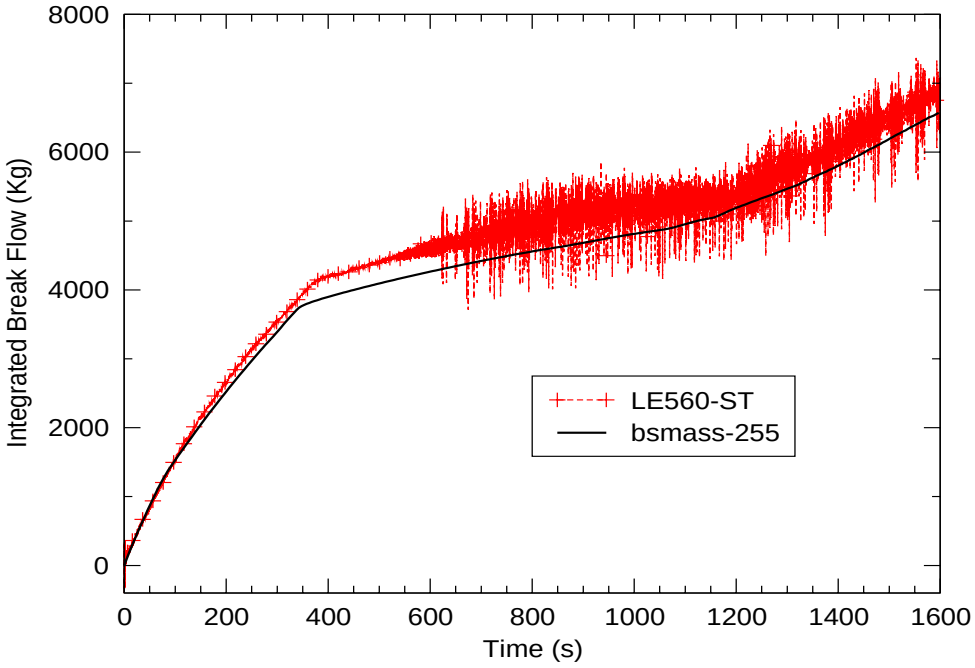

Figure C.5-35. Integrated Break Flow

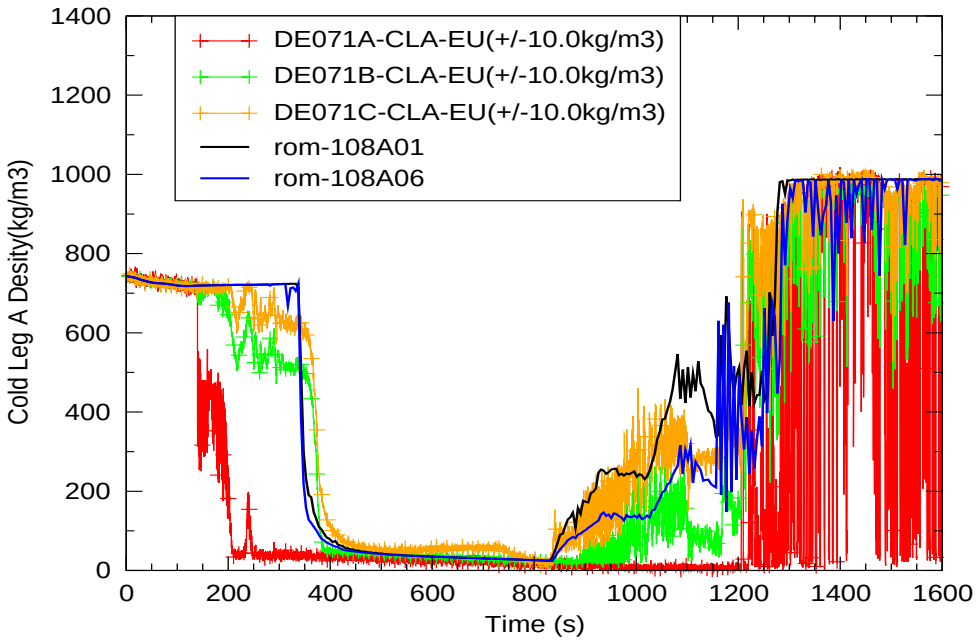

Figure C.5-36. Cold-Leg Density, Loop-A

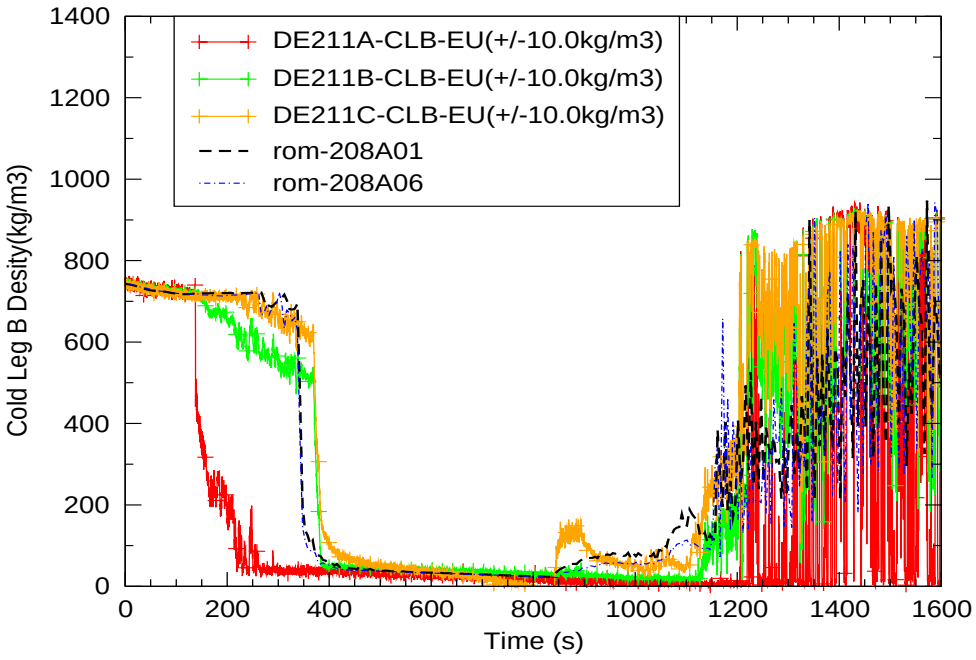

Figure C.5-37. Cold-Leg Density, Loop-B

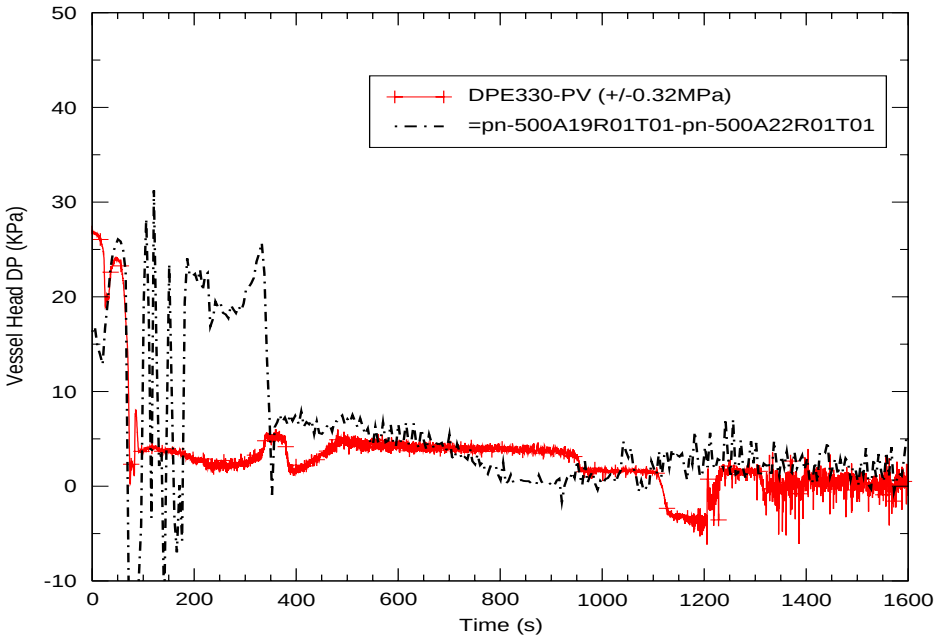

Figure C.5-38. Differential Pressure in Upper Head

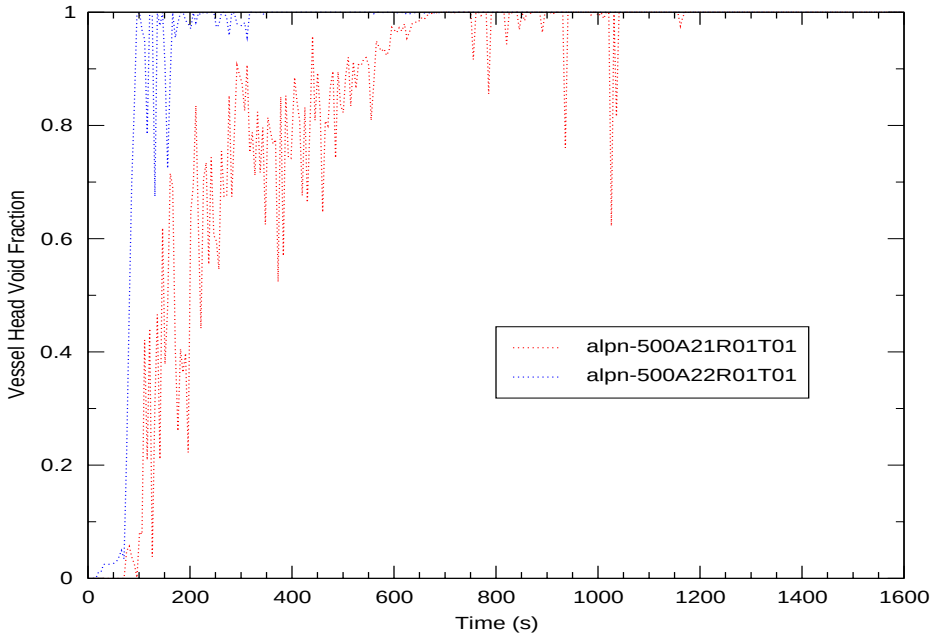

Figure C.5-39. Vessel Void Fraction

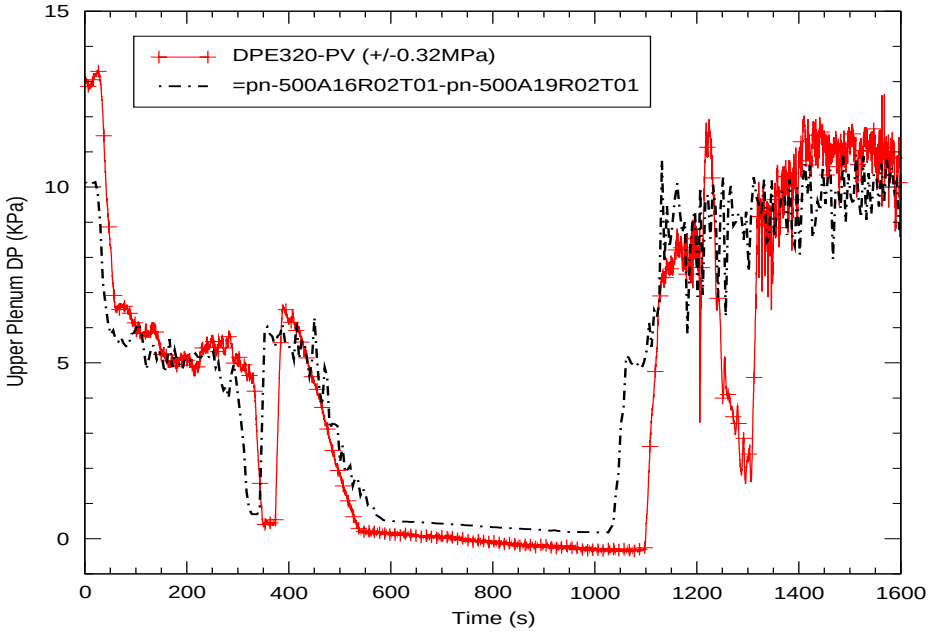

Figure C.5-40. Differential Pressure in Upper Plenum

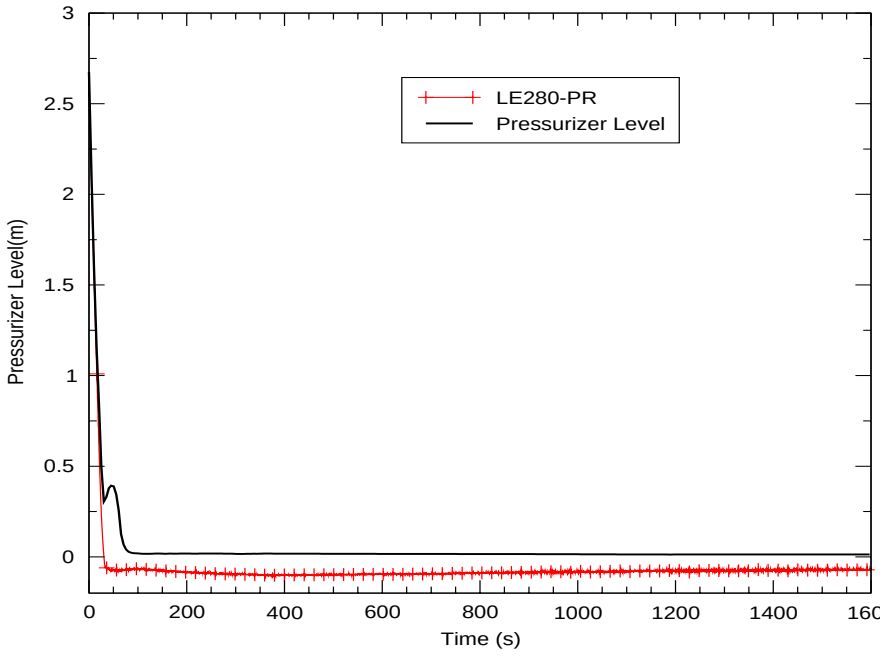

Figure C.5-41. Pressurizer Level

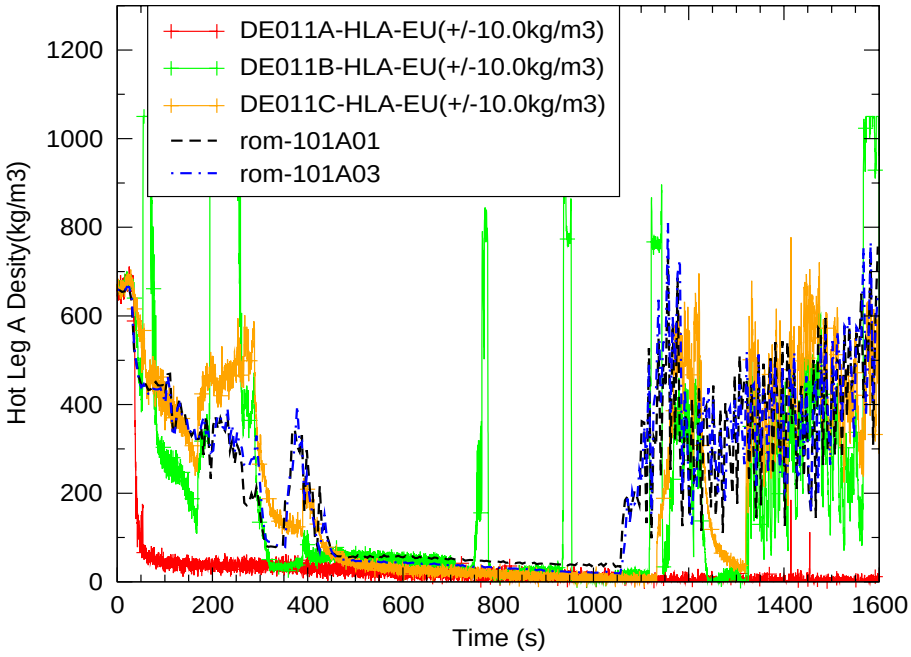

Figure C.5-42. Hot-Leg Density, Loop-B

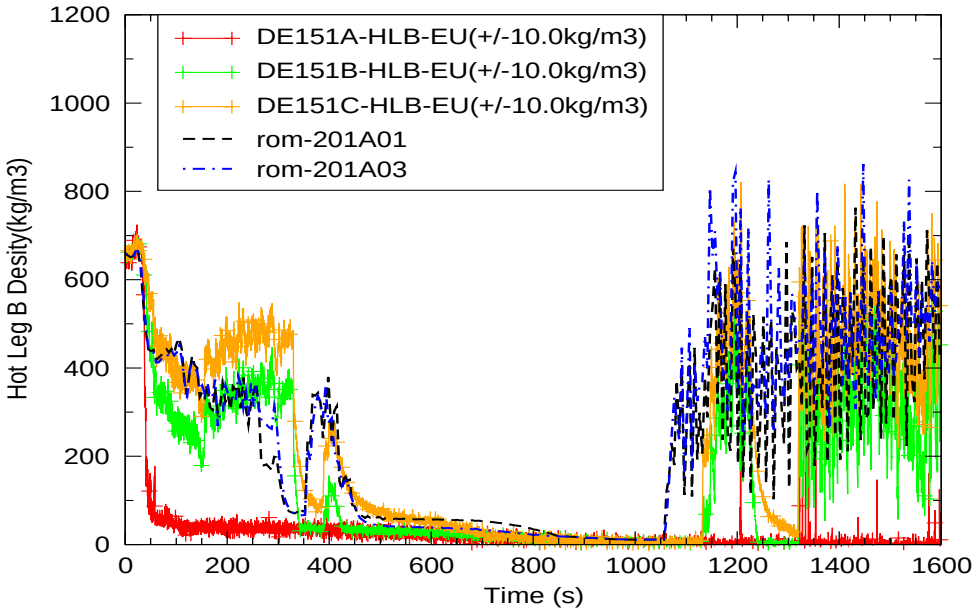

Figure C.5-43. Hot-Leg Density, Loop-B

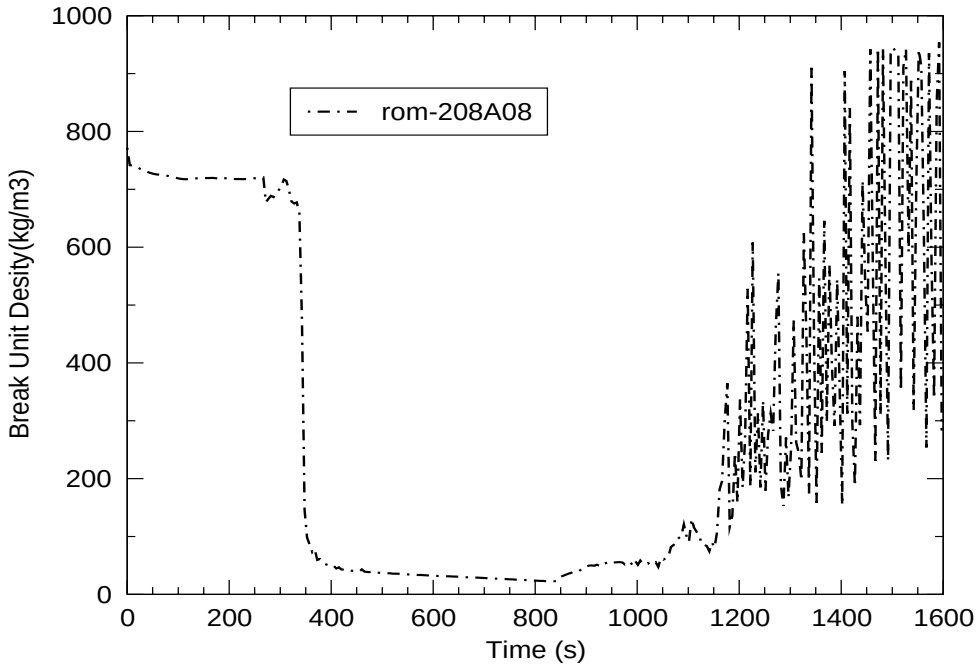

Figure C.5-44. Break Unit Density

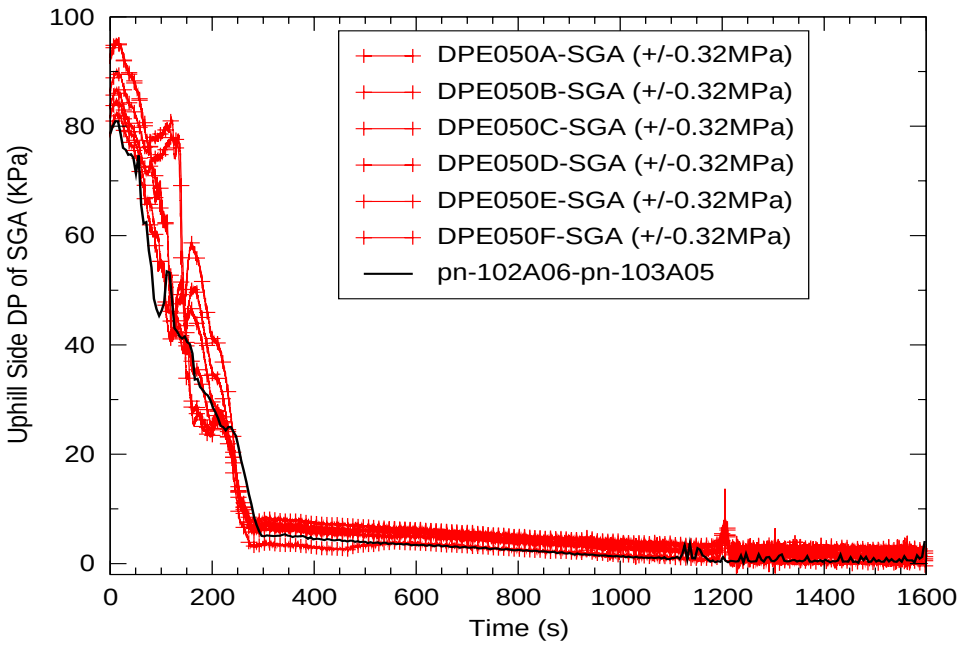

Figure C.5-45. Differential Pressure on uphill side of SGA Tubes

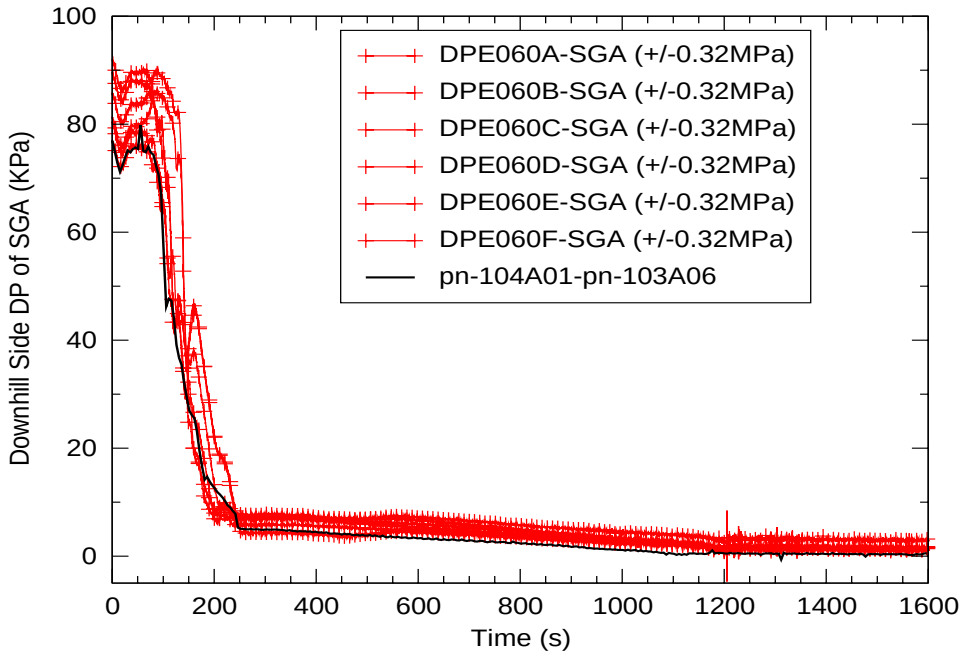

Figure C.5-46. Differential Pressure on downhill side of SGA Tubes

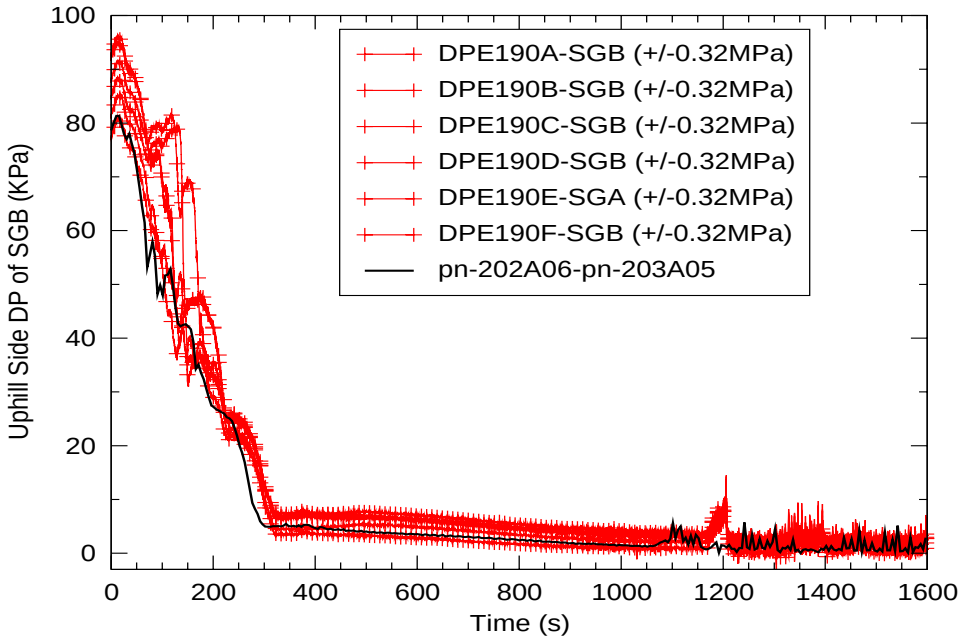

Figure C.5-47. Differential Pressure on uphill side of SGB Tubes

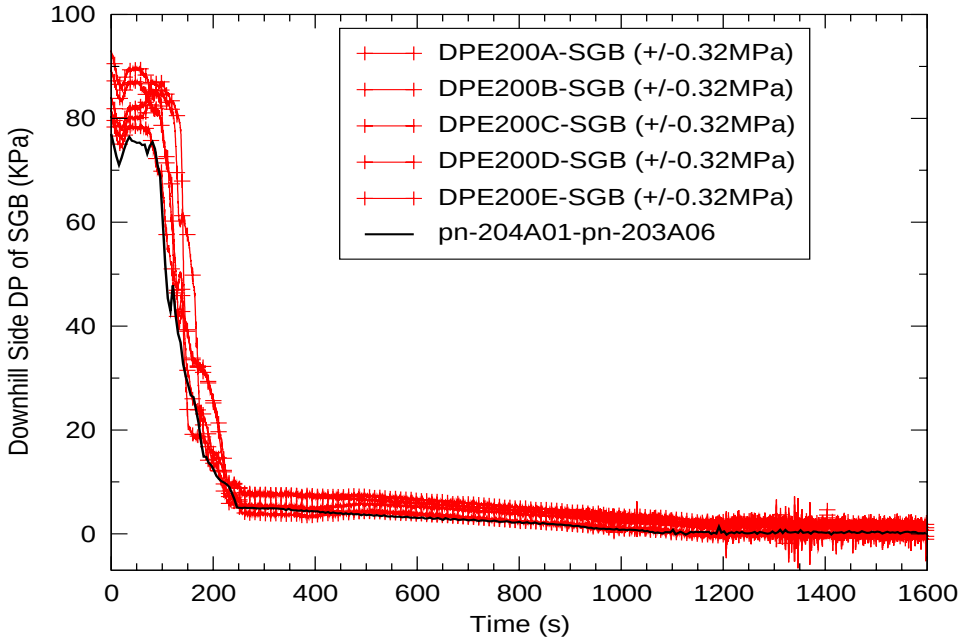

Figure C.5-48. Differential Pressure on downhill side of SGA Tubes

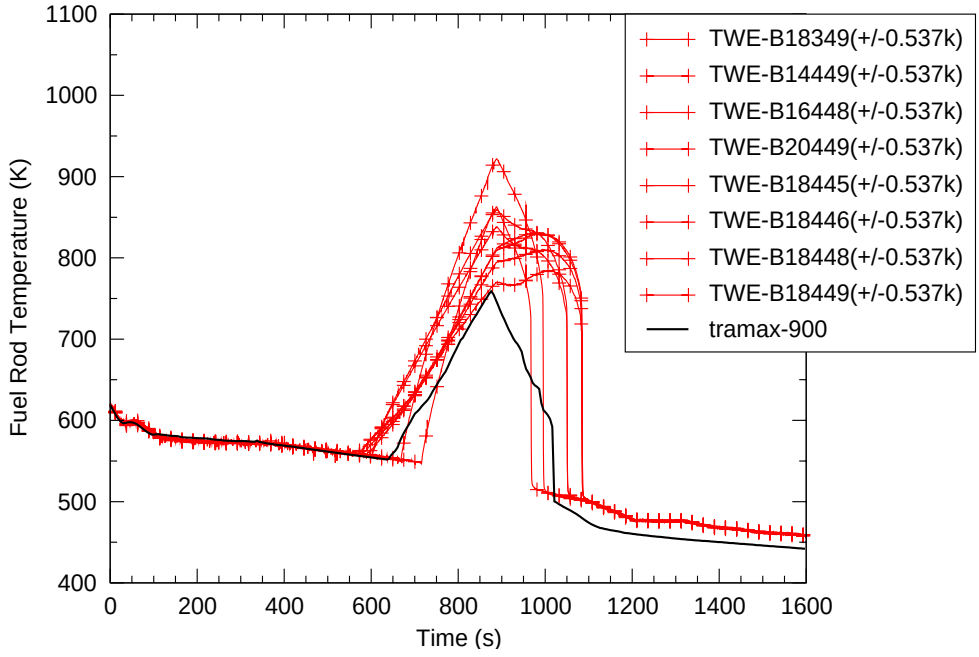

Figure C.5-49. Fuel Rod Temperature

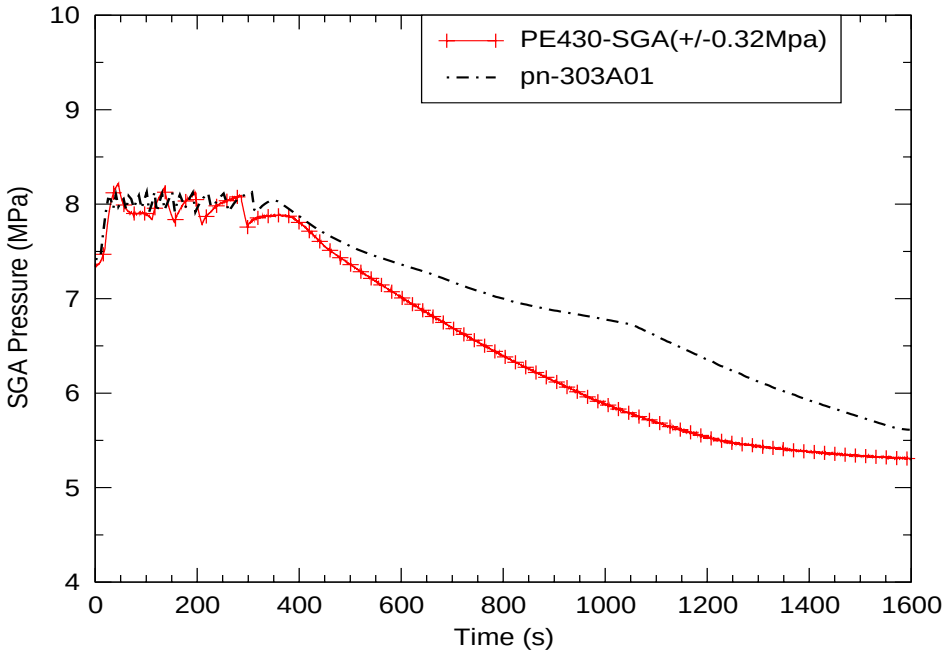

Figure C.5-50. Steam Generator Pressure, Loop-A

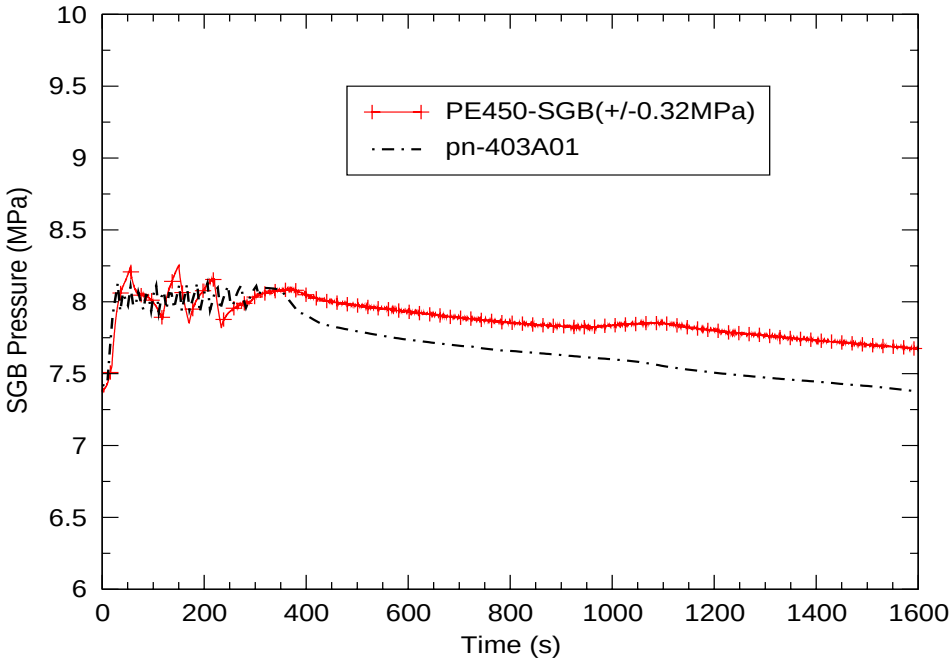

Figure C.5-51. Steam Generator Pressure, Loop-B

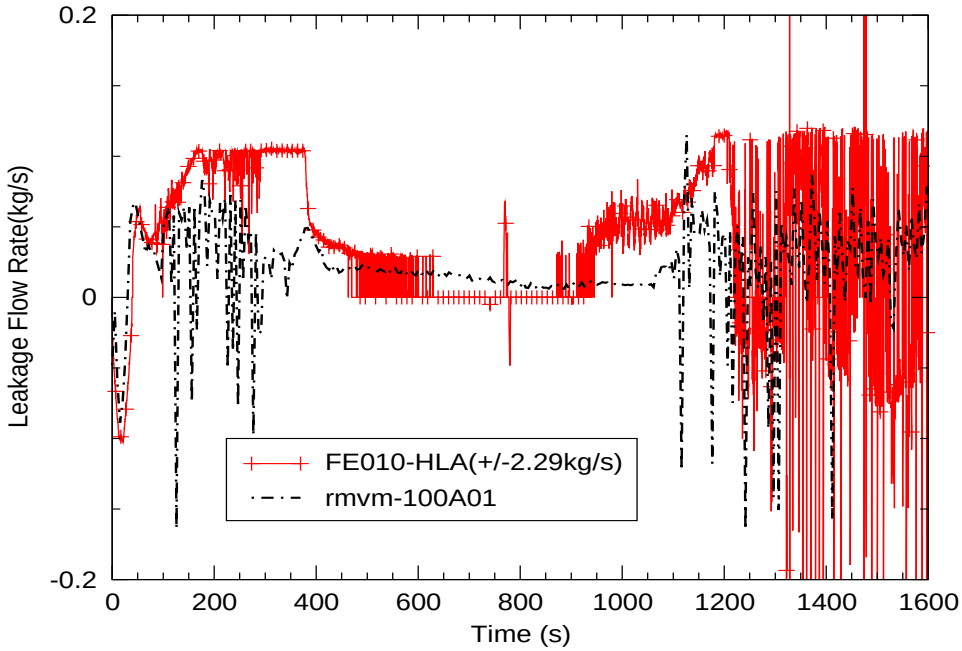

Figure C.5-52. Hot-leg Bypass Leakage, Loop-A

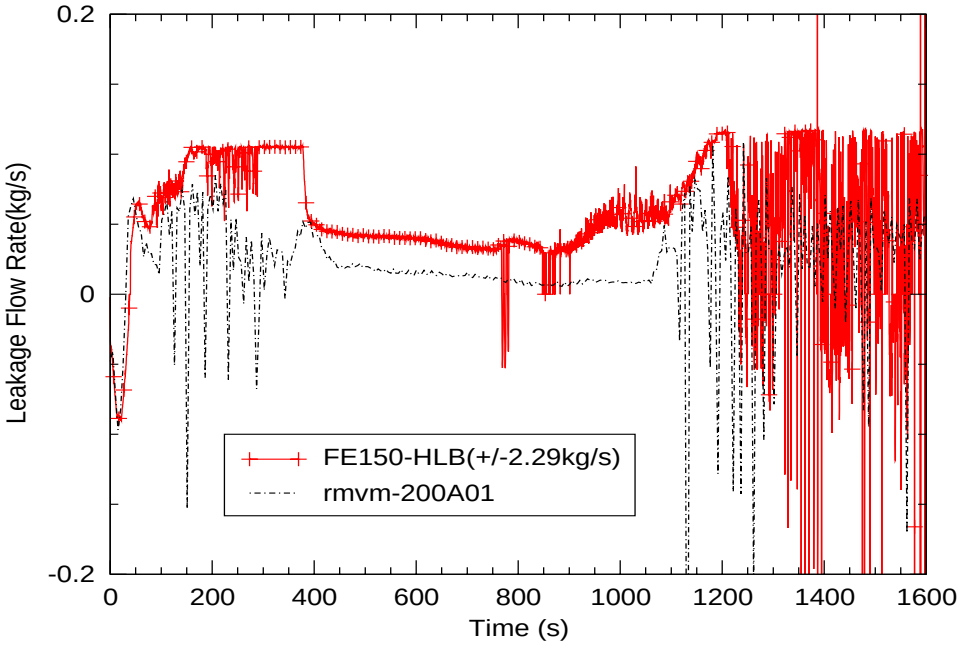

Figure C.5-53. Hot-leg Bypass Leakage, Loop-B

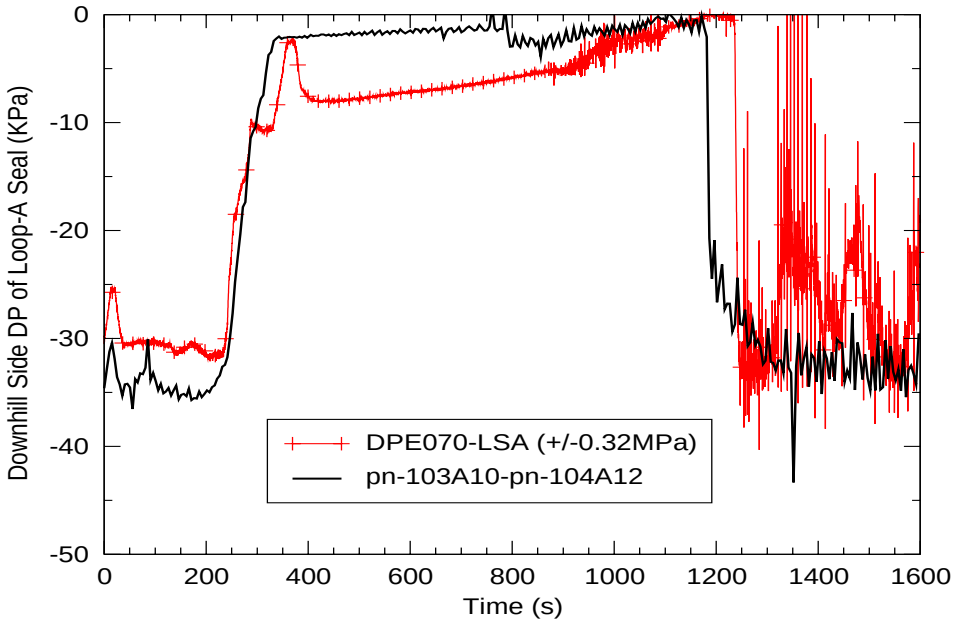

Figure C.5-54. Differential Pressure along downhill side of Loop-A Seal

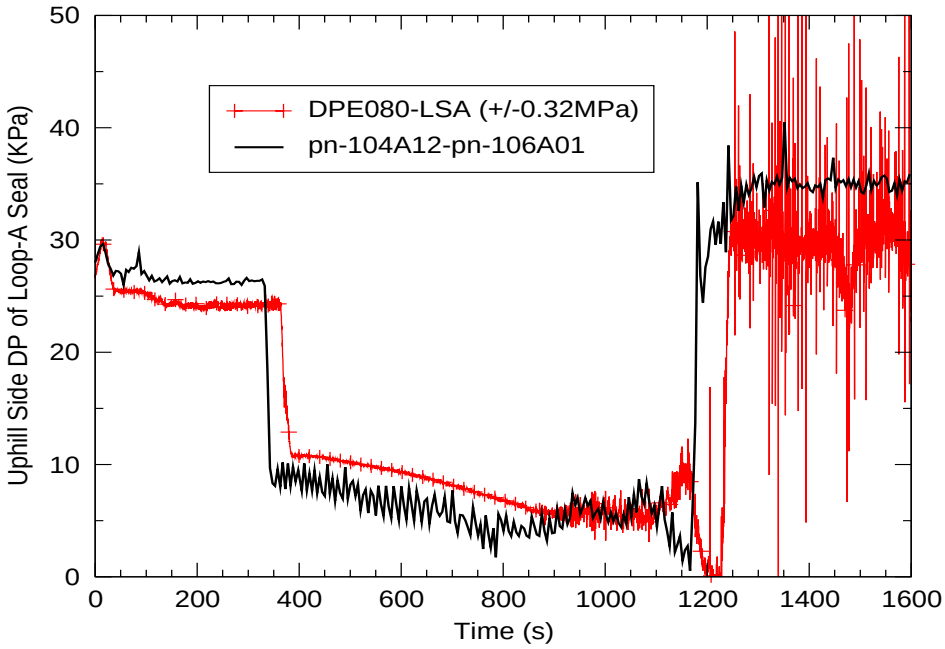

Figure C.5-55. Differential Pressure along uphill side of Loop-A Seal

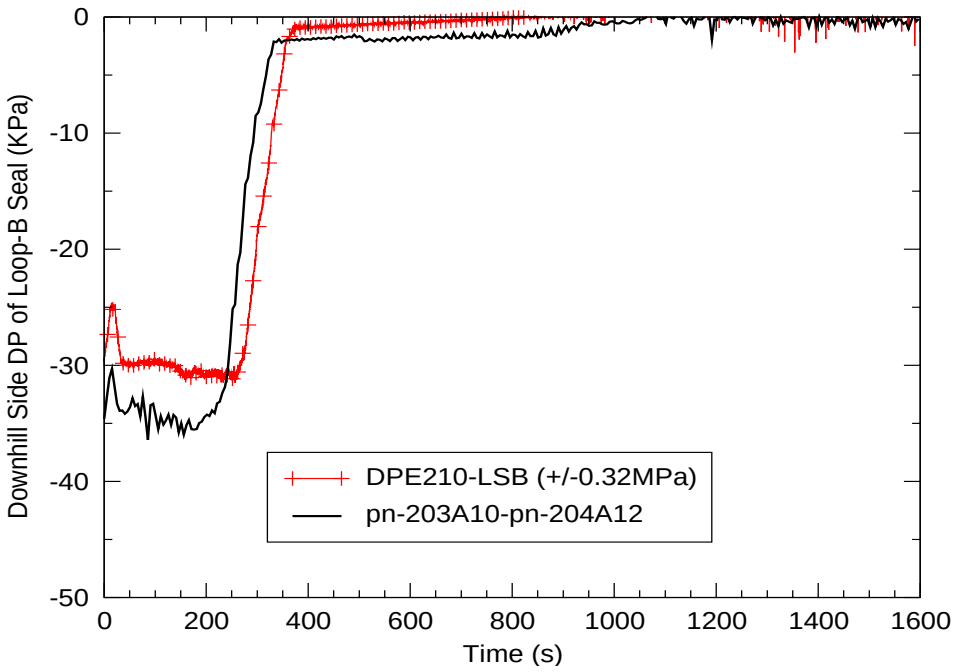

Figure C.5-56. Differential Pressure along downhill side of Loop-B Seal

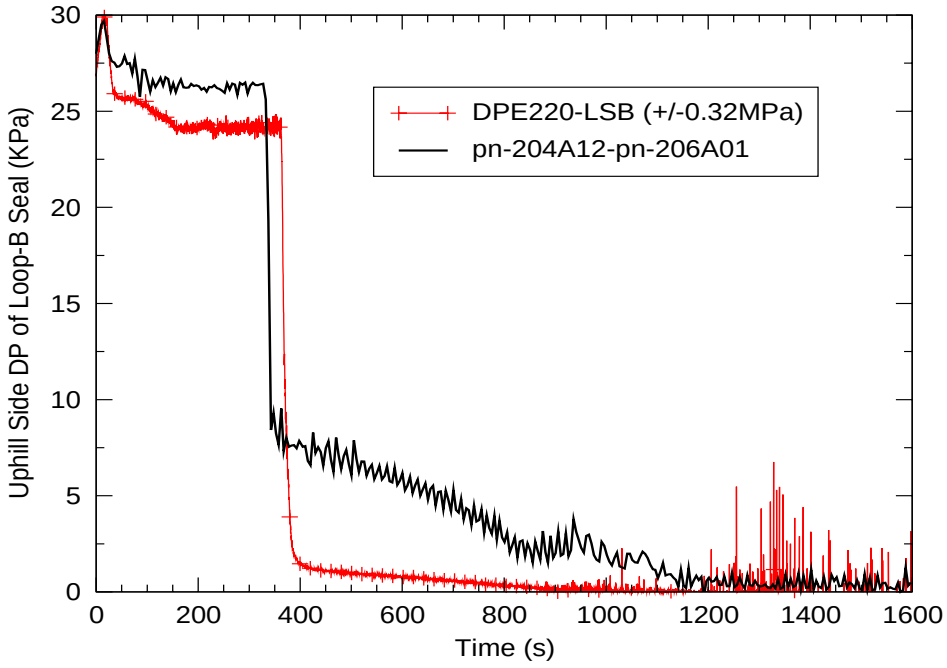

Figure C.5-57. Differential Pressure along uphill side of Loop-B Seal

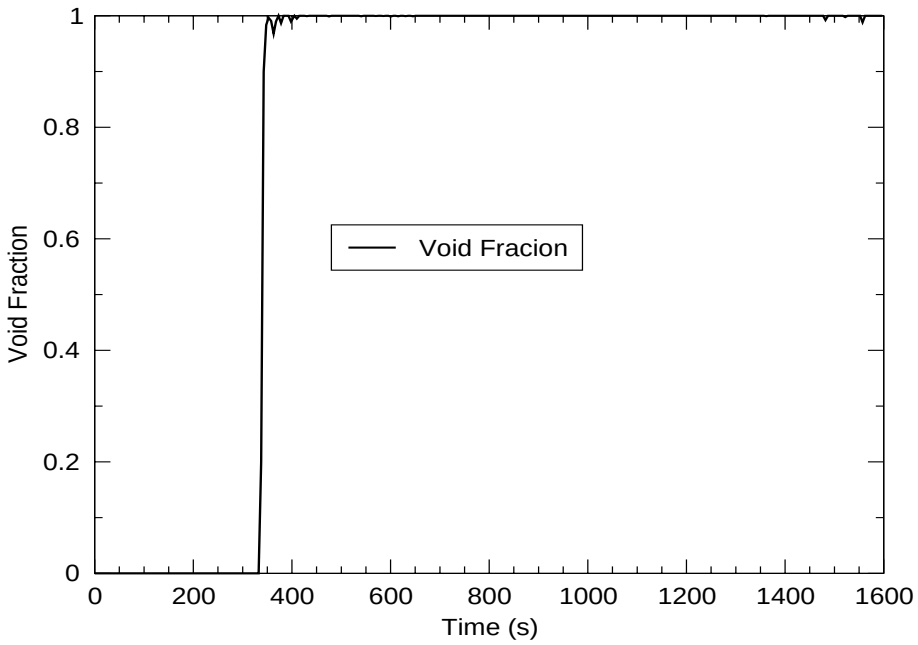

Figure C.5-58. Void Fraction in at Pump-B Inlet

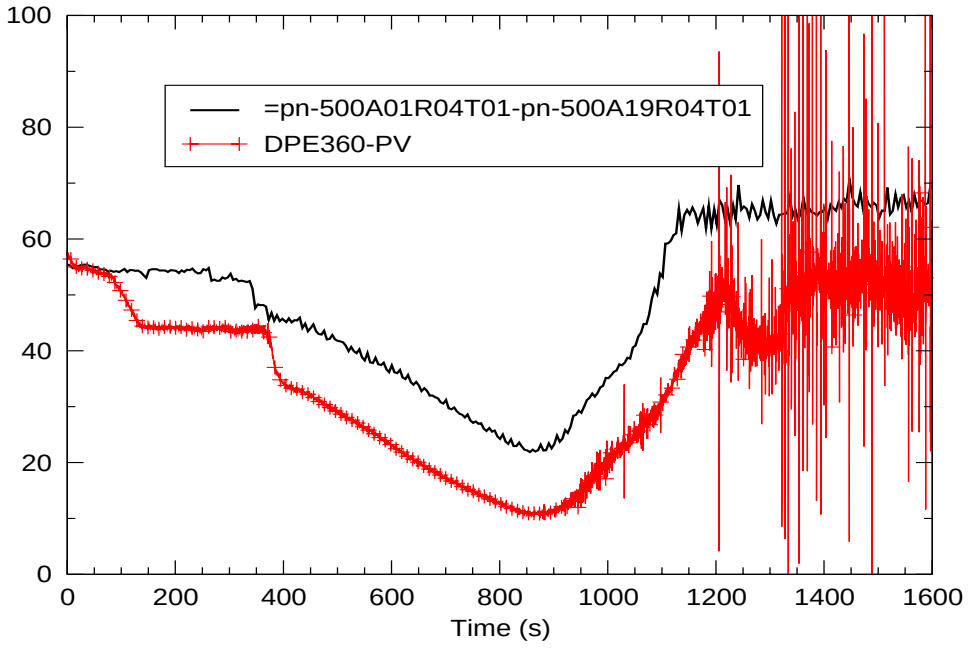

Figure C.5-59. Downcomer Differential Pressure

C.5.5.1.5. Conclusions

Table 5.3 of this report, as well as Reference 8 lists four criteria used in the code validation: *Excellent Agreement, Reasonable Agreement, Minimal Agreement, Insufficient Agreement*. *Reasonable agreement* is defined as:.

> "*Reasonable Agreement* applies when the code exhibits minor deficiencies. Overall, the code provides an acceptable prediction. All major trends and phenomena are predicted correctly. Differences between calculated values and data are greater than those deemed necessary for excellent agreement. The calculation will frequently lie outside but near the specified or inferred uncertainty bands of the data. However, the correct conclusions about trends and phenomena would be reached if the code were used in similar applications. The code models and/or facility model noding should be reviewed to see if improvements can be made."

Based on the PIRT analysis of each characteristic phase encountered during this test, it is evident that the TRACE simulation results presented for SB-CL-01 meet the definition of a *Reasonable Agreement* throughout the transient event for all phenomena ranked high in the applied SBLOCA PIRT.

The most significant discrepancies were as follows:

1. The loop seals clear approximately 50 seconds earlier than in the test.
2. Cold-leg temperatures trend significantly lower after accumulator injection. This appears to be due to the inability of the one-dimensional pipe component to capture the three-dimensional temperature distribution resulting from the mixing of the cold-leg and accumulator-injection fluid.
3. After ECCS injection, the level in the core is predicted to be approximately 20% higher than the measurement. This appears to be due to the lower cold-leg fluid temperatures, and thereby higher cold-leg fluid density.
4. Hot-leg bypass flow is under-predicted by approximately 0.05 kg/s.
5. During the first 350 seconds of the transient, the liquid content in the upper head is over-predicted.
6. After the loop seals clear, more liquid is predicted to remain in the uphill portion of the Loop-Seal B than shown in the data.
7. During the blowdown phase, the data shows a drop in downcomer level that is not predicted with the TRACE model. As a result, the predicted downcomer level remains

approximately 10 kPa higher than the data. For the remaining phases, however, the major events, such as loop-seal clearance, dryout, accumulator injection, are adequately captured.

The majority of the discrepancies appear to be do to either the coarseness in nodalization of certain model components or to inaccuracies in certain component geometries. The only potential code problem appears to be in obtaining accurate temperature distributions resulting from mixing in 1-D components.

C.5.5.2. Simulation of SB-CL-05

SB-CL-05 case was a 5% cold leg break test. The break unit was located on the side of the cold leg in Loop B. Two input decks were developed for the transient analysis: one constrained steady-state (CSS) input deck and one transient input deck. The CSS deck contains most of the model information and plant control procedures. The CSS input deck is used to obtain initial plant conditions for transient calculations.

The control system and control procedures of the ROSA-IV facility were designed to accommodate a wide range of plant operational transients and accident scenarios. The TRACE control procedure was derived from a series of SBLOCA tests.

SB-CL-05 test conditions and control actions implemented in the TRACE transient analysis are listed below.

C.5.5.2.1. SB-CL-05 Test Conditions

Some of the test conditions or control procedures were different from those in the reference PWR reactor. Special control procedures or test conditions were designed to account for some scaling issues in the design of the test facility (Refs.1, 7).

Table C.5.3 summarizes the plant initial conditions. In the test, it was assumed that a loss-of-offsite power occurred concurrently with reactor scram. At the same time, a failure of one of the two diesel-generators for the emergency coolant and auxiliary feedwater pumps was assumed. Table C.5.9 summarizes the operational setpoints for Run SB-CL-05. Table C.5.10 provides the event sequence recorded by the facility instrumentation system; individual items are specified below.

- Coolant pumps

Upon the initiation of the break, the pump speed was increased before the pump started to coast down following the reactor scram signal (Ref. 7). The pump impeller rotation speed after the initiation of break is demonstrated in Figure C.5-60 and Figure C.5-61. The dashed line is the

pump curve obtained in the TRACE simulation of SB-CL-05. The solid line is the measured pump curve in the SB-CL-05 test.

- Reactor trip and core power after break

As indicated in Figure C.5-61, the reactor was tripped 12 seconds after the break was initiated. Two power curves are demonstrated in Figure C.5-62. The solid line is the measured power curve in the SB-CL-05 test. The dashed line is the power curve obtained in the transient simulation.

- Emergency Core Cooling System (ECCS)

During the SB-CL-05 transient, the subsystems of the ECCS system were actuated in the manner given in Table C.5.9 and Table C.5.10. For each loop, the ECCS subsystems injected water into the loop through the same nozzle (Figure C.5-3). In the test, the desired ratio of the ACC injection flow into the loop A cold leg to the ACC injection flow into the loop B cold leg was 3:1. Assuming the ratio was maintained, the ACC injection flow rate into each loop can be calculated based on the discharging flow rate of the ACC tank, which is derived from the ACC tank level measurement (LE14). Figure C.5-63 displays the calculated ECCS injection flow rate into each loop, which is the sum of the injection flow of the ECCS subsystems (high pressure charging and high pressure injection).

- Auxiliary Feedwater System

After the main feedwater was cut off, the auxiliary feedwater system was actuated with delay to supply water to the SG's secondary side. The auxiliary system of the test facility used a single pump and branched piping of unequal hydraulic resistance. In SB-CL-05, the auxiliary feedwater was supplied only to loop B for the first 1370 seconds and then switched to loop A.

- Pressurizer heaters

Based on the test data, power supply to the pressurizer heaters was cut off with the initiation of break.

C.5.5.2.2. TRACE Control Procedure

The control procedure for the TRACE model is simplified by using a strategy outlined at the beginning of this chapter. As a result, the TRACE control procedure mainly consists of a number of trips. In general, a trip is initiated either by time or the system pressure. Specifically

1. At time 0, the break is initiated and the pressurizer heater power is cut off.
2. The pump speed is increased after the break and coasts down with the reactor trip as demonstrated in Figure C.5-60.

3. The reactor is tripped when the system pressure reaches 12.97 MPa. Figure C.5-62 displays the measured power curve after the break and the power curve obtained from the transient calculation.
4. The Safety Injection (SI) signal is generated when the system pressure reaches 12.27 MPa. With a delay of 12 seconds (high pressure charging system) and 17 seconds (high pressure injection) respectively, the Emergency Core Cooling System (ECCS) is actuated. The HPSI and LPSI systems are modeled as boundary conditions. The accumulators are represented in the TRACE model as the two pressurized water tanks connected to their respective cold leg, where flow injection through the check valve is activated when system pressure is below 4.51 MPa.
5. Main steam line valve closure, main feedwater cutoff, and auxiliary feedwater are initiated with proper time delays following the reactor trip.

Table C.5.9. Operational Setpoints for Run SB-CL-05

	Setpoint
Reactor scram signal	12.97 MPa (System pressure)
Pump coast down	With reactor scram
Safety Injection (SI) signal	12.27 MPa (system pressure)
High Pressure charging	12 seconds after SI signal
High Pressure injection	17 seconds after SI signal
Accumulator injection	4.51 MPa
Low Pressure Injection	1.29 MPa
Main feedwater cutoff	With reactor scram
Turbine throttle valve closure	With reactor scram
Auxiliary feedwater ON	28 seconds after reactor scram

Table C.5.10. Chronology of Events for Run SB-CL-05

Events	Time (s)
Break	0
Reactor trip	12
Main Steam Line Valve Closure	15
Safety Injection Signal	17
SG Feedwater stop	18
High Pressure Charging Injection	31
High Pressure Safety Injection	34
Auxiliary feedwater ON	40
Core Uncovery	120 -155
Loop Seal clearing	~140
Primary/Secondary Pressure Reversal	~180
Reactor coolant pump stop	266

Table C.5.10. Chronology of Events for Run SB-CL-05

Accumulator Injection ON	417
Accumulator Injection OFF	1447
End of data	1800

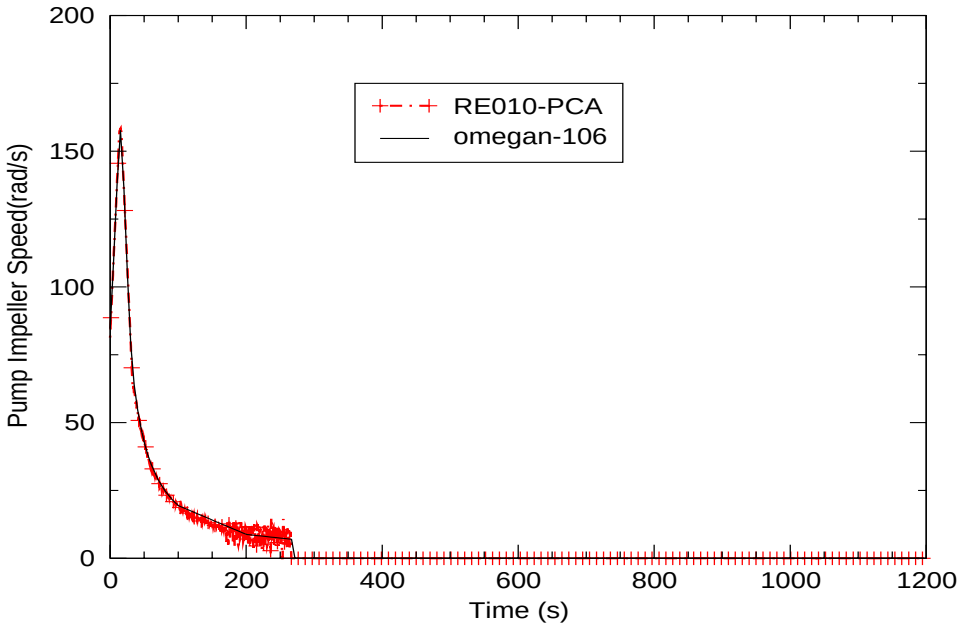

Figure C.5-60. Pump-A Speed

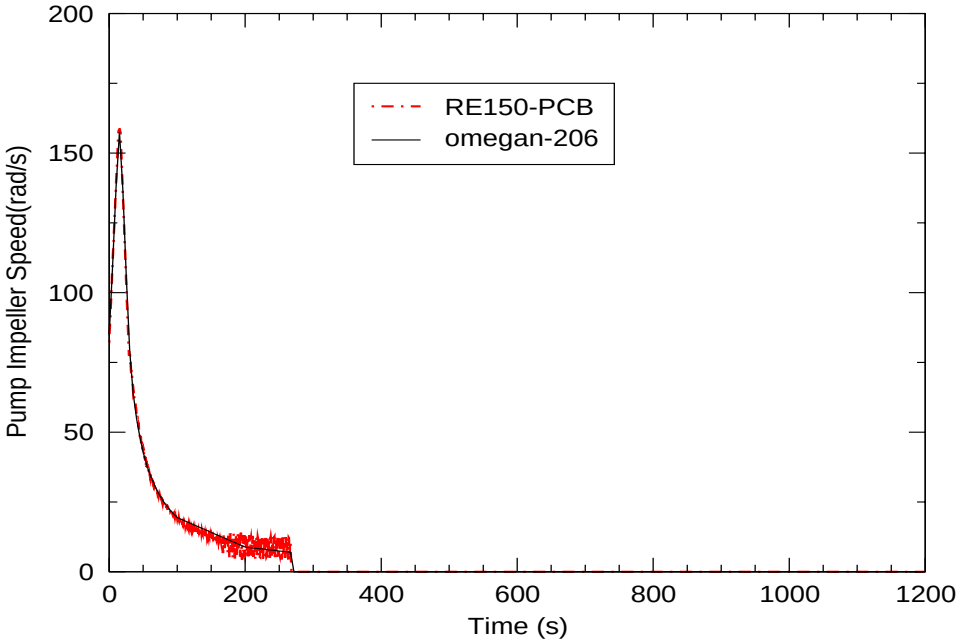

Figure C.5-61. Pump-B Speed

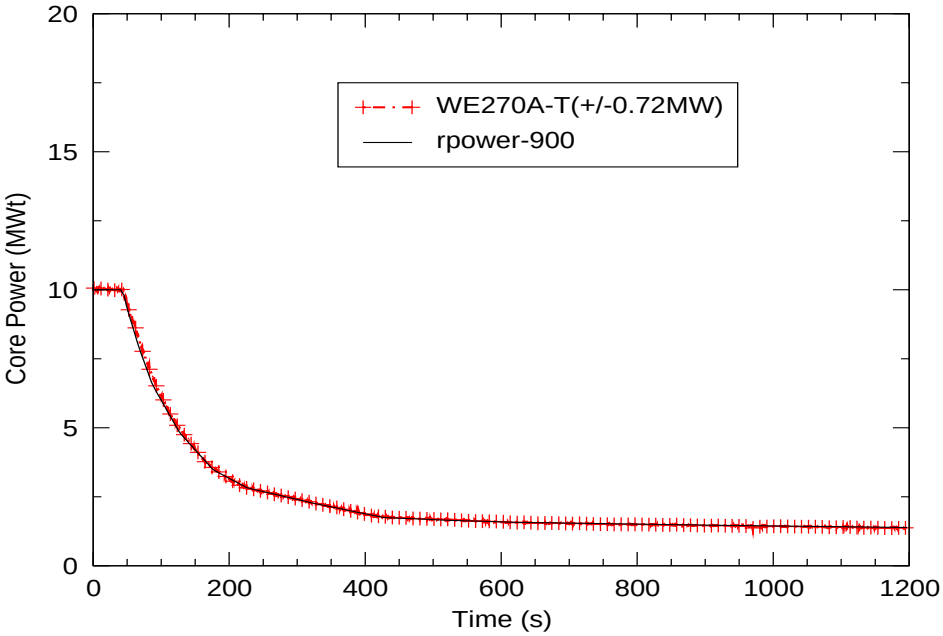

Figure C.5-62. Core Power

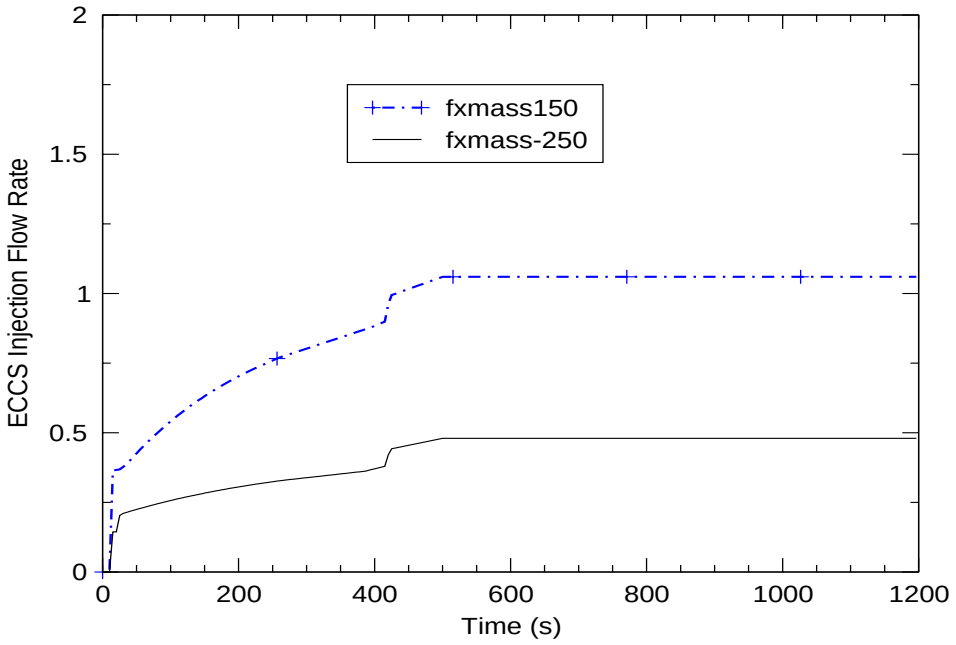

Figure C.5-63. ECCS Injection

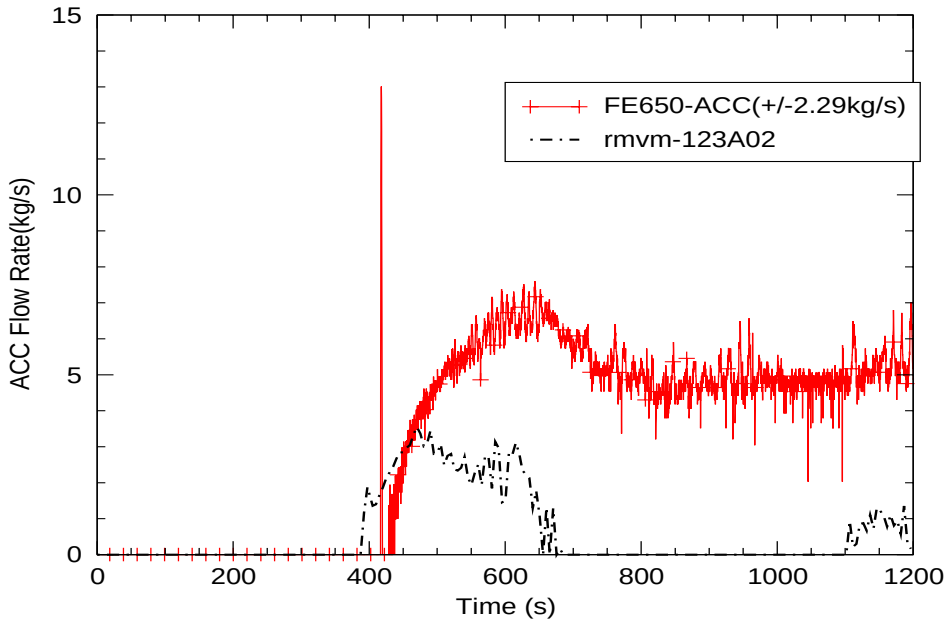

Figure C.5-64. Accumulator-A Injection

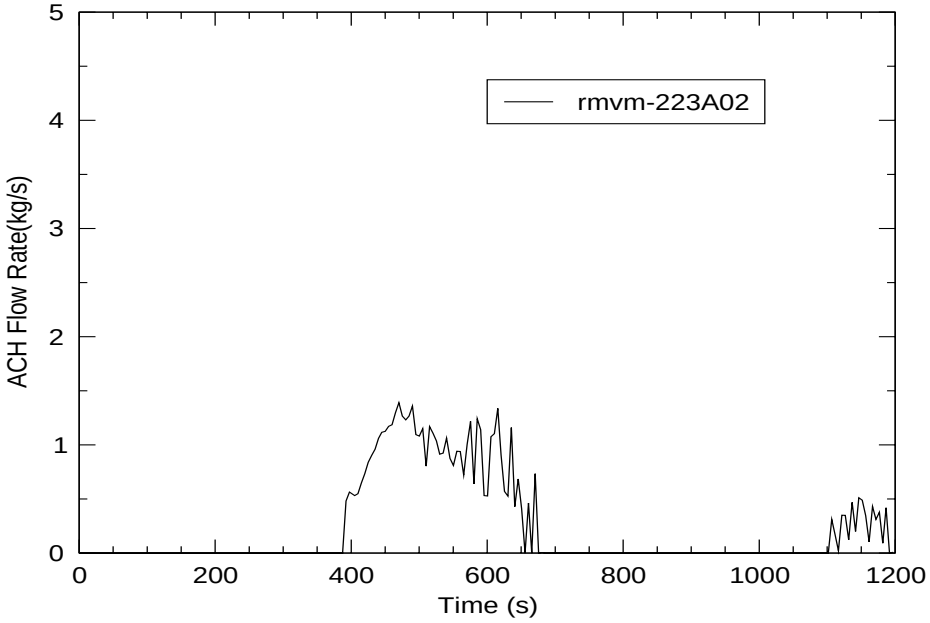

Figure C.5-65. Accumulator-B Injection

C.5.5.2.3. Experimental Observations

The main objective of test SB-CL-05 was to investigate the thermal-hydraulic mechanisms of early core uncovery and heatup. Early core uncovery may be caused by a manometric effect resulting from an imbalance between the water hold up in the upflow and downflow sections of the primary coolant system in the steam generator U-tubes (Ref. 7). Table C.5.11 lists the event sequence recorded by the facility's instrumentation system during the test.

Soon after the start of the transient, the pressure started to drop rapidly and the core power decay curve was initiated at a pressurizer pressure of 12.97 MPa (corresponding to reactor scram) together with a closure of the MSIV, starting of the programmed pump speed curve, and termination of the main feedwater to the steam generators.

The safety injection signal occurred at 17 seconds at the pressurizer pressure of 12.27 MPa. Thus, the charging pump and the high-pressure injection pump began emergency coolant injections at 31 and 34 seconds, respectively. The secondary pressure increased to and remained at approximately 8 MPa due to the SG relief valve operation. The SG secondary-side water mass inventory was maintained at the initial level by the auxiliary feedwater supply activated at 40 seconds.

In spite of the HPIS actuation, the core became temporarily uncovered in the time interval from 120 s to 155 s after the break Consequently, the maximum heater rod temperature increased by

about 100 K above its steady state value. This temporary core uncovery occurred immediately before loop seal clearing.

Both loops experienced loop seal clearing at about 140 s, which led to a core level recovery. Loop seal clearing allowed a mixture of steam and water to discharge from the break, which in turn reduced the break mass flow rate but accelerated the depressurization of the primary loop. At about 180 s after the break, the primary loop pressure decreased below the steam generator secondary side pressure. Thereafter, the steam generators no longer served as heat sinks, and the energy removal from the primary system was by coolant discharge through the break.

C.5.5.2.4. Transient Analysis

The SB-CL-05 transient calculation was performed for 1200 seconds. The transient simulation results and the comparison to the test data are presented in Figure C.5-60 to Figure C.5-94 In these figures, the test data is plotted in solid, colored lines with symbols and the calculation results are plotted in sold black or blue lines without symbols.

C.5.5.2.4.1. System Behavior

The overall primary system behavior determines the boundary conditions of the transient event since most of the control signals are based on the system pressure setpoints. The predicted system pressure is in good agreement (in accordance with the acceptance criteria (Ref. 8)) with the data as demonstrated in Figure C.5-66. Therefore, the sequence of the events based on the system pressure setpoints are also in good agreement with the test data.

Table C.5.11 displays the comparison of the sequence of the events for the SB-CL-05 simulation results and the test data.

Table C.5.11. Sequence of the Event Comparison for SB-CL-05 Test

Event	Test Data	TRACE Model
Break	0 sec	0b[a]
Reactor Trip	12 sec	12 sec
Main Steam Line Valve Close	15 sec	15 sec
Safety Injection Signal	17 sec	17 sec
SG Feedwater Stop	18 sec	18 sec
High Pressure Charging Injection	31 sec	31 sec
High Pressure Safety Injection	34 sec	34 sec
Auxiliary Feedwater On	40 sec	40 sec
First Core Uncovery	120 – 145 sec	125 – 145 sec
Loop-A Seal Begins Clearing[b]	~ 140 sec	~ 140 sec
Loop-B Seal Begins Clearing[b]	~ 140 sec	~ 140 sec
Primary/Secondary Pressure Reversal	~ 180 sec	~ 180 sec
Reactor Coolant Pumps (PC-A/B) Stop	266 sec	265 sec
Accumulator Injection On	417 sec	390 sec
End Time	1800 sec	1200 sec

a. The break starts at time 0.

b. The beginning of loop-seal clearance is the time at which the differential pressure across the uphill portion of the loop seal begins to rapidly descend toward zero.

C.5.5.2.4.2. Analysis Results

As discussed in **Section C.5.5.**, the PIRT (Ref. 6) identifies the highly-ranked phenomena for each phase of the transient. To evaluate the performance of TRACE, each phase will be discussed separately, and the TRACE-simulation results for the highly-ranked phenomena will be compared to the data. The principal Figure of Merit (FOM) of the transient event is the core collapsed liquid level (CCL). The core collapsed level is measured as the core differential pressure as demonstrated in Figure C.5-67.

Certain input parameters, such as decay heat, core power, and feedwater temperature, are taken directly from the test data as boundary conditions. Therefore, although they are identified as important in some of the phases, they will not be discussed in terms of code performance.

Blowdown phase

The blowdown phase is marked by a rapid depressurization of the primary coolant system until the hot coolant begins to flash into steam. The rate of depressurization is strongly influenced by the rate and enthalpy of the break flow, and it changes when flashing and boiling start in the core. In this phase, the most important parameters defining the evolution of the transient are decay heat, primary side heat transfer, critical break flow, and the flow regime upsteam of the break flow.

In the test, the blowdown phase lasted from 0 to 90 seconds. Throughout this time, good agreement is observed between the simulation results for each of the highly-ranked parameters and the test data. The core pressure is shown in Figure C.5-66, and the core differential pressure (DP) is shown in Figure C.5-67. Primary side heat transfer is evaluated using the fluid temperature in the steam generator (SG) tubes and the cold legs. These parameters can be seen in Figure C.5-68 through Figure C.5-71. The integrated break flow shown in Figure C.5-72 is used in evaluating critical break flow, and cold-leg-density predictions, shown in Figure C.5-73 and Figure C.5-74, are used to evaluate the flow regime upstream of the break. The data for the density comparisons is taken from three densitometers located along the cross-sections of the cold legs.

Other key results in this phase are the DPs in the upper head and upper plenum, the pressurizer level, and the flow regime in the hot legs. These results will be discussed to further illuminate the evolution of the transient during this phase and to thoroughly evaluate the code.

Figure C.5-75 shows the vessel-head DP. Here, the depressurization can be observed, but unlike the data, the code is predicting large negative DPs. The cause of these large oscillations is unclear, as the void fraction in the upper head appears to evolve as expected. As can be seen in Figure C.5-76, liquid flashes to vapor in the uppermost level of the upper head, Level 22; the void fraction in the center cell, Level 21, gradually progresses toward single-phase vapor as the liquid

level decreases; and liquid remains in the lowest cell, Level 20, throughout the blowdown phase. It is apparent, however, that the code is adequately capturing the fluid dynamics occurring within the upper plenum; Figure C.5-77 shows excellent agreement between the calculated upper-plenum DP and the data.

As for the pressurizer level, the code produces excellent agreement with the data. As shown in Figure C.5-78, the rate at which the level descends is matched throughout the phase. The only discrepancy appears to be due to an instrument-scale error, which indicates a negative level.

The flow regimes in the hot legs are evaluated in terms of hot-leg fluid density. Figure C.5-79 and Figure C.5-80 show the code predicting the correct fluid densities.

Natural Circulation phase

The natural-circulation phase begins at the end of the pump coastdown and ends when the buoyancy forces caused by differences in loop-fluid densities are no longer able to overcome the flow resistance of the loop components. In the experiment, the natural-circulation phase began at around 91 s and lasted until around 115 s. The beginning of this phase can be seen in Figure C.5-67 as the second momentary interruption in depressurization, just before the final stage of level depression in the core. The measurable highly-ranked processes in this phase are the FOM, decay heat, the counter-current flow in the upper-plenum region, critical break flow, and break upstream flow regime.

Over this period, the predicted primary-system pressure, Figure C.5-66, is greater than the data. Once the simulated depressurization is interrupted, the subsequent drop in pressure is not as rapid as the measurements. The calculated core DP, Figure C.5-67, remains in good agreement.

As for the remaining highly-ranked parameters, there continues to be good agreement between the predictions and the data. Based on the good agreement in upper-plenum DP shown in Figure C.5-77, it can be inferred that the code is adequately simulating the counter-current flow in the upper-plenum; the predicted break flow, shown in Figure C.5-72, is still in agreement with data; and the predicted cold-leg densities (Figure C.5-73 and Figure C.5-74) continue to show the presence of single-phase liquid.

Other parameters of interest during this phase are U-bend voiding, fuel rod temperature, and secondary-side pressure. Voiding in the U-bends of the SG tubes, which is indicative of the state of primary-side heat transfer, can be evaluated in terms of SG-tube DP. Figure C.5-81 through Figure C.5-84 show the SG-tube DPs along the uphill and downhill sides of each set of SG-tubes. These figures give an indication of the degree of voiding occurring in the tubes, and they show excellent agreement between the simulation and the data.

The temperature of the fuel can be seen in Figure C.5-85. As the natural circulation phase progresses, the temperature of the fuel gradually decreases. As shown in the figure, the code accurately captures this decrease.

Figure C.5-86 and Figure C.5-87 show comparisons of predicted and measured pressures from the shell-side of each SG. During this phase, the pressure fluctuates as a result of the relief valves opening and closing. The opening and closing times of the modeled valves are different than the test, leading to the different oscillation frequency.

Loop Seal Clearing phase

The loop seal clearing phase begins when the trapped primary-side steam volume reaches the top of the loop seal piping. From this point, the steam volume depresses the liquid in the downhill side of the loop seal and in the core until a minimum core level is reached. As steam moves through the seal to the break plane, the liquid it displaces is forced into the core, quenching the heatup caused by the drop in core level. In the test, this sequence of events occurred between 116 and 150 seconds.

The highly ranked processes in this phase are listed as follows:

1. Decay heat
2. Mixture level in the core region
3. Hot-leg downcomer gap flow
4. Counter-current flow and CCFL in Upper Plenum region
5. SG primary-side heat transfer in the U-tubes
6. SG primary-side flow resistance
7. SG primary-side tube voiding
8. Flow regime/entrainment in the pump suction / loop seal
9. Critical break flow

The mixture level in the core is related to the core DP shown in Figure C.5-67. The prediction continues to be in excellent agreement with the data. Such agreement also results in the accurate prediction of the fuel heatup shown in Figure C.5-85.

Figure C.5-88 and Figure C.5-89 show the calculated mass flow leaking from the hot legs to the downcomer. Because of the relatively large break size, the under-prediction of this flow, by approximately 0.05 kg/s, had no affect on the occurrence of maximum level depression.

Flow processes in the upper plenum and the SG-tubes continue to be simulated accurately. Evidence of this can be seen in Figure C.5-77, which continues to show excellent agreement in the upper-plenum DP; and in Figure C.5-81 through Figure C.5-84, which continue to show good agreement in SG-tube DP.

Figure C.5-90 through Figure C.5-93 show the DP comparisons along the uphill and downhill sides of the loop seals. In each of these figures, the rate of fluid motion through each part of the seals is in excellent agreement with the data. A key discrepancy, however, is the amount of liquid predicted to remain in the uphill portion of the loop seals after the initial flushing of fluid. This fluid gradually dissipates over a period of about 400 seconds.

As the loop-seal clearing phase progresses, the flow in the loop-seals and cold legs changes composition. Figure C.5-73 and Figure C.5-74 show the code accurately predicting the occurrence of this phase change in the cold legs. Moreover, Figure C.5-72 shows the break flow changing from single-phase liquid to a two-phase mixture.

Boil Off phase

As the transient evolves, the primary system continues to loose inventory and the core inventory continues to boil. During the test, this boil-off phase lasted from 151 to 416 s. The highly-ranked processes in this phase are listed below:

1. Fuel Decay heat and local power
2. Mixture level in the core
3. Horizontal stratification and condensation in the cold leg
4. Downcomer mixture level
5. Critical break flow

Figure C.5-67 shows the code predicting a slightly higher level in the core following clearance of the loop seals, but agreement with the data appears good throughout the remainder of this period.

As for horizontal stratification and condensation in the cold legs, based on the cold-leg density results shown in Figure C.5-73 and Figure C.5-74, the code is predicting the correct flow regimes. However, as can be seen in Figure C.5-70 and Figure C.5-71, the temperature in the cold legs begins to drop considerably below the data. A potential reason for this discrepancy appears to be an error in determining the temperature distribution in the cold leg following injection of the accumulators.

Like the core level, the level in the downcomer is represented by DP measurements. As seen in Figure C.5-94, the predicted level in the downcomer follows the downward trend of the data. However, these results remain higher than the measurements, a condition that appears to be due to the under-predicted level decrease that occurred during the blowdown phase.

The break flow in this phase continues to be in excellent agreement with the data (Figure C.5-72).

Also of note during this phase are the SG pressures. Figure C.5-86 and Figure C.5-87 show the calculated pressures gradually diverging from the data as the phase progresses. The differences, however, are not unacceptably large.

Core Recovery phase

The final stage of this transient is the core-recovery phase. During this phase, safety systems inject liquid into the core to establish and maintain core cooling. For this particular test, HPIS and LPIS are available and HPIS injects at 34 seconds into the transient.

The highly ranked processes in the recovery-phase (416s – 900s) are as listed below:

1. Fuel Decay heat and local power
2. Mixture level in the core
3. Downcomer mixture level
4. Critical break flow

Unlike the data, at the beginning of this phase, the code appears to predict the start of a core dryout. Following the injection of the accumulators at around 417 seconds, the predicted level in the core, shown in Figure C.5-67, drops for about 100 seconds then rebounds. The reduction in level appears to follow a reduction in the upper-plenum level shown in Figure C.5-77, which occurred between 350 and 415 seconds. This can be seen in the hot-leg density results shown in Figure C.5-79 and Figure C.5-80. The hot-leg density calculated during this period drops dramatically, signifying the increased presence of vapor emanating from the vessel. This level decrease was abated by the accumulator injection.

The excessive level increase in the core appears to be caused by the difficulty of the code in accurately simulating the mixing process occurring in the cold legs as a result of accumulator injection. As can be seen in Figure C.5-70 and Figure C.5-71, following the accumulator injection, the cold leg temperatures are significantly under predicted. This, however, goes against the cold-leg density predictions shown in Figure C.5-73 and Figure C.5-74 and the accumulator injection results shown in Figure C.5-64 and Figure C.5-65. The predicted accumulator injection is significantly under-predicted; yet, the predicted density results are similar to the data. Moreover, the density values are indicative of two-phase fluid, but the corresponding temperature of the cold-leg mixtures are much lower than the saturation temperature.

As with the core level, the cold, denser fluid leaving the cold leg and entering the downcomer causes the downcomer mixture level to rise excessively. Figure C.5-94 shows the rise in calculated downcomer level outpacing the measurements after accumulator injection.

At around 700 seconds, the over-estimation of vapor in the cold legs manifests as a reduction in break flow. Figure C.5-72 shows that around this time, the predicted break flow trends lower than the data scatter.

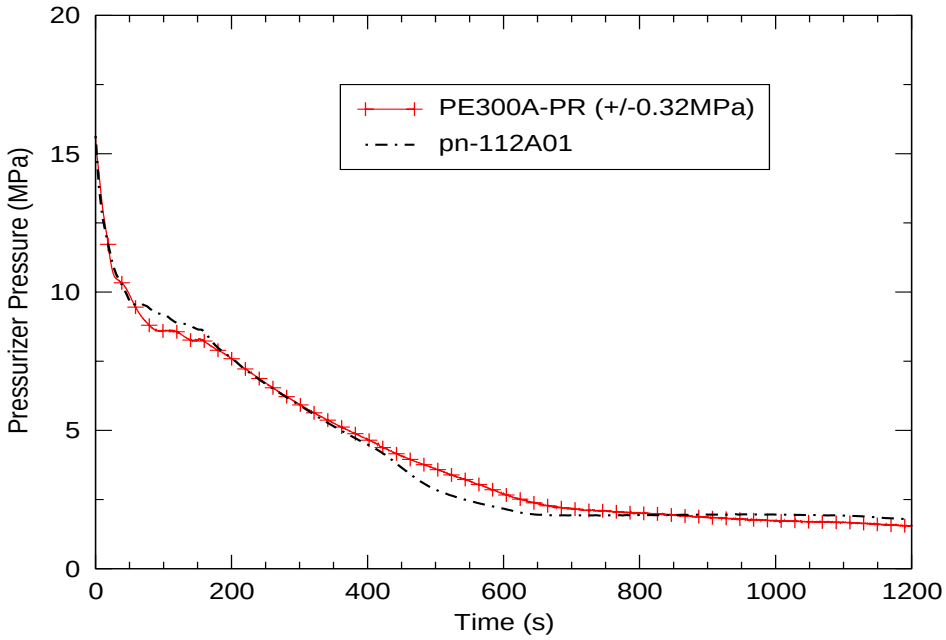

Figure C.5-66. Pressurizer Pressure

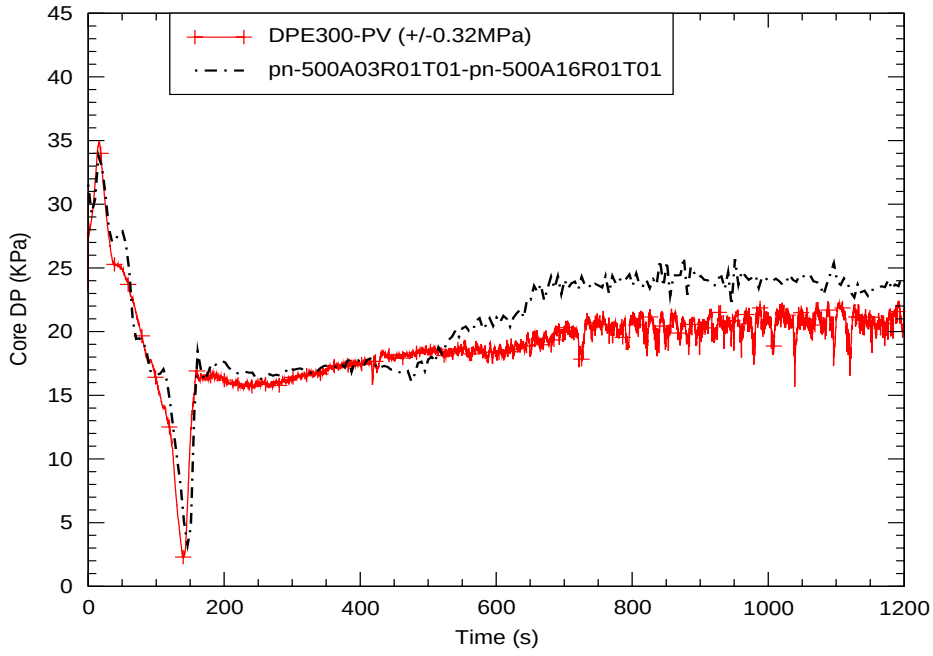

Figure C.5-67. Reactor Core Differential Pressure

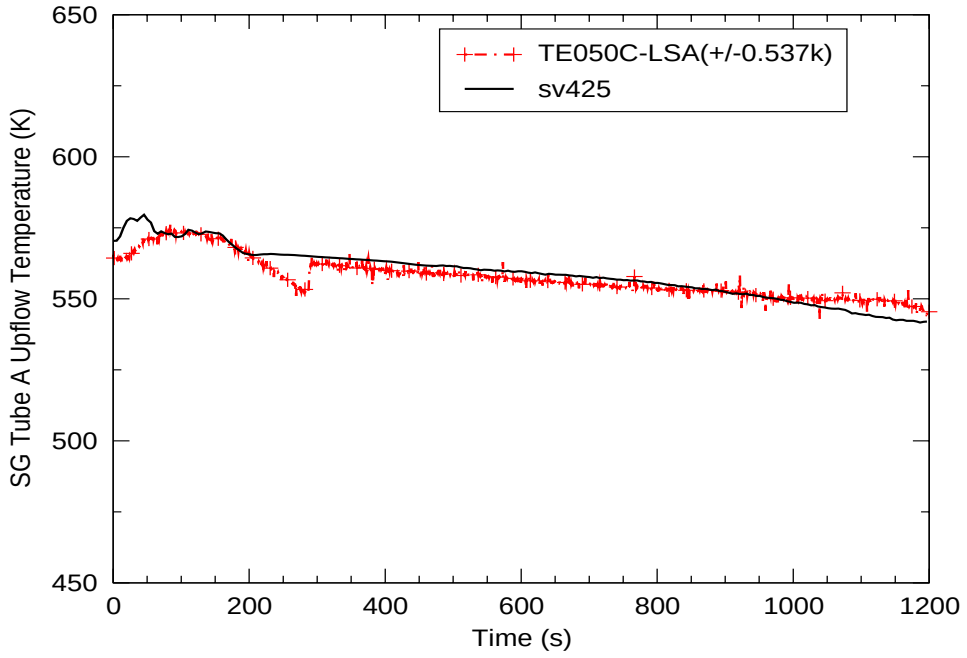

Figure C.5-68. Steam-Generator-Tube Liquid Temperature, Upflow Side, Loop-A

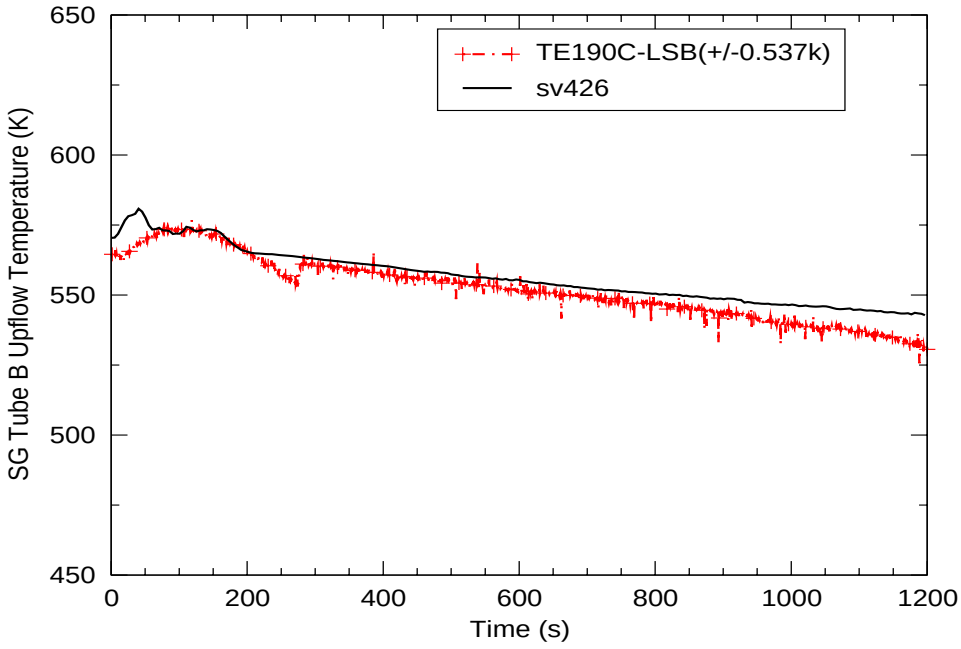

Figure C.5-69. Steam-Generator-Tube Liquid Temperature, Upflow Side, Loop-A

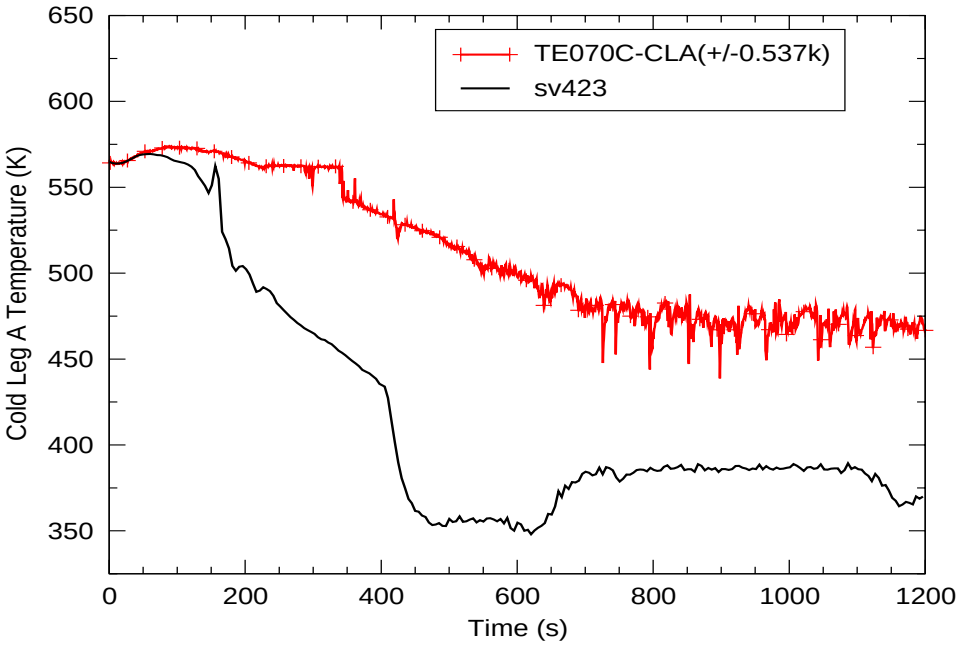

Figure C.5-70. Cold Leg Temperature, Loop-A

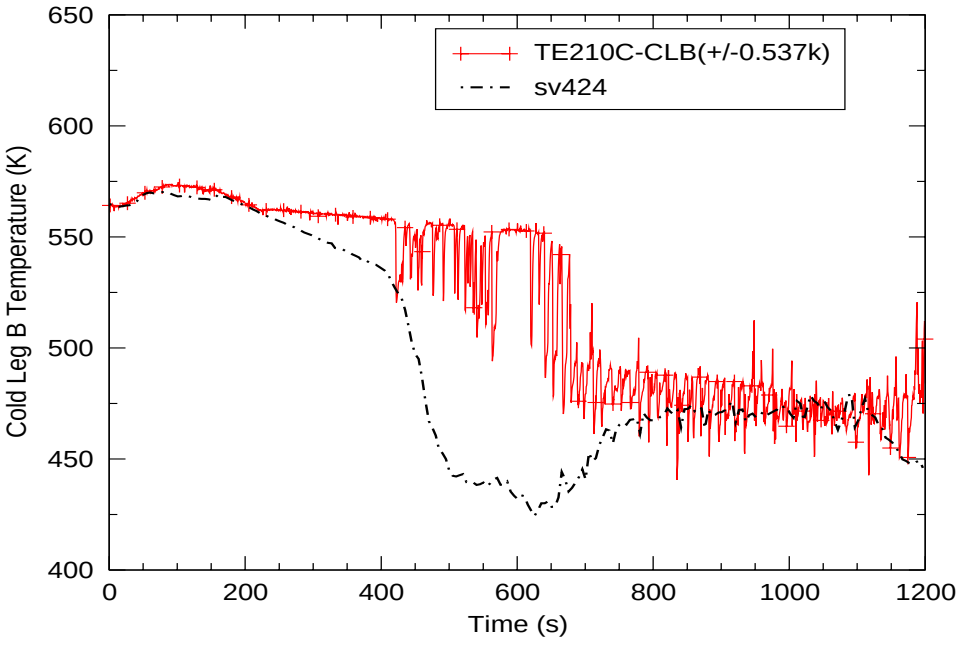

Figure C.5-71. Cold Leg Temperature, Loop-A

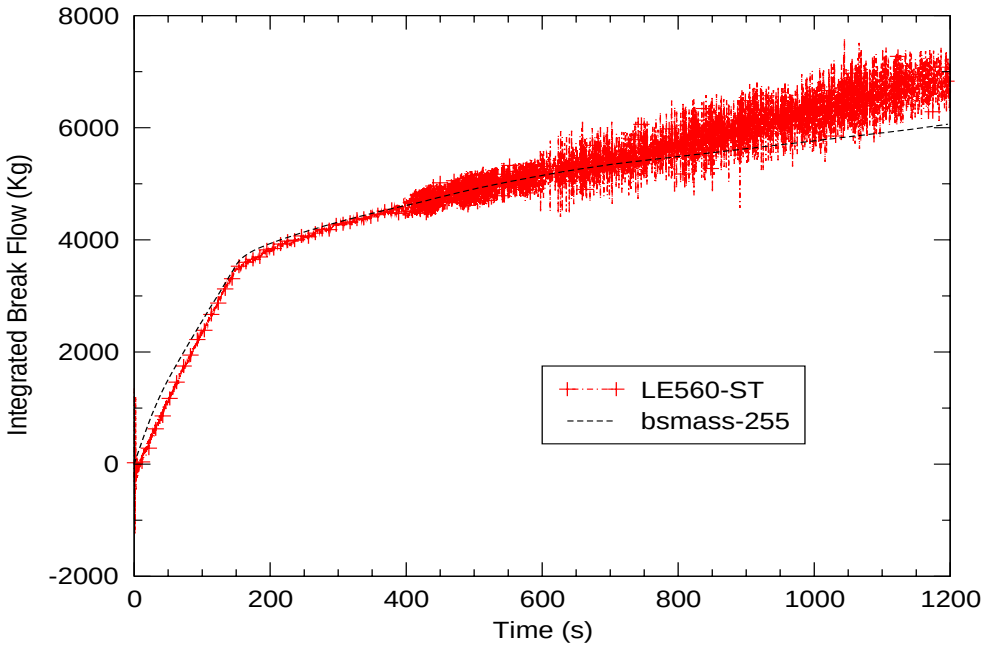

Figure C.5-72. Integrated Break Flow

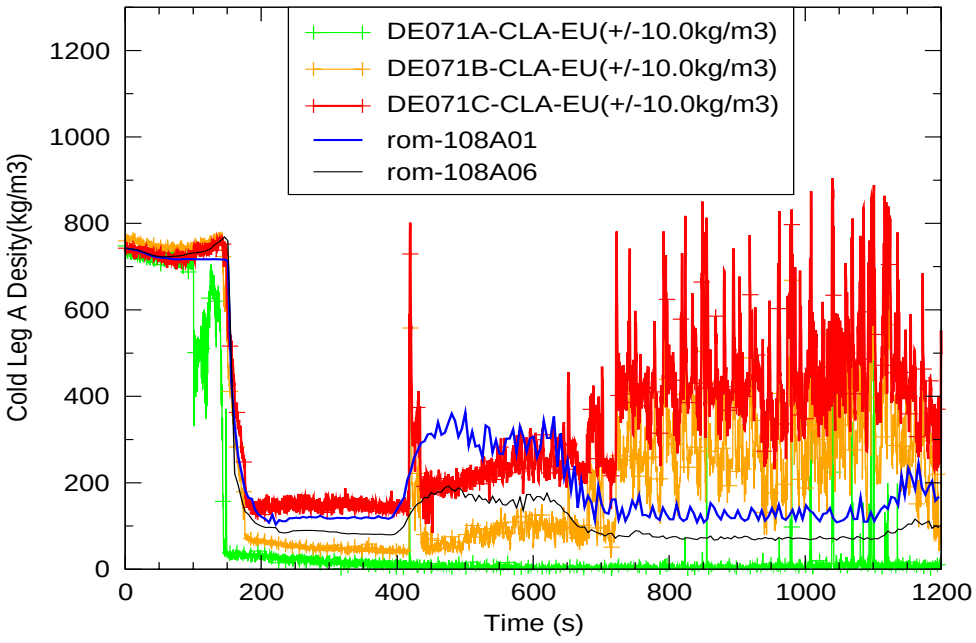

Figure C.5-73. Cold-Leg Density, Loop-A

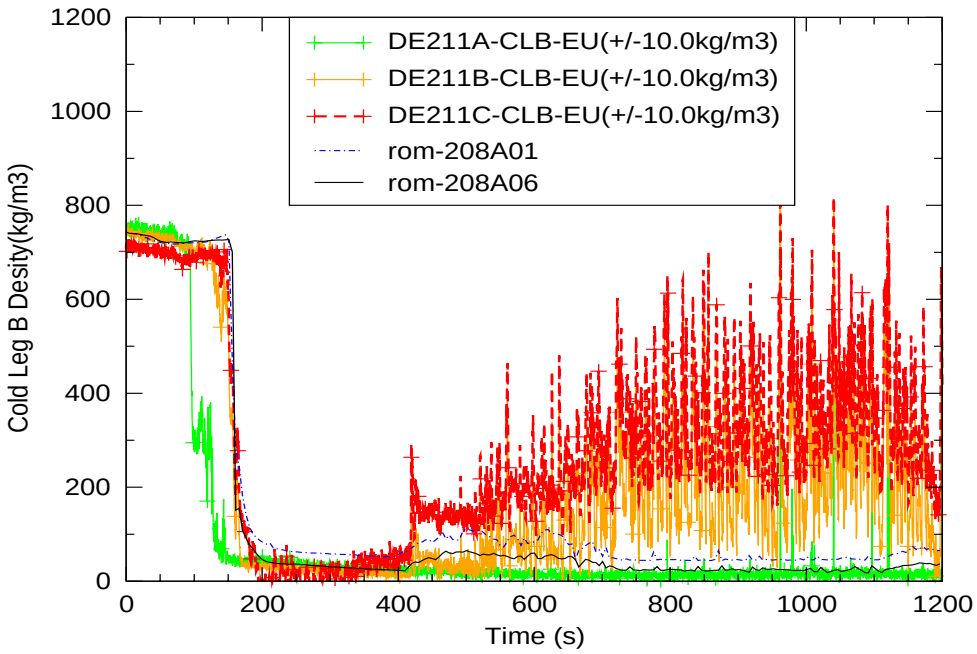

Figure C.5-74. Cold-Leg Density, Loop-B

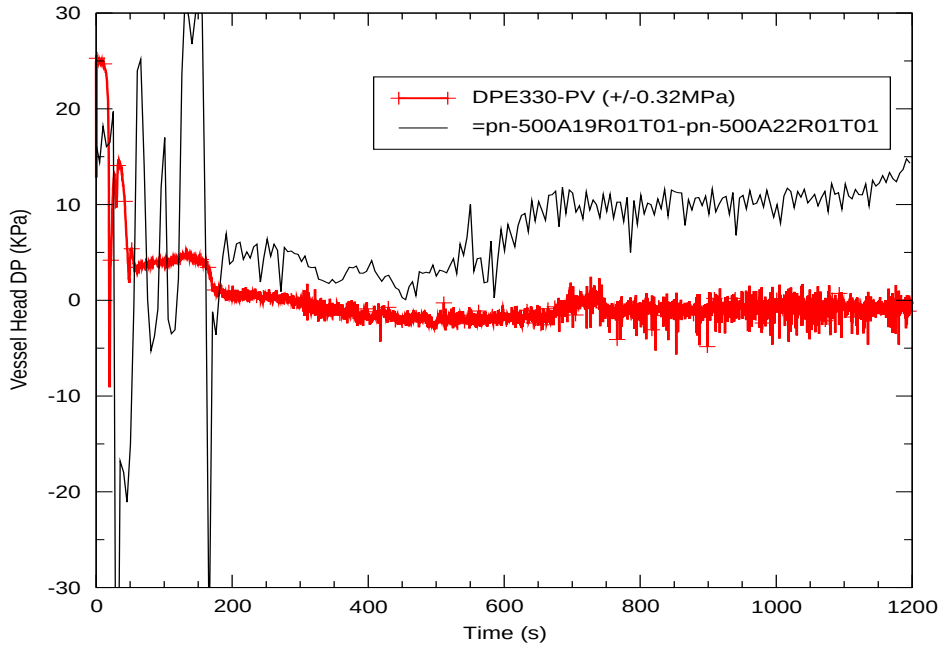

Figure C.5-75. Differential Pressure in Upper Head

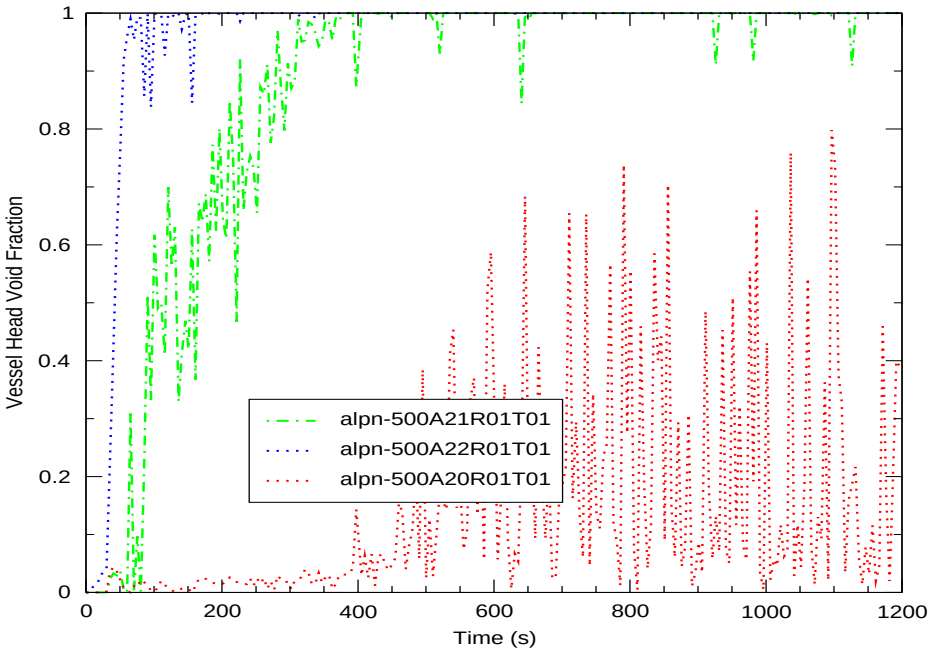

Figure C.5-76. Vessel Void Fractions

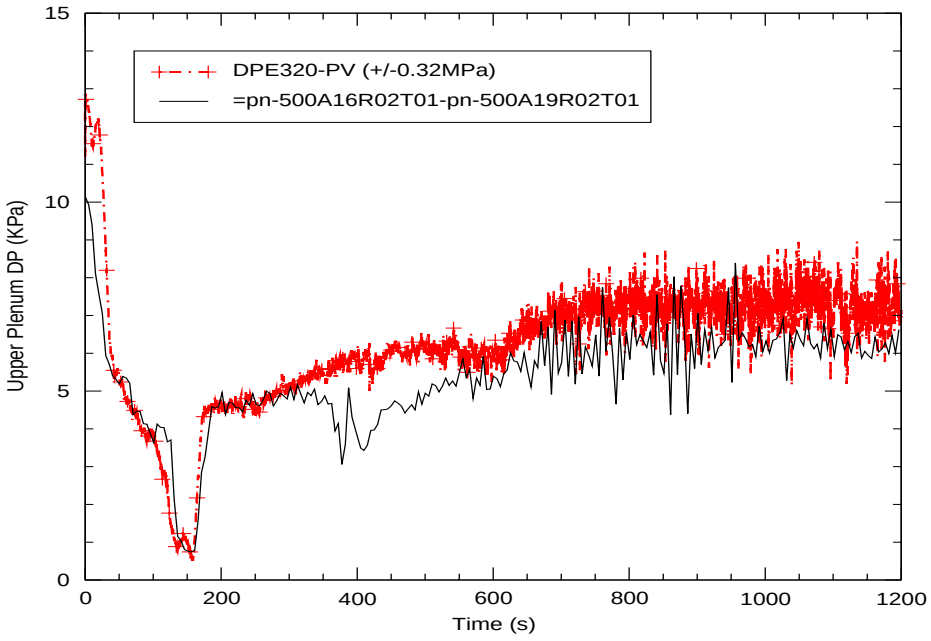

Figure C.5-77. Upper Plenum Differential Pressure

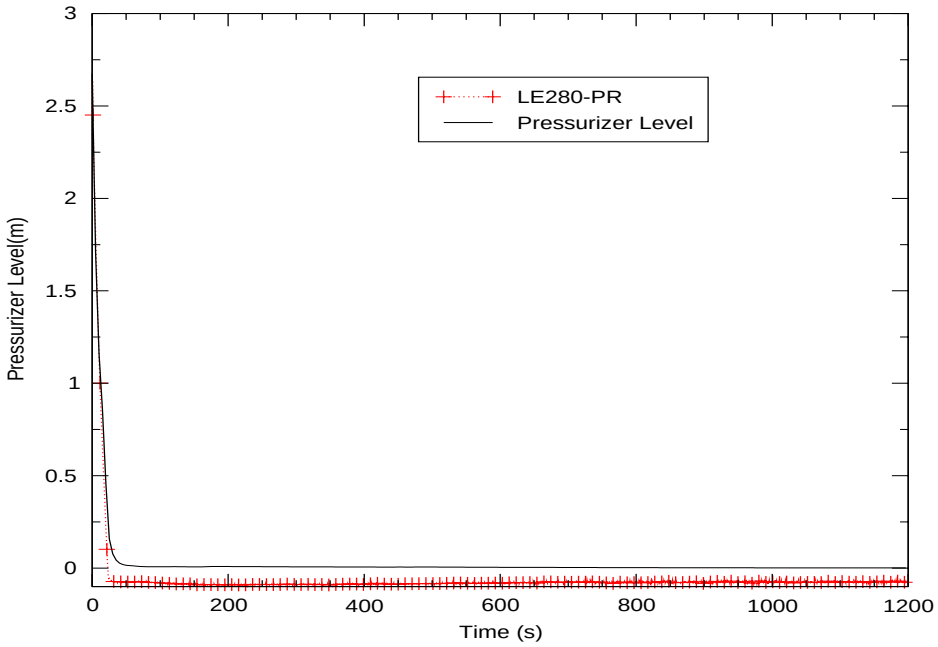

Figure C.5-78. Pressurizer Level

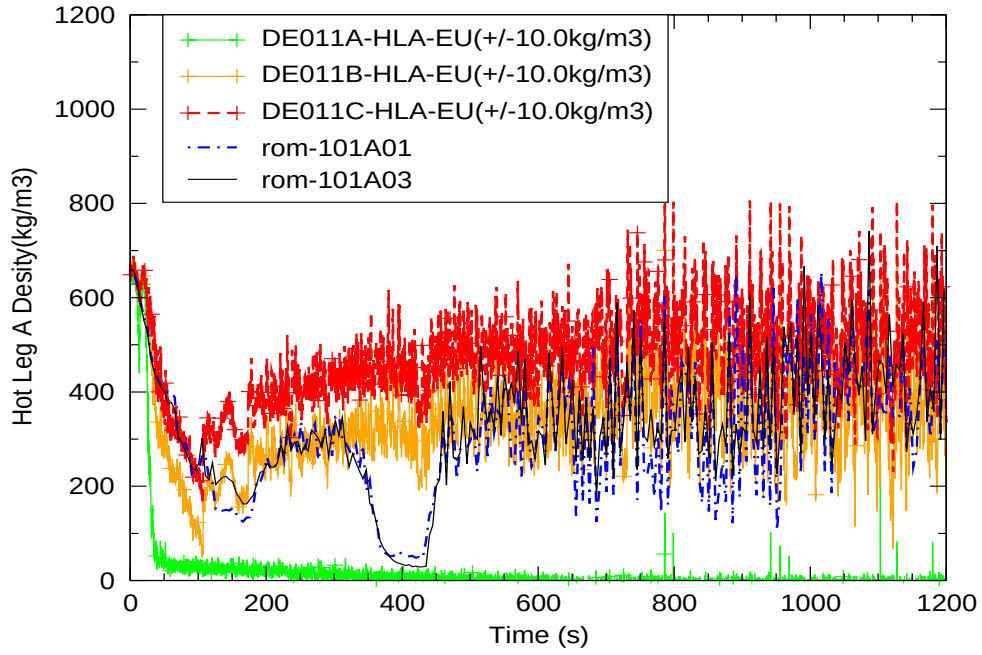

Figure C.5-79. Hot-Leg Density, Loop-A

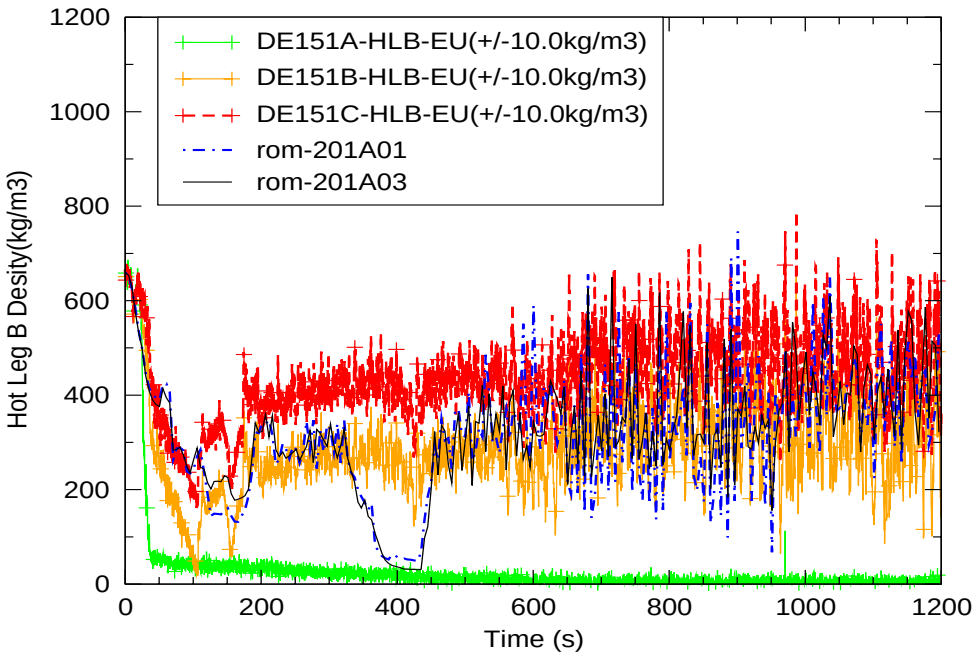

Figure C.5-80. Hot-Leg Density, Loop-B

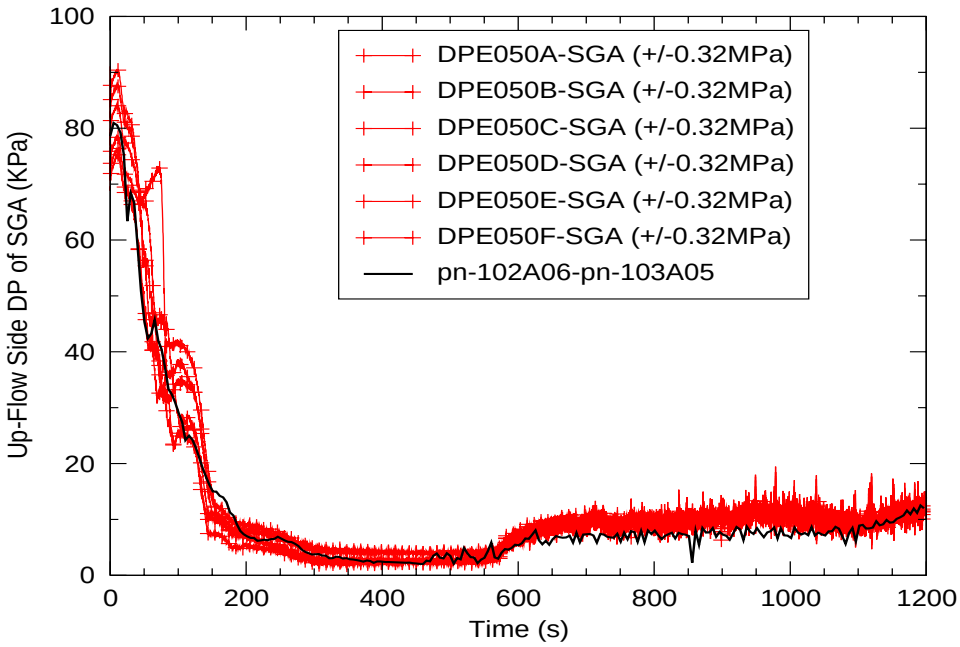

Figure C.5-81. Differential Pressure along uphill side of Steam Generator, Loop-A

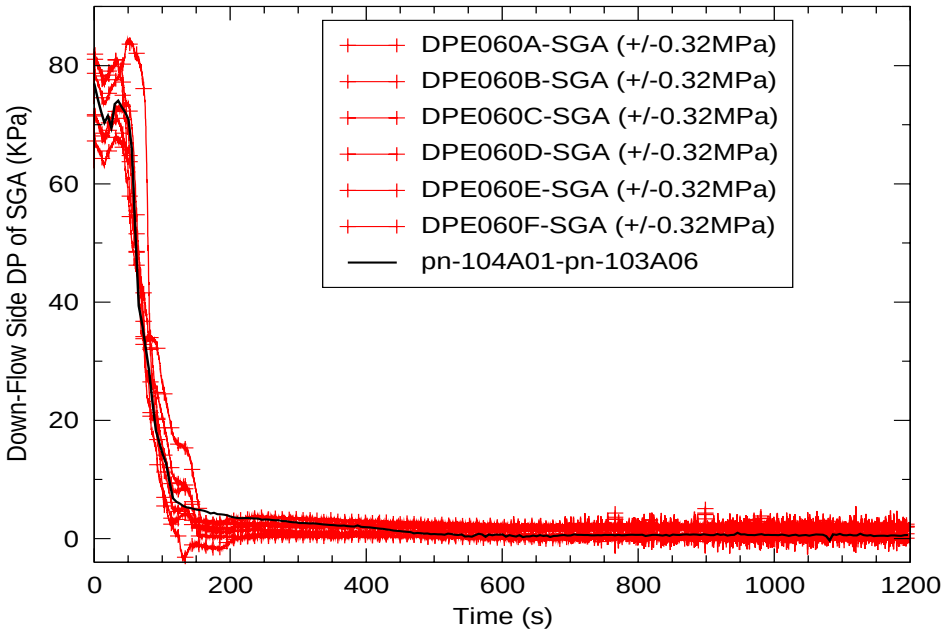

Figure C.5-82. differential Pressure along downhill side of Steam Generator, Loop-A

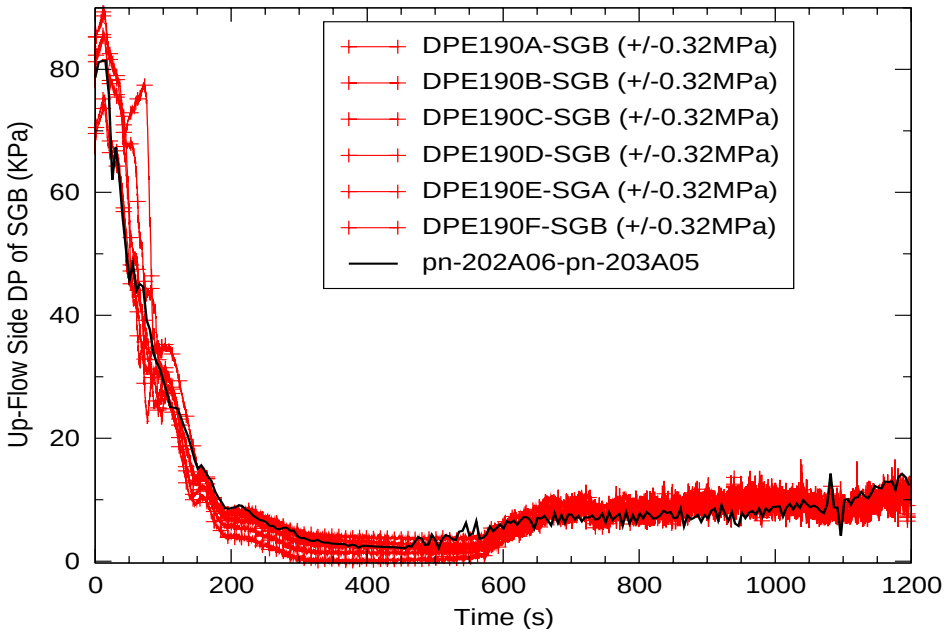

Figure C.5-83. Differential Pressure along uphill side of Steam Generator, Loop-B

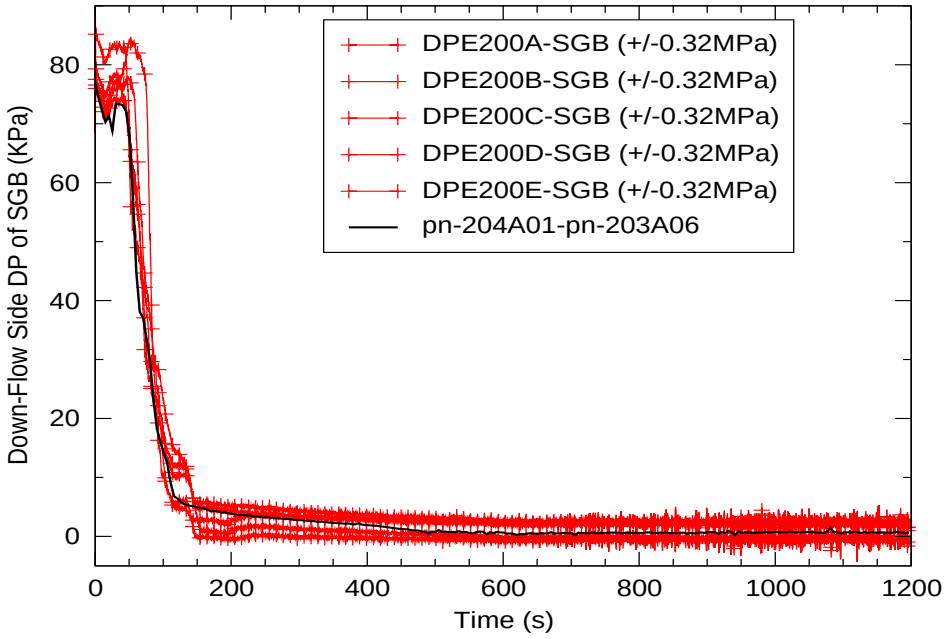

Figure C.5-84. Differential Pressure along downhill side of Steam Generator, Loop-B

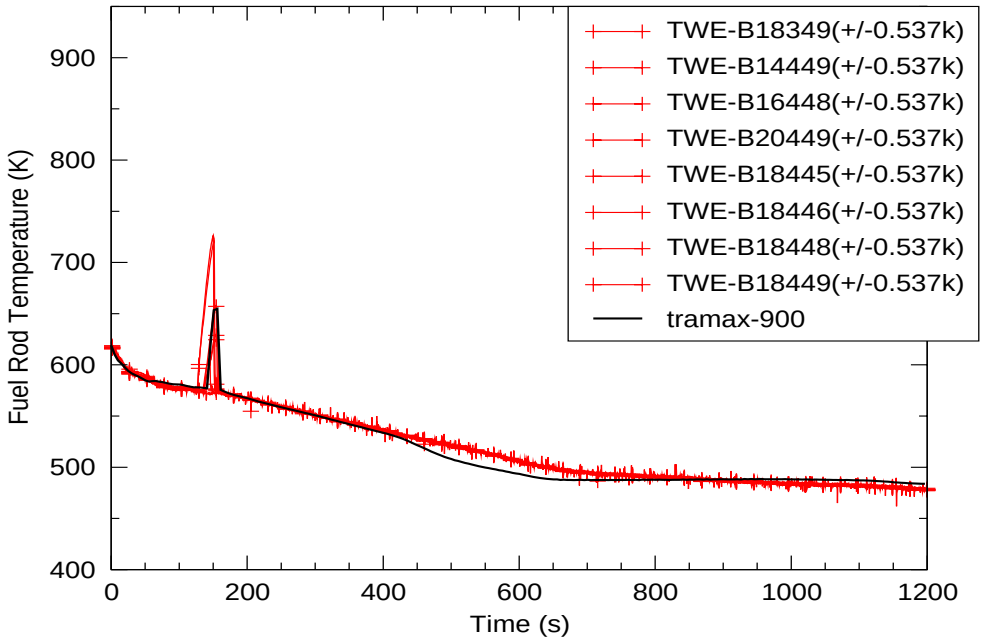

Figure C.5-85. Fuel Rod Temperature

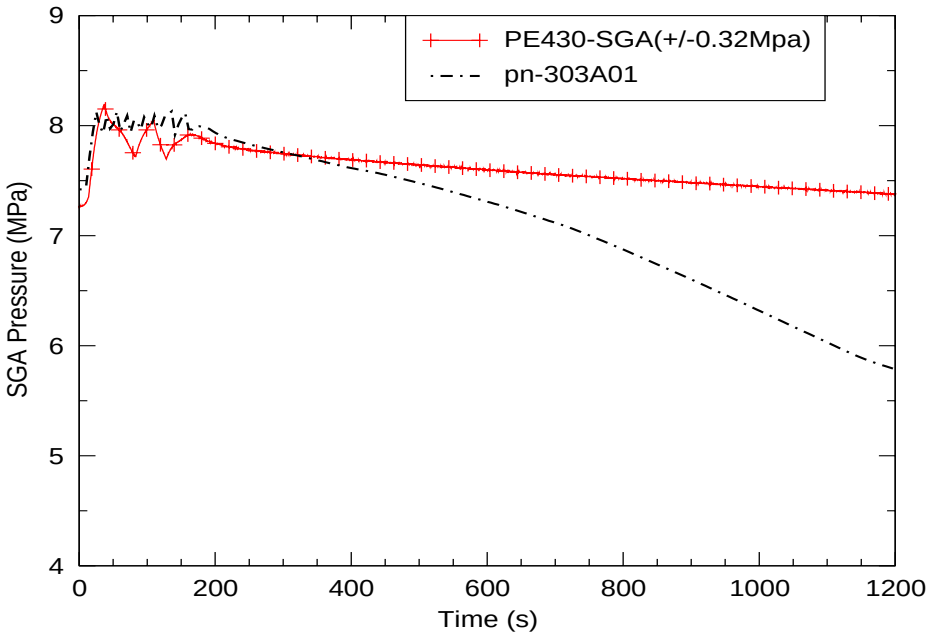

Figure C.5-86. Steam Generator Pressure, Loop-A

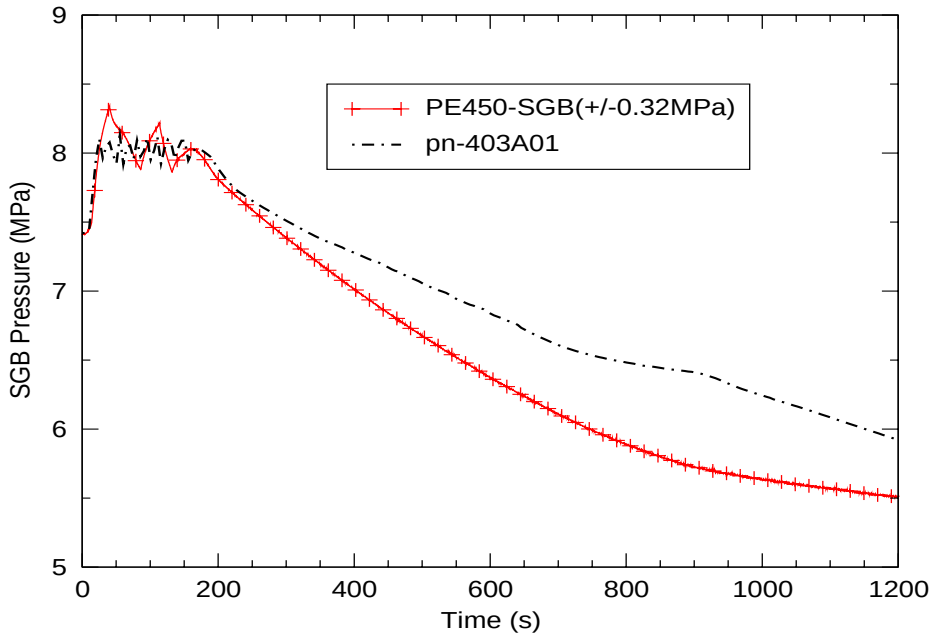

Figure C.5-87. Steam Generator Pressure, Loop-B

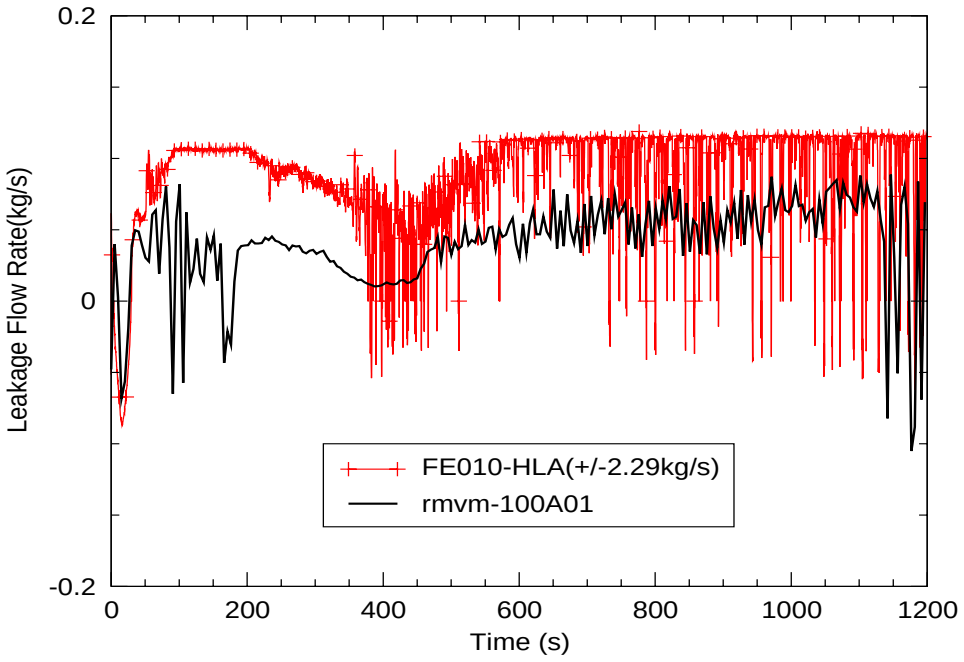

Figure C.5-88. Hot-Leg Bypass Leakage, Loop-A

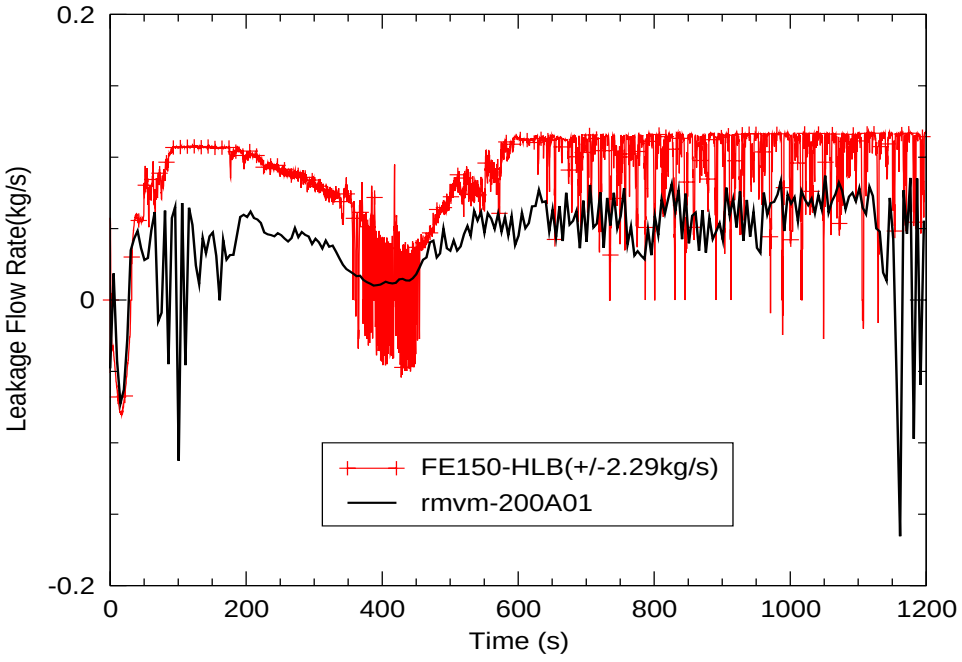

Figure C.5-89. Hot-Leg Bypass Leakage, Loop-B

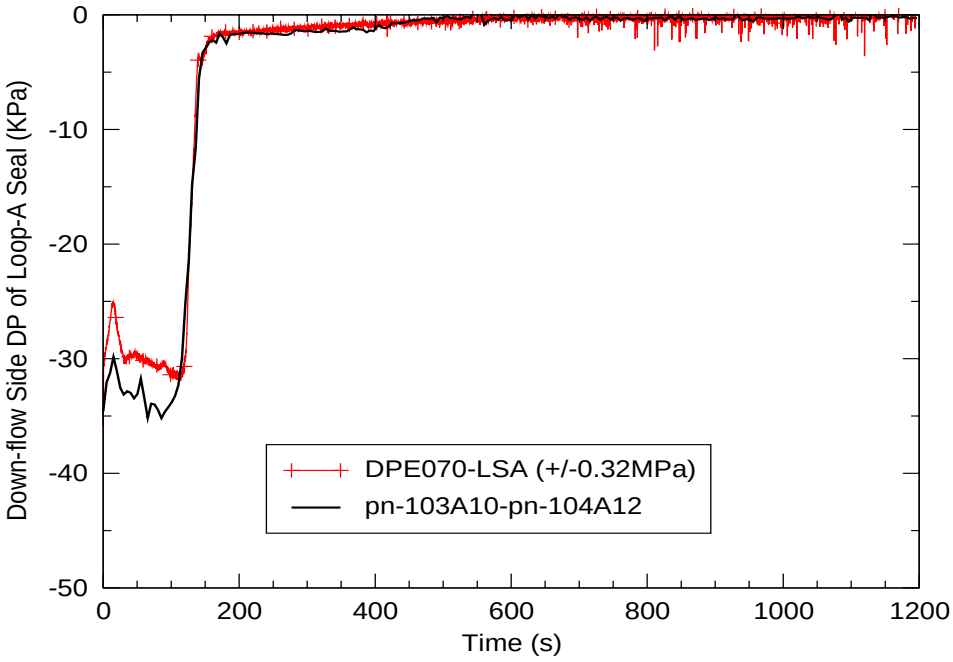

Figure C.5-90. Differential Pressure along downhill Side of Loop-A Seal

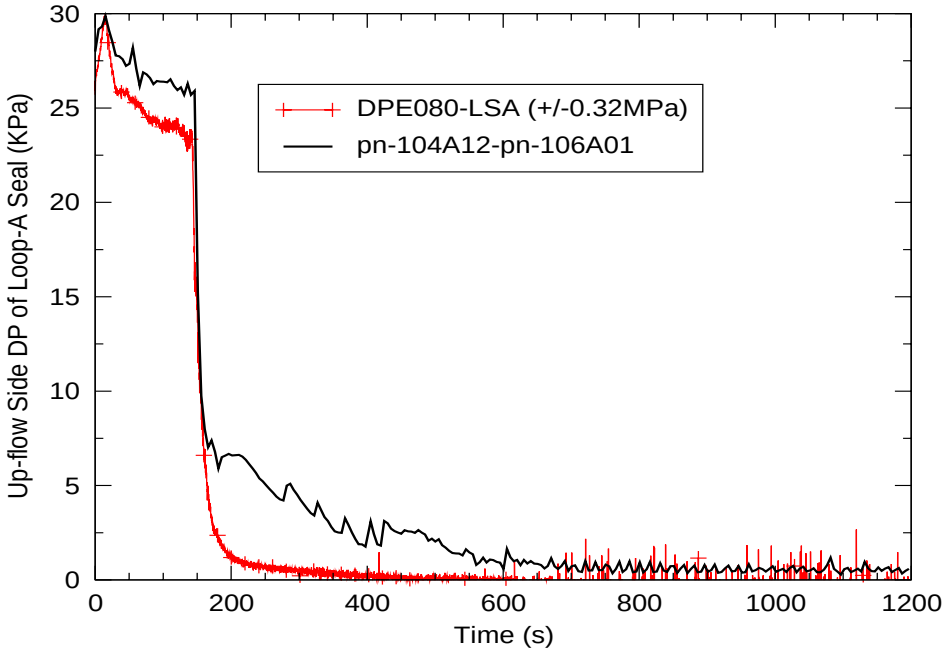

Figure C.5-91. Differential Pressure along uphill Side of Loop-A Seal

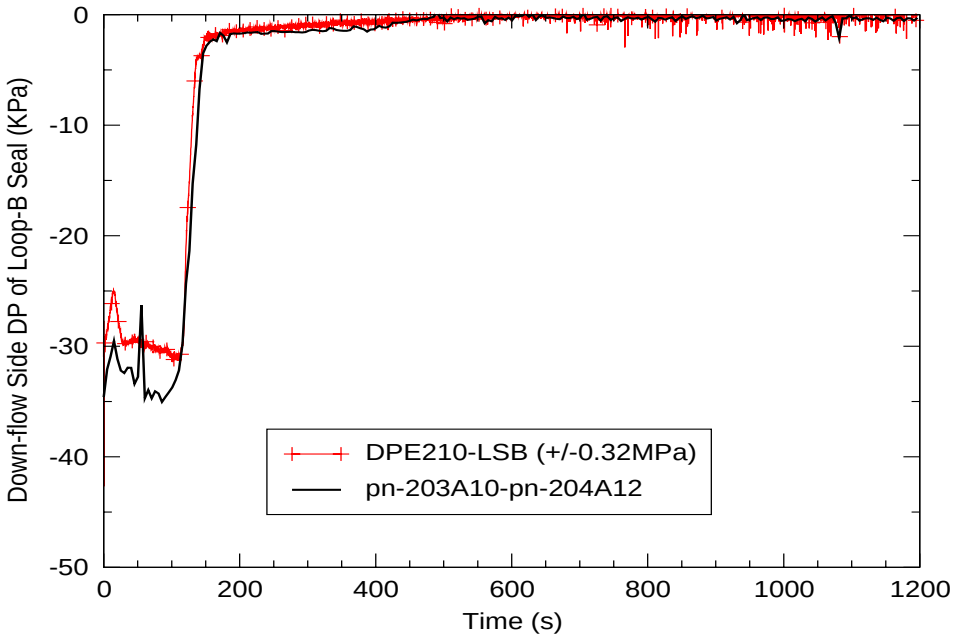

Figure C.5-92. Differential Pressure along downhill Side of Loop-B Seal

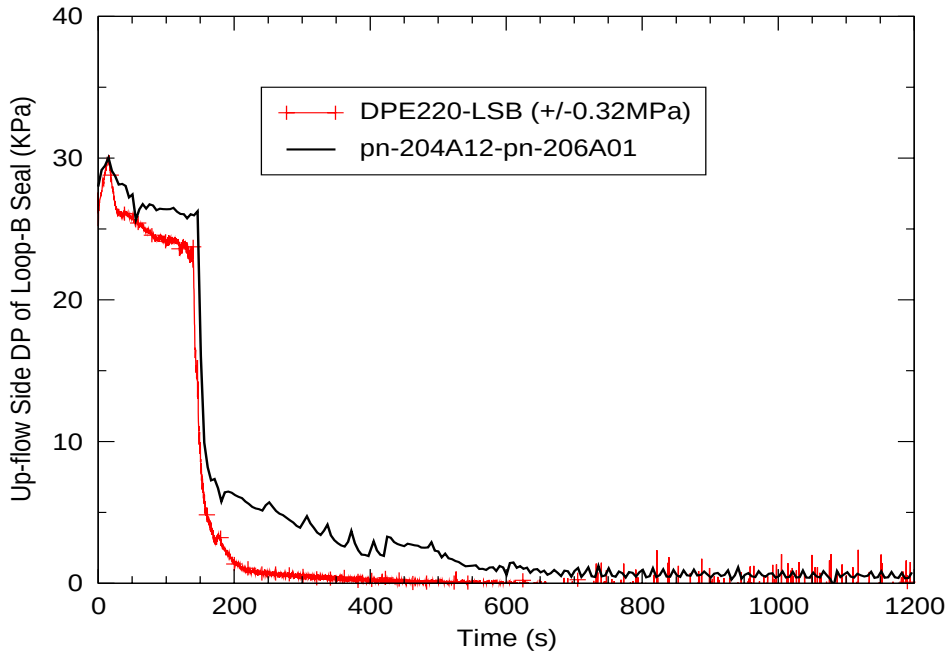

Figure C.5-93. Differential Pressure along uphill Side of Loop-B Seal

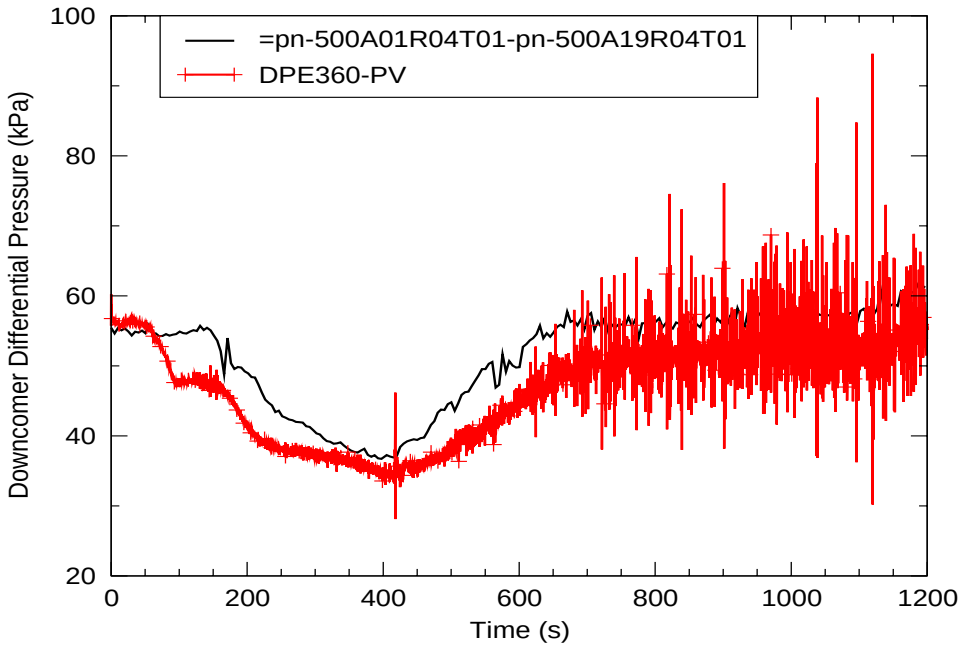

Figure C.5-94. Differential Pressure in Downcomer

C.5.5.2.5. Conclusions

Table 5.3 of this report, as well as Reference 8 lists four criteria used in the code validation: *Excellent Agreement, Reasonable Agreement, Minimal Agreement, Insufficient Agreement*. *Reasonable agreement* is defined as:.

> "*Reasonable Agreement* applies when the code exhibits minor deficiencies. Overall, the code provides an acceptable prediction. All major trends and phenomena are predicted correctly. Differences between calculated values and data are greater than those deemed necessary for excellent agreement. The calculation will frequently lie outside but near the specified or inferred uncertainty bands of the data. However, the correct conclusions about trends and phenomena would be reached if the code were used in similar applications. The code models and/or facility model noding should be reviewed to see if improvements can be made."

Based on the PIRT analysis of each characteristic phase encountered during this test, it is evident that the TRACE simulation results presented for SB-CL-05 meet the definition of *Reasonable*

Agreement throughout all phases of the transient event for all phenomena ranked high in the applied SBLOCA PIRT.

The most notable discrepancies are as follows:

1 Unlike the test, the core began to uncover just before accumulator injection. No signs of such an uncovery is apparent in the data.

2 Predicted cold-leg mixture temperatures are significantly under-predicted after loop-seals clear and after accumulator injection.

3 Hot leg-to-downcomer bypass flow is approximately 0.05 kg/s lower than the data.

4 A small amount of liquid is predicted to remain in the uphill portion of the loop seals after the initial flush of fluid.

5 Accumulators inject approximately 30 seconds early.

6 Flow regime upstream of the break was inaccurately predicted, resulting in the under-prediction of the total amount of mass leaving the break by approximately 500kg.

7 Throughout most of the transient, the liquid level in the vessel-head was over-predicted.

8 Unlike the test, no decrease in downcomer level is predicted to occur during the blowdown phase.

The majority of these items do not appear to be related to a code deficiency, but rather to inaccuracies or over-simplification in the input model. The one potential code problem appears to be in determining the temperature distribution that results from the mixing of the accumulator-injection and cold-leg fluids following accumulator injection. Based on the corresponding void fractions and the mixture density, the mixture temperatures in the cold legs should be higher, closer to the vapor or steam-saturation temperatures. The reduced temperature appears to propagate to the downcomer and the vessel, where it manifests as increased fluid density and level.

C.5.5.3. Simulation of SB-CL-14

Test SB-CL-14 followed the scenario for a 10% break in the side of the Loop-B cold leg, with available low-pressure ECCS injection, unavailable high-pressure ECCS injection, and available auxiliary feedwater. Two input decks were developed for the transient analysis: one constrained steady-state (CSS) input deck and one transient input deck. The CSS deck contains most of the model information and plant control procedures. The CSS input deck is used to obtain initial plant conditions for transient calculations.

The control system and control procedures of the ROSA-IV facility were designed to accommodate a wide range of plant operational transients and accident scenarios. The TRACE control procedure was derived from a series of SBLOCA tests.

SB-CL-14 test conditions and control actions implemented in the TRACE transient analysis are listed here.

C.5.5.3.1. SB-CL-14 Test Conditions

Some of the test conditions or control procedures were different from those in the reference PWR reactor. Special control procedures or test conditions were designed to account for some scaling issues in the design of the test facility (Refs.1, 7).

The plant initial conditions are summarized in Table C.5.3. In the test, it was assumed that a loss-of-offsite power occurred coincident with reactor scram. Also, failure of one of the two diesel-generators for the emergency coolant and auxiliary feedwater pumps was assumed. Table C.5.12 summarizes the operational setpoints for Run SB-CL-14. Table C.5.13 gives the event sequence recorded by the facility instrumentation system. Some specific information is given below for individual items.

- Coolant pumps

Upon the initiation of the break, the pump speed was increased before the pump started to coast down following the reactor scram signal (Ref. 7). The pump impeller rotation speed after the initiation of break is shown in Figure C.5-95 and Figure C.5-96. The dashed line is the pump curve obtained in the TRACE simulation of SB-CL-14. The solid line is the measured pump curve in the SB-CL-14 test.

- Reactor trip and core power after break

As indicated in Table C.5.13, the reactor was tripped 7 seconds after the break was initiated. Two power curves are shown in Figure C.5-97. The solid line is the measured power curve in the SB-CL-14 test. The dashed line is the power curve obtained in the transient simulation.

- Emergency Core Cooling System (ECCS)

During the SB-CL-14 transient, the subsystems of the ECCS system were actuated in the manner given in Table C.5.12 and Table C.5.13. For each loop, the ECCS subsystems injected water into the loop through the same nozzle (Figure C.5-3). In the test, the desired ratio of the ACC injection flow into the loop A cold leg to the ACC injection flow into the loop B cold leg was 3:1. Assuming the ratio was maintained, the ACC injection flow rate into each loop can be calculated based on the discharging flow rate of the ACC tank, which is derived from the ACC tank level measurement (LE14). Figure C.5-98 show the calculated ECCS injection flow rate into each loop, which is the sum of the injection flow of the ECCS subsystems (high pressure charging and high pressure injection).

- Auxiliary Feedwater System

In SB-CL-14, the auxiliary feedwater was not actuated.

- Pressurizer heaters

Based on the test data, power supply to the pressurizer heaters was cut off with the initiation of break.

C.5.5.3.2. TRACE Control Procedure

Using the strategy outlined at the beginning of this chapter, the control procedure for the TRACE model is simplified. As a result, the TRACE control procedure mainly consists of a number of trips**.** In general, a trip is either initiated by time or by the system pressure. Specifically:

1. At time 0, the break is initiated and the pressurizer heater power is cut off.
2. The pump speed is increased after the break and coasts down with the reactor trip as shown in Figure C.5-95 and Figure C.5-96.
3. The reactor is tripped when the system pressure reaches 12.97 MPa. Figure C.5-97 shows the measured power curve after the break and the power curve obtained from the transient calculation.
4. The Safety Injection (SI) signal is generated when the system pressure reaches 12.27 MPa. However, the high pressure portion of the Emergency Core Cooling System (ECCS) was not actuated (assumed failed). The LPIS system were modeled as a boundary condition actuated by the appropriate setpoint (system pressure). The accumulators were modeled as the two pressurized water tanks connected to each cold leg, where flow injection through the check valve is activated when the system pressure is below 4.51 MPa.
5. Main steam valve closure and main feedwater cutoff are initiated by reactor trip. Auxiliary feedwater was assumed failed.

Table C.5.12. Operational Setpoints for Run SB-CL-14

Event	Setpoint
Reactor scram signal	12.97 MPa (System pressure)
Pump coast down	Upon reactor scram
Safety Injection (SI) signal	12.27 MPa (system pressure)
High Pressure charging	Not actuated
High Pressure Injection	Not actuated

Table C.5.12. Operational Setpoints for Run SB-CL-14

Accumulator injection	4.51 MPa
Low Pressure Injection	1.29 MPa
Main feedwater cutoff	With reactor scram
Turbine throttle valve closure	With reactor scram
Auxiliary feedwater initiation	Not actuated

Table C.5.13. Chronology of Events for Run SB-CL-14

Events	Time (s)
Break	0
Reactor trip	7
Main Steam Line Valve Closure	10
Safety Injection Signal	11
SG Feedwater stop	11
Loop Seal clearing	78-120
Primary/Secondary Pressure Reversal	~87
Accumulator Injection ON to Loop B	199
Accumulator Injection ON to Loop A	200
Reactor coolant pumps stop	263
Accumulator Injection OFF to Loop B	443
Accumulator Injection OFF to Loop A	446
Low Pressure Injection System ON	862
End	1289

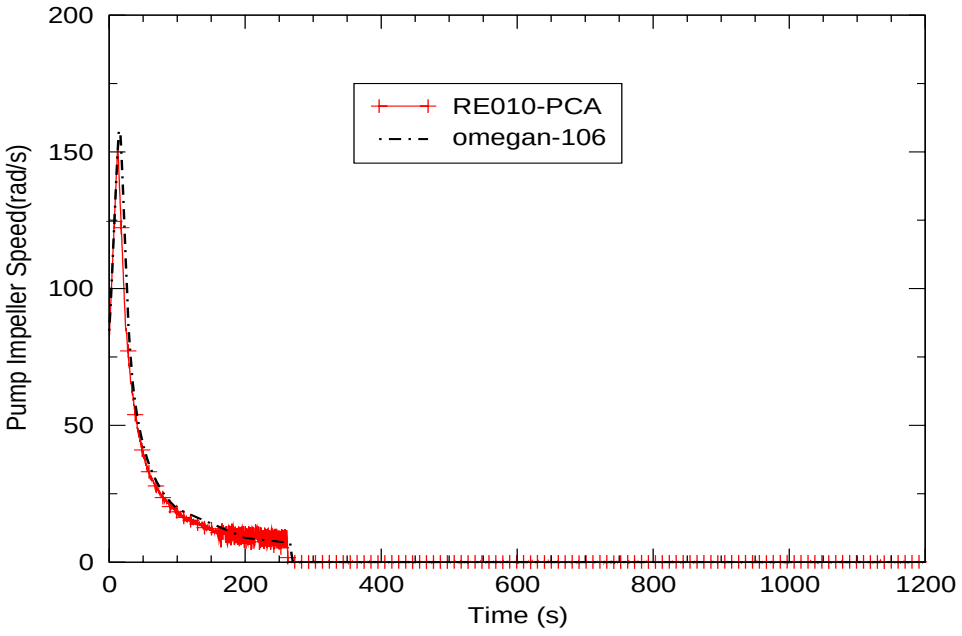

Figure C.5-95. Pump A Impeller Speed After Break

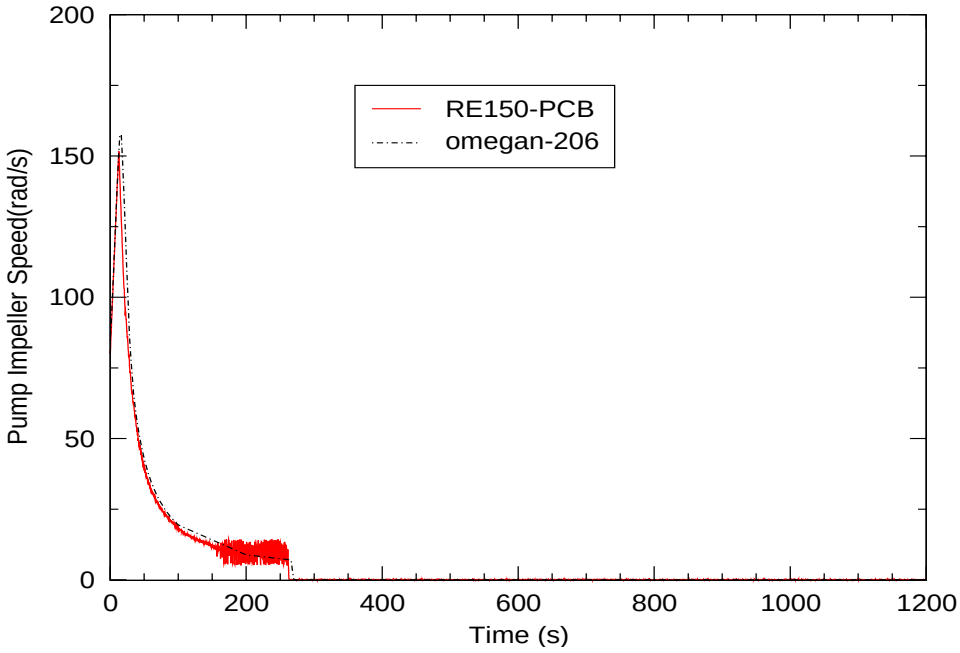

Figure C.5-96. Pump B Impeller Speed After Break

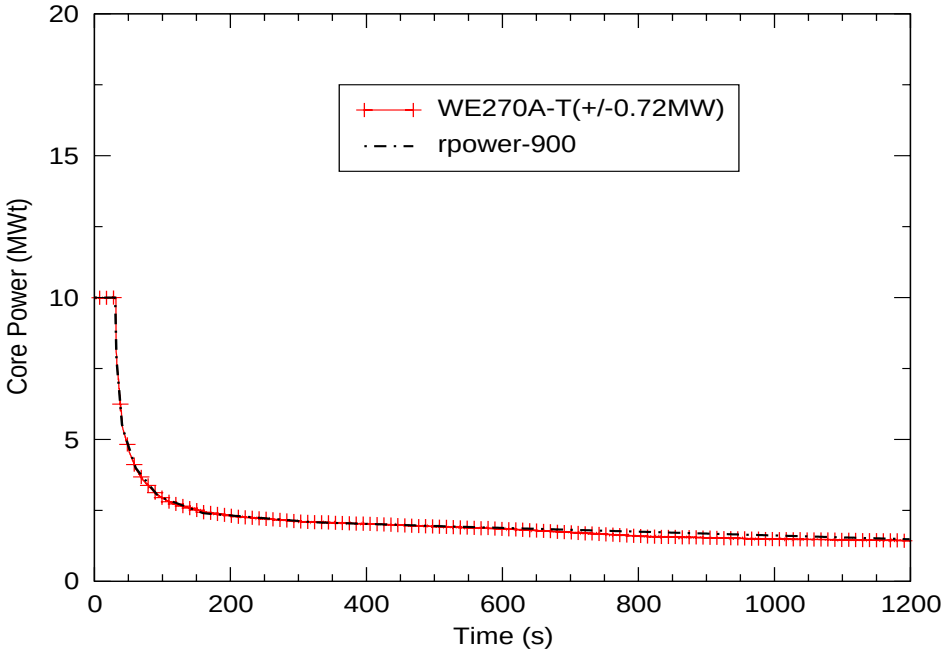

Figure C.5-97. Core Power after Break

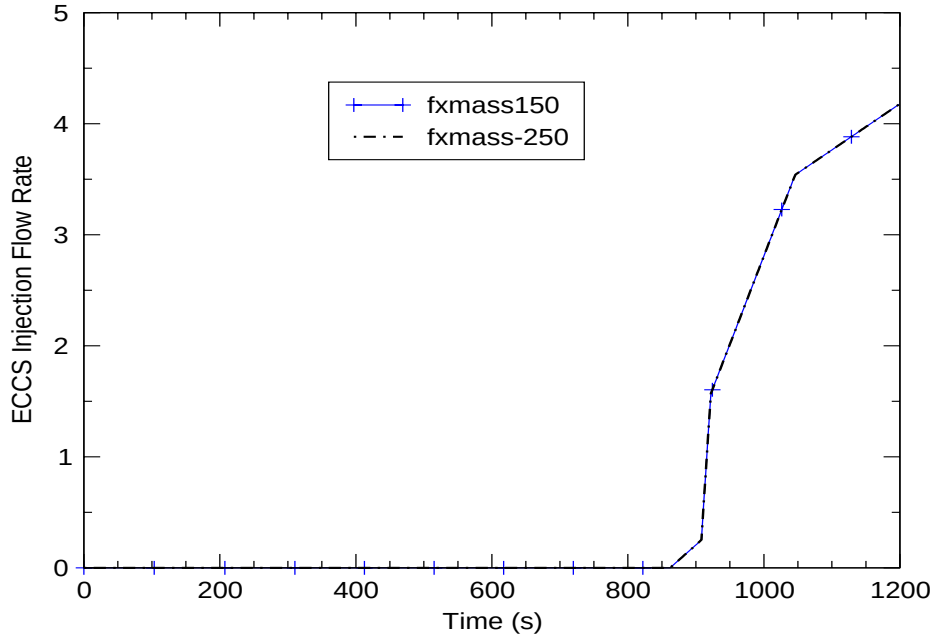

Figure C.5-98. ECCS Injection Flowrates for Loop A and Loop B

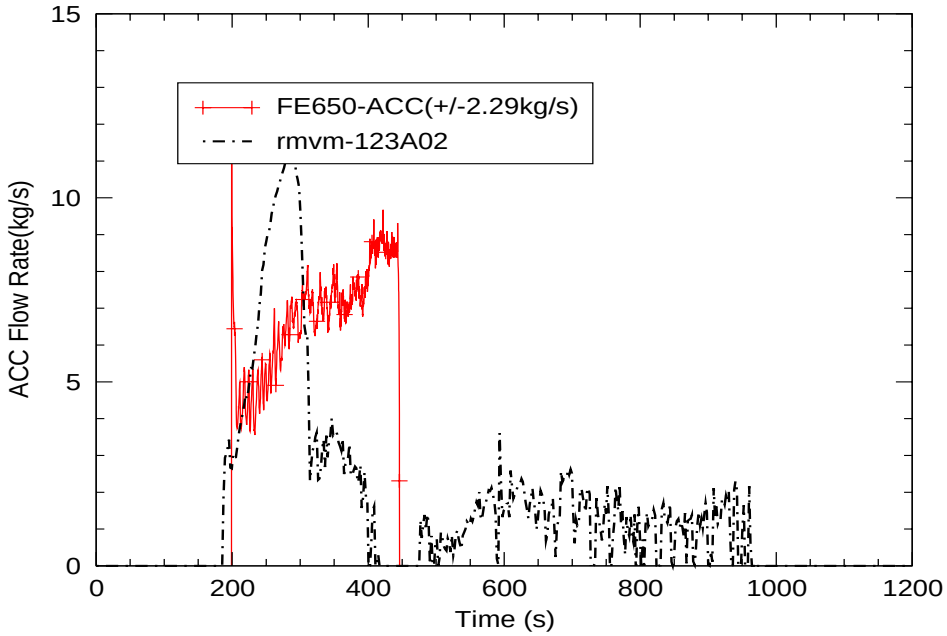

Figure C.5-99. Accumulator Injection Flow to Cold Leg A

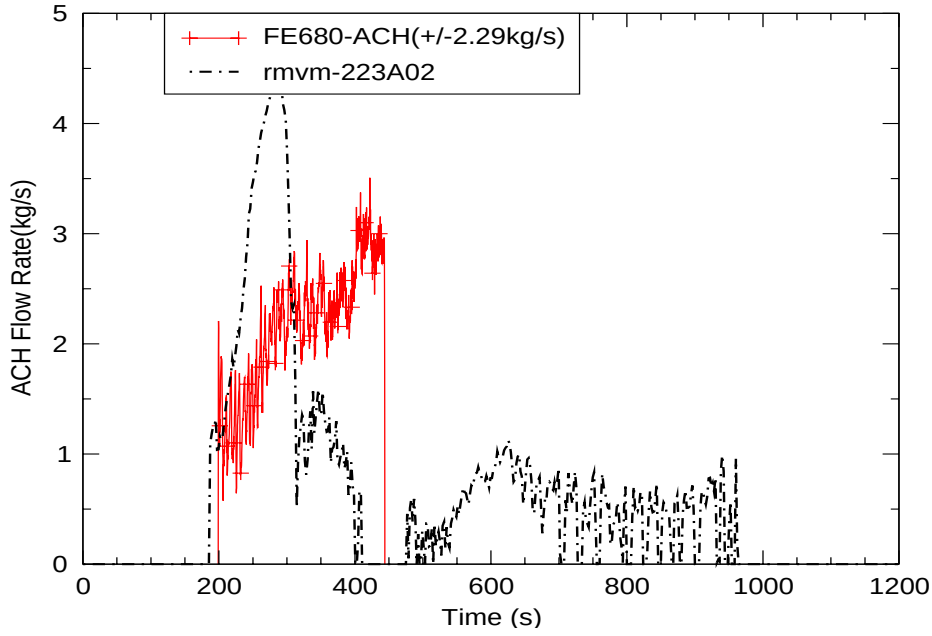

Figure C.5-100. Accumulator Injection Flow to Cold Leg B

C.5.5.3.3. Experimental Observations

The main objective of test SB-CL-14 was to investigate the thermal-hydraulic mechanisms of early core uncovery and heatup. Early core uncovery may be caused by a manometric effect resulting from an imbalance between the water hold up in the upflow and downflow sections of the steam generator U-tubes (Ref. 7). Table C.5.14 lists the event sequence recorded by the facility's instrumentation system during the test.

After the start of the transient, the pressure started to drop rapidly and the core power decay curve was initiated at a pressurizer pressure of 12.97 MPa together with the closing of the MSIV, starting of the programmed pump speed curve, and termination of the main feedwater to the steam generators.

The safety injection signal occurred at 11 seconds at a pressurizer pressure of 12.27 MPa. However, the charging pump and the high-pressure injection pump were assumed failed, respectively. The secondary pressure increased to and remained at approximately 8 MPa due to the SG relief valve operation.

At about 80 s after the break, the primary loop pressure decreased below the steam generator secondary side pressure. Thereafter, the steam generator no longer served as heat sinks and the energy removal from the primary system was through the discharge of the coolant from the break.

With no HPSI actuation, the core became temporarily uncovered in the time interval from 60 to 80 s after the break. The maximum heater rod temperature reached was about 40 K higher than at steady state. The core uncovery occurred just before loop seal clearing.

Both loops experienced loop seal clearing at about 120 s, which led to a recovery of core liquid level. Loop seal clearing allowed mixture of steam and water to escape from the break, which in turn reduced the mass flow rate and accelerated the depressurization of the primary loop.

C.5.5.3.4. Transient Analysis

The SB-CL-14 transient calculation is performed for 1200 seconds. The simulation results and the comparison to the test data are presented in Figure C.5-95 to Figure C.5-129. In these figures, the test data is plotted in solid, colored lines with symbols, and the calculation results are plotted with solid black or blue lines without symbols.

C.5.5.3.4.1. System Behavior

The overall primary system behavior determines the boundary conditions of the transient event since most of the control signals are based on the system pressure setpoints. The predicted system pressure is in good agreement (in accordance with the acceptance criteria (Ref.8)) with the data as shown in Figure C.5-103. Therefore, the sequence of events based on the system pressure setpoints are also in good agreement with the test data.

Table C.5.14 shows the comparison of the sequence of events for SB-CL-14 simulation results and the test data.

Table C.5.14. Sequence of the Event Comparison for SB-CL-14 Test

Event	Test Data	TRACE Model
Break	0 sec[a]	0 sec
Reactor Trip	7 sec	7 sec
Main Steam Line Valve Close	10 sec	10 sec
Safety Injection Signal	11 sec	11 sec
SG Feedwater Stop	11 sec	11 sec
Loop-A Seal Begins Clearing[b]	92 secs	89 secs
Loop-B Seal Begins Clearing[b]	90	85 secs
Core Uncovery	45 - 450 secs	45 - 300 secs
Primary/Secondary Pressure Reversal	87 sec	90 sec
Accumulator Injection B(A) ON	199 (200) sec	190 sec
Reactor Coolant Pumps Stop	263 sec	263 sec
Low Pressure Injection ON	862 sec	862 sec
End Time	1200 sec	1200 sec

a. The break starts at time 0

b. The beginning of loop-seal clearance is the time at which the differential pressure across the uphill portion of the loop seal begins to rapidly descend toward zero.

C.5.5.3.4.2. Analysis Results

As discussed in **Section C.5.5.**, the PIRT (Ref. 6) identifies the high-ranked phenomena for each phase of the transient. To evaluate the performance of TRACE, each phase will be discussed separately, and the TRACE-simulation results for the highly-ranked phenomena will be compared to the data. The principal Figure of Merit (FOM) of the transient event is the core collapsed liquid level (CCL). The core collapsed level is measured as the core differential pressure as demonstrated in Figure C.5-102.

Certain input parameters, such as decay heat, core power, and feedwater temperature, are taken directly from the test data as boundary conditions. Therefore, although they are identified as important in some of the phases, they will not be discussed in terms of code performance.

Blowdown phase

The blowdown phase is marked by a rapid depressurization of the primary coolant system until the hot coolant begins to flash into steam. The rate of depressurization is strongly influenced by the rate and enthalpy of the break flow, and it changes when flashing and boiling start in the core. In this phase, the most important parameters defining the evolution of the transient are decay heat, primary side heat transfer, critical break flow, and the flow regime upsteam of the break flow.

In the test, the blowdown phase lasted from 0 to 75 seconds. Throughout this time, good agreement is observed between the simulation results for each of the highly-ranked parameters and the test data. The calculated pressurizer pressure in Figure C.5-101 and the calculated core differential pressure (DP) in Figure C.5-102 are in good agreement with the data. Good agreement is also shown in terms of primary-side heat transfer, which can be seen in Figure C.5-103 through Figure C.5-106. These figures show comparisons of the fluid temperatures in the SG tubes and the cold legs, respectively. During the first 50s, the predicted SG-tube temperatures progress to higher values than the data, but they settle down into agreement as the phase progresses. As for critical break flow and the flow regime upstream of the break, Figure C.5-107 shows excellent agreement between the predicted integrated break flow and the data. The density of the fluid in the cold legs is evaluated to determine the flow regime upstream of the break. Excellent agreement can be seen in Figure C.5-108 and Figure C.5-109, which shows densitometer readings taken at three locations over the cross-sections of the cold legs.

Other key results in this phase are the DPs in the vessel head and upper plenum, the pressurizer level, and the flow regime in the hot legs. Figure C.5-110 shows the vessel-head DP. Here, the depressurization can be observed, but unlike the data, the code predicts a more severe negative DP at the start of the transient. The predicted DP rebounds and stabilizes, somewhat, but it remains negative. This discrepancy, primarily, appears to be the result of rapidly changing mass flows in the upper head, which causes significant oscillations in the void fraction. In Figure C.5-111, the void fraction in level 21 of the upper head oscillates considerably as it moves toward single phase vapor.

Other pressure indicators do not appear to have been affected in the same manner as the upper head. The calculated upper plenum DP, shown in Figure C.5-112, is in good agreement with the data. There is also good agreement between the calculated and measured pressurizer level. In Figure C.5-113, both code and data show the pressurizer emptying within the first 50 seconds.

The flow regimes in the hot legs are evaluated in terms of hot-leg fluid density. Figure C.5-114 and Figure C.5-115 both show that the code is predicting the correct fluid densities. Because of the size of the break, the fluid in the hot legs immediately changes from single-phase liquid to a two-phase mixture.

Loop Seal Clearing phase

The loop seal clearing phase begins when the trapped primary-side steam volume reaches the top of the loop seal piping. From this point, the steam volume depresses the liquid in the downhill side of the loop seal and in the core until a minimum core level is reached. As steam moves through the seal to the break plane, the liquid it displaces is forced into the core, quenching the heatup caused by the drop in core level. In the test, this sequence of events occurred between 76 and 100s.

The highly ranked processes in this phase are listed as follows:

1. Decay heat
2. Mixture level in the core region
3. Hot-leg downcomer gap flow
4. SG primary-side heat transfer in the U-tubes
5. SG primary-side flow resistance
6. SG primary-side tube voiding
7. Flow regime/entrainment in the pump suction / loop seal
8. Horizontal stratification in the cold leg
9. Critical break flow

The mixture level in the core is related to the core DP shown in Figure C.5-102**.** At approximately 76s, there is a sharp increase in DP that indicates the clearance of the loop seals. In the figure, the predicted maximum core-level depression is about 2 kPa lower than the measurement and the level after the loops clear is about 2 kPa lower. This agreement, however, is adequate and also results in the timely prediction of the brief fuel heatup shown in Figure C.5-127.

Figure C.5-116 and Figure C.5-117 show the calculated leakage flows from Hot leg A and Hot leg B to be lower than the measured amount. During this phase, there appears to be considerable fluctuation in the leakage flow, with the flow reversing at several instances.

Heat transfer, voiding, and flow resistance in the SG tubes is evaluated using the DP predictions shown in Figure C.5-118 through Figure C.5-121. The results on both the uphill and downhill portions of the SG tubes are in excellent agreement with the data.

Figure C.5-122 through Figure C.5-125 show the DP comparisons along the uphill and downhill sides of the loop seals. The uphill portion of the loop seals includes the pump suction piping. These figures show the simulated loop seals clearing just a few seconds early. Also, Figure C.5-123 and Figure C.5-125 show the presence of a small amount of liquid in the loop seals after the initial flushing. This liquid gradually moves out of the seals after about 200 seconds.

The degree of horizontal stratification in the cold-legs is of interests because of its baring on the flow regime upstream of the break. Without an explicit means of displaying horizontal stratification, an analysis of the fluid density upsteam of the break gives a rough indication of the flow regime. It is apparent from the cold-leg-density results in Figure C.5-108 and Figure C.5-109 that the code is predicting the correct flow regime at the pump suction and upstream of the break.

As the loop seals clear, the break flow transitions from single-phase liquid to a two-phase mixture. Figure C.5-107 shows the predicted time of this transition to be the same as the test measurement.

Boil Off phase

As the transient proceeds, the primary system continues to loose inventory and the core inventory continues to boil. During the test, this boil-off phase lasted from 101 to 200s. The highly-ranked processes in this phase are listed below:

1. Fuel Decay heat and local power
2. Mixture level in the core
3. Horizontal stratification and condensation in the cold leg
4. Downcomer mixture level
5. Critical break flow

During the second half of this phase, Figure C.5-102 shows that unlike the data, the simulated core DP decreases by about 3 kPa, indicating a drop in CLL that reaches well into the core. This unexpected decrease appears to be due to a small heatup that causes steam in the upper plenum to flash. This can be seen in Figure C.5-111 as the spike in the upper plenum void fraction at around 200s. The CLL decrease is abated by the accumulator injection at 200 seconds, and the CLL recovers.

As for horizontal stratification and condensation in the cold legs, based on the cold-leg density results shown in Figure C.5-108 and Figure C.5-109, the code is predicting the correct flow regimes. Also, the cold-leg temperatures shown in Figure C.5-105 and Figure C.5-106 continue to be in excellent agreement with the data.

Like the core level, the level in the downcomer is represented by DP measurements. As seen in Figure C.5-126, the predicted level in the downcomer remains almost constant throughout the blowdown phase, unlike the data. However, the code does reasonably well in predicting the pressure drop associated with the clearance of the loop seals and the boil-off period.

The simulated break flow shown in Figure C.5-107 appears to begin trending consistently lower than the data.

Also of note during this phase are the SG pressures. In both Figure C.5-128 and Figure C.5-129, the calculated pressure becomes approximately 0.2 MPa greater than the data during the loop-seal-clearing phase and remains so throughout the remainder of the transient.

Core Recovery phase

The final stage of this transient is the core-recovery phase. During this phase, safety systems inject liquid into the core to establish and maintain core cooling. For this particular test, HPIS is not available, but LPIS injects when system pressure drops to 1.29 MPa.

The highly ranked processes in the recovery-phase (201 s – 1200 s) are listed below:

1. Fuel Decay heat and local power
2. Mixture level in the core
3. Downcomer mixture level
4. Critical break flow

Following the injection of the accumulators at around 200s, the level in the core, shown in Figure C.5-102, rebounds too aggressively and settles at a level that is significantly higher than the data. One possible reason for this is the overly aggressive accumulator injection flow shown in Figure C.5-101 and Figure C.5.102. Another reason is the over-predicted density of the fluid leaving the cold leg and entering the vessel. Apparently, the temperature distribution resulting from the mixing of the accumulator-injection and cold-leg fluid is not being accurately captured. Figure C.5-107 and Figure C.5-108 both show the under-predicted cold-leg temperatures after the accumulators inject. Based on the density of the fluid in the cold legs, the mixture temperatures should be closer to the steam saturation or vapor temperatures. However, the low temperatures are propagating into the downcomer and vessel, where they manifest as increased fluid density and level.

According to Figure C.5-107, the predicted break flow is consistently lower and doesn't change phase at the same times as the data. However, by the end of the transient, the same amount of mass is predicted to have left the break as measured in the test.

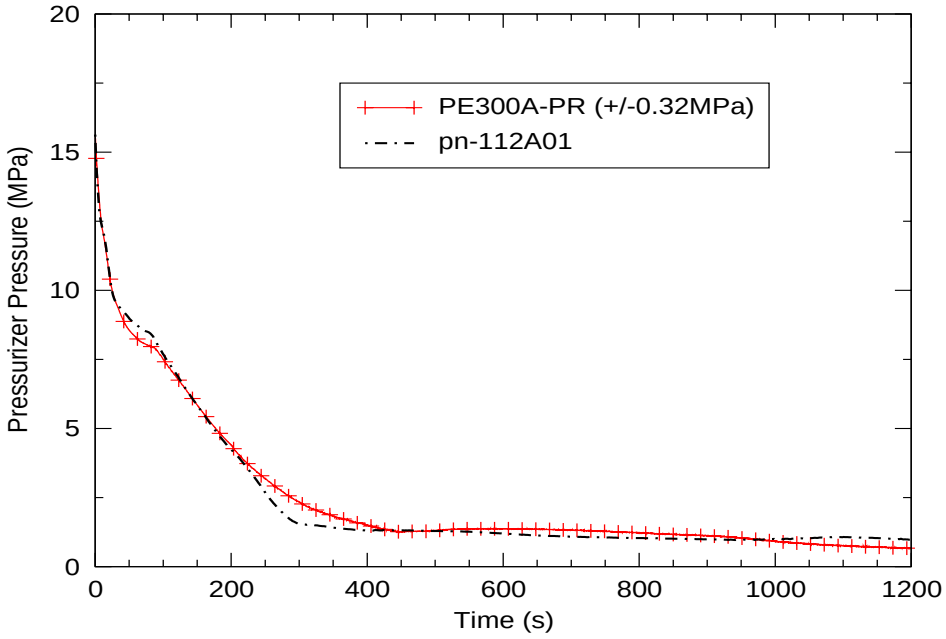

Figure C.5-101. Pressurizer Pressure

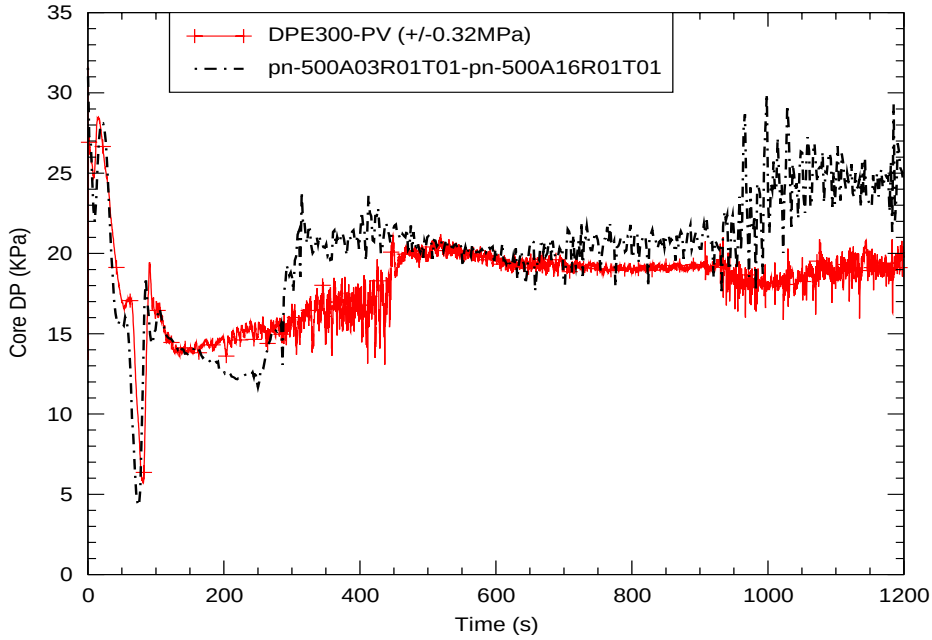

Figure C.5-102. Reactor Core Differential Pressure

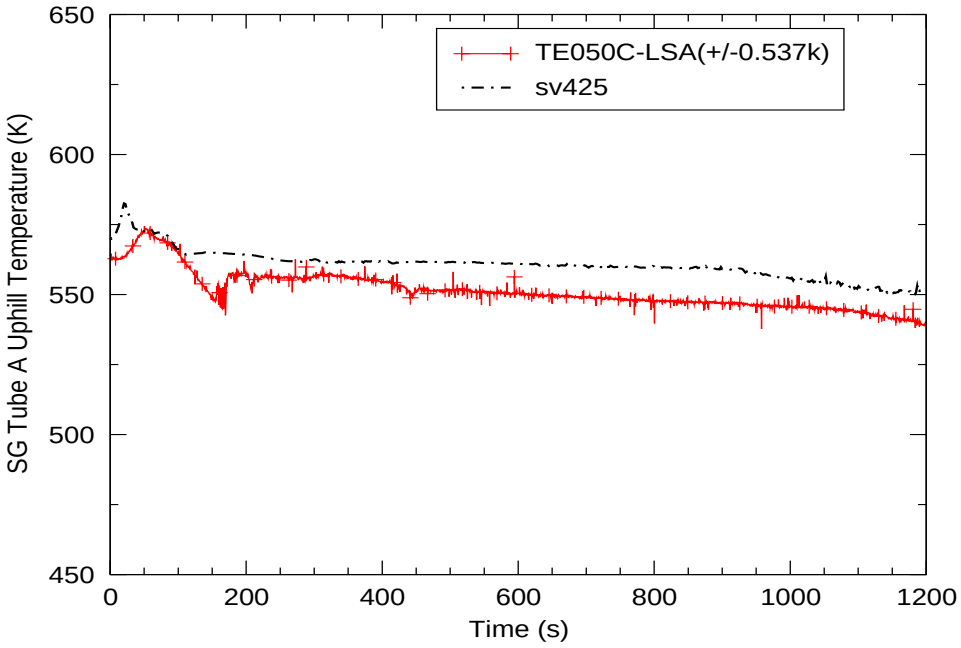

Figure C.5-103. Fluid Temperature on uphill Side of Loop-A Steam Generator

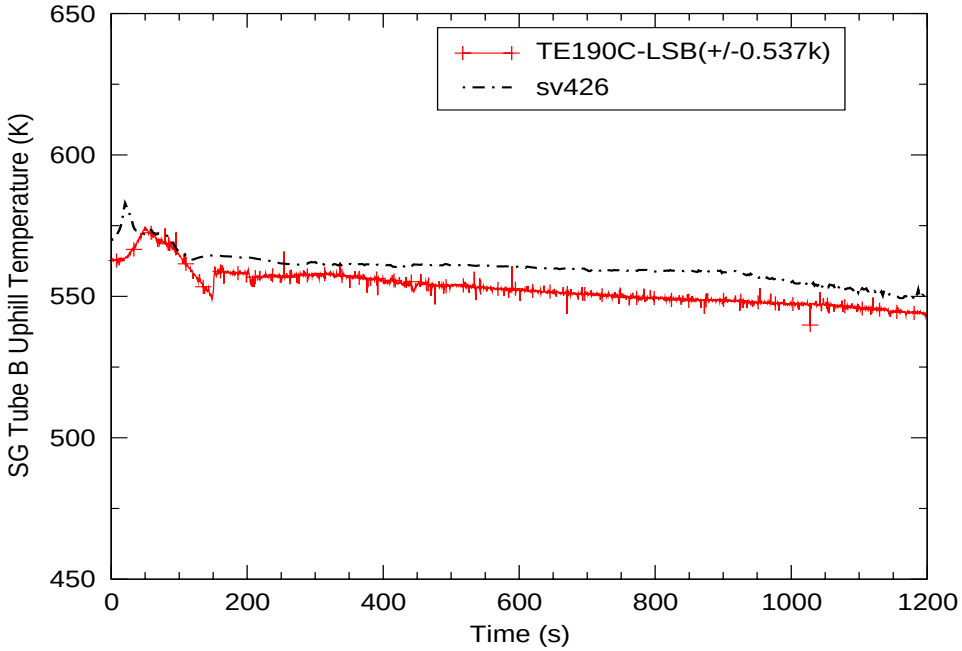

Figure C.5-104. Fluid Temperature on uphill Side of Loop-B Steam Generator

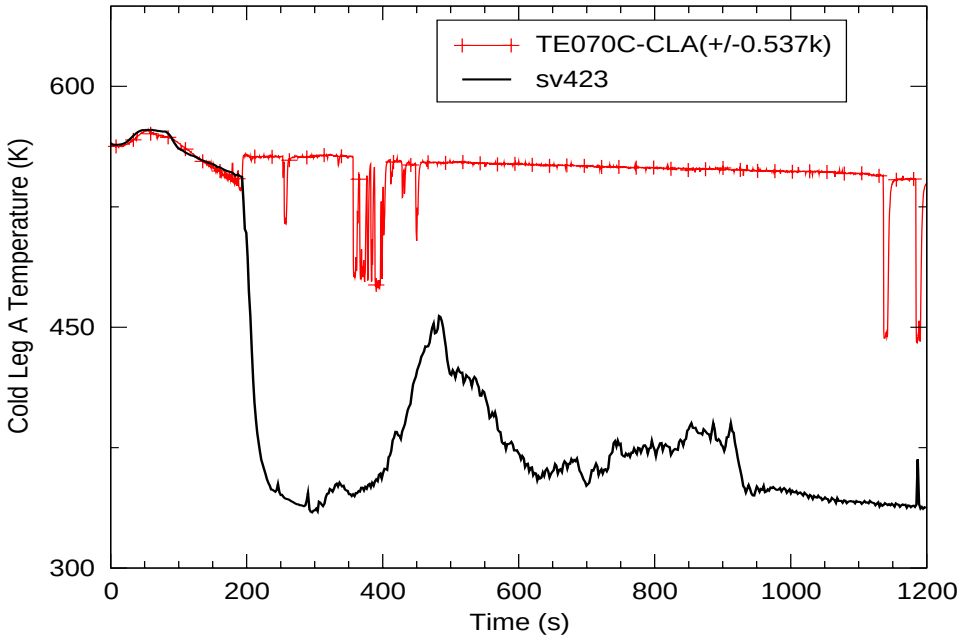

Figure C.5-105. Fluid Temperature in Loop-A Cold Leg

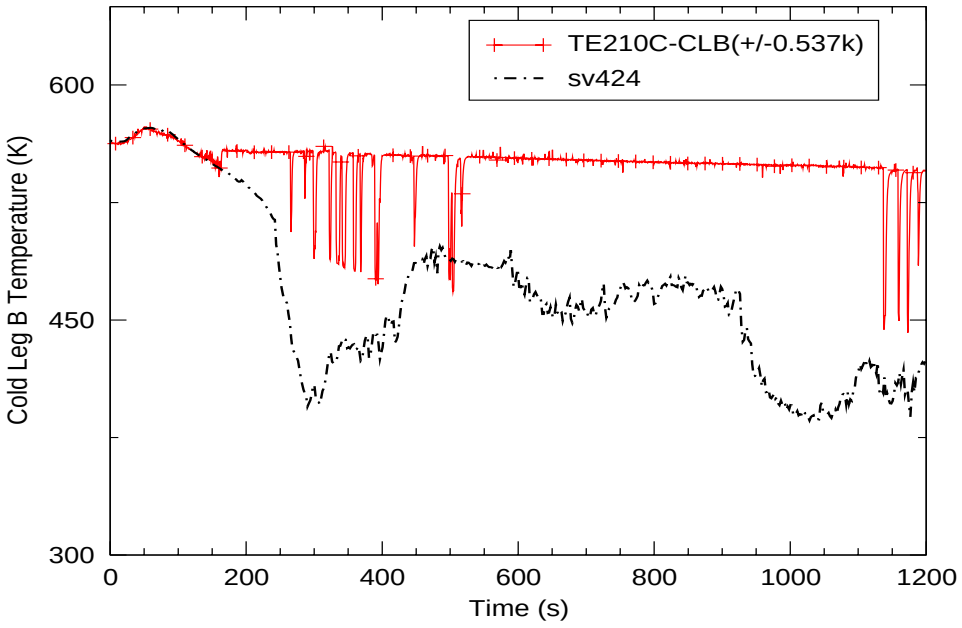

Figure C.5-106. Fluid Temperature in Loop-B Cold Leg

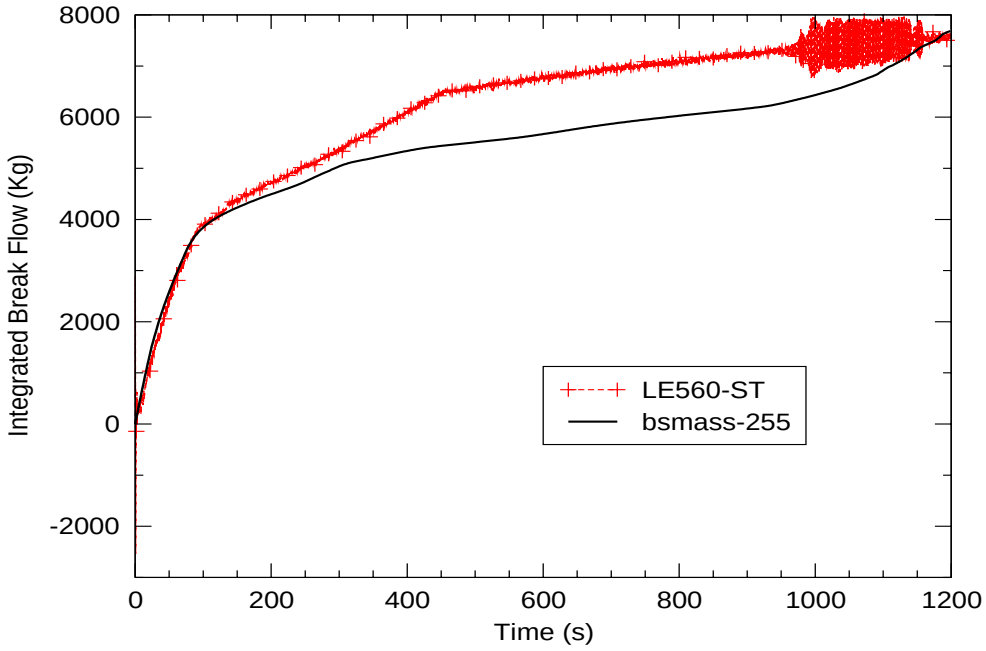

Figure C.5-107. Integrated Break Flow

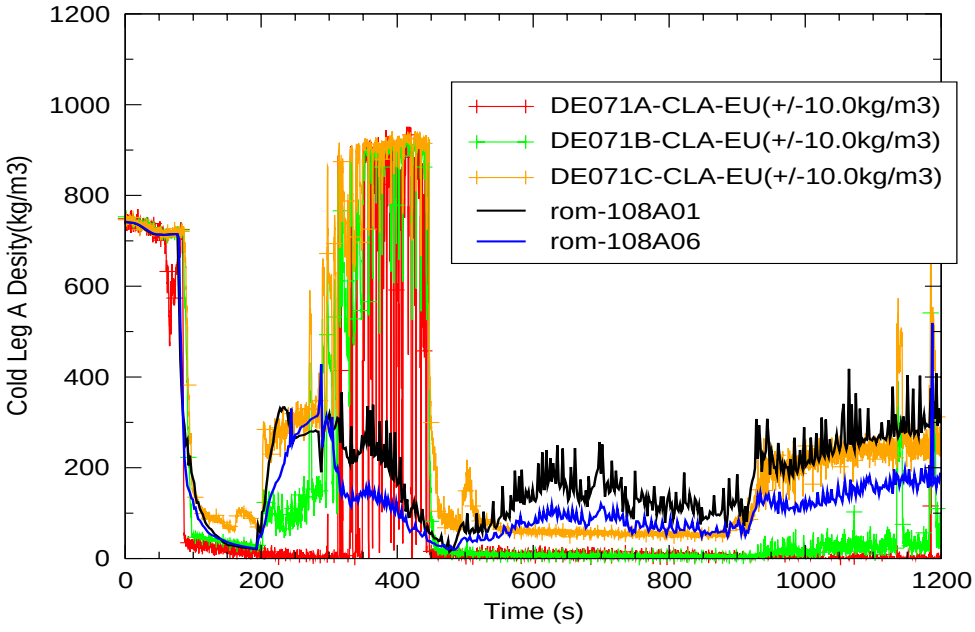

Figure C.5-108. Fluid Density in Loop-A Cold Leg

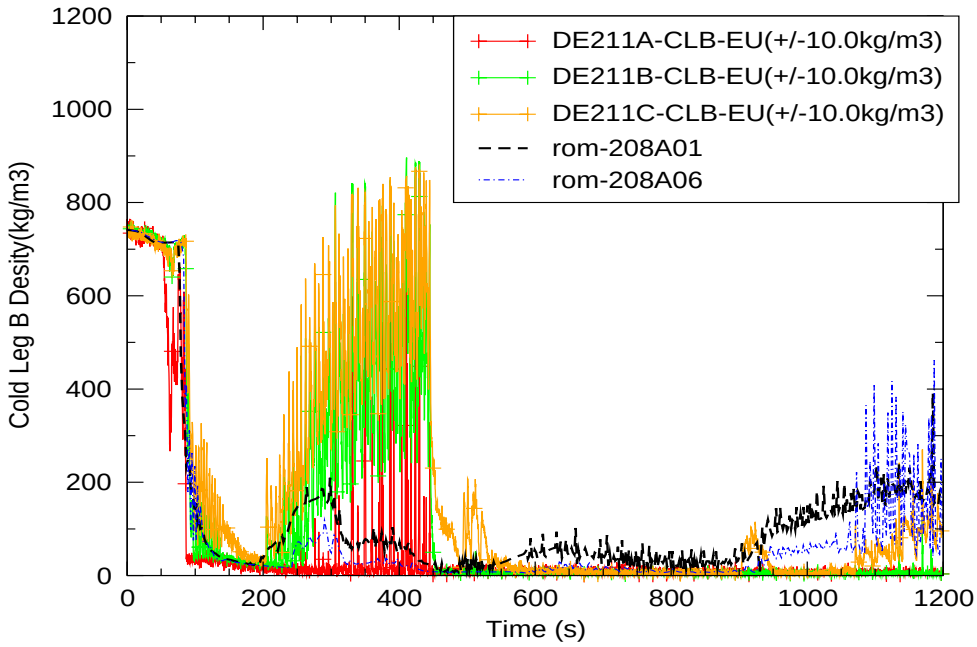

Figure C.5-109. Fluid Density in Loop-B Cold Leg

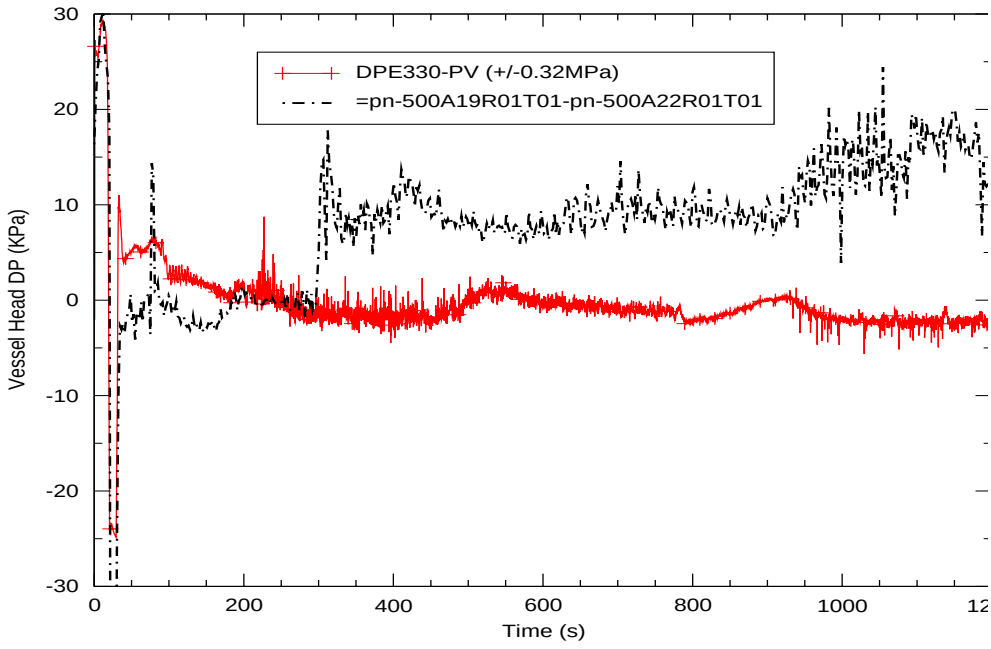

Figure C.5-110. Upper-Head Differential Pressure

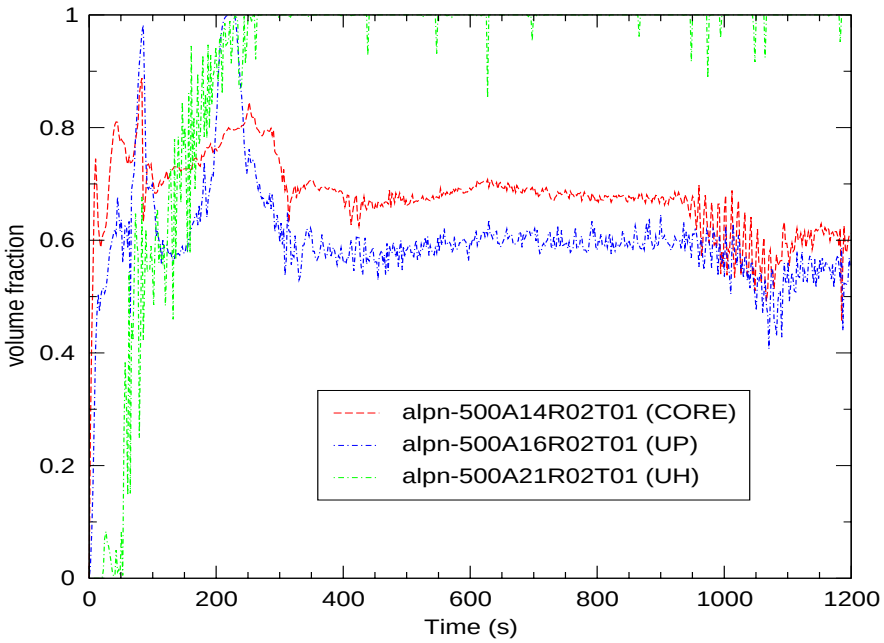

Figure C.5-111. Void Fraction in the Core (CORE), the Upper Plenum (UP), and the Upper Head (UH) Regions of the Vessel

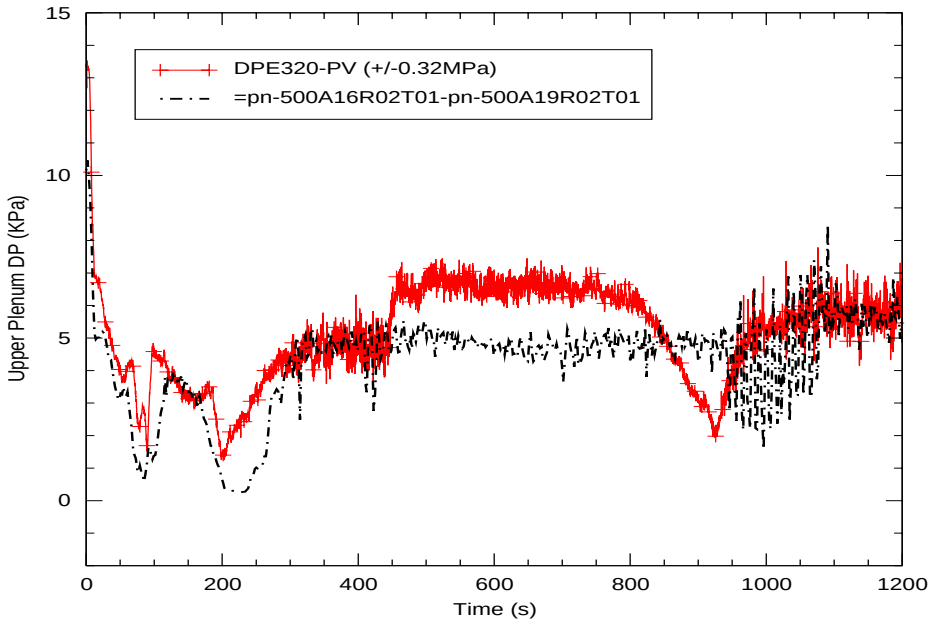

Figure C.5-112. Upper-Plenum Differential Pressure

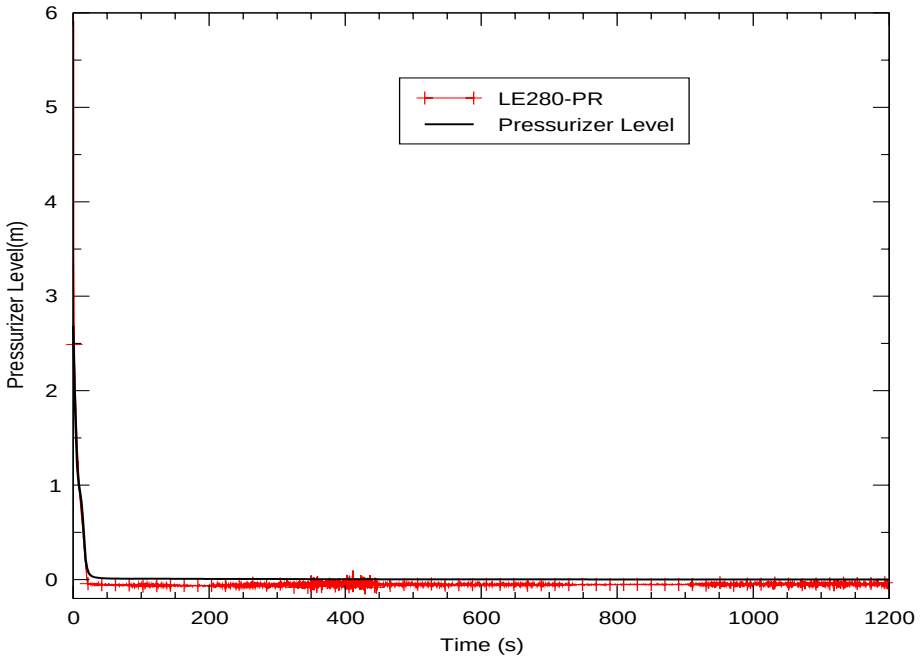

Figure C.5-113. Pressurizer Level

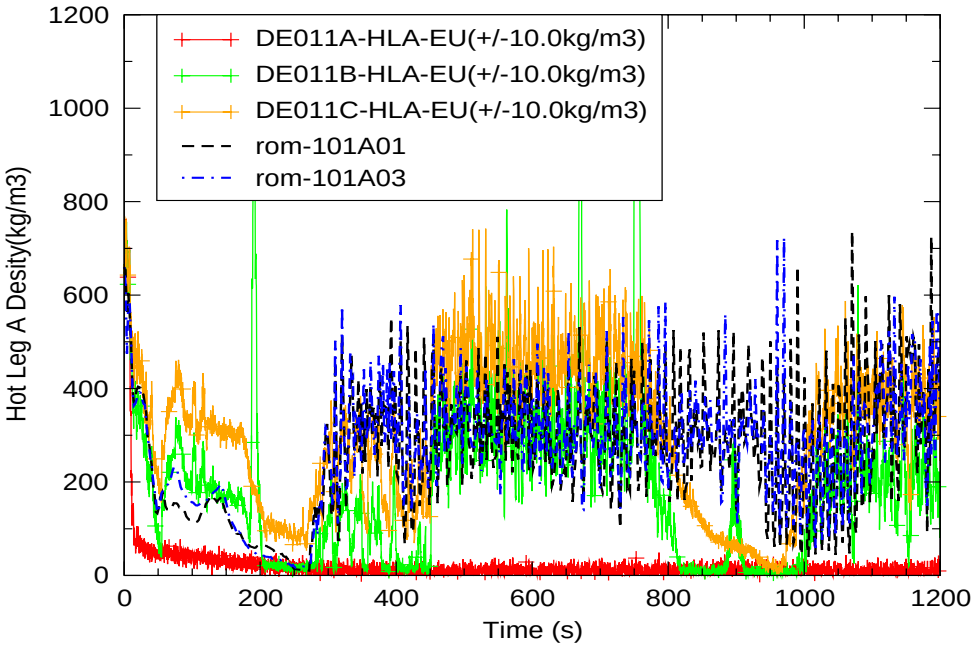

Figure C.5-114. Fluid Density in Loop-A Hot Leg

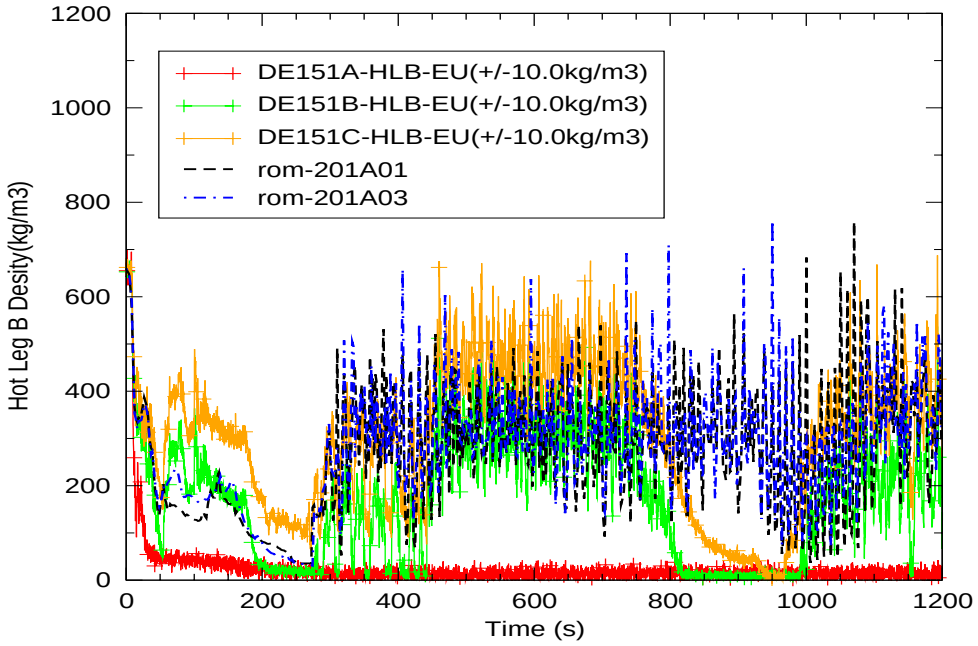

Figure C.5-115. Fluid Density in Loop-B Hot Leg

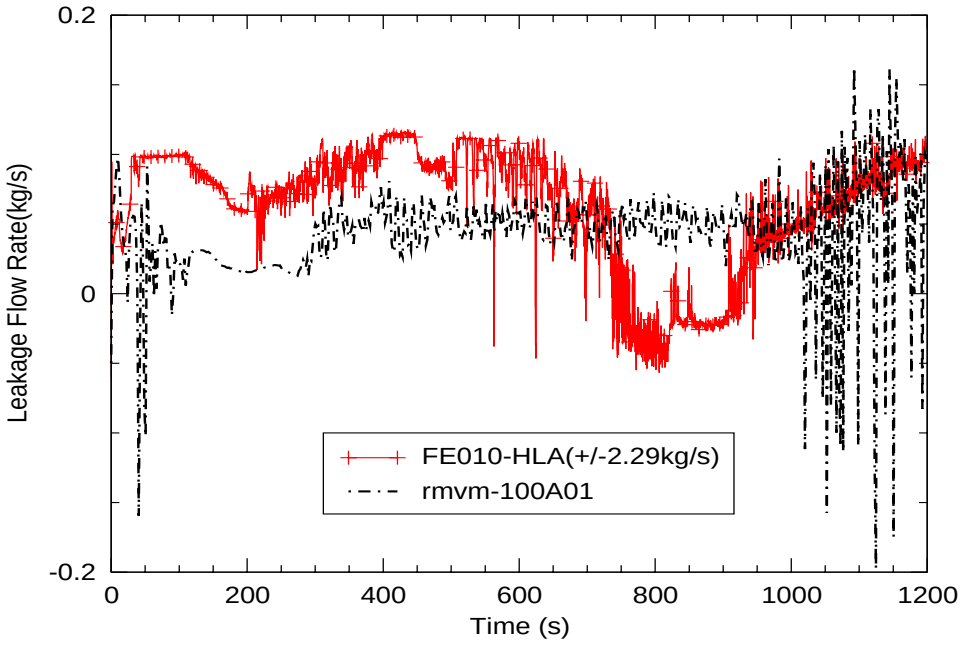

Figure C.5-116. Loop-A Hot-Leg Bypass Leakage

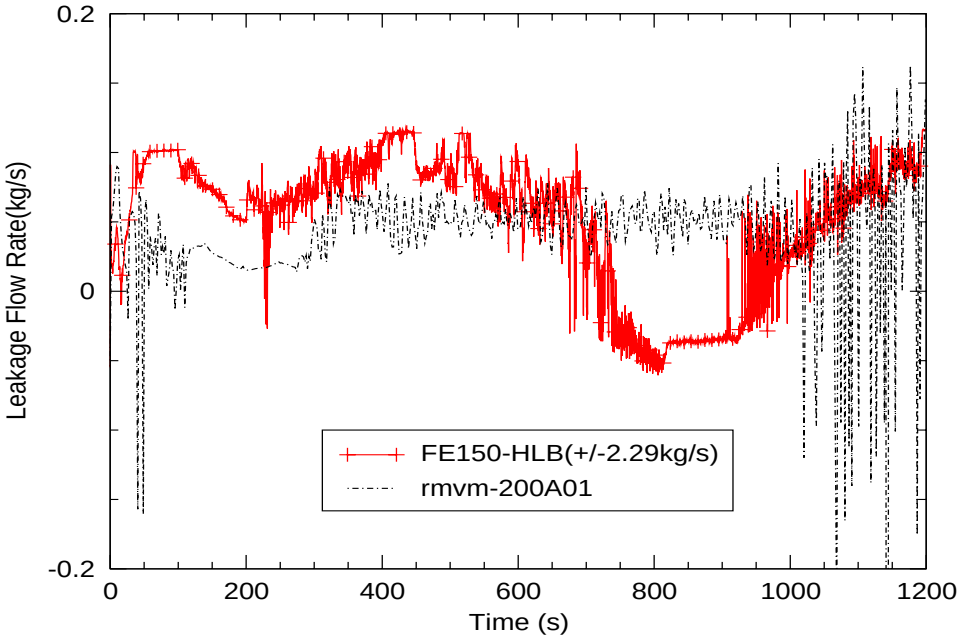

Figure C.5-117. Loop-B Hot-Leg Bypass Leakage

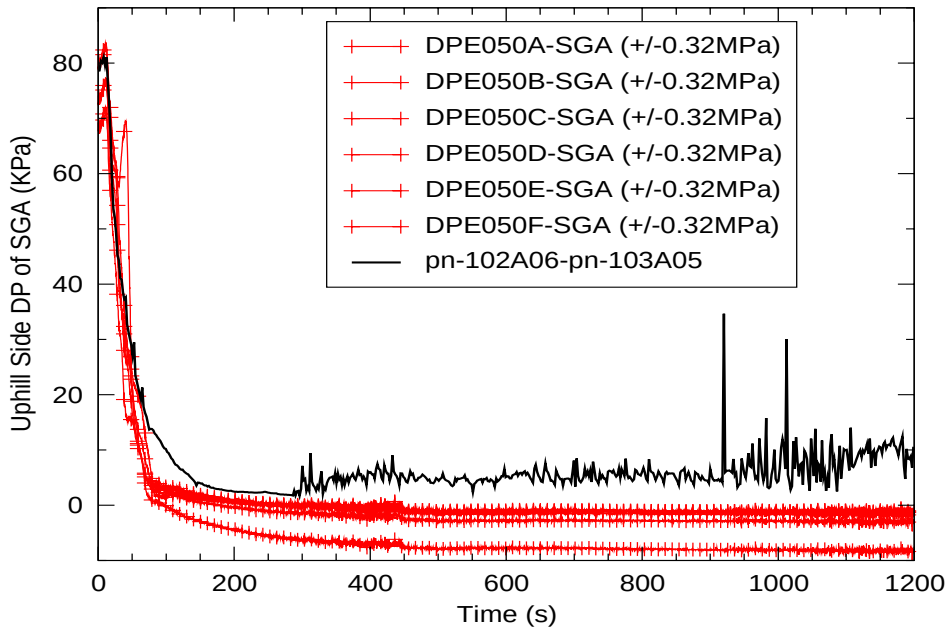

Figure C.5-118. Differential Pressure on uphill side of Loop-A Steam Generator

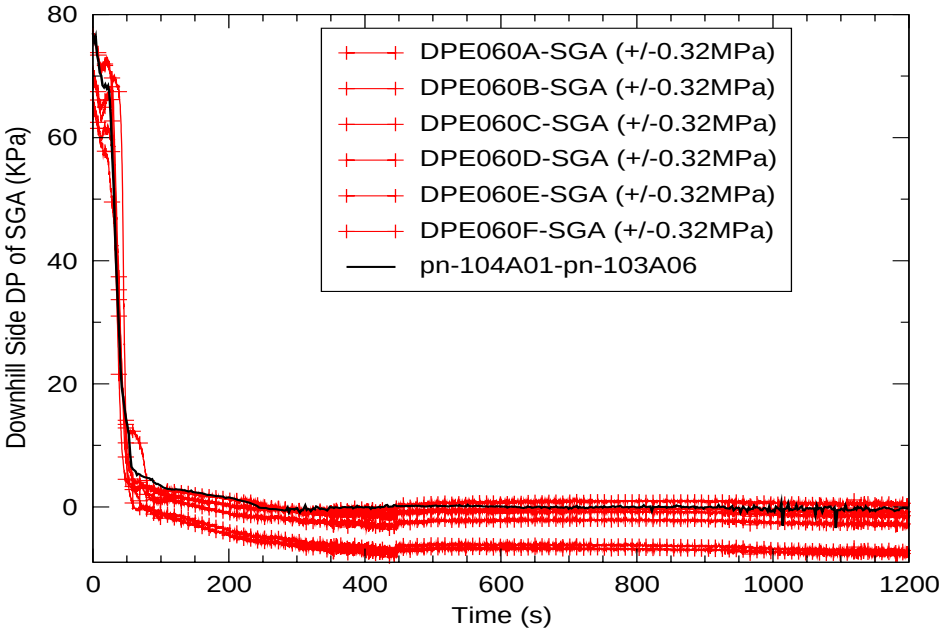

Figure C.5-119. Differential Pressure on downhill side of Loop-A Steam Generator

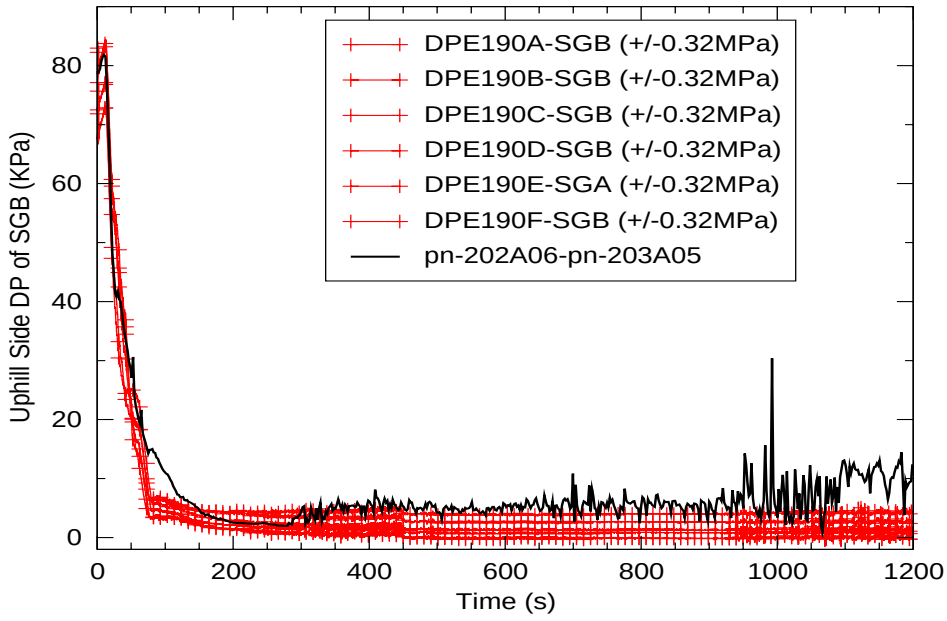

Figure C.5-120. Differential Pressure on uphill side of Loop-B Steam Generator

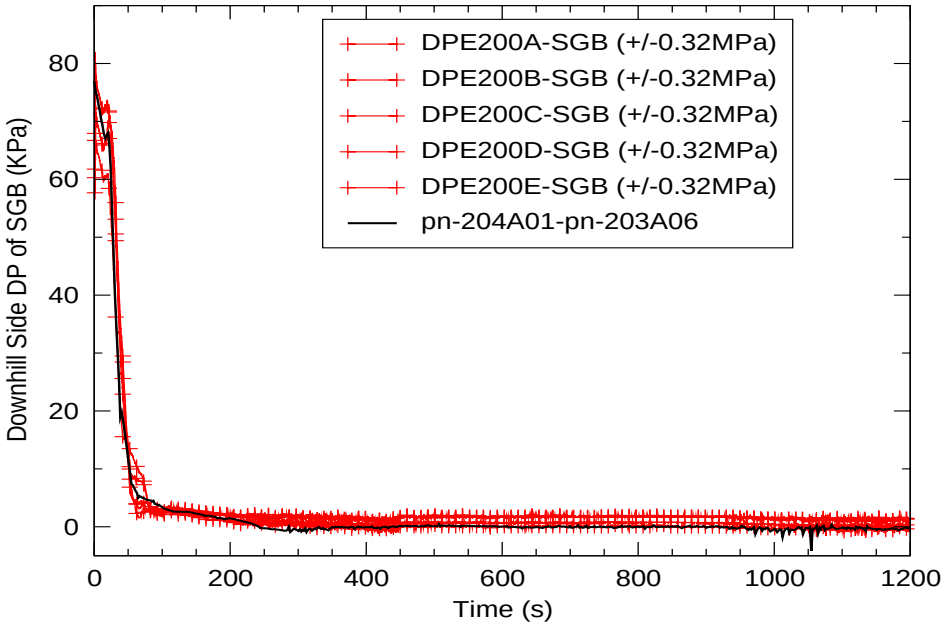

Figure C.5-121. Differential Pressure on downhill side of Loop-B Steam Generator

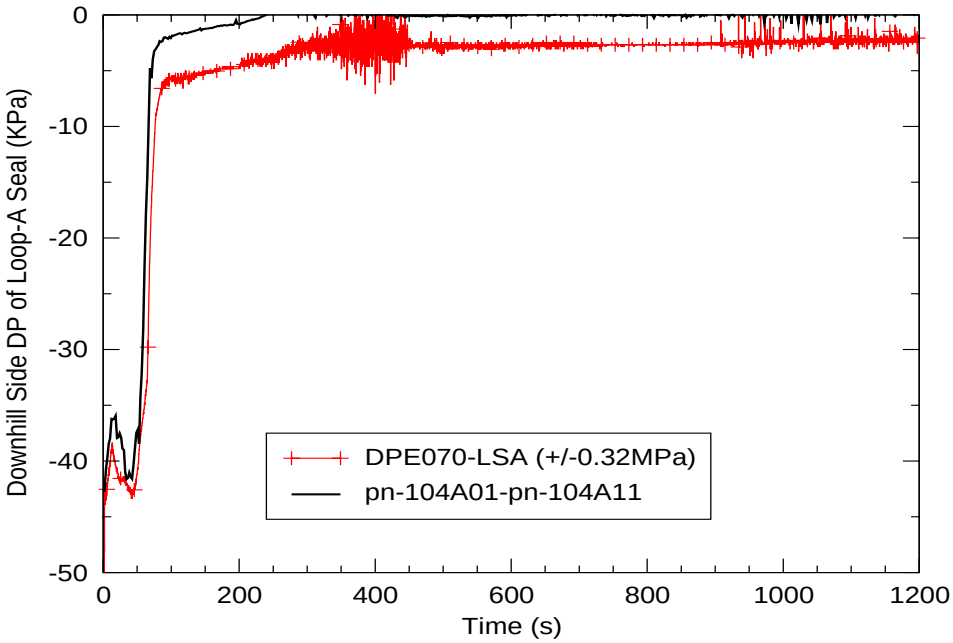

Figure C.5-122. Differential Pressure along downhill Side of Loop-A Seal

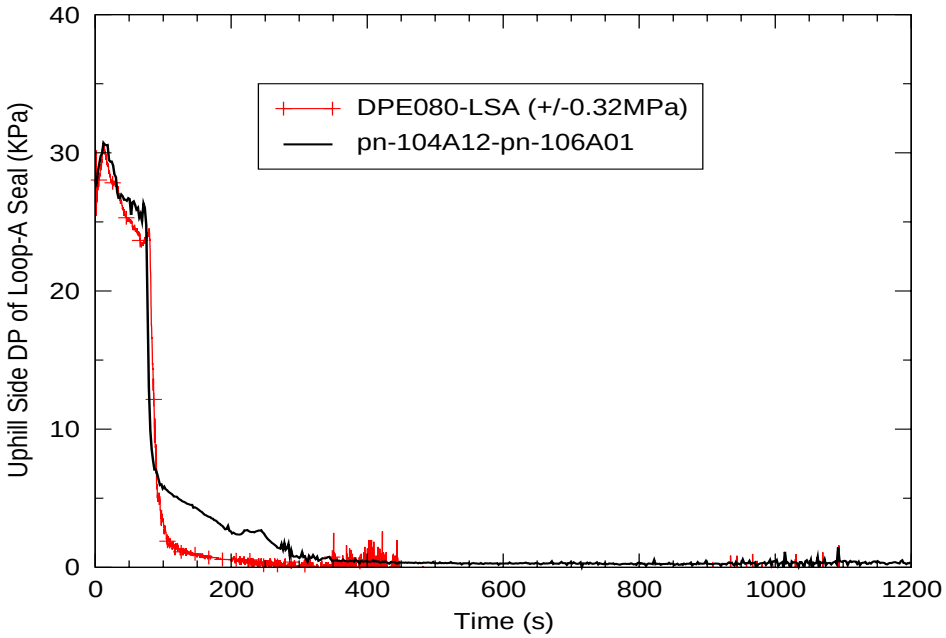

Figure C.5-123. Differential Pressure along uphill Side of Loop-A Seal

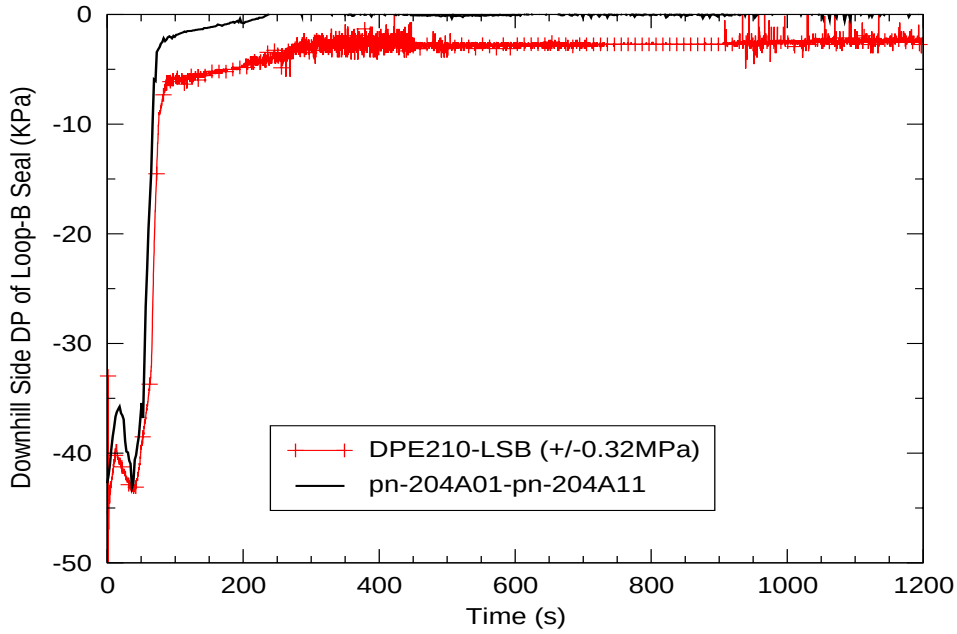

Figure C.5-124. Differential Pressure along downhill Side of Loop-B Seal

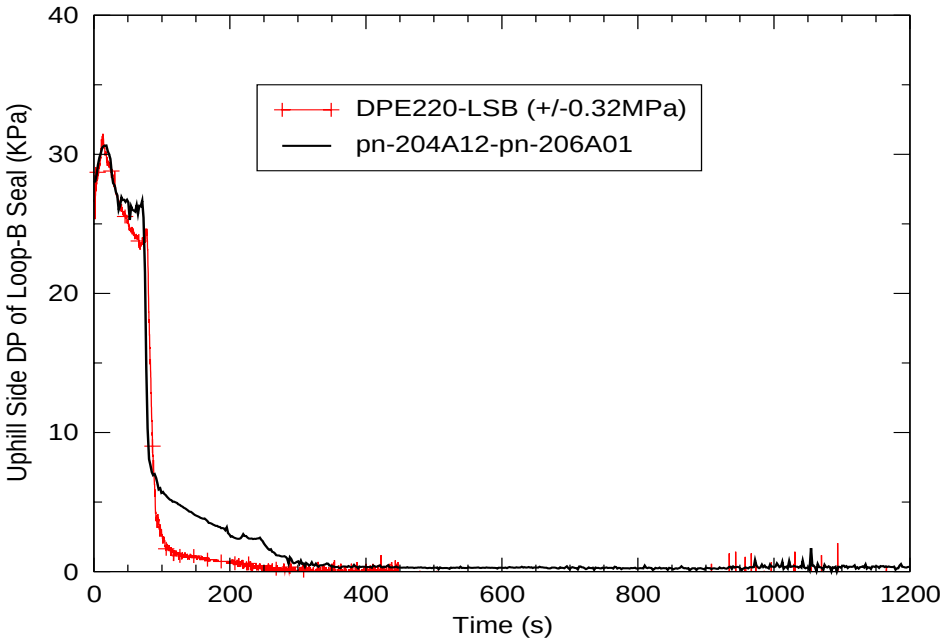

Figure C.5-125. Differential Pressure along uphill Side of Loop-B Seal

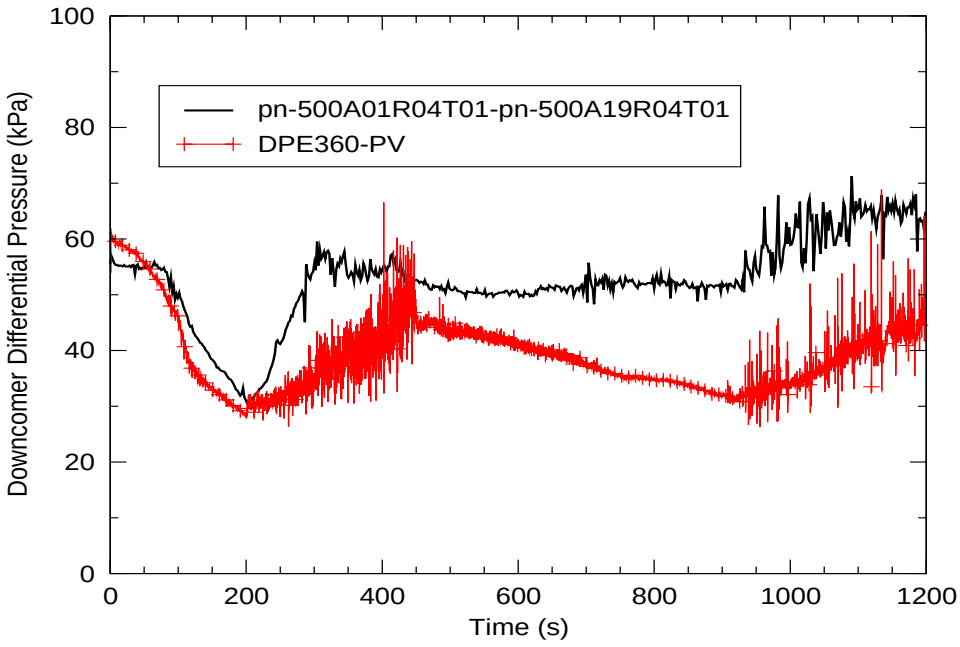

Figure C.5-126. Downcomer Differential Pressure

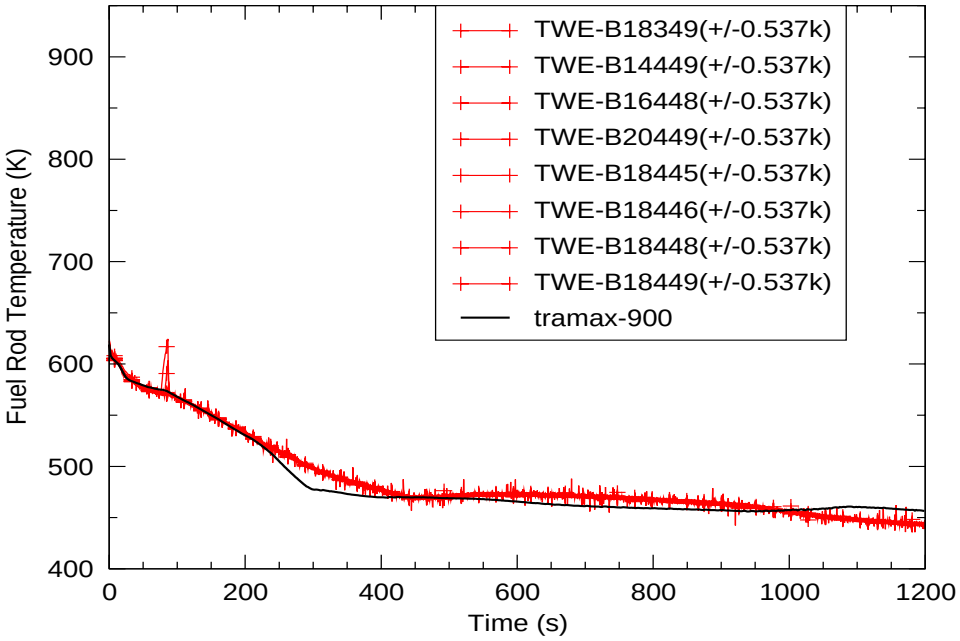

Figure C.5-127. Fuel Rod Temperature

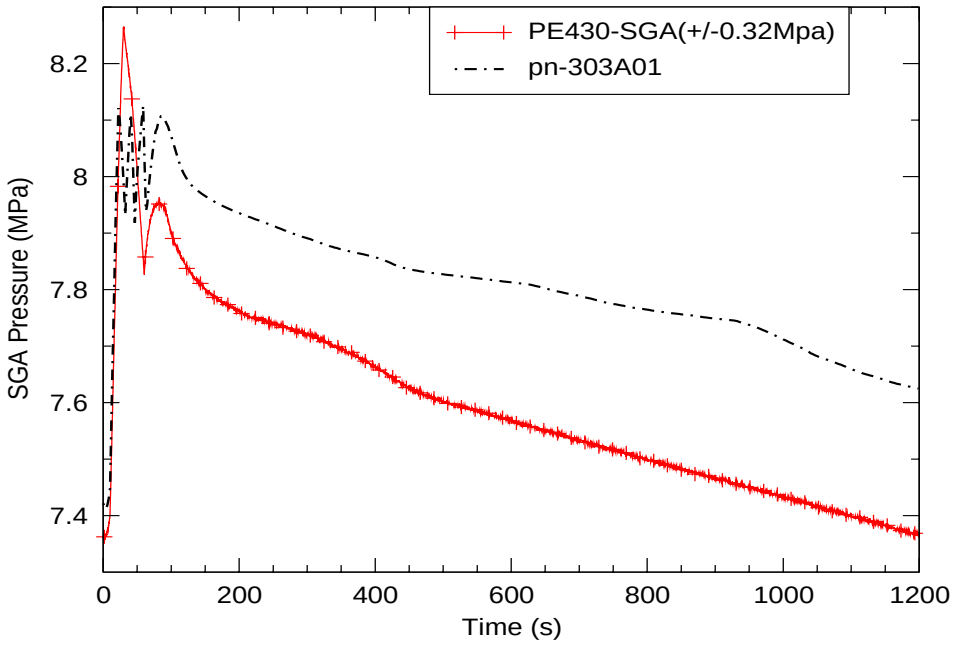

Figure C.5-128. Pressure in Loop-A Steam Generator

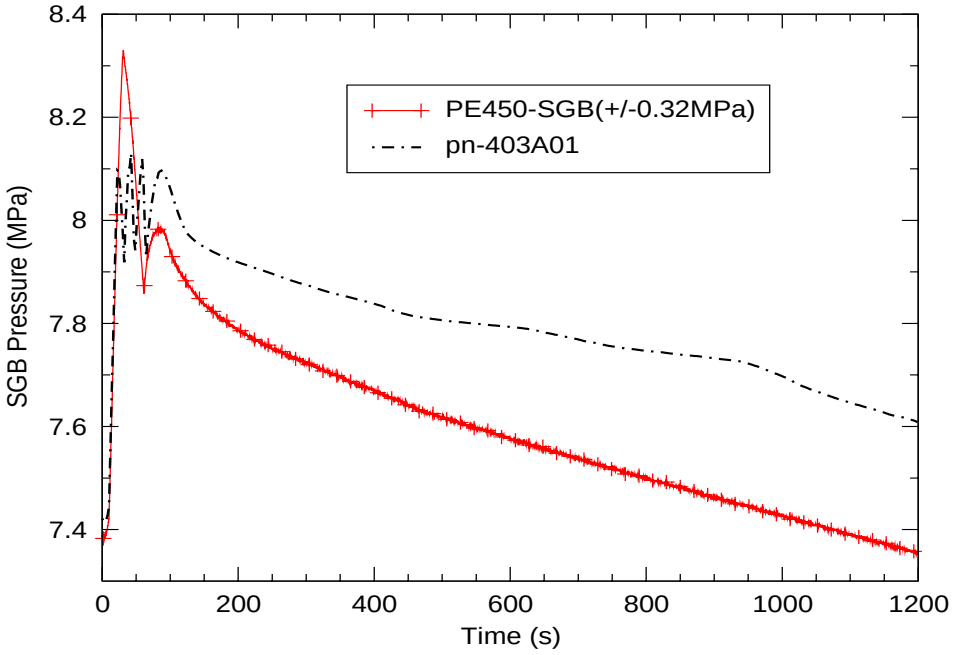

Figure C.5-129. Pressure in Loop-B Steam Generator

C.5.5.3.5. Conclusions

Table 5.3 of this report, as well as Reference 8 lists four criteria used in the code validation: *Excellent Agreement, Reasonable Agreement, Minimal Agreement, Insufficient Agreement*. *Reasonable agreement* is defined as:.

> "*Reasonable Agreement* applies when the code exhibits minor deficiencies. Overall, the code provides an acceptable prediction. All major trends and phenomena are predicted correctly. Differences between calculated values and data are greater than those deemed necessary for excellent agreement. The calculation will frequently lie outside but near the specified or inferred uncertainty bands of the data. However, the correct conclusions about trends and phenomena would be reached if the code were used in similar applications. The code models and/or facility model noding should be reviewed to see if improvements can be made."

Based on the PIRT analysis of each characteristic phase encountered during this test, it is evident that the TRACE simulation results presented for SB-CL-14 meet the definition of a *Reasonable Agreement* throughout the transient event for all phenomena ranked high in the applied SBLOCA PIRT.

The most significant discrepancies are as follows

1 Mixing in the cold leg following accumulator injection was incorrectly captured, resulting in the under-prediction of cold-leg mixture temperatures and densities. The colder temperatures were propagated to the downcomer and the vessel, where they manifest as higher than expected fluid densities and levels.

2 Accumulator-injection mass flux was too high initially and was initiated approximately 10 seconds early.

3 Prior to accumulator injection, the core began to uncover unexpectedly. This was not seen in the data.

4 Predicted DP in the vessel-head remained about 10 kPa higher than the data

5 Hot-leg bypass leakage flow approximately 0.05 kg/s lower than the data

6 Following accumulator injection and throughout the remained of the transient, liquid hold-up predicted to occur in SGA.

7 Loop seals do not clear completely after the initial flush; A small amount of liquid, which dissipates over a period of 200 seconds, is predicted to remain.

8 After accumulator injection, downcomer liquid level is over-predicted.

9 Slight fuel-rod temperature rise occurring a approximately 75 seconds is not predicted to occur.

C.5.5.4. Simulation of SB-CL-15

SB-CL-15 case is a 0.5% cold leg break test. The break unit is located at the bottom side of the cold leg in Loop B. Two input decks were developed for the transient analysis: one constrained steady-state (CSS) input deck and one transient input deck. The CSS deck contains most of the model information and plant control procedures. The CSS input deck is used to obtain initial plant conditions for transient calculations.

The control system and control procedures of the ROSA-IV facility were designed to accommodate a wide range of plant operational transients and accident scenarios. The TRACE control procedure was derived from a series of SBLOCA tests.

SB-CL-15 test conditions and control actions implemented in the TRACE transient analysis are listed here.

C.5.5.4.1. SB-CL-15 Test Conditions

Some of the test conditions or control procedures were different from those in the reference PWR reactor. Special control procedures or test conditions were designed to account for some scaling issues in the design of the test facility (Refs.1, 7).

The plant initial conditions are summarized in Table C.5.3. In the test, it was assumed that a loss-of-offsite power occurred coincident with reactor scram. In addition, coincident failures were assumed failing the high pressure charging system, HPSI, and auxiliary feedwater system. Table C.5.15 summarizes the operational setpoints for Run SB-CL-15. Table C.5.16 gives the event sequence recorded by the facility instrumentation system. Some specific information is given below for individual items.

- Coolant pumps

Upon the initiation of the break, the pump speed was increased before the pump started to coast down following the reactor scram signal (Ref. 7). The pump impeller rotation speed after break is shown in Figure C.5-130 and Figure C.5-131. The dashed line is the pump curve obtained in the TRACE simulation of SB-CL-15. The solid line is the measured pump curve in the SB-CL-15 test. The test data showed that the pump speed was manually increased right before the transient test.

- Reactor trip and core power after break

As indicated in Table C.5.16, the reactor was tripped 84 seconds after the break was initiated. Two power curves are shown in Figure C.5-132. The solid line is the measured power curve in the SB-CL-15 test. The dashed line is the power curved obtained in the transient simulation. The simulated reactor trip was delayed due to the slower depressurization. It took longer time to reach the reactor trip setpoint in the simulation.

- Emergency Core Cooling System (ECCS)

During the SB-CL-15 transient, no ECCS system injected coolant. As mentioned above, coincident failures of the charging system and HPSI were assumed.

- Auxiliary Feedwater System

In SB-CL-15, the auxiliary feedwater was assumed failed for both steam generators.

- Pressurizer heaters

Based on the test data, power supply to the pressurizer heaters was cut off with the initiation of the reactor trip, which was 84 seconds after the break initiation.

C.5.5.4.2. TRACE Control Procedure

Using the strategy outlined at the beginning of this chapter, the control procedure for the TRACE model is simplified. As a result, the TRACE control procedure mainly consists of a number of trips**.** In general, a trip is either initiated by time setpoints or by the system pressure. Specifically:

At time 0, the break is initiated. The pressurizer heater power is maintained for 84 seconds.

The pump speed is increased after the break and coasts down with the reactor trip as shown in Figure C.5-130 and Figure C.5-131.

The reactor is tripped when the system pressure reaches 12.97 MPa. Figure C.5-132 shows the measured power curve after the break and the power curve obtained from the transient calculation.

The Safety Injection (SI) signal is generated as the system pressure reaches 12.27 MPa. The Emergency Core Cooling System (ECCS) is assumed failed in the transient.

Main steam line valve closure and main feedwater cutoff are initiated with proper time delays following the reactor trip.

Table C.5.15. Operational Setpoints for Run SB-CL-15

	Setpoint
Reactor scram signal	12.97 MPa (System pressure)
Pump coast down	With reactor scram
Safety Injection (SI) signal	12.27 MPa (system pressure)
High Pressure charging	Failed
Accumulator injection	4.51 MPa
Low Pressure Injection	1.29 MPa
Main feedwater cutoff	With reactor scram
Turbine throttle valve closure	With reactor scram
Auxiliary feedwater initiation	Failed

Table C.5.16. Chronology of Events for Run SB-CL-15

Events	Time (s)
Break	0
Main Steam Line Valve Closure	80
SG Feedwater stop	80
Reactor trip	84
High Pressure Charging Injection	Assumed failed
High Pressure Safety Injection	Assumed failed
Auxiliary feedwater ON	Assumed failed
Reactor coolant pump stop	341
1st Core uncovery	1750 -1880
Loop seal clearing	1876 - 1883

Table C.5.16. Chronology of Events for Run SB-CL-15

2nd Core uncovery	1980 - 2190
Primary/Secondary pressure reversal	2145
Accumulator Injection on	-
Core power tripped OFF	2596

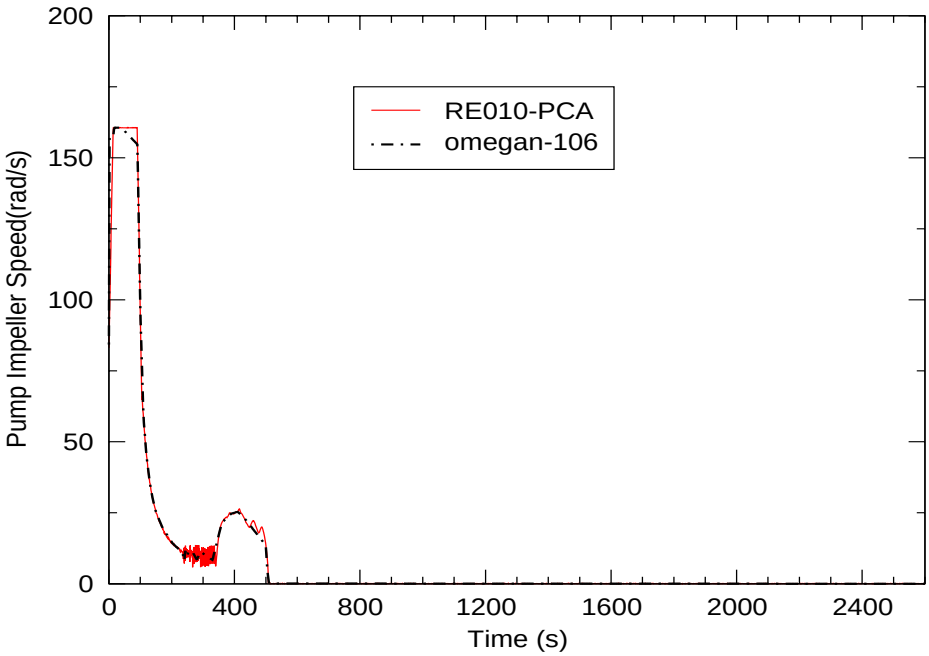

Figure C.5-130. Pump A Impeller Speed After Break

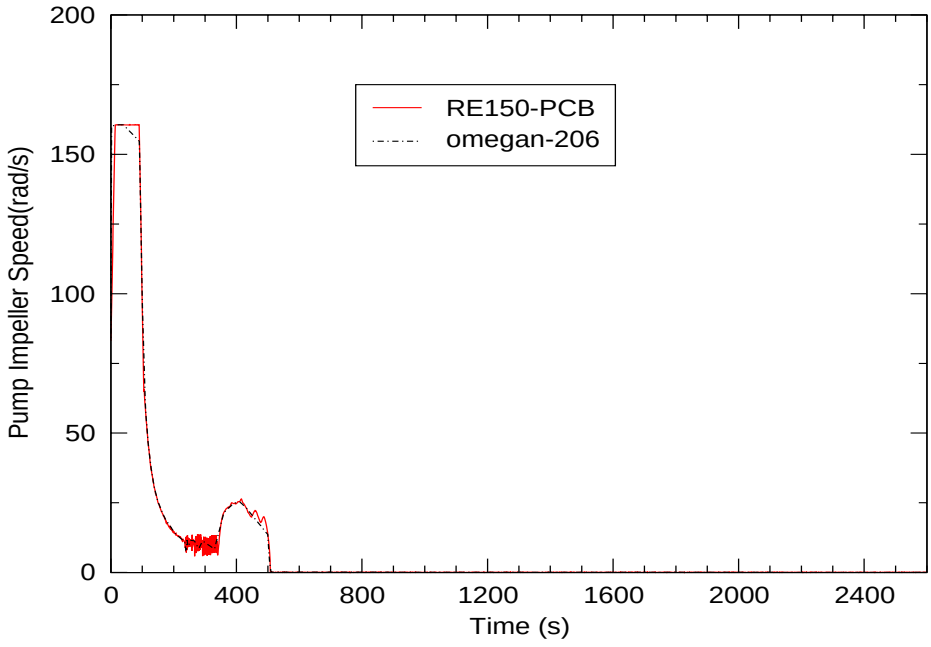

Figure C.5-131. Pump B Impeller Speed After Break

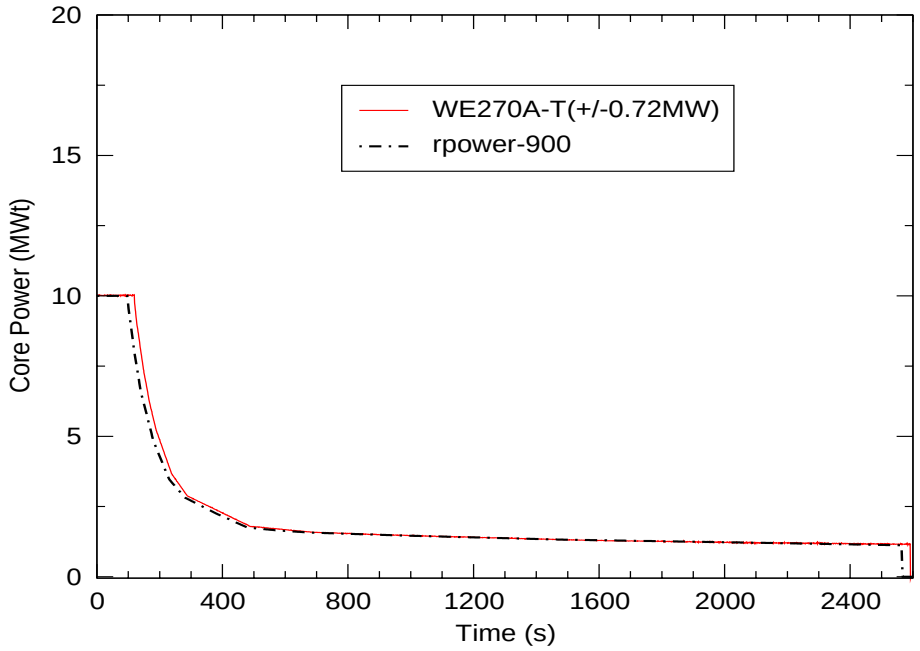

Figure C.5-132. Core Power after Break

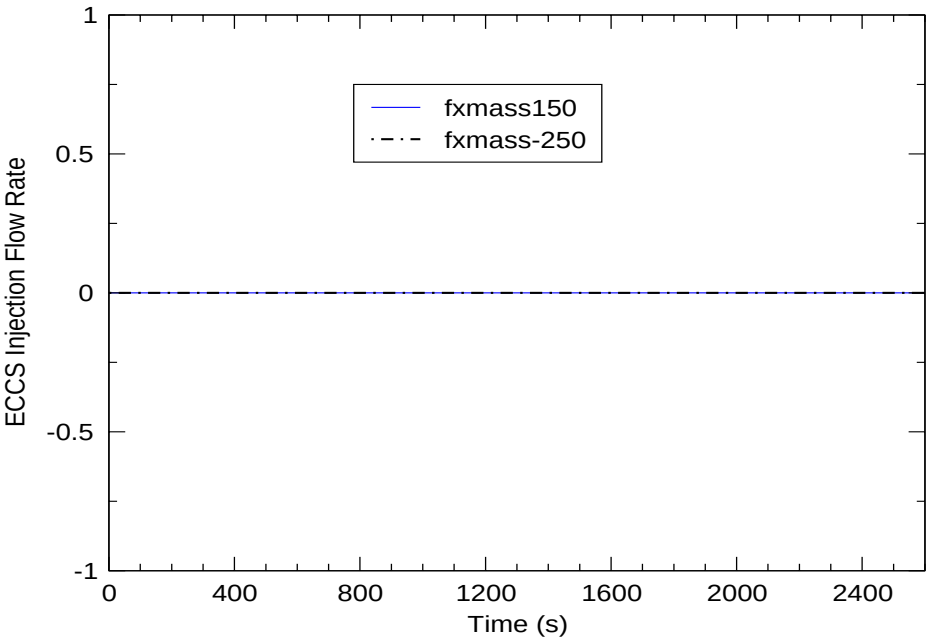

Figure C.5-133. ECCS Injection Flowrates for Loop A and Loop B

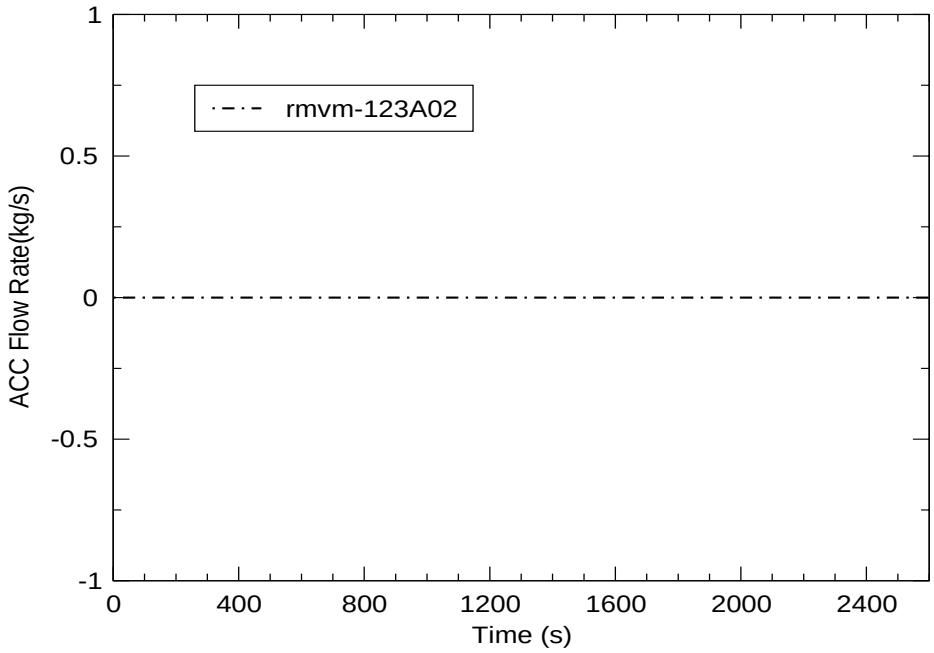

Figure C.5-134. Accumulator Injection Flow to Cold Leg A

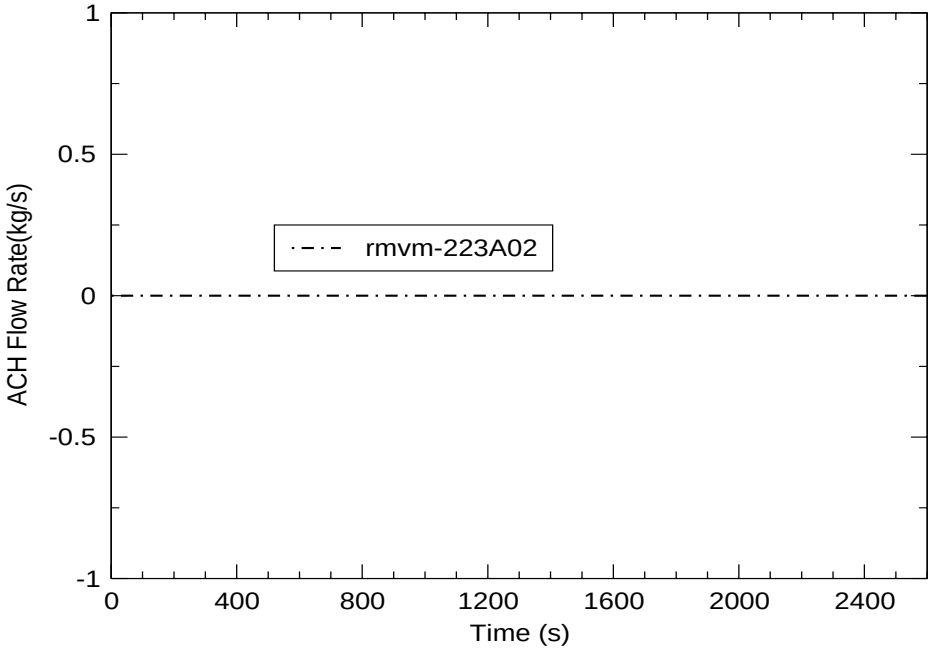

Figure C.5-135. Accumulator Injection Flow to Cold Leg B

C.5.5.4.3. Experimental Observations

The main objective of the test SB-CL-15 was to investigate the thermal-hydraulic mechanisms of early core uncovery and heatup. Early core uncovery may be caused by a manometric effect resulting from an imbalance between the water hold up in the upflow and downflow sections of the primary side of the steam generators (Ref. 7). Table C.5.17 lists the event sequence recorded by the facility's instrumentation system during the test.

Soon after the start of the transient, the pressure started to drop and the core power decay curve was initiated at a pressurizer pressure of 12.97 MPa together with the closing of the MSIV, starting of the programmed pump speed curve, and termination of the main feedwater to the steam generators.

The safety injection signal occurred at 12.27 MPa. However, the high-pressure charging system and HPSI were assumed failed. Auxiliary feedwater was also assumed not available.

The depressurization became slower after the pressure reached about 8 MPa since the secondary pressure was kept at about 8 MPa. The primary pressure remained at this value throughout the experiment and began to decrease only after the secondary side bleed was initiated.

Both loops experienced loop seal clearing at about 1880 s, which substantially recovered the water level in the core. Somewhat later, further coolant boil-off led to a second core uncovery.

C.5.5.4.4. Transient Analysis

The SB-CL-15 transient calculation was performed for 2800 seconds. However, the experiment terminated at 2596 seconds when the core power was tripped off. The transient simulation results and the comparison to the test data are presented in Figure C.5-130 to Figure C.5-164. In these figures, the test data is plotted in solid, colored lines with symbols and the calculation results are plotted with solid black or blue lines without symbols.

C.5.5.4.4.1. System Behavior

The overall primary system behavior determines the boundary conditions of the transient event, since most of the control signals are based on the system pressure setpoints. The predicted system pressure was higher than the test data during the blowdown phase (0 - 410 seconds) as shown in Figure C.5-136. Therefore, the sequence of events, such as reactor trip, based on the system pressure setpoints were delayed during that period of time.

Table C.5.17 shows the comparison of the sequence of events for the SB-CL-15 simulation and the corresponding test data.

Table C.5.17. Sequence of the Event Comparison for SB-CL-15 Test

Event	Test Data Time (sec)	TRACE Model Time (sec)
Break	0	0[a]
Main Steam Line Valve Close	80	80
SG Feedwater Stop	80	80
Reactor Trip	84	80
Reactor Coolant Pumps (PC-A/B) Stop	341	340
First Core Uncovery	1750 -1900	1490 - 1590
Loop-A Seal Began Clearing[c]	1883	Did not clear
Loop-B Seal Began Clearing[c]	1876	1525[b]
Primary/Secondary Pressure Reversal	2145	~1850
Second Core Uncovery	2175 -2596	2160-2600
End Time	2800	2600

a. The break starts at time 0.

b. Cleared partially

c. The beginning of loop-seal clearance is the time at which the differential pressure across the uphill portion of the loop seal begins to rapidly descend toward zero.

C.5.5.4.4.2. Analysis Results

As discussed in **Section C.5.5.**, the PIRT (Ref. 6) identifies the high ranked phenomena for each phase of the transient. To evaluate the performance of TRACE, each phase will be discussed separately, and the TRACE-simulation results for the highly-ranked phenomena will be compared to the data. The principal Figure of Merit (FOM) of the transient event is the core collapsed liquid level (CCL). The core collapsed level is measured as the core differential pressure as demonstrated in Figure C.5-137.

Certain input parameters, such as decay heat, core power, and feedwater temperature, are taken directly from the test data as boundary conditions. Therefore, although they are identified as important in some of the phases, they will not be discussed in terms of code performance.

Blowdown phase

The blowdown phase is marked by a rapid depressurization of the primary coolant system until the hot coolant begins to flash into steam. The rate of depressurization is strongly influenced by the rate and enthalpy of the break flow, and it changes when flashing and boiling start in the core. In this phase, the most important parameters defining the evolution of the transient are decay heat, primary side heat transfer, critical break flow, and the flow regime upsteam of the break flow.

In the test, the blowdown phase lasted from 0 to 410 seconds. Throughout this time, the simulation results follow the general trends of the data, but several discrepancies are noted which have an affect in the later phases of the transient. The calculated pressurizer pressure in Figure

C.5-136 is shown to be slightly under-predicted throughout most of the phase, but at around 400 seconds, the pressure settles at a value approximately 0.5 MPa higher than the data. For the core DP, the prediction shown in Figure C.5-137 is 5kPa less than the data at the start of the transient, but it comes into agreement with the data when the reactor SCRAMS at around 80 seconds. Good agreement, however, is shown in terms of primary-side heat transfer, which can be seen in Figure C.5-138 through Figure C.5-141. These figures show comparisons of the fluid temperatures in the SG-tubes and the cold legs, respectively. As for critical break flow and the flow regime upstream of the break, Figure C.5-142 shows a slight over prediction in break flow, but overall, the agreement is reasonable. The density of the fluid in the cold legs is evaluated to determine the flow regime upstream of the break. Figure C.5-143 and Figure C.5-144 show densitometer readings taken at three locations over the cross-sections of the cold legs. These figures show excellent agreement between the simulation and the data.

Other key results are the DPs in the vessel head and upper plenum, the pressurizer level, and the flow regime in the hot legs. Figure C.5-145 shows the vessel-head DP. Here, the depressurization can be observed, but unlike the data, the code is predicting large negative pressure oscillations. These oscillations appear to be due to the oscillations in upper-head void fraction seen in Figure C.5-146. This erratic behavior is not seen in the calculated upper-plenum DP shown in Figure C.5-147, where there is good agreement with the data.

Figure C.5-148 shows good agreement between the calculated and measured pressurizer levels. The only apparent difference is the over-prediction of the degree of voiding in the bend of the SG U-tubes. This flow resistance halts the decent of the pressure at around 100s, causing the temporary level increase to be more pronounced.

The flow regimes in the hot legs are evaluated in terms of hot-leg fluid density. Figure C.5-149 and Figure C.5-150 both show that the code is predicting mixture densities that fall within the range of the densitometer readings.

Natural Circulation phase

The natural-circulation phase begins at the end of the pump coastdown and ends when the buoyancy forces caused by differences in loop-fluid densities are no longer able to overcome the flow resistance of the loop components. In the experiment, the natural-circulation phase is the longest lasting phase of the transient, spanning from 411 seconds to around 1750 seconds. The measurable highly-ranked processes in this phase are the FOM, decay heat, the counter-current flow in the upper-plenum region, and critical break flow, and break upstream flow regime.

Throughout most of this phase, the calculated pressure is in reasonable agreement with the data. The most notable discrepancy, however, is the early termination of the natural circulation phase (Figure C.5-137); at around 1525 seconds, the loop seals are predicted to begin clearing, approximately 350 seconds too early. This discrepancy is caused by the difference between the predicted and measured primary-system pressures shown in Figure C.5-136.

The presence of counter-current flow or counter-current flow limiting (CCFL) in the upper plenum is evaluated by looking at the upper plenum DP. Figure C.5-147 continues to show reasonable agreement between the prediction and the data during this phase, implying that the steaming rates, which are produced by the prescribed decay heat boundary condition, are leading to accurate predictions of void fraction and counter current flow in the upper plenum.

As for break flow and the flow regime upstream of the break, Figure C.5-142 shows the predicted break flow in excellent agreement with the data. It is expected that such good agreement would indicate the accurate prediction of the flow regime upstream of the break, which is evaluated using cold-leg density results from a location upstream of the break. However, this is not the case. The cold-leg density comparisons in Figure C.5-143 and Figure C.5-144 show the calculated flow regime remaining single-phase liquid until around 1700 seconds then instantly changing to single-phase vapor. The data show the flow regime changing from single-phase liquid to a two-phase mixture at around 800 seconds. This is another result of the pressure discrepancy sited earlier.

Other parameters of interest during this phase are U-bend voiding, fuel rod temperature, and secondary-side pressure. Voiding in the U-bends of the SG tubes, which is indicative of the state of primary-side heat transfer, can be evaluated in terms of SG-tube DP. Figure C.5-151 through Figure C.5-154 show the SG-tube DPs along the uphill and downhill sides of each set of SG tubes. Throughout the first 900 seconds in the transient, these figures show good agreement between the simulation and the data. After 900 seconds, more liquid is predicted to remain in the uphill and downhill sides of SGA and in the downhill side of SGB than in the data.

Figure C.5-155 shows the progression of the fuel temperature over the natural circulation phase. The fuel heatup is predicted to occur prematurely because of the early prediction of core-level depression. However, the magnitude of the heatup is commiserate with the data.

The shell-side SG pressures are shown in Figure C.5-156 and Figure C.5-157. These figures show good agreement between the code and the data. The only discrepancy is the cycling frequency of the valves. It must be noted, however, that due to inconsistencies in the data report, the manual opening of the SGB relief valve was not modeled in this assessment. As can be seen in Figure C.5-157, at around 2100 seconds, the pressure in SGB begins to decrease unexpectedly, but according to the data report, the opening of the relief valve was not performed until after the initial test run had been completed. As a result, the subsequent decreases in primary-system pressure and temperature that are not simulated by the code are not addressed as discrepancies.

Loop Seal Clearing phase

The loop seal clearing phase begins when the trapped primary-side steam volume reaches the top of the loop seal piping. From this point, the steam volume depresses the liquid in the downhill side of the loop seal and in the core until a minimum core level is reached. As steam moves through the seal to the break plane, the liquid it displaces is forced into the core, quenching the heatup caused by the drop in core level. In the test, this sequence of events occurred between 1876 and 1883 seconds.

The highly ranked processes, relevant to this phase, that will be discussed are listed as follows:

1. Decay heat
2. Mixture level in the core region
3. Hot-leg downcomer gap flow
4. SG primary-side heat transfer in the U-tubes
5. SG primary-side flow resistance
6. SG primary-side tube voiding
7. Flow regime/entrainment in the pump suction / loop seal
8. Critical break flow

As stated previously, discrepancies in predicting the evolution of the primary-system pressure leads to the loop seals clearing approximately 350 seconds earlier than the data. Therefore, between 1870 and 1890 seconds, Figure C.5-137 shows the core level already recovered and holding relatively steady.

Figure C.5-158 and Figure C.5-159 show the calculated leakage flows from both hot legs, respectively. Though similar in magnitude, the predicted leakage flow is extremely oscillatory, and unlike the data, it appears to change flow direction at around 100 seconds into the transient. The measured leakage doesn't change flow direction until around 700 seconds, and it appears to be inadequately low.

Heat transfer, voiding, and flow resistance in the SG tubes is evaluated using the DP predictions shown in Figure C.5-151 through Figure C.5-154. In these figures, the predictions match the downward trend of the data quite reasonably. The slight over-prediction in DP, which is shown to occur from around 1100 seconds until the end of the transient, appears to be caused by a difference in measurement location.

Figure C.5-160 through Figure C.5-163 show the DP comparisons along the uphill and downhill sides of the loop seals. The uphill portion of the loop seals includes the pump suction piping. These figures show the simulated loop seals clearing early. As expected, the point at which the loop seals begin to clear is approximately 350 seconds sooner than the data. Comparing the behavior observed in both loop seals, it appears that the predicted DP in LSA more closely resembles the LSB data; in the test, when the initial rush of fluid ensues, the DP in LSB plummets to less than 5kPa. This behavior is similar to what is predicted to occur in LSA. This is also the case for the LSA prediction: in the test, the DP across LSB drops only 10 kPa before recovering, while the predicted LSA DP shows only a momentary decrease.

During this phase, the break flow changed from single-phase liquid to a two-phase mixture during the latter part of the previous phase. In Figure C.5-142, this transition is predicted to occur approximately 200 seconds sooner, and as the phase progresses, the break flow is under-predicted.

Boil Off phase

As the transient proceeds, the primary system continues to loose inventory and the core inventory continues to boil. During the test, this boil-off phase lasted from around 1890 to 2596 seconds. The relevant highly-ranked processes that will be discussed are listed below:

1. Fuel Decay heat and local power
2. Mixture level in the core
3. Downcomer mixture level
4. Critical break flow
5. Break upstream flow regime

At this stage in the transient, the behavior of the most important parameters is mostly a continuation of the previous phase. Exceptions are the mixture level in the core, downcomer DP, and fuel temperature.

According to the data shown in Figure C.5-137, after the core-mixture level is recovered, only 100 seconds or so elapse before the core begins to uncover again. This reversal in level is not predicted to occur as rapidly, resulting in a predicted level that is approximately 5 kPa higher than the data.

Similar agreement is also shown in Figure C.5-164 for the downcomer level, where it is also apparent that the decrease in downcomer level during the natural-circulation phase was not predicted; the level stays relatively constant until the loop seals begin to clear.

As seen in Figure C.5-155, the final fuel heatup is delayed with respect to the data. This delay occurs because of the delay in falling core level mentioned earlier.

Core Recovery phase

No core recovery phase was simulated for this test. There was no ECCS injection, and in addition, the test was terminated at 2596 seconds by tripping off power to the core heaters.

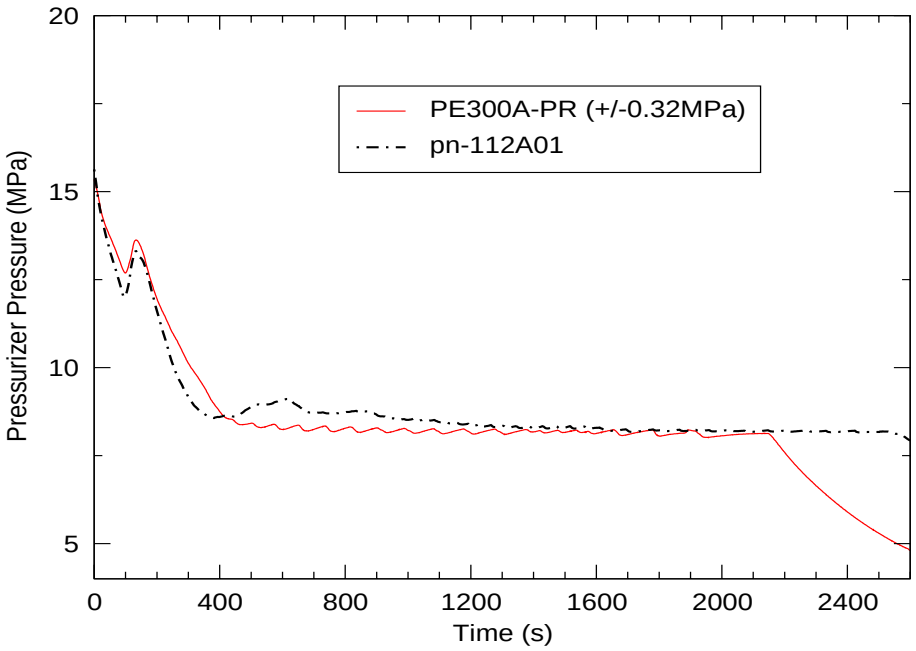

Figure C.5-136. Pressurizer Pressure

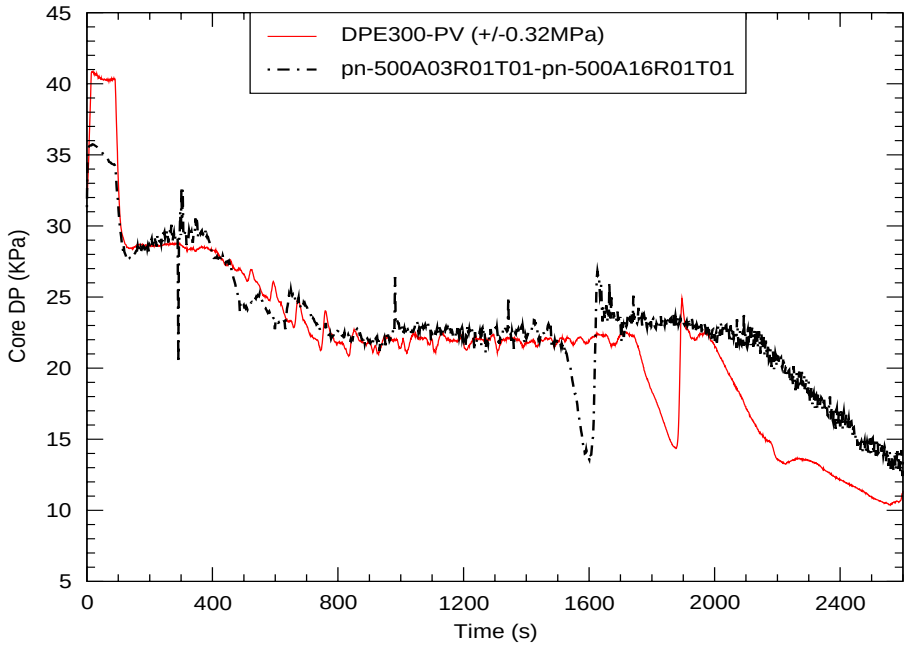

Figure C.5-137. Reactor Core Differential Pressure

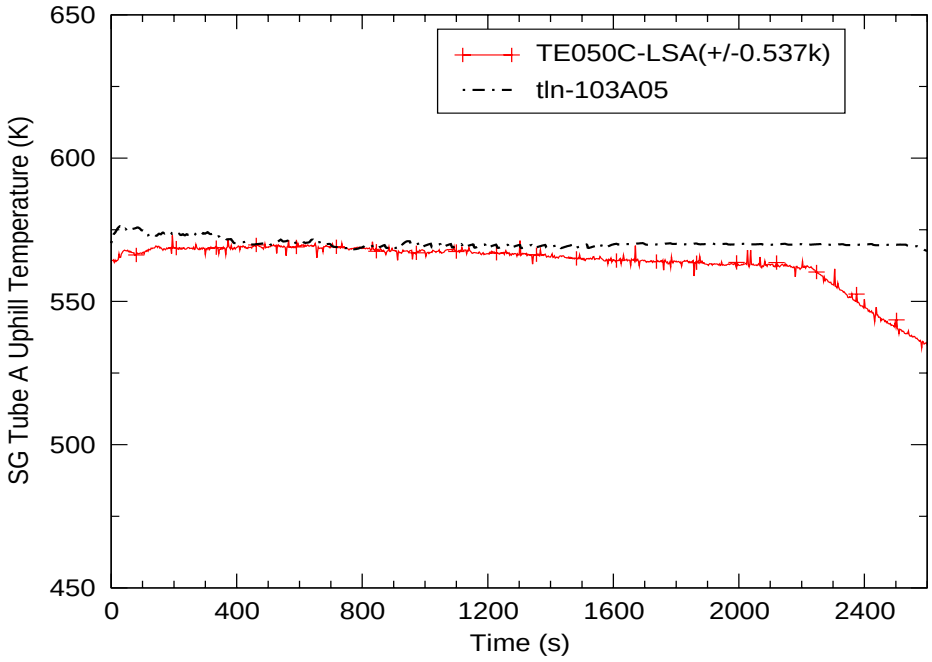

Figure C.5-138. Fluid Temperature in Loop-A Steam Generator Tubes

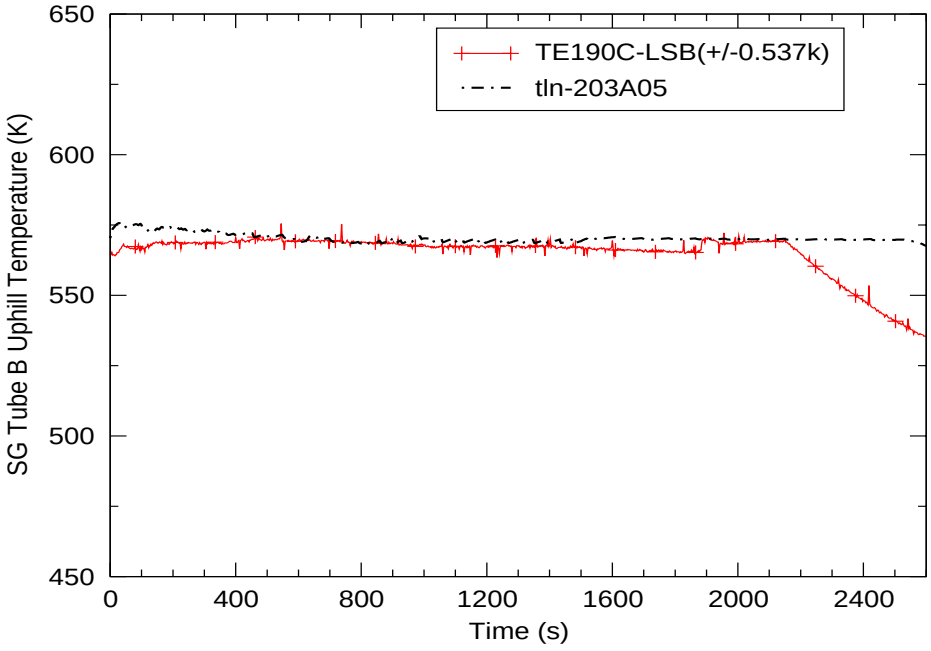

Figure C.5-139. Fluid Temperature in Loop-B Steam Generator Tubes

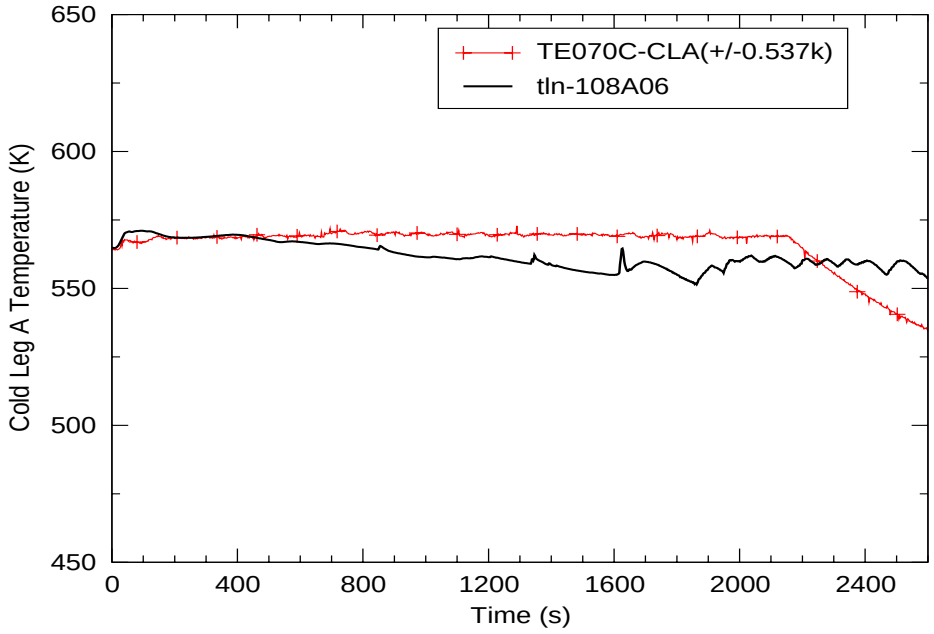

Figure C.5-140. Fluid Temperature in Loop-A Cold Leg

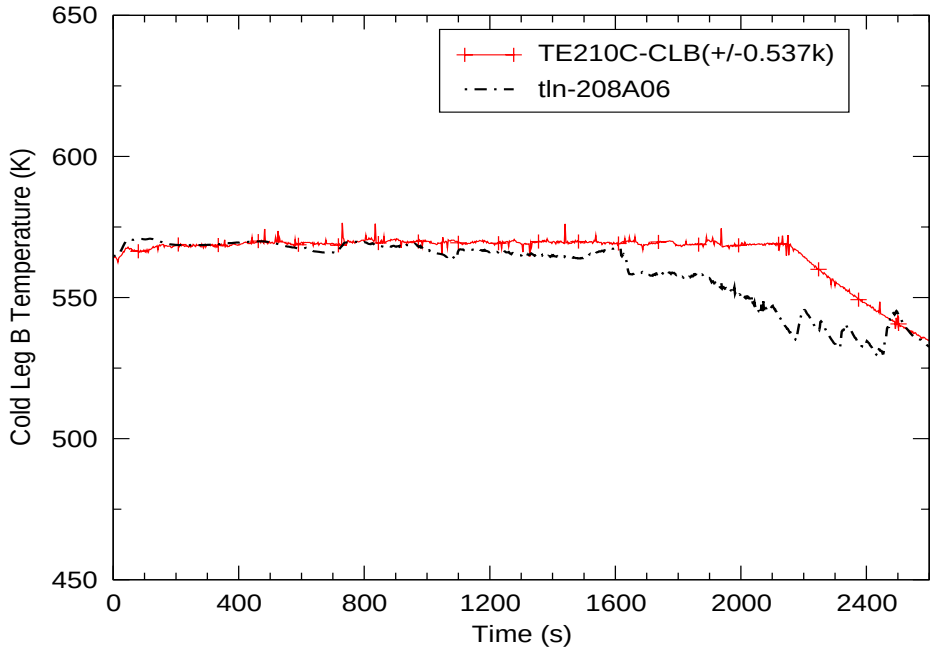

Figure C.5-141. Fluid Temperature in Loop-B Cold Leg

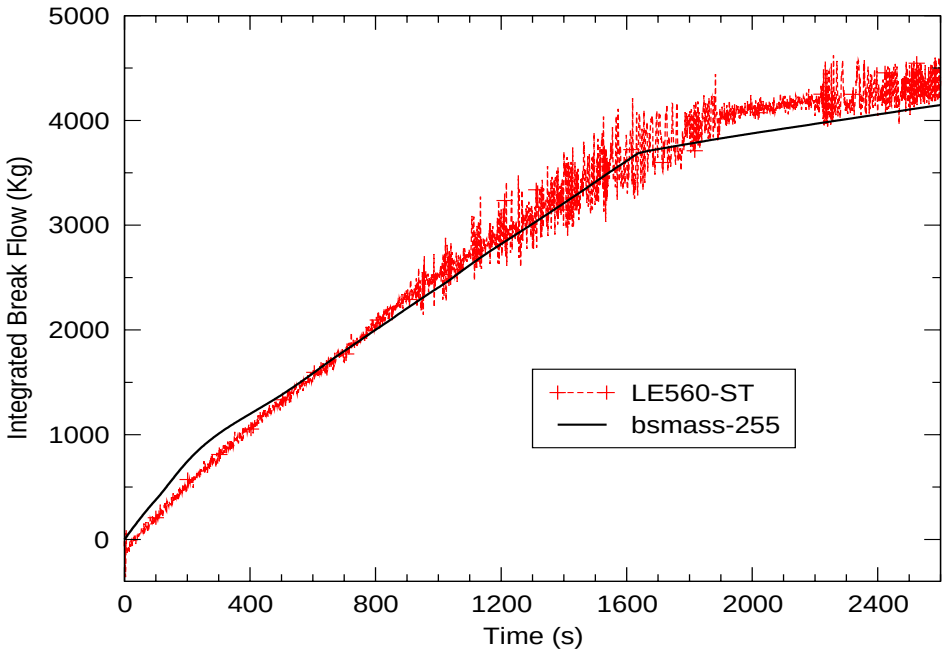

Figure C.5-142. Integrated Break Flow

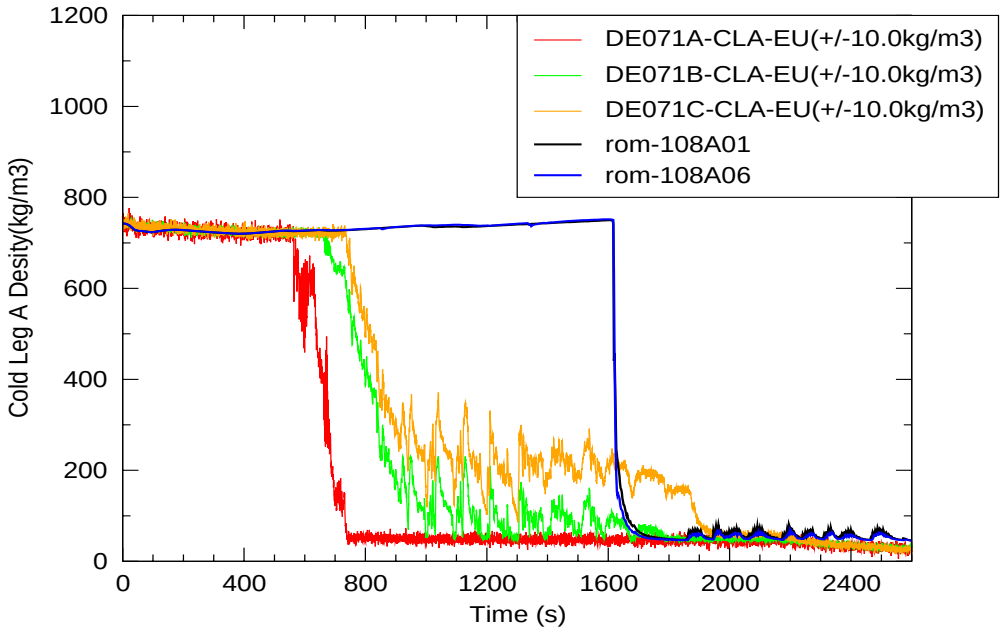

Figure C.5-143. Fluid Density in Loop-A Cold Leg

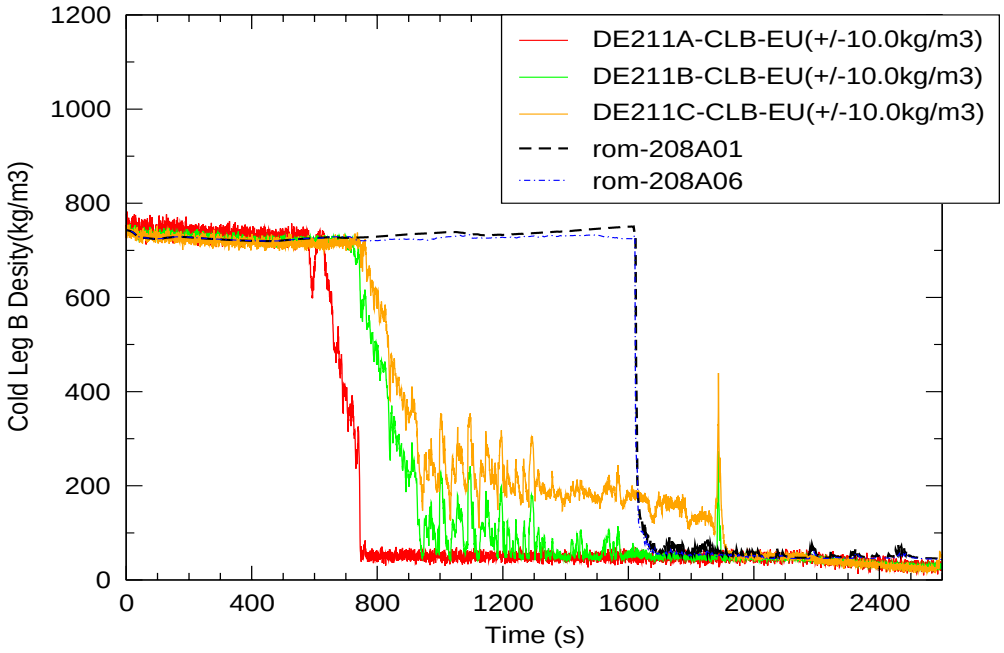

Figure C.5-144. Fluid Density in Loop-B Cold Leg

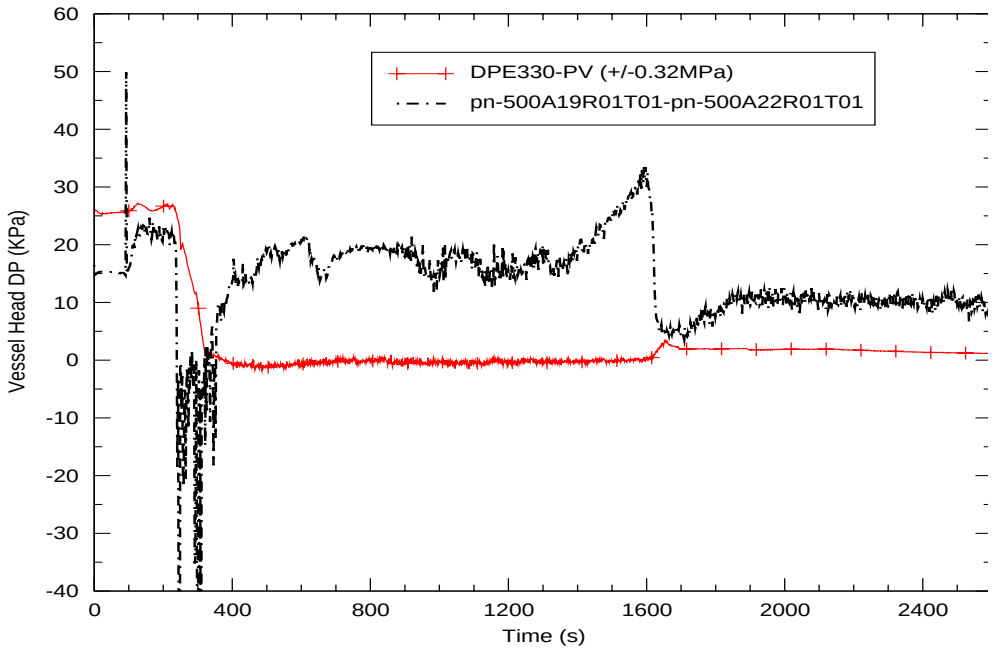

Figure C.5-145. Upper Head Differential Pressure

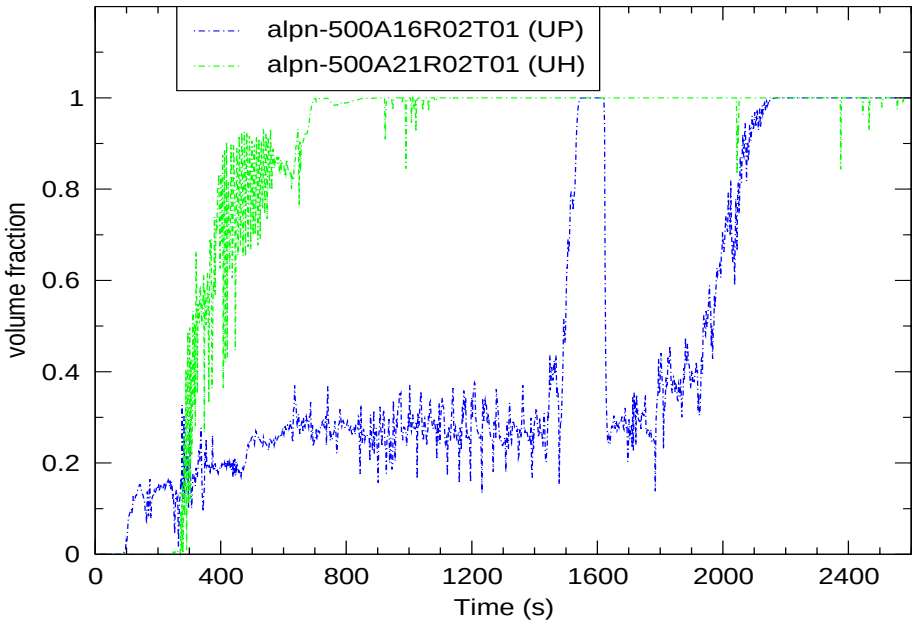

Figure C.5-146. Void Fraction in the Upper Plenum (UP) and Upper Head (UH)

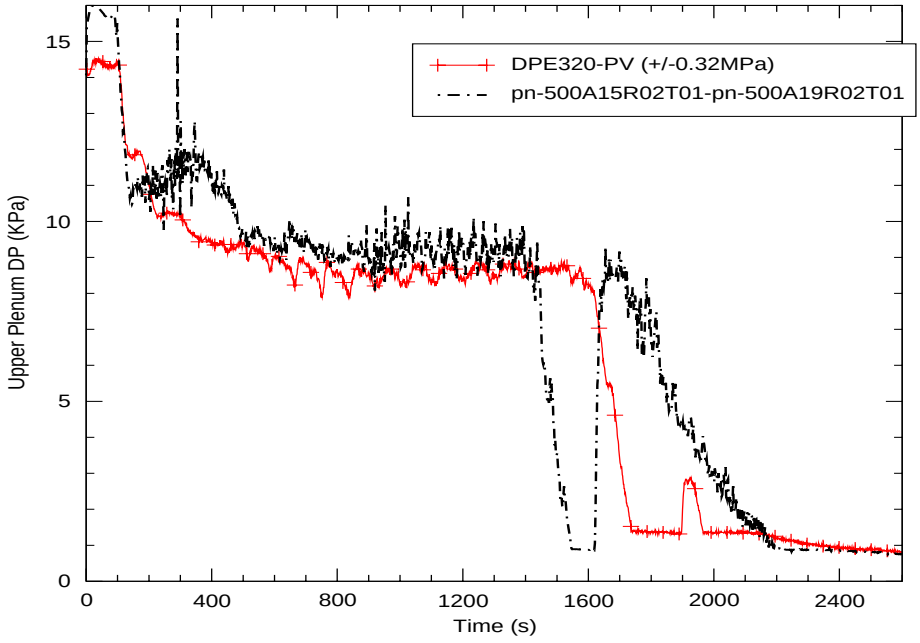

Figure C.5-147. Upper Plenum Differential Pressure

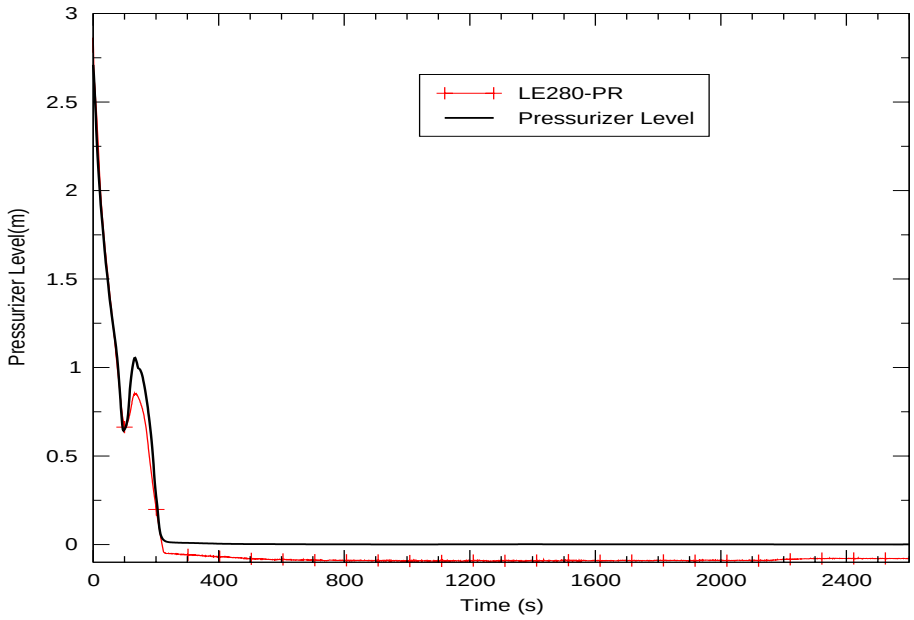

Figure C.5-148. Pressurizer Level

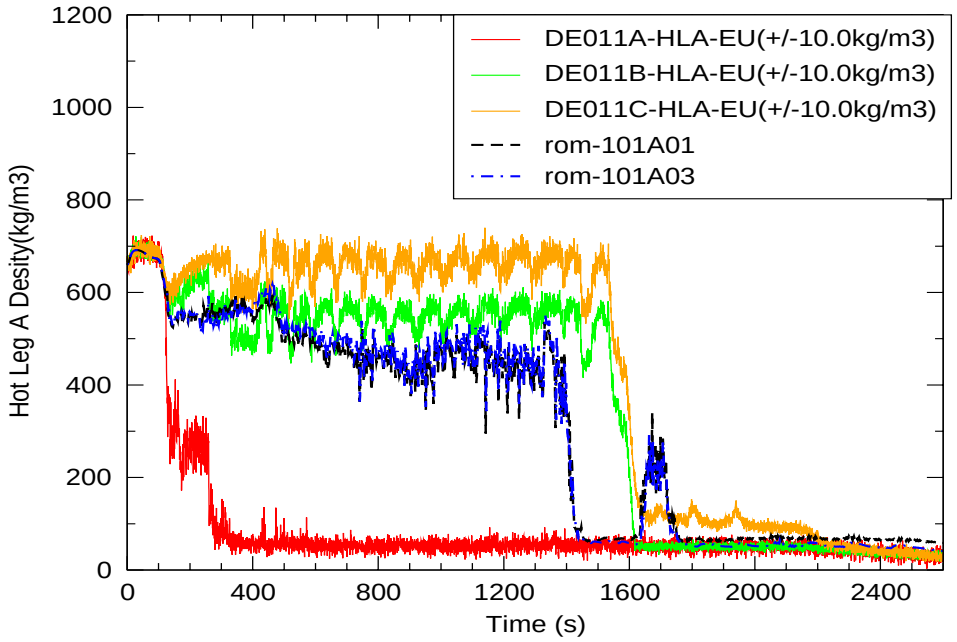

Figure C.5-149. Fluid Density in Loop-A Hot Leg

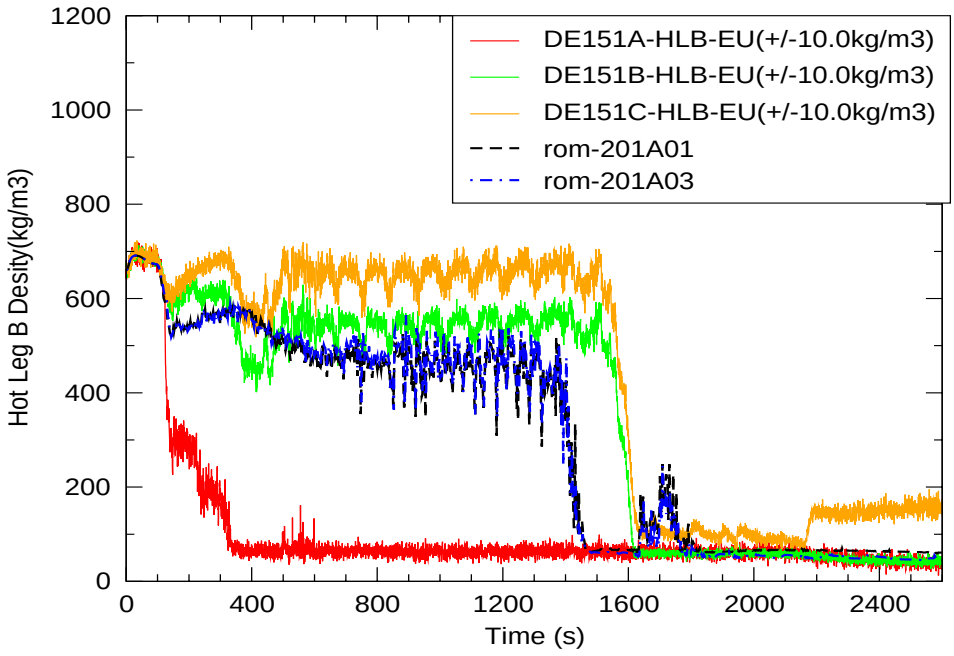

Figure C.5-150. Fluid Density in Loop-B Hot Leg

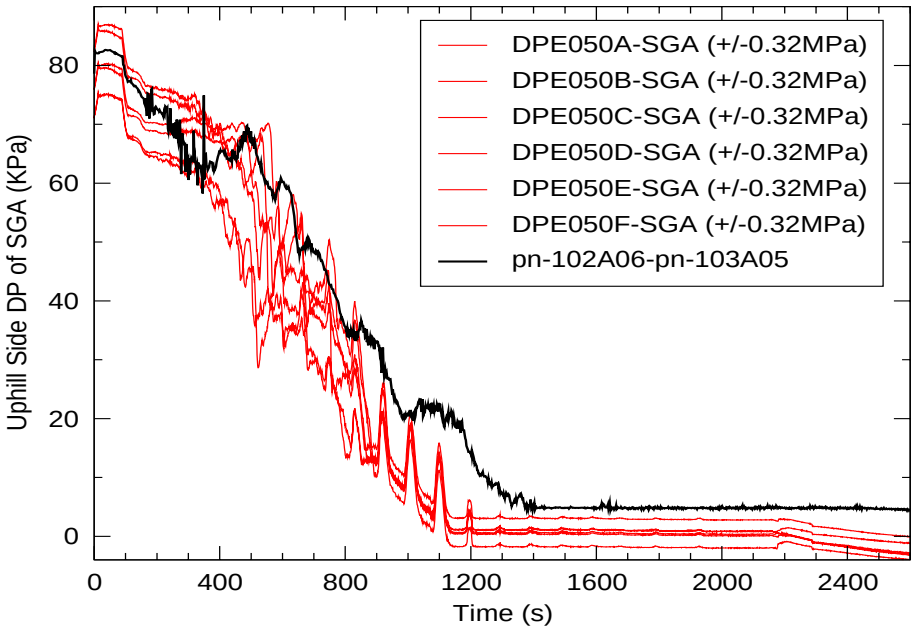

Figure C.5-151. Differential Pressure along uphill Side of Loop-A Steam Generator Tubes

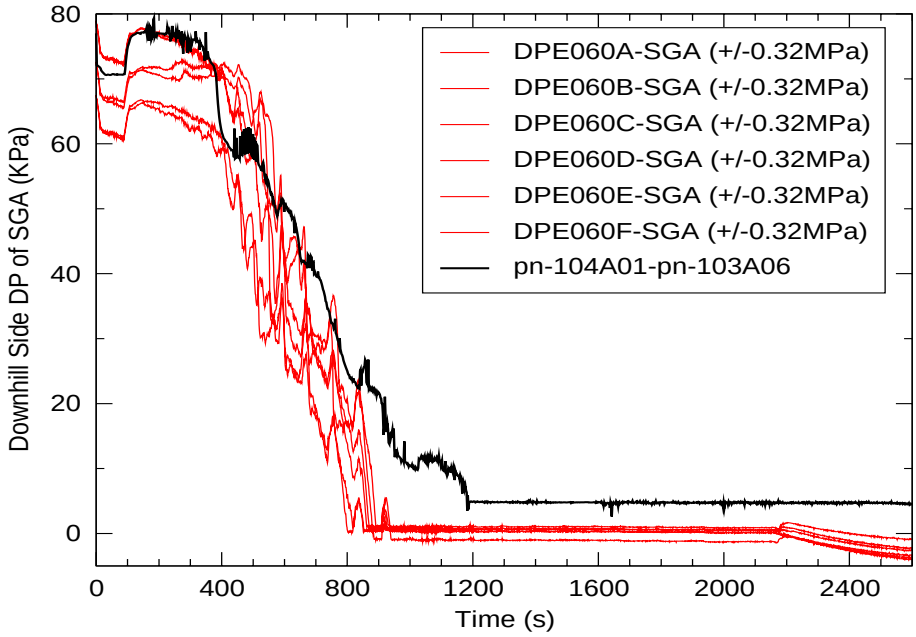

Figure C.5-152. Differential Pressure along downhill Side of Loop-A Steam Generator Tubes

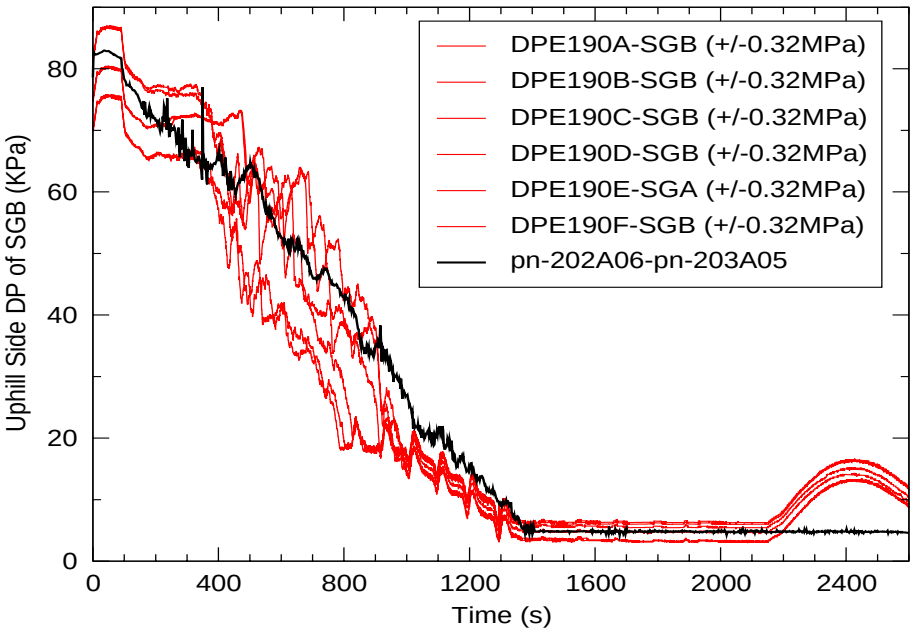

Figure C.5-153. Differential Pressure along uphill Side of Loop-B Steam Generator Tubes

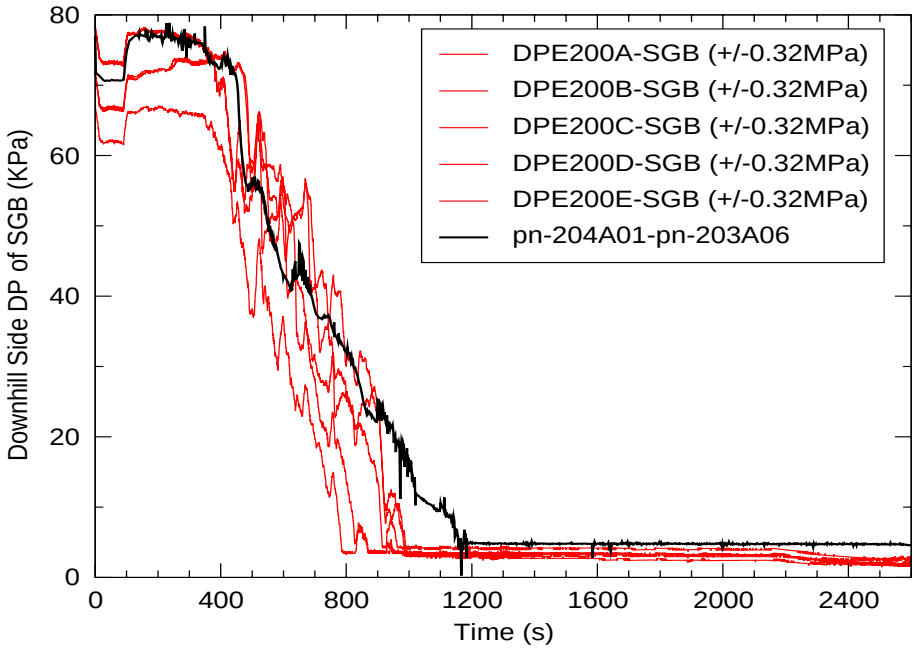

Figure C.5-154. Differential Pressure along downhill Side of Loop-B Steam Generator Tubes

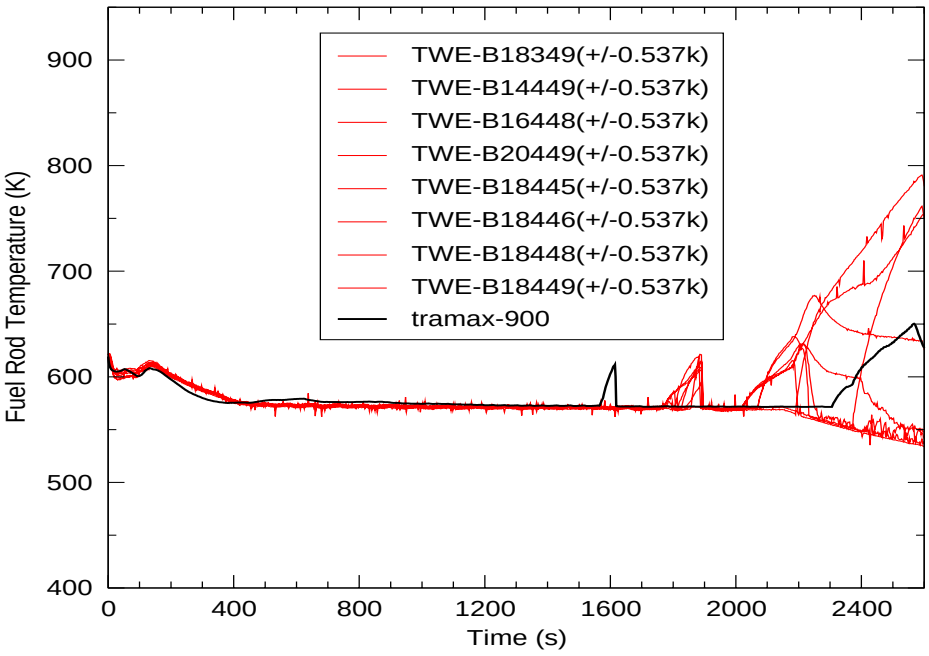

Figure C.5-155. Fuel Rod Temperature

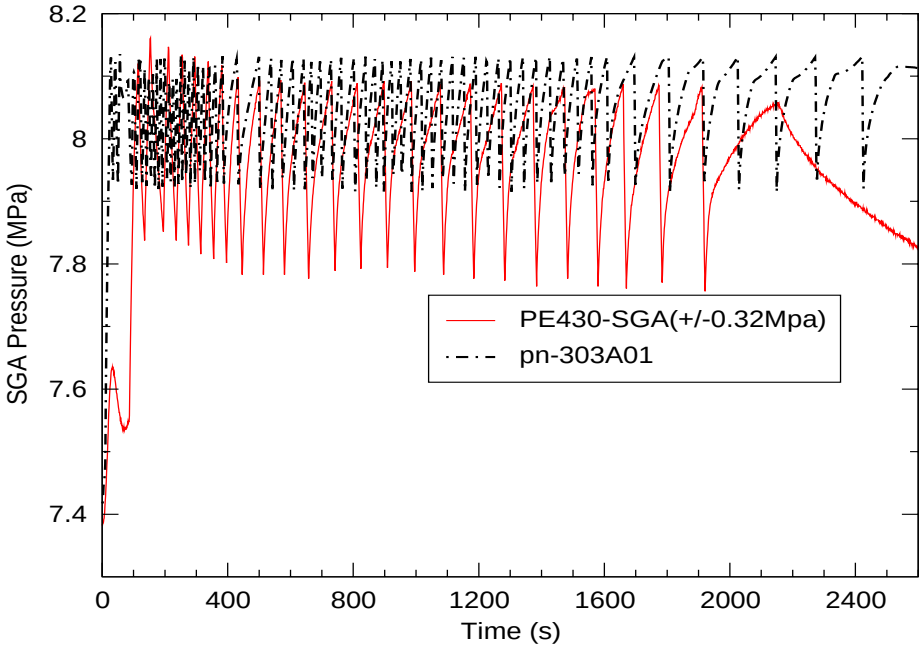

Figure C.5-156. Pressure in Loop-A Steam Generator

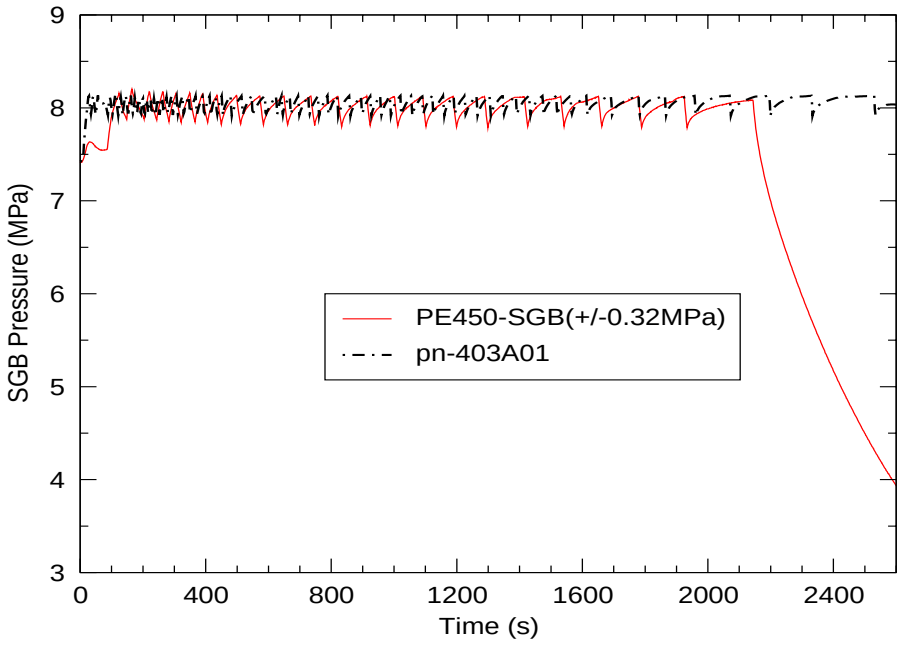

Figure C.5-157. Pressure in Loop-B Steam Generator

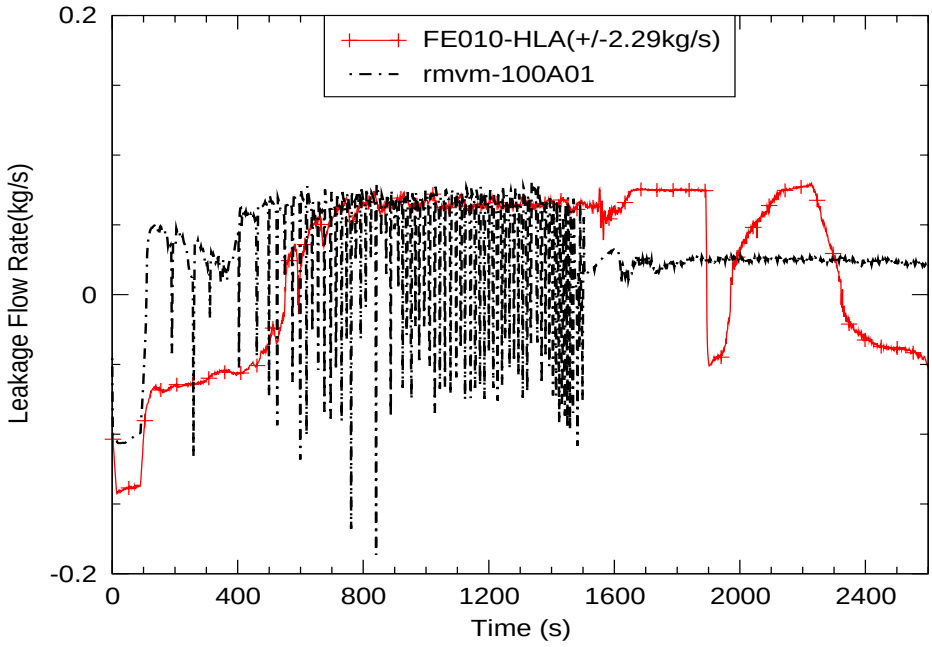

Figure C.5-158. Hot-Leg Bypass Leakage, Loop-A

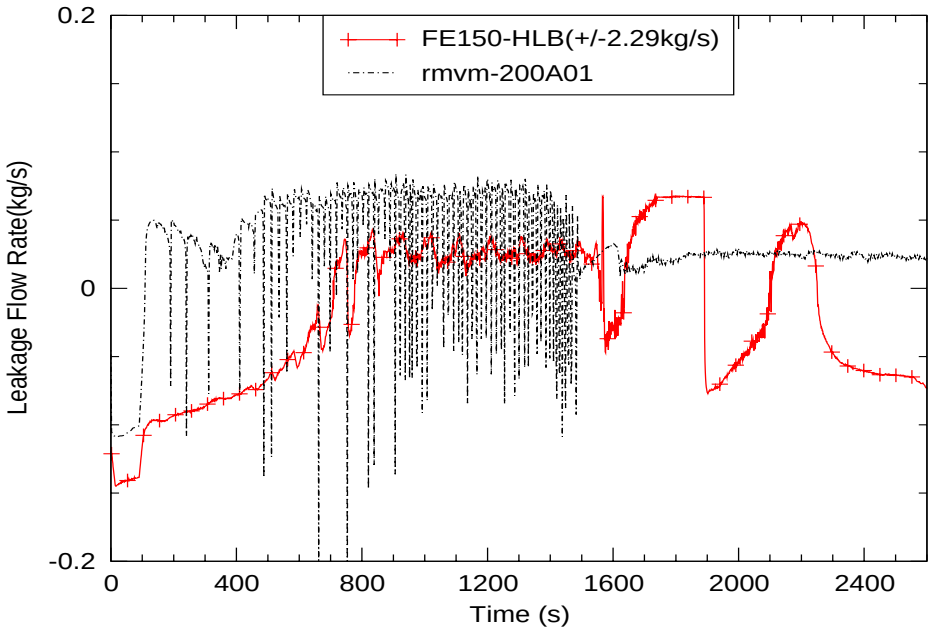

Figure C.5-159. Hot-Leg Bypass Leakage, Loop-B

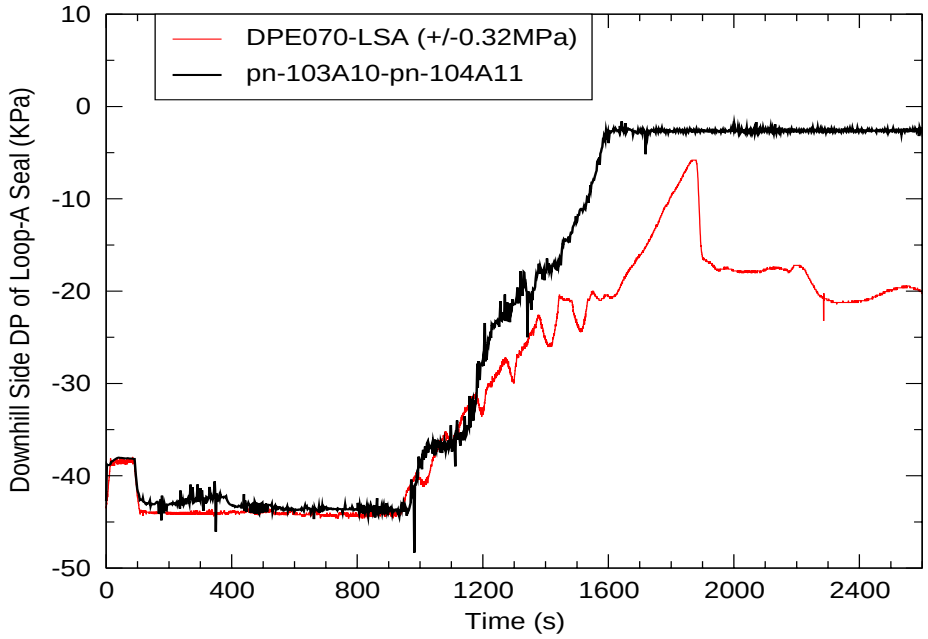

Figure C.5-160. Differential Pressure along downhill Side of Loop-A Seal

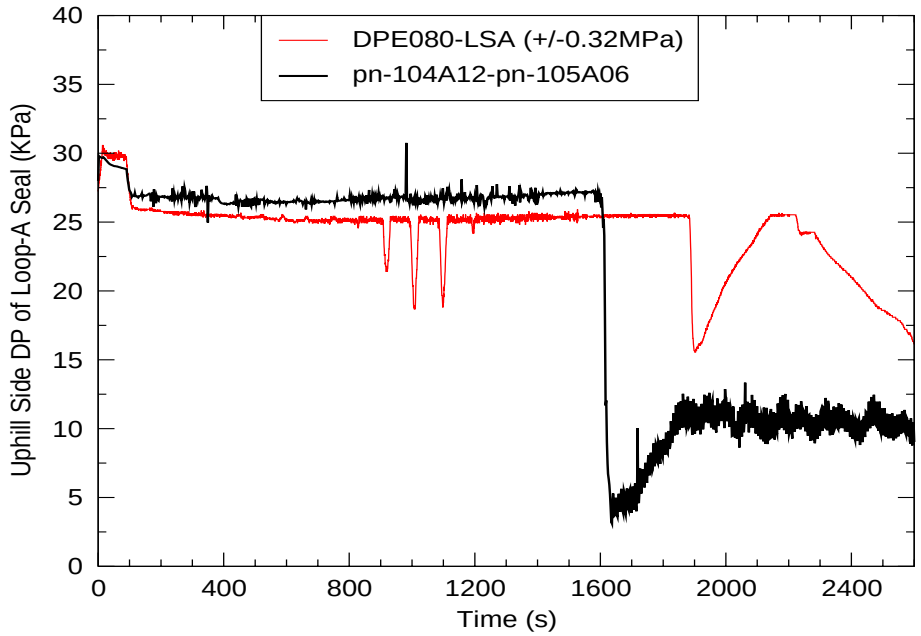

Figure C.5-161. Differential Pressure along uphill Side of Loop-A Seal

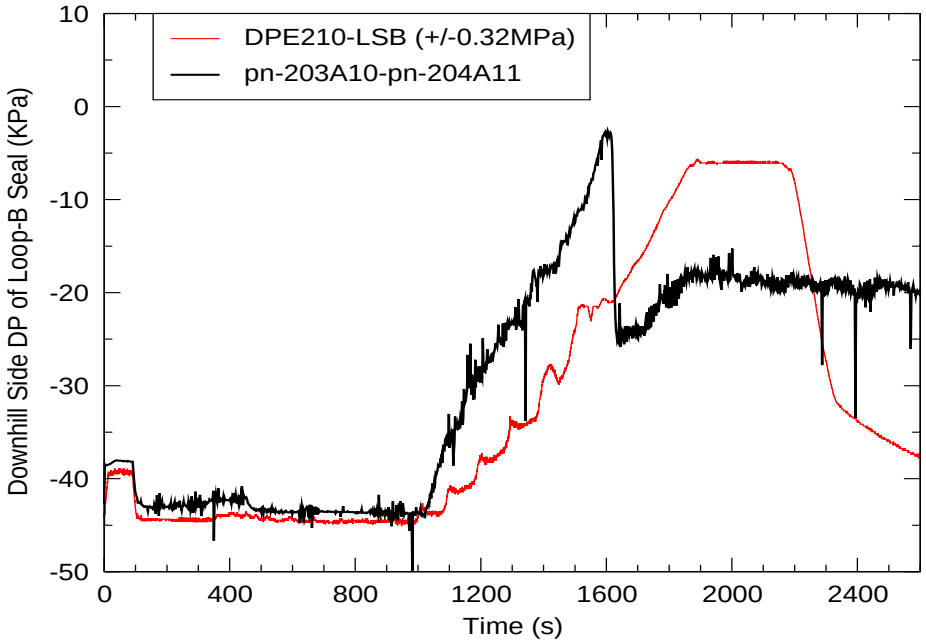

Figure C.5-162. Differential Pressure along downhill Side of Loop-B Seal

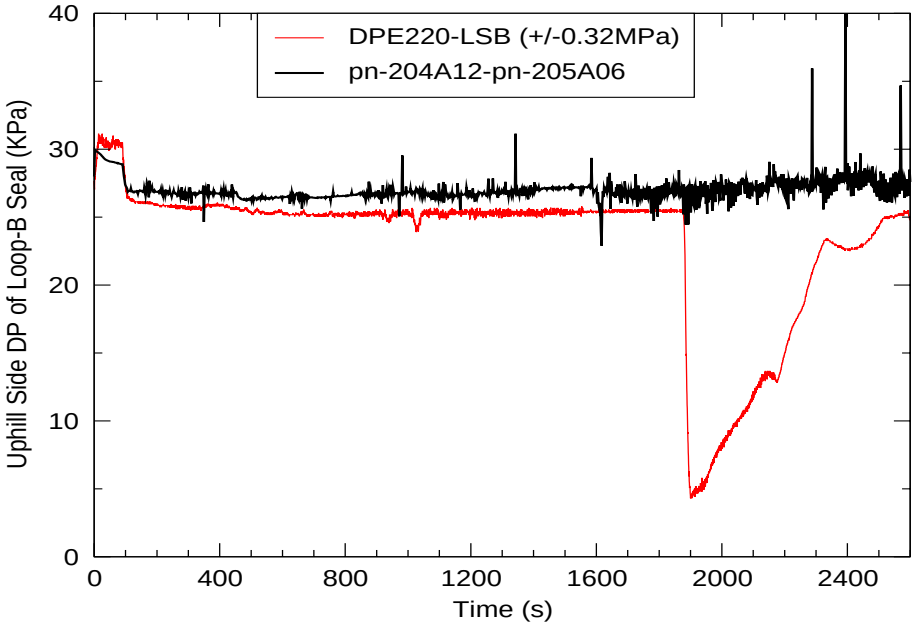

Figure C.5-163. Differential Pressure along uphill Side of Loop-B Seal

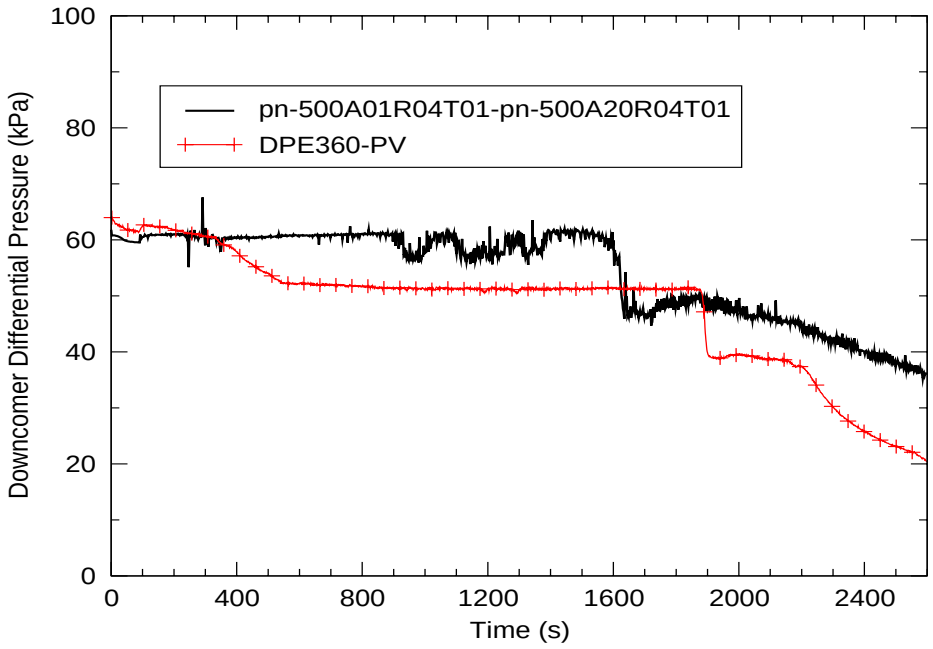

Figure C.5-164. Downcomer Differential Pressure

C.5.5.4.5. Conclusions

Table 5.3 of this report, as well as Reference 8 lists four criteria used in the code validation: *Excellent Agreement, Reasonable Agreement, Minimal Agreement, Insufficient Agreement*. *Reasonable agreement* is defined as:.

> "*Reasonable Agreement* applies when the code exhibits minor deficiencies. Overall, the code provides an acceptable prediction. All major trends and phenomena are predicted correctly. Differences between calculated values and data are greater than those deemed necessary for excellent agreement. The calculation will frequently lie outside but near the specified or inferred uncertainty bands of the data. However, the correct conclusions about trends and phenomena would be reached if the code were used in similar applications. The code models and/or facility model noding should be reviewed to see if improvements can be made."

Based on a PIRT-based analysis of each characteristic phase encountered during Test SB-CL-15, it is evident that the TRACE simulation results meet the definition of *Reasonable Agreement* for all highly-ranked phenomena throughout the course of the transient.

Reasonable agreement was obtained in spite of the following discrepancies:

1. Core predicted to uncover approximately 350 seconds too early
2. Predicted pressure following blowdown phase is higher than the data

3. Hot leg-to-downcomer bypass flow reverses direction too early
4. Unlike the data, liquid holdup is predicted to occur in SGA during natural circulation phase.
5. Predicted behavior in LSA and LSB appear to corresponding with the opposite loop-seal data channels: the LSA prediction is similar to the LSB data and the LSB prediction is similar to the LSA data.

All of these items are indicative of inaccuracies in the input model, not code deficiencies.

C.5.5.5. Simulation of SB-CL-16

SB-CL-16 case is a 0.5% cold leg break test. The break unit is located at the top of the cold leg in Loop B. Two input decks were developed for the transient analysis: one constrained steady-state (CSS) input deck and one transient input deck. The CSS deck contains most of the model information and plant control procedures. The CSS input deck is used to obtain initial plant conditions for transient calculations.

The control system and control procedures of the ROSA-IV facility were designed to accommodate a wide range of plant operational transients and accident scenarios. The TRACE control procedure was derived from a series of SBLOCA tests.

SB-CL-16 test conditions and control actions implemented in the TRACE transient analysis are listed here.

C.5.5.5.1. SB-CL-16 Test Conditions

Some of the test conditions or control procedures were different from those in the reference PWR reactor. Special control procedures or test conditions were designed to account for some scaling issues in the design of the test facility (Refs.1, 7).

The plant initial conditions are summarized in Table C.5.3. In the test, it was assumed that a loss-of-offsite power occurred coincident with reactor scram. In addition, coincident failures were assumed failing the high pressure charging system, HPSI, and auxiliary feedwater system. Table C.5.18 summarizes the operational setpoints for Run SB-CL-16. Table C.5.19 gives the event sequence recorded by the facility instrumentation system. Some specific information is given below for individual items.

- Coolant pumps

Upon the initiation of the break, the pump speed was increased before the pump started to coast down following the reactor scram signal (Ref. 7). The pump impeller rotation speed after break is

shown in Figure C.5-165 and Figure C.5-166. The dashed line is the pump curve obtained in the TRACE simulation of SB-CL-16. The solid line is the measured pump curve in the SB-CL-16 test. The simulated pump speed follow the pump curve from the steady-state condition which could not match the test data.

- Reactor trip and core power after break

As indicated in Table C.5.19, the reactor was tripped 84 seconds after the break was initiated. Two power curves are shown in Figure C.5-167. The solid line is the measured power curve in the SB-CL-16 test. The dashed line is the power curve obtained in the transient simulation. The simulation reactor trip was delayed due to slower depressurization. It took longer time to reach the reactor trip setpoint in the simulation.

- Emergency Core Cooling System (ECCS)

During the SB-CL-16 transient, there was no automatic actuation of the ECCS systems. The operator actuated the high-pressure charging and HPSI systems manually as a part of the recovery procedure. In ROSA-IV, the ECCS subsystems injected water into each loop through the same loop nozzle (Figure C.5-2). Figure C.5-168 shows the calculated ECCS injection flow rate into each loop, which is the sum of the injection flow of the ECCS subsystems (high pressure charging and high pressure injection).

- Auxiliary Feedwater System

In SB-CL-16, the auxiliary feedwater was assumed failed for both steam generators.

- Pressurizer heaters

Based on the test data, power supply to the pressurizer heaters was cut off with the initiation of the reactor trip, which was 84 seconds after the break initiation.

C.5.5.5.2. TRACE Control Procedure

Using the strategy outlined at the beginning of this chapter, the control procedure for the TRACE model is simplified. As a result, the TRACE control procedure mainly consists of a number of trips**.** In general, a trip is either initiated by time or by the system pressure. Specifically:

At time 0, the break is initiated and the pressurizer heater power is cut off after a 75 seconds delay.

The pump speed is increased after the break and coasts down with the reactor trip as shown in Figure C.5-165 and Figure C.5-166.

The reactor is tripped when the system pressure reaches 12.97 MPa. Figure C.5-167 shows the measured power curve after the break and the power curve obtained from the transient calculation.

The Safety Injection (SI) signal is generated as the system pressure reaches 12.27 MPa. The Emergency Core Cooling System (ECCS) was actuated manually at 2558 seconds. The HPSI/ LPSI systems were simply modeled as boundary conditions.

Main steam line valve closure and main feedwater cutoff are initiated with proper time delays following the reactor trip.

Table C.5.18. Operational Setpoints for Run SB-CL-16

	Setpoint
Reactor scram signal	12.97 MPa (system pressure)
Pump coast down	With reactor scram
Safety injection (SI) signal	12.27 MPa (system pressure)
High pressure charging ON	2558 seconds (part of recovery)
High pressure safety injection ON	2558 seconds (part of recovery)
Accumulator injection	4.51 MPa
Low pressure injection	1.29 MPa
Main feedwater cutoff	With reactor scram
Turbine throttle valve closure	With reactor scram
Auxiliary feedwater initiation	Assumed failed

Table C.5.19. Chronology of Events for Run SB-CL-16

Events	Time (s)
Break	0
Main steam line valve closure	80
SG Feedwater stop	80
Reactor trip	84
Reactor coolant pump stop	341
Core uncovery	1750~1950
Loop seal clearing	1895
High pressure charging injection ON	2558
High pressure safety injection ON	2558
Primary/Secondary pressure reversal	2652
Experiment terminated	2800

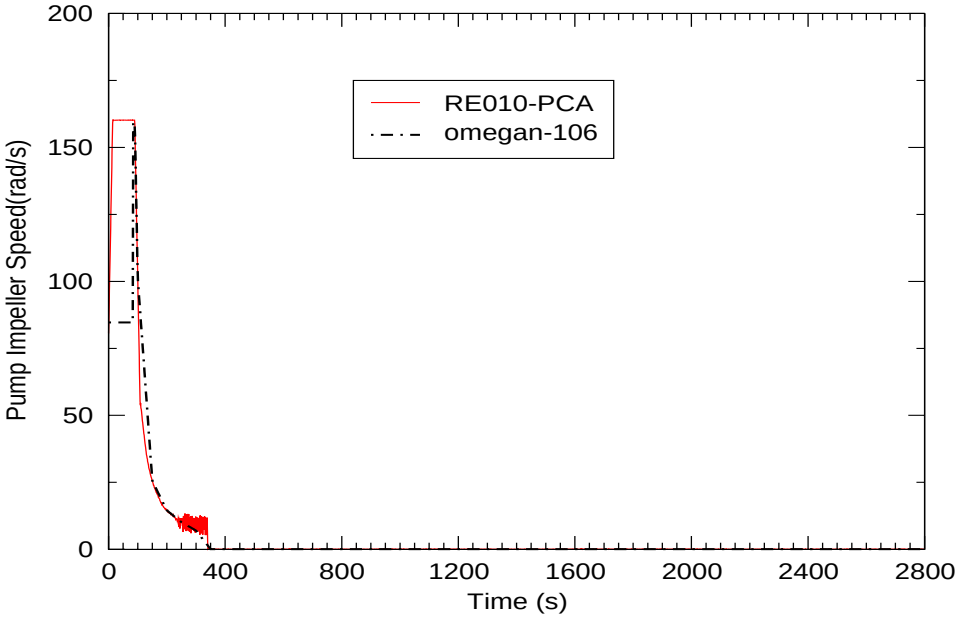

Figure C.5-165. Pump A Impeller Speed After Break

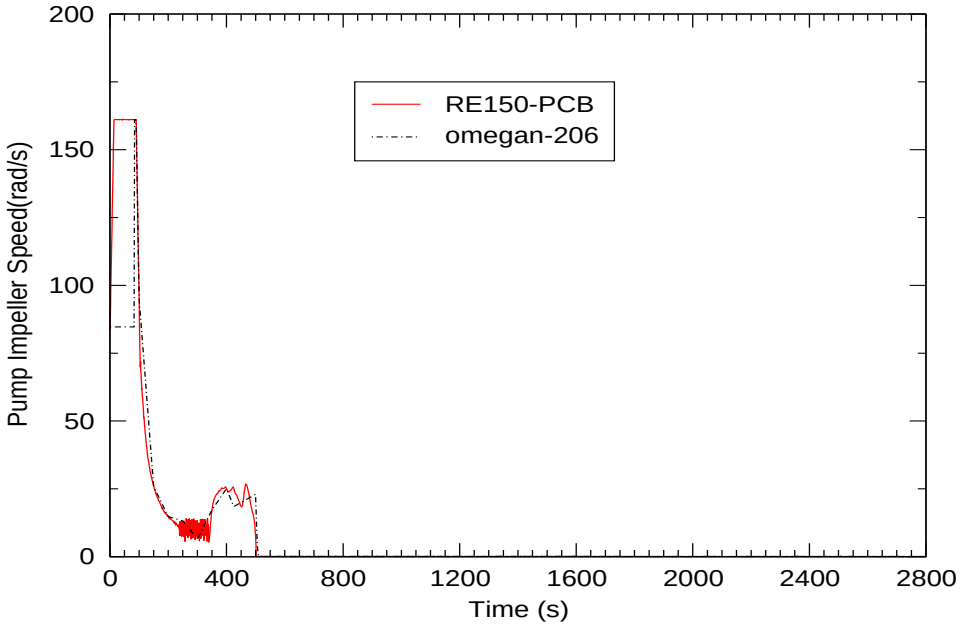

Figure C.5-166. Pump B Impeller Speed After Break

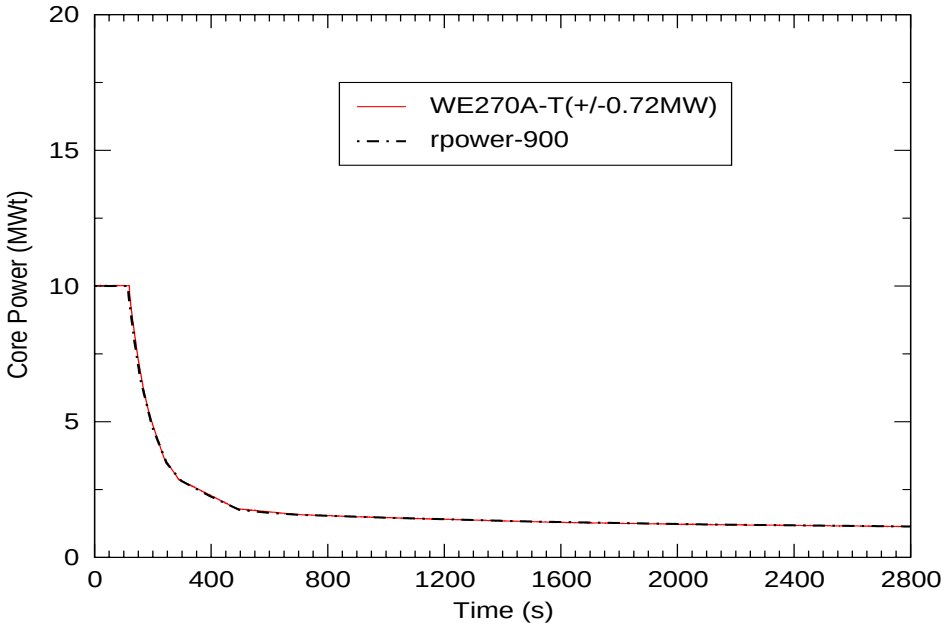

Figure C.5-167. Core Power after Break

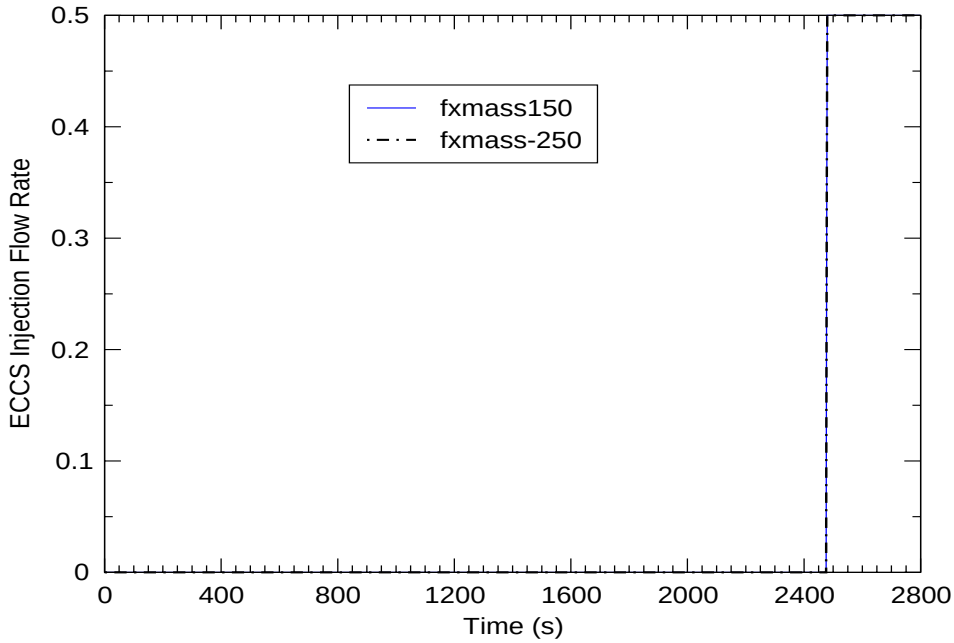

Figure C.5-168. ECCS Injection Flowrates for Loop A and Loop B

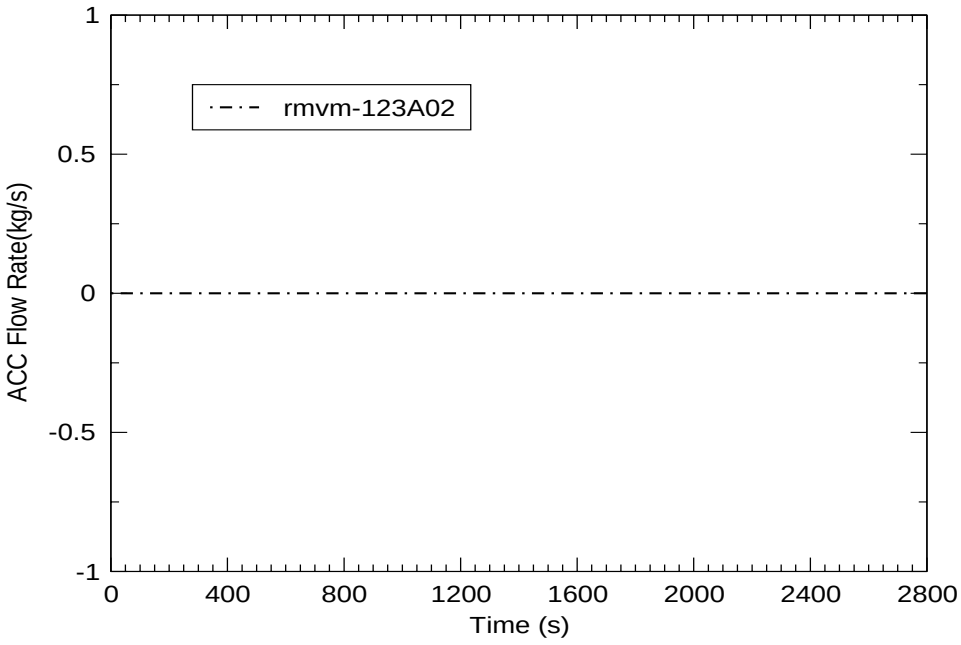

Figure C.5-169. Accumulator Injection Flow to Cold Leg A

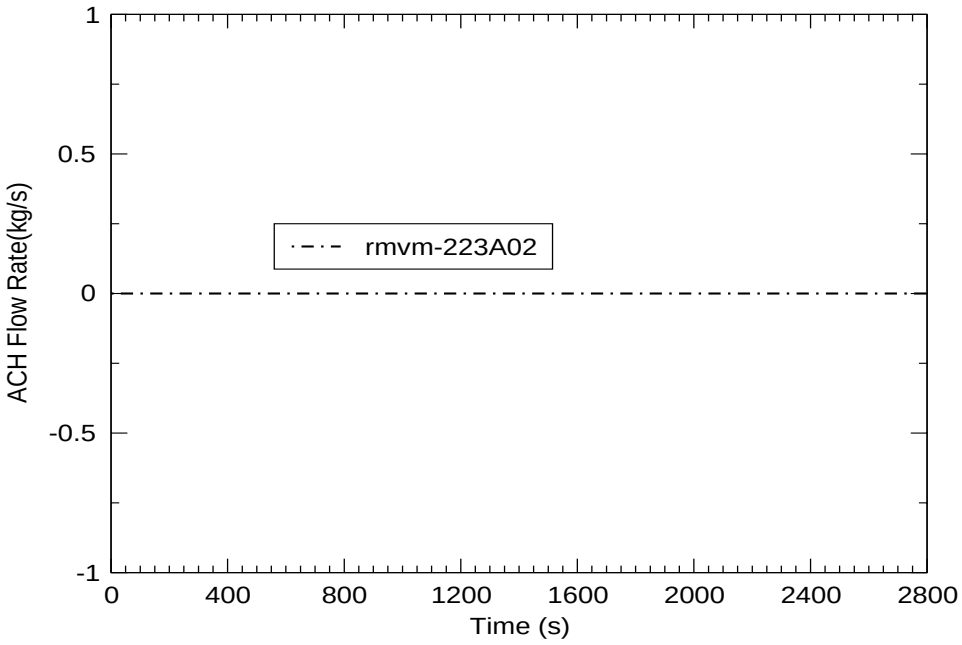

Figure C.5-170. Accumulator Injection Flow to Cold Leg B

C.5.5.5.3. Experimental Observations

The main objective of the test SB-CL-16 was to investigate the thermal-hydraulic mechanisms of early core uncovery and heatup. Early core uncovery may be caused by a manometric effect resulting from an imbalance between the water hold up in the upflow and downflow sections of the steam generator U-tubes (Ref. 7). Table C.5.20 lists the event sequence recorded by the facility's instrumentation system during the test.

After the SBLOCA transient started, the primary pressure started to drop and the core power decay curve was initiated at a pressurizer pressure of 12.97 MPa together with the closing of the MSIV, starting of the programmed pump speed curve, and termination of the main feedwater to the steam generators.

The safety injection signal occurred at 12.27 MPa. However, the high-pressure charging and HPSI systems were assumed failed. Auxiliary feedwater was also not available in this event.

The primary system depressurization became slower after pressure reached about 8 MPa since the secondary pressure was kept about 8 MPa. The primary pressure remained at about 8 MPa through out the experiment and started to decrease when the core power was tripped off to terminate the experiment.

Both loops experienced loop seal clearing at about 1890 seconds, which led to core liquid level recovery. The coolant boil-off period started shortly after, since no ECCS coolant was injected.

C.5.5.5.4. Transient Analysis

The SB-CL-16 transient analysis was performed for 2800 seconds. The transient simulation results and comparison to the test data are presented in Figure C.5-165 to Figure C.5-199. In these figures, the test data are plotted in colored lines with symbols and the calculation results are plotted in the black or blue solid lines without symbols.

C.5.5.5.4.1. System Behavior

The overall primary system behavior determines the boundary conditions of the transient event since most of the control signals are based on the system pressure setpoints. The predicted system pressure is higher than the test data from 75 - 550 seconds as shown in Figure C.5-171. Therefore, the sequence of the events which are based on the system pressure setpoints is delayed in comparison to the test data.

Table C.5.20 shows comparison of the sequence of the event for SB-CL-16 simulation results and the test data.

Table C.5.20. Sequence of the Event Comparison for SB-CL-16 Test

Event	Test Data Time (sec)	TRACE Model Time (sec)
Break	0	0[a]
Main Steam Line Valve close	80	80
SG Feedwater stop	80	80
Reactor trip	84	80
Reactor Coolant Pumps (PC-A/B) stop	341	340
First core uncovery	1750-1950	1450-1580
Loop seal clearing (Loop A)[b]	1896	1575
Loop seal clearing (Loop B)[b]	1895	Not Cleared
Primary/Secondary pressure reversal	2145	2500
Second core uncovery	2250-2550	2150-2510
High Pressure Charging Injection	2558	2558
High Pressure Safety Injection	2558	2558
End time	2800	2800

a: The break starts at time 0.

b. The beginning of loop-seal clearance is the time at which the differential pressure across the uphill portion of the loop seal begins to rapidly descend toward zero.

C.5.5.5.4.2. Analysis Results

As discussed in **Section C.5.5.**, the PIRT (Ref. 6) identifies the high ranked phenomena for each phase of the transient. To evaluate the performance of TRACE, each phase will be discussed separately, and the TRACE-simulation results for the highly-ranked phenomena will be compared to the data. The principal Figure of Merit (FOM) of the transient event is the core collapsed liquid level (CCL). The core collapsed level is measured as the core differential pressure as demonstrated in Figure C.5-172.

Certain input parameters, such as decay heat, core power, and feedwater temperature, are taken directly from the test data as boundary conditions. Therefore, although they are identified as important in some of the phases, they will not be discussed in terms of code performance.

Blowdown phase

The blowdown phase is marked by a rapid depressurization of the primary coolant system until the hot coolant begins to flash into steam. The rate of depressurization is strongly influenced by the rate and enthalpy of the break flow, and it changes when flashing and boiling start in the core. In this phase, the most important parameters defining the evolution of the transient are decay heat, primary side heat transfer, critical break flow, and the flow regime upsteam of the break flow.

In the test, the blowdown phase lasted from 0 to 450 seconds. Throughout this time, the simulation results follow the general trends of the data, but several discrepancies are noted which have an affect in the later phases of the transient. The calculated pressurizer pressure in Figure C.5-171 is shown to be slightly under-predicted throughout most of the phase, but at around 400 seconds, the pressure settles at a value approximately 0.5 MPa higher than the data. For the core DP, the prediction shown in Figure C.5-172 is about 10 kPa less than the data at the start of the transient, but it comes into agreement with the data when the reactor SCRAMS at around 80 seconds. Good agreement is also shown in terms of primary-side heat transfer, which can be seen in Figure C.5-173 through Figure C.5-176. These figures show comparisons of the fluid temperatures in the SG tubes and the cold legs, respectively. As for critical break flow and the flow regime upstream of the break, Figure C.5-177 shows a slight over-prediction in break flow, but overall, the agreement is reasonable. The density of the fluid in the cold legs is evaluated to determine the flow regime upstream of the break. Figure C.5-178 and Figure C.5-179 show densitometer readings taken at three locations over the cross-sections of the cold legs. These figures show excellent agreement between the simulation and the data.

Other key results are the DPs in the vessel head and upper plenum, the pressurizer level, and the flow regime in the hot legs. Figure C.5-180 shows the vessel-head DP. Here, the depressurization can be observed, but unlike the data, the code is predicting large negative pressure oscillations. These oscillations appear to be due to the oscillations in upper-head void fraction seen in Figure C.5-181 This erratic behavior is not seen in the calculated upper-plenum DP shown in Figure C.5-182, where there is reasonable agreement with the data.

Figure C.5-183 shows good agreement between the calculated and measured pressurizer levels. The only apparent difference is the over-prediction of the degree of voiding in the SG-tube U-bend. This flow resistance halts the decent of the pressure at around 100 seconds, causing the temporary level increase to be more pronounced.

The flow regimes in the hot legs are evaluated in terms of hot-leg fluid density. Figure C.5-184 and Figure C.5-185 both show that the code is predicting mixture densities that fall within the range of the densitometer readings.

Natural Circulation phase

The natural-circulation phase begins at the end of the pump coastdown and ends when the buoyant forces caused by differences in loop-fluid densities are no longer able to overcome the flow resistance of the loop components. In the experiment, the natural-circulation phase is the longest lasting phase of the transient, spanning from 451 seconds to around 1890 seconds. The measurable highly-ranked processes in this phase are the FOM, decay heat, the counter-current flow in the upper-plenum region, and critical break flow, and break upstream flow regime.

Throughout most of this phase, the calculated pressure is in reasonable agreement with the data. The most notable discrepancy, however, is the early termination of the natural circulation phase (Figure C.5-172); at around 1500 seconds, the loop seals begin to clear approximately 300

seconds too early. This discrepancy is caused by the difference between the predicted and measured primary-system pressures shown in Figure C.5-171.

The presence of counter-current flow or counter-current flow limiting (CCFL) in the upper plenum is evaluated by looking at the upper plenum DP. Figure C.5-182 continues to show reasonable agreement between the prediction and the data during this phase, implying that the steaming rates, which are produced by the prescribed decay heat boundary condition, are leading to accurate predictions of void fraction and counter current flow in the upper plenum.

As for break flow and the flow regime upstream of the break, Figure C.5-177 shows the predicted break flow in good agreement with the data. However, the cold-leg density comparisons in Figure C.5-178 and Figure C.5-179 show evidence of the early core-level depression. Vapor is predicted to reach the colds leg much sooner than the data. This is another result of the discrepancy in primary-system pressure discuss earlier.

Other parameters of interest during this phase are U-bend voiding, fuel rod temperature, and secondary-side pressure. Voiding in the U-bends of the SG tubes, which is indicative of the state of primary-side heat transfer, can be evaluated in terms of SG tube DP. Figure C.5-186 through Figure C.5-189 show the SG-tube DPs along the uphill and downhill sides of each set of SG-tubes. Throughout the first 900 seconds in the transient, these figures show good agreement between the simulation and the data. After 900 seconds, more liquid is predicted to remain in the uphill and downhill sides of SGA and in the downhill side of SGB than in the data.

Figure C.5-190 shows the progression of the fuel temperature over the natural circulation phase. The fuel heatup is predicted to occur prematurely because of the early prediction of core-level depression. However, the magnitude of the heatup is commiserate with the data.

The shell-side SG pressures are shown in Figure C.5-191 and Figure C.5-192. These figures show good agreement between the code and the data. The only discrepancy is the cycling frequency of the valves.

Loop Seal Clearing phase

The loop seal clearing phase begins when the trapped primary-side steam volume reaches the top of the loop seal piping. From this point, the steam volume depresses the liquid in the downhill side of the loop seal and in the core until a minimum core level is reached. As steam moves through the seal to the break plane, the liquid it displaces is forced into the core, quenching the heatup caused by the drop in core level. In the test, this sequence of events occurred between 1891 and 1900 seconds.

The highly ranked processes, relevant to this phase, that will be discussed are listed as follows:

1. Decay heat
2. Mixture level in the core region

3. Hot-leg downcomer gap flow
4. SG primary-side heat transfer in the U-tubes
5. SG primary-side flow resistance
6. SG primary-side tube voiding
7. Horizontal stratification in the cold leg
8. Critical break flow

As stated previously, discrepancies in predicting the evolution of the primary-system pressure leads to the loop seals clearing too early. Therefore, between 1890 and 1900 seconds, Figure C.5-172 shows the core level already recovered and holding relatively steady.

Figure C.5-193 and Figure C.5-194 show the calculated leakage flows from both hot legs, respectively. Though similar in magnitude, the predicted leakage flow is extremely oscillatory.

Heat transfer, voiding, and flow resistance in the SG tubes is evaluated using the DP predictions shown in Figure C.5-186 through Figure C.5-189. In these figures, the predictions match the downward trend of the data quite reasonably.

Figure C.5-195 through Figure C.5-198 show the DP comparisons along the uphill and downhill sides of the loop seals. The uphill portion of the loop seals includes the pump suction piping. These figures show the simulated loop seals clearing early. As expected the point at which the loop seals begin to clear is approximately 300 seconds sooner than the data.

During this phase, the break flow changes from single-phase liquid to two-phase mixture. In Figure C.5-177, this transition is predicted to occur approximately 300 seconds.

Boil Off phase

As the transient proceeds, the primary system continues to loose inventory and the core inventory continues to boil. During the test, this boil-off phase lasted from 1901 to 2558 seconds. The highly-ranked processes in this phase are listed below:

1. Fuel Decay heat and local power
2. Mixture level in the core
3. Horizontal stratification and condensation in the cold leg
4. Downcomer mixture level
5. Critical break flow

At this stage in the transient, the behavior of the most important parameters is mostly a continuation of the previous phase. Exceptions are the mixture level in the core, downcomer DP, and fuel temperature.

Early core-level depression notwithstanding, the predicted core DP (Figure C.5-172) follows the trend of the data. After the loop seals clear, the level in the core is maintained for several hundred seconds before the core again begins to uncover. ECCS injects after this second core uncovery.

In terms of downcomer level (Figure C.5-199), the primary discrepancy appears to be the unpredicted decrease in level that occurs in the previous phase; the level stays relatively constant until the loop seals begin to clear.

As seen in Figure C.5-177, the final fuel heatup is delayed with respect to the data. This delay occurs because of the delay in falling core level mentioned earlier.

Core Recovery phase

The core recovery phase started at 2558 seconds when the operator actuated the high-pressure charging system and HPSI to cool down the system and prevent overheating of the rods. Both the simulation results and the test data show the core recovery and the decrease of the fuel rod temperature after the ECCS injection.

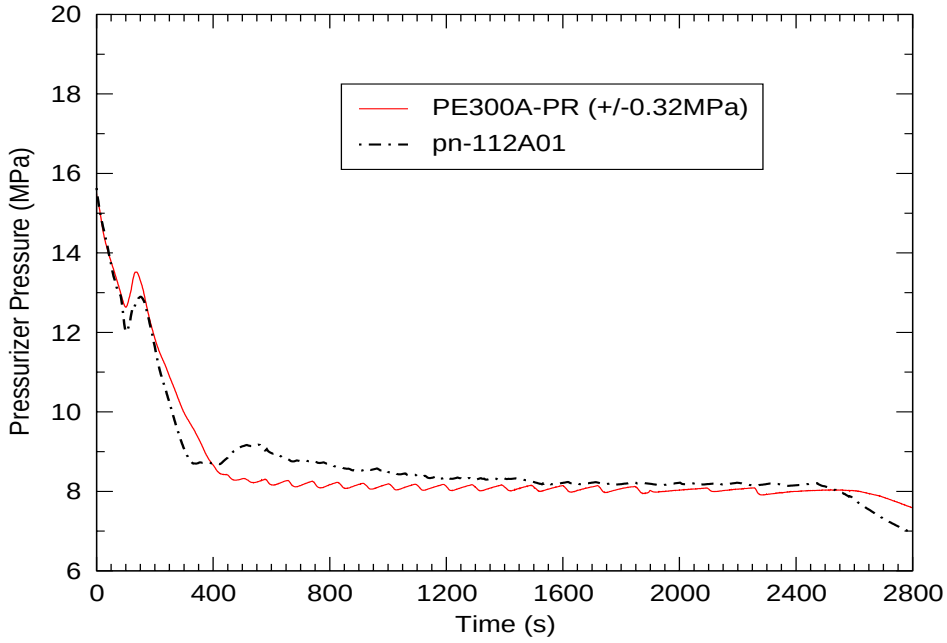

Figure C.5-171. Pressurizer Pressure

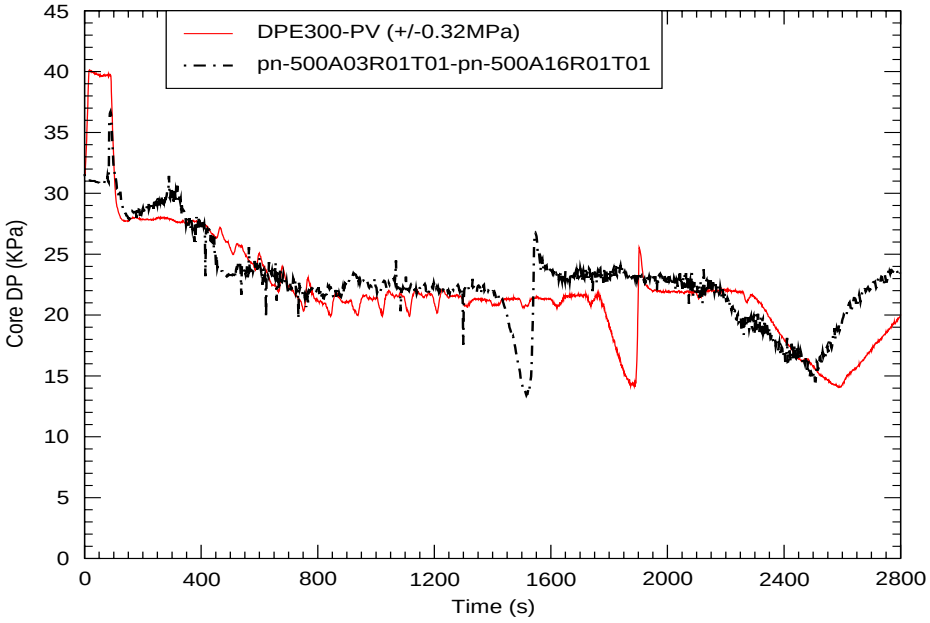

Figure C.5-172. Core Differential Pressure

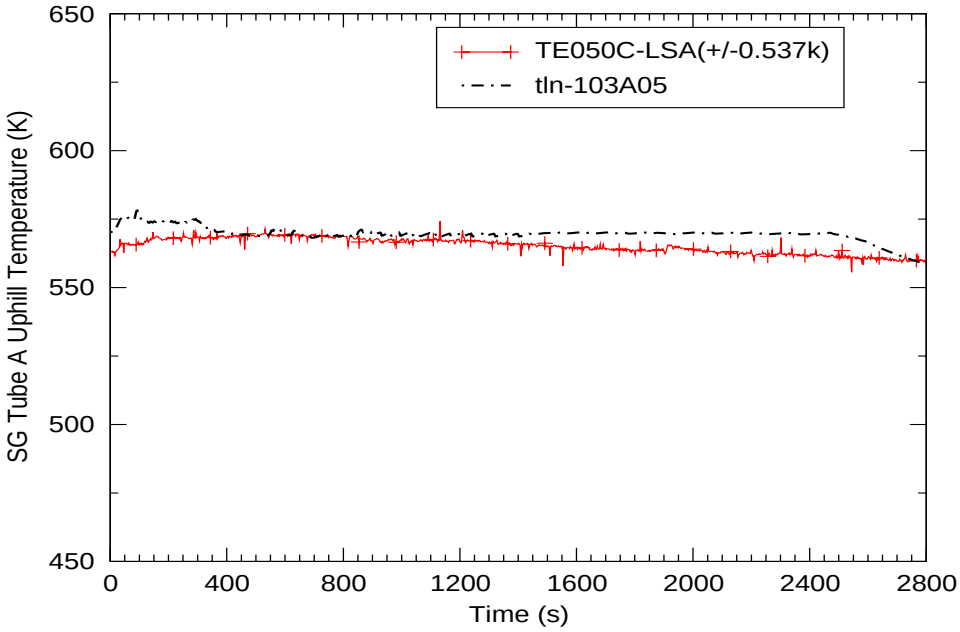

Figure C.5-173. Fluid Temperature in uphill Side of Loop-A Steam Generator

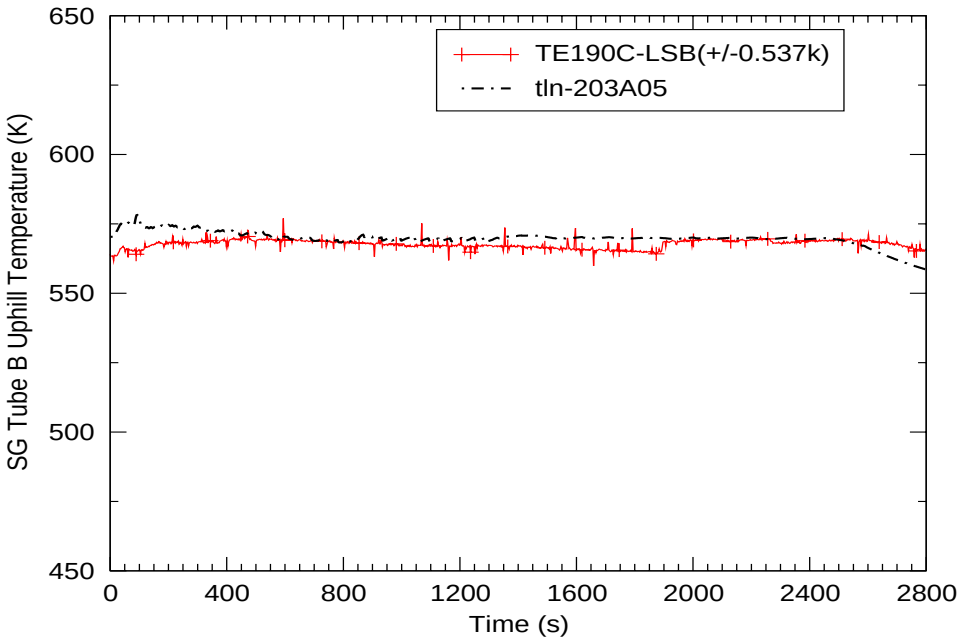

Figure C.5-174. Fluid Temperature in uphill Side of Loop-B Steam Generator

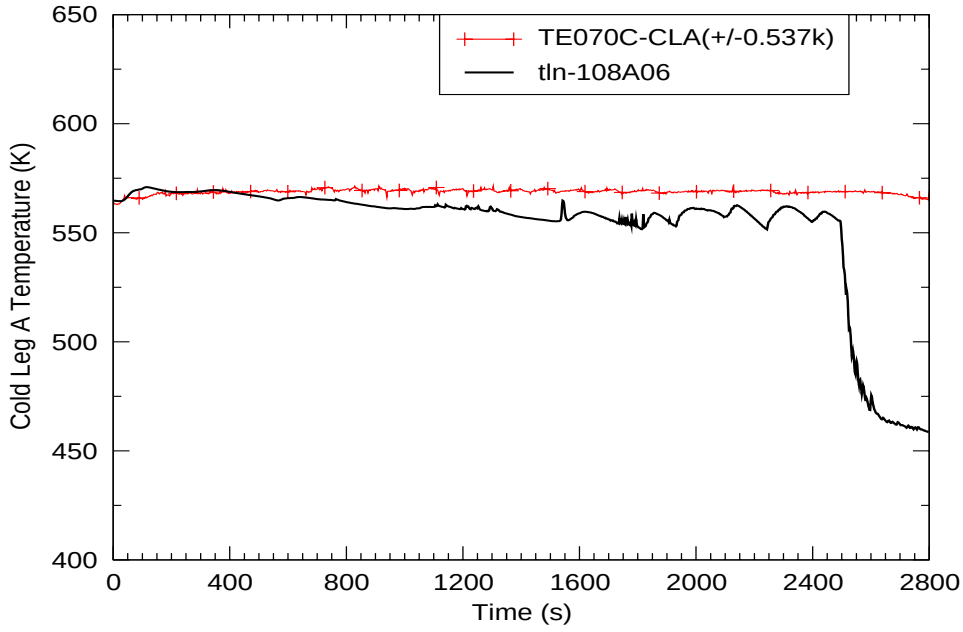

Figure C.5-175. Fluid Temperature in Loop-A Cold Leg

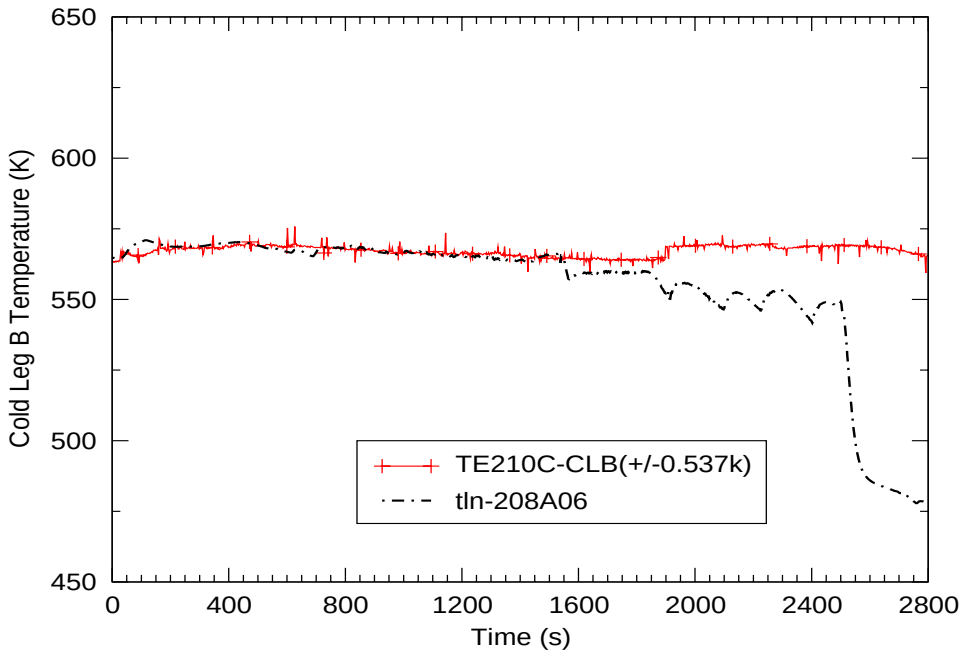

Figure C.5-176. Fluid Temperature in Loop-B Cold Leg

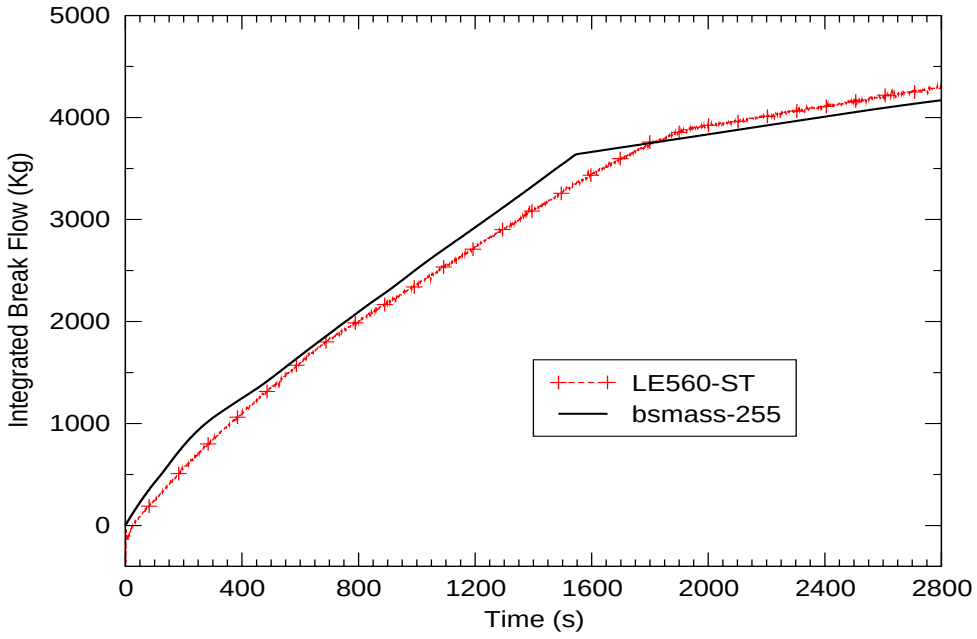

Figure C.5-177. Integrated Break Flow

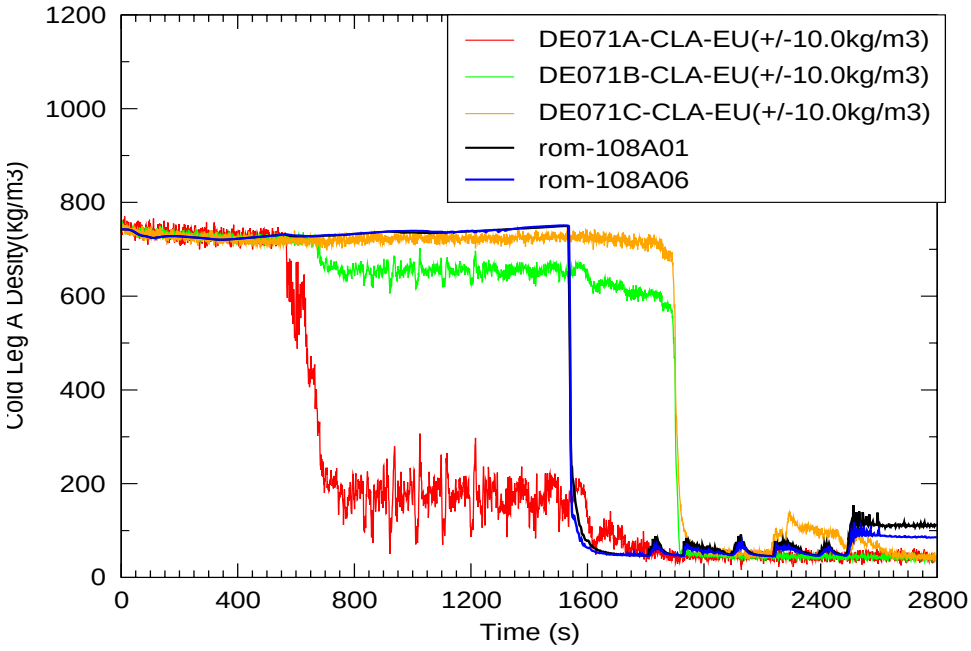

Figure C.5-178. Fluid Density in Loop-A Cold Leg

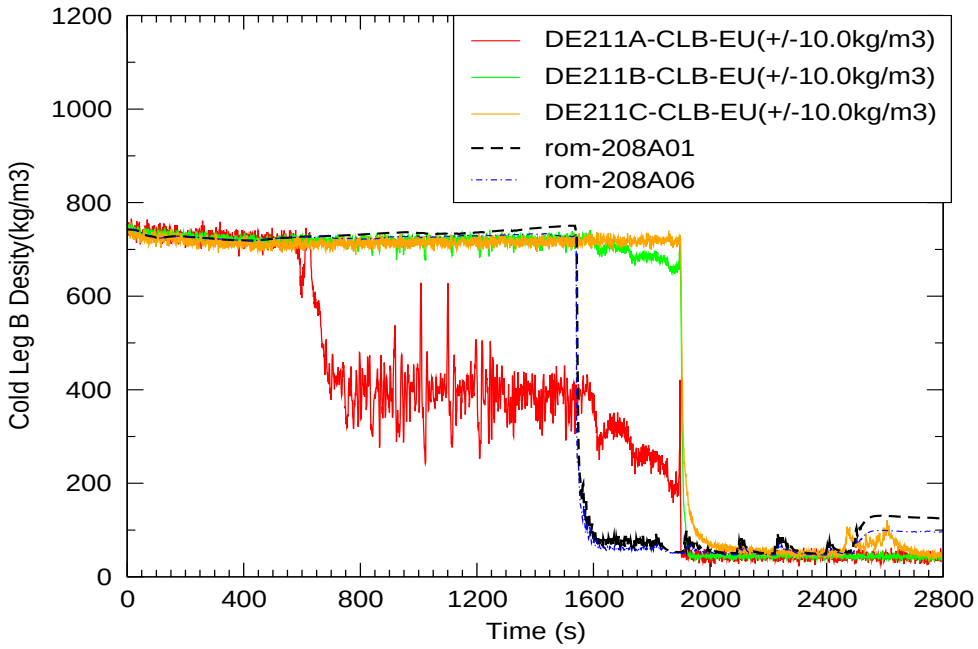

Figure C.5-179. Fluid Density in Loop-A Cold Leg

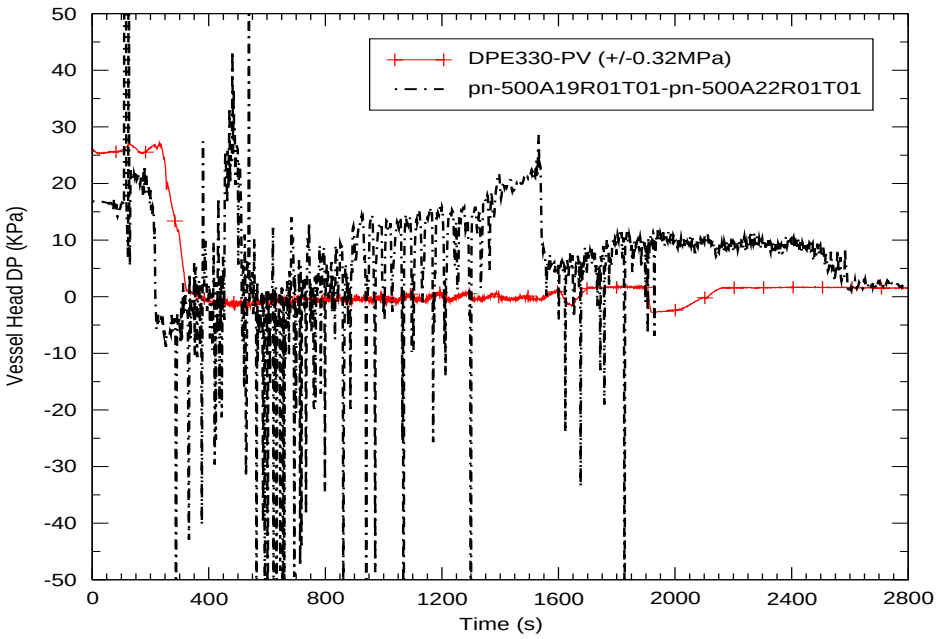

Figure C.5-180. Upper Head Differential Pressure

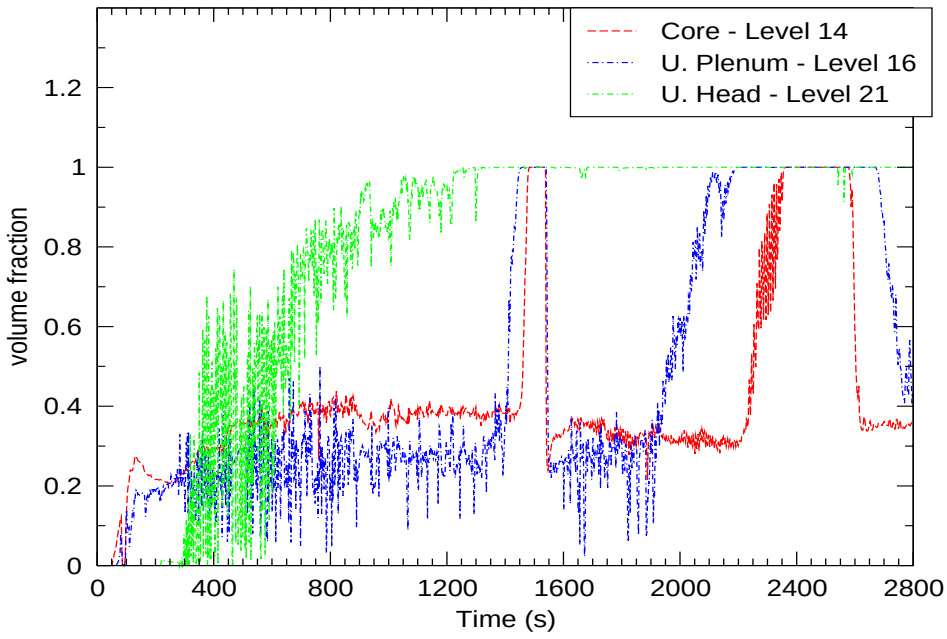

Figure C.5-181. Void Fractions in the Core (CORE), Upper Plenum (UP), and Upper Head (UH)

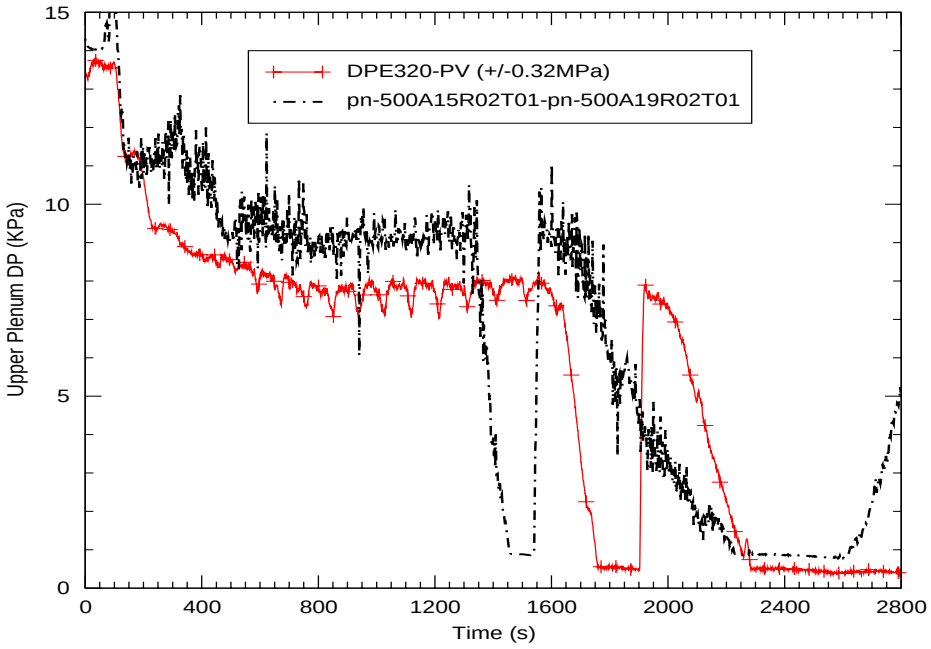

Figure C.5-182. Upper Plenum Differential Pressure

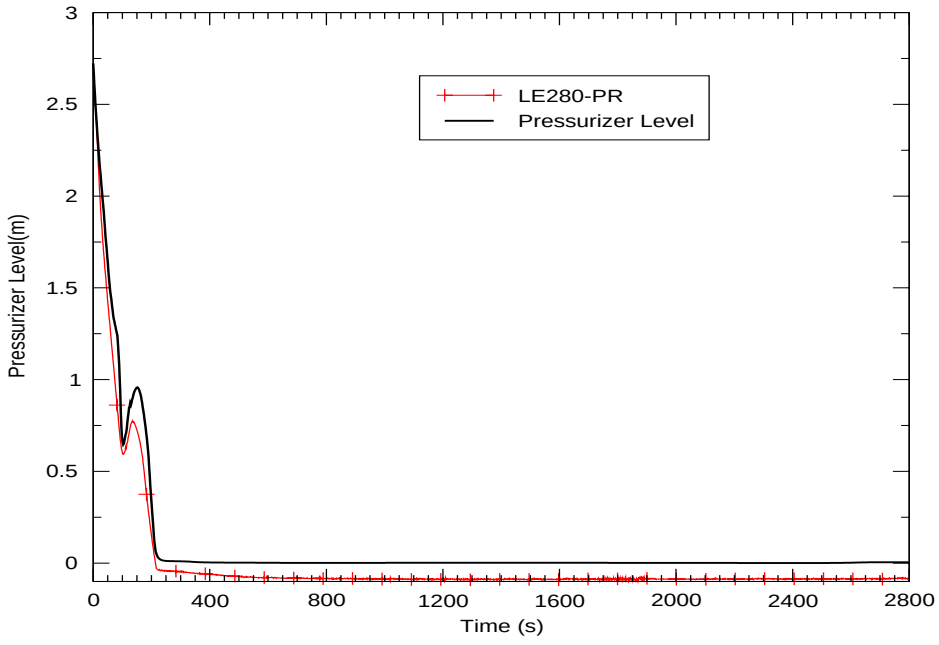

Figure C.5-183. Pressurizer Level

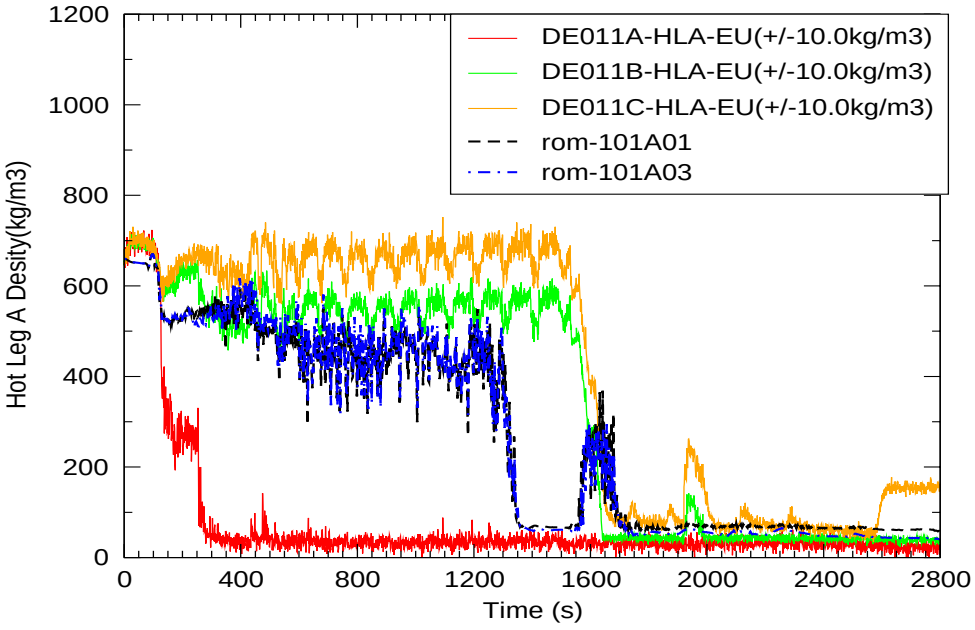

Figure C.5-184. Fluid Density in Loop-A Hot Leg

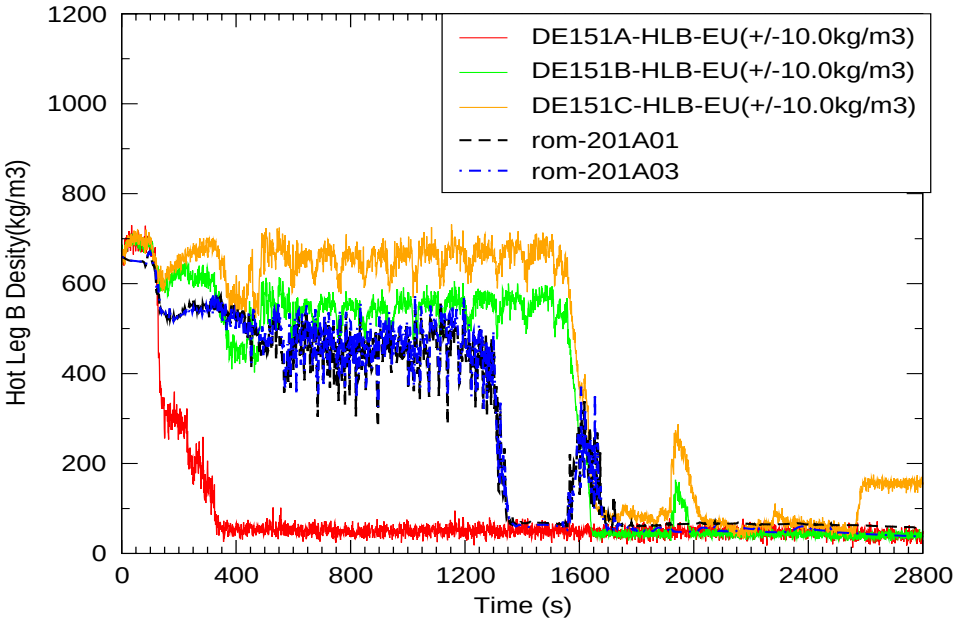

Figure C.5-185. Fluid Density in Loop-B Hot Leg

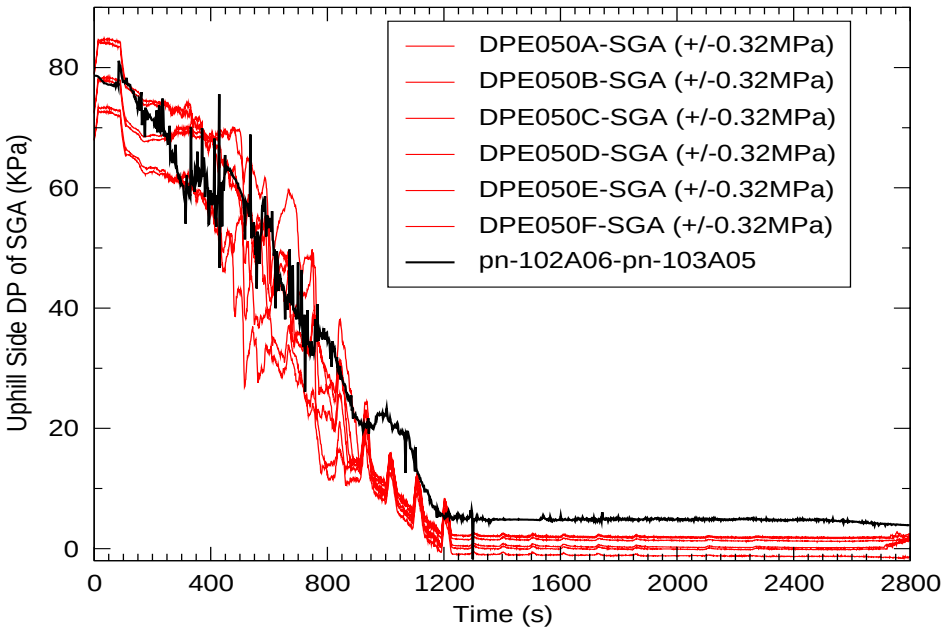

Figure C.5-186. Differential Pressure Along uphill Side of Loop-A Steam Generator

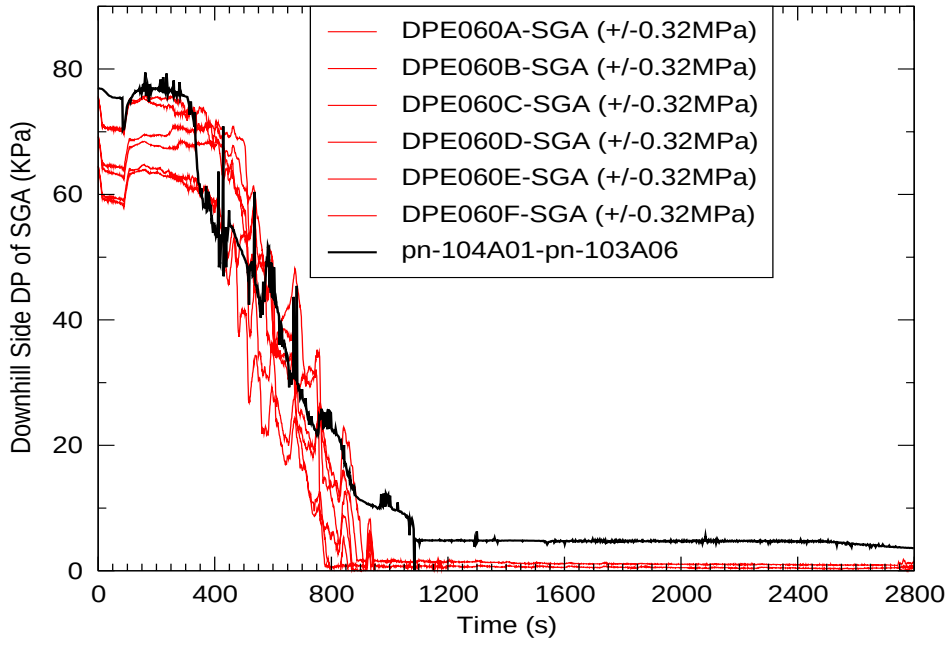

Figure C.5-187. Differential Pressure Along downhill Side of Loop-A Steam Generator

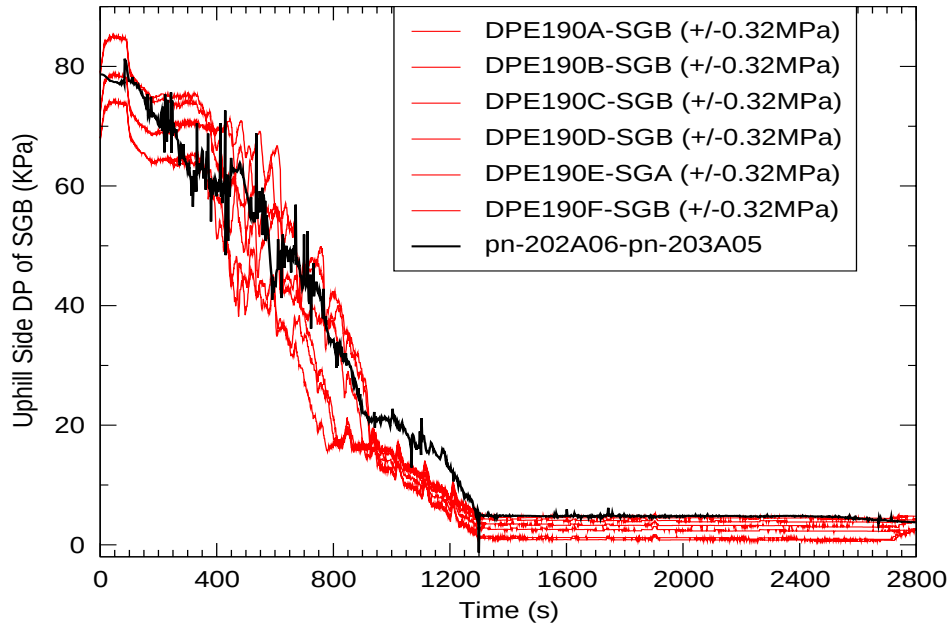

Figure C.5-188. Differential Pressure Along uphill Side of Loop-B Steam Generator

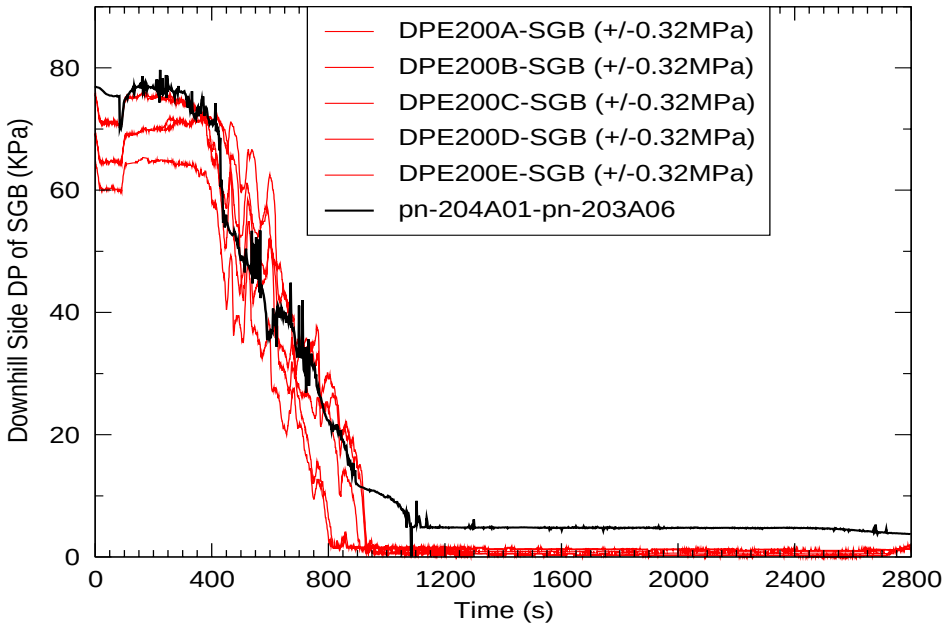

Figure C.5-189. Differential Pressure Along downhill Side of Loop-B Steam Generator

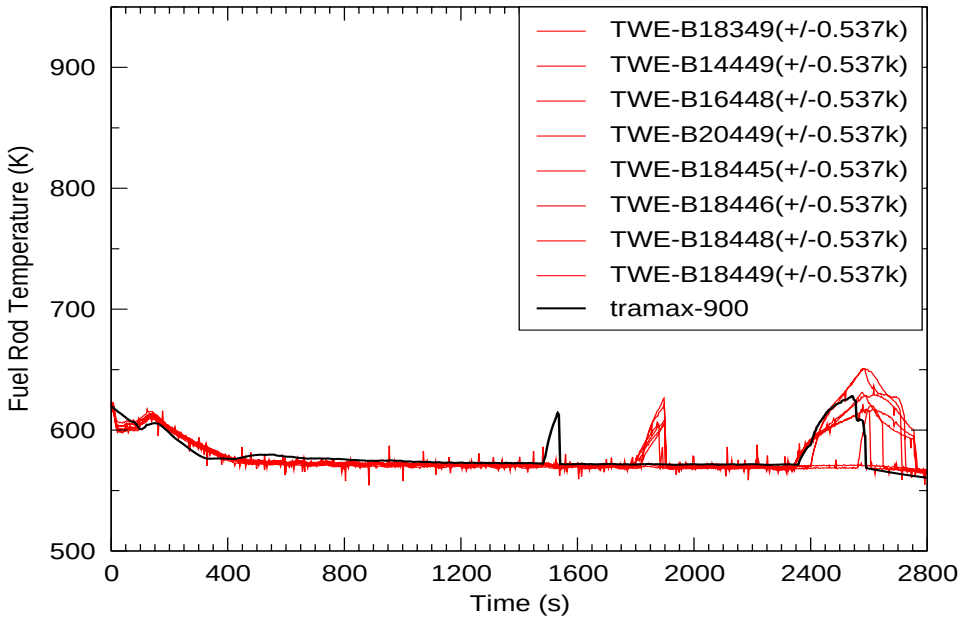

Figure C.5-190. Fuel Rod Temperature

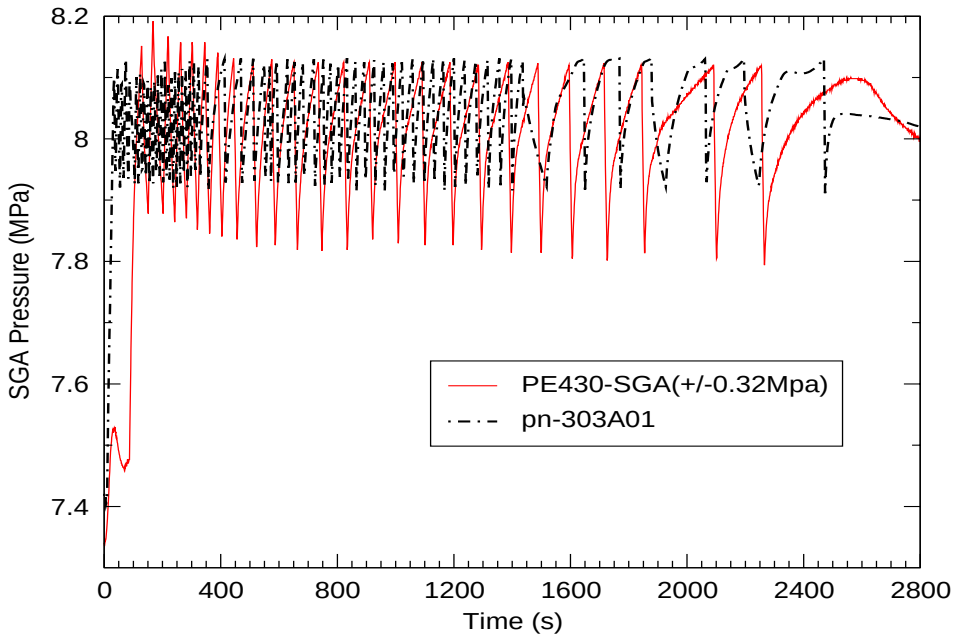

Figure C.5-191. Secondary-side Pressure in Loop-A Steam Generator

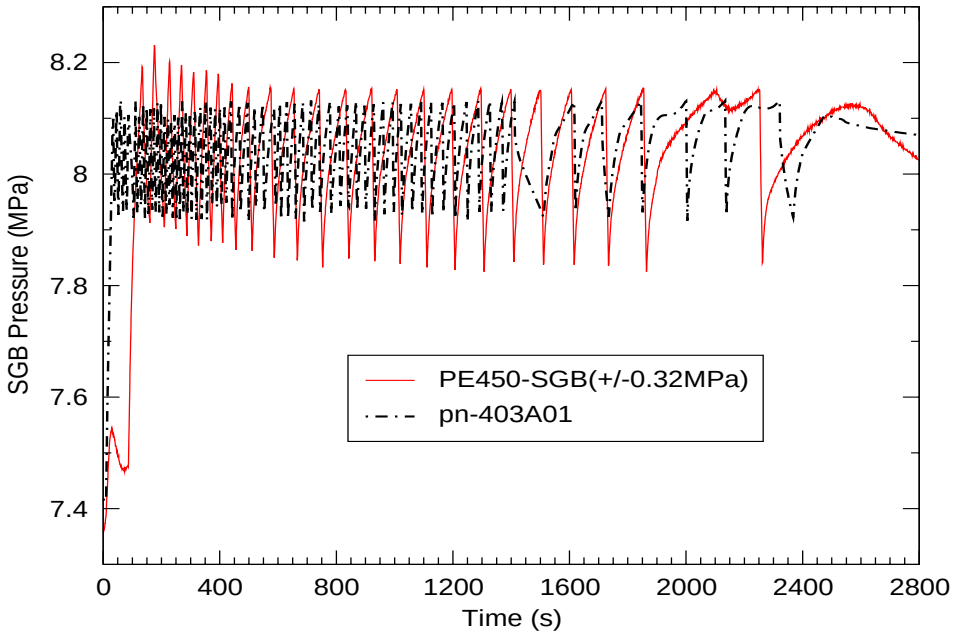

Figure C.5-192. Secondary-side Pressure in Loop-B Steam Generator

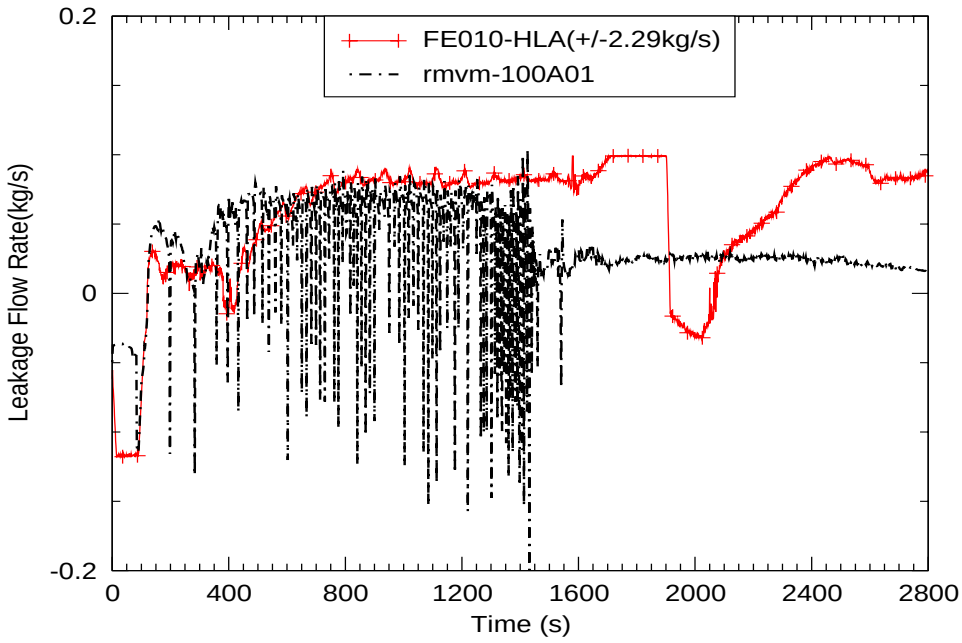

Figure C.5-193. Hot-Leg Bypass Leakage, Loop-A

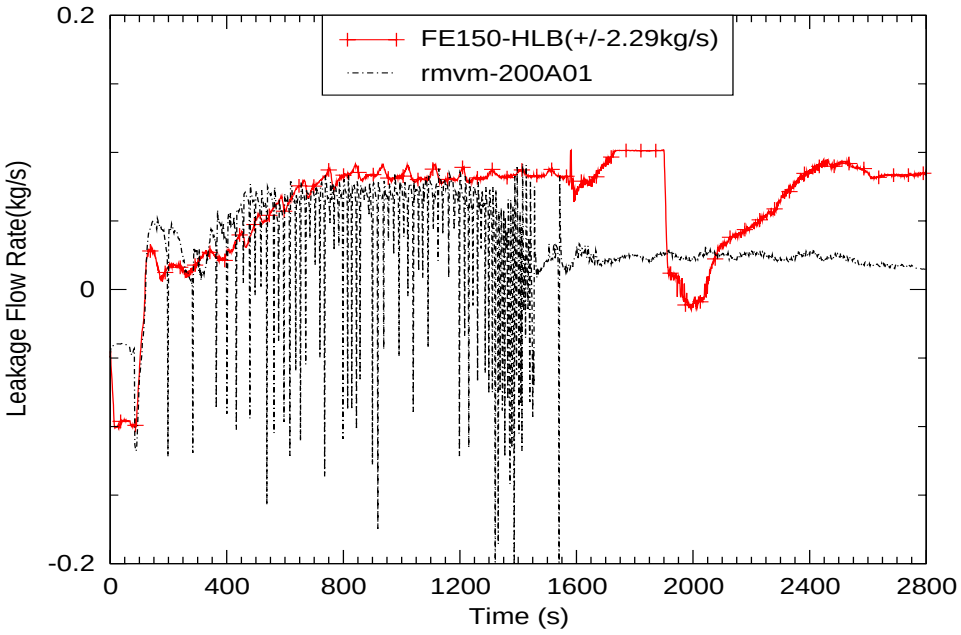

Figure C.5-194. Hot-Leg Bypass Leakage, Loop-B

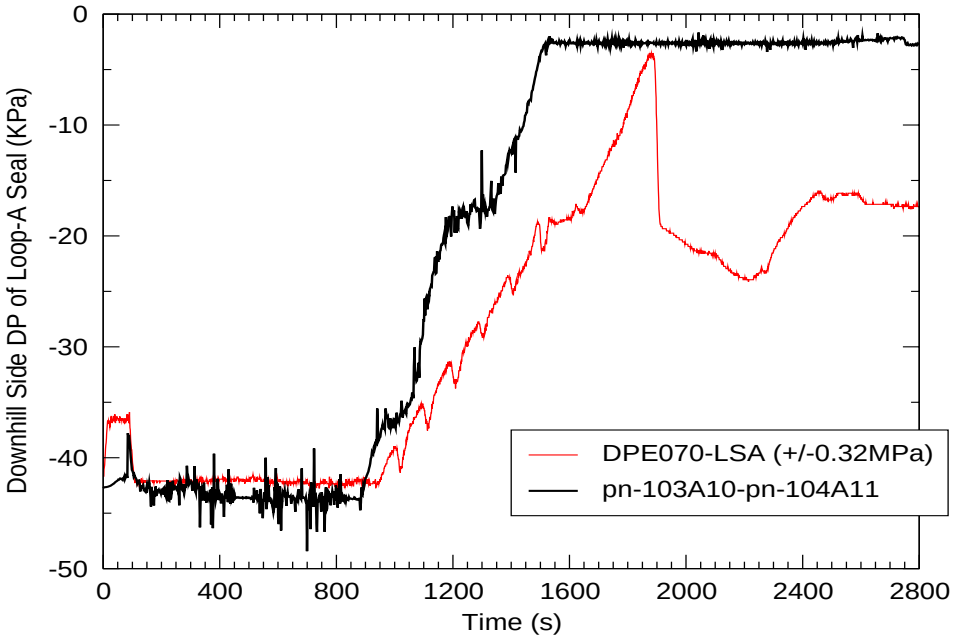

Figure C.5-195. Differential Pressure Along downhill Side of Loop-A Seal

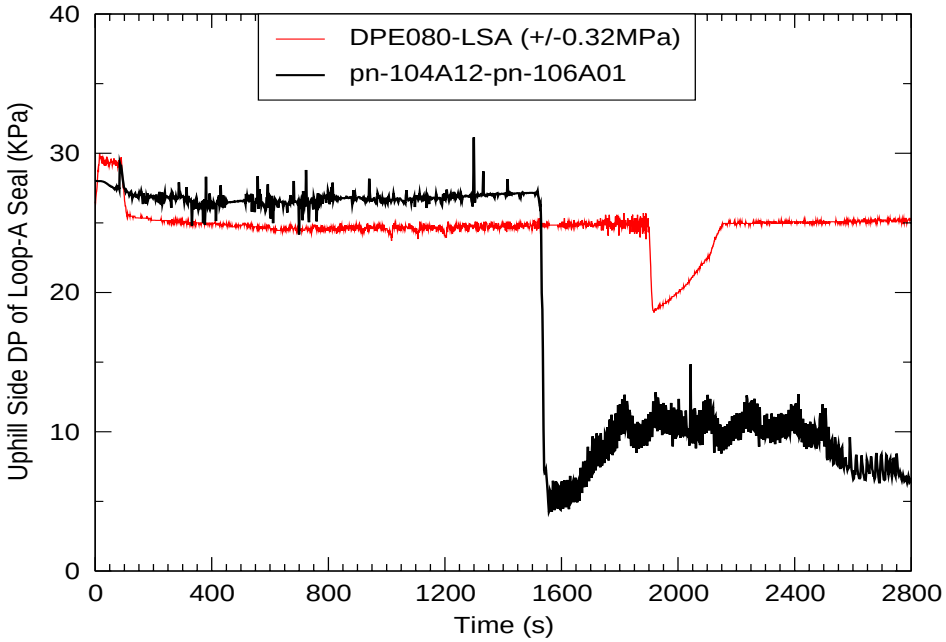

Figure C.5-196. Differential Pressure Along uphill Side of Loop-A Seal

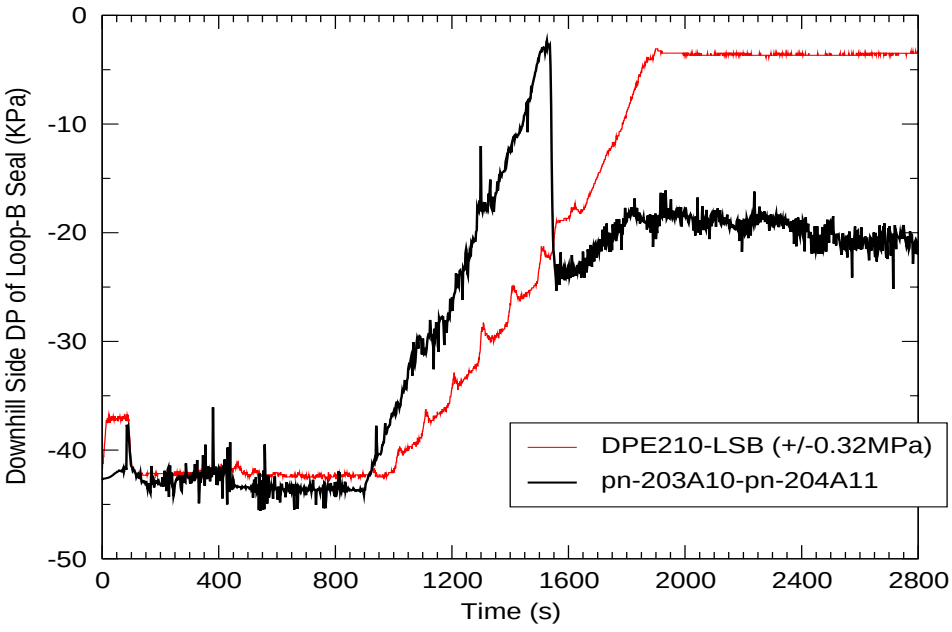

Figure C.5-197. Differential Pressure Along downhill Side of Loop-B Seal

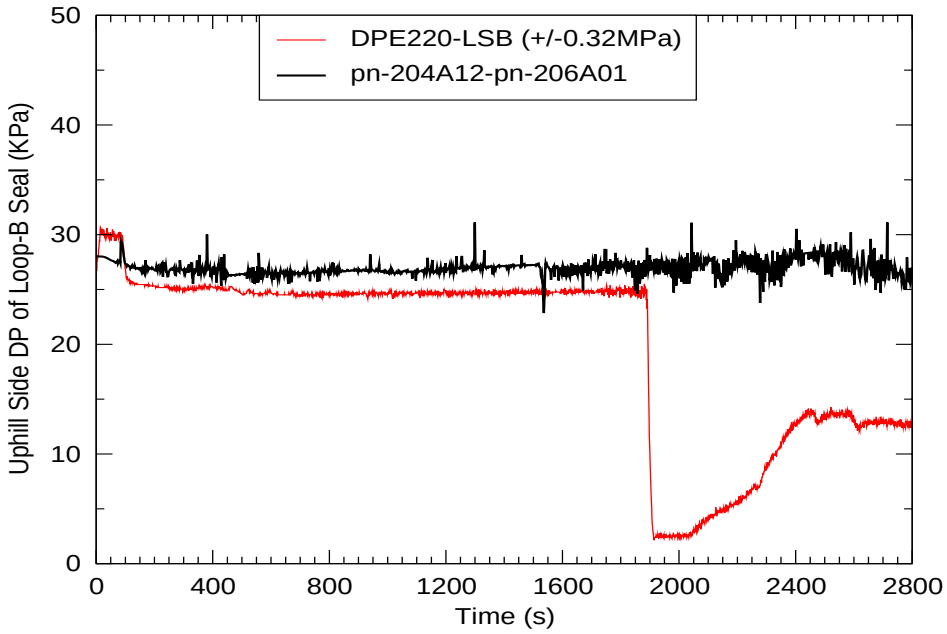

Figure C.5-198. Differential Pressure Along uphill Side of Loop-B Seal

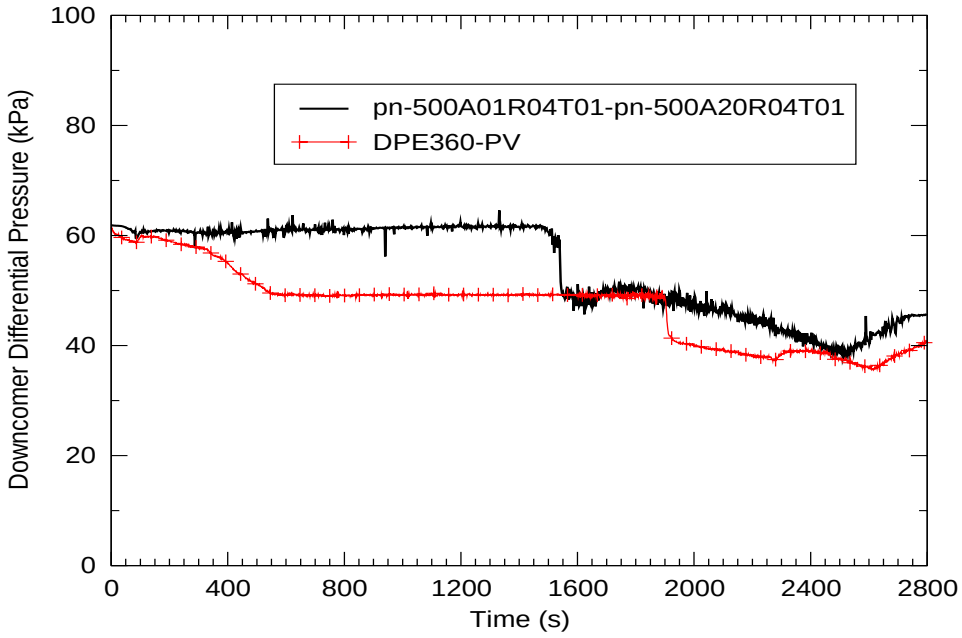

Figure C.5-199. Downcomer Differential Pressure

C.5.5.5.5. Conclusions

Table 5.3 of this report, as well as Reference 8 lists four criteria used in the code validation: *Excellent Agreement, Reasonable Agreement, Minimal Agreement, Insufficient Agreement*. *Reasonable agreement* is defined as:.

> "*Reasonable Agreement* applies when the code exhibits minor deficiencies. Overall, the code provides an acceptable prediction. All major trends and phenomena are predicted correctly. Differences between calculated values and data are greater than those deemed necessary for excellent agreement. The calculation will frequently lie outside but near the specified or inferred uncertainty bands of the data. However, the correct conclusions about trends and phenomena would be reached if the code were used in similar applications. The code models and/or facility model noding should be reviewed to see if improvements can be made."

Based on the PIRT analysis of each characteristic phase encountered during this test, it is evident that the TRACE simulation of test SB-CL-16 meets the definition of *Reasonable Agreement* for all highly-ranked phenomena during each phase of the transient.

Reasonable agreement was obtained in spite of the following discrepancies:

1. Core predicted to uncover approximately 350 seconds too early
2. Predicted pressure following blowdown phase is higher than the data
3. Hot leg-to-downcomer bypass flow reverses direction too early
4. Unlike the data, liquid holdup is predicted to occur in SGA during natural circulation phase.
5. Predicted behavior in LSA and LSB appear to corresponding with the opposite loop-seal data channels: the LSA prediction is similar to the LSB data and the LSB prediction is similar to the LSA data.

C.5.5.6. Simulation of SB-CL-18

SB-CL-18 case was a 5% cold leg break test. The break unit was located on the side of the cold leg in Loop B. Two input decks were developed for the transient analysis: one constrained steady-state (CSS) input deck and one transient input deck. The CSS deck contains most of the model information and plant control procedures. The CSS input deck is used to obtain initial plant conditions for transient calculations.

The control system and control procedures of the ROSA-IV facility were designed to accommodate a wide range of plant operational transients and accident scenarios. The TRACE control procedure was derived from a series of SBLOCA tests.

SB-CL-18 test conditions and control actions implemented in the TRACE transient analysis are listed below.

C.5.5.6.1. SB-CL-18 Test Conditions

Some of the test conditions or control procedures were different from those in the reference PWR reactor. Special control procedures or test conditions were designed to account for some scaling issues in the design of the test facility (Refs.1, 7).

The plant initial conditions are summarized in Table C.5.3. In the test, it was assumed that a loss-of-offsite power occurred concurrently with reactor scram. At the same time, a failure of one of the two diesel-generators for the emergency coolant and auxiliary feedwater pumps was assumed. Table C.5.21 summarizes the operational setpoints for Run SB-CL-18. Table C.5.22 gives the event sequence recorded by the facility instrumentation system. Some specific information is given below for individual items.

- Coolant pumps

Upon the initiation of the break, the pump speed was increased before the pump started to coast down following the reactor scram signal (Ref. 7). The pump impeller rotation speed after the initiation of break is demonstrated in Figure C.5-200 and Figure C.5-201. The dashed line is the pump curve obtained in the TRACE simulation of SB-CL-18. The solid line is the measured pump curve in the SB-CL-18 test.

- Reactor trip and core power after break

As indicated in Table C.5.23, the reactor was tripped 12 seconds after the break was initiated. Two power curves are shown in Figure C.5-202. The solid line is the measured power curve in the SB-CL-18 test. The dashed line is the power curve obtained for the transient simulation. The power level in the test remained at 10 MWt beyond 12 seconds to allow the test curve to catch up with the scaled decay curve.

- Emergency Core Cooling System (ECCS)

During the SB-CL-18 transient, the subsystems of the ECCS system were actuated in the manner given in Table C.5.21 and Table C.5.22 For each loop, the ECCS subsystems injected water into the loop through the same nozzle. In the test, the desired ratio of the ACC injection flow into the loop A cold leg to the ACC injection flow into the loop B cold leg was 3:1. Assuming the ratio was maintained, the ACC injection flow rate into each loop could be calculated based on the discharging flow rate of the ACC tank, which was derived from the ACC tank level measurement (LE14). Figure C.5-203 shows the calculated ECCS injection flow rate into each loop, which is

the sum of the injection flow of the ECCS subsystems (high pressure charging and high pressure injection).

- Auxiliary Feedwater System

After the main feedwater was cut off, the auxiliary feedwater system was actuated with delay to supply water to the SG's secondary side. The auxiliary system of the test facility used a single pump and branched piping of unequal hydraulic resistances. In SB-CL-18, the auxiliary feedwater was assumed to fail.

- Pressurizer heaters

Based on the test data, power supply to the pressurizer heaters was cut off with the initiation of the break.

C.5.5.6.2. TRACE Control Procedure

Using the strategy outlined at the beginning of this chapter, the control procedure for the TRACE model is simplified. As a result, the TRACE control procedure mainly consists of a number of trips**.** In general, a trip is initiated either by time or the system pressure. Specifically,

1. At time 0, the break is initiated and the pressurizer heater power is cut off.
2. The pump speed is increased after the break and coasts down with the reactor trip as shown in Figure C.5-200 and Figure C.5-201.
3. The reactor is tripped when the system pressure reaches 12.97 MPa. Figure C.5-202 shows the measured power curve after the break and the power curve obtained from the transient calculation.
4. The Safety Injection (SI) signal is generated as the system pressure reaches 12.27 MPa. With a 12-second delay, the Emergency Core Cooling System (ECCS) is actuated. The accumulator injection to the cold leg was actuated when the primary system pressure dropped below 4.51 MPa. The HPSI and LPSI systems were modeled as boundary conditions. The same approach is adopted in this work.
5. Main steam line valve closure, main feedwater cut off and auxiliary feedwater are initiated with proper time delays following the reactor trip.

Table C.5.21. Operational Setpoints for Run SB-CL-18

	Setpoint
Reactor scram signal	12.97 MPa (System pressure)
Pump coast down	With reactor scram
Safety Injection (SI) signal	12.27 MPa (system pressure)
High Pressure charging	Assumed failed
Accumulator injection	4.51 MPa
Low Pressure Injection	1.29 MPa
Main feedwater cutoff	With reactor scram
Turbine throttle valve closure	With reactor scram
Auxiliary feedwater	Assumed failed

Table C.5.22. Chronology of Events for Run SB-CL-18

Events	Time (s)
Break	0
Reactor trip	9
Safety Injection Signal	12
Main Steam Line Valve Closure	14
SG Feedwater stop	16
First Core Uncovery	120~155
Loop Seal clearing	~140
Primary/Secondary Pressure Reversal	~180
Reactor coolant pumps stop	265
Second Core Uncovery	420-540
Accumulator Injection ON	455

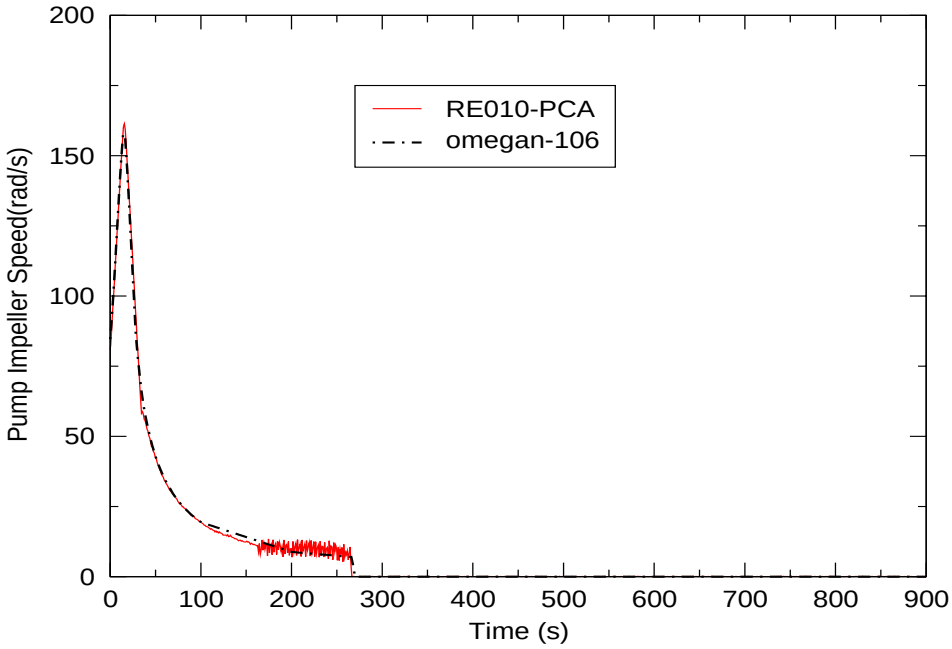

Figure C.5-200. Pump A Impeller Speed After Break

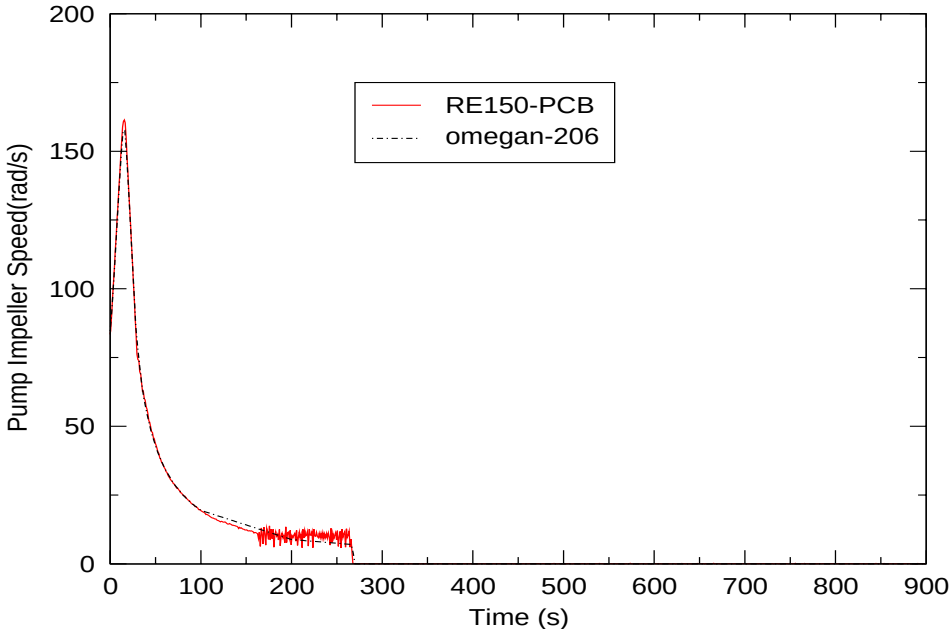

Figure C.5-201. Pump B Impeller Speed After Break

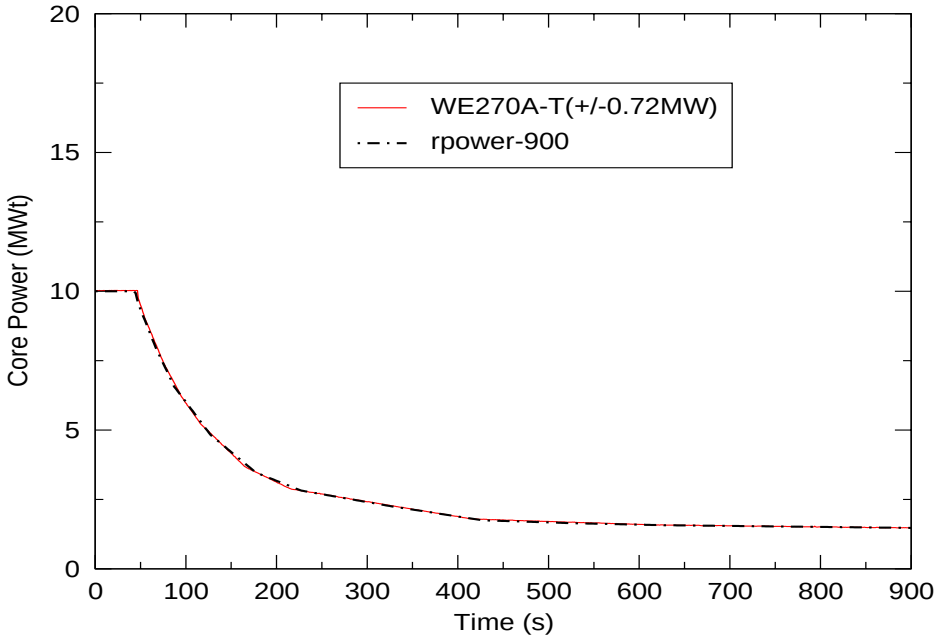

Figure C.5-202. Core Power after Break

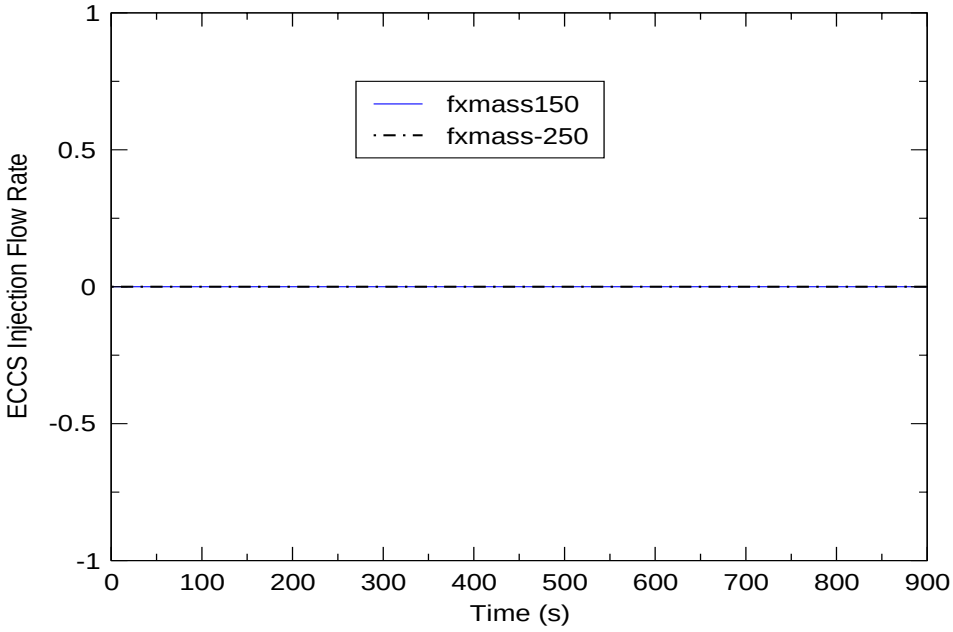

Figure C.5-203. ECCS Injection Flowrates for Loop A and Loop B

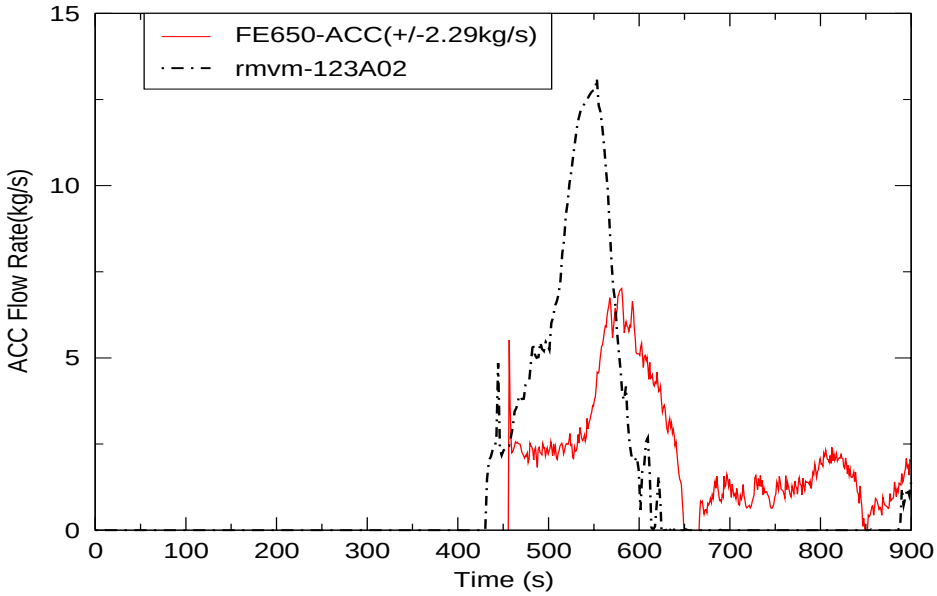

Figure C.5-204. Accumulator Injection Flow to Cold Leg A

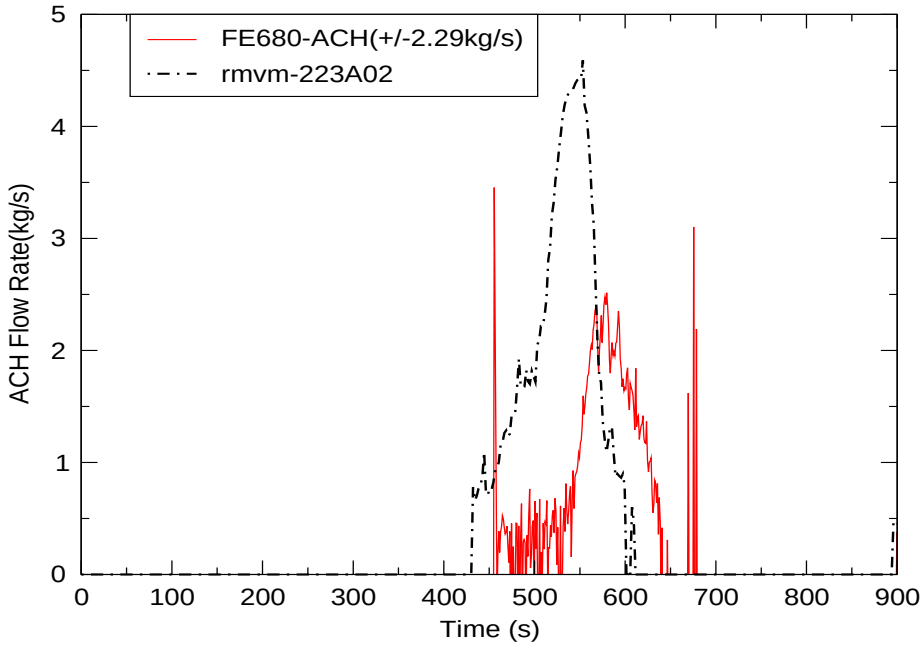

Figure C.5-205. Accumulator Injection Flow to Cold Leg B

C.5.5.6.3. Experimental Observations

The main objective of test SB-CL-18 was to investigate the thermal-hydraulic mechanisms of early core uncovery and heatup. Early core uncovery may be caused by a manometric effect resulting from an imbalance between the water hold up in the upflow and downflow sections of the primary coolant in the steam generator U-tubes, loop seals (Ref. 7). Table C.5.23 lists the event sequence recorded by the facility's instrumentation system during the test.

Soon after the start of the transient, the pressure started to drop rapidly and the core power decay curve was initiated at a pressurizer pressure of 12.97 MPa together with a closure of the MSIV, starting of the programmed pump speed curve, and termination of the main feedwater to the steam generators.

The safety injection signal was initiated at the system pressure of 12.27 MPa. The high-pressure charging and the high-pressure injection pumps were assumed unavailable. Auxiliary feedwater was also unavailable in this event.

Since there was no safety injection until the accumulator started injecting at about 455 seconds (as well as redistribution of water in the primary system (Ref. 4)), the core became temporarily uncovered in the time interval from 120 to 150 s after the break initiation. Consequently, the maximum heater rod temperature increased by about 190 K above its steady-state value. The core uncovery occurred just prior to loop seal clearing. The core level was recovered upon clearing the loop A upflow seal at 150 seconds.

The process of loop seal clearing took place between 85 - 180 s, with the loop A seals being cleared at 150 s and loop B at 180 s, respectively. Loop seal clearing allowed a two-phase mixture of steam and water to discharge from the break, which in turn reduced the break mass flow rate but accelerated the depressurization of the primary loop. At about 180 s, the primary loop pressure decreased below the steam generator secondary side pressure. Thereafter, the steam generator no longer served as heat sinks and the energy removal from the primary system was by coolant discharge through the break.

The core was uncovered again at about 400 seconds due to vessel inventory boil-off, and the heater rods in the upper part of the core experienced superheating up to about 80 K. Due to the depressurization of the primary system, the accumulators were automatically actuated at 455 seconds to fill the system. It is noticed that accumulator injection flow was off by 1 kg/sec from the test data because the initial value started at -1 kg/sec. The core level was recovered at about 540 seconds.

C.5.5.6.4. Transient Analysis

The SB-CL-18 transient calculation was performed for 900 seconds. The transient simulation results and the comparison to the test data are presented in Figure C.5-200 to Figure C.5-234. In these figures, the test data is plotted in solid, colored lines with symbols and the calculation results are plotted with solid black or blue lines without symbols.

C.5.5.6.4.1. System Behavior

The overall primary system behavior determines the boundary conditions of the transient event since most of the control signals are based on the system pressure setpoints. The predicted system pressure was in good agreement (in accordance with NRC-established acceptance criteria (Ref. 8)) with the data as shown in Figure C.5-206. Therefore, the sequence of the events based on the system pressure setpoints are also in good agreement with the test data.

Table C.5.23 shows the comparison of the sequence of the events for SB-CL-18 simulation results and the test data.

Table C.5.23. Sequence of the Event Comparison for SB-CL-18 Test

Event	Test Data Time (sec)	TRACE Model Time (sec)
Break	0[a]	0
Reactor Trip	~ 9	~ 9
Safety Injection Signal	~ 12	~ 12
Main Steam Line Valve Close	14	14
SG Feedwater Stop	16	16
First Core Uncovery	110 – 150	110 – 150
Loop-A Seal Began Clearing	~ 150	~ 220
Loop-B Seal Began Clearing	~ 180	~ 200
Primary/Secondary Pressure Reversal	~ 180	~ 220
Reactor Coolant Pumps (PC-A/B) Stop	265	265
Second Core Uncovery	400 – 540	325 - 530
Accumulator Injection On	455	420
End Time	900	900

a. The break starts at time 0.

C.5.5.6.4.2. Analysis Results

As discussed in **Section C.5.5.**, the PIRT (Ref. 6) identifies the high ranked phenomena for each phase of the transient. To evaluate the performance of TRACE, each phase will be discussed separately, and the TRACE-simulation results for the highly-ranked phenomena will be compared to the data. The principal Figure of Merit (FOM) of the transient event is the core collapsed liquid level (CCL). The core collapsed level is measured as the core differential pressure as demonstrated in Figure C.5-207.

Certain input parameters, such as decay heat, core power, and feedwater temperature, are taken directly from the test data as boundary conditions. Therefore, although they are identified as important in some of the phases, they will not be discussed in terms of code performance.

Blowdown phase

The blowdown phase is marked by a rapid depressurization of the primary coolant system until the hot coolant begins to flash into steam. The rate of depressurization is strongly influenced by the rate and enthalpy of the break flow, and it changes when flashing and boiling start in the core. In this phase, the most important parameters defining the evolution of the transient are decay heat, primary side heat transfer, critical break flow, and the flow regime upsteam of the break flow.

In this test, the blowdown phase lasted from 0 to 150 seconds. Throughout this time, good agreement is observed between the simulation results for each of the highly-ranked parameters and the test data. The core pressure is shown in Figure C.5-206, and the core differential pressure (DP) is shown in Figure C.5-207. Primary side heat transfer is evaluated using the fluid temperature in the steam generator (SG) tubes and the cold legs. These parameters can be seen in Figure C.5-208 through Figure C.5-211. The integrated break flow shown in Figure C.5-212 is used in evaluating critical break flow, and cold-leg-density predictions, shown in Figure C.5-213 and Figure C.5-214 are used to evaluate the flow regime upstream of the break. The data for the density comparisons is taken from three densitometers located along the cross-sections of the cold legs.

Other key results in this phase are the DPs in the upper head and upper plenum, the pressurizer level, and the flow regime in the hot legs. These results will be discussed to further illuminate the evolution of the transient and to thoroughly evaluate the code.

The upper-head DP and upper-plenum DP are shown in Figure C.5-215 and Figure C.5-216, respectively. Over the entire period of the transient, both figures show the code predicting the general trends of the data. In this initial phase, however, the calculated upper-head DP oscillates severely over the first 125 seconds, and the negative values seem to indicate that liquid is being held-up in the upper head. The calculated upper-plenum DP is free of oscillations, however, the level decrease shown here does not occur as rapidly as in the test.

Upon initiation of the break, the level in the pressurizer plunges to zero in approximately 25 seconds. In Figure C.5-220, the predicted level-decreases is in excellent agreement with the measurement.

The flow regimes in the hot legs are evaluated in terms of hot-leg fluid density. Figure C.5-219 and Figure C.5-220 both show excellent agreement between the code and the data.

Loop Seal Clearing phase

The loop seal clearing phase begins when the trapped primary-side steam volume reaches the top of the loop seal piping. From this point, the steam volume depresses the liquid in the downhill side of the seal and in the core until a minimum core level is reached. As steam moves through the seal to the break plane, the liquid it displaces is forced into the core, quenching the heatup caused by the drop in core level. In the test, this sequence of events occurred between 136 and 180 seconds.

The highly ranked processes to be discussed in this phase are listed as follows:

1. Decay heat
2. Mixture level in the core region
3. Hot-leg downcomer gap flow
4. SG primary-side heat transfer in the U-tubes
5. SG primary-side flow resistance
6. SG primary-side tube voiding
7. Flow regime/entrainment in the pump suction / loop seal
8. Critical break flow

The core DP (Figure C.5-207) is in excellent agreement with the data. The code accurately depicts the affect of loop-seal-clearance on the core level. As a result of this accuracy, the fuel heat, shown in Figure C.5-231, is predicted to occur at approximately the same time and within the same temperature range as the data.

The hot-leg to downcomer gap flow, or hot-leg bypass flow, can influence the rate or level of the maximum core-level depression. However, in Figure C.5-221 and Figure C.5-222, about 0.05 kg/s less flow is predicted to leak from the hot legs to the downcomer. Based on the excellent agreement in core level, this shows that the hot-leg bypass did not significantly influence the maximum core-level depression.

Differential pressures along the SG tubes are used to evaluate SG primary-side heat transfer, flow resistance, and tube voiding. Figure C.5-223 and Figure C.5-226 show the differential pressures along the upflow and downhill sides the SG tubes. These figures show excellent agreement between the code and the data, and they confirm that the heat transfer, flow resistance, and void fraction in the tubes are being accurately simulated.

Differential pressures along the loop seals are used to evaluate loop-seal behavior. Figure C.5-227 through Figure C.5-230 show the differential pressures along the uphill and downhill sides the loop seals. Each of these figures show the accurate prediction of the timing of the beginning of the loop seal clearance. Unlike the data, however, the uphill portions of the seals are not predicted to clear completely. After the initial flushing of liquid, the larger than expected DP at around 175 seconds is indicative of the presence of a significant amount of liquid.

The density in the portion of the cold leg upstream of the break, CELL 208A01, is used to evaluate the flow regime upstream of the break. Figure C.5-213 and Figure C.5-214 show the calculated mixture densities in cold legs A and B, respectively. The predictions are in excellent agreement with the data.

The calculated break flow shown in Figure C.5-212 is in reasonable agreement with the data. During this phase, the predicted break flow changes from liquid to vapor at approximately the same time as the data, but the predicted mass leaving the break is about 1000 kg less than was measured at that time.

Boil Off phase

As the transient proceeds, the primary system continues to loose inventory and the core inventory continues to boil. During the test, this boil-off phase lasted from 181 to 454 seconds. The highly-ranked processes to be discussed in relation to this phase are listed below:

1. Fuel Decay heat and local power.
2. Mixture level in the core region
3. Downcomer mixture level
4. Critical break flow
5. Break upstream flow regime.

Throughout most of this phase, the core level (Figure C.5-207) is in excellent agreement with the data. However, at around 325 seconds, the second core uncovery is predicted to occur. This is approximately 50 seconds earlier than the test.

Horizontal stratification and condensation in the cold legs is evaluated by comparing the predicted and measured fluid densities in the colds. Figure C.5-213 and Figure C.5-214 continue to show excellent agreement between code and data; thus confirming that the correct flow regime and fluid composition are being simulated.

The downcomer level is evaluated as differential pressure in the downcomer. As shown in Figure C.5-231, the predicted downcomer level does not drop as it should during the blowdown phase, but it abruptly decreases as the loop seals clear, and thereafter (but at a DP approximately 5 kPa higher than the data) it follows the downward trend of the data. A possible cause of the higher than expected level increase following the accumulator injection appears to be due to an under-prediction in cold-leg mixture temperature shown in Figure C.5-210 and Figure C.5-211. This apparent under-prediction, coupled with inconsistent density predictions shown in Figure C.5-213 and Figure C.5-214, seem to indicate a code problem in determining the correct temperature distribution as a result of the mixing occurring in the cold legs. The lower temperatures are being propagated to the downcomer and the vessel and resulting in higher-than-expected liquid levels.

The agreement between the predicted and measured break flow (Figure C.5-212) remains only reasonable. Although it continues to follow the trend of the data, its magnitude remains consistently lower.

Also of note during this phase are the fuel temperate and SG shell-side pressures. At around 400 seconds the core begins to uncover and the fuel temperature begins to rise. As shown in Figure C.5-232, the code accurately captures the fuel heatup in terms of both timing and magnitude. At this point in the transient, the steam generators are no longer heat sinks but are transferring heat to the primary system. Figure C.5-233 and Figure C.5-234 show that at around 175 seconds, after the loop seals have cleared and the core liquid level has been restored, the predicted SG pressures do not fall as rapidly as in the test, remaining approximately 0.2 MPa higher throughout the transient.

Core Recovery phase

In the core recovery phase (455 - 900 seconds), the injection from both accumulators starts at 455 seconds. As a result, the core mixture level begins to recover. This is depicted in Figure C.5-207**,** which shows the measured and simulated core differential pressure. (It is noted that in the simulation, the accumulator injection occurred about 50 seconds earlier.) The temperature excursion of in the fuel rods which began prior to entering the recovery phase still continues and reaches (at its maximum) about 80 K superheat. Because of recovering core level, the fuel rods will be gradually quenched and their temperature increase will turn over (Figure C.5-232). The period of the longest dryout lasts about 120 seconds.

The highly ranked processes in this phase are listed below.

1. Fuel Decay heat, and local power.
2. Mixture level in the core region
3. Horizontal stratification and condensation in the cold leg
4. Downcomer mixture level
5. Critical break flow
6. Break upstream flow regime.

Following the injection of the accumulators at 455 seconds, the level in the core, shown in Figure C.5-207, rebounds too aggressively and settles at a level that is significantly higher than the data. There are several factors that appear to contribute to this result. The first obvious cause is the over-predicted accumulator injection flow shown in Figure C.5-204 and Figure C.5-205. These flows appear to be almost twice the measured flow. A second factor appears to be the prediction of colder-than-expected-liquid in the cold legs following accumulator injection. And finally, a third factor is the under predictions of the break flow. With less mass leaving the system, the level in the core will be higher. All of the factors influencing the core level also influence the downcomer level.

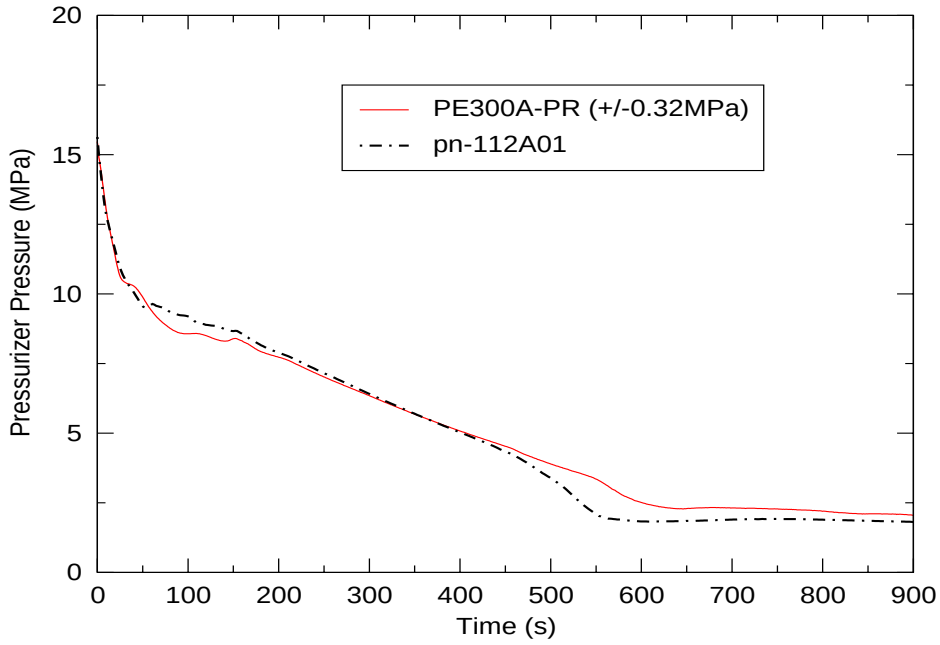

Figure C.5-206. Pressurizer Pressure

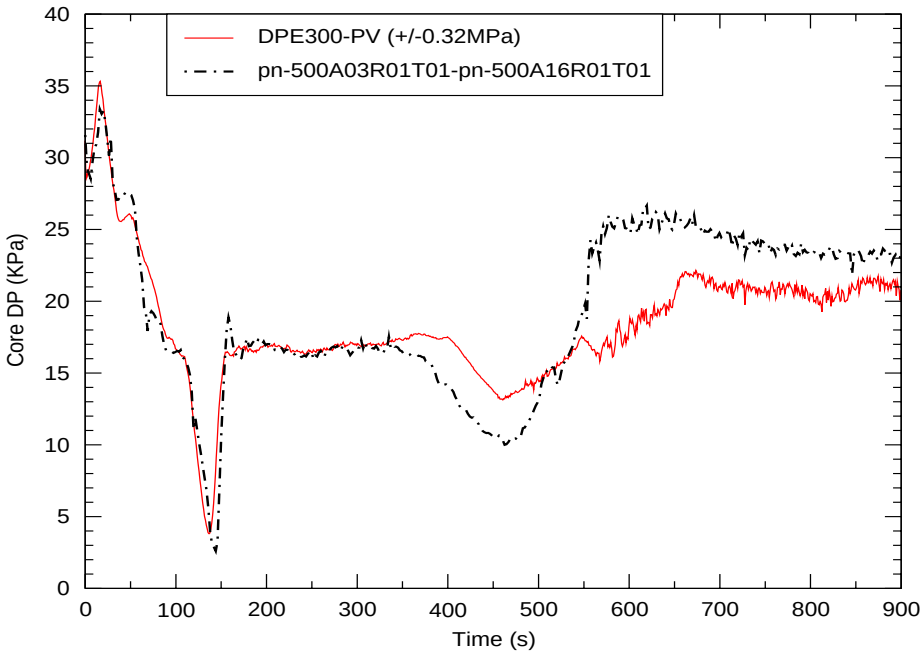

Figure C.5-207. Reactor Core Differential Pressure

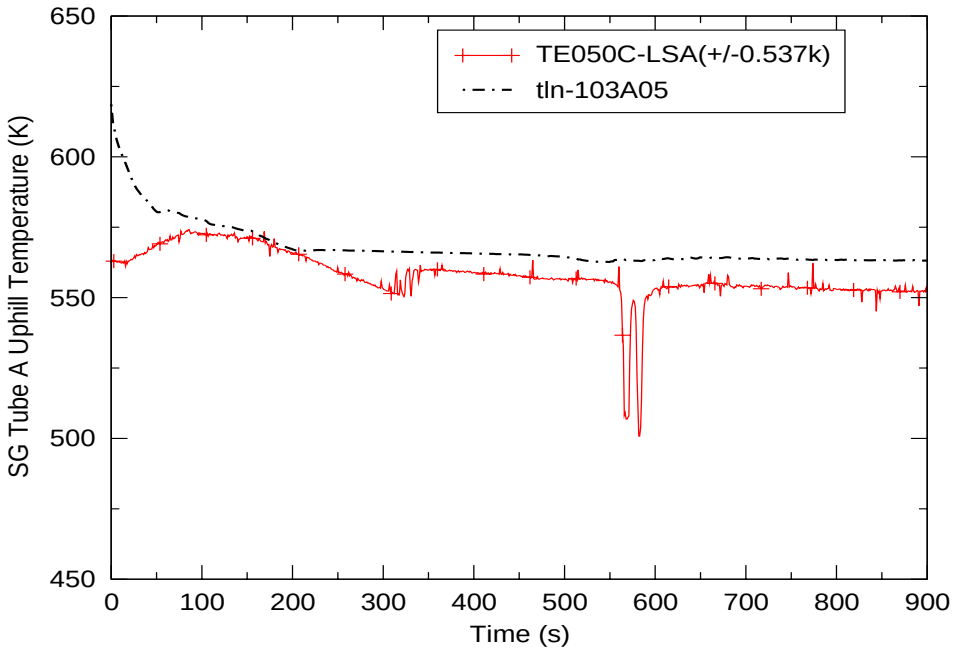

Figure C.5-208. Fluid Temperature in Loop-A Steam Generator Tubes

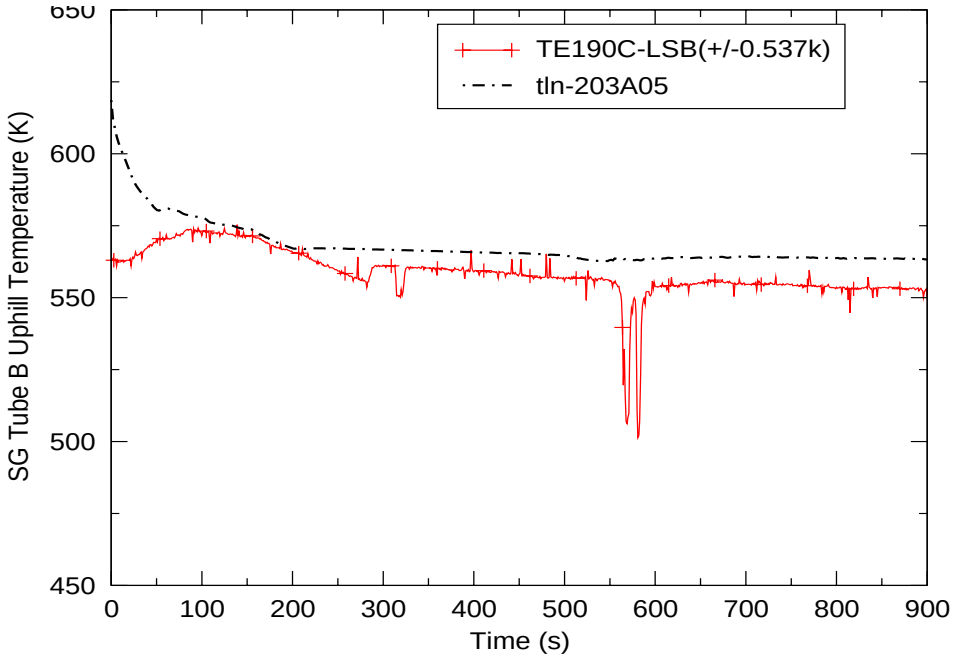

Figure C.5-209. Fluid Temperature in Loop-B Steam Generator Tubes

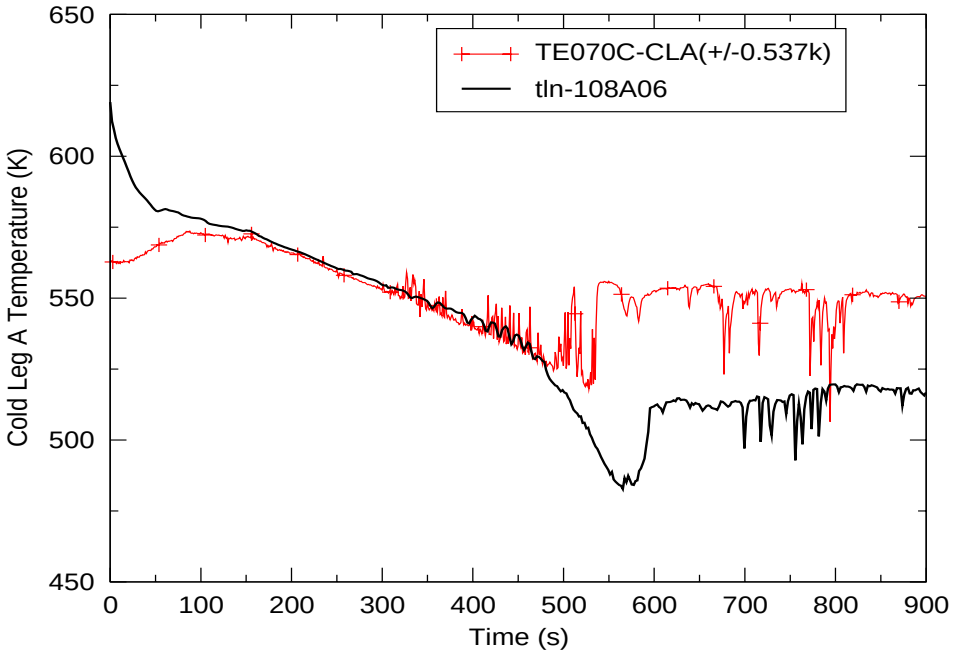

Figure C.5-210. Fluid Temperature in Loop-A Cold Leg

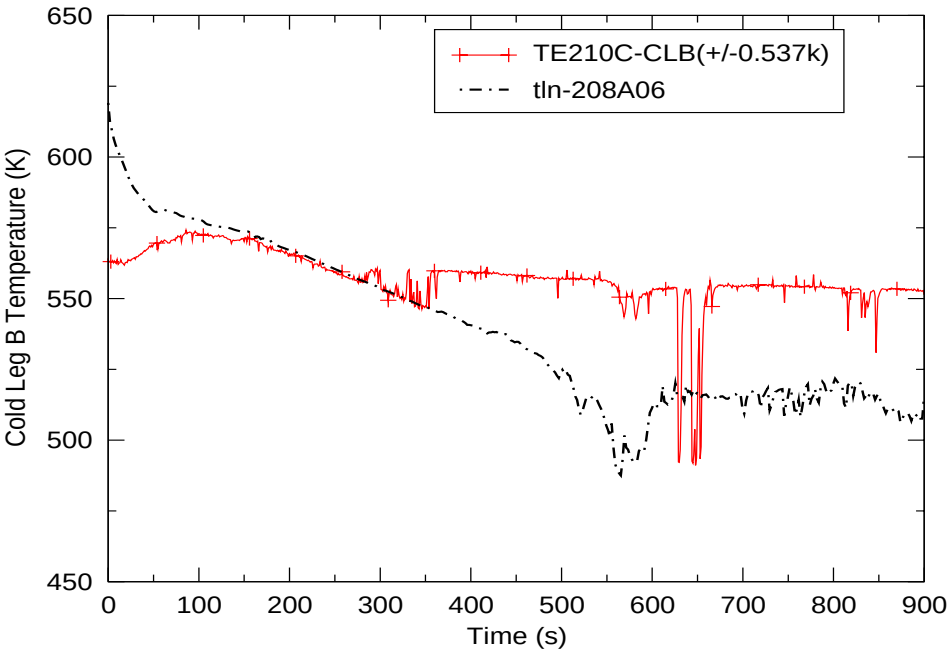

Figure C.5-211. Fluid Temperature in Loop-B Cold Leg

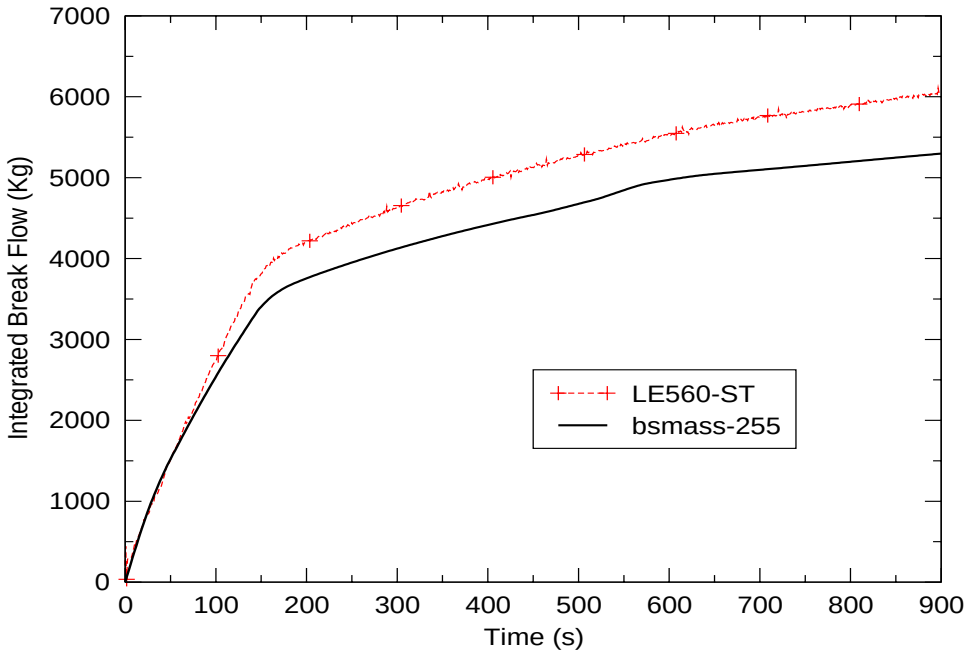

Figure C.5-212. Integrated Break Flow

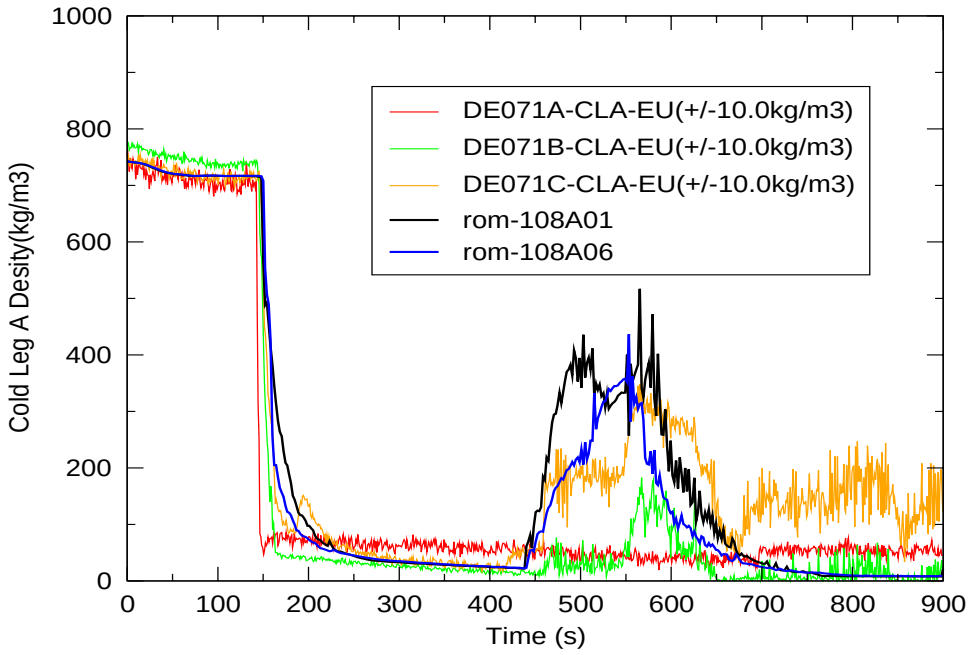

Figure C.5-213. Fluid Density in Loop-A Cold Leg

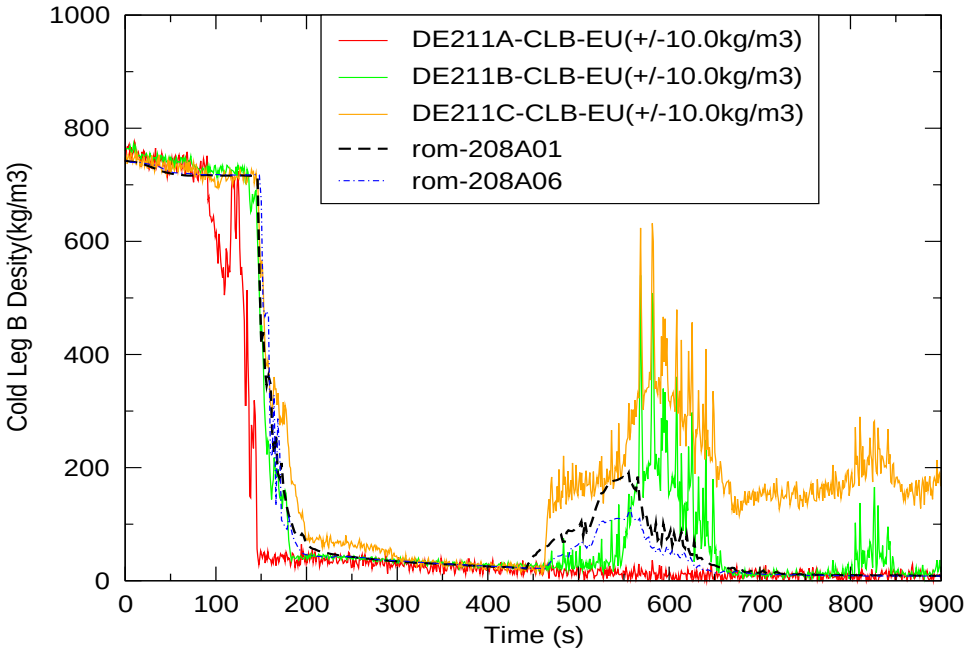

Figure C.5-214. Fluid Density in Loop-B Cold Leg

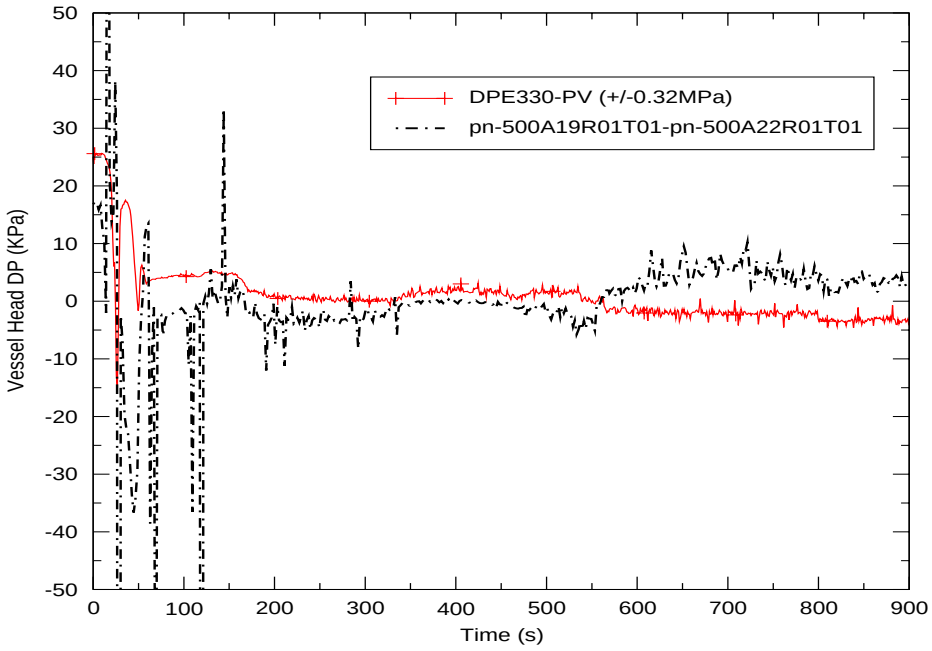

Figure C.5-215. Upper Head Differential Pressure

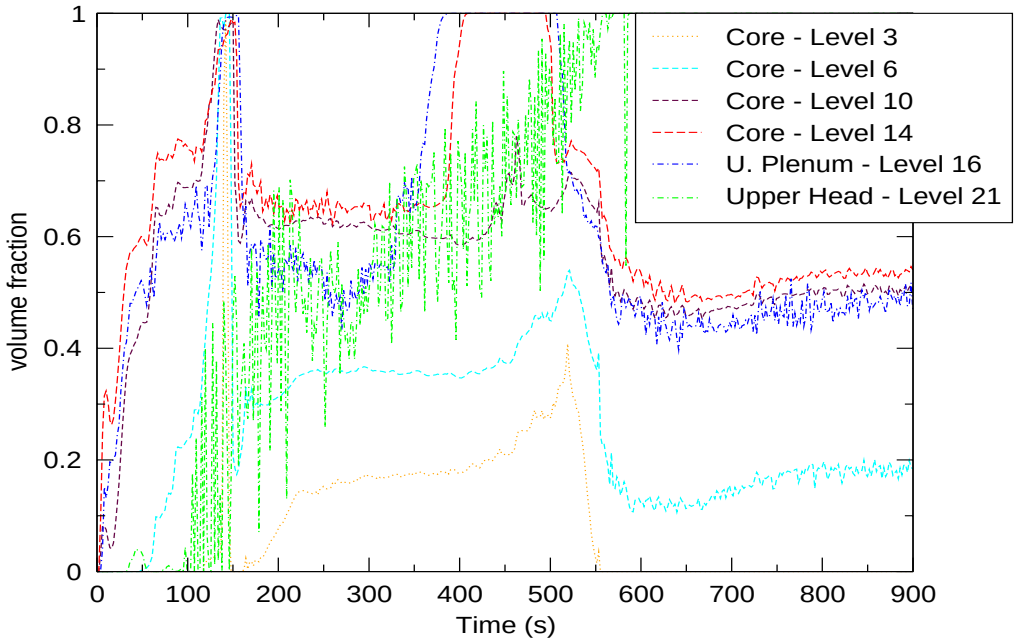

Figure C.5-216. Void Fraction in the Core (500A03-500A14), Upper Plenum (500A16), and Upper Head (500A21)

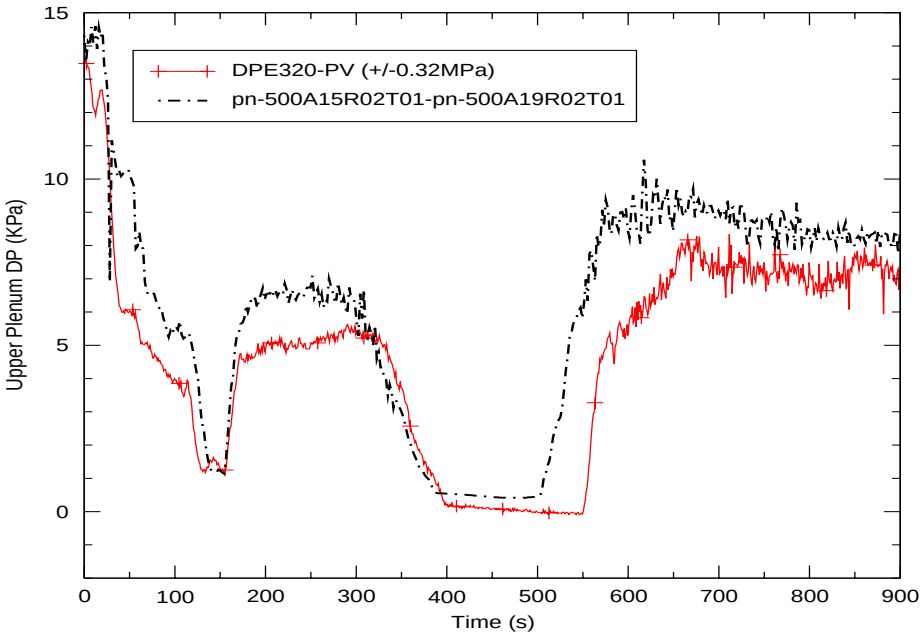

Figure C.5-217. Upper Plenum Differential Pressure

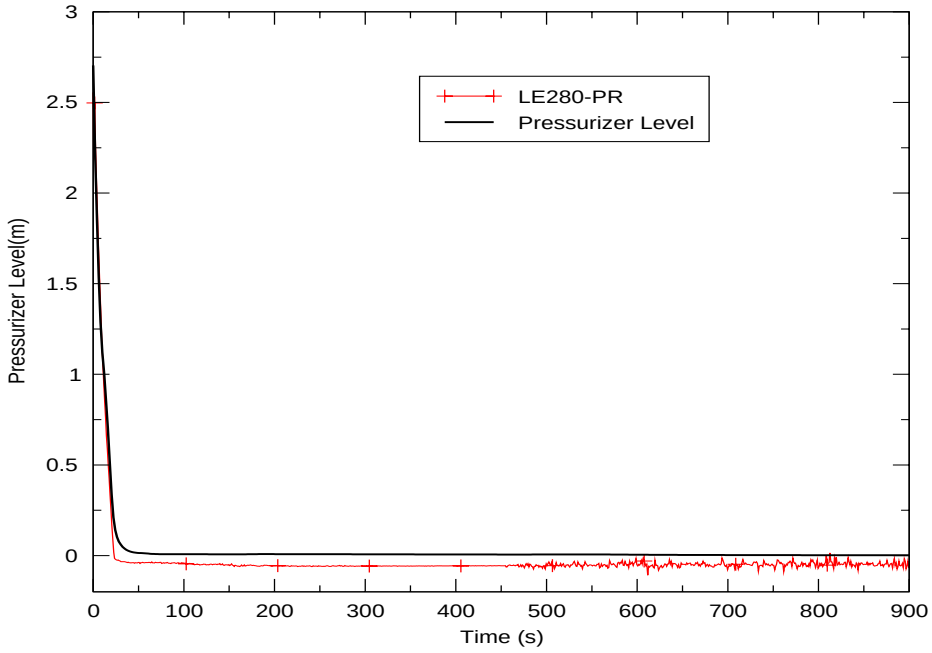

Figure C.5-218. Pressurizer Level

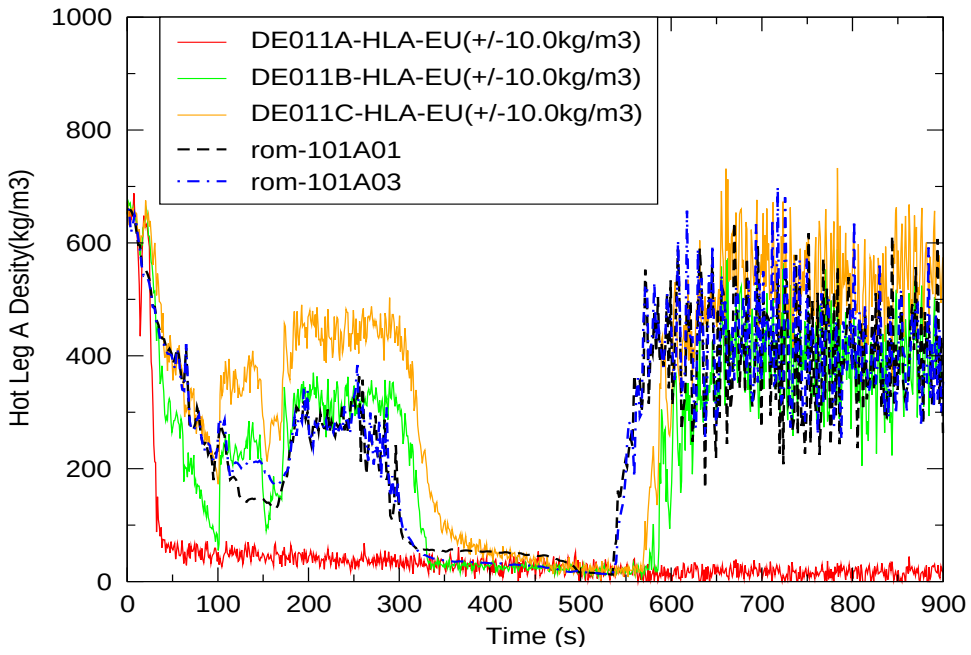

Figure C.5-219. Mixture Density in Loop-A Hot Leg

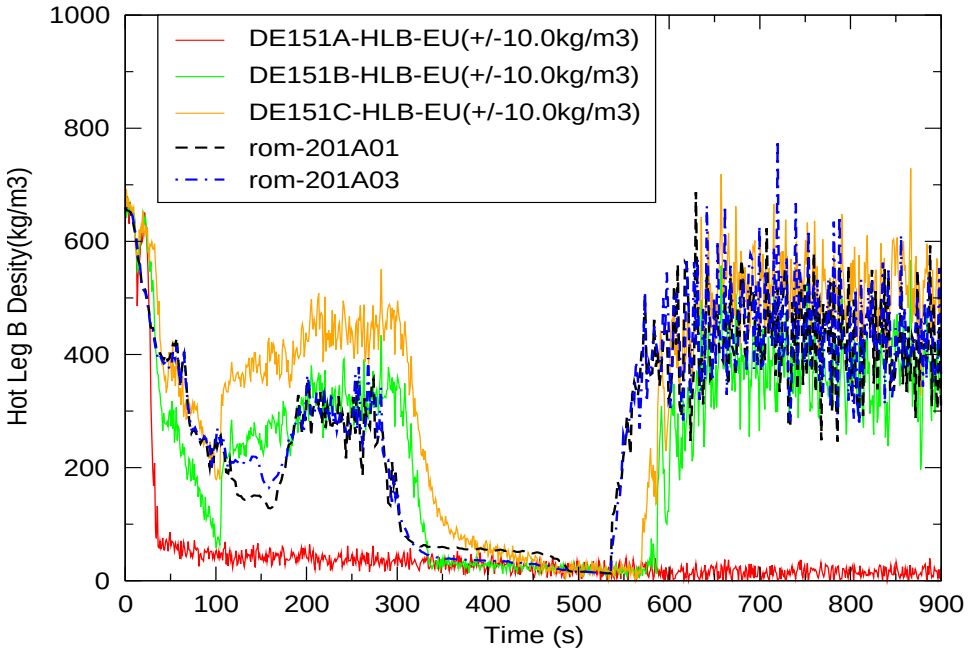

Figure C.5-220. Mixture Density in Loop-B Hot Leg

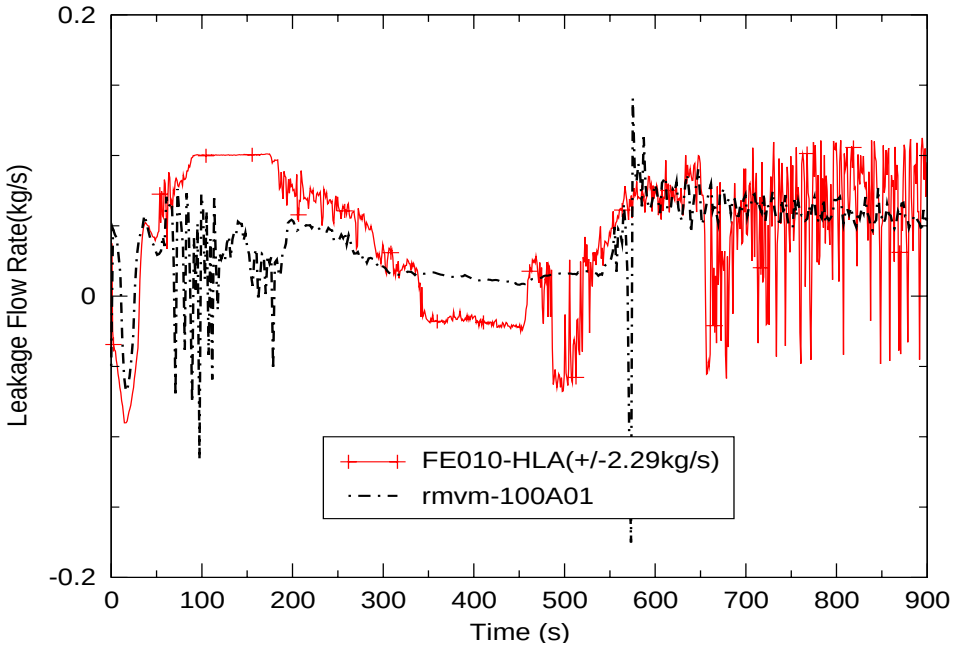

Figure C.5-221. Hot-Leg Bypass Leakage, Loop-A

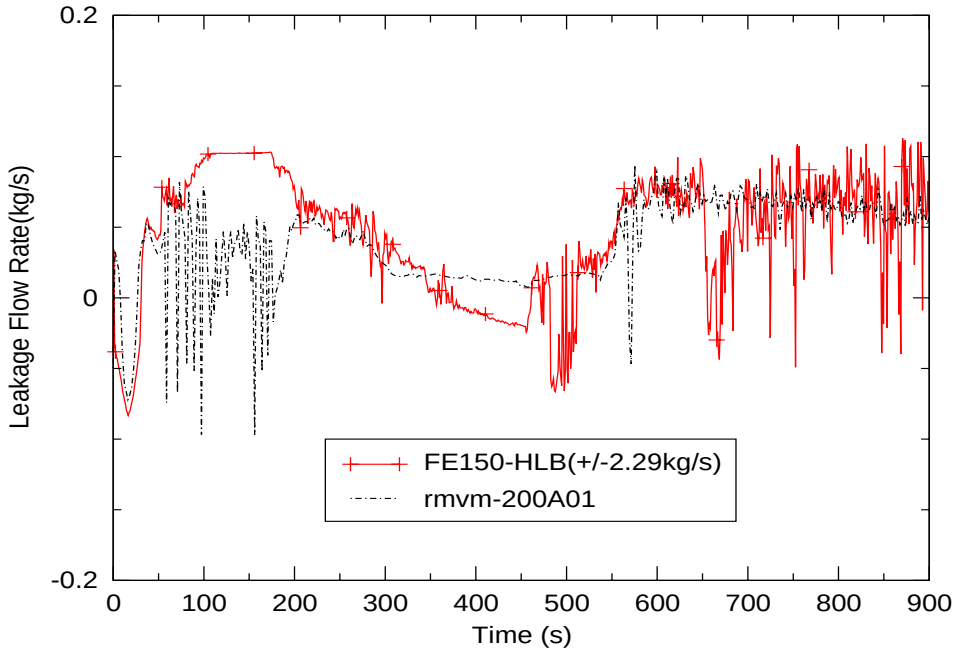

Figure C.5-222. Hot-Leg Bypass Leakage, Loop-B

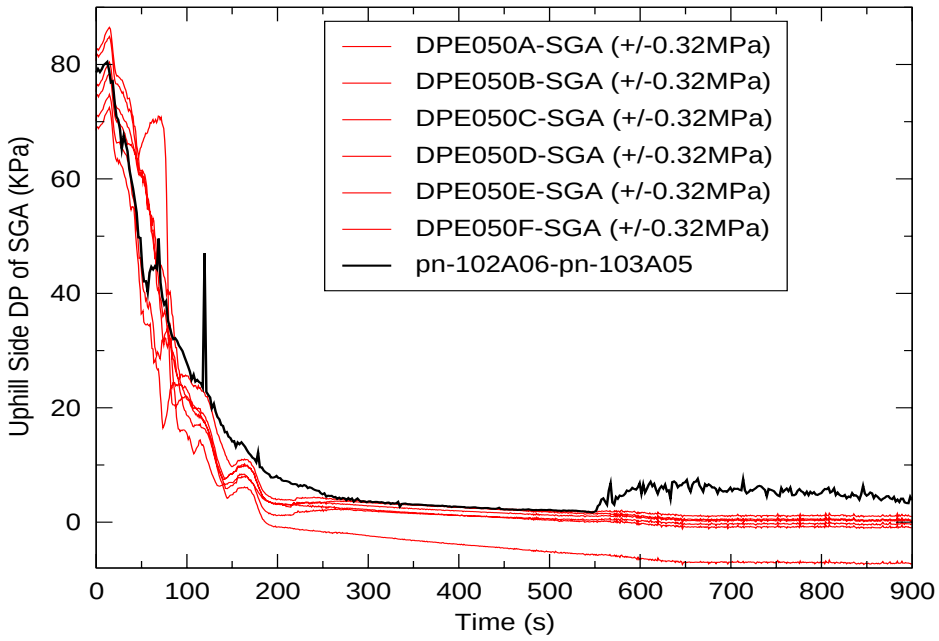

Figure C.5-223. Differential Pressure Along uphill Side of Loop-A Steam Generator Tubes

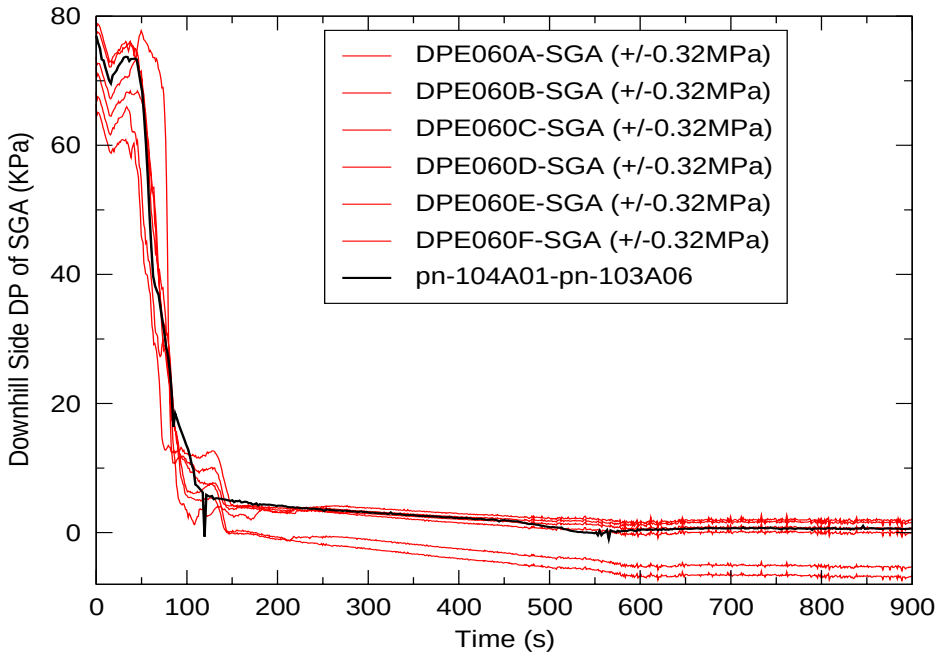

Figure C.5-224. Differential Pressure Along downhill Side of Loop-A Steam Generator Tubes

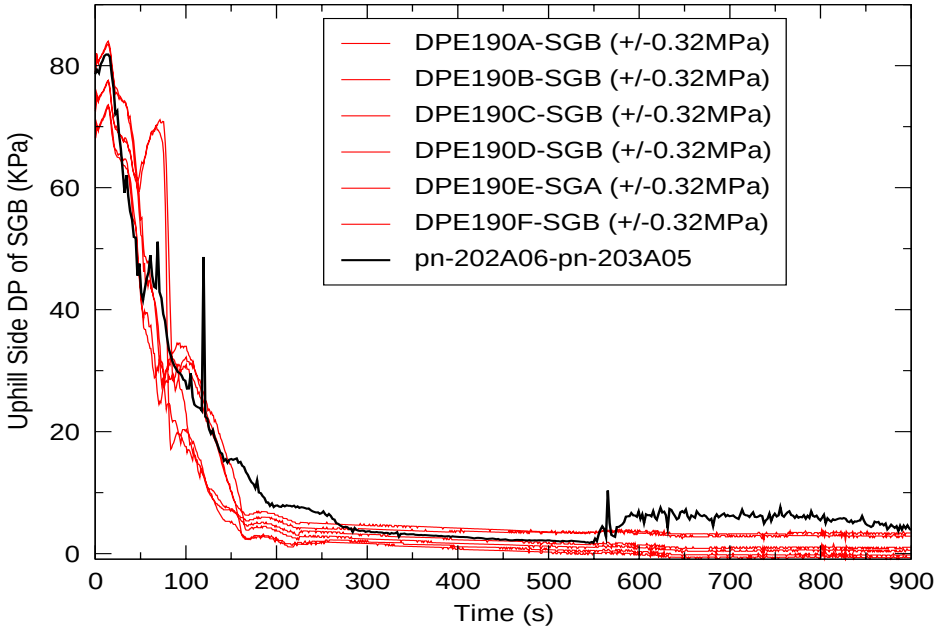

Figure C.5-225. Differential Pressure Along uphill Side of Loop-B Steam Generator Tubes

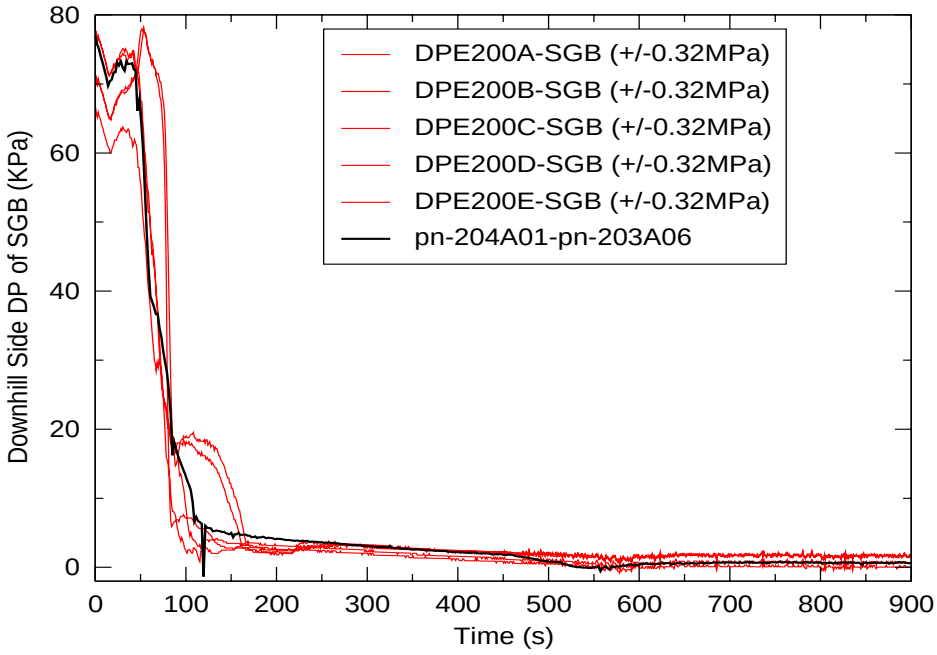

Figure C.5-226. Differential Pressure Along downhill Side of Loop-B Steam Generator Tubes

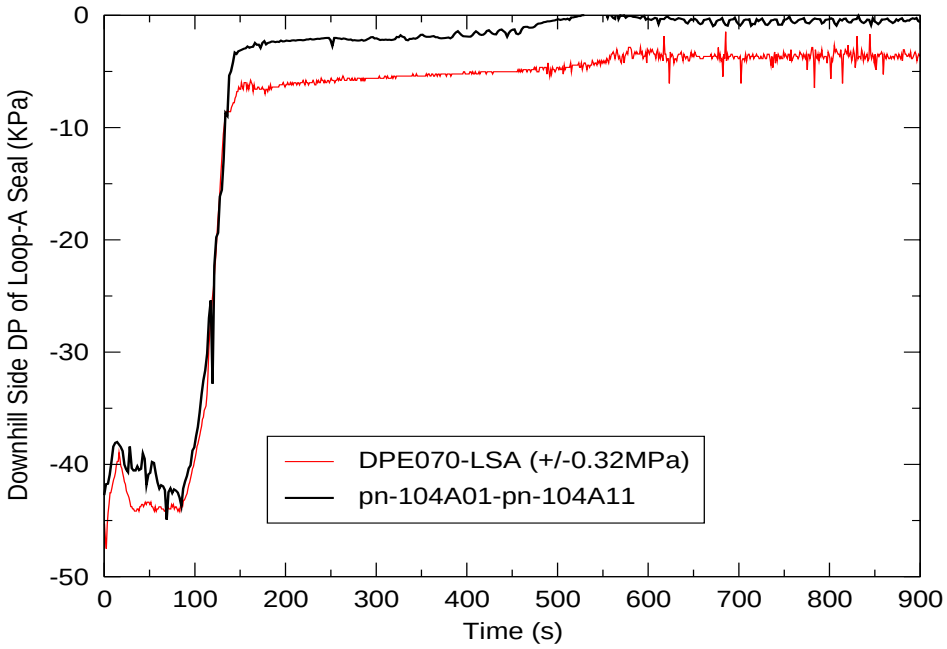

Figure C.5-227. Differential Pressure Along downhill Side of Loop-A Seal

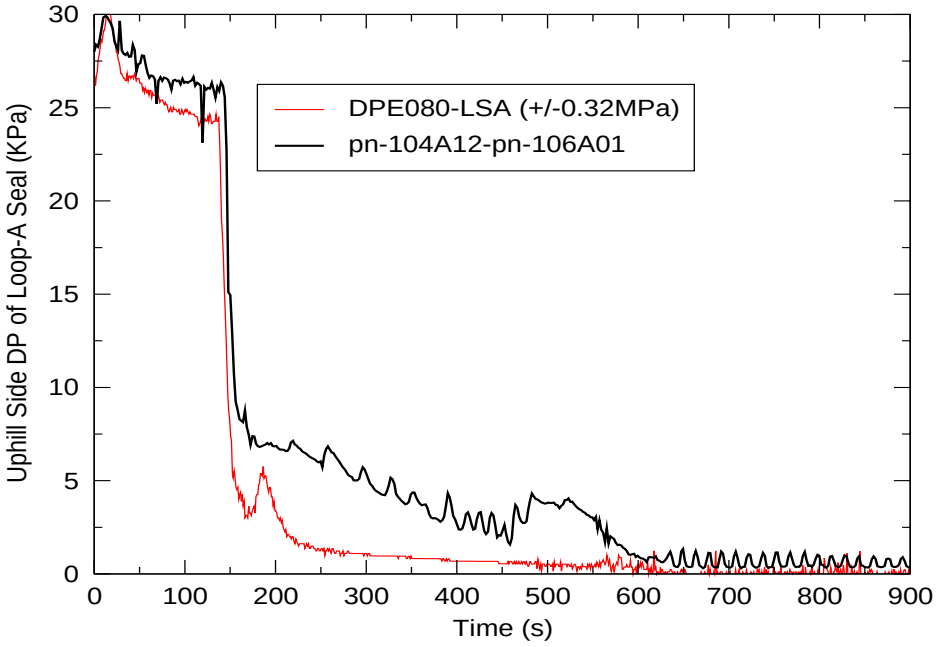

Figure C.5-228. Differential Pressure Along uphill Side of Loop-A Seal

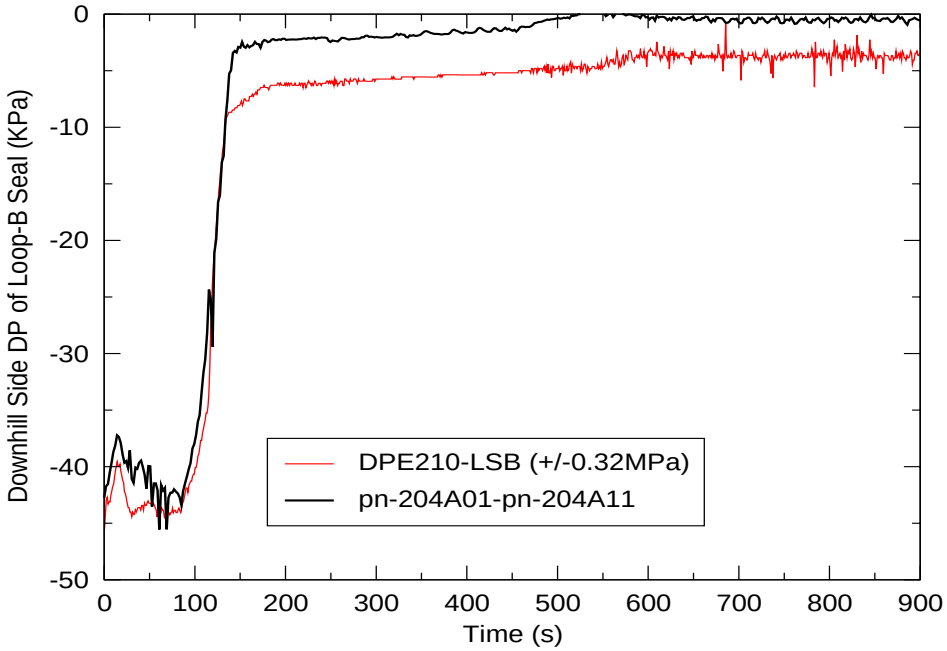

Figure C.5-229. Differential Pressure Along downhill Side of Loop-B Seal

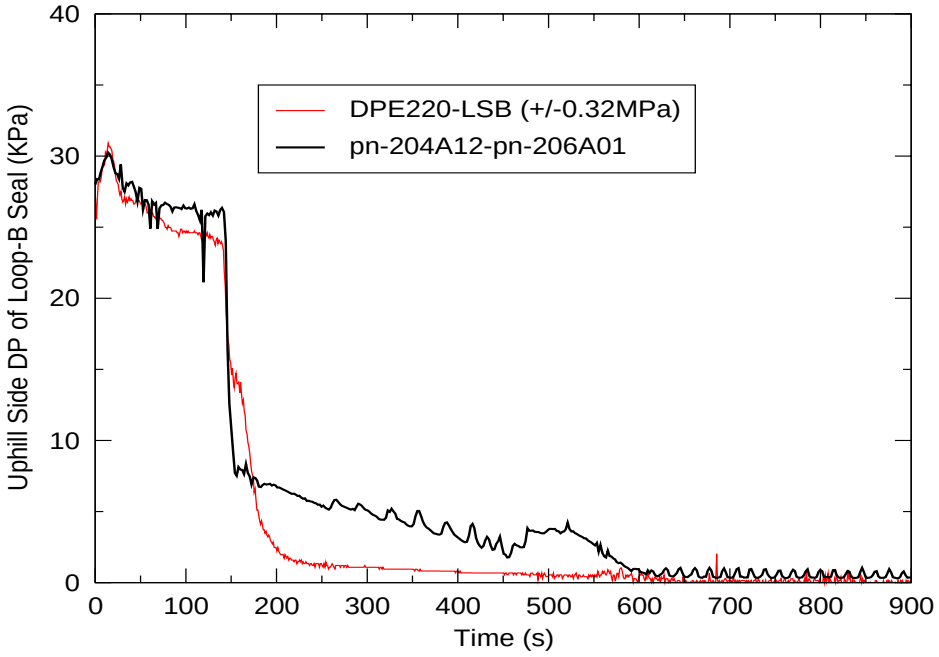

Figure C.5-230. Differential Pressure Along uphill Side of Loop-B Seal

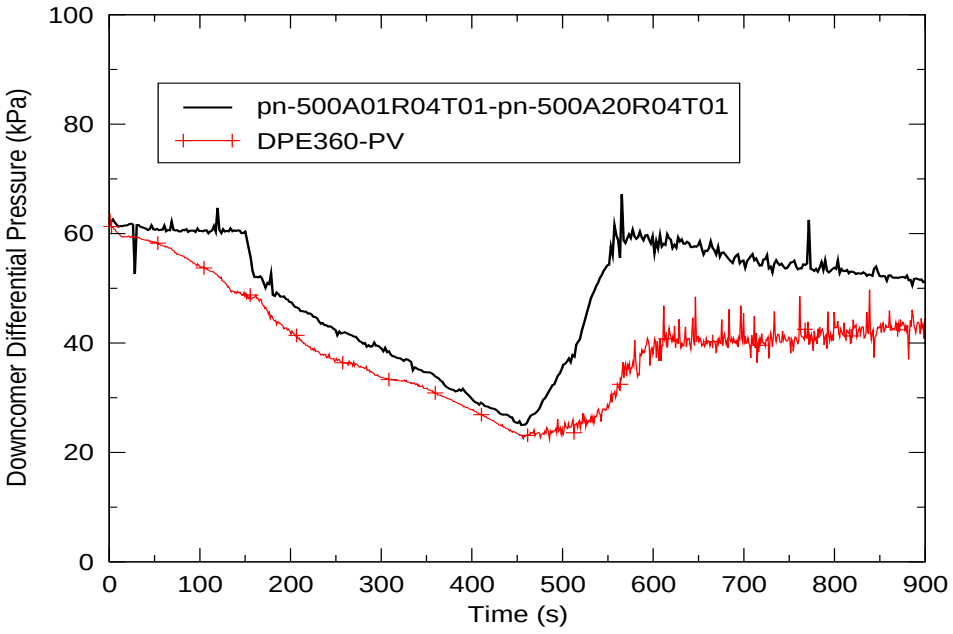

Figure C.5-231. Downcomer Differential Pressure

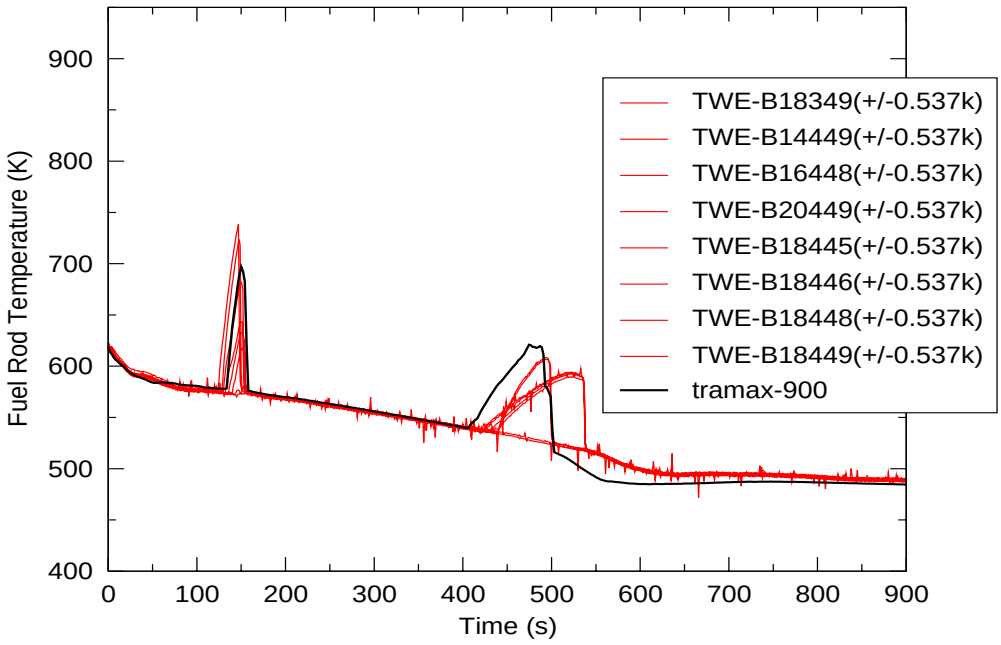

Figure C.5-232. Fuel Rod Temperature

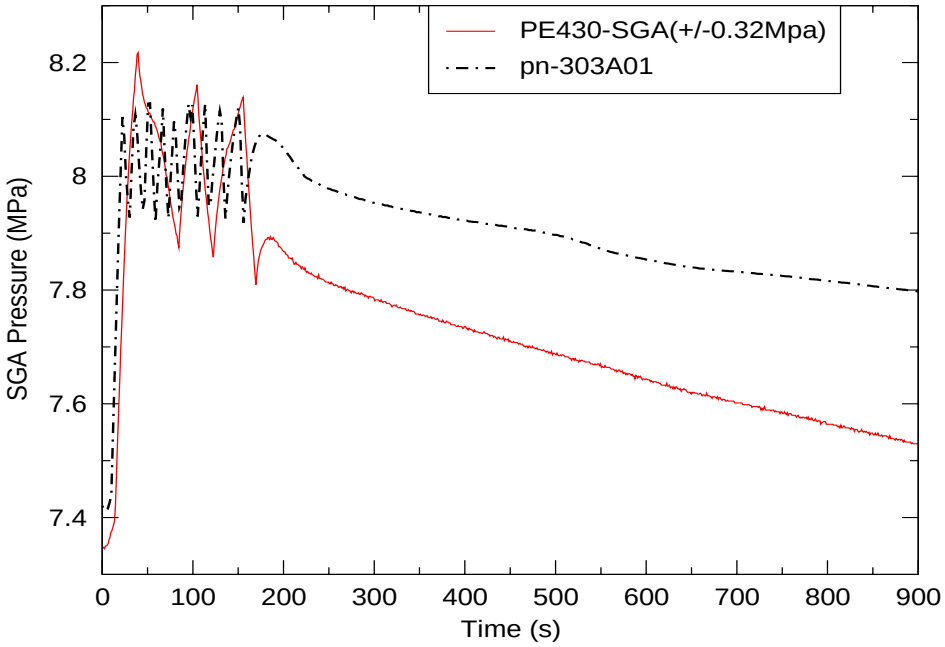

Figure C.5-233. Shell-side Pressure in Loop-A Steam Generator

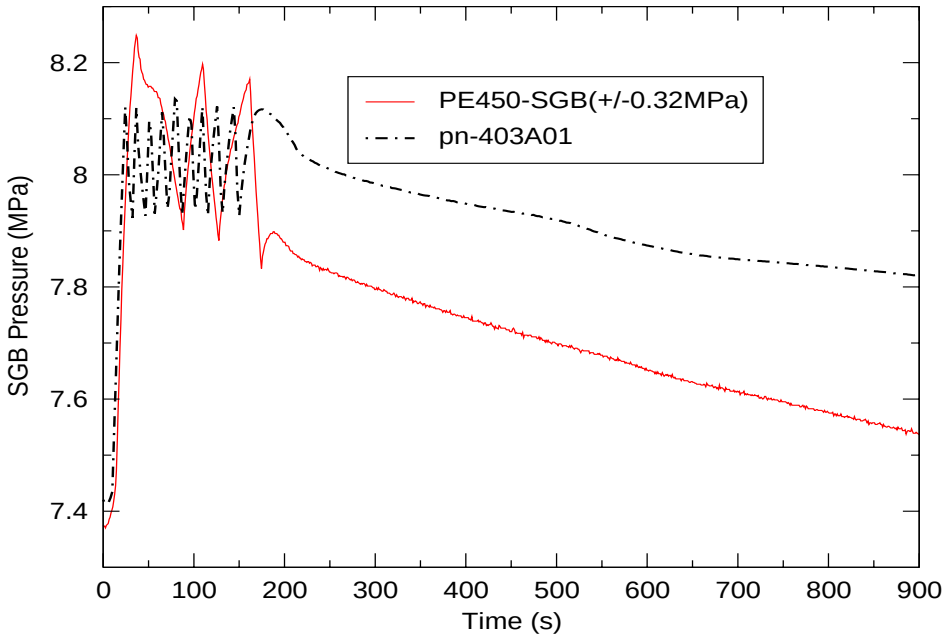

Figure C.5-234. Shell-side Pressure in Loop-B Steam Generator

C.5.5.6.5. Conclusions

Table 5.3 of this report, as well as Reference 8 lists four criteria used in the code validation: *Excellent Agreement, Reasonable Agreement, Minimal Agreement, Insufficient Agreement*. *Reasonable agreement* is defined as:.

> "*Reasonable Agreement* applies when the code exhibits minor deficiencies. Overall, the code provides an acceptable prediction. All major trends and phenomena are predicted correctly. Differences between calculated values and data are greater than those deemed necessary for excellent agreement. The calculation will frequently lie outside but near the specified or inferred uncertainty bands of the data. However, the correct conclusions about trends and phenomena would be reached if the code were used in similar applications. The code models and/or facility model noding should be reviewed to see if improvements can be made."

Based on the PIRT analysis of each characteristic phase encountered during this test, it is evident that the TRACE simulation results presented for SB-CL-18 meet the definition of *Reasonable Agreement* throughout all phases of the transient for all phenomena ranked high in the applied SBLOCA PIRT.

The majority of these items do not appear to be related to a code deficiency, but rather to inaccuracies or over-simplifications in the input model. The one potential code problem appears

to be in determining the temperature distribution that results from the mixing of the accumulator-injection and cold-leg fluids following accumulator injection. Based on the corresponding void fractions and mixture densities, the mixture temperatures in the cold legs should be higher, closer to the vapor or steam-saturation temperatures. The reduced temperatures appear to propagate to the downcomer and the vessel, where they manifest as increased fluid density and level.

C.5.6. Assessment Results Summary

Six (6) selected ROSA-IV SBLOCA tests were simulated using the TRACE V5.0 code. In these tests, four different break sizes (0.5%, 2.5%, 5%, and 10%) and three break orientations (top, side, and bottom) were investigated. Based on all of the results generated, the performance of TRACE in simulating these tests can be evaluated in terms of break size and separated into two groups: tests with break sizes larger than 0.5% and the two tests with the 0.5% break. To judge agreement between the simulations and tests, the results of a SBLOCA PIRT were used. This enabled the assessment to be focused on the phenomena and their physical variables that were ranked high in the level of importance by the SBLOCA PIRT.

For the tests with break sizes larger than 0.5%, the accurate prediction of the primary-system pressure as the transient evolved lead to good agreement between the calculated and measured FOM, particularly over the first two phases of the transient, the blowdown and natural circulation or loop-seal clearance phases. As shown in Figure C.5-235, the rate of the blowdown depressurization and the timing and magnitude of the subsequent core-level depression are matched quite well for the 5.% and 10% breaks, with a slightly premature level depression occurring for the smaller 2.5% break. This good agreement is the result of the accurate simulation of several other processes, such as primary to the secondary heat transfer and break flow. It also, in turn, leads to good agreement in fuel temperature predictions.

The primary discrepancies appear just before and shortly after accumulator injection. In tests SB-CL-05, SB-CL-14, and SB-CL-18, there appears to be a delayed affect of the accumulator injection flow, which results in a noticeable drop in core level before the injecting flows begin to aid in core recovery. Then, once the core level begins to rise, it does so too quickly, giving the indication of too much liquid injection. A look at Figure C.5-236 suggests that the accumulator system can be modeled better to bring about better agreement; however, in the SB-CL05 results, the injection flow is significantly under-predicted, yet the subsequently predicted core level surpasses the core-level measurement. Therefore, there appears to be a problem with the code related to establishing and propagating the correct temperature distribution of the mixed cold-leg and accumulator-injection flows. As shown in Figure C.5-237, almost immediately after the accumulator inject, the temperature in the cold legs plummet to near the injection fluid temperature of 322 K. In the tests, the temperature drop does not occur as quickly, nor does it reach temperatures as low. This possibly causes the fluid in the downcomer and the core to become more dense, and thus, give indications of higher levels.

The results for the 0.5% break tests were not as good, but they did not present any previously undisclosed code errors. The main problem appears to be in the prediction of the primary-system pressure. Although the agreement between the calculation and the data does not appear unreasonable, the locations and the time over which the differences remained resulted in the predicted core uncovery occurring approximately 350 seconds earlier than expected and inaccurate behavior in the loop seals. It appears that the prolonged unfolding of the transient, as a result of the relatively small break size, magnified any inaccuracies in model geometry, causing inaccurate fluid characterizations at key times during the transient.

Overall, considering both categories of tests, the TRACE V5.0 code, and dispute a potential code problem and certain modeling issues, predicted the ROSA-IV SBLOCA transients reasonably well, achieving *Reasonable Agreement* for all major phenomena.

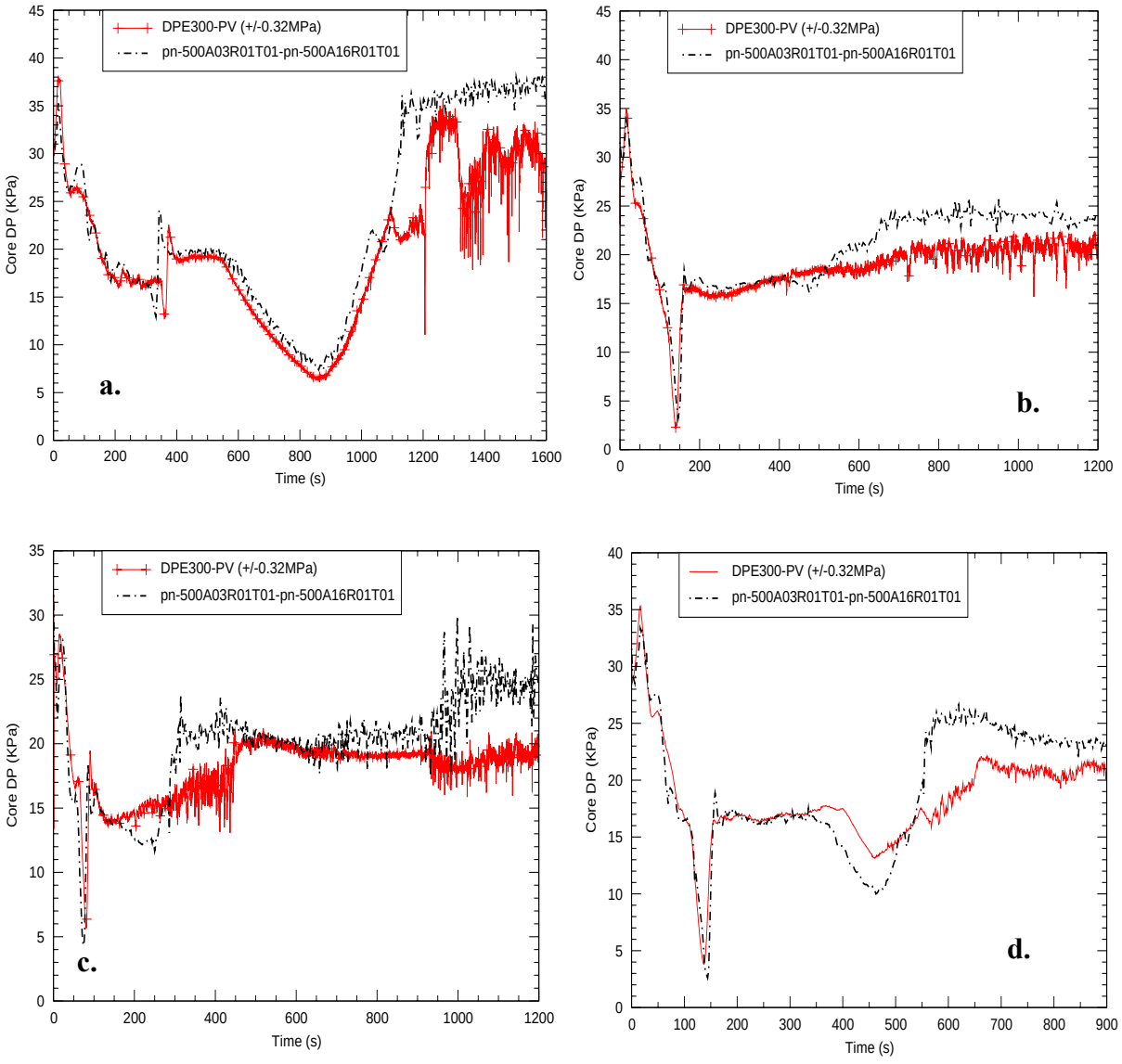

Figure C.5-235. Core Differential Pressure from Tests (a) SB-CL-01, (b) SB-CL-05, (c) SB-CL-14, and (d) SB-CL-18

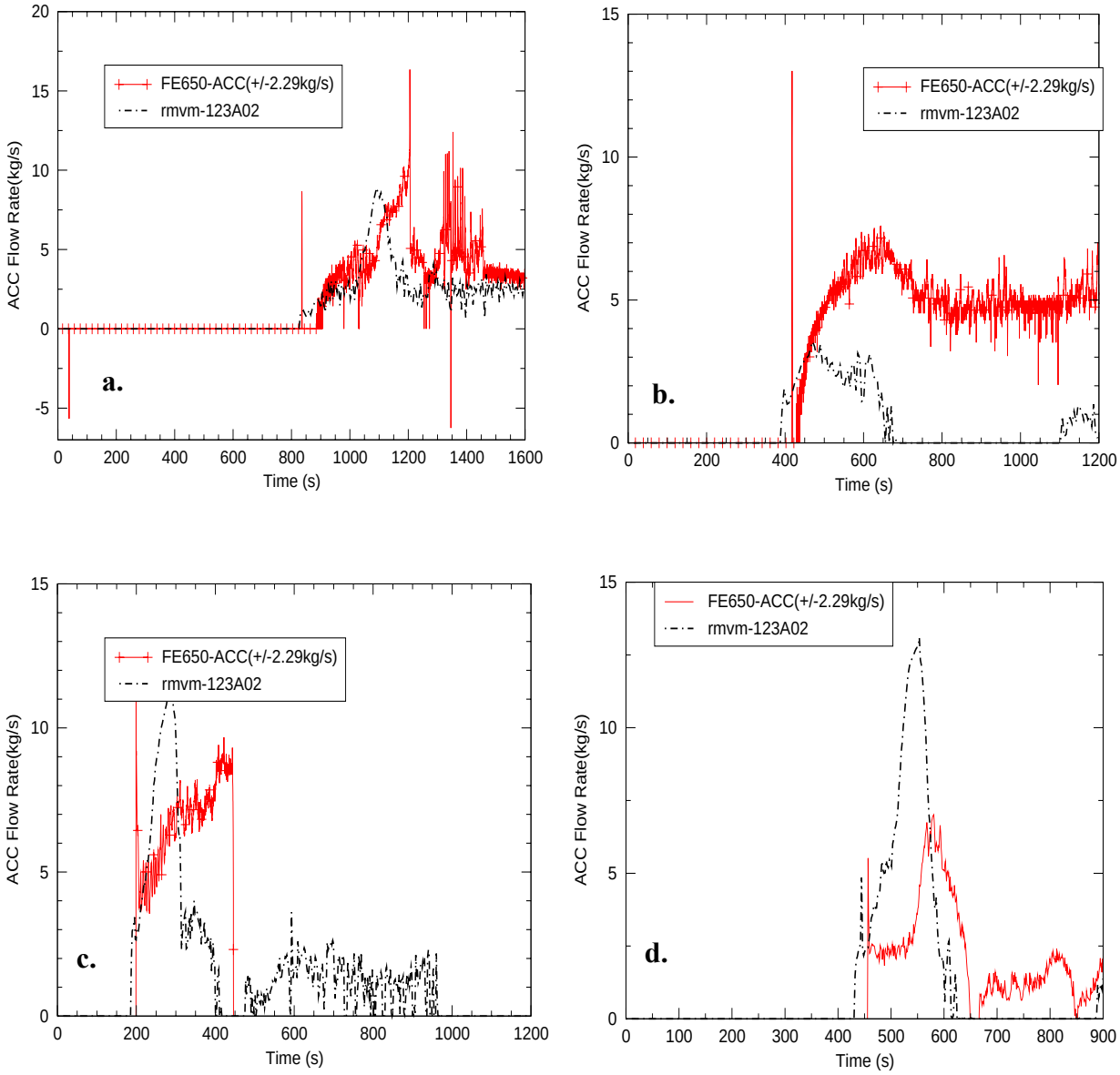

Figure C.5-236. Accumulator Injection, Tank A, from Tests (a) SB-CL-01, (b) SB-CL-05, (c) SB-CL-14, and (d) SB-CL-18

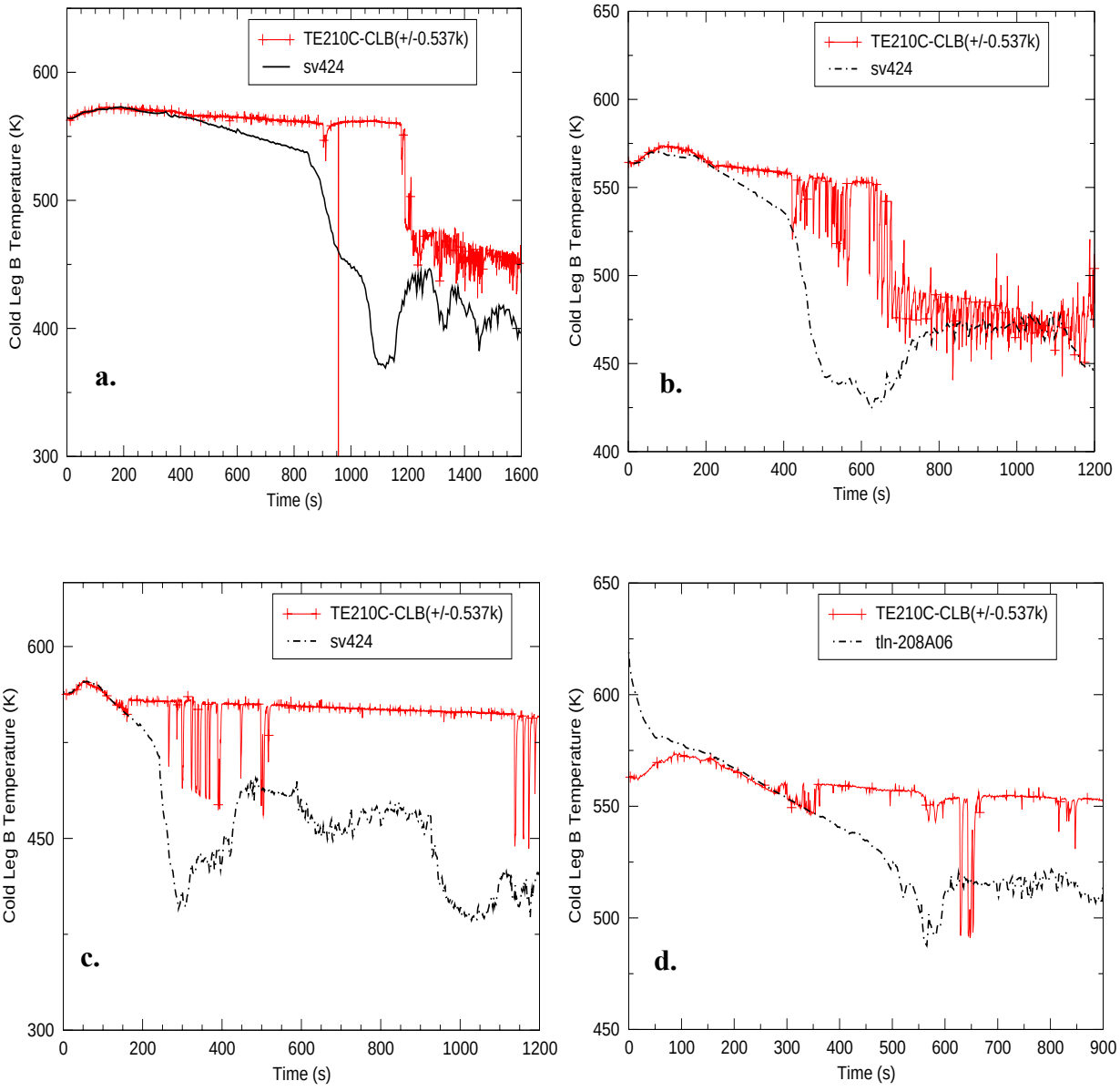

Figure C.5-237. Cold Leg B Temperatures from Tests (a) SB-CL-01, (b) SB-CL-05, (c) SB-CL-14, and (d) SB-CL-18

C.5.7. References

1 *ROSA-IV Large Scale Test Facility* (LSTF) *System Description*, JAERI – M 84-237, January 1985.

2 *System Description for the ROSA/AP600 and ROSA-V Configurations (for the 3rd Installed Core)*, JAERI-memo, 08-70, The ROSA-V Group, March 1996.

3 *TRAC-PF1/MOD2 Model for ROSA/AP600 1 Inch Small-Break LOCA, SCIE-NRC-252-96, Rev 2*, Scientech Inc., December 1998.

4 R.R. Schultz, E.E. Motley, et. al, *Calculation Notebook for a TRAC-P Vessel Model of the ROSA-IV LSTF*, Los Alamos National Laboratory, December 1985.

5 *Supplemental Description of ROSA-IV/LSTF with No.1 Simulated Fuel-Rod Assembly*, The ROSA-IV Group, September 1989.

6 Bajorek, S. M., Ginsberg, A., Shimeck, D., Ohkawa K., Young, M., Hochreiter, L., Griffith, P., Hassan, Y., Fernandez, T., Speyer, D.,"Small Break Loss of Coolant Accident Phenomena Identification and Ranking Table (PIRT) for Westinghouse Pressurized Water Reactors," Ninth International Topical Meeting on Nuclear Reactor Thermal Hydraulics (NURETH-9), San Francisco, October, 1999.

7 Y. Koizumi et al., *ROSA-IV/LSTF 5% Cold Leg Break LOCA Experiment Data Report, RUN SB-CL-05*, JAERI-memo 61-056, March 1986.

8 F. Odar, *Software Quality Assurance Procedures for NRC Thermal Hydraulic Codes*, NUREG-1737, December 2000.

9 Simulation of ROSA-IV SB-CL-05 Test Using the TRACE Computer Code, June 2004.

C.6. Semiscale Small Break LOCA Tests

Author(s): William Krotiuk[1], Mark Bolander[2]

Affiliation: [1]U.S. Nuclear Regulatory Commission, [2]Information Systems Laboratories, Inc.

Code Version: TRACE V5.0

Platform and Operating System: Intel x86, Windows XP

C.6.1. Introduction

The Semiscale experimental facility program was sponsored by the U.S. Nuclear Regulatory Commission (USNRC) and the Department of Energy (DOE), and conducted at the Idaho National Engineering and Environmental Laboratory (INEEL) during the late 1960 to late 1980 time period. Tests S-NH-1 and S-NH-2 (Ref. 1) were Small Break Loss of Coolant Accident (SBLOCA) tests with complete loss of all High Pressure Injection System (HPIS). This accident scenario results in a primary system leak continuing after scram with no automatic safety system available to inject Emergency Core Cooling (ECC) water until the primary system pressure decreases to the accumulator discharge pressure. Test S-NH-1 simulated a 0.5% cold leg pipe break. Test S-NH-2 simulated a 2.1% cold leg pipe break. The two different break sizes resulted in similar core heatup responses during the SBLOCA tests, but with different transient timing of events. The Semiscale facility hardware configuration for the NH test series was labeled as Mod-2C. Tests S-NH-1 and S-NH-2 were simulated with TRACE. The purpose of the assessment was to verify the code's ability to predict the phenomenon occurring in the primary and secondary sides of the test facility during the transient. The TRACE calculated results are compared to Semiscale test data.

The input models for Semiscale SBLOCA tests S-NH-1 and S-NH-2 were developed by Information Systems Laboratory (ISL) and executed using earlier TRACE Version 4263. This document reports the results of the execution of TRACE Version 5.0 Release Candidate 3 using the original inputs prepared by ISL.

C.6.2. Semiscale Facility Description

A facility and instrumentation description for these tests is given in Reference 2. Semiscale configuration Mod-2C was scaled to a four loop pressurized water reactor. The facility was built with a 1/1 vertical length scaling and 1/1705 volume scaling. The intact loop was sized to represent three lumped loops and the broken loop was sized to represent the single fourth loop. The core was represented by a 5x5 electrically heated bundle with two unpowered rods. Core power was 2 MW.

An isometric sketch of the Mod-2C hardware is shown in Figure C.6-1 Mod-2C hardware included a vessel downcomer external to the vessel so that wall surface area could be minimized while maintaining the scaled downcomer flow area. The broken loop steam generator also had an external downcomer. Both steam generators were of the inverted U tube design. The intact loop steam generator had 6 tubes and the broken loop steam generator had only 2 tubes.

C.6.3. TRACE Model Description

A TRACE input model of the Semiscale facility used in an earlier assessment study for the small break NH test series (Ref. 3) was used as the base model for this assessment. All of the major flow paths of the facility were modeled. There were several modifications made to the base model that include removing unneeded components, merging the components that made up the vessel into one VESSEL component, and merging the components that made up the pressurizer into one PIPE component. A detailed description of the model modifications is given in Reference 4.

The TRACE nodalization of the Semiscale small break test facility is shown in Figure C.6-2 There are a total of 104 components: 55 hydro components, 48 heat structure components and one power component. Six control system models were used during the steady-state calculations to drive the TRACE model to the desired steady-state initial conditions. The control systems are: intact and broken loop flow controllers, intact and broken loop steam generator steam dome pressure controllers, and intact and broken loop steam generator secondary side mass controllers. Miscellaneous controllers were implemented to calculate system mass and various operator actions taken during the tests. The control system is composed of 345 elements. There are 147 Signal Variables, 176 Control Blocks and 22 Trips. A detailed description of the base model is given in Reference 3.

C.6.4. Tests Simulated with TRACE

Semiscale small break tests S-NH-2 and S-NH-1 were simulated with TRACE.

The S-NH-2 transient was a 2.1% cold leg SBLOCA test, with all HPI unavailable. This small break transient resulted in reactor scram, Main Steam Isolation Valve (MSIV) closure, Feedwater (FW) trip and recirculation pump trip shortly after break initiation due to a low pressurizer pressure trip. The primary system lost coolant through the small break in the cold leg pipe. With

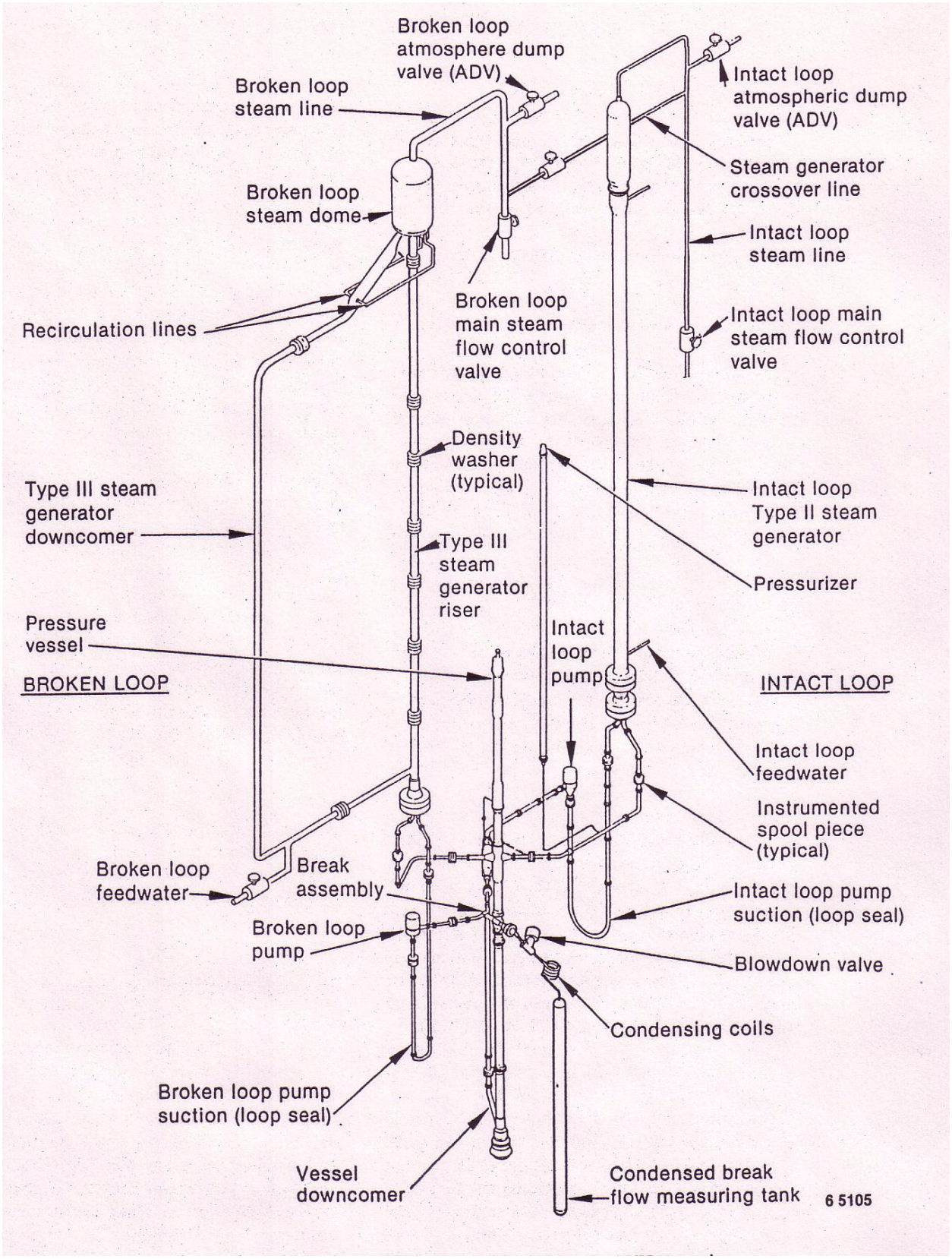

Figure C.6-1. Semiscale Facility.

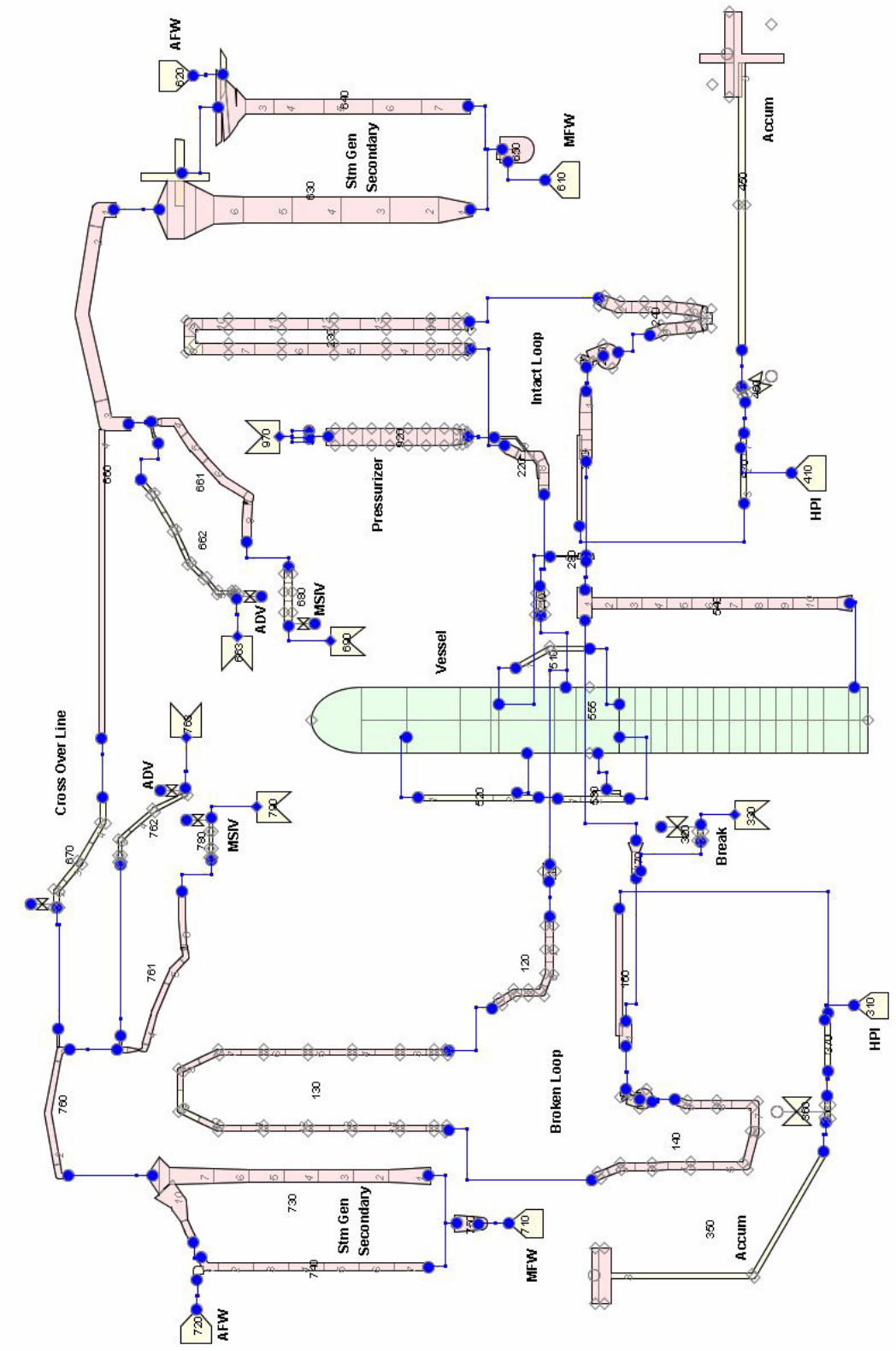

Figure C.6-2. TRACE Nodalization Scheme of the Semiscale Test Facility for the NH (small break) Series Tests.

complete loss of HPI, no safety injection water was available to replenish the primary system inventory until the primary system pressure decreased to the accumulator setpoint of 4.24 MPa. The primary system transitioned from forced flow, to single phase natural circulation flow, to two-phase natural circulation flow, and then to reflux natural circulation. The pressurizer water inventory drained and water level in the reactor vessel decreased. To prevent heater rod damage if the core region became significantly uncovered prior to accumulator injection, Test S-NH-2 was planned to have operators initiate recovery operations by manually latching open the Steam Generator (SG) Atmospheric Dump Valves (ADVs) when the fuel heatup resulted in the Peak Clad Temperature (PCT) reaching 811 ^{o}K. Opening the ADVs would blow down the SGs, resulting in SG pressure less than primary system pressure. This recovery scheme would enable the SGs to resume removing heat from the primary system and depressurize the primary system to less than the accumulator injection pressure. The accumulators have sufficient capacity to refill the primary system with water and reflood the core to terminate the fuel heatup. Test S-NH-2 lasted 2500 seconds.

The S-NH-1 test was the same transient scenario as S-NH-2, except S-NH-1 was a much smaller break size. The break size for test S-NH-1 was a 0.5% cold leg break. As in test S-NH-2, all HPI was unavailable. This small break transient resulted in reactor scram, MSIV closure, FW trip and recirculation pump trip shortly after break initiation due to a low pressurizer pressure trip. The primary system lost coolant through the small break in the cold leg pipe. With complete loss of HPI, there was no other safety injection water available to replenish the primary system inventory until the primary system pressure decreased to the accumulator set point of 4.24 MPa. The primary system transitioned from forced flow, to single phase natural circulation flow, to two-phase natural circulation flow, and then to reflux natural circulation flow. The pressurizer water inventory drained and water level in the reactor vessel decreased. To prevent heater rod damage if the core region became significantly uncovered prior to accumulator injection, Test S-NH-1 was planned to have operators initiate recovery operations by manually latching open the SG ADVs when the fuel heatup resulted in PCT reaching 811 ^{o}K. Opening the ADVs would blow down the SGs, resulting in SG pressure less than primary system pressure. This recovery scheme would enable the SGs to resume removing heat from the primary system and depressurize the primary system to less than the accumulator injection pressure. The accumulators have sufficient capacity to refill the primary system with water and reflood the core to terminate the fuel heatup. Test S-NH-1 lasted 5200 seconds.

C.6.4.1. Simulation of Test S-NH-2.

A summary of the initial conditions from the Semiscale S-NH-2 experiment and the TRACE code calculated initial conditions is shown in Table C.6.1 The S-NH test series initial conditions were obtained from Table 1 of Reference 1 and from the recorded test data files for S-NH-2 in the NRC databank. The uncertainty values for the measured test data were obtained from Table VII of Reference 5.

The timing of important events during the S-NH-2 transient are compared to TRACE predictions in Table C.6.2. The Semiscale NH test series results report (Ref. 1), does not contain any sequence of events tables to document the timing of trips and events that occurred during the tests. The

Semiscale times reported in Table C.6.2 were obtained from various text sections of the NH test series results report and from the recorded test data file. TRACE was executed longer (3000 s) than the test duration (2500 s) in order to capture the second core heatup.

Table C.6.1. Initial Conditions for Test S-NH-2 .

Parameter	Measured Data	TRACE
Pressurizer Pressure (MPa) - (pn-920A10)	15.58 ± 0.07	15.58
Pressurizer Liquid Level (m) - (sv800)	2.53 ±0.25	2.52
Core Power (MW) - (rpower-998)	1.998 ± 0.02	1.998
Core Δ Temperature (^{o}K) - (tln-555A16R01T01 - tln-555A03R01T01)	37.7 ± 3.3	40.4
Intact Loop Cold Leg Temperature (^{o}K) - (tln-270A03)	548.9 ± 3.3	547.6
Intact Loop Hot Leg Temperature (^{o}K) - (tln-210A01)	587.4 ± 3.3	587.2
Broken Loop Cold Leg Temperature (^{o}K) - (tln-170A01)	551.4 ± 3.3	548.8
Broken Loop Hot Leg Temperature (^{o}K) - (tln-110A01)	586.8 ± 3.3	587.2
Intact Loop Flow (l/s) - (cb270)	9.07 ± 0.033	9.07
Broken Loop Flow (l/s) - (cb170)	3.23 ± 0.033	3.23
Intact Loop Cold Leg Pressure (MPa) - (pn-270A03)	15.77 ± .0.07	15.78
Broken Loop Cold Leg Pressure (MPa) - (pn-170A01)	15.79 ± .0.07	15.78
Downcomer to upper head Bypass flow (% of total core flow) - (rmvm-280A04 / (rmvm-270A02 + rmvm-170A02))	3.14	3.10
Intact Loop Steam Generator secondary pressure (MPa) - (pn630A09)	4.82 ± 3.3	4.82
Broken Loop Steam Generator secondary pressure (MPa) - (pn730A08)	4.56 ± 3.3	4.56
Intact Loop Steam Generator steam flow (kg/s) - (rmvm-630A10)	0.77	0.786
Broken Loop Steam Generator steam flow (kg/s) - (rmvm-730A09)	0.24 ±0.05	0.27
Intact Loop Steam Generator feedwater flow (kg/s) - (fxmass-610)	0.77	0.775
Broken Loop Steam Generator feedwater flow (kg/s) - (fxmass-710)	0.24	0.27
Intact Loop Steam Generator secondary mass (kg) - (cb100)	68	68.4
Broken Loop Steam Generator secondary mass (kg) - (cb200)	24	23.6
Intact Loop Pump Speed (rpm) - (omegan-250)	2208	2202 [a]
Broken Loop Pump Speed (rpm) - (omegan-150)	1539	1531
Intact Loop Feedwater Temperature (^{o}K) - (tln-610A01)	487.8 ± 3.3	487.8
Broken Loop Feedwater Temperature (^{o}K) - (tln-710A01)	484.2 ± 3.3	484.2
Intact Loop Accumulator Temperature (^{o}K) - (tln-450A03)	300 ± 3.3	302
Broken Loop Accumulator Temperature (^{o}K) - (tln-350A03)	unknown ± 3.3	302

a. Pump speed was adjusted to obtain the desired loop flow rate

Table C.6.2. Key Events for SemiScale Test S-NH-2

Key Event	Time Data (s)	Time TRACE (s)
Break Initiation	~ 0.0	0.0
Pressurizer Pressure Low Pressure Trip at 13.1 MPa (signal for MSIV trip, steam line crossover valve closure and power scram) - (trip-170, trip-150)	~ 18.69	18.9
MSIV Closure Trip, Intact Loop - (trip-680)	18.69<t<21.52	18.9
MSIV Closure Trip, Broken Loop - (trip-780)	15.86<t<18.69	18.9
Power Scram - (trip-150)	18.69<t<21.52	21.9
Pressurizer Pressure Low Pressure Trip at 12.6 MPa (safety injection signal) - (pn-920A01)	~ 19.78	23.8
Feedwater Trip Off - (fxmass610, fxmass710)	18.69<t<21.52	24.3
Start Aux FW, Intact Loop / Broken Loop - (trip-620 / trip-720)	18.69<t<21.52	24.1/24.2
Main Coolant Loop Pumps Trip - (omegan-250, omegan-150)	21.52<t<24.34	25.9
HPIS Initiated Intact Loop / Broken Loop	unavailable	unavailable
Pressurizer Empty - (cb360)	~ 50	~ 40 - 60
Break flow transitions from liquid to two-phase flow - (alpn-320A01)	~ 175	228
Intact Loop Seal Clears - (alpn-240A07)	~ 620	~ 1287
Broken Loop Seal Clears - (alpn-140A07)	never	~ 520
Break uncovers, break flow transitions to all steam flow - (alpn-320A01)	~ 620	~ 647 - 743[a]
First Core Heatup Begins - (tsurfo-951A09)	846.7	965
Operator action, BL SG Aux FW Off - (trip-720)	~ 965	965
Intact Loop steam dump valve (ADV) latched open - (trip-662)	1086.9<t<1089.8	1208.3
Broken Loop steam dump valve (ADV) latched open - (trip-762)	1084.1<t<1086.9	1208.3
Operator action, BL SG Aux FW On - (trip-720)	~ 1118	1118
Accumulator Injection, Intact Loop / Broken Loop - (rmvm460A02 / rmvm360A02)	1171.7 / 1185.9	1258 / 1152
Minimum core collapsed water level; distance from bottom of core - (cb577)	~ 1200 [b] (0.84 m)	1287 (0.41 m)
First PCT - (tsurfo-951A09)	1296.1 (983 ^{o}K)	1293 (880 ^{o}K)
Second Core Heatup Begins - (tsurfo-951A09)	2078.9	2355
Second PCT - (tsurfo-951A09)	2497.2 (1089 ^{o}K)	NA
End of Test	2497	3000 [c]

a. Reference 1 specifies break uncovery at 620 seconds based on the upstream break density plot, Figure 29. The Semiscale break flow data (MDOT*BREAK) shows break flow transitions to steam flow by ~700 seconds. TRACE break uncovery is based on break void fraction transition from 0.95 to 0.99.

b. scaled from Figure 35 in Reference 1.

c. The TRACE analysis was executed to 3000 seconds problem time in order to capture the second core heatup which was predicted to begin at 2355 seconds which is about 276 s after the test measurement.

C.6.4.1.1. Core Power

The TRACE decay heat curve used was obtained from the TRACE simulation of Semiscale test S-LH-2, as documented in Reference 6. The Semiscale NH test series core power was augmented by a continuous 22kW during the transients to make up for excessive environmental heat loss, unaccounted for by the external heaters (Ref. 1). The TRACE model does not simulate the primary system heat loss to the environment, therefore, the decay heat curve data from test S-LH-2 was used for the TRACE model. Test S-LH-2 reportedly did not use augmented core power. Figure C.6-3 compares the TRACE calculated core power response with the Semiscale test data.

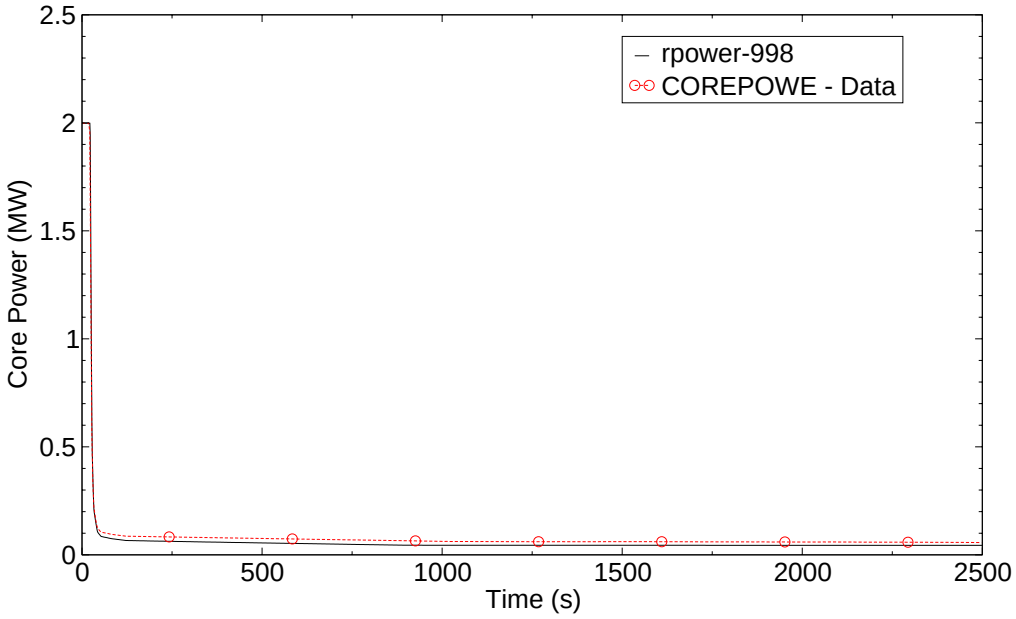

Figure C.6-3. Core Power Comparison - Test S-NH-2.

C.6.4.1.2. Break Flow

A comparison of the predicted break mass flow rate to the measured data is shown in Figure C.6-4 The Semiscale experimental break simulator was attached to the side of the cold leg pipe which is represented by a TEE in TRACE. The TRACE offtake model was active at the side arm. The TRACE predicted break flow rate agrees well with the Semiscale data. The TRACE initial break flow spike is larger in magnitude than the Semiscale data. The Semiscale data is the recorded condensate mass collected in the break collection tank, located downstream of the break and condensing coils. The TRACE plotted mass flow rate is at the break orifice location. The Semiscale break flow data should be slightly delayed and have a damped response, in comparison to the TRACE calculated break flow.

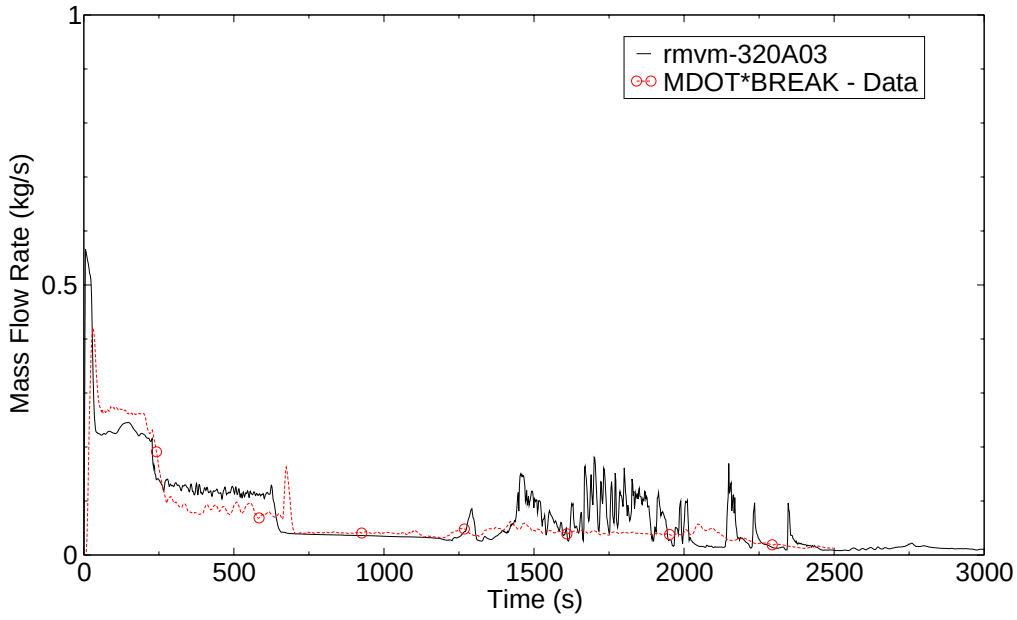

Figure C.6-4. Break Mass Flow Rate Comparison - Test S-NH-2.

At about 228 seconds, the TRACE calculated break flow transitioned from liquid flow to two-phase flow. By about 250 seconds, the void fraction at the break was just below 80% as shown in Figure C.6-5 When the break transitions to a higher void fraction the break vapor velocity increased as shown in Figure C.6-6 The flow becomes choked and remained choked throughout most of the transient.

The break flow is relatively constant until about 680 seconds when the break flow transitioned from two-phase to mostly all steam flow. The predicted transition from two-phase to single phase steam occurs earlier when compared to the data. The flow spike in the data appears to be as result of a slug of water reaching the break as the loop seals cleared. The flow spike is not observed in the calculation.

The predicted integrated break mass flow rate is compared to data in Figure C.6-7 The mass leaving the system through the break compares reasonably well with the data until about 1400 seconds when TRACE predicts larger flow rate than the data.

C.6.4.1.3. Primary System Pressure.

The TRACE calculated primary system pressure response agrees reasonably well with the measured data as shown in Figure C.6-8 Phenomenon affecting the primary system pressure response include break flow rate, decay heat, pump coast down and fluid flashing as the system pressure approached saturation. During the early part of the blowdown the predicted pressure

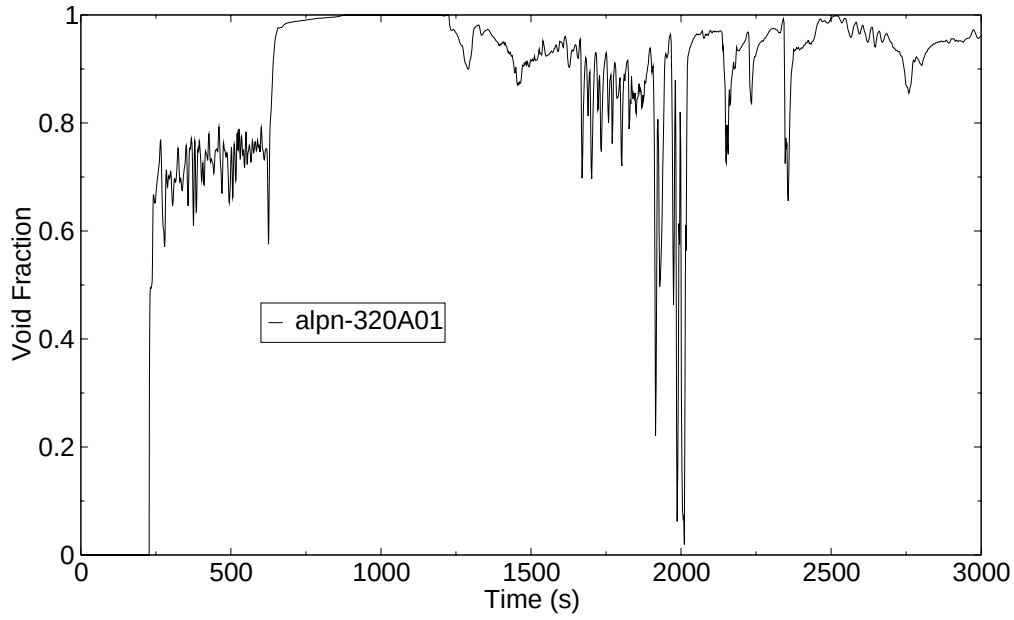

Figure C.6-5. Predicted Break Void Fraction - Test S-NH-2.

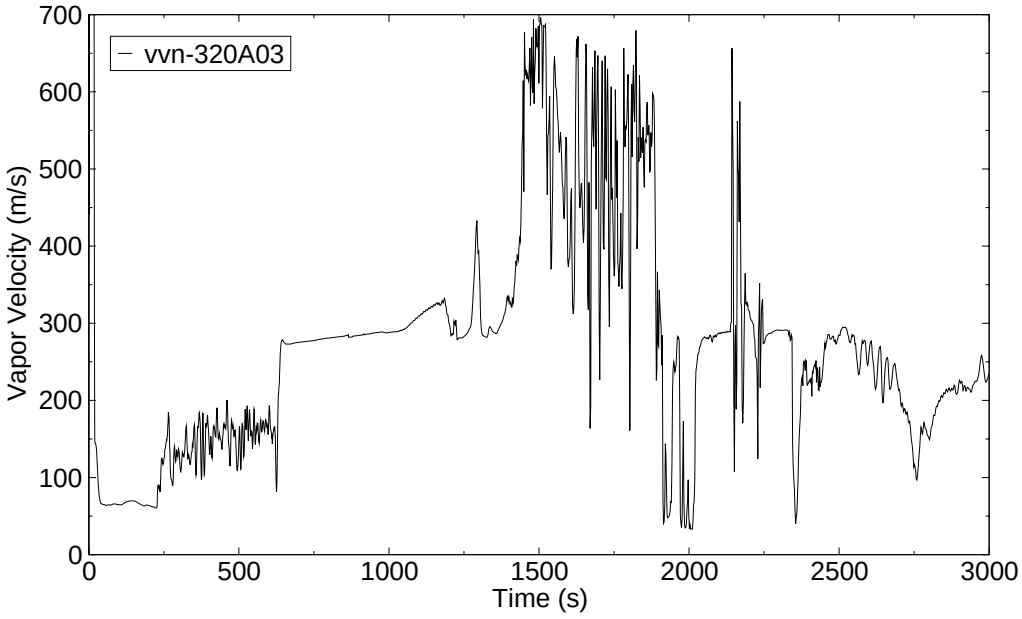

Figure C.6-6. Predicted Vapor Velocity at the Break - Test S-NH-2.

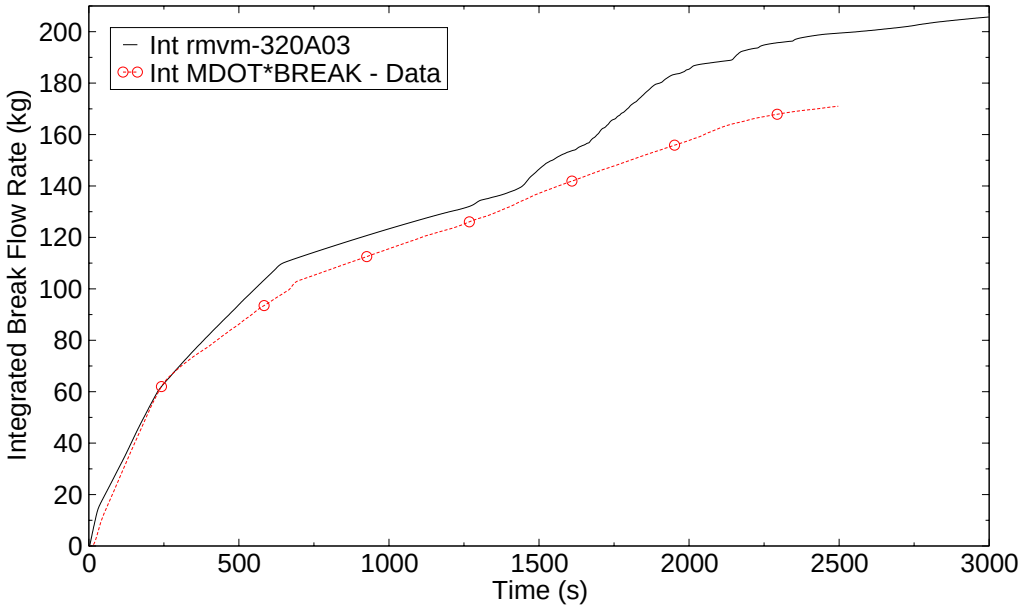

Figure C.6-7. Integrated Break Mass Flow Rate Comparison - Test S-NH-2.

response matches quite well with the data. After the pumps coast down and the system approaches saturation conditions, the predicted pressure is higher than the data. This is consistent with the break mass flow rate which is under predicted by the code. After transitioning to two-phase flow at the break, the depressurization rate increased more than the data and by about 500 seconds the predicted response was nearly the same as the data.

At about 1088 seconds, the clad temperature reached 811 ^{o}K in the experiment and the operators manually opened the steam line atmospheric depressurization valves (ADVs). The secondary side pressure rapidly decreased dropping below the primary side pressure making the steam generators a heat sink for the primary. The primary side depressurization rate increased. By 1171 seconds the primary pressure had decreased below the accumulator pressure and the accumulators began to inject cold water into the cold legs. In the calculation, the ADVs were not opened until about 1208 seconds when the predicted rod clad temperature reached 811 ^{o}K. When the primary pressure is predicted to drop below the accumulator pressure at about 1258 seconds, the accumulator injection into the cold legs was initiated. With the injection of the cold accumulator water entering the primary system, the primary depressurization rate increased. After about 1400 seconds, the predicted pressure is below the measured pressure response which is consistent with the larger break flow rate predicted by TRACE.

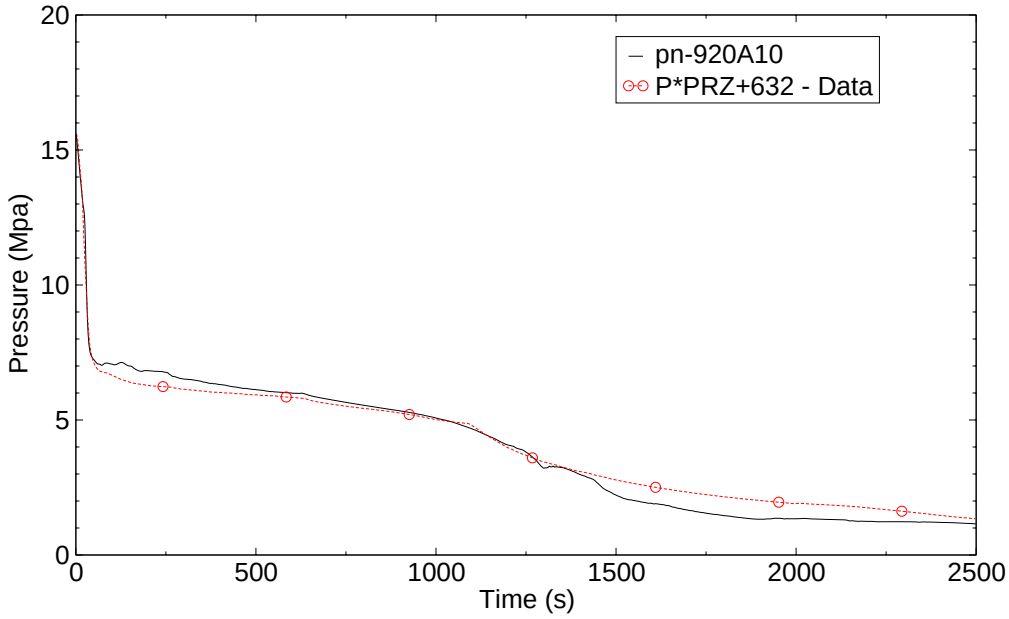

Figure C.6-8. Pressurizer Pressure Comparison - Test S-NH-2.

C.6.4.1.4. Pressurizer Differential Pressure

The predicted pressurizer differential pressure response compared to data is shown in Figure C.6-9 The pressurizer liquid level response is inferred from the differential pressure. The predicted response agrees well with the measured data. This agreement of pressurizer differential pressure is a good confirmation that the predicted break flow rate is generally in good agreement with the test for the early transient time period. The prediction shows the pressurizer emptying at about the same time as in the test. There was some uncertainty in the initial pressurizer water level in the measured data as pointed out in Reference 3.

C.6.4.1.5. Primary Pump Run Back

Pump speed tables for the intact and broken loop pumps were input to the TRACE model based on the S-NH-2 transient data. Speed was modulated by the TRACE steady-state controllers to set the loop flow. Consequently, the predicted initial speed differs slightly from the data. The pumps were tripped on low pressurizer pressure. The test data indicates that the pumps were tripped to run back sometime between 21.52 and 24.34 seconds. The simulation tripped the pumps to run back at 25.9 seconds. It appears that, after the low pressurizer pressure trip, the pump speed was power controlled and power to the pumps was turned off at about 60 seconds in the test. Figure C.6-10 and Figure C.6-11 show the pump run back transient results for the intact and broken loops, respectively.

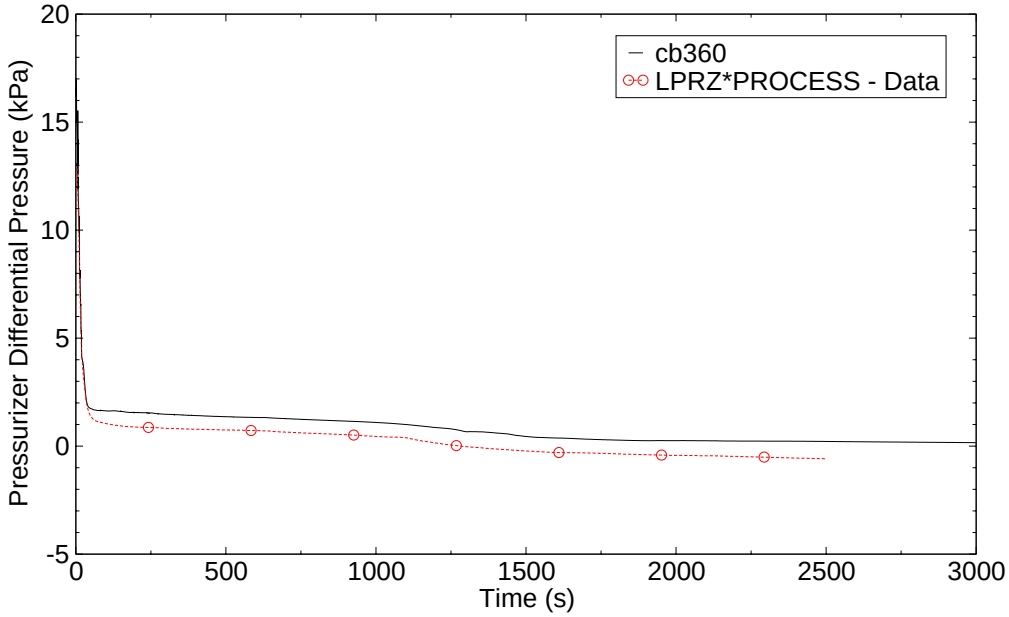

Figure C.6-9. Pressurizer Water Level Comparison - Test S-NH-2.

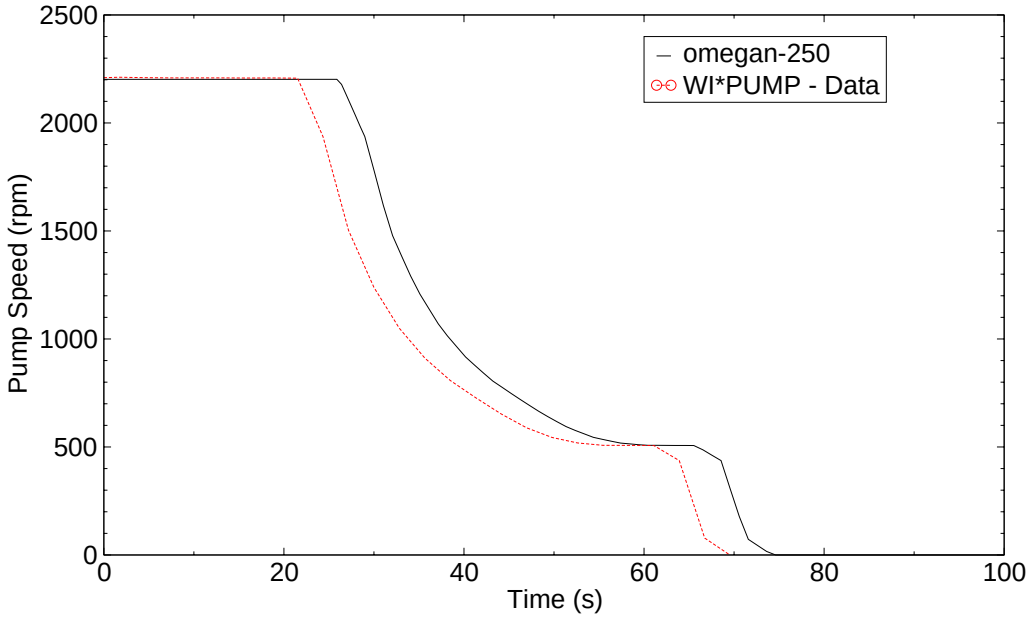

Figure C.6-10. Intact Loop Pump Speed Comparison - Test S-NH-2.

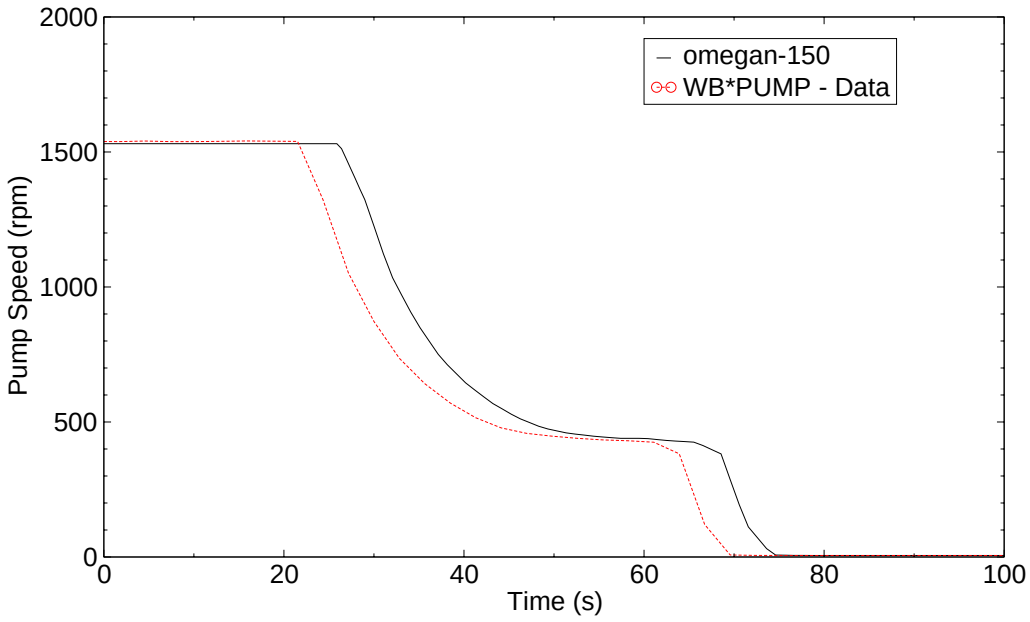

Figure C.6-11. Broken Loop Pump Speed Comparison - Test S-NH-2.

C.6.4.1.6. Steam Generator Pressure

Pressure comparisons in the intact and broken loop steam dome are shown in Figure C.6-12 and Figure C.6-13, respectively. The MSIV closure trip resulted in a rapid pressure increase. Although the predicted secondary pressure response is significantly greater in magnitude than the test data, the pressure did not reach the relief valve set point of 7.22 MPa. The predicted response during the first 1000 seconds seems reasonable. Heat loss to the environment was reported in Reference 2. External heaters were attached to the system to compensate for the heat loss. However, external heaters were not applied to the secondary side. A possible reason the predicted steam dome pressure rose higher than the data after the MSIV closure was due to the environmental heat loss from the secondary side that was not included in the model. Therefore, the amount of subcooling in the predicted secondary side fluid was less making the steam generation rate higher resulting in a higher predicted pressure.

The steam line ADVs were manually latched open in the experiment at about 1088 seconds due to operator response to rod clad temperature reaching 811 ^{o}K. The same operator response was built into the TRACE input model; however, the ADVs in the calculation were not opened until about 1208 seconds. The predicted depressurization rate after the ADV opened in the intact loop steam generator follows the trend of the data, indicating the predicted ADV flow rate matched the experimental flow rate reasonably well. (The ADV flow rate was not measured in the experiment, therefore, a direct comparison with predictions is not possible.) After 2000 seconds the predicted pressure in the intact loop matched the data quite well. The depressurization rate in the broken

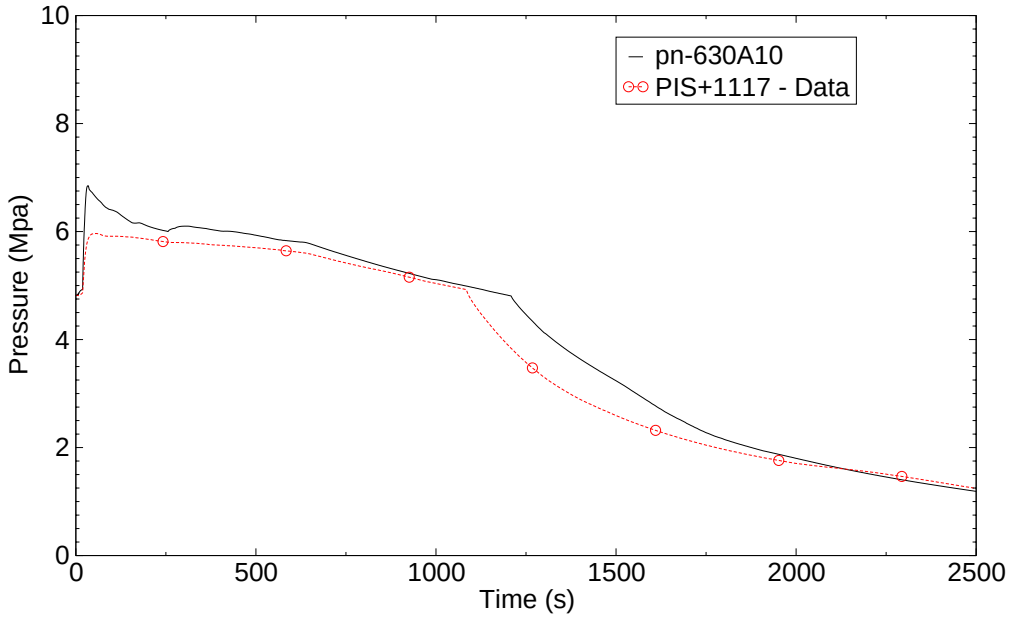

Figure C.6-12. Intact Loop Steam Generator Secondary Side Pressure Comparison - Test S-NH-2.

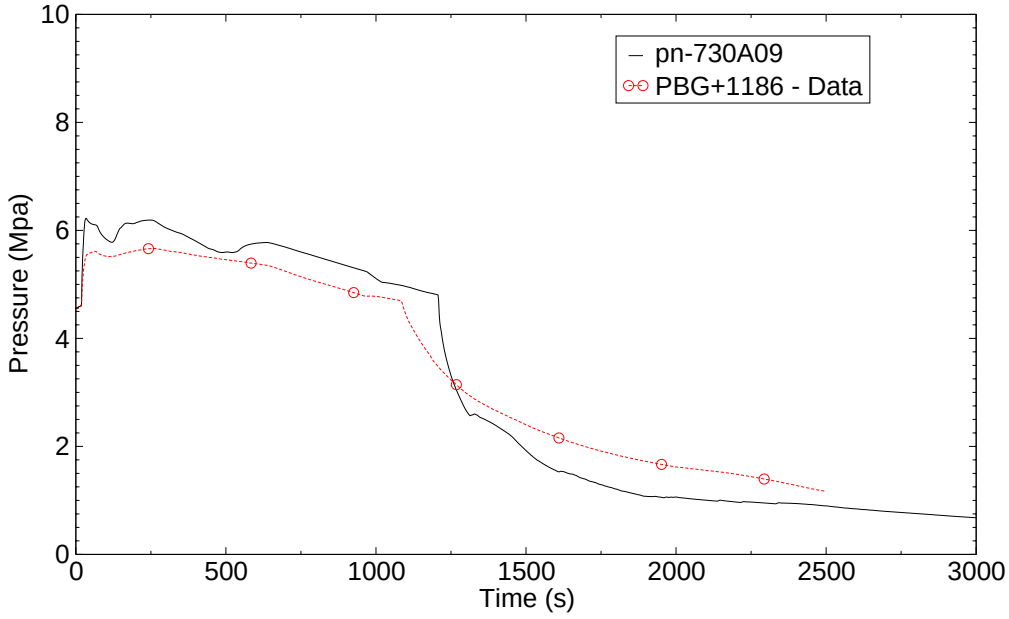

Figure C.6-13. Broken Loop Steam Generator Secondary Side Pressure Comparison - Test S-NH-2.

loop steam generator after the ADV was opened was initially higher than the data. After about 1500 seconds the broken loop steam generator pressure was predicted to be below the data, but the depressurization rate was close to the data. Overall, the predicted broken loop steam generator blowdown rate has similar trends as the intact loop.

C.6.4.1.7. Pump Suction Loop Seal Clearing

As water drains and flashes from the primary system piping during the small break blowdown, natural circulation ceases in the loops. The remaining water settles into the pump suction loop seal pipe and forms a water plug that prevents steam from flowing through the loops. Steam pressure builds up behind the water plug and depresses the core water level. Loop seal clearing is important because it increases the core water level. When sufficient steam pressure builds upstream of the loop seal water plug, the plug is pushed out through the pump and allows steam to flow freely around the loop. Subsequently, the differential pressure between the vessel downcomer and the core equalize. This results in a core water level increase and downcomer water level decrease. As a result of loop seal clearing, the break flow transitions from two-phase flow to steam flow. Reference 1 reports that the Semiscale broken loop did not clear and that the intact loop cleared at 620 seconds during the S-NH-2 test.

Vessel liquid level measurement LV-13M-578 is defined in Reference 2 as the difference between pressure taps in the upper plenum (0.13 m below the cold leg centerline) and the lower plenum (5.78 m below the cold leg centerline)[1]. The corresponding measurement locations in the TRACE model are approximately VESSEL axial level 1 and axial level 17. Control block 560 was used to obtain the pressure difference between these two locations. The point of loop seal clearing is evident in both the measured data and the prediction as shown in Figure C.6-14 (620 seconds for the measured data and about 650 seconds for the TRACE prediction). The predicted vessel level trend and timing agrees reasonably well with the Semiscale data. The TRACE calculation cleared the broken loop seal; in comparison the intact loop is cleared in the Semiscale test. However, at about 1287 seconds the intact loop seal began is predicted to void (Figure C.6-15).

C.6.4.1.8. Accumulator Flow Rates

In the S-NH test series all HPI flow was unavailable, therefore, no ECC water was available until the primary system pressure decreased to the accumulator injection setpoint of 4.24 MPa. The accumulator flow rates are a function of the pressure difference between the accumulator and the cold leg injection location. Comparisons of the predicted and measured accumulator mass flow rates for the intact and broken loops are shown in Figure C.6-16 and Figure C.6-17, respectively. The timing of the accumulator initiation agrees with the data.

1. It appears the pressure taps were hooked up to yield a negative pressure difference. Therefore, the data was inverted for the comparison. Additionally, it appears there was an offset in the DP tap calibration. consequently, an offset of 75.28 kPa was added to the data curve so the data and calculation matched at time zero.

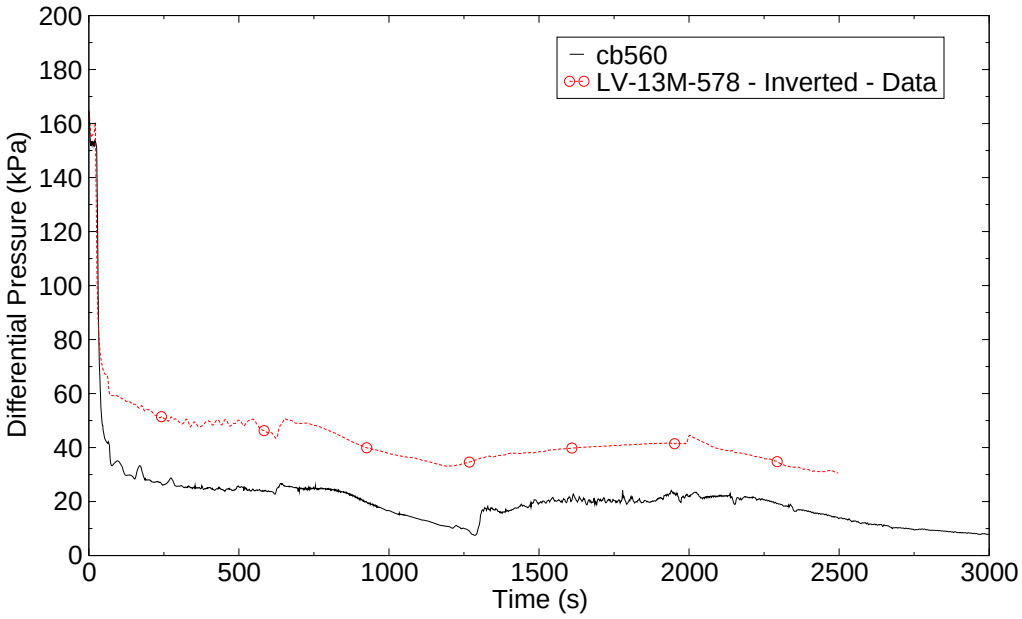

Figure C.6-14. Vessel Lower Plenum to Upper Plenum Differential Pressure Comparison - Test S-NH-2.

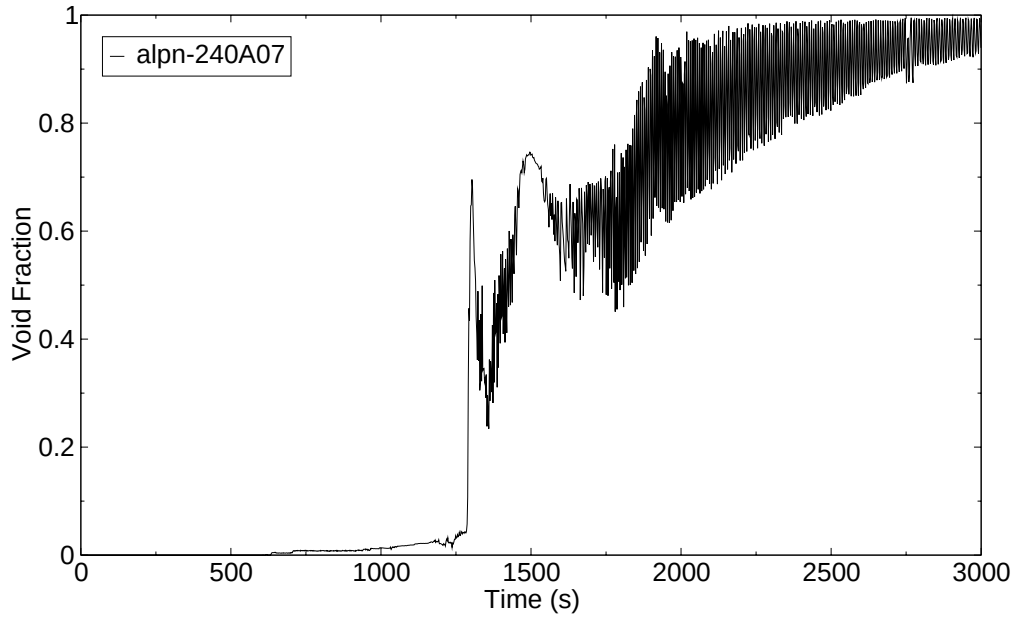

Figure C.6-15. Predicted Void Fraction in the Bottom of the Intact Pump Loop Seal - Test S-NH-2.

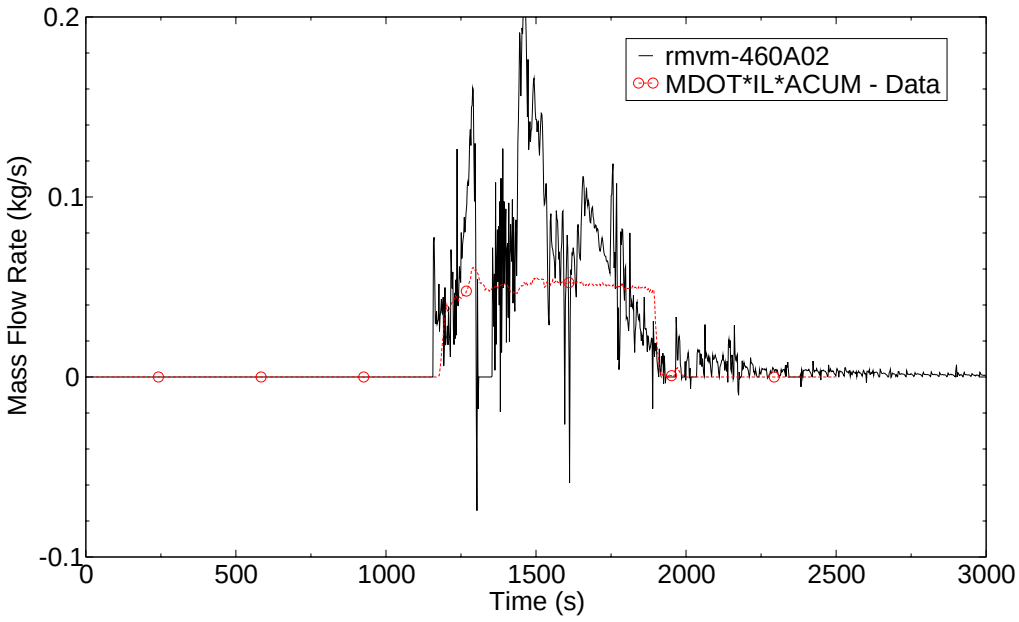

Figure C.6-16. Intact Loop Accumulator Injection Flow Rate Comparison - Test S-NH-2.

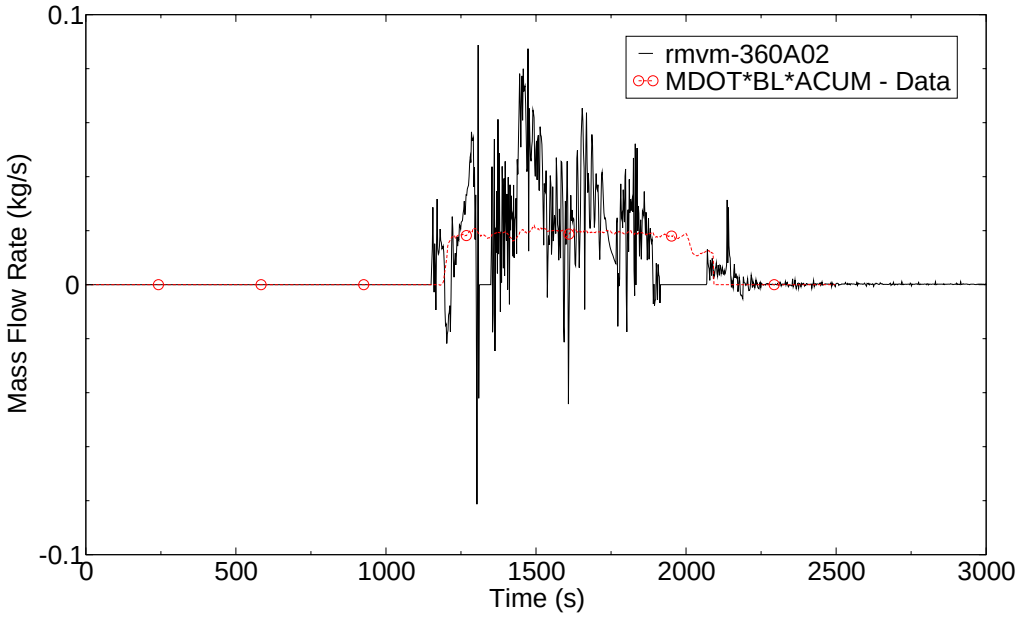

Figure C.6-17. Broken Loop Accumulator Injection Flow Rate Comparison - Test S-NH-2.

C.6.4.1.9. Rod Clad Temperature

A comparison of the heater rod cladding temperature near the top and at the core mid plane are shown in Figure C.6-18 and Figure C.6-19, respectively. The predicted rod temperature does not depart from nucleate boiling (DNB) until after DNB is observed in the experiment. At the upper core elevation, the rod heat-up is slower than the data. Additionally, the predicted peak clad temperature is on the order of 100 ^{o}K lower than the data. Although the predicted break mass flow rate is reasonable (see Figure C.6-4) there appears to be a different mass distribution throughout the system in the calculation than in the experiment. An examination of the core fluid density at elevations 3.42, 2.53 and 1.83 m shown in Figure C.6-20 through Figure C.6-22 indicate a higher predicted froth level in the core, thus keeping the rods cooler. Once the level began to drop in the core (see Figure C.6-23 and Figure C.6-24) the rods began to heat-up. There was enough liquid entrainment in the core that the predicted rod temperature at the top of the core heated up at a much slower rate than the data shows. After accumulator flow was established the core was flooded and the rods quenched.

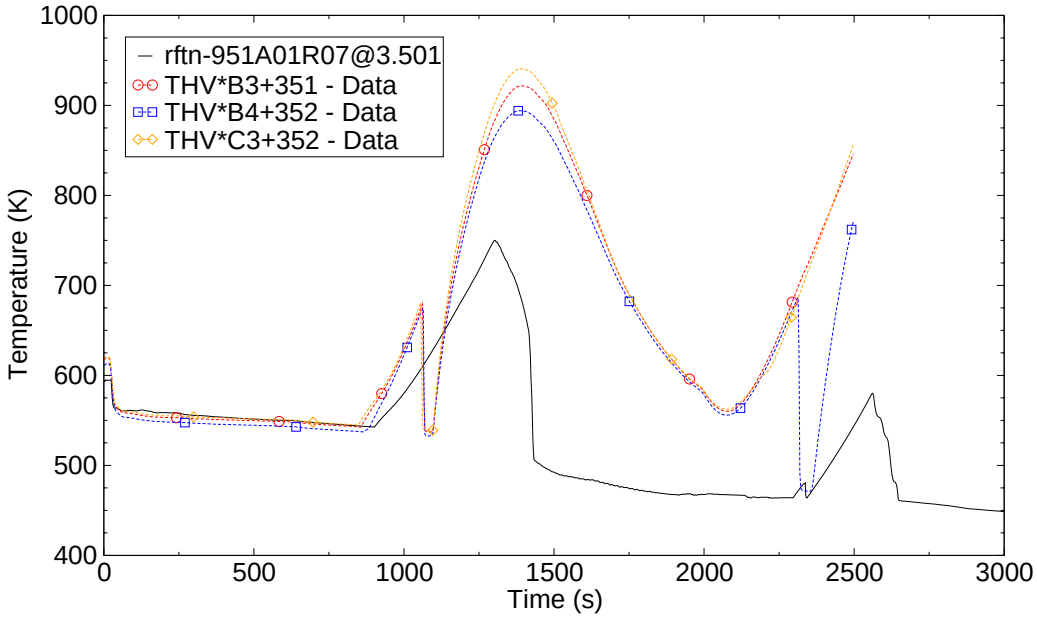

Figure C.6-18. Rod Clad Temperature Comparison at 3.5 m - Test S-NH-2.

The second rod heat-up predicted by the code occurs significantly after data measurements. Once the accumulators emptied in the experiment, the core level began to decrease and the rods began to heat-up. The experiment was terminated before the system pressure reached the low pressure injection set point. There was sufficient fluid remaining in the core region in the calculation (see Figure C.6-24) that the rods remained quenched longer; however, a second rod heat-up is predicted about 276 seconds after the measured rod heat-up time.

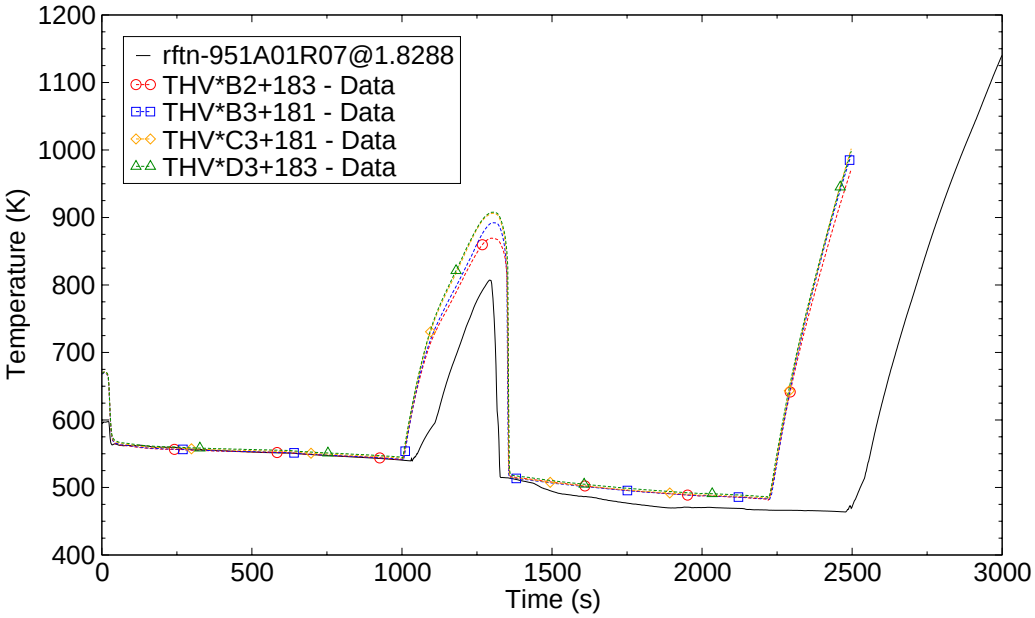

Figure C.6-19. Rod Clad Temperature at the Core Mid-plane - Test S-NH-2.

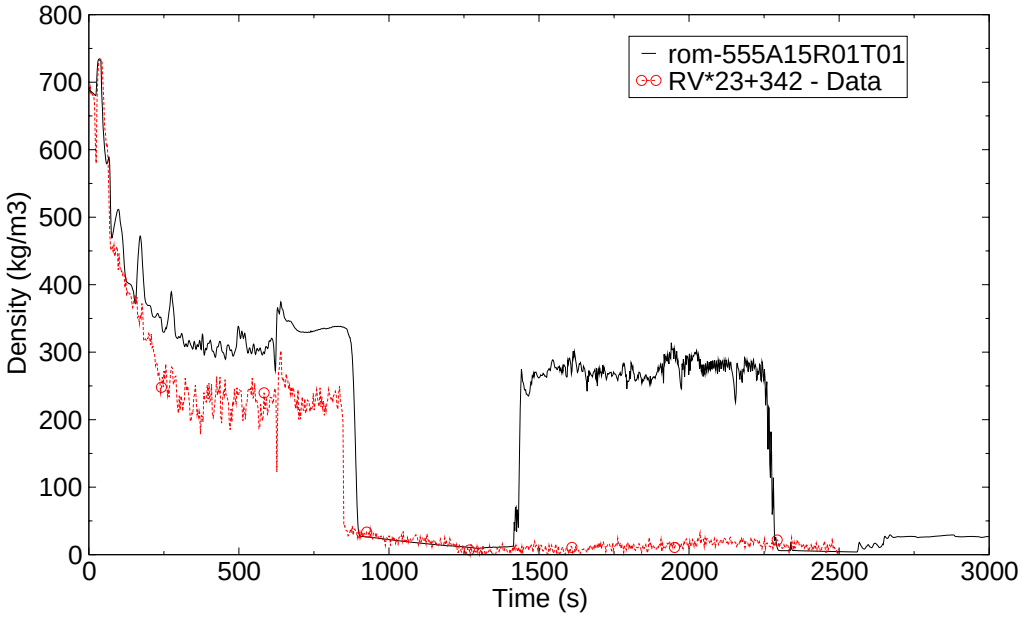

Figure C.6-20. Fluid Density in the Core Region at the 3.42 m elevation - Test S-NH-2.

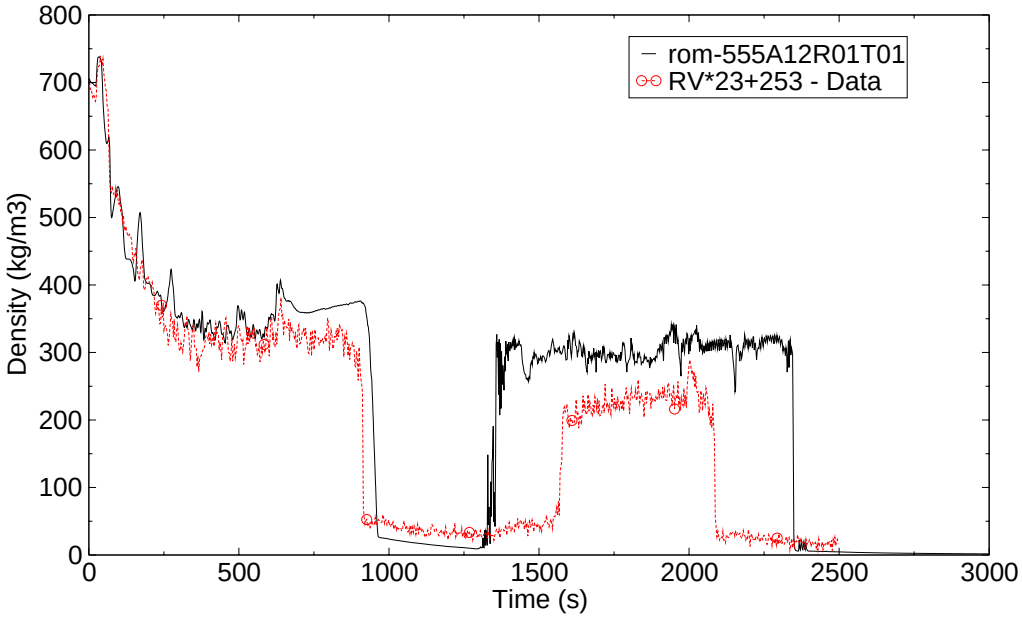

Figure C.6-21. Fluid Density in the Core Region at the 2.53 m elevation - Test S-NH-2.

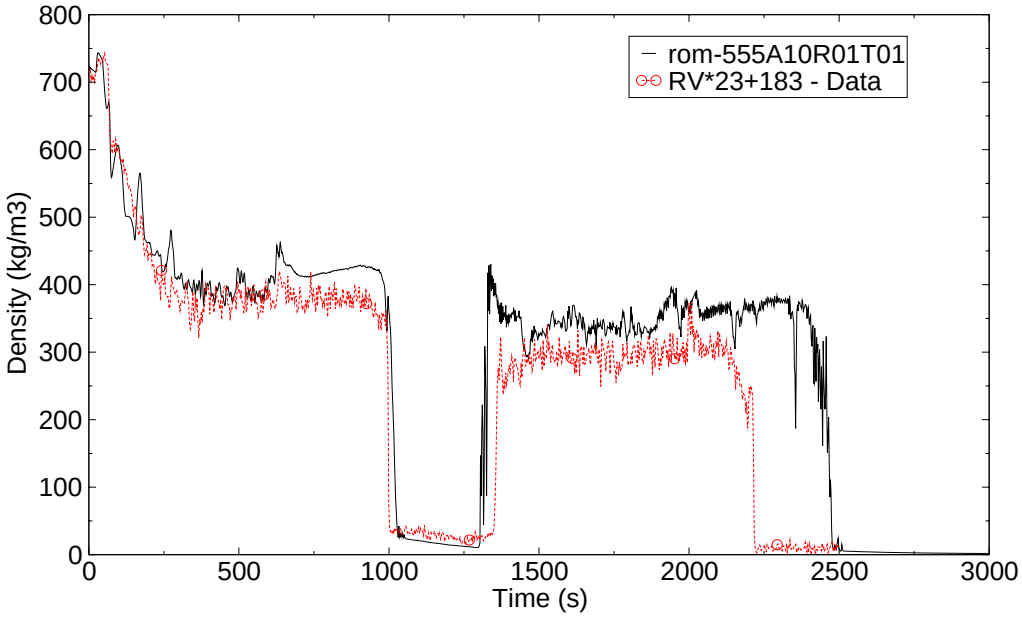

Figure C.6-22. Fluid Density in the Core Region at the 1.83 m elevation - Test S-NH-2.

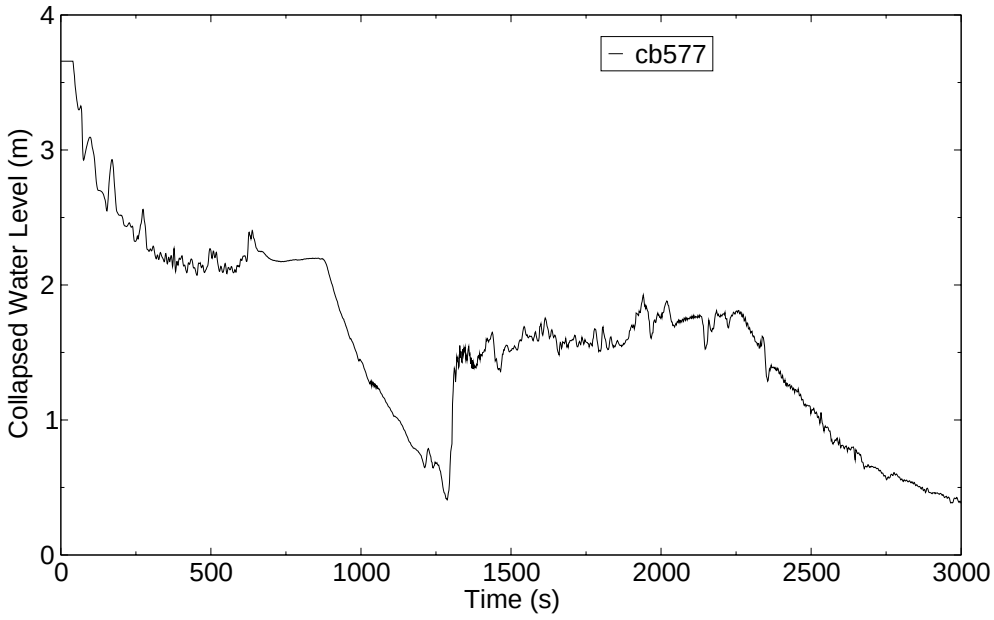

Figure C.6-23. Predicted Core Level - Test S-NH-2.

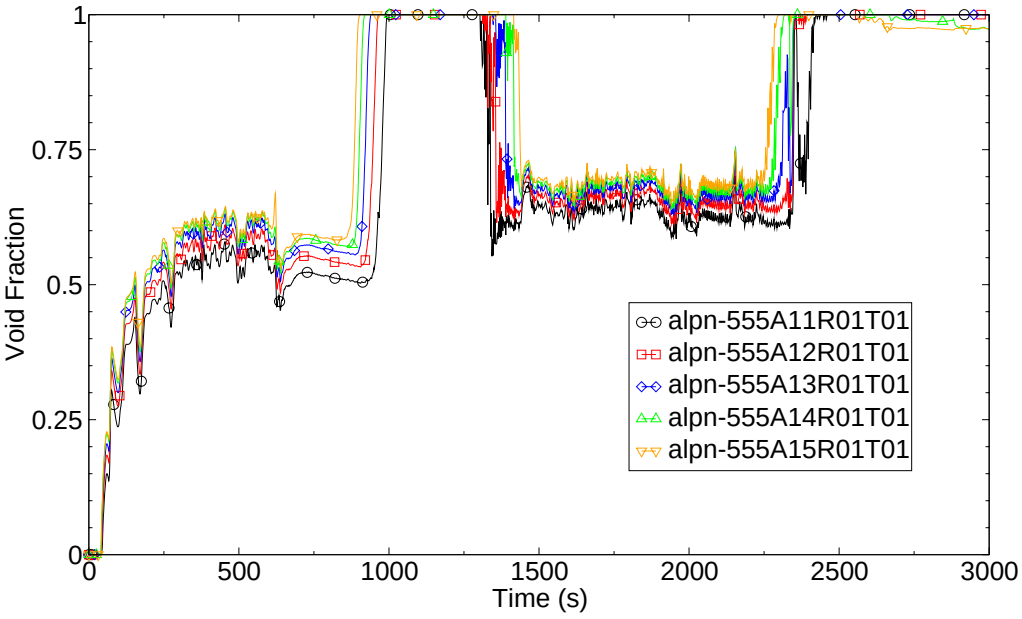

Figure C.6-24. Predicted Upper Core Void Fractions - Test S-NH-2.

C.6.4.2. Simulation of Test S-NH-1

For Semiscale SBLOCA Test S-NH-1 the TRACE input model was revised and adjusted accordingly to simulate the S-NH-1 transient initial conditions. A summary of the initial conditions from the Semiscale S-NH-1 experiment and the TRACE code calculated initial conditions is shown in Table C.6.3. The S-NH test series initial conditions were obtained from Table 1 of Reference 1 and from the recorded test data files for S-NH-1 in the NRC databank. The uncertainty values for the measured test data were obtained from Table VII of Reference 5.

The timing of important events during the S-NH-1 transient compared to the TRACE predicted event timing is shown in Table C.6.4 The Semiscale NH test series results report (Ref. 1), does not contain any sequence of events tables to document the timing of trips and events that occurred during the tests. The Semiscale times reported in Table C.6.4 were obtained from various text sections of the NH test series results report and from the recorded test data file.

Table C.6.3. Initial Conditions for Test S-NH-1

Parameter	Measured Data	TRACE
Pressurizer Pressure (MPa) - (pn-920A10)	15.64 ± 0.07	15.64
Pressurizer Liquid Level (m) - (sv800)	2.59 ±0.25	2.59
Core Power (MW) - (rpower-998)	2.0 ±0.02	2.0
Core Δ Temperature (K) - (tln555A16R01T01 - tln-555A03R01T01)	37.55 ± 3.3	40.3
Intact Loop Cold Leg Temperature (^{o}K) - (tln-270A03)	548.1 ± 3.3	546.9
Intact Loop Hot Leg Temperature (^{o}K) - (tln-210A01)	586.3 ±3.3	586.57
Broken Loop Cold Leg Temperature (^{o}K) - (tln-170A01)	550.9 ±3.3	548.1
Broken Loop Hot Leg Temperature (^{o}K - (tln-110A01))	586.4 ±3.3	586.57
Intact Loop Flow (l/s) - (cb270)	9.06 ±0.033	9.06
Broken Loop Flow (l/s) - (cb-170)	3.25 ±0.033	3.25
Intact Loop Cold Leg Pressure (MPa) - (pn-270A03)	15.82 ± .0.07	15.85
Broken Loop Cold Leg Pressure (MPa) - (pn-170A01)	15.83 ± .0.07	15.84
Downcomer to upper head Bypass flow (% of total core flow) - (rmvm-280A04 / (rmvm-270A02 + rmvm-170A02))	2.75	2.67
Intact Loop Steam Generator secondary pressure (MPa) - (pn630A09)	4.76 ± 3.3	4.76
Broken Loop Steam Generator secondary pressure (MPa) - (pn730A08)	4.50 ± 3.3	4.50
Intact Loop Steam Generator steam flow (kg/s) - (rmvm-630A10)	0.83	0.797
Broken Loop Steam Generator steam flow (kg/s) - (rmvm-730A09)	0.25 ±0.05	0.274
Intact Loop Steam Generator feedwater flow (kg/s) - (fxmass-610)	0.83	0.787
Broken Loop Steam Generator feedwater flow (kg/s) - (fxmass-710)	0.23	0.278
Intact Loop Steam Generator secondary mass (kg) - (cb100)	73	73.4
Broken Loop Steam Generator secondary mass (kg) - (cb200)	23	22.5
Intact Loop Pump Speed (rpm) - (omegan-250)	2201	2202 [a]
Broken Loop Pump Speed (rpm) - (omegan-150)	1540	1540

Table C.6.3. Initial Conditions for Test S-NH-1 (Continued)

Parameter	**Measured Data**	**TRACE**
Intact Loop Feedwater Temperature (^{o}K) - (tln-610A01)	493.4 ± 3.3	493.4
Broken Loop Feedwater Temperature (^{o}K) - (tln-710A01)	493.7 ± 3.3	493.7
Intact Loop Accumulator Temperature (^{o}K) - (tln-450A03)	301 ± 3.3	302
Broken Loop Accumulator Temperature (^{o}K) - (tln350A03)	310 ± 3.3	302

a. Pump speed was adjusted to obtain the desired loop flow rate

Table C.6.4. Key Events for SemiScale Test S-NH-1 .

Key Event	**Time Data (s)**	Time TRACE (s)
Break Initiation	~ 0.0	0.0
Pressurizer Pressure Low Pressure Trip at 13.1 MPa (signal for MSIV trip, steam line crossover valve closure and power scram) - (trip-170, trip150)	~ 69.16	70.2
MSIV Closure Trip, Intact Loop / Broken Loop - (trip-680 / trip-780)	67.06<t<72.83	70.2 / 70.2
Power Scram - (trip-150)	67.06<t<72.83	73.2
Pressurizer Pressure Low Pressure Trip at 12.6 MPa (safety injection signal) - (pn-920A01)	~ 73.21	81.7
Feedwater Trip Off - (fxmass610, fxmass710)	72.83<t<78.59	84
Start Aux FW, Intact Loop / Broken Loop - (trip-620 / trip-720)	72.83<t<78.59	82.2 / 82.3
Pumps Trip - (trip-140, trip-145)	72.83<t<78.59	84.2
HPIS Initiated, Intact Loop / Broken Loop	unavailable	unavailable
Pressurizer Empty - (cb360)	~ 113	~ 135
Break flow transitions from liquid to two-phase flow - (alpn-320A01)	~ 1100	~ 744
Intact Loop Seal Clears - (alpn-240A07)	never	~ 4330
Broken Loop Seal Clears - (alpn-140A07)	never	never
Break uncovers, break flow transitions to all steam flow - (alpn-320A01)	never	periodic[a]
Operator action, BL SG Aux FW Off - (trip-720)	~ 1080	1080.1
Core Heatup Begins - (tsurfo-951A08)	2325.3	~ 3638
Operator action, BL SG Aux FW On - (trip-720)	~ 2394	2394.1
Intact Loop steam dump valve (ADV) latched open - (trip-662)	~ 2642	3876.4
Broken Loop steam dump valve (ADV) latched open - (trip-762)	~ 2630	3876.4
Accumulator Injection, Intact Loop / Broken Loop - (rmvm460A02 / rmvm360A02)	~ 2838 / ~ 2878	~ 3990 / ~ 3985
Minimum core collapsed water level; distance from bottom of core - (cb577)	~2900 [b] (1.04 m)	~ 4140 (0.627 m)
PCT - (tsurfo-951A08)	3022.4 (916.1 ^{o}K)	3889 (818.2 ^{o}K)
Final Rod Rewet	~ 3290	~ 4336
End of Test	5194	5200

a. Break uncovery is difficult to define. Reference 1, page 40 says NH-1 break flow never becomes 100% steam. However, density measurements RB*79B, M, T and RB*74B, M indicate broken loop cold leg density was possibly all steam for a brief period, approximately 2200 to 2400 seconds. The calculated void fraction at the break exceeded 0.95 at 1055 s, at 1572 s, between 1692 s and 2559 s, and at 3844 s.
b. Scaled from Figure 24 in Reference 1.

C.6.4.2.1. Break Flow Rate

Figure C.6-25 shows the predicted and measured mass flow rate out of the break orifice. The TRACE predicted break flow rate agrees quite well with the measured data until the predicted break flow transitions from liquid flow to two-phase flow at approximately 744 seconds. The initial break flow spike in the calculation is larger in magnitude than the data. The data is the recorded condensate mass collected in the break collection tank located downstream of the break and condensing coils. Therefore, break flow data is expected to be slightly delayed and have a damped response in comparison to the TRACE calculated break flow.

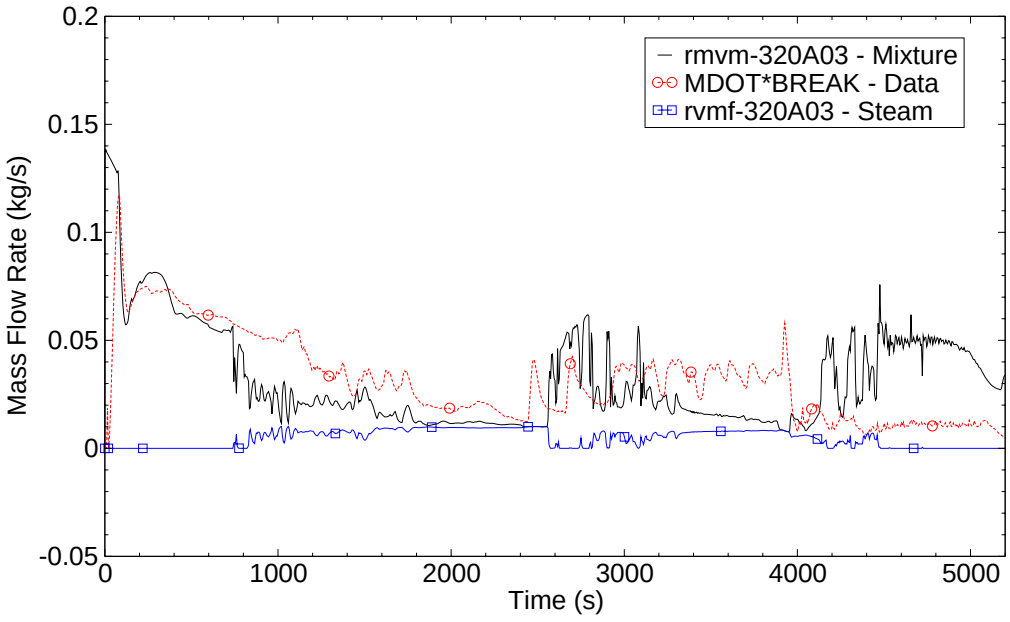

Figure C.6-25. Break Mass Flow Rate Comparison - Test S-NH-1.

When the recirculation pumps stop rotating, 130 seconds for the experiment and 139 seconds for the calculation, the TRACE simulation repressurized more than shown in the data resulting in a greater increase in the predicted break mass flow.

At approximately 744 seconds, the calculated break flow starts to transition from liquid flow to two-phase flow. The transition is evident as the predicted steam flow becomes positive on the

curve labeled rvmf-320A03 - Steam in Figure C.6-25 By about 735 seconds, the driving head for natural circulation was lost and subsequently the calculated broken loop flow became stagnant whereas the measured flow rate in the broken loop remained positive as shown in Figure C.6-26 The positive flow resulted in more entrained liquid exiting the break in the experiment. The flow exiting the break in the calculation was coming from the external downcomer and was mostly steam since the predicted void fraction at the break exceeded 90%. Consequently, the calculated break flow was significantly less than the measured break flow after this time. The smaller predicted break flow rate resulted in a higher predicted system pressure, more liquid inventory in the vessel and a delay in the core dryout, and rod heatup. The broken loop flow did not stagnate in the experiment until about 2031 seconds (Figure C.6-26) and then only for a short time.

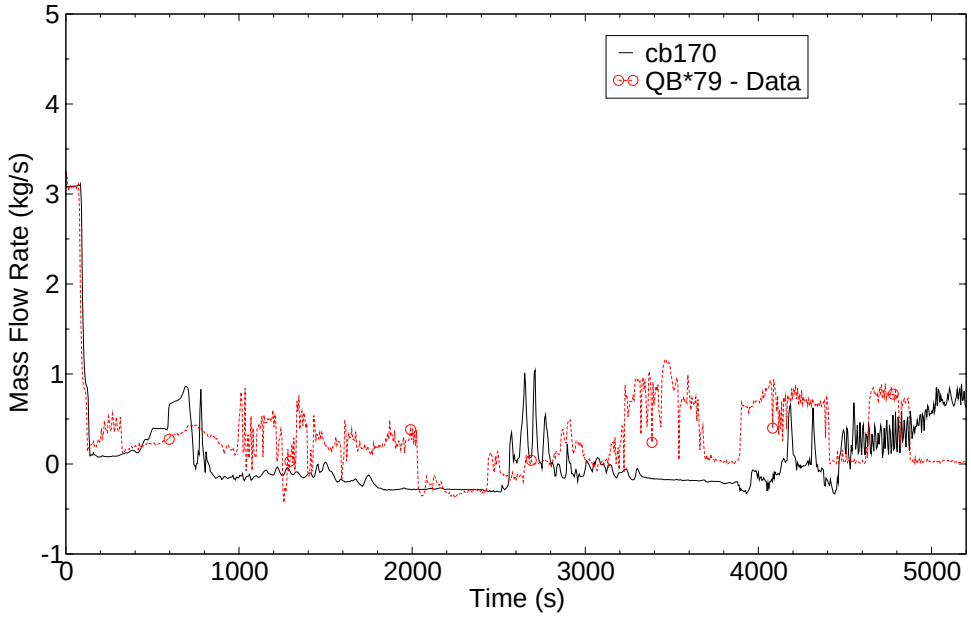

Figure C.6-26. Broken Loop Cold Leg Flow Rate Comparison - Test S-NH-1.

The predicted integrated break mass flow rate is compared to data in Figure A.99.1-27. The predicted mass leaving the system through the break compares reasonably well with the data to about 1000 seconds. After 1000 seconds the mass leaving the system is under predicted. Consequently, the system pressure is over predicted.

C.6.4.2.2. Primary System Pressure

The calculated primary system pressure response agrees very well with the Semiscale initial pressure decrease as the pressurizer drains, as shown in Figure C.6-28, due to the primary system liquid blowdown through the break and the core power scram. After the recirculation pumps stopped the primary system began a short repressurization. The repressurization was caused by flashing in the vessel upper plenum and core which increased the primary system steam volume at

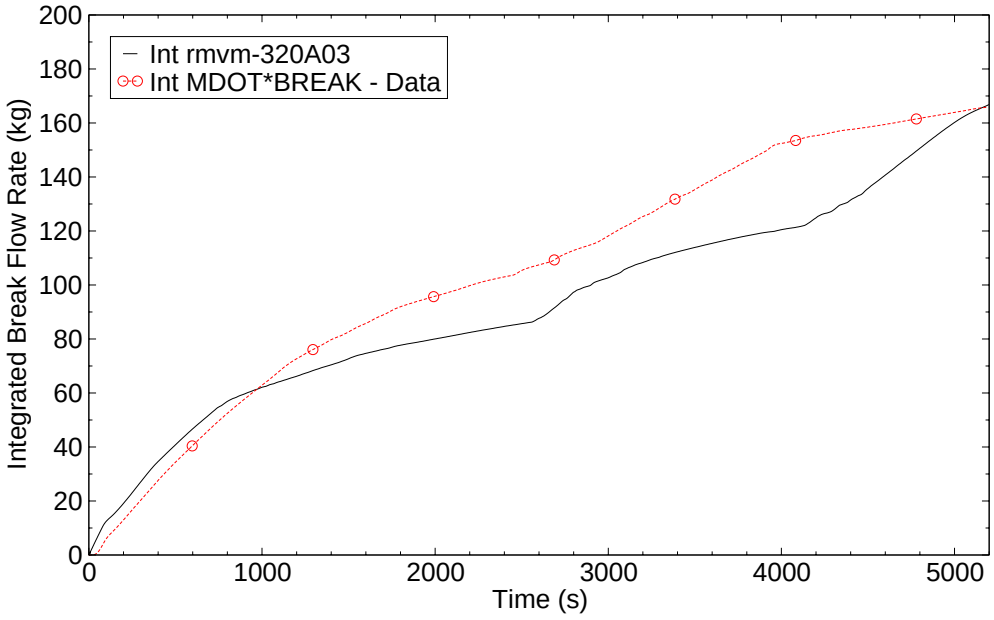

Figure C.6-27. Integrated Break Flow Rate Comparison - Test S-NH-1.

a faster rate than was being lost through the break. The simulation repressurizes significantly more than the test data and the calculated primary system pressure remains higher than the test data for the remainder of the transient. The transient simulation event timing is off track after this time period, as compared to the test. The predicted accumulator injection pressure reaches 4.24 MPa approximately 1150 seconds later than the test data.

C.6.4.2.3. Pressurizer Differential Pressure

The pressurizer differential pressure comparison is shown in Figure C.6-29 The pressurizer liquid level response is inferred from the differential pressure. The predicted pressurizer differential pressure response agrees well with the test data. However, as the pressurizer nears empty the predicted primary system repressurizes for a short time. During the repressurization (~100 seconds), an increase in the pressurizer water level is observed in the calculation. This behavior is not evident in the test data indicating that the repressurization is not as significant.

C.6.4.2.4. Primary Pump Speed Run Back

Pump speed tables for both the intact and broken loop pumps were input to the TRACE model based on the Semiscale S-NH-1 transient data. Pump speed was used by the TRACE steady-state controllers to set the desired loop flow rate. Consequently, the TRACE initial pump speeds differ slightly from the data. The pumps were tripped on low pressurizer pressure. The test data

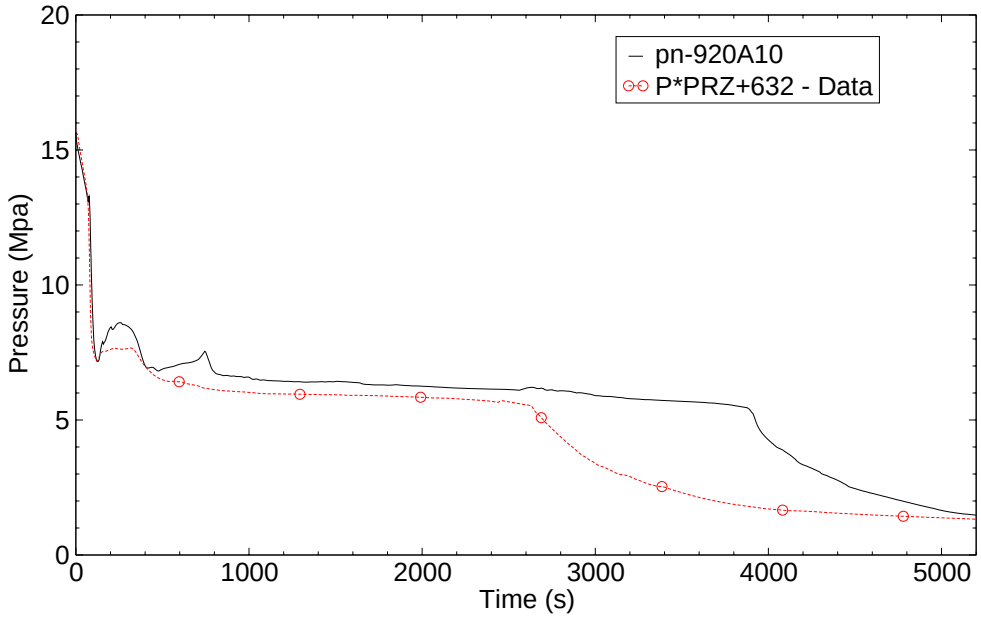

Figure C.6-28. Pressurizer Pressure Comparison - Test S-NH-1.

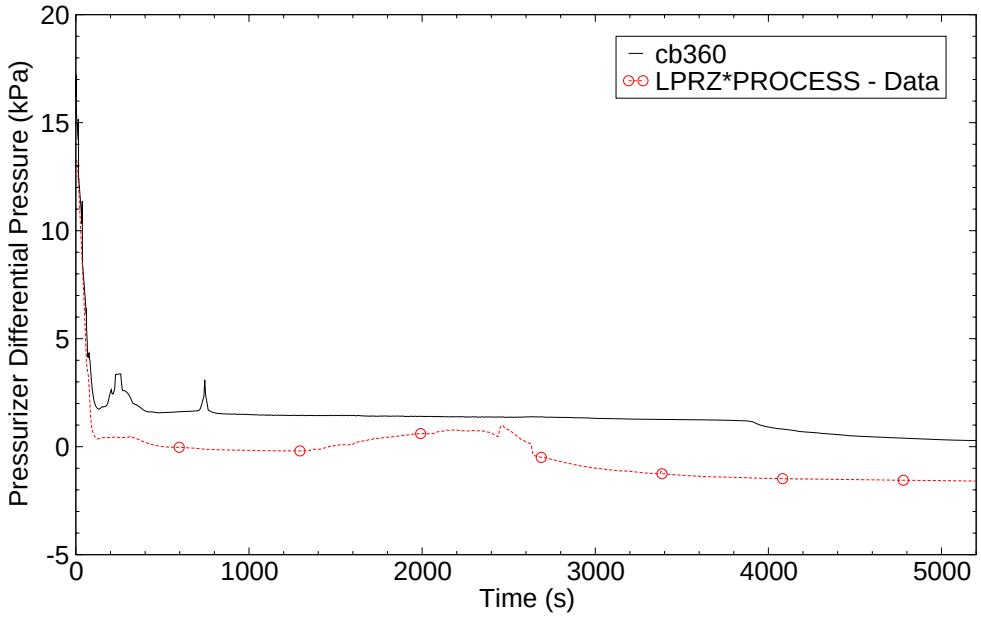

Figure C.6-29. Pressurizer Differential Pressure Comparison - Test S-NH-1.

indicates that the pumps were tripped to run back sometime between 72.83 and 78.59 seconds. The simulation tripped the pumps to run back at about 84 seconds. It appears that after the low pressurizer pressure trip, the Semiscale pump speed was power controlled and power to the pumps was turned off at about 115 seconds in the Semiscale test. Figure C.6-30 and Figure C.6-31 show the pump run back transient results for the intact and broken loop, respectively

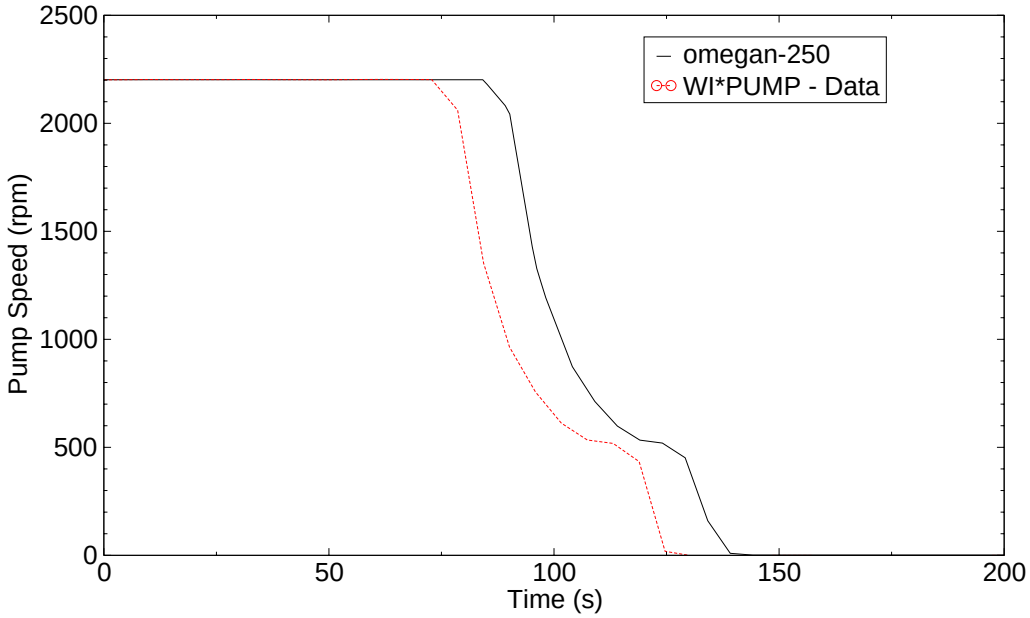

Figure C.6-30. Intact Loop Pump Speed Comparison - Test S-NH-1.

C.6.4.2.5. Steam Generator Secondary Pressure Response

Pressure in the intact and broken loop steam generator steam dome is shown in Figure C.6-32 and Figure C.6-33, respectively. The MSIV closure trip resulted in both SGs experiencing a rapid pressure increase. As in the S-NH-2 test, the predicted steam generator pressure in both the intact and broken loops increase in response to the MSIV closure and is significantly greater in magnitude than the test data. However, the predicted steam generator pressures do not reach the relief valve set point of 7.22 MPa. Before approximately 2600 seconds the calculated steam generator pressure response follows the trend of the data. At about 2630 seconds the operator opens the intact and broken loop secondary side ADVs to blowdown the secondary side pressure in response to core heater rod PCT reaching 811 ^{o}K. Because the predicted primary system pressure decay and clad heatup was greatly delayed, the predicted opening of the ADVs was also greatly delayed by approximately 1240 seconds. Both predicted pressure responses would have been close to the data had it not been for the initial over pressurization.

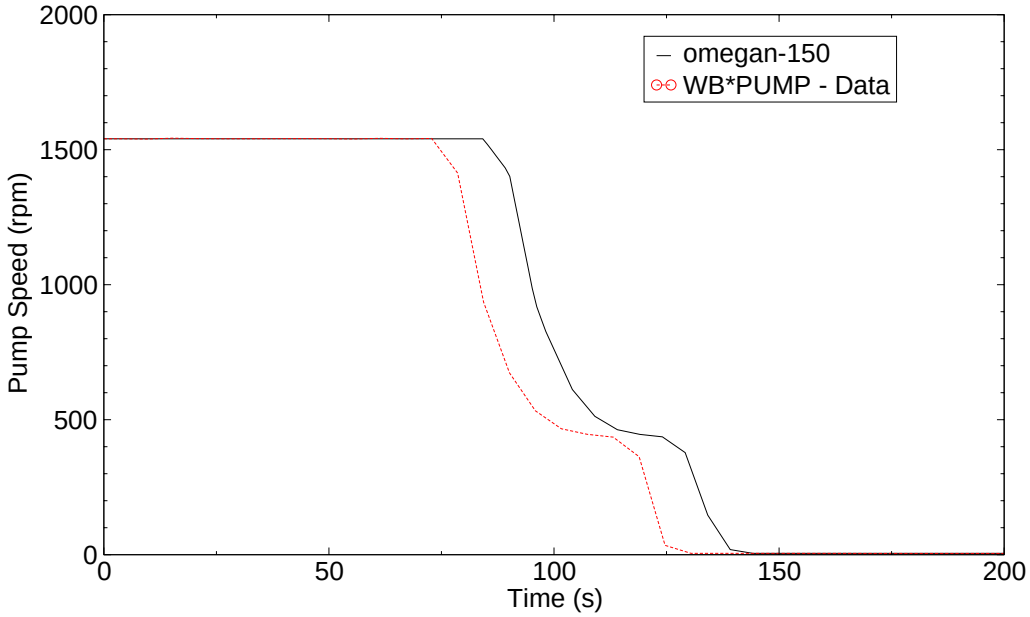

Figure C.6-31. Broken Loop Pump Speed Comparison - Test S-NH-1.

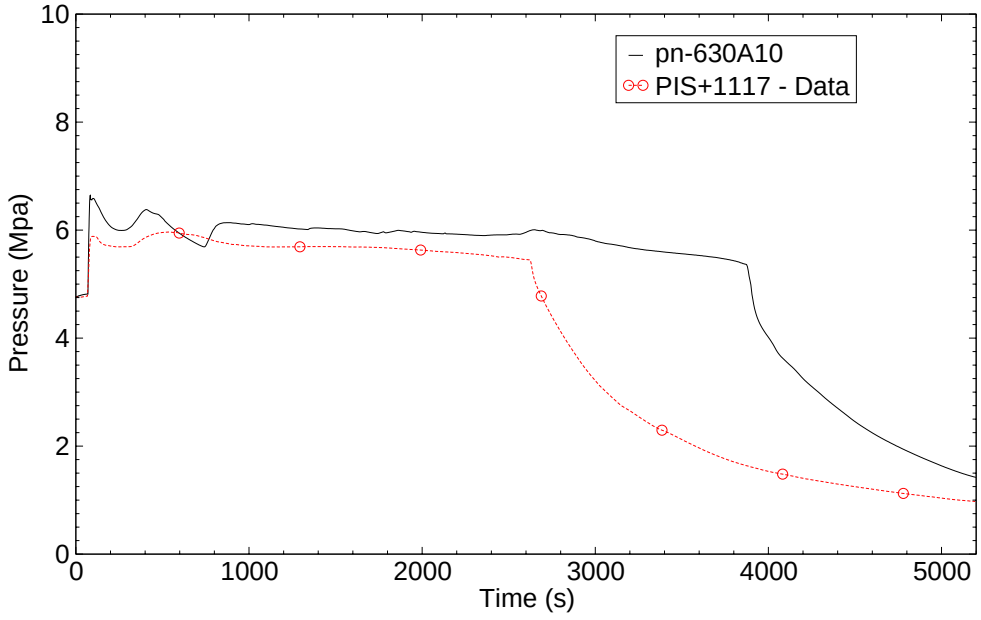

Figure C.6-32. Intact Loop Steam Generator Secondary Side Pressure Comparison - Test S-NH-1.

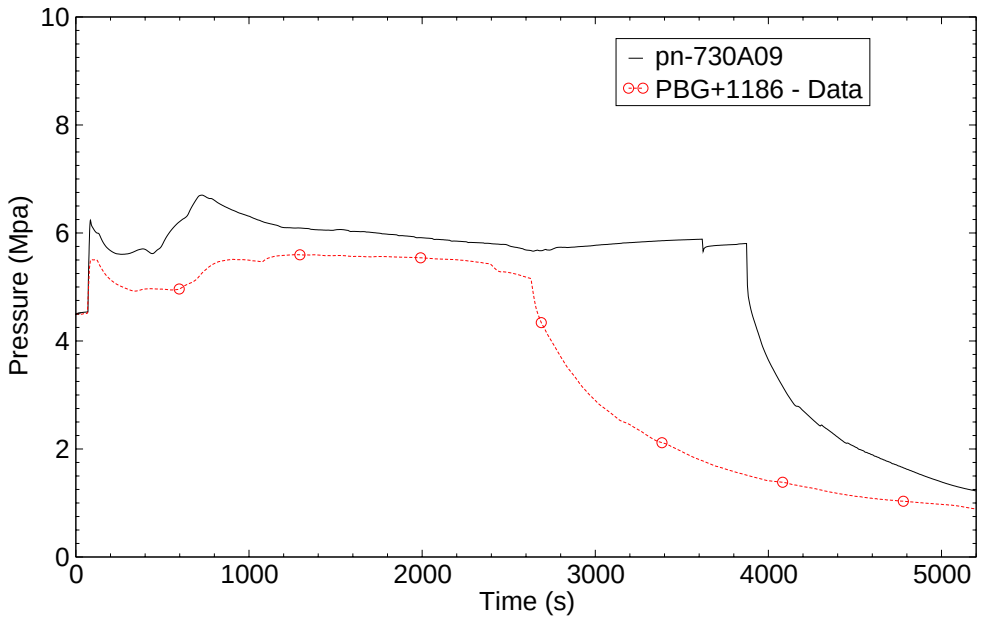

Figure C.6-33. Broken Loop Steam Generator Secondary Side Pressure Comparison - Test S-NH-1.

C.6.4.2.6. Pump Suction Loop Seal Clearing

The Semiscale S-NH results report, Reference 1, states that the S-NH-1 test did not experience a loop seal clearing event. In contrast, the S-NH-1 simulation did predict clearing of the intact loop pump suction loop seal after 4300 seconds as shown in Figure C.6-34 (Cells 6 and 7 are the cells in the bottom of the loop seal). However, by this time, the S-NH-1 simulation behavior had already missed several key events compared to the test data. The test data shows that core heatup had already begun at 2325 seconds. By the time the simulation predicted loop seal clearing occurs, the TRACE simulation and the Semiscale test data are on different transient event paths. It can not be concluded that the predicted loop seal clearing in the intact loop pump suction piping is incorrect, but it can be concluded that the TRACE simulation of the S-NH-1 transient and the test data are on divergent transient paths.

C.6.4.2.7. Bypass Flow Rate

The Semiscale NH results report (Ref. 1), states that the NH-1 test bypass flow reverses direction and drains the vessel upper head region into the downcomer region during the time period of 106 seconds to 280 seconds. This is shown in comparison to the TRACE calculated bypass flow in Figure C.6-35. The TRACE calculated bypass draining agrees fairly well with the Semiscale data.

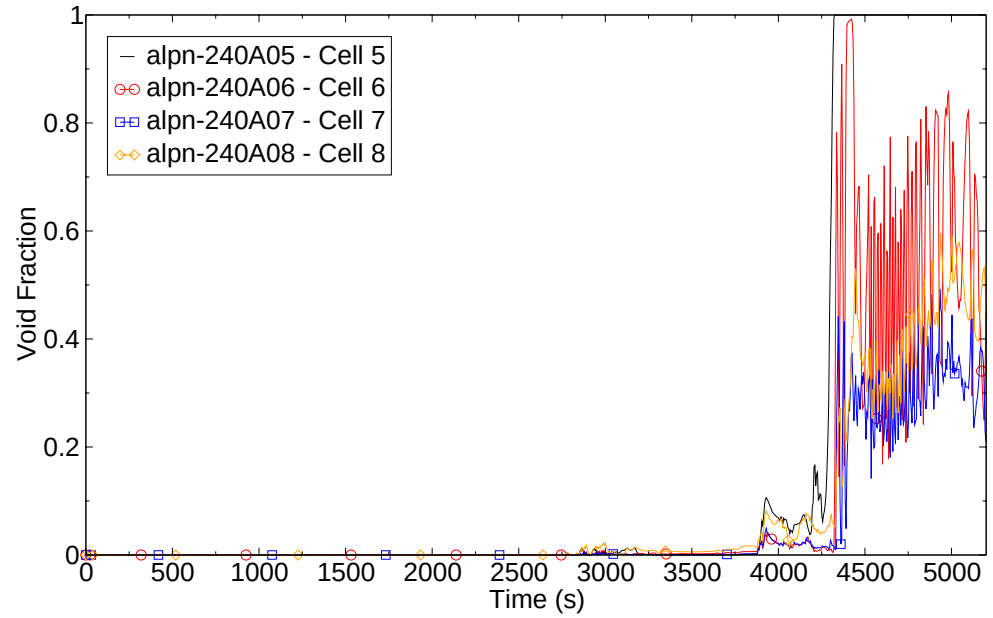

Figure C.6-34. Intact Loop Pump Suction Pipe Void Fraction Prediction - Test S-NH-1.

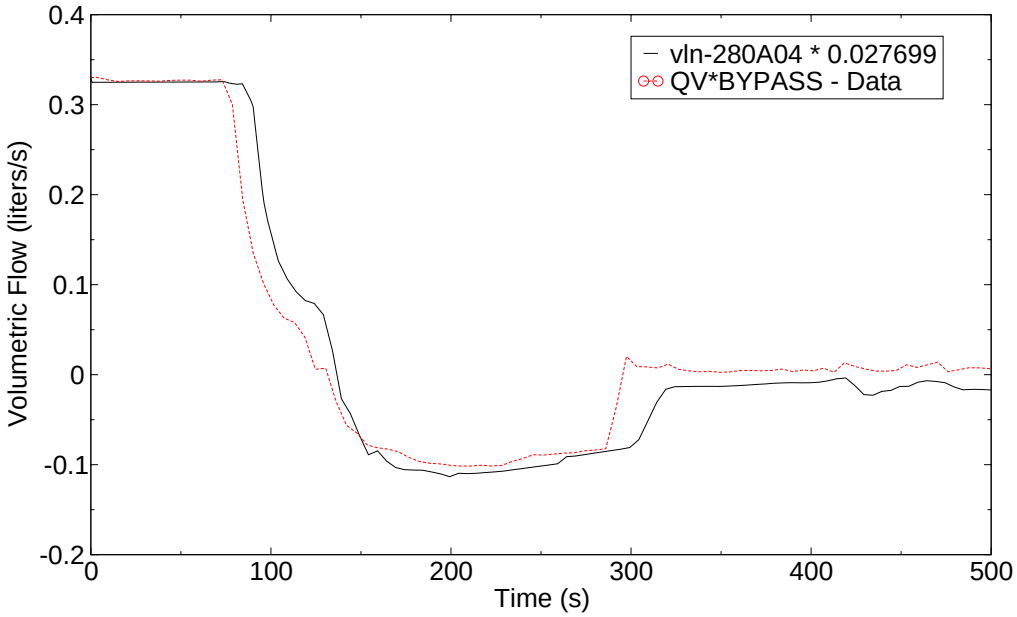

Figure C.6-35. Predicted and Measured Bypass Flow Rates - Test S-NH-1.

C.6.4.2.8. Accumulator Flow Rates

In the S-NH test series all HPI flow was unavailable, therefore, no ECC water was available until the primary system pressure decreased to the accumulator injection setpoint of 4.24 MPa. The accumulator flow rates are a function of the pressure difference between the accumulator and the cold leg injection location. A comparison of the predicted and measured accumulator mass flow rates for the intact and broken loops are shown in Figure C.6-36 and Figure C.6-37, respectively. Since the predicted pressure response was higher than the data (see **Section C.6.4.2.2.**) the timing of accumulator injection was off by over 1150 seconds. The predicted accumulator flow rates are comparable in magnitude to the test data.

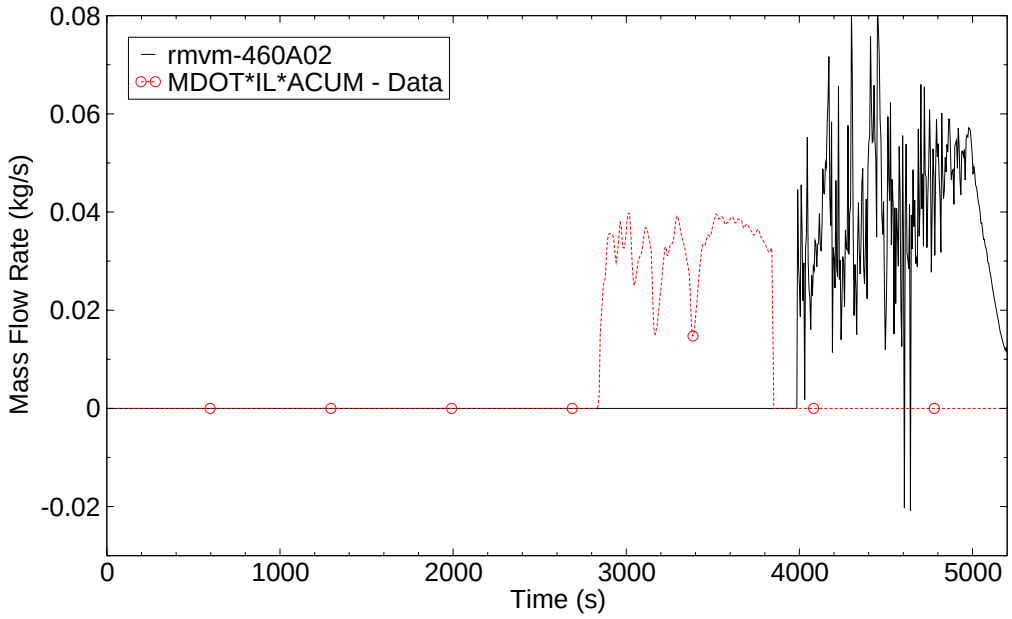

Figure C.6-36. Intact Loop Accumulator Mass Flow Rate Comparison - Test S-NH-1.

C.6.4.2.9. Rod Clad Temperature

The magnitude of the predicted core dryout is in reasonable agreement with the data, but the rod peak clad temperature is under predicted by about 98 °K. Since the predicted system pressure response was higher than the measured data, the calculated event timing is greatly delayed. The calculated primary system water mass lost through the break is much less than the Semiscale test data as inferred in Figure C.6-25 With more mass in the primary system the timing for core dryout and clad heatup were greatly delayed in the calculation.

The NH series of tests directed the operators to latch open the steam generator ADVs when the PCT reached 811 °K. Opening the ADVs resulted in secondary system blowdown and

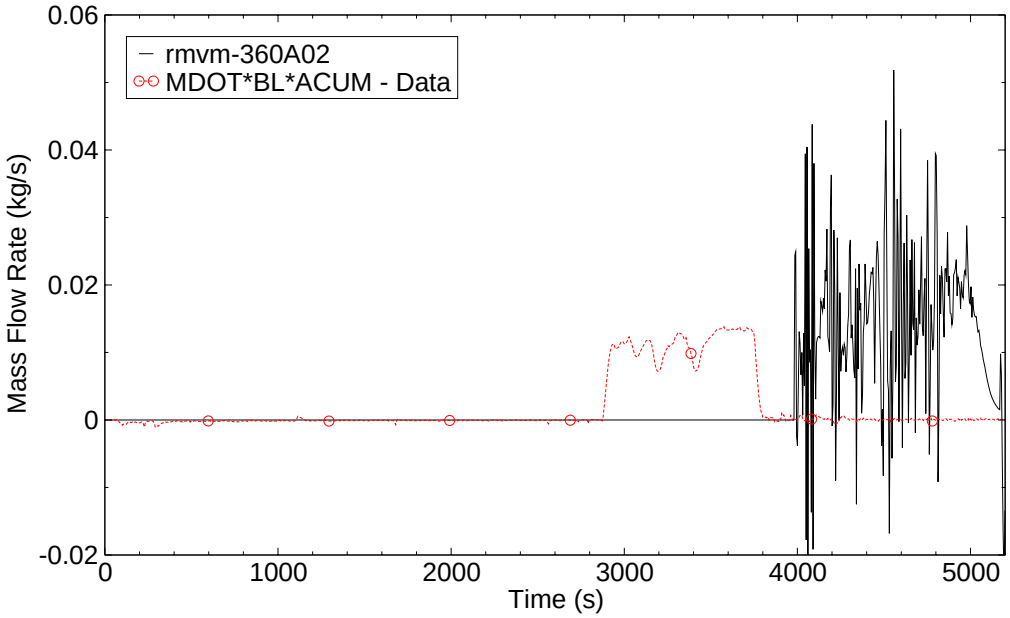

Figure C.6-37. Broken Loop Accumulator Mass Flow Rate Comparison - Test S-NH-1.

depressurization which increased the primary to secondary side heat transfer. Subsequently this action resulted in primary side cooldown and depressurization of the accumulator discharge pressure. The accumulator water discharges into the primary system loop piping, drains to the reactor vessel, rewets the heater rods, and terminates the clad heatup.

Figure C.6-38 shows the predicted and measured rod maximum peak clad temperature. The calculated PCT (818 ^{o}K) is about 98 ^{o}K less than the measured peak clad temperature (916 ^{o}K).

The predicted collapsed water level in the core is shown in Figure C.6-39 The calculated core collapsed water level decreased to about 0.6 meters above the bottom of the heated core at approximately 4140 seconds. Reference 1 reports the vessel collapsed water level dropped to about -392 cm below the cold leg centerline elevation at approximately 2900 seconds. This is equivalent to 1.04 meters above the bottom of the core. It is expected that with a lower predicted collapsed liquid level a higher rod temperature excursion would ensue. However, the peak clad temperature predicted by the code is 98 ^{o}K less. Figure C.6-40 shows the predicted void fraction in the top five cells in the core region, and Figure C.6-41 through Figure C.6-43 show rod clad temperature comparisons at the mid-plane 2.286 m above the bottom of the heated core and at the top of the core, respectively. While the upper part of the core shows complete voiding the rod temperature excursion is minimal, in fact only a small temperature excursion is noted at the top of the core whereas the data shows the rods peaking at around 810 ^{o}K. The lower calculated clad temperature response could possibly be caused by the prediction of too much entrainment or by an insufficient critical heat flux prediction by the code, or by a combination of both concerns.

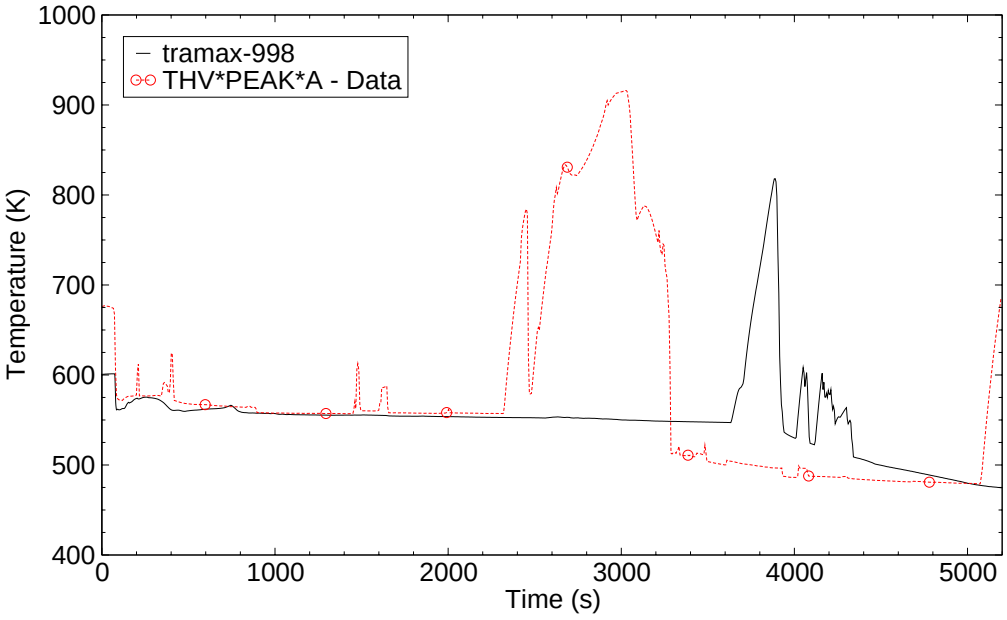

Figure C.6-38. Predicted and Measured Rod Peak Clad Temperature Comparison - Test S-NH-1.

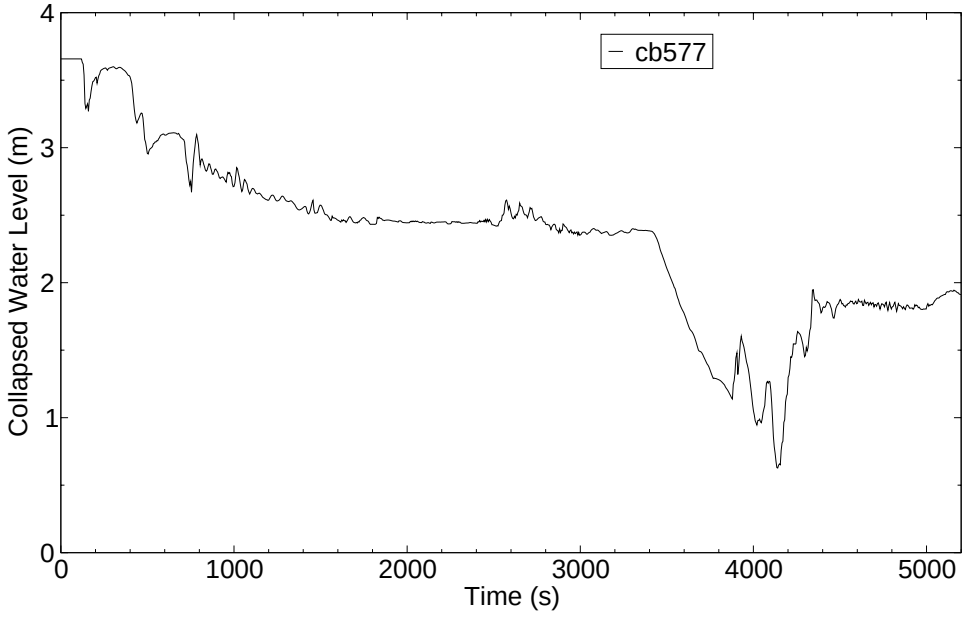

Figure C.6-39. Predicted Core Collapsed Liquid Level - Test S-NH-1.

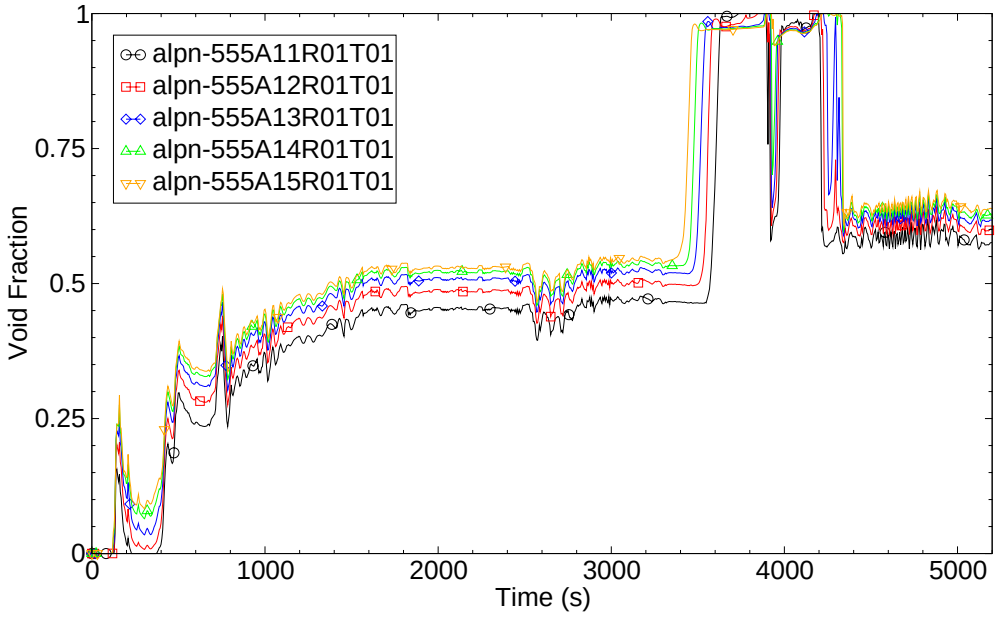

Figure C.6-40. Predicted Core Void Fraction in the Upper Half of the Core - Test S-NH-1.

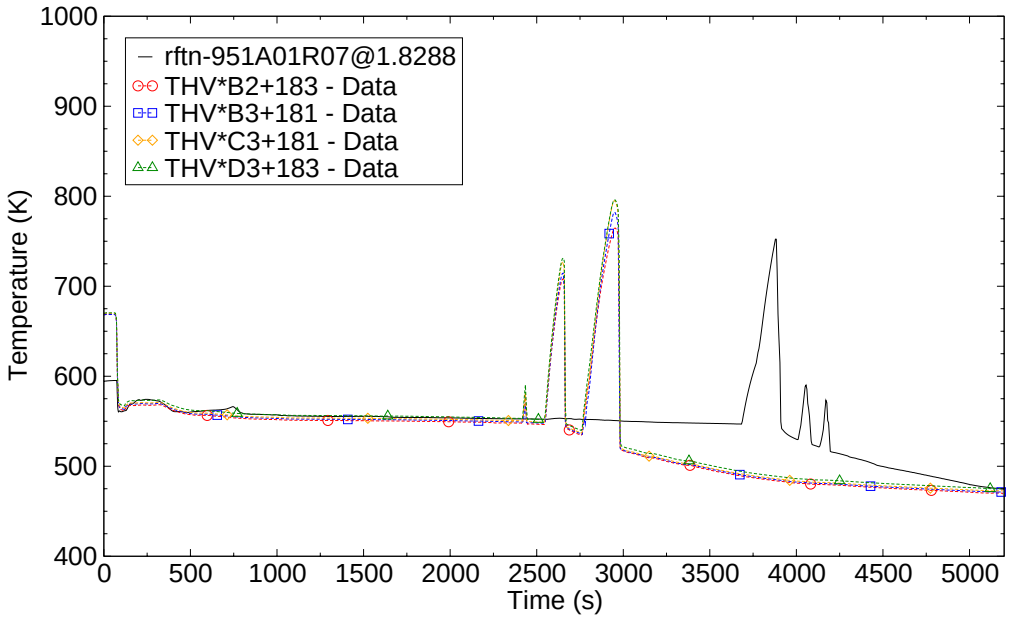

Figure C.6-41. Rod Clad Temperature Comparison at the Core Mid-plane (1.83 m) - Test S-NH-1.

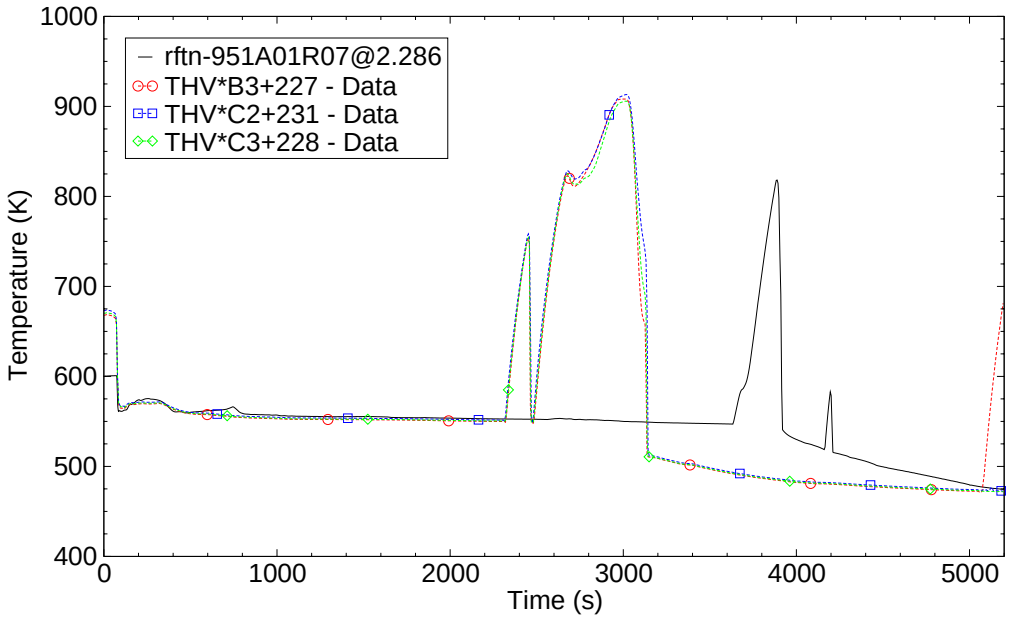

Figure C.6-42. Rod Clad Temperature Comparison at the 2.286 m Elevation - Test S-NH-1.

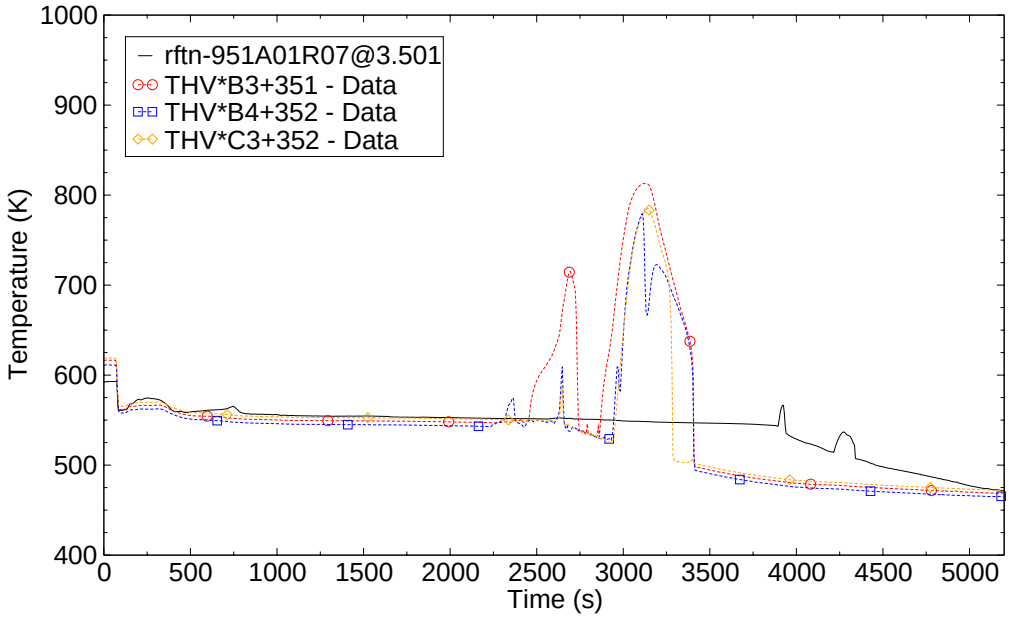

Figure C.6-43. Rod Clad Temperature Comparison at the Top of the Core (3.05 m) - Test S-NH-1.

At about 3990 seconds the primary system pressure dropped below the accumulator pressure and accumulator water injection began. The accumulator injection water quickly rewets the core and the rods quench. The data show a second rod heatup near the end of the transient. However, because of the delay in the predicted timing of events, a second rod heatup was not predicted by the code before the transient was terminated.

C.6.4.3. Figures of Merit

Peak clad temperature along the core axis was chosen as a figure of merit to illustrate how well the code predicts the measured data. Measured versus predicted peak clad temperature for tests S-NH-1 and S-NH-2 are shown in Figure C.6-44 and Figure C.6-45, respectively. In each simulation TRACE under predicts the peak clad temperature, more so in the upper half of the core. Although the predicted core dryout seems to be consistent with the data, the heater rods do not heatup as fast as the rod in the experiment and do not reach the maximum cladding temperature. Possible reasons for the differences between the predicted and measured rod behavior include the prediction of too much entrainment and insufficiencies in the critical heat flux prediction.

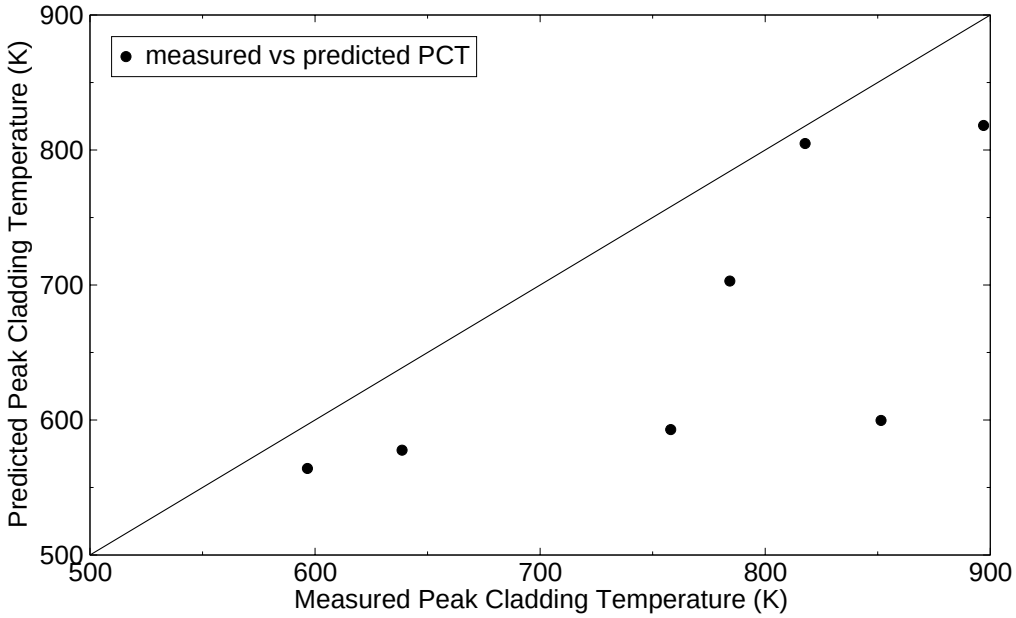

Figure C.6-44. Measured Versus Calculated Peak Clad Temperature - Test S-NH-1.

Core fluid density is an indicator of liquid level in the core. Measured core fluid density versus calculated core fluid density at three different elevations are shown in Figure C.6-46 and Figure C.6-47 for tests S-NH-1 and S-NH-2, respectively. The data shows rod heat up occurs at about 2325 and 5080 seconds for test S-NH-1, and at about 850 and 2080 seconds for test S-NH-2. The

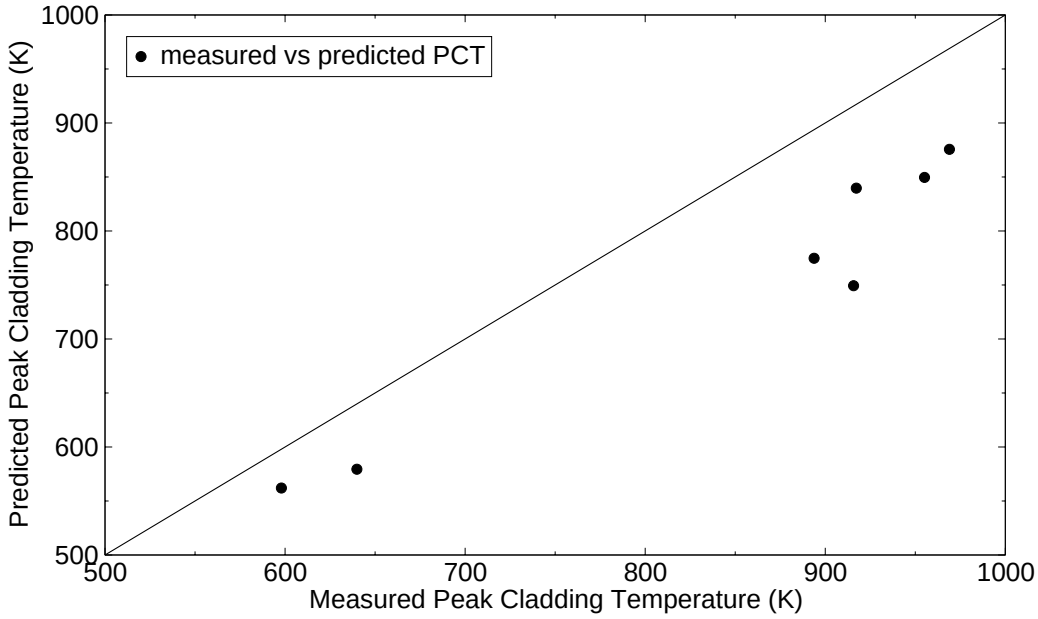

Figure C.6-45. Measured Versus Calculated Peak Clad Temperature - Test S-NH-2.

core fluid density prior to rod heat up is reasonably predicted. The delay in the predicted core heat up is evident in the fluid density comparisons.

C.6.5. Assessment Results Summary

The TRACE simulation of Semiscale test S-NH-2 compared well to the data. The timing of most events occurring during the transient were predicted fairly well, except for the actuation of the steam line ADVs. The ADVs were opened manually when the peak rod temperature reached 811 ^{o}K. The calculated rod temperature excursion was delayed and the ADVs were not opened until about 120 seconds after the operator action in the experiment.

The calculated rod clad temperature heatup was slower at the upper elevation in the core region and the code under predicted the peak clad temperature. Although the calculated core dry out appeared reasonable, there was sufficient cooling that the rod temperatures did not peak as high as the data. Possible reasons include the prediction of too much liquid entrainment during the core boil off and deficiencies in the critical heat flux calculated by the code.

The TRACE simulation of Semiscale test S-NH-1 was not as good as the simulation of test S-NH-2. The break flow rate was under predicted resulting in an over prediction of the system pressure. The data showed the broken loop flow rate did not stagnate and liquid was entrained out the break. However, in the simulation the broken loop stagnated. Subsequently, the break flow

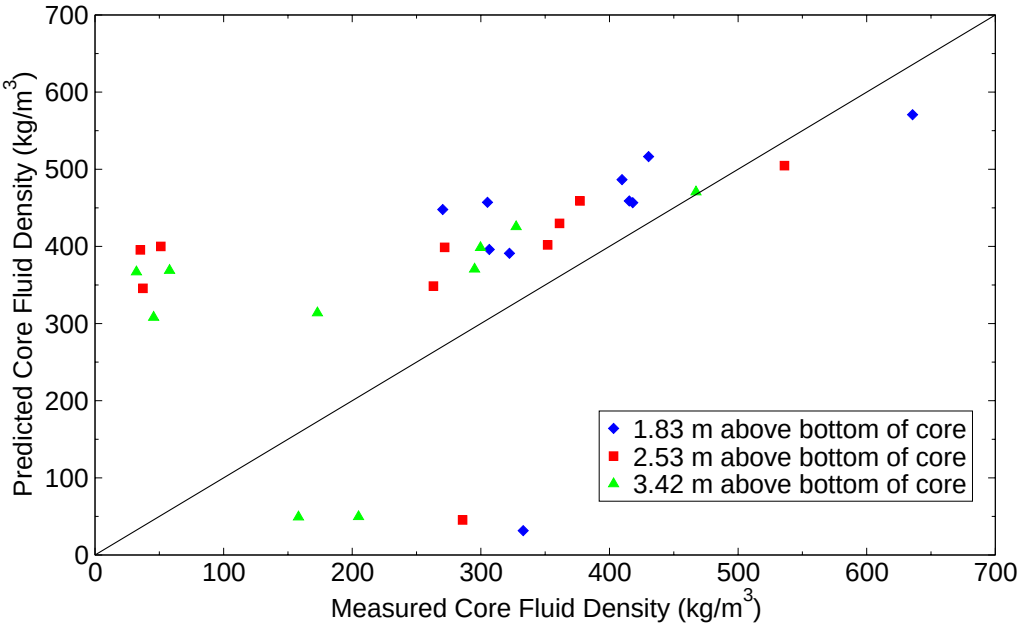

Figure C.6-46. Measured versus Calculated Core Fluid Density - Test S-NH-1.

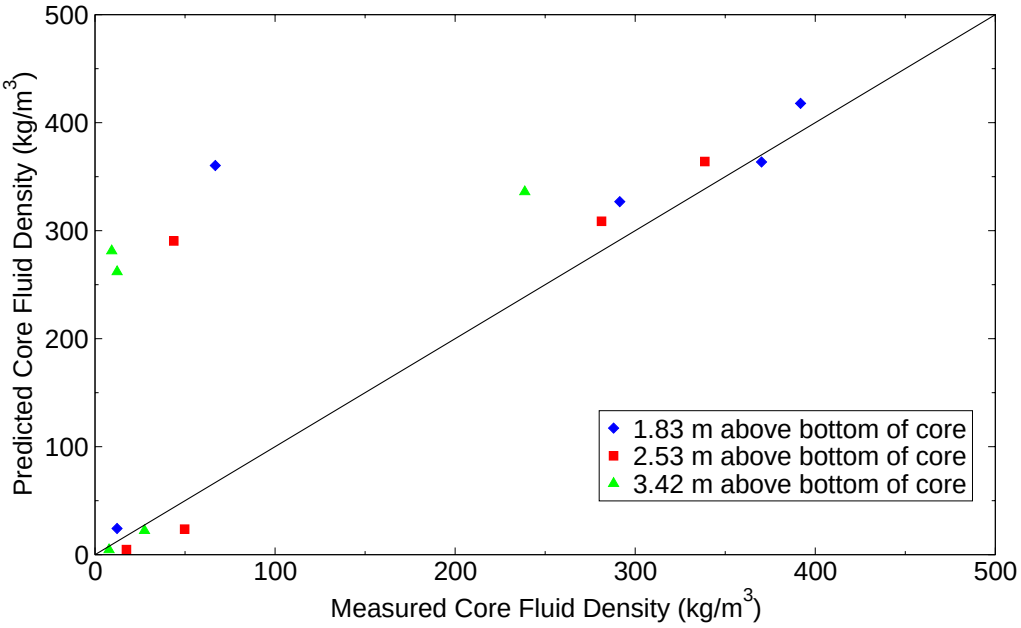

Figure C.6-47. Measured versus Calculated Core Fluid Density - Test S-NH-2.

became mostly steam flow and more liquid remained in the system. With more liquid in the system there was a delay in the core boil off and consequently a delay in the rod heatup. When the rods began to heat-up similar behavior was observed as was observed in the simulation of test S-NH-2, i.e. the heatup was slowed and the predicted PCT was lower. Rod temperature predicted near the top of the core only had a short lived heatup. Possible reasons for the rod heatup behavior include the prediction of too much entrainment and deficiencies in the critical heat flux calculated by the code.

Semiscale SBLOCA Tests S-NH-2 and S-NH-1 were executed using TRACE Version 5 Release Candidate 3 on 32 bit PCs using both the Windows XP and Linux operating systems. The executions using the Windows and Linux operating systems predicted similar results for both tests. Consequently, it was concluded that Semiscale SBLOCA Tests S-NH-2 and S-NH-1 could be run using either a Windows XP or Linux operating system.

C.6.6. References

1 John E. Streit, *"*Results of Semiscale Mod-2C Small-Break Loss-of-Coolant Accident Without HPI (S-NH) Experiment Series," NUREG/CR-4793, EGG-2482, January 1987.

2 E. Klingler and K. E. Sackett, *"*The Semiscale Mod-2C Small-Break (.5% and 2.1%) Configuration Report for Experiments S-NH-1, S-NH-2, S-NH-3, and S-NH-5," EGG-RTH-7323, July 1986.

3 J. Atchison, "TRACE Comparison to Semiscale Test NH-1 and NH-2 Data," ISL-NSAD-TR-03-23, December 2003.

4 M. Bolander, "TRACE Calculation Notebook for Semiscale Tests S-NH-1 and S-NH-2," March 2006.

5 Morris L. Patton, *"*Semiscale Mod-3 Test Program and System Description," NUREG/CR-0239, TREE-NUREG-1212, July 1978.

6 Rex Shumway, "TRACE Comparison to Semiscale Test LH-1 and LH-2 Data," ISL-NSAD-TR-03-20, September 2003.

C.7. Semiscale Natural Circulation Tests

Author(s): William Krotiuk[1], David Caraher[2]

Affiliation: [1]U.S. Nuclear Regulatory Commission, [2]Information Systems Laboratories, Inc.

Code Version: TRACE V5.0

Platform and Operating System: Intel x86, Windows XP

C.7.1. Introduction

TRACE simulations for two Semiscale natural circulation tests (S-NC-2 and S-NC-3) have been run and compared with experimental data. The objective of these code-to-data comparisons is to evaluate TRACE capabilities for predicting the single and two-phase natural circulation phenomena in an integral facility.

The inputs models for Semiscale natural circulation tests S-NC-2 and S-NC-3 were developed by Information systems Laboratory (ISL) and executed using TRACE V4.261. This document reports the results of the execution of TRACE V5.0 using the original inputs prepared by ISL.

C.7.2. Test Facility Description

Natural circulation experiments were performed in the Semiscale Mod-2A test facility, a small-scale model of the primary system of a four-loop PWR nuclear power generating plant (scaling factor 1/1705). The Mod-2A system incorporates the major components of a PWR including steam generators, vessel, downcomer, pumps, pressurizer, and loop piping. Detailed descriptions of the Semiscale Mod-2A test facility and operation procedure are given in References 1 through 3. All of the natural circulation experiments and the data are summarized in Reference 4. The data used in this report are from that reference. It should be noted that the data given in the quick look reports differs from the data given in Reference 4 in that the primary system mass inventory percentages are lower in Reference 4.

The natural circulation experiments used a single-loop configuration consisting of the intact loop with steam generator and a vessel/downcomer, as shown in Figure C.7-1. In the single-loop configuration, the intact loop pump was replaced with a spool piece containing an orifice that

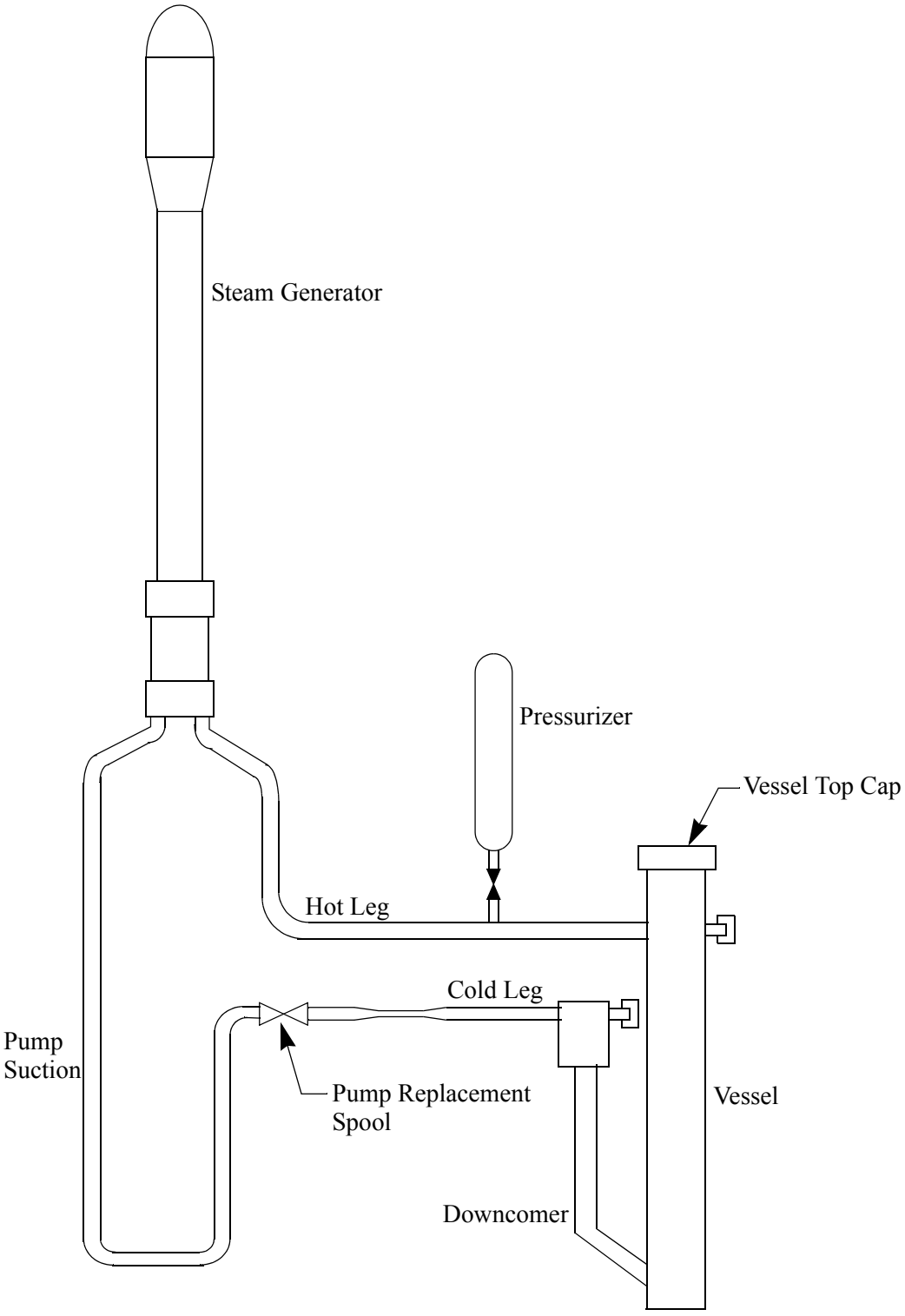

Figure C.7-1. Semiscale Mod-2A Single-loop Configuration

simulated the hydraulic resistance of a locked pump rotor. In addition, the vessel was modified from the normal Mod-2A configuration by removing the vessel upper head to ensure a uniform heatup of the entire system and to avoid condensation in upper-head structures (the upper vessel was capped).

Ten test series made up the Semiscale natural circulation experiments. The various phenomena simulated in these test series included: transition from single-phase to two-phase to reflux natural circulation modes by varying primary side system mass; effect of steam generator secondary side mass inventory on two-phase natural circulation; effect of secondary conditions on reflux; effect of non condensable gas (nitrogen) on both reflux and two-phase, single, and two-loop effects; transient small break LOCAs; and ECCS effects.

C.7.3. TRACE Model Description

The calculations reported here were performed using the TRACE V5.0 computer code. The starting-point TRACE facility model for this assessment was the RELAP5 model employed for the RELAP5 developmental assessment simulations performed in 2001 (Ref. 6). The RELAP5 model was converted to a TRACE base model using the SNAP/TRACE deck conversion process. The resulting deck was then modified as follows:

1. SJC components were removed so the deck was more readable.
2. All fric input was converted back to loss factor input so that the correspondence of the RELAP5 and TRACE decks was easy to see.
3. Unneeded components were removed.
4. All the components representing the vessel were combined into a VESSEL component.
5. grav terms were modified as necessary so all circulation paths were closed in TRACE.
6. Signal variables, control blocks, and trips were created to control feedwater flow and to control the PUMP components which are used to reduce the mass inventory in both the primary and secondary sides.

After the TRACE base deck was created it was cloned numerous times so that each steady-state data point for case 2 of test S-NC-2 and case 3 of test S-NC-3 could be simulated. A total of 16 TRACE decks were created for test S-NC-2 simulations. These decks differ only in the specification of how much mass is to be drained from the primary system. Ten TRACE decks were created for test S-NC-3 simulations. These decks differ only in the specification of how much mass is to be drained from the secondary system.

Loss factors were specified in the base RELAP5 input such that RELAP5 matched the experimental loop flow for the 100% primary system mass case for test S-NC-2. All loss coefficients in the TRACE decks were taken from RELAP5 deck for S-NC-2.

The TRACE nodalization of the Semiscale natural circulation test facility is depicted in Figure C.7-2. The TRACE input is documented in Reference 7.

C.7.4. Tests Simulated

The 60 kW power level cases for tests S-NC-2 and S-NC-3 were used to assess TRACE. The S-NC-2 test examined single-phase, two-phase, and reflux steady-state modes by varying the primary side system mass at different core powers (30, 60, and 100 kW) with a constant steam generator secondary side condition. The S-NC-3 test examined primary side two-phase natural circulation behavior under varying steam generator secondary side mass inventory at a core power of 62 kW.

C.7.4.1. Simulation of Test S-NC-2

The core power level used in this TRACE assessment study was 60 kW (S-NC-2, Case 2). At this power level, 16 different steady-state conditions were achieved. Each steady-state was at a different primary side mass inventory that ranged from 100% down to 55% full. The primary system pressure was allowed to vary as the system was drained (the pressurizer was valved out) while the steam generator secondary pressure was held constant and acted as an effective heat sink throughout the test. The test data for S-NC-2, case 2 show that for mass inventories between 97% and 100% the primary system behavior was similar to single-phase natural circulation. Further reductions in primary system mass resulted in two-phase natural circulation. In this regime the loop flow increased rapidly as the system mass was decreased, peaking at a primary system mass of about 88%, and slowly falling off as the mass inventory declined. When the primary side mass inventory was decreased below 66 to 70% the system transitioned from two-phase natural circulation to the reflux mode of cooling. The reflux mode of natural circulation is a two-phase state roughly characterized by a vapor-continuous condition entering the inlet of the steam generator tubes with counter-current liquid flow returning to the vessel.

The rapid increase in measured loop flow as the primary system mass was decreased below 97% is due to boiling in the core and vapor flowing into the steam generator tubes and condensing before reaching the top of the u-tubes. This lowers the density of the hot leg of the natural circulation loop while the density in the cold leg remains unchanged. When the system mass is lowered sufficiently vapor is carried over the top of the steam generator u-tubes, lowering the density of the cold leg of the loop. The mismatch of the hot and cold legs of natural circulation loop is thus diminished and loop flow decreases.

Figure C.7-4 through Figure C.7-6 show the calculated results compared to data for mass flow rate, hot leg fluid temperature, primary side steam generator outlet fluid temperature, and primary system pressure. All but one of the calculations resulted in a steady-state mass flow. One

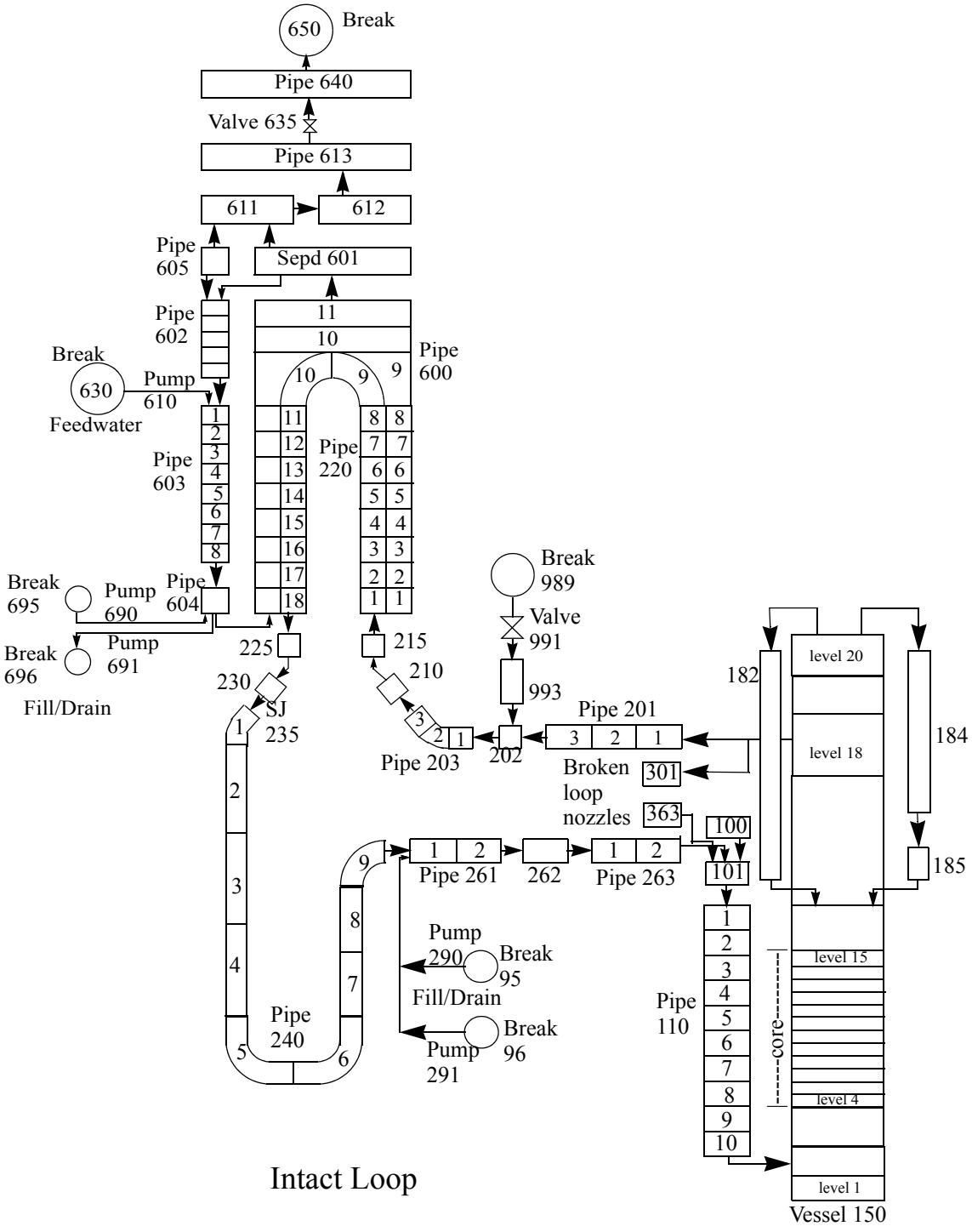

Figure C.7-2. Schematic of the TRACE Semiscale Natural Circulation Tests' Model

calculation point predicted an oscillatory steady-state condition. The black band on Figure C.7-4 illustrates the range of the flow oscillations for this point. The calculated flow results underpredict data between the 76% and 88% mass inventory points. At least part of the reason for the higher measured flows for these points is due to the external heaters used on the pump suction piping in the tests. It was noted in the tests (p 46, Ref. 2) that, for the 73% primary system mass case, the mass flow dropped from 0.38 kg/s to 0.20 kg/s when the pump suction external heater was turned off. Having the heaters on reduced the fluid density in the upside of the pump suction u-bend and thus increased the flow. It is suspected that a similar effect occurred for the system mass cases which had the pump suction heaters on. The heaters were turned off for system masses below 72%. Only the heaters off data point is shown for the 73% system mass data point in Figure C.7-4

According to Reference 2 reflux cooling was observed for system inventories less than about 66%. The TRACE simulation of the 66% system mass case showed intermittent reflux in the hot leg while both the 61% and 56% system mass simulations showed steady countercurrent flow in the hot leg - steam flowing to the SG and liquid returning to the vessel. In this regard the TRACE simulations are in agreement with the experimental data.

The disagreements between TRACE and measured pressures and temperatures are mostly a result of differences between computed and measured loop flows. The exceptions to this are the computed steam generator outlet temperatures in the 69 - 86% mass inventory range (Figure C.7-5). The low temperatures for these points were calculated by TRACE because of a heat transfer regime change for some of the heat structures representing the downside of the SG tubes. Heat transfer switched from forced convection to condensation, thereby resulting in a pooling of cool liquid at the SG outlet.

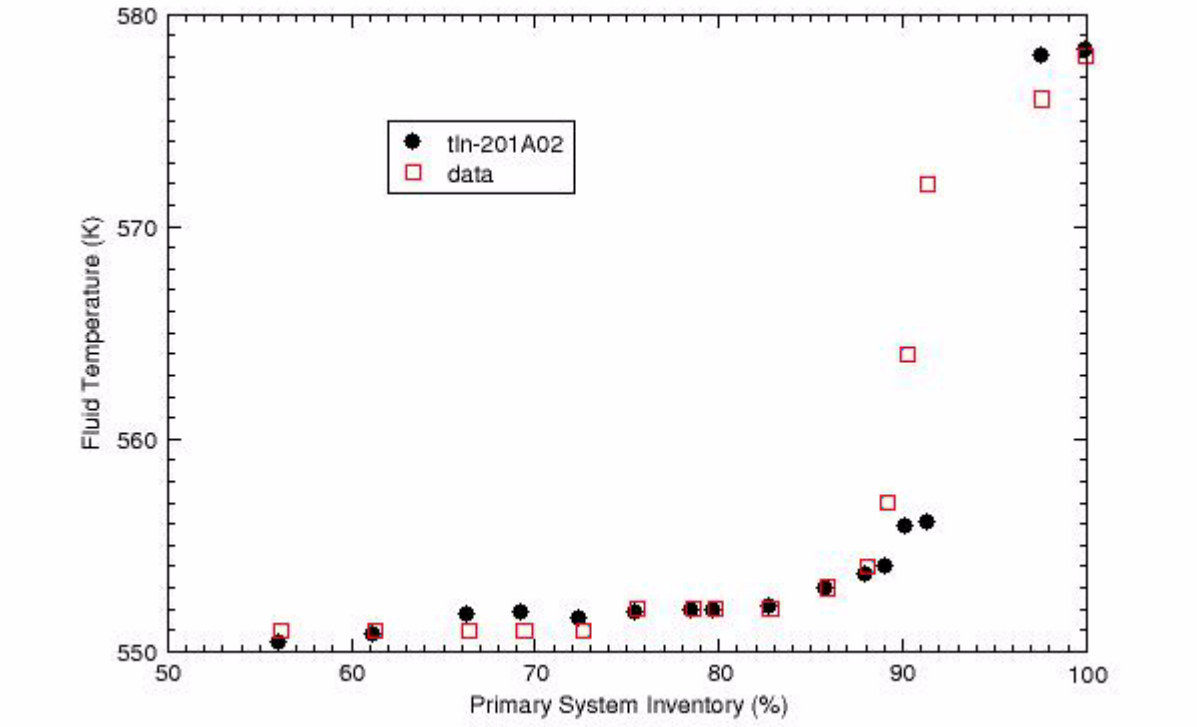

Figure C.7-3. Measured and Calculated Hot Leg Temperatures at the 60 kW Power Level for Test S-NC-2

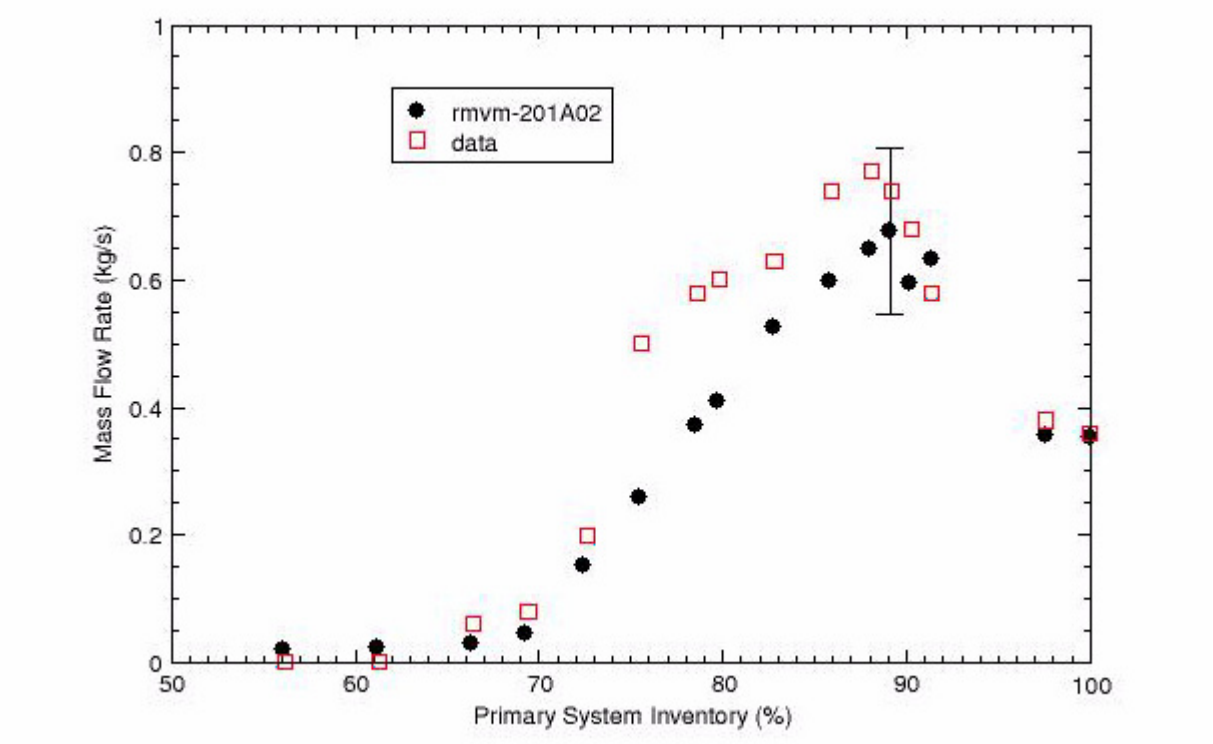

Figure C.7-4. Measured and Calculated Mass Flow Rates at the 60 kW Power Level for Test S-NC-2

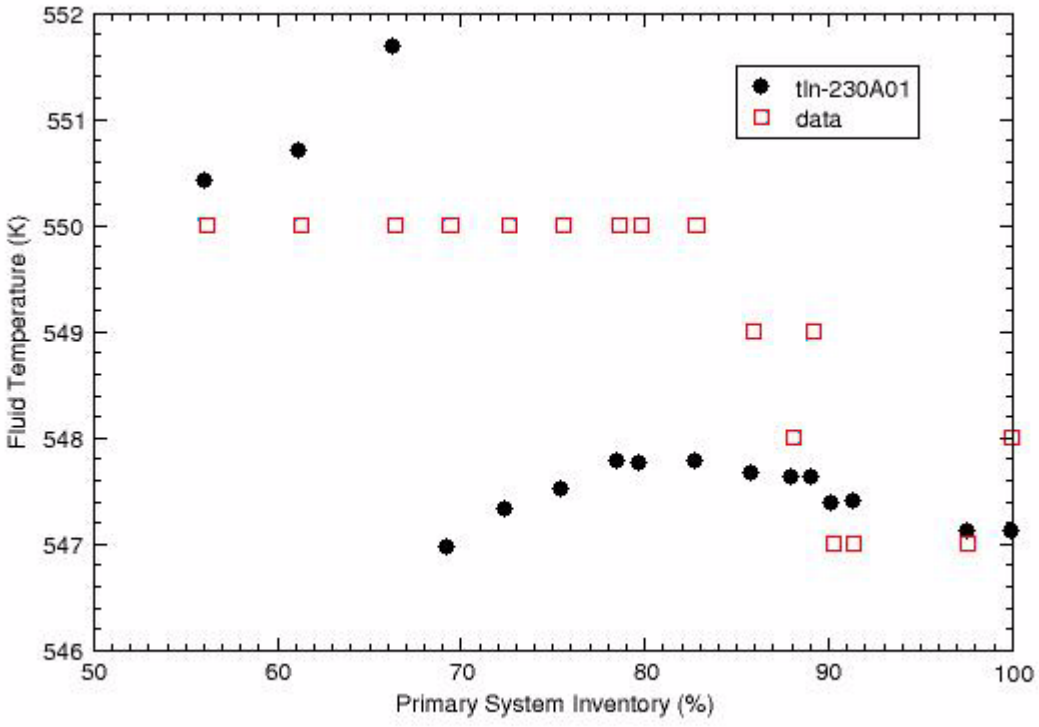

Figure C.7-5. Measured and Calculated Steam Generator Outlet Temperatures at the 60 kW Power Level for Test S-NC-2

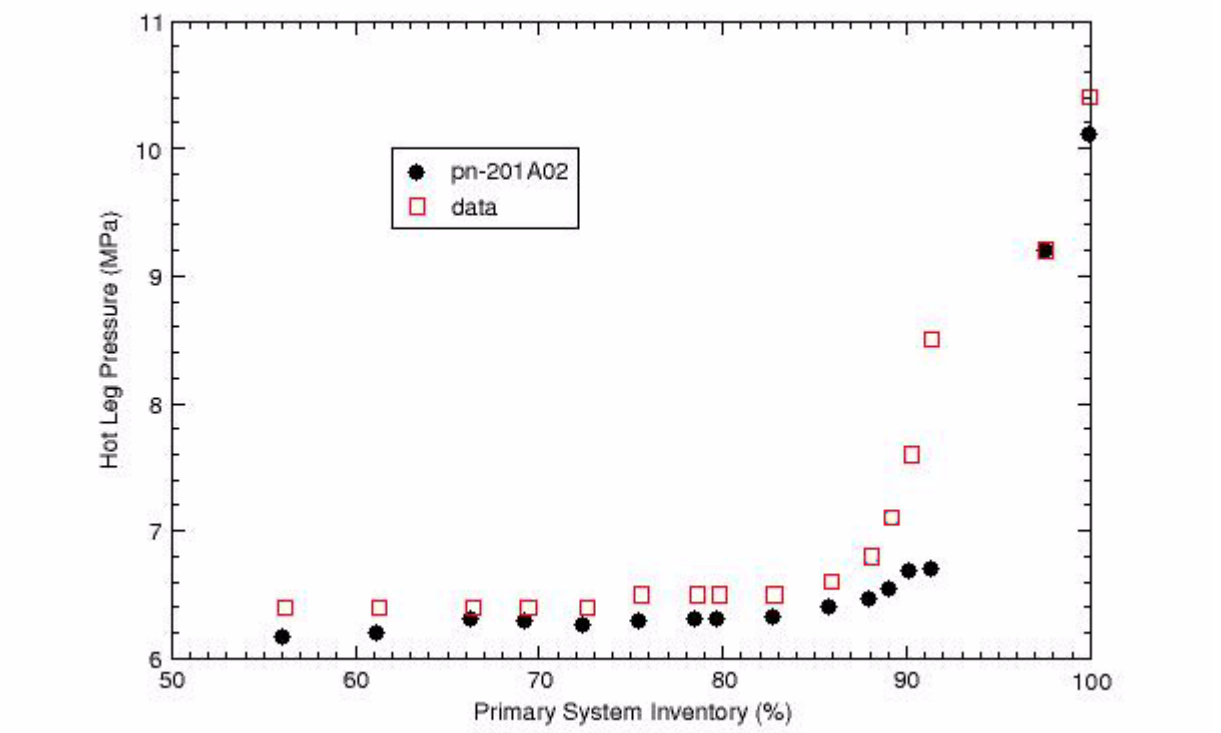

Figure C.7-6. Measured and Calculated Hot Leg Pressures at the 60 kW Power Level for Test S-NC-2

C.7.4.2. Simulation of Test S-NC-3

The core power level used in this TRACE assessment was 62 kW (S-NC-3, Case 3). At this power level, 9 different steady-state conditions were achieved. Each steady-state was at a primary side mass inventory of 89.2% full but with different amounts of liquid in the steam generator secondary side. The primary system pressure was allowed to vary as the system was drained (the pressurizer was valved out) to the 89.2% level. By varying the steam generator secondary mass the effective heat transfer area between the primary to secondary systems was changed. Results were tabulated as a function of collapsed liquid level in the steam generator.

It should be noted that the simulations of S-NC-3 were done with an 89.2% primary system mass inventory even though the test data indicate a level of 91.8% (Table B-5, Ref. 4). The reason for this is that the inventory level (91.8%) quoted for case number 10 in Table B-5, Ref. 4 is inconsistent with the stated flow rate of 0.75 kg/s. Table B-3 of Ref. 4 shows that a primary system mass inventory of 91.8% would correspond to a flow rate of about 0.55 kg/s, while a flow rate of 89.2% would correspond to a flow rate of 0.74 kg/s. This inconsistency in the data report was resolved by using a mass inventory of 89.2% in the TRACE simulations.

Figure C.7-7 through Figure C.7-10 compare the calculated results with data for mass flow rate, hot leg fluid temperature, primary side steam generator outlet fluid temperature, and primary system pressure versus the steam generator collapsed liquid level above the tube sheet. The average height (tube sheet to top of u-bend) of the six steam generator tubes is 9.4 m.

The measured mass flow rate and the fluid temperature at the primary side steam generator outlet in the region from 1 to 4 meter steam generator collapsed level was oscillatory. The minimum and maximum of the oscillations observed are shown in Figure C.7-7 and Figure C.7-9 The calculated mass flow rate fell close to or within the oscillatory data range when the SG collapsed liquid level was less than 5 meters. The calculated mass flow generally slightly under predicts data for SG collapsed liquid levels between about 4 and 9 meters. For lower levels the data showed that the primary-to-secondary heat transfer was degraded thus diminishing the heat removal capability of the steam generator. Consequently, the driving potential (density difference between the core and SG tubes' upside and the SG tubes' downside) was diminished and the mass flow rate slowed. TRACE calculated reasonable heat transfer capability for all tests. The higher mass flow rates in TRACE for SG collapsed liquid levels below 5 meters resulted in lower calculated fluid temperatures and a lower primary system pressure relative to the data, as shown in Figure C.7-8 through Figure C.7-10

For every case, TRACE calculated that all the vapor entering the steam generator tubes was completely condensed. The void fraction of the flow entering the tubes, 32% dropped below 2% prior to reaching the bend in the SG tubes. A steady-state flow of a low void fraction mixture was established in TRACE for SG collapsed liquid levels below 9 meters, and an oscillatory flow of a low void fraction mixture, as indicated by the maximum-minimum band range indicated on Figure C.7-7**,** was established in TRACE for levels above 9 meters. The data exhibited a fairly periodic stalling and unstalling of the flow amongst the six SG tubes. This behavior was attributed to formation and collapse of a steam bubble in the u-bend of the various SG tubes.

Although not presented here, a sensitivity study of the SG tubes nodalization was conducted in a previous analysis performed using TRACE Version 4.261. Replacing the first two nodes of both component 220 and 600 with 8 nodes had no effect upon computed results. A sensitivity study was also done in which the 6 SG tubes were modeled as 3 groups: two long, two short, and two intermediate. Modeling the tubes in this manner resulted in the same computed results as when the tubes were all lumped together.

C.7.5. Assessment Results Summary

The TRACE simulations of Semiscale natural circulation tests S-NC-2 are in good agreement with the experimental data overall. For the flow data, there are differences between calculated and measured flows for several data points. This discrepancy is attributed to the effect of heat addition by the external heaters on the pump suction piping during the test. TRACE also calculated an oscillatory steady-state flow conditions for a primary system mass inventory of about 89%.

For test S-NC-3 the agreement between TRACE and the data is good for secondary system collapsed liquid levels less than 5 meters (average height of the six u-tubes is 9.4 m). However, TRACE slightly under predicts flowrate at higher liquid levels. TRACE calculated a steady flow through the SG tubes for all of the data points below a collapsed level of about 9 meters, and oscillatory steady-state conditions above 9 meters. The test data exhibited periodic stalling and unstalling of the SG tubes' flows for secondary side collapsed levels below 5 m.

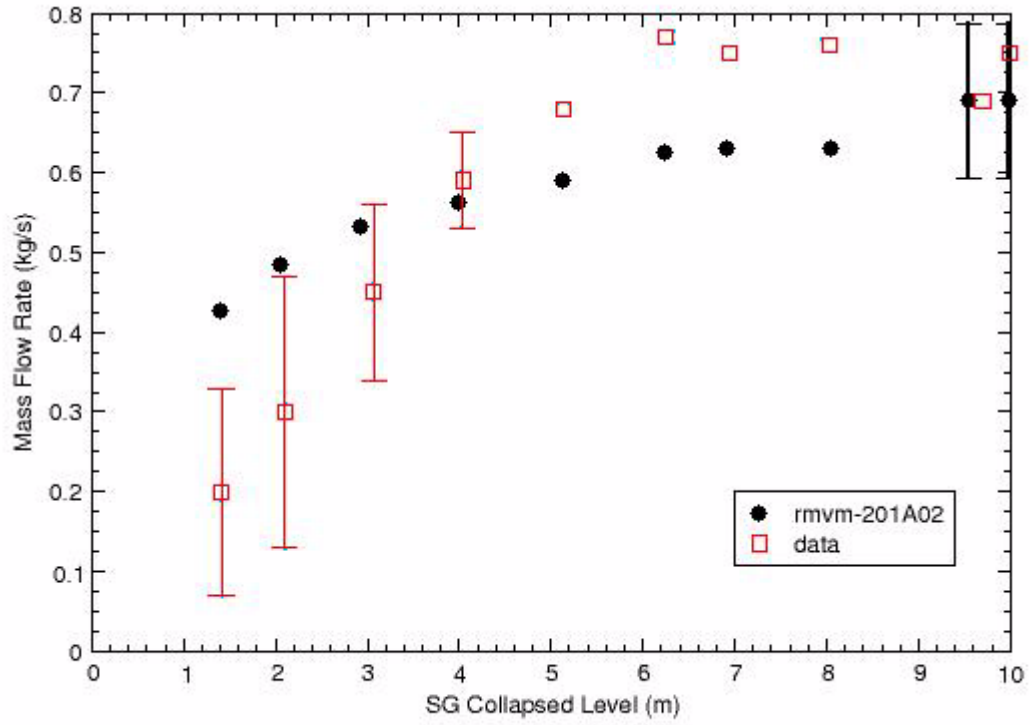

Figure C.7-7. Measured and Calculated Primary System Mass Flow Rate Versus Steam Generator Secondary Collapsed Level for Test S-NC-3

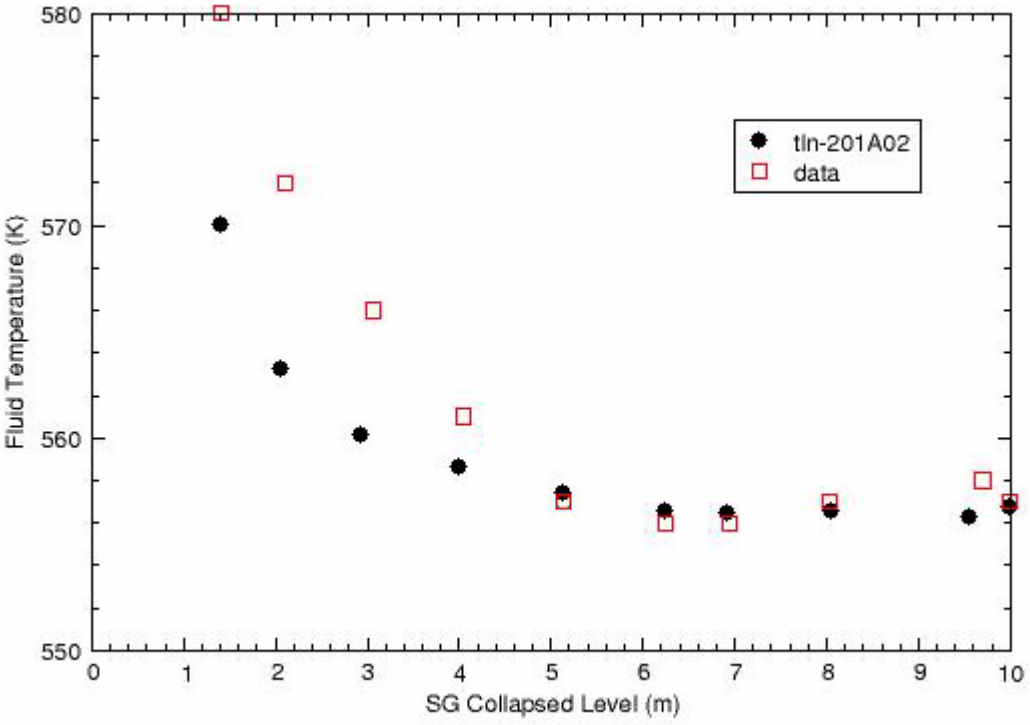

Figure C.7-8. Measured and Calculated Primary Side Hot Leg Fluid Temperature Versus Steam Generator Secondary Side Collapsed Level for Test S-NC-3

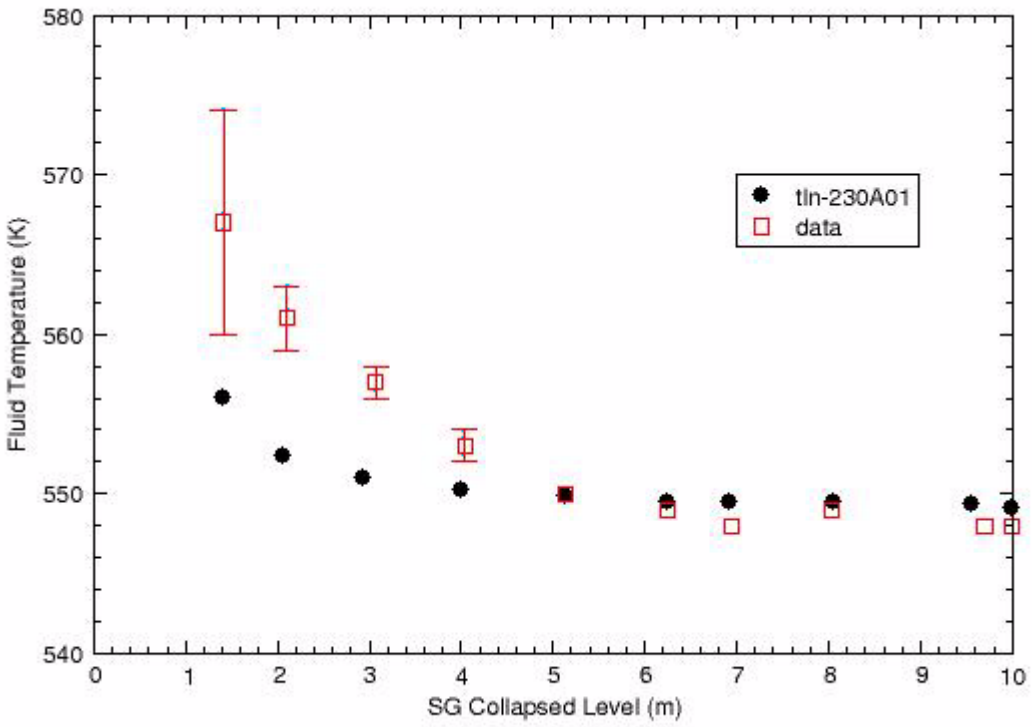

Figure C.7-9. Measured and Calculated Primary Side Steam Generator Outlet Temperature Versus Steam Generator Secondary Side Collapsed Level for Test S-NC-3

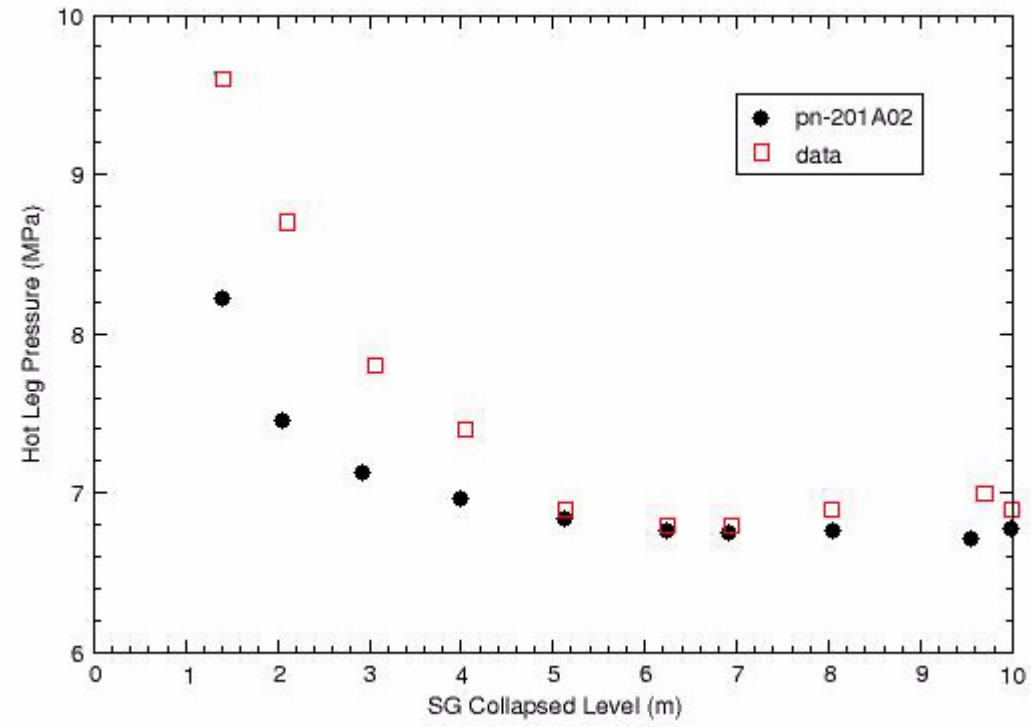

Figure C.7-10. Measured and Calculated Primary System Pressure Versus Steam Generator Secondary Side Collapsed Level for Test S-NC-3

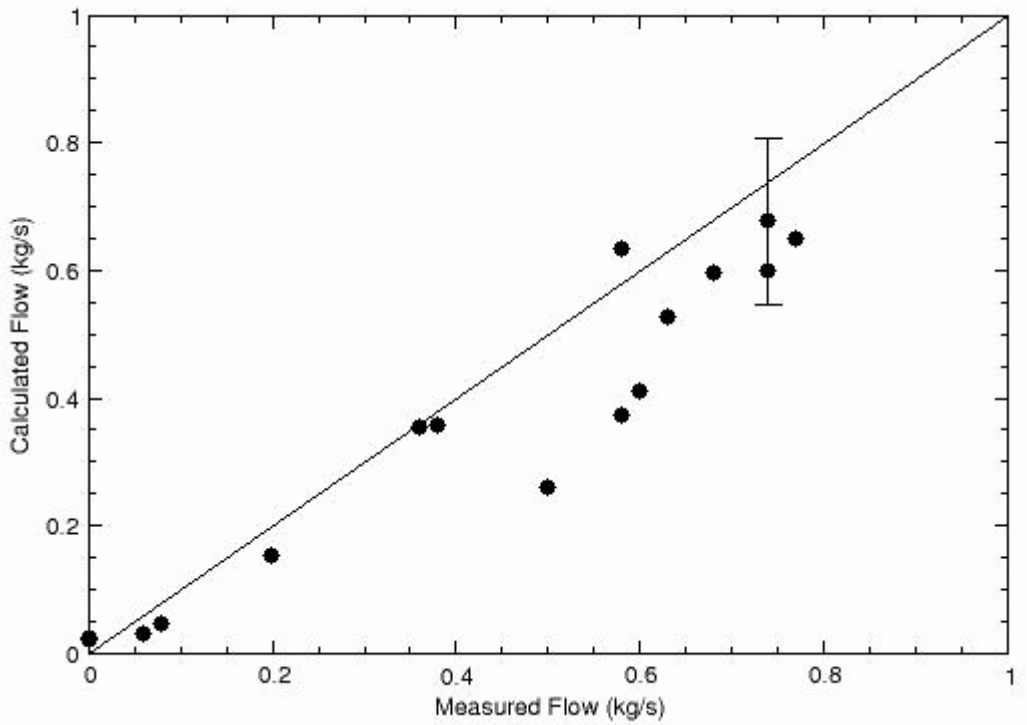

Figure C.7-11. Calculated versus Measured Flows for Test S-NC-2

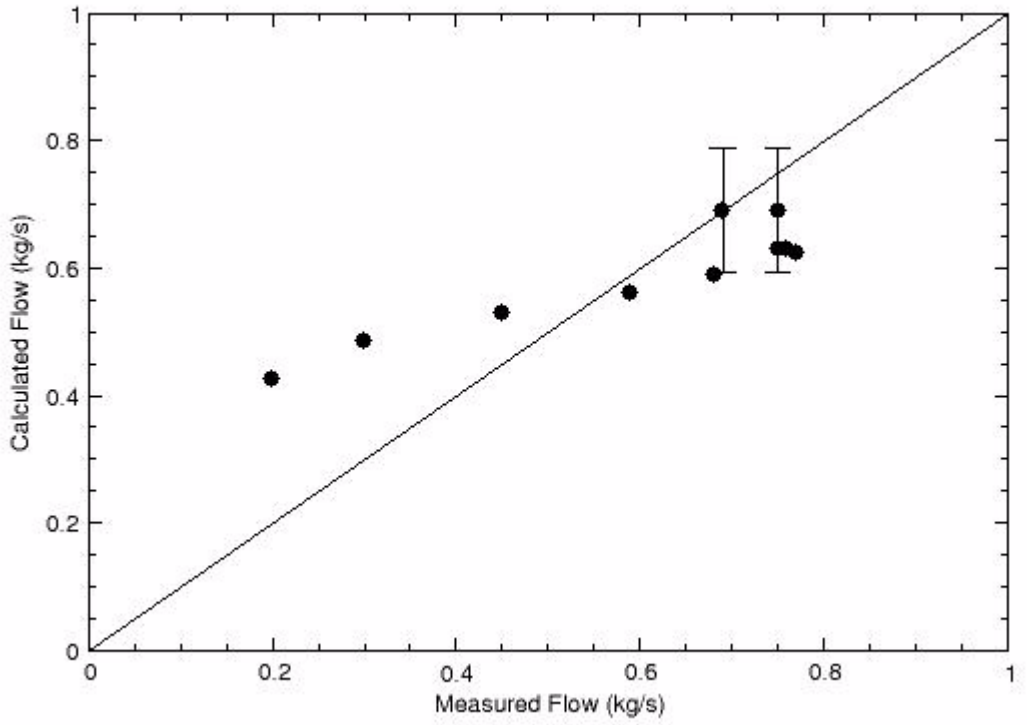

Figure C.7-12. Calculated versus Measured Flows for Test S-NC-3

C.7.5.1. Figures of Merit

The agreement of loop flows with measured flows was adopted as a figure of merit for the natural circulation tests. Figure C.7-11 illustrates the figure of merit for tests S-NC-2 and Figure C.7-12 shows it for test S-NC-3..

C.7.6. References

1 System Design Description for the Mod-A Semiscale System, Addendum 1, "Mod-A Phase I Addendum to Mod-3 System Design Description," EG&G Idaho, Inc., December 1980.

2 G. G. Loomis, et. al., "Quick Look Report for Semiscale Mod-2A Test S-NC-2," EGG-SEMI-5507, July 1981.

3 G. G. Loomis, et. al., "Quick Look Report for Semiscale Mod-2A Test S-NC-3," EGG-SEMI-5522, August 1981

4 G. G. Loomis and K. Soda, "Results of the Semiscale MOD-2A Natural Circulation Experiments," NUREG/CR-2335, September 1982.

5 R. A. Dimenna, "RELAP5 Analysis of Semiscale Mod-A Single-Loop Single-Component Steady-State Natural Circulation Tests," EGG-SEMI-6315, June 1983

6 RELAP5/MOD3.3 Code Manual, Vol. III: Developmental Assessment Problems, NUREG/CR-5535/Rev 1. December 2001

7 D. Caraher, TRACE Calculation Notebook for the Semiscale MOD-2A Natural Circulation Experiments, Information Systems Laboratories, Inc., March 2003.

C.8. BETHSY Test 9.1B and Test 6.2

Author(s): William Krotiuk[1], Weidong He[2] and Donald Palmrose[2]

Affiliation: [1]U.S. Nuclear Regulatory Commission, [2]Advanced Systems Technology and Management, Inc.

Code Version: TRACE V5.0

Platform and Operating System: Intel x86, Windows XP

C.8.1. Introduction

The objective of this work is to assess the ability of V5.0 of the TRACE code to calculate the thermal-hydraulic response to a small break loss-of-coolant accident (SBLOCA) phenomena as simulated in the BETHSY test facility. TRACE code calculations are compared with experimental data from BETHSY Test 9.1b and Test 6.2TC. This report describes the following assessment activities:

• Identification of the phenomena occurring in the BETHSY test facility.

• Development of the TRACE input for each test.

• Development of acceptance criteria.

• Comparison of code calculations with the test data.

• Identification of potential code deficiencies.

BETHSY Test 9.1b (i.e., International Standard Problem No. 27 or ISP-27) simulated a 0.5% (5.08 cm or 2-inch) cold leg break without available high pressure injection system (HPIS) (Ref. 1). The break was simulated by a side-oriented break nozzle (L/D=13.6) which was located on the Loop 1 cold leg, 0.332 m downstream of the outlet flange of the Loop 1 pump. Additional break geometry information is given in Reference 1. A quick acting valve with an 1 second opening time was used for initiating the transient. The following major phenomena were observed during this test:

• Single- and two-phase flow through a break nozzle,

• Reactor coolant pump operation during two-phase flow,

• Primary and secondary depressurization,

• Natural circulation and reflux cooling,

• Loop seal clearing,

• Core boiloff,

• Accumulator injection, and

• Low Pressure Injection System (LPIS) injection operation.

This transient results in a large core uncovery and fuel heat-up, requiring the implementation of an "Ultimate Procedure" which should be applied as soon as the unavailablity of HPIS is known (Ref. 1). The test simulated a reactor scram in combination with a lengthy reactor coolant pump coastdown followed by a simulated operator action to depressurize the steam generator secondary sides once core thermocouples detected significant heat-up. Specifically, the three steam generator steam dumps to atmosphere were fully opened when the maximum core heater rod cladding temperature reached 723 ^{o}K. Depressurization of the steam generator secondary sides allows the primary coolant system to depressurize to the point of accumulator injection followed by low pressure injection system (LPIS) actuation. The test was terminated when the primary coolant system reached a safe state for the actuation of the residual heat removal system (RHRS).

BETHSY Test 6.2TC simulated a 5.0% (15.24 cm or 6 inch) cold leg break without available HPIS (Ref. 2). The break was simulated by a side-oriented break nozzle (L/D=10) which was located on the Loop 1 cold leg just downstream of the outlet for the Loop 1 pump. The accumulator on Loop 1 is isolated during this test. The following major phenomena were observed during Test 6.2TC:

• Single- and two-phase flow through a break nozzle,

• Primary and secondary depressurization,

• Natural circulation and reflux cooling,

• Loop seal clearing,

• Core boiloff, and

• Accumulator injection.

The pumps rotors were locked once they were tripped during the transient (i.e., there was no pump coastdown time). Accumulator injection began and was terminated prior to the injection of

nitrogen into the primary coolant system. No steam generator auxiliary feedwater was used during the test and the steam generator U-tubes remained covered throughout the transient. The transient continued and was terminated when unmitigated core heat-up began.

This report represents the culmination of several previous assessments against interim TRACE code versions (Refs 3, 4). The TRACE inputs for Test 9.1b and Test 6.2TC used for the current assessment were essentially the same ones documented in Reference 4, with very minor modication to add some diagnostic signal variables for extracting the integrated accumulator flows.

C.8.2. Test Facility Description

BETHSY is a scaled model of a three loop 2775 MWt, 900 MWe CP1 FRAMATOME pressurized water reactor (PWR) with 17 x 17 fuel bundles. BETHSY was specifically designed to study PWR accident transients, and to contribute to verification of the CATHARE code and Emergency Operating Procedures (EOP) (Refs. 5, 6). The overall scaling factor, 1/100, is the result of a compromise between costs and the need for an adequate representation of a commercial reactor. Elevations are 1/1 in order to preserve the gravitational heads.

The facility is designed to operate over the full range of primary system (0.1 MPa to 17.2 MPa) and secondary system (0.1 to 8 MPa) pressures and corresponding fluid temperatures. The core power is limited to 10% of the nominal scaled value, i.e. 3 MW for the 428 full length indirectly-heated 17 x 17 geometry heater rods which make up the core. Electrically heated rods in the core can reach 1273 ^{o}K, and the facility structures (vessel and piping) are designed to withstand high temperatures (873 ^{o}K below 10 MPa). This allows for the study of recovery procedures in severely impaired cooling conditions.

The BETHSY primary system has three identical loops, each one is equipped with a main coolant pump capable of delivering up to the nominal flow rate, and an active steam generator. Each of the three steam generators is equipped with 34 U-tubes of the same radial dimensions and height stepping as the reference steam generator. The U-tubes are also arranged to preserve the secondary side hydraulic diameter and the tube lane is true to scale (Ref. 6).

Every primary and secondary engineered safety system is simulated. This includes high and low pressure injection systems, accumulators (one per loop), pressurizer spray and relief circuits, auxiliary feedwater system, and steam dump to the atmosphere and to the condenser.

Special attention has been focussed on the problem of heat losses, which may cause undesirable distortions especially in the case of steady-state or slow transient tests. The entire primary side as well as steam generators are equipped with trace heaters.

The measurement system includes more than 1200 instruments to provide detailed information on on both primary and secondary side thermal-hydraulic phenomena. For example, about 70 primary fluid temperature measurements are distributed along several U-tubes of Steam

Generator No. 1 (SG 1). Finally, a computerized control system, organized according to the principle of distributed microcomputers, enables tests and associated Emergency Operating Procedures (EOPs) to be conducted in the automatic mode.

C.8.3. TRACE Model Description

The TRACE input model for BETHSY Test 9.1b was developed from a RELAP5 input. The Idaho National Engineering Laboratory developed this RELAP5 input to analyze ISP-27 (Ref. 2). This RELAP5 input model was converted for the NRC into a TRACE input using the SNAP graphical user interface program with appropriate manual corrections. This TRACE input was used to assess TRACE Version 4.036 against the BETHSY Test 9.1b data from ISP-27 (Ref. 3). This TRACE input, herein called the original BETHSY input, was the starting point for this TRACE assessment task.

As part of a previous task, the original BETHSY input was reviewed against the TRACE Version 4.190 user guidelines and checked with TRACE Version 4.190. Two major modifications were determined to be necessary to meet the TRACE user guidelines and to properly run under V4.190. Namely, the pressure vessel model, an assembly of 1-D components, was replaced by a 3-D VESSEL component and the steam generator model was renodalized using TEE components for the downcomer and steam dome segments. Other modifications were made to the signal variables and control blocks to accommodate the new pressure vessel model and the modified steam generator nodalization to obtain the BETHSY Test 9.1.b input. All other parts of the original BETHSY input remain unchanged. The description of the original BETHSY input provided in Sections 3 and 4 of Reference 3 still applies to unchanged sections of the BETHSY input; namely the primary loops, pressurizer, steam line piping, break model, safety injection (accumulators and low pressure safety injection), and control systems. Loop nodalization diagrams from Reference 3 are reproduced in Figure C.8-1 and Figure C.8-2. The reader is referred to Reference 3 for the description for these unchanged sections. These steps resulted in the final BETHSY input which was used for the current assessment.

The input for BETHSY Test 6.2TC was developed from the BETHSY Test 9.1.b input. The input for BETHSY Test 6.2TC has the same nodalization as Test 9.1.b, but the initial conditions, control procedures, and break model were modified to reflect the Test 6.2TC test conditions.

The remainder of this section discusses the 3-D VESSEL component and the modified steam generator model used in the current assessment. Detailed geometric information was obtained from the BETHSY Data Base document (Ref. 7).

C.8.3.1. VESSEL Component

The BETHSY pressure vessel is modeled with a PIPE component (PIPE 400) and a VESSEL component (VESSEL 420) as shown in Figure C.8-3. PIPE 400 provides three side junctions at Cell 4 for the three cold legs. Cells 4 to 13 of PIPE 400 represent the external portion of the downcomer of the pressure vessel and Cells 1 to 3 model the downcomer-to-vessel head bypass.

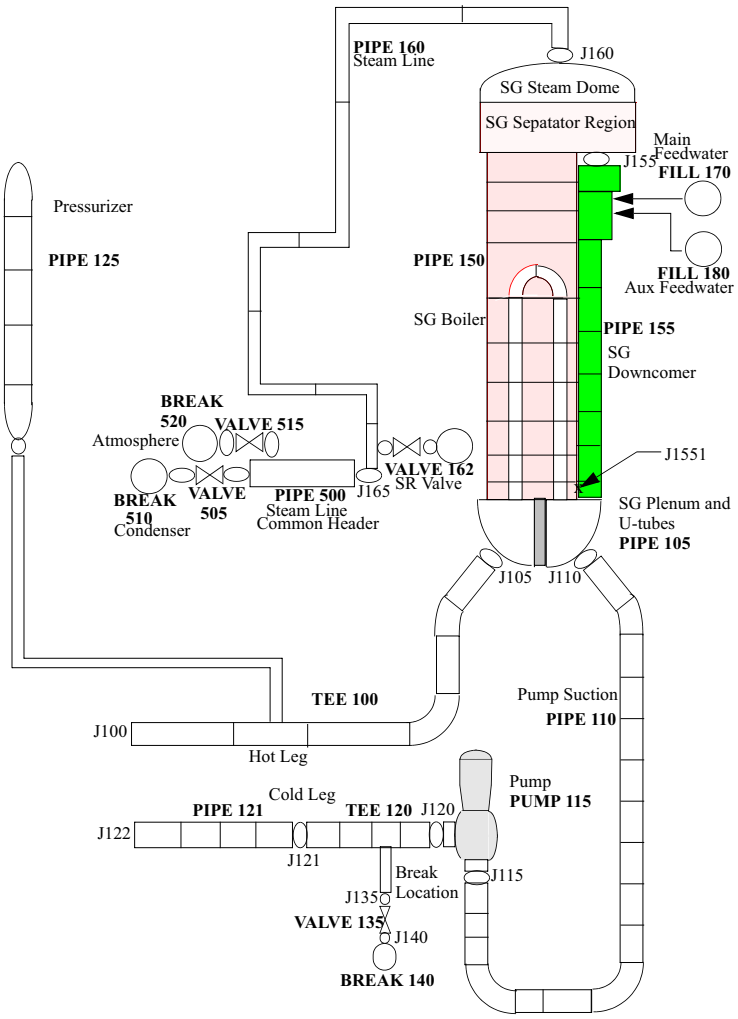

Figure C.8-1. TRACE BETHSY Loop 1 Nodalization

The lower end and top end of PIPE 400 connect to the lower plenum and upper head of the VESSEL component, respectively. The VESSEL heat structure arrangement and power rod nodalization are shown in Figure C.8-4.

VESSEL component 420 models the lower plenum, core, core bypass, upper plenum and upper head sections of the BETHSY pressure vessel. As shown in Figure C.8-3, the VESSEL component consists of 24 levels (L), 5 radial rings (R), and 3 azimuthal sectors. The lower plenum is modeled with four levels (L1-L4); the core section nine levels (L5-L13); the upper plenum eight levels (L14-21); and the upper head three levels (L22-24). Even though the core power is uniform in the radial direction, five rings are used to accommodate the lower plenum, core bypass and upper plenum structure, and radial dimension changes from the bottom to the top of vessel. Three azimuthal sectors are used to match the three hot legs connections to the vessel.

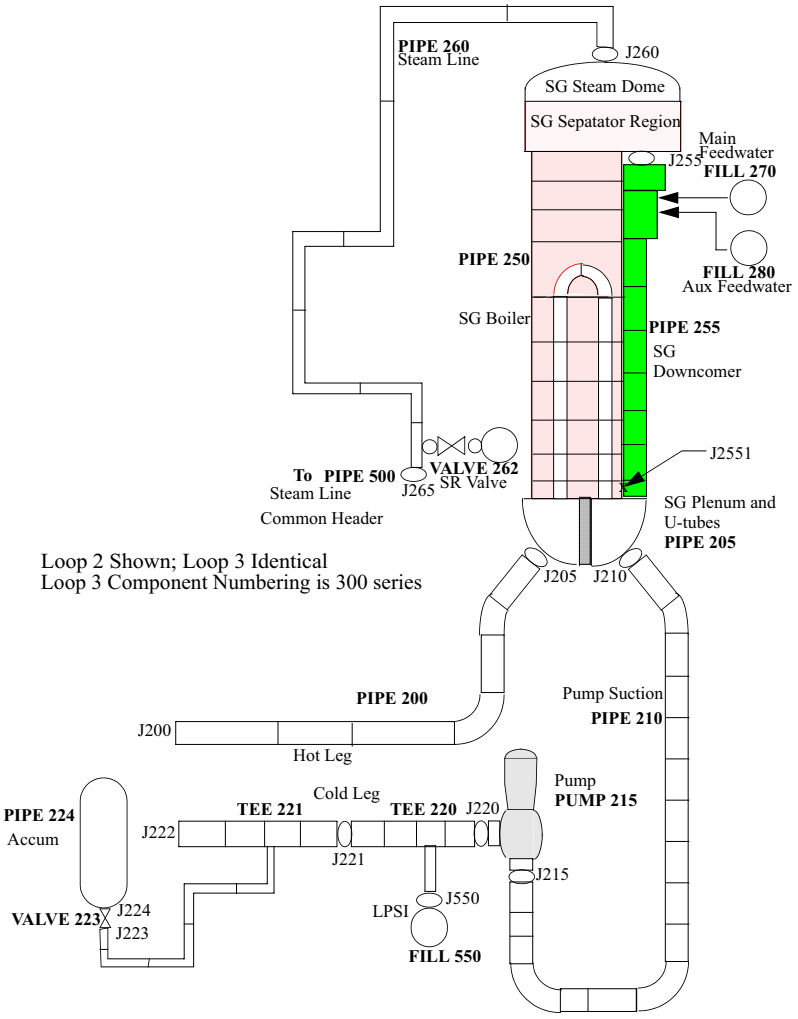

Figure C.8-2. TRACE BETHSY Loop 2/3 Nodalization

The lower plenum is modeled with four levels (L1 - L4).

- Level 1 corresponds to BETHSY pressure vessel volume V1 as shown on the schematic of the BETHSY vessel (Refs. 7, 8),
- Level 2 corresponds to BETHSY pressure vessel volumes V2+V3+V4, and
- BETHSY pressure vessel volume V5 is split into L3 and L4. Ring 4 of L3 and L4 represents the annular downcomer section. The external downcomer pipe is connected to the annular downcomer at level 4 as shown in the nodalization scheme. The cells in Ring 5 of L3 and L4 are null cells (no flow in or out).

The core section comprises of nine levels (L5-L13).

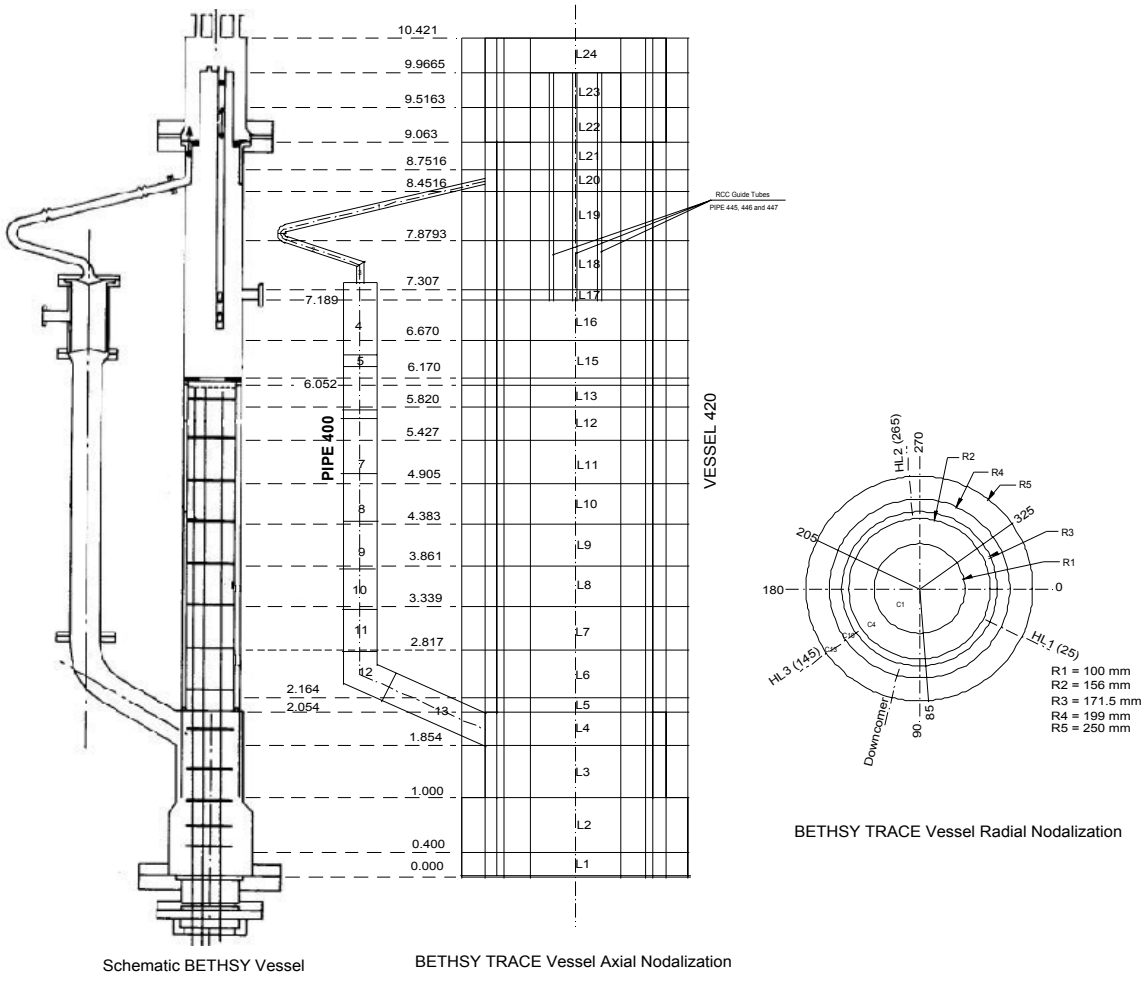

Figure C.8-3. TRACE BETHSY Vessel Nodalization

- Levels from L6 to L12 correspond to the heated section of the heater rods,
- The BETHSY core was provided with 9 spacer grids. Except for the first spacer grid at the core inlet, their locations correspond to related level boundary locations in the VESSEL model,
- R1 and R2 represent the core section. The core power is uniform in radial direction and the core could be represented by one ring. However, a second ring is introduced mainly to accommodate the internal structure at the upper portion of the upper plenum,
- R3 is used to represent the core bypass (volume between the core baffle and the vessel inner wall), and
- Cells in R4 and R5 are null cells (no flow in or out).

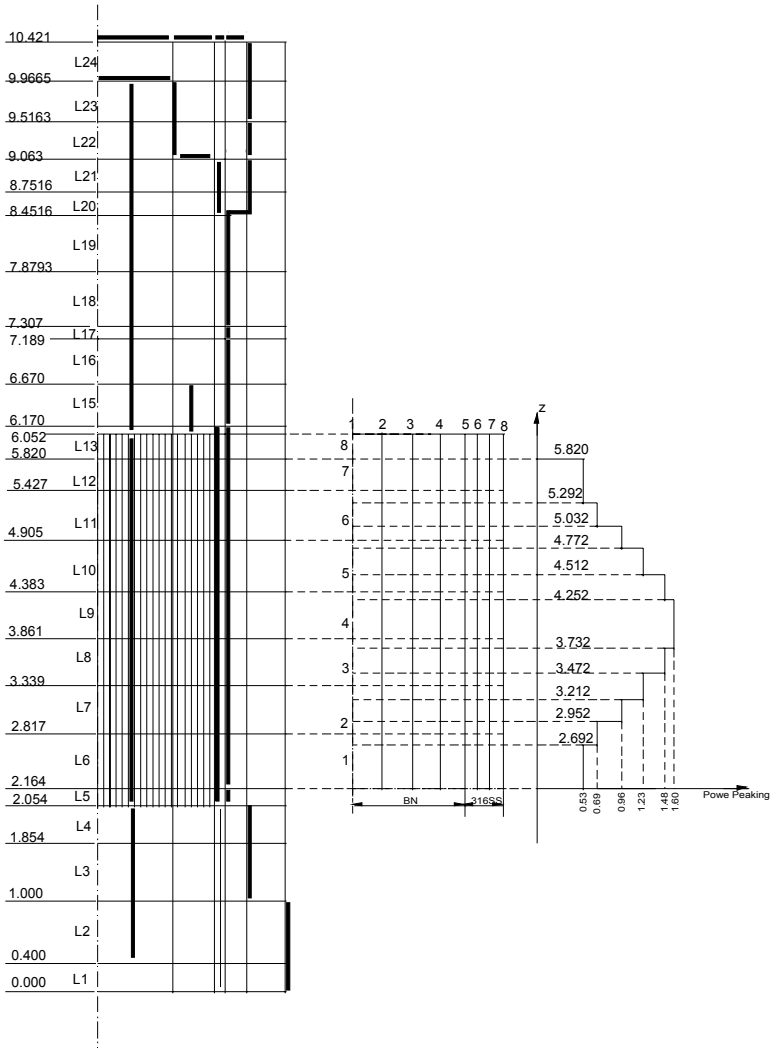

Figure C.8-4. TRACE BETHSY Vessel HTSTR Arrangement and Power Rod Nodalization

The upper plenum comprises of eight levels (L14-L21). The upper plenum provides sources (junctions) connecting the VESSEL to hot legs (three sources), RCC guide tubes and upper head-downcomer leakage path.

- Hot leg connections are located at Level 17 and outer surface of R3, with each connected to one sector,

- The upper boundary of L15 provides three sources, with each in one sector of R1, to connect 3 PIPE components representing the RCC guide tube, and

- The BETHSY pressure vessel annular volume, V5 (connected to the pipe simulating the leakage path from downcomer to the upper head), is represented with Ring 4 at Level 20. Physi-

cally, V5 was inside the vessel wall. However, Ring 3, which relates to the core bypass, cannot accommodate the flow area of V5 in the z direction. In the vessel model, V5 is shifted to Ring 4.

The upper head comprises of three levels (L22, L23, and L24). The lower boundary of Level 24 provides three sources, with each in one sector of R1, to connect 3 PIPE components representing the RCC guide tube.

C.8.3.2. Steam Generators

The steam generator nodalization for the BETHSY TRACE model is shown in Figure C.8-5 along with the physical arrangement of a BETHSY steam generator. It consists of a combination of PIPE and TEE components. The nodalization basis (number of nodes and their respective elevations) can be referenced to the previous RELAP5 and TRACE work. The TRACE components and layouts were selected to avoid use of side and leakage path junctions. This approach uses the existing component cell information in combination with standard modeling practice. To avoid the use of side/leakage junctions, an additional TEE component was added to permit the connection of the Feedwater system with the Main and Auxiliary Feedwater sources in one steam generator downcomer cell.

C.8.4. BETHSY Tests Simulated with TRACE

C.8.4.1. Simulation of BETHSY Test 9.1b

C.8.4.1.1. BETHSY Test 9.1b Steady-State Conditions

The steady-state or initial conditions for BETHSY Test 9.1b were obtained by running a 100 second null transient. The input model was initialized with the steady-state values used from the reference model (Ref. 3). The VESSEL component was initialized with the steady-state values obtained in running as stand-alone model as part of developing this component model. Table C.8.1 lists the initial conditions measured by BETHSY Test 9.1b and calculated by the TRACE code. The table shows good agreement between the TRACE calculated and the measured initial conditions. Figure C.8-6 through Figure C.8-13, which plot key parameters for the 100 second null transient, indicate that steady-state conditions are achieved at the end of the null transient. In addition, the calculated initial conditions agree well with the code predictions documented in Reference 3.

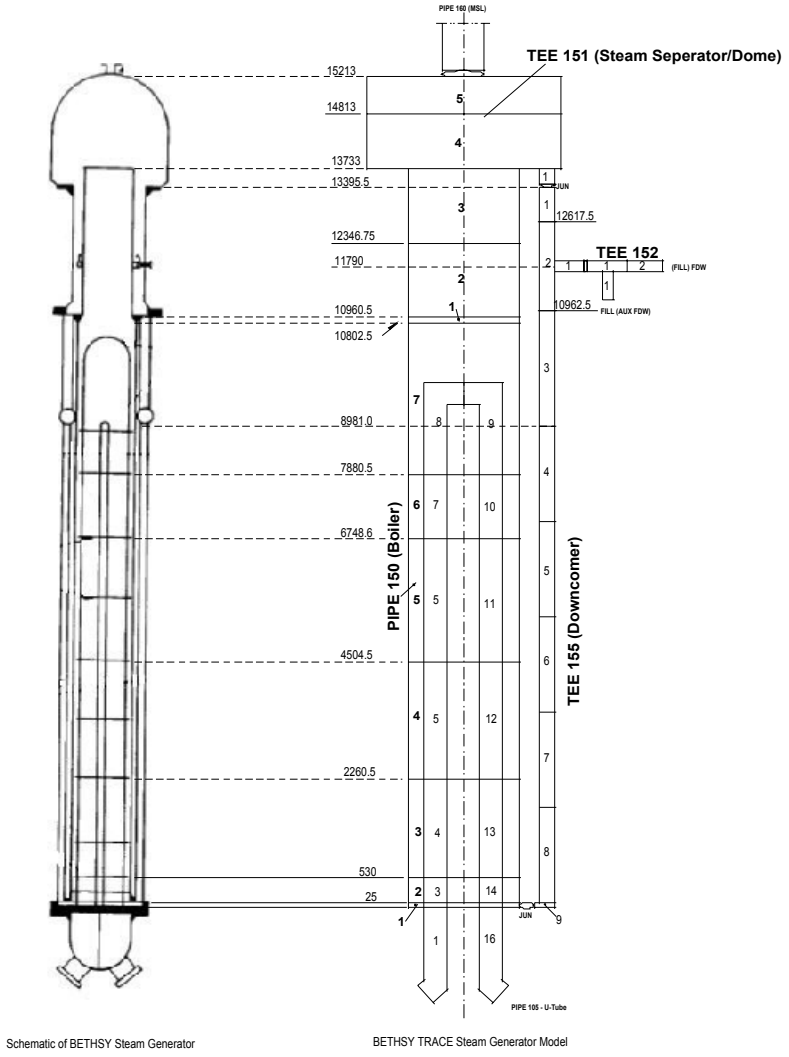

Figure C.8-5. TRACE BETHSY Steam Generator Model

Table C.8.1. BETHSY Test 9.1b Initial Conditions

Parameter	**Measured**[a]	**TRACE**
Core power (kW) - (rpower-999)	2864 +/-30	2864
Pressurizer Pressure (MPa) - (pn-125A05, sv2)	15.51 +/-0.09	15.50
Pressurizer level (m) - (cb505)	4.08 +/-0.1	4.198
Pump 1 rotational speed (rpm) - (omega115)	308 (from test data)	310.97
a - Source: Refs. [3, 8] and BETHSY Test Data b - Volume check performed for the VESSEL component and found to be in good agreement with design data		

Table C.8.1. BETHSY Test 9.1b Initial Conditions

Parameter	Measured[a]	TRACE
Core inlet temperature (K) - (tln-110A01, tln-210A01, tln-310A01)	559.99 +/-0.5	561.3
Core outlet temperature (K) - (tln-100A01, tln-200A01, tln-300A01)	565.4 (from test data) +/-0.5	564.9
Primary coolant inventory (kg)	1960 +/-40	NA[b]
Steam generator pressure (MPa) - (pn-151A04, pn-251A04, pn-351A04)	6.91 +/-0.4	6.90
Steam generator water level (m) - (cb110, cb210, cb310)	13.45 +/-0.05	13.73
Feedwater temperature (K) - (tln-170A01, tln-270A01, tln-370A01)	491.15 +/-2	493.15
Vessel downcomer flowrate (kg/s) - (rmvm-400A14)	150 +/-5	144.2
a - Source: Refs. [3, 8] and BETHSY Test Data b - Volume check performed for the VESSEL component and found to be in good agreement with design data		

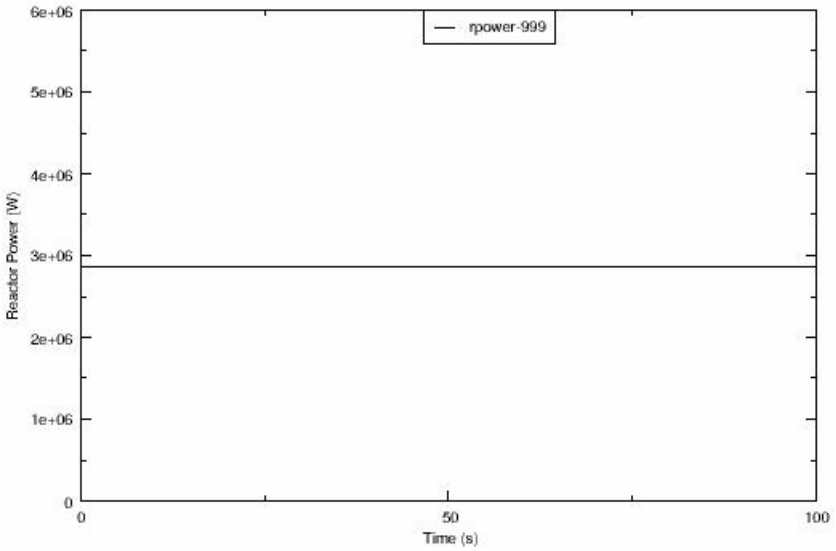

Figure C.8-6. Reactor Power

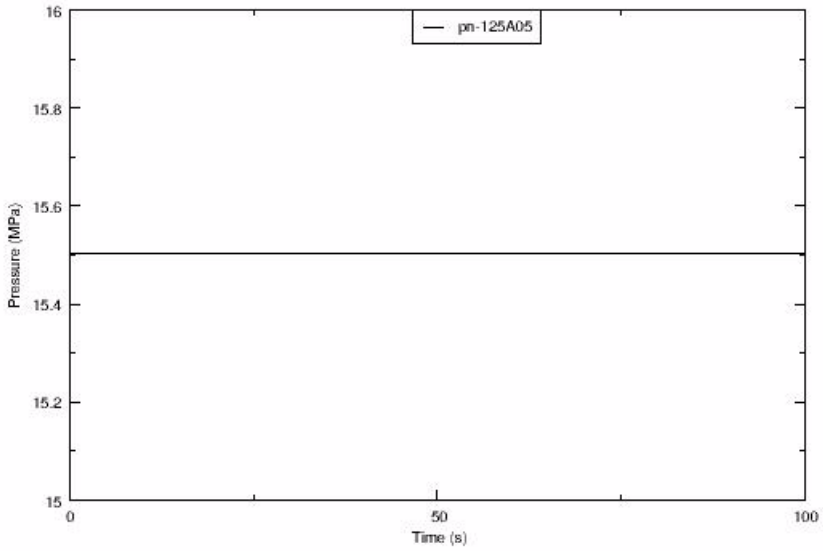

Figure C.8-7. Pressurizer Pressure

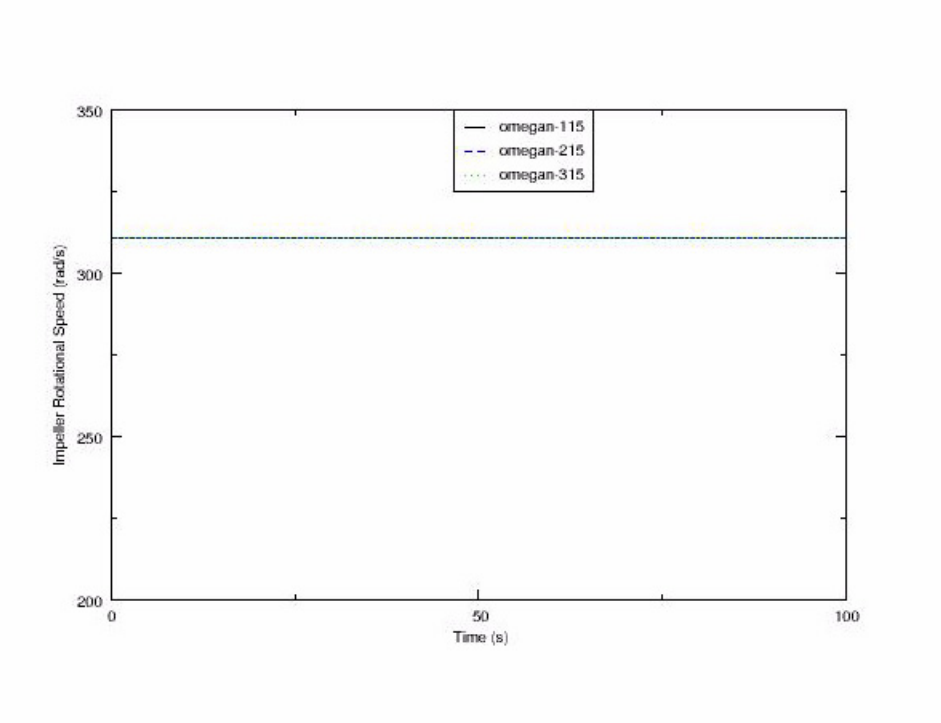

Figure C.8-8. Reactor Coolant Pump Impeller Rotational Speed

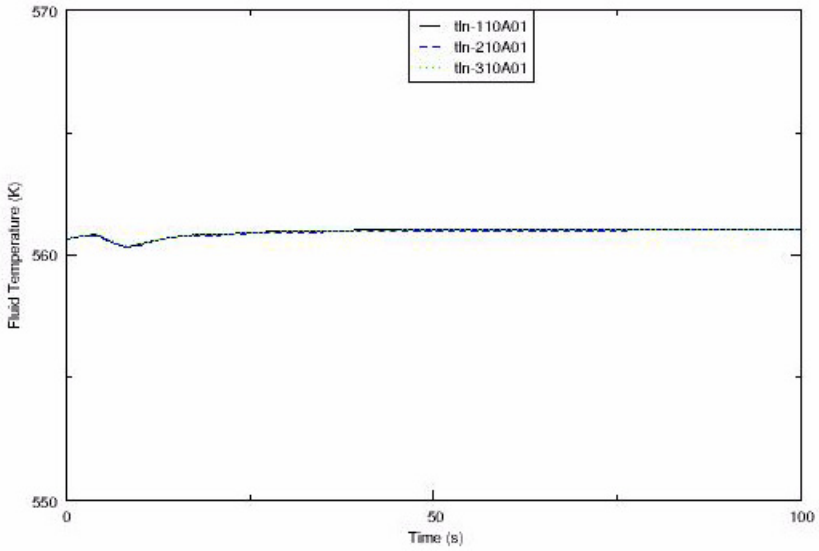

Figure C.8-9. Cold Leg Coolant Temperature

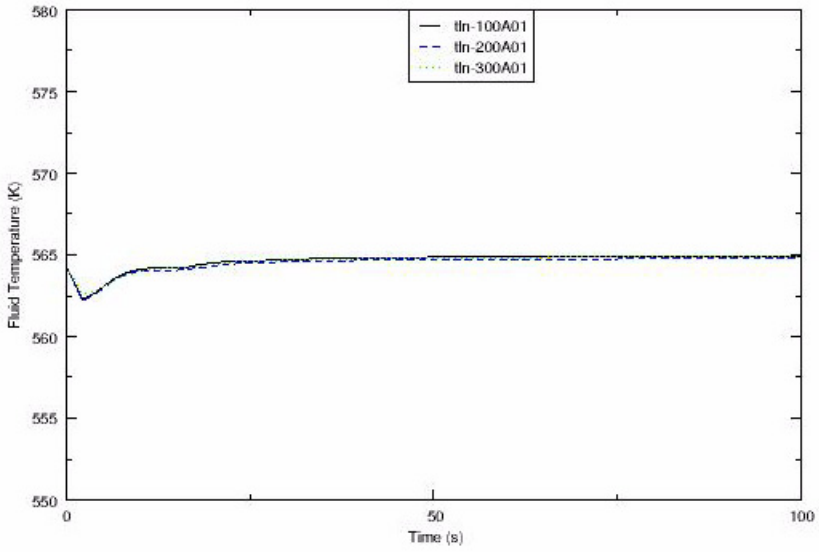

Figure C.8-10. Hot Leg Coolant Temperature

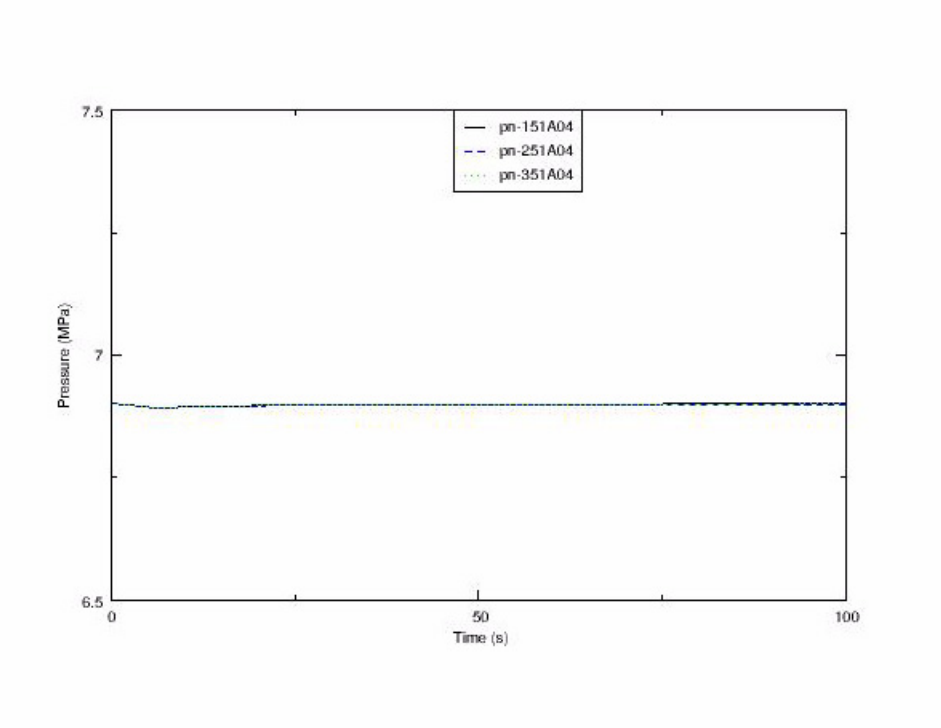

Figure C.8-11. Steam Generator Steam Dome Pressure

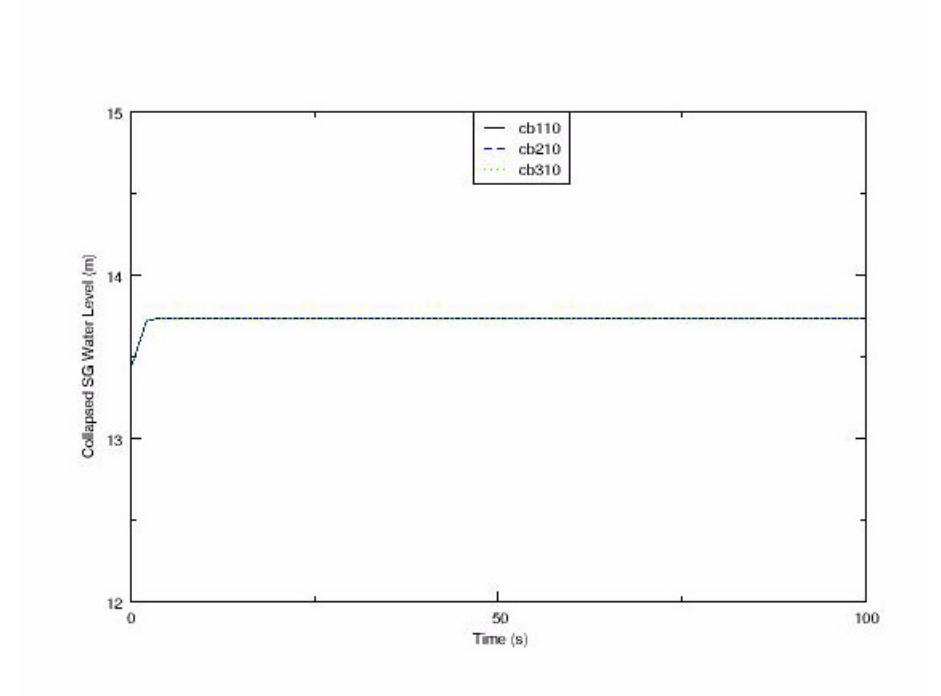

Figure C.8-12. SG Collapsed Water Level

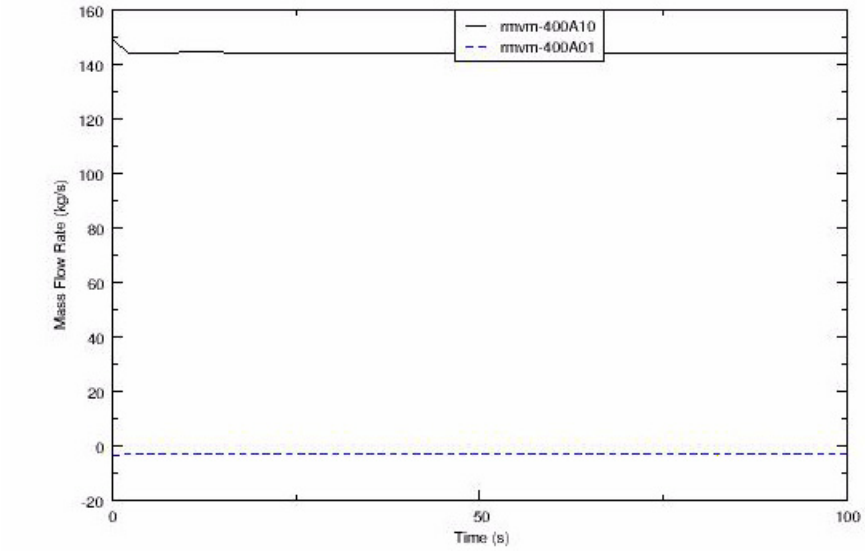

Figure C.8-13. Downcomer Mass Flow and Downcomer-to-Vessel Head Bypass Mass Flow

C.8.4.1.2. BETHSY Test 9.1b Transient Results

The duration of BETHSY Test 9.1b transient is approximately 8200 seconds. For this TRACE assessment, the calculation was terminated at 8300 seconds after start of the transient due to the completion of the most significant events. Table C.8.2 lists major events and their timing observed in the experiment and as predicted by the TRACE code calculation. The experiment results were from the NRC Data Bank File 9.1b.bin, which contains a subset of data from the experiment. This subset of data was used for assessment purposes in ISP-27.

Table C.8.2. BETHSY Test 9.1b Event Chronology

Event	Experiment [a] (seconds)	TRACE (seconds)
Break initiation	0	0
Pressurizer pressure equals 13.1 MPa; Scram signal - (trp440)	41	36.5
Pressurizer is empty - (level cb505)	50	46
Pressurizer pressure = 11.9 MPa; Safety injection signal (SIS) - (trp450, trp451)	54	51
Core power decay starts (17 seconds after scram signal) - (trp440 + 17)	58	53.5
Main feedwater off, turbine bypass - (fxmass-170, fxmass-270, fxmass-370)	59	54.3

Table C.8.2. BETHSY Test 9.1b Event Chronology

Event	Experiment [a] (seconds)	TRACE (seconds)
Auxiliary feedwater on (30 seconds after SIS signal) - (trp450, trp451 + 30)	82	81
Pump coastdown starts (300 seconds after SIS) - (trp450, trp451 + 300)	356	351
End of pump coastdown - (omega115)	917	969
Start of the first core level depletion - (alpn-420A12R03T01)	1830	1585
First loop seal clearing in Loop 2- (alpn-210A11)	1944	1588
Start of second core uncovery - (alpn-420A12R03T01)	2180	1944
Ultimate procedure initiated - (sv725)	2562	2574
Atmospheric steam dump opening (Valve VAGV3; simulates all three steam dump valves opening) - (area-515)	2567	2574
Loop seal reformation in Loop 2- (alpn-210A11)	2750	1599
Pressurizer pressure = 4.16 MPa; Accumulator injection starts - (trp401)	2962	2983
Second loop seal clearing in Loop 2 - (alpn-210A11)	3040	2974
Maximum core clad heatup - (tramax-950)	3053 (996 ^{o}K)	2978 (951 ^{o}K)
Loop seal reformation in Loop 2 - (alpn-210A11)	3680	3296
Pressurizer pressure = 1.5 MPa; Accumulator isolated - (trp401)	3831	3719
Pressurizer pressure = 0.91 MPa; LPIS) - (pn-125A05, sv2, fxmass550)	5177	4675
End of test (TRACE calculation ended)	8200 - 8330	8300

a. Reference 3

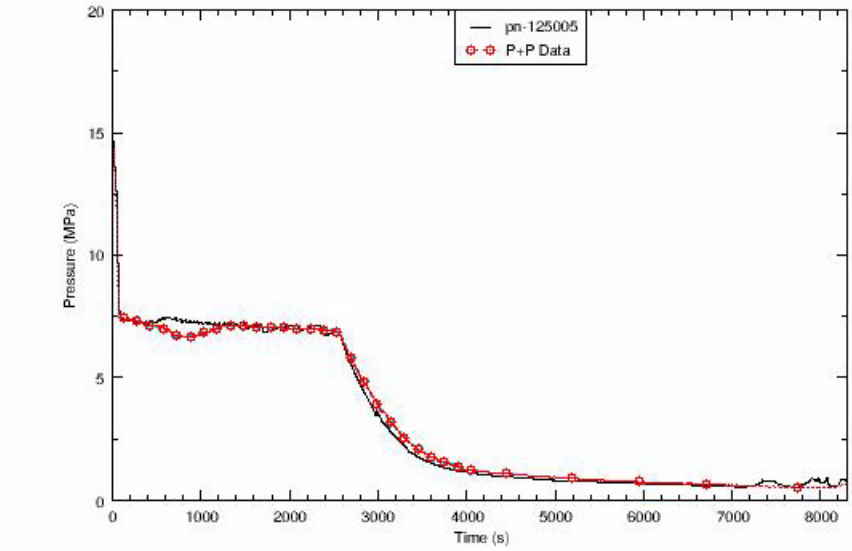

Figure C.8-14. Primary System Pressure

Experimental Observations

Various thermal-hydraulic codes including Anthet, Cathare, Dynamika, Notrump, RELAP5 Mod2, RELAP5 Mod3, RELAP4 Mod6, Tech-M4, and TRAC (Ref. 1) were evaluated using thermal-hydraulic analysis problem ISP-27 which was based on BETHSY Test 9.1b. Participants first performed blind calculations to see how well their codes and modeling practices could capture the test facility response. Post-test calculations were also performed to assess how the blind calculations could be modified to obtain greater agreement with test results. The ISP-27 report will be used as the basis for the discussion of the test results in this section (Ref. 1) because the objective of the ISP-27 report was to compare analysis predictions from thermal-hydraulic codes to the BETHSY Test 9.1b test data.

The BETHSY Test 9.1b transient is initiated by the opening of the quick-acting ball valve on the break piping attached to Cold Leg 1 just downstream of that loop's pump discharge. Primary system depressurization proceeds rapidly until the primary-side pressure approaches the secondary-side pressure. Once the pressurizer empties at about 50 seconds into the transient, the primary system pressure tends to follow the secondary-side pressure but at a value that is slightly higher to accommodate removal of core energy. A small depression in secondary side pressure, with a corresponding reduction in primary side pressure, occurred in the experiment between about 500 and 1250 seconds. This depression appears to be caused by a reduction in recirculation flow rate in the steam generator secondary side with a increased subcooling in the steam generator risers (Ref. 1).

The test data shows the upper plenum begins to drain about 190 seconds and the mixture level reaches the hot leg nozzles at about 400 seconds. The downflow and upflow sides of steam generator U-tubes are empty at 1100 and 1240 seconds respectively, and the pressure vessel level restarts depleting simultaneously with the level drop in the downflow side of loop seals. At 1310 seconds the mixture level in the upper plenum has decreased enough to create an unblocked vapor path to upper head via the guide tube. Vapor then flows to the cold legs via the upper head-to-downcomer bypass. Void fractions as high as 60% appear upstream of the break resulting in a drastic reduction of the break flow rate.

Loop seal clearing occurs at 1944 seconds only in loop 2 when the first core depression stops, even though there is a symmetric level drop in each of the three loop seal's downflow side. After this time the core level recovers with loop seal refilling.

A second pressure vessel level depression (or core uncovery) begins at 2180 seconds as a result of core boil off and continued loss of the primary system coolant through the break. (HPIS was not available in this test.) The Ultimate Procedure (UP) was initiated at 2562 seconds when the maximum heater rod cladding temperature reaches 723 ^{o}K.

The opening of the three steam generator atmospheric dumps results in a rapid blowdown of the secondary side with intense condensation occurring in the steam generator U-tubes. This leads to a reformation of liquid in the loop seals and a fall back of liquid into the core. The primary pressure follows the secondary side rapid depressurization. The accumulator injection begins at 2962 seconds, stops the primary side mass reduction, and results in a second clearing of the loop seal in Loop 2 at approximately 3040 seconds. The pressure vessel level starts to recover at about the same time.

This inflow to the core causes the cladding temperatures to turn around at 3053 seconds. The pressure vessel mixture level reaches the top of the core approximately 300 seconds after the accumulator injection at about 3260 seconds. This mixture level remains roughly constant after accumulator isolation until actuation of the LPIS. At approximately 5177 seconds, the primary system pressure reaches the set point of LPIS injection, 0.91 MPa, which actuates the LPIS and proceeds to fill the loops with subcooled liquid. Stable conditions are achieved by 8200 to 8300 seconds after break opening for the startup of the Residual Heat Removal System and the transition to shutdown conditions.

The ISP-27 report did specifically cite some core heat transfer phenomenon during the second core uncovery prior to and after initiation of Ultimate Procedure (Ref. 1):

"Before the fast depressurization of primary and secondary sides, heater rod temperatures at a given elevation are rather uniform, heat transfer in the uncovered part of the core being especially due to the upflow of vapour."

And

"After the Ultimate Procedure is initiated, the central part of the core receives a rather significant downward flow rate of liquid coming from condensation in the upflow side of steam generator U-

tubes [i.e., reflux flow via the hot legs], and cooling is well improved compared with the outer rows of heater rods which are mainly cooled by vapour."

Past models of BETHSY applied 1-D components for the pressure vessel and could not capture this post-Ultimate Procedure flow pattern. Because a VESSEL component, with the core and upper plenum modeled with two rings and three azimuthal zones, was used in the current assessment, the post-Ultimate Procedure flow pattern will be specifically investigated.

Overall TRACE Simulation Response

As shown in Table C.8.2, the TRACE calculation did capture the times for most of the key transient events. The primary system pressure response as compared to the measured system pressure is shown in Figure C.8-14 where the overall TRACE prediction is consistent with the experiment. The critical parameter for obtaining accurate event times and predicting system response during the TRACE calculation is the break mass flow. The break mass flow affects core water inventory and heat transfer. The heat removal from the core determines the time when the maximum heater rod temperature reaches the setpoint to initiate Ultimate Procedure (i.e., 723 ^{o}K). Ultimate Procedure actions drive the system response, through primary system heat removal by forced blowdown of the steam generators, and also rapidly reaches the setpoints to initiate safety injection flows from the accumulators and LPIS. After Ultimate Procedure initiation, another key parameter driving system response is the rate of steam generator depressurization. This parameter establishes the rate of change in primary system pressure, which affects the timing of safety injection.

Based on these observations, the break mass flow is a significant factor which determines the TRACE code's effectiveness in predicting the proper BETHSY system response (pressure, core heat transfer, timing of Ultimate Procedure initiation), and the rate of steam generator depressurization which affects the timing of accumulator and LPIS injection. The following discussion assesses the appropriateness of these key parameters as calculated by TRACE and describes the component or system parameter responses which affect their behavior.

Break Mass Flow

In the BETHSY Test 9.1b, the break nozzle is located on the cold leg 1, 332 mm downstream of the outlet flange of the reactor coolant pump (Ref. 1). The break is side-oriented, namely the axis of the nozzle is horizontal and perpendicular to the cold leg axis. The break nozzle geometry for BETHSY Test 9.1b is shown in the schematic drawing of Figure C.8-15. The break opening is controlled through a quick acting ball valve with an operating time of 1.0 second. In the TRACE calculation, the same break model used in the reference deck was applied for this TRACE assessment (Ref. 3). The schematic of the TRACE break model is given in Figure C.8-16. Modeling sensitivities were investigated for their ability to match the experimental break mass flow.

The break mass flow rate and integrated break mass flow rate are shown in Figure C.8-17 and Figure C.8-18. Figure C.8-17 demonstrates that the predicted break mass flow has varying degrees of agreement with the data at different time frames during the transient:

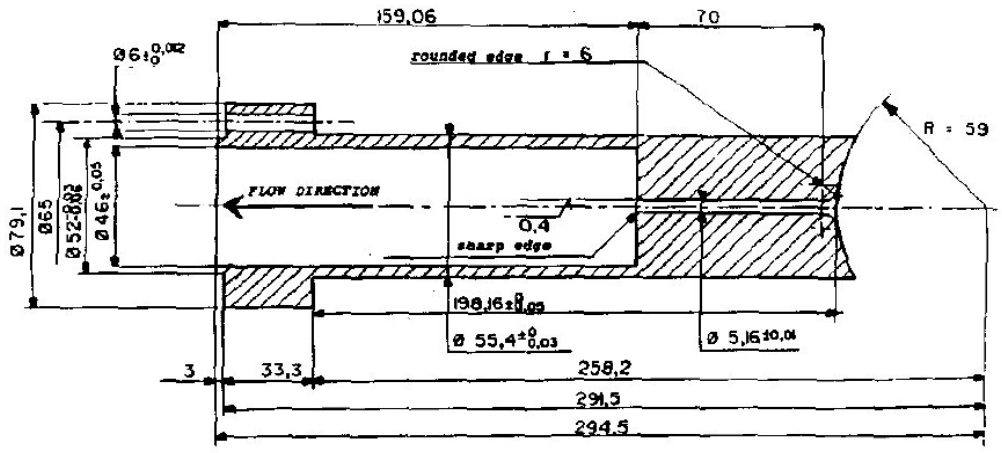

Figure C.8-15. Break Nozzle Geometry for BETHSY Test 9.1b (Ref. 1)

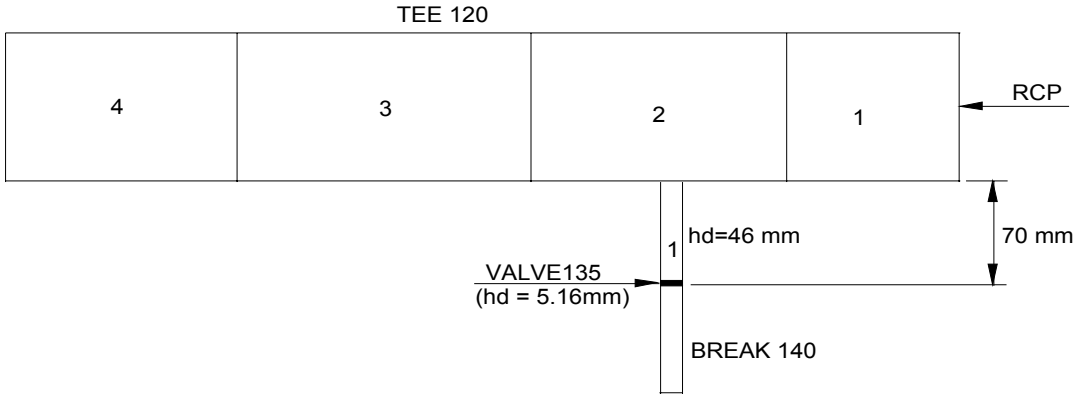

Figure C.8-16. TRACE Break Nozzle Schematic for BETHSY Test 9.1b (Ref. 3)

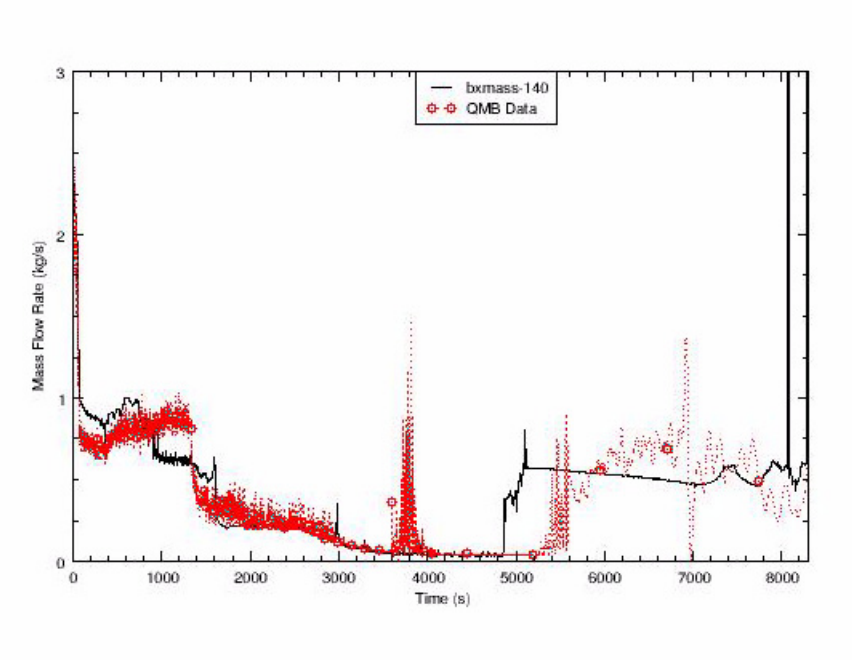

Figure C.8-17. Break Flow Rate

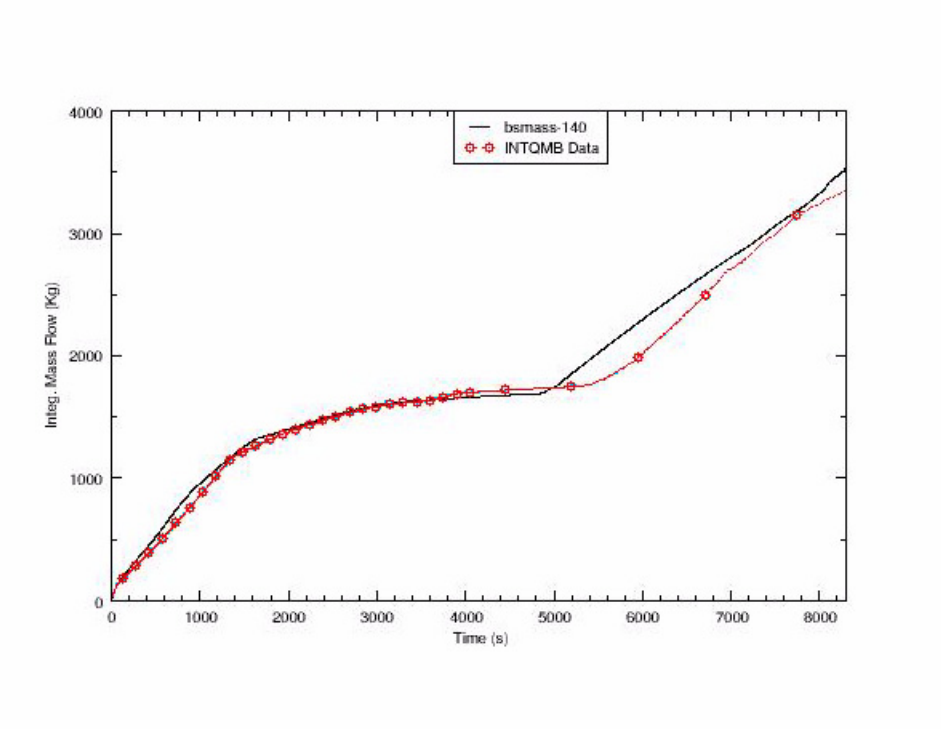

Figure C.8-18. Integrated Break Flow

- 0 - 750 seconds

In this initial transient period, the predicted break mass flow is close to but slightly higher than the data. The break cold leg possesses single-phase flow in the test, and low void fraction two-phase flow in the simulation as shown by Figures C.8-19, C.8-20, and C.8-21 The voiding calculated by TRACE is due to local void flashing.

- 750 - 1375 seconds

For this time frame, the calculated break mass flow is lower than the measured data. As shown in Figures C.8-19, C.8-20, and C.8-21, the cold leg for the experiment is still single-phase flow, or low void fraction two-phase flow. In contrast, TRACE calculates the cold leg in transition from single-phase flow to two-phase flow.

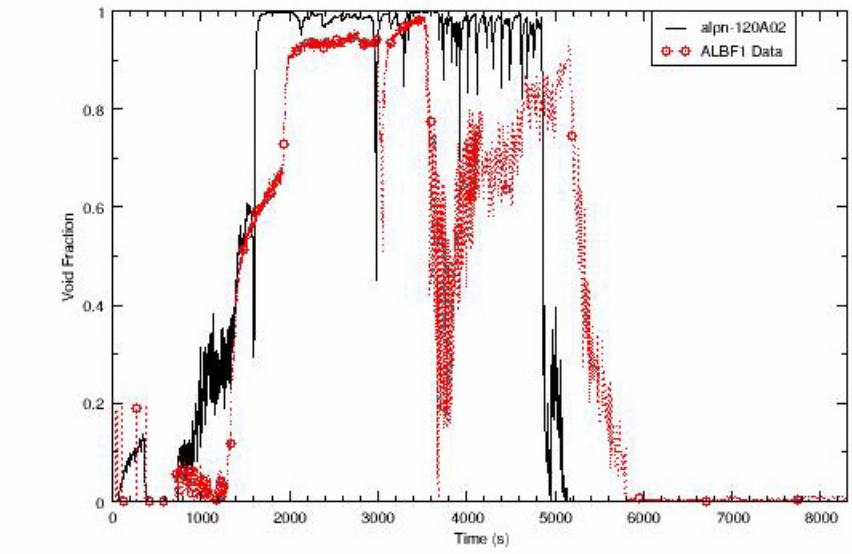

Figure C.8-19. Void Fraction in Loop 1 Cold Leg

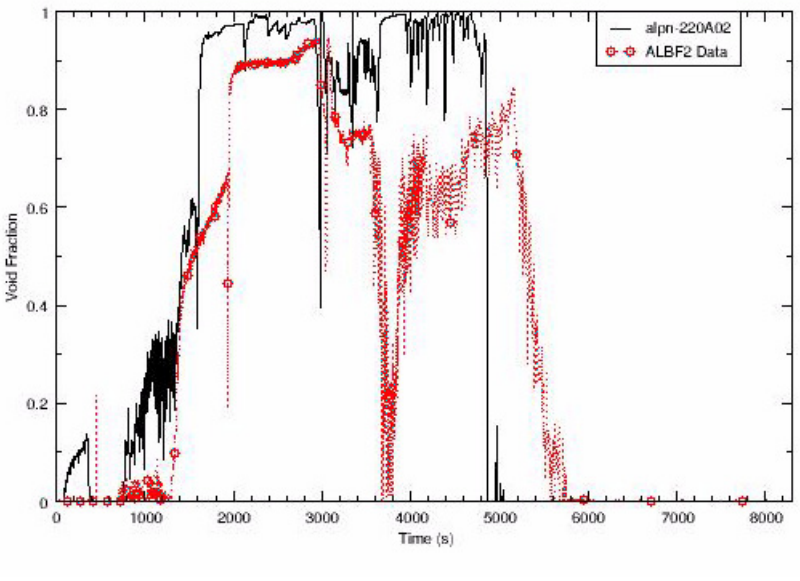

Figure C.8-20. Void Fraction in Loop 2 Cold Leg

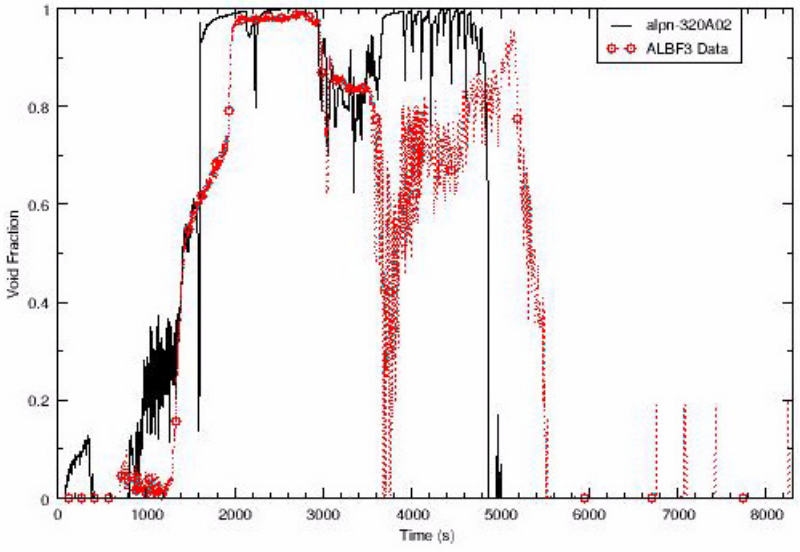

Figure C.8-21. Void Fraction in Loop 3 Cold Leg

- 1375 - 2050 seconds

In this time frame, the calculated break mass flow rate is initially higher than test data and begins to approaches the test data at about 1600 seconds.

At about 1375 second, the data shows a sharp decrease in break flow rate. Afterward, the break flow decreases at a slow rate until approximately 2050 seconds. The differential pressure in the upper plenum (see Figure C.8-22) indicates the mixture level in the upper plenum is approaching the bottom of the control rod guide tubes resulting in the establishment of the flow path from the upper plenum to the cold legs through the vessel upper head. The cold leg starts the transition from single-phase to two-phase flow (see Figures C.8-19, C.8-20, and C.8-21).

In the TRACE simulation, the break mass flow rate is relatively constant from about 1375 second to 1600 second. During this period, the void fraction in the cold leg is also relatively constant. From 1600 to 2050 seconds, the mixture level in the upper plenum is decreasing and approaching the bottom of the control rod guide tubes. The flow path from the upper plenum to the cold leg through the vessel upper head is established. As a result, the void fraction in the cold leg increases rapidly resulting in the calculated decrease in break mass flow.

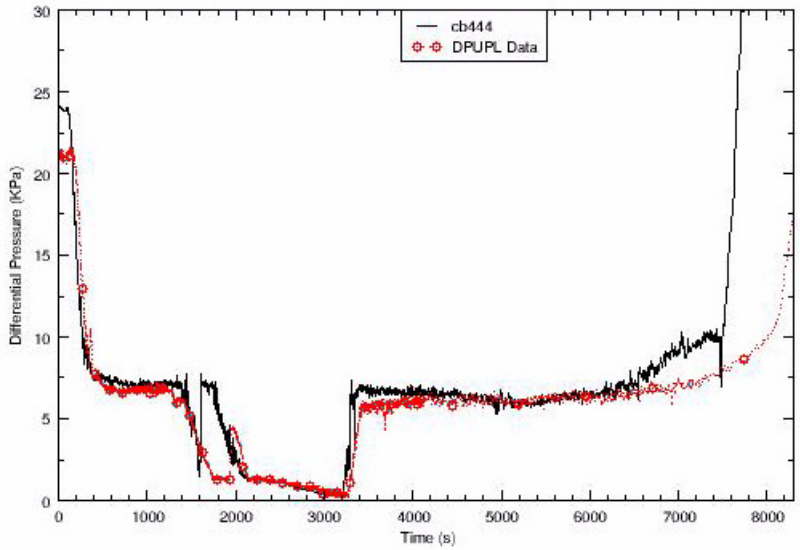

Figure C.8-22. Vessel Upper Plenum Differential Pressure

- 2050 - 3600 seconds

During this time, the predicted break flow is in a good agreement with data. By 3600 seconds, the accumulator injection is almost finished in both the test and simulation. However, the accumulator injection has not affected the fluid regime in the broken cold leg. As show in Figure C.8-19 the cold leg is still single-phase vapor.

- 3600 - 5200 seconds

The TRACE calculation shows a good agreement with the experiment for most of this time frame. Shortly after 3600 seconds until 4100 seconds in the test the void fraction in the broken cold leg drops sharply. The broken leg is filled with water for a brief period as shown in Figure C.8-19. As the result, the break flow rate increases and then drops to a small value when the cold leg becomes two-phase flow again both in the test and the simulation. The TRACE calculation does not show the large void fraction drop and temporary break mass flow rate increase exhibited in the test data after 3600 seconds.

- 5150 second - 8000 seconds

This time frame corresponds with the LPIS injection period. The LPIS injection starts at 5177 seconds in the test and 4676 seconds (cb455) in the calculation. Shortly after the LPIS starts, the broken cold leg starts the transition from the two-phase to single-phase flow, and the break flow starts to increase both in the test and the calculation. The calculation predicts an earlier increase in break flow rate than the data, but TRACE results show a good prediction for break flow rate during the LPIS phase after the break flowrate increase.

Primary System Pressure

The calculated primary system pressure provides reasonable agreement with the test data up to the initiation of the Ultimate Procedure at approximately 2560 second (see Figure C.8-14). As in the experiment, the primary system pressure is slightly higher than the secondary side pressure once the pressurizer completely empties. However, TRACE did not capture the slight drop in system pressure from 480 to 1300 seconds. In the TRACE calculation, the Ultimate Procedure is initiated at 2574 seconds once the maximum heater rod cladding temperature reaches 723 ^{O}K. The calculation of the Ultimate Procedure initiation time is close to the experiment value.

Upon the Ultimate Procedure initiation, the primary pressure follows the secondary pressure of the steam generators and depressurizes rapidly as shown in Figure C.8-14 and Figure C.8-23. As indicated in Figures C.8-24, C.8-25, and C.8-26, steam is calculated to be removed from the steam generators at a rate close to the experimental measurement, resulting in good agreement between the calculated and measured pressure curves in Figure C.8-14.

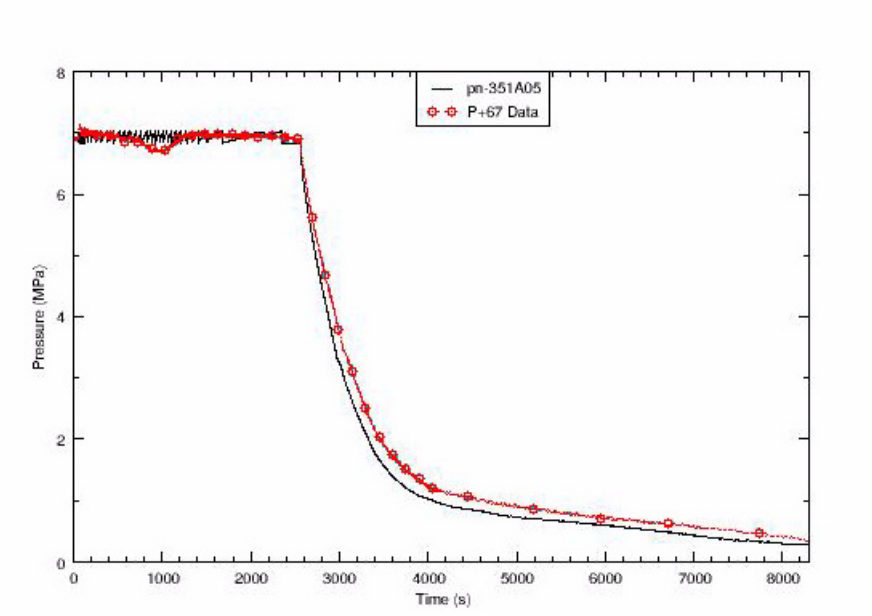

Figure C.8-23. SG3 Secondary Side Pressure

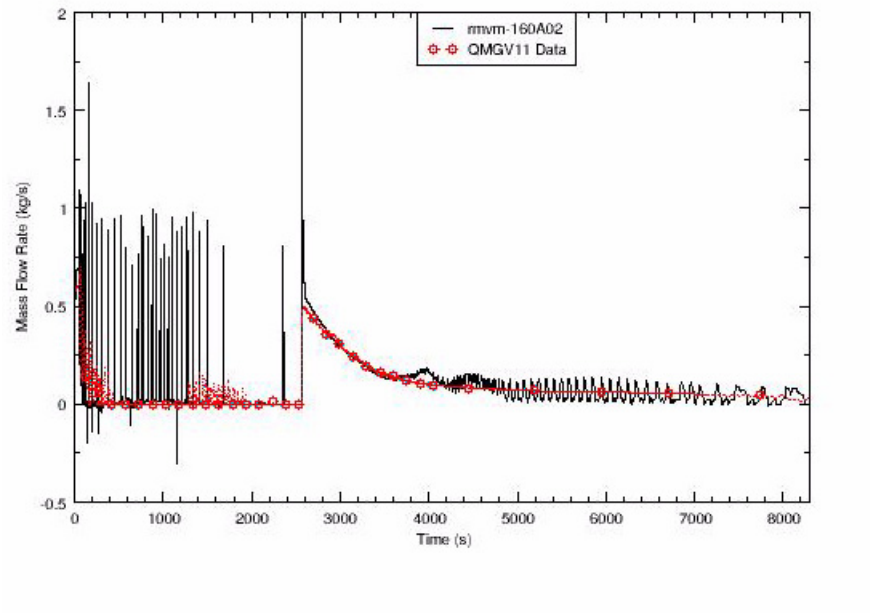

Figure C.8-24. Steam Dump Flow Rate from SG1

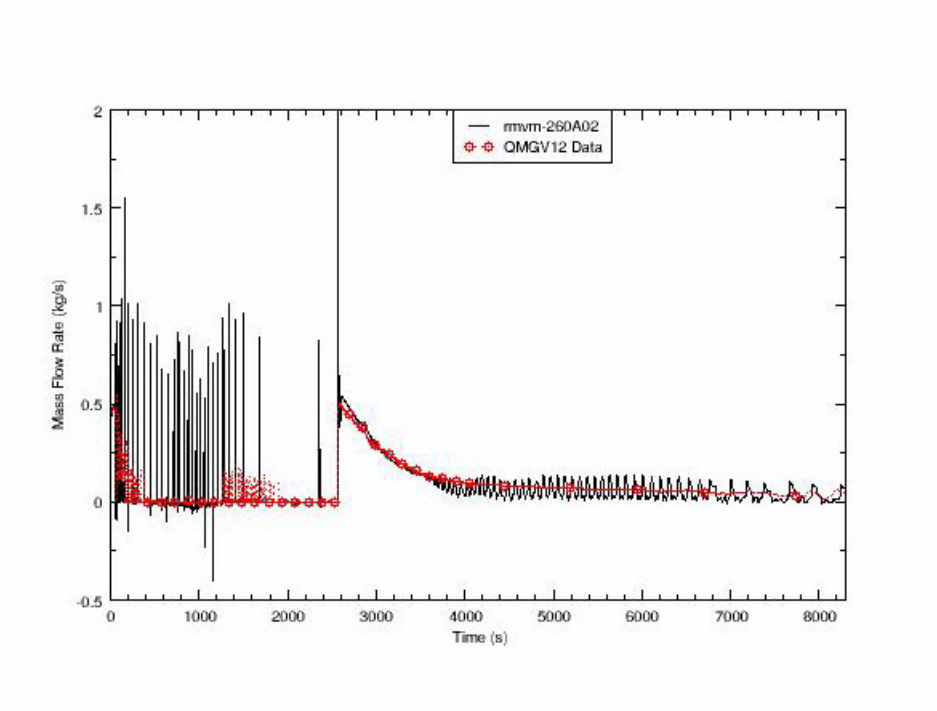

Figure C.8-25. Steam Dump Flow Rate from SG2

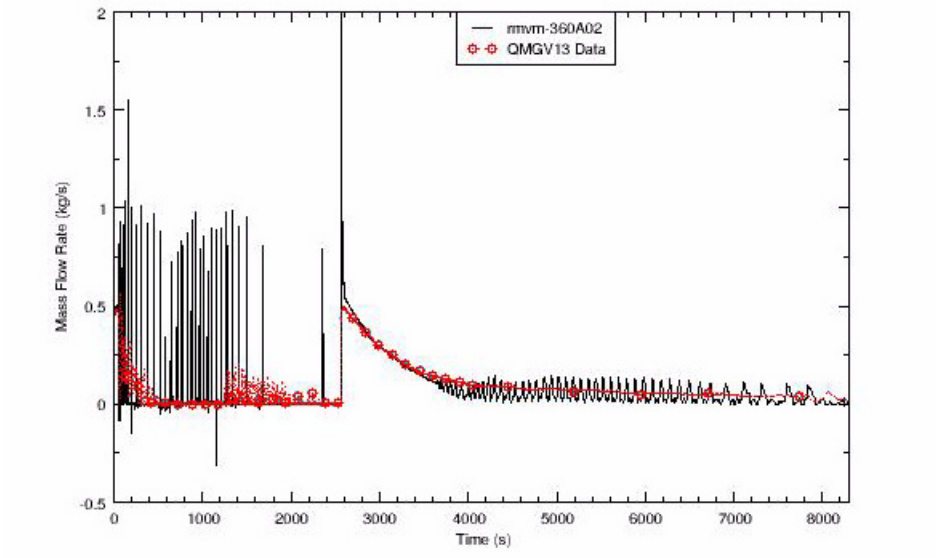

Figure C.8-26. Steam Dump Flow Rate from SG3

Core Liquid Level Depression and Core Heatup

The core level depression is represented by the core differential pressure response shown in Figure C.8-27. In the test, the core level depression occurred twice and the core level recovered respectively at about 1940 seconds and 3020 seconds, concurring with the first and second loop seal reformation. The TRACE calculation also predicts that the core level depression occurs twice with about the same minimum collapsed liquid levels as in the test. In the calculation, the core level recovers respectively at about 1588 seconds and 2974 seconds, corresponding with the times of the first and second loop sealing clearings (Figure C.8-29 through Figure C.8-34). Both in the test and the calculation, there is an instantaneous core level recovery at the moment the loop seal clearing occurs.

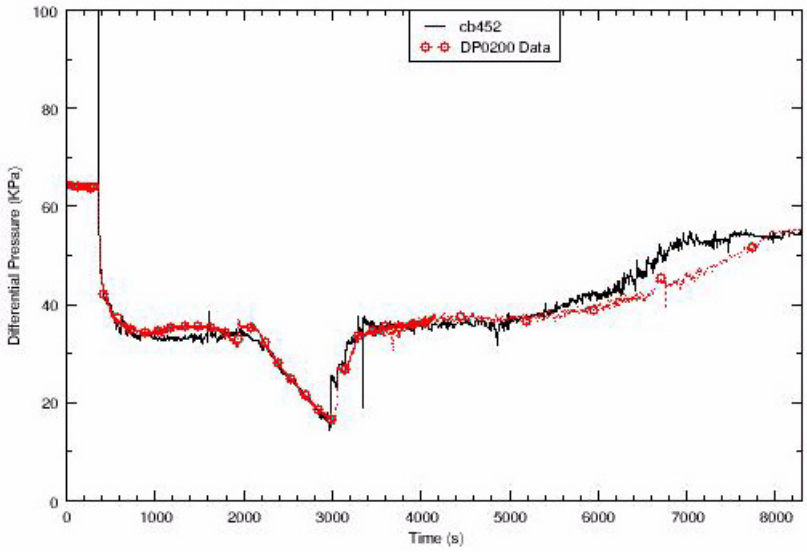

Figure C.8-27. Core Differential Pressure

Figure C.8-28 displays the maximum heater rod cladding temperature for the TRACE calculation (i.e., the heater rod that initiates Ultimate Procedure), and three heater rod cladding temperatures from the test. Two of three measured temperatures are from inner core locations and the third is a heater rod cladding temperature at the core periphery. The TRACE temperature response shown in Figure C.8-28 is similar to the experimental response. Prior to the rise in cladding temperature, the distribution across the core is fairly uniform and there is good agreement between the TRACE calculation and measurements. Once heatup occurs, the TRACE calculation predicts a similar response as for the inner core heater rods of the experiment. For both the experiment and TRACE calculation the heat up turns around quickly. Also, the duration of the temperature excursion are approximately the same for the experiment and the TRACE calculation. The only significant

difference between the TRACE calculation and the experiment is the observation that the TRACE calculation did not capture the larger temperature excursion by the heater rod(s) at the core periphery. For this TRACE model, the six powered HTSTRs represent the average heater rods in each VESSEL cell. The BETHSY facility has 426 heater rods in the core, but only a small number of the heater rods temperature measurements are provided in the NRC Data Bank.

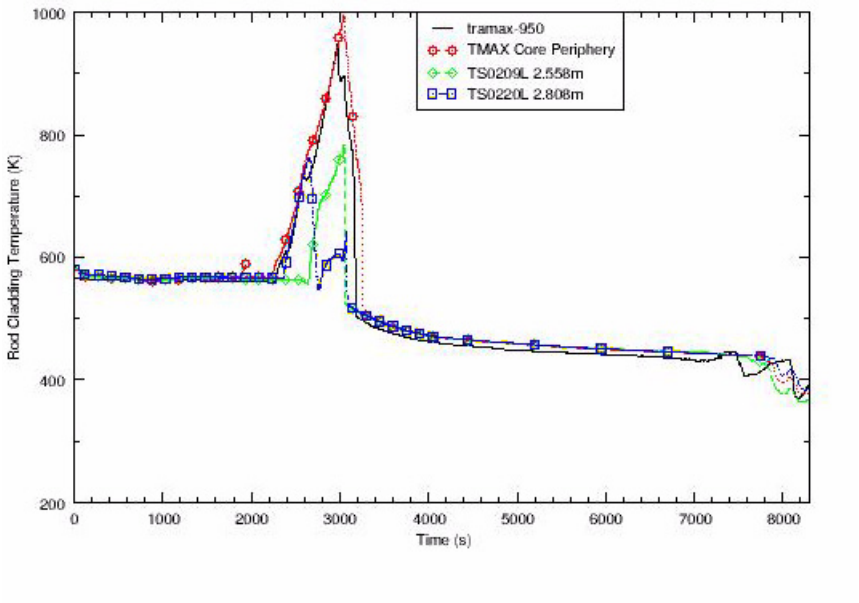

Figure C.8-28. Fuel Rod Cladding Temperature

Loop Seal Clearing

Figures C.8-29 through C.8-34 provide the predicted and measured differential pressures of the upflow and downflow sides of the loop seals for each of the three loops. The predicted loop seal clearing behavior is similar to that shown in References 1 and 3. In general, the TRACE code does not predict the loop seal clearing in the same manner as seen in the test data. The previous code calculations also either did not predict loop seal clearing or predicted delayed clearings. For the code calculations this behavior was attributed to the early onset of two-phase discharge at the break. Interestingly, the predicted loop 2 seal clearing is in good agreement with the loop 3 seal clearing in the test, while the predicted loop 3 seal clearing is in better agreement with the loop 2 seal clearing in the test. The predicted downflow side differential pressure of Loop 1 is in good agreement with the test data.

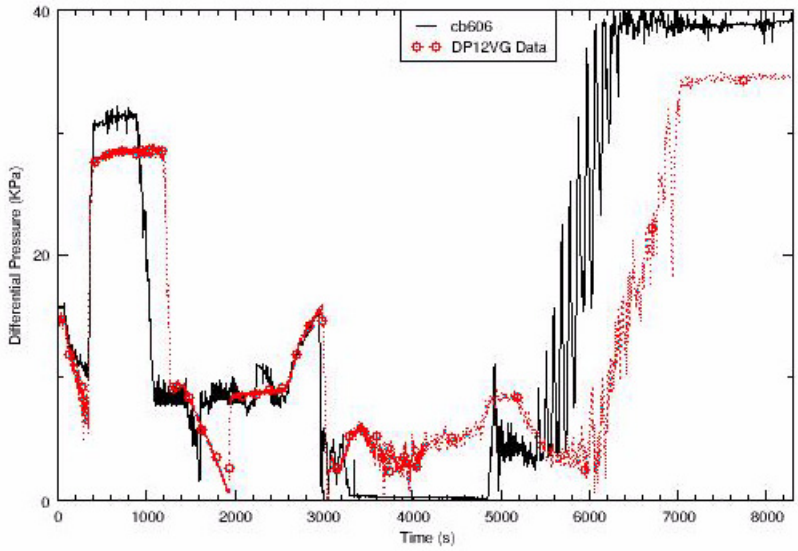

Figure C.8-29. Loop 1 Seal Downflow Side Differential Pressure

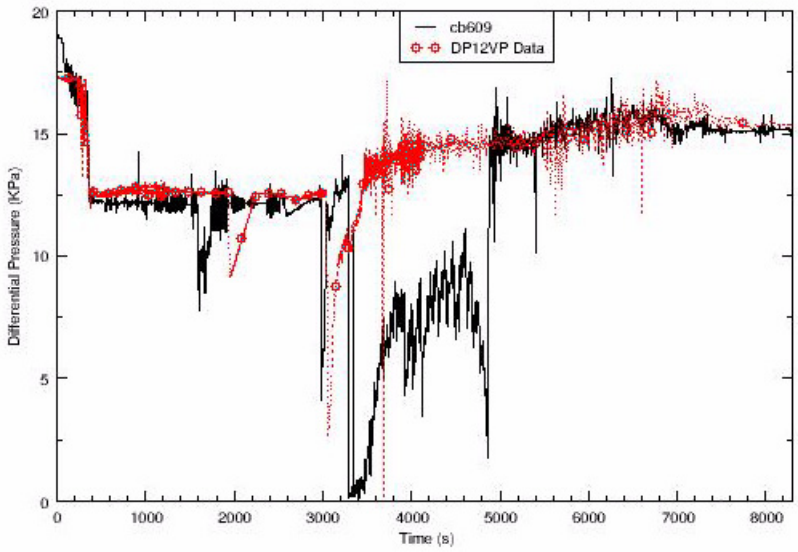

Figure C.8-30. Loop 1 Seal Upflow Side Differential Pressure

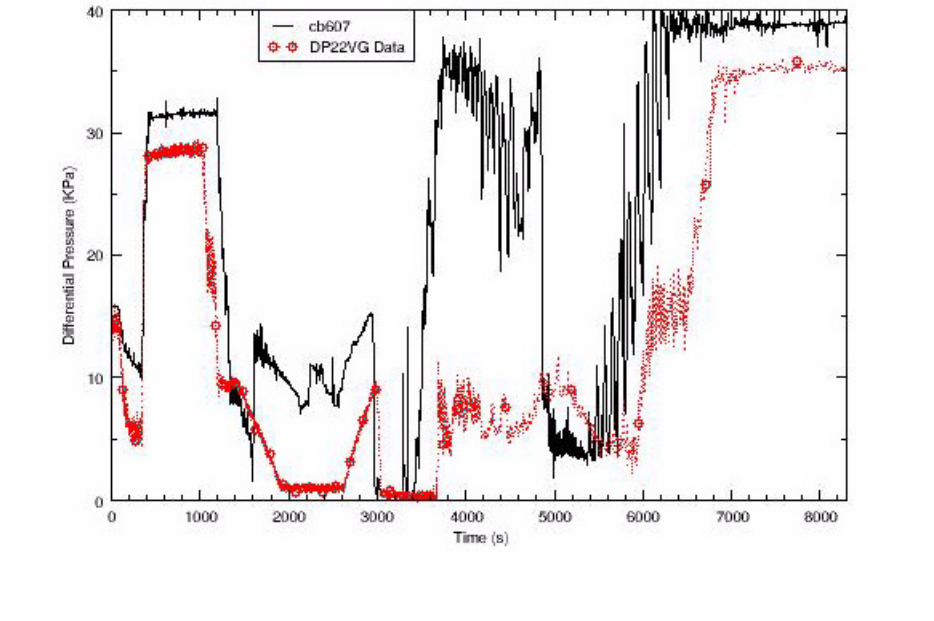

Figure C.8-31. Loop 2 Downflow Side Differential Pressure

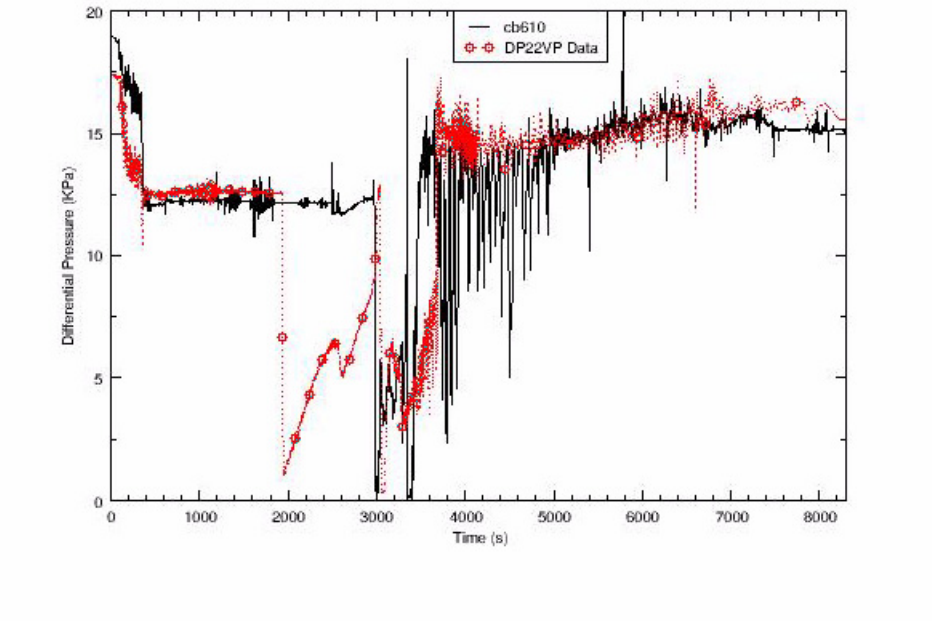

Figure C.8-32. Loop 2 Seal Upflow Side Differential Pressure

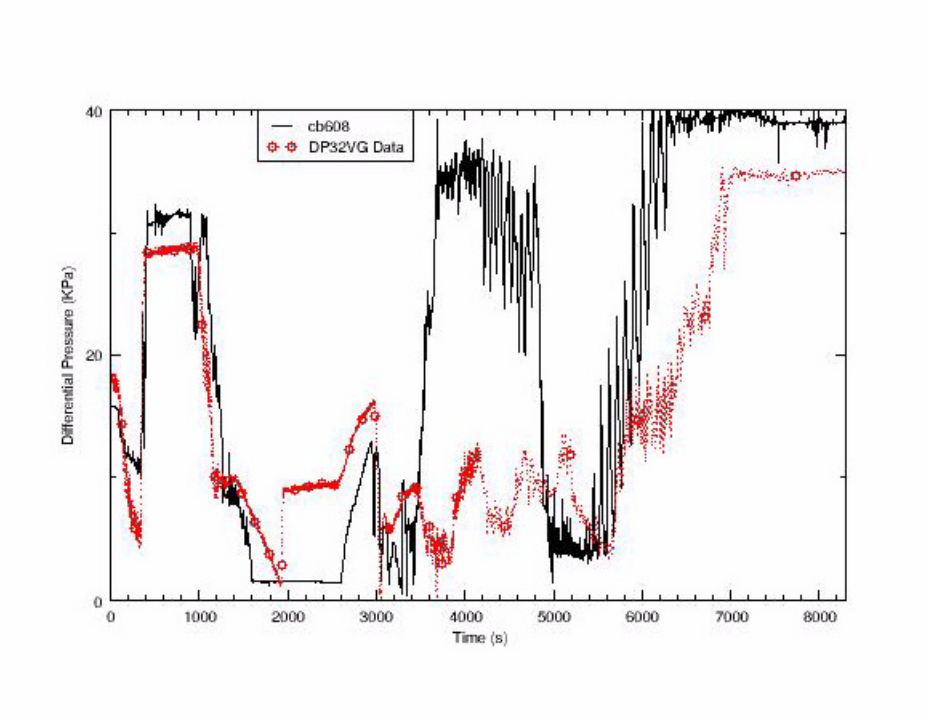

Figure C.8-33. Loop 3 Seal Downflow Side Differential Pressure

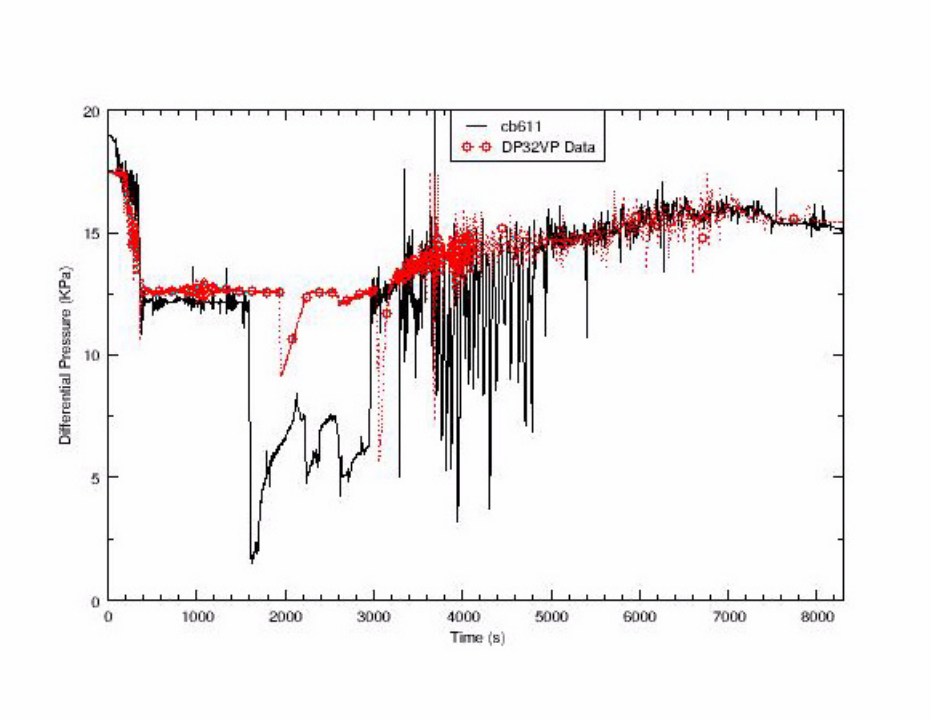

Figure C.8-34. Loop 3 Upflow Side Differential Pressure

ECC Injection

For BETHSY Test 9.1b, the HPIS is not available, and only two out of three accumulators and LPIS pumps are available. An accumulator tank is attached to the cold legs of the two intact loops, Loop 2 and Loop 3. The accumulator injection begins when the primary loop pressure drops to 4.2 MPa and is isolated when the primary loop pressure reaches 1.5 MPa. As for the accumulators, LPIS injection is only provided through the cold legs of Loop 2 and Loop 3. LPIS injection is initiated when the primary system pressure reaches 0.91 MPa. The TRACE calculation gives a good prediction of accumulator injection and LPIS injection as shown in Figure C.8-35 and Figure C.8-36.

Figure C.8-35 shows the accumulator tank inventory predicted by TRACE and measured during the test. Compared to the test, the calculated accumulator injection is slightly delayed corresponding to the slight delay in initiation of the Ultimate Procedure as discussed earlier. The calculated accumulator injection also is terminated slightly earlier due to the slightly overpredicted pressure toward the end of the accumulator injection phase.

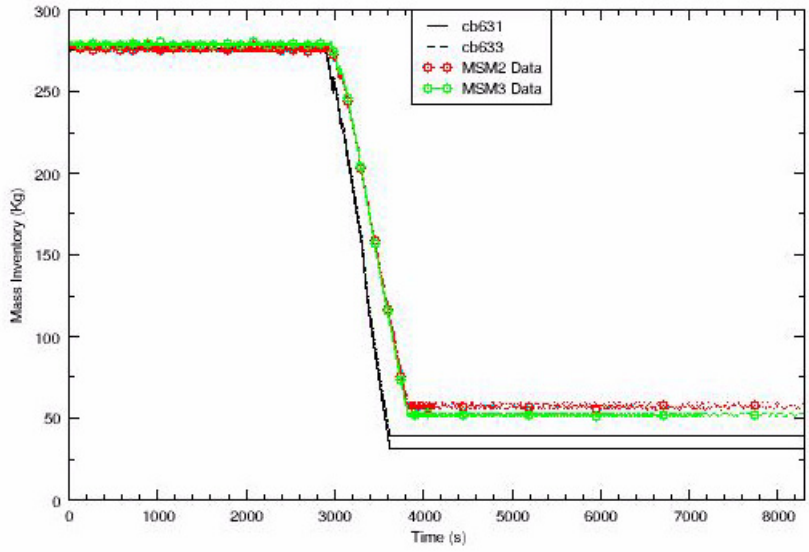

Figure C.8-35. Accumulator Inventory

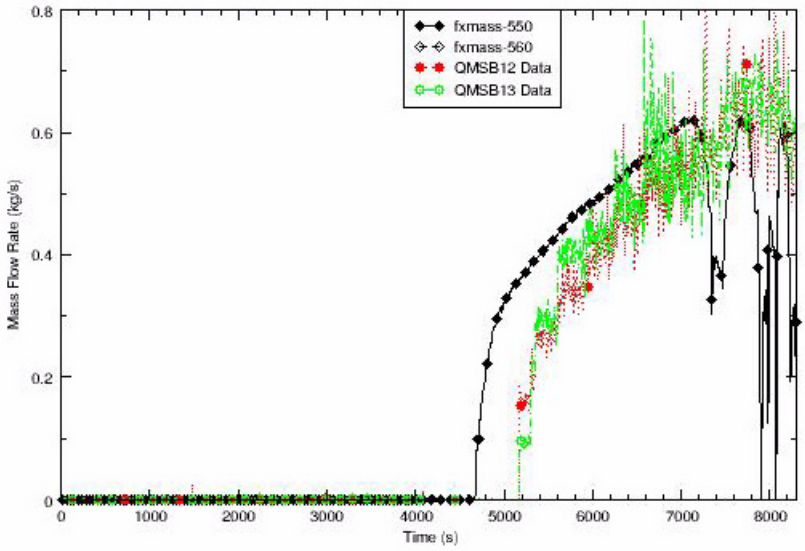

Figure C.8-36. LPSI Injection Flow

Figure C.8-36 plots the LPIS injection flow rates into Loop 2 and Loop 3. As mentioned early, the LPSI injection starts earlier than in the test. After the start of the measured injection flow, the TRACE calculation predicts an injection flow slightly higher than the test data.

Summary

In general, TRACE code performs relatively well in predicting the BETHSY Test 9.1b conditions and the calculation results have as good or better agreement than the result reported in prior analyses. During the early portion of the execution, TRACE employed time steps of about 0.05 seconds. After approximately 3000 seconds into the transient, TRACE required slightly smaller time-step sizes of about 0.02 seconds in order to achieve numerical convergence. The total execution time was about 12 hours.

C.8.4.2. Simulation of BETHSY Test 6.2TC

As presented in Reference 9, BETHSY Test 6.2TC was performed on July 5, 1989. This was a companion test to the ROSA-IV SB-CL-21 experiment performed two months later in September 1989. The intent was to compare the behaviors of the two facilities of different scales for an "intermediate" cold leg break transient. One key physical phenomena to be assessed during the LOCA transients in each facility was the core liquid level depression behavior before loop seal clearing.

C.8.4.2.1. BETHSY Test 6.2TC Initial Conditions

The TRACE inputs for BETHSY Test 6.2TC was developed from the BETHSY Test 9.1.b deck used in this report. The BETHSY Test 6.2TC TRACE model has the same nodalization as the BEHTSY Test 9.1.b TRACE model, but the initial conditions, control procedures and break model were modified to reflect the Test 6.2TC conditions. Two TRACE inputs were created. The first input is used to obtain the steady-state results, including the steady-state controllers for the pump impeller speed control. The other input is used to perform the transient calculation using the restart file from the steady-state execution. This second deck turns off the pump speed controllers and implements the pump coastdown curve.

The initial conditions for Test 6.2TC were obtained by running a 400 second null transient of the first input. A summary of the initial conditions from the BETHSY Test 6.2TC and the TRACE code calculated initial conditions are listed in Table C.8.3. As shown in the table, the TRACE calculated initial conditions agree well with the test conditions. Key parameters are plotted in Figure C.8-37 through Figure C.8-44, which indicate that the calculation reach the steady-state at the end of the null transient.

Table C.8.3. BETHSY Test 6.2TC Initial Conditions

Parameter	Measured[a]	TRACE
Core power (kW) - (rpower-999)	2863 +/–30	2863
Pressurizer Pressure (MPa) - (pn-125A05, sv2)	15.38 +/-0.15	15.50
Pressurizer level (m) - (cb505)	7.45 +/-0.2	7.286
Pump 1 rotational speed (rpm) - (omega115)	238 +/-6	219.2[b]
Core inlet temperature (K) - (tln-110A01, tln-210A01, tln-310A01)	557.2 +/-0.4	559.0
Core outlet temperature (K) - (tln-100A01, tln-200A01, tln-300A01)	588.2 +/-0.4	590.9
Primary coolant inventory (kg)	1984 +/-50	NA[c]
Steam generator pressure (MPa) - (pn151A04, pn-251A04, pn-351A04)	6.84 +/-0.07	6.849
Steam generator water level (m) - (cb110, cb210, cb310)	11.1+/-0.05	11.98
Feedwater temperature (K) - (tln-170A01, tln-270A01, tln-370A01)	523.1 +/-4	523.1
Upper head temperature - (tln-420A24R01T01, tln-420A24R01T02, tln420A24R01T03)	577.0	577
Heat loss (kW)	54.82	NA

a - Source: Reference 9 and Reference 10
b - Pump speed set to obtain flows, differential pressures, and temperatures
c - Volume check performed for the VESSEL component and found to be in good agreement with design data

Table C.8.3. BETHSY Test 6.2TC Initial Conditions

Parameter	Measured[a]	TRACE
Total flow (kg/s) - (rmvm-100A01 + rmvm-200A01 + rmvm-300A01)	16.81 (calculated from core power)	16.41
Downcomer to upper head flow (kg/s or %) - (rmvm-400A01)	0.047 / 0.28%	0.062 / 0.38%

a - Source: Reference 9 and Reference 10
b - Pump speed set to obtain flows, differential pressures, and temperatures
c - Volume check performed for the VESSEL component and found to be in good agreement with design data

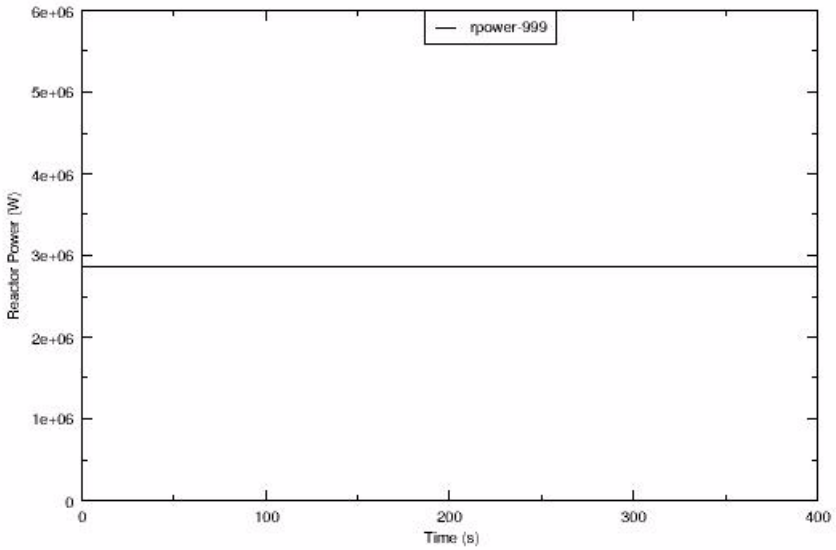

Figure C.8-37. Reactor Power

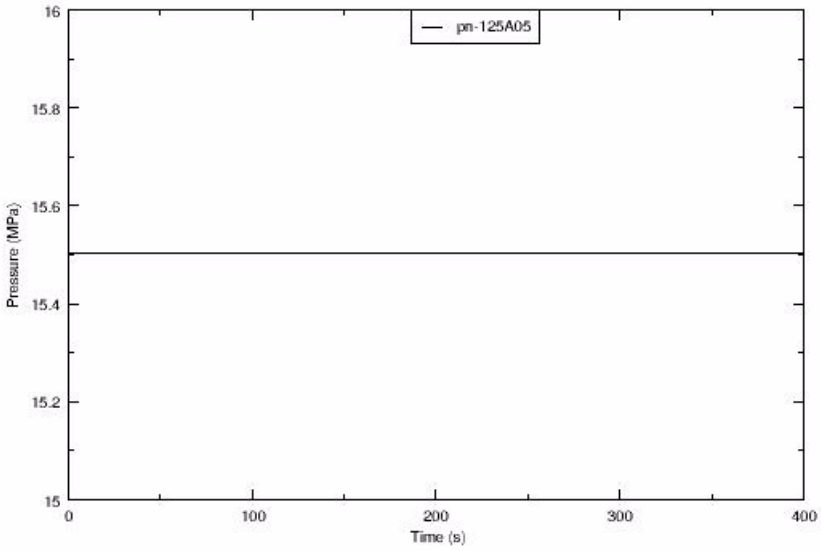

Figure C.8-38. Pressurizer Pressure

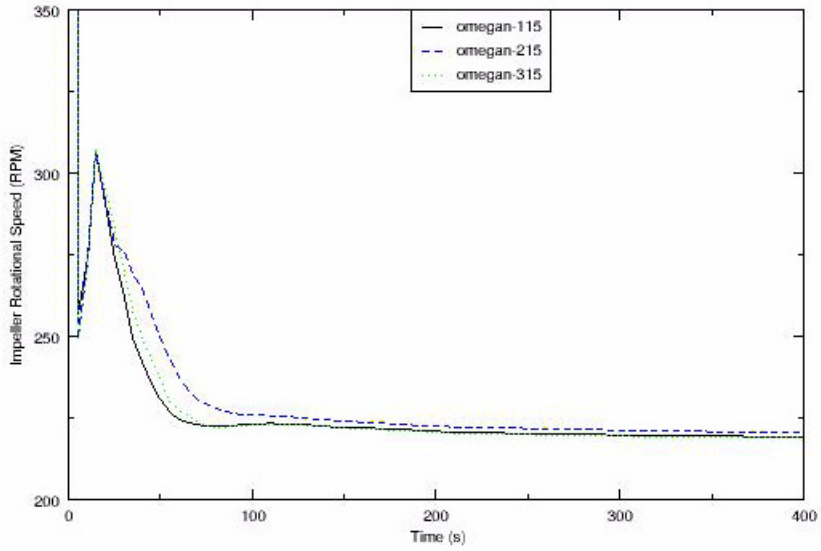

Figure C.8-39. Pump Impeller Rotation Speed

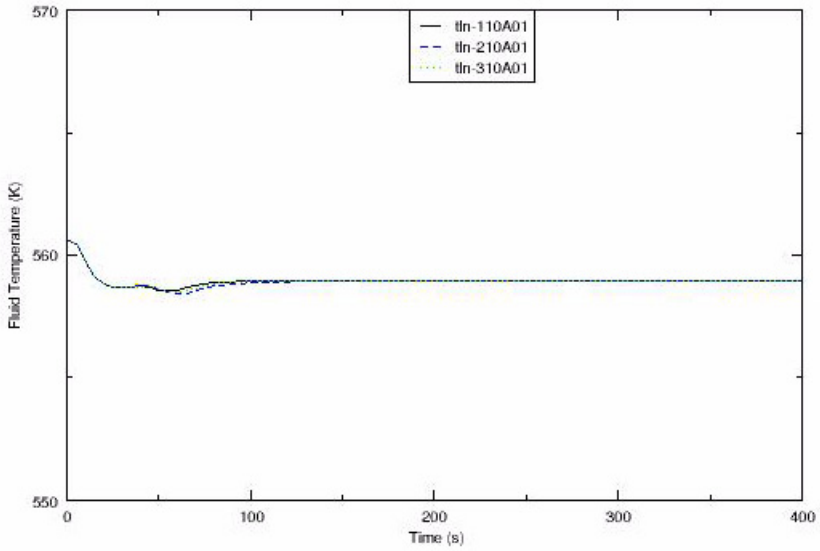

Figure C.8-40. Cold Leg Temperature

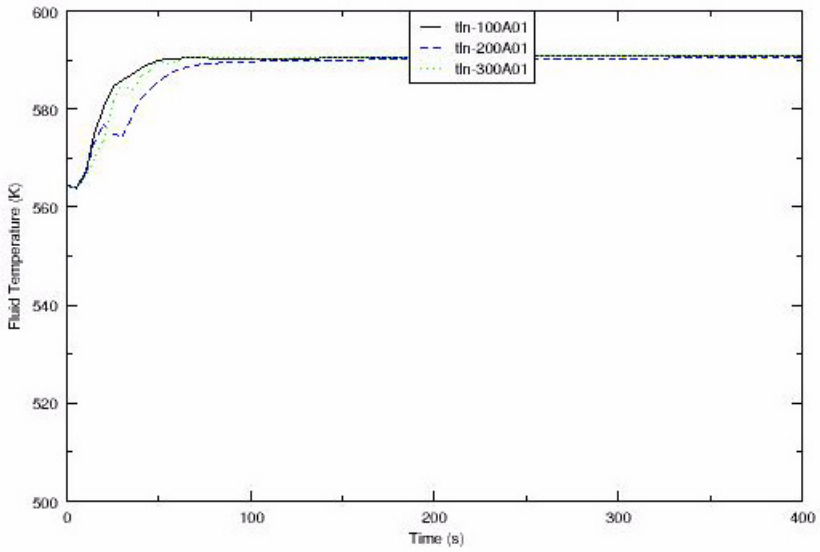

Figure C.8-41. Hot Leg Temperature

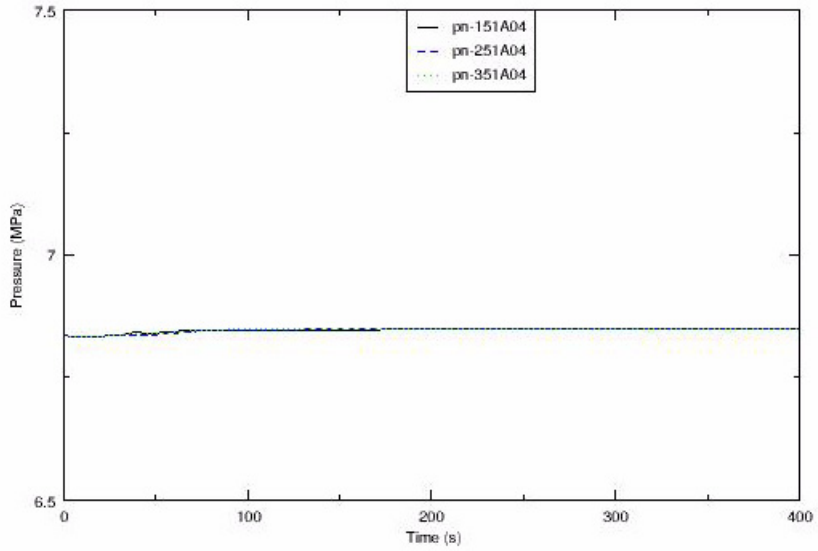

Figure C.8-42. SG Steam Dome Pressure

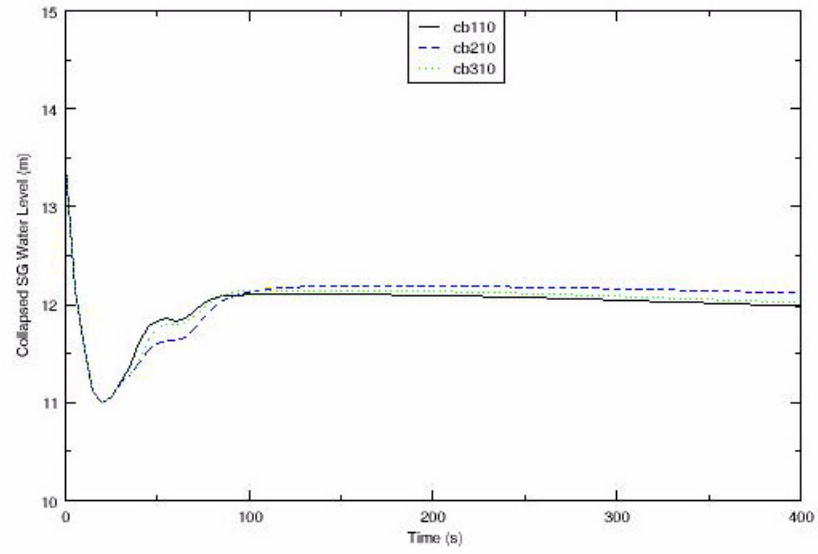

Figure C.8-43. SG Water Level

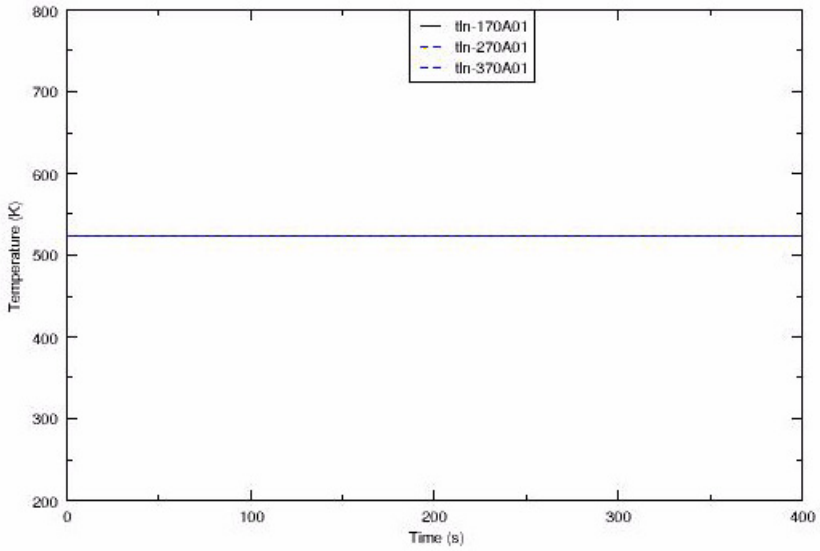

Figure C.8-44. SG Feedwater Temperature

C.8.4.2.2. BETHSY Test 6.2TC Transient Results

BETHSY Test 6.2TC was a 2000 second transient that was terminated when the pressurizer pressure decreased below 0.7 MPa. For this TRACE assessment, the calculation bombed at 2080 seconds, but executed sufficiently long to capture the test's transient behavior. Table C.8.4 lists the major system events with their timing observed in the experiment and as predicted during the TRACE code calculation. The test data used for the comparison were from the NRC Data Bank File 6.2TC.bin, which contains a subset of data from the experiment.

Table C.8.4. BETHSY Test 6.2TC Event Chronology

Event	Experiment (seconds)[a]	TRACE (seconds)
Break open	0	0
Reactor scram signal - (trp440)	8	18.5
Safety injection signal - (trp450)	12	36
Loop seal clearing	134	135
Primary/Secondary pressure reversal	172	155

a - Source: Reference 9

Table C.8.4. BETHSY Test 6.2TC Event Chronology

Event	Experiment (seconds)[a]	TRACE (seconds)
Accumulator #2 injection - (trp402)	345 ~ 948	313 ~ 760
Accumulator #3 injection - (trp402)	345 ~ 976	313 ~ 760
Pressurizer pressure < 0.7 MPa - (pn125A05, sv2)	2179	1815
a - Source: Reference 9		

Experimental Observations

Overall, core uncovery appears three times during the experiment with four distinct time periods.

1. 0 to 134 seconds: Low-quality two-phase blowdown period until loop seal clearing.

As described in (Ref. 10), after the break opening the upper part of the RCS gradually fills with steam. The liquid seals on the side of the break with downflow of the cold legs, and on the reactor vessel side of the break were established, preventing the steam from the core region to flow along the loops toward the break. The pressure buildup in the upper parts of the RCS causes voiding in the cold legs from the steam generator side and in the reactor vessel, until the lowest point of the cold legs loop seal was reached. Then loop seal clearance occurred.

2. 134 to 345 seconds: High-quality two-phase blowdown until the beginning of accumulator injection.

With loop seal clearing, a rapid increase in core liquid level follows. This is attributed to a manometric head balance between the downcomer and the core (Ref. 9). The downcomer head pushes fluid into the core resulting in the increase in the collapsed core water level. Depressurization is observed again because the break is uncovered. Collapsed core water level now decreases until accumulator actuation.

3. 345 to 945 seconds: Accumulator injection.

Accumulator actuation increases the core liquid level and primary water inventory until injection flow ends.

4. 945 to 2000 seconds: Boil-off until the end of the experiment.

This time period is characterized by redistribution of coolant, boil-off, and monatomic level decrease until the test is stopped once the pressurizer pressure is less than 0.7 MPa (Ref. 9).

Overall TRACE Simulation Response

As shown in Table C.8.4, the TRACE calculation did capture the times for most of the key transient events. As for BETHSY Test 9.1b, the critical parameter for obtaining accurate event

times and predicting system response during the TRACE calculation is the break mass flow. The break mass flow affects core water inventory and, for this test, the timing of core heatup. The following discussion is primarily assesses the break flow during the TRACE calculation and describes the affected component or system parameter responses.

Break Flow

In the BETHSY Test 6.2TC, the break nozzle is located on the cold leg of Loop 1. The break is side-oriented, namely the axis of the nozzle is horizontal and perpendicular to the cold leg axis. The break nozzle has an inner diameter of 15.48 mm and a length of 154.8mm (L/D = 10). The break opening is controlled through a quick-acting ball valve. The schematic of the TRACE break model is given in Figure C.8-45.

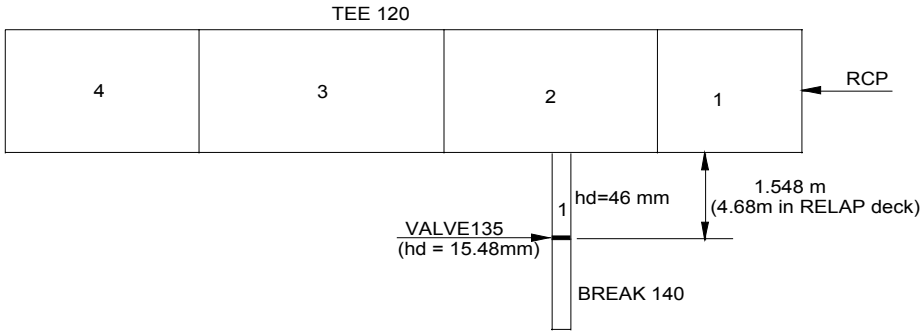

Figure C.8-45. TRACE Break Model

The calculated integrated flow rate is given in Figure C.8-46 along with the data. The TRACE calculated break mass flow rate is given in Figure C.8-47; a break mass flow rate was not provided in the data file.

The slope of the integrated break flow rate represents the break flow rate. According to Figure C.8-46, the predicted break flows are in good agreement in the time period from 0 to 150 seconds and slightly overpredicted for the period from 150 to 220 sec. The region upstream of the break is single-phase liquid flow during the 0 to 150 second period and single-phase vapor flow after about 2200 seconds as shown in Figure C.8-48. In the two-phase period, approximately 150 to 220 seconds, the calculation overpredicts the break flow.

Figure C.8-48 shows the calculated void fraction (alpn-120002) and the measured void fraction (AL131, AL132 and AL133) in the broken cold leg upstream of the break. The figure indicates that the calculation provides an excellent prediction of the cold leg voiding process. This figure also shows a sudden decrease in calculated void fraction from approximately 0.8 to 0.7 indicating the passage of a liquid slug through the break. This is a likely contributor to the higher integrated break flow seen in Figure C.8-46.

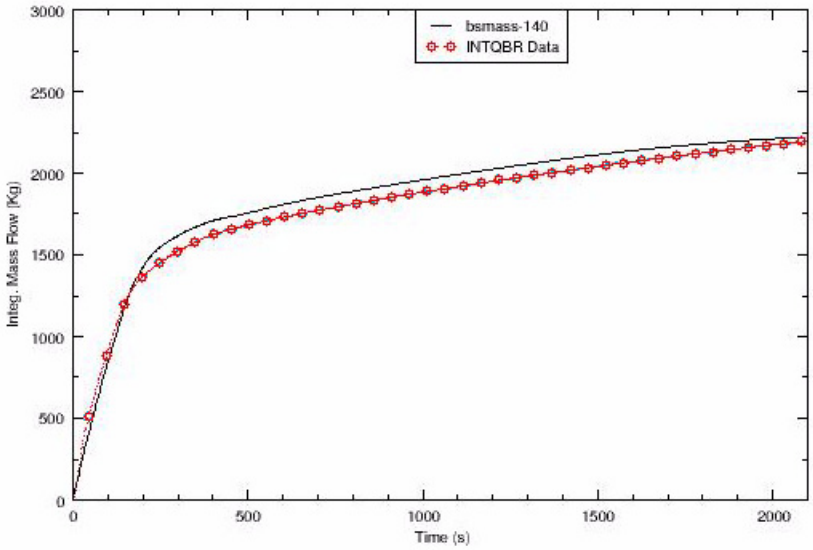

Figure C.8-46. Integrated Break Flow

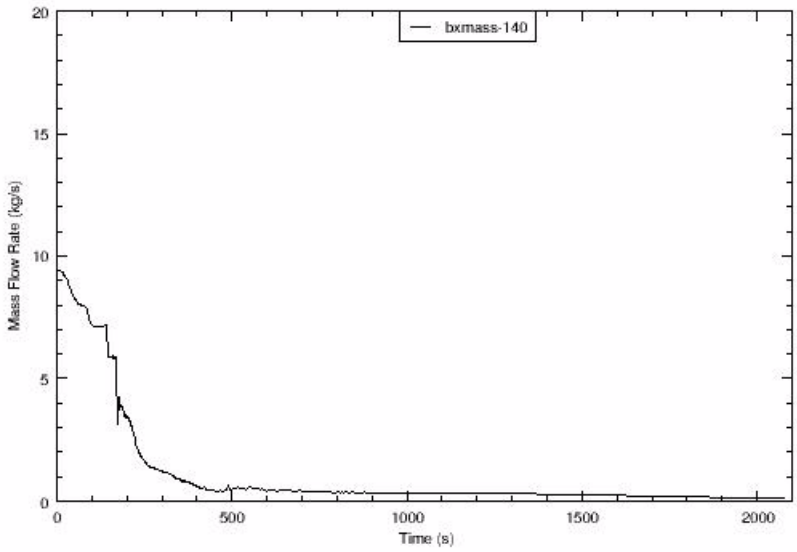

Figure C.8-47. Break Mass Flow Rate

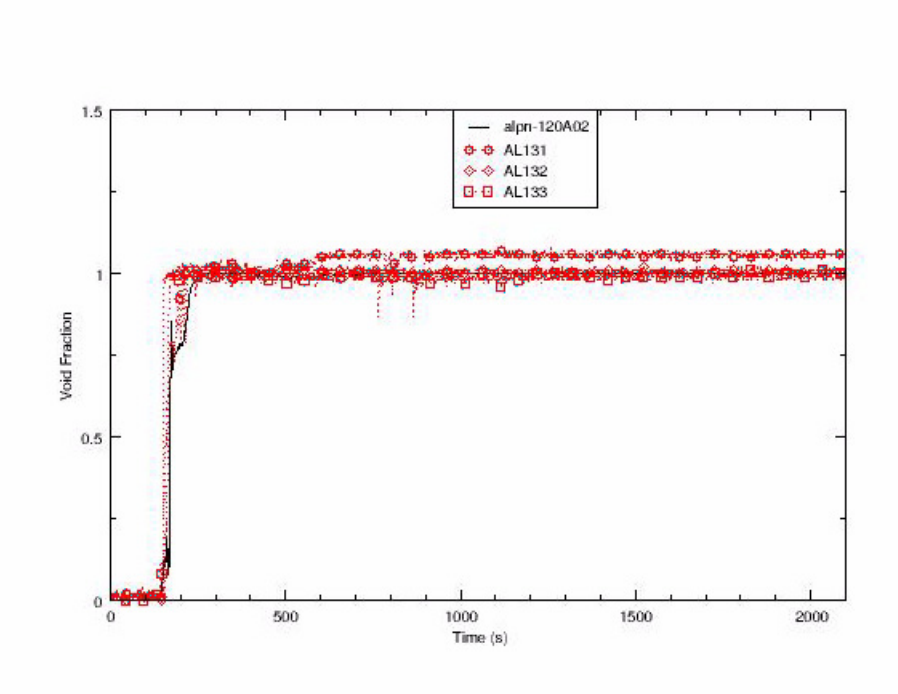

Figure C.8-48. Void Fraction of the Cold Leg of Loop 1

Primary System Pressure

The TRACE calculated primary system pressure is shown in Figure C.8-49 along with the data. After the break opens, primary system depressurization proceeds rapidly until the primary-side pressure approaches the secondary-side pressure and the pressurizer is emptied at approximately 50 seconds. In this phase, the system pressure is overpredicted. The sensitivity study shows that the depressurization rate is dependent on the initial liquid level in the pressurizer. With a lower initial liquid level, the predicted pressure will be improved.

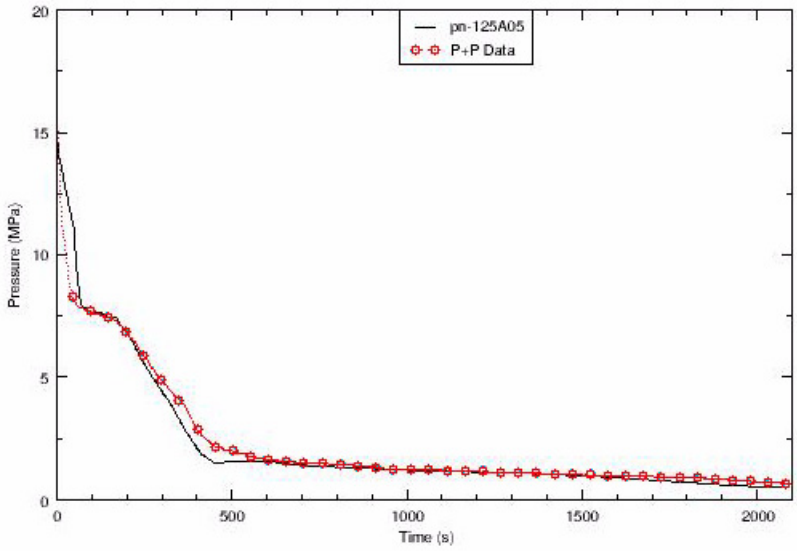

Figure C.8-49. Pressurizer Pressure

In the calculation and the test, the primary-side and secondary-side pressure reversals occur at about the same time, approximately 175 seconds, as shown in Figure C.8-50. Between 0 and 75 seconds, the predicted system pressure is lower than the test data. This behavior results from the underprediction of the steam generator secondary side pressure (see Figure C.8-50).

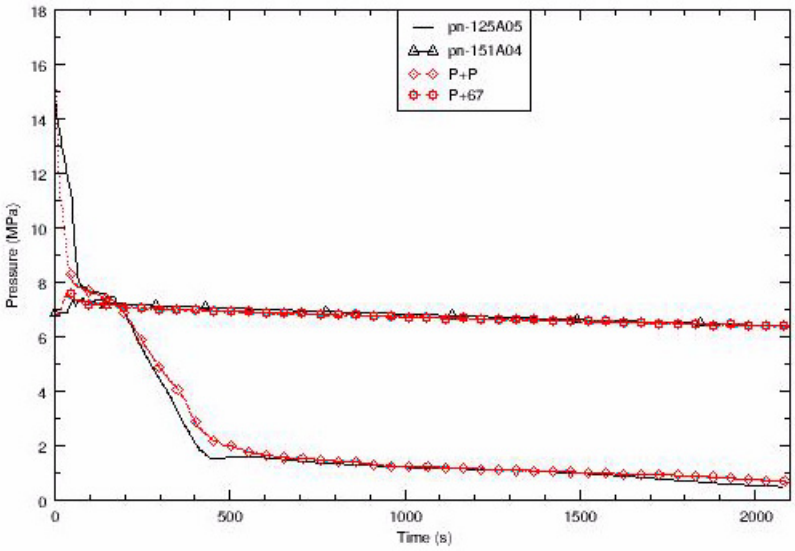

Figure C.8-50. SG Steam Dome Pressure vs Pressurizer Pressure

In the time period from 175 to 600 seconds, the calculation underpredicts the primary system pressure. In this phase, the primary pressure is dependent on the heat transfer from the steam generators but is primarily determined by the coolant loss (or integrated break flow). The underprediction of the primary system pressure is mainly due to overprediction of the break flow from 150 to 220 seconds into the transient as discussed earlier. One of the consequence of underpredicting the primary system pressure is an early initiation of the accumulator injection. After 600 seconds, the predicted system pressure is in good agreement with the data.

Core Liquid Level Depression

The core differential pressure is used to represent the core liquid level depression. Figure C.8-51 shows the core differential pressures predicted by TRACE and given in the test data.

According to Figure C.8-51, the test data indicates a rapid core liquid depression following the break which is the result of loss of the coolant mass and flashing in the primary system. The core liquid reaches a minimum value at approximately 135 seconds just before the loop seal clearing as discussed later in this section. The minimum core liquid level is dependent on the manometric effect, especially the liquid holdup in the steam generator U-tube upflow side and in the loop seals. Following loop clearing, the core liquid level starts to recover instantaneously. The core liquid level recovery continues to approximately 175 seconds. After 175 seconds, the core liquid level continues to decrease until the accumulator injection starts at 345 seconds. As the result of

the accumulator injection, the core liquid level starts to increase from 365 seconds to 700 seconds. Then the core liquid level remains constant until core boiloff starts at 1625 second.

As shown in Figure C.8-51, the calculation gives a good prediction of the core level depression and recovery in the first 100 seconds after the break. From 100 to 275 seconds, the predicted core liquid level over predicts the data. Following the accumulator injection, the core liquid level starts to increase and remains at a roughly constant level after approximately 500 seconds until the predicted core boiloff begins at 1250 seconds. In the calculation, the core boiloff starts earlier than in the test. This is caused by the overprediction the integrated break flow.

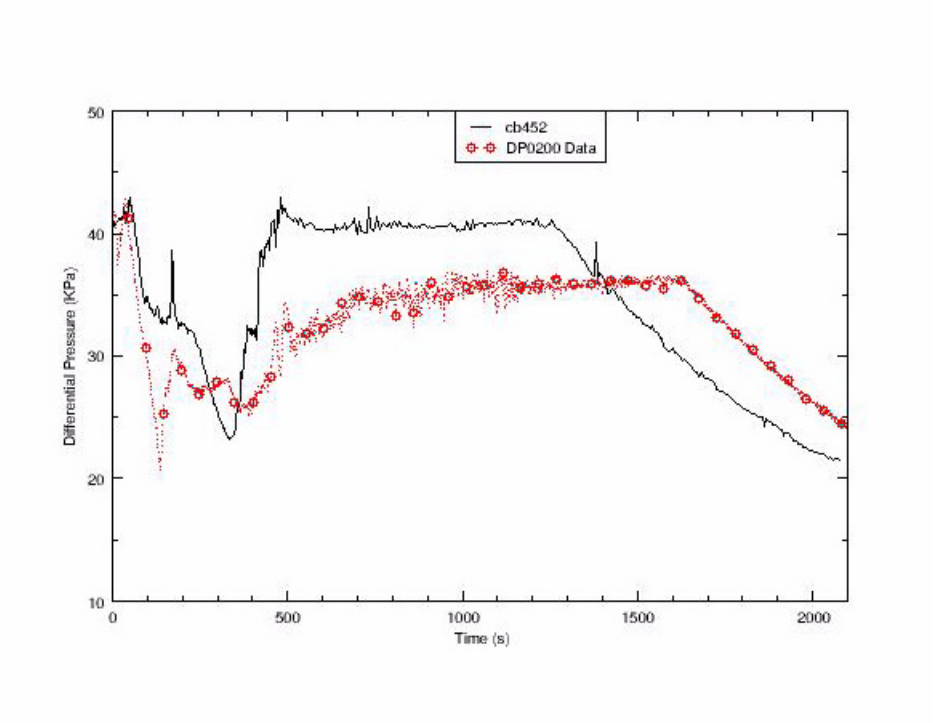

Figure C.8-51. Core Differential Pressure

Core Heatup

In the test, core heatup was first observed around 140 seconds after the break and again late during the core boiloff phase at approximately 2159 seconds as shown in Figure C.8-52. The first core heat up lasts only a very short period corresponding to the core level depression at 135 seconds. In the calculation, the core heatup occurs at approximately 330 seconds when the core has the minimum liquid level during the transient. In the core boiloff phase, the calculated core heatup starts early, at approximately 1330 seconds, in part due to the greater amount of liquid mass sent through the break as discussed earlier.

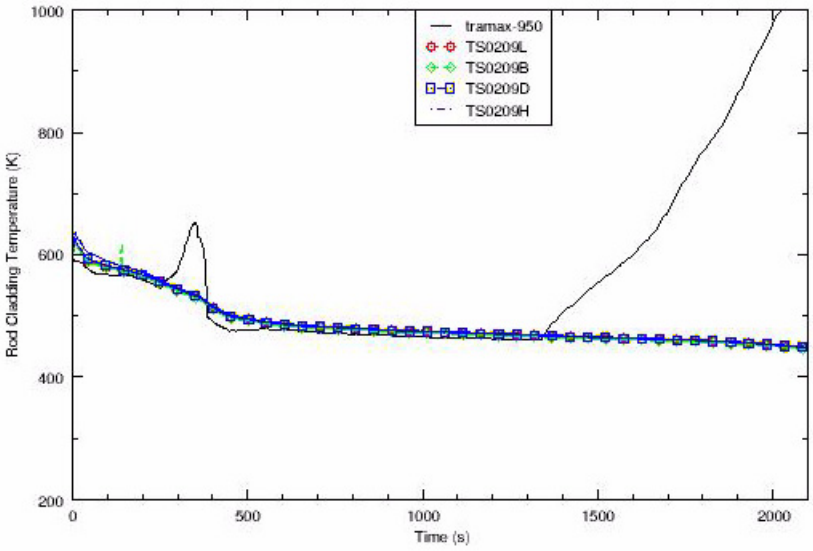

Figure C.8-52. Rod Cladding Temperature

Loop Seal Clearing

The differential pressures of the upflow and downflow sides of the loop seals for the three loops are given in Figure C.8-53 to Figure C.8-58. The calculation results show good agreement with the test data except for some difference in predicting the clearing of the upflow side of Loop 3 seal.

In the experiment the loop seal clearings of the three loops occur almost simultaneously at 135 seconds with some liquid hold-up in the upflow side of the loop seals, the section between the reactor coolant pump and the bottom of the cross leg.

The code provides a good prediction on the loop seal clearing phenomena, especially for the loop seal clearings of Loop 1 and Loop 2. However, in the calculation, the clearing of the upflow side of the Loop 3 seal is postponed by about 250 seconds.

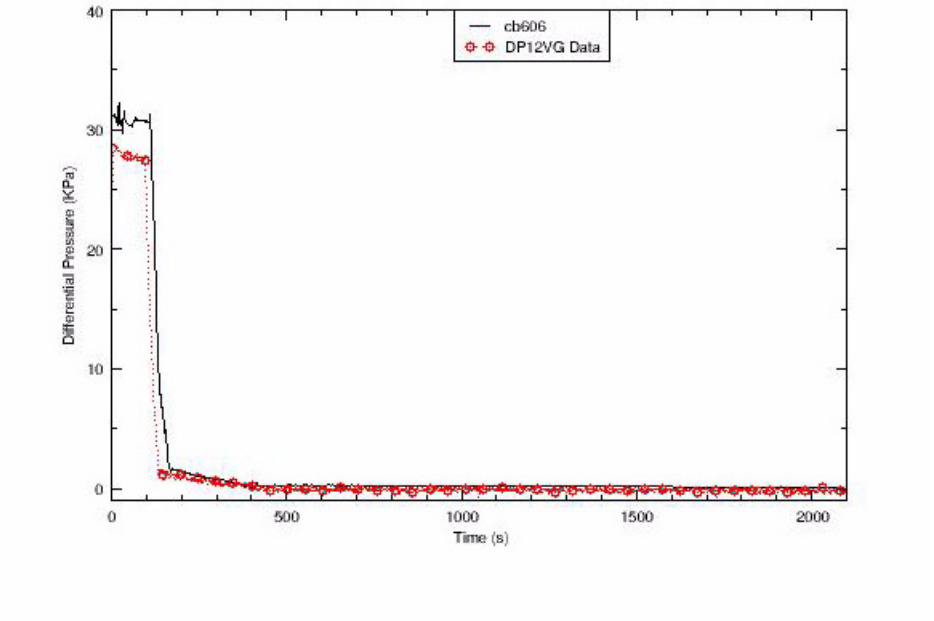

Figure C.8-53. Loop 1 Seal Downflow Side Differential Pressure

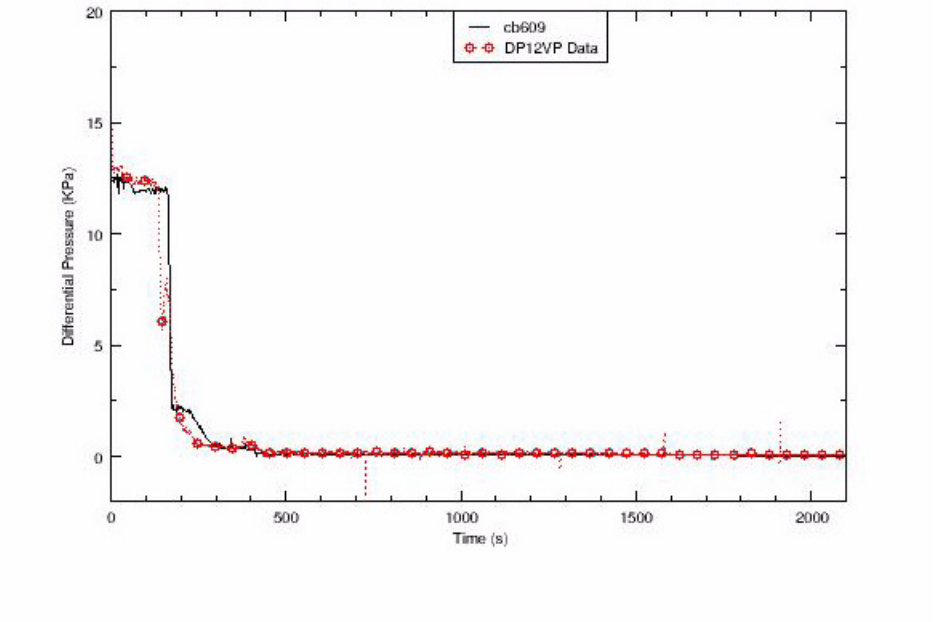

Figure C.8-54. Loop 1 Seal Upflow Side Differential Pressure

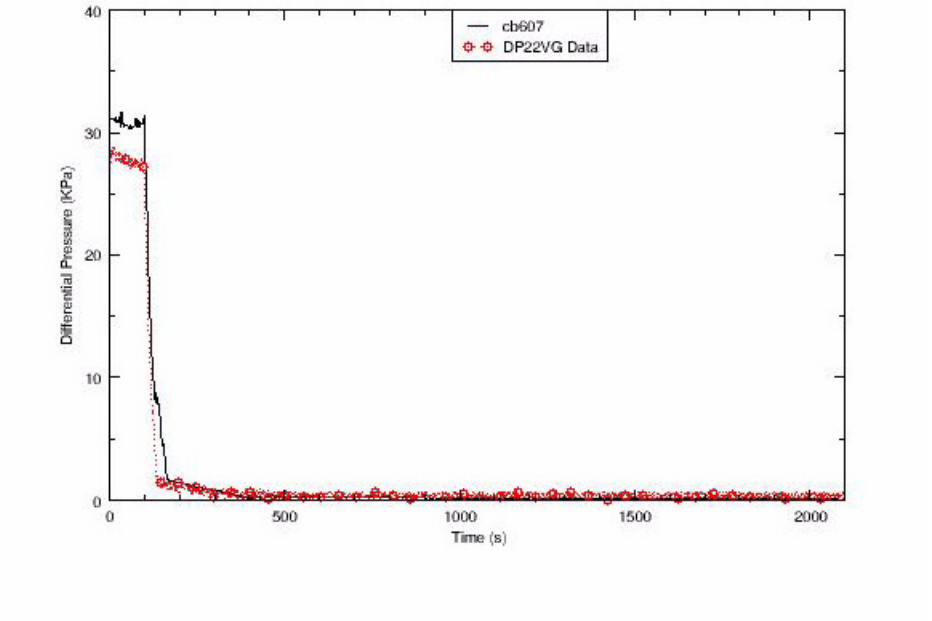

Figure C.8-55. Loop 2 Seal Downflow Side Differential Pressure

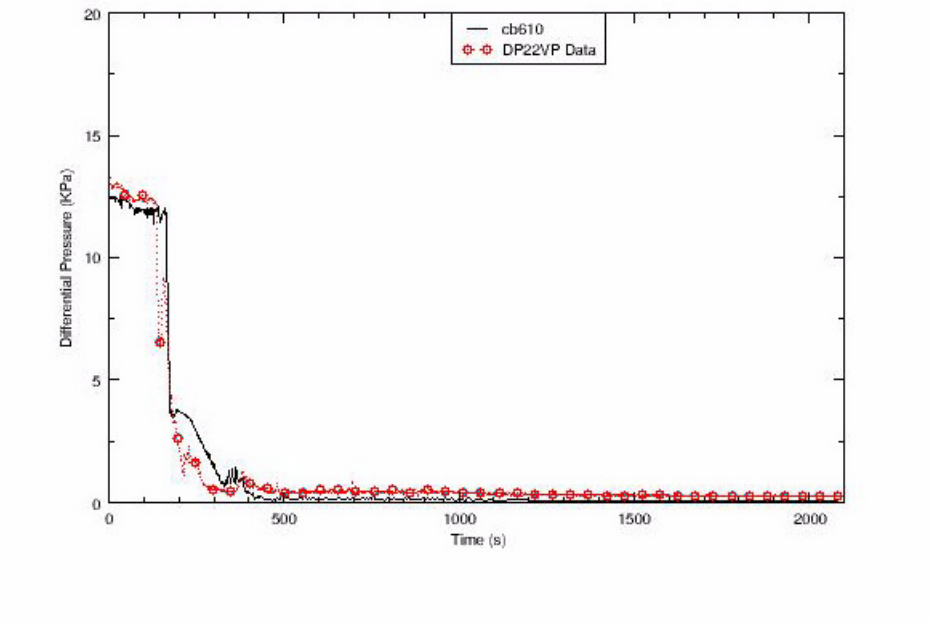

Figure C.8-56. Loop 2 Seal Upflow Side Differential Pressure

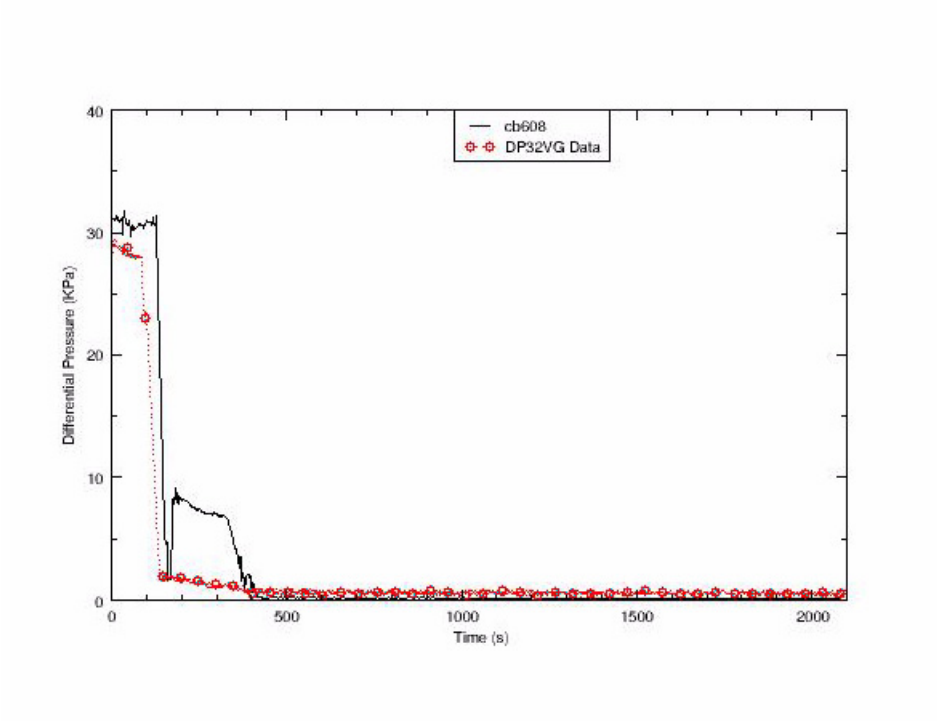

Figure C.8-57. Loop 3 Seal Downflow Side Differential Pressure

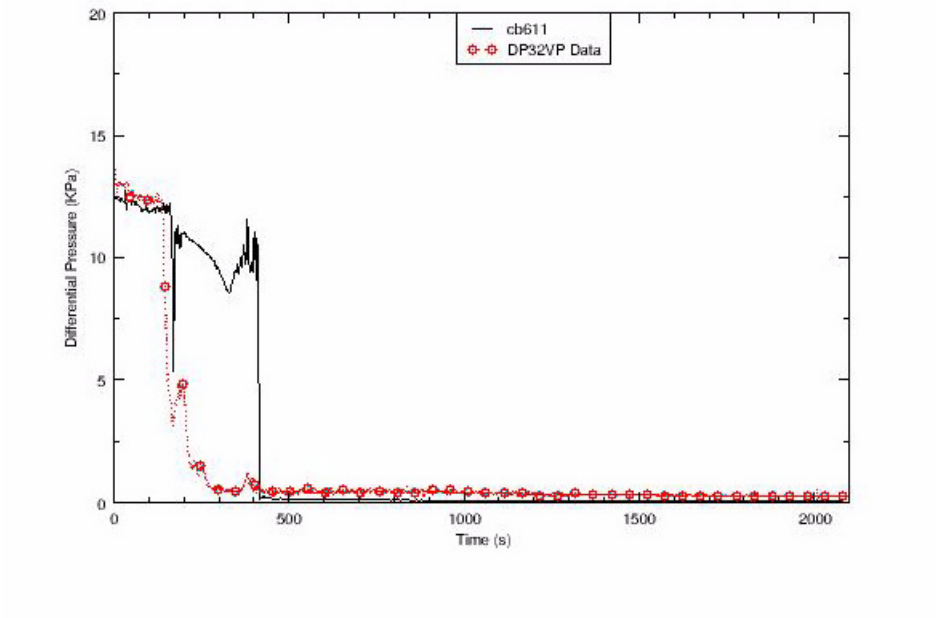

Figure C.8-58. Loop 3 Seal Upflow Side Differential Pressure

Differential Pressures in the Upflow and the Downflow Sides of Steam Generator U-Tubes

The differential pressures in the upflow and the downflow sides of the steam generator U-tubes are shown in Figure C.8-59 to Figure C.8-64. The calculation results are in a good agreement with the test data. Both in the calculation and in the test, draining of the down flow side of the steam generator U-tubes proceeds faster than the upflow side of the steam generator U-tubes. Draining of the down flow side of the steam generator U-tubes is completed at about the time loop seal clearing occurs, approximately 135 seconds. The complete draining of the upflow side of the steam generator U-tubes is postponed and occurs roughly between 150 and 200 seconds, corresponding to the core liquid level recovery after the first core liquid level depression.

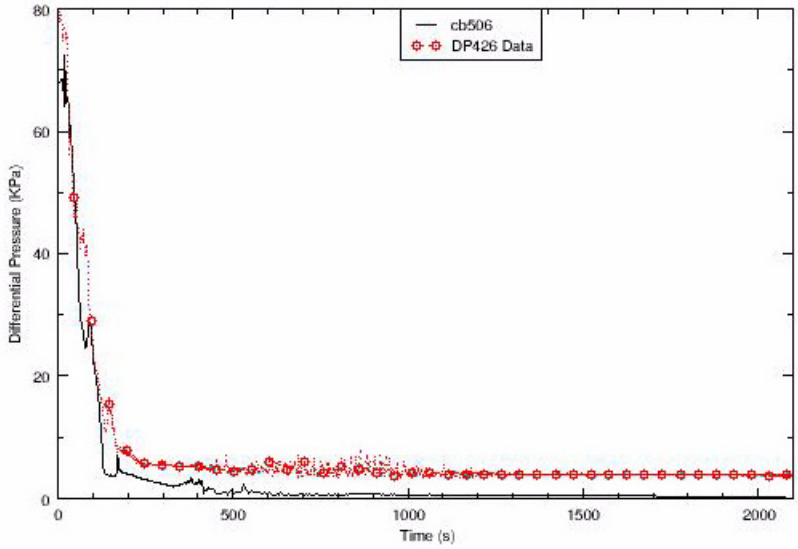

Figure C.8-59. SG1 U-Tube Upflow Side Differential Pressure

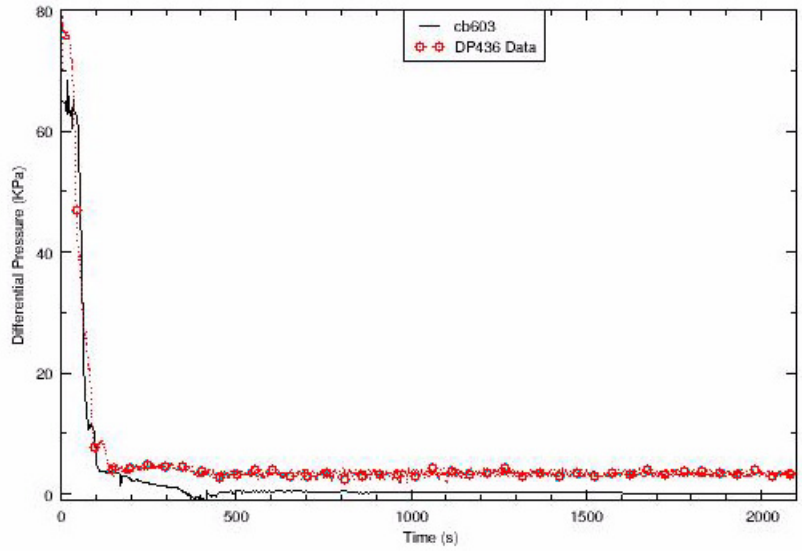

Figure C.8-60. SG 1 U-Tube Downflow Side Differential Pressure

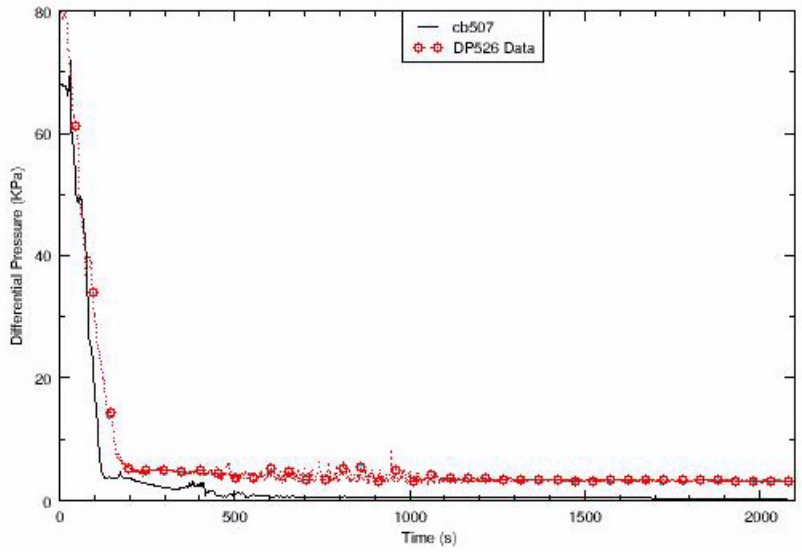

Figure C.8-61. SG2 U-Tube Upflow Side Differential Pressure

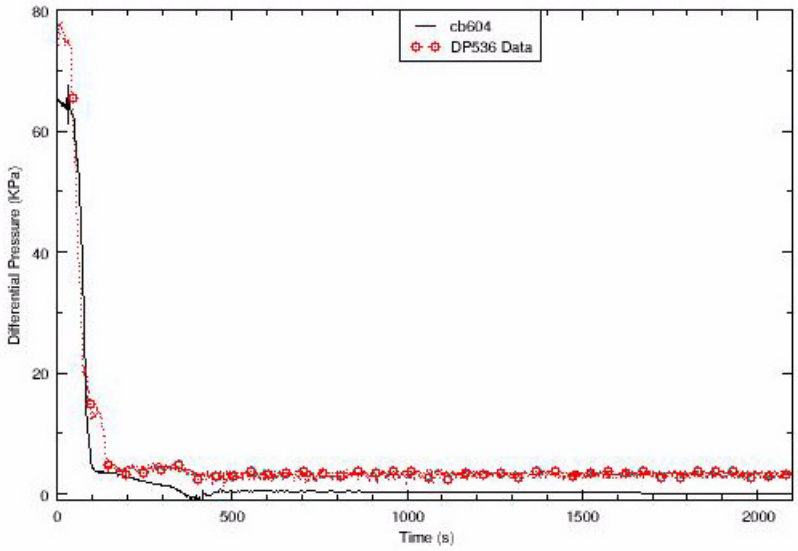

Figure C.8-62. SG2 U-Tube Downflow Side Differential Pressure

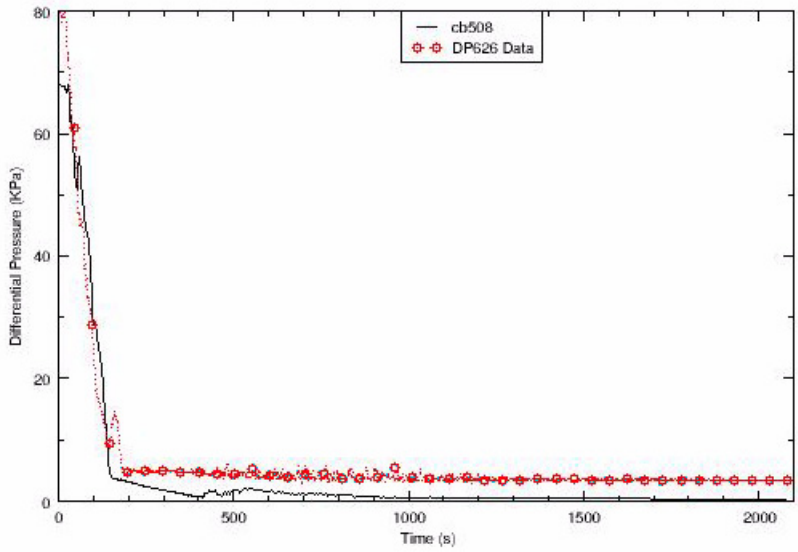

Figure C.8-63. SG3 U-Tube Upflow Side Differential Pressure

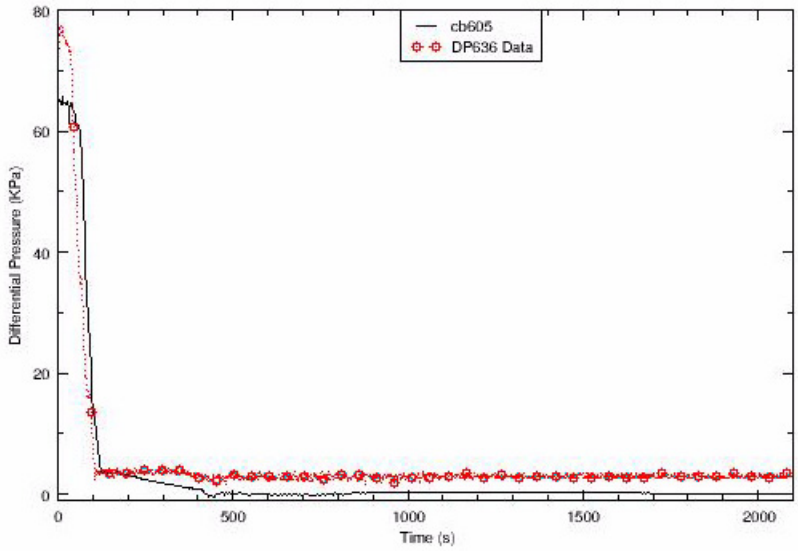

Figure C.8-64. SG3 U-Tube Downflow Side Differential Pressure

ECC Injection

In the BETHSY Test 6.2TC, the HPIS and LPIS are not available. An accumulator tank is attached to the cold legs of the two intact loops, Loop 2 and Loop 3. The accumulator injections start when the primary loop pressure drops to 4.2 MPa and stops when the water level in the accumulator tanks reaches 0.6 m.

Calculated and measured integrated accumulator injection flows into both loops are shown in Figure C.8-65. In the test, the accumulator injection starts at 345 seconds and is isolated at approximately 950 seconds. In the calculation, the accumulator injection begins at about 350 seconds and is isolated at about 650 seconds. As indicated in Reference 9, the combination of the larger amount of water inventory loss out the break and the earlier time that the accumulators complete their injection results in the earlier calculated core heatup at approximately 1330 seconds.

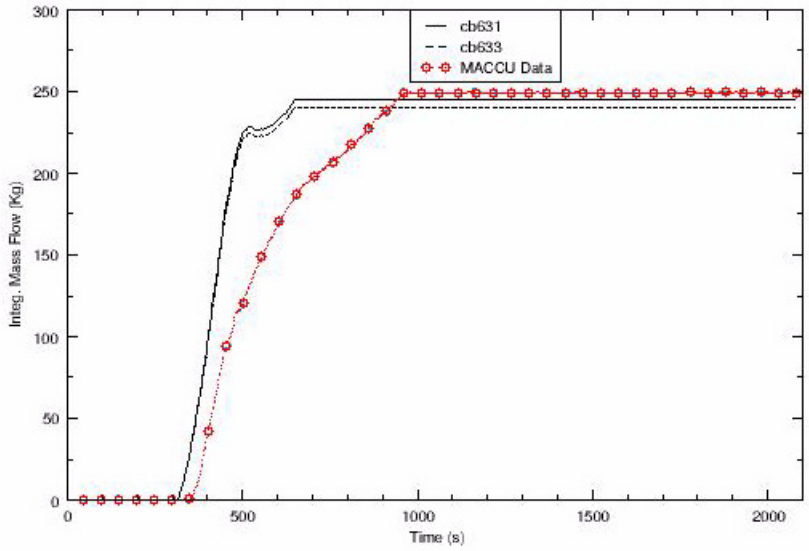

Figure C.8-65. Integrated Accumulator Injection Flow

Summary

The overall results calculated in this study are similar to the results obtained in Reference 9 where the RELAP5/MOD3 code was used to simulate BETHSY Test 6.2TC. As previously discussed, the differences between the calculations and data result primarily from the overprediction of the integrated break flow. The execution used time steps of about 0.02 seconds throughout the transient. The total execution time for the problem was about 3 hours.

BETHSY Test 6.2TC was also run using TRACE Version 5.0 Release Candidate 3 on a 32-bit PC with a Linux operating system. The Windows and Linux executions both bombed prior to reaching the total (steady-state and transient) problem end time of 2600 seconds. The Windows execution bombed at a total problem time of 2479.6 seconds, and the Linux run bombed at 2451.9 seconds. The calculated results from the Linux run were very similar to those obtained using the TRACE executions on a PC using Windows XP. Consequently, it can be concluded that it is acceptable to run the BETHSY Test 6.2TC on a PC using either the Windows XP or Linux operating systems.

C.8.5. Assessment Summary for BETHSY Tests 9.1b and 6.2TC

Two LOCA tests were simulated using Version 5.0RC3 of the TRACE thermal-hydraulic code. The calculated results generally agree reasonably well with the test data. Although timing of the

key events, such as core uncovery, loop seal clearing, etc. in each of the simulations differed when compared to the available test data, the difference is not too large and the events were captured reasonably well.

Break flow was the most important parameter which resulted in differences between calculations and data. For BETHSY Test 9.1b, differences in predicted and measured behavior result from TRACE predicting two-phase flow earlier at the break location when the measured flow is still liquid. Because the physical layout of the break nozzles for BETHSY Tests 9.1b and 6.2TC are horizontal side connections to the cold leg, the flow in this cold leg could be highly stratified, especially for Test 9.1b. For Test 6.2TC with a larger break size, TRACE overpredicted the integral break flow during an early time period when both the calculation and the test are transitioning from single-phase to two-phase break flow. The TRACE offtake model could be the principal source for the deviations in break flow. This phenomenon has also been observed in simulations of other integral tests (Refs. 9, 12).

The prediction of the heater rod cladding temperatures during core heatup also differed with test data for both test simulations. For Test 9.1b, the differences between predictions and data are related to water inventory and distribution in the pressure vessel. The timing of core heatup is more of a concern for Test 6.2TC.

The principal core heatup occurs in Test 9.1b prior to and shortly after initiation of Ultimate Procedure when inventory levels are the lowest. Prior to the Ultimate Procedure, the radial temperature distribution is relatively even. Once the Ultimate Procedure is initiated, the temperature response in the test differs between the inner region and the periphery of the core. This difference was attributed to accumulation of liquid in the upper plenum with draining into the central or inner region of the core while steam flowed upward along the core periphery. While the inner core temperatures quickly turned around following initiation of the Ultimate Procedure, the temperatures continued to rise along the core periphery until accumulator injection was able to reverse and bring uniformity in the core's radial temperature distribution. The TRACE model does have an inner and periphery core region with heater rods. Thus, there is the potential to capture the difference in temperature response across the core. However, the BETHSY facility's heater rods in each azimuthal and ring section of the TRACE model were lumped into one rod as recommended by user guidance. Additionally, the TRACE code would also have to accurately capture the complex counter-current flow pattern, namely liquid flowing down in the inner core region with steam flowing upward, for a core with a potentially large L/D ratio (i.e., BETHSY's heated core L/D is approximately 10.7 while the reference core L/D is likely closer to 1).

In Test 6.2TC, core heatup occurs towards the end of the transient when enough inventory has boiled off as a result of the larger break size, the continued isolation of the steam generators because no Ultimate Procedure was initiated, and the unavailability of LPIS. Because TRACE overpredicts the inventory loss out the break and an earlier accumulator injection, the beginning of the final core heatup occurs earlier than in Test 9.1b. This early timing of the final core heatup has also been observed in at least one other calculation due to larger integrated break flow and the earlier depletion of the accumulator (Ref. 8).

Applying the acceptance criteria presented in NUREG-1737 for reactor plant system transient analysis, the results of the TRACE simulation of BETHSY Test 9.1b and Test 6.2TC shows the code can provide *Reasonable Agreement*. The same LOCA phenomena observed in each test were predicted by TRACE with the principal differences being the timing of the phenomena. These results are also consistent with previous thermal-hydraulic code calculations (Refs 1,3,4,9,10).

C.8.6. References

1 OECD/NEA/CSNI International Standard Problem No. 27, "BETHSY Experiment 9.1B 2 inch Cold Leg Break without HPSI and with Delayed Ultimate Procedure," Comparison Report, Volume 1, NEA/CSNI/R(R92)20, November 1992.

2 Information Systems Laboratories (ISL), "RELAP5/MOD3.3 Code Manual Volume VII: Summaries and Reviews of Independent Code Assessment Reports," Nuclear Safety Analysis Division, Information Systems Laboratories, Inc., prepared for the U.S. Nuclear Regulatory Commission, December 2001.

3 Bolander, M., "TRACE Comparison to BETHSY Test 9.1B (ISP-27)," ISL-NSAD-TR-03-25, Nuclear Safety Analysis Division, Information Systems Laboratories, Inc., prepared for the U.S. Nuclear Regulatory Commission, December 2003.

4 Weidong He and Don Palmrose, "TRACE Simulation of BETHSY Test 9.1B and Test 6.2," Advanced Systems Technology and Management, Inc. prepared for U.S. Nuclear Regulatory Commission, ADAMS Accession Number ML0617106180, January 31, 2006

5 Centre D'etudes Nucleaires De Grenoble (CEA), "BETHSY General Description," SETh/LES/90-97, Equipe BETHSY, Document collectif, Grenoble, France, April 1990.

6 Joint Research Center (JRC), European Commission, "The BETHSY Facility, an important part of the french strategy for PWR accident management," STRESA: Storage of Thermal Reactor Safety Analysis Data, <http://asa2.jrc.it/stresa_cea/Specific/BETHSY/bethsy-Fac.htm> (Accessed 10/3/2005).

7 Bazin, P., "BETHSY Data Base," SETh-LES-87-27, Equipe BETHSY, Document collectif, Grenoble, France, March 1988.

8 U.S. Nuclear Regulatory Commission, "NRC Data Bank: BETHSY Test 9.1b," Filename 9.1b.bin, Dated July 1, 2005.

9 Chung, Y., et al., "Assessment of RELAP5/MOD3 Using BETHSY 6.2TC 6-Inch Cold Leg Side Break Comparative Test," NUREG/IA-0131, U.S. Nuclear Regulatory Commission, October 1996.

10 Petelin, S., and B. Koncar, "RELAP5/MOD3.2 Assessment on the BETHSY 6.2TC SBLOCA Test," 4th Regional Meeting, Nuclear Energy in Central Europe, Bled, Slovenia, September 7-10, 1997.

11 U.S. Nuclear Regulatory Commission, "NRC Data Bank: BETHSY Test 6.2," Filename 6.2.bin, Dated July 1, 2005.

12 Advanced Systems Technology and Management, Inc., "TRACE Version 4.150 Simulation of ROSA-IV Tests: Final Report." prepared for the U.S. Nuclear Regulatory Commission, April 15, 2005

BWR Large Break Integral Tests

C.9. SSTF Tests EA3.1 Run 111 and EA3.3-1 Run 119

Author(s): Weidong He, Millan Straka and Dave Ebert

Affiliation: Advanced Systems Technology and Management, Inc.

Code Version: TRACE V5.0

Platform and Operating System: Intel x86, Windows XP

C.9.1. Introduction

The objective of this work is to assess the ability of the TRACE code.to calculate loss-of-coolant accident (LOCA) thermal-hydraulic phenomena as simulated in the Steam Sector Test Facility (SSTF). In this report, TRACE code calculations are compared with experimental data from SSTF Test EA 3.1 Run 111 and Test EA 3.3-1 Run 119.

A series of tests were conducted in the SSTF to study thermal-hydraulic phenomena during the refill/reflood phase of hypothesized boiling water reactor (BWR) loss-of-coolant accidents, including separate effect tests and system response tests (Ref. 1). Test EA3.1 Run 111 was a system transient response test and was conducted to study controlling phenomena related to the BWR/4 ECCS configuration (Ref. 1). It simulated a 1.0-m design basis accident (DBA) break (or 100% recirculation line break). Test EA3.3-1 Run 119 was identical to Test EA3.1/111 except that it simulated a 0.73-m DBA break with some variations in the initial conditions (e.g., mass inventory distribution in the system). The main purpose of Test EA3.3-1/119 was to investigate the sensitivity of the system response to the break size. The phenomena of interest in these two tests include counter-current flow limiting (CCFL), ECCS injection mixing in the upper plenum and lower plenum, parallel channel phenomena, etc (Refs 4, 5).

C.9.2. Test Facility Description

SSTF was a full-scale mock-up of a 30^{o} sector of a GE BWR/6-218 (624 bundles) design (Ref. 3). A schematic of the SSTF test section is shown in Figure C.9-1. The 30^{o} sector internals are housed in the SSTF pressure vessel, which serves as a pressure envelope.

The 30^{o} sector provides an accurate representation of the reference BWR/6 reactor through the use of prototypical hardware and geometry. It simulates major regions of the reference reactor

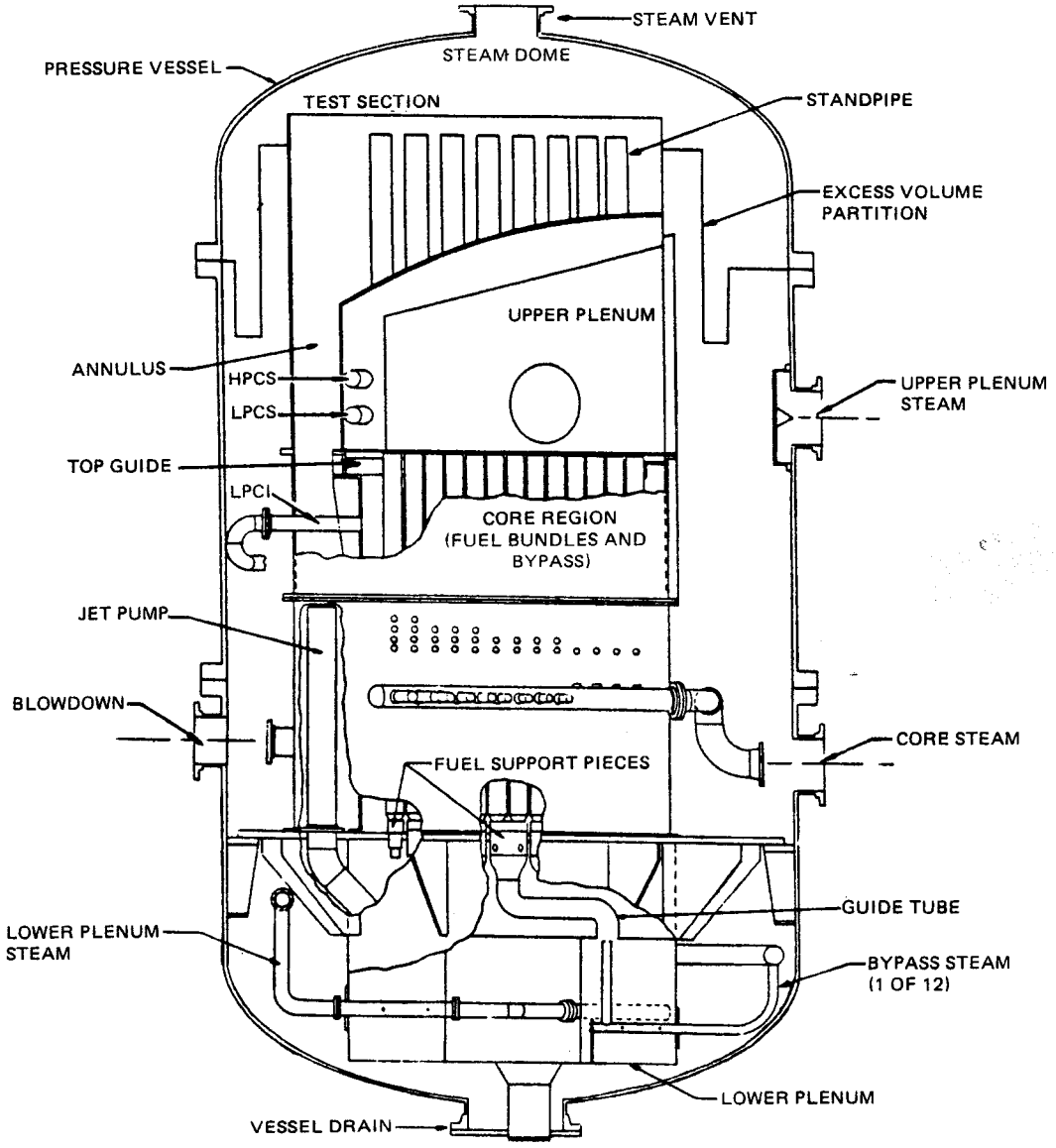

Figure C.9-1. SSTF Test Section Schematic

design such as the steam dome, steam separator, reactor core, core bypass, downcomer, lower plenum, control rod guide tubes and jet pump volumes, etc.

The upper plenum is a full-scale mockup of the 30^{o} sector of the reference upper plenum. Standpipes simulating the steam separators extend up from the shroud. The upper and lower core-spray spargers are full scale mockups of the 30^{o} sector of the reference BWR/6-218 High Pressure Core Spray (HPCS) and Low Pressure Core Spray (LPCS) spargers with regard to size, curvature

and location of the nozzles. An LPCS lower header representative of BWR/4,5 design was installed to simulate BWR/4 and BWR/5 ECCS configurations. The Low Pressure Core Injection (LPCI) system was setup to simulate LPCI in a BWR/6 (providing injection into the core bypass region) or a BWR/4 (providing injection into the recirculation pump drive line).

The core region is full scale in the cross section and is about 5 feet shorter than the BWR reference design, including fifty-eight (58) mock fuel bundles in the 30^{o} sector. The radial locations of the bundles and bypass are shown in Figure C.9-2. Decay heat in the bundles was simulated by injecting steam into the core region. The bundle steam flow factors are listed in Table C.9.1.

Table C.9.1. SSTF Bundle Steam Flow Factors (Ref. 4)

Bundle Location[a]	Steam Factors[b]	Bundle Location	Steam Factors
1, 8	0.365	29, 34	0.699
2, 7	0.641	30, 33	1.283
3, 6	0.664	31, 32	1.283
4, 5	0.664	35, 38	1.294
9, 16	0.297	36, 37	1.294
10, 15	0.985	39, 42	1.260
11, 14	1.008	40, 41	1.283
12, 13	1.031	43, 46	0.989
17, 22	1.145	44, 45	1.283
18, 21	1.180	47, 50	0.601
19, 20	1.191	48, 49	1.271
23, 28	1.059	51, 52	1.271
24, 27	1.248	53, 54	1.191
25, 26	1.271	55, 56	0.847
		57, 58	0.404

a - See Figure C.9-2

b - Bundle steam injection = (total core steam injection) x (bundle steam factor)/58

Twelve (12) volume-scaled guide-tube regions are provided. The lower plenum volume represents the scaled volume of the reference lower plenum volume outside the guide tubes. Liquid flashing in the lower plenum and the guide tube volumes are simulated by injecting adiabatic steam into these regions.

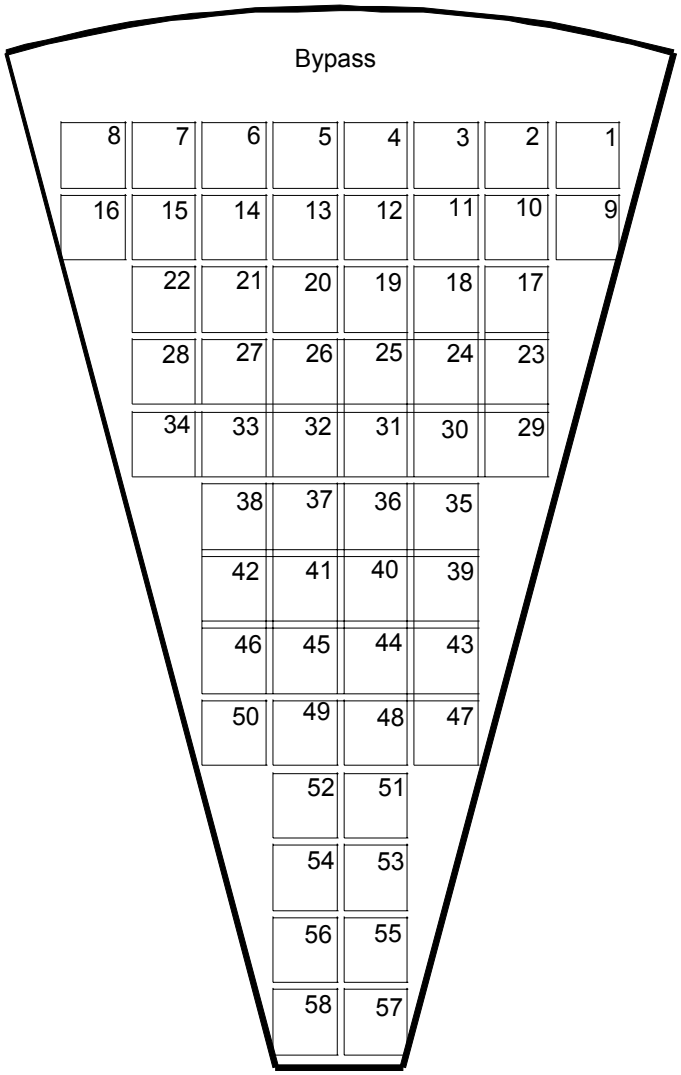

Figure C.9-2. Channel Arrangement in the 30-Degree Sector

C.9.3. TRACE Model Description

The TRACE input model for simulation of SSTF Test EA3.1 Run 111 was developed from a TRAC-BWR transient model (Ref. 7). The TRAC-B input model was converted into a TRACE input deck by utilizing the NRC Symbolic Nuclear Analysis Package (SNAP). The TRACE input model was reviewed against the original TRAC-B model to ensure consistency. Major modelling changes included one level added both in the lower plenum region and in the bypass region. A number of signal variables and control blocks were created for mass inventory calculations.

The TRACE input model for SSTF Test EA3.3-1 Run 119 was developed from the TRACE deck for Test EA3.1 Run 111. The steady-state calculation was conducted with the boundary conditions of EA 3.3-1 Run 119 (e.g., system pressure, steam injection rates) to obtain the initial conditions for the transient simulation.

The TRACE SSTF nodalization scheme is shown in Figure C.9-3. Table C.9.2 summarizes the components in the SSTF TRACE model, representing the SSTF core, core bypass, upper plenum, lower plenum, guide tube volumes, annular downcomer volume, steam injection systems, ECCS injection, etc.

The 30^{o} sector reactor is modeled with a VESSEL component of a slab geometry. The VESSEL consists of four rings and fourteen levels. The first three rings represent the lower plenum (Levels 1-5), core bypass (Levels 6-10), upper plenum (Levels 11-13), and steam dome (Level 14). The fourth ring (Level 6 - Level 13) is the annulus downcomer, housing the simulated jet pumps.

The individual bundles are lumped into three groups, each represented by a TRACE TEE/CHAN combination and each coupled with one of the first three rings of the VESSEL component as shown in Figure C.9-3 The combination simulates both the core steam injection and the bundle/ bypass leakage paths.

The twelve facility guide tubes are modeled as two lumped PIPE components, located in Rings 1 and 2 of the lower plenum. Both PIPEs are connected to FILL components simulating the guide tube steam injection. The sparger piping used in the facility to inject steam into the lower plenum is modeled with FILL/PIPE combinations for each radial rings in the lower plenum. The two facility inactive jet pumps are lumped together and modeled with a single TRACE TEE component. The side tube of the TEE component provides the LPCI FILL junction.

The TRACE break model was taken from the reference TRACB model (Ref. 7). PIPE 77 is modified to have 10 cells, and a single junction break valve (VALVE 79) is added to control the initiation of the transient.

The modeled ECCS includes LPCS and LPCI. The LPCS injection system is modeled as a PIPE/ FILL combination connected to the VESSEL upper plenum peripheral ring (Ring 3) at Level 12 (Figure C.9-3). The LPCI FILL is connected to the drive line of the recirculation loop. The ECCS FILL mass flow rates are modeled as function of the system pressure.

The boundary conditions to simulate the steam injection into the fuel bundles, guide tubes, and lower plenum are modeled with generalized FILL components. The steam injection rates and conditions are determined as a function of time according to the test data.

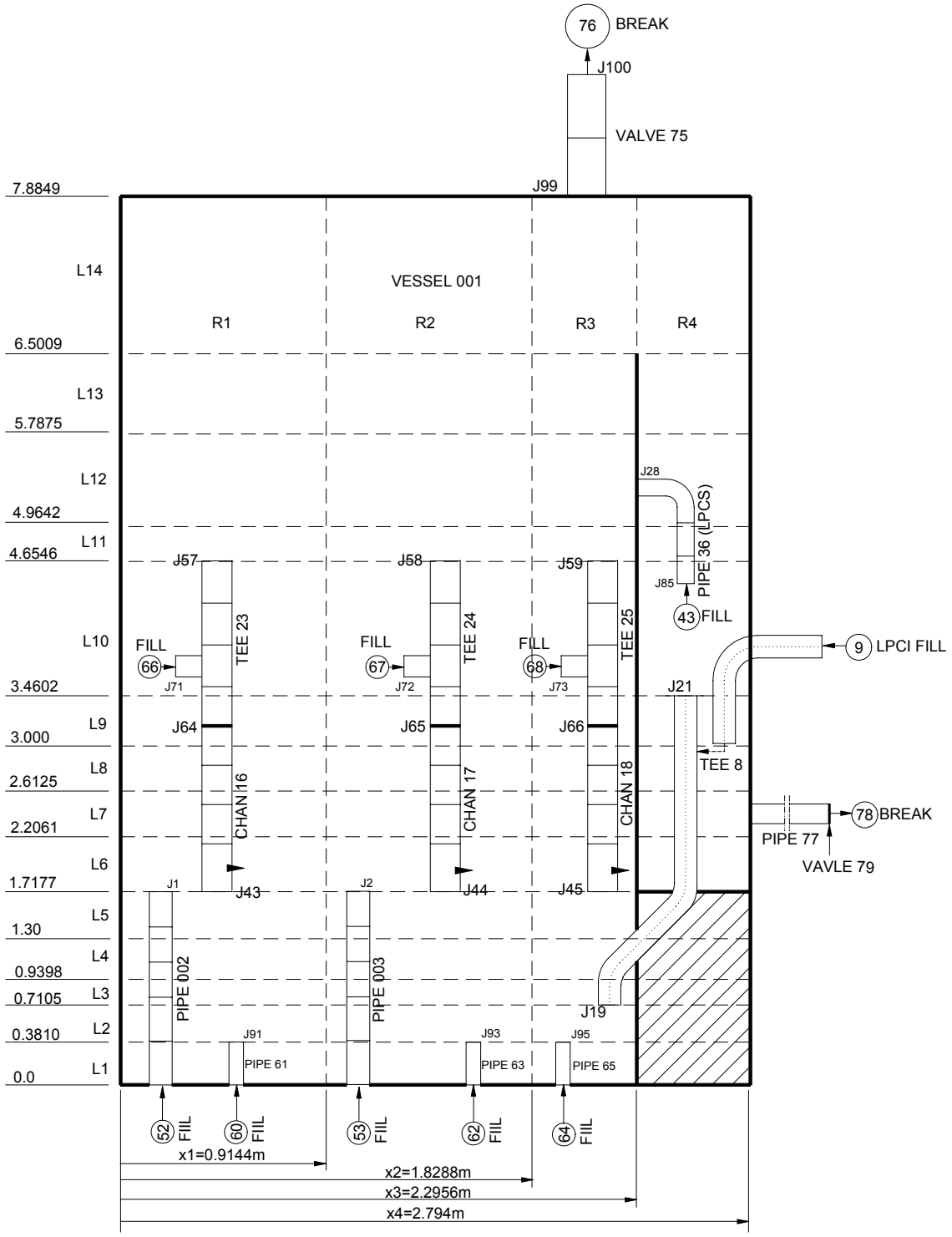

Figure C.9-3. TRACE SSTF Nodalization

Table C.9.2. Components in the SSTF TRACE Model

SSTF Test Section Regions	TRACE Component
SSTF 30-Degree Test Sector (Lower Plenum, Bypass, Downcomer, Upper Plenum, Steam Dome)	VESSEL 001
Channel Components	CHAN 016/TEE 023, CHAN 017/TEE024, and CHAN 018/TEE 025
BRW/4 Jet Pumps	TEE 008
LPCS	FILL 043, PIPE 036
LPCI	FILL 009
Vessel Steam Vent	VALVE 075, BREAK 076
Core Steam Injection	FILL 066, FILL 067 and FILL 068
Lower Plenum Steam Injection	FILL 060/PIPE 061, FILL 062/PIPE 063, and FILL 064/PIPE 065
Guide Tubes	PIPE 002, PIPE 003
Guide Tube Steam Injection	FILL 052, FILL 053
Break Unit	PIPE 077, VALVE 079, BREAK 078

C.9.4. Tests Simulated with TRACE

This section presents the TRACE simulation results of SSTF Test EA3.1 Run 111 and Test EA3.3-1 Run 119. Both tests were conducted to study the controlling phenomena during the refill/reflood phase of the BWR LOCAs. The initial conditions for the tests were typical for the refill/reflood phase. Test EA3.1 Run 111 simulated a 1.0-DBA break transient. Test EA3.3-1 Run 119 simulated a 0.73-DBA break transient. Otherwise, the test conditions for the two tests were essentially identical (Ref. 5). The controlled boundary conditions in the tests were ECCS injection flow rates, programmed as a function of the systems pressure, and steam injection decay curves.

In the experiment, the tests were initiated by activation of the test initiation sequencer control system which automatically activated key equipment actions (test loop isolation, opening of blowdown valve, activation of ECCS, etc.). The blowdown transient and resultant refill-reflood response proceeded without additional control system action until steady system conditions were achieved. In the remainder of this section, TRACE calculation results are compared with the test data.

C.9.4.1. Simulation of Test EA 3.1 Run 111

C.9.4.1.1. Test EA 3.1 Run 111 Initial Conditions

The TRACE simulation performs a 300-second steady-state calculation, followed by a 300-second transient calculation. The 300-second steady-state calculation generates the initial condition for the transient calculation. The calculated initial conditions are listed in Table C.9.3 for Test EA3.1 Run 111. As shown in the table, a majority of the parameters is within data uncertainty range. The core bundle initial mass is slightly outside the data uncertainty range. There is a large difference in the guide tube initial mass between the data and the TRACE calculation. With the current CCFL correlation constants and the geometry setup for the guide tube model, it was found that in the steady state calculation, the guide tube mass always settled at ~1273.6 Kg, given the steam injection flow equal to the test data. The guide tube was taken from the original TRACB model. Currently, the information available does not provide an adequate basis to change the guide tube model (e.g., CCFL correlation constants, geometry).

Table C.9.3. Test EA3.1 Run 111 Initial Conditions

Regions	**Data**[a]	**TRACE Calculated**
Vessel pressure (KPa)	1034.21	1035.31
Core steam flow (kg/s)	6.93	6.9206
Lower plenum steam flow (kg/s)	5.98	5.8812
Guide tube steam flow (kg/s)	3.91	3.9688
Upper plenum (kg)	0	15.42
Core bypass (kg)	373.0 ± 33	353.7
Core bundles (kg)	347.5 ± 33	415.88
Lower plenum (kg)	1618.0 ± 59.1	1593.64
Guide tubes (kg)	721.4 ± 51.3	1273.6
Annular downcomer (kg)	325.4 ± 13.3 (278.0[b])	271.3

a - Table 1, Reference 6
b - NRC databank file for SSTF Test EA3.1 Run 111

C.9.4.1.2. Test EA 3.1 Run 111 Transient Results

This section presents the transient results. The parameters of interest include the system pressure response, break flow, and mass distribution in the system.

System Pressure Response

The system pressure (the upper plenum pressure) response is shown in Figure C.9-4 The system pressure is underpredicted until 180 ascends when both the calculated system pressure and measured pressure approach the atmospheric pressure.

The system depressurization is the combined effect of system blowdown and steam condensation induced by ECCS injection. In this calculation, the overprediction in the depressurization rate is mainly caused by the condensation in the upper plenum as the result of the LPCS injection. The underpredicted liquid temperature in the lower plenum also contributes to the accelerated depressurization. Figure C.9-5 and Figure C.9-6 show the measured and calculated liquid temperatures in the periphery region and the apex region of the upper plenum along with saturated temperatures. It shows that LPCS injection results in large subcooling in the periphery region in the calculation in comparison to the test data. In the apex region, liquid temperature closely follows the saturation temperature both in the test and calculating. Figure C.9-7 and Figure C.9-8 give the liquid temperatures in the lower plenum. The underpredicted liquid temperature in the lower plenum is caused by the underpredicted temperature of LPCI injection liquid out of the JETP into the lower plenum as shown in Figure C.9-9

Figure C.9-10 and Figure C.9-11 show the ECCS response (LPCS and LPCI injection flow rates). The predicted ECCS injection flows agree well with the data.

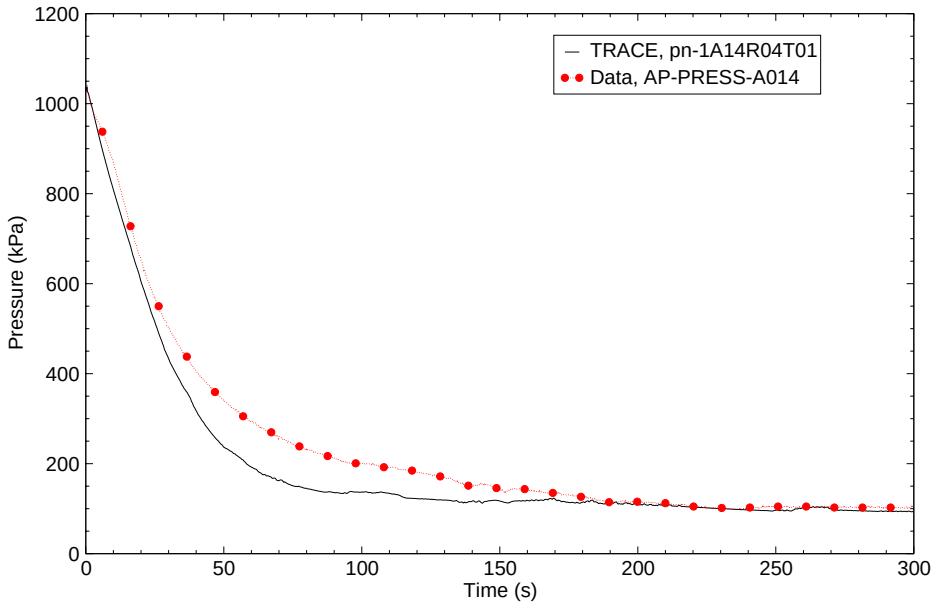

Figure C.9-4. SSTF EA3.1 Run 111 - System Pressure Response

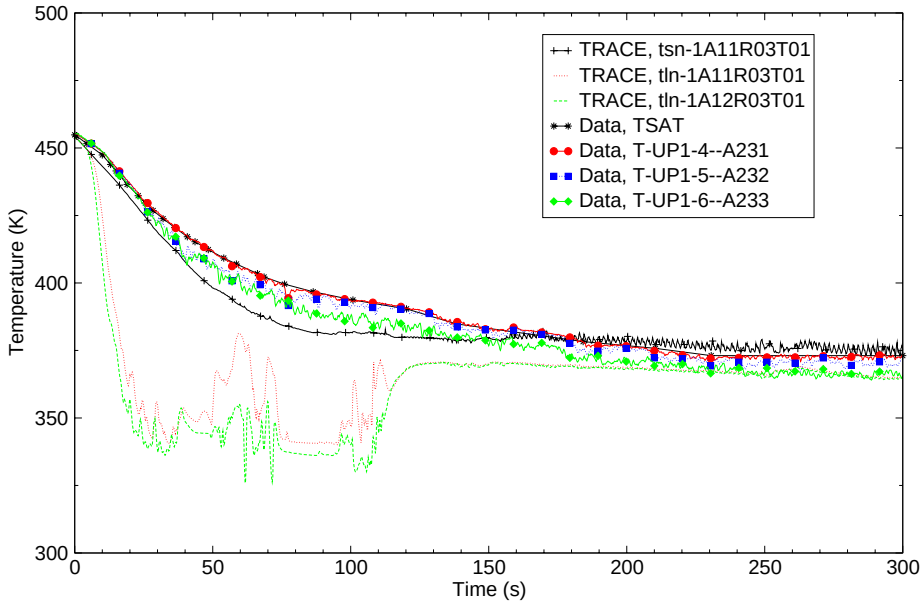

Figure C.9-5. SSTF EA3.1 Run 111 - Liquid Temperature in the Periphery of the Upper Plenum

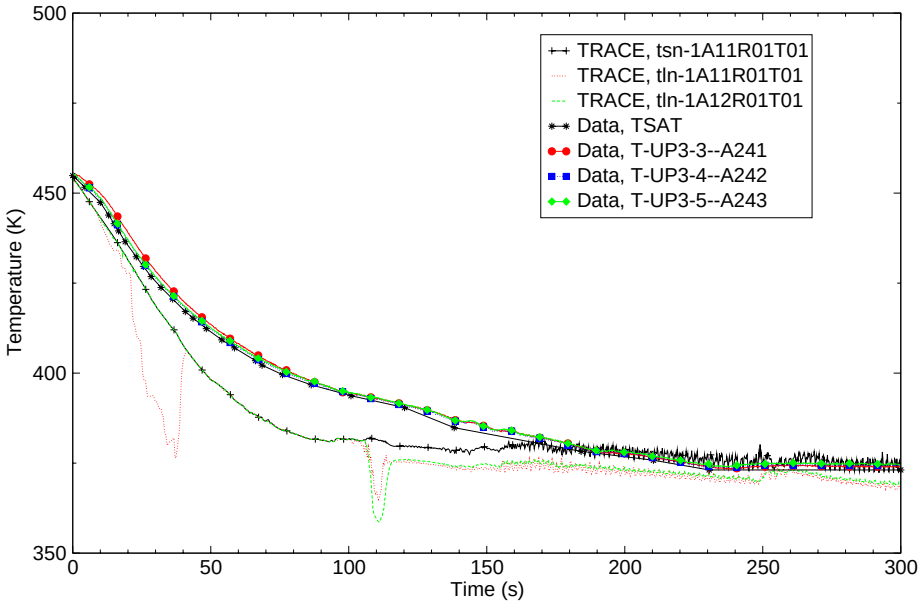

Figure C.9-6. SSTF EA3.1 Run 111 - Liquid Temperature in the Apex of the Upper Plenum

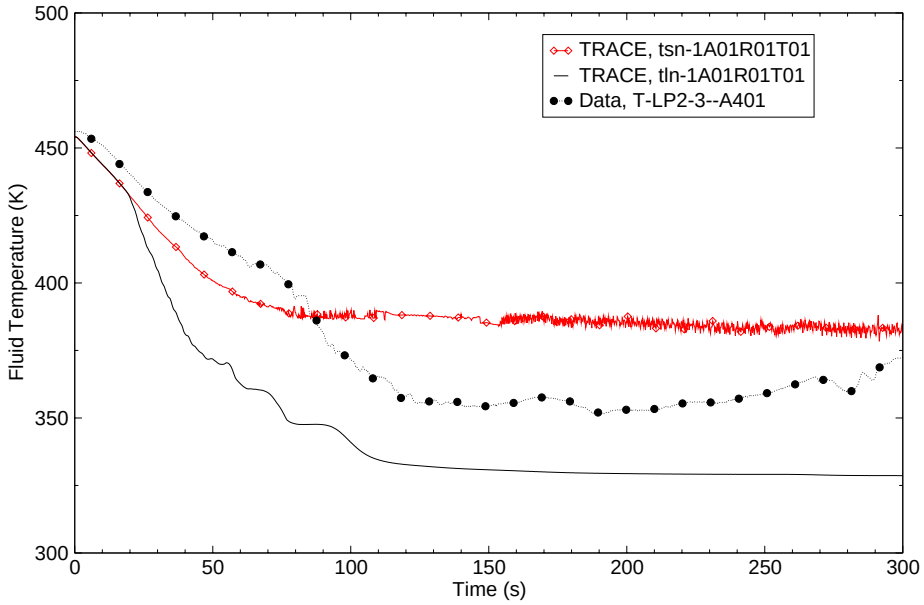

Figure C.9-7. SSTF EA3.1 Run 111 - Fluid Temperature in the Bottom Portion of Lower Plenum

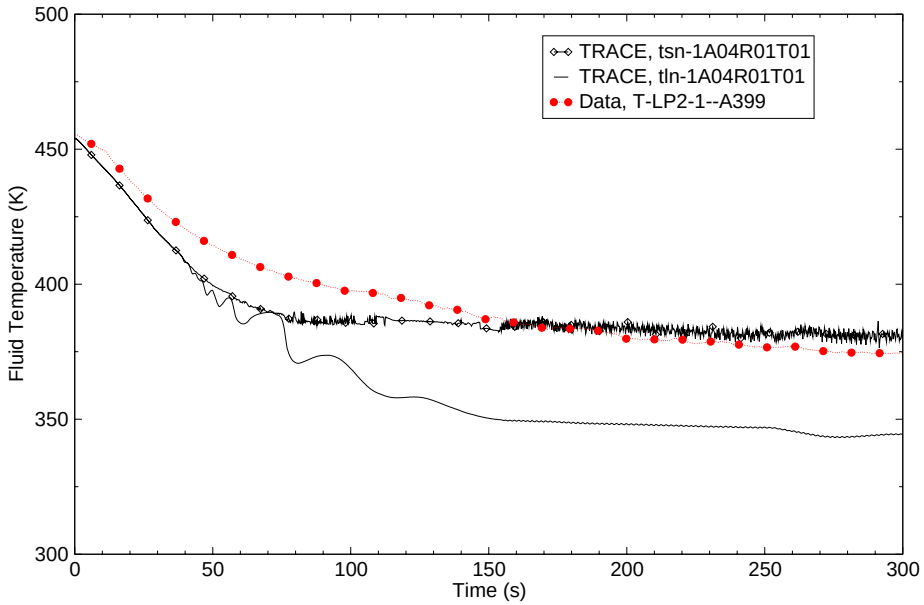

Figure C.9-8. SSTF EA3.1 Run 111 - Fluid Temperature in the Upper Portion of Lower Plenum

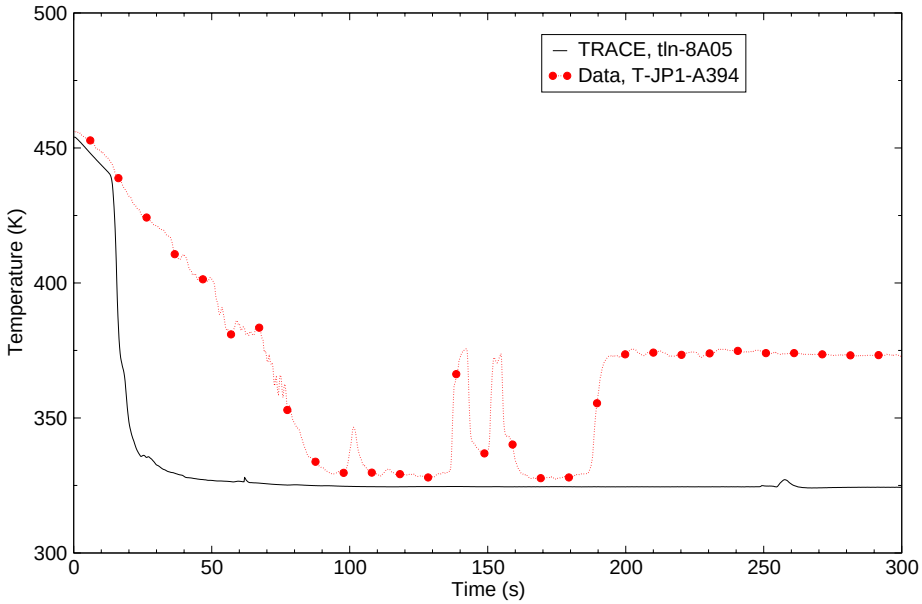

Figure C.9-9. SSTF EA3.1 Run 111 - Liquid Temperature at JETP Exit

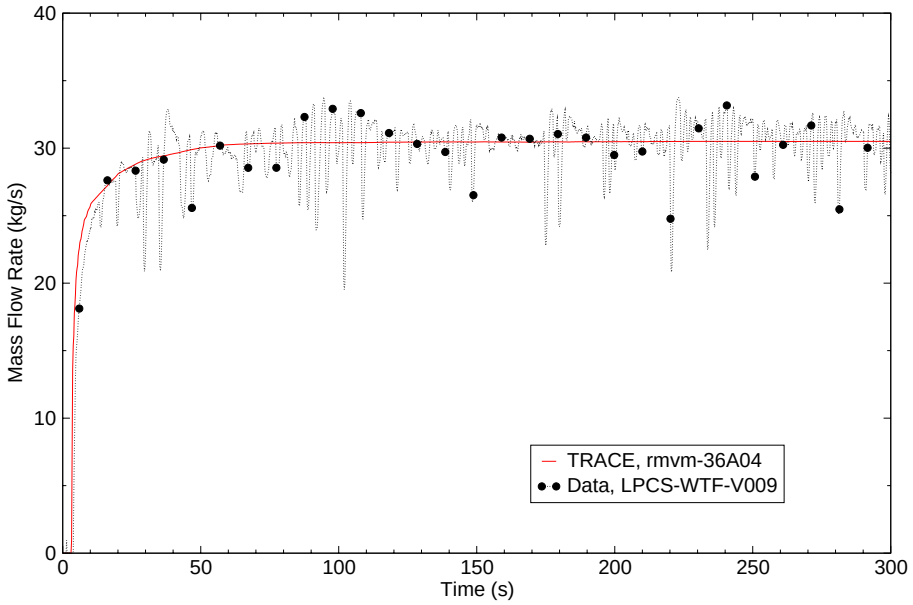

Figure C.9-10. SSTF EA3.1 Run 111 - LPCS Response

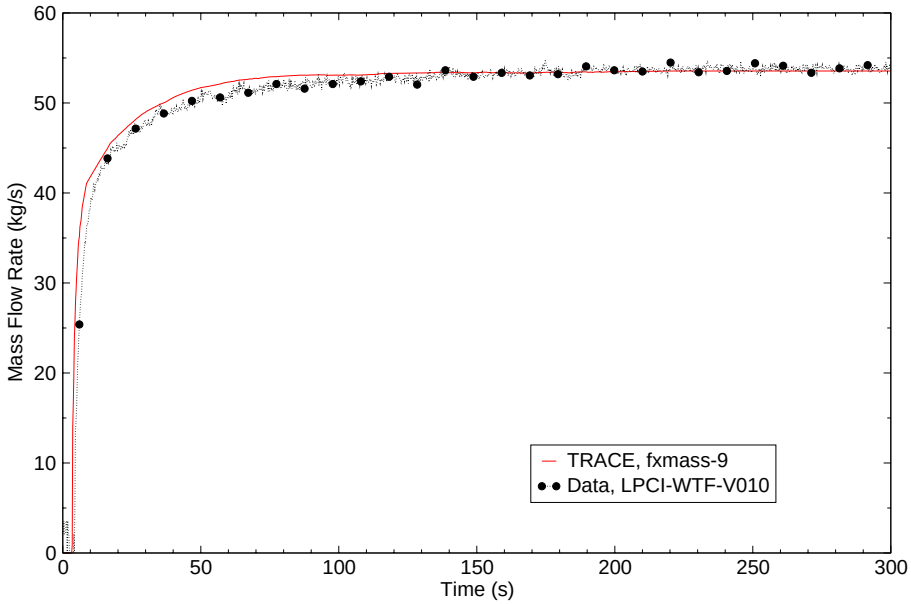

Figure C.9-11. SSTF EA3.1 Run 111 - LPCI Response

Break Flow

Figure C.9-12 shows the calculated break flow rate vs. the test data. The break flow rate is mainly affected by the void fraction in the downcomer at the recirculation line elevation. The predicted break flow is in good agreement in the first 90 seconds when the break flow is in the high void two phase or is single-phase steam. At ~90 seconds, the test data shows a sharp increase in the break flow rate while in the TRACE simulation the break flow increase is postponed until about 110 seconds. This occurs because, in the test, the transition from the single-phase to two-phase flow occurred around 90 seconds, while in the simulation this transition occurs at around 110 seconds after break, which is confirmed by the liquid levels both in the JETP and in the downcomer (Figure C.9-13 and Figure C.9-14).

Mass Distribution

This subsection presents the calculated mass distribution in the SSTF system, namely, the mass inventory change in the lower plenum, the bundle, the core bypass and the upper plenum. In the following discussion, both differential pressure (in centimeter water) and absolute mass (kg) are used to represent the mass inventory of each region. The mass inventory values are only available for the core and core bypass from the test data file.

Figure C.9-15 shows the differential pressures in the lower plenum region. Figure C.9-16 gives the TRACE calculated mass in the lower plenum region. According to Figure C.9-14, the predicted lower plenum differential pressures are in good agreement with the test data. (The

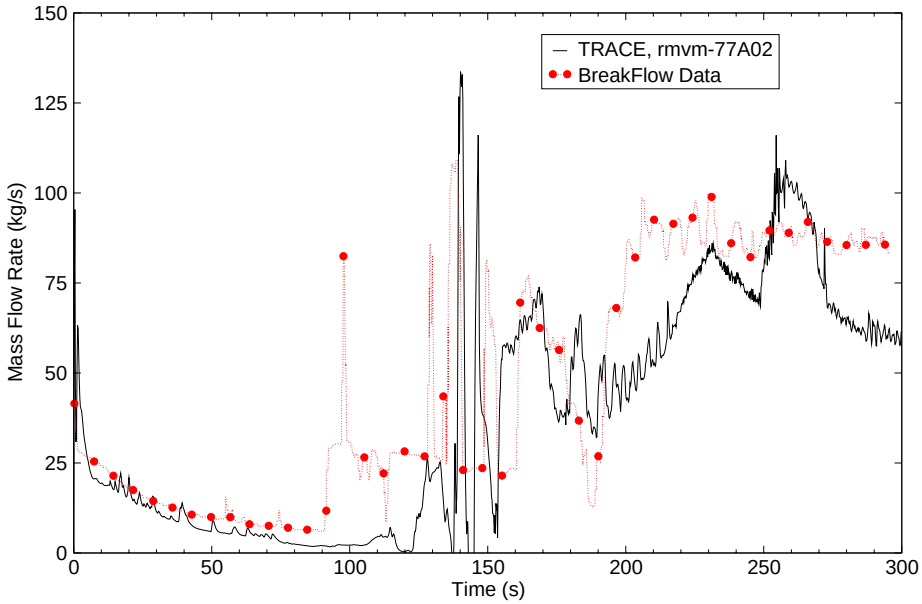

Figure C.9-12. SSTF EA3.1 Run 111 - Break Flow

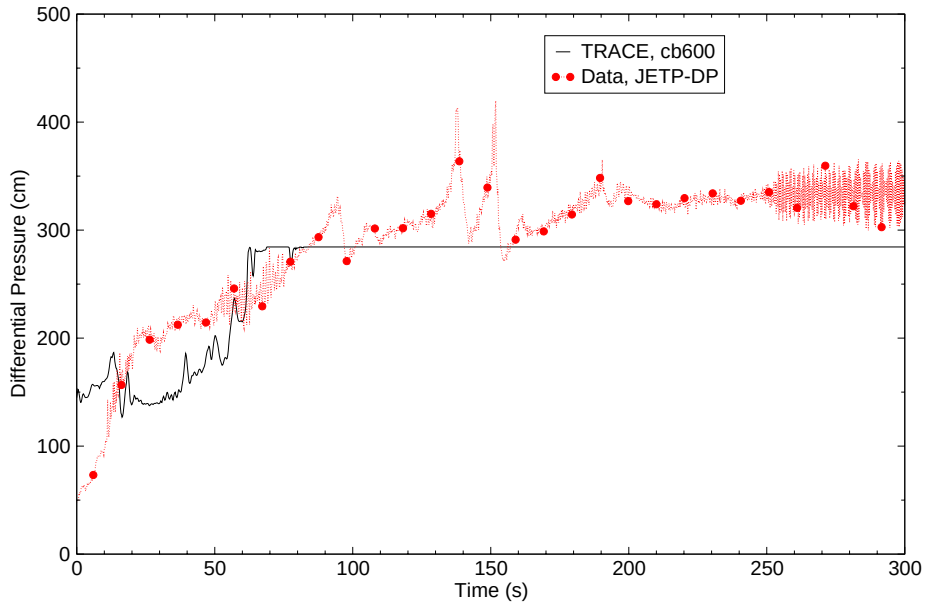

Figure C.9-13. SSTF EA3.1 Run 111 - JETP Differential Pressure

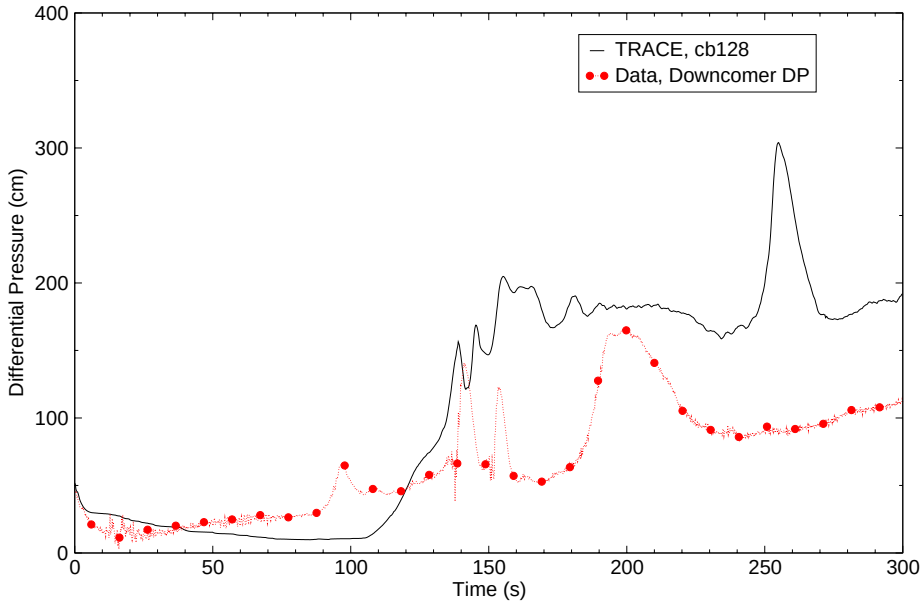

Figure C.9-14. SSTF EA3.1 Run 111 - Downcomer Differential Pressure

differential pressure taps for the periphery region covers ~1.25 m vs. ~1.5 m covered by the differential pressure taps for the apex and center regions of the lower plenum in the test facility.) The mass inventory experiences an initial decrease both in the data and in the calculation due to the system depressurization. A few seconds afterward, the mass starts to increase steadily with LPCI injection initiation. Around 80 seconds after break, the lower plenum completely fills with liquid.

Figure C.9-17 shows the calculated differential pressures in CHAN 16/TEE 23 (in the apex), CHAN 17/TEE 24 (in the middle) and CHAN 18/TEE 25 (at the periphery) along with the measured differential pressures in Bundles 54, 26 and 4 (Figure C.9-2). The calculated total mass in the bundles is shown along with the measured core mass in Figure C.9-18. In general, the calculated results follow the data trend well. The bundles start to fill shortly after the ECCS initiation and are completely filled at ~110 seconds both in the test and in the calculation. Figure C.9-17 also shows some discrepancies exists between the calculated results and the data. The data shows that the refill/reflood process in the three bundles (B54, B26 and B4) at the apex, middle and periphery is similar. In the calculation, the bundle refill at the periphery (CHAN 18/TEE 25) agrees well with the test data while the refill of the middle bundle (CHAN 17/TEE 24) and the apex bundle (CHAN 16/TEE 23) are delayed.

Figure C.9-19 shows the differential pressures in the core bypass region. Figure C.9-20 shows the mass inventory of the core bypass. The measured bypass differential pressures shows fluctuations for ~120-240 seconds. This is related to the refill process of the guide tube as shown in Figure C.9-21, which gives the differential pressure measurements in two guide tubes. The difference

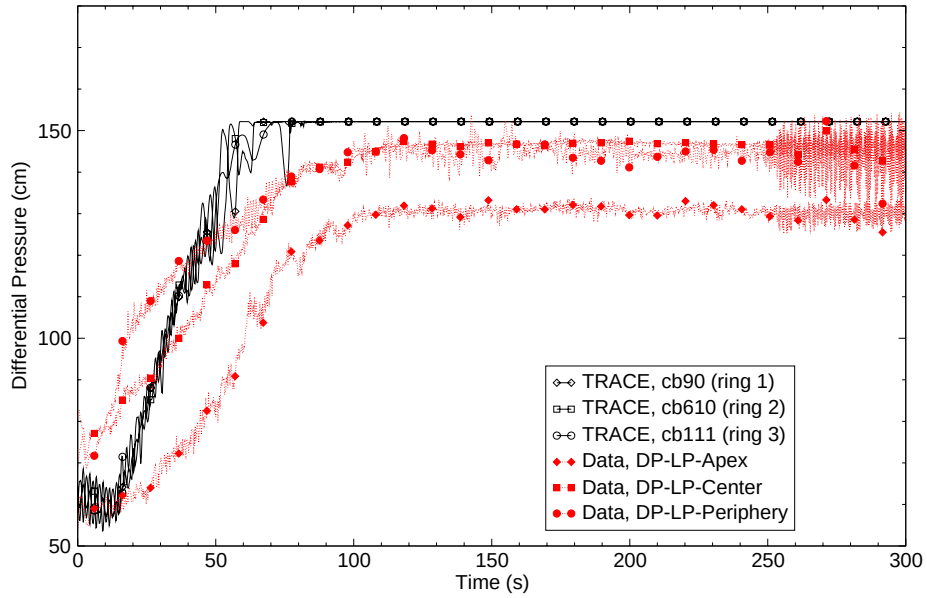

Figure C.9-15. SSTF EA3.1 Run 111 - Lower Plenum Differential Pressure

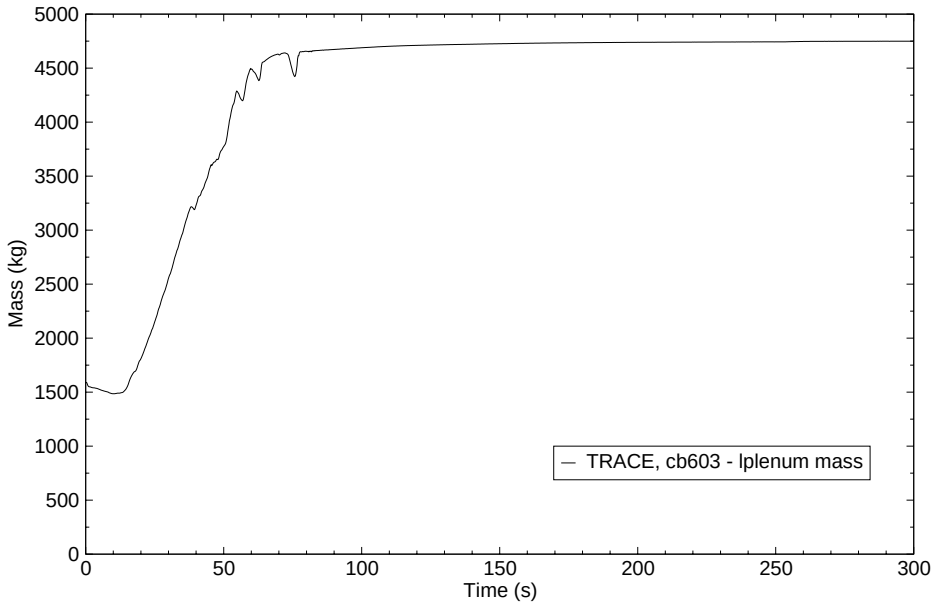

Figure C.9-16. SSTF EA3.1 Run 111 - Lower Plenum Mass

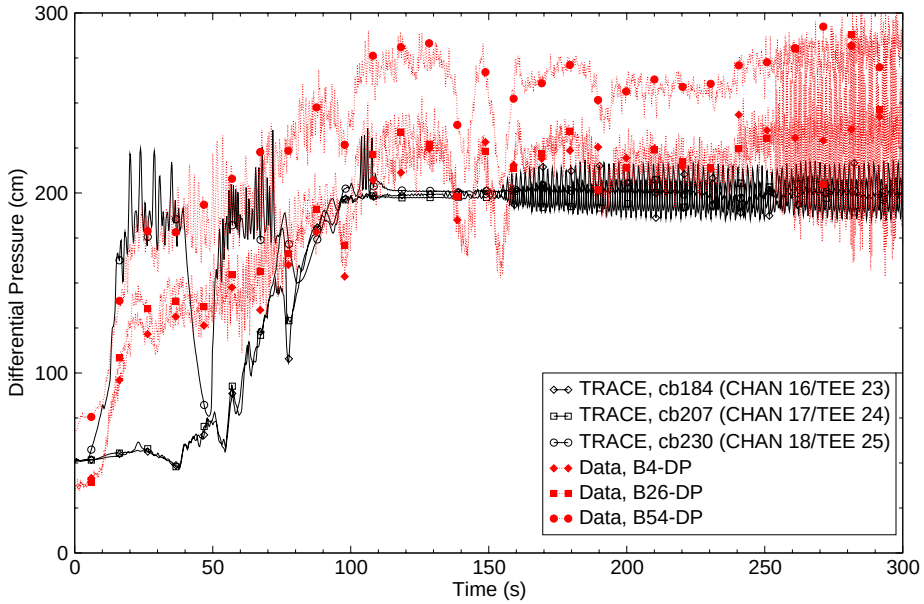

Figure C.9-17. SSTF EA3.1 Run 111 - Bundle Differential Pressure

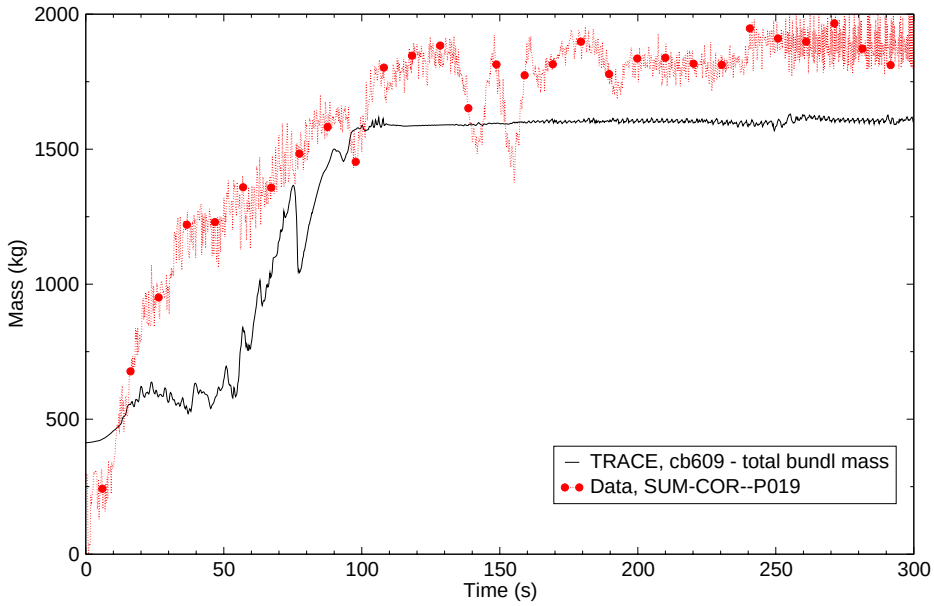

Figure C.9-18. SSTF EA3.1 Run 111 - Mass in the Bundle

between the calculated and measured guide tube differential pressures are attributed to the difference in the calculated and test initial condition in the guide tubes as shown in Table C.9.3.

The measured and calculated upper plenum liquid level is shown in Figure C.9-22, and Figure C.9-23 shows the calculated mass in the upper plenum. Figure C.9-22 gives the calculated and measured differential pressures in the apex and periphery regions of the upper plenum. The data shows that CCFL breakdown occurs at the upper core plate at ~90 seconds and the differential pressures in the apex and periphery regions follows a similar pattern. In the calculation, for the first ~70 seconds the differential pressure change in the periphery differs from that in the apex. Following the LPCS initiation, liquid starts to build up in the periphery region and CCFL breakdown at the upper core plate breakdown occurs at ~30 seconds in this region. The calculated differential pressure in the apex region indicates that there is almost no LPCS fluid mass propagating to this region until ~100 seconds. The calculated differential pressures indicate that liquid starts to build up after ~100 seconds and more liquid is accumulated in the upper plenum than that in the test, which is largely attributed to underprediction of the break flow rate from ~90 seconds afterward on average.

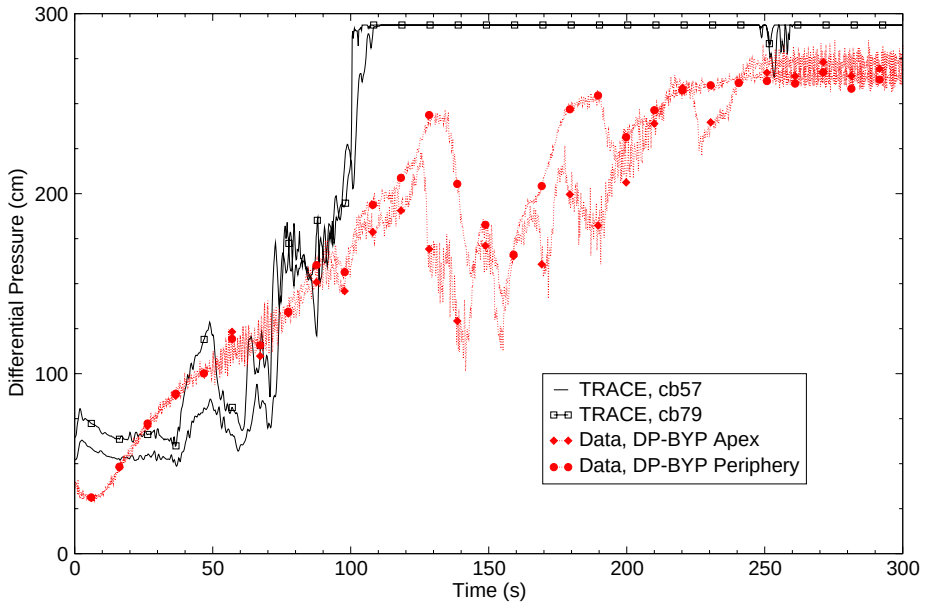

Figure C.9-19. SSTF EA3.1 Run 111 - Bypass Differential Pressure

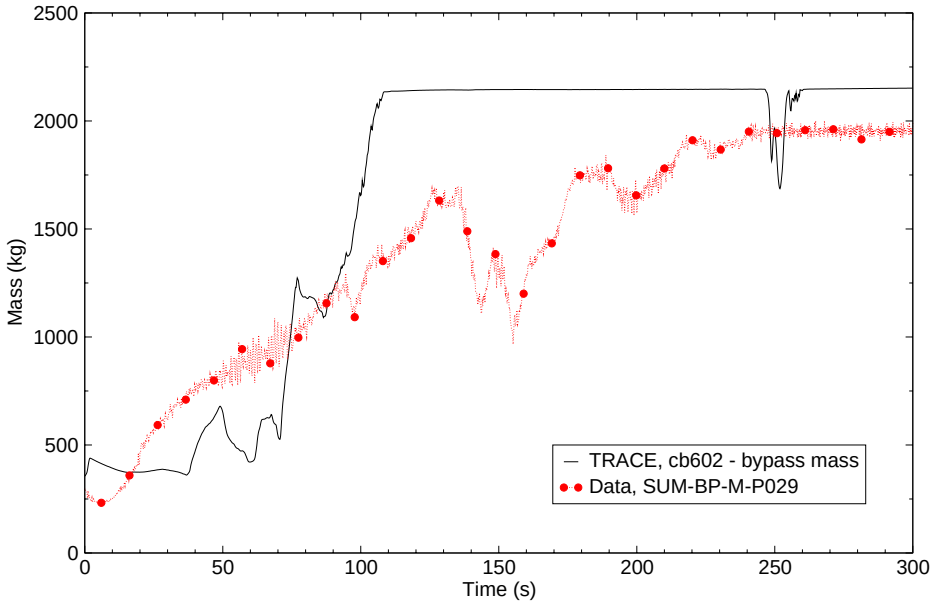

Figure C.9-20. SSTF EA3.1 Run 111 - Mass in the Bypass Region

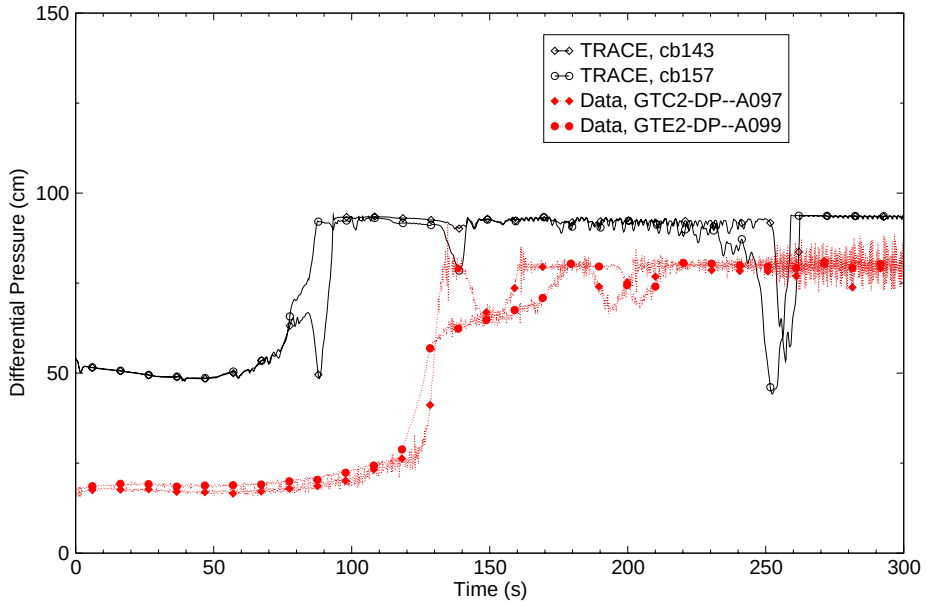

Figure C.9-21. SSTF EA3.1 Run 111 - Guide Tube Differential Pressure

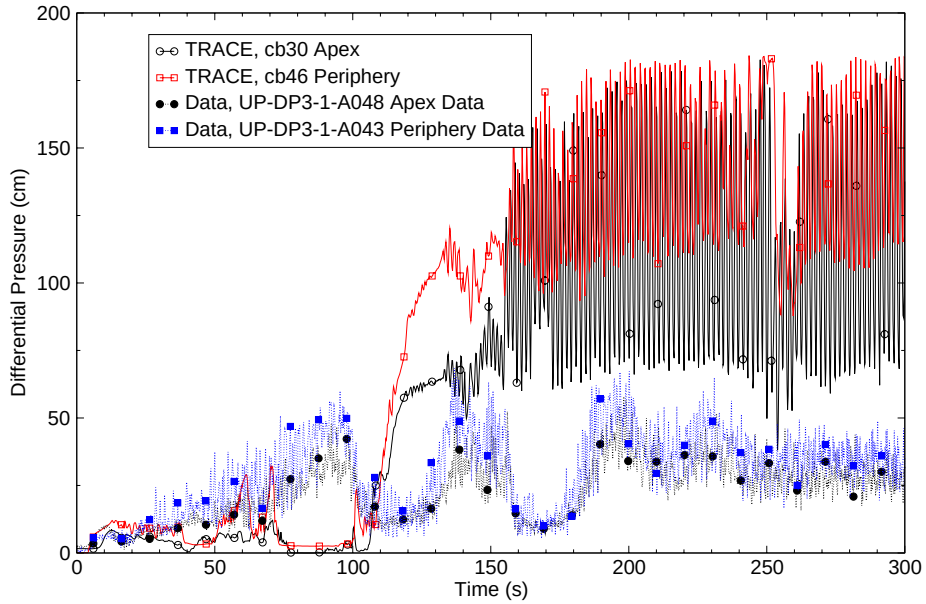

Figure C.9-22. SSTF EA3.1 Run 111 - Upper Plenum Differential Pressure

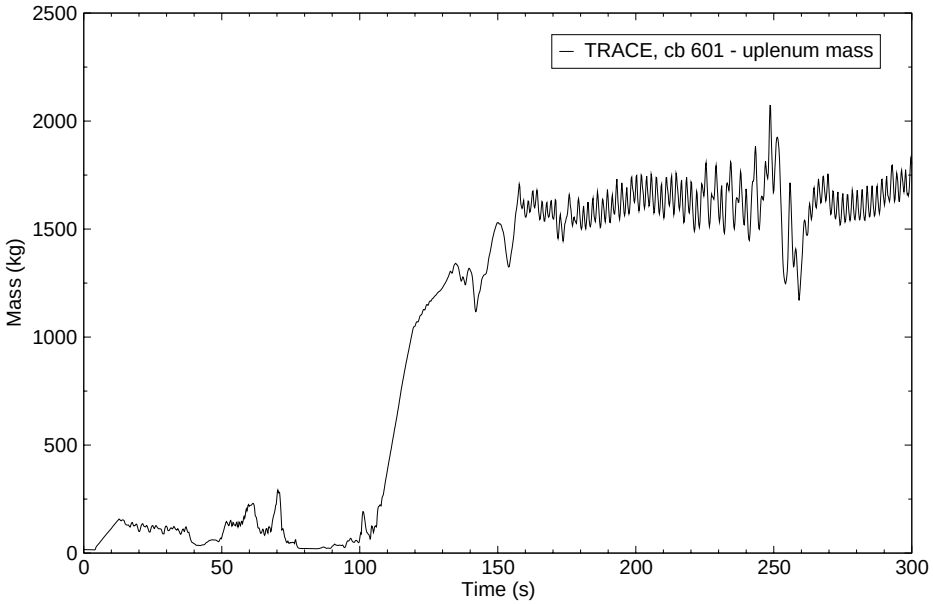

Figure C.9-23. SSTF EA3.1 Run 111 - Mass in the Upper Plenum

C.9.4.2. Simulation of Test EA3.3-1 Run 119

C.9.4.2.1. Test EA 3.3-1 Run 119 Initial Conditions

The TRACE calculated initial conditions for EA3.3-1 Run 119 are listed in Table C.9.4 in comparison with the test data. As shown in the table, the calculated values are in good agreement with the data except for the guide tube mass inventory. The TRACE initial conditions are satisfactory for the transient simulation of Test EA3.3-1 Run 119.

Table C.9.4. Test EA3.3-1 Run 119 Initial Conditions

Regions	Data	TRACE Calculated
Vessel pressure (KPa)	1024.5[a]	1025.26
Core steam flow (kg/s)	6.93[b]	6.921
Lower plenum steam flow (kg/s)	5.44[b]	5.351
Guide tube steam flow (kg/s)	3.128[b]	3.175
Upper plenum (kg)	21.5[a]	12.84
Core bypass (kg)	329.0 ± 33 a	312.76
Core bundles (kg)	370.2 ± 33 a	384.73
Lower plenum (kg)	2156.5 ± 59.1 a	2079.86
Guide tubes (kg)	1109.0 ± 51.3 a	1364.04
Annular downcomer (kg)	158.9 ± 13.3 a	159.1

a - NRC data bank file for Test EA3.3-1 Run 119; the uncertainty ranges in mass inventory are assumed to be the same as in Test EA3.1 Run 111 (Table C.9.3)

b - Table A-4, Reference 2

C.9.4.2.2. Test EA 3.3-1 Run 119 Transient Results

As mentioned on page C-505, Test EA 3.3-1 Run 119 was essentially identical to EA 3.1 Run 111, except for the break size. The smaller break size in EA 3.3-1 Run 119 causes the system to depressurize more slowly. However, the overall impact of the break size has no pronouced effect on the system refill-reflood response (Ref. 5). The TRACE calculation results for EA 3.3-1 Run 119 show similar performance as for EA 3.1 Run 111. Therefore, this section will not repeat the discussion but presents the plots of major parameters. The plots presented in this section include:

1. Figure C.9-24 - System pressure response

2. Figure C.9-25 - Break flow: the measured break flow rate is not available from the test data file.

3. Figure C.9-26 through Figure C.9-29 - Mass in the lower plenum, core, core bypass and upper plenum regions: the test data is available for the mass in these regions; therefore, the differential pressure plots are not presented.

4. Figure C.9-30 and Figure C.9-31 - LPCS and LPCI injection flow rates.

C.9.5. Assessment Results Summary

Two SSTF system effect tests (EA3.1 Run 111 and EA3.3-1 Run 119) were simulated using TRACE Code Version 5.0. The simulation results generally agree reasonably well with the test data.

The major deviations in both simulations (e.g., underpredicted pressure, bundle refill, CCFL breakdown timings at the upper core plate) are attributed to LPCS injection. An improved LPCS model that generates a more realistic LPCS injection liquid distribution in the upper plenum is expected to improve the simulation globally.

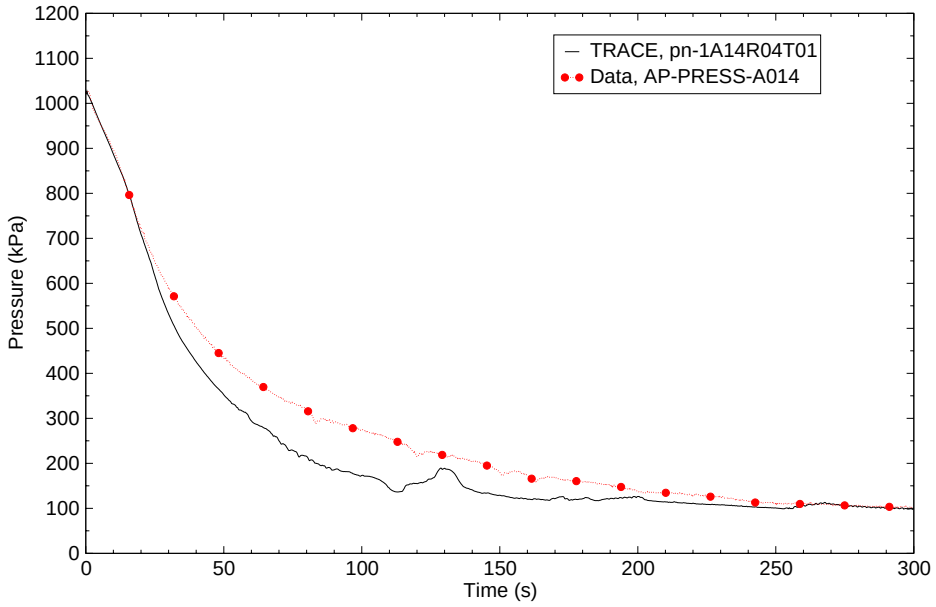

Figure C.9-24. SSTF EA3.3.1 Run 119 - System Pressure Response

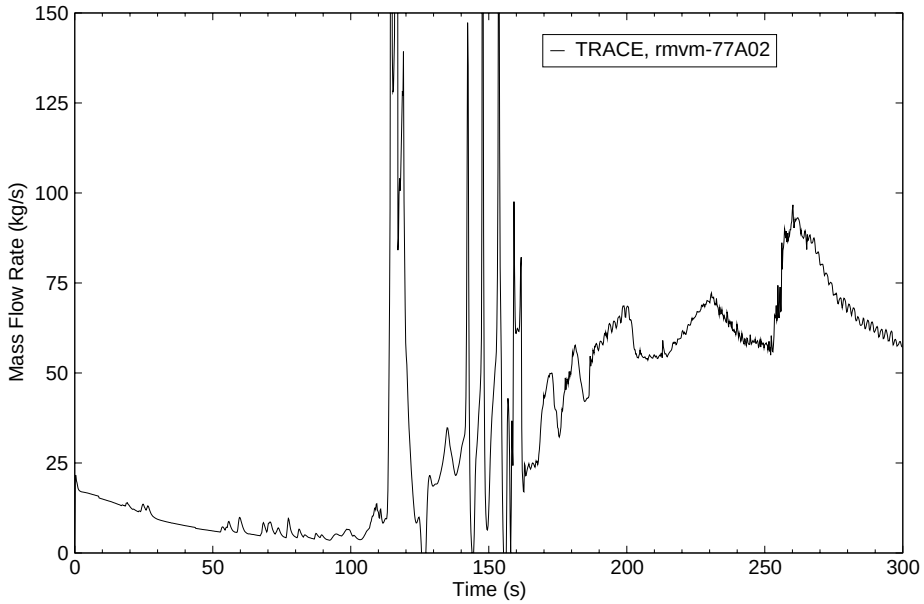

Figure C.9-25. SSTF EA3.3.1 Run 119 - Break Flow

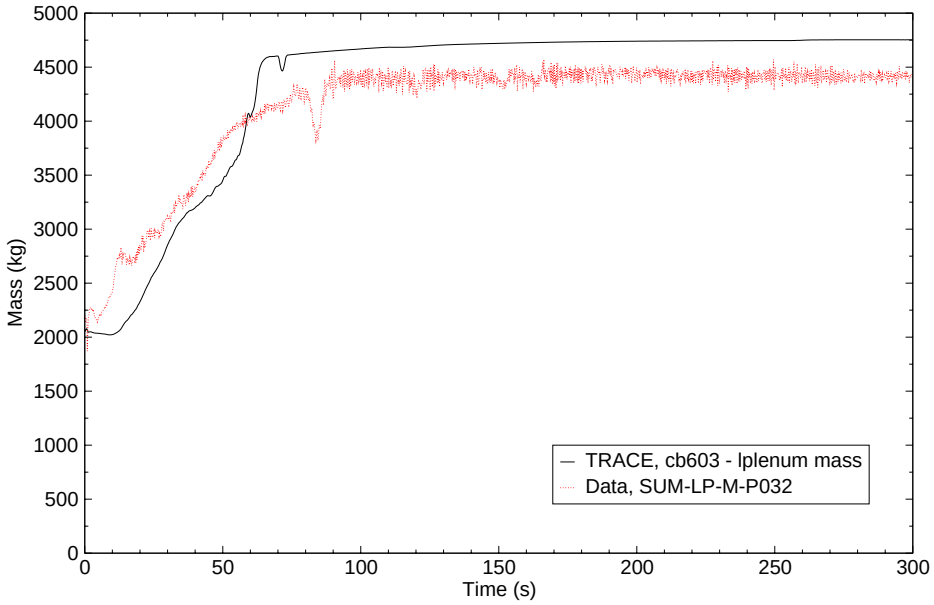

Figure C.9-26. SSTF EA3.3.1 Run 119 - Lower Plenum Mass

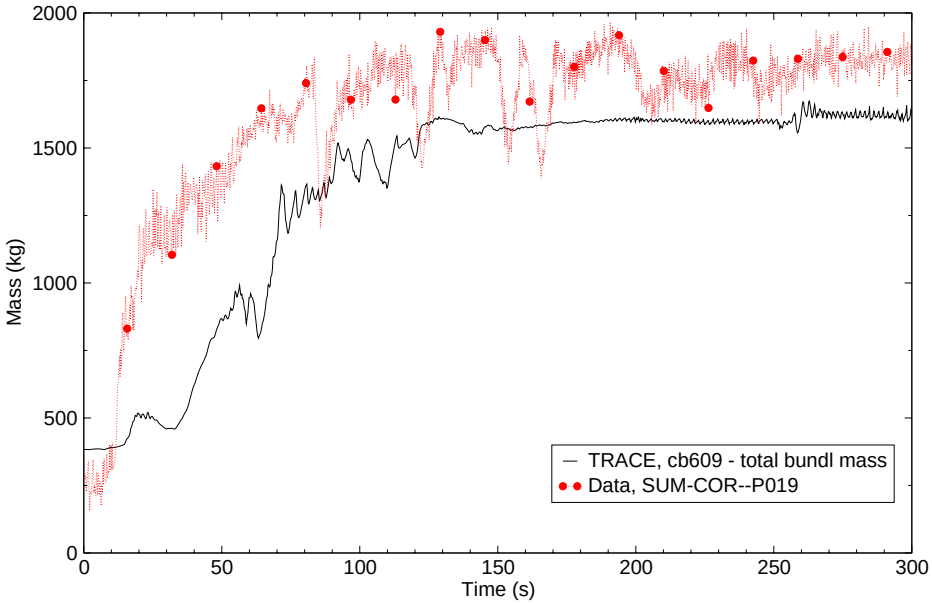

Figure C.9-27. SSTF EA3.3.1 Run 119 - Mass in the Bundle

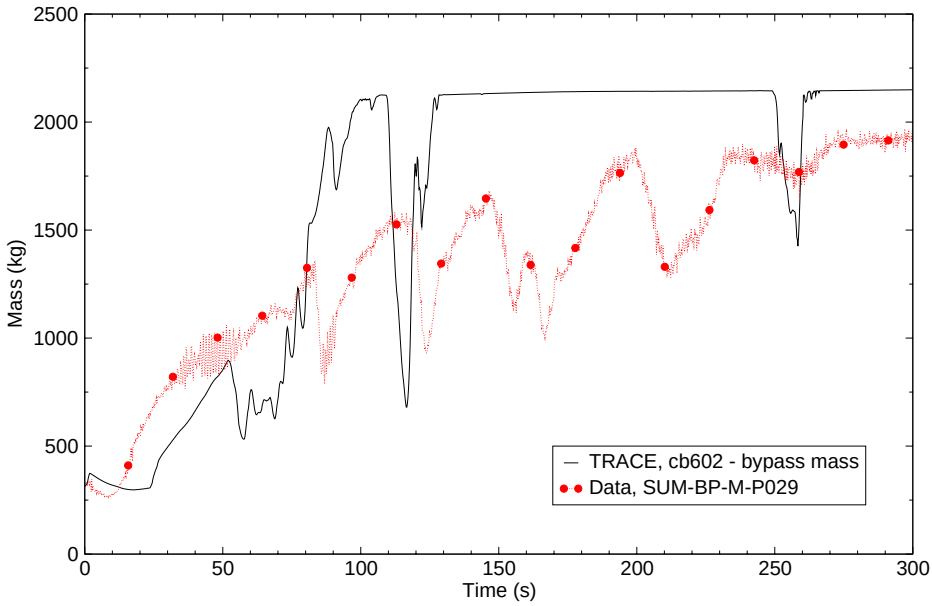

Figure C.9-28. SSTF EA3.3.1 Run 119 - Bypass Mass

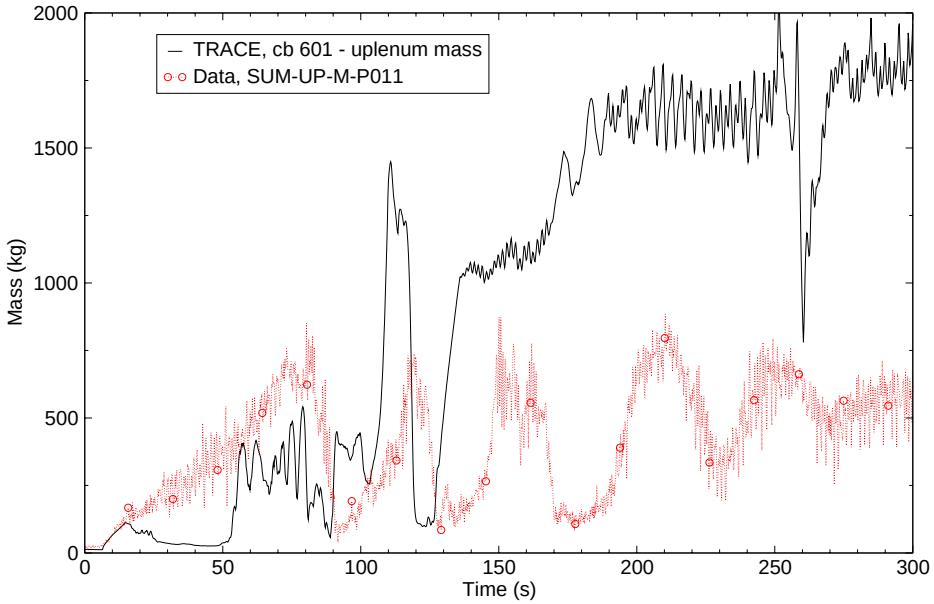

Figure C.9-29. SSTF EA3.3.1 Run 119 - Upper Plenum Mass

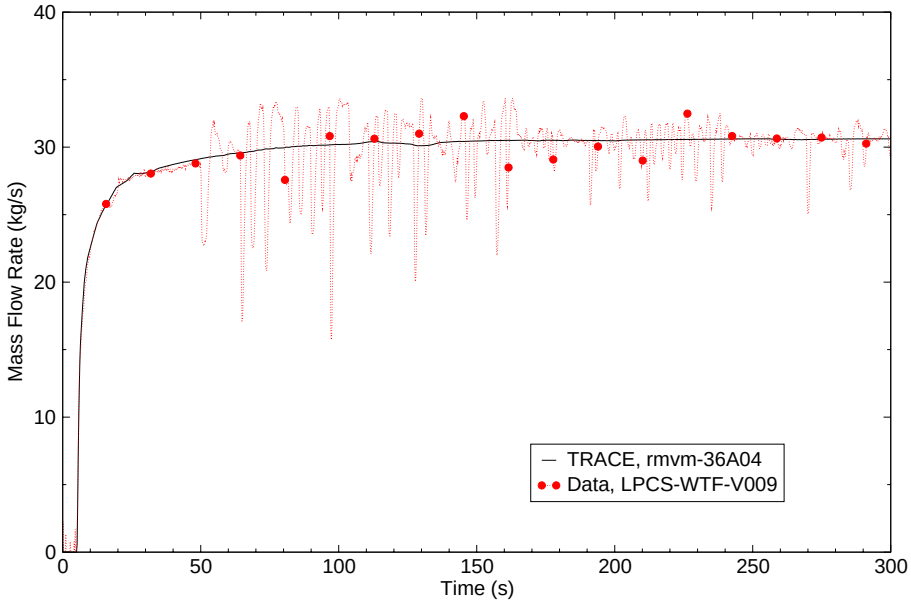

Figure C.9-30. SSTF EA3.3.1 Run 119 - LPCS Response

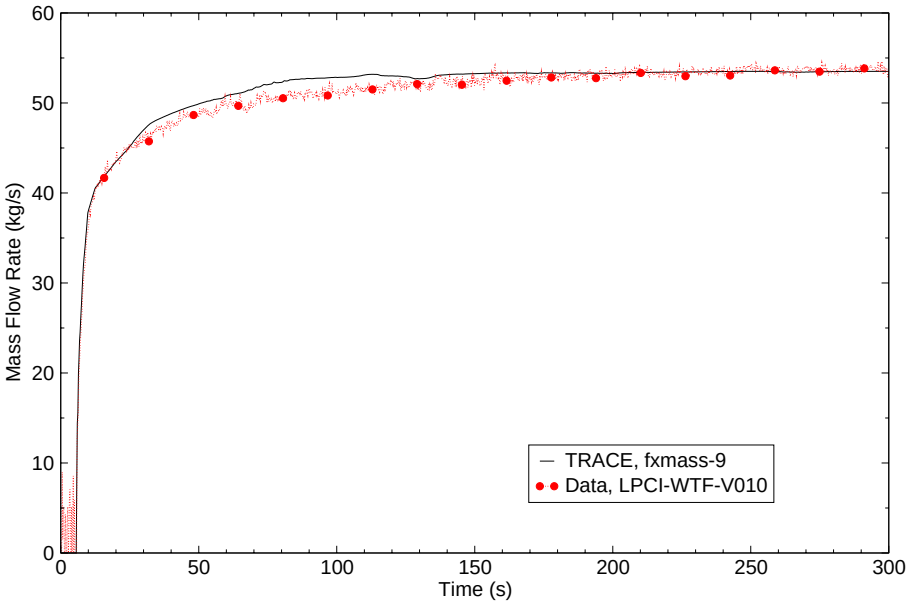

Figure C.9-31. SSTF EA3.3.1 Run 119 - LPCI Response

C.9.6. References

1 D. G. Schumacher, “BWR Refill-Reflood Program Task 4.4 - CCFL/Refill System Effects Tests (30^{o} Sector) - Experimental Task Plan”, NUREG/CR-1846, July 1981.

2 T. Eckert, "SSTF Operational Summary Report", DTR 516.8206, General Electric, June 1982.

3 Mati Merio, "BWR Refill-Reflood Program 30^{o} SSTF Facility Description", NUREG/CR-2133, Interim Report, September 1982.

4 J. A. Findlay, “BWR Refill-Reflood Program Task 4.4 - CCFL/Refill System Effects Tests (30^{o} Sector), Evaluation of ECCS Mixing Phenomena”, NUREG/CR-2786, May 1983.

5 D. G. Schumacher, et al, “BWR Refill-Reflood Program Task 4.4 - CCFL/Refill System Effects Tests (30^{o} Sector) SSTF System Response Test Results”, NUREG/CR-2568, April 1983.

6 James Low, "TRAC-BD1 (Version 12) Assessment Using SSTF BWR/4 Data", EGG-NTAP-6298, May 1983.

7 Mark A. Bolander, et al, “Simulation of Steam Sector Test Facility Test EA3.1 Run 111 - Report Task Order No. 6 Task 4", ISL, February 2003.

C.10. FIST Tests 6SB2c and 6SB1

Author(s): Millan Straka, Weidong He, and David Ebert

Affiliation: AdSTM

Code Version: TRACE V5.0

Platform and Operating System: Intel x86, Windows XP

C.10.1. Introduction

A series of BWR integral simulation tests performed in the Full Integration Simulation Test (FIST) facility (Refs 1, 2) provides test data that can be used to assess thermal-hydraulic system codes. The objective of this work is to compare the calculations from one such code, TRACE, against the data from selected FIST tests. In particular, the two tests simulated were: 1) Test 6SB2C - 0.05 ft^2 recirculation line break without High Pressure Core Spray (HPCS), and 2) Test 6SB1 - similar to Test 6SB2C, but with a stuck open Safety Relief Valve (SRV) in addition.

C.10.2. Test Facility Description

The FIST facility was scaled to a GE BWR/6-218 standard plant (Ref. 2). The test facility flow schematic is presented in Figure C.10-1 and the key vessel fluid volumes in Figure C.10-2. The FIST height was full scale, but its fluid volumes and flow areas were scaled 1/624. This corresponds to a single bundle in FIST versus 624 in a BWR/6. Therefore, the bundle fluid flow conditions can be considered typical of a BWR/6. The only significant compromise in scaling had to be made with the overscaling of the FIST vessel metal mass and therefore stored heat. (The vessel metal mass of the facility was several times greater than scaling a BWR/6.)

The full-size bundle with electrically heated rods simulated the reactor fuel assembly. A centrifugal separator with a dryer provided steam-water separation with pressure drop characteristics of a BWR/6. The FIST facility included two recirculation loops, each driving its own jet pump housed in the downcomer pipe, external to the main vessel. Blowdown piping lines were included in one of the recirculation loops to simulate the recirculation loop pipe breaks.

The feedwater system provided capability for steady-state operation, capable of delivering a make-up water at BWR rated temperature and scaled flow rates. Other systems included in the facility simulated Reactor Core Isolation Cooling (RCIC), High Pressure Core Spray (HPCS),

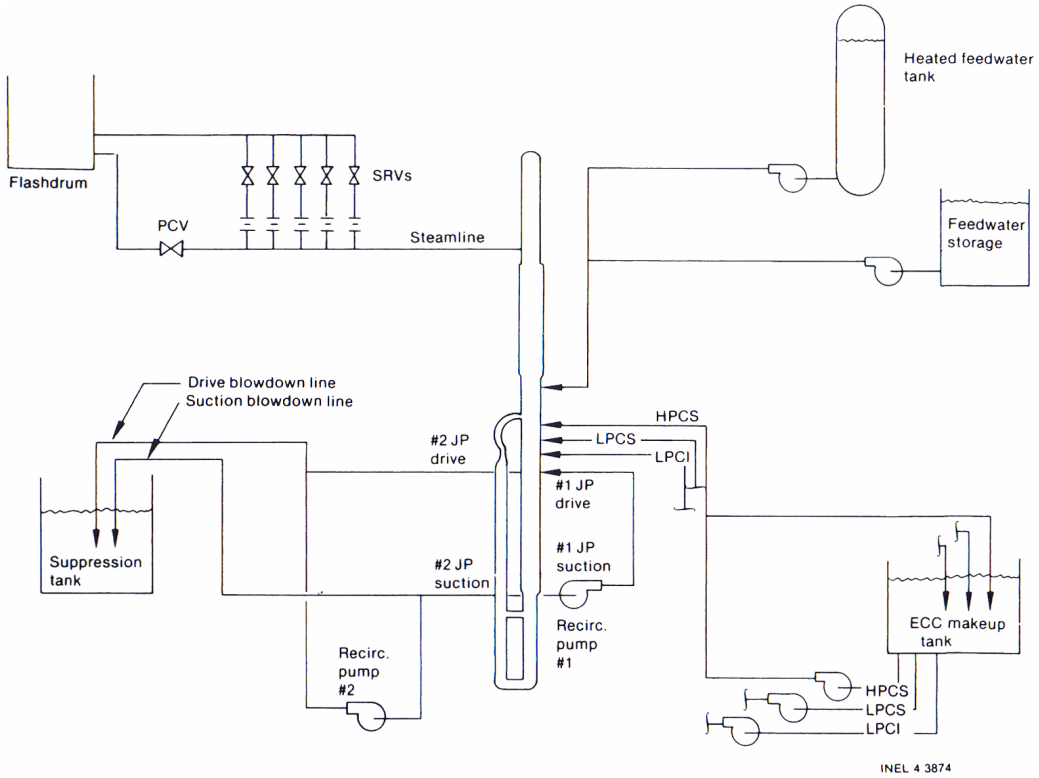

Figure C.10-1. FIST Test Facility Flow Schematic

Low Pressure Core Spray (LPCS) and Low Pressure Coolant Injection (LPCI) systems. The Safety Relief Valves (SRV) and Automatic Depressurization System (ADS) were also included with scaled flow areas and pressure set-points typical of a BWR/6.

A complete description of the facility, its instrumentation, and data acquisition can be found in the facility description report (Ref. 2).

C.10.3. TRACE Model Description

A sketch of the TRACE model used in the simulations is shown in Figure C.10-3. This model was developed from an older model used during assessment of an earlier TRACE version (then called TRAC-M) (Ref. 3). The model has 67 components and 32 junctions. The FIST vessel is described with the TRACE component VESSEL with 2 radial rings. The 1-D components inside the VESSEL component are a guide tube (PIPE), one BWR channel (CHAN), a separator (SEPD), and two jet pumps (JETP). Each recirculation loop has one pump (PUMP) and two isolation valves (VALVE). Both valves are tripped closed 20 seconds into the transient to trap excess fluid and improve scaling. In addition, the broken loop uses the TEE components in order to connect a PUMP suction and a PUMP discharge break simulation.

A detail of the nodalization used in the CHAN component is shown in Figure C.10-4 below.

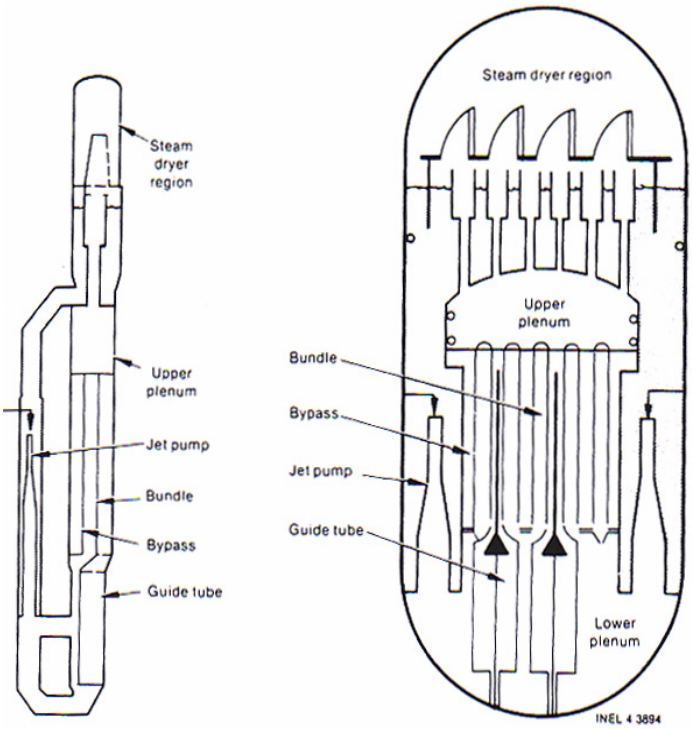

Figure C.10-2. FIST Vessel Fluid Volumes

C.10.4. Tests Simulated with TRACE

Both FIST tests simulated a BWR/6 recirculation suction line break of 0.05 ft^2 with HPCS assumed to be unavailable. (Test 6SB1 had, in addition, stuck open one SRV.) It is noted that since the initial bundle power levels are different, some of the initial conditions are also different.

Since the system response during these two test is very similar, Test 6SB2C will be briefly described with differences between the two tests noted later. After achieving steady-state in desired conditions, the test was initiated with opening of the break valve, start of bundle power decay, trip of the recirculation pumps, and trip of feedwater. When the setpoint water level low (L1) in the downcomer (DC) was reached, the main steam isolation valve (MSIV) was closed, and the ADS activated. After reaching the respective low pressure setpoints, LPCS and LPCI began to inject ECC water. Decrease in the DC water level and bundle is due to depletion of water through the pipe break and steam production.

The ADS actuation lead to flashing and significant level swell initially, but the mixture level receded as the depressurization rate decreased. Further decrease of the mixture level lead to a bundle uncovery with subsequent heater rod dryout. Upon initiation of LPCS and LPCI the bundle started to reflood - mainly via leakage from the bypass and upper plenum core spray (after the counter current flow limit, CCFL, at the upper tie plate broke down). After the bundle was

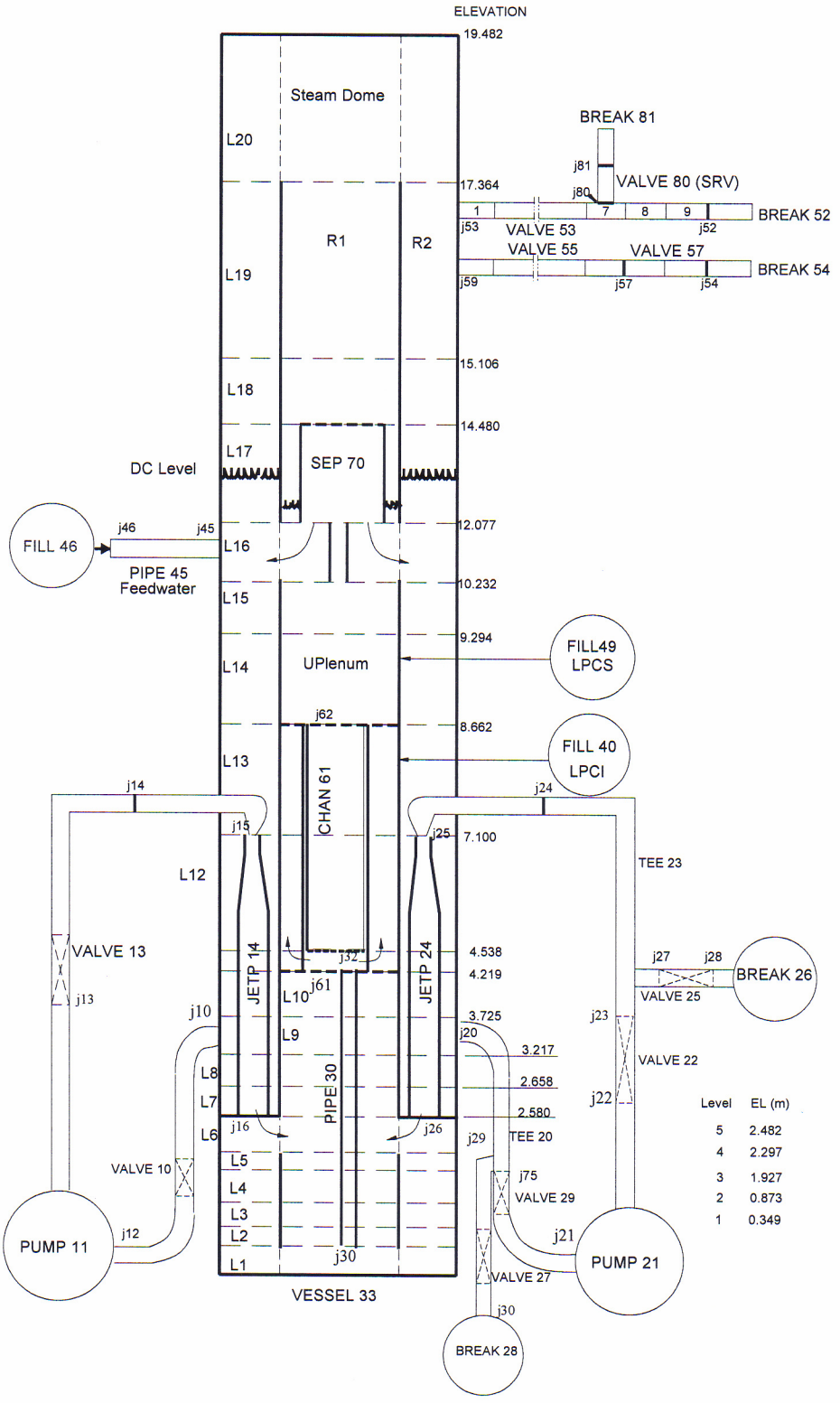

Figure C.10-3. TRACE Model Sketch

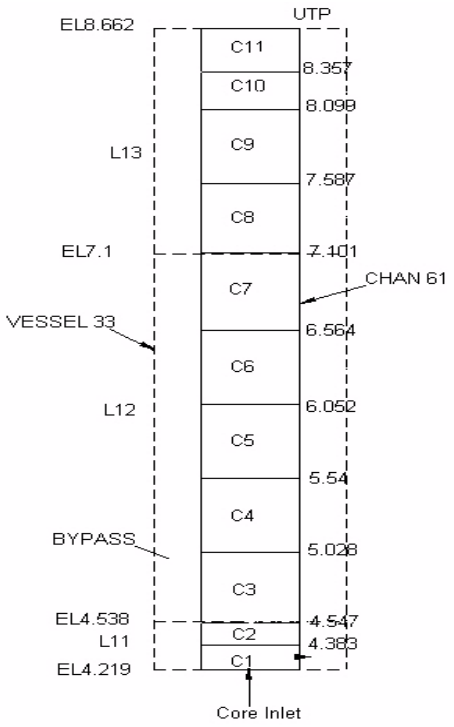

Figure C.10-4. FIST Channel Component Nodalization (all dimensions in m)

reflooded, the subcooled ECC water arrived at the core inlet causing a CCFL breakdown at the side entry orifice (SEO) which in turn enabled a lower plenum refill.

In Test 6SB1, one SRV was opened 45 sec after the MSIV closure (but before the ADS actuation). It remained open for the rest of the transient. Similarly to 6SB2C, bundle uncovery caused rods to heatup, but it was less severe - mainly due to a lower power in this test (4.64 MW versus 5.05 MW in 6SB2C).

The sequence of controlling events for each respective test and its TRACE simulation are presented in Table C.10.2 and Table C.10.4.

C.10.4.1. Simulation of Test 6SB2C

The steady-state FIST conditions before the test and conditions reproduced by the 6SB2C TRACE model are shown in Table C.10.1.

Table C.10.1. Parameters for Test 6SB2C

Parameter	Test 6SB2C	TRACE
Bundle power, MW	5.05 ± 0.01	5.05
Steam dome pressure, MPa	7.23 ± 0.05	7.23
Core flow, kg/s	19.05 ± 0.10	19.04
Channel flow, kg/s	not given	18.83
Bypass flow, kg/s	not given	1.55
Downcomer water level[a], m	10.8 ± 0.10	10.8
Steam flow rate, kg/s	2.62 ± 0.03	2.68
Feedwater flow rate, kg/s	2.62 ± 0.05	2.69
Feedwater temperature, K	484 ± 2	484
Jet pump 1 flow rate, kg/s	8.85	8.84
Jet pump 2 flow rate, kg/s	10.2	10.2
Downcomer temperature, K	550.9 ± 2	551.6
ECCS temperature, K	305.4	305.4
HPCS pump	off	off
LPCS pump	on	on
LPCI pump	on	on

[a] relative to the lower jet pump support plate

The sequence of key events and the comparison between the test and TRACE are shown in Table C.10.2. The test starts (at t = 0 sec) with opening of the break, feedwater shut-off, recirculation pump (RCP) trip, and bundle power trip. (The electric power begins to follow the reactor decay curve.) The loss of the vessel coolant inventory is mainly due to the break flow depicted in Figure C.10-6 (No measurement is available for comparison.) The trip on the DC water level L1 (@ 6.179 m) causes a closure of the MSIV (Figure C.10-5) and activation of the ADS timer. The key event in the time period up to the actuation of the ADS, at 180 sec in the TRACE calculation, is reversal of the bypass flow and establishment of a bypass-bundle coolant circulation loop which gradually ceases at about 118 sec due to increasing voidage in the bypass (Figure C.10-9).

The ADS actuation (at 195 and 180 secs in the test and the TRACE calculation, respectively) gives rise to massive flashing inside the vessel, including the lower plenum (Figure C.10-8). Associated with flashing is entrainment of liquid from the lower portions of the vessel into the upper plenum (Figure C.10-11). This period of time (until about the time of the ECCS injection start) is characteristic of a sharply reduced break flow, bundle uncovery, further bypass drainage, and occurrence of CCFL. The break flow reduction is shown in Figure C.10-6 (no test data are available). The bundle uncovery is depicted in Figure C.10-10 in terms of the measured and calculated differential pressure. It is noticed that TRACE calculates a shorter uncovery. The

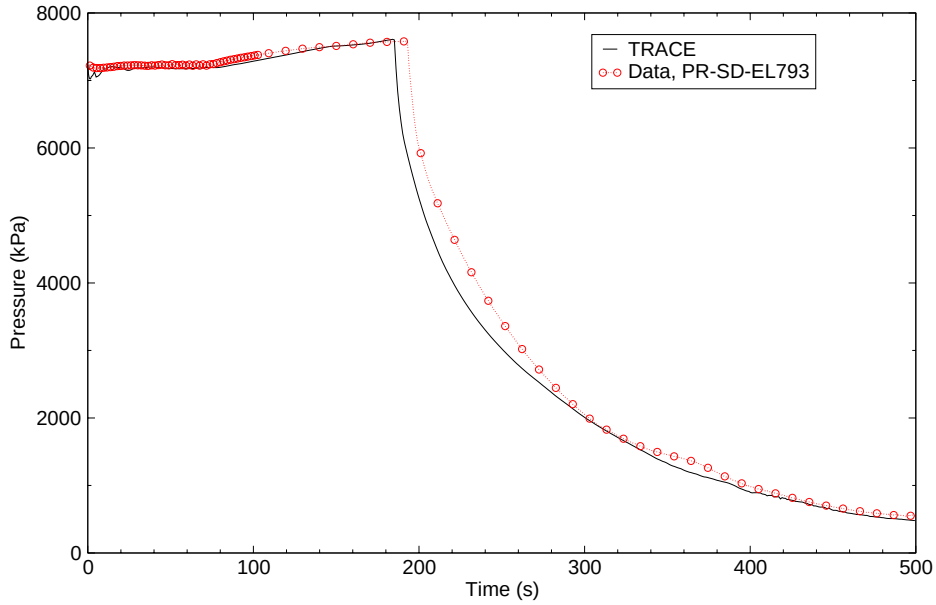

Figure C.10-5. FIST 6SB2C - Pressure Vessel Steam Dome Pressure

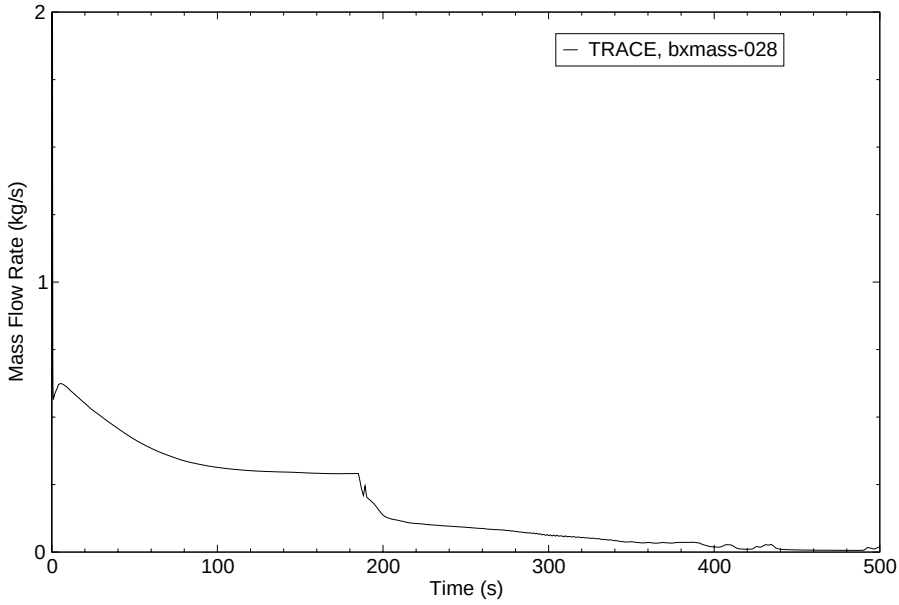

Figure C.10-6. FIST 6SB2C - Break Flow Rate

reason is that the liquid entrained in the initial period of depressurization and deposited in the upper plenum trickles down into the bundle and bypass due to insufficient

Table C.10.2. Sequence of Key Events in Test 6SB2C and TRACE Simulation

Events (sec)	**Test 6SB2C**	**TRACE**
Break initiation	0	0
Bundle power trip	0	0
Feedwater trip	0	0
Recirculation pump trip	0	0
Recirculation line isolation	20	20
Level 1 reached	75	56
MSIV closure	77	-
ADS opens	195	180
Bundle uncovery starts	237	187
Rod heatup starts	250	272
LPCS injection begins	310	308
LPCI injection begins	335	328
Bundle reflood starts	370	330
Bundle reflood finished	420	440
SEO CCFL breakdown	465	435[a]
Lower plenum refilled	465	470
End of test/simulation	510	500

[a] SEO flow remains toward lower plenum

CCFL (or lack of it) which has not been observed in the experiment (see the relatively short temporary increase of the differential pressure measurement in the upper plenum in (Figure C.10-11).

The time period after the low pressure ECCS begins injecting coolant is marked by increased reversed channel-bypass leakage flow which provides for reflooding of the bundle (Figure C.10-10). It is noted that during this time period there is no downflow into the bundle from the upper plenum which remains empty (Figure C.10-11). After about 440 sec the gradually increasing ECC flow begins to refill all vessel compartments (see Figures C.10-7 through C.10-11).

During the period of bundle uncovery, there are prolonged periods of dryout (see Figures C.10-12 through C.10-17) lasting - depending upon the dryout elevation - well past the onset of the bundle level recovery. The shift of about 25 sec between the measured and calculated dryouts corresponds to the shift observed between the measured and calculated bundle uncovery (Figure

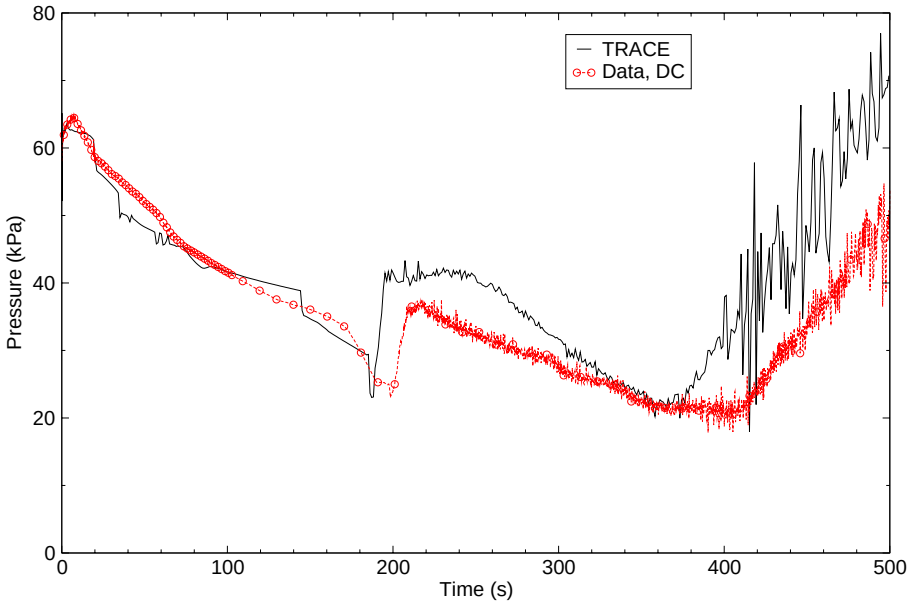

Figure C.10-7. FIST 6SB2C - Downcomer Differential Pressure

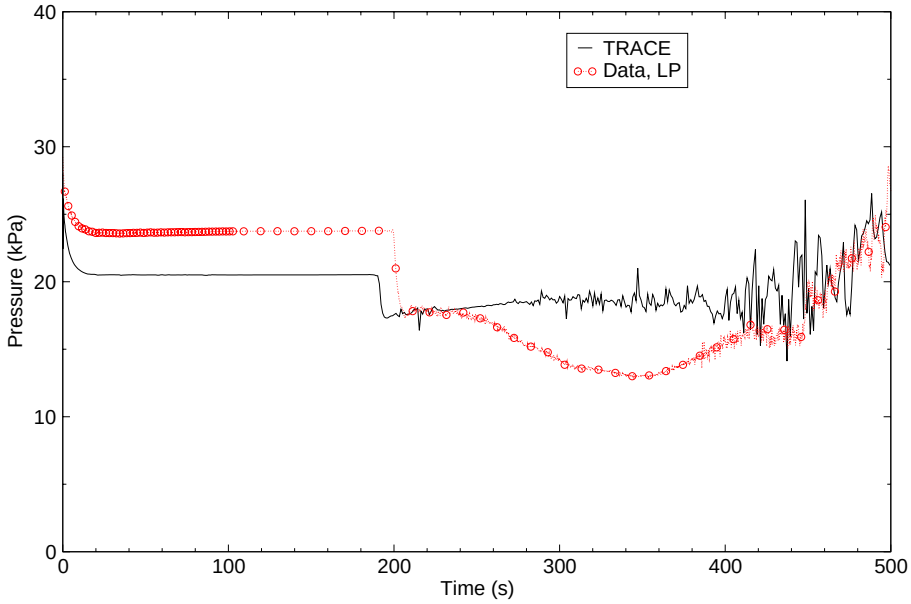

Figure C.10-8. FIST 6SB2C - Lower Plenum Differential Pressure

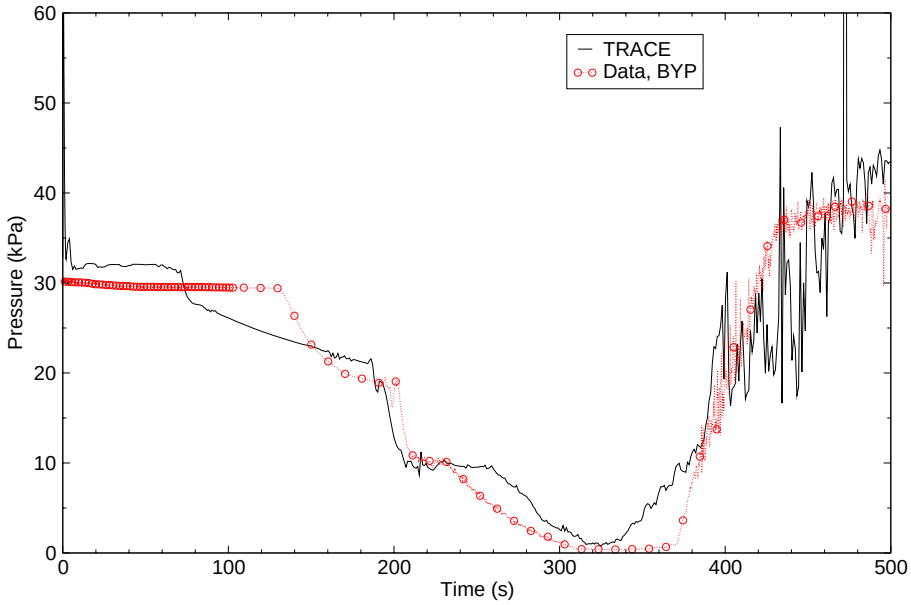

Figure C.10-9. FIST 6SB2C - Bypass Differential Pressure

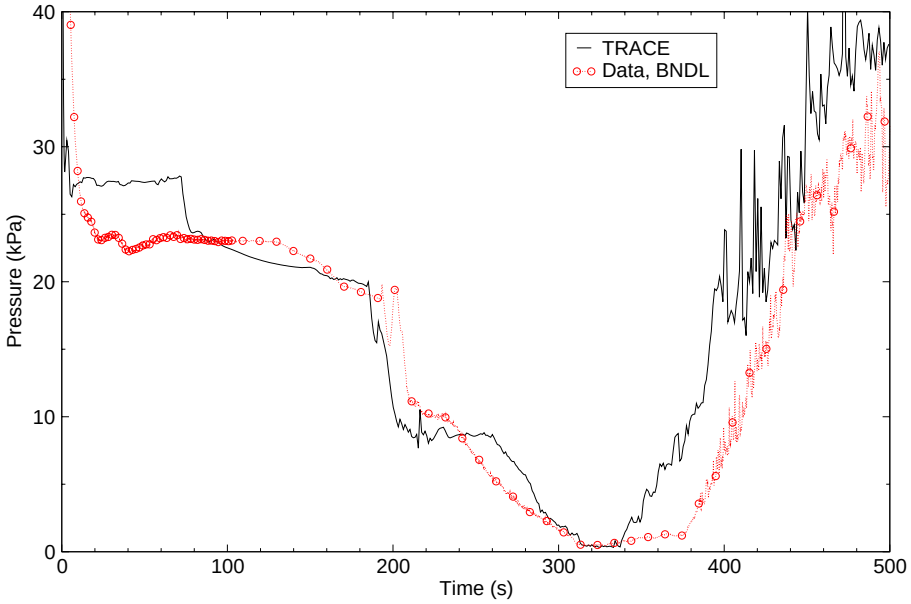

Figure C.10-10. FIST 6SB2C - Bundle Differential Pressure

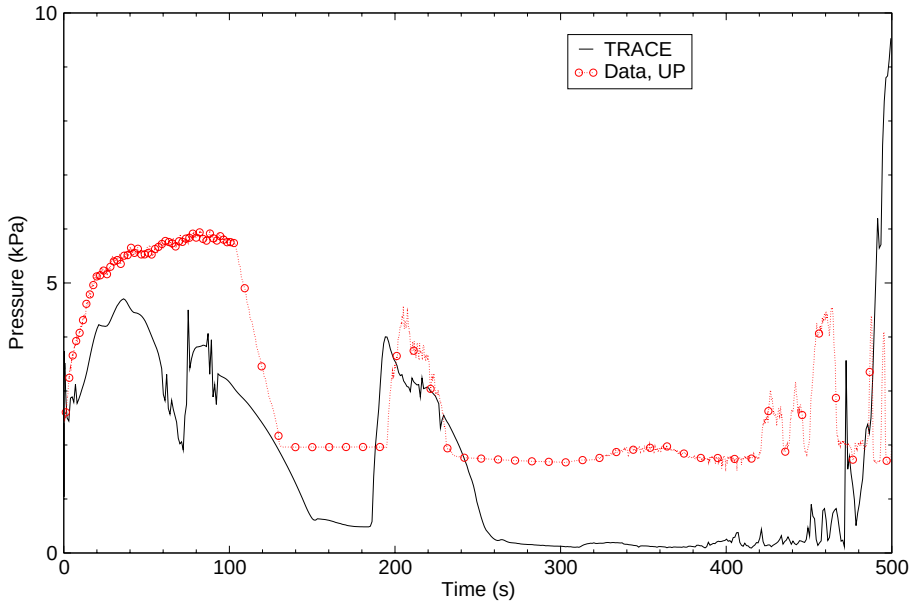

Figure C.10-11. FIST 6SB2C - Upper Plenum Differential Pressure

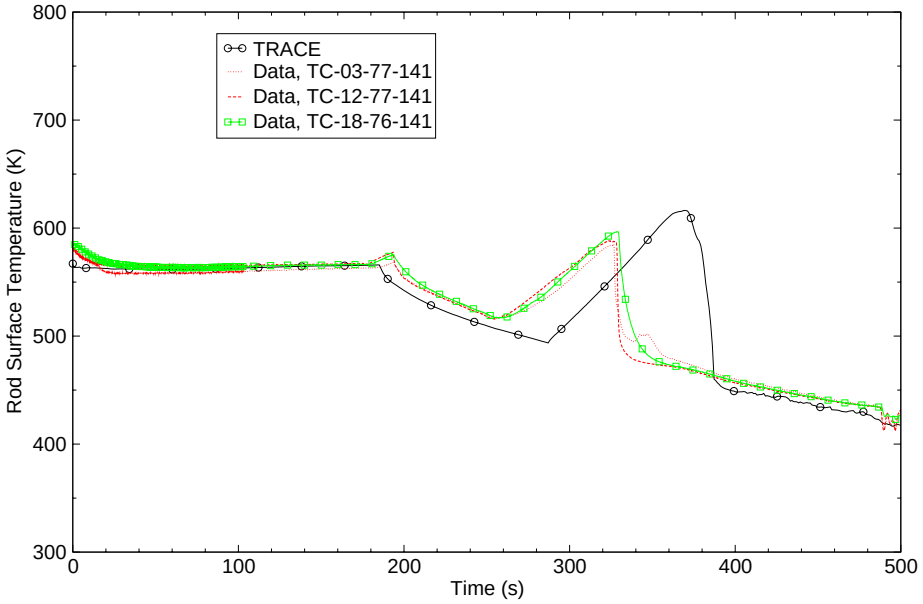

Figure C.10-12. FIST 6SB2C - Rod Surface Temperatures-Elevation 141 Inches

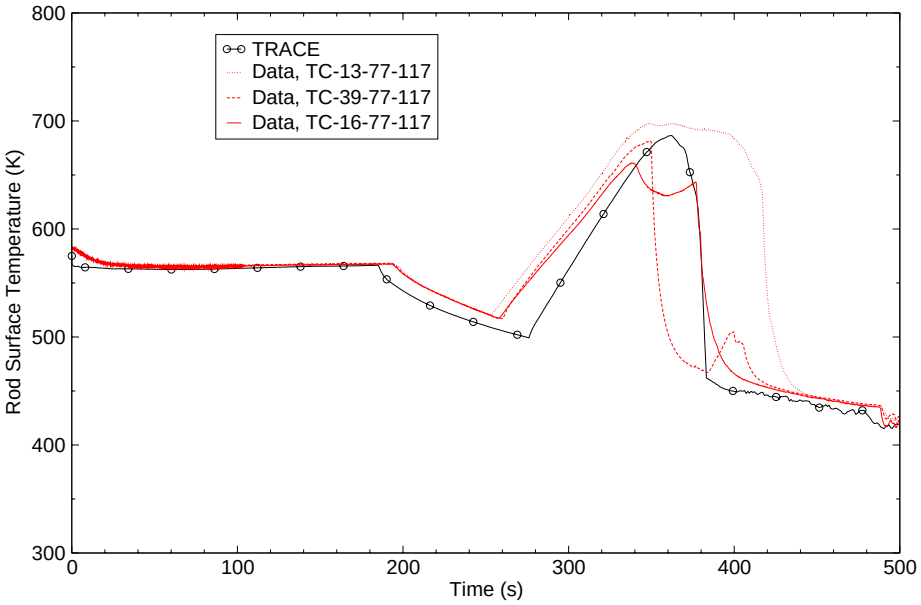

Figure C.10-13. FIST 6SB2C - Rod Surface Temperatures-Elevation 117 Inches

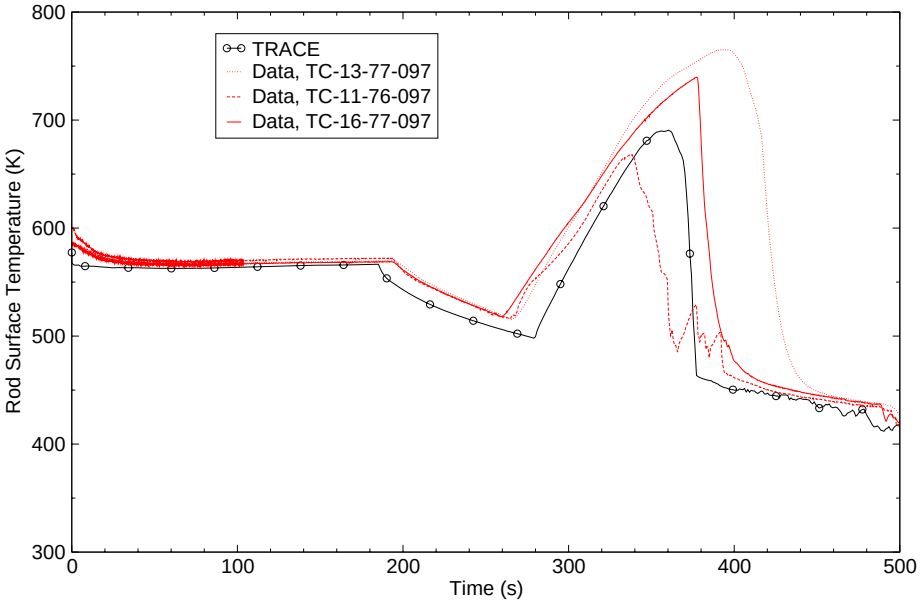

Figure C.10-14. FIST 6SB2C - Rod Surface Temperatures-Elevation 97 Inches

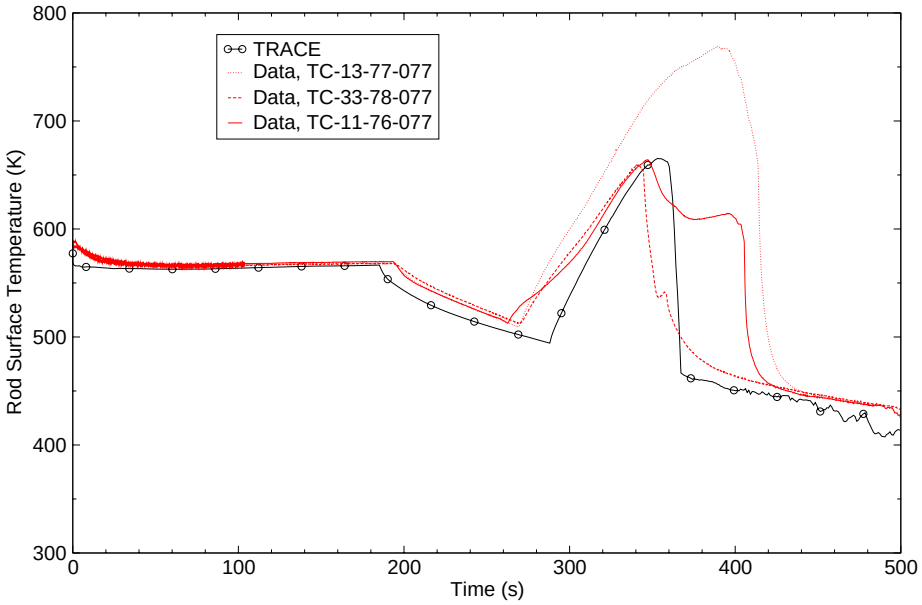

Figure C.10-15. FIST 6SB2C - Rod Surface Temperatures-Elevation 77 Inches

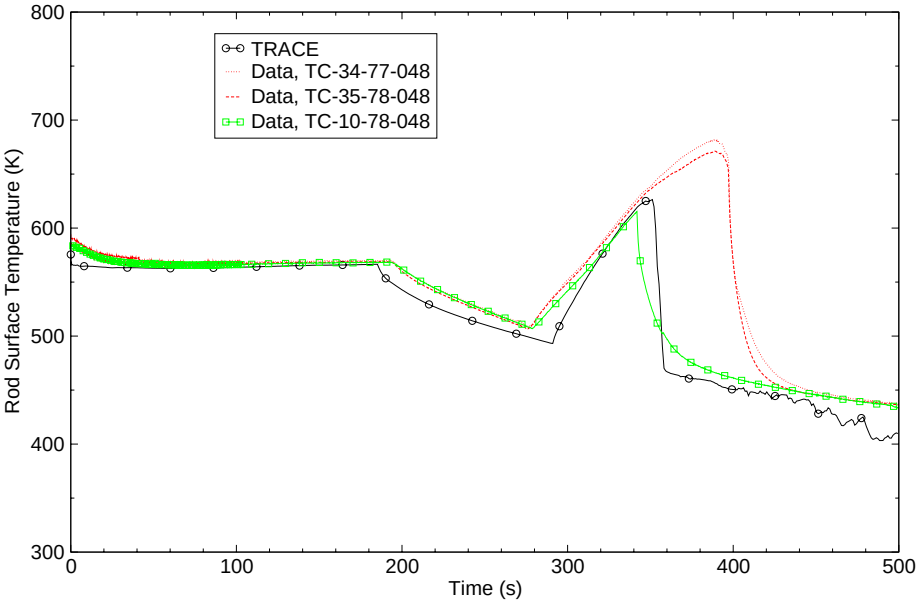

Figure C.10-16. FIST 6SB2C - Rod Surface Temperatures-Elevation 48 Inches

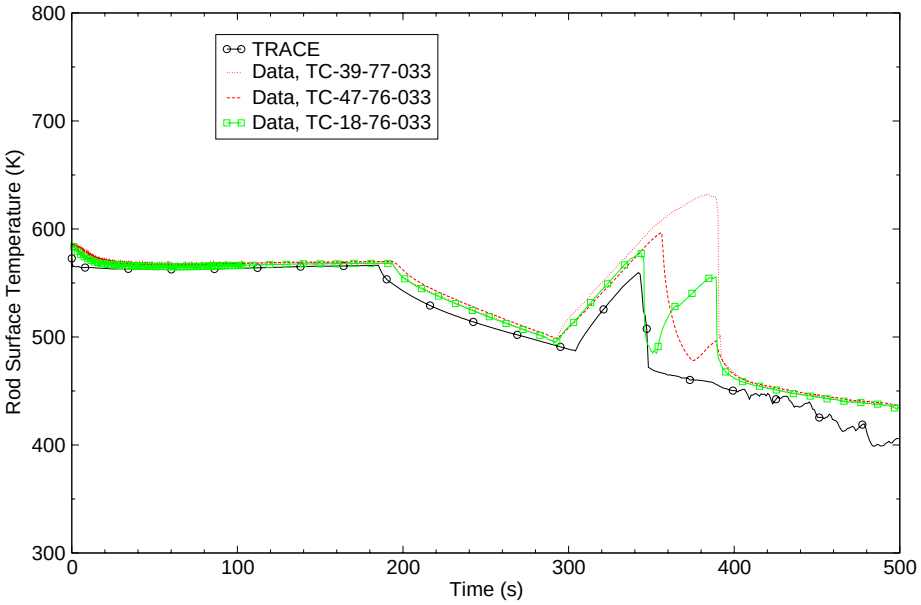

Figure C.10-17. FIST 6SB2C - Rod Surface Temperatures-Elevation 33 Inches

C.10-10). The maximum peak clad temperature (PCT) measured in this test is 779 K compared to TRACE calculated 685 K (Figure C.10-13). In the test the quench front proceeded from both the bottom and top of the bundle while in the simulation the bottom reflood only is observed (see Figures C.10-12 through C.10-17).

C.10.4.2. Simulation of Test 6SB1

The FIST conditions before the test 6SB1 and the steady-state conditions reproduced by the TRACE model are shown in Table C.10.3

Table C.10.3. Initial Conditions in Test 6SB1 and TRACE Model

Parameter	**Test 6SB1**	**TRACE**
Bundle power, MW	4.64 $\pm$ 0.01	4.64
Steam dome pressure, MPa	7.17 $\pm$ 0.5	7.17
Core flow, kg/s	17.23 $\pm$ 0.10	17.20
Channel flow, kg/s	not given	17.01

[a] relative to the lower jet pump support plate

Table C.10.3. Initial Conditions in Test 6SB1 and TRACE Model

Parameter	Test 6SB1	TRACE
Bypass flow, kg/s	not given	1.73
Downcomer water level[a], m	10.8 ± 0.10	10.8
Steam flow rate, kg/s	2.41 ± 0.03	2.44
Feedwater flow rate, kg/s	2.41 ± 0.05	2.48
Feedwater temperature, K	484 ± 2	484
Jet pump 1 flow rate, kg/s	8.61	8.60
Jet pump 2 flow rate, kg/s	8.61	8.60
Downcomer temperature, K	550.9 ± 2	550.9
ECCS temperature, K	322.0	322.0
HPCS pump	off	off
LPCS pump	on	on
LPCI pump	on	on

[a] relative to the lower jet pump support plate

Key events and the comparison between the test and the TRACE code are shown in Table C.10.4 Generally, governing phenomena reproduced by TRACE and the code performance are similar to what was observed in the simulation of Test 6SB2C.

The system pressure is shown in Figure C.10-18. It starts diverging from the measurement at the time SRV #1 is calculated to open (110 sec). This indicates that the calculated breakflow is overestimated which is corroborated by the fact that the L1 setpoint is reached by about 18 sec earlier in the TRACE calculation (Table C.10.4). The major depressurization occurs after the ADS opens which leads to the low pressure ECCS initiation (Table C.10.4).

The discussion of the results of the 6SB2C simulation in terms of the differential pressures in the downcomer, lower plenum, bypass, bundle, and upper plenum (Figures C.10-19 through C.10-23) is valid for this test as well.

Table C.10.4. Sequence of Key Events in Test 6SB1 and TRACE Simulation

Events (sec)	Test 6SB1	TRACE
Break initiation	0	0
Bundle power trip	0	0
Feedwater trip	0	0
Recirculation pump trip	0	0

[a]SEO flow remains toward lower plenum

Table C.10.4. Sequence of Key Events in Test 6SB1 and TRACE Simulation

Events (sec)	Test 6SB1	TRACE
Recirculation line isolation	20	20
Level 1 reached	85	67
MSIV closure	87	69
SRV #1 opens	130	110
ADS opens	190	170
Bundle uncovery starts	196	172
Rod heatup starts	250	270
LPCS injection begins	290	308
LPCI injection begins	320	331
Bundle reflood starts	355	333
Bundle reflood finished	420	457
SEO CCFL breakdown	435	421[a]
Lower plenum refilled	450	470
End of test/simulation	485	500

[a]SEO flow remains toward lower plenum

During the period of bundle uncovery, there is a prolonged period of rod dryouts lasting - depending upon the dryout elevation - past the onset of the bundle level recovery. At upper elevations, the calculated dryout temperatures are overestimated by as much as 70 K. The maximum peak clad temperature (PCT) measured in this test was 655 K (see instrumentation ID TC-13-77-077 in Figure C.10-27), as compared to 658 K which was calculated in TRACE (see Figure C.10-25). Similarly as in Test 6SB2C, quenching proceeds in the calculation from the bottom up. The most upper node is quenched intermittently from the top (Figure C.10-24).

C.10.5. Assessment Results Summary

Two FIST SBLOCA tests were simulated using TRACE Code Version 5.0. Both the simulation trend and results agree reasonably well with the test data. A shift in timing of key events is noted and is attributed to calculated breakflow. All key events and sequences of thermal hydraulic phenomena were captured, e.g. depressurization, vessel flashing, channel uncovery, rod dryout, etc.

The major deviation between the tests and their simulation was associated with predicting the degree of bundle uncovery. In the simulation of Test 6SB1, the bundle was calculated to uncover only partially. This prediction defect appears to be associated with the amount of liquid entrainment and its deposition during the ADS blowdown and occurrence of CCFL at the bundle inlet (SEO), the upper tie plate and the bypass top. With the initiation of the ADS blowdown, a

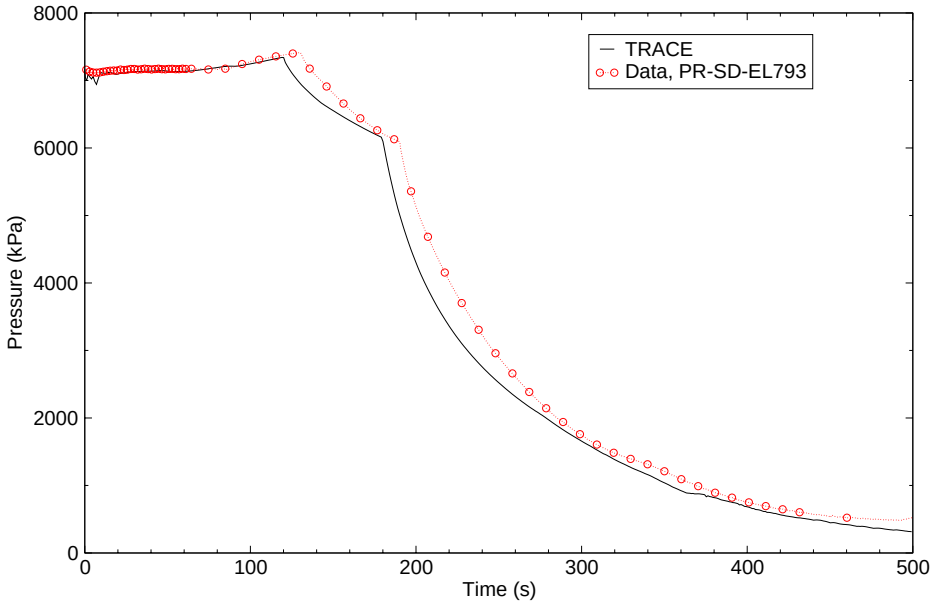

Figure C.10-18. FIST 6SB1 - Pressure Vessel Steam Dome Pressure

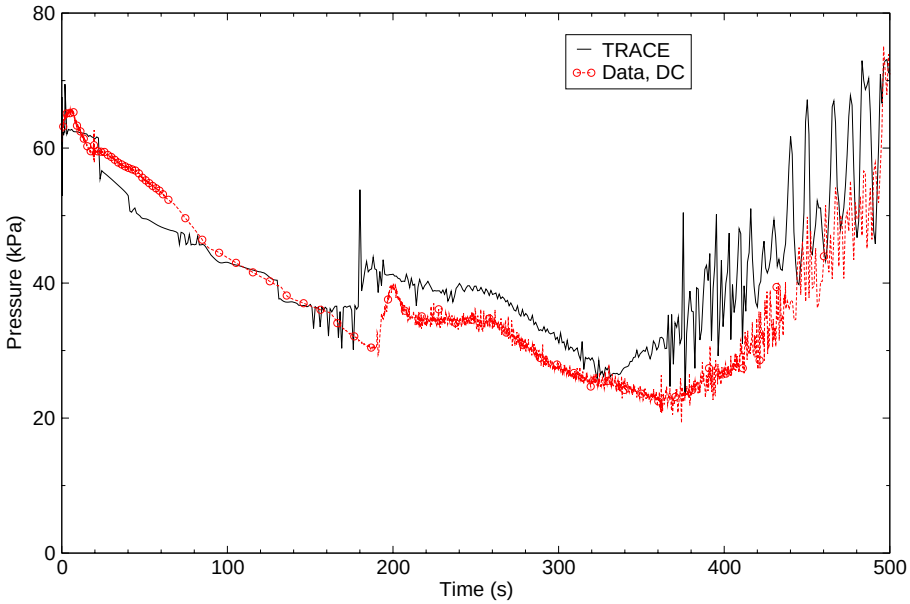

Figure C.10-19. FIST 6SB1 - Downcomer Differential Pressure

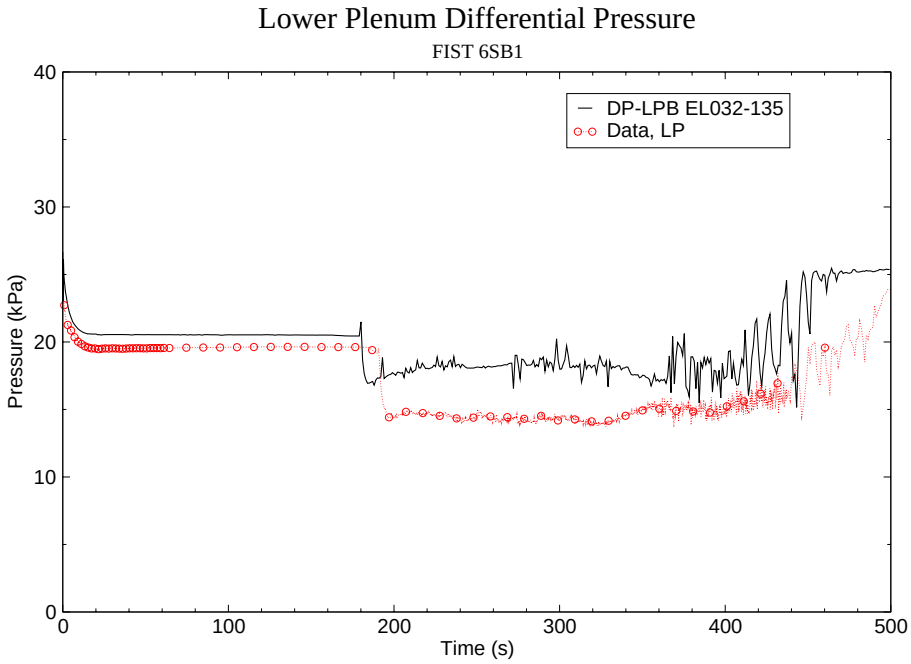

Figure C.10-20. FIST 6SB1 - Lower Plenum Differential Pressure

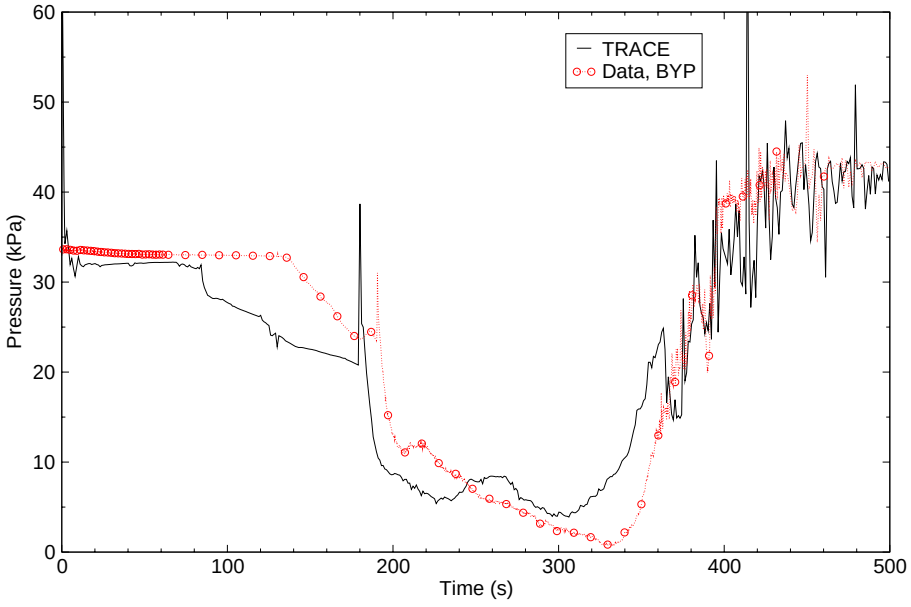

Figure C.10-21. FIST 6SB1 - Bypass Differential Pressure

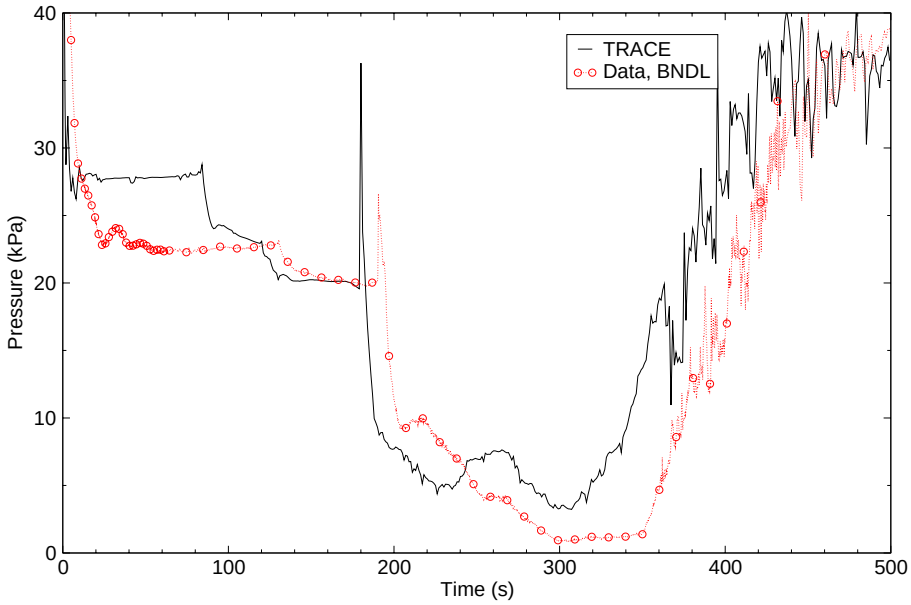

Figure C.10-22. FIST 6SB1 - Bundle Differential Pressure

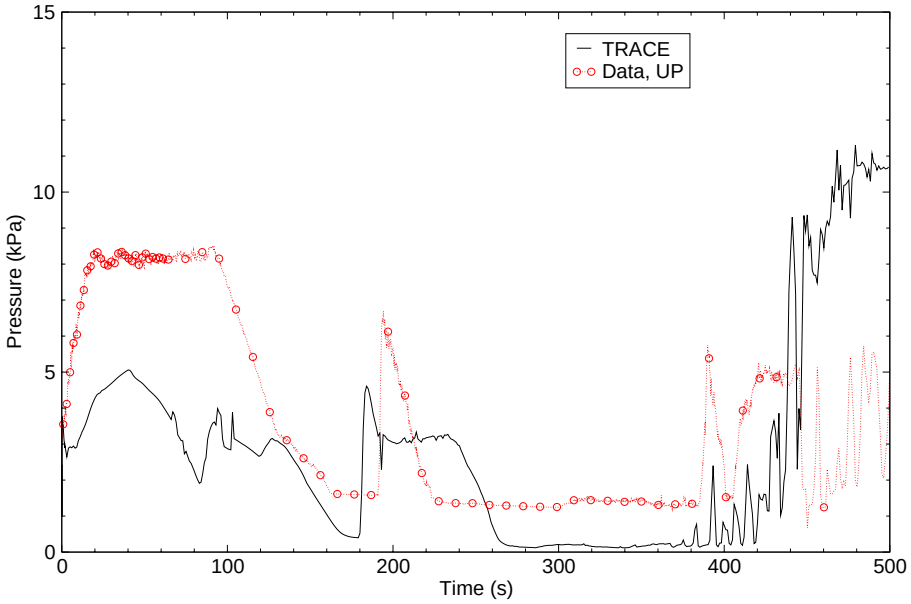

Figure C.10-23. FIST 6SB1 - Upper Plenum Differential Pressure

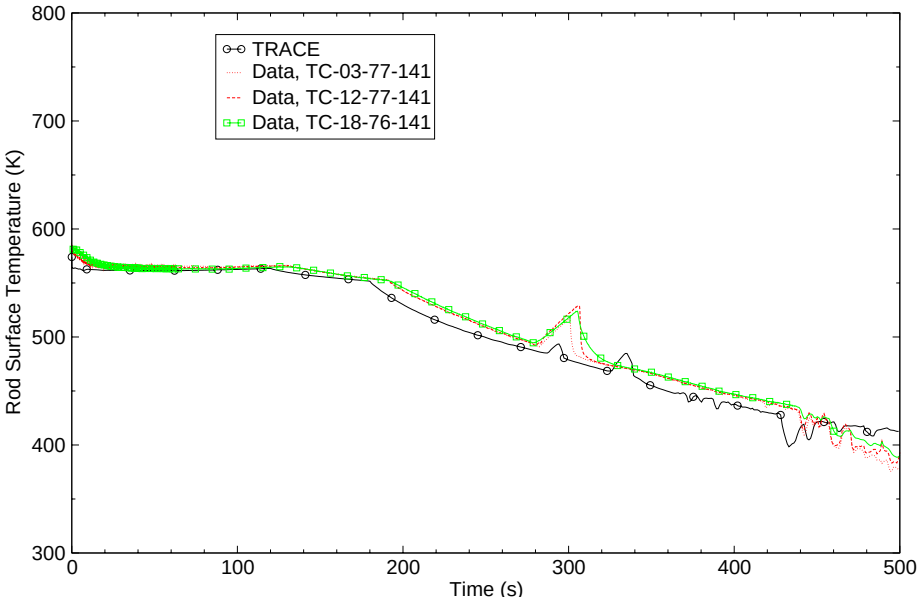

Figure C.10-24. FIST 6SB1 - Rod Surface Temperatures-Elevation 141 Inches

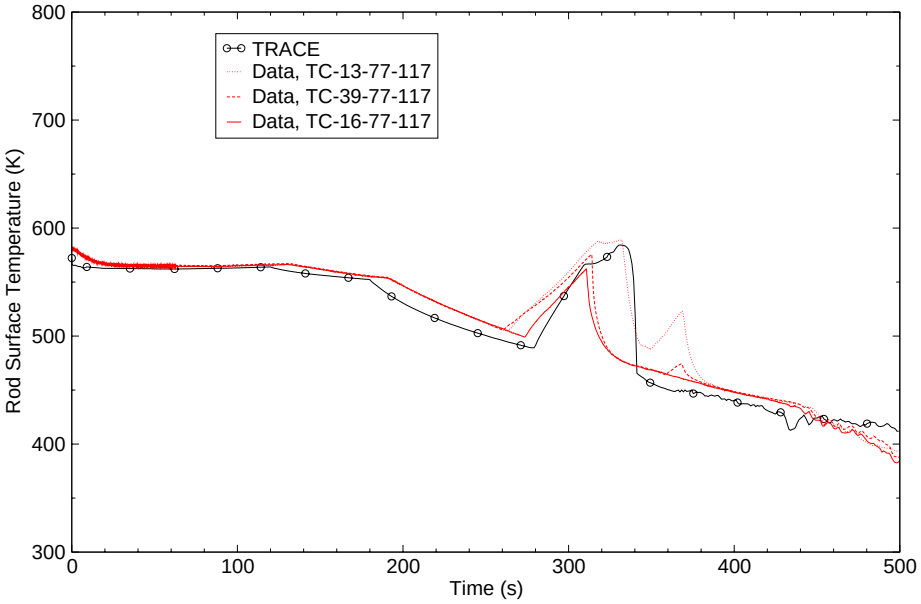

Figure C.10-25. FIST 6SB1 - Rod Surface Temperatures-Elevation 117 Inches

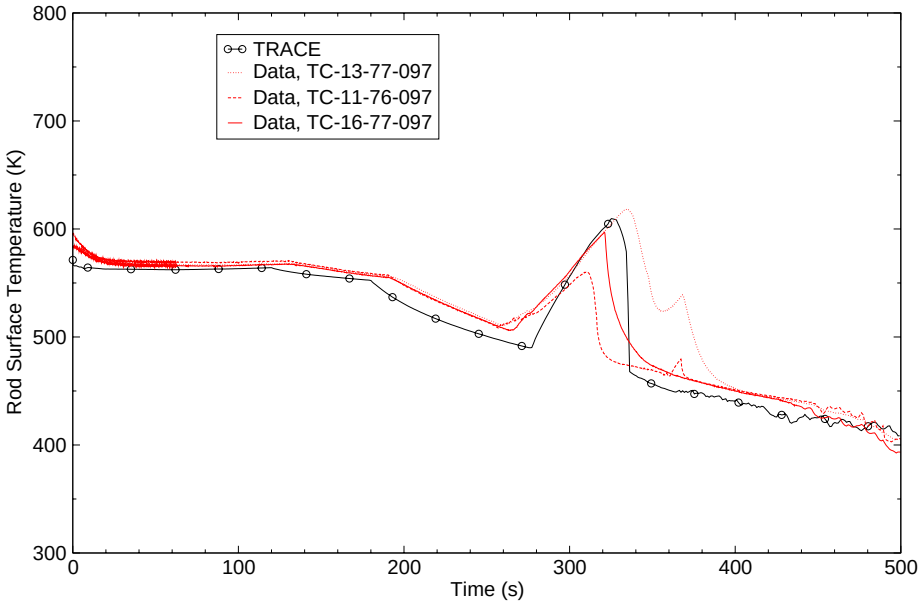

Figure C.10-26. FIST 6SB1 - Rod Surface Temperatures-Elevation 97 Inches

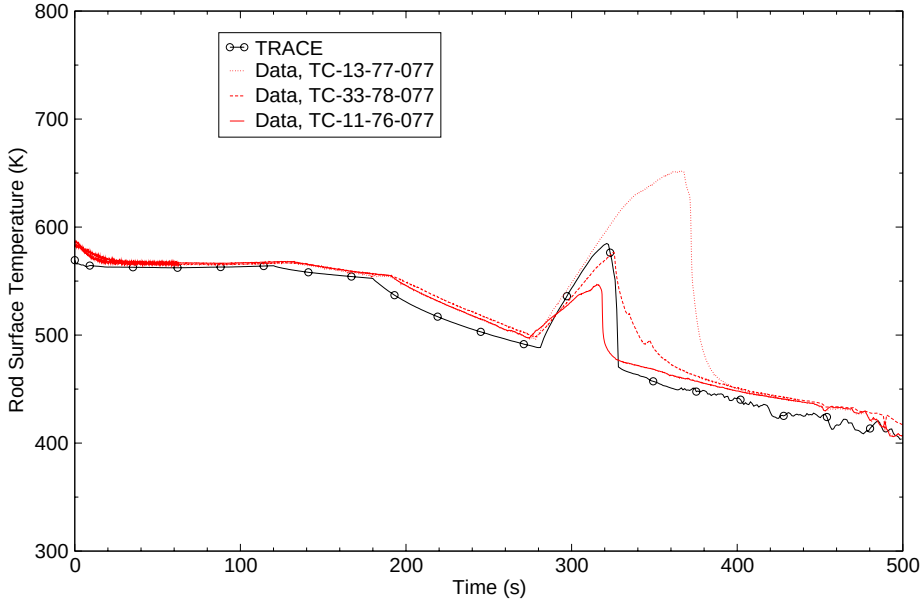

Figure C.10-27. FIST 6SB1 - Rod Surface Temperatures-Elevation 77 Inches

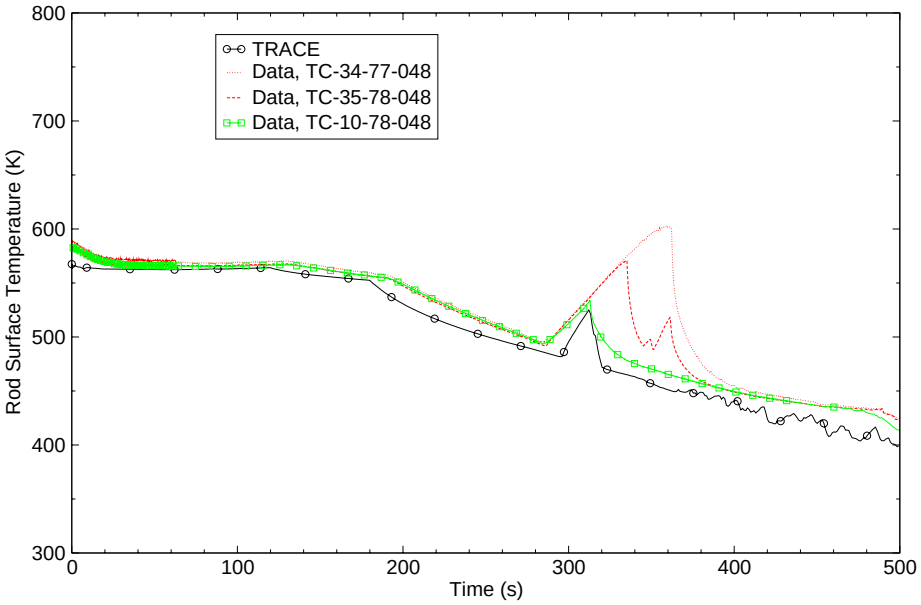

Figure C.10-28. FIST 6SB1 - Rod Surface Temperatures-Elevation 48 Inches

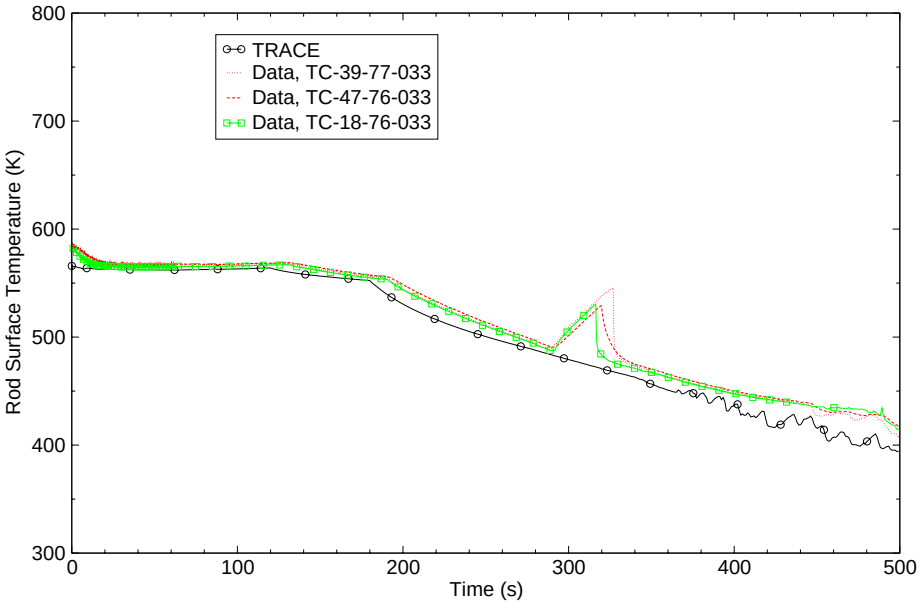

Figure C.10-29. FIST 6SB1 - Rod Surface Temperatures-Elevation 33 Inches

large amount of water was calculated to be deposited in the upper plenum, which provided a small but steady supply of water to the bundle until it all drained. This did not occur in tests. The quench front in the TRACE calculation proceed from the bottom up while in tests both the bottom up and top down reflood was observed.

C.10.6. References

1 W.S. Hwang, Md. Alamgir, and W.A. Sutherland, "BWR Full Integral Simulation Test (FIST) Phase 1 Test Results", NUREG/CR-3711, EPRI NP-3602, GEAP-30496, September 1984.

2 A.G. Stephens, "BWR Full Integral Simulation Test (FIST) Program Facility Description Report", NUREG/CR-2576, EPRI NP-2314, GEAP-22054, September 1984.

3 R. W. Shumway, and M. A. Bolander, "TRAC-B & TRAC-M Comparison to FIST Small Break Test 6SB2C", Task Order No. 6 Task 4, ISL-NSAD, March 2002.

BWR Small Break Integral Tests

C.11. TLTA Test 6425 Run 2 and Test 6424 Run 1

Author(s): Weidong He, Millan Straka, and David Ebert

Affiliation: Advanced Systems Technology and Management, Inc.

Code Version: TRACE V5.0

Platform and Operating System: Intel x86, Windows XP

C.11.1. Introduction

The objective of this work is to assess the capability of the TRACE V5.0 thermal-hydraulics code to calculate large break loss-of-coolant accident (LBLOCA) thermal-hydraulic phenomena in a boiling water reacter (BWR), as simulated in the Two-Loop Test Apparatus (TLTA) facility (Ref. 1). TRACE code calculations are compared with experimental data from TLTA Test 6425 Run 2 and Test 6424 Run 1.

TLTA Large Break Test 6425 Run 2 and Test 6424 Run 1 provides valuable integral system loss-of-coolant response data in a scaled BWR facility. Test 6425 Run 2 was an average power (5.05 MW), average Emergency Core Cooling (ECC) flow and nominal ECC temperature test to simulate a double-ended rupture of a recirculation line (Ref. 2). Test 6424 Run 1 was similar to the Test 6425 Run 2 but with a peak power (6.49 MW) (Ref. 2). The key events and governing phenomena of interest in these tests include critical flow, counter current flow limitation (CCFL), core heatup, ECCS injection, etc.

C.11.2. Test Facility Description

TLTA is a single electrically heated bundle facility, a 1/624 volume scaled version of a standard BWR/6-218 in. reactor (Ref. 1). The core is of full length. The TLTA vessel was not of full length as was FIST (Ref. 3).

A schematic of the facility is shown in Figure C.11-1 The system models major regions and components in a BWR, such as the lower plenum, core, core bypass, upper plenum, steam separator, steam dome, downcomer, jet pumps and recirculation loops. The LOCA depressurization tests are initiated by breaking rupture disks in the suction and drive line of recirculation loop 2. The ECCS simulation consists of HPCS, LPCS and LPCI. The single bundle core is simulated by 62 electrically heated rods and two water rods in the 8 x 8 lattice. Figure

C.11-2 shows the bundle configuration. The bundle provides a peak power of 6.50 MW. Figure C.11-3 gives the instrumentation diagram for the facility.

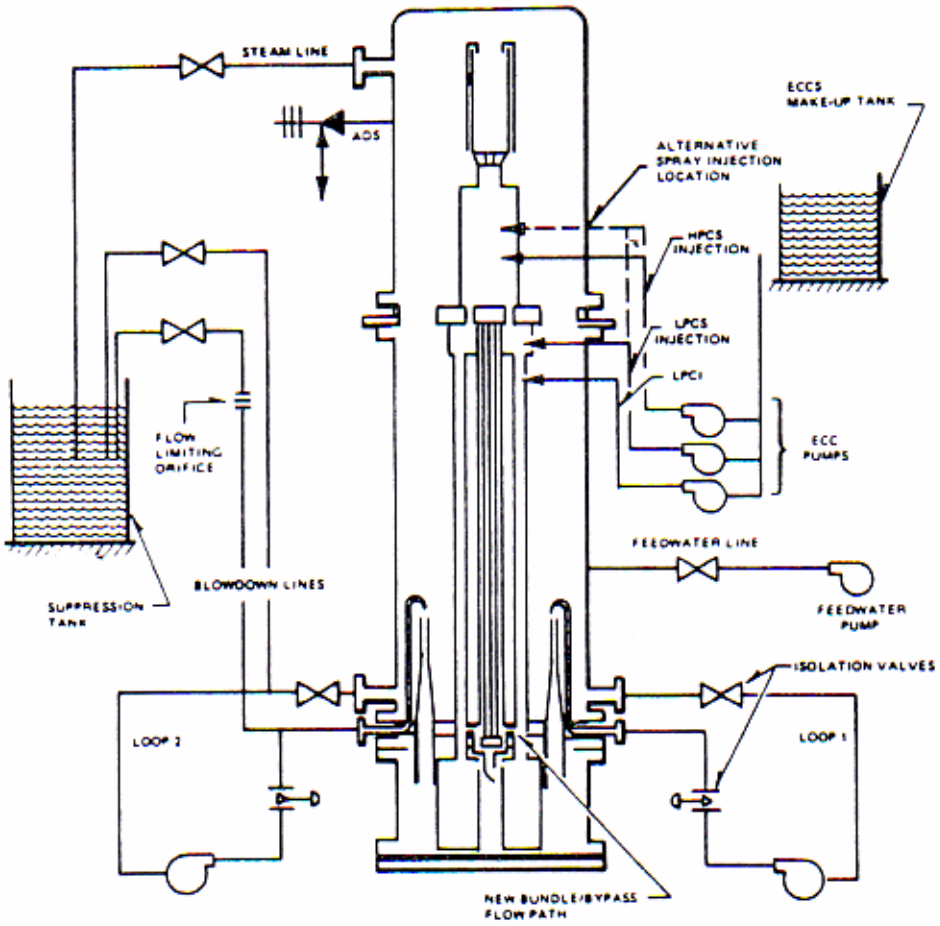

Figure C.11-1. Two-Loop Test Apparatus Configuration (TLTA-5A) (Ref. 4).

C.11.3. TRACE Model Description

The TRACE input deck for simulation of TLTA Test 6425/2 was developed from a TRACB input deck (Ref. 5). The TRACB input deck was converted into a TRACE input deck using the NRC Symbolic Nuclear Analysis Package (SNAP). The TRACE input deck was reviewed against the original TRACB deck and was used to simulate Test 6425/2 in this study.

The TRACE input decks for simulation of Test 6424/1 were obtained by modifying the TRACE input deck for Test 6245/2 to accommodate the test conditions of Test 6424/1, e.g. control procedures (pressure control, level control and recirculation flow control) developed to obtain the Test 6424/1 initial conditions.

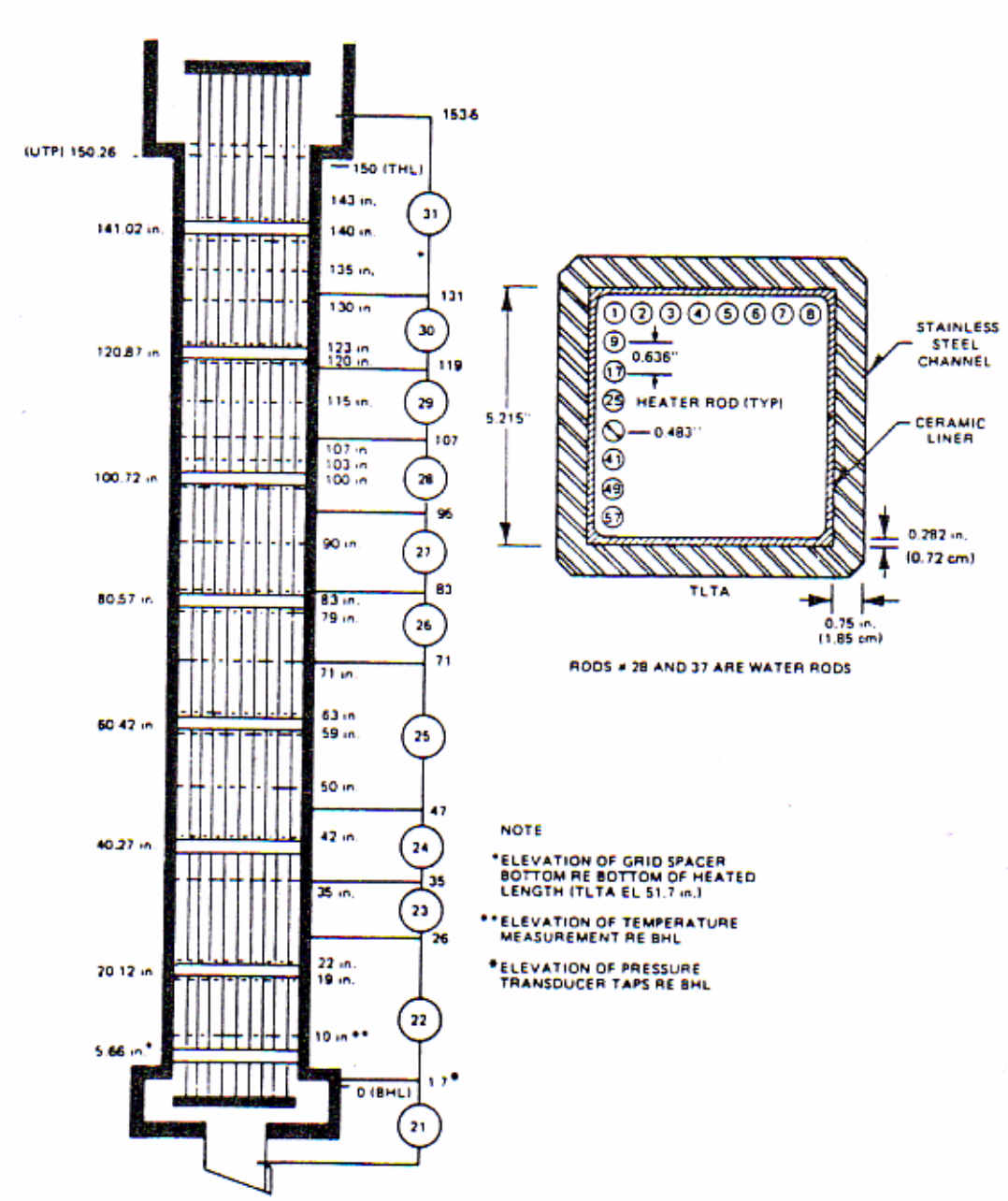

Figure C.11-2. Bundle Temperature and Differential Pressure Measurements in TLTA (Ref. 4).

The TRACE TLTA nodalization scheme is shown in Figure C.11-4. Table C.11.1 lists the components used in the TRACE model. This model consists of components representing the TLTA vessel, the single electrically heated bundle, the two recirculation loops, the ECCS systems,

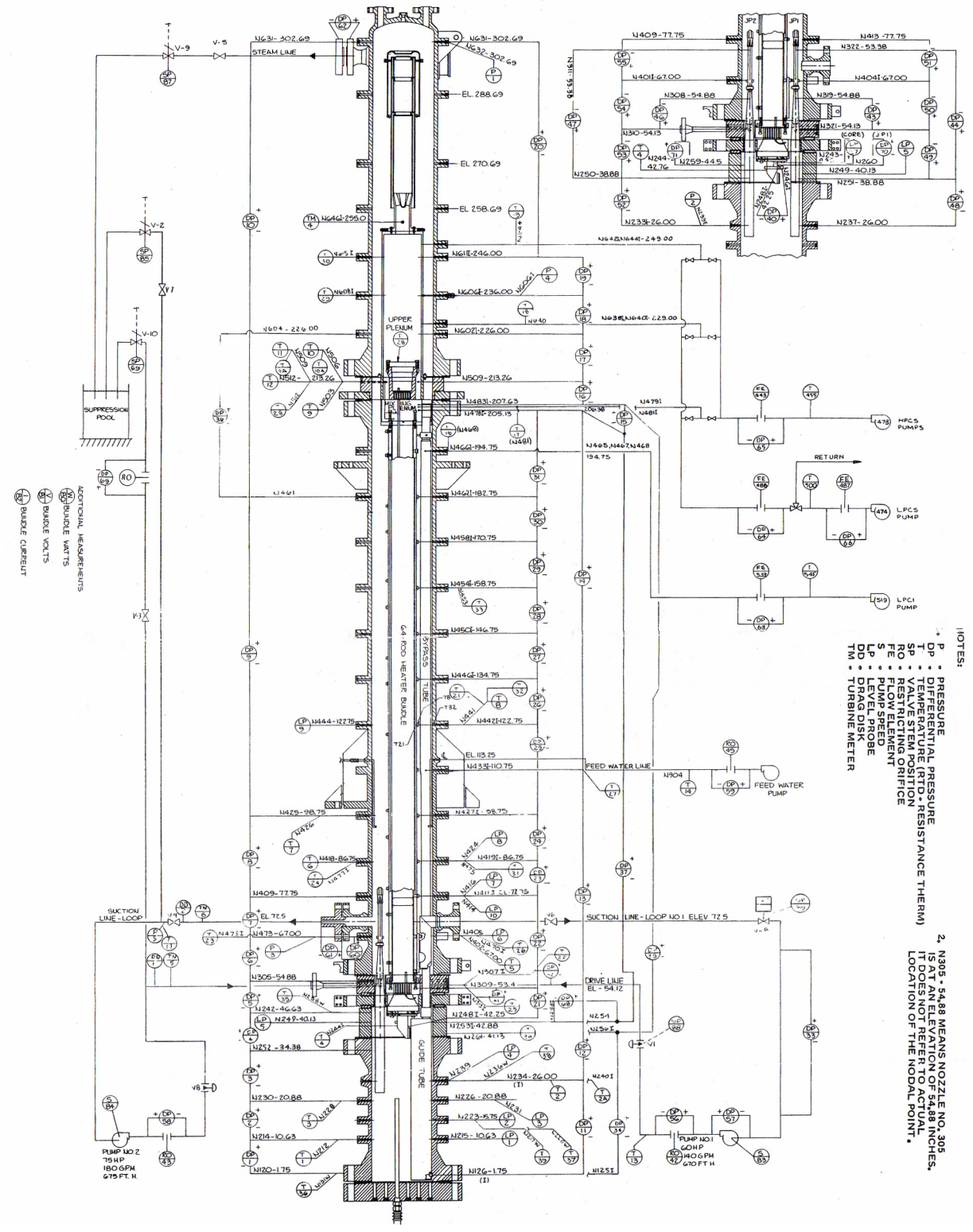

Figure C.11-3. TLTA-5A Instrumentation (Ref. 2).

the break configuration, the main steam line and the feedwater system. The remainder of this section discusses TLTA vessel and TLTA channel nodalization.

Table C.11.1. TLTA Facility TRACE Components

TLTA Region	TRACE Components
Break lines	TEE 23, VALVE 37, BREAK 38, TEE 20, VALVE 27, BREAK 28
Broken loop suction line	TEE 20
Broken loop drive pump	PUMP 21
Broken loop drive line isolation valve	VALVE 22
Broken loop drive line	TEE 23
Broken loop jet pump	JETP 24
Intact loop suction line	PIPE 10
Intact loop suction line isolation valve	VALVE 11
Intact loop drive pump	PUMP 12
Intact loop drive line isolation valve	VALVE 13
Intact loop jet pump	JETP 14
Heated bundle	CHAN 61
Guide tube	TEE 31
Feedwater line	FILL 46, PIPE 47
Main steam line	Test 6425: PIPE 51, FILL 52 (Serving as MSIV); Test 6424: VALVE 51, VALVE 52, BREAK 53
HPCS line	PIPE 45, FILL 44
LPCS line	PIPE 43, FILL 42
LPCI line	PIPE 41, FILL 40
Vessel and internals	VESSEL 33
Lower plenum	Levels 1-5, Rings 1 and 2
Downcomer	Levels 6-18, Ring 2
Bypass	Levels 6-14, Ring 1
Mixing plenum	Levels 15-16, Ring 1
Upper plenum	Levels 17-18, Ring 1
Steam separator	Level 19, Ring 1
Steam Dome	Level 20, Rings 1 and 2

C.11.3.1. TLTA Vessel Nodalization

The TLTA vessel is modeled with a TRACE vessel component (VESSEL 33) as shown in Figure C.11-4. The VESSEL component models the lower plenum, core bypass, downcomer, upper plenum, stand pipes, separator, dryer, and steam dome sections of the TLTA facility vessel. The

VESSEL component has 20 axial levels, two radial rings and one theta sector. The locations of two rings coincide with the boundary between the core and the downcomer and with the outer boundary of the vessel. The 20 levels correspond to the lower plenum, bypass, upper plenum and steam separator - dome regions.

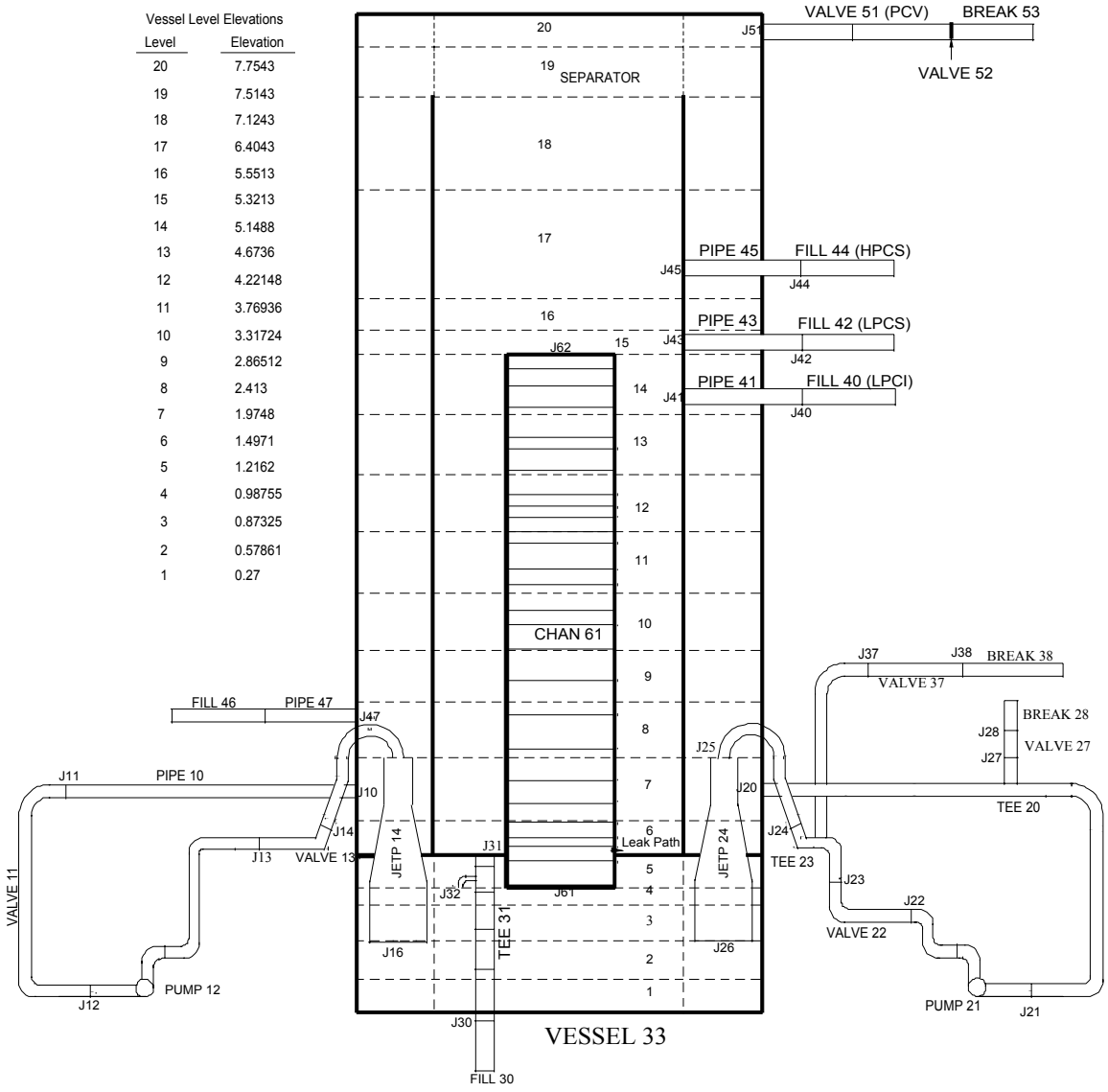

Figure C.11-4. TLTA Nodalization

The bottom five levels in Rings 1 and 2 comprise the lower plenum. The core bypass is modeled with Levels 6 through 14 in Ring 1. Levels 15 through 18 in Ring 1 model the mixing plenum and the upper plenum. Liquid separation is modeled in Level 19. The downcomer is modeled with Levels 6 through 18 in Ring 2. The steam dome is comprised of Level 20.

The communications among various vessel cells are either through open flow areas or through other 1-D components. The 1-D components are the fuel bundle connecting the lower and upper plenum, the guide tube connecting the bypass and the lower plenum, and jet pumps connecting the lower plenum and the downcomer. Other external connections (sources) include the recirculation lines, feedwater line, the HPCS line, the LPCI line, the LPCS line and the main steam line.

C.11.3.2. TLTA Bundle Nodalization

The TLTA single rod bundle is modeled with a CHAN component (CHAN 61). The nodalization diagram for CHAN 61 is shown in Figure C.11-5 The inlet and outlet of the CHAN component are connected to the upper boundary of Levels 4 and 14 of the VESSEL component (Figure C.11-4).

The CHAN component has 26 axial cells. Cell 2 provides a side junction simulating the leakage path from the channel to the TLTA facility vessel. Cells 3 through 26 correspond to the heated length.

Figure C.11-6 represents the rod grouping configuration modeled in the CHAN component (Ref. 5). The CHAN component models five rod groups. One rod group represents the two water rods, and the other four rod groups represent the 62 powered rods. The breakdown of the rod grouping and the average radial peaking factors is shown in Figure C.11-6. The axial power profile is shown in Figure C.11-7.

C.11.4. Tests Simulated with TRACE

The initial conditions are listed in Table C.11.2 for TLTA Test 6425/2 and Test 6424/1. As shown in the table, besides the difference in the power level, there are differences between the two tests in other parameters, e.g. downcomer water level, steam flow rate, bundle inlet flow rate, etc. It is also noted that the steam flow rate was much greater than the feadwater flow rate for both tests.

Table C.11.3 lists major controlled events. Controlled events here refer to the events that are designed and controlled to be similar to those predicted for a reactor counterpart. In Test 6425/2 and Test 6424/1, controlled parameters include the bundle power, steam line flow, ECC injection flow characteristics, recirculation pump coast down, and feedwater flow. As indicated in Table C.11.3, major controlled events and their timings are essentially the same for the two tests.

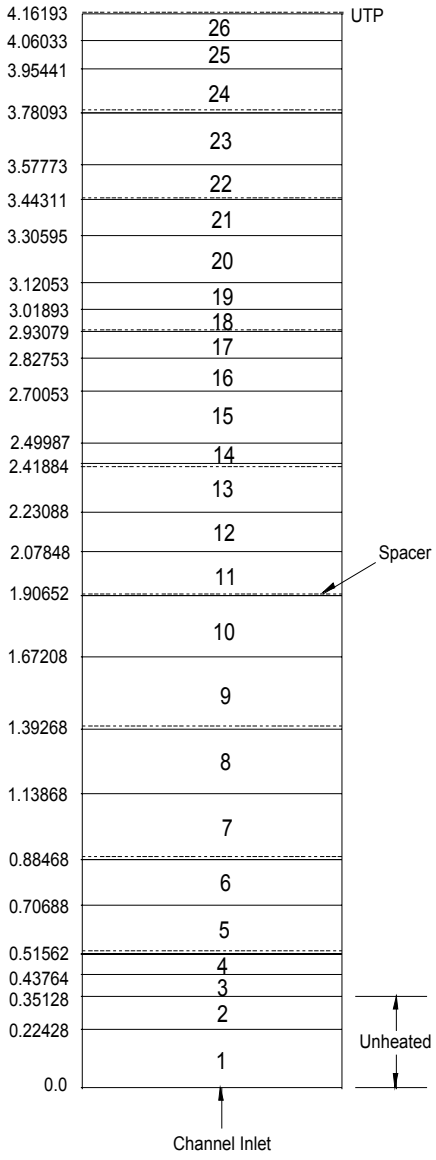

Figure C.11-5. TLTA Bundle Nodalization (Ref. 5).

C.11.4.1. Simulation of Test 6425 Run 2

C.11.4.1.1. Test 6425/2 Initial Conditions

A summary of the initial conditions from the experiment and the TRACE input model are shown in Table C.11.4 As indicated in Table C.11.4, the initial conditions of the TRACE simulation agree well with the test conditions being within the uncertainty range of the measurements.

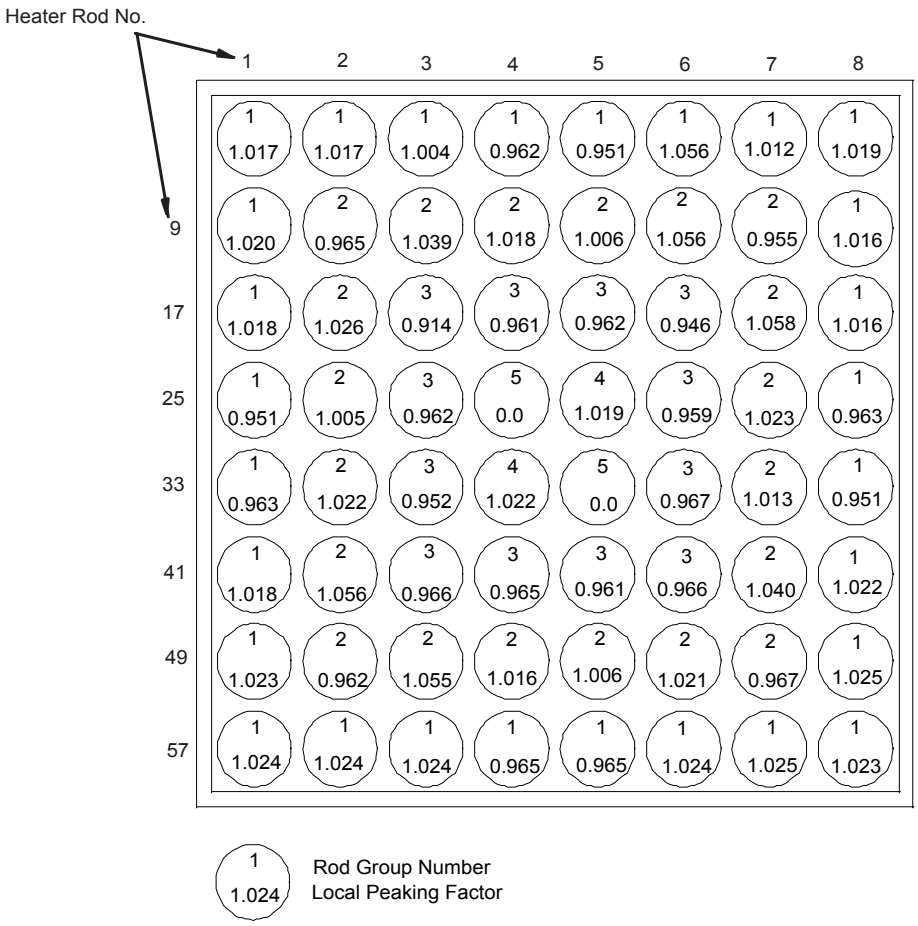

Rod Group No.	No. Rods in Group	Average Peaking Factor
1	28	1.00350
2	20	1.01545
3	12	0.95675
4	2	1.02050
5	2	0.00000

Figure C.11-6. Rod Group Configuration (Ref. 5)

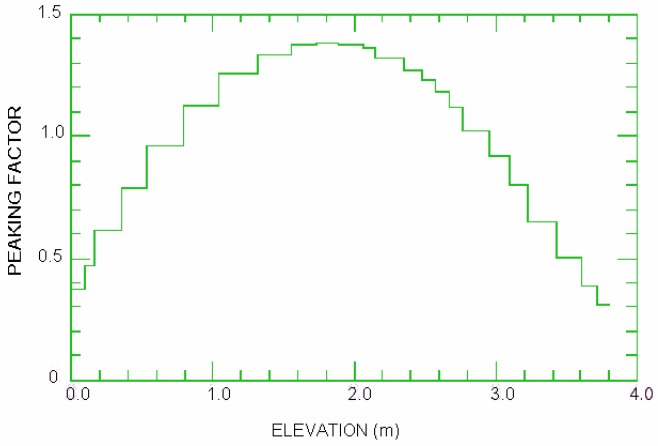

Figure C.11-7. TLTA Rod Axial Peaking Factor (Ref. 5)

Table C.11.2. Initial Conditions for Test 6425/2 and Test 6424/1

Parameter	**TLTA Test 6425 Run 2** [b]	**TLTA Test 6424 Run 1** [b]
Core power (MW)	5.05 ± 0.03	6.49 ± 0.03
Steam dome (MPa)	7.198 ± 0.034	7.281 ± 0.034
Lower plenum pressure (MPa)	7.384 ± 0.034	7.45 ± 0.0344
Initial water level (m) [a]	1.85 ± 0.15	3.15 ± 0.1524
Bundle inlet to outlet DP (KPa)	77 ± 14	137.9 ± 13.79
Steam flow (kg/s)	2.7 ± 0.454	3.6288 ± 0.4536
Feedwater flow (kg/s)	0.5 ± 0.136	0.50 ± 0.136
Drive pump 1 flow (kg/s)	4.1 ± 0.454	3.17 ± 0.4536
Drive pump 2 flow (kg/s)	3.8 ± 0.454	3.6288 ± 0.4536
Jet pump 1 flow (kg/s)	10 ± 0.907	6.35 ± 0.9072
Jet pump 2 flow (kg/s)	9 ± 0.907	8.165 ± 0.907
Bundle inlet flow (kg/s)	18 ± 2.27	13.15 ± 2.268

a - Relative to jet pump support plate
b - Reference 2

Table C.11.3. Times of Controlled Events

Events	**Test 6425 Run 2** [a] **(second)**	**Test 6424 Run 1** [a] **(second)**
Break valves opern	0.0	0.0

a - Reference 2

Table C.11.3. Times of Controlled Events

Events	Test 6425 Run 2 [a] (second)	Test 6424 Run 1 [a] (second)
Bundle power decay initiated	0.5	0.5
Feedwater flow stops	0.5	0.5
Steamline valve completely closed	9.0	8.0
Loop 1 isolated	20.0	20.0
HPCS injection begins	27.0	27.0
LPCS and LPCI activated	37.0	37.0
LPCS flow begins	64.0	64.0
LPCI flow begins	75.0	71.0
End of the test	400.0	400.0
a - Reference 2		

Table C.11.4. TRACE Initial Conditions for Simulation of Test 6425 Run 2

Parameter	Test Conditions [a]	TRACE
Core power (MW)	5.05 ± 0.03	5.05
Steam dome (MPa)	7.198 ± 0.034	7.2
Lower plenum pressure (MPa)	7.384 ± 0.034	7.39
Initial water level (m)	1.85 ± 0.15	1.852
Bundle inlet to outlet DP (KPa)	77 ± 14	90.5
Steam flow (kg/s)	2.7 ± 0.454	2.64
Feedwater flow (kg/s)	0.5 ± 0.136	0.5
Drive pump 1 flow (kg/s)	4.1 ± 0.454	4.04
Drive pump 2 flow (kg/s)	3.8 ± 0.454	3.95
Jet pump 1 flow (kg/s)	10 ± 0.907	9.63
Jet pump 2 flow (kg/s)	9 ± 0.907	9.39
Bundle inlet flow (kg/s)	18 ± 2.27	18.08
a - Reference 2		

C.11.4.1.2. Test 6425/2 Transient Simulation Results

Table C.11.5 lists the key events observed in the test and in the TRACE calculation. As shown in the table, major events and governing phenomena occur in the first 150 seconds or so, when the

bundle liquid level recovery is completed. Discussion of transient results in this section will focus on this time frame.

System Pressure and Break Flow

The calculated and measured system pressures are depicted in Figure C.11-8 The pressure calculated by TRACE matches the measured system pressure closely in the first ~14 seconds. Afterward and until ~250 seconds, the TRACE calculation underpredicts the system pressure.

The break flow rate data are not available in the test data file. The suction line and driveline break flow data in Figure C.11-9 and Figure C.11-10 is from a previous work (Ref. 5). The break flow data was verified using the break flow plots provided in Reference 2. The integrated total break flow data in Figure C.11-11 was derived from the suction line and driveline break flow data.

Figure C.11-11 shows that the integrated total break flow calculated by TRACE agrees well with the data, which may indicate that the underprediction of the system pressure is due to factors other than the break flow. The fact that the calculation starts to underpredict the system pressure (after ~14 seconds) before HPCS injection is initiated at 27 seconds (Table C.11.5) may exclude the condensation induced by HPCS injection water as causation of the underprediction of the system pressure.

Differential Pressures

- Differential Pressure in the Lower Plenum

Figure C.11-12 gives the measured differential pressure in the lower plenum and the calculated differential pressure. The test data shows that for the first 12 seconds the lower plenum is of solid water. The flashing starts at 12 seconds and the differential pressure drops rapidly until ~30 seconds. Afterward and until the end of the test (400 seconds), the differential pressure (or water level) maintains roughly constant, which is an indication of strong CCFL at the bundle side entry orifice (SEO) throughout the test.

Compared to the test data, the TRACE calculation predicts the data trend reasonably well for 0-260 seconds. In the calculation, the bulk flashing occurs at 12 seconds, followed by a period of rapid loss of coolant in the lower plenum until ~30 seconds. The calculated differential pressure drops faster and is settled at a lower value in comparison to the test data for ~12-30 seconds. From ~100 to 130 seconds, the lower plenum sees a slow inventory recovery, which corresponds to the upper plenum starting to dump water the into the bypass at ~100 seconds (Figure C.11-13), the bypass refill (Figure C.11-14) and the core reflooding (Figure C.11-15) during this period. In the calculation, strong CCFL at the bundle SEO is observed for ~0-100 seconds and intermitted CCFL is observed from ~100 seconds until ~260 seconds when refill of the lower plenum occurs.

- Differential Pressure in the Upper Plenum

Figure C.11-13 gives the measured differential pressure and the calculated differential pressure in the upper plenum. It is observed from the test data: 1) In the first ~4 seconds after break, the water level in the upper plenum drops rapidly and then settled at a roughly constant value; 2) At ~14 seconds, the water level experiences certain recovery due to flashing in the lower plenum and guide tube, and then stays at a constant value on average; 3) CCFL at the bypass top breakdown occurs around 110 seconds and the liquid in the upper plenum is completely dumped into the bypass and core by ~130 seconds; 4) after ~130 seconds, no liquid from HPCS and LPCS is accumulated in the upper plenum.

The calculated differential pressure in the upper plenum is in a good agreement with the test data until ~230 seconds. From ~230 seconds on, it indicates some liquid from HPCS and LPCS accumulates in the upper plenum.

- Differential Pressure in the Bypass

Figure C.11-14 gives the measured differential pressure and the calculated differential pressure in the bypass. The calculated differential pressure is in reasonable agreement with the test data. The bypass liquid level experiences a temporary recovery at ~16 seconds due to void flashing in the lower plenum and the guide tube. The water level in the bypass reaches its minimum at ~70 seconds in the test and 50 seconds in the calculation. At ~100 seconds, a rapid refill occurs in the bypass as a result of the upper plenum dumping coolant into the bypass. The bypass refill is completed at ~120 seconds.

The measured differential pressure indicates the bypass experiences a liquid level depression and recovery during ~280-330 seconds (Figure C.11-14). The measured bundle differential pressure (Figure C.11-15) shows that the bundle also experience a liquid level depression and recovery during ~280-350 seconds.However, the test data can not explain where the coolant lost in the bypass and bundle goes especially for 280 - 320 seconds since there is not an increase in the measured differential pressure observed in the lower plenum for this time frame.

- Differential Pressure in the Bundle

Figure C.11-15 gives the measured differential pressure and the calculated differential pressure in the bundle. The calculated differential pressure is in an excellent agreement with the test data up to ~165 seconds. Afterward, the calculated bundle liquid level settles on average at a lower value than the test data.

As shown in Figure C.11-15, after the initial rapid decrease in the bundle liquid level, a temporary recovery occurs at ~15 seconds due to the lower plenum flashing. Then the bundle level continues to decrease until it is almost empty at ~50 seconds. The bundle refill starts at ~100 seconds,

coinciding with the bypass refill. The bundle refill is mainly through the leakage path from the bundle to the bypass. The bundle refill proceeds in a slower pace than the bypass refill as shown in Figure C.11-14 and Figure C.11-15. From ~165 to 400 seconds, the calculated liquid level is lower than the test data.

Rod Cladding Temperatures

Figure C.11-16 through Figure C.11-20 show TRACE calculated and measured cladding temperatures of the heater rods in Group 1 (Figure C.11-6) at five different elevations. The calculated steam-water saturation temperature is also given in these figures. In these plots, each measured rod temperature trace is identified with rod position in the bundle, elevation and power peaking factor. For example, "P07-E130-0.946" means that the temperature trace was measured at elevation 130 inches (relative to the bottom of the heated section) from a rod located at position 07 and its peaking factor of the rod is 0.946. The rod position numbering scheme and peaking factors are shown in Figure C.11-6.

As indicated in Figure C.11-6, the rods in the same group may have different peaking factors, which explains in part the observation that measured temperatures at the same elevation for different rods of the same group may differ. For example, Figure C.11-16 gives the rod cladding measurements at elevation 130 inches for three rods. Rod P33 has a temperature excursion (of no significance) at ~40-70 seconds while Rods P07 and P57 shows no temperature excursion. The heaters rods in the TRACE model represent group-averaged behavior. Considering these factors, it can be concluded from Figure C.11-16 through Figure C.11-20 that the predicted rod cladding temperatures are in reasonable agreement with the measured rod temperatures in term of the magnitude and timing of cladding temperature excursion.

At the same time, it is also noticed that the predicted rod temperatures are typically lower than the measured values outside rod cladding temperature excursion durations. When dryout is not occurring, rods are cooled by steam-water mixture and cladding temperatures follow local saturation temperatures, which in turn are function of local pressures. The underprediction in the system pressure leads to the underprediction of the rod cladding temperature.

Table C.11.5. Sequence of events for TLTA 6425 Run 2

Event	Experiment[b] (seconds)	TRACE (seconds)
Break Initiation (Blowdown valves open)	0	0
Bundle Power Trip	0.5	0.5
Blowdown loop jet pump flow reverses	0.5	0.75

a. void fraction is 50% at 10.0 s and 90% at 25 s at the recirculation suction
b. Reference 2

Table C.11.5. Sequence of events for TLTA 6425 Run 2

Event	Experiment[b] (seconds)	TRACE (seconds)
Feedwater flow stops	0.5	0.5
Bypass flow reverses	1.7	3.3
Jet pump suction uncovers	6.7	~7.0
Steamline valve completely closed	9.0	9.0
Recirc. suction line begins to uncover	9.4	~10.0-25.0[a]
Lower plenum bulk flashing begins	11.0	12.0
Core inlet uncovers (SEO)	20	~14-19
Loop 1 isolated	20	20
HPCS injection begins	27	27
Lower plenum mixture level reaches jet pump exit	35	~20-35
LPCS flow begins	64	64
LPCI flow begins	75	75
Bundle begins to refill	114	~110
Bypass region refilled	125	~120
CCFL breaks down at upper tie plate	~100	~100
Bundle recovery	150	~150
End of test	400	400

a. void fraction is 50% at 10.0 s and 90% at 25 s at the recirculation suction
b. Reference 2

C.11.4.2. Simulation of Test 6424/1

C.11.4.2.1. Test 6424/1 Initial Conditions

One challenge in obtaining the initial conditions for TRACE simulation of Test 6424/1 is that the test was not operated at the steady state before the break valves were opened, as indicated by the mismatch between feedwater flow and steam flow (Table C.11.6). The TLTA facility did not have a feedwater heating system, and as a result, the feedwater water temperature (~294.0K) was much lower than that in a typical BWR plant (~500K). In order to achieve desired fluid parameter distribution and scaled steam flow rate, the feedwater flow of Test 6424/1 was controlled at a lower value.

Due to lack of detailed information on the operation procedure to establish the initial conditions in the test, a steady state calculation is conducted to establish initial conditions for the TRACE

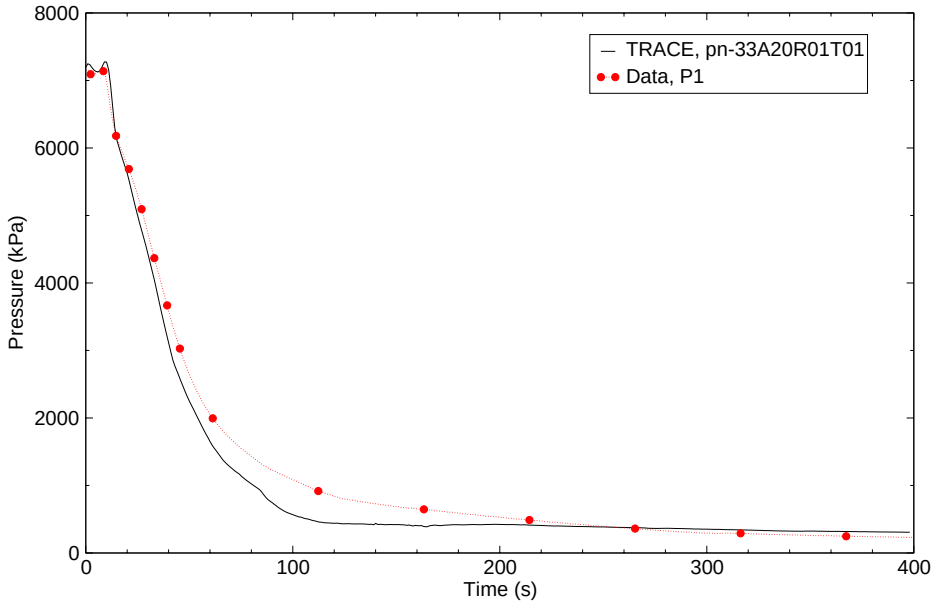

Figure C.11-8. TLTA Test 6425/Run 2 - Vessel Steam Dome Pressure

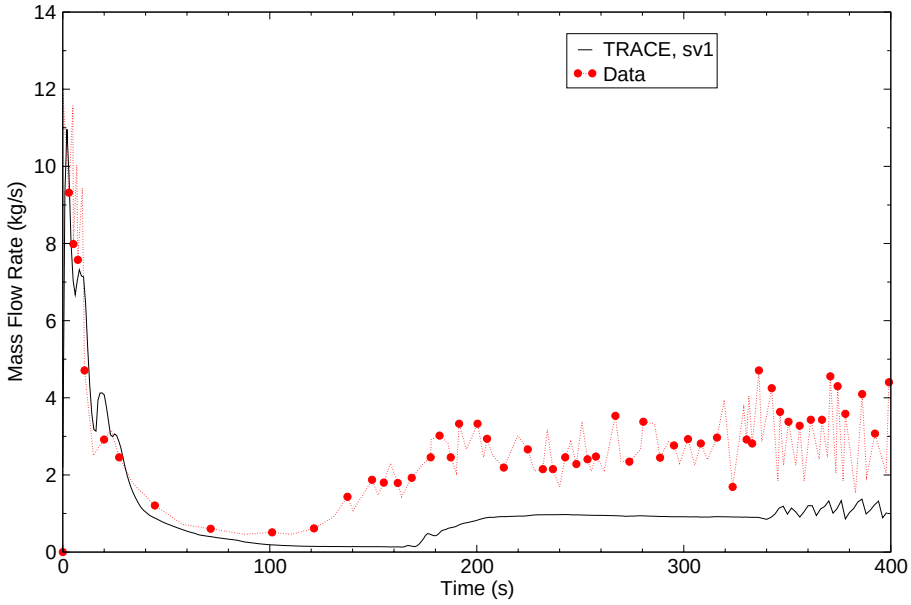

Figure C.11-9. TLTA Test 6425/Run 2 - Suction Line Break Flow Rate

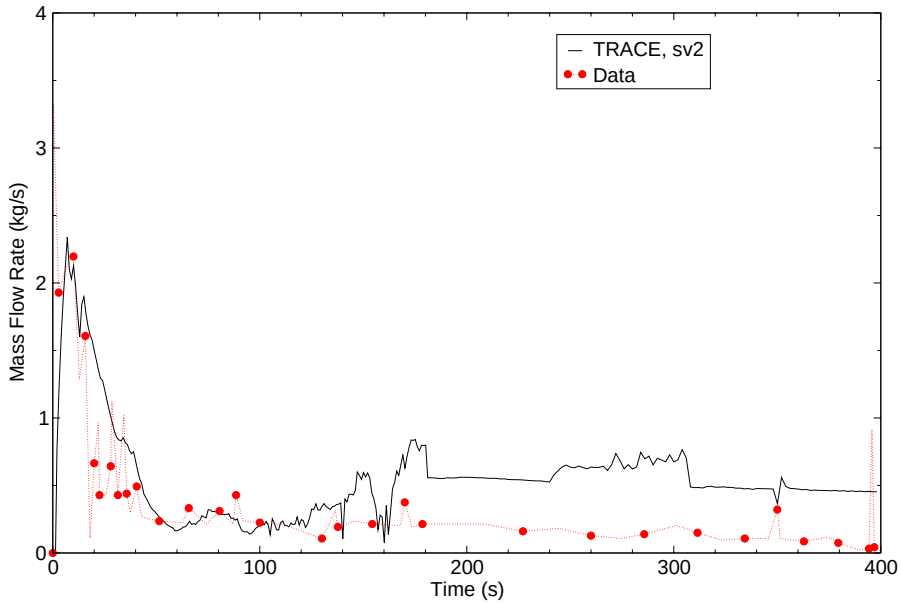

Figure C.11-10. TLTA Test 6425/Run 2 - Driveline Break Flow Rate

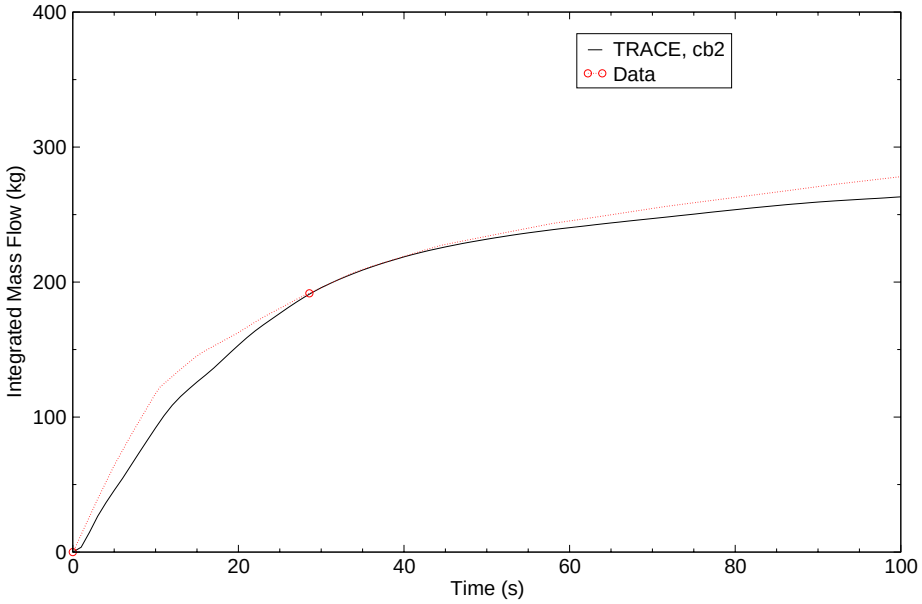

Figure C.11-11. TLTA Test 6425/Run 2 - Integrated Total Break Flow Rate

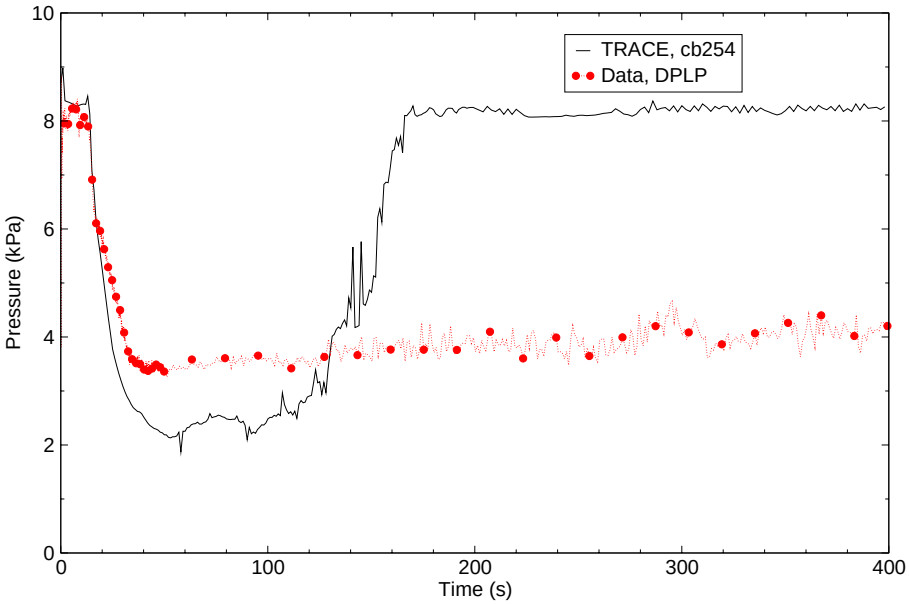

Figure C.11-12. TLTA Test 6425/Run 2 - Lower Plenum Differential Pressure

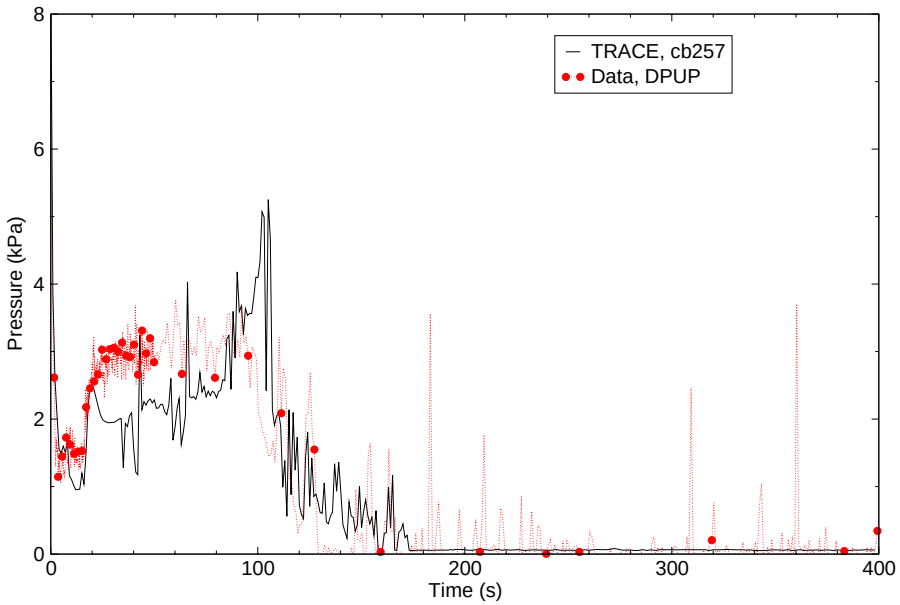

Figure C.11-13. TLTA Test 6425/Run 2 - Upper Plenum Differential Pressure

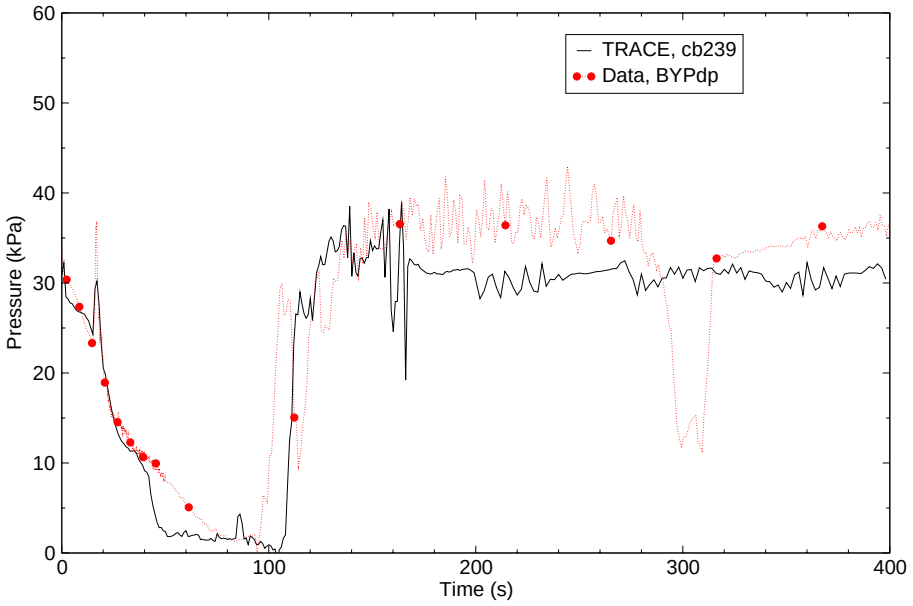

Figure C.11-14. TLTA Test 6425/Run 2 - Bypass Differential Pressure

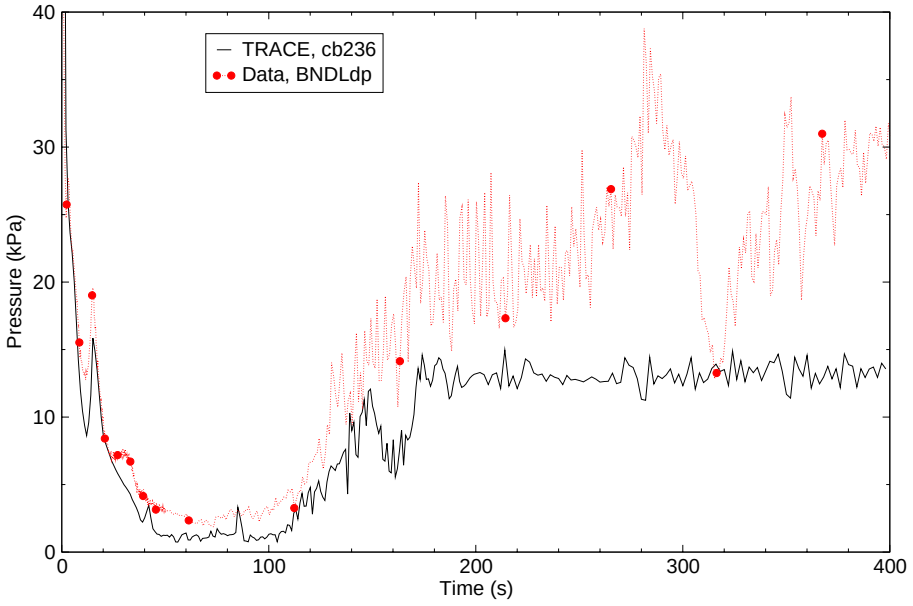

Figure C.11-15. TLTA Test 6425/Run 2 - Bundle Differential Pressure

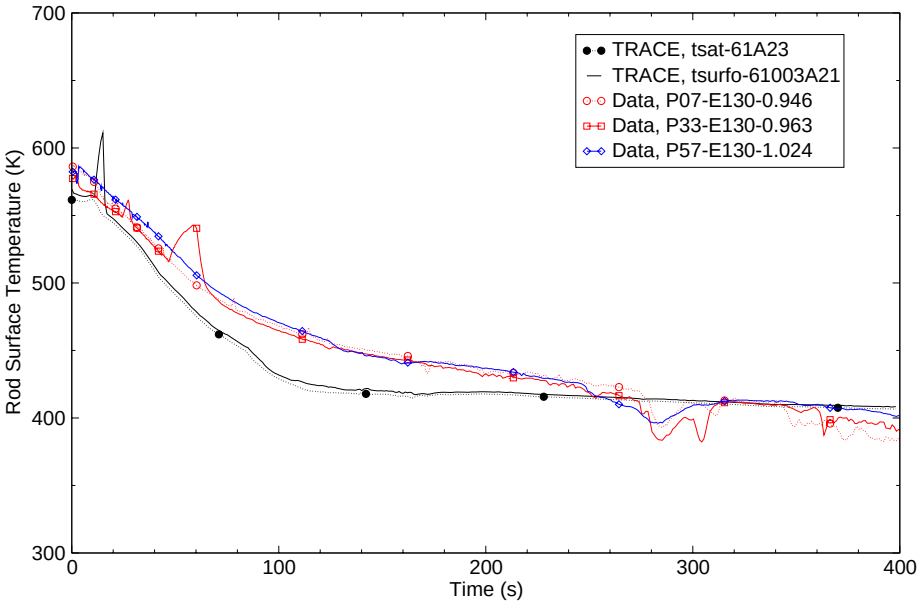

Figure C.11-16. TLTA Test 6425/Run 2 - Rod Cladding Temperatures at Elevation 130 Inches

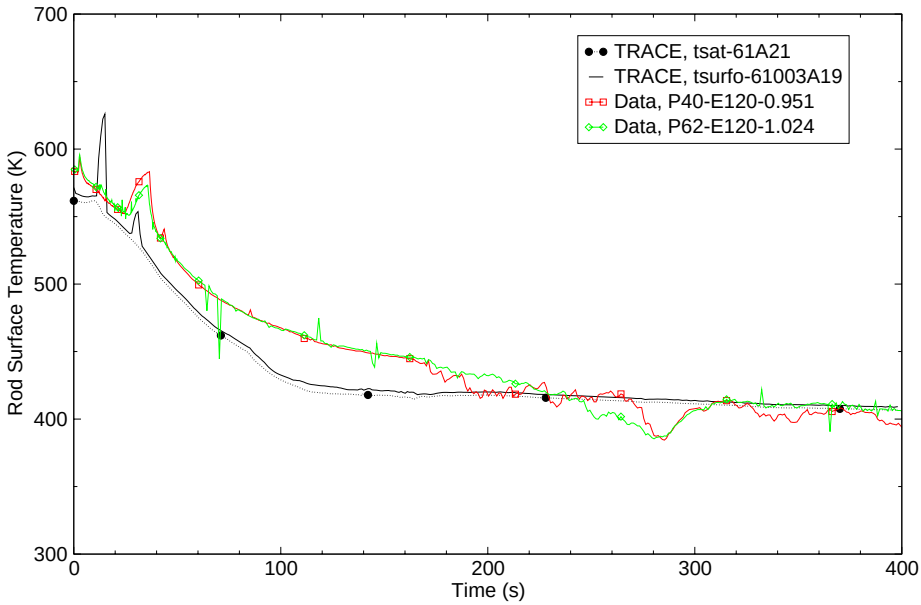

Figure C.11-17. TLTA Test 6425/Run 2 - Rod Cladding Temperature at Elevation 120 Inches

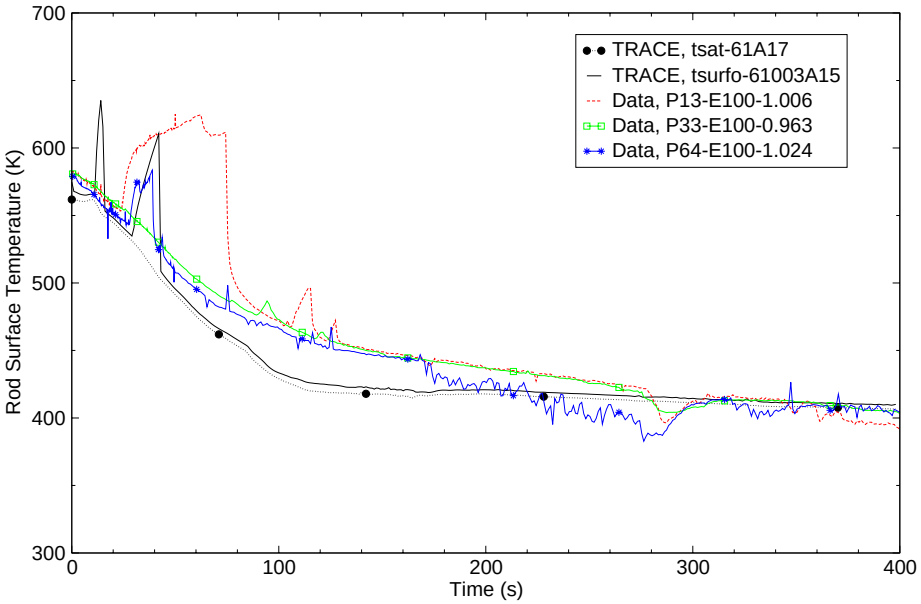

Figure C.11-18. TLTA Test 6425/Run 2 - Rod Cladding Temperature at Elevation 100 Inches

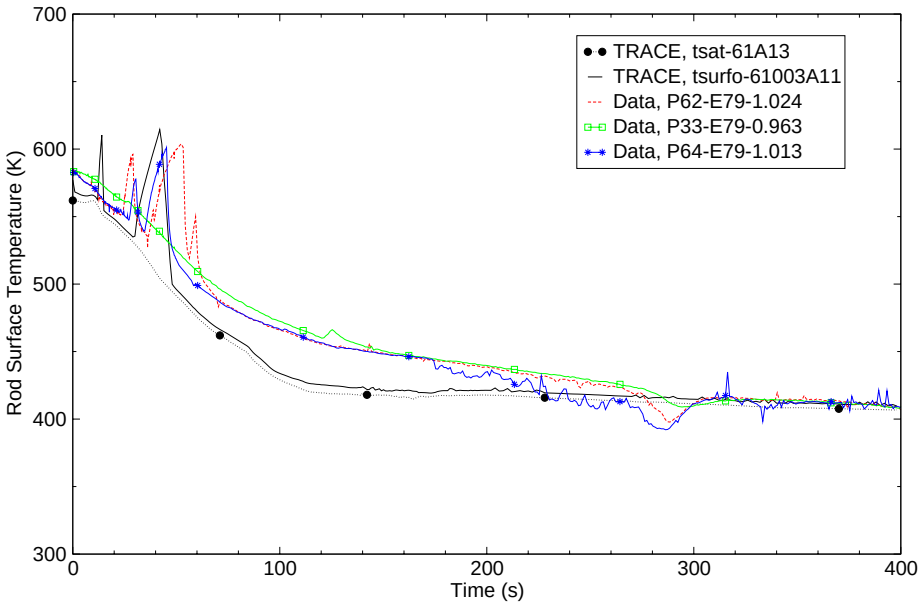

Figure C.11-19. TLTA Test 6425/Run 2 - Rod Cladding Temperature at Elevation 79 Inches

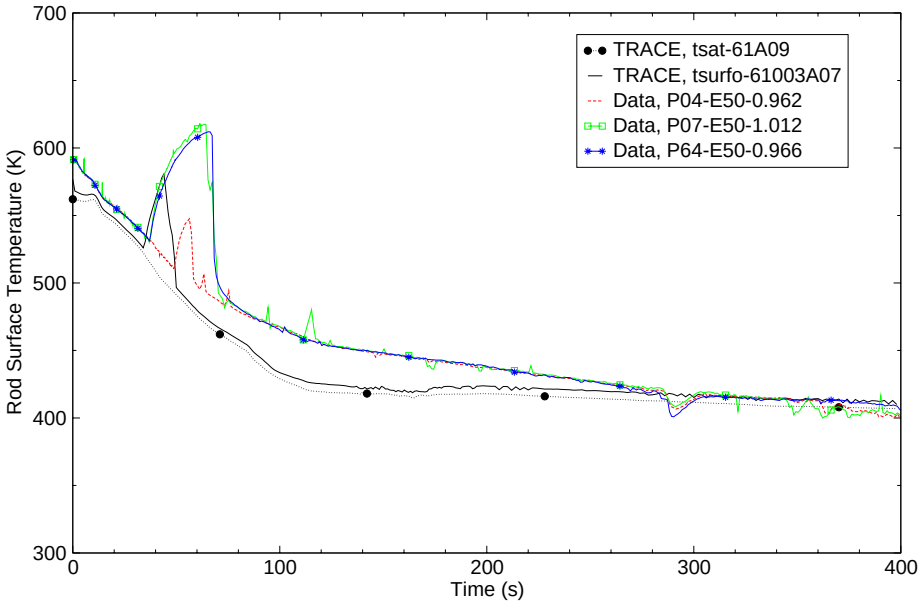

Figure C.11-20. TLTA Test 6425/Run 2 - Rod Cladding Temperature at Elevation 50 Inches

transient calculation. In the TRACE steady-state calculation, the feedwater temperature is raised to 500K whereby the feedwater flow matches the test steam flow rate. Control logics for pressure, water level and JETP flow are employed to achieve desired system parameters (e.g., system pressure, steam flow rate, dowcomer water level) that are close to the test data.

A summary of the initial conditions from the experiment and the TRACE steady-state calculation are listed in Table C.11.6

Table C.11.6. TRACE Initial Conditions for Simulation of Test 6424 Run 1

Parameter	**Test Condition** [a]	**TRACE**
Core power (MW)	6.49 ± 0.03	6.49
Steam dome (MPa)	7.281 ± 0.034	7.281
Lower plenum pressure (MPa)	7.45 ± 0.0344	7.504
Initial water level (m)	3.15 ± 0.1524	3.15
Bundle inlet to outlet DP (KPa)	137.9 ± 13.79	114.5
Steam flow (kg/s)	3.6288 ± 0.4536	3.612

a. Reference 2

b. In the transient simulation, feedwater flow is set at 0.5 Kg/s and feedwater temperature is 294 K for 0-0.5 sec.

Table C.11.6. TRACE Initial Conditions for Simulation of Test 6424 Run 1

Parameter	Test Condition [a]	TRACE
Feedwater flow (kg/s)	0.50 ± 0.136	3.612 [b]
Drive pump 1 flow (kg/s)	3.17 ± 0.4536	3.60
Drive pump 2 flow (kg/s)	3.6288 ± 0.4536	4.256
Jet pump 1 flow (kg/s)	6.35 ± 0.9072	6.346
Jet pump 2 flow (kg/s)	8.165 ± 0.907	8.160
Bundle inlet flow (kg/s)	13.15 ± 2.268	13.776
Lower plenum fluid temperature (K)	546 (averaged)	548 (averaged)

a. Reference 2
b. In the transient simulation, feedwater flow is set at 0.5 Kg/s and feedwater temperature is 294 K for 0-0.5 sec.

C.11.4.2.2. Test 6424/1 Transient Simulation Results

Table C.11.7 lists the key events observed in the test and in the TRACE calculation. As shown in the table and discussion followed in this section, major events and governing phenomena occur in the first 150 seconds or so, by which the bundle and bypass liquid level recovery has completed. Discussion of transient results in this section will focus on this time frame.

System Pressure and Break Flow

The calculated and measured system pressures are shown in Figure C.11-21 The temporary system pressurization in the blowdown phase is due to isolation of the main steam line. The calculation underpredicts the system pressure from ~20 seconds on.

The suction break flow and the drive line break flow rates are shown in Figure C.11-22 and Figure C.11-23. The calculated break flow rates (the suction line and drive line) agree reasonably well with the test data in the first 100 seconds or beyond. However, it is noticeable that the break flow rates are over-estimated ~10-30 seconds when the break flow regime transitions from the single-phase liquid to single-phase vapor. This overprediction in the break flow during this time frame also is reflected on the integrated total flow as shown in Figure C.11-24 (slope of the integrated total break flow represents the total break flow).

Differential Pressures

- Differential Pressure in the Lower Plenum

Figure C.11-25 gives the measured differential pressure and the calculated differential pressure in the lower plenum. The test data shows that for the first 14 seconds the lower plenum is of solid water. The flashing starts at 14 seconds and the differential pressure drops rapidly until ~39

seconds. Afterward and until the end of the test, the differential pressure (or water level) maintains roughly constant, which is an indication of strong CCFL present at the bundle SEO throughout the test.

Compared to the test data, the TRACE calculation predicts the data trend reasonably well for 0-250 seconds. In the calculation, the bulk flashing occurs at 16 seconds, followed a rapid decrease in the liquid level of the lower plenum until 36 seconds. The calculated differential pressure drops faster and is settled at a lower value in comparison to the test data for ~16-36 seconds. For ~90-160 seconds, the lower plenum experiences a slow inventory recovery, which follows the upper plenum starting to dump water (Figure C.11-26), and refill of the bypass (Figure C.11-27) and the bundle (Figure C.11-28) starting at ~85 seconds.

- Differential Pressure in the Upper Plenum

Figure C.11-26 gives the measured differential pressure and the calculated differential pressure in the upper plenum. It is observed from the test data: 1) In the first ~4 seconds after break, the water level in the upper plenum drops rapidly and then settled at a roughly constant value (close to empty); 2) At ~20 seconds, the water level experiences certain recovery, which coincides with a temporary liquid level increase in the bypass at ~20 seconds; 3) After the initiation of LPCS at 63 seconds, the liquid level sees a steady increase up to ~90 seconds when CCFL at the bypass top breakdown occurs and the liquid in the upper plenum starts to drain into the bypass; 4) after ~105 seconds, intermitted liquid level buildup is observed in the upper plenum.

The calculated differential pressure in the upper plenum agrees reasonably well with the test data. However, some discrepancies exist between the calculation and the measurements. The initiation of LPCS injection at 63 seconds, introduces liquid level oscillations, which, instead of leading to a steady increase in the liquid level as in the test, results in an early temporary CCFL breakdown at ~85 seconds. After ~105 seconds, liquid level oscillations are observed as in test but in general the calculated liquid level is higher than the measured.

- Differential Pressures in the Bypass and the Bundle

Figure C.11-27 gives the measured differential pressure and the calculated differential pressure in the bypass. The calculated differential pressure is in reasonable agreement with the test data. Figure C.11-28 gives the measured differential pressure and the calculated differential pressure in the bundle. The calculated differential pressure is in an excellent agreement with the test data up to ~150 seconds. Afterward, the calculated bundle liquid level settles on average at a lower value than the test data. It is also observed that in the calculation the bundle water level has a large spike around 300 seconds for ~30 seconds. This is due to the upper plenum dumping the liquid into the bundle through the bundle exit between ~290-300 seconds (Figure C.11-26)

<u>Rod Cladding Temperatures</u>

Figure C.11-29 through Figure C.11-33 show TRACE calculated and measured cladding temperatures of the heater rods in Group 1 at five different elevations. Figure C.11-30, Figure C.11-32, and Figure C.11-33 indicate that the TRACE calculation gives very good rod cladding temperatures at elevations 120 inches, 79 inches, and 50 inches. Figure C.11-29 gives the predicted and calculated cladding temperatures at the top of the heater rods. Though the calculation shows temperature excursions in the first 20 seconds, the predicted peak temperatures are much lower than the measurements. Figure C.11-31 gives the calculated rod cladding temperature and the measured temperatures from four heater rods at elevation 100 inches. In the test, all the four rods experienced multiple cladding temperature excursions.

Considering that 1) the calculated rod temperature represents averaged-group rod behavior and 2) the CHAN component is one-dimensional and is not designed to capture localized two-dimensional thermal-hydraulic phenomena, the TRACE calculated rod cladding temperature agree reasonably well with the test data.

Table C.11.7. Sequence of events for TLTA 6424 Run 1

Event	Experiment (seconds) [a]	TRACE (seconds)
Break Initiation (Blowdown valves open)	0.0	0.0
Bundle Power Trip	0.5	0.5
Feedwater flow stops	0.5	0.5
Bypass flow reverses	1.2	5.5
Steamline valve completely closed	8.0	8.0
Lower plenum bulk flashing begins	14	16
Loop 1 isolated	20	20
HPCS injection begins	27	27
Lower plenum mixture level reaches jet pump exit	34	~25-40
LPCS flow begins	63	63
LPCI flow begins	71	71
Bundle begins to refill	90	~100
End of experiment	400	400
a - Reference 2		

C.11.5. Assessment Results Summary

Two BWR LBLOCA tests were simulated using TRACE Code Version 5.0. The simulation results generally agree reasonably well. Major events and thermal hydraulic phenomena were captured, e.g. CCFL, break flow, lower plenum flashing, etc. The timings of major events were

well predicted in general. In both simulations, the system pressure was underpredicted. This may relate to the prediction of break flow and/or flashing calculation in the system.

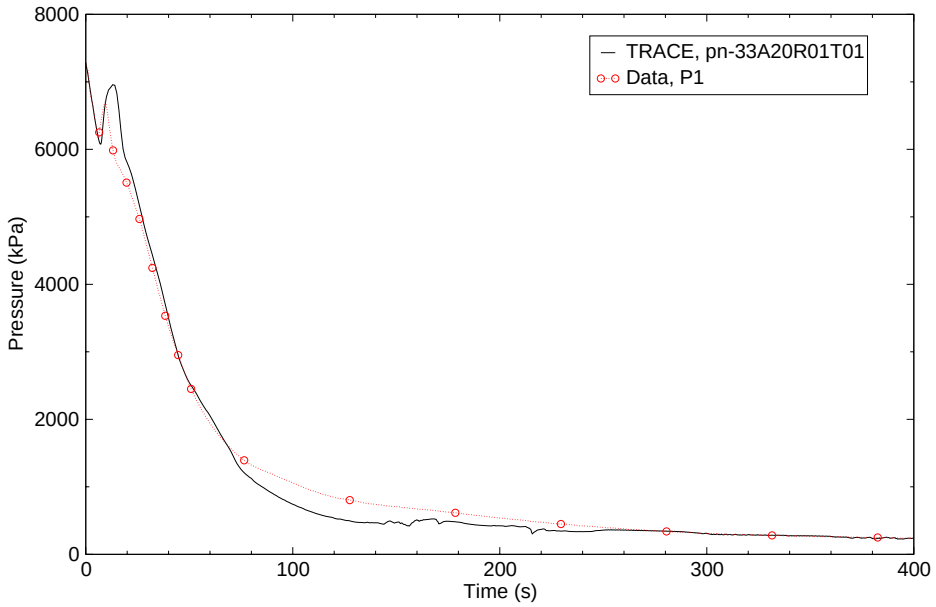

Figure C.11-21. TLTA Test 6424/Run 1 - Vessel Steam Dome Pressure

C.11.6. References

1 L.S. Lee, G. L. Sozzi and S.A. Allison, "BWR Large Break Simulation Tests - BWR Blow-down/Emergency Core Cooling Program", Vol. 1, NUREG/CR-2229, March 1981.

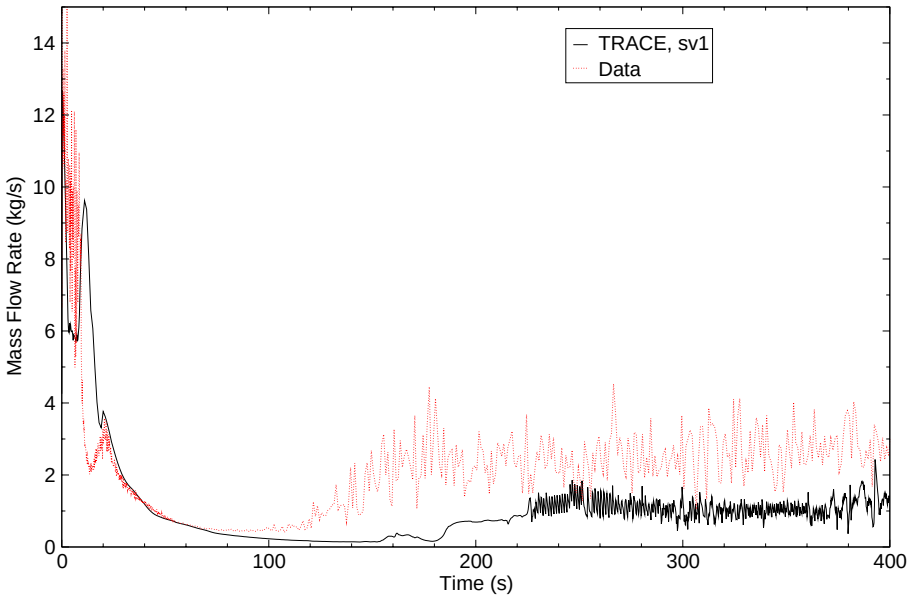

Figure C.11-22. TLTA Test 6424/Run 1 - Suction Line Break Flow Rate

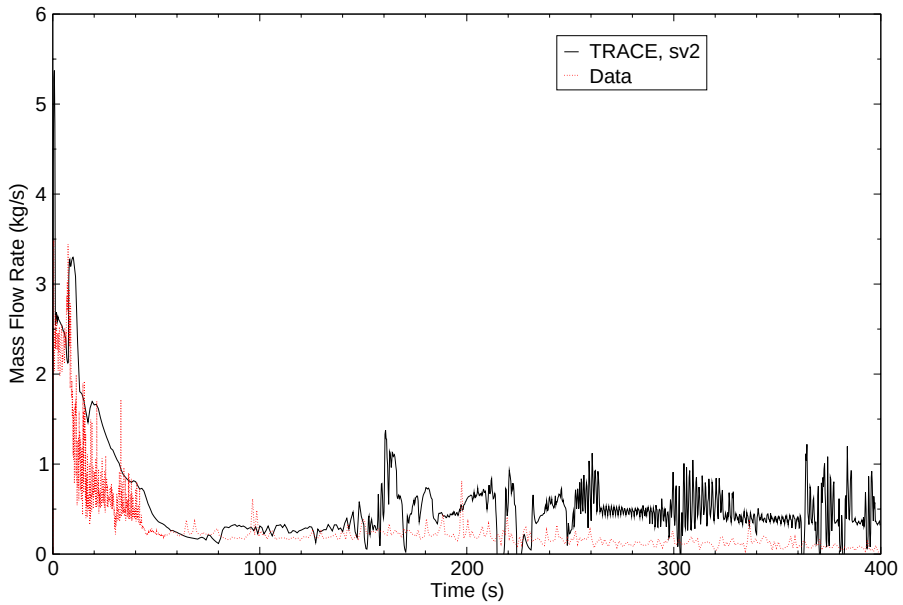

Figure C.11-23. TLTA Test 6424/Run 1 - Driveline Break Flow Rate

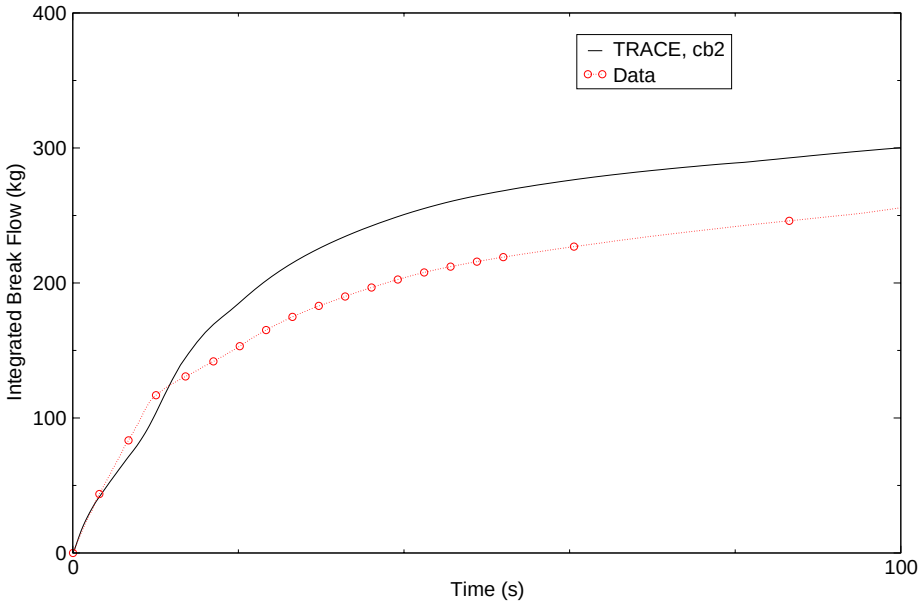

Figure C.11-24. TLTA Test 6424/Run 1 - Total Integrated Break Flow Rate

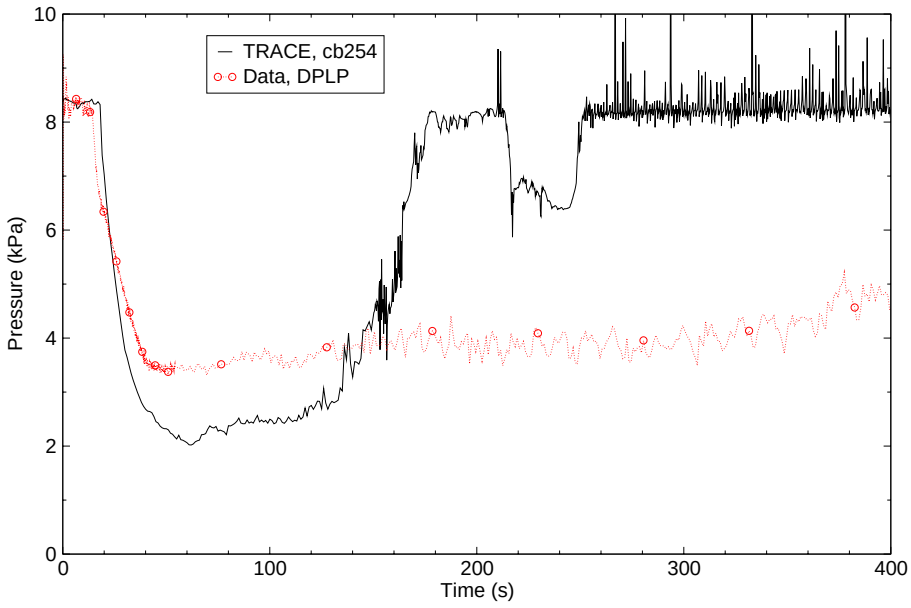

Figure C.11-25. TLTA Test 6424/Run 1 - Lower Plenum Differential Pressure

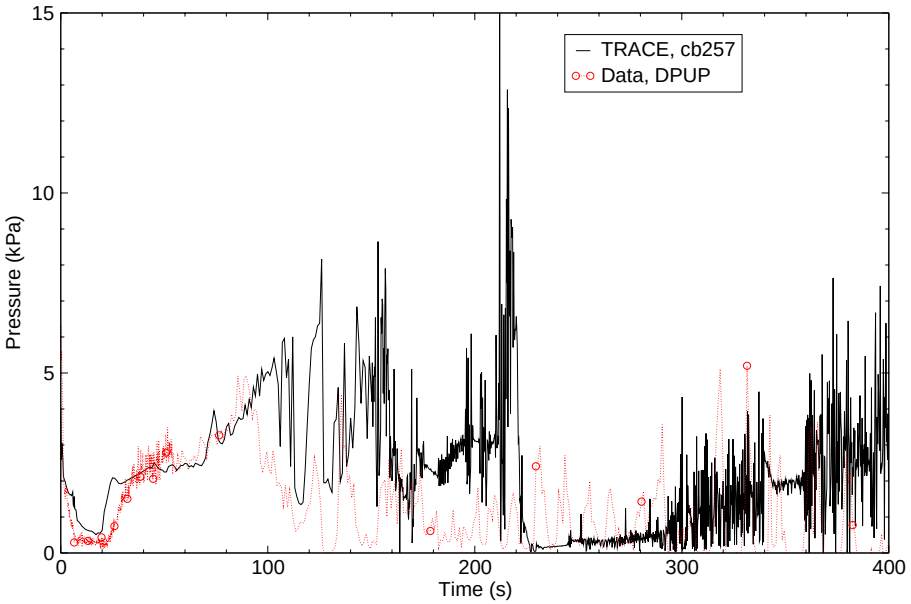

Figure C.11-26. TLTA Test 6424/Run 1 - Upper Plenum Differential Pressure

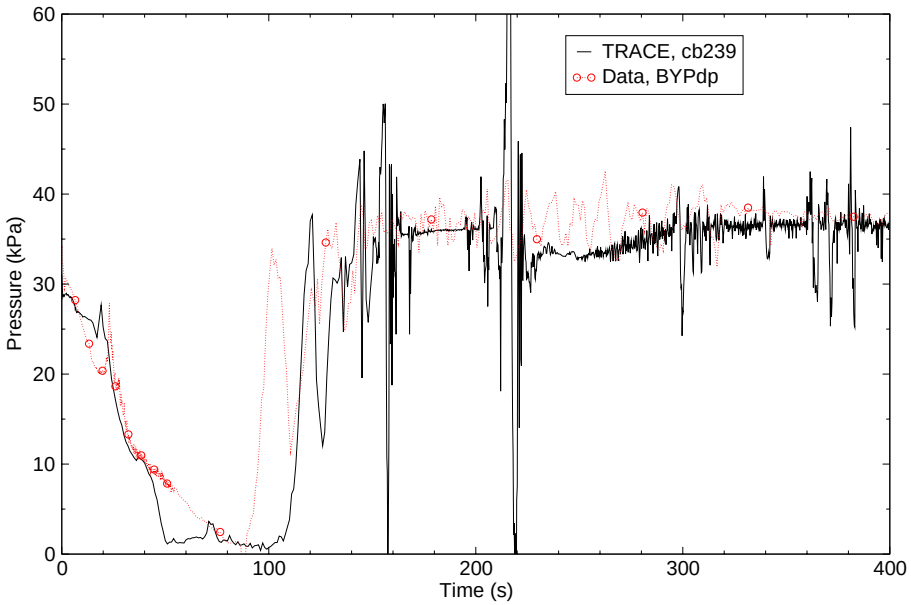

Figure C.11-27. TLTA Test 6424/Run 1 - Bypass Differential Pressure

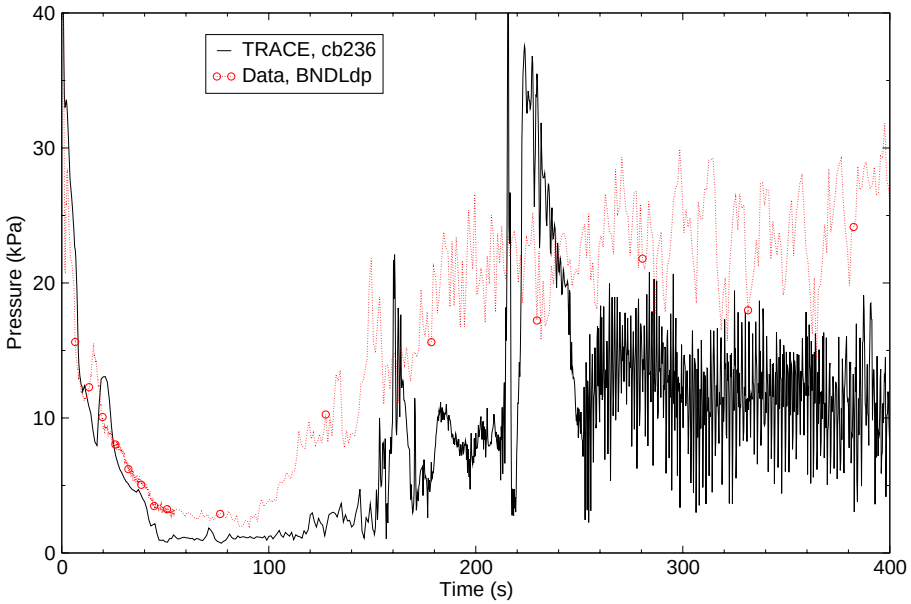

Figure C.11-28. TLTA Test 6424/Run 1 - Bundle Differential Pressure

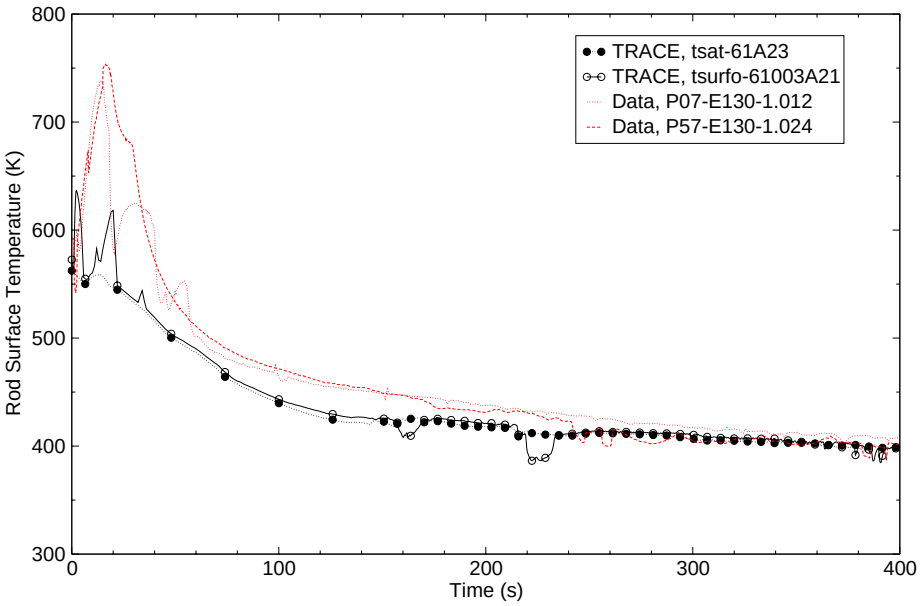

Figure C.11-29. TLTA Test 6424/Run 1 - Rod Temperatures at Elevation 130 Inches

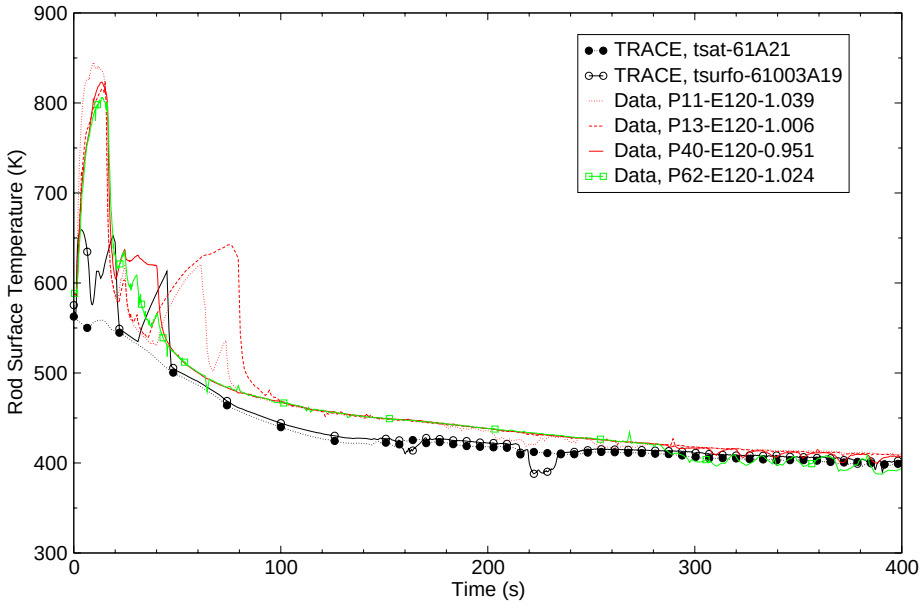

Figure C.11-30. TLTA Test 6424/Run 1 - Rod Cladding Temperature at Elevation 120 Inches

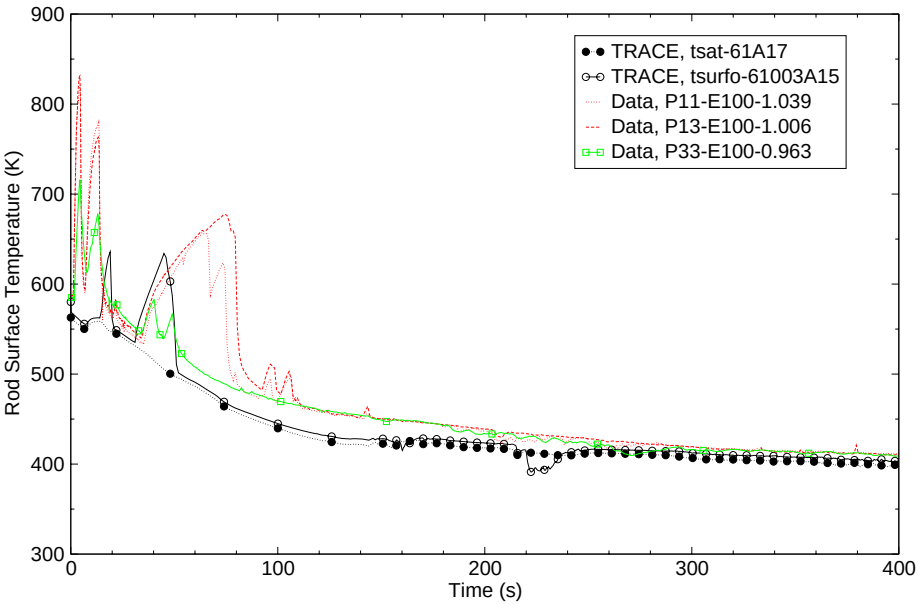

Figure C.11-31. TLTA Test 6424/Run 1 - Rod Cladding Temperature at Elevation 100 Inches

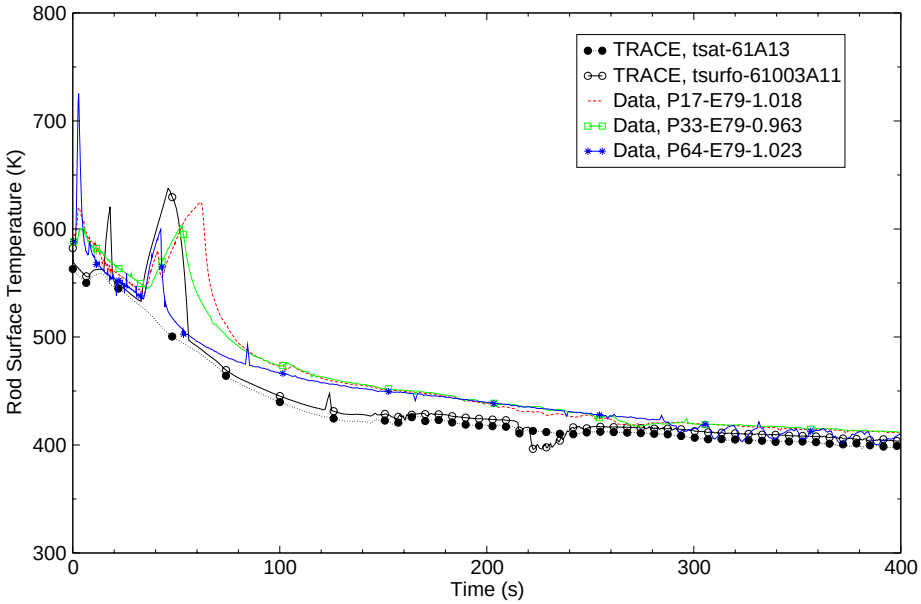

Figure C.11-32. TLTA Test 6424/Run 1 - Rod Cladding Temperature at Elevation 79 Inches

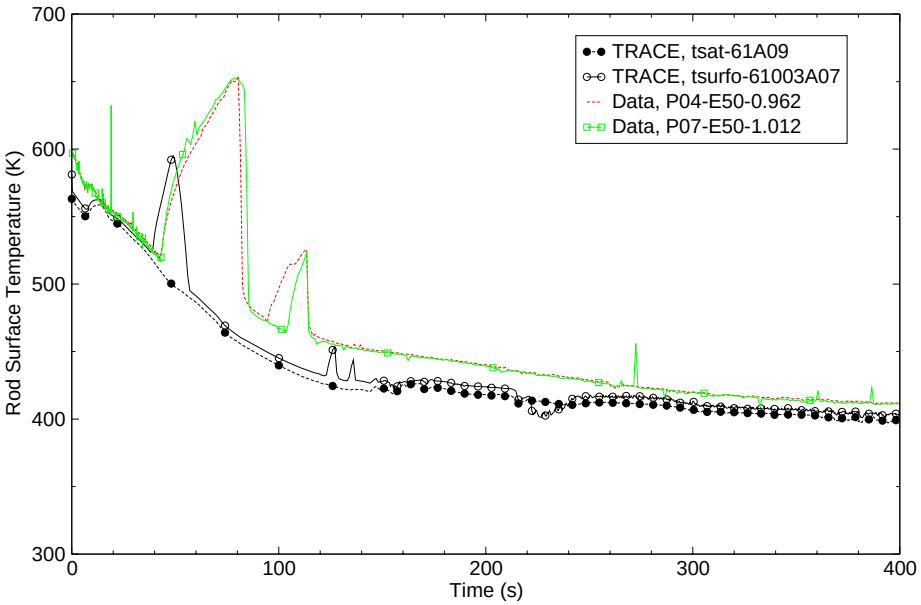

Figure C.11-33. TLTA Test 6424/Run 1 - Rod Cladding Temperature at Elevation 50 Inches

2 L.S. Lee, G. L. Sozzi and S.A. Allison, "BWR Large Break Simulation Tests - BWR Blow-down/Emergency Core Cooling Program", Vol. 2, NUREG/CR-2229, March 1981.

3 A.G. Stephens, "BWR Full Integral Simulation Test (FIST) Program - Facility Description Report", NUREG/CR-2576, Nuclear Regulatory Commission, General Electric Company and Electric Power Research Institute, December 1982.

4 Md. Alamgir, "BWR Refill-Reflood Program Task 4.8 - TRAC-BWR Model Qualification for BWR Safety Analysis Final Report", NUREG/CR-2571, General Electric Company, San Hose, CA, October 1983.

5 Bolander, M., "Simulation of TLTA Large Break Test 6425 Run 2" - Report Task Order No. 6 Task 4, ISL-NSAD-TR-03-03, Nuclear Safety Analysis Division, Information Systems Laboratories, Inc., prepared for the U.S. Nuclear Regulatory Commission, February 2003.